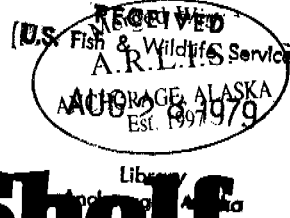


Environmental Assessment of the Alaskan Continental Shelf

Annual Reports of Principal Investigators
for the year ending March 1978

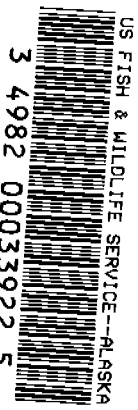
Volume X. Transport



On Reserve



U.S. DEPARTMENT OF COMMERCE
National Oceanic and Atmospheric Administration



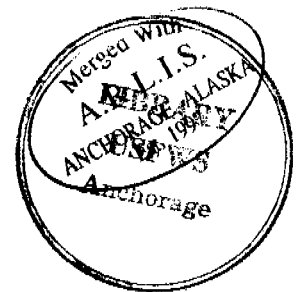
VOLUME I	RECEPTORS -- MAMMALS BIRDS
VOLUME II	RECEPTORS -- BIRDS
VOLUME III	RECEPTORS -- BIRDS
VOLUME IV	RECEPTORS -- FISH, LITTORAL, BENTHOS
VOLUME V	RECEPTORS -- FISH, LITTORAL, BENTHOS
VOLUME VI	RECEPTORS -- MICROBIOLOGY
VOLUME VII	EFFECTS
VOLUME VIII	CONTAMINANT BASELINES
VOLUME IX	TRANSPORT
VOLUME X	TRANSPORT
VOLUME XI	HAZARDS
VOLUME XII	HAZARDS
VOLUME XIII	DATA MANAGEMENT

ARLIS

Alaska Resources
Library & Information Services
Anchorage, Alaska

GC
85.2
.A4
ES7
1978
V.10

Environmental Assessment of the Alaskan Continental Shelf



Annual Reports of Principal Investigators
for the year ending March 1978

Volume X. Transport

Outer Continental Shelf Environmental Assessment Program
Boulder, Colorado

October 1978

U.S. DEPARTMENT OF COMMERCE
National Oceanic and Atmospheric Administration

U.S. DEPARTMENT OF INTERIOR
Bureau of Land Management

ARLIS
Alaska Resources
Library & Information Services
Anchorage, Alaska

DISCLAIMER

The National Oceanic and Atmospheric Administration (NOAA) does not approve, recommend, or endorse any proprietary product or proprietary material mentioned in this publication. No reference shall be made to NOAA or to this publication furnished by NOAA in any advertising or sales promotion which would indicate or imply that NOAA approves, recommends, or endorses any proprietary product or proprietary material mentioned herein, or which has as its purpose an intent to cause directly or indirectly the advertised product to be used or purchased because of this publication.

ACKNOWLEDGMENT

These annual reports were submitted as part of contracts with the Outer Continental Shelf Environmental Assessment Program under major funding from the Bureau of Land Management.

TRANSPORT

Contents

<u>RU #</u>	<u>PI - Agency</u>	<u>Title</u>	<u>Page</u>
257	Stringer, W. - Geophysical Inst. Univ. of Alaska Fairbanks, AK	Morphology of Beaufort, Chukchi and Bering Seas Near Shore Ice Conditions by Means of Satellite and Aerial Remote Sensing	1
265	Shapiro, L. - Geophysical Inst. Univ. of Alaska Fairbanks, AK	Development of Hardware and Procedures for <u>In-</u> <u>Situ</u> Measurement of Creep in Sea Ice	221
267	Belon, A. - Geophysical Inst. Univ. of Alaska Fairbanks, AK	Operation of an Alaskan Facility for Applications of Remote-Sensing Data to OCS Studies	260
289	Royer, T. - Inst. of Marine Science (IMS) Univ. of Alaska Fairbanks, AK	Circulation and Water Masses in the Gulf of Alaska	292
367	Reynolds, R. - Pacific Marine Environmental Lab/NOAA Seattle, WA	Near-shore Meteorology	324
435	Leendertse, J. - Rand Corp. Liu, S. Santa Monica, California	Modeling of Tides and Circulations of the Bering Sea	569
519	Leavitt, E. - Polar Science Center Univ. of WA Seattle, WA	Coastal Meteorology of the Alaskan Arctic Coast	580
526	Matthews, J. - Geophysical Inst. Univ. of Alaska Fairbanks, AK	Characterization of the Nearshore Hydrodynamics of an Arctic Barrier Island - Lagoon System	607

<u>RU #</u>	<u>PI - Agency</u>	<u>Title</u>	<u>Page</u>
529	Naidu, A. - IMS Univ. of Alaska Fairbanks, AK	Sediment Characteristics, Stability, and Origin of the Barrier Island-Lagoon Complex, North Arctic Alaska	628
530	Cannon, P. - Dept. of Geology Univ. of Alaska Fairbanks, AK	The Environmental Geology and Geomorphology of the Barrier Island - Lagoon System along the Beaufort Sea Coastal Plain from Prudhoe Bay to the Colville River	687
531 (Annual Rpt.)	Mungall, J. - Dept. of Ocean- ography Texas A&M Univ. College Station, Texas	Oceanographic Processes in a Beaufort Sea Barrier Island-Lagoon System: Numerical Modeling and Current Measurements	732
531 (Quarterly Rpt.)	Mungall, J. - Dept. of Ocean- ography Texas A&M Univ. College Station, Texas	Oceanographic Processes in a Beaufort Sea Barrier Island-Lagoon System: Numerical Modelling and Current Measurements	831
536	Frank, M. - Naval Arctic Laursen, G. Research Lab. Barrow, AK	Development and Operations of a Remote Sensing Data Acquisition Platform for OCS Studies	835
540	Nummedal, D. - Dept. of Geology et al. Univ. of S. C. Columbia, SC	Oil Spill Vulnerability of the Beaufort Sea Coast	853
541/550	Coachman, L. - Univ. of WA et al. Seattle, WA Charnell, R. - PMEL/NOAA et al. Seattle, WA	Norton Sound/Chukchi Sea Oceanographic Processes (N-COP)	860

ANNUAL REPORT

Contract #03-5-022-55
Research Unit #257
Reporting Period 1 April 1977 -
31 March 1978
Number of pages 223
Additional maps 46

Morphology of Beaufort, Chukchi and Bering Seas
Near Shore Ice Conditions by Means of Satellite
and Aerial Remote Sensing

Principal Investigator

William J. Stringer
Geophysical Institute
University of Alaska
Fairbanks, Alaska 99701

Assisted by

Stephen A. Barrett
Linda Schreurs

Table of Contents

List of Figures

- I. Summary of Objectives, Conclusions and Implications with Respect to OCS Oil and Gas Development
- II. Introduction
 - A. General nature and scope of study
 - B. Specific objectives
 - C. Relevance
- III. Current State of Knowledge
- IV. Study Area
 - A. Geographic area
 - B. Physical setting
 - C. Climate
- V. Sources, Methods and Rationale of Data Collection
 - A. Selection of sources for analysis
 - B. Mapping technique
 - C. Creation of composite data products
 - D. Ground truth
 - E. Applicability of techniques developed to other places where near shore ice is a hazard
- VI. Results
 - A. Interpretation of ice maps
 - B. Beaufort sea results
 - C. Chukchi sea results
 - D. Bering sea results
- VII. Discussion
 - A. Capabilities
 - B. Limitations
 - C. Discussion of the detectability of Ice Islands
- VIII. Conclusions
 - A. Beaufort Sea
 - B. Chukchi Sea
 - C. Bering Sea

Milestone Chart

- IX. Summary of Fourth Quarter Operations
 - A. Ship or Laboratory Activity
 - B. Problems Encountered/Recommended Changes
 - C. Estimate of Funds Expended
- X. List of References

Appendix A

List of Figures

<u>No.</u>	
V-1	Beaufort Sea Image Location Map: Images 1222-1239
V-2	Beaufort Sea Image Location Map: Images 1312-1329
V-3	Beaufort Sea Image Location Map: Images 1330-1347
V-4	Beaufort Sea Image Location Map: Images 1582-1599
V-5	Beaufort Sea Image Location Map: Images 1600-1619
V-6	Beaufort Sea Image Location Map: Images 1636-1654
V-7	Beaufort Sea Image Location Map: Images 1690-1707
V-8	Beaufort Sea Image Location Map: Images 1708-1725
V-9	Beaufort Sea Image Location Map: Images 1726-1743
V-10	Beaufort Sea Image Location Map: Images 1942-1960
V-11	Beaufort Sea Image Location Map: Images 2147-2164
V-12	Beaufort Sea Image Location Map: Images 2165-2182
V-13	Beaufort Sea Image Location Map: Images 2273-2290
V-14	Beaufort Sea Image Location Map: Images 2381-2398
V-15	Beaufort Sea Image Location Map: Images 2399-2416
V-16	Beaufort Sea Image Location Map: Images 2435-2452
V-17	Beaufort Sea Image Location Map: Images 2525-2542

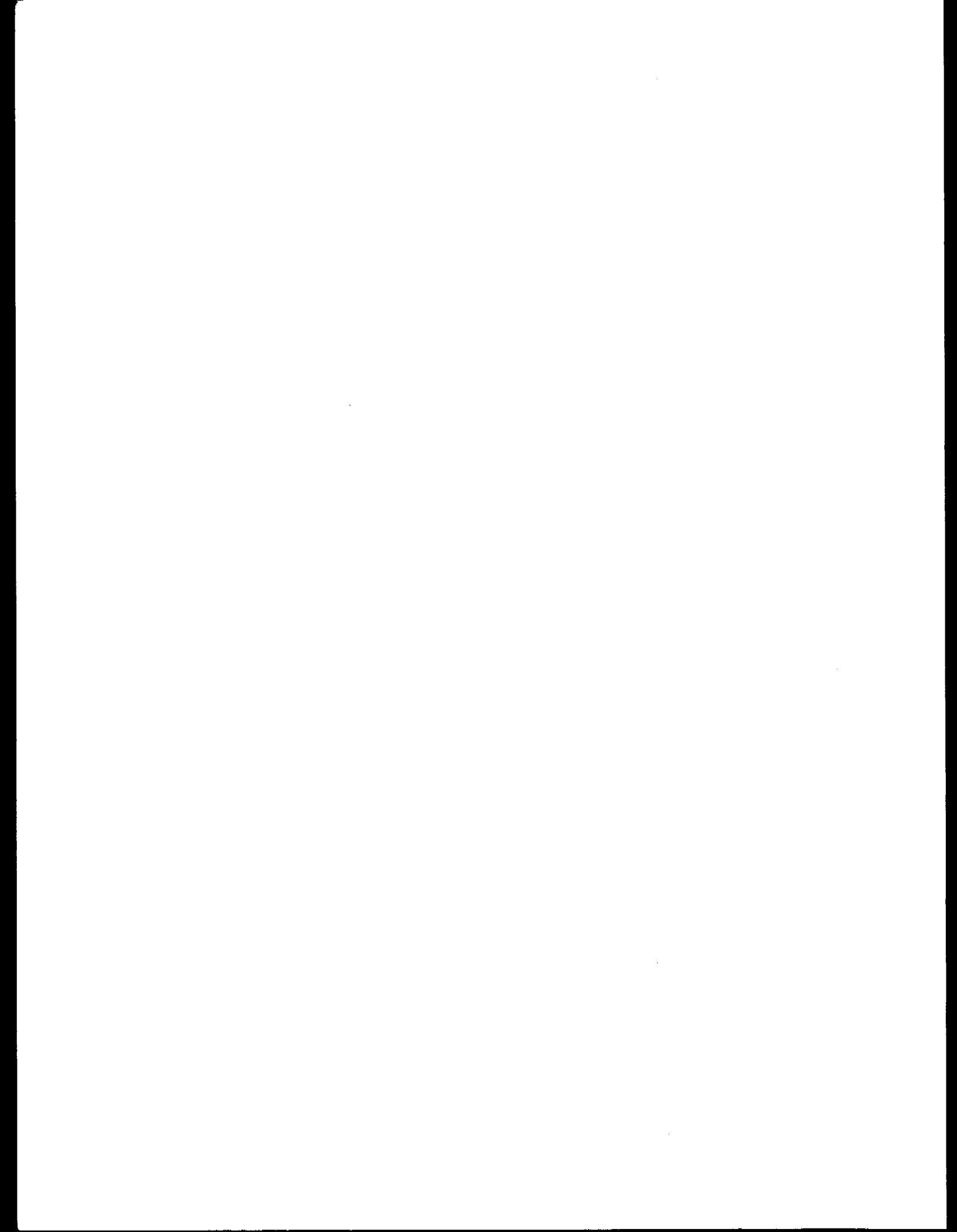
- V-18 Beaufort Sea Image Location Map:
Images 2543-2560
- V-19 Beaufort Sea Image Location Map:
Images 2741-2758
- V-20 Beaufort Sea Image Location Map:
Images 2759-2776
- V-21 Beaufort Sea Image Location Map:
Images 2777-2794
- V-22 Beaufort Sea Image Location Map:
Image 2795-2812
- V-23 Beaufort Sea Image Location Map:
Images 2813-2830
- V-24 Beaufort Sea Image Location Map:
Images 2831-2848
- V-25 Beaufort Sea Image Location Map:
Images 2849-2866
- V-26 Beaufort Sea Image Location Map:
Images 2867-2884
- V-27 Beaufort Sea Image Location Map:
Images 2885-2902
- V-28 Beaufort Sea Image Location Map:
Images 5804-5821
- V-29 Beaufort Sea Images Location Map:
Images 2903-2920
- V-30 Beaufort Sea Images Location Map:
Images Ascending Node Images (Nighttime)
- V-31 Chukchi Sea Image Location Map:
Images 1222-1239
- V-32 Chukchi Sea Image Location Map:
Images 1258-1275
- V-33 Chukchi Sea Image Location Map:
Images 1312-1329
- V-34 Chukchi Sea Image Location Map:
Images 1492-1509
- V-35 Chukchi Sea Image Location Map:
Images 1582-1599
- V-36 Chukchi Sea Image Location Map:
Images 1618-1635

- V-37 Chukchi Sea Image Location Map:
Images 1672-1689
- V-38 Chukchi Sea Image Location Map:
Images 1690-1707
- V-39 Chukchi Sea Image Location Map:
Images 1816-1833
- V-40 Chukchi Sea Image Location Map:
Images 1942-1959
- V-41 Chukchi Sea Image Location Map:
Images 1978-1995
- V-42 Chukchi Sea Image Location Map:
Images 2075-2092
- V-43 Chukchi Sea Image Location Map:
Images 2128-2145
- V-44 Chukchi Sea Image Location Map:
Images 2272-2290
- V-45 Chukchi Sea Image Location Map:
Images 2291-2308
- V-46 Chukchi Sea Image Location Map:
Images 2381-2398
- V-47 Chukchi Sea Image Location Map:
Images 2399-2416
- V-48 Bering Sea Image Location Map:
Images 2444-2461
- V-49 Bering Sea Image Location Map:
Images 2390-2407
- V-50 Bering Sea Image Location Map:
Images 2372-2389
- V-51 Bering Sea Image Location Map:
Images 2102-2119
- V-52 Bering Sea Image Location Map:
Images 1942-1954
- V-53 Bering Sea Image Location Map:
Images 1664-1681
- V-54 Bering Sea Image Location Map:
Images 1592-1609
- V-55 Bering Sea Image Location Map:
Images 1574-1591

V-56	Bering Sea Image Location Map: Images 1286-1303	
V-57	Bering Sea Image Location Map: Images 1232-1249	
VI-1	1973 Contiguous Ice Edge Map--Beaufort Sea	MS*
VI-2	1974 Contiguous Ice Edge Map--Beaufort Sea	MS
VI-3	1975 Contiguous Ice Edge Map--Beaufort Sea	MS
VI-4	1976 Contiguous Ice Edge Map--Beaufort Sea	MS
VI-5	1977 Contiguous Ice Edge Map--Beaufort Sea	MS
VI-6	Late Winter Contiguous Ice Edge Map--Beaufort Sea	MS
VI-7	Early Spring Contiguous Ice Edge Map--Beaufort Sea	MS
VI-8	Late Spring--Early Summer Contiguous Ice Edge Map--Beaufort Sea	MS
VI-9	1973 Ridge System Map--Beaufort Sea	MS
VI-10	1974 Ridge System Map--Beaufort Sea	MS
VI-11	1975 Ridge System Map--Beaufort Sea	MS
VI-12	1976 Ridge System Map--Beaufort Sea	MS
VI-13	1977 Ridge System Map--Beaufort Sea	MS
VI-14	Composite Ridge System Map--Beaufort Sea	MS
VI-15	Composite Stationary Ice Map--Beaufort Sea	MS
VI-16	1973 Open Water Map--Beaufort Sea	
VI-17	1974 Open Water Map--Beaufort Sea	
VI-18	1975 Open Water Map--Beaufort Sea	
VI-19	1976 Open Water Map--Beaufort Sea	
VI-20	1977 Open Water Map--Beaufort Sea	
VI-21	1973 Contiguous Ice Edge Map--Chukchi Sea	MS
VI-22	1974 Contiguous Ice Edge Map--Chukchi Sea	MS
VI-23	1975 Contiguous Ice Edge Map--Chukchi Sea	MS
VI-24	1976 Contiguous Ice Edge Map--Chukchi Sea	MS

VI-25	Late Winter Contiguous Ice Edge--Chukchi Sea	MS
VI-26	Mid-spring Contiguous Ice Edge--Chukchi Sea	MS
VI-27	Late Spring--Early Summer--Chukchi Sea	MS
VI-28	Average Late Winter Contiguous Ice Edge--Chukchi Sea	MS
VI-29	Average Mid-spring Contiguous Ice Edge--Chukchi Sea	MS
VI-30	Average Late Spring--Early Summer Ice Edge--Chukchi Sea	MS
VI-31	Migration of Average Seasonal Edge of Contiguous Ice - Chukchi Sea	MS
VI-32	1973 Ice Ridge System Map--Chukchi Sea	MS
VI-33	1974 Ice Ridge System Map--Chukchi Sea	MS
VI-34	1975 Ice Ridge System Map--Chukchi Sea	MS
VI-35	1976 Ice Ridge System Map--Chukchi Sea	MS
VI-36	Composite Ridge System Map--Chukchi Sea	MS
VI-37	Bering Sea Migration of Contiguous Ice Edge	MS
VIII-1	Beaufort Sea Late Fall--Early Winter Morphology Map	MS
VIII-2	Beaufort Sea Mid-winter--Late Spring Morphology	MS
VIII-3	Beaufort Sea Ice Hazard Map	MS
VIII-4	Chukchi Sea Mid-winter Morphology Map	MS
VIII-5	Chukchi Sea Early Spring Morphology Map	MS
VIII-6	Chukchi Sea Late Spring Morphology Map	MS
VIII-7	Chukchi Sea Ice Hazard Map	MS
VIII-8	Bering Sea Morphology Map	MS

* MS -- These maps are in the attached map section.



I. Summary of Objectives, Conclusions and Implications with Respect to OCS Oil and Gas Development

The objective of this research unit is to develop a morphology of near shore ice along the Beaufort, Chukchi and Bering coasts of Alaska, and identify those features which may represent hazards imposed by ice conditions on OCS oil and gas development.

Winter and spring Beaufort and Chukchi Sea near-shore ice conditions have been analyzed for 1973, 1974, 1975, 1976, and 1977. The chief objective of this analysis was to assess hazards related to activities associated with offshore petroleum developments.

Landsat imagery has been utilized to map major ice features related to regional ice morphology. Following this, significant features from individual Landsat image maps have been combined to yield regional maps of major ice ridge systems for each year of study and maps of flaw lead systems for representative seasons during each year of study. These regional maps have, in turn, been used to prepare seasonal ice morphology maps.

The seasonal ice morphology maps show, in terms of a zonal analysis, regions of statistically uniform ice behavior. The behavioral characteristics of each zone have been described in terms of coastal processes and bathymetric configuration.

Based on the combined seasonal morphologies, a zonal analysis of potential hazards related to offshore petroleum development has been made for the Chukchi and Beaufort seas. The hazards addressed are: safety of field personnel performing offshore geologic reconnaissance, large-scale displacement or deformation of fast ice sheet, the probability of formation of large ice ridge systems which could bring large forces to bear on offshore structures, and the possible fate of an under-ice oil spill.

The general conclusion is that near shore sea ice behavioral patterns are similar from year to year thereby yielding some predictability in terms of offshore sea ice hazards to oil and gas development.

The implications are that geographical zones of different design and construction criteria can be established in the offshore areas taking into consideration the probability of damage to the structure by adverse ice conditions and the relative risk imposed to the adjacent ecosystems.

II. Introduction

A. General nature and scope of study

Environmental concerns stemming from the possibility of petroleum-related development on the Alaskan Continental Shelf have brought about great interest in Alaskan coastal processes. The distinctive feature of the arctic coasts of Alaska is that for a significant portion of the year these coastal waters are covered by ice. Clearly, an understanding of the dynamic morphology of ice in near shore areas is essential to an assessment of environmental and personnel risks imposed by offshore petroleum developments. The goal of this project has been to develop a synoptic picture of ice behavioral patterns along the Alaskan coast and to describe this morphology in such a way that the environmental and human risks can be identified.

Obviously the greatest ice-related influence on environmental hazards arising from petroleum development in ice-frequented waters arises from containment of petroleum under or within the ice. For this reason, it is necessary to develop a morphology of near shore ice characteristics and address this problem through those characteristics.

A second hazard related to ice, although not environmental, is the hazard personnel and equipment are subjected to when using ice as platform in exploratory work. This risk can be evaluated through determination of persistence of ice sufficiently stable to act as an exploration platform.

The possibility of deposition of petroleum on the undersurface of arctic ice, its possible toxic effects and the ultimate fate of such a deposition should be considered. The problems involved include:

- 1) entrapment of light, water-soluble fractions of petroleum under the ice barrier with resulting prolonged high concentration of these known toxic agents,
- 2) difficulty in detection and delineation of the extent of the spill,
- 3) possible transport of petroleum beneath the ice or with ice during dynamic events, and
- 4) clean-up difficulties caused by combinations of 1 through 3 and possible danger to personnel and equipment during dynamic ice events.

Ice conditions vary significantly depending on season and geographic location. Although the morphology presented later will be more complex, for the sake of this introduction two major zones of ice in near shore areas need be considered. These are:

- 1) The "fast ice zone", the area generally shoreward of the 20-meter isobath with quite stable ice much of the ice year. (December through June.)
- 2) The "shear zone", the area generally extending some distance beyond the 20-meter isobath. In this zone the ice potentially can undergo shear to the point of failure and move with respect to the fast ice at any time.

Within each zone the year can be broken into several behavioral periods. These are:

<u>Month</u>	<u>Fast Zone Period</u>	<u>Shear Zone Period</u>
Oct.	<u>Freeze-up:</u> Ice freezes in place or is driven into near shore areas and piled. Grounded ridges formed out to the 20-meter isobath. The result is a stable sheet of fast ice.	<u>Freeze-up:</u> Complex process with periods possibly including pack ice, new ice pans, open water, etc. Result is nearly complete covering of ocean with ice not stable and subject to motion.
Nov. Dec. Jan. Feb.	<u>Stable:</u> Ice within zone is stable with few leads resulting from shear. Cracks can occur resulting from temperature-related tension and tidal processes. Opening and closing of these cracks can cause micro-ridging.	<u>Semi-stable:</u> Static ice can extend several tens of km seaward beyond fast ice for several weeks at a time. Ice can fail in shear at any time.
Mar. Apr. May.	Ice grows in thickness approaching 2 meters by end of period.	<u>Shearing and refreezing:</u> Ice more prone to shearing events and failure adjacent to edge of grounded ridges. However, after failure with cessation of motion, tendency for ice cover to be reestablished by freezing.
June July	<u>Decay and break-up:</u> Solar flux sufficiently great to initiate melting. Grounded ridges break up, fast ice melts close to shore, breaks up and melts farther offshore.	<u>Close pack:</u> successive shearing events break-up ice into pans of various size. Refreezing does not take place. Ice subject to significant displacement resulting from currents and winds.
Aug. Sept.	<u>Ice Free:</u> Area generally of ice except for grounded remnants and blown-in pack ice.	<u>Ice Free:</u> Area generally free of ice except for blown-in pack ice and grounded features including ice islands.

B. Specific Objectives

Specifically, this comprehensive morphology includes a synoptic picture of the development and extent of fast ice, the construction and location of pressure and shear ridges, the location and persistence of grounded ice features including ice islands, stamuki, ridges and hummock fields and the interrelationships among these phenomena.

In addition, this comprehensive morphology is interpreted in terms of hazards related to petroleum development.

C. Relevance

The relevance of ice-related environmental hazards to petroleum development should be considered in terms of four major phases of petroleum-related activities: Exploration I, Exploration II, Development and Production. Each of these phases has particular ice-related problems.

a. Exploration I. This activity is mainly geologic mapping by seismic crews. Currently seismic mapping is being carried out in the Beaufort Sea using fast ice as an operational platform rather than using boats during the relatively short and undependable open water season. Although few, if any, environmental hazards are created by this activity, hazards are imposed on the crews performing such work. The ice morphology developed here has been interpreted in terms of persistence of various ice zones and the period (if any) that exploration activities can be carried out from the ice within these zones.

b. Exploration II. During this phase, test wells are drilled--very likely from temporary structures including man-made gravel islands, anchored drill ships, movable platforms, etc. The choice of temporary structure used will depend in part on the morphological behavior of the ice in the location where a test well is desired. For instance, areas with a high incidence of hummock fields and shear ridging would be poor locations for anchored drill ships and might require artificial islands. A poor choice here might result in higher exploration costs and possibly environmental risk resulting from petroleum products spilled by damaged exploration equipment.

c. Development. During this phase, permanent structures are constructed for drilling of permanent wells and extraction facilities. Collector pipelines are laid and other permanent facilities are constructed. The considerations involved in the placement of these structures include the probability of ice piling around and upon man-made islands, ridge keel gouging of pipelines and also the effect of the facility on the morphology of near shore ice and this in turn on the quality and nature of habitats.

The information provided here will obviously yield information about ice piling and the probability of bottom plowing. Through the morphology of near shore ice including the dynamics of ice behavior near natural obstructions to ice motions, descriptive models of the impact of the creation of man-made islands on the morphology of near shore ice can be developed. This can then in turn be related to impact on near shore habitats.

d. Production. This phase of petroleum-related activities would take place over a span of many years. Consideration has to be given to the probability of adverse ice conditions over a period as long as twenty years and how these conditions relate to structures designed to support pumping and piping of crude petroleum. Within this period the greatest environmental hazards would arise from the possibility of a large oil spill. Because of the ice cover on the ocean most of the year, there is a great probability that a spill will become associated with the ice. In addition the presence of ice may even enhance the probability of a petroleum spill during the ice season. The ice morphology presented in this report has been interpreted in terms of the fate of an oil spill created at a time when it could become incorporated into the ice and at times when spilled oil would become trapped under the ice: what transport might take place, how much spreading might occur, how long entrapment might last, and when release might occur. Also based on the morphology developed, consideration has been given to favorable locations for production facilities and to anticipation of techniques which may be used to deal with specific spills through prediction of the ice behavior to be expected within statistically-determined zones of uniform behavior of ice. Finally, consideration has been given to

possible destruction of underwater facilities as a result of ocean-floor plowing by grounded sea ice features within each statistically-determined zone of uniform ice behavior.

III. Current State of Knowledge

With the exception of site-specific studies performed by other investigators concerning locations of ridges and ice edge locations, this report represents the public domain state of knowledge of the coastal-wide morphology of near-shore ice conditions as outlined in Section II.B.

IV. Study area

A. Geographic area

The area of this study can be divided into two different regions. The first region consists of the Beaufort Chukchi Seas, extending from Demarcation Point in the eastern Beaufort Sea to Nome on the south side of the Sea-ward Peninsula. This region encompasses approximately 2500 kilometers of coastline, extending from approximately 141° to 169° west longitude and 64°30' to 71°30' north latitude. The coastline is irregular in shape, consisting of numerous bays, points, capes, and lagoons. The lagoons are bordered on the seaward side by long, narrow islands less than 4 meters elevation.

There is little human habitation in this region, especially along the Beaufort Sea coast. Nome, Kotzebue, Barrow, and Prudhoe Bay are the major population centers with populations of 3000, 4000, and 1000 respectively. There is one year-round native village with a population of approximately 200 along the Beaufort Sea coast east of Barrow, located in the Colville Delta. The only other permanent human habitations along this coast are three military Distant-Early-Warning stations at Lonely, Oliktok Point and Barter Island and the oil fields at Prudhoe Bay. However, there are several native villages along the coast between Barrow and Nome, most having populations less than 100 persons.

The second region consists of the Bering Sea, extending from Bering Strait in the north to the Aleutian Islands in the south. This region overlaps slightly with the Beaufort-Chukchi region from Bering Strait to Nome.

The Bering Sea region encompasses approximately the same length of coast line as the Beaufort-Chukchi region, extending from approximately 157° to 168° west longitude and 53°30' to 65°40' north latitude. The coast line is very irregular in shape and consists of numerous bays, points and capes as well as several large islands, notably Nunivak and St. Lawrence Is. Several large rivers empty into the Bering Sea, including the Yukon, Kuskikwim, and Kuichak Rivers.

Major settlements in the region consist of Nome, Unalakleet, Bethel, Cape Newenham, Dillingham, King Salmon, Naknek and Cape Sarichef. There are numerous other villages and encampments in the region, having populations less than 100 persons.

B. Physical setting. The bathymetry varies significantly in the area of study. In the Beaufort Sea the 80-meter isobath is approximately 70 kilometers offshore from Barrow to Demarcation Point and is the approximate edge of the continental shelf. The sea floor drops off very sharply from there to depths of 4000 meters.

The bathymetry of the Chukchi Sea is quite different from that of the Beaufort Sea. The maximum depth of the Chukchi Sea is approximately 70 meters. However, for most of the Beaufort and Chukchi Seas the bathymetry is not known accurately, especially the shelf areas of the Beaufort Sea.

The Pacific Gyre and the Bering Strait current are the major currents in the Beaufort and Chukchi Seas. The Pacific Gyre is a large clockwise flow of water that dominates the water currents in the Western Arctic Ocean. It results in an east-to-west flow of water in the Beaufort Sea. The Pacific Gyre does not directly affect the flow of water in the Chukchi Sea. The Chukchi currents are dominated by the northerly flow of water through the Bering Strait and into the Arctic Ocean.

The amount of tidal fluctuation varied significantly throughout the study area. At Point Barrow the range of the diurnal tide (the difference between mean higher high water and mean lower low water) is 12 centimeters (0.4 feet) along the entire Beaufort Sea coast from Barrow to Demarcation Point. However, the tides in the southern part of the Chukchi Sea are much greater; the diurnal range at Kiwalik in Kotzebue Sound is approximately 80 centimeters (2.7 feet) and at Nome is approximately 50 centimeters. These are still relatively small fluctuations but they may measurably affect the ice conditions along the coast. The size of the tidal fluctuations is a function of the latitude; the tides generally decrease in size with increasing latitude.

The amount of daylight, i.e., the period from sunrise to sunset, undergoes large seasonal variations at high latitudes. At Barrow, the northern most point of land in this study, the sun does not set during the summer months from late May to late July, while the sun is below the horizon from approximately late November to late January. The conditions at Nome, the most southerly point in the study area, are similar although not as extreme.

The bathymetry for the Bering Sea is similar to that of the Chukchi Sea except that with the presence of more and large rivers the sedimentation rate is higher and the shallow regions extend farther offshore, notably in Norton Sound and Kuskokwim Bay. The depths range to 40 fathoms (80 meters) for most of the sea but drops off rather sharply to 2000 fathoms (4000 meters) south of 56° north latitude.

The surface water currents vary from summer to winter in the Bering Sea. During the summer the currents flow predominantly north through the Bering Strait. A small counter clockwise gyre exists in Norton Sound. However, during the winter only part of the currents appear to flow north through the Bering Strait. The major current flow consists of a large counter clockwise flow up the Alaska coast and down the Siberian coast. The small gyre in Norton Sound has disappeared. (All current data is from the BLM-OCSEAP Climatic Atlas, Bering Sea, Vol. III, 1977.)

The tidal fluctuations in the Bering Sea are even greater than in the Beaufort-Chukchi region. The diurnal tide (mean higher high water to mean lower low water) fluctuations vary from 36.6 centimeters on St. Lawrence Island to 689 centimeters at the mouth of the Naknek River. These fluctuations are sufficient to significantly affect the winter ice conditions along the coast.

The annual variations in daylight hours are less extreme in this region than in the Beaufort Sea region. At the Bering Strait, the amount of daylight varies from continuous (i.e., the sun does not set) from 12 to 30 June to approximately three hours on December 22. However, in the southern part of the Bering Sea, the daylight hours vary from seventeen hours on June 20 to seven hours on December 22.

C. Climate. The climatic conditions along the Beaufort Sea coast are relatively uniform from Barrow to Barter Island. The mean annual temperature at Barrow is -12.6°C with a record maximum of +26°C and a record minimum of -49°C. The normal yearly water equivalent precipitation at Barrow is 12.4 centimeters with an average yearly humidity of 80 percent. The mean yearly snowfall is 72.6 centimeters. The average windspeed at Barrow is 18.9 km/hr from the east; the maximum wind velocity was 93 km/hr from the west. The prevailing wind directions are from the east-northeast to east-southeast.

The weather conditions at Barter Island are similar to those at Barrow. The Barter Island mean annual temperature is -12°C with a maximum of $+26^{\circ}\text{C}$ and a record low of -51°C . The normal yearly water equivalent precipitation is 17.9 centimeters with a normal yearly snowfall of 113 centimeters. The humidity at Barter Island averages 80 percent. The average windspeed is 21.0 km/hr with a record maximum of 130 km/hr. The prevailing winds are from the west from January through April and from the east from May through December.

The climate along the Chukchi Sea coast from Barrow to Nome is warmer, wetter, and somewhat more variable than along the Beaufort Sea coast. The climatic conditions at Kotzebue are similar to those along the Beaufort coast. However, Kotzebue, being farther south, is somewhat warmer with a mean annual temperature of -6.2°C . The record maximum and minimum temperatures are $+20^{\circ}\text{C}$ and -47°C , respectively. Kotzebue receives slightly more precipitation than Barter Island, 22.3 cm water equivalent per year and 120 cm of snowfall per year. However, the humidity is slightly lower at Kotzebue, averaging 78 percent. The yearly average windspeed is 20.8 km/hr from the east with a maximum recorded windspeed of 149 km/hr from the southeast. The prevailing winds are from the west from May through August and out of the east the remainder of the year.

Nome is on the Bering Sea side of the Seward Peninsula and therefore has weather somewhat different than that of the areas described above. The mean annual temperature at Nome is -5.1°C with a record high of $+25^{\circ}\text{C}$ and a record low of -39°C . The precipitation at Nome is nearly twice as great as at anywhere in the Chukchi or Beaufort Seas. The normal yearly water equivalent precipitation at Nome is 41.8 centimeters. However, the amount of snowfall is 137 centimeters, only slightly greater than at Barter Island and Kotzebue; a larger percentage of the precipitation occurs in the form of rain. Despite the higher precipitation, the average yearly humidity at Nome is 72 percent, considerably less than at Kotzebue or Barrow. The average windspeed at Nome is 17.3 km/hr from the north, off the hills of the Seward Peninsula. The maximum recorded windspeed at Nome was 88 km/hr from the southwest. Although the average yearly prevailing winds are from the north, the monthly averages are more variable. From December through March the winds are from the east, from the north April through May, from the west-southwest from June through August, and from September through November are again from the north.

The monthly mean temperatures for the Bering Sea range from -18°C in February to $+12^{\circ}$ in July with extremes ranging from -36° to $+22^{\circ}\text{C}$. The higher temperatures are generally to the south.

The mean annual total water equivalent precipitation along the Bering Sea coast ranges between approximately 50 to 100 centimeters. The snowfall ranges from 70 to 200 centimeters annually.

The wind speeds average 20 km/hr along the coast with some areas recording windspeeds in excess of 100 km/hr. The predominant wind directions vary from due north to southeast.

V. Sources, Methods and Rationale of Data Collection

A. Selection of Scenes for Analysis

The primary sources of data for this study were Landsat I and Landsat II band-7 imagery. Landsat acquired images of the same 160 kilometer square area once every eighteen days. In the high latitudes of the Beaufort and Chukchi Seas, overlap of succeeding days' images of up to 80 percent occurs. In the Beaufort Sea, a given area may be imaged up to four days in a row. In the Chukchi Sea and Bering Sea the overlap decreases with decreasing latitude so that in the Nome vicinity, an area will be imaged up to three days in a row. Twelve days' images are required for continuous coverage from Demarcation Point to Point Barrow. A minimum of six days' images are required to continuously cover the Chukchi Sea coast line from Point Barrow to Nome.

Each eighteen-day Landsat cycle was used as a data set. Several cycles of images were mapped for each year from 1973 through 1976, depending on the availability of the images. Landsat does not obtain imagery from approximately mid-November to early February in the Beaufort and Chukchi Seas because the sun does not rise above the horizon at those latitudes during that time. Consequently, February is the earliest that images are available for these areas. Cycles of Landsat images were mapped for the following periods, depending on availability of images: (1) midwinter (mid-to-late February to early March); (2) late winter (mid-to-late March); (3) early spring (late March to late April); (4) late spring (May to mid-June); (5) summer (late June to mid-July); (6) late summer (late July to mid-August); and (7) late fall to early winter (late October to mid-November).

The choice of Landsat cycles used for this study depended primarily upon the cloud cover of the scenes of each cycle and the number of images available. Some Landsat scenes were not available from NASA due to dense cloud cover. Other images with up to eighty percent cloud cover were obtained from NASA but not used. The usefulness of the images in a cycle was determined on an image-by-image basis. Two criteria were used. First, there needed to be enough coastline showing on the image to match a coastline overlay to the image. Generally, if even a small section of the coastline or coastal river was visible on the image, the image could be lined up with the overlay, using the latitude and longitude marks on the image. The latitude and longitude marks were not usable by themselves due to the difference in projections of the Landsat image and the Lambert conic conformal map overlay. The second criteria required that significant ice detail be visible through the cloud cover. "Significant" ice detail varied from scene to scene. For example, a low-contrast scene with moderate cloud cover but showing open leads in the ice has informational value whereas a scene with the same cloud conditions but not showing open leads may be useless for ice mapping. Generally, Landsat cycles with fewer than five usable scenes were not considered for detailed analysis. Exceptions included scenes used in stationary ice and open water maps (see below).

The Landsat cycles used in this study are shown in Figures V-1 through V-18 for the Beaufort Sea Figures V-19 through V-35 for the Chukchi Sea, and Figures V-19 through V-30 for the Bering Sea. The location, area and extent of each scene and the scene identification numbers are shown.

B. Mapping Technique

The images chosen for analysis were obtained at a scale of 1:500,000 from the EROS Data Center, Sioux Falls, South Dakota. The EROS Data Center produces 1:1,000,000 scale, 1:500,000 scale and 1:250,000 scale black and white prints of available Landsat imagery as standard products. The 1:1,000,000 scale images were too small to accurately map details while the 1:250,000 scale imagery was too expensive. Therefore, the 1:500,000 scale imagery was chosen as a compromise between cost and resolution of detail.

General overlays of the Beaufort Sea, Chukchi Sea and Bering Sea coastlines including the major rivers were drawn in ink on clear acetate. The base maps used for the overlays were the 1:500,000 scale sectional aeronautical charts. These maps are published by the U.S. Department of Commerce using the Lambert conformal conic projection (standard parallels 49°20' and 54°40'). This projection is the closest to the Landsat projection found. The error in locating points on the Landsat image using the base map overlay is approximately a kilometer.

The technique used in mapping the ice on each Landsat image is as follows. First, the base map overlay was placed onto the image and the two were lined-up as closely as possible. Then a blank sheet of clear acetate was placed over the base map overlay. The coastline and rivers were drawn onto the blank acetate. Then the ice features were also drawn onto this acetate from the Landsat image. Finally, the bathymetry obtained from National Ocean Survey (formerly Coast and Geodetic Survey) nautical charts was drawn onto the map.

The initial interpretation was made using a blue-line copy of the acetate map. The distinguishable ice features, such as flaw leads, ridge systems, areas of smooth ice, etc., were identified primarily from Landsat image but other data (see below) were also used. The interpreted results were then transferred to a copy of the original acetate ice map in the form of labeling nomenclature which was then reduced to page size (approximately 1,000,000 scale) for publication. These annotated ice maps of each Landsat image were the preliminary data products.

C. Creation of Composite Data Products

The preliminary ice maps of the individual Landsat scenes were used to create secondary, composite data products. The first generation of composite data products consisted of maps of edge of contiguous ice and of ridge systems for the Beaufort, Chukchi and Bering Seas.

A composite map showing the edge of contiguous ice, defined as the seaward boundary of the currently stationary ice was made for each Landsat cycle. The composite for each cycle was prepared by making a mosaic of the maps of the scenes in the cycles and outlining the contiguous ice edge. When the ice conditions were rapidly changing the significant changes in the edge of contiguous ice were observed from one day to the next, the edge of ice on the latest image was used in the composite map. The mosaic was then transferred to mylar, drawing in the contiguous ice edge, the 20-meter isobath, the coastline and the major rivers. Each composite map of contiguous ice edges contained either the data of all of the cycles for each year studied or the data for each season for all the years studied. Four years' data were used, 1973 through 1976, and, generally, three seasons, winter, early spring, and late spring - early summer. In addition, a map showing the average ice edge and the variation from the average was made for each season. Finally, the averages of the

three seasons were combined on one map to show the seasonal migration of the ice edge. The above maps are discussed in Section VI.

Yearly composite maps of the ridge systems visible on the Landsat imagery were made using the same method used for making the contiguous ice edge maps. One composite map was made for each ice year from 1973 through 1976. The four composite maps were compiled into one map of "all-time" ridge systems. These maps are discussed in Section VI.

The second generation of data products utilizing the preliminary and composite ice maps consists of ridge density maps, sea ice morphology maps and ice hazard maps for the Beaufort and Chukchi Seas. The ridge density maps were prepared from the all-time ridge system maps by visually delineating the areas of differing ridge density. The sea ice morphology maps were prepared from various sources including contiguous ice edge composite maps, ice ridge density maps and other data listed below. Morphology maps were prepared for the late fall to early winter ice season (approximately October to early March) and the midwinter to late spring ice season (approximately mid-March to late May - early June). The morphology maps contain information on the various ice conditions such as average edge of ice, fast ice, ridge occurrences, areas of smooth ice, fast-moving ice, hummock fields, etc. The ice hazard maps used all of the above sources of data for determining the type and location of ice conditions that may be hazardous to offshore structures and ship traffic. The hazards include areas of heavy ridging, continuously changing ice conditions, ice islands, etc. The ice hazard maps are discussed in detail in Section VIII of this report.

Other data products, compiled directly from Landsat imagery, included maps of stationary ice and open water. The term "stationary ice" as used here defines ice that was observed to have remained unmoved by wind and currents during breakup of the near shore ice from one Landsat cycle to the next. Stationary ice is either grounded or attached to grounded ice. The stationary-ice maps were prepared by superimposing two images of the same location, but acquired at different times, on a viewing screen. The ice which had not moved during the time interval between the two images was mapped by placing a sheet of mylar over the viewing screen and tracing the outlines of the stationary ice onto the mylar. One such map was made for each year from 1973 through 1976 (see Section VI for the Beaufort Sea only).

The open-water maps show the progressive increase in open water occurring in the near shore areas from the start of the melt season until the end of summer for the years 1973 through 1976 for the Beaufort Sea. The open-water maps were prepared by overlaying a sheet of mylar on each Landsat image and tracing the outline of the extent of the open water. Data from all available imagery were used. One map was made for each year showing the annual migration of the edge of the open water. The maps are discussed further in Section VI.

D. Ground Truth

This project has conducted numerous aerial reconnaissances along the Beaufort and Chukchi coasts with the objective of relating ice conditions and features with patterns observed on Landsat images. This effort was always placed at a disadvantage because of the six-week to two-month delay between Landsat data acquisition and the availability of hard copy imagery for reconnaissance purposes. Hence, only the most stable ice could be compared directly with imagery. In areas of unstable

ice it was necessary to note and photograph ice conditions during the reconnaissance and wait two months for the comparison process. The difficulty with this was that nearly always the reconnaissance overlooked a feature of apparent significance on the Landsat imagery.

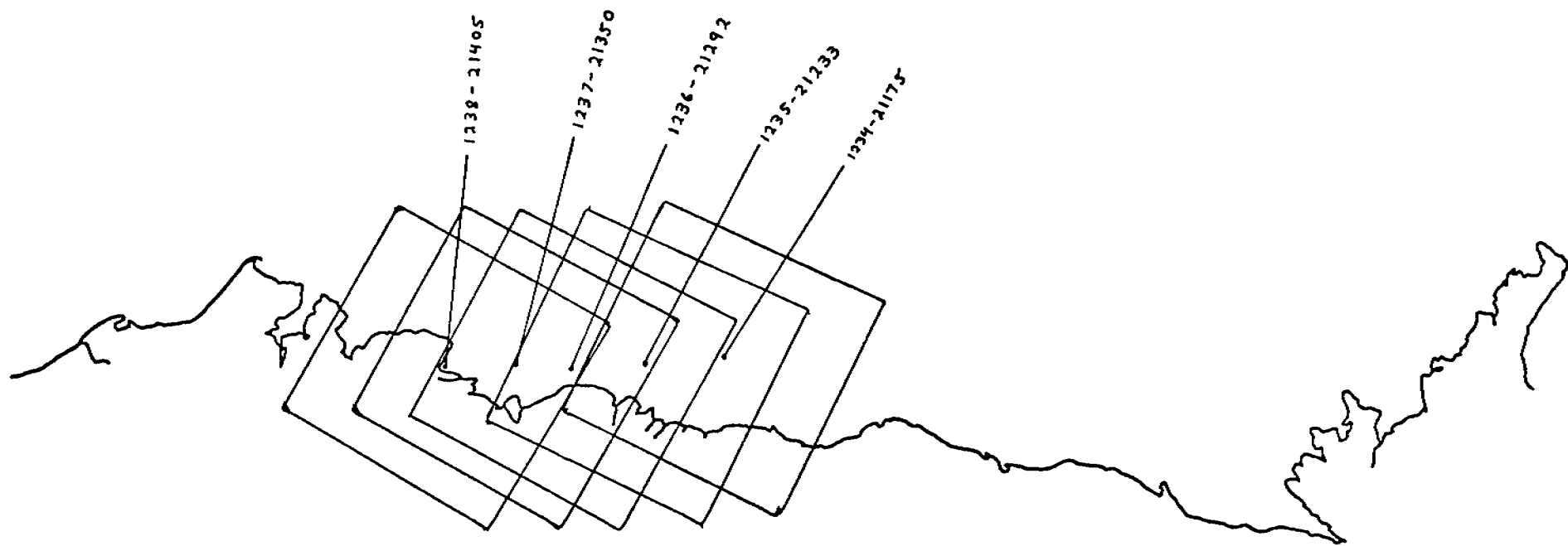
In general, it was found that while major ice features (for instance, ridge systems 50 m wide and 10 km long) can nearly always be identified on Landsat imagery, smaller features cannot be identified with any degree of regularity. The chief parameters here were found to be solar elevation angle, degree of snow cover and haze. It is not always apparent upon inspection of a single Landsat image that haze, for instance, is diminishing detectability of ice features. Often this only became apparent upon inspection of two overlapping images from successive days.

Perhaps the most useful ground truth information was obtained in June of 1974 when we obtained 1:20,000 scale panchromatic photography along a several hundred km flight line in the Beaufort Sea, followed a few days later by a NASA U-2 flight obtaining 1:120,000 scale color infrared photography and the acquisition of a good-quality Landsat image a few days later. On this data, it was possible to conclusively relate measurable ice features with patterns identified on Landsat imagery.

E. Applicability of Techniques Developed to Other Places Where Near Shore Ice is a Hazard.

The chief utility of Landsat data was found to be the detection of large ridge systems and lead openings by direct observation and observation of ice piling and shearing events largely by inference. The analysis of the ice hazards depends on the gathering of sufficient data to make possible the development of a synoptic picture of ice conditions. This, in turn, depends on two factors: the commitment of the spacecraft for data acquisition and a sufficiently adequate number of cloud and haze free occasions when data could be obtained.

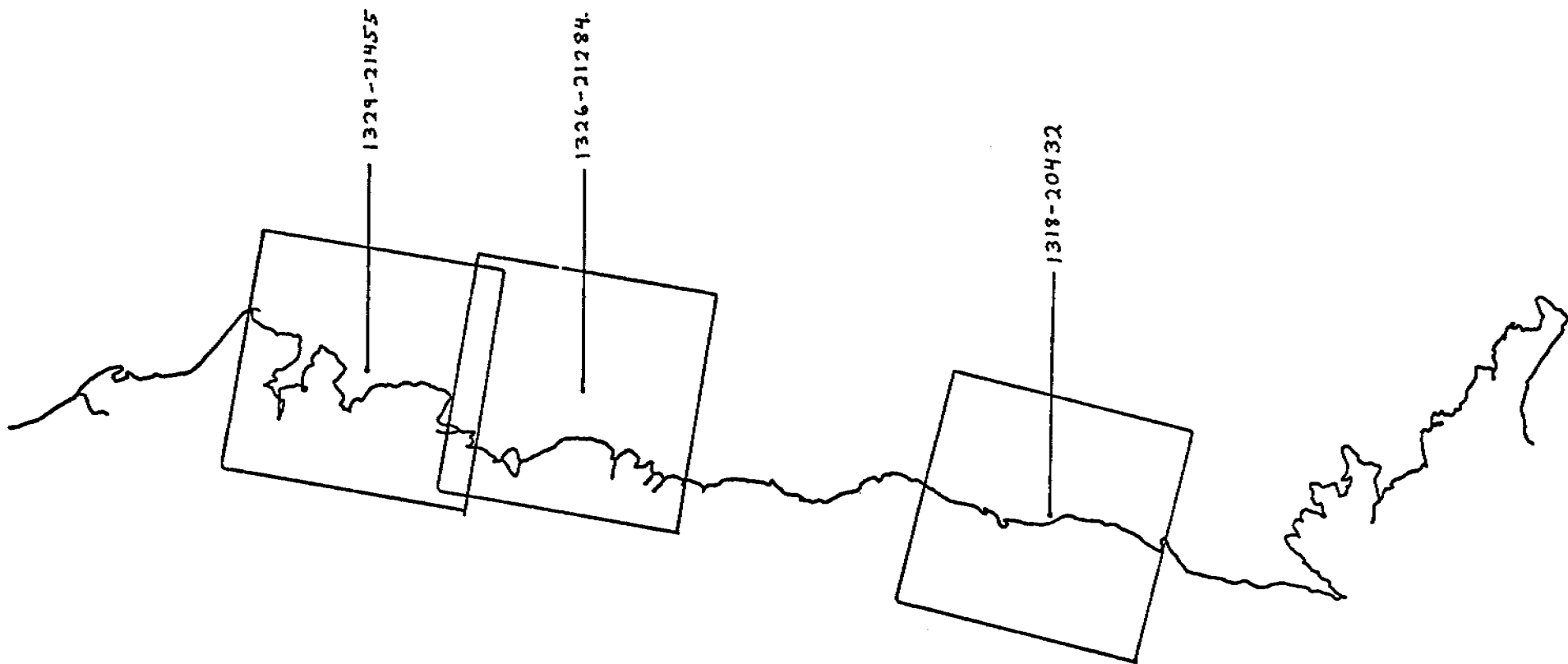
Other than data availability two other factors need be considered: the nature of the hazard and the size of the area under consideration. The techniques used here have been developed to determine rather large zones of somewhat broad hazard description.



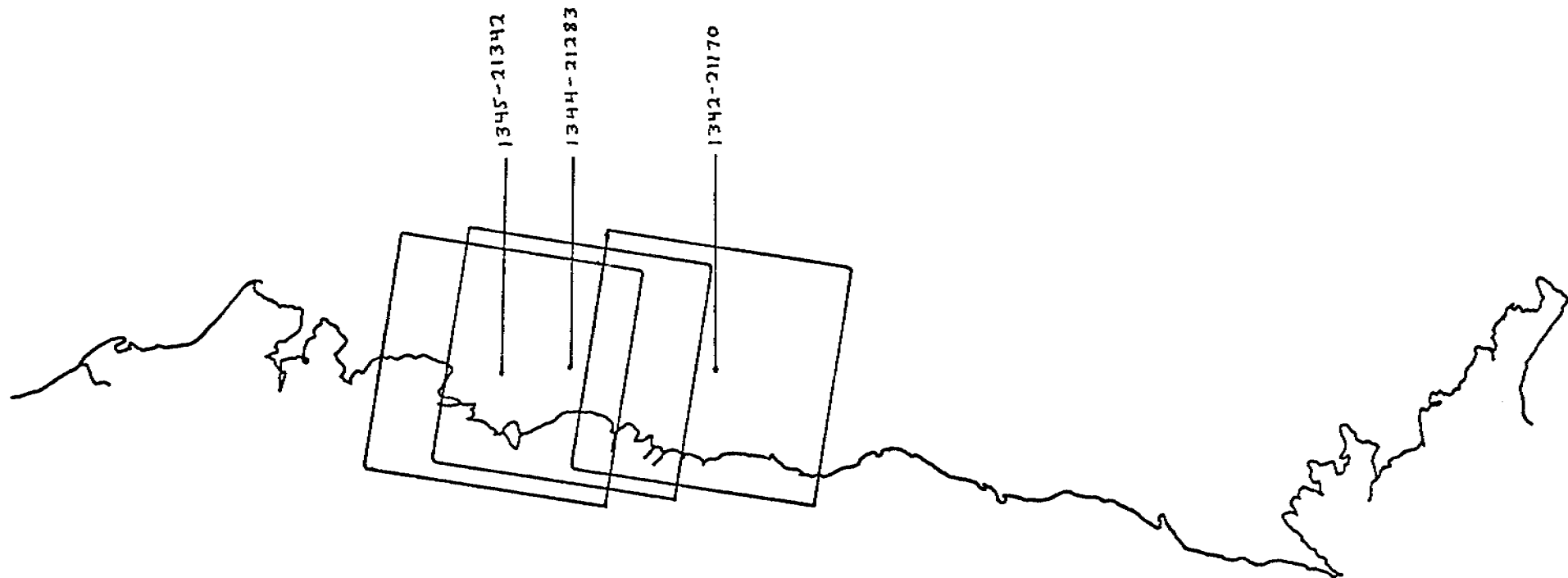
BEAUFORT SEA

MARCH 2 - MARCH 19, 1973

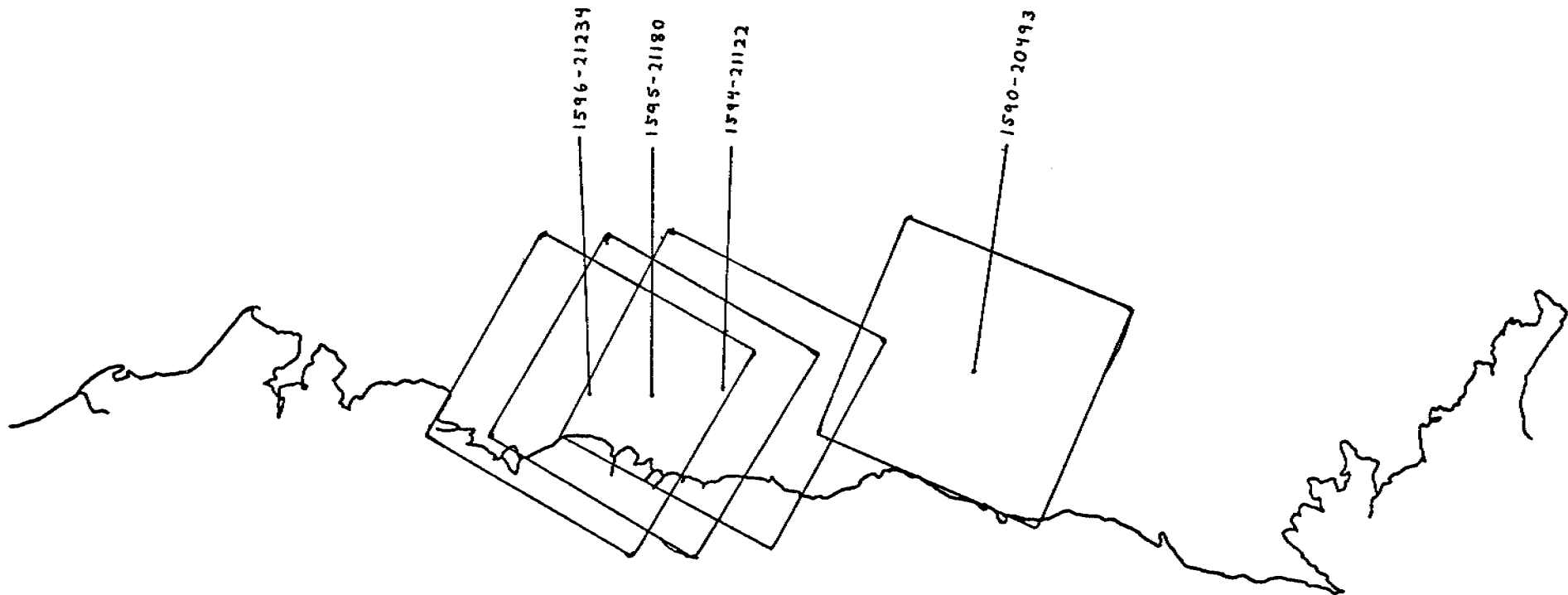
IMAGES: 1222 to 1239



BEAUFORT SEA
31 MAY - 17 JUNE 1973
Images: 1312 - 1329



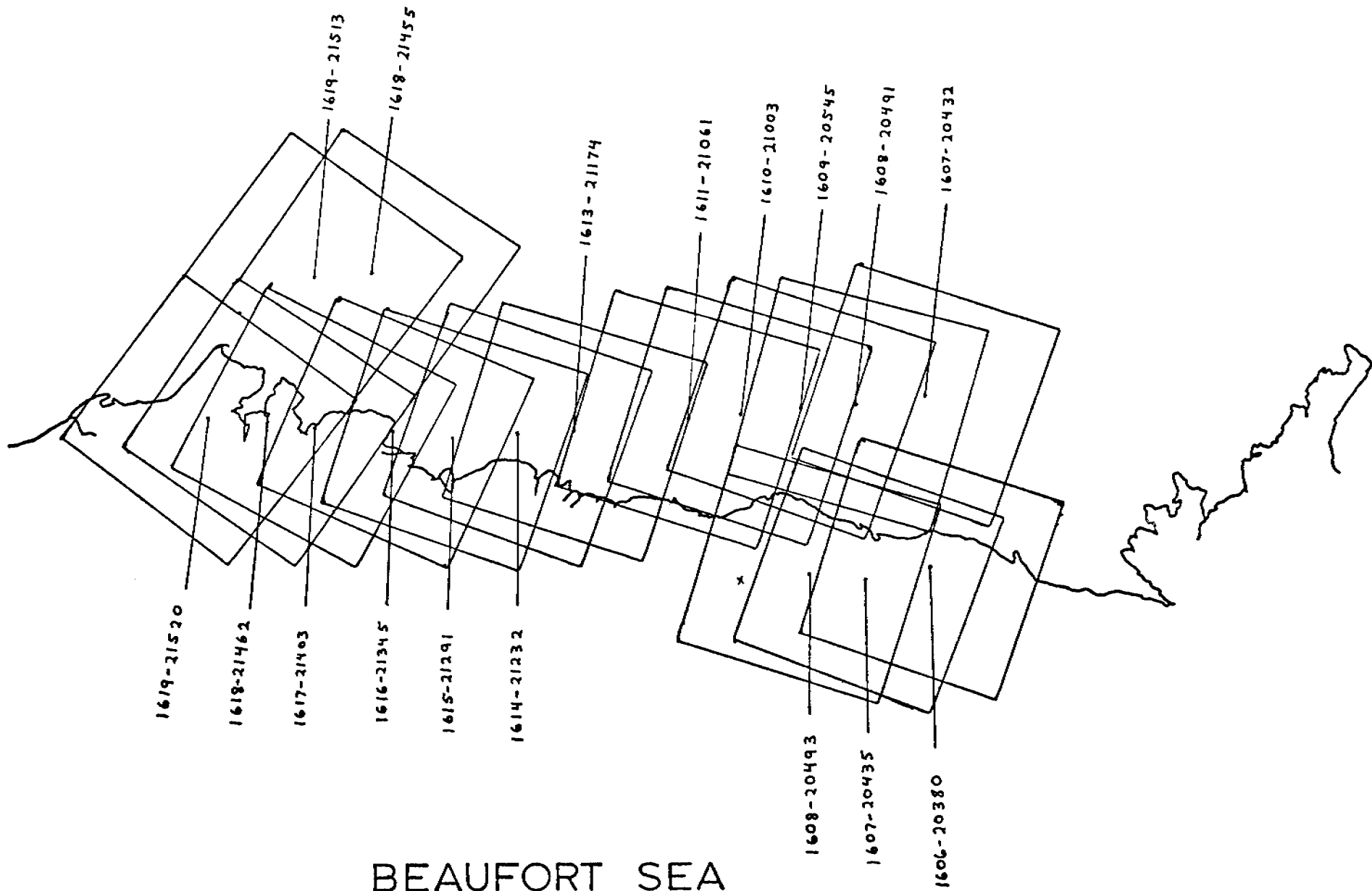
BEAUFORT SEA
18 JUNE-5 JULY 1973
1330 - 1347



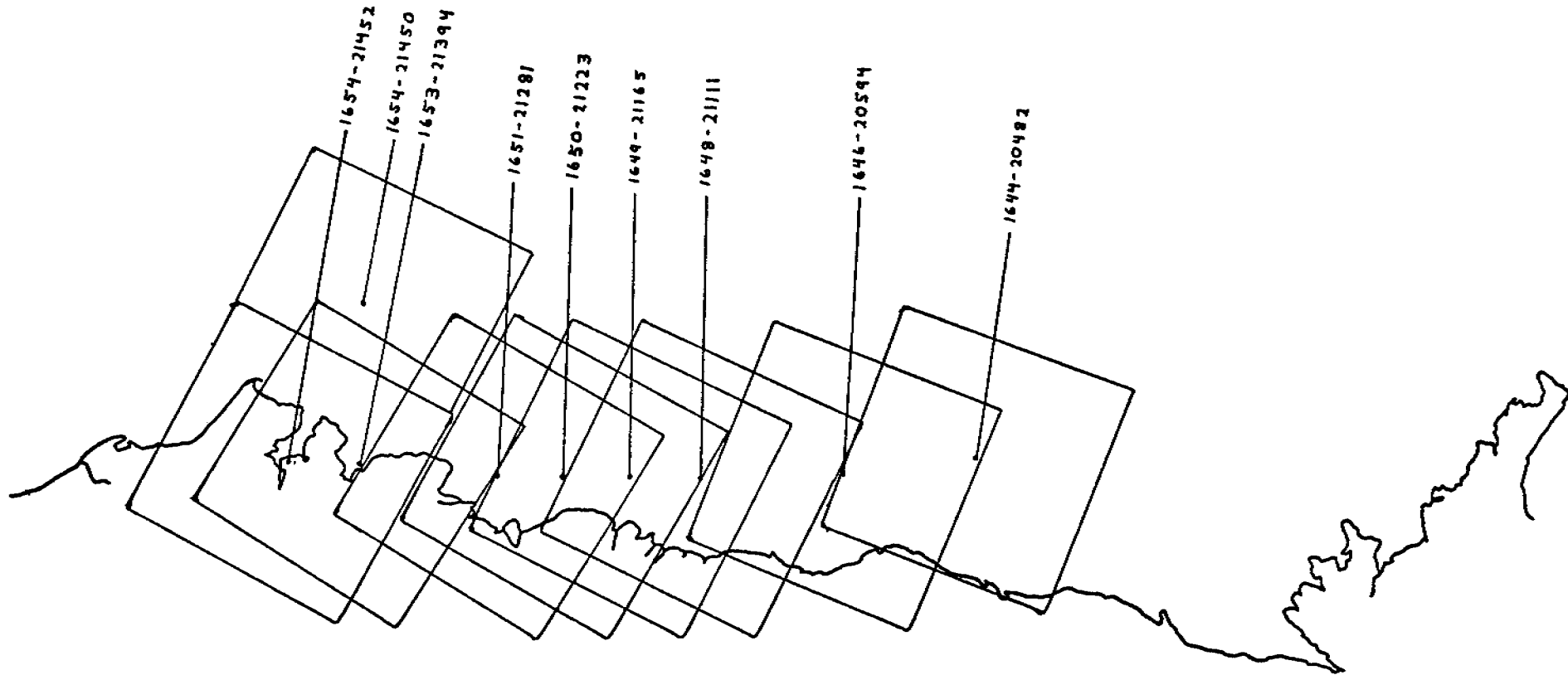
BEAUFORT SEA

FEBRUARY 25 - MARCH 14, 1974

IMAGES: 1582 to 1599



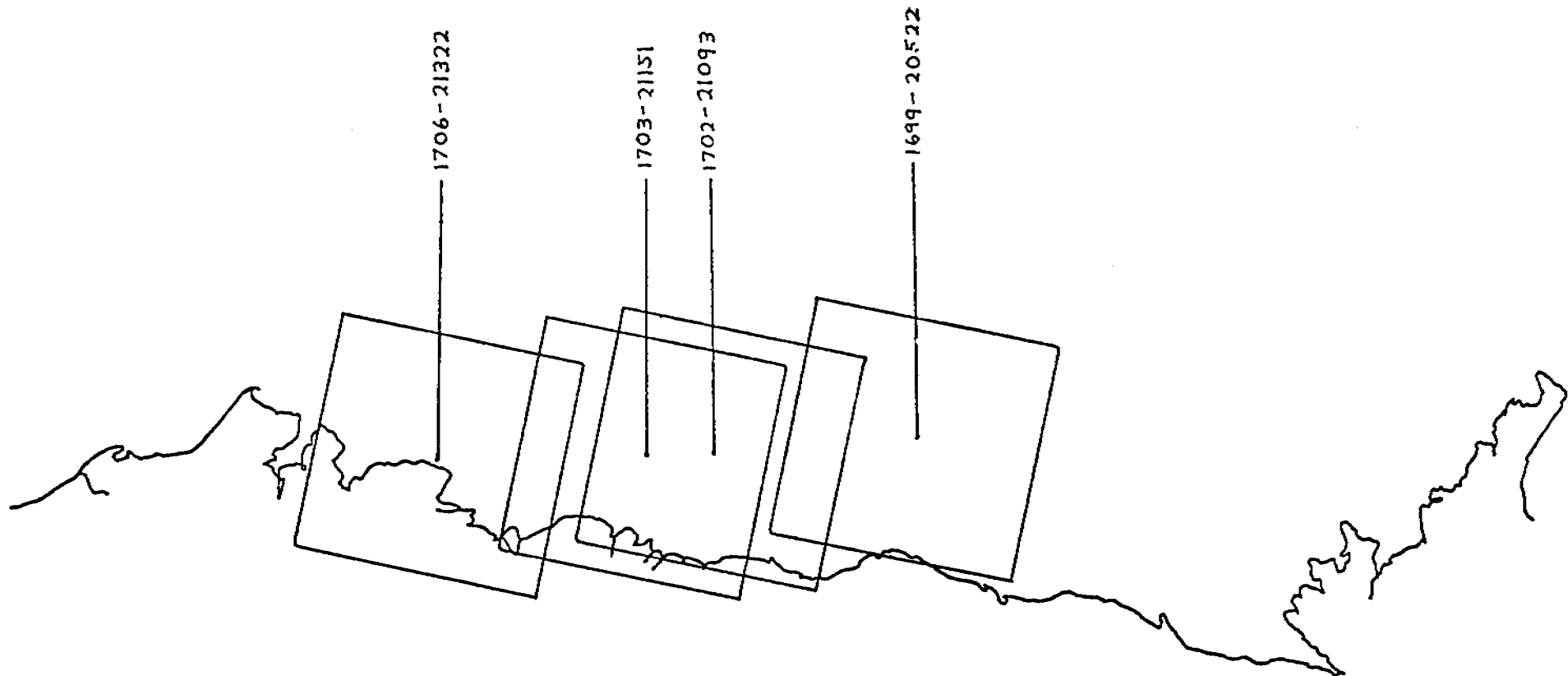
BEAUFORT SEA
 MARCH 15 - APRIL 3, 1974
 IMAGES: 1600 to 1619



BEAUFORT SEA

APRIL 20 - MAY 8, 1974

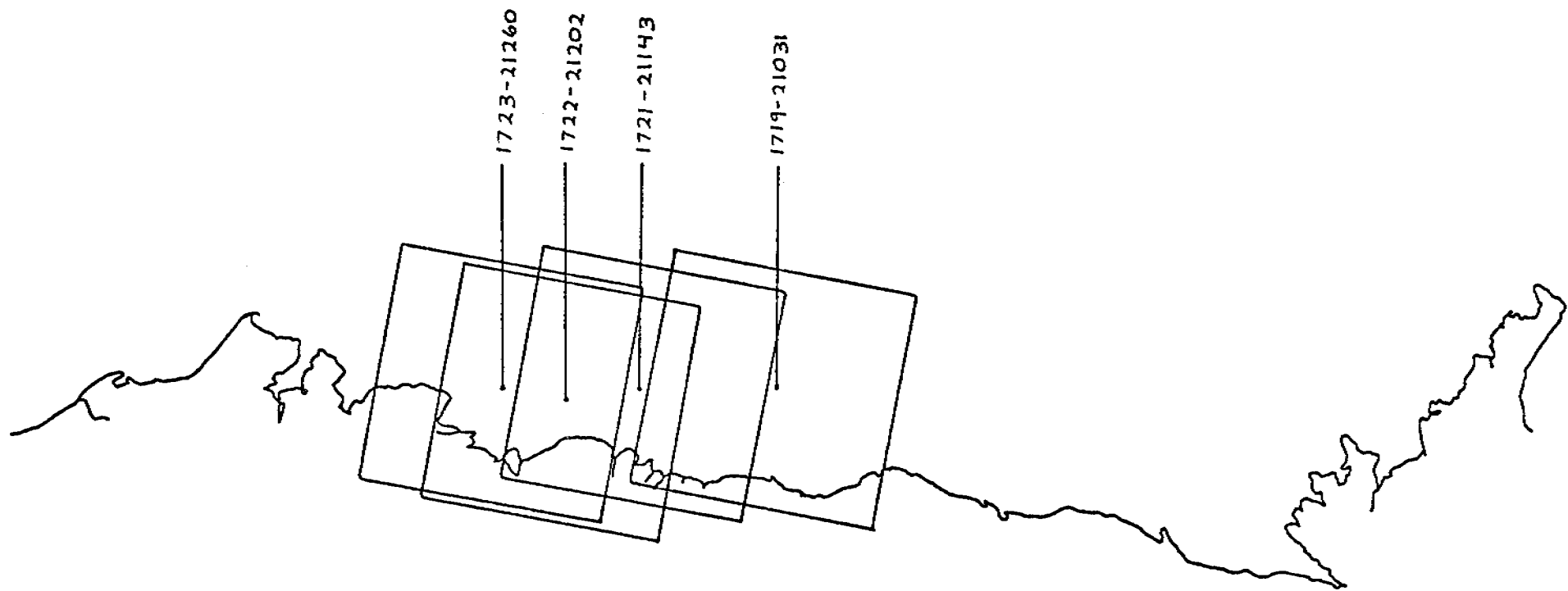
IMAGES: 1636 to 1654



BEAUFORT SEA

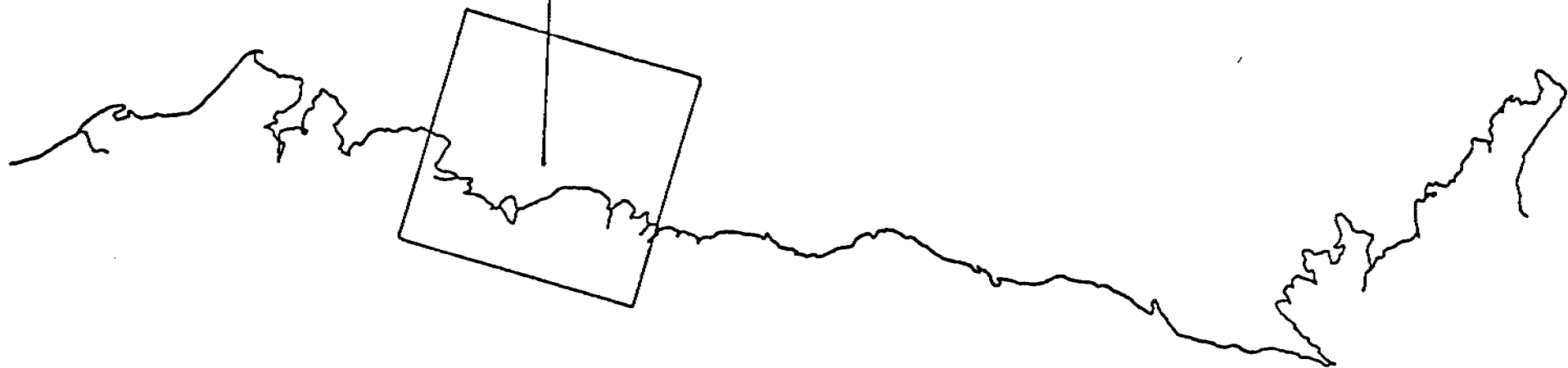
13 JUNE - 30 JUNE 1974

Images: 1690-1707



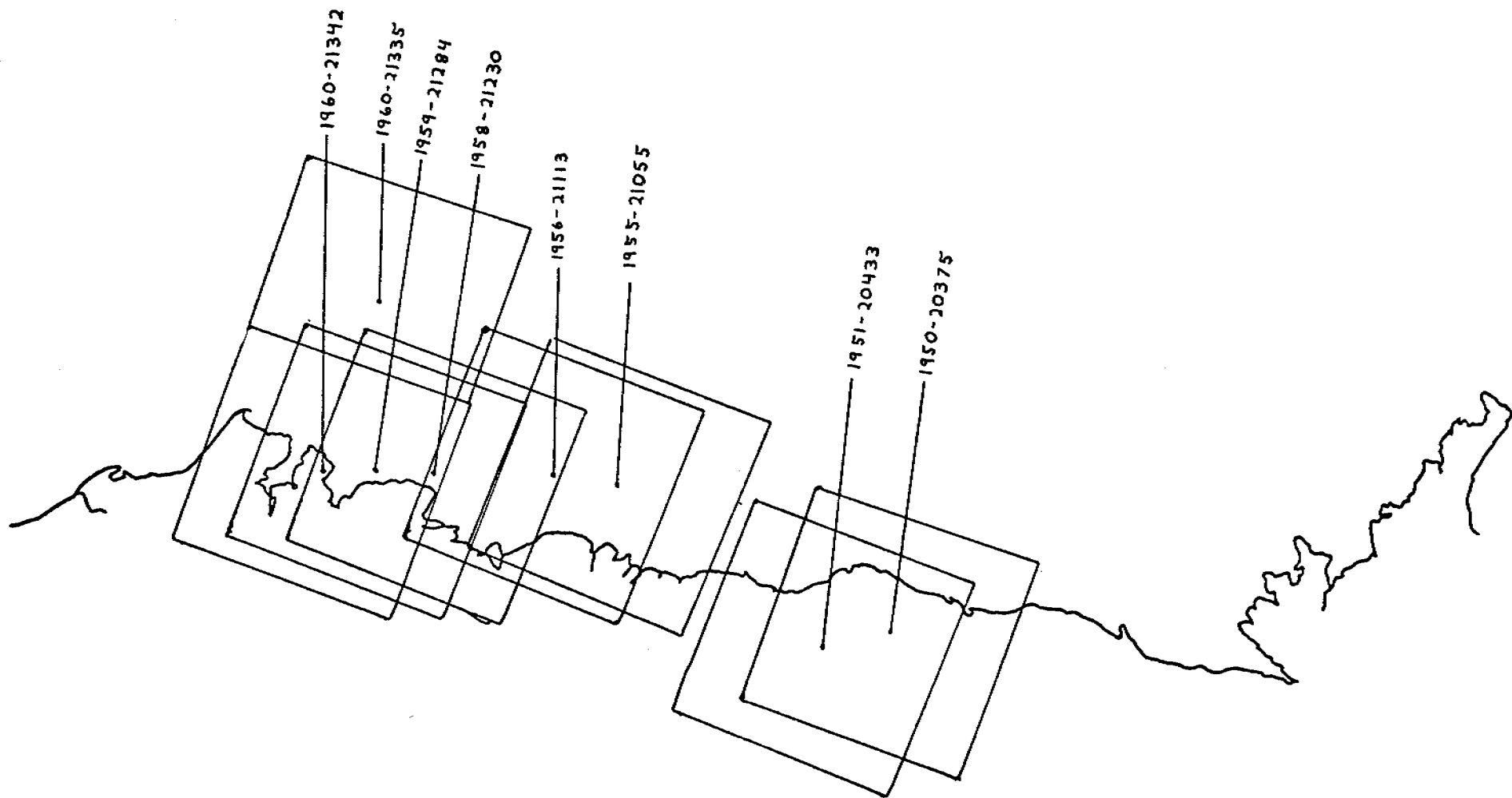
BEAUFORT SEA
1 JULY - 18 JULY 1974
1708-1725

4 bits - 0471

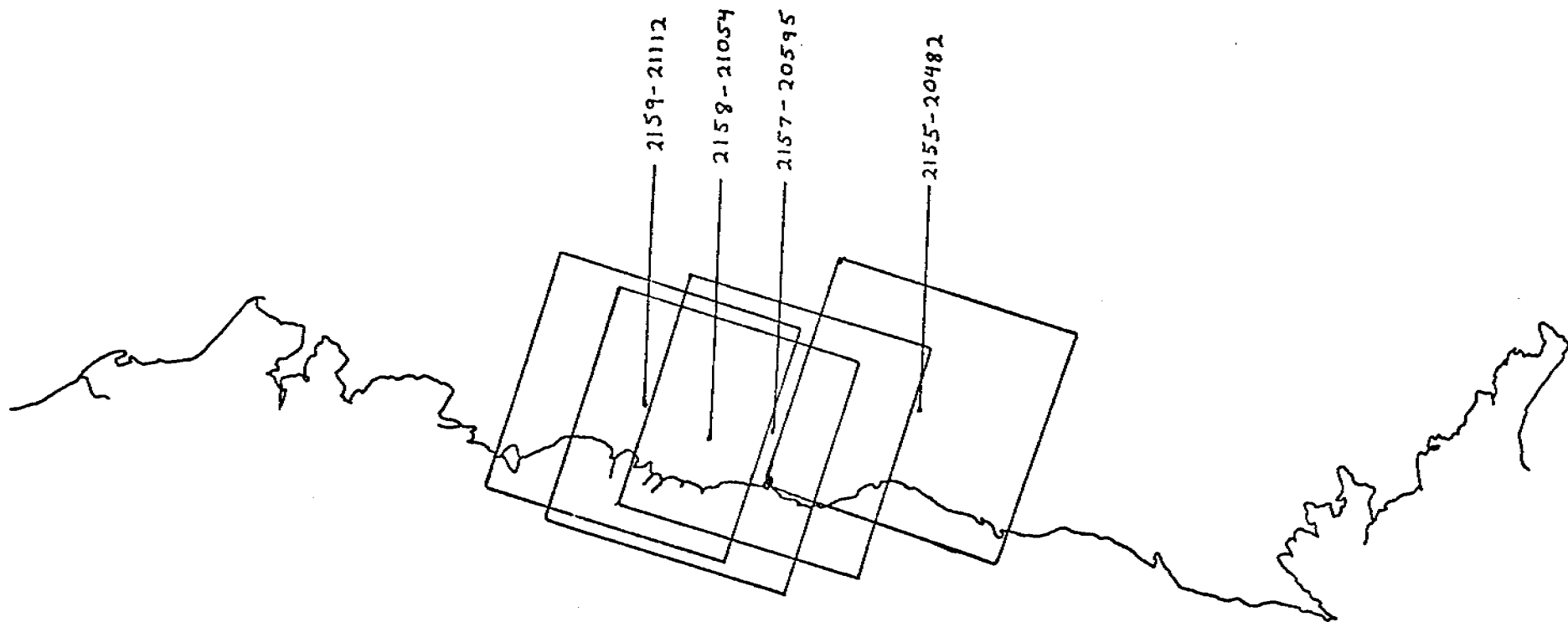


29

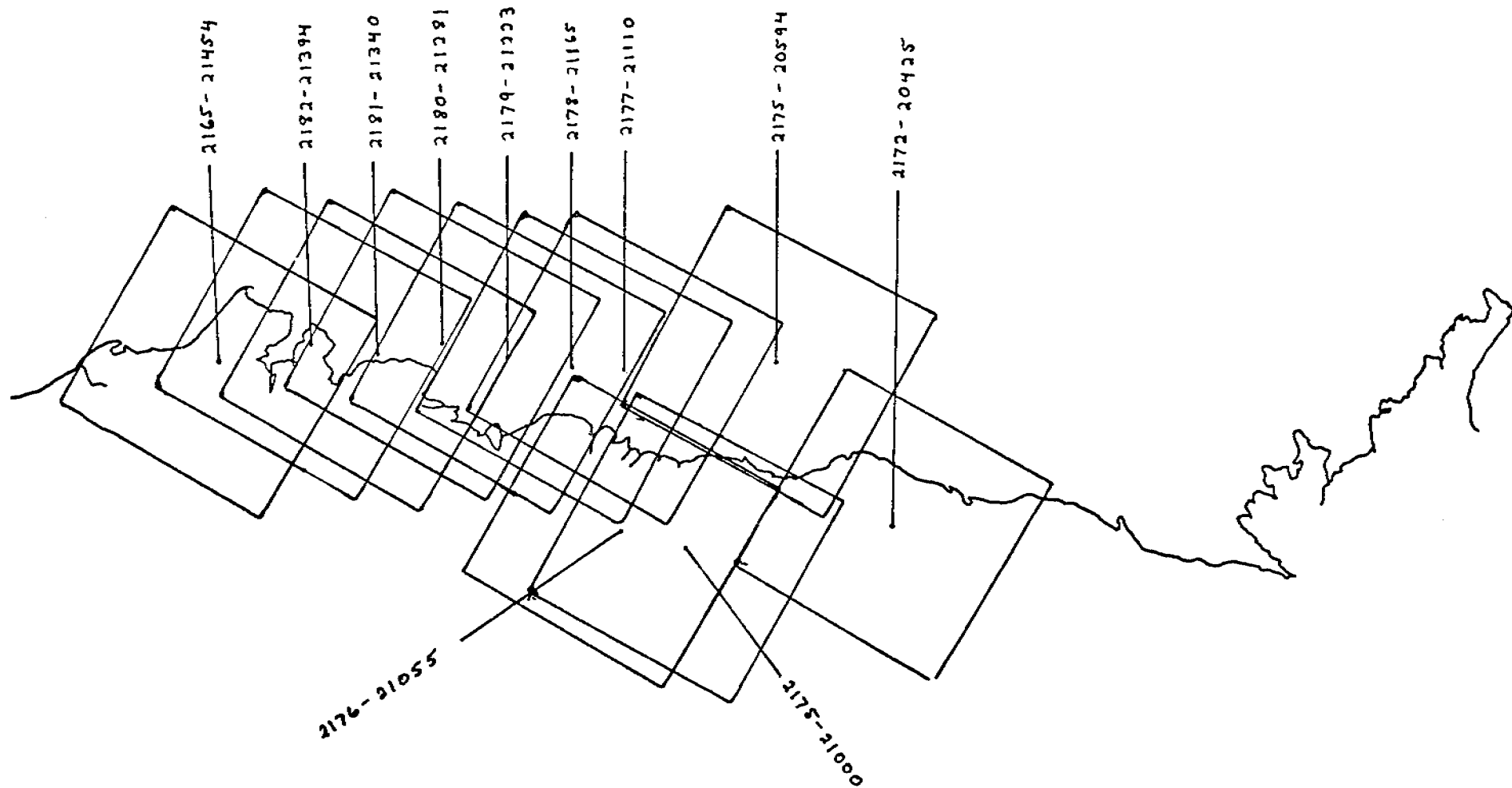
BEAUFORT SEA
19 JULY - 5 AUGUST 1974
Images: 1726 - 1743



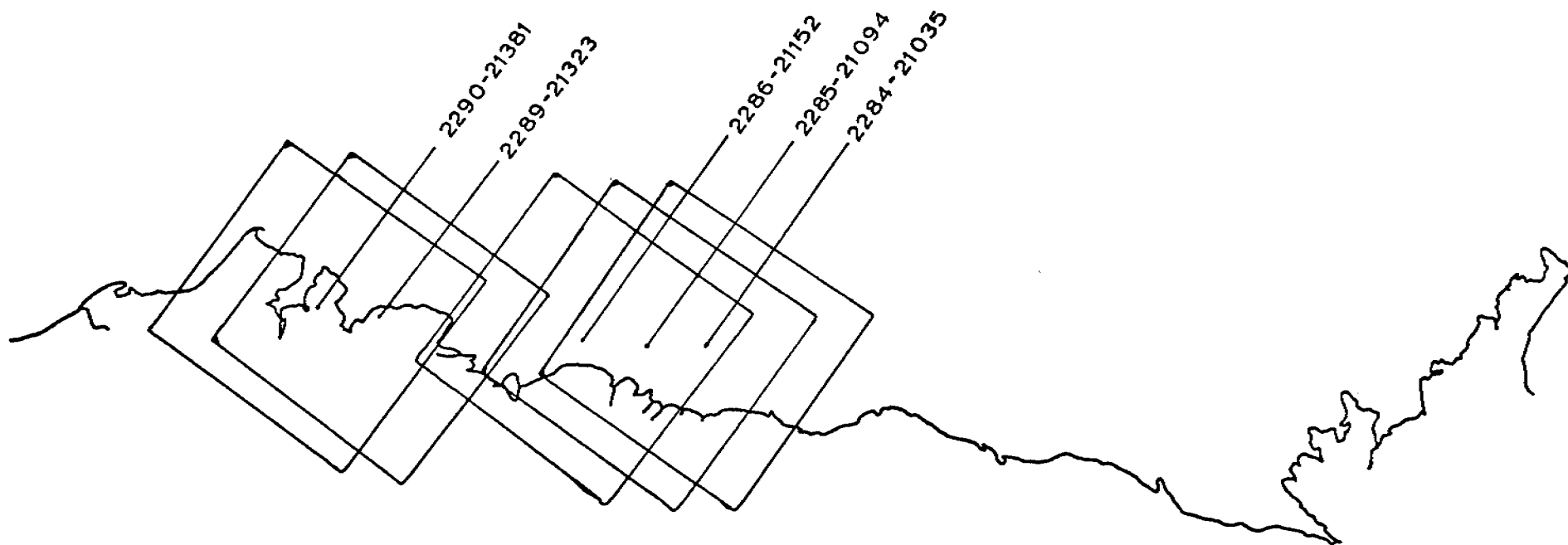
BEAUFORT SEA
FEBRUARY 20 - MARCH 10, 1975
IMAGES: 1942 to 1960



BEAUFORT SEA
18 JUNE - 5 JULY 1975
Images: 2147-2164



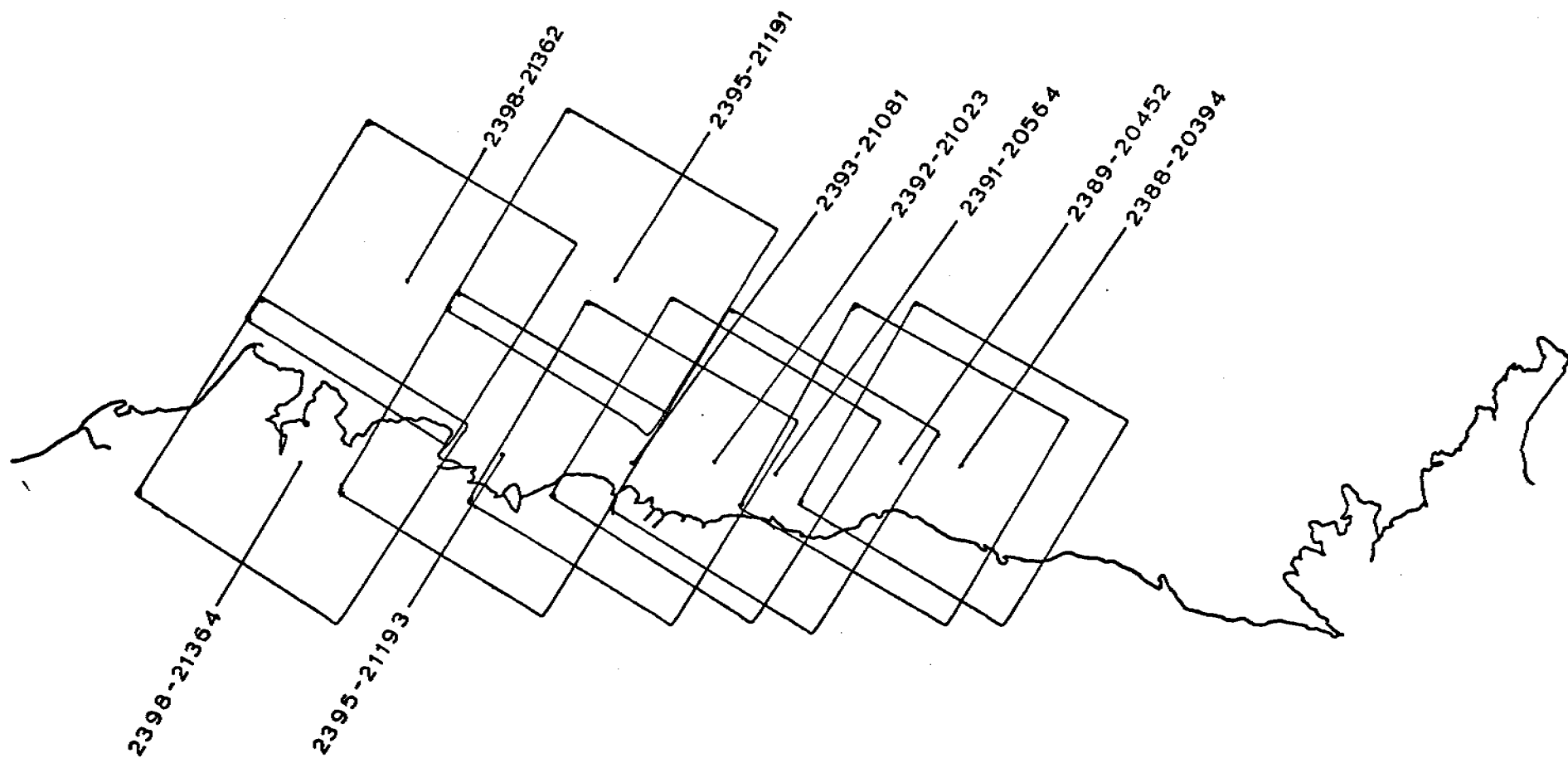
BEAUFORT SEA
6 JULY - 23 JULY 1975
Images 2165 - 2182



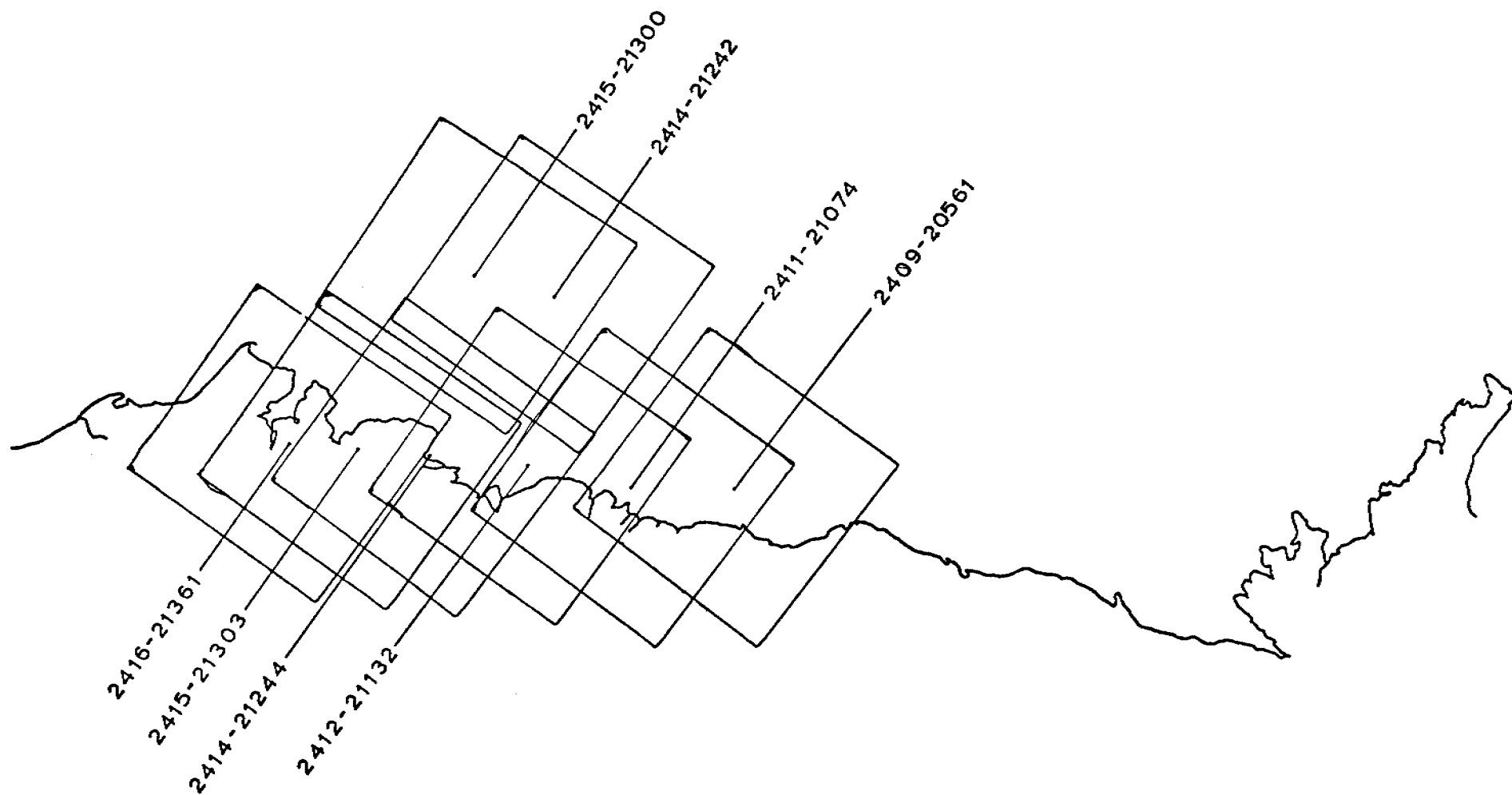
BEAUFORT SEA

22 OCTOBER - 8 NOVEMBER
1975

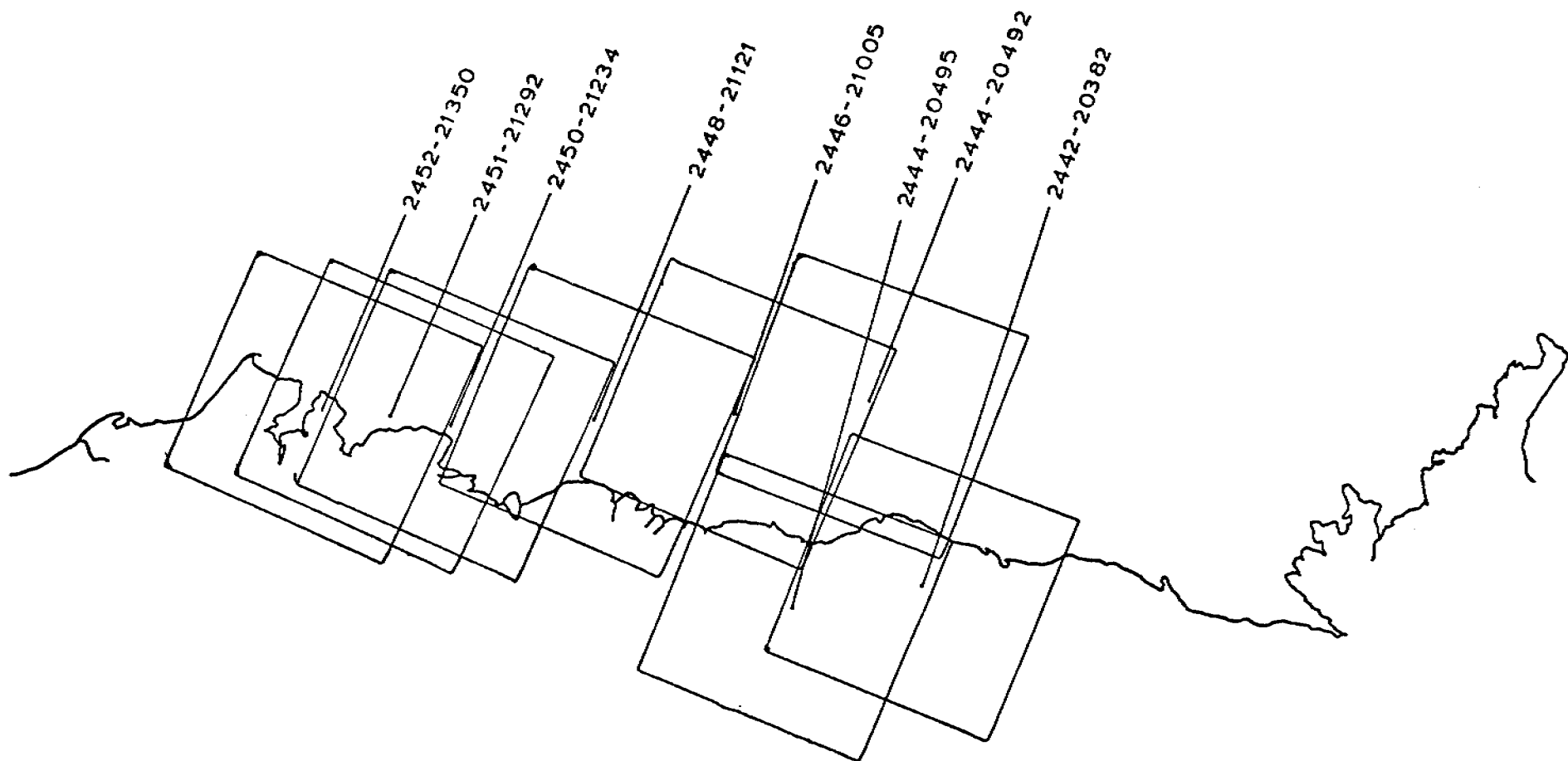
IMAGES: 2273 - 2290



BEAUFORT SEA
6 to 23 FEBRUARY 1976
IMAGES: 2381-2398



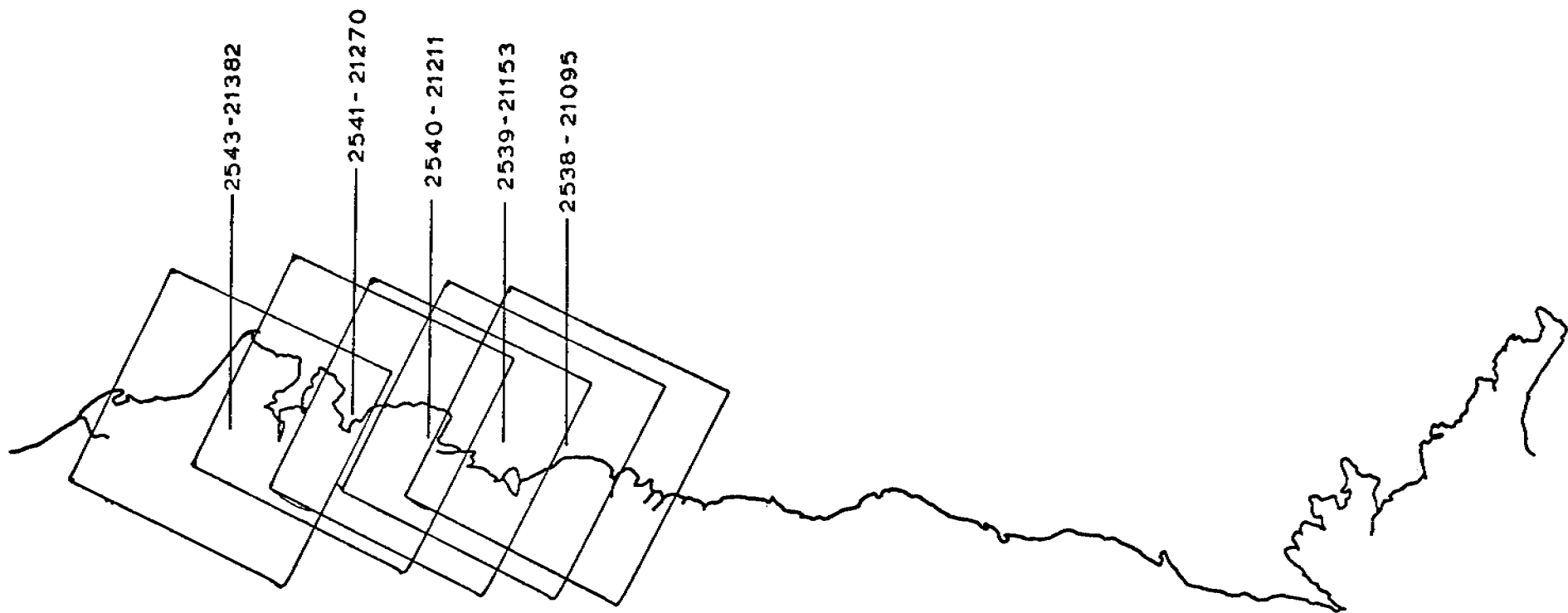
BEAUFORT SEA
24 FEBRUARY to 12 MARCH 1976
IMAGES: 2399 - 2416



BEAUFORT SEA

31 MARCH to 17 APRIL 1976

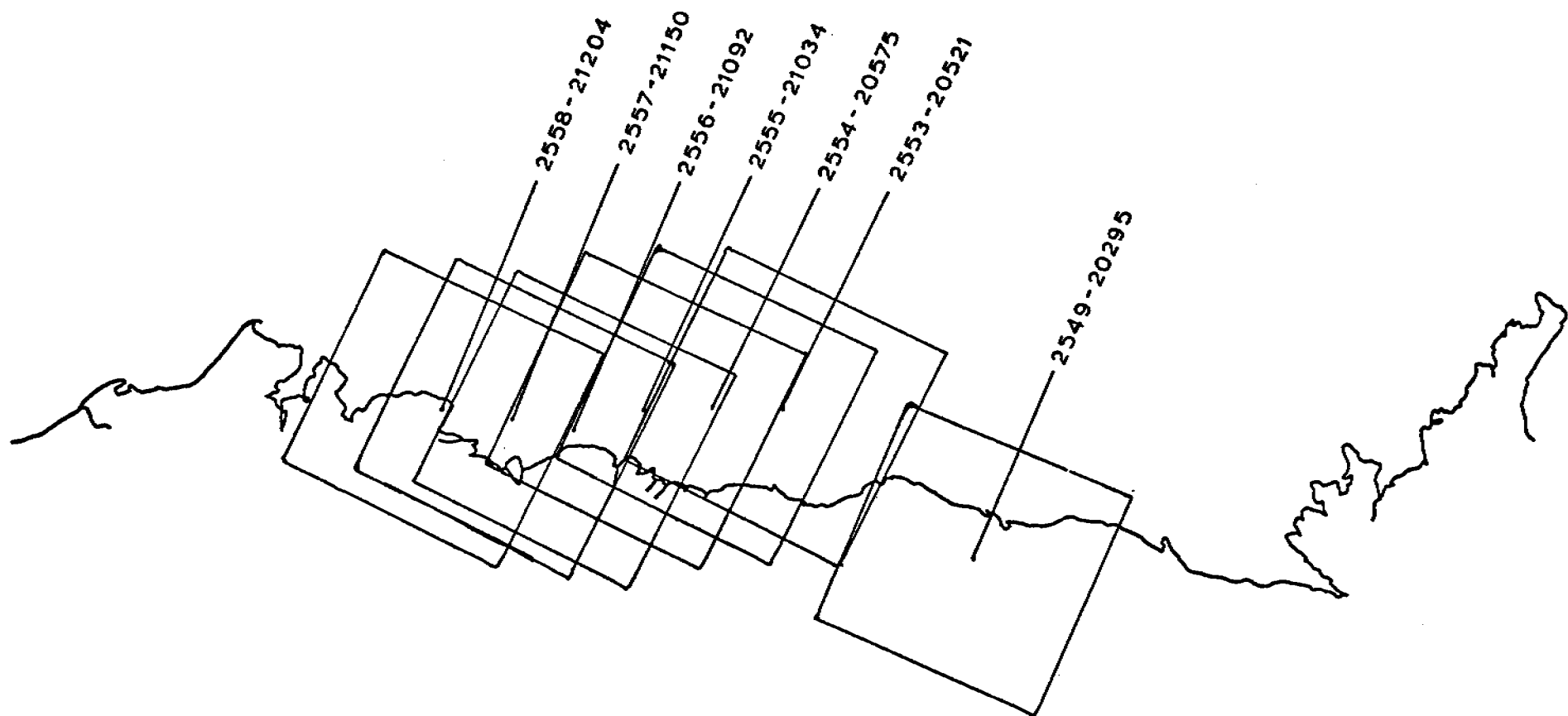
IMAGES: 2435-2452



BEAUFORT SEA

30 JUNE - 17 JULY 1976

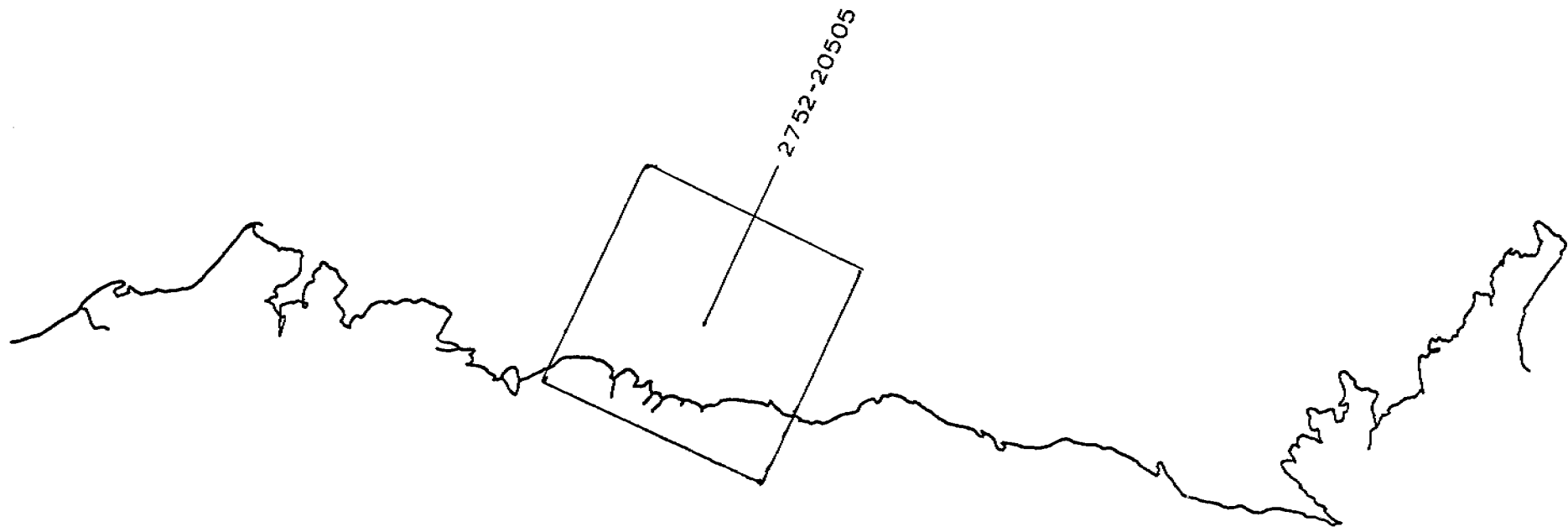
IMAGES: 2525 - 2542



BEAUFORT SEA

18 JULY to 4 AUGUST 1976

IMAGES: 2543-2560

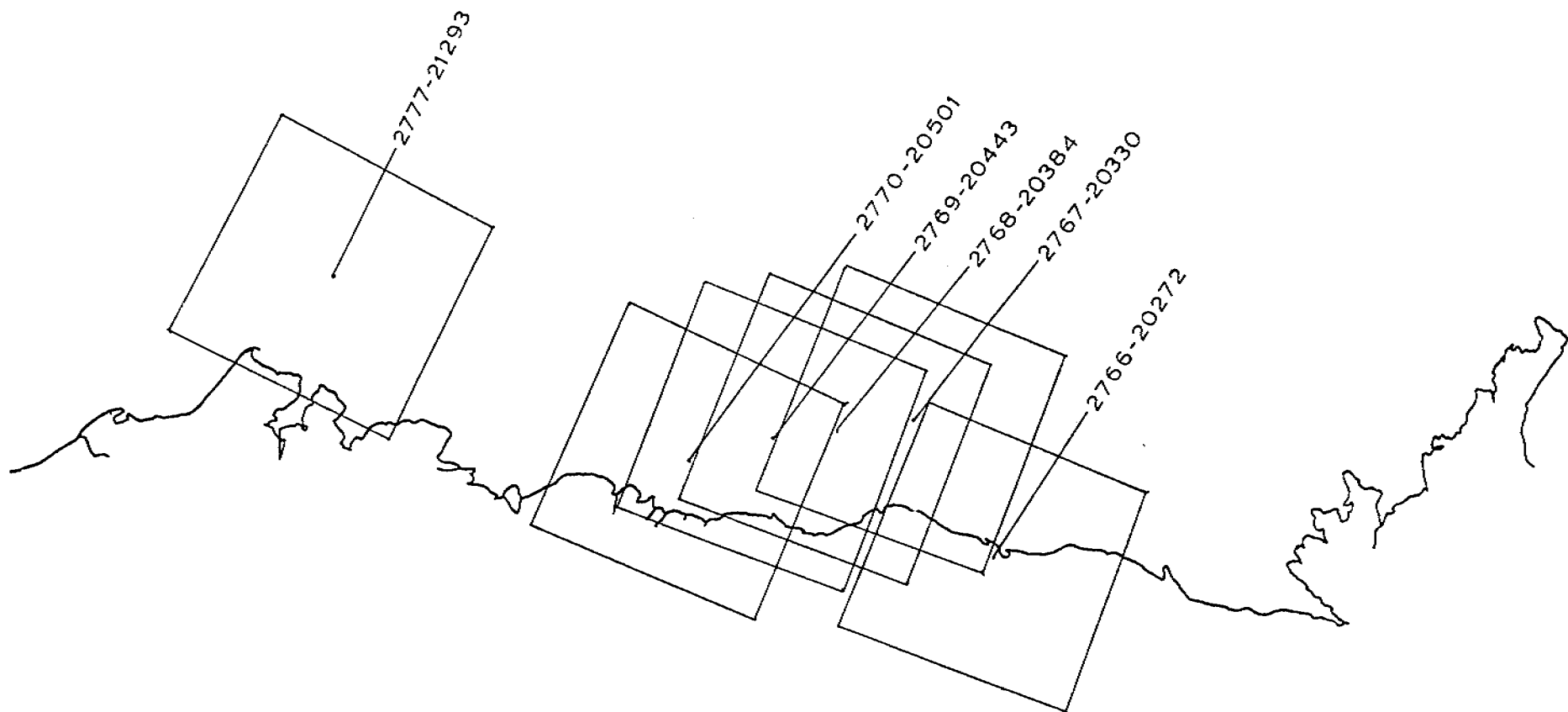


2752-20505

BEAUFORT SEA

1-18 FEBRUARY 1977

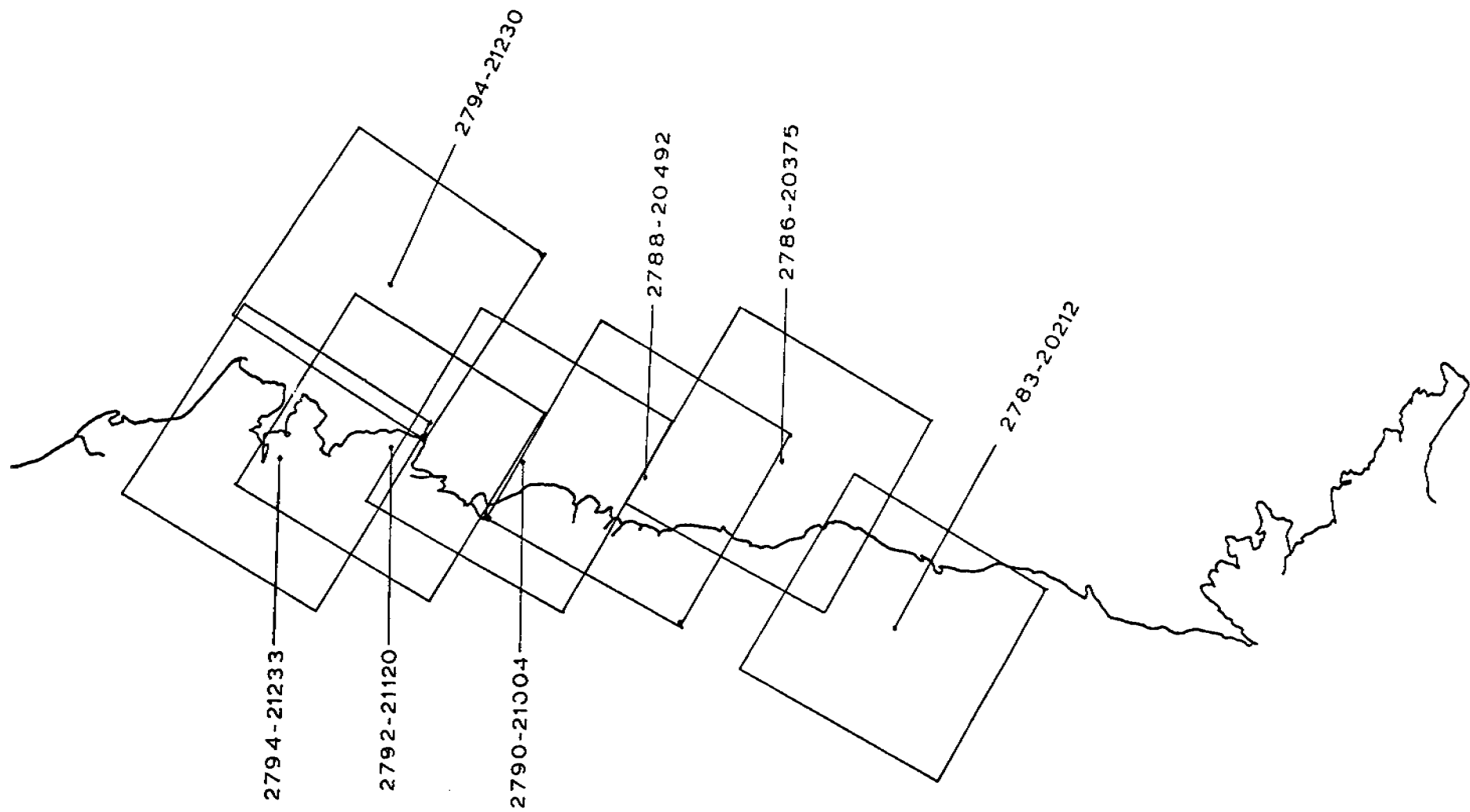
CYCLE 2741-2758



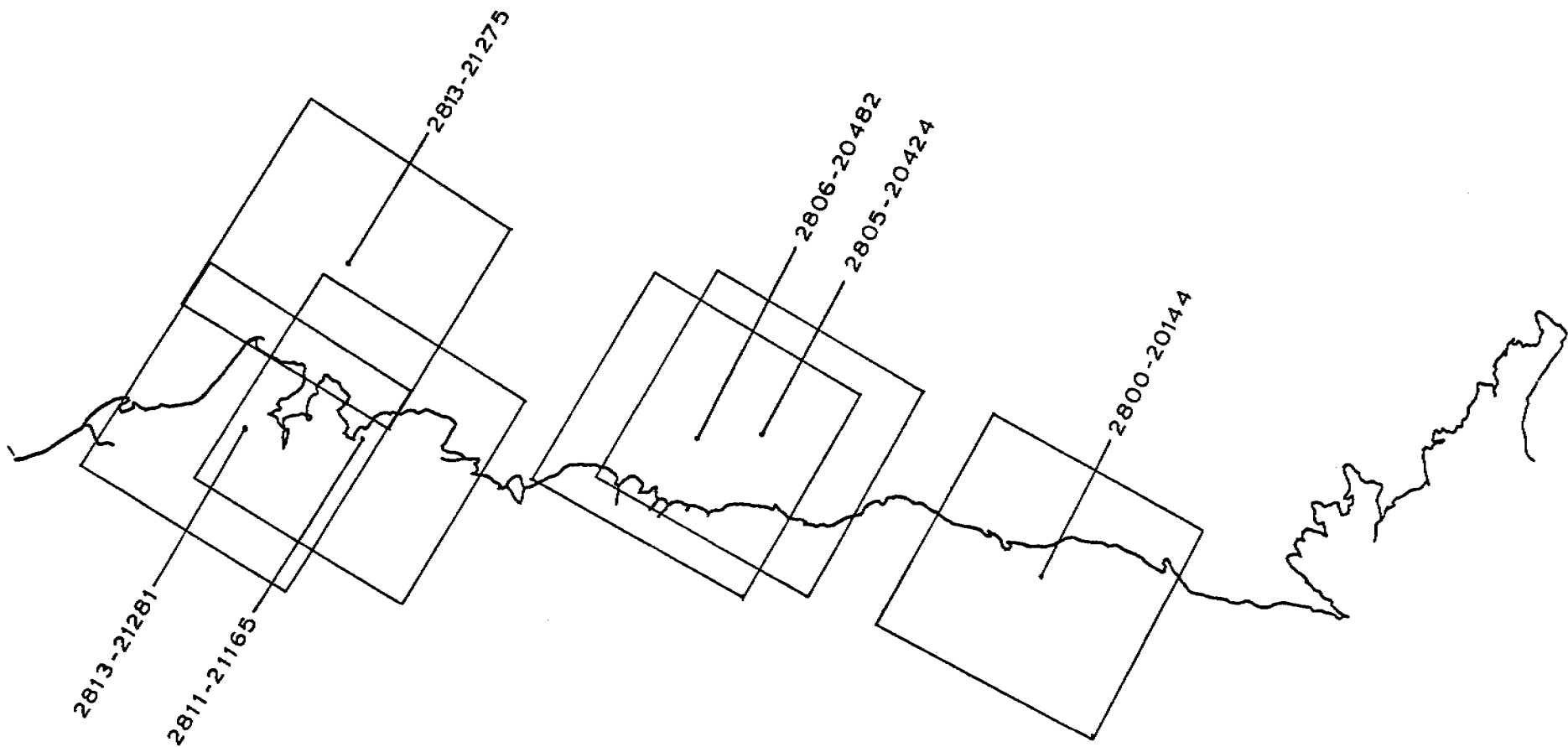
BEAUFORT SEA

19 FEBRUARY - 8 MARCH 1977

CYCLE 2759-2776



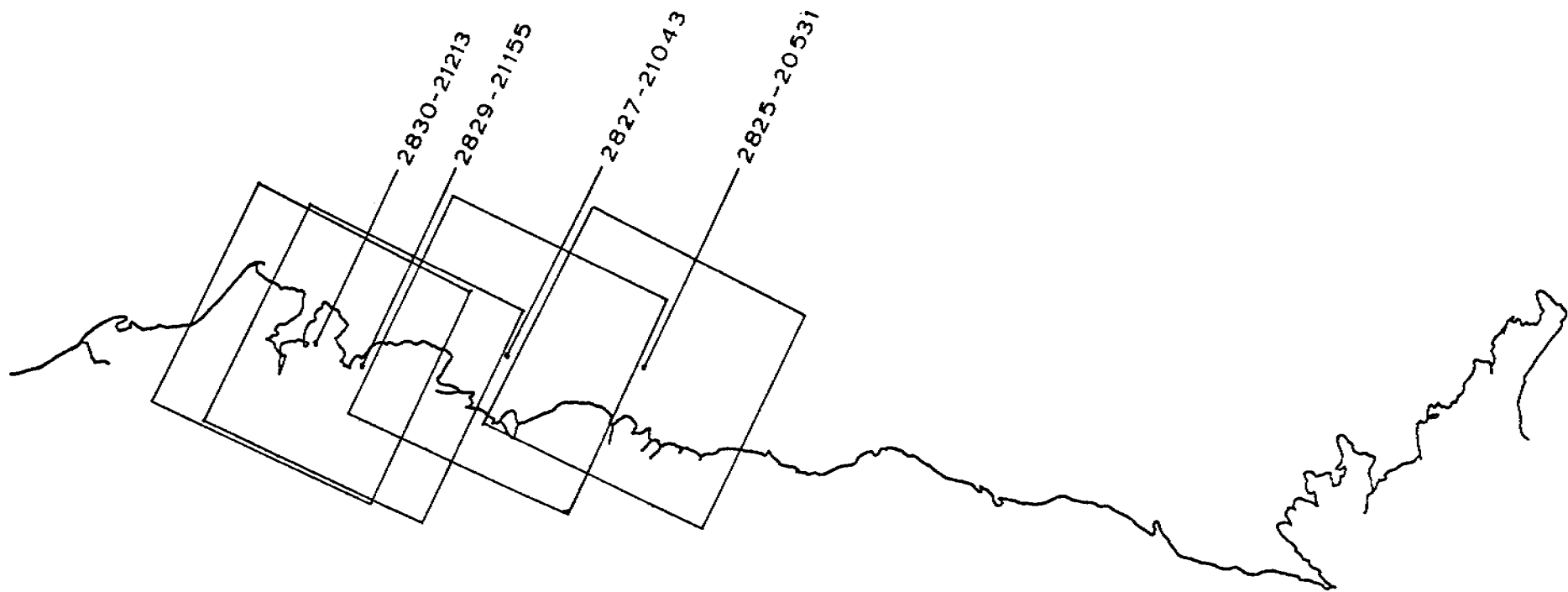
BEAUFORT SEA
9-26 MARCH 1977
CYCLE 2777-2794



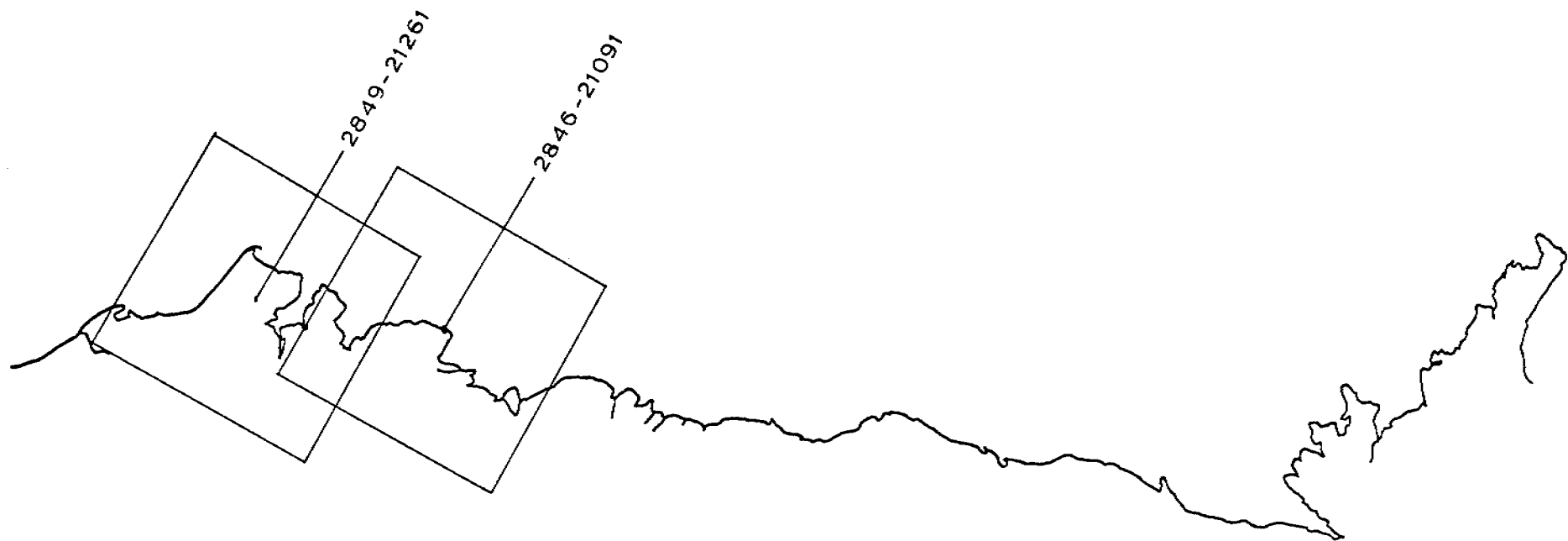
BEAUFORT SEA

27 MARCH - 13 APRIL 1977

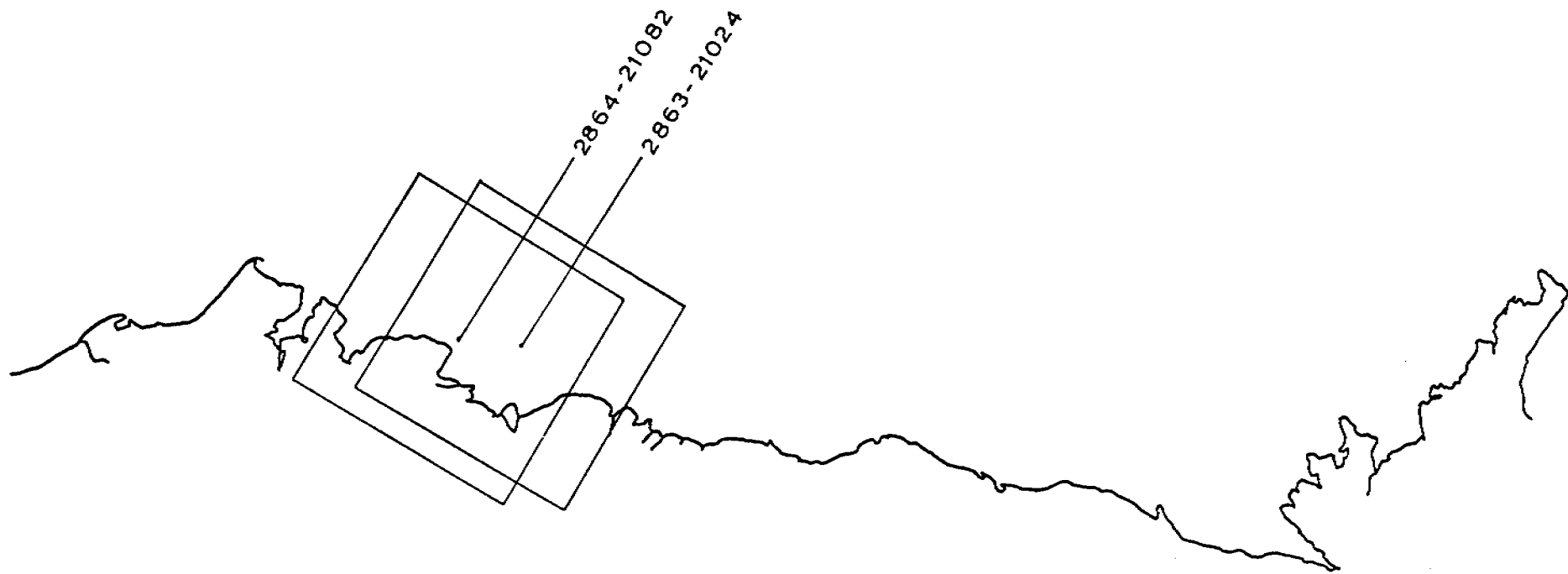
CYCLE 2795 - 2812



BEAUFORT SEA
14 APRIL-1 MAY 1977
CYCLE 2813-2830



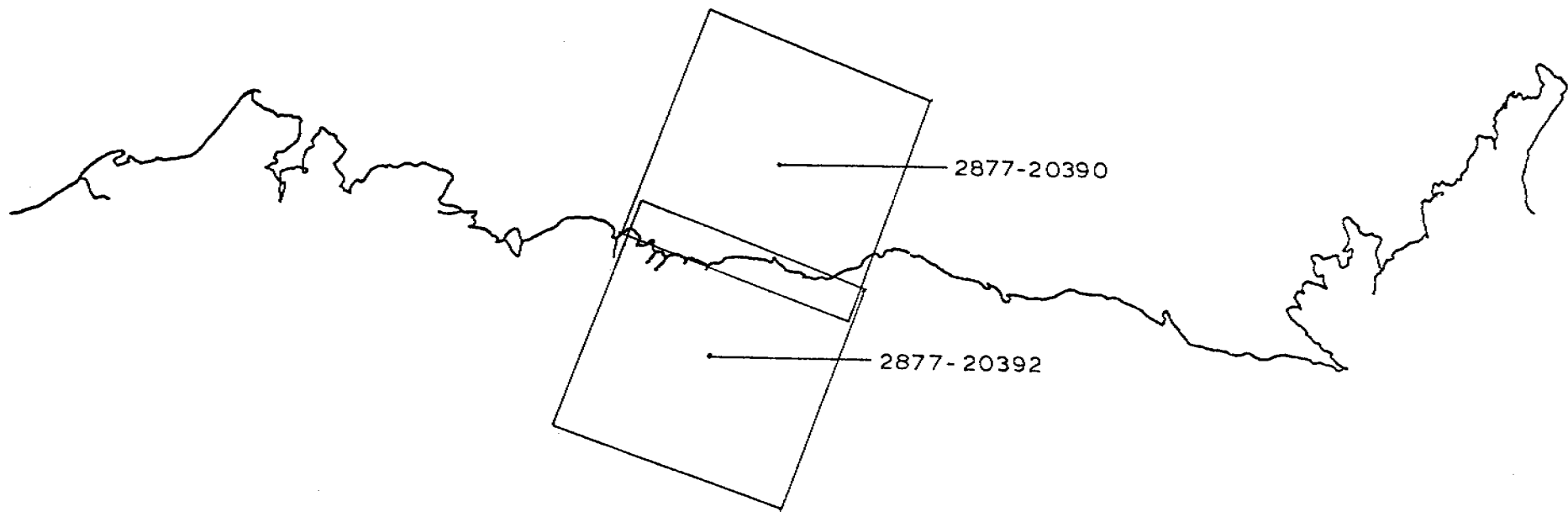
BEAUFORT SEA
2-19 MAY 1977
CYCLE 2831-2848



BEAUFORT SEA

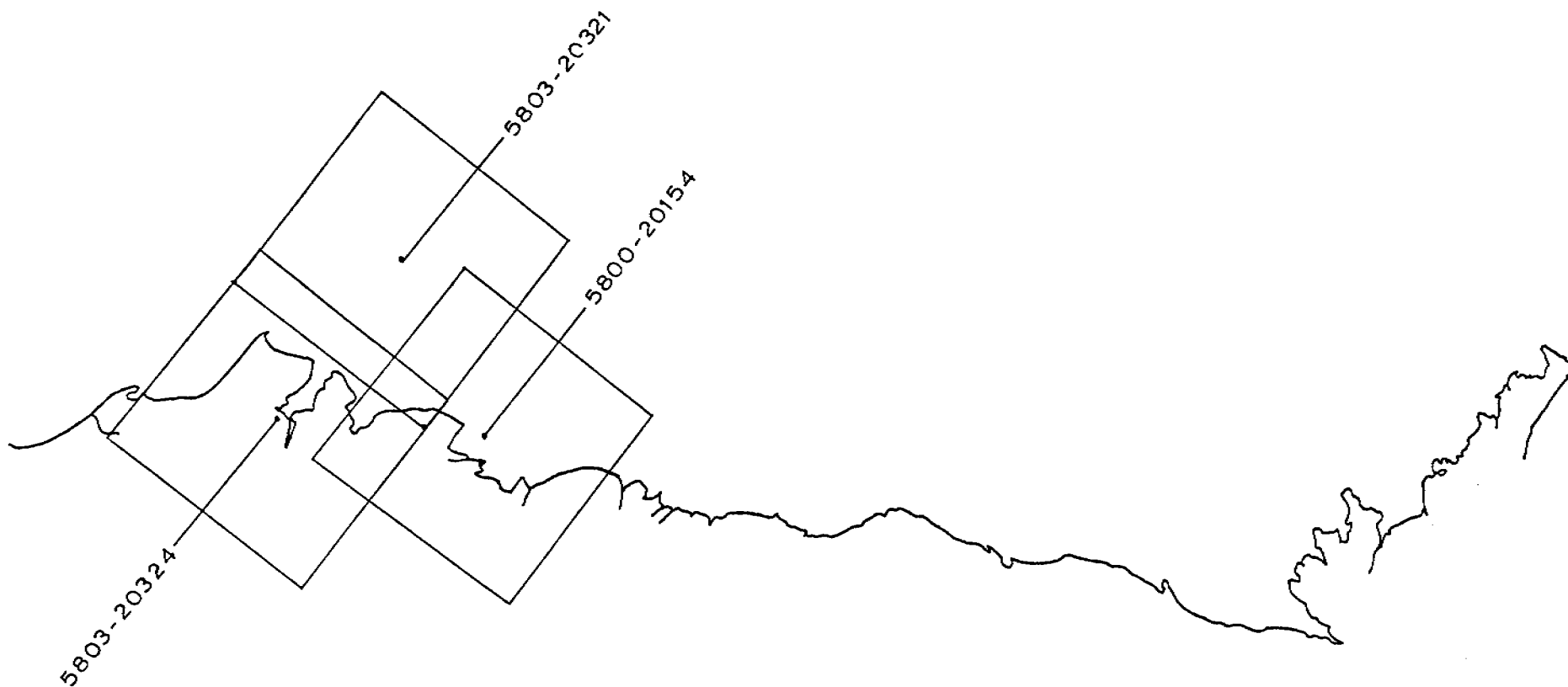
20 MAY - 6 JUNE 1977

CYCLE 2849-2866



BEAUFORT SEA
7-24 JUNE 1977
CYCLE 2867-2884

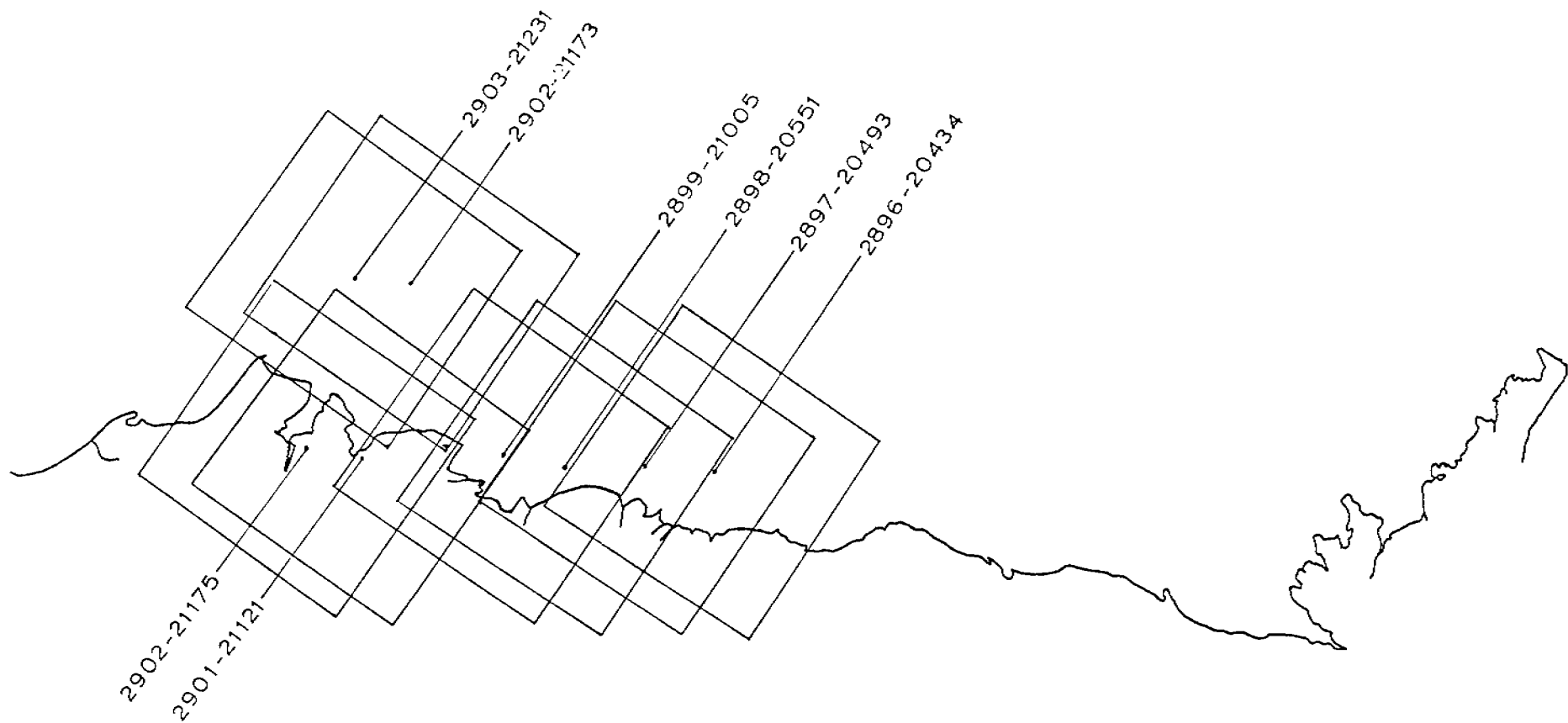
47



BEAUFORT SEA

13-30 JUNE 1977

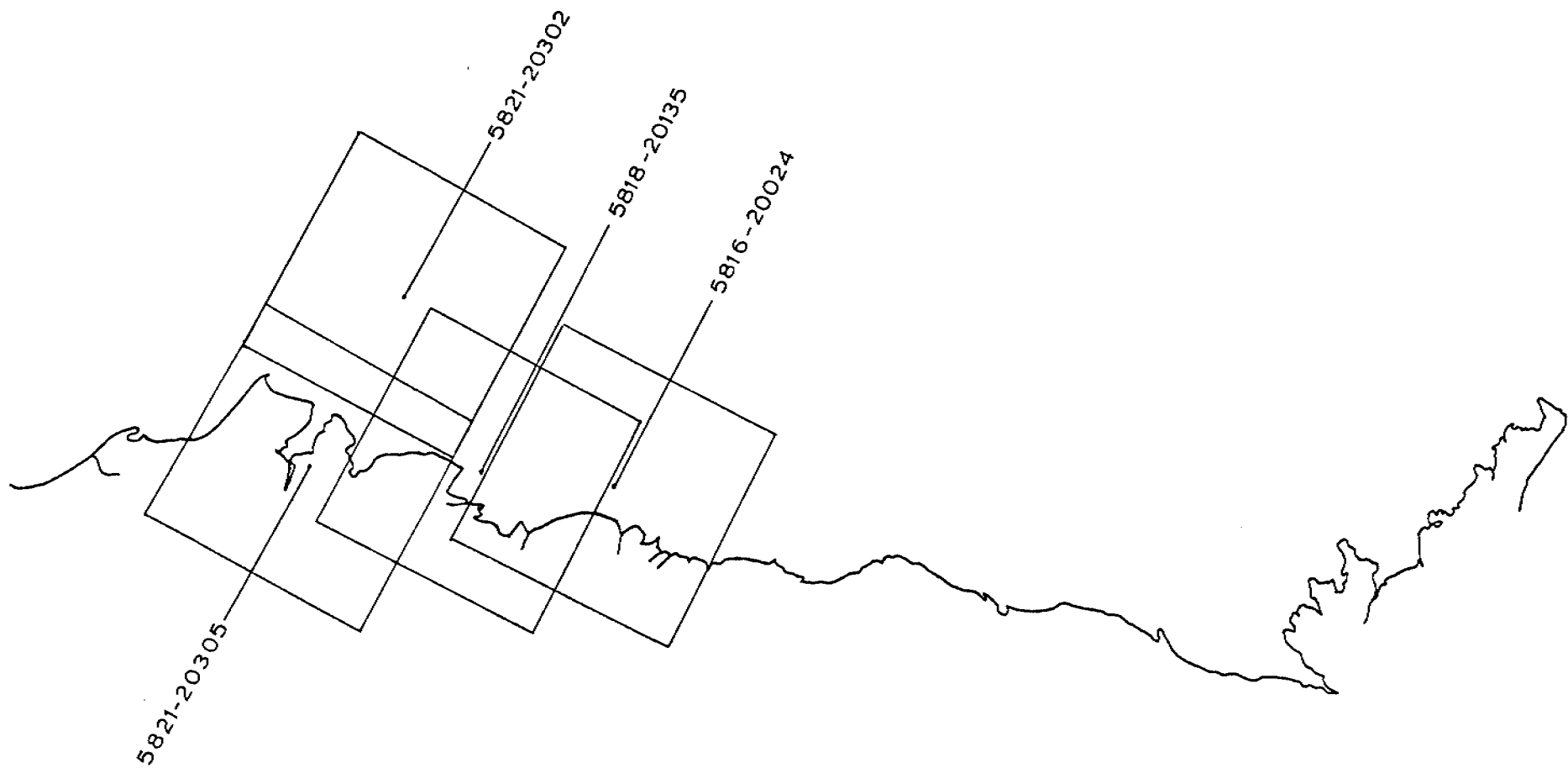
CYCLE 5786 - 5803



BEAUFORT SEA

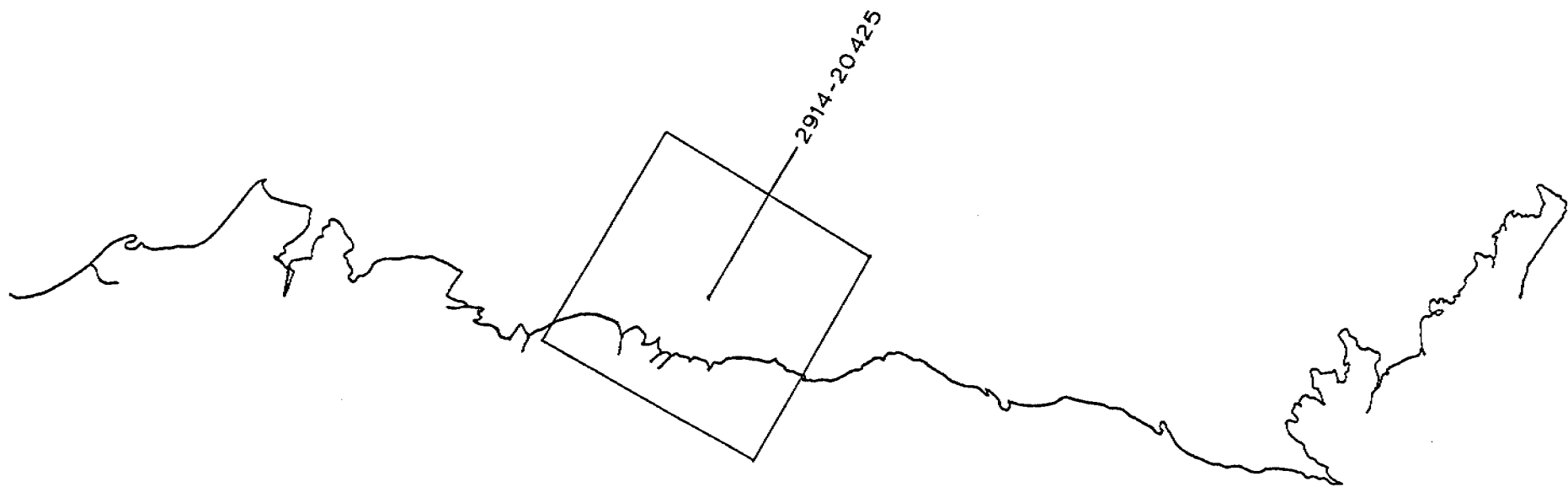
25 JUNE-12 JULY 1977

CYCLE 2885-2902



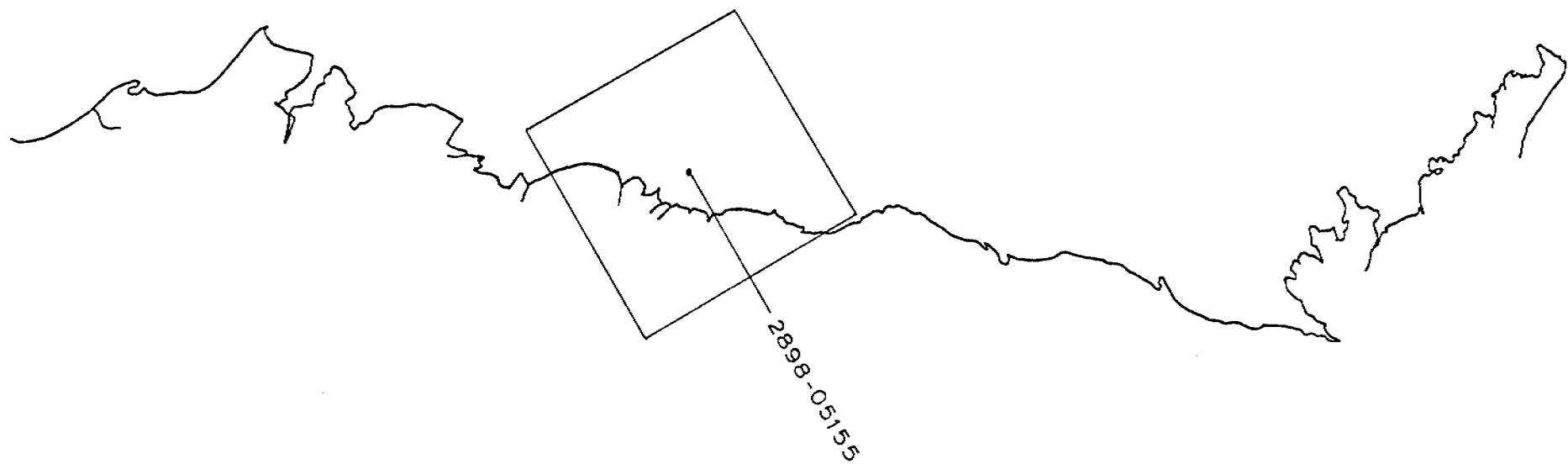
BEAUFORT SEA
1-18 JULY 1977
CYCLE 5804-5821

50



BEAUFORT SEA
13-30 JULY 1977
CYCLE 2903-2920

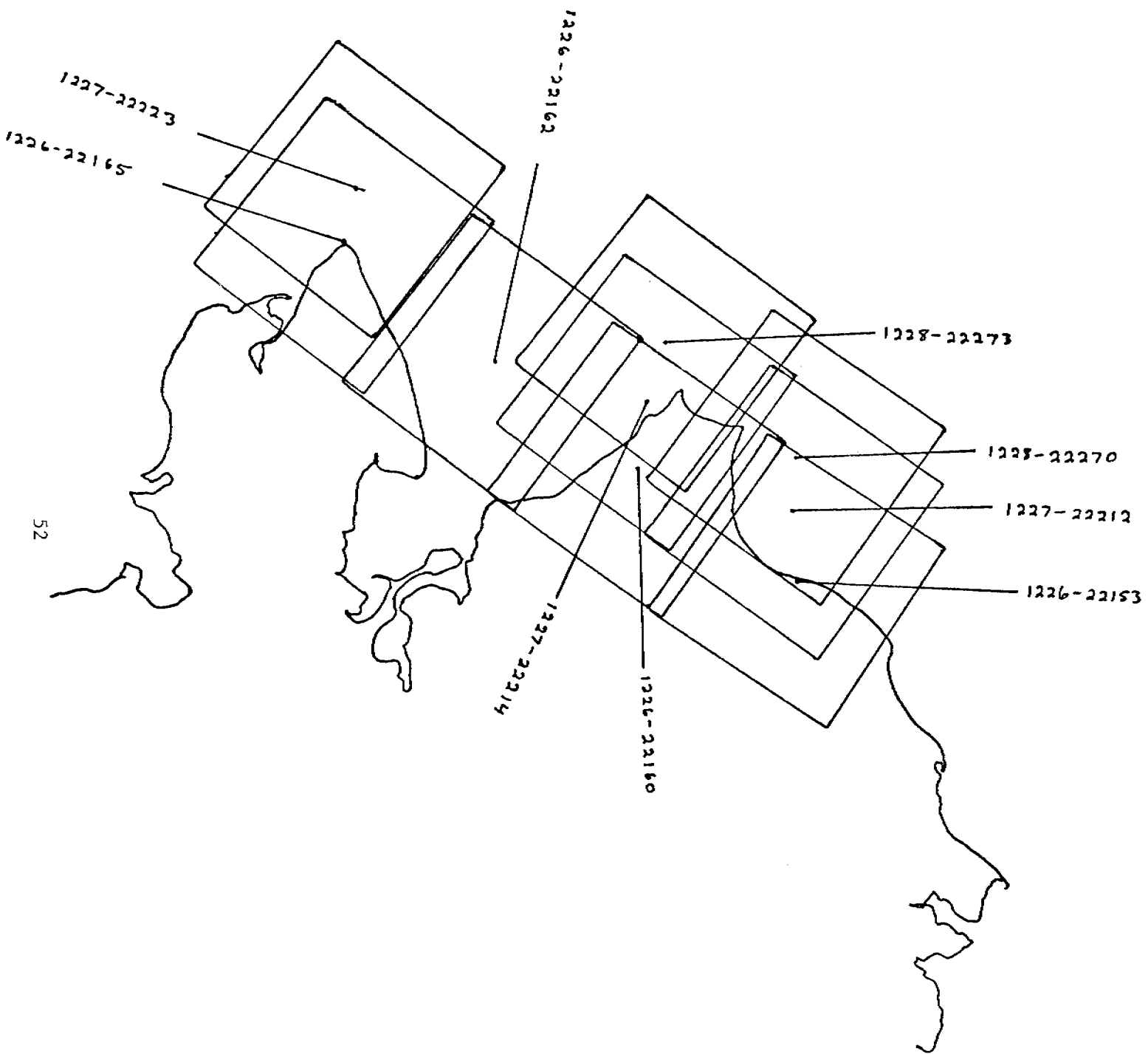
51



BEAUFORT SEA

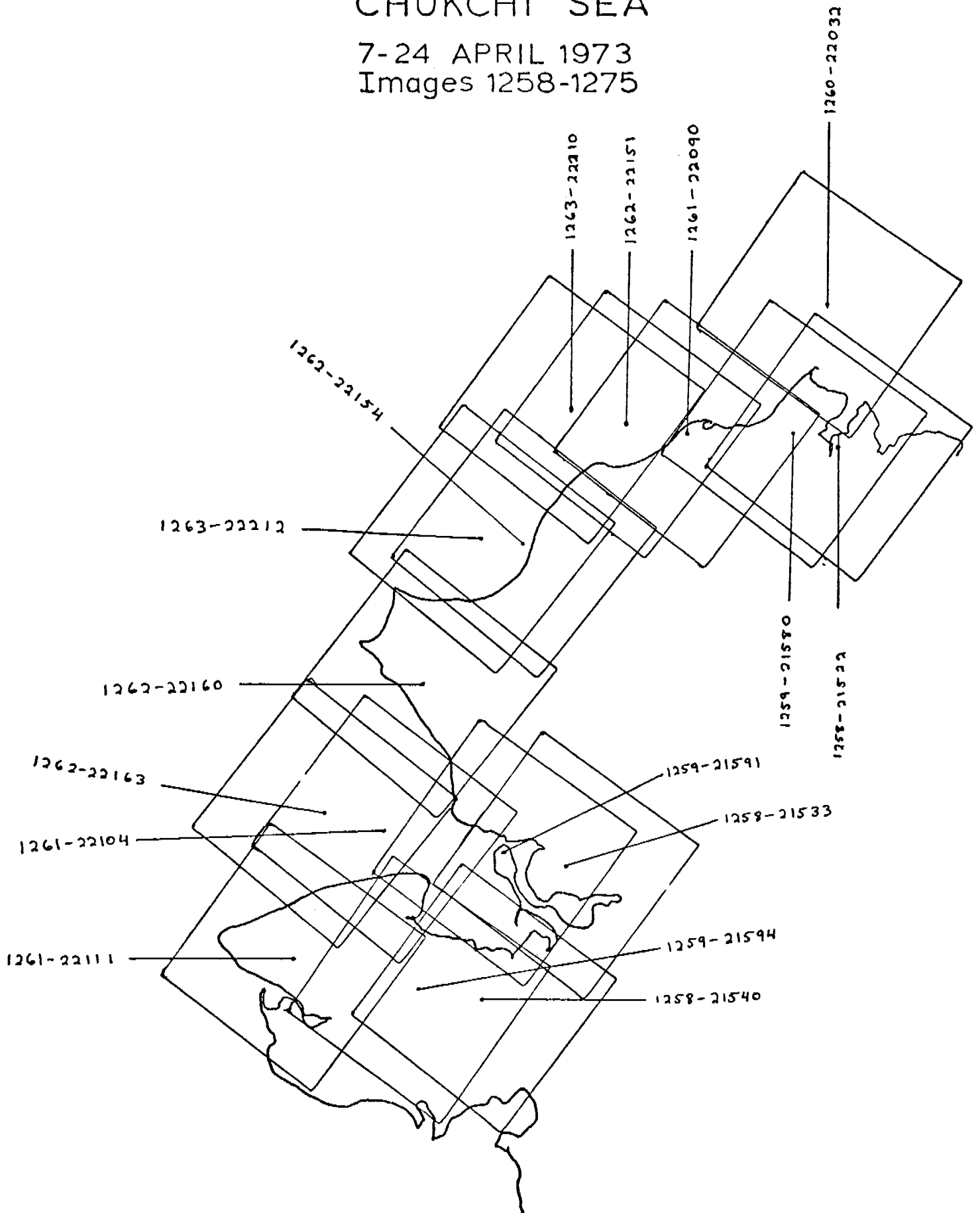
ASCENDING NODE
8 JULY 1977

CHUKCHI SEA
2 - 19 MARCH 1973
Images 1222 - 1239



CHUKCHI SEA

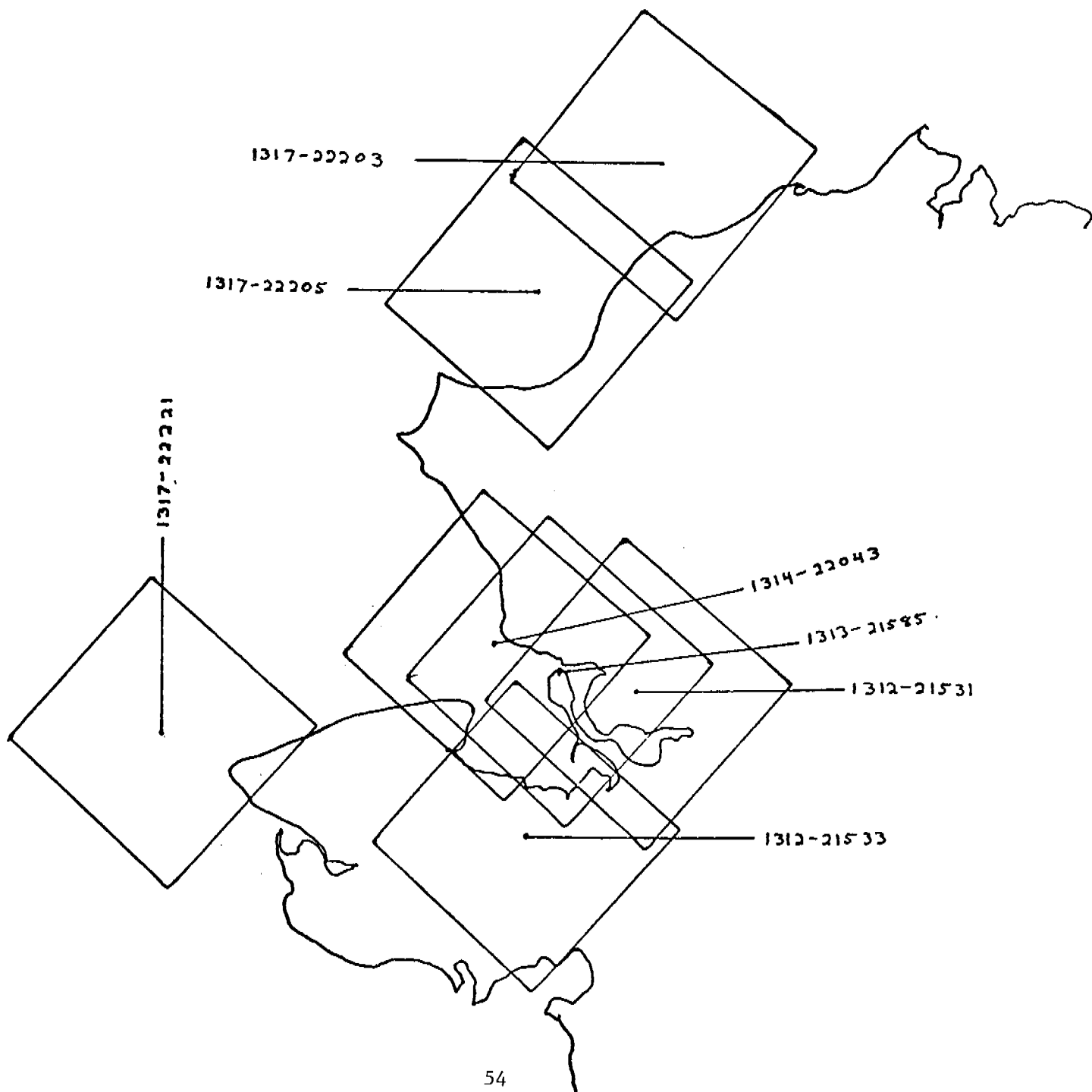
7-24 APRIL 1973
Images 1258-1275



CHUKCHI SEA

31 MAY-17 JUNE 1973

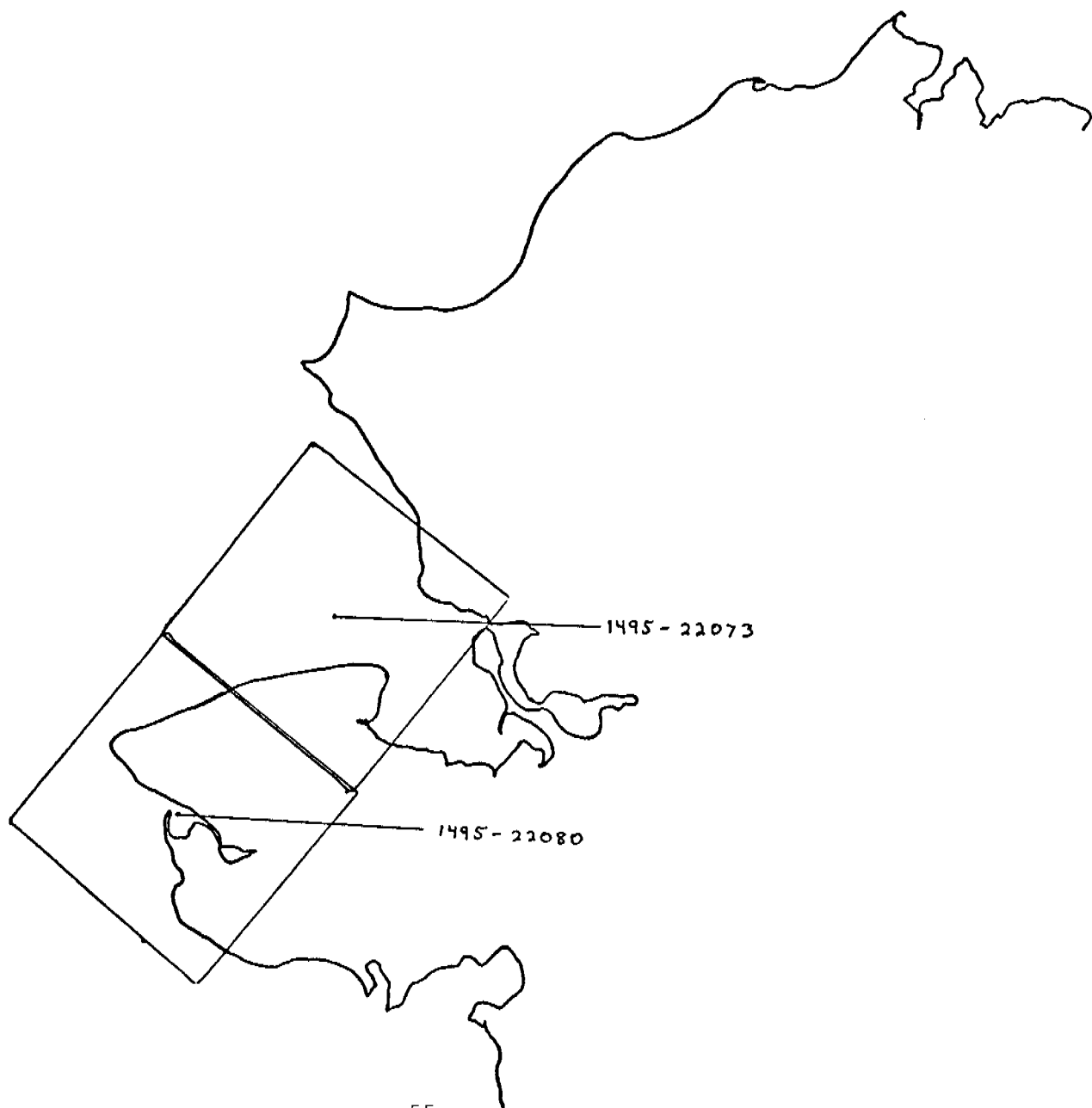
Images 1312-1329



CHUKCHI SEA

27 NOVEMBER-14 DECEMBER
1973

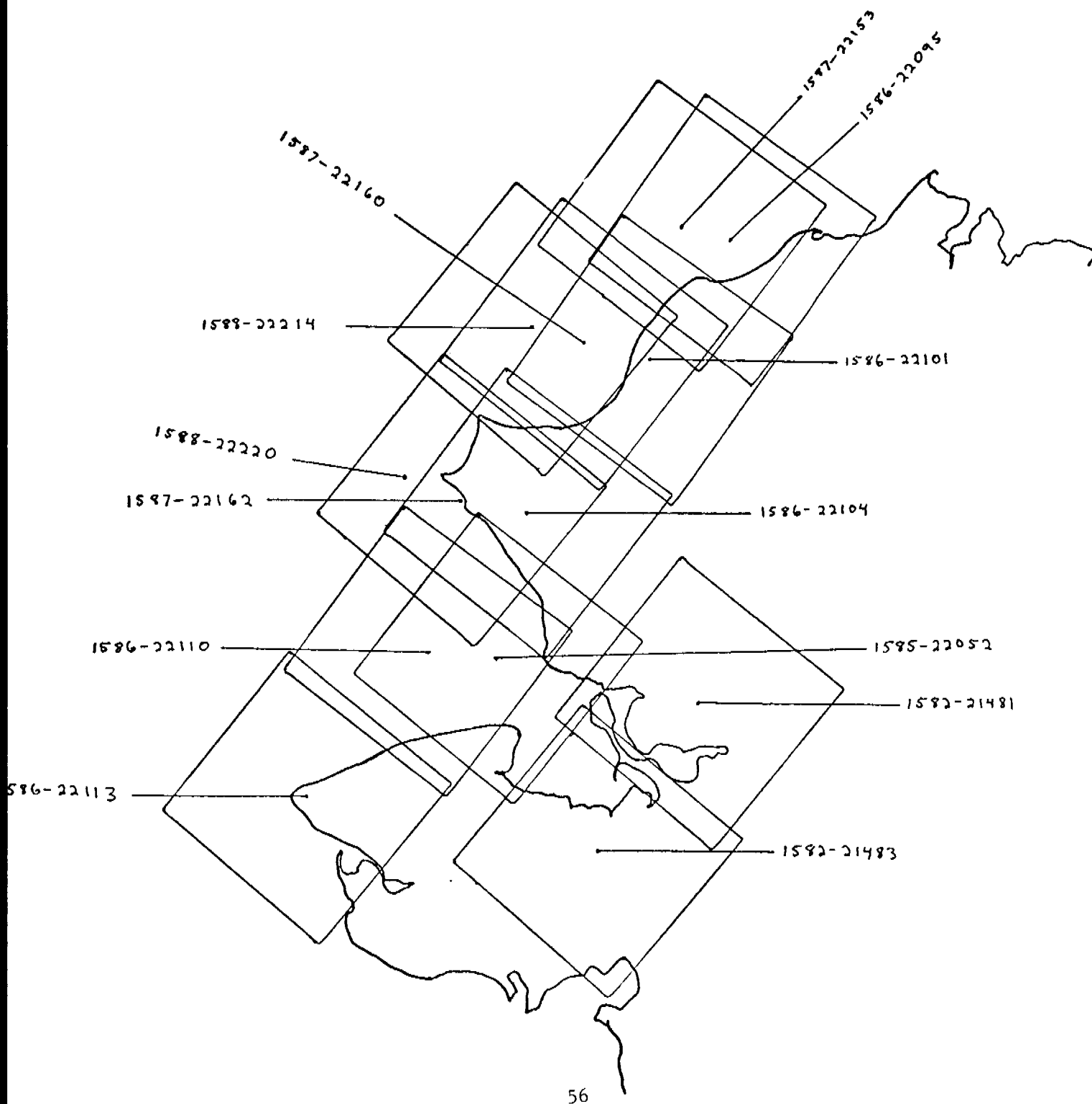
Images 1492-1509



CHUKCHI SEA

25 FEBRUARY-14 MARCH
1974

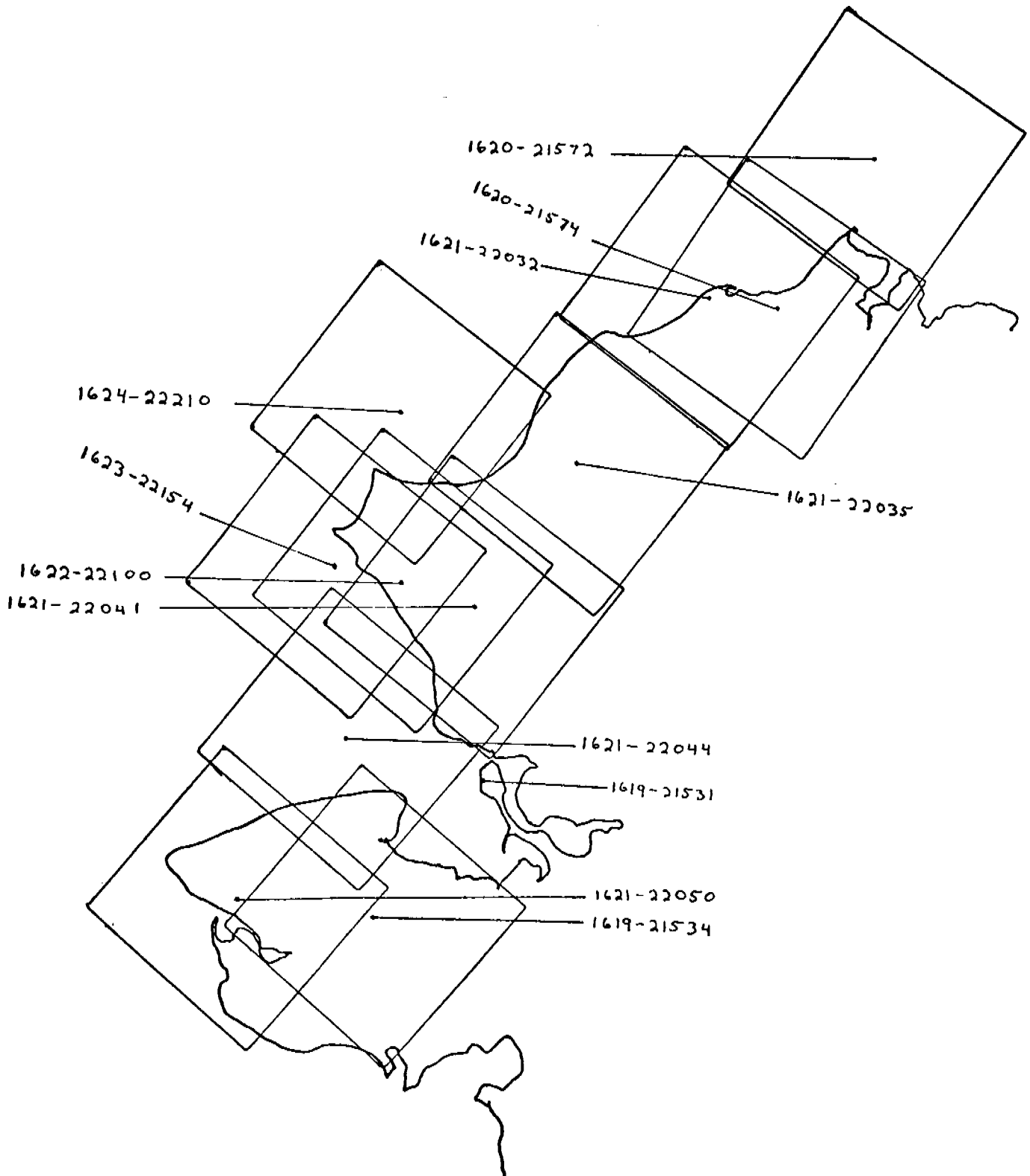
Cycle 1582-1599



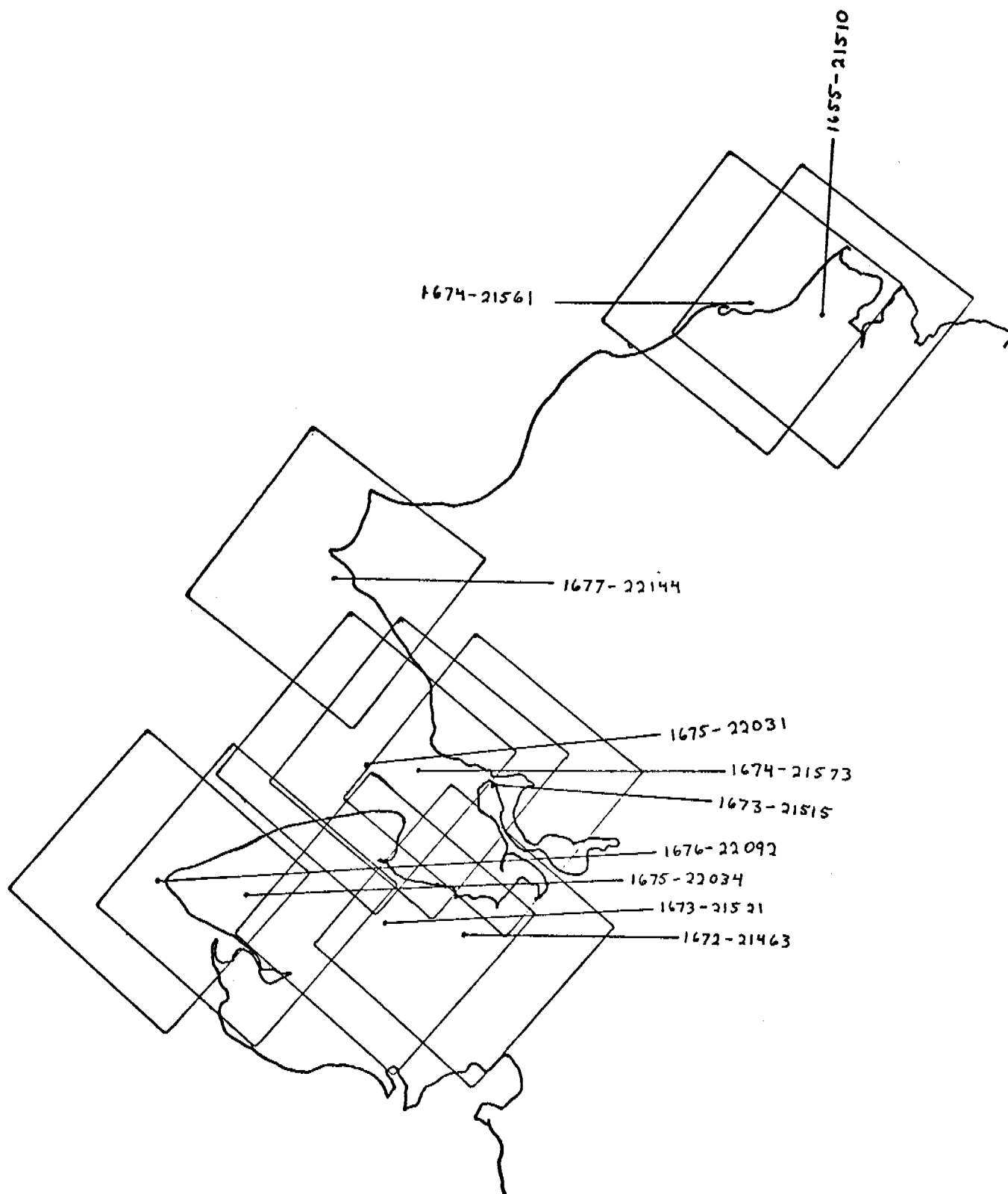
CHUKCHI SEA

2-19 APRIL 1974

Cycle 1618-1635



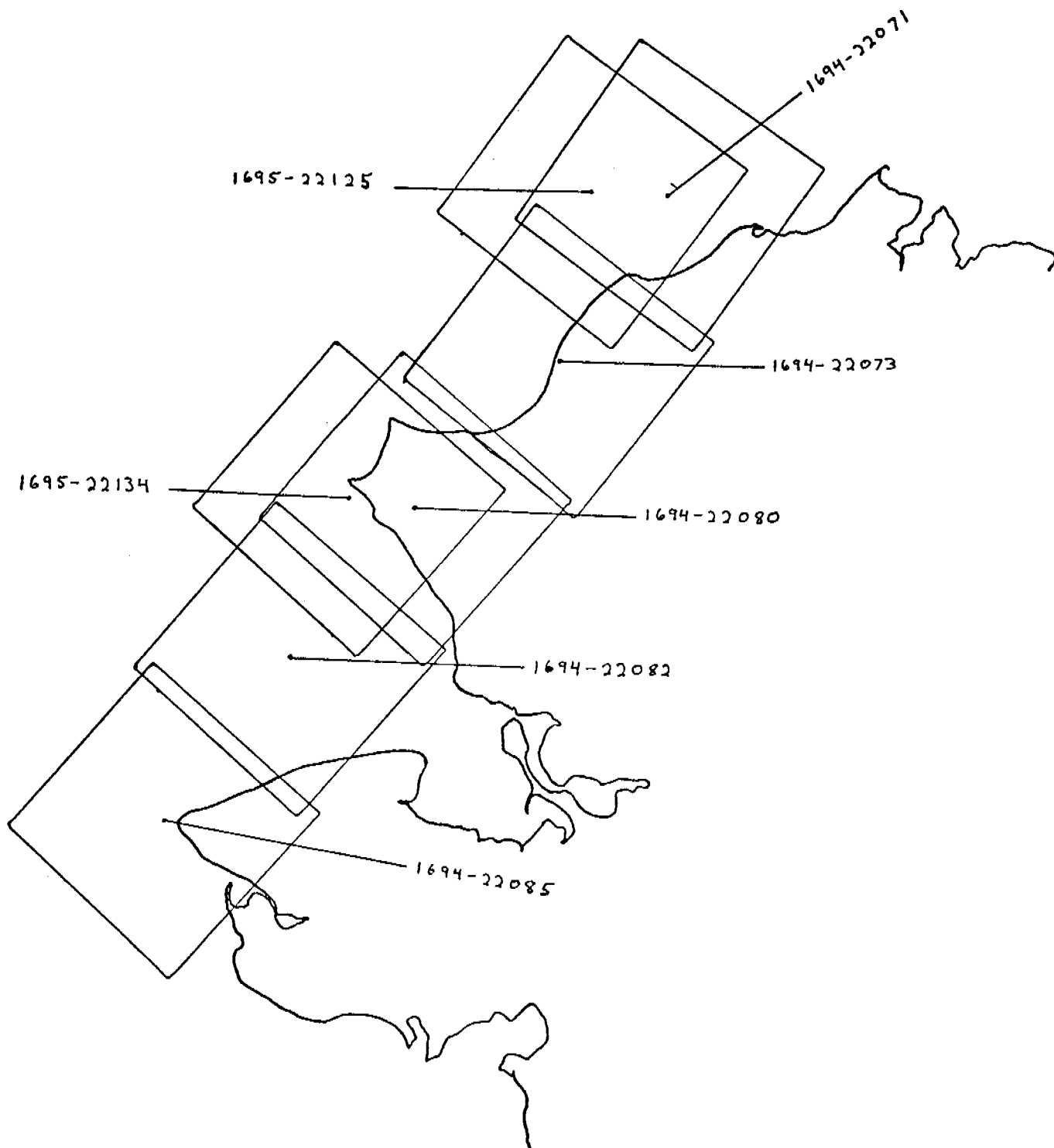
CHUKCHI SEA
26 MAY - 12 JUNE 1974
Cycle 1672 - 1689



CHUKCHI SEA

13-30 JUNE 1974

Cycle 1690-1707

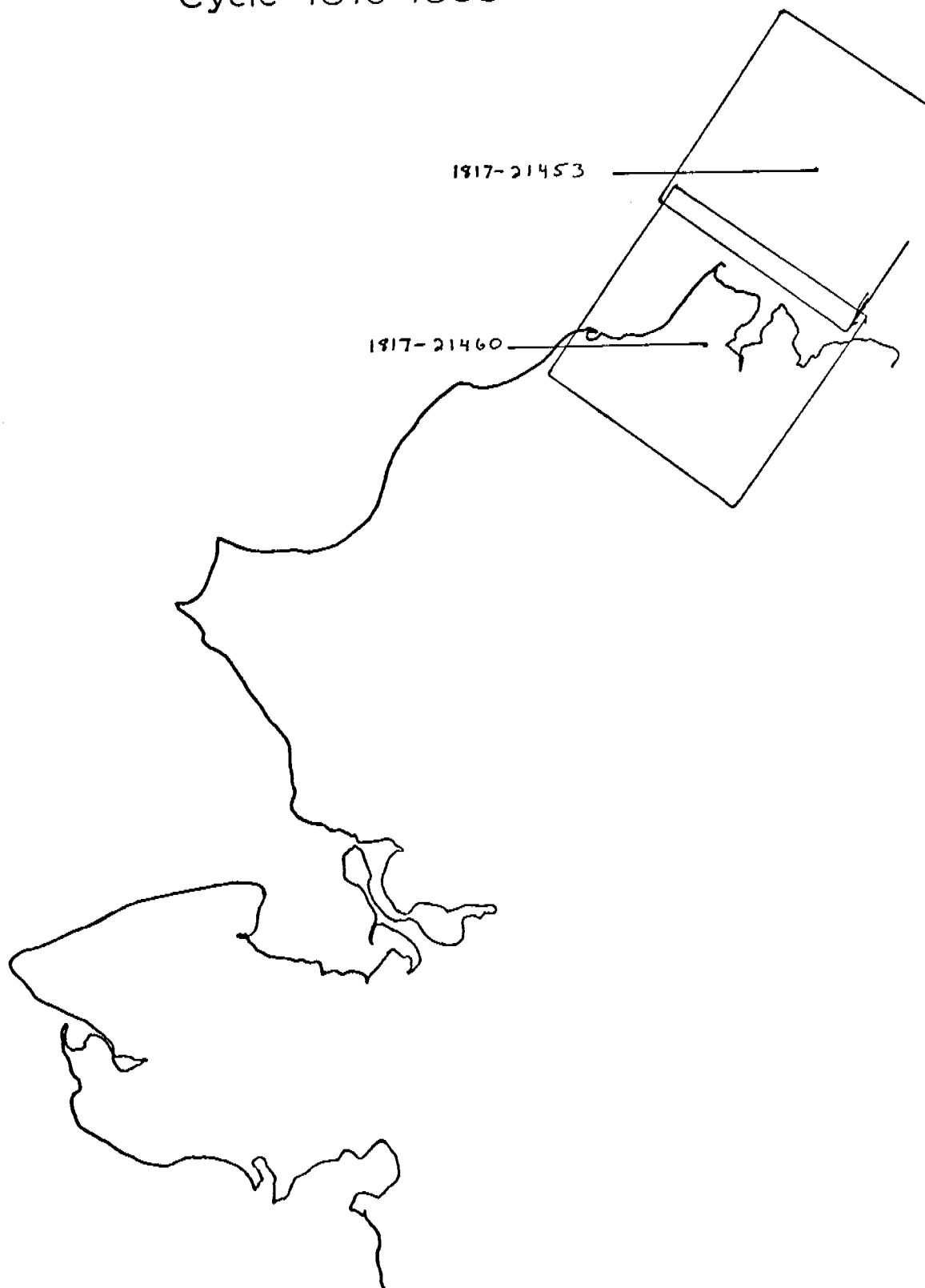


CHUKCHI SEA

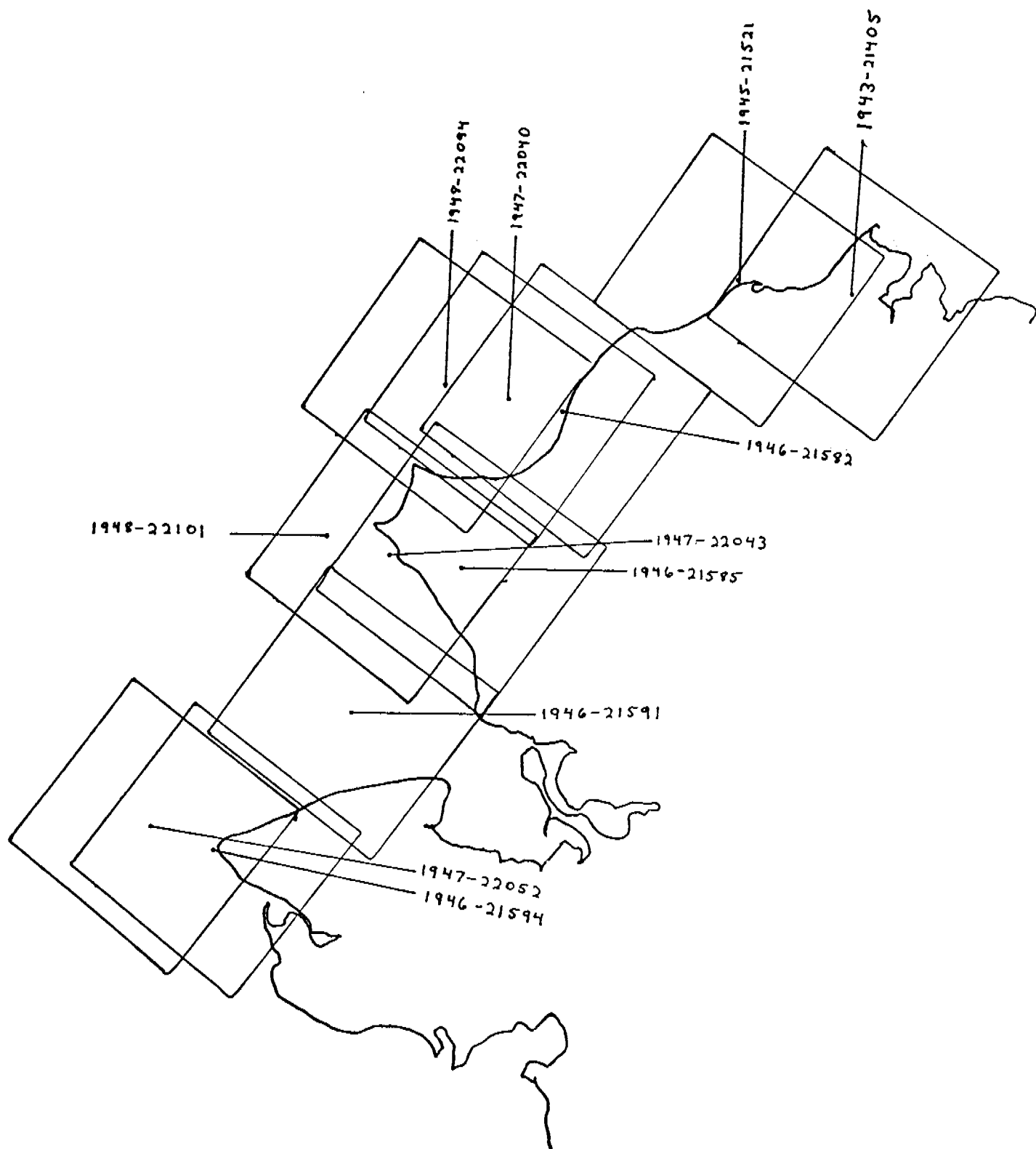
17 OCTOBER-3 NOVEMBER

1974

Cycle 1816-1833



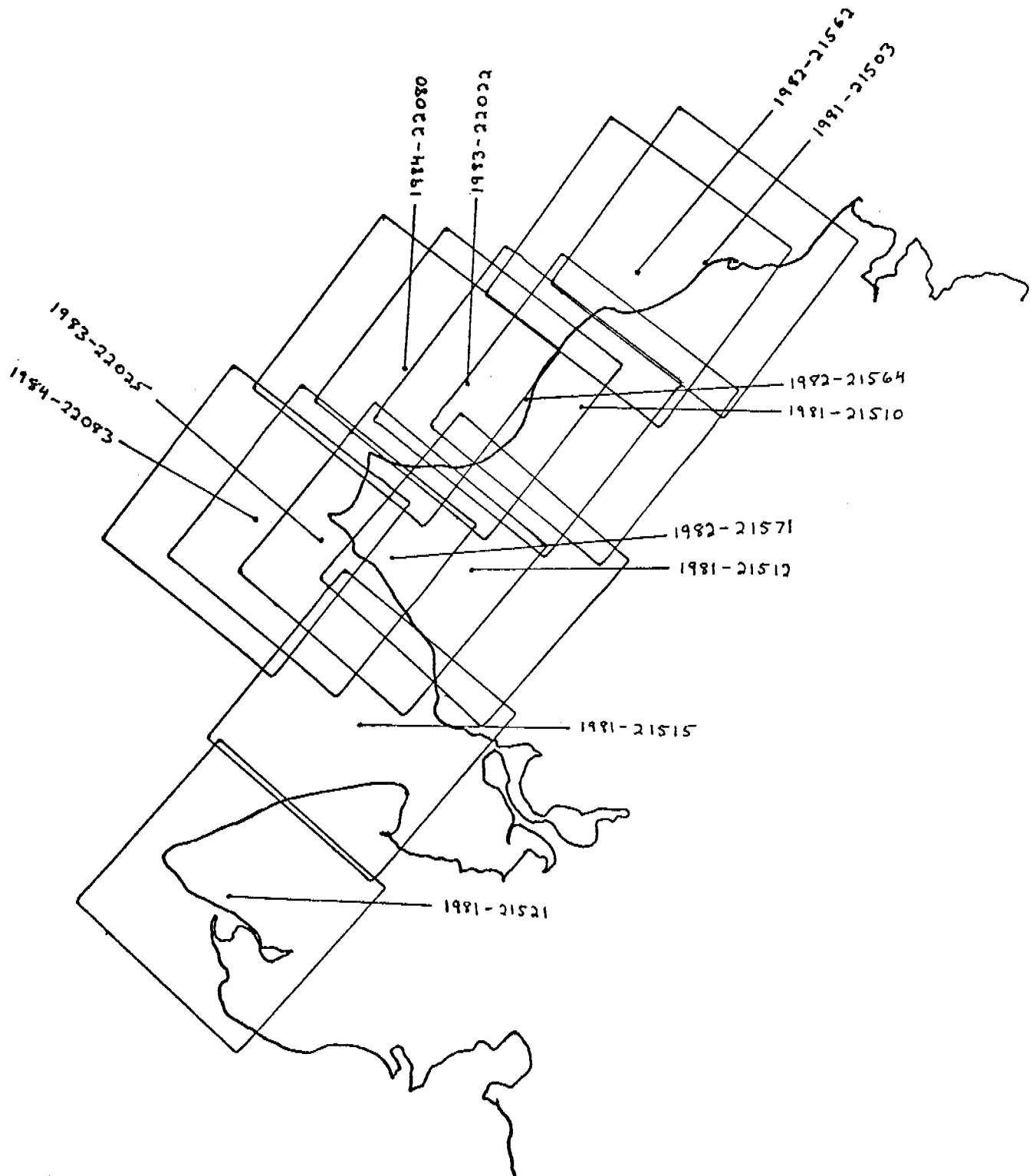
CHUKCHI SEA
20 FEBRUARY - 9 MARCH 1975
Cycle 1942-1959



CHUKCHI SEA

28 MARCH-14 APRIL 1975

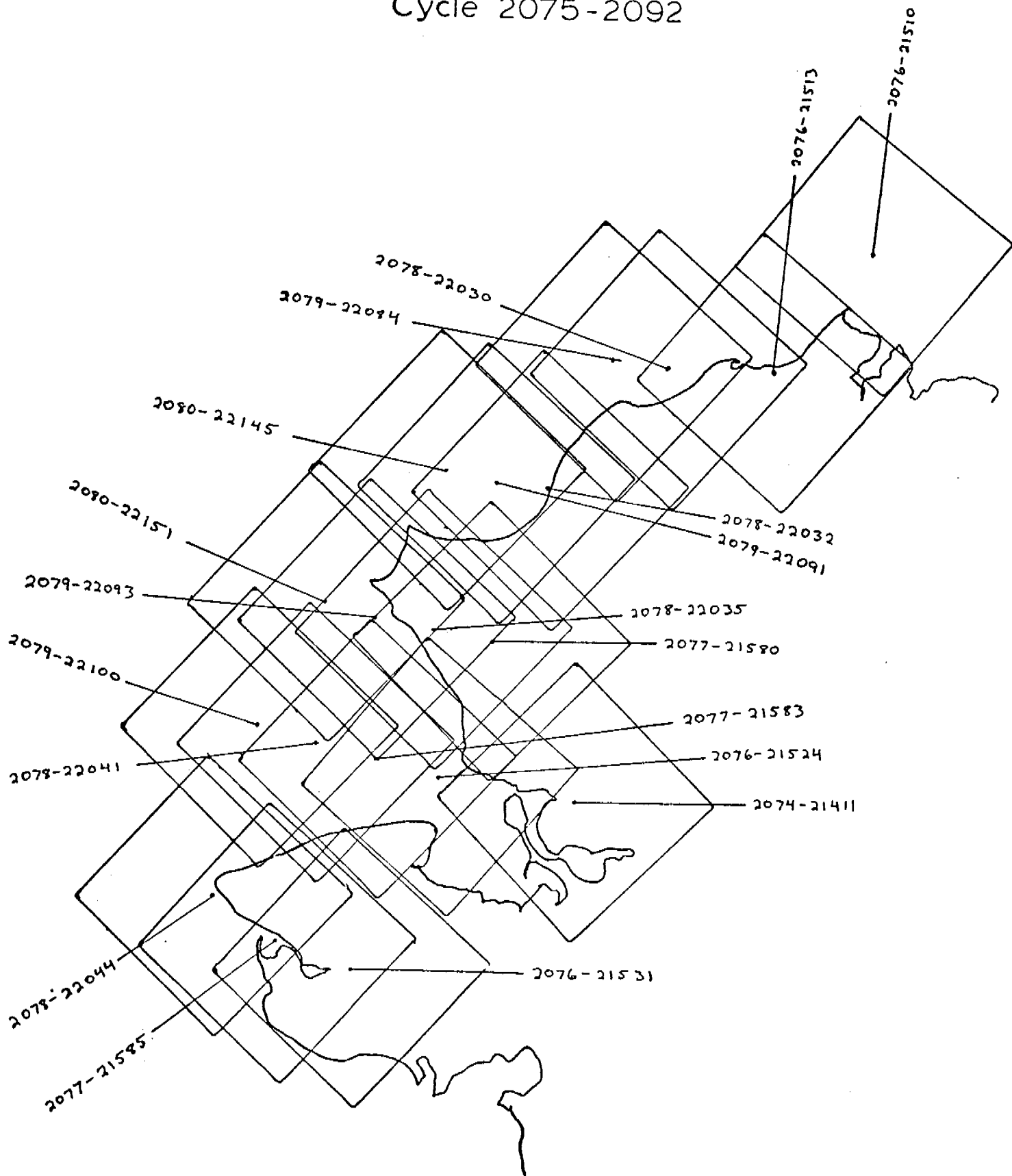
Cycle 1978 - 1995



CHUKCHI SEA

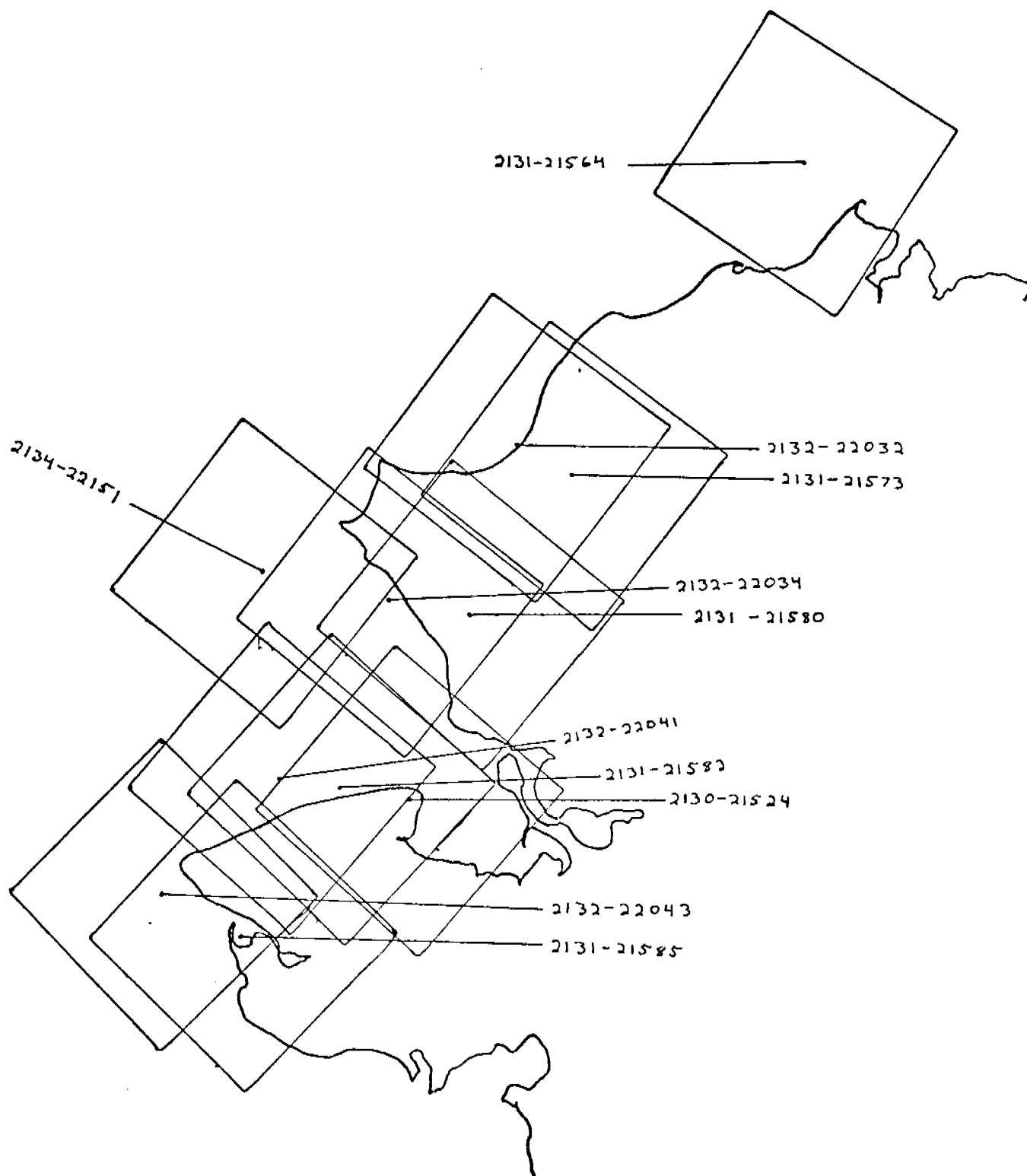
6-23 APRIL 1975

Cycle 2075-2092



CHUKCHI SEA

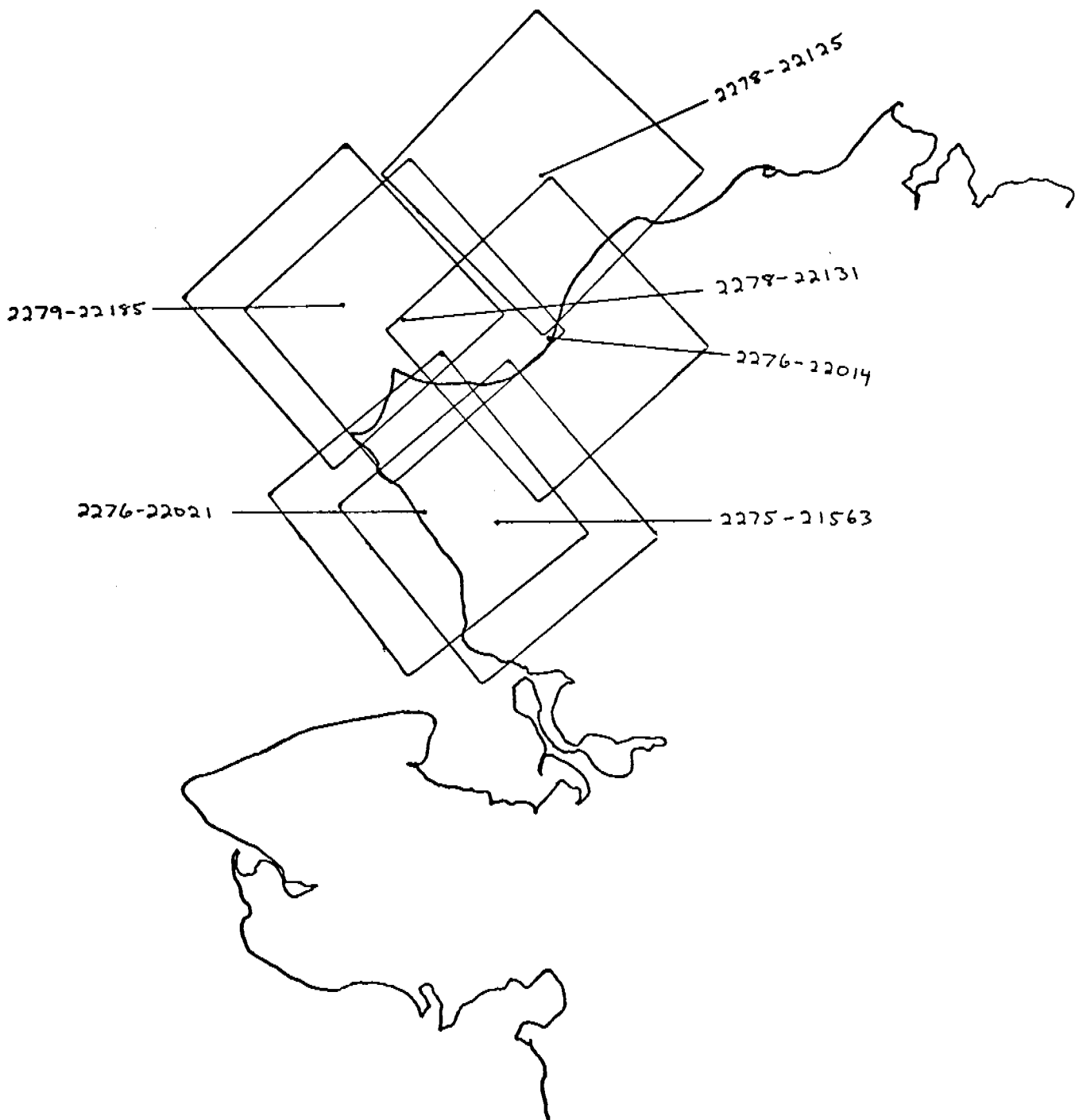
30 MAY-16 JUNE 1975
Cycle 2128-2145



CHUKCHI SEA

21 OCTOBER - 8 NOVEMBER 1975

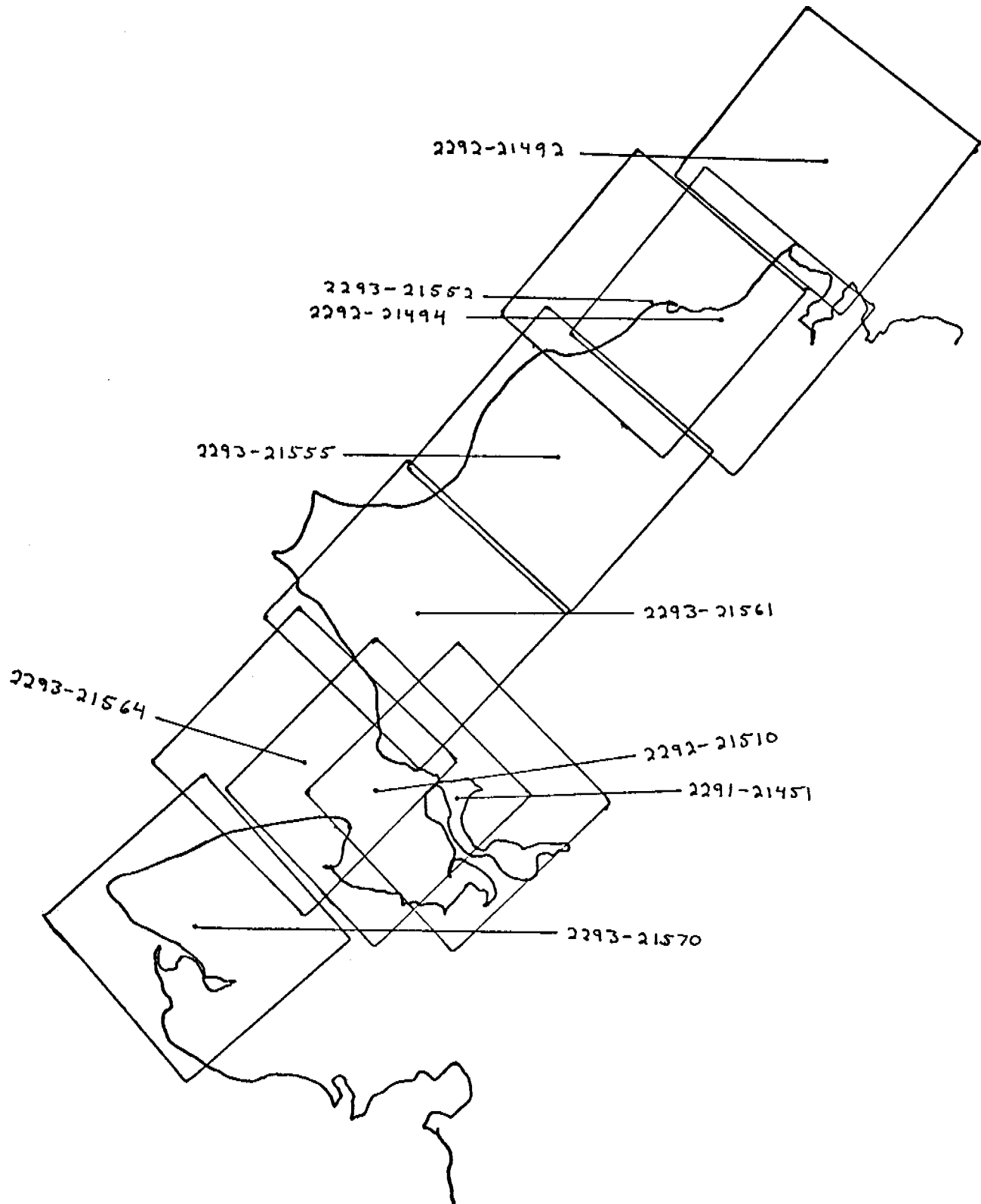
Cycle 2272-2290



CHUKCHI SEA

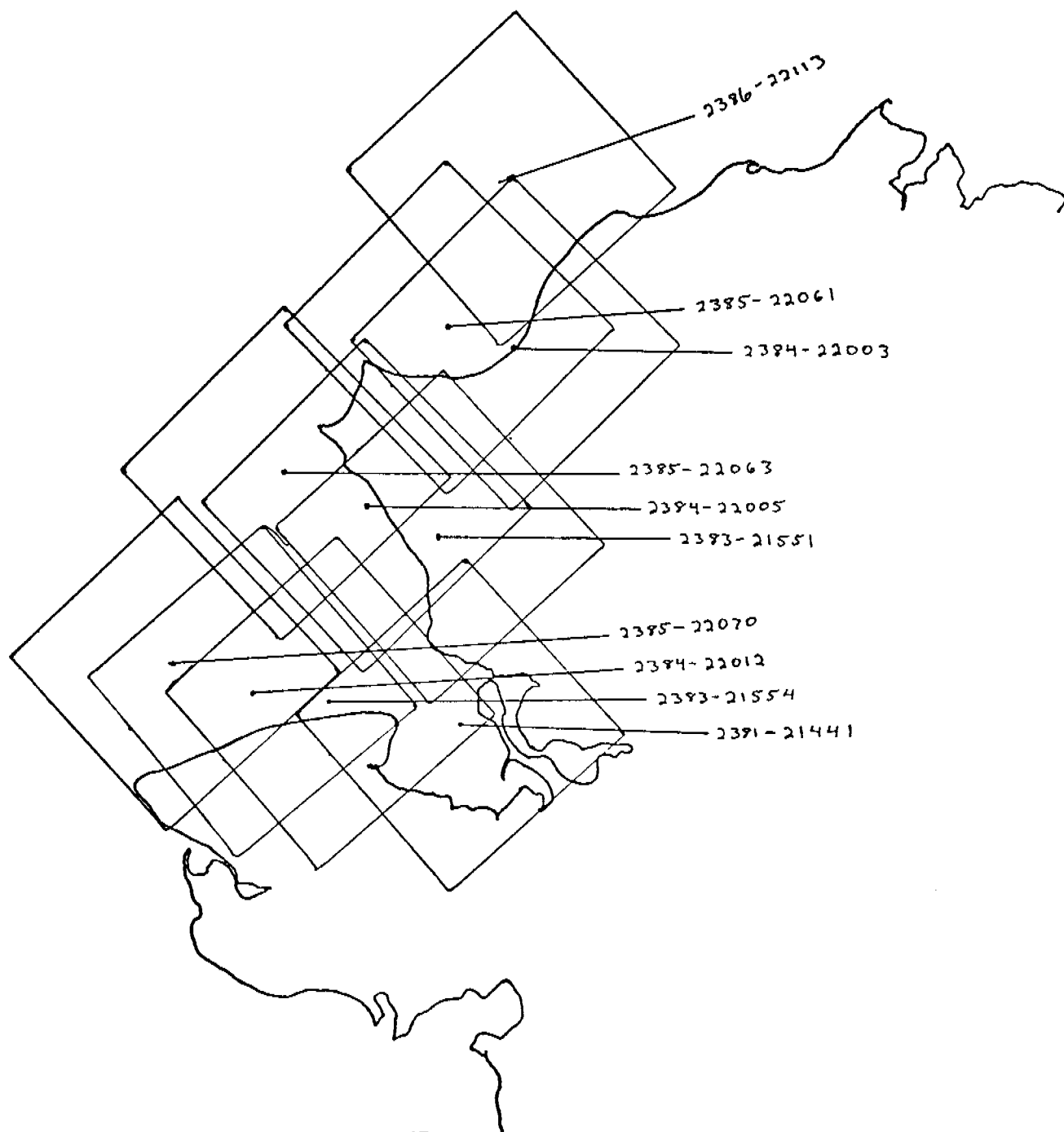
9-26 NOVEMBER 1975

Cycle 2291-2308



CHUKCHI SEA

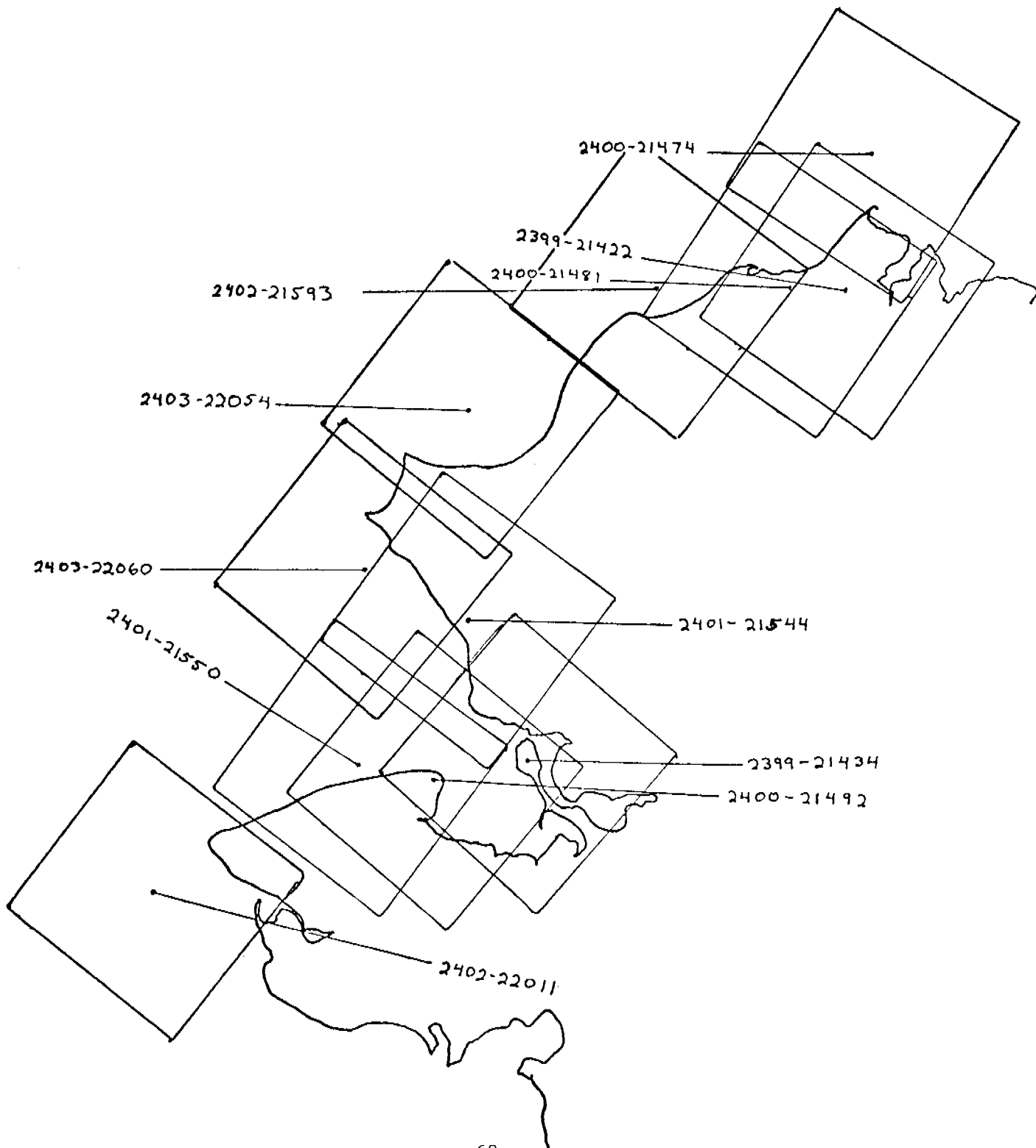
6-23 FEBRUARY 1976
Cycle 2381-2398

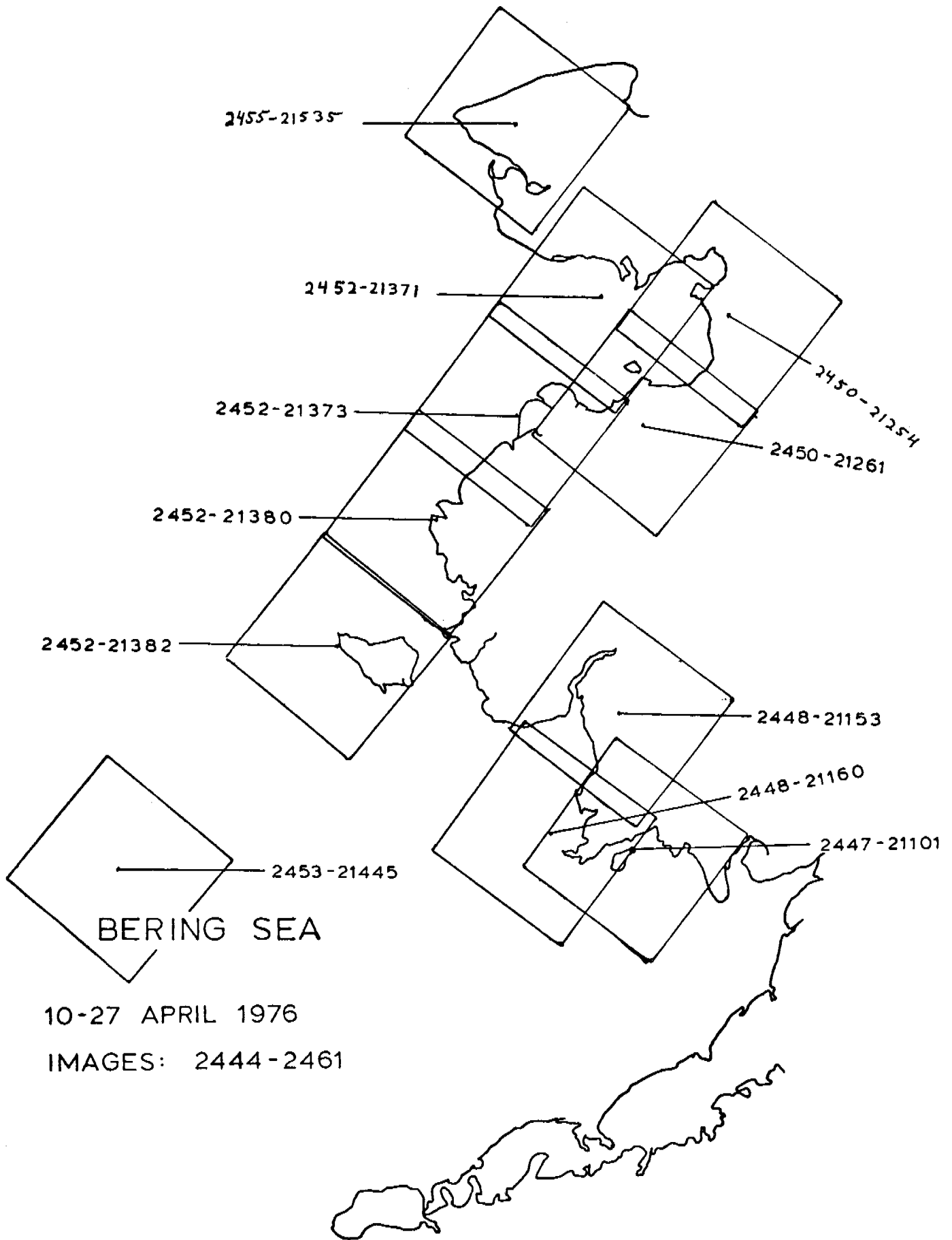


CHUKCHI SEA

24 FEBRUARY - 12 MARCH 1976

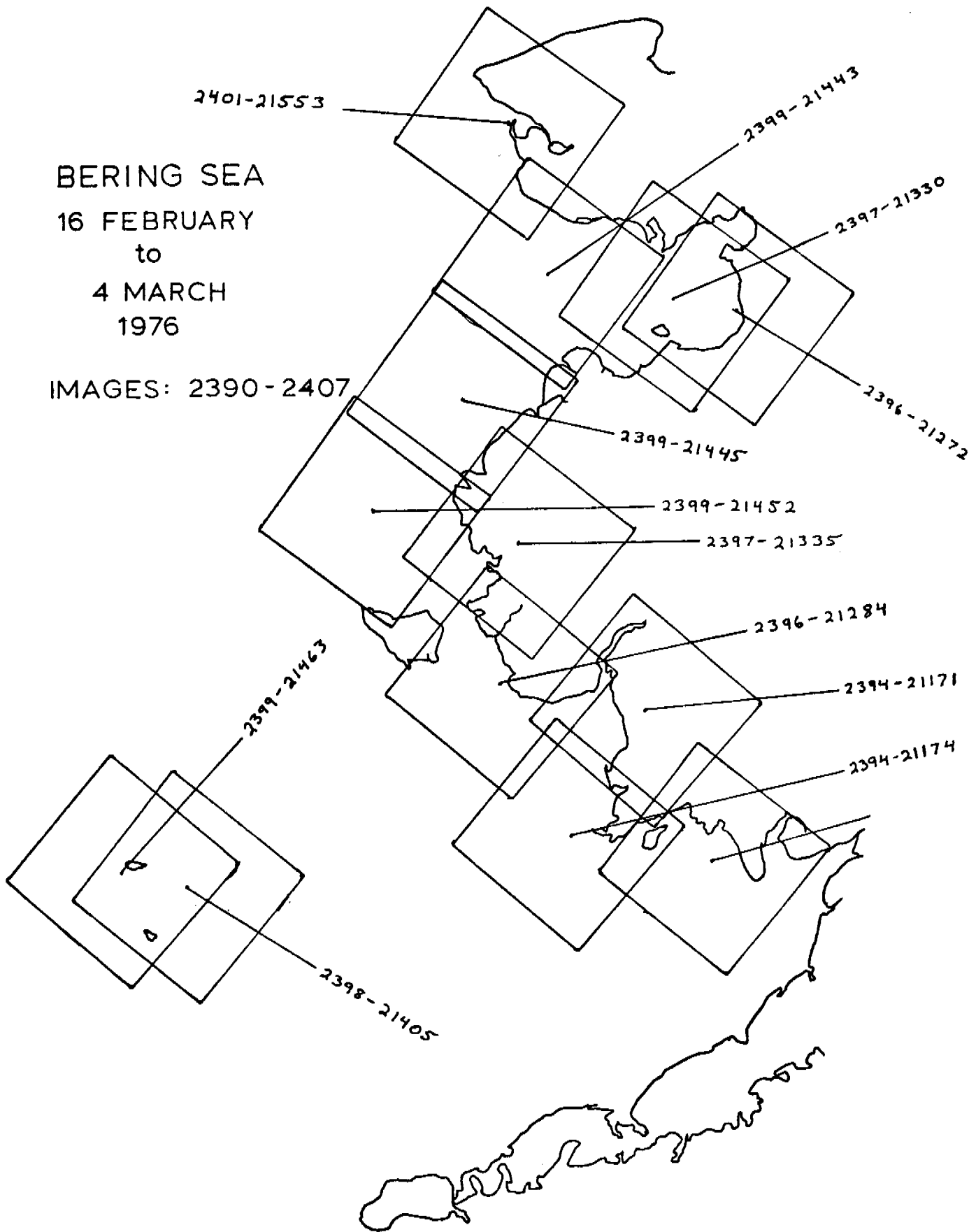
Cycle 2399 - 2416

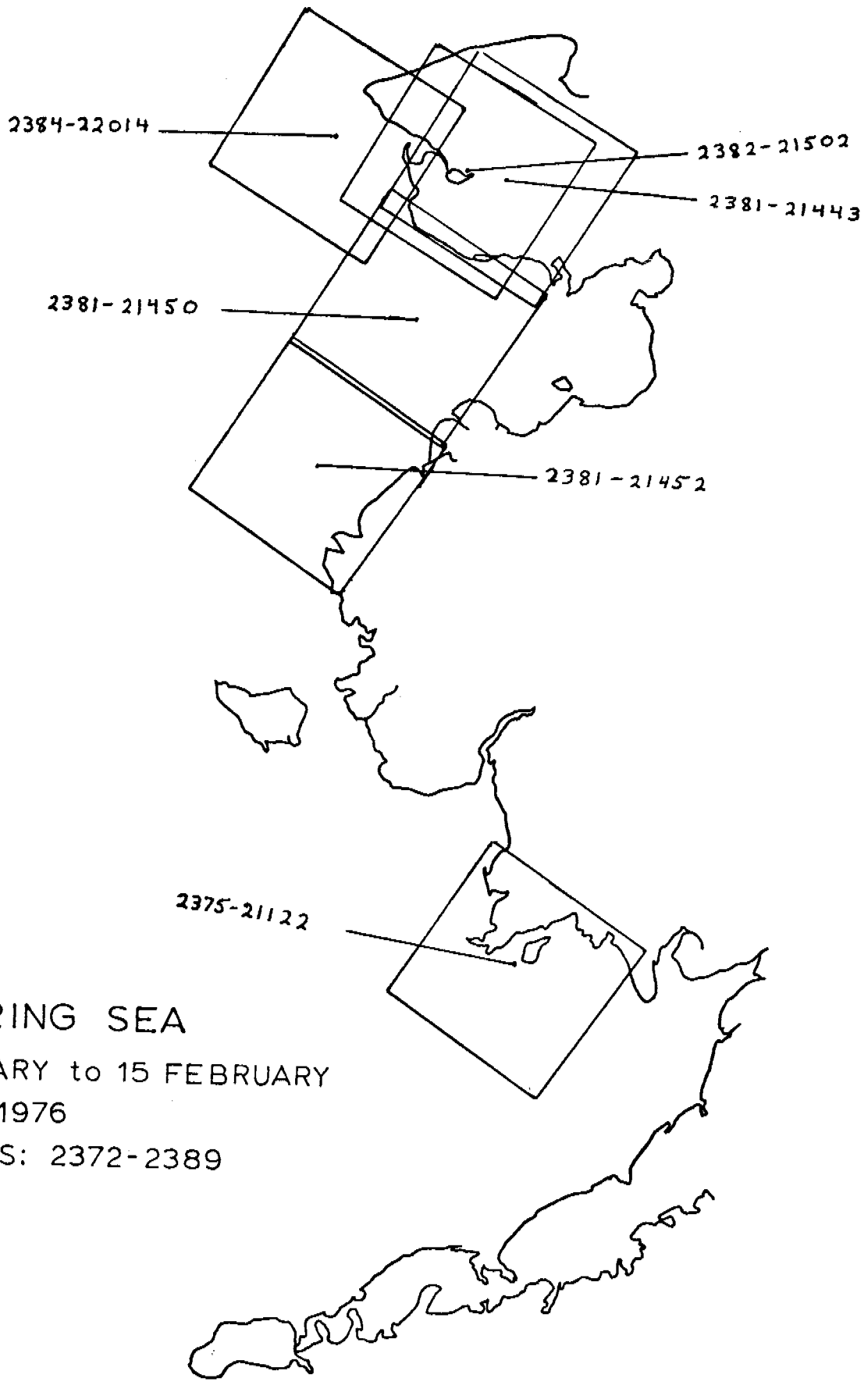




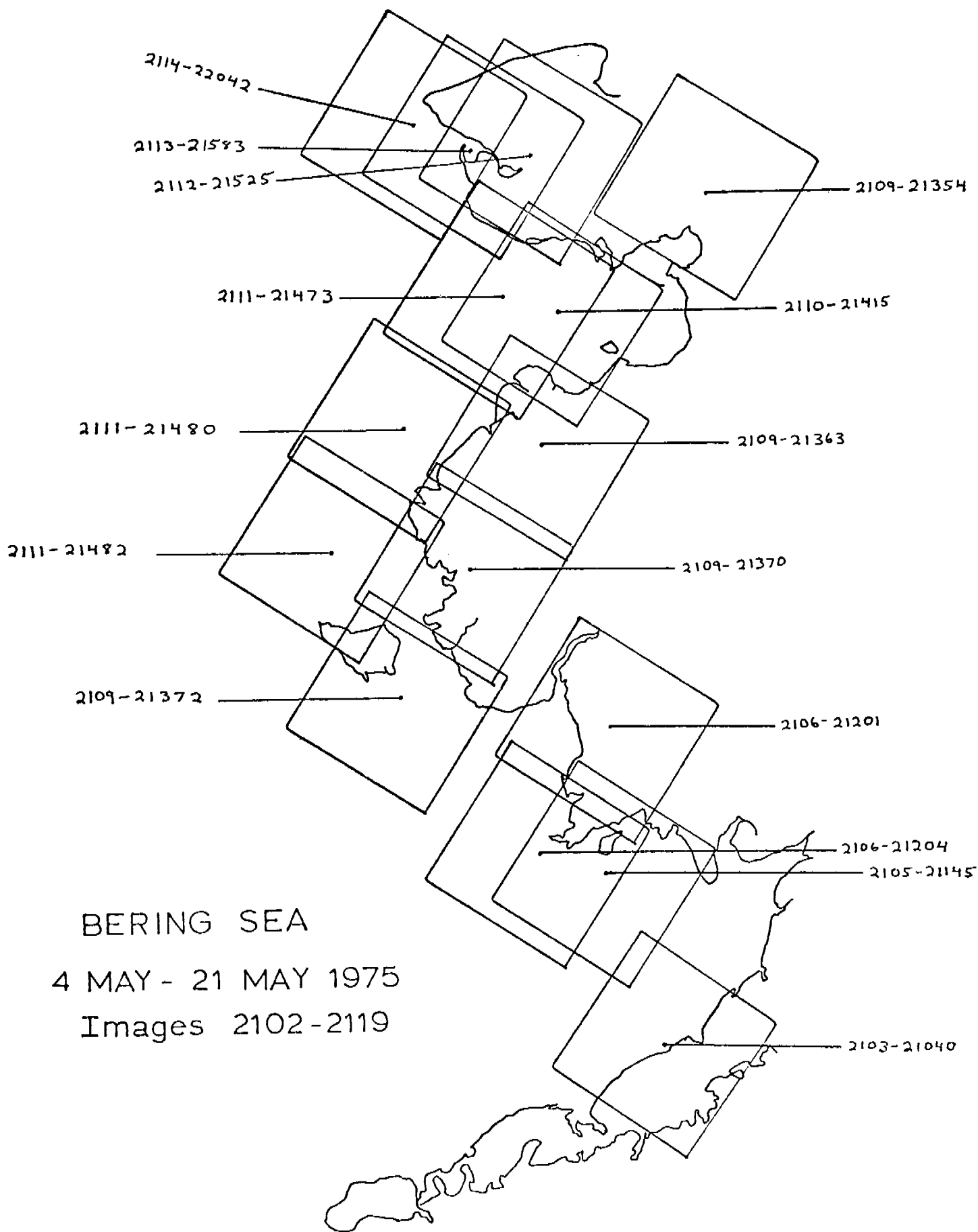
BERING SEA
16 FEBRUARY
to
4 MARCH
1976

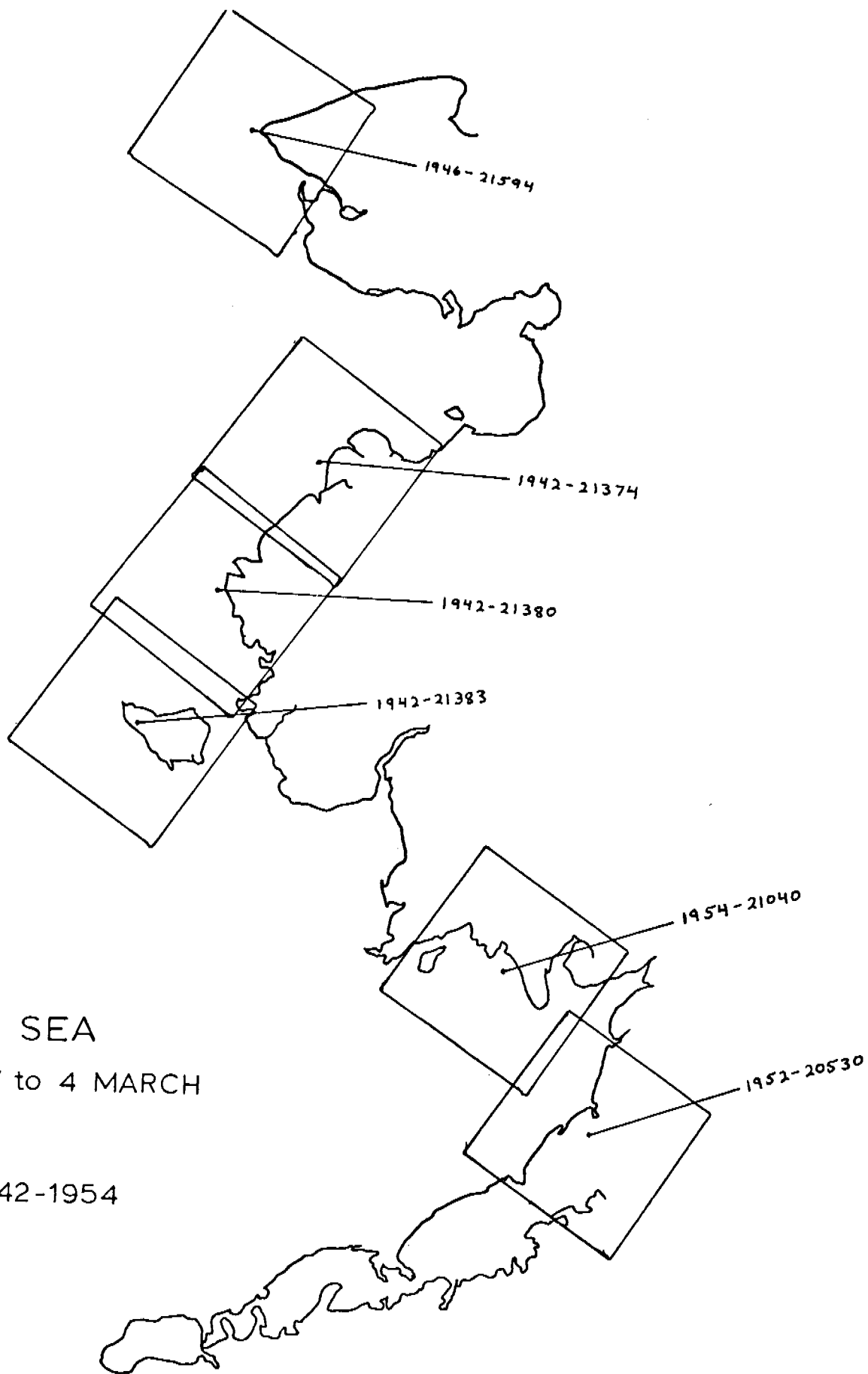
IMAGES: 2390 - 2407





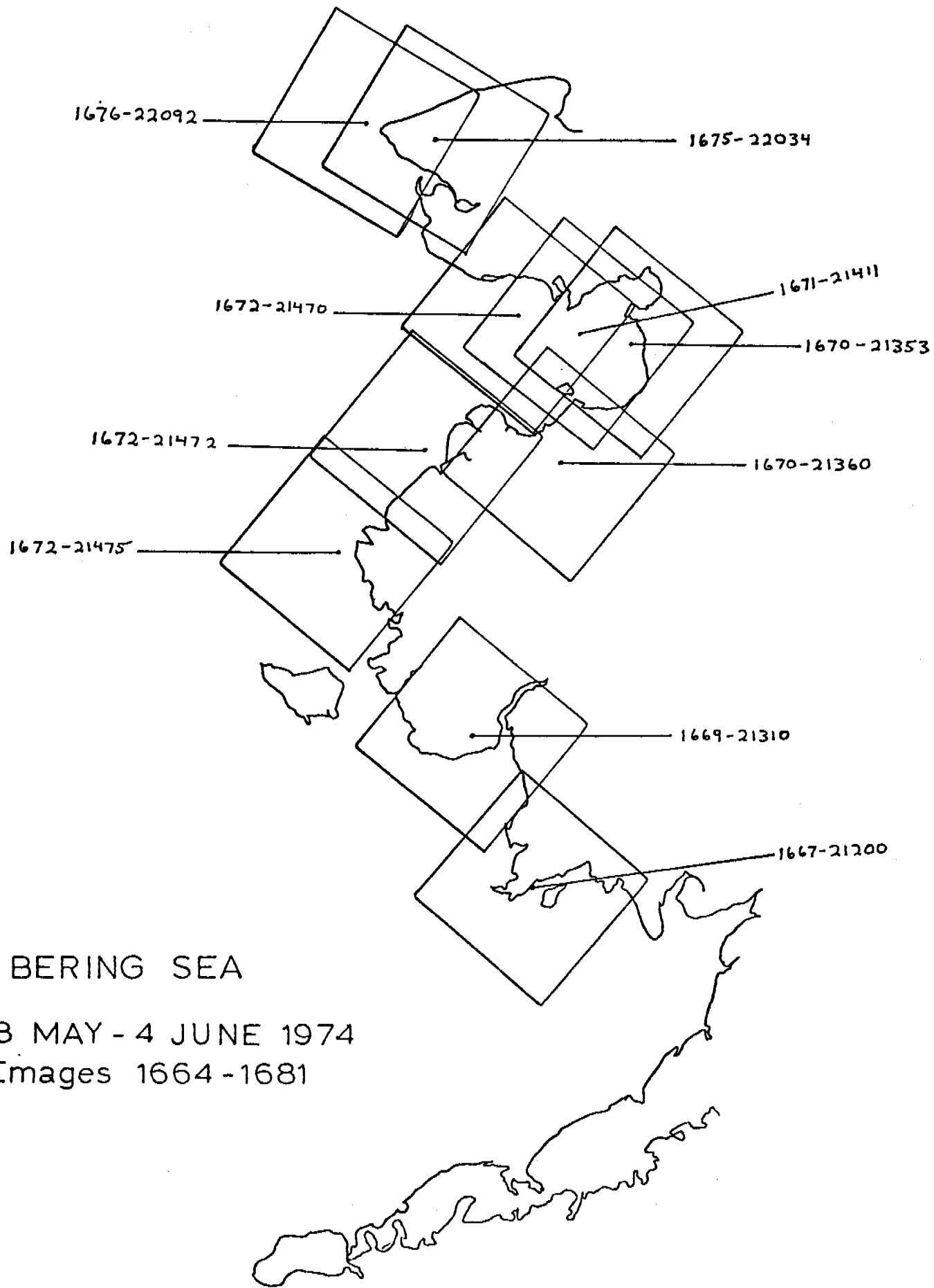
BERING SEA
29 JANUARY to 15 FEBRUARY
1976
IMAGES: 2372-2389





BERING SEA
20 FEBRUARY to 4 MARCH
1975

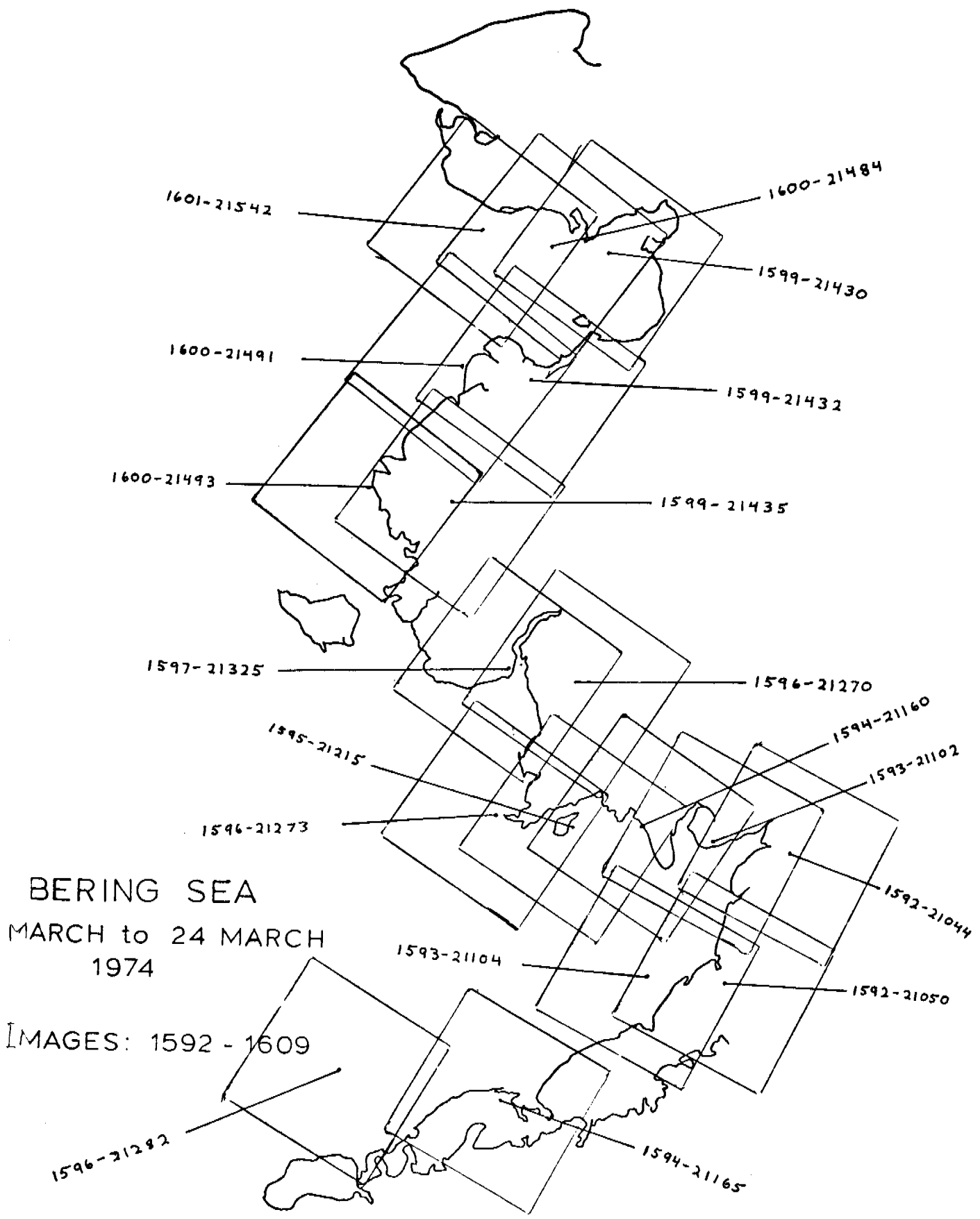
IMAGES: 1942-1954



BERING SEA

18 MAY - 4 JUNE 1974

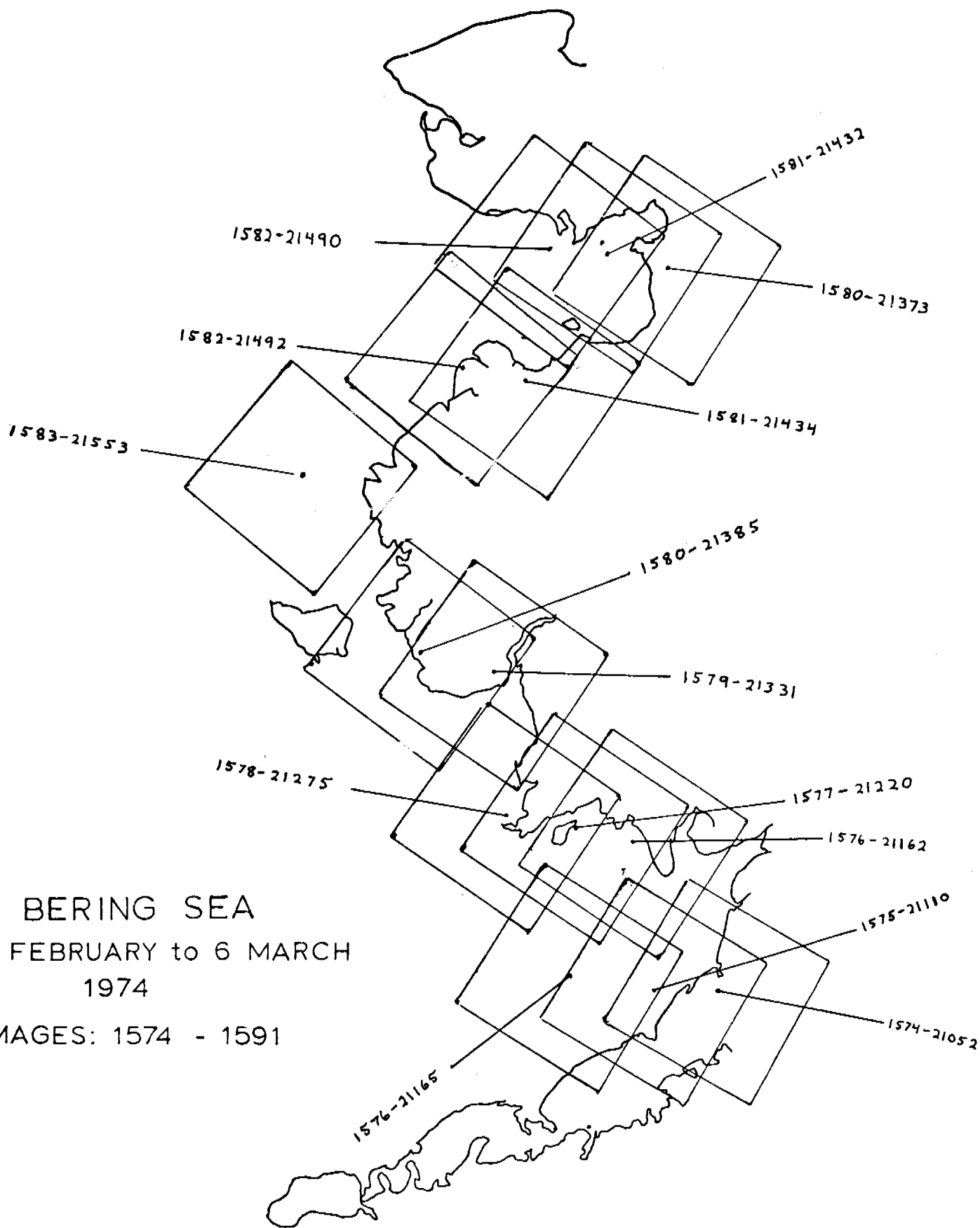
Images 1664 - 1681

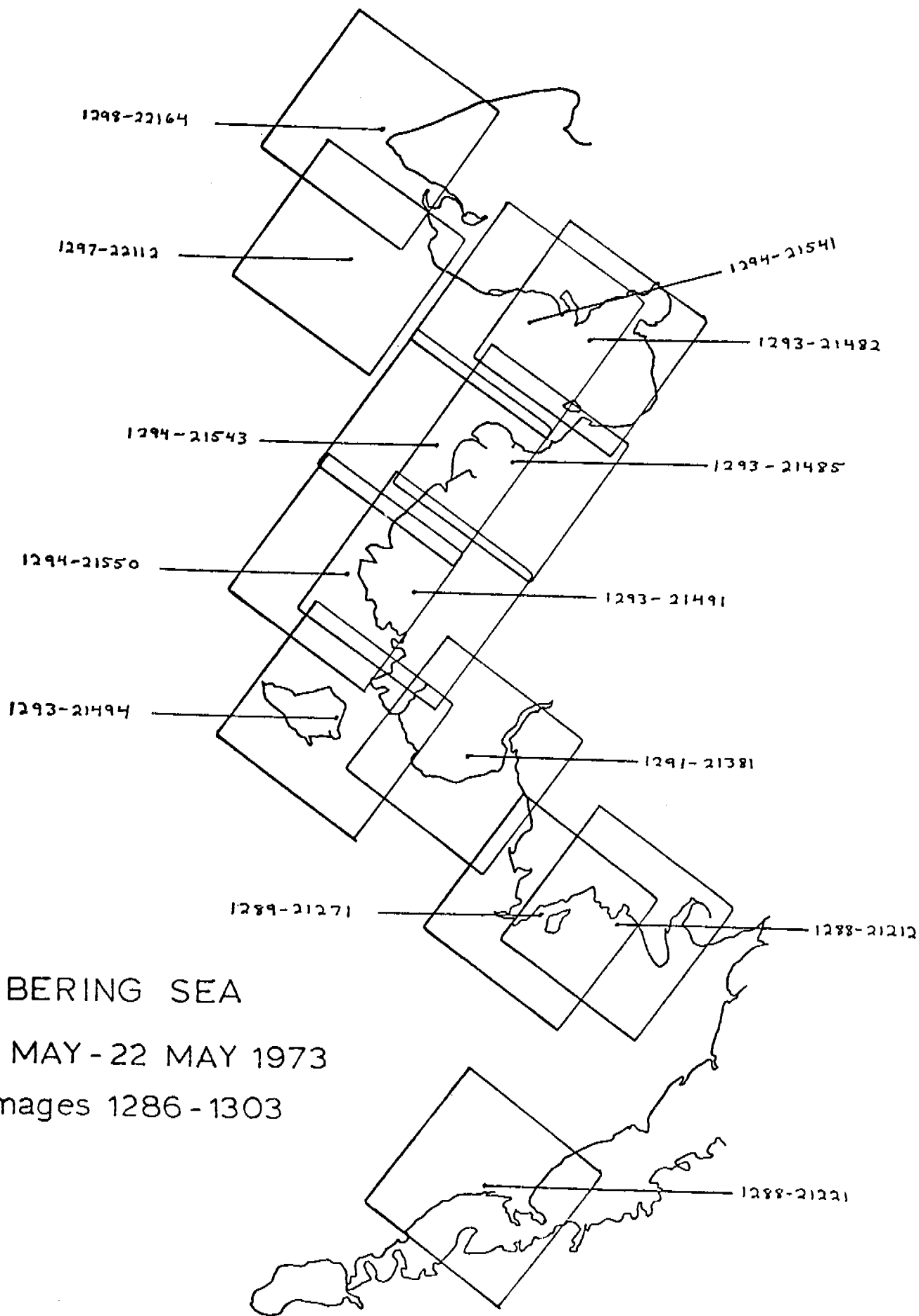


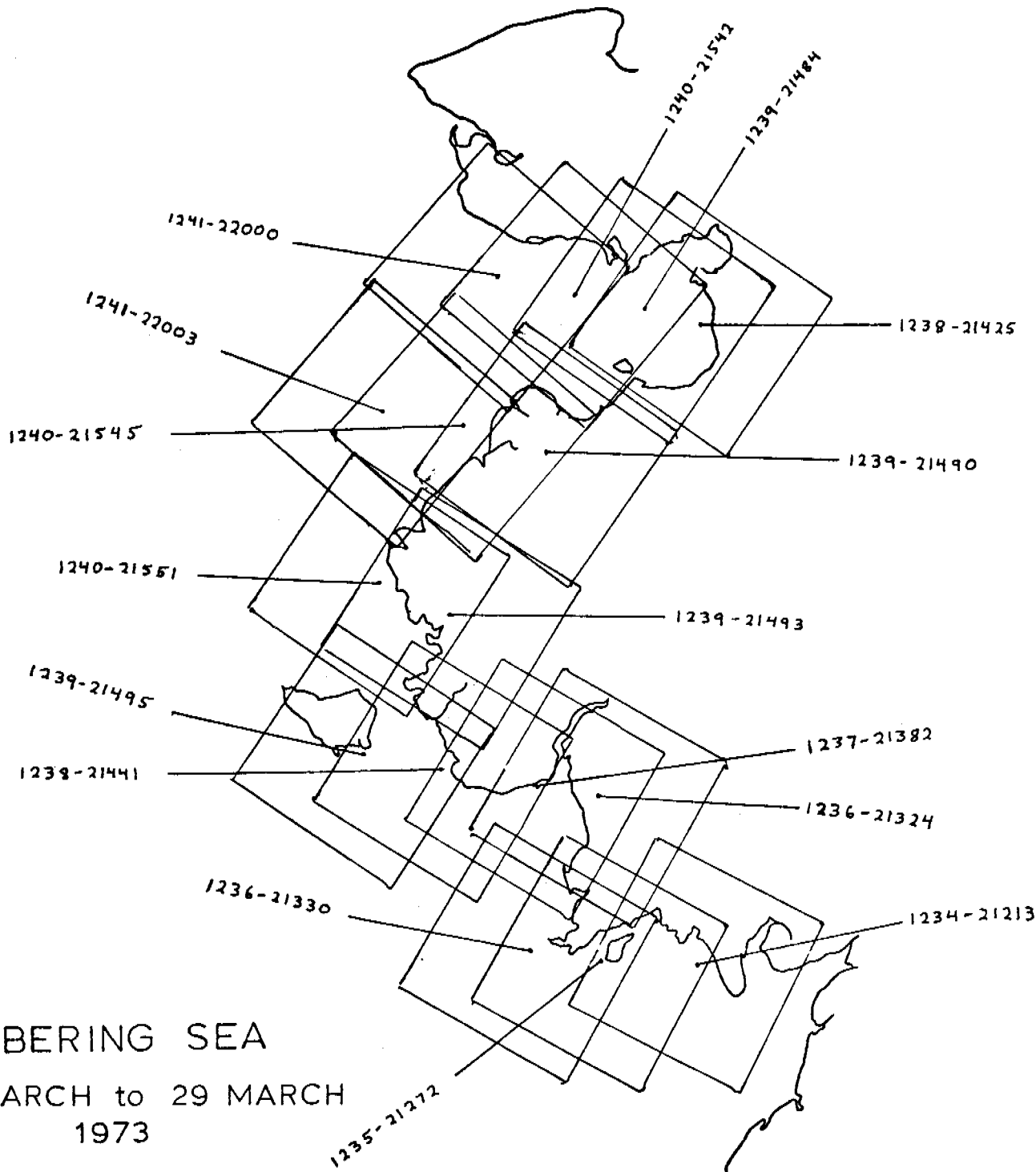
BERING SEA
 MARCH to 24 MARCH
 1974

IMAGES: 1592 - 1609

BERING SEA
17 FEBRUARY to 6 MARCH
1974
IMAGES: 1574 - 1591







BERING SEA
 12 MARCH to 29 MARCH
 1973

IMAGES: 1232 - 1249

VI. Results

A. Interpretation of Ice Maps

1. Selection of ice features pertinent to morphology. The individual maps of each Landsat scene were examined and annotated in terms of ice conditions observed on the sequence of images to which the individual image belonged. This exercise served to develop a historical perspective of ice behavior along that portion of coast. Descriptive histories, even with associated maps do not in themselves constitute a morphological description of ice behavior. In particular, the salient features of several year's ice dynamics must be compared to determine the patterns of ice behavior.

In order to accomplish this task, the maps which had been prepared were examined to find the mapped characteristics which could be compared from season-to-season and year-to-year.

One obvious class of characteristics found was large ridge systems. Ground truth exercises, described in section VD, had shown that maps based on Landsat imagery could be expected to show the locations of large ridge systems with a good degree of confidence.

A second class of characteristic found useful for development of a near shore ice morphology was the location of the seaward edge of contiguous ice. The term "contiguous ice" is used rather than "fast ice" because of the widespread useage of the term "fast ice" by various authors to describe a variety of conditions related to near shore ice. "Contiguous ice" means ice contiguous with the shore and continuous to the first break. Often the first break is the flaw lead. However, it could be the edge of open ocean or a polynya. For brevity these maps are labeled "ice edge maps."

These two classes of features, recorded on as frequent a schedule as possible were found to be a suitable basis for formulating a near shore ice morphology related to hazardous conditions. Their utility is discussed in the next two sections.

2. Edge of contiguous ice. The edge of contiguous ice is often the boundary between "pack ice" and "shore fast ice." However, it should be realized that within a short period of time, the edge of contiguous ice can vary by tens of kilometers. This is particularly true off the Beaufort coast where the edge of contiguous ice has been observed to range from the 20-meter isobath to a point 30 to 40 km seaward. The cause of these extensions appears to be an absence of sufficient winds, currents and interval forces within the ice sheet to keep individual pans within the pack ice from freezing together. This condition can persist for several weeks before sufficient forces exist for failure to take place along lines considerably closer to shore.

When observing conditions similar to these, some observers define the "fast ice" as being defined by the ice called "contiguous" here. Others insist that the true "fast ice" is defined by the ice which would remain adjacent to shore after a major shearing event and subsequent failure of the ice sheet. Those who use the latter definition generally associated well-grounded ridge systems and other ice features with this stable edge of ice. Our results have shown sufficient exceptions to this association to cause us to not use this definition except in the most general sense and develop ice descriptions for each zone which can be identified to have uniform ice behavior.

Maps showing edge of contiguous ice have been made showing ice edges for different dates in 1973, 1974, 1975, 1976, 1977. These data have then been combined from each year showing late winter, early spring, and late spring average ice edge maps, and where appropriate, these average seasonal maps have been combined to show the seasonal migration of the average ice edge.

3. Ridge system maps. Ridge system maps are useful in several ways leading to development of a near shore ice morphology. Ridges located within the existing contiguous ice sheet observed on the earliest available Landsat images each year, serve as a record of earlier, unobserved, ice event. Where they are grounded, ridges often--but not always--serve as anchoring points for the near shore ice sheet. By mapping ridges created for each year and comparing year-to-year it is possible to determine variability of dynamic ice events from one year to the next. Compilation of several years' ridge data onto one map shows the persistent locations of this type of feature, at the same time implying year-to-year persistence of the conditions responsible for ridge creation.

B. BEAUFORT SEA RESULTS

1. Contiguous Ice Edge Maps

a. Yearly Ice Edge Maps: For each year of study a single map has been prepared showing the edge of contiguous ice for each Landsat cycle yielding useful data. Throughout these maps it should be noted that generally the contiguous ice edge is not mapped for late spring. This is often because near shore flooding and melting had occurred, destroying the contiguous aspect of the near shore ice although vast areas remain in place. These vast areas of ice have been mapped under the heading; "stranded ice."

1). 1973 (Figure III-1)

i. 2-19 March Landsat cycle. During this time the edge of contiguous ice was quite far off shore. The individual Landsat image maps drawn for these dates merely indicate that the edge of ice is beyond their boundaries. This information is indicated here in terms of a series of lines indicating that the edge of ice was no closer to shore than these lines.

ii. 31 May--17 June. Where it could be identified the edge of contiguous ice has been mapped.

2). 1974 (Figure VI-2)

i. 25 February--14 March. Shown by a dashed line, the edge of ice is never far from the 20-meter isobath except in the vicinity of Camden Bay. Compare this edge with the edge for 2-19 March the previous year.

ii. 15 March--3 April. Indicated by the dotted line, the edge of ice has remained very nearly constant except for the eastern Beaufort where it is now considerably closer to shore.

iii. 20 April--8 May. Indicated by alternating dots and dashes, contiguous ice was well off shore during this period and only the shoreward limit is shown here for much of the Beaufort Sea.

iv. 13-30 June. Shown by a line consisting of two dashes followed by a single dot, the edge of ice shows some agreement with earlier ice edges but also indications of the advanced season and decay of ice in Harrison Bay.

3). 1975 (Figure VI-3)

i. 20 February--10 March. Only one good Landsat cycle was found for this year showing the edge of contiguous ice. During this time there is an indication that the edge of ice had been considerably farther off shore until just recently and was now nearly coincident with the 20-meter isobath for much of the Beaufort coast.

4). 1976 (Figure VI-4)

i. 22 October--8 November. This ice edge, shown by a dashed line is the only extensive ice edge data obtained in the fall season during the entire study. It shows the edge of contiguous ice roughly coincident with the 20-meter isobath along the western Beaufort and significantly seaward of that line east of Harrison Bay.

ii. 6-23 February. This ice edge is indicated by a dotted line. For most of the Beaufort coast, the edge of contiguous ice is beyond the area mapped by the individual Landsat images. Only in the vicinity of Barrow is the actual ice edge mapped.

iii. 24-12 March. This ice edge is shown by a sequence of dots and dashes. For a good portion of the Beaufort coast this line is nearly parallel to the 20-meter isobath--tending however, to bridge over indentations in this contour.

5). 1977 (Figure VI-5)

i. 12 February-9 March. This Landsat cycle yielded ice edge data between February 26 and March 9 across the eastern and western portions of the Alaskan Beaufort Coast. It is interesting to note that except at Barrow, this ice edge is significantly far seaward of the 20-meter isobath. It appears reasonably safe to assume that the ice edge for these dates extends across the unobserved area directly linking the two observed portions. At Barrow the ice edge does coincide with the 20-meter isobath.

ii. 9-26 March. Data indicates that the contiguous ice edge for these dates is even further from shore than during the previous Landsat cycle with the exception of the Barrow vicinity where the ice edge is in the same location.

iii. 27 March -14 April. This Landsat cycle yielded data from Barter Island to eastern Harrison Bay and From Barrow eastward to SMith Bay. The eastern portion is considerably shoreward of previous ice edges and very nearly coincides with the 20-meter isobath. Off Barrow the ice edge has remained coincident with the 20-meter isobath. However, to the east of Barrow the edge of contiguous ice now curves around Point Barrow shoreward of the 20-fathom isobath to a location that remains constant throughout the ice year.

iv. 14 April-01 May. Data for this Landsat cycle begins opposite the Canning River and continues beyond Barrow. Now, the edge of contiguous ice is nearly coincident with the 20-meter isobath along the entire coast where even it is observed.

v. 2 May-30 June. The edge of contiguous ice was observed during this period across the central Beaufort coast. During this time it was again located significantly far seaward of the 20-meter isobath.

vi. 25 June-15 July. Data for this Landsat cycle exists between July 6 and July 8. During this time the ice edge was observed off the Beaufort coast between the Canning and Colville Rivers. On July 7 the ice edge was again found far off shore. Shortly following that, on the 6th it was again located along the 20-meter isobath.

iv. 31 March-17 April. The observed edge of contiguous ice for this date is shown by a line consisting of a dash followed by two dots.

The data indicate that during this Landsat cycle the edge of contiguous ice moved considerably shoreward. The earlier images obtained in the eastern Beaufort show the edge of contiguous ice far off shore while the later images show the ice edge much closer to its normal position. Comparison of data obtained on March 12 and 14 show this to actually be the case in the central portion of the Beaufort Sea.

b. Seasonal Ice Edge Maps: The data representing the various edges of contiguous ice have been recompiled for each season yielding sufficient information to warrant analysis: late winter (February-March), early spring (June-July) and late spring--early summer (June-July). The reason for these groupings is obvious; to determine whether each season can be characterized by a single, generalized ice edge representing that season. The results of this analysis will be discussed in order of season.

1). Late Winter Ice Edge. Data from the following Landsat cycles are utilized: 2-19 March 1973, 25 February-14 March 1974, 20 February-10 March 1975, and 24 February-12 March 1965. These ice edges, with the exception of the 1973 data show a good degree of similarity--running parallel and off shore from the 20-meter isobath, and bridging across landward indentations of the 20-meter isobath. The 1973 ice edge has been discussed previously--it was located very far off shore, well beyond the near shore area (Figure VI-5).

2). Early Spring Ice Edge. Data from the following Landsat cycles were utilized: 15 March-3 April 1974, 31 March-17 April 1976. It is difficult to justify a characterization of ice during this period by means of only two recorded ice edges. However, the indication appears to be that of similarity with the late winter ice edge. The most striking deviation is in the western Beaufort where the 1976 data show the ice edge closer to the 20-meter isobath than any other data--indicating that during early spring at least a degree of variability in ice edge in this region (Figure VI-6).

3). Late Spring--Early Summer Ice Edge. The following Landsat cycles were utilized: 31 May--17 June 1973 and 13-30 June 1974. Again, while it is difficult to justify conclusions drawn from just two data sets, it is worth noting that the 31 May--17 June data coincide with the 20-meter isobath in the western Beaufort. This location is somewhat landward of the bulk of other ice edge data in this region but it does not represent a highly significant deviation. East of Harrison Bay the 1973 data strike significantly seaward. However, this is not considered to be a seasonal morphological feature; other data have shown that this phenomenon can occur in any season. What this does show, however, is that this can occur even this late in the ice season.

The mid-June 1974 data are the only ice edge information representing contiguous ice which show the decay of near shore ice to points well within the 20-meter isobath. This is only true for mid Harrison Bay to points westward. To the east of Harrison Bay the edge of contiguous ice is again located roughly along the 20-meter isobath (Figure VI-7).

2. Ridge System Maps

a. Yearly Ridge System Maps: For each year of study a single map of the Beaufort coast has been prepared from the individual Landsat image maps showing the ridges observed during that year. No

attempt has been made here to identify the date of formation of each ridge. The object of this mapping exercise was to identify those locations where ridging does occur in order to relate this phenomenon with bathymetric features including depth and isobath configuration. Mapping on a yearly basis was performed in order to provide information regarding year-to-year persistence in location and severity.

1). 1973 Ridge System Map: This map shows a cluster of major ridges offshore between Prudhoe Bay and Harrison Bay and a few ridges very close to shore in the western Canadian Beaufort. The ridges mapped well inside Harrison Bay are located in shallow waters and were very likely created at time of freeze-up (Figure VI-8).

2). 1974 Ridge System Map: Here ridges were found throughout the length of the Beaufort coast. Of particular note are two prominent hummock fields in outer Harrison Bay where the complex of ridge ice have been represented by a series of dots covering the area of the hummock field. Also worthy of note is the fan-shaped focus of ridges centered on the headland just east of Camden Bay (Figure VI-9).

3). 1975 Ridge System Map: Not many ridges were mapped for this year. However, in consistency with the previous two years, the greatest density of ridging occurs well offshore between Prudhoe and Harrison Bay (Figure III-10).

4). 1976 Ridge System Map: Again, as in 1974, major ridges were found throughout the length of the Beaufort coast. It is interesting to note these ridges are almost entirely located beyond the 20-meter isobath. This is a strong indication that these ridges were formed after early winter. Again, as in previous years, the greatest ridge density occurs offshore between Harrison and Prudhoe Bays. Again, the fan-shaped assembly of ridges occurs in Camden Bay (Figure VI-11).

b. Composite Ridge System Map: This map shows the combined ridge systems for 1973, 1974, 1975, and 1976. Here ridge density trends noted on the yearly ridge maps become more clear (Figure VI-12):

1). The greatest density along the Beaufort coast is found far offshore between Harrison and Prudhoe Bay.

2). A secondary maximum ridge density occurs in a fan-shaped pattern in eastern Camden Bay.

3). There is an indented area across inner Harrison Bay with a moderate tendency toward ridging.

4). A cluster of ridges occurs seaward of Midway and Cross Islands with a tendency toward greater density between the islands and the 20-meter isobath.

5). The focus of the fan-shaped ridge cluster in eastern Camden Bay is located significantly landward from the 20-meter isobath.

3. Stationary Ice Maps

a. Stationary vs. Contiguous Ice

During winter along the Beaufort Sea coast, large ridges form in a zone parallel to the shore. These ridges have keel depths sufficient to cause grounding out to approximately the 20-meter bathymetric contour. This zone of grounded ridges varies between a few kilometers and many tens of kilometers in width and effectively shields the smoother ice inshore from the effects of pack ice motion. The zone of immobile ice is usually referred to as the "fast ice zone."

When summer break up occurs, these grounded ridges are often the last ice forms to dislodge. These areas were not mapped in terms of edge of contiguous ice because they are not contiguous with the shore.

Yet the ice does remain bottom fast and is an important part of the near shore ice regime. Three questions need to be answered regarding these stationary ice areas. 1) Where are these areas located? 2) Do they occur in the same locations each year? and 3) How long do they last in the summer?

b. Method of Analysis

The data base used in this study of stationary ice was Landsat band-7, 70 mm imagery projected onto a screen at 1:500,000 scale. The projection device used was an International Imaging Systems additive colorviewer. In order to determine which ice was stationary, two images taken at different times of the same area were projected simultaneously onto a screen. The two images were lined up by matching coastal features visible on both images. A transparent overlay with the coastline and major rivers drawn in was then laid on the screen. The areas where the ice had not moved were then traced onto the overlay.

c. Problems of Analysis

Images of the Beaufort Sea are not readily available in the mid and late summer because the area is often covered by clouds. As a consequence, only two or three sets of images for each year were available. This made repeat coverage from year to year not generally possible.

There were also problems determining which was stationary ice and which ice had moved. Because the margin of error due to the difference in projection of the Landsat image and the overlay maps was approximately 1 km, ice that appeared to move less than 1 km was generally considered to be stationary.

The time period between images was also important. Generally, if the images were one Landsat cycle (18 days) apart, the ice could be considered stationary if it had not moved. However, occasionally the only sequence of images available were only a day or two apart. Small drift rates during these times were difficult to observe.

d. Composite Stationary Ice Map (Figure VI-13)

Four years' data were analyzed for stationary ice - 1973, 1974, 1975, and 1976. The data were combined on one map extending from Point Barrow to Herschel Island. The smallest stationary ice object plotted was approximately a kilometer in diameter. Analysis of this map shows that:

1). Stationary ice is generally located inshore of the 20-meter bathymetric contour. Inshore areas that are generally clear of stationary ice include the majority of Harrison Bay and the immediate river mouth vicinities.

2). Areas where stationary ice recurs were difficult to determine because of insufficient data. One area where it recurs and seems to last most of the summer is along the 20-meter contour north of the Colville River in Harrison Bay. Each year a large hummock field forms, causing a seaward bulge in the edge of the fast ice that persists until late summer. Another area where stationary ice was seen to recur was between Oliktok Point and the Sagavomirktok River, extending from shore to the 20-meter contour.

3). In 1976, stationary ice was last seen to exist on 2 August only in a small area west of Harrison Bay. The next image of the area was not obtained until 20 August (one Landsat cycle later). By then, the stationary ice had disappeared completely. Therefore, it can be concluded that stationary ice is generally gone by mid-August. One exception to this was seen in 1974. A large piece of a ridge system

north of Oliktok point was observed to remain throughout the summer of 1974 and was still there in the spring of 1975. However, it did not remain as stationary ice in 1975.

4. Open Water Maps

Maps of open water of the Beaufort Sea were prepared at 1:500,000 scale from Landsat imagery. There were prepared in three sections extending from Point Barrow to Demarcation Point for the years 1973 through 1977. The open water was mapped from the Landsat image by overlaying a prepared mylar base map onto the image and drawing the boundaries of the open water on the mylar. A different symbol was used for each Landsat scene for which open water was mapped. In addition, the date of the image was indicated on the mylar with a line drawn to the open water area.

The open water maps shown the chronological increase in open water extent for each season, usually starting sometime in June and continuing through August, when the nearshore region generally became clear of ice. An area was considered to be open water if it contained no stationary ice and less than 50 percent floes smaller than 1 kilometer in diameter. Cases where ice moved into an area after it had been mapped as open water were not indicated.

5. Ice Island Observations and Frequency

a. Ice Islands - background

For approximately thirty years the existence of "ice islands" in the Arctic Ocean--particularly in the Pacific Gyre has been established. These features are tabular floes of freshwater ice ranging in size from dimensions on the order of km downwards. Their thickness can be as great as 35 m. It has been reasonably well established that they originate from the Ellesmere Ice sheet. The number and size distribution of these features are not known. The Ellesmere Ice sheet does not calve continuously and it is possible that all existing ice islands were created in a small number of calving events. Ice islands ablate at the exposed surface and could be expected to possess a relatively long lifetime. However, there have been several observations of grounded ice islands along the Beaufort coast having broken into several pieces. Further, at least one large ice island has been observed to exit the gyre and enter the Atlantic Ocean.

Ice islands have been considered to constitute a threat to offshore facilities because their bulk is capable of obtaining a momentum many times greater than any conventional floe. For this reason it would be very useful to be able to develop statistical data representing their number, size distribution, and frequency of occurrence in nearshore Beaufort waters.

b. Results of Analysis of Imagery for Ice Island Data

Because of the potential value derived from determining statistical information concerning ice islands, each Landsat image used was examined explicitly for evidence of ice islands. It was thought that even if no ice islands could be observed directly, large ice islands would drift differentially from pack ice because of their deep draft and leave an identifying wake in their trail. (This is the case for the large ice feature located on Hanna's Shoal--see Section D.)

Unfortunately, no ice islands were observed directly or indirectly on the Landsat imagery. On two occasions stranded and broken-up ice islands were observed along the Beaufort coast during aerial reconnaissance operations. In both cases the broken-up island was approximately 300 m in diameter.

Attempts were made to identify these ice features on Landsat imagery. Positive identification could not be made in either case. In the first case, the ice island was observed well inside the contiguous ice between Admiralty and Smith Bays (1974). The exact position was difficult to determine however, because of rather poor navigation equipment on the aircraft used. The second ice island was observed during a 1976 photographic reconnaissance trip. It was located well by navigational equipment on board the aircraft and also by its location with respect to other ice features in the vicinity. Both grounded ice islands were located in water on the order of 20 m in depth. (These results are discussed in Section VC.)

C. CHUKCHI SEA RESULTS

1. Contiguous Ice Edge Maps

a. Yearly Ice Edge Maps: For each year of study a single map has been prepared showing the edge of contiguous ice for each Landsat cycle yielding useful data.

1). 1973 (Figure VI-14)

i. 2-19 March. Available data is shown by a dashed line. Later seasonal ice maps will show the ice edge data for this date to be rather unusual in the outer Kotzebue Sound region. Usually on this date the edge of contiguous ice is located well off shore--bridging across the mouth of the Sound as far west as Shismaref. Here the edge of ice appears to cross the mouth at Cape Krusenstern. It should also be noted that between Point Hope and Cape Lisburne there is a portion of coast where the edge of contiguous ice coincides with the shore.

ii. 7-24 April. Available data is shown by a series of dots. Again as will be seen later, the edge of ice is considerably landward of its normal location in Kotzebue Sound during this period. Again, although in a slightly different location, the edge of

contiguous ice coincides with the shore line in the vicinity of Cape Lisburne.

iii. 31 May-17 June. These data are shown by a line of dots and dashes. Note that by this time much of Kotzebue Sound is free of ice and several less protected areas are free of ice at this time.

2). 1974 (Figure VI-15)

i. 25 February--14 March. Contiguous ice edge data for this date are shown as a series of dashes. Note how far out into outer Kotzebue Sound this ice edge is found, yet it nearly touches the shore south of Point Hope and again approaches the shore near Cape Lisburne. Beyond Cape Lisburne this ice edge remains far off shore until it reaches Cape Franklin.

ii. 2-19 April. Ice edge data for these dates are shown as a series of dots. Generally closer to shore, the ice edge for this date follows the shoreline configuration more closely than did the earlier ice edge. Note that at Cape Lisburne this ice edge does meet the coast.

iii. 26 May--12 June. Represented by alternating dots and dashes, the ice edge on this date is generally closer to shore than the dotted line representing the April ice edge. In some places, however, the contiguous ice edge even for this late date can be found

seaward of the earlier edge--indicating that the edge of ice does not merely retreat with advancing season.

iv. 13-30 June. Contiguous ice edge data for this date are represented by a sequence consisting of two dots and a dash. Note that this ice edge is the most seaward of the four plotted for this year in the region just southeast of Point Hope. This ice is most likely pans which have been driven into this location and compacted somewhat. Farther north, the ice edge for this date can be seen to be quite close to shore except at Pt. Franklin where the April ice edge was actually closer to shore.

3). 1975. Note the unusually close similarity between the ice edges shown for this year (Figure VI-16).

i. 20 February--9 March. Data for this period are represented by a series of dashes. Again, as in previous years, this earliest ice edge extends farthest seaward in outer Kotzebue Sound and off Cape Lisburne.

ii. 28 March--14 April. The contiguous ice edge for this Landsat cycle is indicated by a line of two dots followed by two dashes. Note that north of Wales, the edge of contiguous ice now extends farther seaward than previously. This occurred as a result of s-ridge build-up of a large hummock field in this location. This ice edge becomes adjacent to the coast south of Point Hope--as do all other ice edges for this year. (None was recorded for late June as was shown for the previous year.) This ice edge also coincides with the coast at Cape Lisburne as March ice edges have done in previous years.

iii. 6-23 April. Ice edge data for this date are shown by a series of dots. This ice edge is similar to the previous ice edge except on the exposed sides of the Seward Peninsula and Cape Lisburne. In both cases the ice edge now extends considerably farther seaward.

iv. 30 May--16 June. Data are shown for this date by a dot-dash sequence. Where these data were available they did not differ greatly from the previous ice edge data.

4). 1976 (Figure VI-17)

i. 6-23 February. Shown by a dashed line, this ice edge differs significantly from other winter ice edges which have been mapped for this period: This ice edge indents far into Kotzebue Sound while previously for this date the edge of ice has been far seaward, well into outer Kotzebue Sound.

ii. 24 February--12 March. Shown by a dot-dash sequence, this ice edge appears similar to ice edges drawn for the same date on previous years. Note that at Cape Lisburne it indicates no ice adjacent to the coast for a considerable distance. To the north, this ice edge generally resembles ice edges drawn for previous years during this period.

iii. 14-31 March. These ice edge data are shown by a sequence of two dots followed by two dashes. While this ice edge resembles others for this period in the vicinity of the Seward Peninsula and Kotzebue Sound it differs somewhat to the north where it is unusually distant from the shore in the vicinity of Cape Thompson and Cape Lisburne. Farther north, between Icy Cape and Pt. Franklin this ice edge advances unusually far seaward followed by a rapid coastward motion. North of Pt. Franklin this behavior is repeated somewhat.

iv. 19 April--6 May. Shown by a series of dots, the contiguous ice edge data for this date are as unusual as the data shown for 6-23 February: Here, instead of indenting toward and into Kotzebue Sound, this ice edge actually bridges across out Kotzebue Sound. It would seem that the winter and spring data were interchanged. Farther to the north, the springtime data continues to exhibit this unusual behavior--remaining far seaward.

b. Seasonal Composite Maps

1). Late Winter. Shown here are the ice edge data for late winter (February-March) Landsat cycles, 1973 through 1976. These data indicate some interesting trends showing areas tending toward a high degree of variability in ice edge location. While one might expect a focusing of ice edge locations at exposed headlands (Wales, Point Hope, Cape Lisburne, Pt. Franklin, and Barrow), Pt. Lay is not similarly exposed but yet the ice edge data there also exhibit this behavior pattern (Figure VI-18).

2). Mid-Spring. Shown here are the ice edge data for mid-spring (April-May) Landsat cycles, 1973 through 1976. Again as with the late winter data there are zones of great location stability and other areas with a high degree of variability. Generally while there appears to be a greater overall uniformity of ice edge location here, less stability is indicated off Point Hope and Point Lay (Figure VI-19).

3). Late Spring--Early Summer. Shown here are the ice edge data for late spring and early summer (May-June) 1973 through 1976. These data show that in some regions (Kotzebue Sound, for instance) there can be a high degree of variability at this time while other locations exhibit a tendency toward more uniform ice edge behavior. Because of the absence of data from each year in some locations, some indicated trends--particularly those toward uniformity should not be considered as particularly strong (Figure VI-20).

c. Average Seasonal Ice Edges

The composite maps of section b have been analyzed to produce a single average ice edge for each season. In addition, the greatest and least bounds of observed ice edge have also been shown in order to document the reliability of the average ice edge for use in morphological modeling and hazard analysis.

1). Late Winter. The average ice edge for February-March passes close to shore at Bering Strait and proceeds toward Kotzebue Sound at a great distance from shore, bridging across the mouth of outer Kotzebue Sound. North of Kotzebue Sound, the average edge is considerably closer to shore than south of the Sound, finally passing just a few km off Pt. Hope and Cape Lisburne. North of Cape Lisburne the average ice edge follows the coastline at some distance until reaching Pt. Franklin, where again the average edge is quite close to shore. The average edge bridges across the coastal indentation between Pt. Franklin and Barrow, passing that point at a distance of approximately 10 km (Figure VI-21).

2). Mid-Spring. The average ice edge for this period does not differ a great deal from the average ice edge for late winter except for a tendency to lie closer to shore in some locations. It is interesting to note that the envelope of greatest and least bounds is much smaller during this season than during late winter--indicating perhaps a steady-state condition during this period. However, the variability in outer Kotzebue Sound is still quite large during this season (Figure VI-22).

3). Late Spring--Early Summer. The average ice edge for this season is generally closer to shore than the previous season's average ice edge. The envelope of maximum and minimum contiguous ice edge locations during this period is generally narrow except for the vicinities of large embayments. For instance, in Kotzebue Sound the envelope is large just as it has been in other seasons--only now it is located even farther inshore (Figure VI-23).

d. Migration of Average Seasonal Edge of Contiguous Ice

This map shows the three seasonal average ice edges described in section c plotted together so that the possibility of a systematic change in ice edge location can be investigated. When considering the relationship between these ice edges, the envelope of maximum and minimum ice edge location must be borne in mind. For instance, both in Kotzebue Sound and north of Cape Lisburne, there is a wide seasonal spatial variation in average ice edge location and the immediate conclusion might well be to consider any apparent seasonal motion of ice edge more significant than opposite Icy Cape where the spatial variation is smaller. However, in Kotzebue Sound the variation envelopes are all quite large so that seasonal average ice edges located relatively close together (late winter and mid-spring for instance) do not indicate a significant variation. North of Cape Lisburne the envelopes are generally small so that some credibility may be given to the mid-spring ice edge being found more seaward than the late winter ice edge. At Icy Cape the variation envelopes are small so that despite the proximity of the average ice edges the seasonal progression shown may have statistical significance.

Bearing these qualifications in mind the following observations can be made from this map (Figure VI-24):

1). At Wales, Point Thompson, Point Hope, Cape Lisburne, and Point Franklin there are at least small stretches of coast where the average ice edge remains at the same distance from shore throughout the three seasons. The mechanisms responsible for the agreement of these average ice edges will be discussed in the development of the Chukchi coastal morphology. It should be noted that at Wales, Point Hope, and Cape Lisburne and Point Franklin the variation envelopes are fairly large indicating that the ice edge varies in location during each season. The agreement in average location at Pt. Thompson between each season indicates that no seasonal trend is to be found in the varying location of ice edge here.

2). North of Cape Lisburne there are significant reaches of coast where the sequence of average ice edge distance from shore varies uniformly with season. That is, late winter is furthest from shore, mid-spring is intermediate, and late spring--early summer is closest to shore.

3). Immediately north of both the Seward Peninsula and Cape Lisburne the ice edge sequence for winter and spring is reversed.

4). The winter and spring sequence are reversed in Kotzebue Sound. However, this trend would not appear if the 6-23 February 1976 data were removed from the late winter data set. This could only be done if some valid justification can be found. The data here should be taken to indicate a high degree of variability of contiguous ice edge in this zone.

d. Chukchi Sea Ice Ridge Systems

1). Yearly Ridge System. These maps show locations of ridge systems which could be recognized on Landsat imagery clearly as ridge systems. The ridges identified are generally s-ridges which are several km long.

i. 1973. Ridges were mapped in only a few locations this year. It is interesting to note that they were found in locations adjacent to headlands in all cases. These headlands were: the tip of the Seward Peninsula at Wales, Point Lay and Point Franklin (Figure VI-25).

ii. 1974. The ridge pattern mapped for 1974 is significantly different from the 1973 pattern. There appears to be a tendency for ridges to be located on the south side of major embayments. The large "V" shaped ridge northeast of Cape Lisburne was formed when ice was driven southward toward the coast. It is interesting to note that although the forces creating this ridge system were compressional the ridges formed under shear failure (Figure VI-26).

iii. 1975. Ridge systems mapped for 1975 were even fewer than previous years. No particular pattern was observed. In the embayment between Barrow and Pt. Franklin a ridge was observed to follow the coast in a way resembling the pattern found between Point Franklin and Icy Cape the previous year. Off Cape Lisburne a long ridge system was found in a position indicating flow of ice across Cape Lisburne. Ridges in this location were not seen previously (Figure III-27).

iv. 1976. Three ridge systems were observed this year north of Bering Strait. They have an interesting similarity in that they all lie "north" of the three major headlands; Seward Peninsula, Cape Lisburne, and Icy Cape (Figure III-28).

2). Ridge System Composite (Figure III-29)

All ridge systems observed and discussed previously are plotted together on this map. There are two objects of this exercise: The first is to indicate where, over a long time period, ridging occurs. The second is to determine whether, when seen together, the individual yearly ridging patterns fit into a single morphological pattern.

The first objective is reflected in the general morphological and hazard maps produced where long term average behavior is under consideration. The second objective will help determine the year-to-year reliability of the morphological picture developed. Under this second category we should note upon examining the ridge systems drawn for each year that the following behavioral patterns emerge:

- i. Generally, the 1976 ridges are the most seaward in all locations.
- ii. The 1973 ridges are the most landward in all locations.

Nevertheless,

i. All the ridges north of the Seward Peninsula form a single pattern as do the ridges off Pt. Lay and Icy Cape and the ridges south of Barrow indicating that although they occurred in different years, they represent a single morphological pattern.

ii. The possible exception to this uniformity is found at Cape Lisburne where the three year's data appear to indicate three distinct patterns.

The general over-all pattern which emerges is that of streamlining along the coast from Barrow to Point Lay with an abrupt seaward shift seaward at that location to a new flowing pattern across the tip of Cape Lisburne followed by a similar pattern across the tip of the Seward Peninsula.

D. Bering Sea Results

1. Contiguous Ice Edge Maps

Ice conditions maps have been compiled from the individual Landsat images shown as figures V-48 through V-57. These maps have been included in previous quarterly and annual reports. Composite contiguous ice edge maps have been compiled but are not yet in manuscript form. The draft copies of these maps have been used to compile the seasonal average ice edges which have, in turn, been placed on a map showing the migration of the seasonal average edge of ice. This map is shown here as figure VI-37. Manuscript copies of the maps described above will be included in the final report for this project. The main object of these maps is to enable the compiling of the seasonal average map so, with time limited, the manuscript form of these intermediate maps has been passed over.

a). Map of Seasonal Migration of Contiguous Ice Edge

This map shows the average edge of contiguous ice for winter, late winter to early spring and mid-to-late spring. Data from the years 1973, 1974, 1975 and 1976 have been averaged to yield these seasonal average ice edges.

In the Chukchi Sea region there is a tendency for winter ice edges to be seaward of later ice edges. This appears to be a result of the rapid freezing possible during the colder winter months. In the Bering Sea region this phenomena only appears to occur in relatively protected areas. In most other areas the average edge of contiguous ice remains relatively constant throughout the ice season with the additional exception of the Yukon Delta. Two factors appear to be responsible for this behavior:

1. Nearly constant ice motion away from shore. This behavior occurs also in the Chukchi sea--notably in the Cape Thompson area where there is also a tendency to maintain a constant edge of contiguous ice. Along the Bering coast ice motion is not impeded to the south with the result that this motion of ice away from shore is much more constant.

2. Tidal ranges along the Bering coast are quite large (see Section IV) with the result that ice can be broken, set adrift and carried seaward. Morphological details resulting from these phenomena are described in section VIII.

VII. Discussion:

A Discussion of the Models Developed to Describe the Extent and Behavior of Near Shore Ice, Their Capabilities and Limitations

A. Capabilities

Despite the limitation indicated above, the models developed in the next section represent the state of knowledge of comprehensive regional ice morphology in the Chukchi, Beaufort, and Bering Seas available in the public domain. Certainly the various zones delineated to describe near shore ice morphology should be considered an initial stage of any assessment of hazards related to activities of the offshore development along these coasts.

The chief capabilities include:

1. an assessment of the relative safety of personnel and equipment operating on offshore ice in the various zones identified.
2. a preliminary assessment of the mid-winter to late spring probability of major ice displacement occurring in the zones identified.
3. a preliminary assessment of the probability of a structure placed in each given zone having to withstand the bearing load of a major ridge system.
4. a preliminary assessment of the probability of subsurface structures being disturbed by bottom plowing by major ridge systems.
5. a zone-by-zone assessment of the fate of a possible under ice petroleum spill.

B. Limitations

The models developed here for Chukchi, Beaufort, and Bering Sea ice morphology are based on statistical analysis of four years' ice data. The models represent an average of conditions observed during only those years. An obvious limitation, then, is the lack of really long-term data and the possibility that the ice during the years observed do not represent long-term average conditions.

In addition, even if by some chance the models do represent the long term average conditions, there is little hint of what variability in conditions should be expected over a span of twenty to thirty years. Hence, it is not certain what range of ice conditions to anticipate during the active life of an off shore oil field.

For instance, during this period of observation the melt season weather conditions have been reasonably mild. Near shore ice has broken up and melted in place. Grounded ridge systems have slowly broken contact with the sea floor and drifted away. We have not had the opportunity to access the potential hazard created if a major storm were to occur during this period when great quantities of highly mobile ice are present in the near shore areas.

Finally, the model developed here is only semi-dynamic in that only a few processes involved in near shore ice morphology have been identified. To develop a dynamic morphology a much more extensive analysis would be necessary.

C. A Discussion of the Detectability of Ice Islands

At the outset of this analysis it was anticipated that ice islands in the pack ice during winter and spring would be detectable because their deep draft would make them susceptible to oceanic currents and to a certain extent drive them through the pack leaving a wake behind. Only on one occasion was anything like this observed and it was not possible to verify the ice island possibility. (Actually, the image was acquired before the initiation of this project.)

As stated earlier in this report, on two occasions, small ice islands were observed apparently grounded in the contiguous ice zone. Both times an attempt was made to locate the islands on Landsat imagery. Neither time could they be found. In both cases, the islands had broken into several fragments.

We now think that the best assessment of the number of ice islands could be made by using summertime imagery of the polar pack. The analysis would consist of looking for large pieces of ice with perhaps a small polynya to one side. Week-by-week observation should show a slightly different trajectory for an ice island over ordinary pack ice.

VIII. Conclusions

A. Beaufort Sea

In this section, the results described in Section VI are interpreted in terms of seasonal morphologies of the Beaufort Sea near shore ice regime. Then, based on these morphologies, an assessment of relative hazards has been made for the Beaufort near-shore area.

The development of a complete near shore morphology should be based on an analysis of statistical data from several years where average conditions and deviations from average conditions have been determined, followed by detailed analysis of specific individual events to test the validity of the conclusions drawn on the basis of the statistical analysis. Here, four years' statistical data has been compiled and related to specific ice events observed during the period of study. Rather than being considered a completed product, this analysis should be considered a starting point for further study.

The ice year has been broken into two periods: Late fall to early winter, and mid-winter to late spring. A map has been prepared for each season showing areas of relatively uniform behavioral characteristics which can then be described for each area. These two periods include the times when ice hazards appear to be greatest. The division was based on splitting the period of formation of the most stable ice from the later period when this ice is essentially static.

1. Beaufort Sea Near Shore Ice Morphology

a. Late fall to Early Winter Morphology: This period includes the time of freeze-up to the establishment of stable ice within the near-shore area. This period roughly corresponds to early November through late January. Unfortunately, very few direct observations of ice conditions during this period are available; in late fall cloudy conditions prevail and between late November and early February no Landsat data is normally obtained because solar depression angles less than $6\frac{1}{4}$ generally do not provide good imagery. However, this project was able to arrange with NASA to obtain imagery at solar depression angles down to $0\frac{1}{4}$ during fall, 1976. These images were found quite useful even at $0\frac{1}{4}$ solar elevation angle.

Other than interpretation of the few fall images which were obtained, the construction of the late fall-early winter morphology was based largely upon inference from later imagery and observation of processes occurring at other times. This morphology is presented in the form of a map of the Beaufort Sea near-shore area showing areas having statistically uniform morphology conditions. These conditions are described in the legend to the map (Figure VIII-1).

Legend - Late Fall to Early Winter Morphology Map

- I. This zone contains generally smooth ice located in water less than 10 meters deep. This ice is often formed in place but it can consist of floes of recently formed ice rafted into location and surrounded by a matrix of younger ice. In the latter case, roughness is not uncommon, especially around the rims of these floes. Leads have often been opened in this area and subsequently frozen over, providing long, broad avenues of smooth ice. These frozen-over leads have often been subjected to compressive forces which have formed pressure ridges within them. The ice within this zone is completely formed by early January; it would be very unusual for lead openings, other than tidal or tension cracks, to occur after this date.
- Shear ridging appears to be at a minimum within this zone, principally because sufficient anchoring mechanisms occur at the edge of this zone, causing stress concentration at outer locations. Because of their large draft, multiyear floes do not penetrate into this zone but tend to pile up along the 10-meter isobath where they ground and become anchors for ice located shoreward.
- IIa-h. These areas are the active shear zone as soon as the anchoring floes are established along the 10-meter isobath. S-ridges form within this zone, adding strength to the newly formed ice sheet. The sheet quickly builds seaward through growth of new ice, attachment of floes, construction of new ridges and grounding of multiyear floes. The dashed line represents the mean seaward boundary of this activity. However, it should be recognized that in the absence of disturbance, ice contiguous with the shore can extend over 100 km seaward, remaining in place for weeks at a time. On the other hand, until the ice in this zone is well stabilized, leads can open and ridging or shear deformation can take place at almost any location within it.
- Pack ice motion is usually from east to west. When forces act to cause compression along the line of contact between moving and stationary ice, s-ridges are formed. This ridging activity appears to be greater in some areas than in others. Details of ridging activity are given in the following subsections.
- IIa. This rather large area stretching from Cape Halkett to Barrow has rather low ridging activity, although lead formation appears to be rather frequent. This would suggest a relative absence of compressive forces along this portion of the coast.
- IIb. Moderate ridging occurs in this this area early in the ice year as a result of ice being driven into Harrison Bay from the east. This activity soon ceases as a result of the increased strength created in the ice. Thereafter, coastal ice motions are deflected along zone IIc.
- IIc. This zone of moderate ridging is created after the increased strength of ice in zone IIb halts motions into Harrison Bay from the east. Because of shoals just shoreward of the 20-meter isobath, large draft multiyear floes act as anchoring mechanisms for the sheet of ice to the shoreward (Zone III). Ridges created in this zone during early winter have a high probability of remaining in place the entire ice year.

- IId. This zone of high ridging frequency begins approximately at the 20-meter isobath and extends seaward to the vicinity of the 40-meter isobath. Ridges in this zone are not well grounded and can be severed by lead formation. However, following such an event, there is a high probability of new s-ridge formation along the boundary of the opened lead. All along this zone, from Mikkelson Bay to a point off Cape Halkett, long highly identifiable s-ridges can be formed by the combination of motion of pack ice toward the west and by compressive forces as it is held against the fast ice.
- IIE. This is a zone of moderate ridge formation extending from the west side of Camden Bay to Mikkelson Bay. It is presumed that, although westward slippage of seaward ice takes place here similar to Zones 11c and 11d, compressive forces are not as great along this section of coast. As a result, s-ridging is less pronounced.
- IIf. This is a zone of high ridging frequency formed largely by compression of pack ice against fast ice as the ice moves either east or west. The compression is created when the moving pack ice encounters ice held fast against the large headland in this vicinity. Note that the zone of high ridging frequency extends considerably shoreward of the 20-meter isobath. It is of interest to note that the prevailing wind at Barter Island shifts from east in November to west in December, returning to east in January and then back to west in February. Hence, these ridges could be created by ice motion in either direction.
- IIg. This area has a low frequency of ridging. One possible explanation for this phenomena is that when winds are from the east, if ice motion in this vicinity takes place, it simply fails in tension and pulls away from the shore with the result that no compressive components exists to form large s-ridges. If, on the other hand, the wind is from the east, the ice piles in compression here and fails in shear to the north, forming Zone 11f. The compression piles are not as visible as s-ridges hence the area is mapped as having a low frequency of ridging.
- IIh. Ridging frequency is increased in this zone as a result of the shoreline being more nearly parallel to the direction of ice motion with the result that east winds can cause creation of s-ridges.
- III. This is an area of low ridging frequency in the middle of outer Harrison Bay. It apparently forms because shoals to the seaward cause grounding of multiyear ice features and pressure ridges. As a consequence large s-ridges form to the seaward of the shoals, providing additional protection.

b. Mid-winter to Late Spring Morphology: The morphology of near-shore ice during this period has been determined by direct observation through Landsat imagery. Many areas with considerable ice activity during the previous period are now static with very little chance of violent deformation. However, tension and tidal cracks appear and "work" as conditions change. Other areas are now static and have very little chance of major failure resulting in s-ridging but have been observed to develop crack patterns suggesting failure under shear. In general, during this period the active edge of ice often moves further from shore than the 60-meter isobath and then returns to that vicinity during dynamic ice events.

The morphology of near-shore ice during this period has been summarized in map form (Figure VIII-2). Based on the statistical data, zones have been delineated which can be described in terms of a uniform ice behavioral pattern within each zone. The behavioral patterns have been described in the following legend.

Legend - Mid-Winter to Late Spring Morphology Map

- I. Stable fast ice. The ice within this classification is usually well formed by the beginning of February. With one possible exception (denoted Ib), the ice in this category is sufficiently stable that flaw leads form to the seaward throughout this period (somewhere within category II). Hence, except for opening and closing of tidal and tension cracks, the ice within this zone is static during this period. The following subdivisions within this zone are based on statistical occurrence of major ridges.
- Ia. Zone of light ridging. Generally overlying shallow waters, this ice is free from major ridges. Often large expanses of very smooth ice can be found.
- Ib. Zone of moderate ridging. A variety of conditions can be encountered reflecting conditions during time of freeze-up. Multi-year floes may be encased in a matrix of new ice. Large floes of worked, first year ice may be broken by smooth, frozen-over lead systems. Pressure ridging can be expected in these areas. There is also a moderate probability of encountering an S-ridge created some time during freeze-up.
- Ic. Zone of intermediate ridging. Ice conditions are similar to those described for zone Id. However, the probability of large S-ridges is considerably increased.
- Id. Zone of severe ridging. The ice in these areas is likely to be first year pack ice and multiyear floes - obviously not formed in their present location. A great deal of ridging and pressuring has taken place, creating large grounded hummock fields in some areas. Note that these areas occur along the seaward boundary of stable fast ice and often at points of inflection of this boundary. These areas are the main anchors of the fast ice system.
- II. Zone of mid-winter - late spring flaw lead formation. The areas within this classification are prone to flaw lead formation at any time during this period. Following flaw lead formation, S-ridging may occur, the lead may freeze over and remain static for weeks at a time, the recently frozen lead may close, creating S- and P-ridges, or the leads may open yet again. However, it is also possible to have an extensive sheet of stable, unbroken fast ice for long periods of time within this zone. Flaw lead formation probability is low at the shoreward boundary of this zone, increases seaward to a maximum probability, then begins to decrease further from shore. The variability of ridge density is the major criterion for the subdivisions within the zone.
- IIa. Zone of moderate ridging with a high probability of flaw lead formation. Ice behavior is related more to the Chukchi Sea morphology than to the Beaufort Sea.
- IIb. Zone of relatively low ridging probability, but prone to flaw lead and polynya formation during this period.
- IIc. Zone of moderate ridging, prone to flaw lead formation during this period.
- IIId. Zone of intermediate prone to flaw lead formation.
- IIe. Zone of flaw lead formation with greatest probability of ridge formation. Very often long S-ridges can be observed running the length of this zone.

- IIf. Zone of flaw lead formation with intermediate ridge formation frequency.
- IIg. Zone of low probability of flaw lead formation with moderate probability of major ridge formation. (Flaw leads are more likely to be formed shoreward of this zone).
- IIh. Zone of flaw lead formation with moderate ridge probability.
- IIi. Zone of flaw lead formation with low ridge probability.
- IIj. Zone of low probability of flaw lead formation with low ridge probability.
- III. Generally zone of pack ice. Usually a flaw lead or recently active flaw lead (currently thinly frozen over) can be found between this zone and zone I. P-ridging is a frequent phenomenon in this zone and S-ridging can occur but the probability is much lower than in the II zones.

2. Hazards Resulting From Beaufort Sea Ice Morphology

Based on the Beaufort Sea seasonal morphologies, an assessment of relative hazard during the several phases of offshore petroleum development has been made. The hazards identified are, of course, related only to those aspects of the general over-all ice morphologies identified here. These hazards include: 1) The relative safety of field crews operating on the ice, 2) Possible ice motion endangering drilling operations from temporary structures (anchored drill ships, ice structures, pile structures, etc.), 3) The probability of ice piling events posing obstruction to rapid surface evacuation from potentially hazardous situations, 4) The potential for ice piling events and subsequent damage to under sea structures from the subsurface structure of the piled ice, and 5) The potential for increased bearing load against bottom-founded structures as a result of piled ice.

Figure VIII-3 shows the Beaufort coast with several major hazard zones delineated. The hazard zones have been chosen on the basis of a rather uniform hazard potential within each zone. The zones have been grouped into 5 major zones based largely on probability of ice edge occurrence and subdivided further largely on the basis of ridging probability. In the caption for Figure VIII-3 each major zone is described followed by descriptions of the subzones.

Legend - Beaufort Sea Ice Hazard Map

- I. This zone represents the most stable ice along the Beaufort coast. After December it is extremely safe for surface travel, (with one possible exception noted later) it has not been observed to fail in shear between December and June (therefore deformations are generally small), and ice piling is at a minimum.

Actually, this zone contains two subzones not shown here determined almost entirely by depth of water. The first subzone consists of water less than two meters in depth. The significance of this zone is that by late winter, the ocean freezes to this depth hence after that date this subzone should be very stable. The second subzone consists of the balance of Zone I and contains depths as great as 10 meters. These two subzones have not been differentiated because the relative hazard between the two has not been considered extremely great.

The greatest source of hazard observed to occur in this zone was the mid-winter formation of thermal tension cracks. These cracks occur generally during very cold temperatures in December and open to a width of 2 to 3 m. Often the new ice formed in the crack is drifted over with snow with the result that it does not equal the thickness of the surrounding ice. On one occasion in Prudhoe Bay a large piece of equipment and its driver were lost when an attempt was made to merely drive across a frozen-over tension crack. There appears to be some repetition from year-to-year of these cracks; one major tension crack appears between Thetis Island and Oliktok Point annually.

Ridging occurs within this zone only early within the ice season with the participating floes generally on the order of 30-40 cm in thickness. Major ocean floor plowing should not be expected from these events. After December and January the active edge of ice is well seaward of this zone. No ice failure events have been observed to occur which indicate deformation within this zone between the end of January and the end of May. It is estimated that an event resulting in 20 m deformation would have been observable by the techniques utilized here.

- II. Like Zone I, this zone consists of stable fast ice during late winter and early spring. However, the relative hazards related to this zone are somewhat greater than those related to Zone I. During the four year observation period reported here, failure to the point of large scale displacement (10 km) was not observed within this zone.

The zone has been subdivided generally in terms of ridge density although not entirely with respect to that attribute. Generally the zone is safe for surface travel during winter and spring. Structures are subjected to varying amounts of ridging, and varying amounts of displacement can take place. However, this is still within the zone of "stable fast ice" generally held in place by grounded ice features along its seaward edges. Oil spilled under this zone should encounter a relatively smooth undersurface and might spread significantly for an under ice spill. This process would be aided by lunar and barometric pumping of water in the confines between the ocean floor and bottom of the ice.

IIa. This zone is adjacent to Zone I and parallels the coast from Barrow to Barter Island. Its chief distinction from Zone I is that within it there is a greater ridging density. During winter and spring few hazards should be encountered by surface operations. The probability of deformation in this zone is greater than in Zone I. During the four-year observation period reported here, failure under apparent shear was observed on only a few occasions within this zone. The failure resulted in crack formation in a stress release pattern with displacements on the order of a kilometer. Complete failure accompanied by s-ridge or lead formation was observed on one occasion and has led to the distinction between Zones IIa and IIb. The probability of lead formation is low and the probability of encountering major obstructions during an attempt to escape lead-forming events is not extremely great.

This zone does contain the shallow areas just seaward of the Barrier Islands, however, and is often seaward of the 10-meter isobath, although generally contained by the 20-meter isobath. The ridge density was observed to be greater than in Zone I and consequently ice piling events by older and thicker ice than in Zone I are likely.

Oil spilled in this zone would encounter a somewhat rough under ice surface and therefore would spread less than in Zone I. Similarly, however, clean-up operations would be hampered by the ice surface roughness.

IIb. This has been designated a separate hazard area from Zone IIa because of one lead-forming event occurring along the dotted line distinguishing these two zones. It is interesting to note that were Zone IIb not recognized, this would be the only significant area in Zone IIa seaward of the 20-meter isobath. However, the one lead-forming event observed indicates that this area is not as stable as the balance of Zone IIa and should be distinguished. Within this zone then, there is greater hazard to surface parties through the possibility of ice failure.

IIc. This is an area of relatively smooth ice surrounded by ice which is statistically rougher in terms of major ridge systems. It has often been found to contain floes of varying ages surrounded by younger ice. Generally, however, both are annual ice. This has been determined to be a zone of relatively low hazard to surface travel. Dynamic ice events appear to be at a local minimum. Deformation and lead formation has not been observed during winter and spring. Oil spilled under this ice might spread but could well be channeled by the smooth undersurface of the newer ice surrounding the older floes.

IIe. These are areas of heavy and moderate ridging respectively, located inshore from the average location of flaw leads. Although statistically quite rough, these areas are quite stable and often contain large areas of grounded ridge systems. The chief hazard to personnel performing surface operations comes from the probability of lead formation, compounded by the difficulty imposed on attempts at rapid escape by the great surface roughness. Clearly in late fall massive ridge-forming events occur here and at least once, an ice island fragment was observed grounded in this vicinity. It would appear, then, that structures placed in these zones could bear the load of ice piled from several meters above the sea surface all the way to the ocean floor.

Oil spilled under this surface would most likely become trapped in many deep pools located between ridge keels and as a result spread less than in other areas.

- IIf. This is a large zone of moderate ridging located largely inshore from the average edge of winter and spring contiguous ice. Hazards to crews performing surface operations vary somewhat depending on proximity to the average location of flaw leads where there is the greatest chance of deformation or lead opening. One arm of this zone extends well into inner Harrison Bay where surface conditions are more stable than at the zones' seaward edge. Some deformation and accompanying displacement has been observed in this region during winter and spring. However, the ice has not been observed to the point of creation of an edge of contiguous ice through flaw lead formation.

Structures placed in this region could be confronted with massive ice piles and, in fact, large hummock fields have been observed in this zone. Oil spilled under this zone would encounter fairly significant resistance to its spreading as a result of the under surface roughness of this zone,

- IIG. This is a zone of severe ridging located shoreward of the shoreward limit of the observed envelope of flaw leads. Located northwest of Cross Island, it is often the site of massive s-ridges formed in November and early December. Many of these ridges are apparently well-grounded and remain in place well into summer. Cracks have been observed here in mid-winter, but the ice has not failed to the point of major lead formation and followed by displacement along the lead.

Surface operations in this area would involve an element of risk related to the chance of lead formation and the relative impediment to surface travel presented by the ice surface. Structures could very well have massive ice piles adjacent to them and available to exert relatively large forces against them.

An oil spill would tend to pool under this ice and have its spread thus retarded.

- IIh. This zone is the east end of an area of severe ridging. This portion lies shoreward of the flaw lead zone. Hazards in this zone are essentially the same as those described for Zone IIG.

- IIIi. This is a rather large zone of moderate ridge density lying shoreward of the shoreward edge of winter and spring contiguous ice. In two places this zone is shoreward of areas of more severe ridging between it and the shoreward edge of contiguous ice while a large area actually borders this edge. A good portion of this zone lies seaward of the 20-meter isobath. This circumstance might raise a question concerning the stability of that portion. Certainly there is very little reason to believe that ridge systems in these rather deep waters are grounded. However, this ice is stable. The apparent reason is coastline geometry.

This area is statistically safe for surface travel. However, considering the above observation, escape precautions should be made when operating beyond the 20-meter isobath.

Structures placed in this zone could encounter major ridging events. Deformation could take place in the exposed region and dislocation is a serious possibility in the region beyond the 20-meter isobath.

Oil spilled under this ice could be expected to pool somewhat because of the moderately rough undersurface.

An additional hazard in this subzone not encountered by other subzones in the II group is the possibility of ice island occurrences because of the large area with water depths greater than 20 meters.

- IIj. This is a zone of severe ridging located shoreward of the flaw lead zone. Because this zone lies seaward of the 20-meter isobath, its stability should be held in question. However, the flaw lead has consistently been observed along its seaward edge. Hence, while surface operations might be performed, precautions should be made to make certain that evacuation could be made quickly.

Structures placed in this zone would not only be endangered by the possibility of major ridge-building events but also by the possibility of ice island transects across the zone during open water and freeze-up periods.

An under ice oil spill located here would probably not spread greatly as a result of the enhanced underwater topography.

- IIk. This is a zone of moderate ridging lying to the east of Barter Island. Like Zone IIj, much of this zone lies seaward of the 20-meter isobath. Hazards described for this zone are essentially the same as those described for IIj except that the probability of a major ridge confronting a structure is diminished and the pooling effect of an underwater oil spill is similarly decreased.

- III. This major zone is defined by the statistical envelope of observed flaw leads. During mid-winter flaw leads quickly freeze over after formation while during late spring they tend to freeze much more slowly and as a result remain active much longer. During the mid-winter periods when the Beaufort flaw lead has frozen in this vicinity, a vast area seaward of this area is often constituted of contiguous ice. The term "flaw lead" loses its significance during this period. However, when a flaw lead does appear it has the greatest probability of occurring within Zone III.

Hazards in Zone III are significantly greater than in Zone II because of the flaw lead probability and because this zone lies almost entirely seaward of the 20-meter isobath making visits of ice islands and other deep-draft ice features very possible. Under ice oil spills located within this zone face a high probability of exposure to the water surface through the creation of flaw leads.

It should be noted that whereas Zone II could be thought of as having a good probability of remaining static throughout winter and spring, with the result that large ridge probabilities could be thought of as indicating stability through grounding and consequent anchoring of ice, a high ridge probability in this region indicates a high probability of instability through flaw lead formation and ridge-building events.

Major ice displacements are possible in this zone at any time associated with lead-forming events and ice deformation. This possibility is found throughout this zone and should be kept in mind in terms of the subzones defined below.

- IIIa. This zone rounds Pt. Barrow joining the Beaufort and Chukchi Seas. It represents an area of moderate ridging and a very narrow focus of flaw lead location. It should be considered extremely hazardous for surface operations. Structures placed in this zone would be confronted by almost constant ridge-building events. An

oil spill located here would be pooled significantly by the ice bottom topography but would also face a high probability of exposure to the water surface and incorporation within the ice over a large area through lead and ridge activity.

IIIb. This is an area of high probability of flaw lead formation with a low probability of ridging. During winter and spring there is often new ice being formed in this vicinity. It should be considered extremely hazardous for surface operations. Structures placed in this zone may very well have a high probability of escaping major ridge-building events. However, their interaction with the often newly-created ice within this zone should be considered carefully. Further, the probability of ice island visits may be enhanced by coastal configuration here. Oil spilled within this zone would have a high probability of incorporation into new ice and transport with pack ice motion.

IIIc. This is a large area of low probability of major ridging oriented parallel to the coast and located far beyond the 20-meter isobath. It should be considered significantly hazardous for surface operations. A structure placed in this zone would have a low probability of encountering a major ridging event but ice island visits would be quite possible. Oil spilled under this zone would not be pooled by major ridges and would have a large probability of incorporation into the pack ice through lead formation.

IIId. This zone runs parallel to the coast for much of the length of the Alaskan Beaufort Sea. It possesses a moderate probability of ridge building events, few impediments to ice island visits and a good chance of being located seaward of the flaw lead. For these reasons the zone should be considered hazardous for each of the activities considered here under "hazards".

IIIe. This is a relatively small zone of moderate probability of major ridging located inshore of Zone IIIf (described next) possessing a high probability of major ridging. It is generally somewhat stable but flaw leads have cut across it. Presuming suitable precautions are taken, surface operations could be performed in this zone. Structures placed here could well be confronted by major ridge-building events while there is a small probability that because of the bathometric configuration, some protection from ice island visits may be afforded. Oil spilled under this zone would very likely be pooled by the bottomside ice configuration.

IIIf. This is a large zone of great probability of major ridging running parallel to the coast from Harrison Bay to Flaxman Island. This zone also has a great probability of containing the flaw lead. And, because it is largely located over waters deeper than 20 meters, there is a good chance of an ice island visit.

Surface operations in this zone should be considered fairly hazardous due to the compounding effect of great ridge density and probability of lead formation events. Structures placed in this zone would be subject to major ridge-building events and at least the potential for ice island visits. Oil spilled under this zone would very likely be pooled significantly by the underside configuration of the ice. However, there would also be a great probability of near future oil incorporation into ice piles through lead formation and ridge-creating events.

- IIIg. This is a narrow zone of light ridging located beyond Zone IIIId. The hazards related to this zone are essentially the same as the hazards in Zone IIIId except that the probability of flaw lead formation between this zone and shore is even greater, and the possibility of an ice island visit is enhanced while the probability of major ridging is decreased.
- IIIh. This is a zone of low probability of major ridge building events but with little obstruction to ice island visits. The probability of a flaw lead formation between a point located in this zone and shore is very great. During lead-forming events there is a good chance that field crews could flee dangerous situations to nearby points but not escape to shore by surface transportation. Structures, while largely free from major ridge-building events could very well be confronted by ice islands. An under ice oil spill would probably spread significantly and soon be introduced into the pack ice.
- IIIj. This zone possesses a low ridging probability and a high probability that flaw leads are located to the shoreward. Hazards are essentially the same as Zone IIIh.
- IV. This zone contains ice with a moderate probability of major ridge formation as a result of ice interaction with the shore, yet there is a high probability that flaw leads will be found shoreward of this zone. Because of the shore-linked aspect of its morphology and hazards, it has been differentiated from Zone V which is essentially pack ice.
- Surface operations in this zone should not be performed without provisions for non-surface evacuation. Structures placed in this zone will be subject to at least a finite probability of major ridge formation, while ice island and floeberg visitations are entirely possible. Oil spilled under this zone would tend to be pooled significantly by major ridges but be subject to introduction to the ocean surface during lead-forming events.
- V. This zone is essentially the pack ice zone. Here, influence of shore on ice morphology and hazards has been reduced to regional influences. In the region north of the Beaufort Sea there are periods of stable ice extending up to six weeks duration. During that time, field operations could be carried out here subject to the provision for non-surface evacuation if necessary. However, the relative danger is actually diminished from that in Zones III and IV because of the smaller chance for major shear deformation in this zone. It is very unlikely structures will ever be placed in this zone. An under ice oil spill would essentially be a spill into pack ice.

B. Chukchi Sea

In this section, the results described in Section VI are interpreted in terms of seasonal morphologies of the Chukchi Sea near shore ice regime. Then based on these morphologies, an assessment of relative hazards has been made for the Chukchi near-shore area.

1. Chukchi Sea Morphology

The ice year has been broken into three periods: mid-winter, early spring and late spring. The morphology of the Chukchi Sea ice is much more dynamic than the Beaufort Sea morphology. While the Beaufort Sea exhibits a vast area of static ice with an occasional much larger area attached, there is an almost constantly active flaw lead along the Chukchi coast with new ice being formed, detached, piled, and transported almost constantly. For that reason the morphology of Chukchi ice has been described in a somewhat different way from the morphology of Beaufort Sea ice.

Figures VIII-3, VIII-4 and VIII-5 contain the morphological description of Chukchi Sea ice behavior. Two fundamental ice features have been utilized to construct these maps: The edge of contiguous ice which essentially coincides with the flaw lead, and large massive ridge systems. In some respects these two ice features are independent of one another; the edge of contiguous ice is, in general, controlled by season--being farther off shore during winter and advancing toward shore with advancing season while the location of large ridge systems appears to be controlled mainly by bathymetric configuration.

Because of this relative independence, the major influence or change in the near shore morphology will be seen to be the changing location of the edge of contiguous ice. Lest this seem an over simplification of the near shore morphological processes, it should be pointed out that at some places a direct relationship has been noted. In particular, north of Bering Strait s-ridges have been observed to build seaward extending the edge of contiguous ice in that direction while elsewhere the edge of contiguous ice is retreating toward shore.

The Chukchi Sea Ice Morphology Maps have a much different appearance than do the Beaufort Sea Maps. One major reason for this is the opportunity for ice to move out Bering Strait. All during the late winter and spring period, ice moving events take place along the Chukchi coast, often creating shear ridges along shoals jutting seaward from the string of capes and headlands which are so prominent along the coast. Increasingly as one travels to the south, the edge of contiguous ice between headlands is more poorly defined and the ice contained is more prone to seaward motion leaving areas of open water behind. In general, there is often a lead system extending the length of the coast from Barrow to Cape Lisburne.

Just south of Cape Lisburne and north of Point Hope is an area with a constantly reformed polynya.

South of Point Hope the effect of ice motion out Bering Strait is even more prominent. Another recurring polynya occurs just southeast of Point Hope formed by southward ice motion. Kotzebue Sound is generally covered by stable ice during much of the ice year, but the presence of a zone of weak and often moving ice just seaward hints that this sheet of ice is probably potentially unstable.

At the southern end of the Chukchi Sea is Bering Strait. Just north of the Strait is a large system of shoals where large extensive shear ridges can be built during ice motion out the Strait.

2. Hazards Resulting From Chukchi Sea Morphology

Based on the Chukchi Sea morphology described in the previous section, the question of hazards related to offshore petroleum development has been addressed. Map IV-7 shows a number of hazard descriptor areas having sufficiently uniform conditions within each area that a hazard description could be written for each area.

The hazards addressed include: the safety of crews and equipment used to perform surface exploratory operations, an assessment of the possible load-bearing ice surface imposed on structures resulting from ice piling events, the possible plowing of the ocean floor by ice piling events, and the possible fate of petroleum spilled in each descriptor area.

The following table describes the hazards related to each of the descriptor areas defined on map IV-7

CHUKCHI SEA ICE HAZARDS

Legend - Chukchi Sea Ice Hazard Map

1. This is an area generally safe for travel from January through early June. Depending on conditions at freeze-up, ice seaward of the islands can vary from smooth to very rough. In front of Barrow, this zone narrows to a strip 200 m wide.

This is not an area of major ridging and surface structures would be subjected to a minimum of hazards resulting from ice piling or keel plowing of the ocean floor.

Fall and early winter oil spills could be transported away or incorporated into permanent ice. From early winter till breakup, under ice spills would remain trapped except for transport through occasional tension and tidal cracks.

2. An area of moderate ridging formed early in the ice year, this area is generally safe for surface travel from January through early June. Chances of lead formation toward seaward with the advance of the season. There is also moderate hazard to structures resulting from ice piling and keel plowing.

Fall and early winter oil spills are very likely to be transported away with ice motion. Later spills are likely to be trapped under the ice and pooled between ridge keels until spring when thawing and breakup of the ice would cause lead pumping and transport of the oil.

3. An area of moderate ridging formed early in the ice year is subject to lead formation with low probability from January through March. Lead formation is very likely after that date. Surface travel is least hazardous during January through March and moderately hazardous at other times. Because of dynamic ice events in this region, this area should not be considered for the location of camps.

Surface and subsurface structures subject to damage by moderate ridging and keel plowing of the sea ice at almost any time during the ice year.

Oil spills would be subject to transport or incorporation into piled ice at any time during the ice season. The longest period during which an oil spill would not be subject to ice motion is on the order of two to three weeks.

4. This is an area subject to moderate ridging activity at any time during the ice season. Since lead formation is frequent during the ice season as well, surface travel is extremely dangerous at any time and is actually less hazardous farther offshore.

Surface and subsurface structures are subject to damage by ice piling and plowing during the entire ice season.

Oil spilled in this region during the ice season would soon become subject to lead pumping and incorporation into ice piles and ridges. There would be a high probability of transport within one week of the spill. Clean-up attempts would be made difficult by the possibility of ice motion.

5. An area of severe ridging seaward of the normal edge of stable ice at any time during the ice season, this is an extremely hazardous area for exploration activities. In addition, surface structures would be constantly subjected to piling events and subsurface structures would be subjected to damage by ice keel plowing.

Oil spilled in this region would very likely be incorporated into piled ice, pumped onto the surface by lead activity and incorporated into newly-forming ice within leads.

6. An area of severe ridging just shoreward of the mid-winter edge of fast ice, this region should not be considered stable. However, during mid-winter, ice here might remain in place two to three weeks at a time. By mid-spring, the boundary of fast ice is located along the shoreward edge of this zone.

The safety of surface operations in this zone is similar to that of Zone 4 except that the increased ridging in Zone 6 would make retreats to safer ice more difficult in case of dangerous ice conditions, and the increased piling in this area increases the probability of parties being caught in truly hazardous situations. Camps should not be established in this area.

Surface and subsurface structures would be subjected to damage by great amounts of ice piling and plowing --- perhaps as severe as any place along the Beaufort/Chukchi coast.

Oil spills generally would be located under mobile ice subject to piling events most of the ice year. However, during mid-winter spills might be trapped under stationary ice for as long as six weeks. Lead formation is a possibility at any time during the ice year.

7. An area of severe ridging just offshore the springtime edge of stable ice. This area is generally stable from mid-winter to mid-spring. Because of the ridging exposure offered ice by the configuration of Point Barrow, even this area should be considered hazardous for prolonged surface activity. (See description of Zone 6). The hazards associated with this zone are similar to Zone 6 except that there is a longer period - up to two to three months - when the ice may not be subject to motion.

8. This area is subject to severe ridging offshore of the late spring edge of contiguous ice yet inshore of the early spring edge of stable ice. The ridges in this zone are formed early in the ice year and generally remain in place until the melt season. Surface exploration activities are not extremely hazardous. However, because of the wide variation in location of the springtime edge of fast ice, the relative safety of this zone is not as great as its counterpart along the Beaufort coast.

Surface and subsurface structures would be subject to damage by ridging and plowing events generally only at the beginning (November-December) and end (June-July) of the ice season.

Oil spills in this zone during November and December could be transported away with near shore ice motion or incorporated into ice piles in the near shore area (within this zone or even inshore of this zone). From December until early June, an under-ice oil spill would most likely remain trapped under the ice in this area. After June sufficient leads and cracks exist that the oil could be pumped to the surface by ice activity.

9. An area of moderate ridging formed early in the ice year, this area is located offshore of the late spring ice edge but inshore of the early spring ice edge. This zone is similar to Zone 2 on the other side of Barrow in terms of hazard. Generally safe for surface travel from January through June. Chances of lead formation increase seaward with the advance of the ice season. Moderate hazard to structures exist resulting from ice piling and ice keel plowing.

Fall and early winter oil spills would probably be transported away with any ice motion. Later spills are likely to be trapped under the ice and pooled between ridge keels until spring.

10. This is an area generally free from major ridges running from south of Barrow to near Pt. Franklin and is located seaward of the late spring ice edge but shoreward of the early spring ice edge. Because of the great statistical variation of the ice edge in this region, the description of this area and Zone 11 should not be considered entirely accurate. One reason for the wide variation of behavior here is the location of these areas in waters considerably deeper than 20 meters, and hence, the absence of significant grounded ice features to provide anchoring mechanisms for fast ice. This situation is reversed on headlands (Pt. Barrow, Pt. Franklin, Icy Cape, etc.) where many of the identified near shore zones are located within the 20-meter isobath.

This area tends to be free from lead activity from mid-winter until mid-spring. However, surface travel should be considered hazardous even at those times because of the wide variation in behavior mentioned above.

Surface and subsurface structures are relatively free from hazards due to major piling and plowing events. Subsurface oil spills may be pooled under stationary ice for up to a month at a time but lead activity and ice motion would eventually result in the pools of oil breaking up and being redistributed.

11. This area, generally free from major ridges, runs from south of Pt. Barrow to north of Pt. Franklin and is located seaward of the early spring ice edge but shoreward of the mid-winter ice edge. Because of the reasons described for Zone 10, the boundaries of this zone are not well defined. The hazards described for Zone 10 also apply to this zone. However, the probability of stationary ice here is even less than in Zone 10 and the possibility is generally restricted to the period December-February.

12. This is a broad zone subject to moderate ridging running from Barrow to Pt. Franklin and located shoreward of the late spring ice edge. Although this is a generally stable zone with some grounded ice features, the relative hazard to surface travel increases as

one progresses seaward. Some lead activity has occurred here during winter months although, statistically, this area is considered stable from December through late June.

Under-ice oil spills would be trapped under generally stable ice from December through June with a low probability of transport or major pumping onto the surface by lead activity.

Surface and subsurface structures would be subjected to hazards due to moderate ice piling and plowing events early (November-December) and late (June-July) in the ice season.

13. This zone of ice extends from shore to the area of moderate ridging and is entirely within the late spring edge of ice, being wide in areas of embayment and narrow across headlands. Although this zone extends along the entire coast it has been divided into smaller zones because some characteristics of the ice change from place to place.

Ice topography in this zone is dependent on conditions at the time of final freeze-up, usually has occurred by the end of December. The ice surface topography will vary from location to location and from year-to-year. The surface can at times be sufficiently smooth for the operation of wheeled vehicles. At other times it consists of a jumbled pile of small plates of ice about 30 cm thick and 2-3 m across presenting a major obstacle for even foot travel. Ridging generally does not occur in this zone and, in fact, usually forms the seaward boundary of this zone.

Structures placed in this zone would be subject to relatively hazardous conditions due to piling and plowing. By the end of the ice year most first year ice is on the order of 2 m thick and as a result considerable expanses of the ice in this zone will be frozen to and into the bottom. This is particularly true in lagoon areas such as Pt. Franklin. Because of this and the long life of the ice zone, under-ice oil spills could spread considerable distances along this zone.

14. This zone adjacent to Pt. Franklin appears to exhibit ice behavioral characteristics somewhat different from ice zones adjacent to other headlands. Very little ridging appears to occur here and the edge of contiguous ice varies little from season to season. This behavior appears to be explained by the fact that the ocean floor profile drops off rapidly to 20 meters along this section of coast and the same profile is maintained much of the length of this region. Hence, ridging resulting from differential motion under compression ("shear ridging") is confined to a very narrow zone and may not be of sufficient extent to be resolvable on a Landsat image. This zone may be quite narrow and consist of a single shear ridge perhaps 50 m wide.

Obviously this zone is hazardous for surface travel because of the high degree of activity within it and structures would be endangered by the constant ice motion.

15. This is a broad zone of moderate ridging located seaward of the late spring edge of contiguous ice but shoreward of the mid-winter ice edge. The statistical variation of the edge of this zone is relatively small, hence, the boundaries of this zone should be considered fairly well-known.

Surface travel in this zone should be relatively safe from December through late March, with increasing risk toward the seaward side. Structures placed here would be exposed to moderate

ridging before December and after March. Underwater oil spills be contained under the ice from December through March and subject to transport at other times.

16. This is a zone of moderate ridging inshore of the late spring edge of ice and located between Pt. Franklin and Icy Cape. This zone is generally stable from December through late March and could be used for surface exploration with a reasonable degree of safety during this period. Structures are subject to ice motion, piling and plowing before December and after April. Under-ice oil spills could be expected to be trapped under the ice.

17. This is a continuation of Zones 13 and 1. Though this zone may be free of ridging, the surface can vary considerably from place-to-place and from year-to-year. (See description of Zone 13).

18. This zone of relatively stable ice between December and February has a high probability of spatial variation. It is located off Icy Cape and seaward of a zone of moderate ridging. While from time-to-time stable contiguous ice exists here, its suitability for surface travel is very poor. It is subject to being broken off at almost any time to join the adjacent pack ice.

This area is subject to ice motions at any time during the ice year with stable ice perhaps two weeks at a time between December and March.

Oil spills under this region would soon be introduced into the pack ice.

19. This is an area of severe ridging located between the early spring and late spring boundaries of contiguous ice. This zone lying off Icy Cape is located over Blossam Shoals with water depths on the order of six meters. Early in the ice year ice grounds on these shoals and remains stranded until the edge of contiguous ice migrates across the shoals with the advance of the ice season. This particular zone includes the stranded piled ice which is broken free between March and May-June.

Under normal conditions surface travel on this zone would be relatively safe between late December and May. Obviously structures located here would be subjected to severe ice piling events during November and December, but after that time structures would be insulated from piling events.

Oil spilled under this region would be trapped under the ice between December and May and would very likely be pooled in many small chambers beneath the piled ice.

The variation in boundary location of this zone is on the order of half the width of the zone itself. Hence while the zone is statistically meaningful the precise position of the zone can vary on the order of its own width.

20. This zone is a region of severe ridging located inshore of the late spring edge of fast ice. This zone is similar to Zone 19. In terms of hazards, the hazard to surface travel in this zone is considerably less than in Zone 19 although during most years the ridging might make travel difficult.

21,22. This is a region of moderate ridging with an adjacent zone of severe ridging located between the mid-winter and early spring edges of ice. This is an active area during the entire ice year with perhaps the exception of a few weeks between December and

March. However, the statistical variation of the location of these zones is sufficiently large so that their precise positions cannot be reliably determined. Also, depending on ice activity, ridges created in these two areas may be broken away to drift with the pack ice.

Generally, these two areas are extremely hazardous for surface travel. Also, structures located within these zones would be subjected to nearly constant piling and plowing except for perhaps one or two periods of several weeks in mid-winter.

Oil spilled under these two regions would soon be transported into the pack ice.

23. A zone of moderate ridging located between the early spring and late spring edges of fast ice, this zone is similar to the adjacent Zone 19 except for ridge density (see description of Zone 19).

24. A zone of mid-winter contiguous ice extending from Icy Cap to Point Lay, this zone lies between the mid-winter and early spring edges of fast ice. However, along this section of the coast the variation of the mid-winter edge of ice is large and the width of this region can vary considerably. For this reason, the existence of this zone should not be depended upon for surface travel.

Structures located in this region would generally be free from ice piling and plowing events. Oil leaked under this area would soon be transported into the pack ice region.

25. This is a zone of reasonably stable contiguous ice located between the early and late spring boundaries of contiguous ice. The statistical variation of the positions of these boundaries is on the order of the width of the zone and hence, its width and precise location can vary from year-to-year. The ice within this zone is generally relatively smooth and free from major ridges. It is formed during early winter (November-December) and is broken up by late spring (April-May).

This area is moderately safe for surface travel in mid-winter with decreasing safety toward the seaward boundary. Structures in general would not be subject to great amounts of piling and plowing although this section of coast should not be considered entirely free from ridging activity. Subsurface oil spills within this zone would generally remain trapped between December and April-May and, because of the lack of ridged ice in this area, might spread considerable distances beneath the ice.

26. This zone is composed of generally ridge-free ice located inshore from the late spring edge of ice and is actually an extension of Zones 13 and 17 farther to the north. However, it widens out in this vicinity and has a somewhat different morphology than Zones 13 and 17.

This zone consists of two sub-zones: ice within the barrier islands and ice outside the barrier islands. Within the barrier islands the ice is essentially lagoon ice. It is generally formed early (November) in the ice year and often melts earlier than ice just seaward of the barrier islands. It is ridge-free but often has working tension and tidal cracks, and in areas less than two meters deep, it is often frozen to the bottom. Because of these characteristics, structures are subject to a minimum of piling and plowing while under water oil spills would remain in place under

the ice for great lengths of time, working to the surface through the tension and tidal cracks. Obviously surface travel in this portion of Zone 26 is quite safe until the ice melts or overflows with melt water.

The portion of Zone 26 outside the barrier islands is generally ridge-free and remains in place until May-June. The statistical variation of its outer boundary is quite large and hence the exact width of this zone measured from the barrier islands will vary from year-to-year. This zone is formed early in the ice year and is generally free of major ridges. Lead activity does not occur until late spring (May-June). The area is generally safe for surface travel with hazard increasing significantly after early spring and with distance from shore. Structures placed in this zone would be subjected to relatively small ridging and plowing events. However, it is very likely that one or more small shear ridges may become frozen into the zone during its time of formation. Oil spilled under this zone is likely to remain until May or June.

27. This is a zone of moderate ridging located between the early and late spring edges of ice. The early and late spring edges of ice converge along this section of coast off Pt. Lay while the mid-winter edge of ice remains much farther offshore. Also, the shoreward statistical variation of the mid-winter edge of ice is quite broad here, generally coinciding with the combined edge of early and late spring fast ice. This small zone is reasonably safe for surface travel until early spring but increasingly hazardous after that time. Structures would be exposed to a moderate amount of ridging and plowing. Underwater oil spills would most likely be trapped under ice here until mid-spring when lead-forming activity would introduce the oil into the pack ice.

28. This zone of moderate ridging is located inshore from the combined early and late spring edges of fast ice. (see description for Zone 27.) This zone is formed during November and December and usually lasts until mid-spring. Early and late spring data show that variations in the boundaries of this zone can cause it to be very narrow with flow leads quite close to shore.

This area should be safe for surface travel from December through early March but with increasing probability of lead formation following that date. Structures placed in this zone are exposed to ice piling and plowing events during November and December. Oil spilled under the surface in this zone would normally remain in place until May when it would be introduced into the pack ice due to breakup of the ice.

29. This is a zone of moderate ridging just seaward of the combined edge of early and late spring contiguous ice. This zone is subject to lead formation generally after early March but the data show that lead formation has occurred at earlier dates. For this reason, surface travel in this area is somewhat dangerous between December and March and increasingly so after that date. The relative danger of surface travel is increased by the occurrence of moderate ridging in the area making rapid travel away from developing hazards difficult.

Structures placed in this area are subject to damage due to ice piling and plowing at nearly all times during the ice season. Oil leaked under this area would be introduced into the pack ice through lead opening activity.

under this zone would soon become incorporated into broken and refreezing pack ice.

30. This zone of generally ridge-free ice is located inshore from the late spring edge of ice and extends from Pt. Lay to Cape Lisburne. This zone is actually an extension of Zone 26 but is much broader and has a somewhat different morphology. Occasionally, ridge-building events can occur within this zone (see Zone 36) but long shear ridges are probably unusual.

This zone should be relatively safe for surface travel between December and April-May except that during severe conditions ice piling can occur within the area. Structures placed in this area would be relatively free from ice piling events and bottom plowing appears to be at a minimum. Under-ice oil spills would normally be trapped under the ice between December and April.

31, 32. These are zones of moderate and severe ridging resulting from motion of ice past Cape Lisburne. Both are located seaward of the mid-winter edge of fast ice and, therefore, not part of the near shore regime. However, these zones have been included in this analysis to help explain the morphology of the nearshore ice.

33. This zone of moderate ridging is located between the mid-winter and early spring edges of fast ice. The variation in width of this zone is on the order of the width of the zone, and therefore, even between mid-winter and early spring the stability of fast ice in this area is uncertain. Therefore, this area is only marginally safe for surface travel. Examination of individual cases shows that the flaw lead is often located within this zone.

Because of water depths in this zone, it is unlikely that structures attached to the bottom would be constructed. However, it appears that any structure located within this area would rarely be free from ice motion for more than two to three weeks. Similarly, oil leaked under the ice in this zone would soon be incorporated into the moving pack ice.

34. This two-part zone of ice, relatively free from ridging is located between the early and late spring edges of contiguous ice. The zone is broken into two subzones by Zone 35. Examination of the statistical variation of both boundaries of this zone indicates that the zone is reasonably significant statistically. Hence, between December and March this area should be reasonably safe for surface travel with the hazard increasing after that time. Structures located in this area should be relatively free from the effects of ice motion from December through March and only flaw lead activity after that time. Oil leaked under the ice in this zone would spread due to the absence of major ridges and be incorporated into flaw leads after March.

35, 36. These two zones are areas of moderate ridging intruding into Zones 30 and 34 and are basically the same. The formation of Zones 35 and 36 decrease the utility of these areas as avenues for surface travel. The mechanism for the creation of this zone is somewhat different from the mechanism responsible for other near shore areas of ridging: while most other ridges in the nearshore area are shear ridges, the ridges in this area are better classified as pressure ridges which are due to ice moving down the Chukchi coast and being driven into the nearshore ice.

37. This is an area of severe ridging located in the vicinity of shoals off Cape Lisburne. This zone is inshore from the average edge of mid-winter contiguous ice but within the range of boundary variation of this zone. Hence, this area should be considered to be the location of early winter ridging with moderate stability from mid-winter to early spring. After that date the edge of contiguous ice generally moves shoreward.

This area could possibly be safe for surface travel from mid-winter to early spring. However, the safety resulting from the relative stability of this ice is negated somewhat by the presence of many ridges which makes rapid surface travel very difficult.

Structures placed in this area would be subject to a great deal of ice piling and bottom plowing events. Oil spilled under the ice in this area would be incorporated into the piled ice and later into the pack ice or introduced into the pack ice via flaw lead activity.

38. This is a zone of moderate ridging located in pack ice and is included in this analysis for completeness.

39. This is a zone of moderate ridging located offshore from the mid-winter edge of contiguous ice and within the boundary of a recurring polynya. The ice within this zone is quite unstable. Surface travel would be very hazardous at anytime. Structures would be constantly subject to moving ice and piling events. Bottom plowing by ice keels should be frequent. Oil spilled under the ice in this zone would rapidly be incorporated into the pack ice.

40. This small zone just off Cape Lisburne is subject to both ridging and polynya formation. It should be considered extremely hazardous for surface operations and structures. Petroleum spilled under this zone would soon be incorporated into new ice subject to transport with pack ice.

41, 42. These are zones of nearly constant production of new ice. This area along with Zones 39 and 40 has been documented more completely in our annual report for 1976. The ice within this zone is almost constantly moving seaward, leaving a polynya adjacent to Cape Lisburne over which new ice continuously forms. The average edge of mid-winter ice runs across this area dividing it into two zones as a result of the very rapid formation of new ice during that period. The shoreward variation of the mid-winter ice runs very close to the shore as do the early and late spring average contiguous ice edges.

This area is particularly unsafe for surface travel at all times. However, there is the interesting possibility that structures placed here might be subject to at least a minimum of ice hazards. Oil spilled here would quickly be incorporated into newly-forming ice and be transported seaward into the pack ice.

43. This zone of moderately stable ice is located just north of Point Hope, over relatively shallow water and within a reasonably stable portion of the late spring edge of contiguous ice. This area should be safe from ridging events and significant bottom plowing. Oil spilled under this zone could be expected to spread a great distance and remain on location between December and May.

44. A zone of intermediately safe ice located between the early spring and late spring edges of contiguous ice. Because of the variation of the boundaries of this zone this zone should be taken

to illustrate the transition between the relatively stable Zone 43 and the unstable Zone 45 described next.

45. This is a small zone located within the average edge of mid-winter contiguous ice and adjacent to the recurring polynya (41 and 42). Generally, this zone exists in this vicinity but its precise location changes frequently. This is an area where newly-formed ice from the adjacent polynya is compacted from time-to-time and at other times broken away. It is generally unsafe for surface travel. Structures placed within this zone would be subject to minor piling events but probably very little bottom plowing. Oil leaked under this zone during December through May will very likely become incorporated into compacted new ice and subsequently enter the pack ice region.

46. In this zone the edge of contiguous ice remains constant throughout the ice season. An apron of ice generally extends seaward from the shore. Pack ice rounding Pt. Hope occasionally in flaw lead activity at the west end of this zone. Statistically the zone varies significantly with the seaward edge migrating occasionally very close to shore. This zone should be moderately safe for surface travel as long as quick access to the shore is maintained. Structures placed in this zone would be subject to a minimum of ridging activity. An oil leak occurring under this area between December and May would spread along the underside of this relatively smooth ice and remain until breakup in late spring or until a flaw lead developed allowing the oil-contaminated ice to drift into the pack ice region.

47. This zone is the location of a recurring polynya formed by the ice within this zone and Zone 46 breaking away and drifting southward (into Zone 48). This area is completely unsafe for surface travel during the ice season. However, a bottom-founded structure would probably encounter a minimum of destructive ice conditions. Oil spilled under this zone would soon be incorporated into newly-formed ice and subsequently into the pack ice.

48. This zone, lying in outer Kotzebue Sound, is an area of ice compaction and growth. New ice created in Zone 47 is driven into area through the ice season. Considerable compaction of the ice is evident on successive Landsat images. The ice in this area is growing in thickness due to both compaction and freezing of new ice.

Surface travel in this area would be extremely hazardous throughout the ice season. Structures placed here would be subject to nearly constant ice piling although bottom plowing may not represent a severe hazard. Oil spilled in this area during the ice season would become incorporated into the thickening and compacting ice and would be slowly transported southward toward Zone 54.

49. This zone of ice is similar to Zone 48 except that it is located between the mid-winter and late spring edges of ice and is stationary for several weeks at a time during this period. The ice within this zone could be used for surface operations during the period December through April providing that provisions for the rapid evacuation of personnel are maintained. Structures placed within this zone would be subject to some ridging and piling of ice at all times. Ocean floor plowing should not represent a major

hazard. Oil spilled under the ice in this zone would become trapped beneath the ice and be transported with the ice during breakup events. The oil could also be subject to lead pumping. The actual length of ice trajectories during these events is relatively small with the result that spills of this nature would probably be retained in the vicinity for the balance of the ice season.

50. This zone of ice is shoreward of the late spring ice edge. Examination of Landsat imagery of this area reveals linear features which are very likely shear ridges running close to and parallel with the shore. Because of the existence of these shear ridges this zone was separated from Zone 46. These ridges are most likely formed during November and December and remain with the ice in this zone until May. During this period surface travel within this zone is relatively safe. Structures placed here may be subject to some ridge-building activity in November and December and some bottom plowing might occur during these events. Oil spilled under the ice could be expected to spread somewhat as a result of the relatively smooth undersurface of the ice in most of this zone. It would then remain in place until April-May.

51. This large zone of relatively stable ice is located inshore of the late spring ice edge including inner Kotzebue Sound. During the period of formation in November-December, dynamic ice events may take place in this zone; pressure and shear ridges may form - particularly in Kotzebue Sound - creating conditions hazardous to structures. Following that period and until April, this surface should be fairly safe for surface travel. Oil spilled here during November-December would most likely be incorporated into the ice somewhere within the zone - depending on the nature of the dynamic ice events during that period. After that time oil would spread out on the relatively smooth undersurface of the ice and remain until breakup around May.

52. A zone of ice within Kotzebue Sound located between the early and late spring edges of fast ice. Analysis of contiguous ice edge variations shows that sometime between early and late spring the ice within this zone is broken up. From December until the ice breaks up this area should be safe for surface travel. Structures placed within this zone would be subject to ridging activity during November-December but generally not after that date. Oil spilled under the ice will remain until springtime breakup events and would only be slowly transported away after that time.

53. This is a zone of moderate ridging located between the mid-winter and early spring average edge of contiguous ice and the late spring average edge of contiguous ice. The ridges in this area could be created at almost any time because of the high statistical variation of this zone. This area is dangerous for surface travel at all times. Structures could be subject to ice piling events and bottom plowing at almost any time. Oil spilled under the ice would soon become incorporated into broken ice within a few weeks of a spill.

54. This is an area of moderate ridging located outside the average mid-winter edge of contiguous ice in outer Kotzebue Sound. The ridges created in this area are largely shear ridges and arise as a result of motion of ice toward Bering Strait. This behavior is largely a continuation of the process originated in Zones 47 and 48.

This area is within the extreme variation boundaries of contiguous ice for mid-winter and early spring and could be considered for surface travel between December and March or April. However, this ice is highly prone to breaking up at all times and therefore surface operations should include contingency plans for rapid retreat from this zone. Structures placed within this zone would be subject to ice piling events at any time. Bottom plowing is also a definite possibility in areas less than 20 meters deep during November through April. Oil leaked under this zone would be trapped in pools between ridge keels and other keels related to the generally rough surface of this zone. However, there is a high probability of ice breakage and subsequent motion of ice allowing lead pumping of oil.

55. This is an area of moderate ridging located beyond the average edge of mid-winter contiguous ice. Shear type ridges are created in this zone largely by ice being pushed out Bering Strait and being compressed against contiguous ice in that process. This area is occasionally within the contiguous ice zone but has a high probability of being sheared or broken free. It is generally a very dangerous area for surface travel. Structures placed within this zone would be subject to almost constant ridging processes and, in locations less than 20 meters in depth, bottom plowing would take place. Oil spilled under the ice in this zone would generally become trapped. However, since the ice in this zone is frequently broken free, such trapped oil would soon be introduced into the pack ice.

56. This area of severe ridging is located offshore from the average edge of mid-winter contiguous ice. This zone is similar to Zone 55 except that the density of ridging and the relative stability is increased, (see description of Zone 55) but not sufficiently to cause this zone to be considered safe for surface operations.

57, 58. These are zones of moderate and severe ridging respectively, located inshore from the average edge of early spring contiguous ice and offshore from the average edge of mid-winter contiguous ice. This situation is reverse from the spatial relationship of these two average edges elsewhere along the coast. Further the statistical variation of the early spring contiguous ice edge is less than the variation of the mid-winter ice edge. These data support the concept of a building-up of stable ice in this area during the winter and early spring parts of the ice season while elsewhere along the coast, maximum build-up generally occurs by mid-winter. Presumably this effect is a result of the nearly constant motion of ice out of Bering Strait creating many parallel s-type ridges along this area of the coast.

This area should be considered for surface travel only in early spring. However, the surface roughness at that time would be a major factor in the relative ability to retreat from dangerous ice conditions. Structures placed in these zones would be subject to pressured ice events during nearly all the ice season. Bottom plowing is also a distinct possibility at nearly all times. Oil spilled under this zone has a high probability of entrapment in pressured ice.

59. This is an area of severe ridging located inshore from the average edges of contiguous ice for mid-winter, early spring and

late spring. Hence, this zone is constructed early (Nov.-Dec.) in the ice year and remains until late spring or early summer. It is very likely that this ice is securely grounded on the relatively shallow (~ 8m) shoals mapped in this area.

Because of its stability, the ice in this zone could be used for surface operations many months of the year. However, the surface roughness should create considerable logistical problems. Structures placed in this zone would usually be subject to ice piling and bottom plowing events early (Nov.-Dec.) in the ice year. Oil spilled under this zone would be incorporated into piled ice between November and December and entrapped under piled ice after that time. Later, during May, such oil would be released into the open water with the break-up of the ice in this zone.

60. This zone contains a great transition of ice conditions within two very short distances between shore and the average edge of contiguous ice. It is interesting to note that not only do the average edges of contiguous ice coincide for each season, but the variations on the seaward of this line are very small indicating a nearly constant ice condition for this zone from December through late May. Further, although linear features parallel to the coast can be identified on many images, it is difficult to establish whether these linear represent ridge systems or boundaries between ice types.

Based on the available information and the morphological behavior pattern of ice moving through Bering Strait, it should be expected that the ice in this zone is formed early in the ice year (December) and might remain until May. Because of the nearly constant motion of ice out Bering Strait, s-type ridges are constructed along the seaward boundary of this zone. However, the variation of the edge of this zone on the landward side of the average position is large, indicating that ridges may be constructed and carried away in an alternating sequence along this portion of the coast. Further, it is likely that the ice adjacent to the shore is rough because of this same process being operative during its formation.

This zone is therefore not entirely safe for surface travel - the relative danger increasing significantly with distance beyond very well grounded ridges. Similarly the ice conditions imposed on structures would vary considerably across this zone. Finally, oil spilled under the ice in this zone would be subject to pooling as a result of the rough undersurface and introduction into the pack ice during the occasional break-off events.

61. This is a zone of relatively smooth, stable ice formed early in the ice year and remaining in place until late spring. It should generally be moderately safe for surface travel from December through May. Structures placed in this zone should be relatively free from ice piling events and bottom plowing. Oil spilled under this zone would be subject to considerable spreading because of the relatively smooth undersurface.

62. This is a zone of moderate ridging and variable stability throughout the ice season. It is generally unsafe for surface travel over long periods of time although brief excursions could be safely carried out providing ice conditions were monitored carefully. Structures in this zone would generally be subject to ice piling

conditions at any time. Oil spilled under this zone would tend to become trapped under the relatively rough undersurface and be introduced into the pack ice during the occasional ice breaking events.

63. This is a broad zone of unstable ice located over relatively shallow waters running from Cape Espenberg to Wales. This zone has some unusual characteristics: the variation of the edges of contiguous ice run adjacent to the shore. Hence the area can be relatively broad at one time and break-up to the shore at other times. This area should be considered unsafe for surface travel. Structures placed within this zone would probably not be exempt from ice piling events for very long periods of time. Oil spilled under this zone would soon become incorporated into broken and refreezing pack ice.

C. Bering Sea

In this section, the results described in section VI are interpreted in terms of a general ice season morphology of Bering Sea ice behavior. Unlike the Beaufort and Chukchi Sea morphologies, the Bering sea near shore area has not yet been subdivided into descriptor areas. Rather, short general descriptions have been written for each significant near shore zone. Such a subdivided will be prepared following further data analysis. A zonal hazards map will follow preparation of the zonal morphology map. This report contains a brief description of the hazards to be considered in the Bering Sea area with some site--specific references.

1. Bering Sea Morphology

Map VIII-8 shows in first draft form the morphological behavior of near shore ice along the Bering sea coast. On this map, the areas with nearly constant contiguous ice edge are delineated with a single line. Areas where significant deviations of average ice edge occurs are shown as shaded. Data for this map are taken largely from map VI-37. Paragraphs describing ice behavior along the Bering coast are situated proximate to the areas being described.

The following behavioral patterns have been observed:

(A.) Contiguous ice located over water depths greater than 20 meters. Generally in the Bering Sea area contiguous ice is found in waters considerably less than 20 meters deep. This is considerably different from the behavior in the Beaufort Sea where the 20-meter isobath is generally taken to represent the stable location of "fast ice". As shown in figure VI-37 there is little seasonal variation in the location of the edge of contiguous ice. We postulate that in the Beaufort and Chukchi seas the rapid freezing rates obtained with very low temperatures coupled with the relative immobility of the ice act to stabilize the ice sheet. In the Bering Sea, daily tidal activity associated with frequent motion away from the coast keeps this process from occurring except in areas where coastal configuration affords unusual protection from one or both of these processes. The following locations are sited as examples:

1. The entrance to Port Clarence where contiguous ice bridges across a narrow inlet of water greater than 20 meters.

2. Eastward from Sledge Island past Nome where Sledge Island and associated shoals serve to anchor contiguous ice and allow it to extend beyond the 20-meter isobath. Large ridges have been formed off Nome on occasions further anchoring the ice in this location.

3. Inner Norton Sound where occasionally contiguous ice forming in the highly protected embayment south of Unalakleet extends over

water greater than 20 meters deep. This ice does not appear to become anchored and is broken off frequently.

4. The north side of Nunivak Island where it appears that protection from southward-moving floes offered by the island configuration allows a sheet of contiguous ice to extend beyond the 20-meter isobath.

(B.) Contiguous ice extends farther seaward with advance of season

Only one major example of this behavior was observed: Along the north side of the Yukon Delta, the early spring contiguous ice edge is located seaward of the winter ice edge. This appears to occur as a result of piling of ice moving into the Bering Sea from Norton Sound. Continual piling on shoals in this area appears to extend the ice edge seaward.

(C.) Contiguous ice located on shoals, extending far seaward but confirmed to waters less than 20 meters deep.

The major example of this behavior is found just south of the Yukon Delta where shoals as shallow as 8 meters appear to anchor contiguous ice as far as 30 km from shore.

(D.) Contiguous ice located on mudflats in rather shallow waters (3-4 meters)

Numerous examples of this behavioral pattern are to be found along the Bering coast. Apparently the tidal fluctuations accompanied by meteorological conditions causing frequent offshore winds cause these areas to be constantly flushed of contiguous ice. New ice is often observed forming just seaward of these locations. Perhaps the best example of this behavior can be seen just west of the mouth of the Kuskokwim River.

(E.) Contiguous ice found as large ridge systems.

This occurs occasionally along the north side of the Alaskan Peninsula where ice blown across Bristol Bay from north to south piles up along the peninsula shore in waters considerably less than 20 meters in depth. These ridge systems can be quite massive and form very quickly.

2. Bering Sea Hazards

(This map has not been compiled as of the date of this annual report.)

MILESTONE CHART

RU #: 257

PI: W. J. STringer

Major Milestones: Reporting, data management and other significant contractual requirements; periods of field work; workshops; etc.

MAJOR MILESTONES	1977						1978								
	O	N	D	J	F	M	A	M	J	J	A	S	O	N	D
Data acquisition	C	O	N	T	I	N	O	U	S						
Ground truth								▲							
"Special Event" map											▲				
Completion of ice edge maps											▲				
"Special Event" maps											▲				
Completion of ridge systems maps											▲				
Completion of hazards maps														▲	
Completion of morphology maps														▲	
Completion of final report															▲

123

△ Planned Completion Date

▲ Actual Completion Date

IX. Summary of Fourth Quarter Operations

A. Ship or Laboratory Activity

1. Ship or field trip schedule - none.
2. Scientific party - none.
3. Methods: Sea ice maps prepared from Landsat imagery by overlaying 1:500,000 scale black and white Landsat print with acetate and tracing ice boundaries. The details of this method were described in earlier quarterly reports.

4. Sample localities - none.

5. Data collected or analyzed: This quarter the 1976-77 Beaufort Sea near shore Landsat data was mapped from hardcopy band 7 imagery at 1:500,000 scale. Particular care, described in earlier reports, has been taken to locate ice features as well as the bathymetric 10-fathom isobath. Half-size (1:1 million scale) reproductions of these maps are reproduced as part of this section of the report as Appendix A.

6. Milestone Chart and data submission schedules (see next page). We have changed the completion date for completion of data products related to the previous year. There are two reasons for this: First, it now takes nearly four months to obtain Landsat data; second, we have found it highly advantageous to analyze an entire year's imagery at one time. Hence, in order to analyze the 1977 ice data for the Beaufort Sea, it was December before the data for July and August could be obtained. The resulting maps are included in this report.

B. Problems Encountered/Recommended Changes

We recommend that side-looking radar data of near shore ice conditions be obtained in the Beaufort Sea during November, December and January and that disciplinary scientists from this and other research units be on hand at Barrow to establish quality control, coverage and related parameters.

C. Estimate of Funds Expended

See Geophysical Institute Business Office Financial Report.

APPENDIX A

BEAUFORT SEA ICE MAPS FOR 1977 ICE SYMBOLS USED AND THEIR MEANING

Listed below are the symbols used to map near shore ice conditions from LANDSAT imagery. This list of symbols has evolved during the mapping project and reflects ice conditions which can be detected on LANDSAT imagery as well as those ice conditions considered important in the understanding of near shore ice dynamics.

A	River Overflow	Used to denote areas where river water has overflowed onto sea ice.
B	Boundary	Denotes boundary between what appears to be two different ice conditions even though the two ice conditions may not be differentiated by the definitions used.
Bn	Broken New Ice	Sheet of new ice which has been broken - usually into an irregular pattern.
Bpn	Broken Pans and New Ice	A sheet of young or first year ice is broken into pans followed by the freezing of the voids to the new ice stage, followed by the breaking of this entire matrix. Several cycles of this process may be evident, but the most recently-formed ice has developed to the new ice stage.
Bpy	Broken Pans and Young Ice	A sheet of young or first year ice is broken into pans followed by the freezing of the voids to the young ice stage followed by the breaking of this entire matrix. Several cycles of this process may be evident, but the most recently-formed ice has developed to the young ice stage.
By	Broken Young Ice	Sheet of young ice which has been broken - usually into an irregular pattern.
C	Contiguous Ice	Ice stationary and continuous from shore without apparent fractures. This ice is at the time of observation fast with respect to the shore. The symbol is placed within large expanses of such ice and along the landward side of the seaward edge of such ice. Contiguous ice is not necessarily bounded on the seaward edge by grounded ice and can therefore extend seaward considerable distances.

X List of References

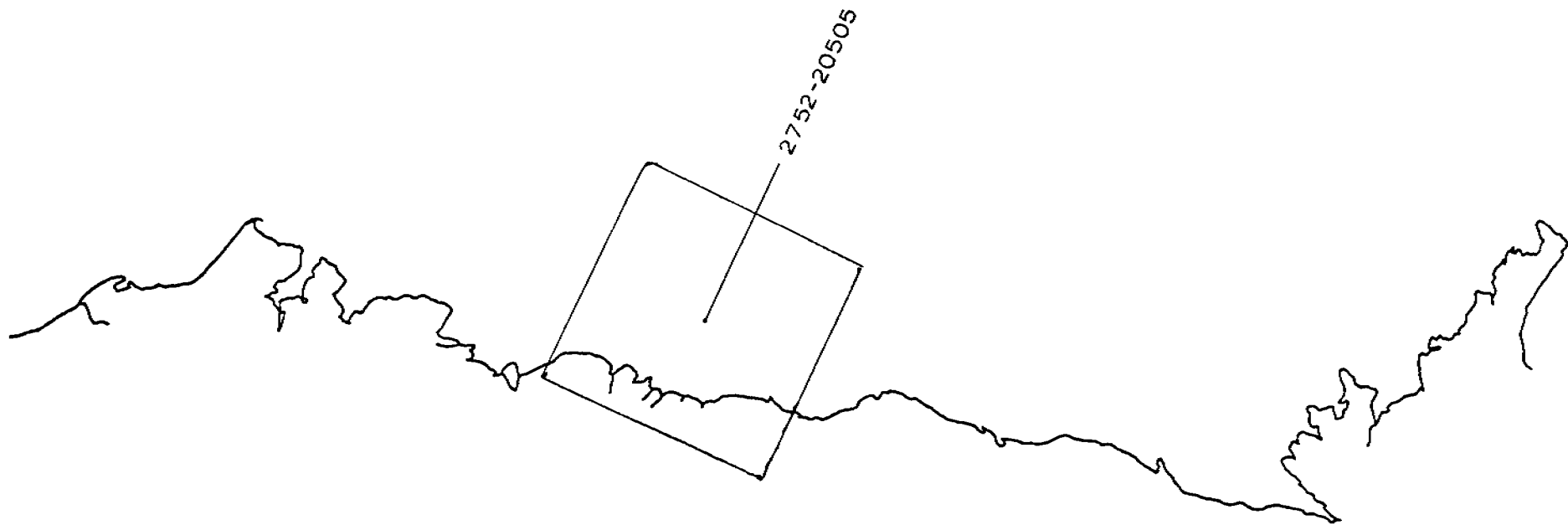
No direct references to other publications are made in this report. This is largely because of the original nature of this statistical analysis. However, use was made of the following publications:

- Ahlnas, K., and G. Wendler, Arctic sea-ice conditions in early spring viewed by satellite, Arctic and Alpine Research, Vol. 9, no. 1, p. 61-72, 1977.
- Fryer, M., Planning marine structure for Alaska's arctic regions, Northern Engineer, 2, p. 17, 1970.
- Kovacs, A., and M. Mellor, Sea ice morphology and ice as a geologic agent in the southern Beaufort Sea, Proceedings of the Symposium on Beaufort Sea Coast and Shelf Research, Arctic Institute of North America, 1974.
- Kovas, Austin, and Anthony J. Gow, Some characteristics of grounded floebergs near Prudhoe Bay, Alaska, CRREL REport 76-34, prepared for NOAA, Sept. 1976.
- Kovacs, Austin, Grounded ice in the fast ice zone along the Beaufort Sea coast of Alaska, CRREL Report 76-32, prepared for NOAA, September 1976.
- Kovacs, A., A. J. Gow, and W. F. Dehn, Islands of grounded sea ice, CRREL Report 76-4.
- Kovacs, Austin, Sea ice thickness rprofiling and under ice oil entrapment, 9th Annual Offshore Technology Conference, Houston, Texas, May 1977.
- Nelson, Richard K., Hunters of the Northern Ice, University of Chicago, Press, 1969.
- Reimnitz, E., and P. W. Barnes, Studies of the inner shelf and coastal sedimentation environment of the Beaufort Sea from ERTS-1, NASA Report no. NASA-CR-132240, p. 3, 1973.
- Reimnitz, Erk, Larry Toimil, and Peter Barnes, Development of the Stamukhi zone and its relationship to arctic shelf processes and morphology, Beaufort Sea, Alaska, U. S. Geological Survey, Menlo Park, California, 1976.
- Searby, Harold W., and Marcelle Hunter, Climate of the north slope Alaska, U. S. Department of Commerce, NOAA, National Weather Service, February 1971.
- Seifert, Richard D., The structure of shorefast ice off the north slope of Alaska, M. S. Theses, University of Alaska, May 1973.
- Shapiro, Lewis H. and John J. Burns, Satellite observations of sea ice movement in the BERING Strait region, preprint, 1975.
- Stringer, W. J., Shorefast ice in vicinity of Harrison Bay, Northern Engineer 5, no. 4, 1974.
- Stringer, W. J., The morphology of Beaufort Sea shorefast ice, Proceedings of the Arctic Institute of North America, December 1974.
- Weeks, W. F., Sea ice conditions in the arctic, AIDJEX Bulletin no. 34, Div. of Marine Resources, University of Washington, December 1976.

Cf	Fractured Contiguous Ice	Contiguous ice which although not separated from shore by an open lead, is fractured by leads - often perpendicular to the shore.
D	Decayed Ice	Rotting or decaying ice, characterized by a dark mottled effect indicating holes and puddling.
F	Floe	Separately identifiable ice floe. Symbol used to denote floes distinctly visible against background even when completely frozen into surrounding ice.
Fw	Floes in Water	Open water with numerous floes of various sizes (see "Up").
Fy	First Year Ice	Ice cover of age and thickness beyond "young" stage. Used principally to denote large expanses of ice in either contiguous or off-shore category. May be composed of single sheet, many pans frozen together, or many pans frozen together, or many pans compressed and frozen together. Thickness on the order of 30-70 cm.
Fyb	First Year Broken	A broken or fragmented expanse of first year ice.
G	Grounded	Ice which clearly appears to be grounded.
H	Hummock Field	Large expanses of piled ice.
I	Young Ice	Ice appearing light grey on LANDSAT imagery. Can be single sheet or exhibit a variety of conditions (broken, compressed, rafted, etc.). Thickness of the order of 10-30 cm.
L	Lead	A lead, usually open, but may be so narrow that this can not be determined. Large leads denoted by two lines showing boundaries, narrow leads denoted by single line.
M	New Ice	Characterized by dark shade of grey, smooth texture, may exhibit a number of conditions (see I). Thickness on the order of 0-10 cm.
N	Newly Frozen Lead or Polyna	Either new or young ice. Symbol usually written within distinct boundary.
O	Old Frozen Lead	A lead with ice sufficiently old to have either turned light grey or be covered

with snow.

P	Partly Frozen Lead	Partly frozen lead. Ice conditions not uniform (as distinct from M) and may vary from new ice to late stages of young ice.
Pn	Pans in Matrix of New Ice	A sheet of ice has broken into pans and the surrounding water has frozen to the new ice stage.
Py	Pans in Matrix of Young Ice	A sheet of ice has broken into pans and the surrounding water has frozen to the young ice stage.
R	Ridge	Denotes shear or pressure ridge or system of ridges.
S	Smooth Ice	Usually used to denote featureless ice of uncertain age in protected areas.
T	Tidal or Tension Cracks	Cracks in near shore ice opened by either tidal action or thermal tension. Identification may be indirect (snow drifts, drainage pattern, etc.).
Up	Unconsolidated Pack	A broken sheet of ice of any age beyond young ice which has been compressed to the point that open water voids are quite small but are not frozen over (see Fw).
W	Water	Open water - symbol often used to denote specific area enclosed by line.
Y	Polynya	More specific than W. Most often used to denote area of open water on lee side of obstruction.
Z	Zone of Shear	Symbol used to denote location of apparent shearing motion on image. The symbol may be specifically located on a lead where shearing motion is taking place, a closed lead where shear piling of ice is apparently occurring or in an ice field where characteristic pattern of leads caused by shearing forces can be seen.

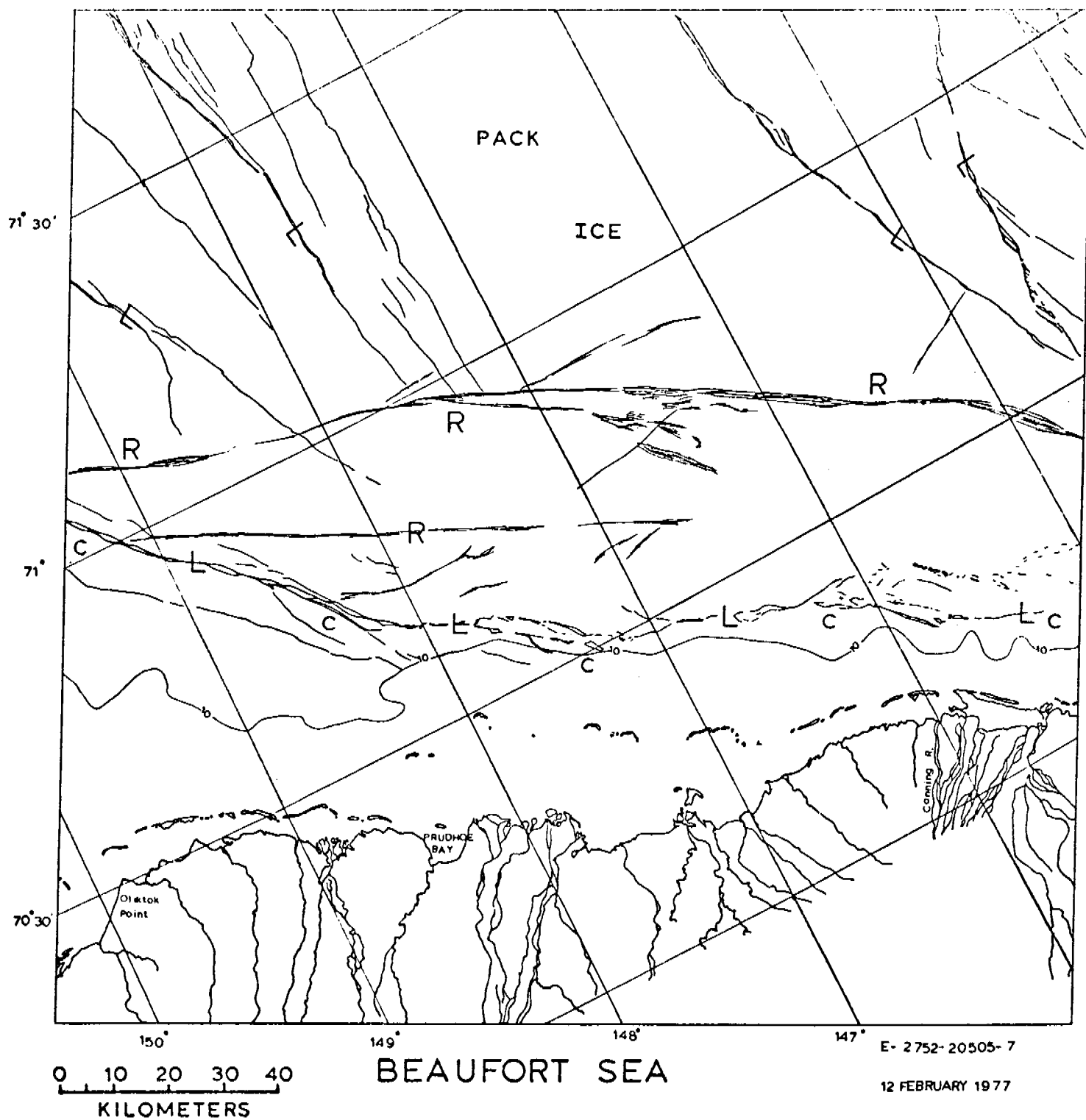


2752-20505

BEAUFORT SEA

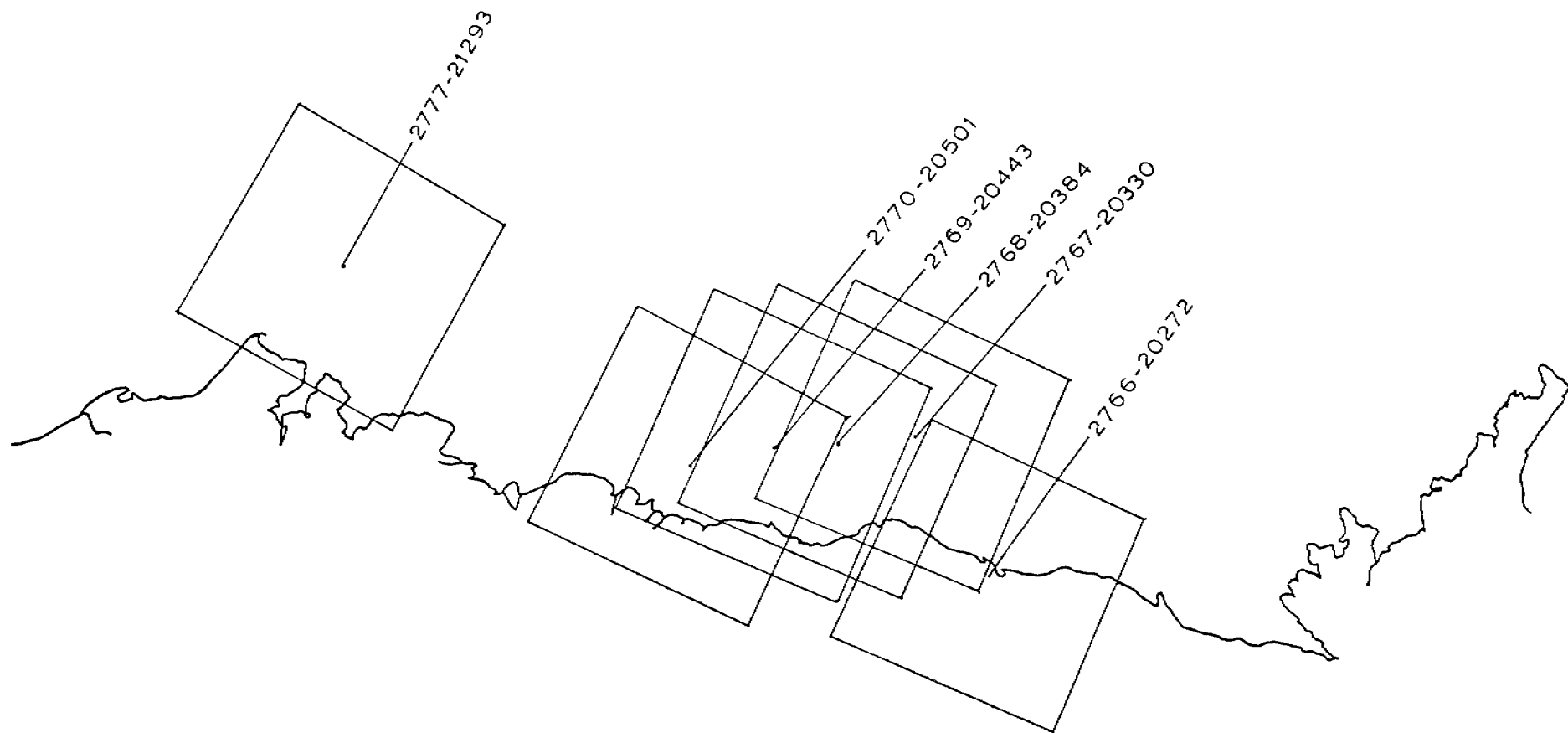
1-18 FEBRUARY 1977

CYCLE 2741-2758



Scene 2752-20505 (12 February 1977)

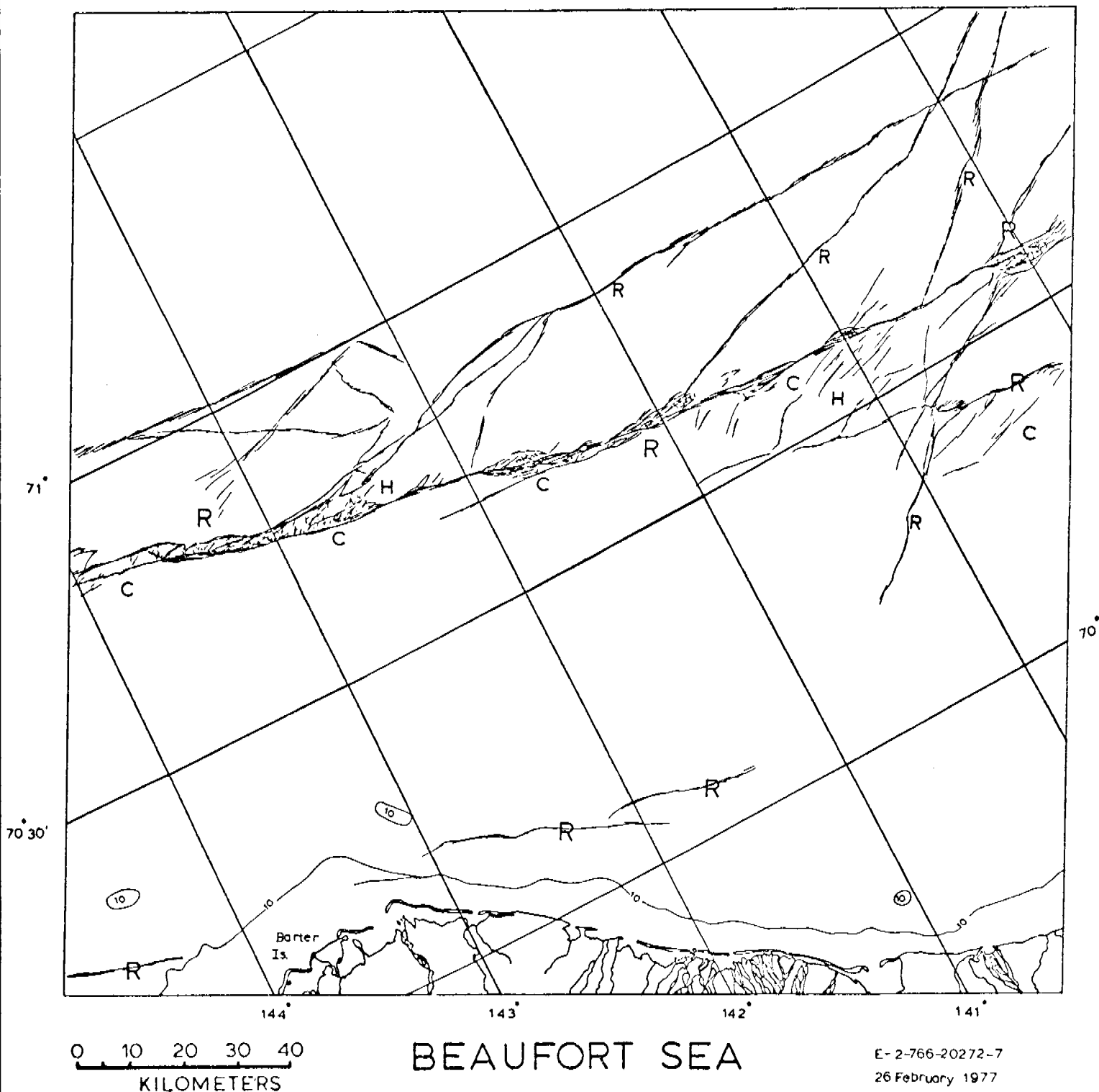
A large ridge system extends from right to left across the center of the image. This ridge system has been in existence for some time as is evidenced by its relatively low contrast with respect to the pack ice and by the existence of several breaks and displacements in the ridge system. The boundary of the most recent movement is a lead system approximately 35 km off shore. The pack ice has moved from left to right (northwest to southeast) with respect to the coastline. This lead system marks the edge of contiguous ice. No detail is visible in the contiguous due to a very thin cloud cover and poor image quality.



BEAUFORT SEA

19 FEBRUARY - 8 MARCH 1977

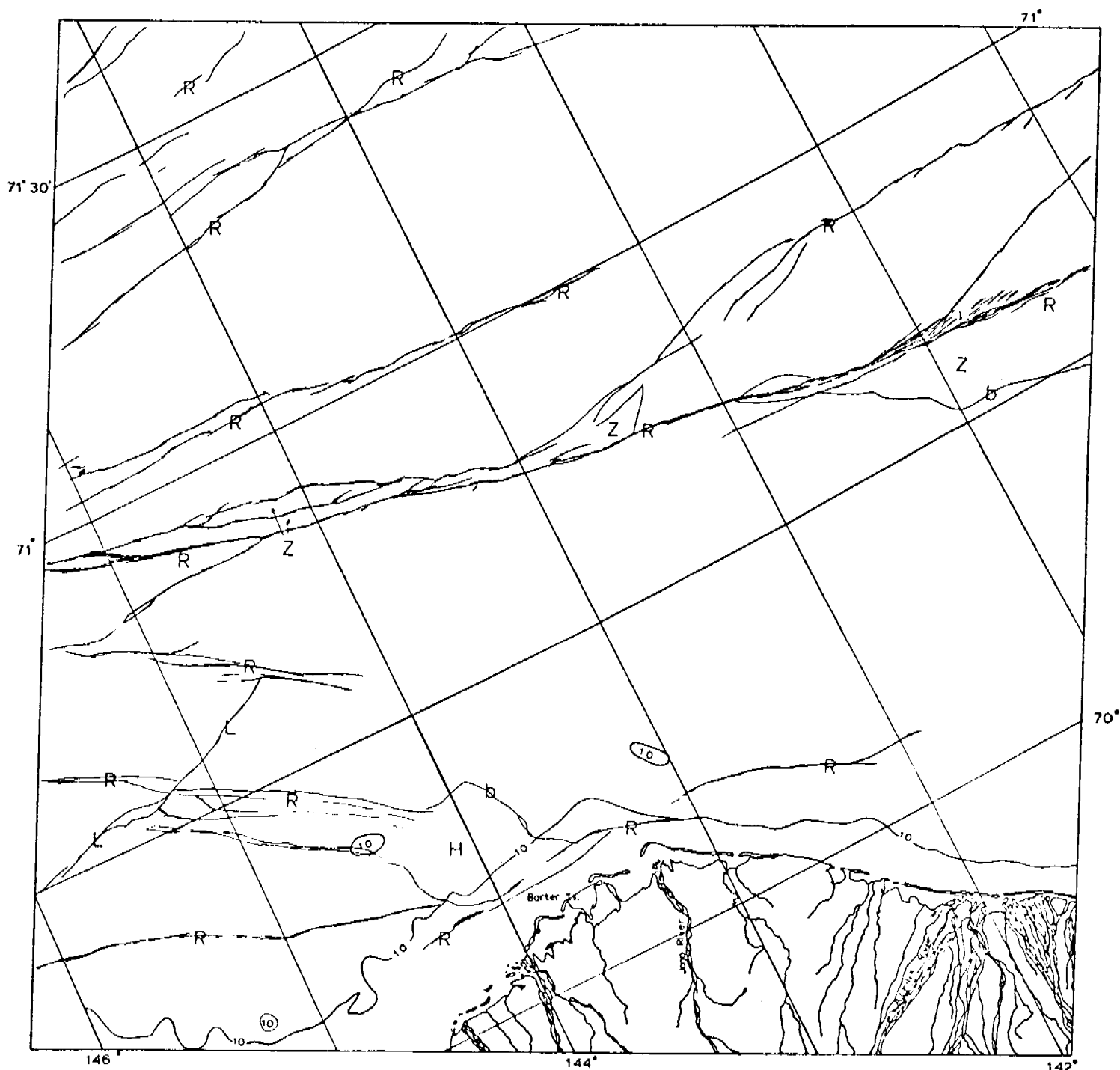
CYCLE 2759-2776



Scene 2766-20272 (26 February 1977)

A large, apparently still active ridge system extends across the image from east to west. The pack ice motion north of the ridge system is moving from west to east. This ridge system forms the edge of contiguous ice, approximately 80 km offshore. There appears to be another ridge system a few kilometers offshore but its extent is obscured by clouds and only parts of it can be seen.

The pack ice north of the large ridge system has undergone much piling, ridging and fracturing, with many ridge systems subordinate to the major one. South of this large system the ice appears to be somewhat less disturbed, but is obscured by clouds and details cannot be seen.



0 10 20 30 40
KILOMETERS

BEAUFORT SEA

E-2-767-20330-7
27 FEBRUARY 1977

Scene 2767-20330 (27 February 1977)

As in the previous days' image, a large ridge system extends approximately east-west across the center of the image. The system appears to be recently active and probably forms the edge of contiguous ice. Large zones of shearing are visible between various ridges in the system. Older ridge systems can be seen nearer to shore. One of these is cut by a refrozen lead (lower left corner of image). An area of what appears to be hummocked and piled ice exists just north of Barter Island.

The ice north of the large, recent ridge system is multiply fractured, piled and ridged. All of the lines on the map represent ridges or ridge systems.

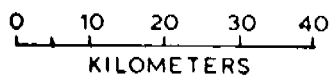
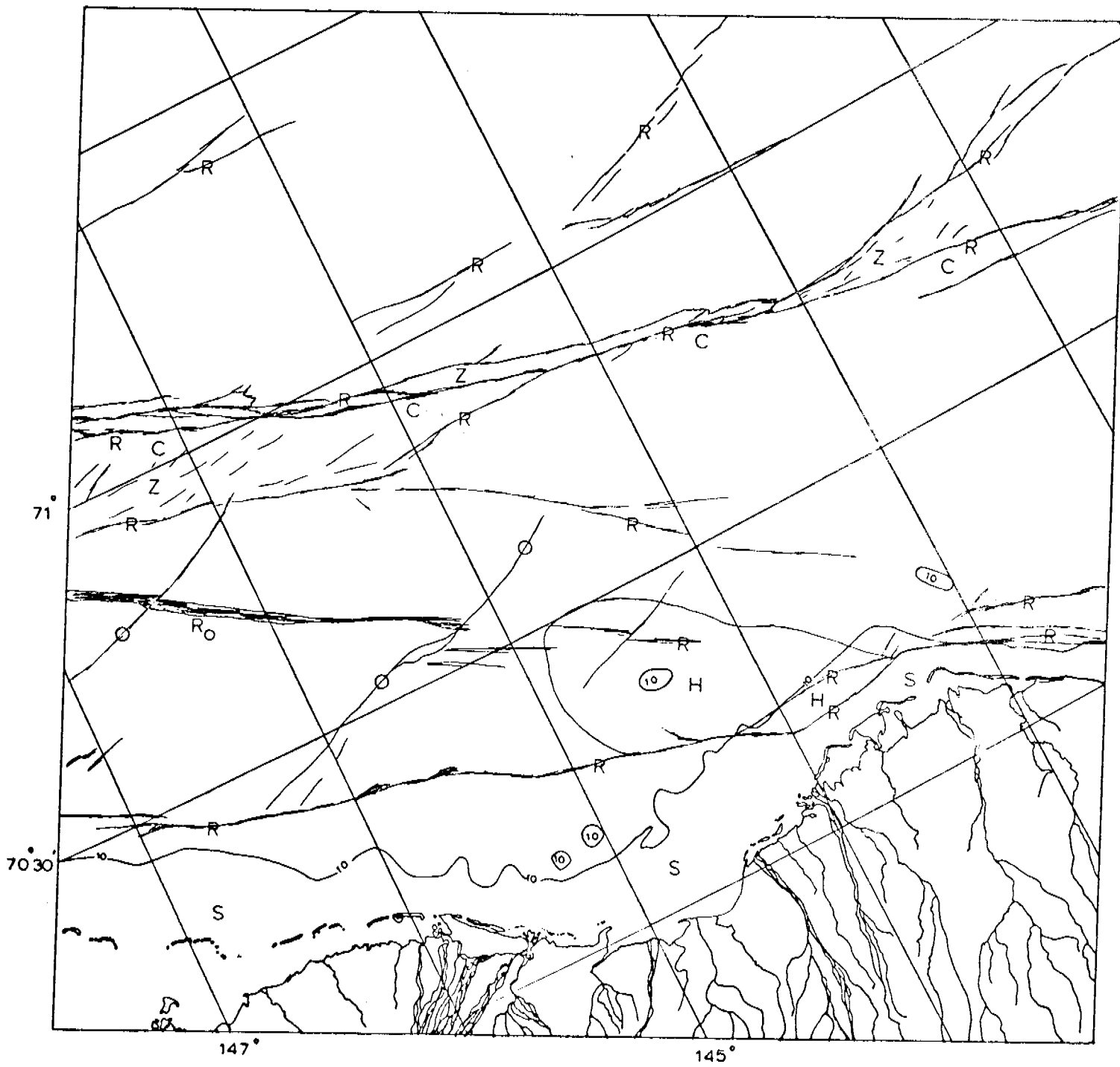
Scene 2768-29384 (28 February 1977)

The large ridge system seen in previous images extends across the upper part of the image. Zones of shear, labeled 'Z', can be seen between subordinate ridges and ridge systems of the larger system. The system is still active on this date and its landward edge probably forms the edge of contiguous ice. The pack ice seaward of this major ridge system is fractured, piled and ridged.

Shoreward of the large ridge system several smaller ridge systems of varying age can be seen. An old ridge system, labeled 'Ro', can be seen approximately 60 km north of the barrier islands in the western half of the image. Several old refrozen leads, labeled 'O', have cut across and displaced sections of the ridge system.

A large area of hummocked ice exists north of Barter Island. This area appears to have been a zone of shear when ridge system Ro was active, although it may have been active more recently.

Relatively smooth ice occupies the area between shore and the most shoreward ridge system, which approximates the 10-fathom (20-meter) bathymetric contour. This area, labeled 'S', has probably seen little activity since freeze-up.

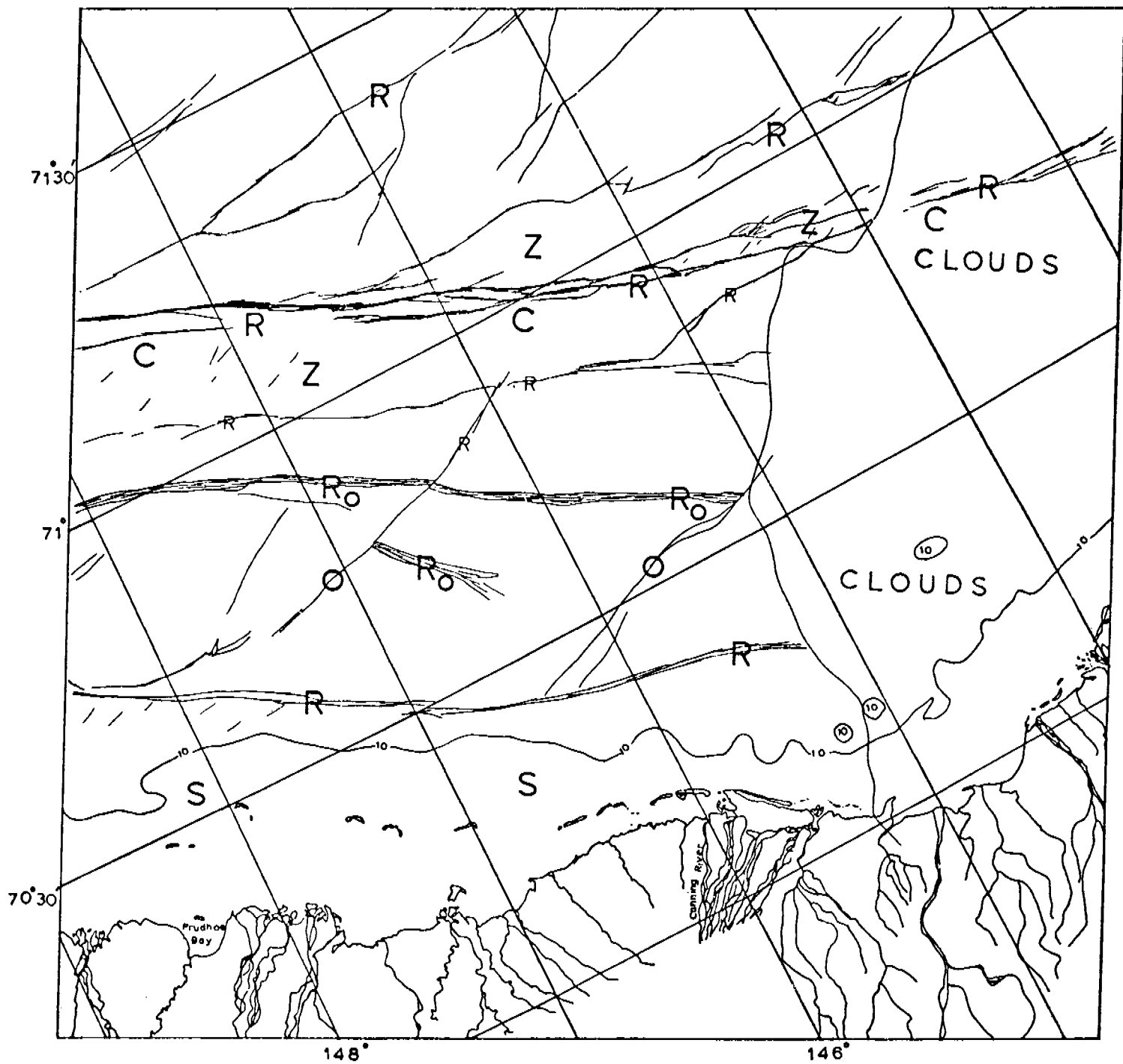


BEAUFORT SEA

E 2-768-20384-7
28 FEBRUARY 1977

Scene 2769-20443 (1 March 1977)

The active ridge system observed in the previous days' images can be seen extending across the top part of the scene. The edge of contiguous ice is the landward edge of the ridge system, but a broad shear zone (labeled 'Z') exists shoreward of the ridge system and the exact boundary of the contiguous ice can not be delineated. Clouds obscure the eastern portion of the image.



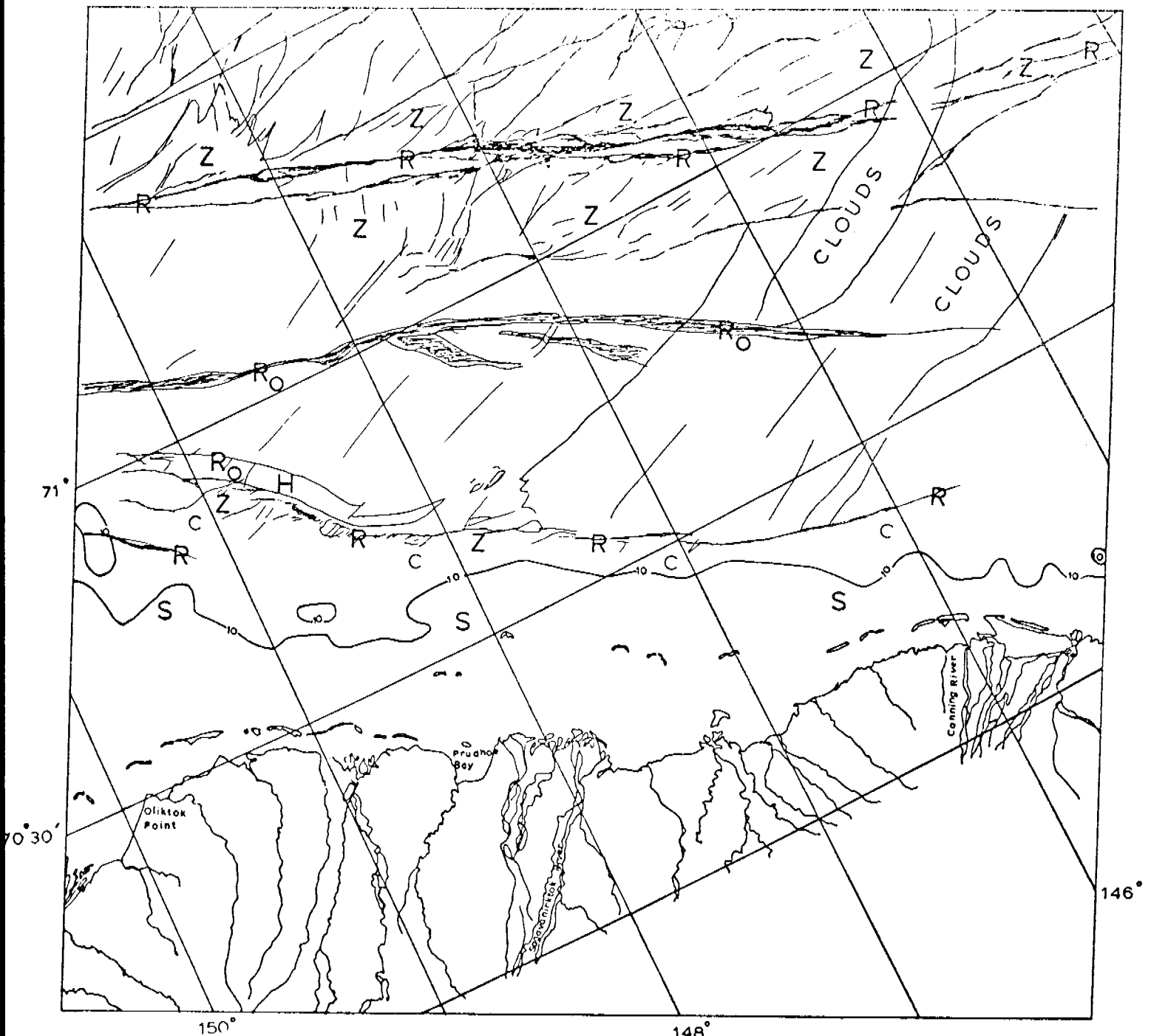
BEAUFORT SEA

E 2-769-20443-7
01 March 1977

Scene 2770-20501 (2 March 1977)

This scene extends from the Canning River to Oliktok Point. The large ridge system noted on previous images still appears to be active at this time. A large shear zone exists on either side of the ridge system. The orientations of the fractures in the shear zones are predominantly northeast-southwest, indicating pack-ice motion from east to west.

The edge of contiguous ice appears to be shoreward of a smaller ridge system just seaward of the 10-fathom bathymetric contour. The ice shoreward of the contiguous ice edge appears smooth.



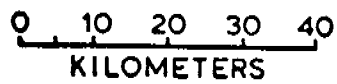
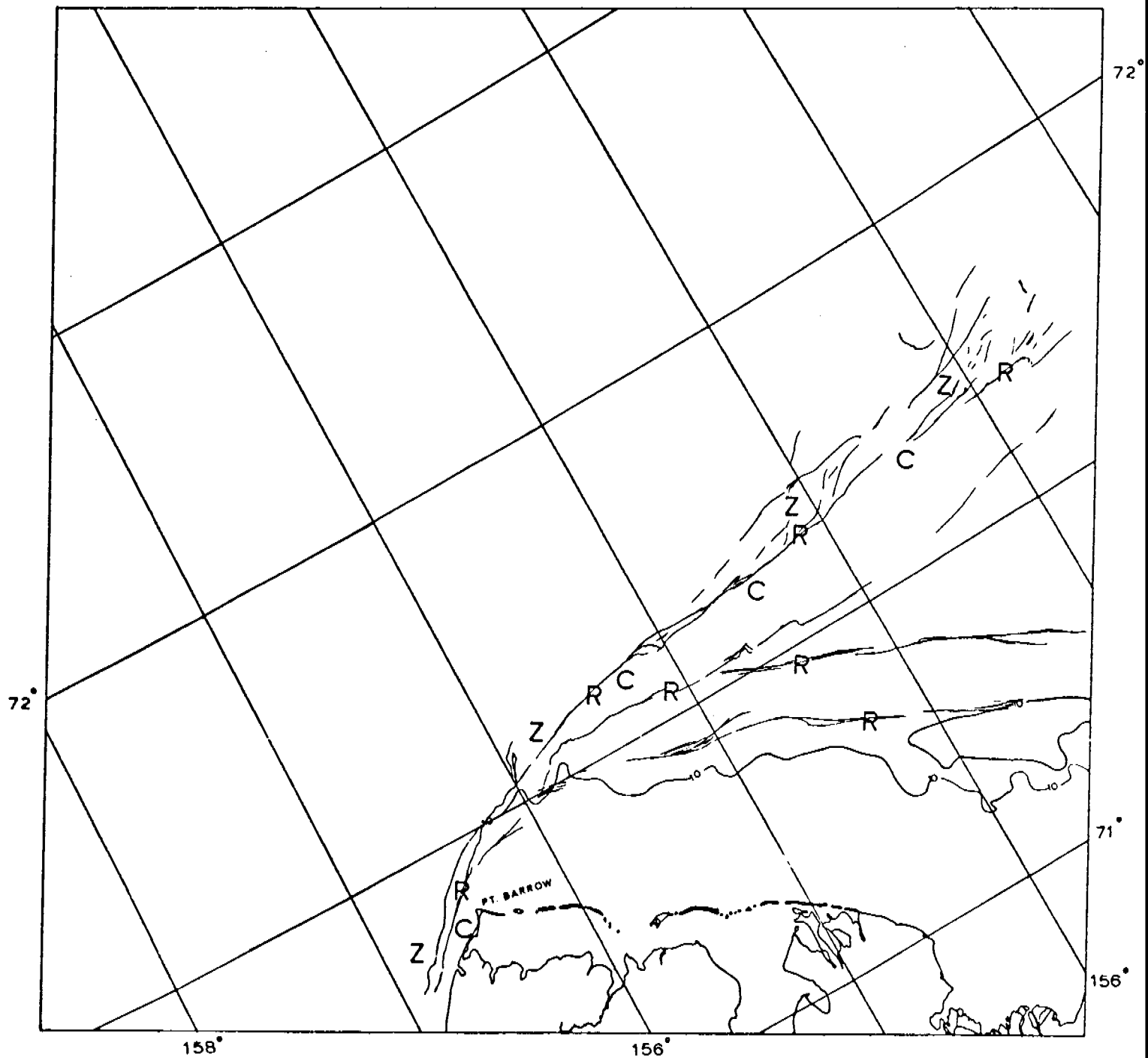
0 10 20 30 40
KILOMETERS

BEAUFORT SEA

E-2-770-20501-7
02 MARCH 1977

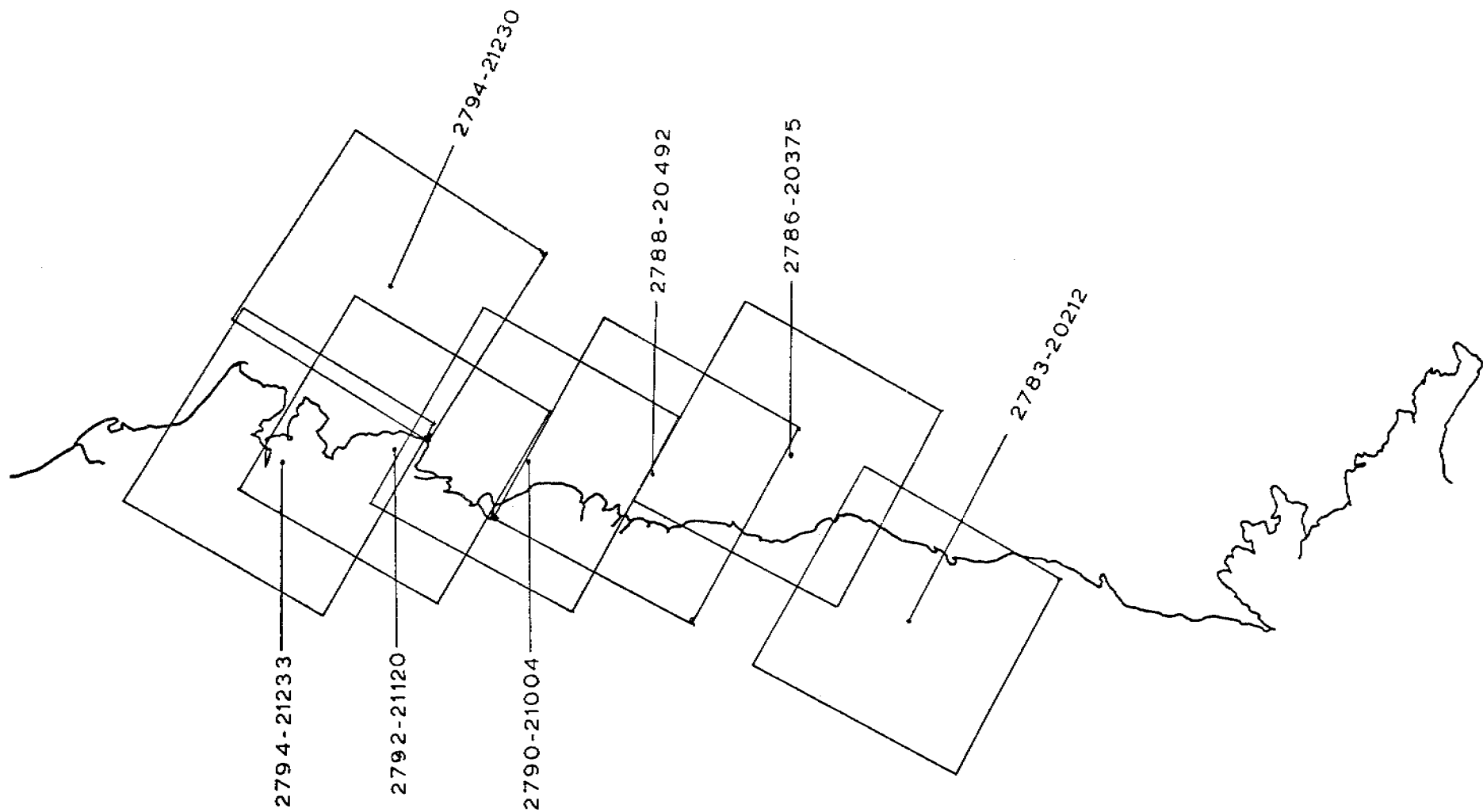
Scene 2777-21293 (9 March 1977)

This scene shows the effect of pack ice moving southwest past Point Barrow. A narrow zone of shear separates the immobile contiguous ice from the moving pack ice. A narrow ridge system can be seen on the shoreward side of the shear zone. Other older ridge systems can be seen inshore of the active ridge system. The ice between the 10-fathom bathymetric contour and the shore appears relatively smooth with respect to the pack ice.



BEAUFORT SEA

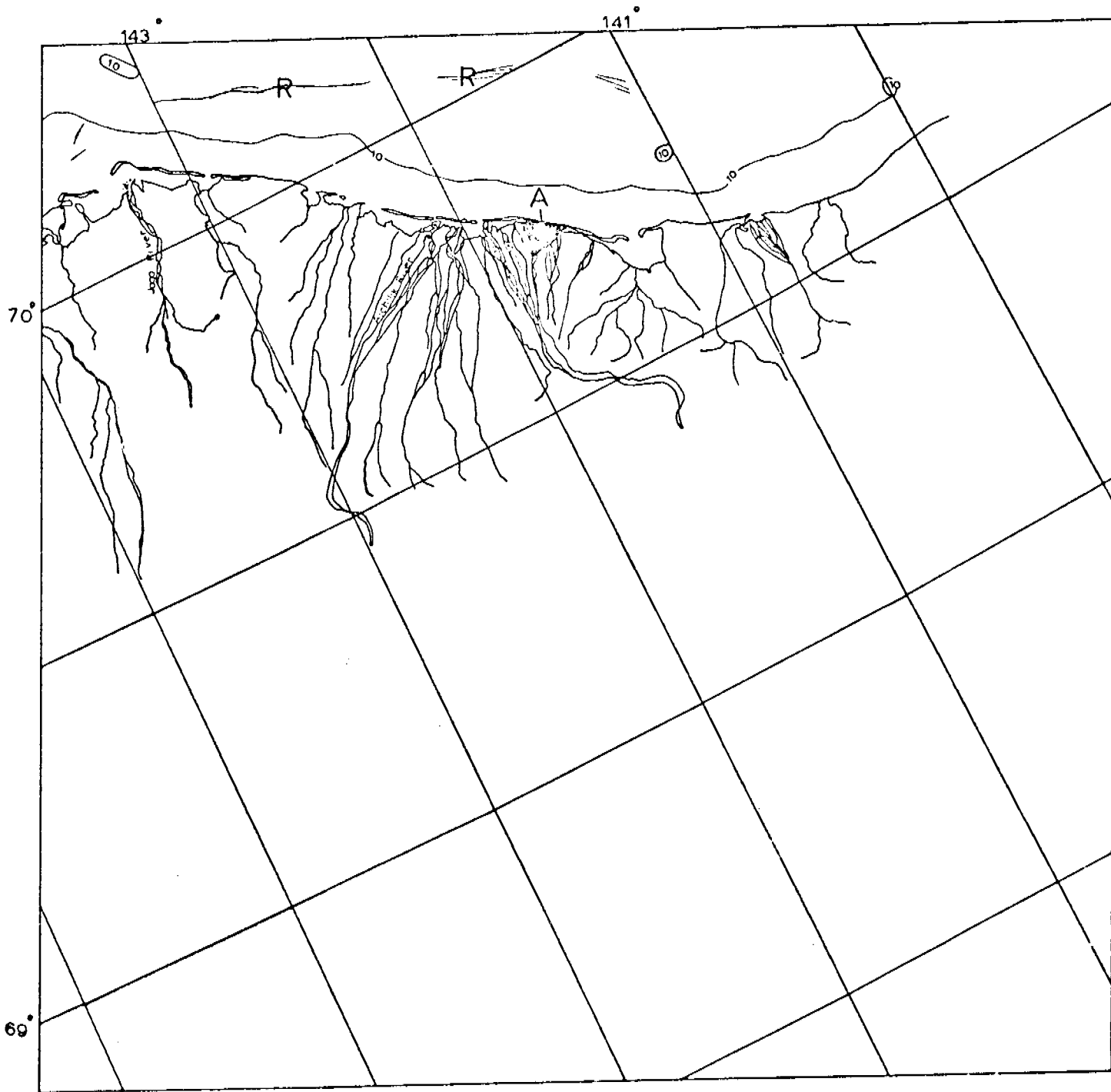
E-2-777-21293-7
09 MARCH 1977



BEAUFORT SEA
9-26 MARCH 1977
CYCLE 2777-2794

Scene 2783-20212 (15 March 1977)

This scene shows a narrow strip of nearshore ice east of Barter Island. The contrast on the ice is very low and consequently very few details are visible. Parts of ridge systems can be seen. River overflow A can be seen on one of the rivers, emptying into a barrier island lagoon. The edge of contiguous ice is beyond the edge of the image.



BEAUFORT SEA

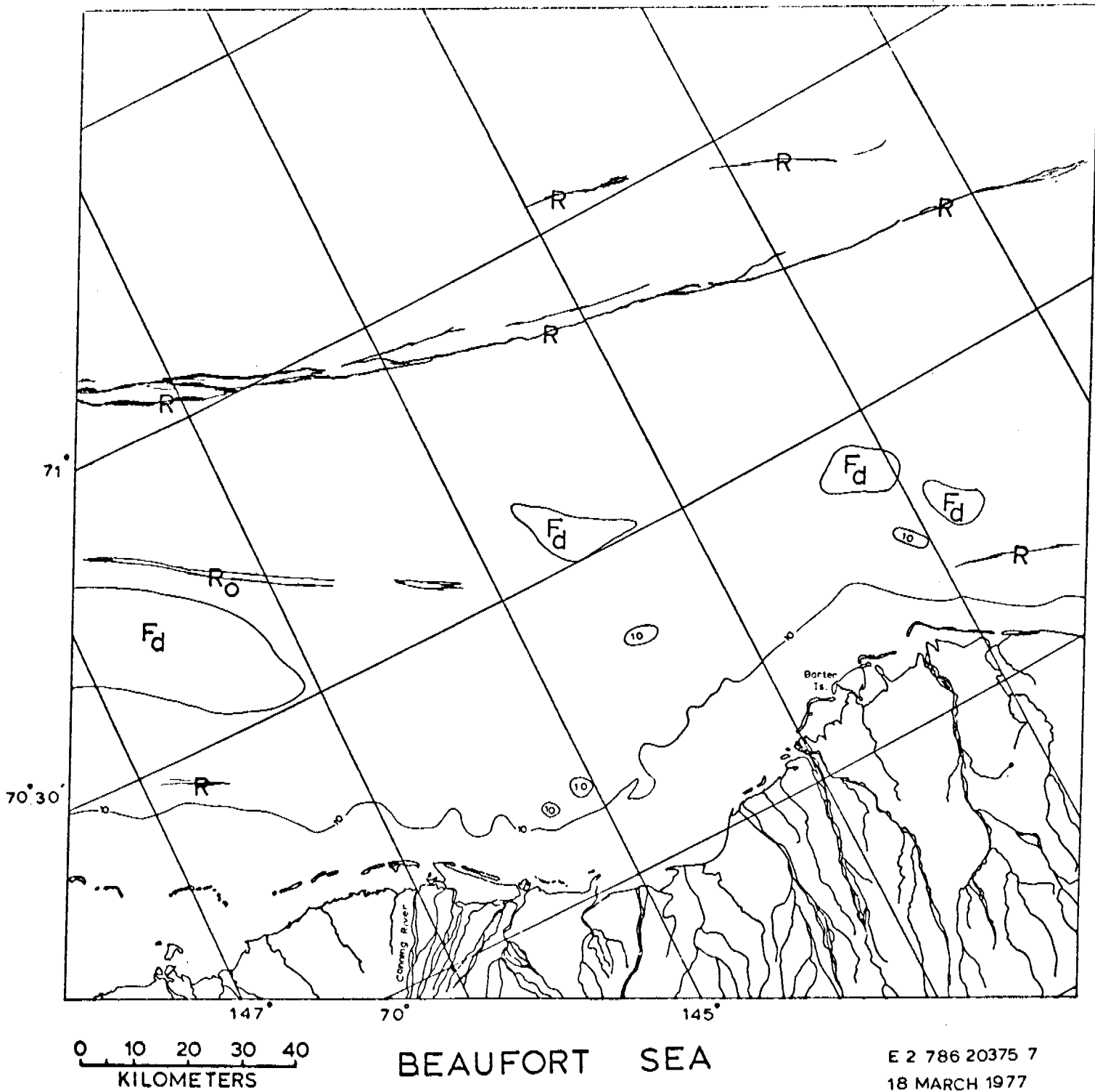
E-2-783-20212-7
15 MARCH 1977

Scene 2786-20375 (18 March 1977)

This scene is mostly obscured by thin clouds and very little detail can be seen. The large ridge system that was active in late February-early March is now apparently inactive. If the large ridge system is inactive, then the edge of contiguous ice extends past the edges of the image.

Short sections of other ridge systems can be seen through the clouds. Little other detail is visible. Dark splotches can be seen on the ice in the lower half of the image but it is unclear whether these are characteristics of the ice or simply cloud shadows so they were not mapped.

Large areas of nearshore pack ice appears to have a significant percentage of dirty ice floes incorporated into it. The areas are labeled 'Fd'.

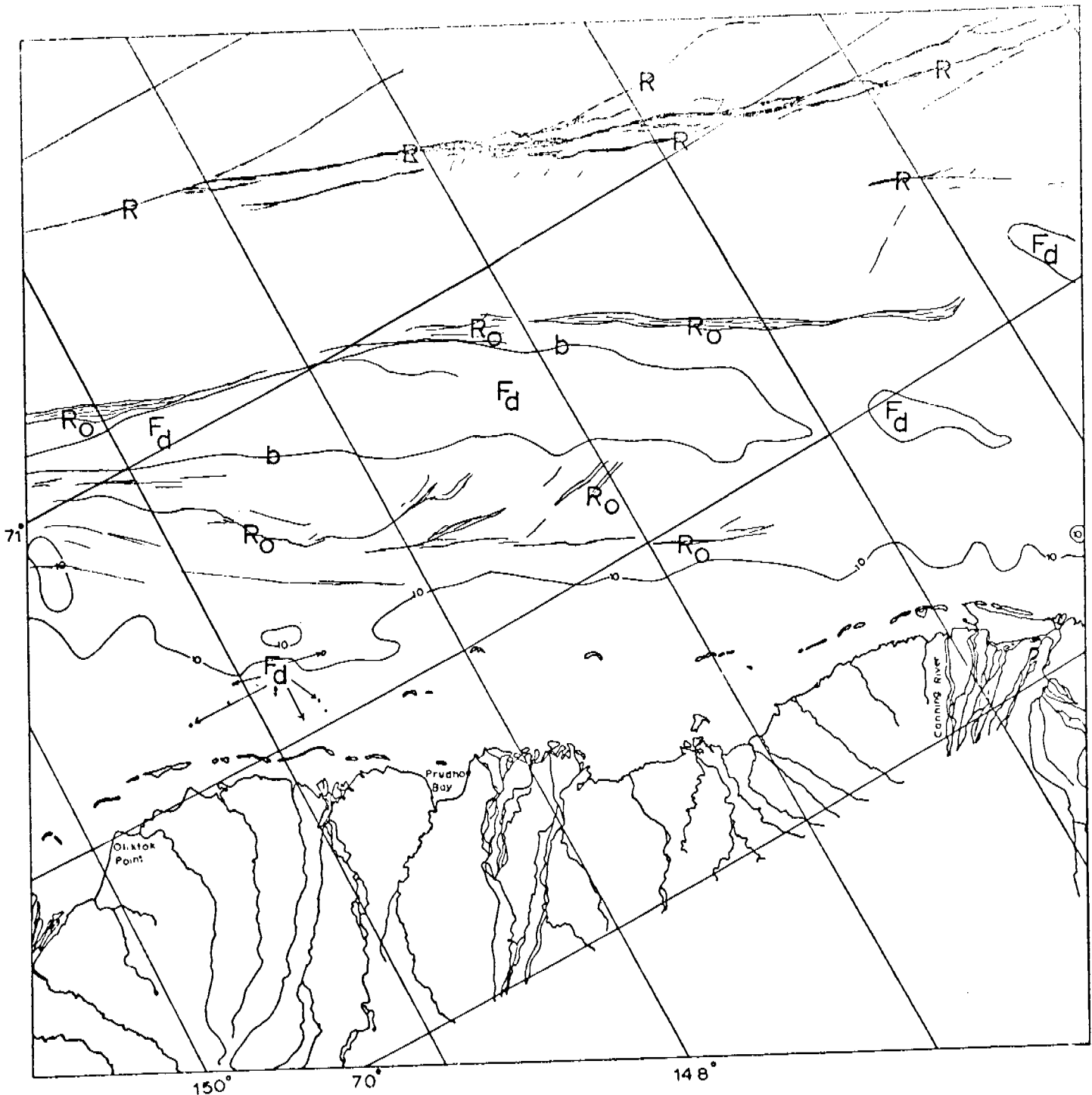


BEAUFORT SEA

E 2 786 20375 7
18 MARCH 1977

Scene 2788-29493 (20 March 1977)

This scene extends from the Canning River to Oliktok Point and approximately 100 kilometers offshore. The large, recently active ridge system is visible in the top of the image. Other older ridge systems are also visible. Large areas of pack ice appear to contain "dirty" ice floes (Fd). Individual dark-colored "dirty" ice floes are indicated by arrows. The ice surface inshore of the 10-fathom bathymetric contour appears relatively smooth. The contiguous ice edge extends beyond the edge of the image since the ridge system is no longer active.

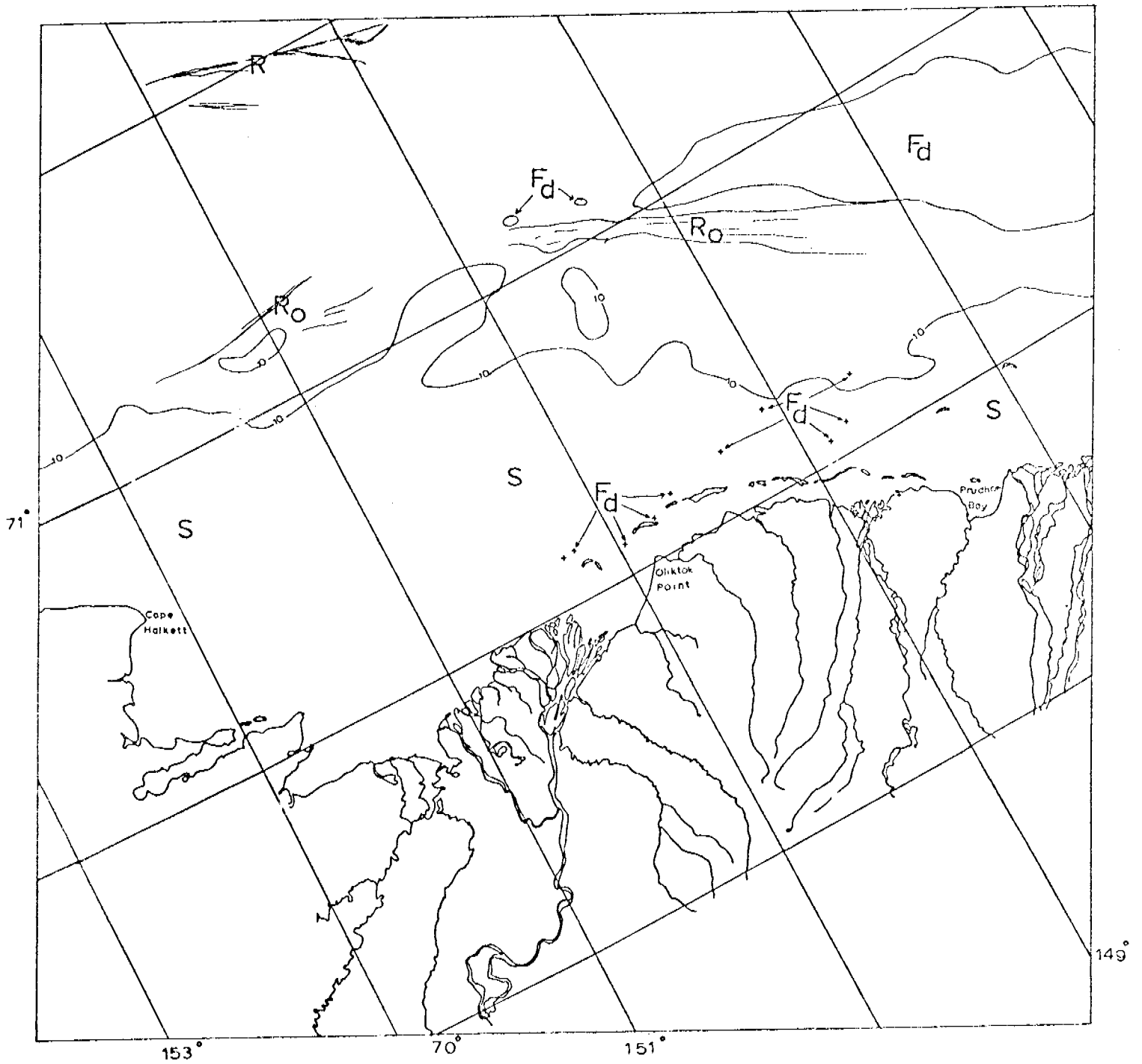


BEAUFORT SEA

E-2-788-20492-7
20 MARCH 1977

Scene 2790-21004 (22 March 1977)

This scene, extending from Prudhoe Bay to Cape Halkett, is partially obscured by clouds, primarily in the northern part of the image over the pack ice. The clouds obscure all but a few sections of the ridge systems. Areas of pack ice containing dirty ice floes can be seen. Individual dirty floes near shore are indicated by '+' marks. The nearshore ice from shore to the 10-fathom bathymetric contour is relatively smooth. The contiguous ice edge extends beyond the limits of the image.



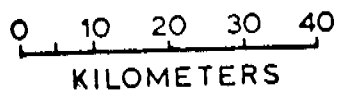
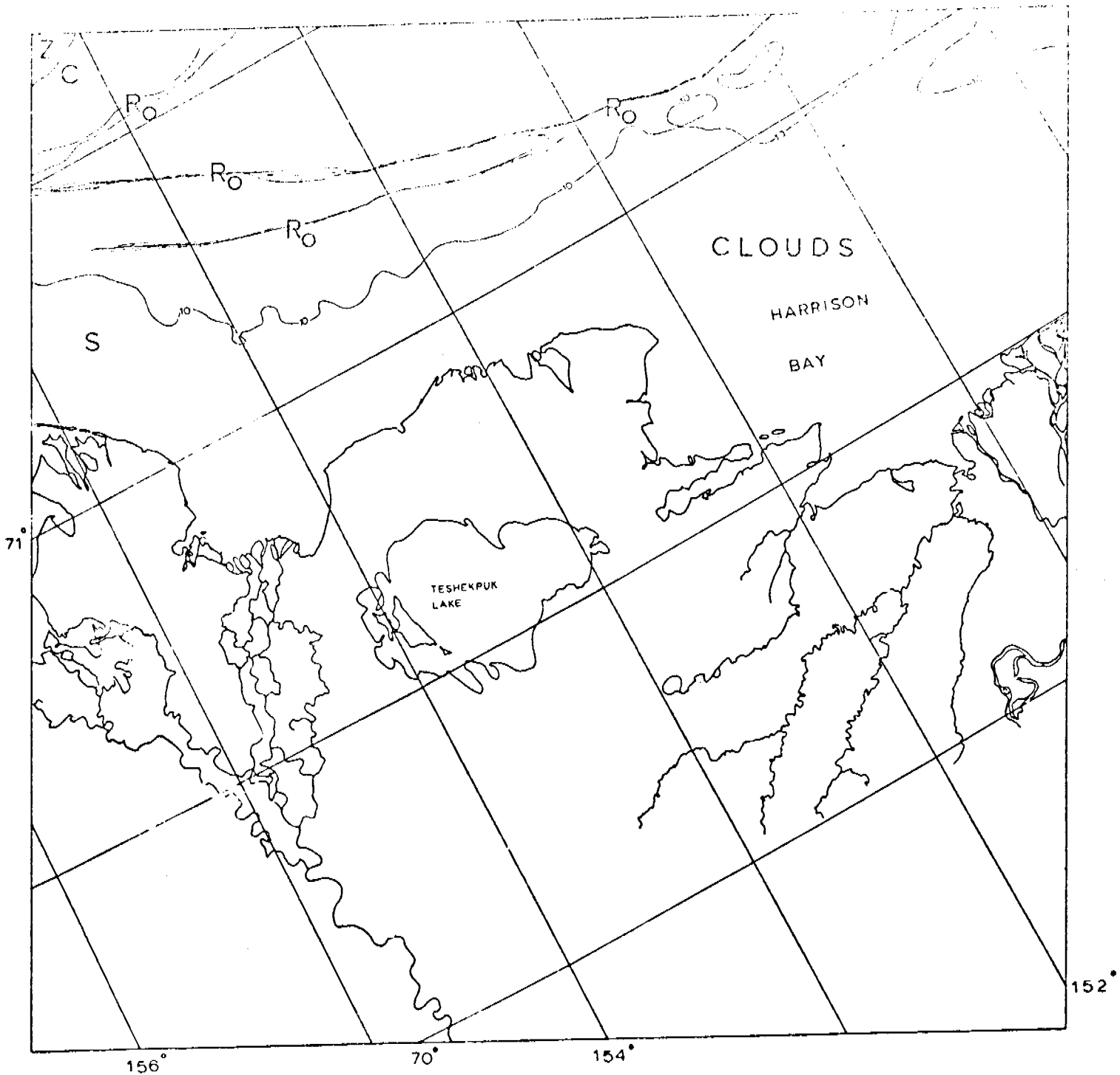
0 10 20 30 40
KILOMETERS

BEAUFORT SEA

E-2-790-21004-7
22 MARCH 1977

Scene 2792-21120 (24 March 1977)

This scene, extending from Harrison Bay to Admiralty Bay, is largely obscured by clouds. The area of Harrison Bay is totally obscured while ridge systems can be seen through the clouds west of Harrison Bay. The nearshore ice appears relatively smooth. In the extreme upper left corner of the image the boundary between the contiguous ice and the pack ice can be seen. The pack ice appears to be undergoing a shearing motion.



BEAUFORT SEA

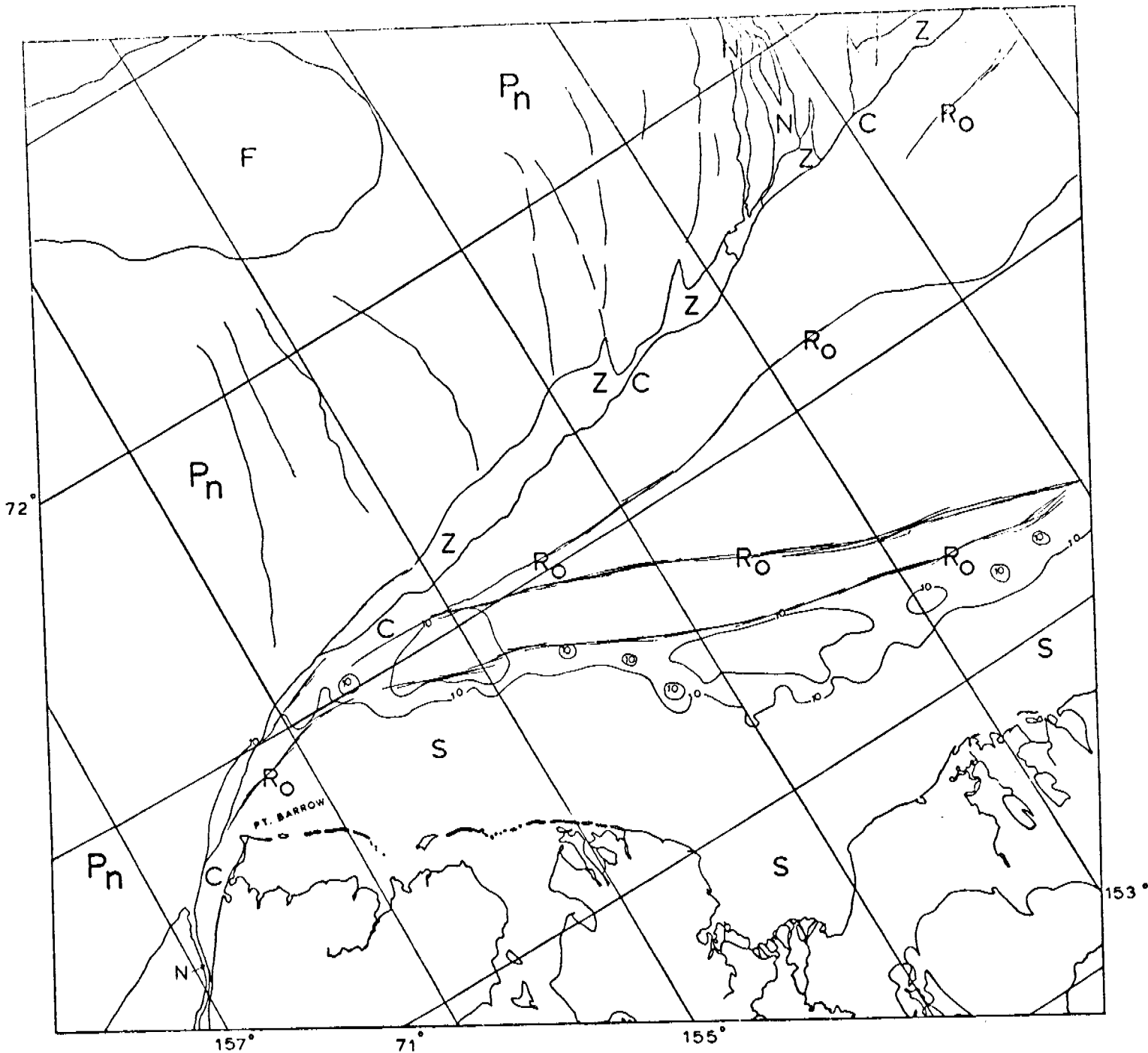
E 2-792-21120-7
24 MARCH 1977

Scene 2794-21230 (26 March 1977)
2794-21233

These scenes in the vicinity of Point Barrow show the result of pack ice moving southwest past Barrow. The pack ice is fractured and broken with the interstitial areas frozen over with new ice. Concentric fracture lines indicate the direction of motion. A large floe exists in the pack ice to the north.

Separating the pack ice from the contiguous ice is a narrow zone of shearing that narrows as it nears Pt. Barrow. South of Barrow the shear zone is replaced by a newly refrozen lead, indicating that the pack ice is moving away from shore.

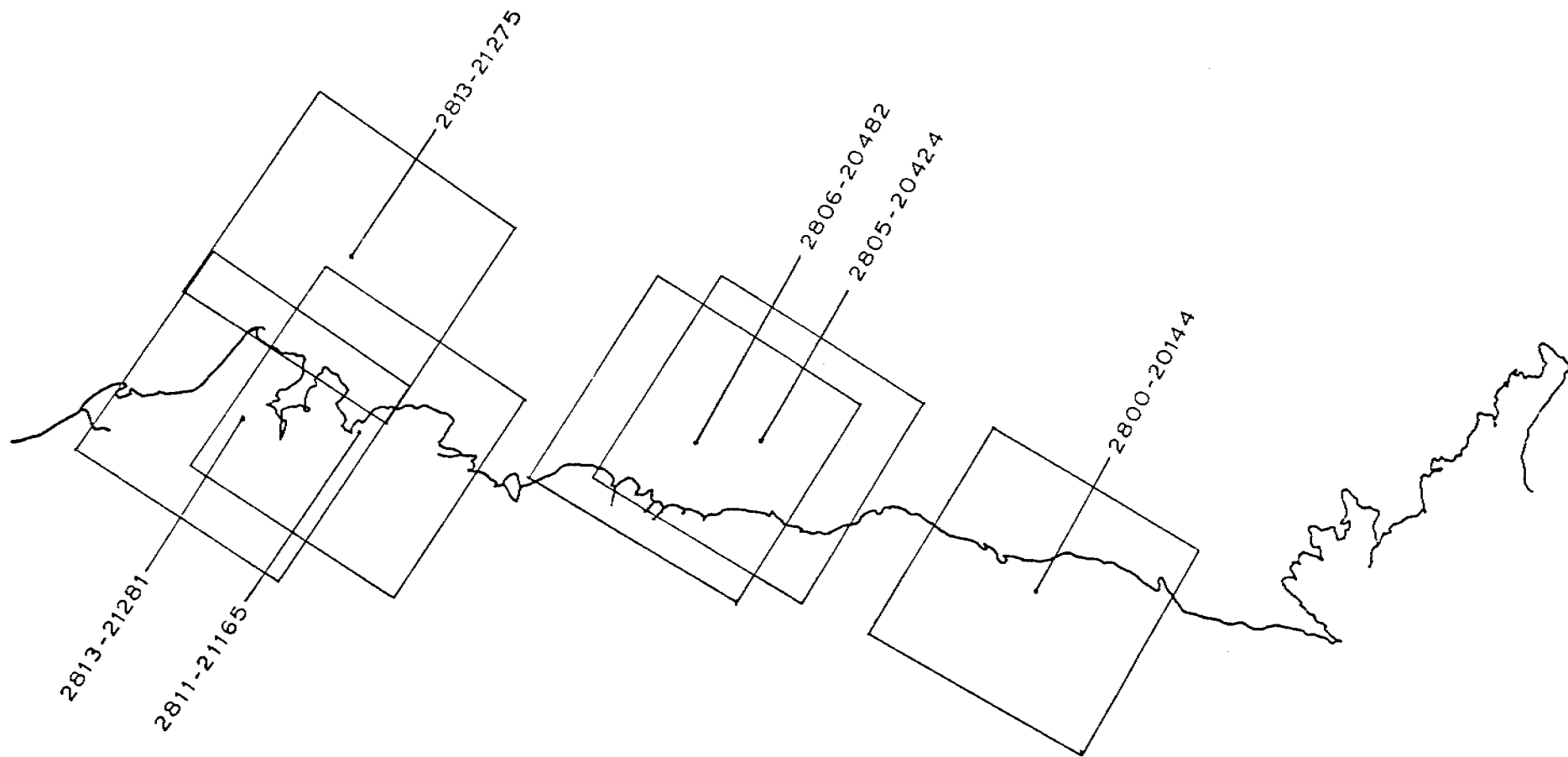
Several old ridge systems can be seen radiating from Pt. Barrow in the contiguous ice. The ice closest to shore appears to be relatively smooth.



0 10 20 30 40
KILOMETERS

BEAUFORT SEA

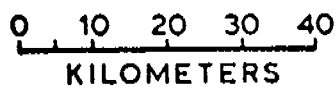
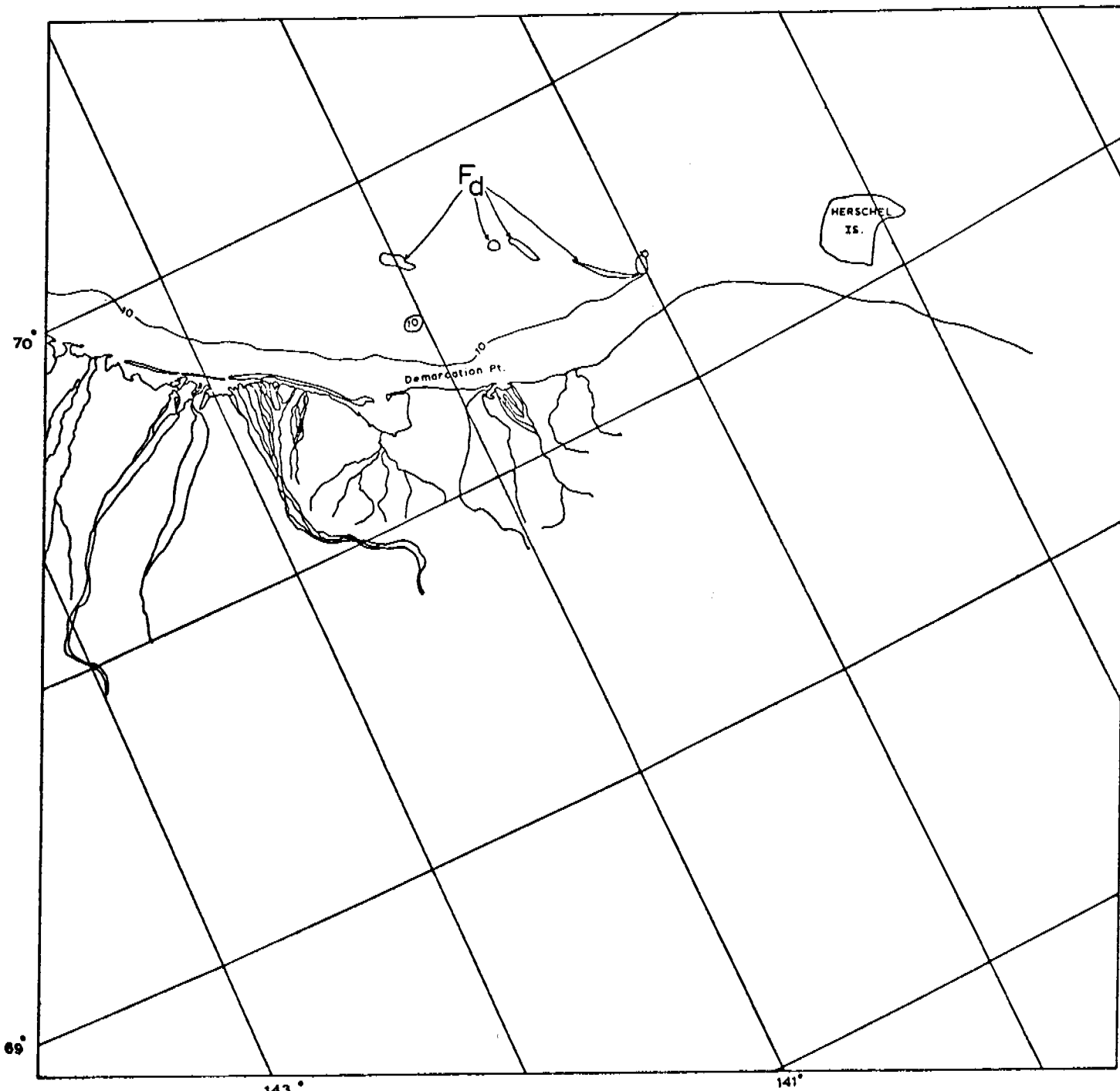
E-2-794-21230-7
E-2-794-21233-7
26 MARCH 1977



BEAUFORT SEA
27 MARCH -13 APRIL 1977
CYCLE 2795 -2812

Scene 2800-20144 (1 April 1977)

This scene shows very little ice detail. Only a few 'dirty' ice floes are visible north of Demarcation Point. There does not appear to be sufficient contrast in the image to see ice detail.

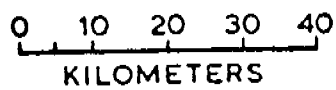
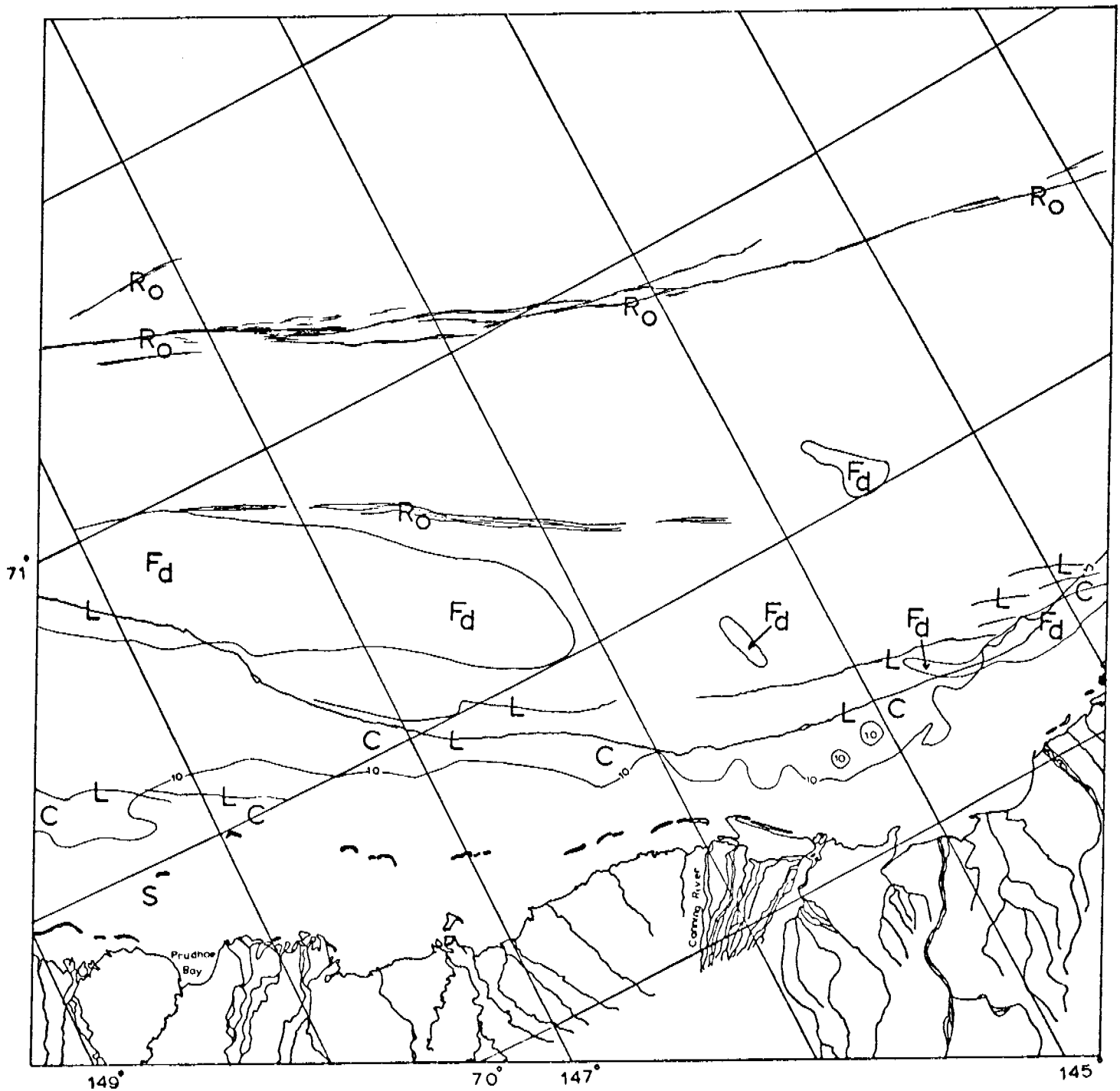


BEAUFORT SEA

E-2-800-20144-7
01 APRIL 1977

Scene 2805-20424 (6 April 1977)

A new lead system has opened up parallel to the coast north of the 10-fathom contour, defining the new edge of contiguous ice. The large ridge system previously active is now considered to be an 'old' ridge system. Other old ridge systems can be seen inshore. Areas of pack ice containing dirty ice (fd) can be seen.

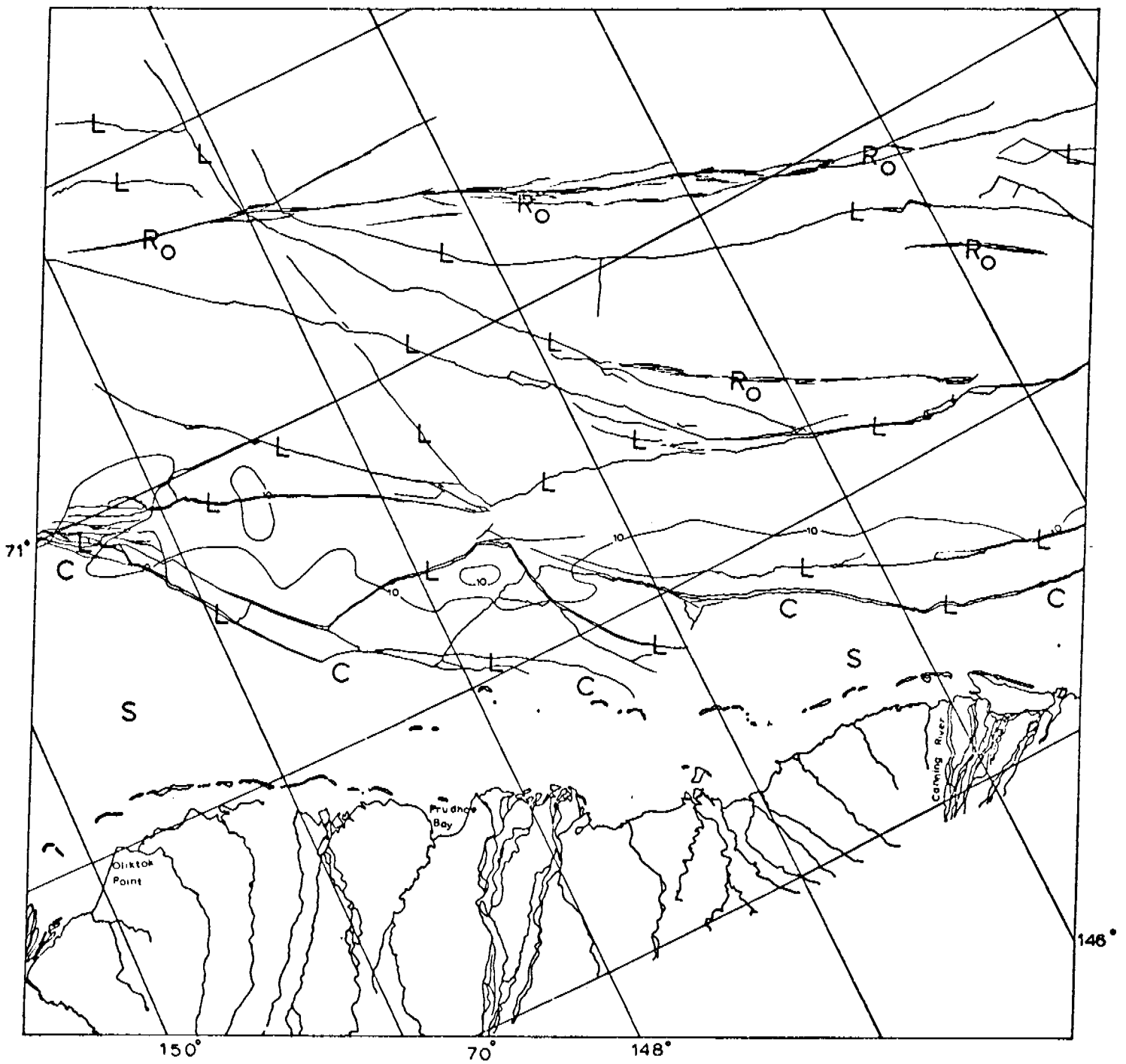


BEAUFORT SEA

E 2 805 20424 7
06 APRIL 1977

Scene 2806-20482 (7 April 1977)

The leads that were seen forming on 6 April (scene 2805-20424) have now developed into a major system of leads extending several tens of kilometers from shore. The more open leads are actually partially frozen over with a thin layer of new ice. The fracture pattern reveals that the ice is moving directly offshore. Older ridge systems are labeled Ro.



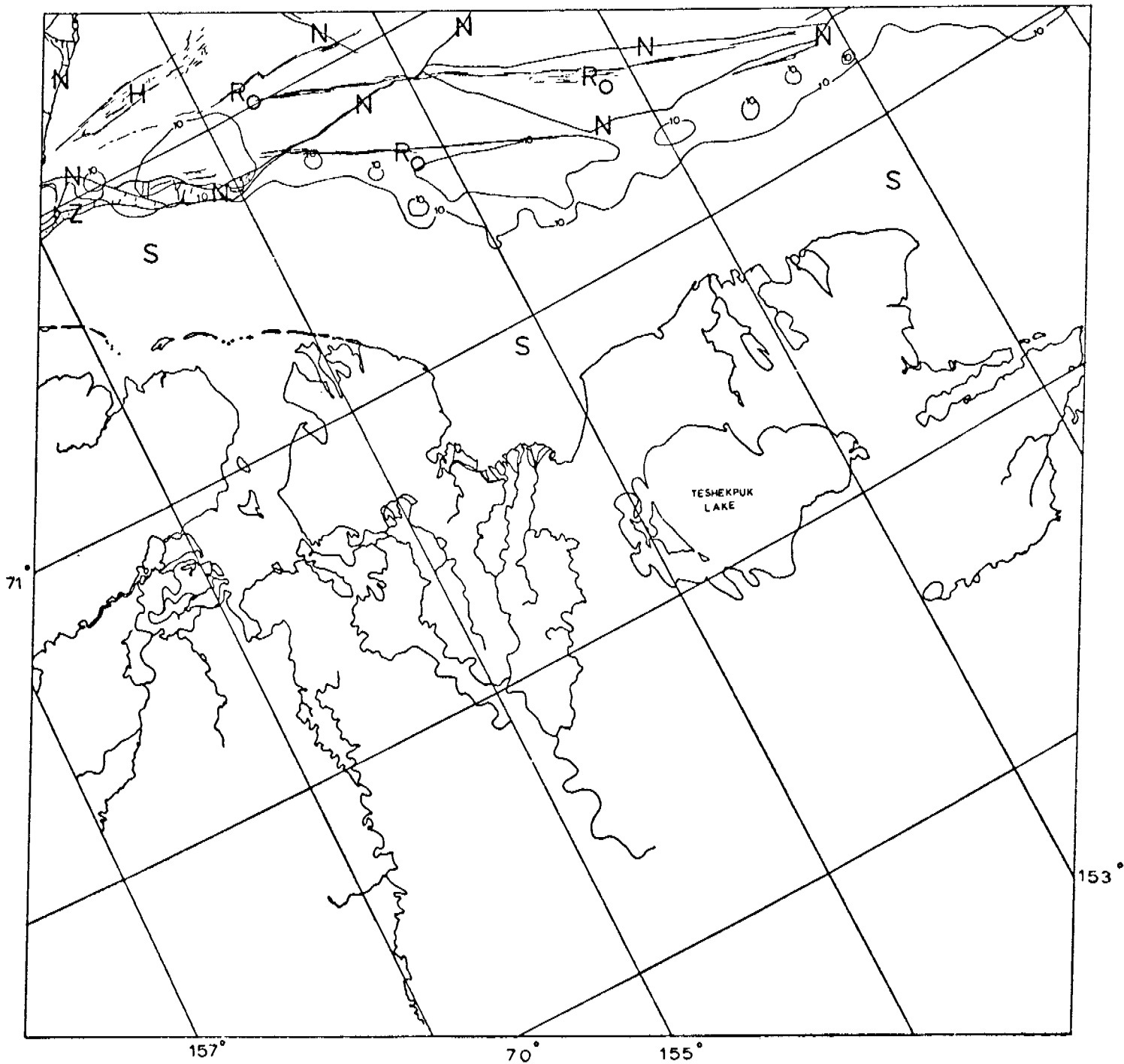
0 10 20 30 40
KILOMETERS

BEAUFORT SEA

E-2-806-20482-7
07 APRIL 1977

Scene 2811-21165 (12 April 1977)

A network of newly frozen leads extends across the top of the scene just north of the 10-fathom bathymetric contour. These leads may be connected with those seen on the April 7 image (scene 2806-20482) and if so, then the whole system may have frozen over and become inactive at this time. Pressure and shear ridging may be taking place within the system and therefore the edge of contiguous ice is not known. The area inshore of the 10-fathom contour is relatively smooth. The ice within the lead system contains several old ridge systems and hummock fields.



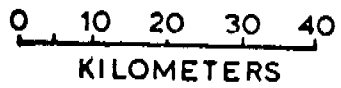
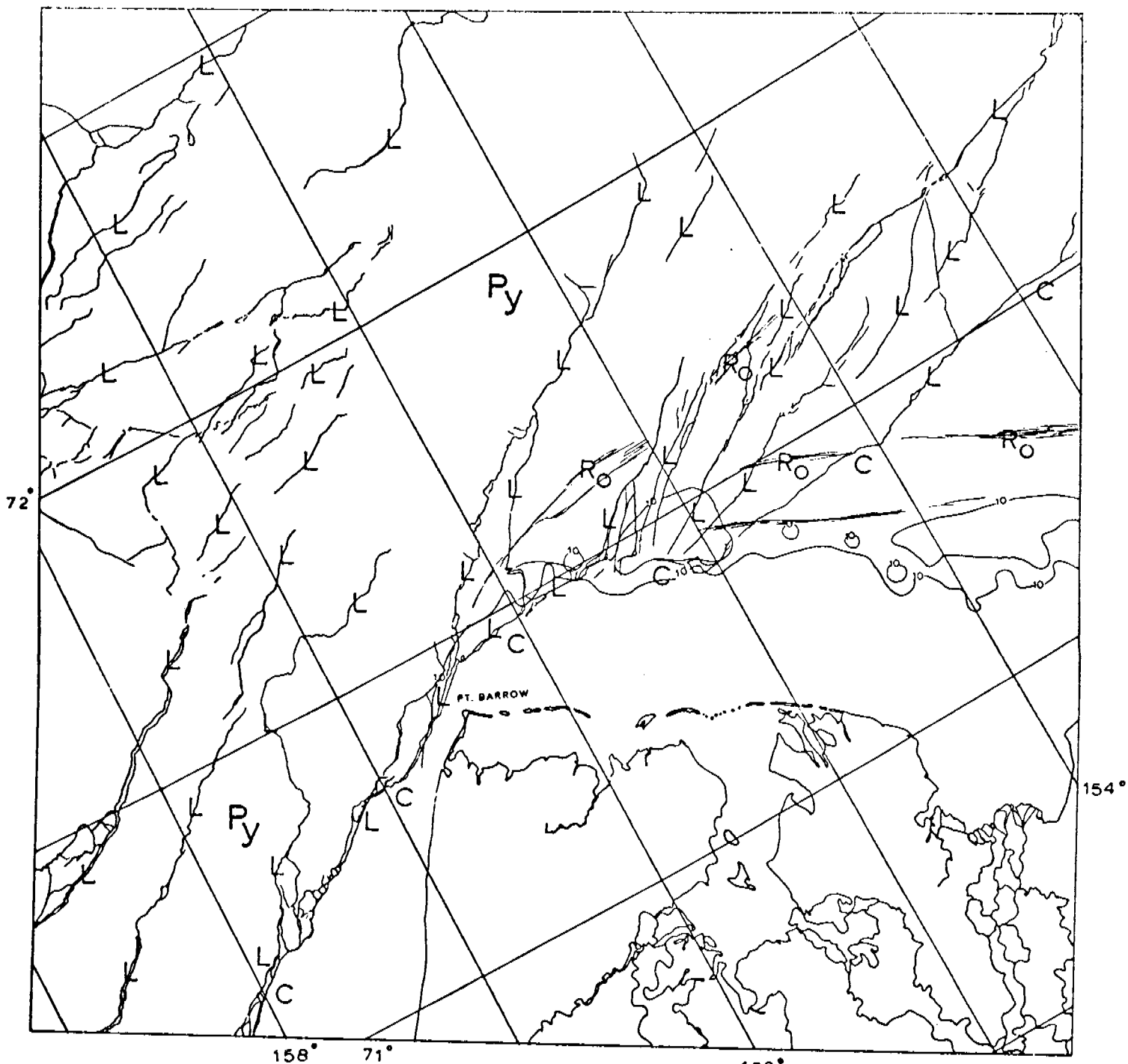
0 10 20 30 40
KILOMETERS

BEAUFORT SEA

E-2-811-21165-7
12 APRIL 1977

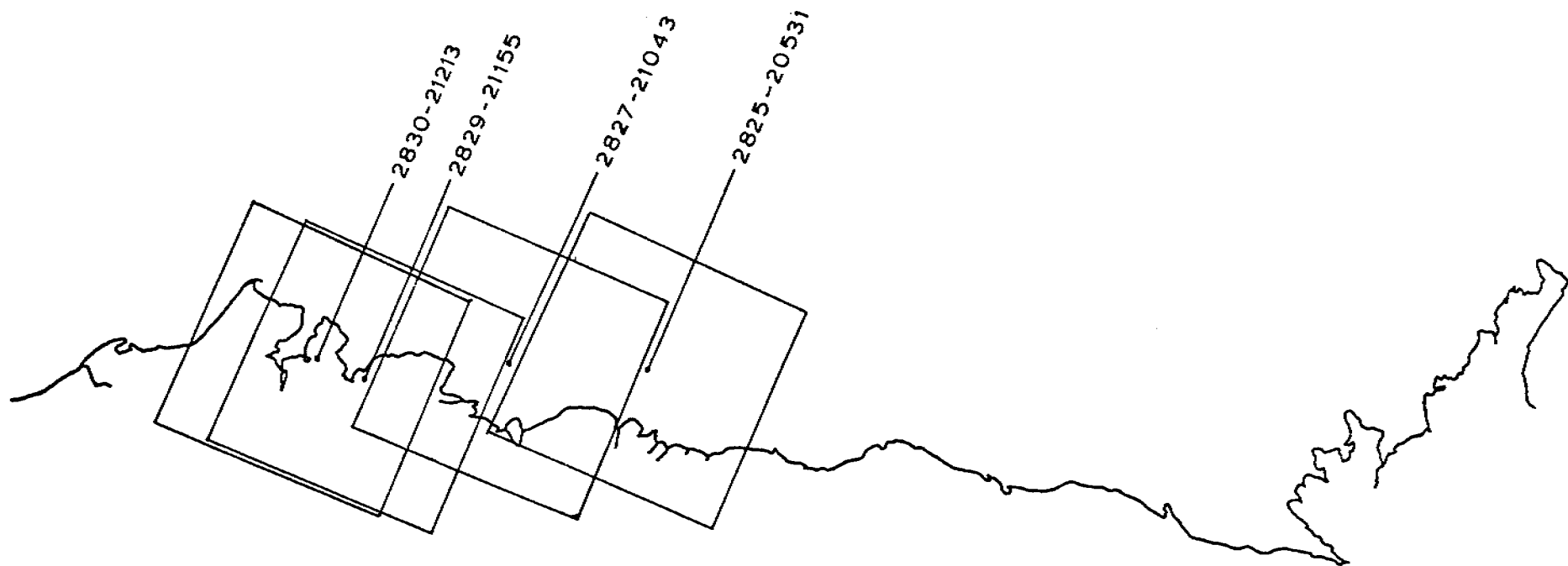
Scenes 2813-21275 (14 April 1977)
2813-21281

The pack ice in these scenes is in motion as can be seen by the large number of open leads (L). The leads northeast of Barrow cut across old ridge systems (Ro). The pack ice at this time appears to be moving northwest. The ice inshore of the edge of contiguous ice in the Beaufort Sea appears to be quite smooth.



BEAUFORT SEA

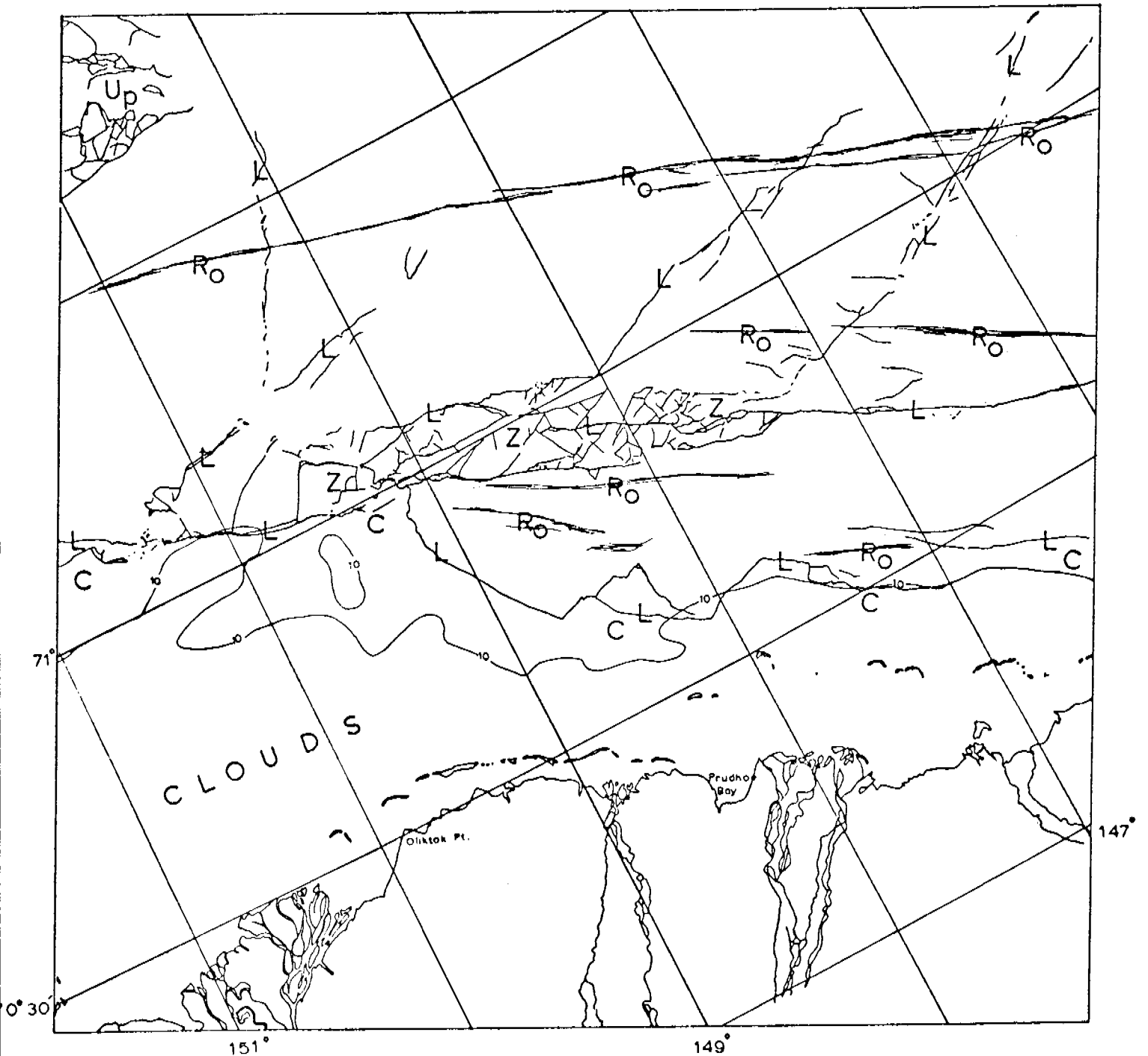
E-2 813-21275-7
 E-2 813-21281-7
 14 APRIL 1977



BEAUFORT SEA
14 APRIL-1 MAY 1977
CYCLE 2813-2830

Scene 2825-20531 (26 April 1977)

The leads in this scene appear to contain open water, indicating that the pack ice is in motion at this time. A broad shear zone exists in the center of the image (labeled 'Z'). The newly-formed leads cut across several old ridge systems. A lead system has opened up inshore of the old ridge system that is visible nearest to shore and defines the present edge of contiguous ice. Clouds obscure the entire area of Harrison Bay from shore to the edge of the contiguous ice zone. The area labeled 'Up' in the upper left corner of the image is broken pack ice with open water between the floes.



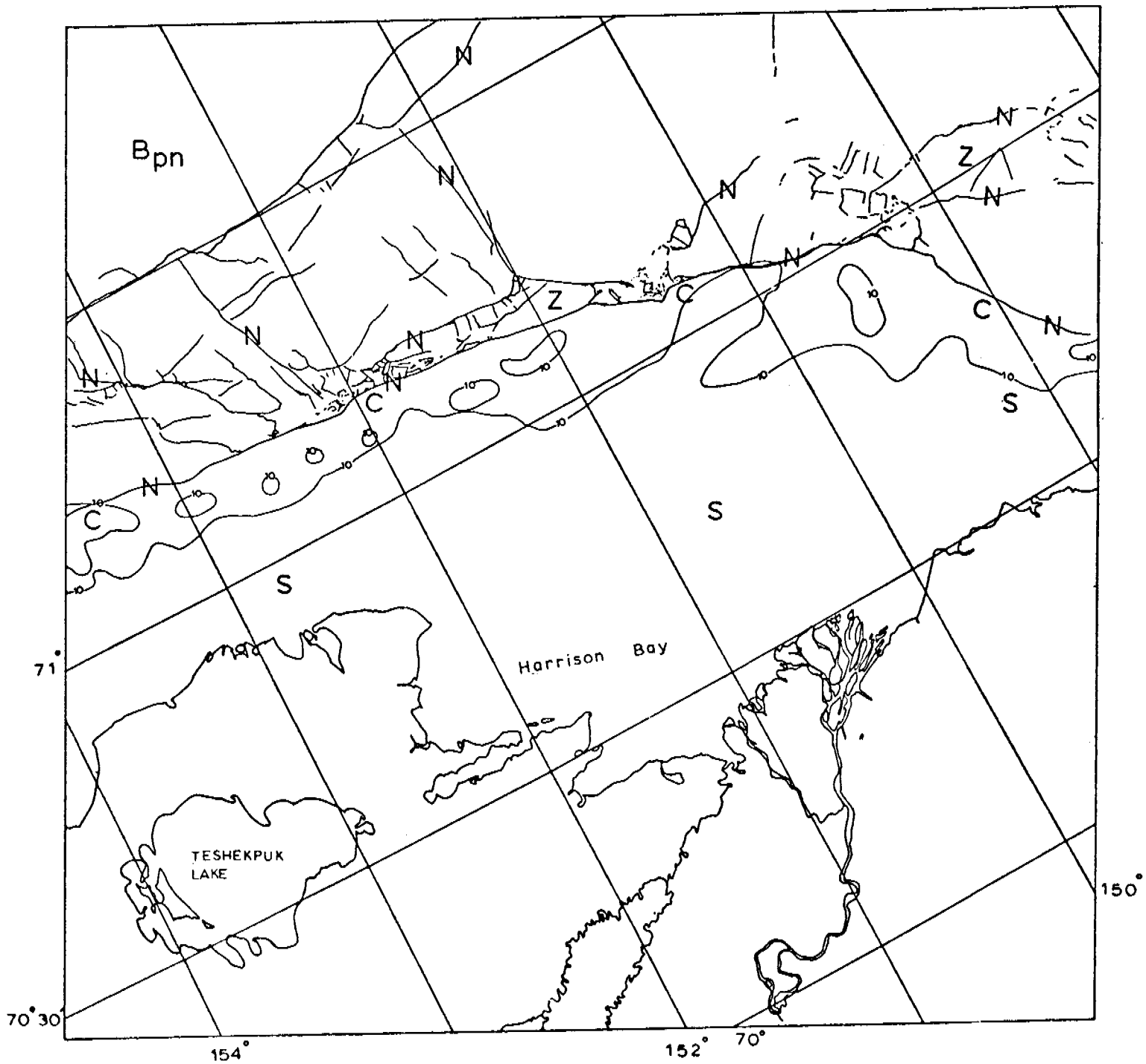
0 10 20 30 40
KILOMETERS

BEAUFORT SEA

E-2-825-20531-7
26 APRIL 1977

Scene 2827-21043 (28 April 1977)

The open leads seen in the image on 26 April 1977 have frozen to the new ice stage (N). The contiguous ice edge is therefore not well defined but is assumed to be along the newly frozen lead that previously defined the contiguous ice edge on 26 April. The ice inshore of the contiguous ice edge appears to be smooth because little detail can be seen.



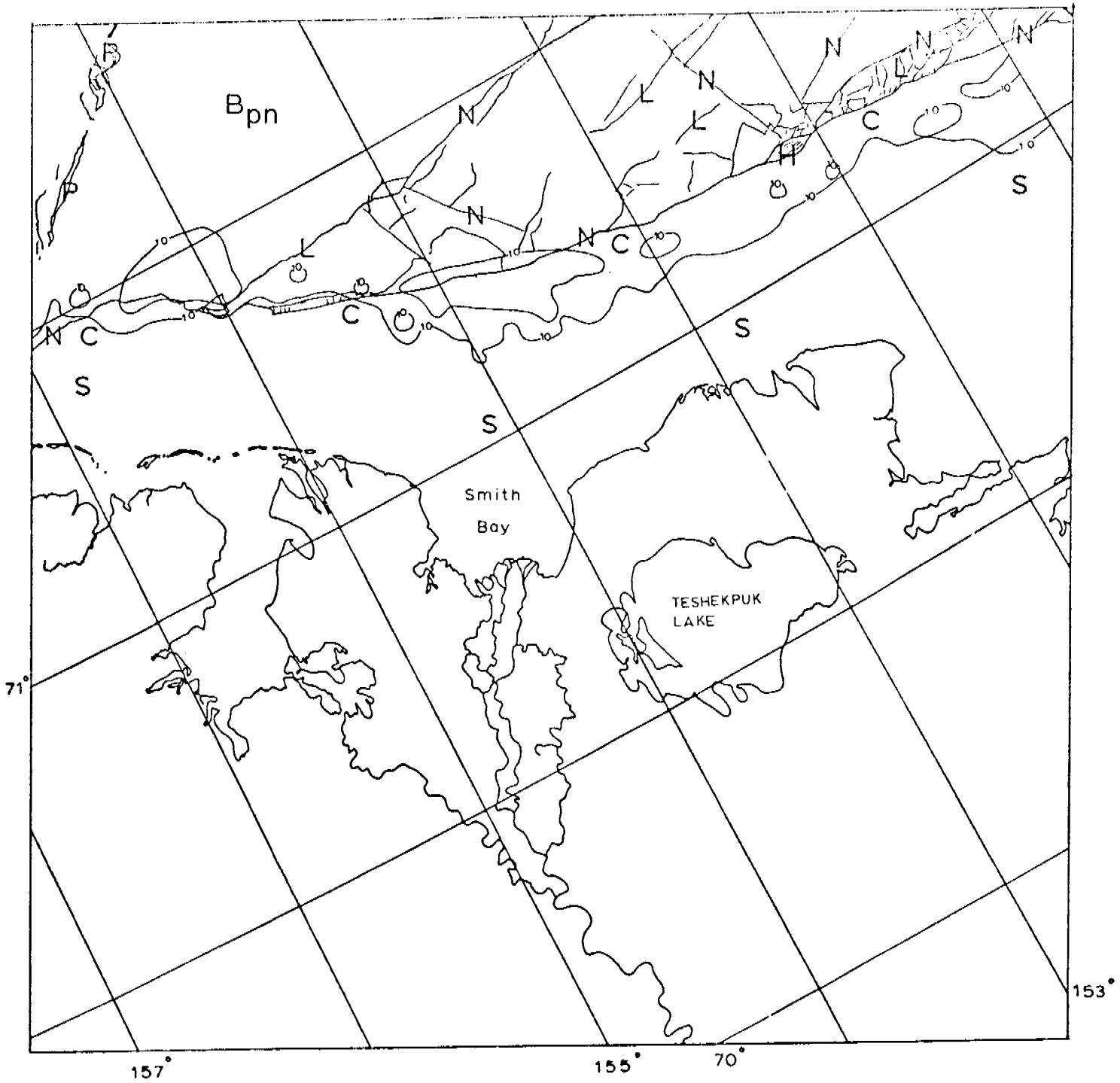
0 10 20 30 40
KILOMETERS

BEAUFORT SEA

E-2 827-21043-7
28 APRIL 1977

Scene 2829-21155 (30 April 1977)

The pack ice is in motion in this scene as evidenced by the open leads. Shearing motion appears to be taking place along the previous edge of contiguous ice. Some leads are difficult to identify as open or newly frozen. The ice inshore of the contiguous ice edge appears to be smooth; this may be due to lack of detail and/or contrast of the image.



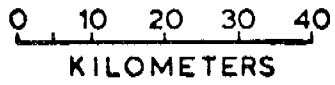
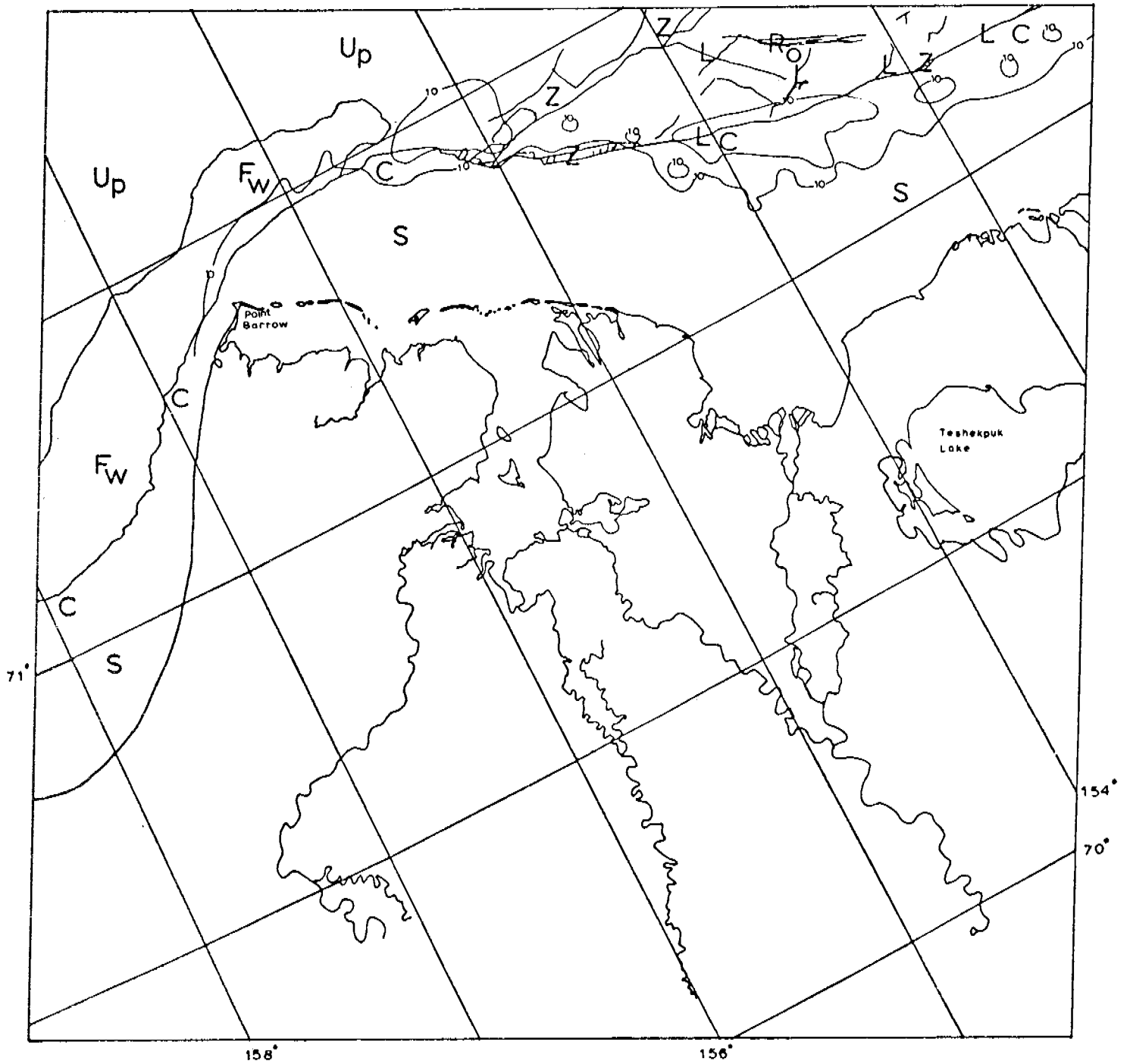
0 10 20 30 40
KILOMETERS

BEAUFORT SEA

E-2-829-21155-7
30 APRIL 1977

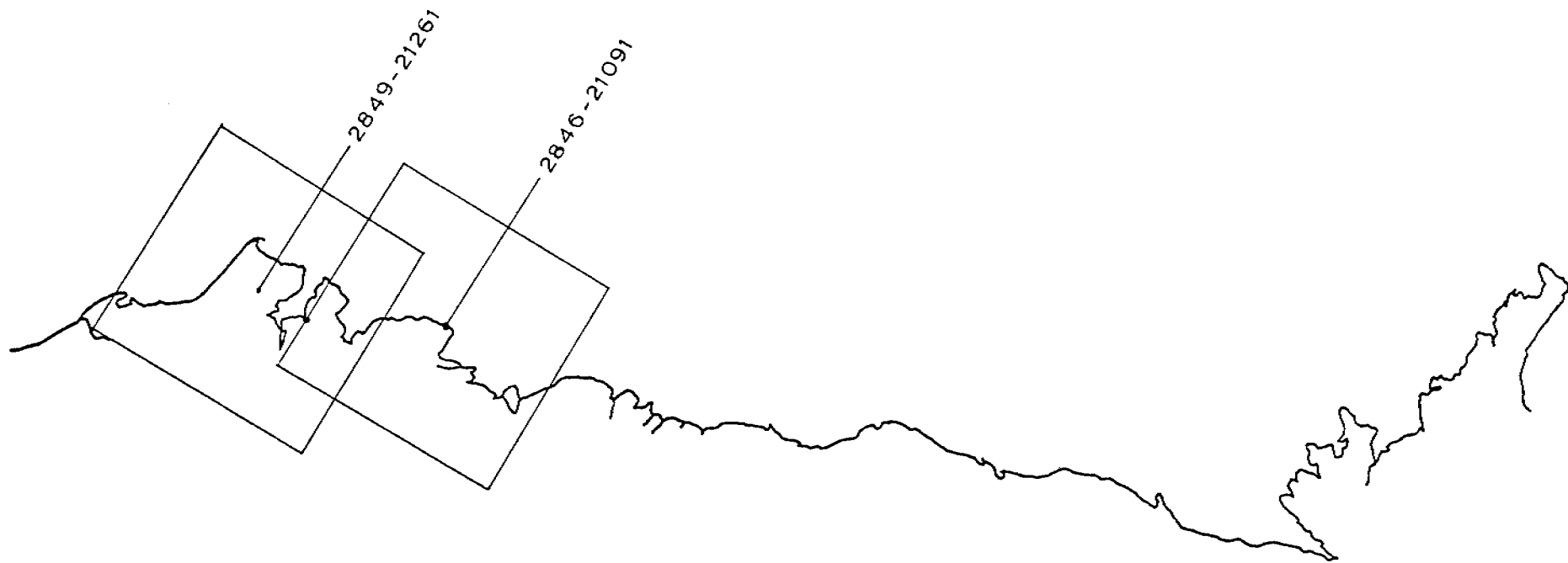
Scene 2830-21213 (1 May 1977)

The contiguous ice edge in this scene closely approximates the location of the 10-fathom bathymetric contour. North of the contiguous ice edge and east of Point Barrow, a wedge of relatively intact pack ice can be seen moving westward. North and west of Point Barrow there is a zone of floes in open water. Further seaward the pack ice is unconsolidated. The ice inshore of the contiguous ice edge appears to be relatively smooth.



BEAUFORT SEA

E 2 830 21213 7
01 MAY 1977



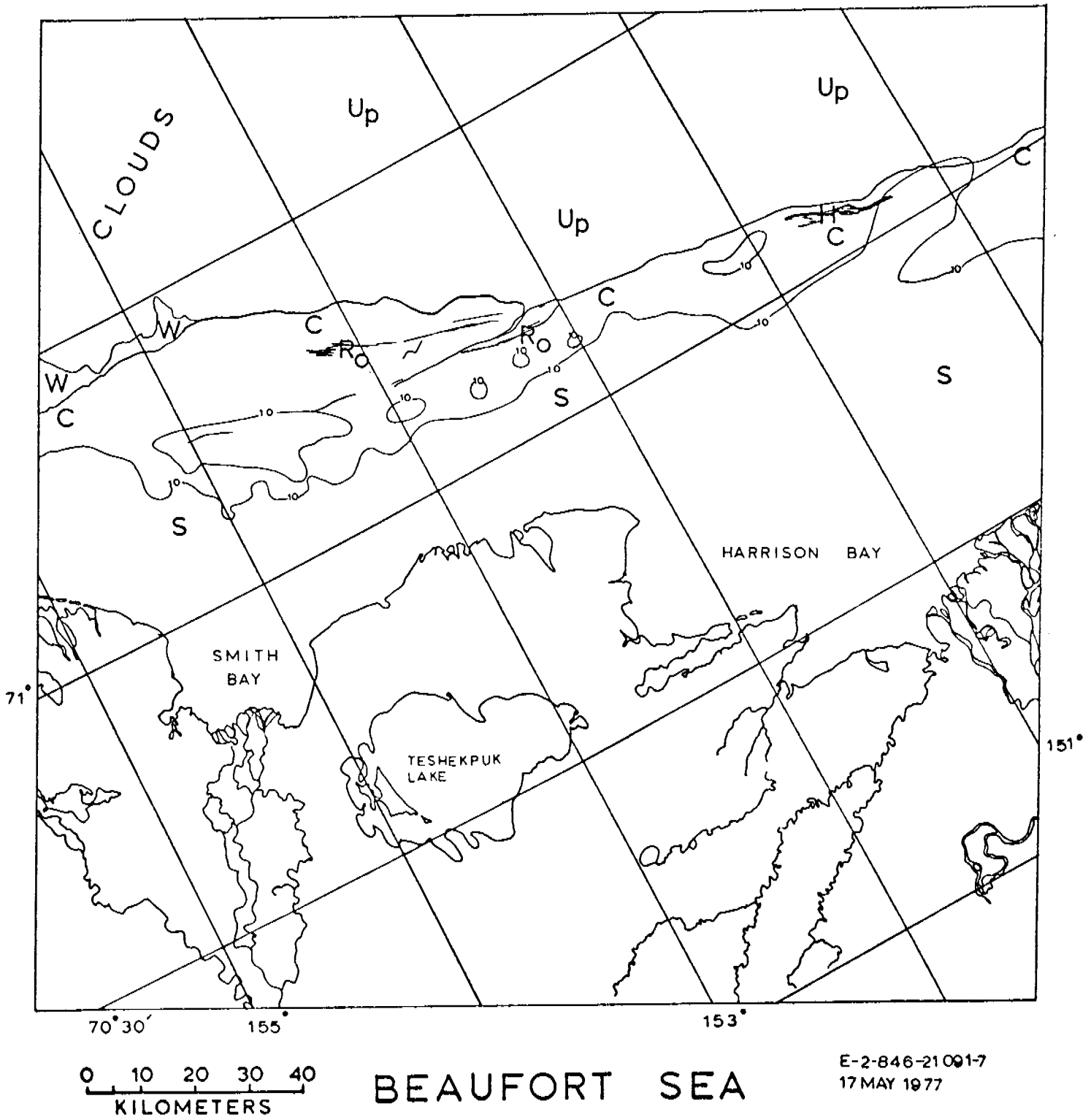
BEAUFORT SEA

2-19 MAY 1977

CYCLE 2831-2848

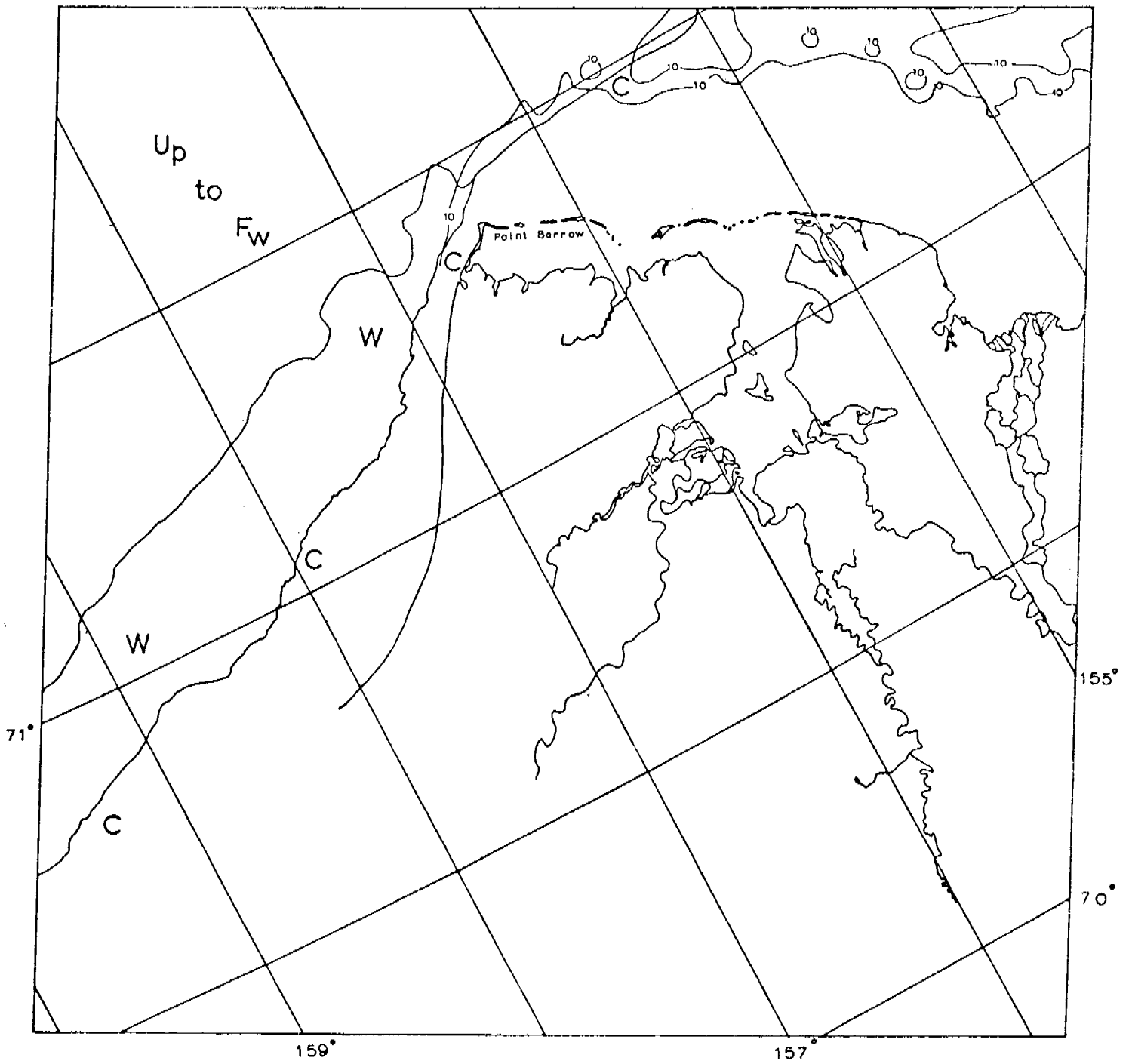
Scene 2846-21091 (17 May 1977)

The boundary between contiguous ice and pack ice is well defined on this image. The pack ice consists of unconsolidated floes in open water. Small areas of ridged and hummocked ice can be seen near the edge of the contiguous ice, which is just north of the 10-fathom bathymetric contour. The contiguous ice appears to be relatively smooth.



Scene 2849-21261 (20 May 1977)

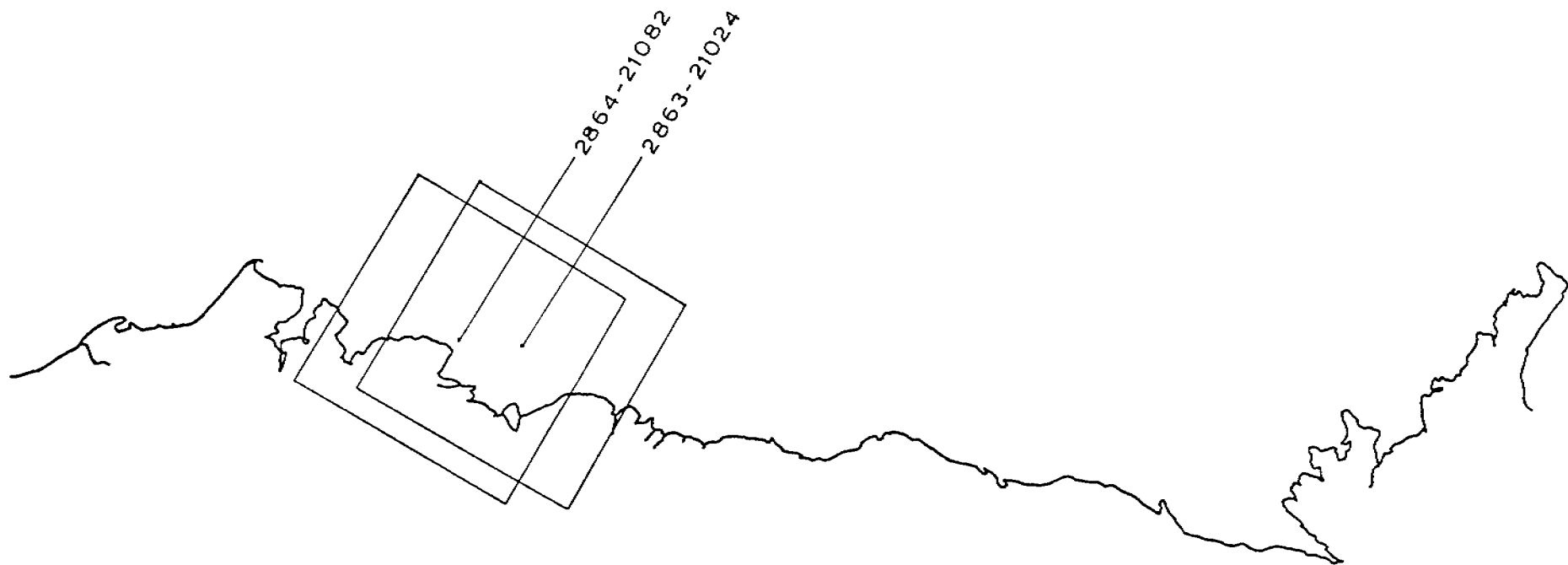
This scene is completely covered by thin clouds. Large scale details only can be seen. The edge of contiguous ice is sharply defined with a large stretch of open water extending from the ice edge to the pack ice. The pack ice varies from unconsolidated pack ice to floes in open water.



0 10 20 30 40
KILOMETERS

BEAUFORT SEA

E 2 849 212617
20 MAY 1977



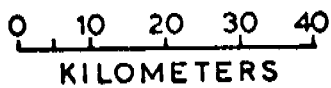
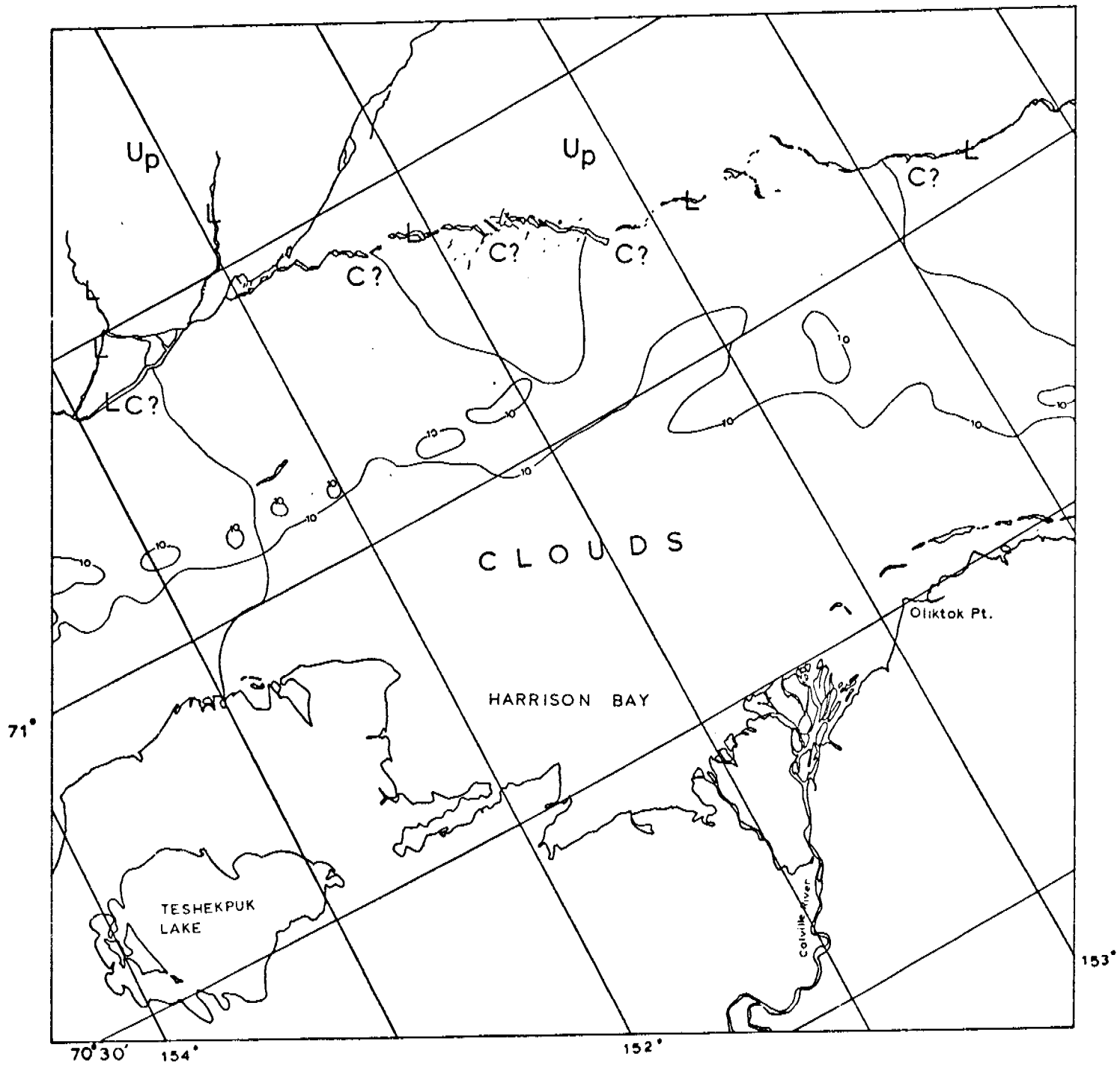
BEAUFORT SEA

20 MAY - 6 JUNE 1977

CYCLE 2849-2866

Scene 2863-21024 (3 June 1977)

Clouds obscure the area of Harrison Bay seaward to several kilometers north of the 10-fathom bathymetric contour. The contiguous ice edge appears to be along a lead opened up near the edge of the clouds. This edge is questionable, however, for two reasons. First, the clouds may obscure the true contiguous ice edge. Second, the pack ice on both sides of the lead appears unconsolidated. The pack ice in the upper left corner of the image is more broken than the rest.

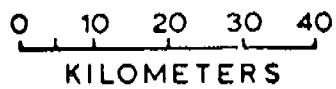
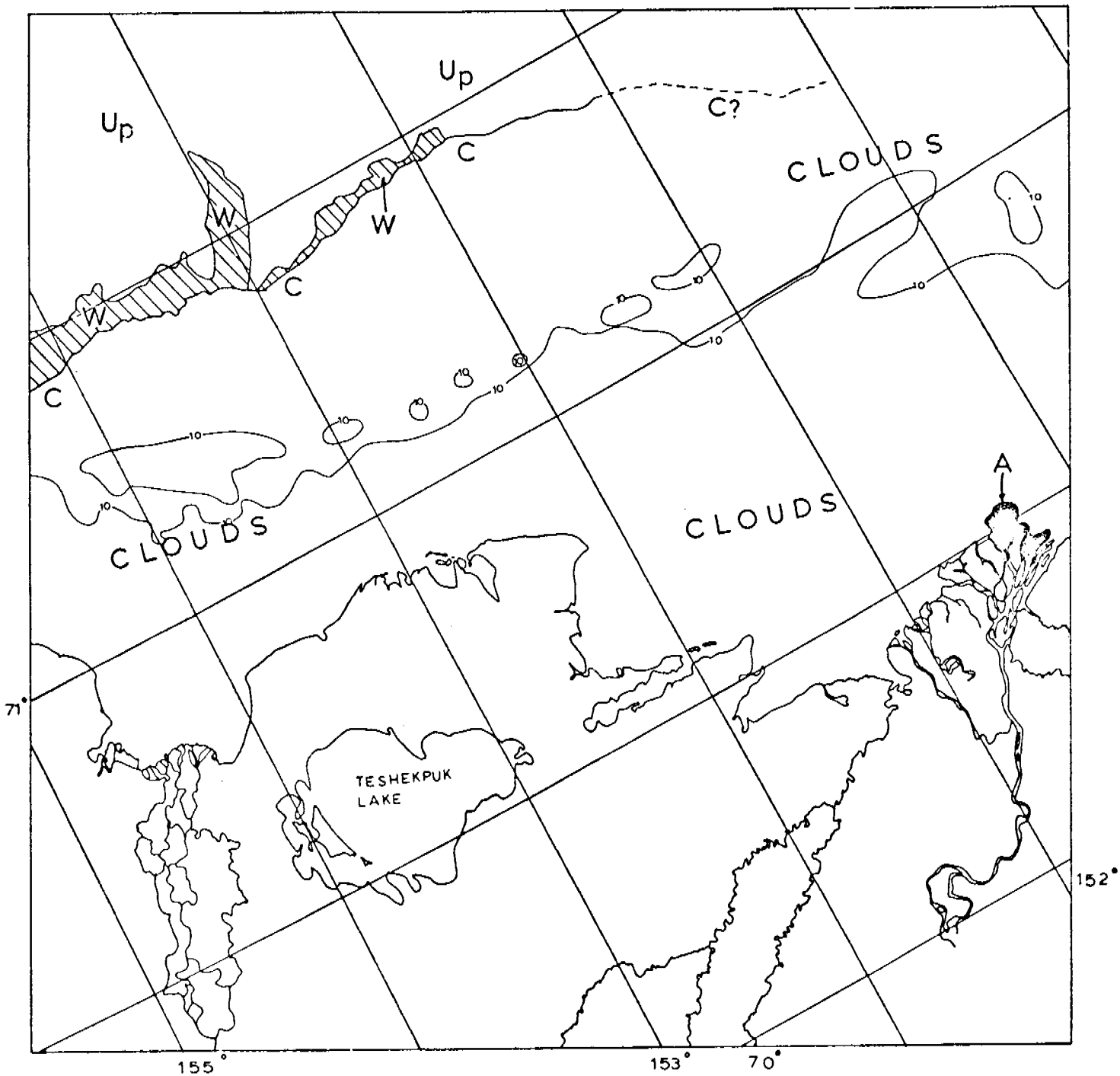


BEAUFORT SEA

E-2-863-21024-7
03 JUNE 1977

Scene 2864-21082 (4 June 1977)

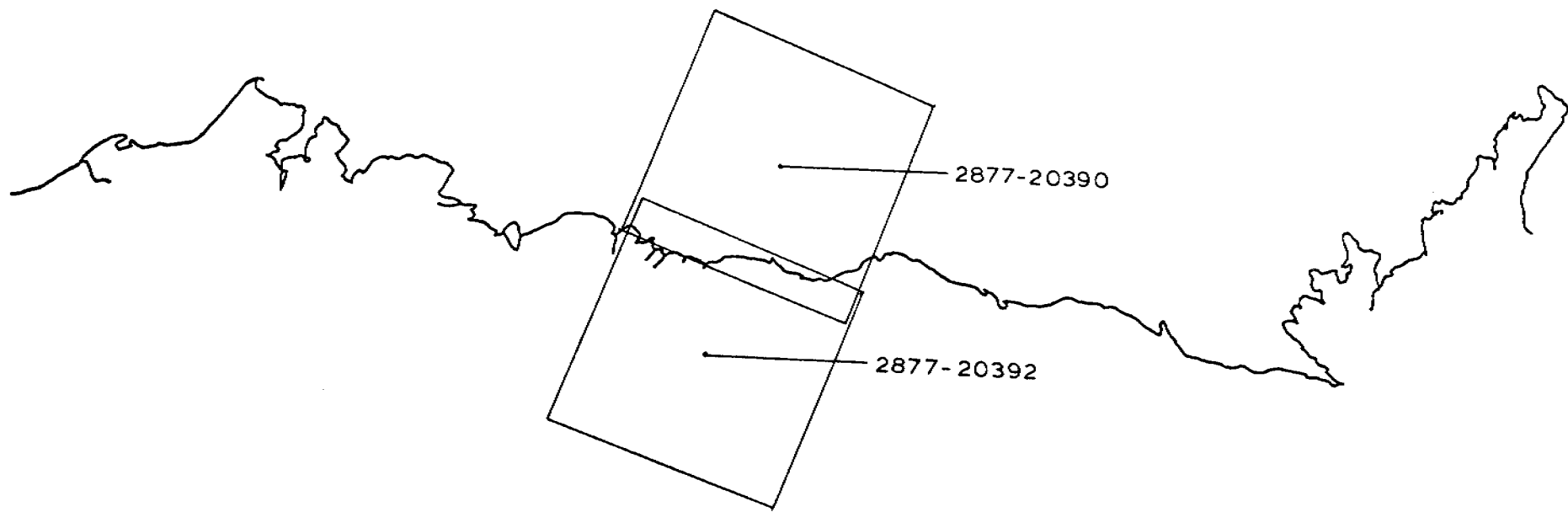
Clouds partially or totally obscure most of the ice detail in this scene. The western part of the contiguous ice edge can be seen but it fades into the clouds to the east. The pack ice north of the contiguous ice edge is broken up. River overflow can be seen at the mouth of the Colville River.



BEAUFORT SEA

E-2-864-21082-7

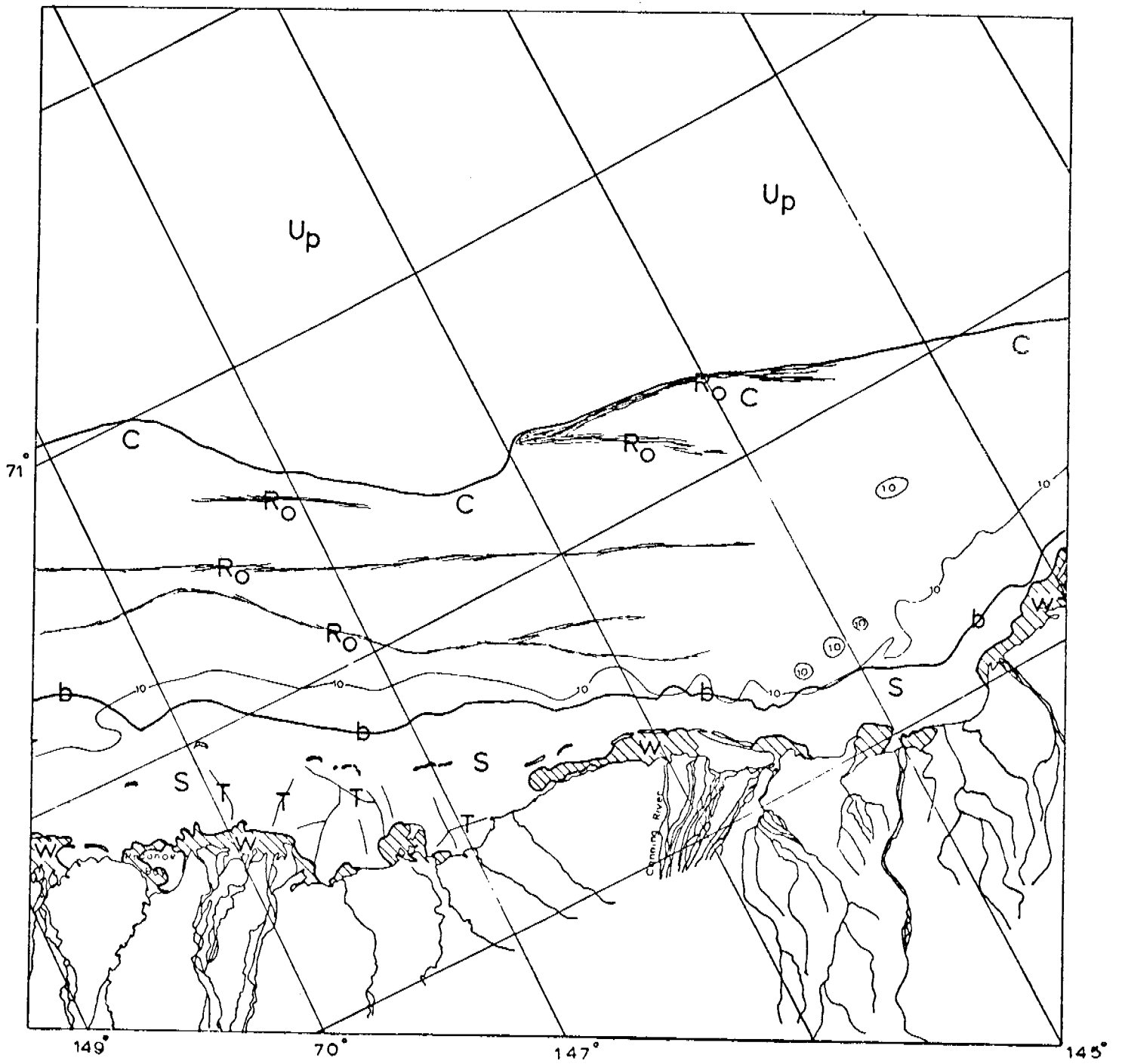
04 JUNE 1977



BEAUFORT SEA
7-24 JUNE 1977
CYCLE 2867-2884

Scenes 2877-20390 (17 June 1977)
2877-20392

The majority of the snow cover on the ice has melted and the fine details of the ice can be seen. There is open water in the vicinity of river mouths. The ice is relatively smooth from shore to boundary 'b'. What appear to be tension or tidal cracks are labeled with a 'T'. From the boundary b to the edge of contiguous ice, the ice has undergone multiple stages of ridging and piling. It is a mass of piled and hummocked ice and old ridges. The major ridge systems that can be distinguished are labeled Ro. The pack ice north of the contiguous ice edge is dense but unconsolidated.



0 10 20 30 40
KILOMETERS

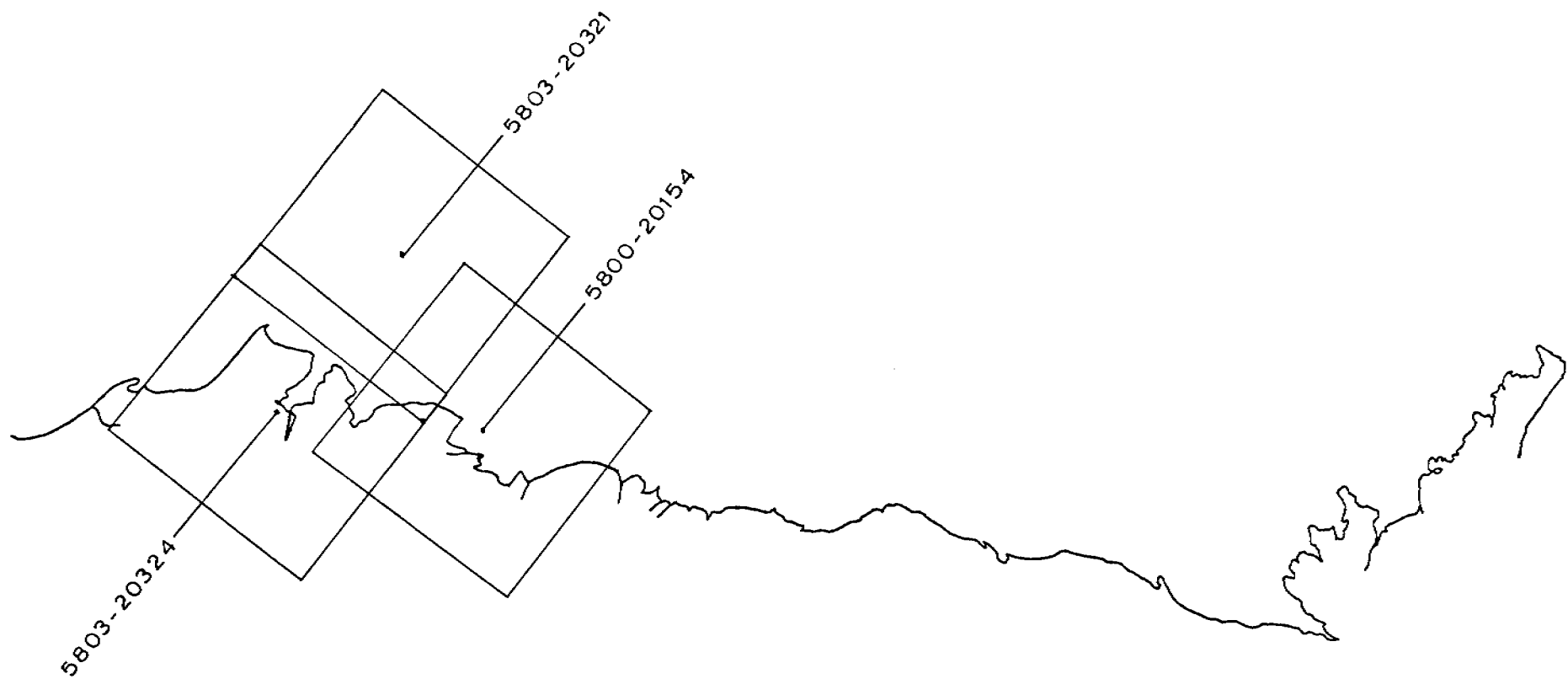
BEAUFORT SEA

E-2 877-20390-7

E-2 877-20392-7

17 JUNE 1977

188



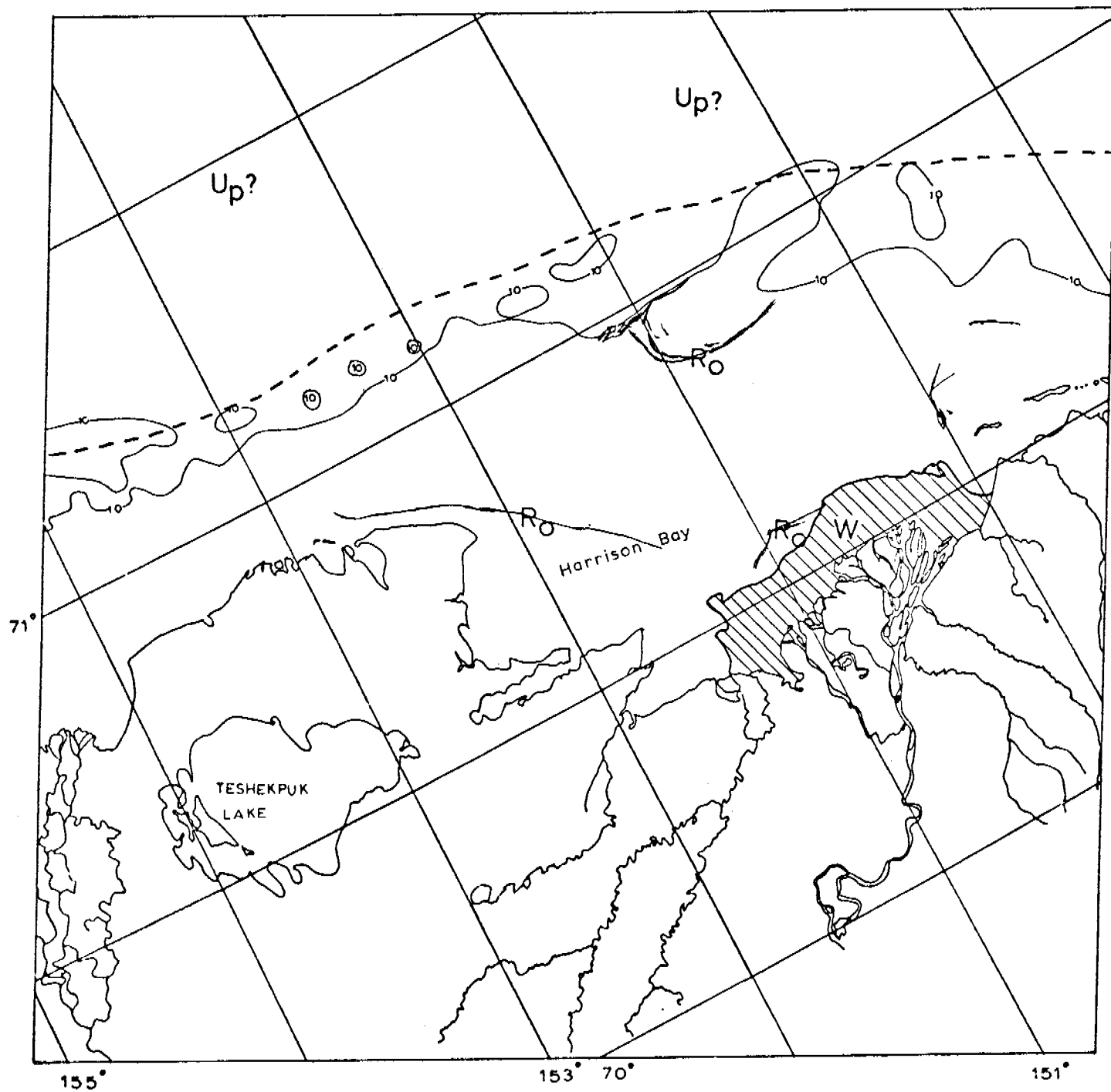
BEAUFORT SEA

13-30 JUNE 1977

CYCLE 5786 - 5803

Scene 5800-20154 (27 June 1977)

This scene of the area of Harrison Bay is obscured by thin clouds and much detail cannot be seen. The boundary between contiguous ice and pack ice cannot be seen and so is approximately located by a dashed line. Patches of open water can be seen in the pack ice which is probably unconsolidated.



0 10 20 30 40
KILOMETERS

BEAUFORT SEA

E-5-800-20154-7
27 JUNE 1977

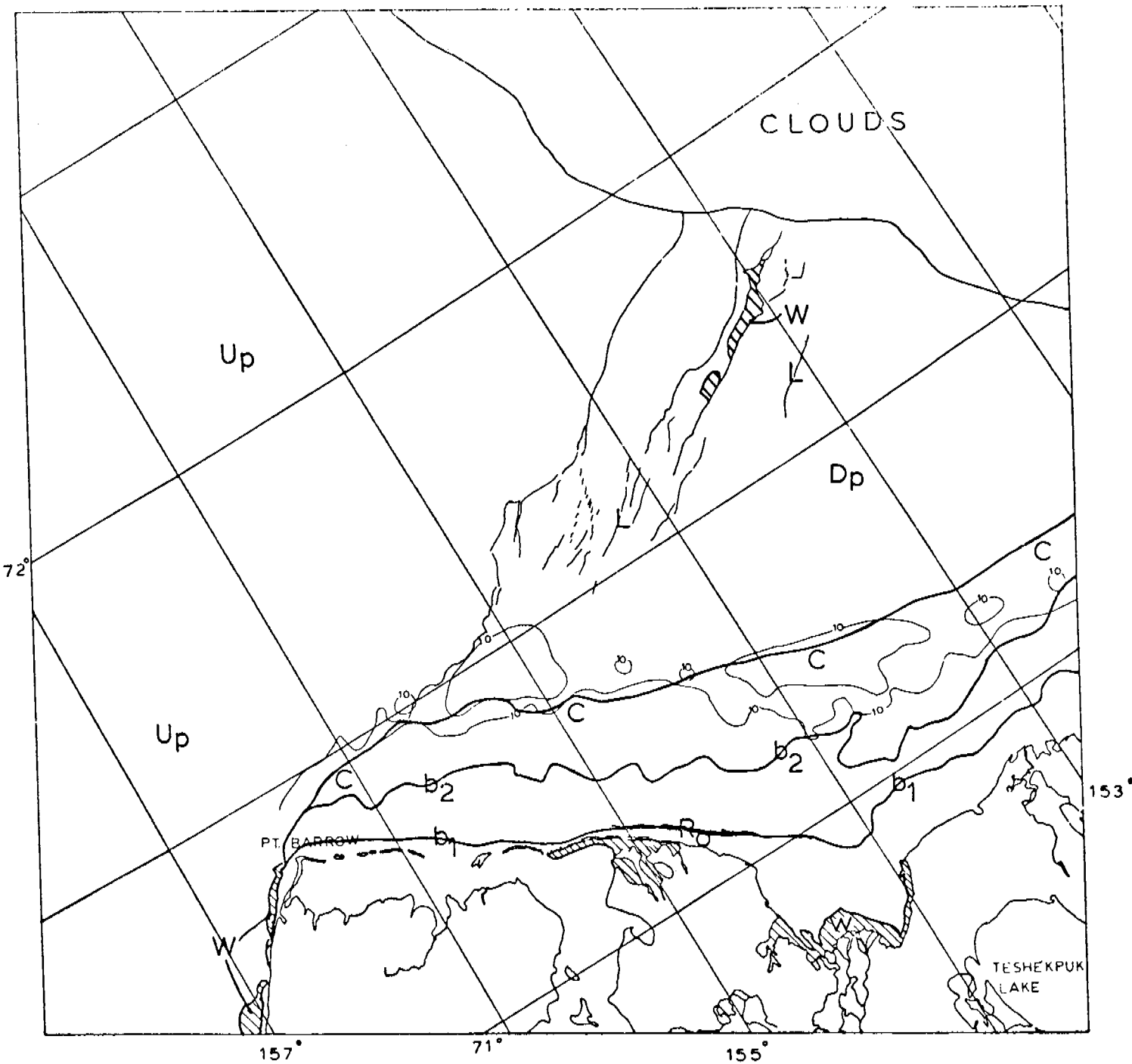
Scenes 5803-20321 (30 June 1977)
5803-20324

Three distinct zones of nearshore ice are visible in this scene. The first zone, extends from shore to boundary b_1 . This zone consists of large areas of smooth ice. This ice probably has not been subject to significant forces since freeze-up the preceding fall. It is now breaking up and open water exists in some areas between shore and the edge of the ice.

The second zone of ice extends between boundaries b_1 and b_2 . This zone consists of small, smooth pans ranging from a couple of kilometers to a few meters in diameter separated by minor ridging. A few small ridges several kilometers long are visible in this area. Also, a large ridge (R_0) separates a portion of the first zone from the second.

The third zone of nearshore ice extends from boundary b_2 to the edge of contiguous ice 'C'. This ice in this zone is very rough and consists of mostly ridges and hummock fields. For the most part individual piling events are impossible to separate. The seaward-most edge of this zone lies approximately along the 10-fathom (20-meter) bathymetric contour and is probably grounded.

Seaward of this zone and east of Barrow the pack ice is partially consolidated. Separating this pack ice from the unconsolidated pack ice to the west is a zone of fracturing indicated by the leads 'L'.



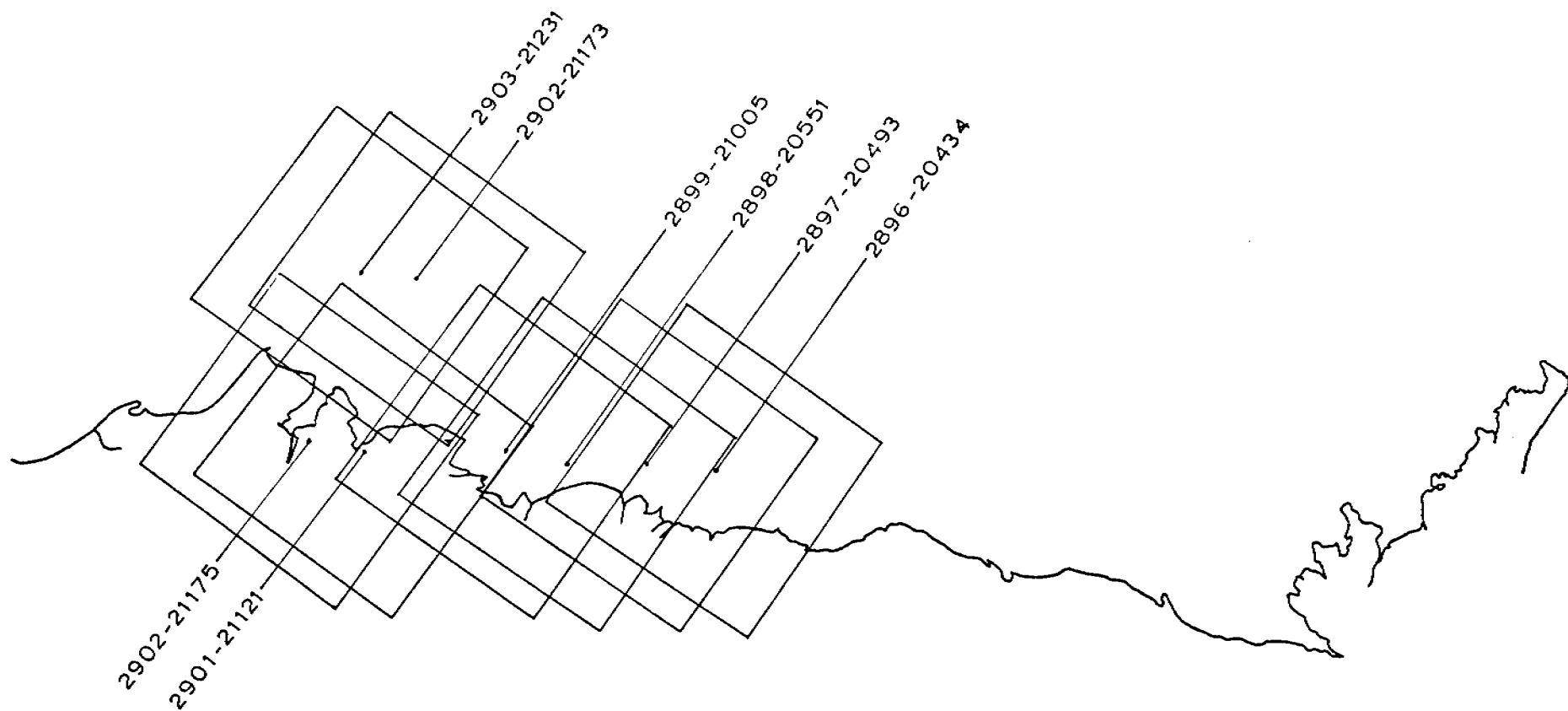
0 10 20 30 40
KILOMETERS

BEAUFORT SEA

E-5-803-20321-7

E-5-803-20324-7

30 JUNE 1977



BEAUFORT SEA

25 JUNE-12 JULY 1977

CYCLE 2885-2902

Scene 2896-20434 (6 July 1977)

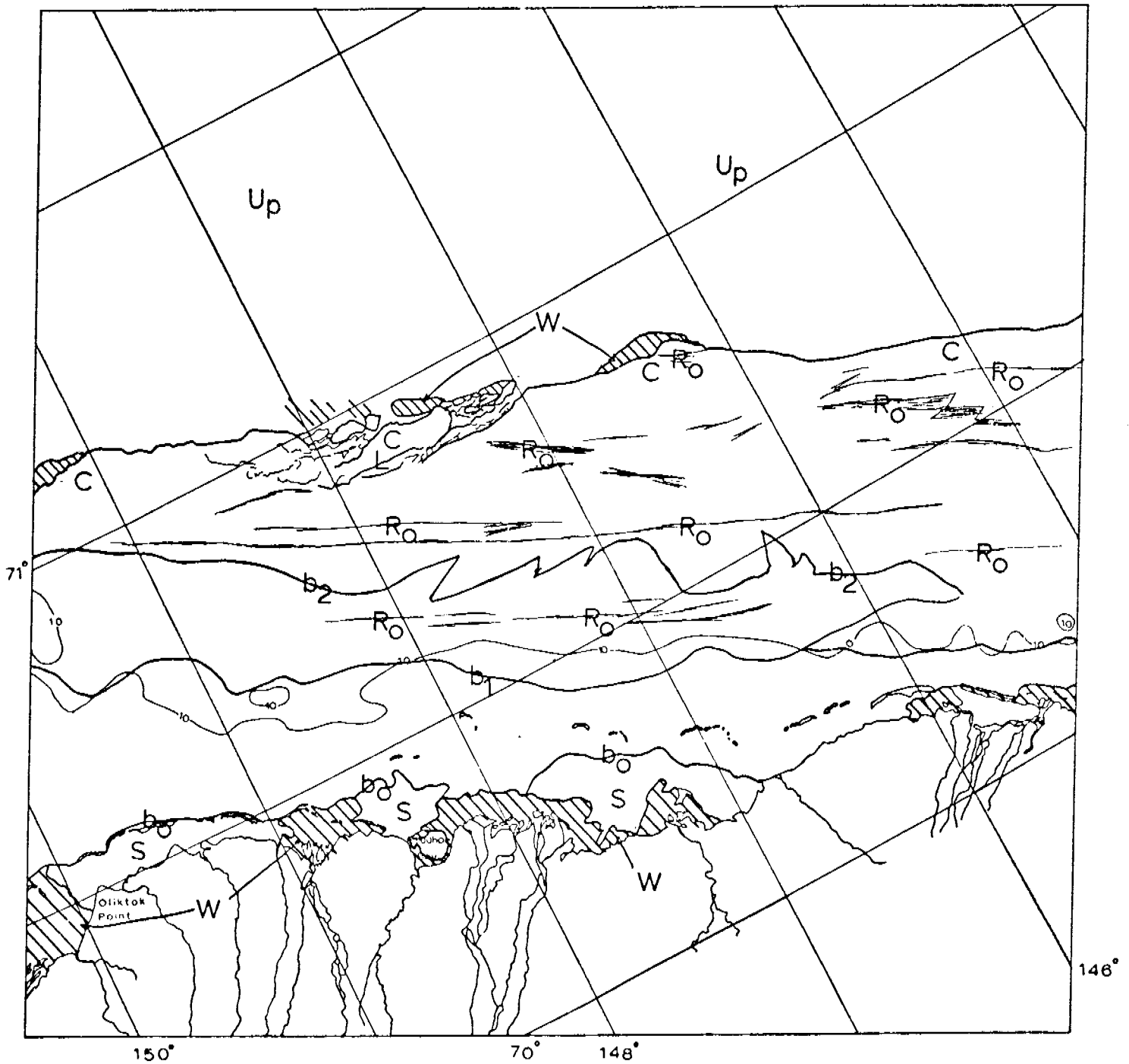
More open water exists at the mouths of the rivers than in the previous Landsat cycle. Approximately fifty percent of the coast is ice free.

The nearshore ice is divided into three zones. The first zone extends from shore (or the edge of the open water) to boundary b_1 which approximates the 10-fathom (20-meter) bathymetric contour. The ice in this zone is smooth compared to the other zones. The ice has probably remained static since freeze-up the previous fall. It consists primarily of flat pans surrounded by low ridges.

The second zone is approximately 20 kilometers wide, between boundaries b_1 and b_2 , but appears to abruptly pinch off to nothing north of the Sagavanirktok River in the right of the image. This zone probably contains the greatest amount of rough ice, i.e., the largest hummock fields and ridge systems, and is probably grounded. This zone has probably been subject to continuous stress since its formation early in the ice season. Major ridge systems that can be seen are labeled Ro.

The third zone of nearshore ice extends from boundary b_2 to the edge 'C' of the stationary ice. The ice in this zone is also quite rough but has not existed as long as zone 2. On the February 12 image (scene 2752-20505) the edge of contiguous ice was in the center of zone 2. However, the edge of the contiguous ice in the 6 July image is approximately defined by the large ridge system seen in the 12 February image. This ridge system appears to have formed not many weeks prior to February 12.

North of the stationary ice the pack ice consists of unconsolidated floes not exceeding a diameter of 10 kilometers. Small patches of open water separate the pack ice from the stationary ice.



BEAUFORT SEA

E-2-896-20434-7
06 JULY 1977

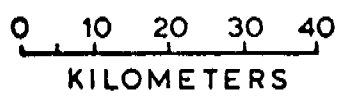
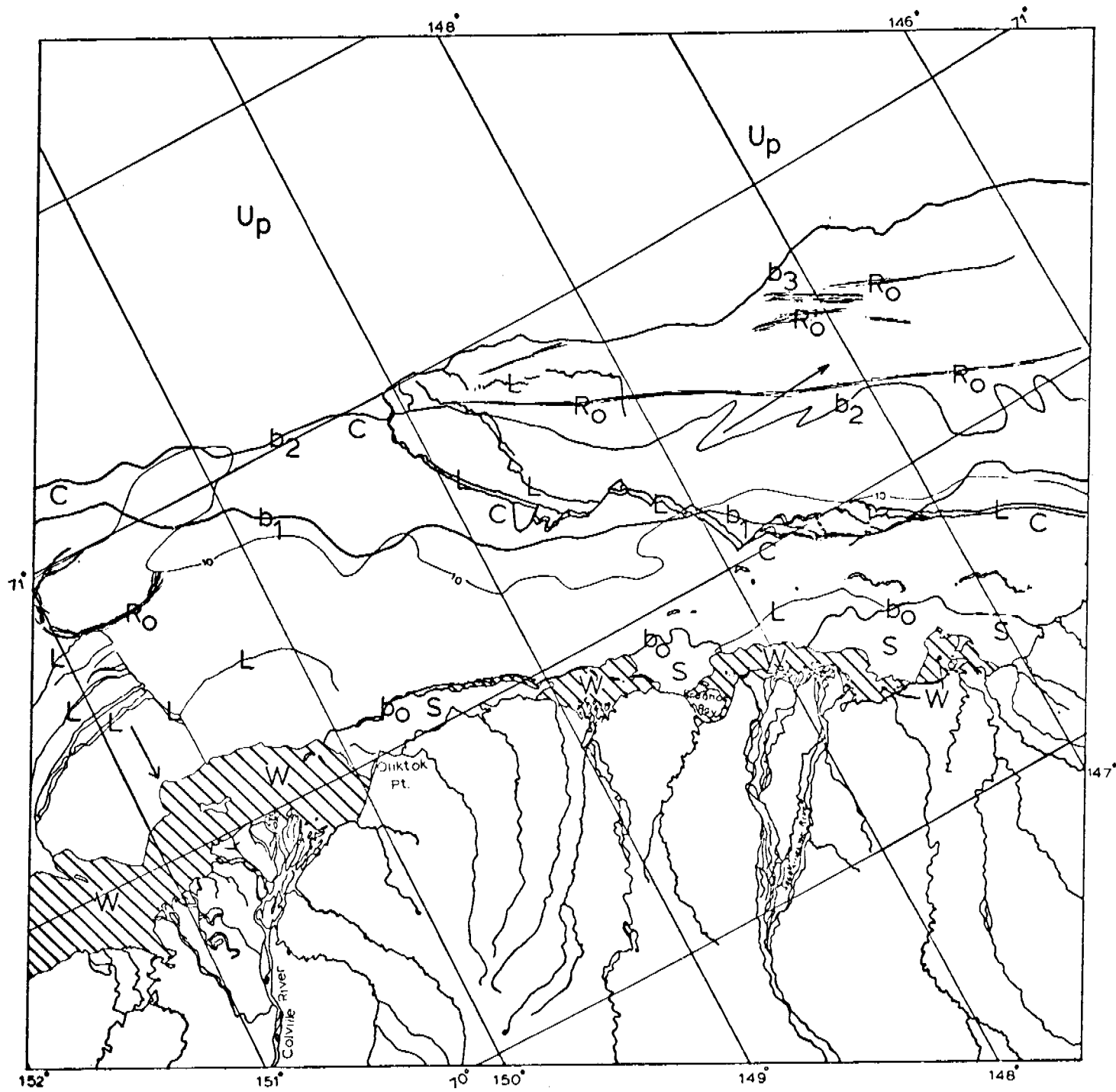
Scene 2897-20493 (7 July 1977)

A large section of the ice that was stationary on 6 July (scene 2896-20434) has broken loose and moved 1 1/2 to 2 kilometers northeast (note arrow). This section is the area between boundaries C and b_3 . The fracturing that forms the lower boundary C cuts across the zone of heavy ridging between boundaries b_1 and b_2 . The shoreward edge of this zone approximately parallels the 10-fathom (20-meter) bathymetric contour and is probably grounded to the sea floor.

A smaller section of ice is seen breaking loose from the main ice sheet in Harrison Bay. This ice appears to have moved south, towards shore (note arrow).

A large semi-circular feature is visible in Harrison Bay at the edge of the image. It appears to be a ridge system and may have formed early in the ice season when a large floe was forced into the thin, young ice forming in Harrison Bay. This feature was not visible on the winter imagery when snow covered the ice and hence the ridges were probably not very high. The nature and origin of this feature is purely speculation as no imagery was available for the period when the feature formed.

The boundary designations are the same as those used previously. The area between shore and b_0 is very smooth ice. From shore or b_0 to b_1 is mostly flat ice with some ridging. The area between boundaries b_1 and b_2 is heavily ridged and piled. This forms the outer boundary of the so-called grounded "shore-fast ice". The ice between boundaries b_2 and b_3 is consolidated pack ice that has undergone substantial ridging and piling and has become attached to the stationary ice. It is not grounded. Beyond this the pack ice is unconsolidated.



BEAUFORT SEA

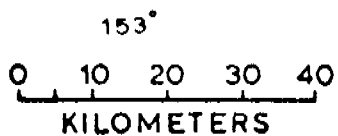
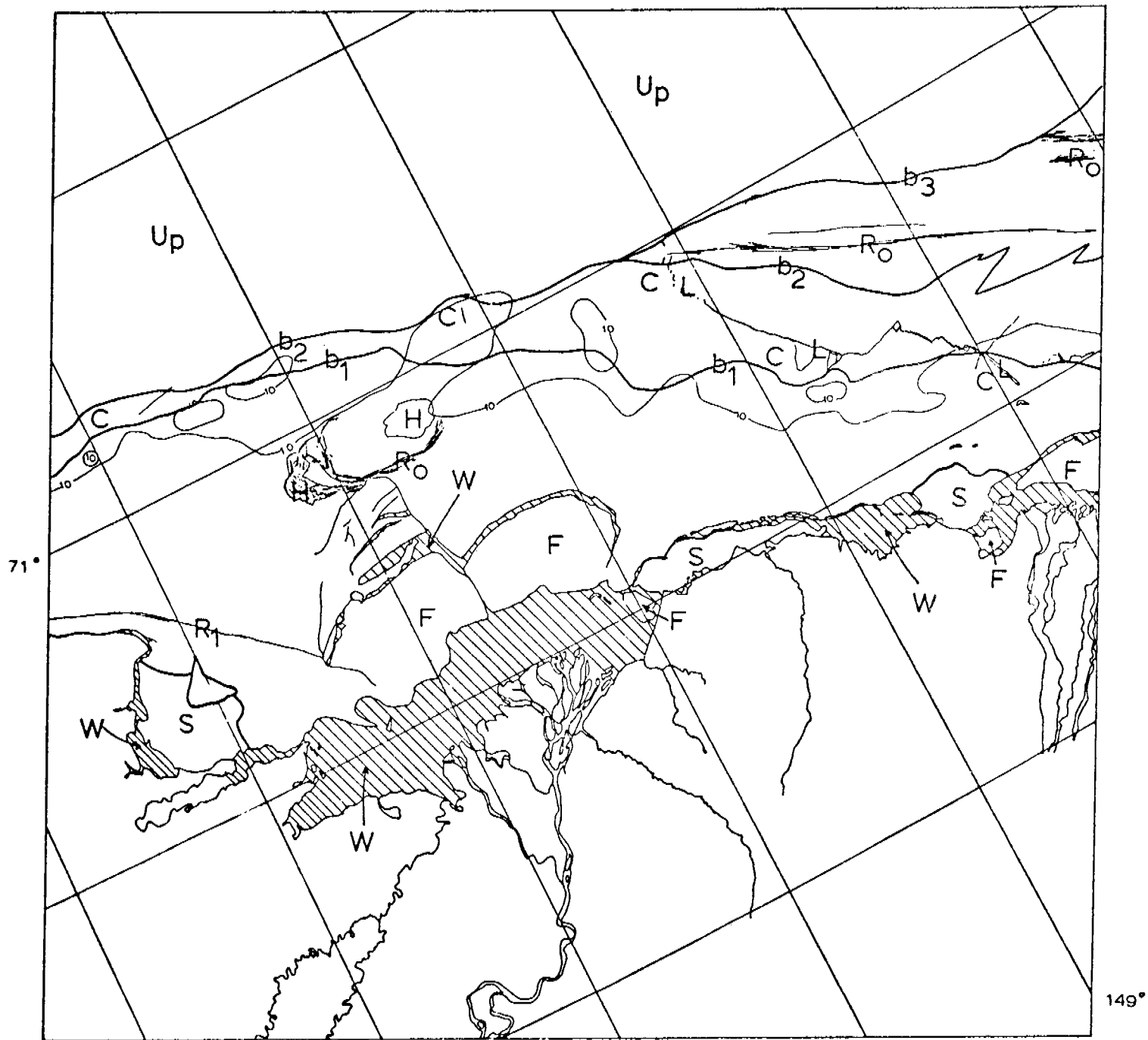
E-2-897-20493-7
7 JULY 1977

Scene 2898-20551 (8 July 1977)

The large lead system paralleling the coast from Oliktok Point eastward has almost closed again. Some other ice movement has taken place inshore of the stationary ice in the areas of open water.

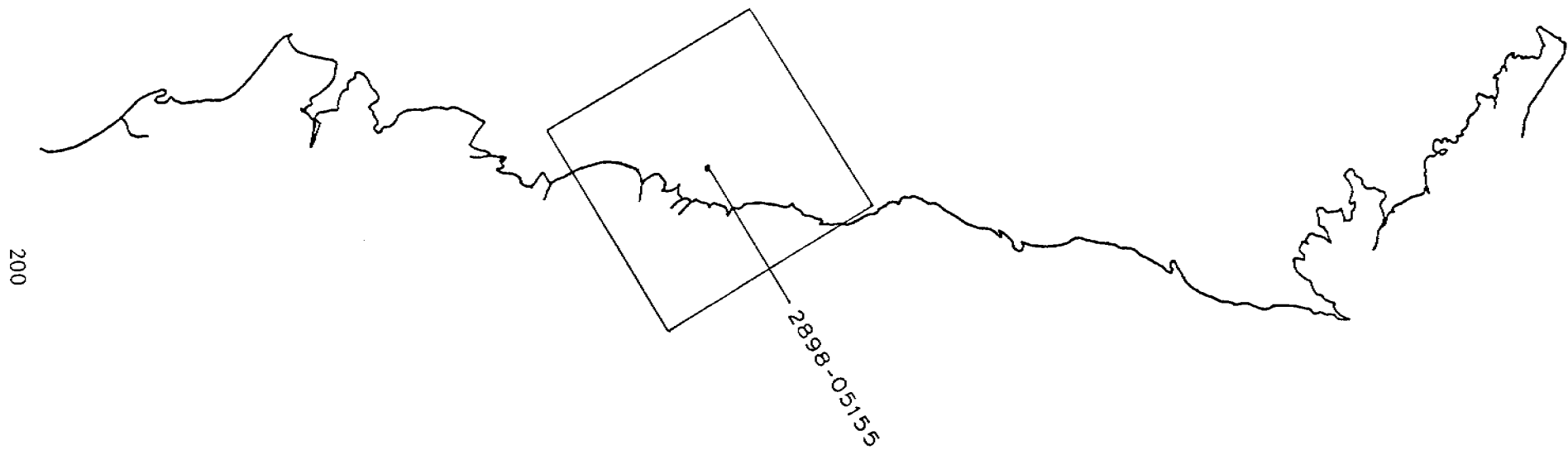
An area of very smooth ice can be seen in western Harrison Bay (labeled 'S'). This area appears very white in the image, indicating that it is well-drained. A triangular-shaped area of ice adjacent to this area appears almost black in the image and indicates an area of dark/poorly-drained and/or clear ice. North of this area is an old ridge, R_1 , which appears to be a single ridge rather than a system.

The ice between boundaries b_1 and b_2 and b_2 and b_3 is essentially the same as previously described. The circular ridge feature in Harrison Bay (R_0) is visible. The outline R_0 approximately overlies the six-fathom bathymetric contour of a high in the ocean floor. The smaller circular feature in the center is apparently a hummock field; it appears white in the image. Another hummock field extends to the west of the ridge feature.



BEAUFORT SEA

E-2-898-20551-7
08 JULY 1977



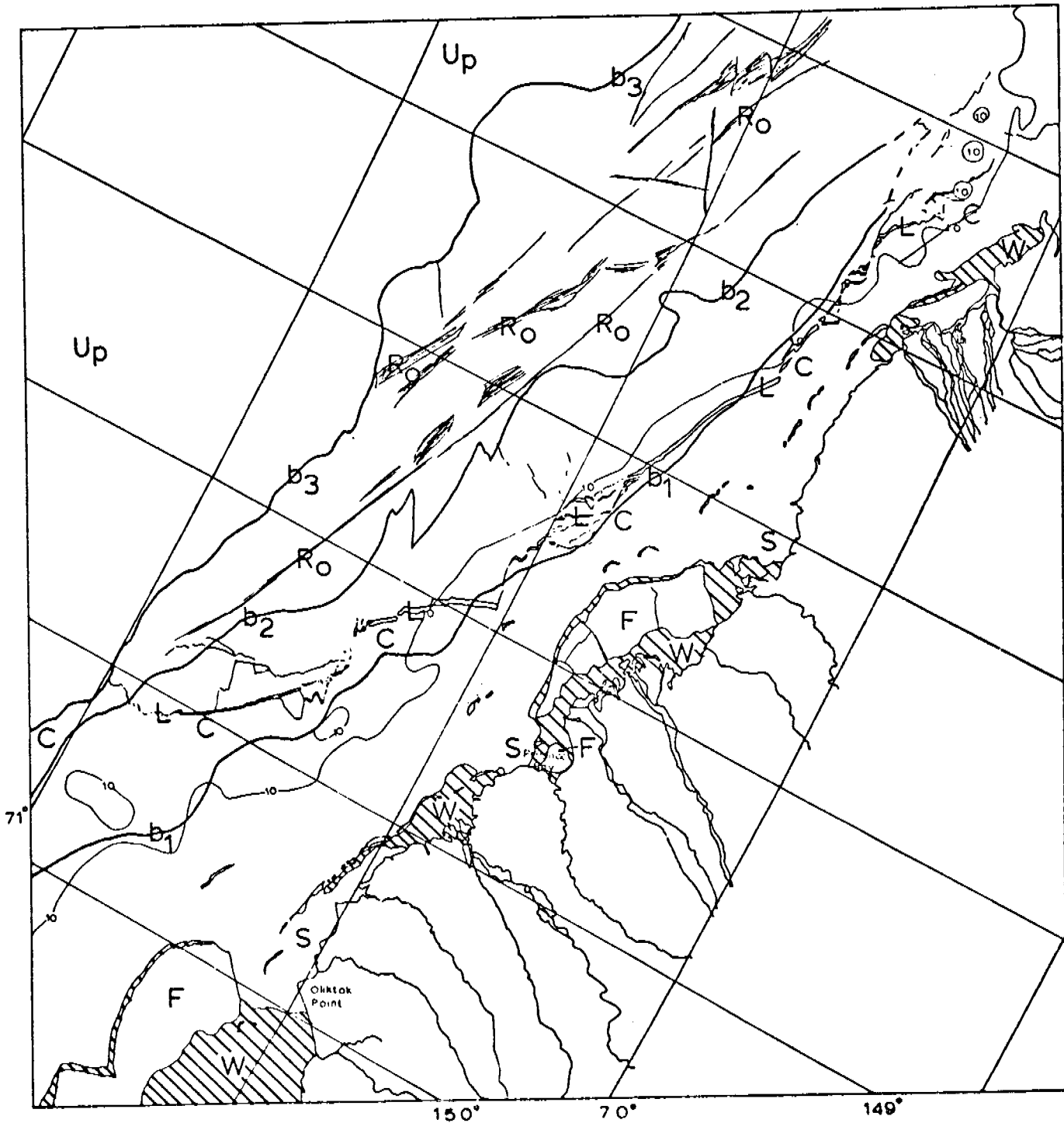
BEAUFORT SEA

ASCENDING NODE
8 JULY 1977

Scene 2898-05155 (8 July 1977)

This scene was obtained in the ascending mode of the spacecraft, i.e., when the satellite was traveling from south to north. The image was obtained at approximately 0515 hrs universal time, 8 July 1977, which is approximately 1915 hrs local time on 7 July 1977. The sun is at an azimuth of 296° with an elevation of 14° compared with the descending mode image azimuth of 158° and elevation of 40° for the same date.

The ice in this scene is basically unchanged from scene 2897-20493 (9 hours earlier). Two small sections of nearshore floating ice, labeled 'F', have moved shoreward. This is the only apparent change from 7 July (see description of previous image 2897-20493).



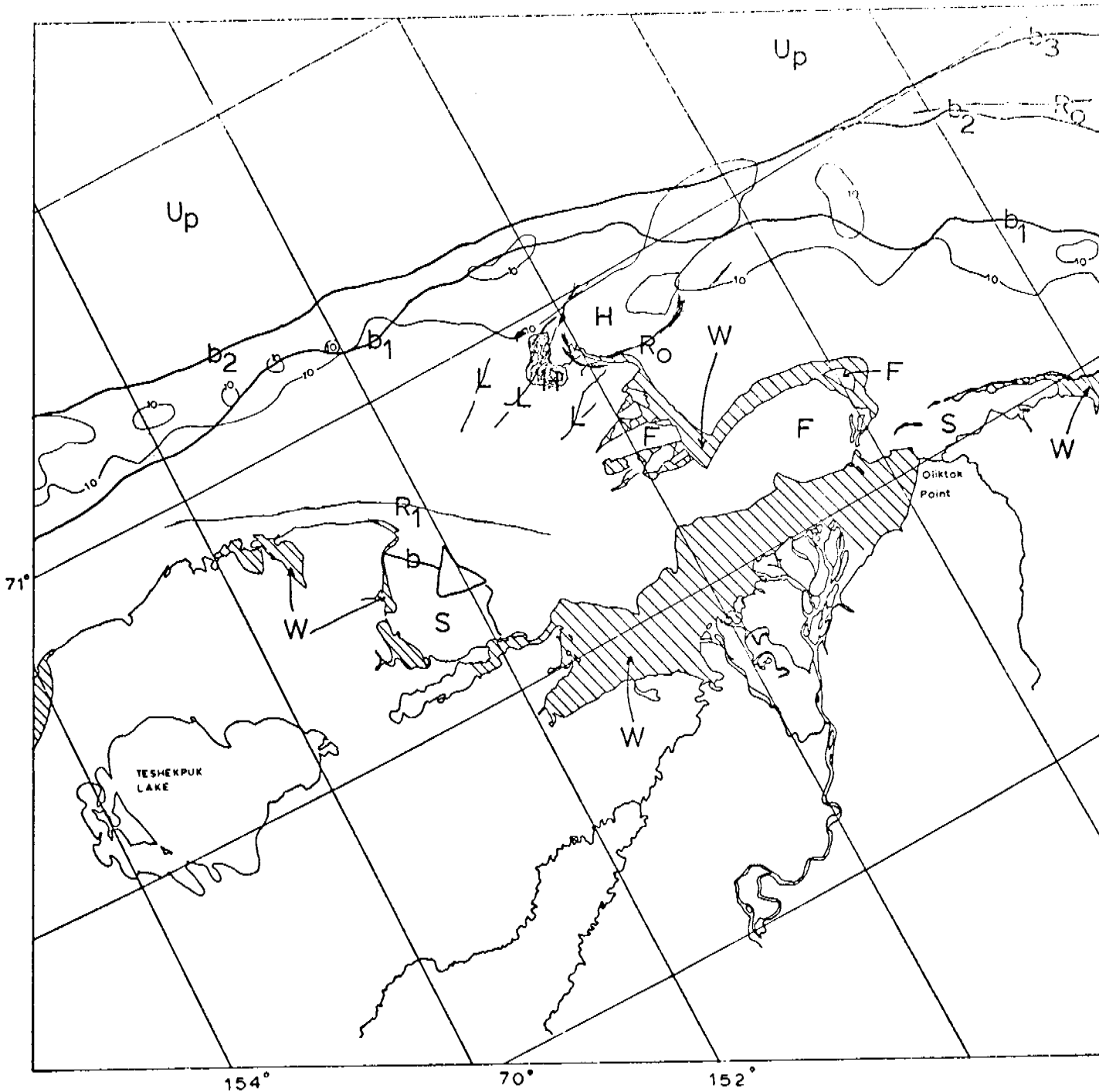
0 10 20 30 40
KILOMETERS

BEAUFORT SEA

E-2898-05155-7
08 JULY 1977

Scene 2899-21005 (9 July 1977)

The general character of the ice has not changed noticeably since the 7 July image (scene 2897-20493). However, the ice in Harrison Bay is breaking up. The fracture patterns and leads have extended into the edge of the circular ridge system that apparently encloses a hummock field grounded on a bathymetric high.



0 10 20 30 40
KILOMETERS

BEAUFORT SEA

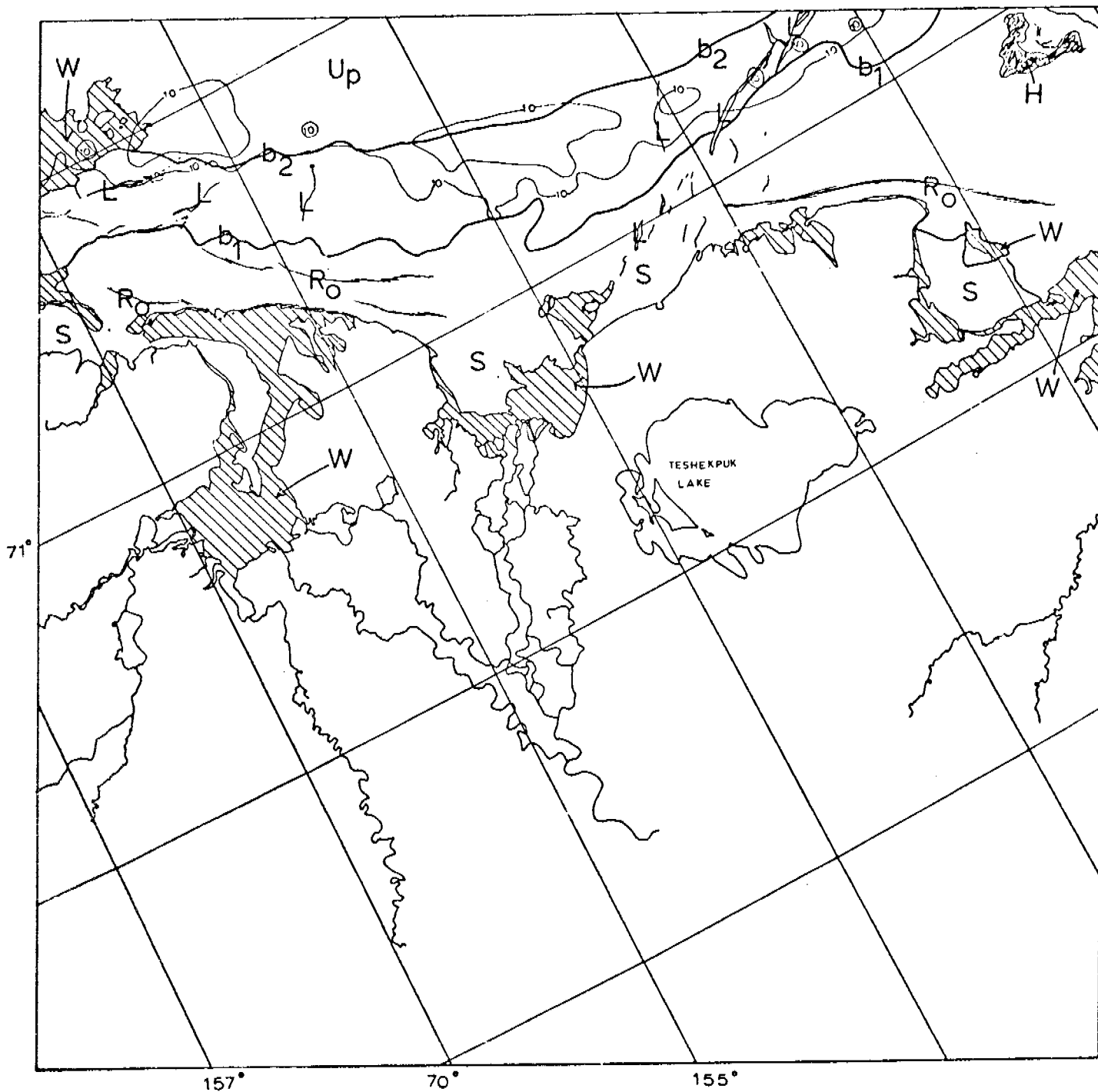
E-2-899-21005-7
09 JULY 1977

Scene 2901-21121 (11 July 1977)

Two distinct zones of stationary ice are visible in this image. The first zone consists of relatively flat ice with light to moderate ridging and piling (probably 10 to 50 percent of the surface is piled). This zone extends from shore (or the edge of open water) to boundary b_1 . Areas of very smooth ice are labeled 'S'. The remains of the large hummock field in Harrison Bay is visible in the upper right corner of the image.

The second zone between boundaries b_1 and b_2 consists of mostly ridged and piled ice (50 to 100 percent of the area). Seaward of boundary b_2 the pack ice appears unconsolidated.

The grounded stationary ice is in the process of breaking up. Large fractures in the ice can be seen and are indicated by 'L'. Open water is denoted by hachured areas.



0 10 20 30 40
KILOMETERS

BEAUFORT SEA

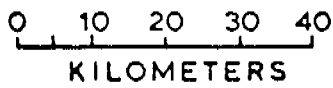
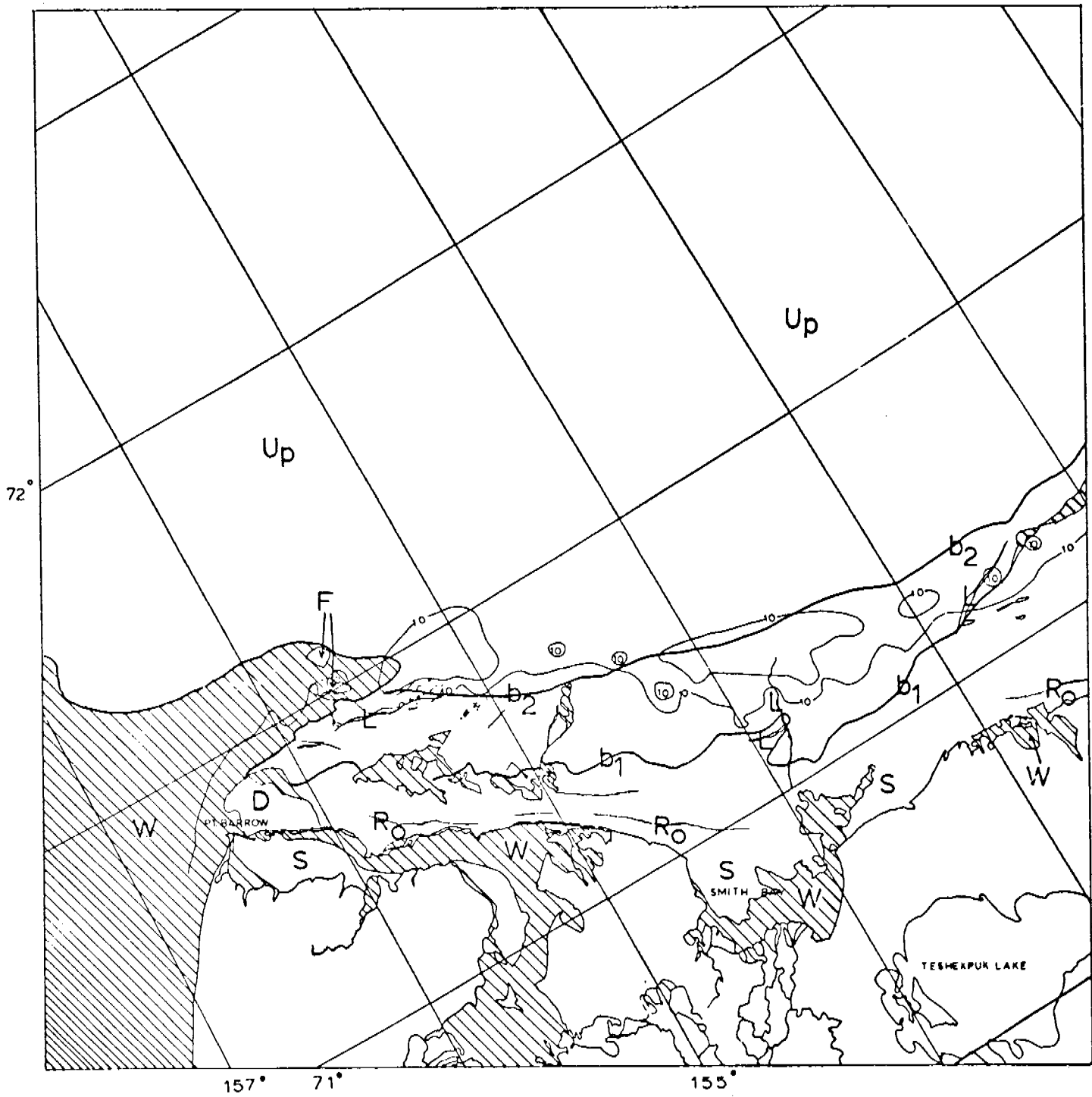
E-2-901-21121-7
11 JULY 1977

Scenes 2902-21173 (12 July 1977)
2902-21175

The nearshore stationary ice in the vicinity of Point Barrow is in the process of breaking up. Large expanses of open water exist between shore and the ice edge and between the relatively smooth ice and the piled ice (separated by boundary b_1). The zone of piled ice between boundaries b_1 and b_2 is also breaking up. Just off Point Barrow the area labeled D is decayed² and partially consolidated nearshore ice.

The pack ice is partially consolidated with fossil remnants of large ridge systems (floebergs) scattered throughout.

Hachured areas are open water.



BEAUFORT SEA

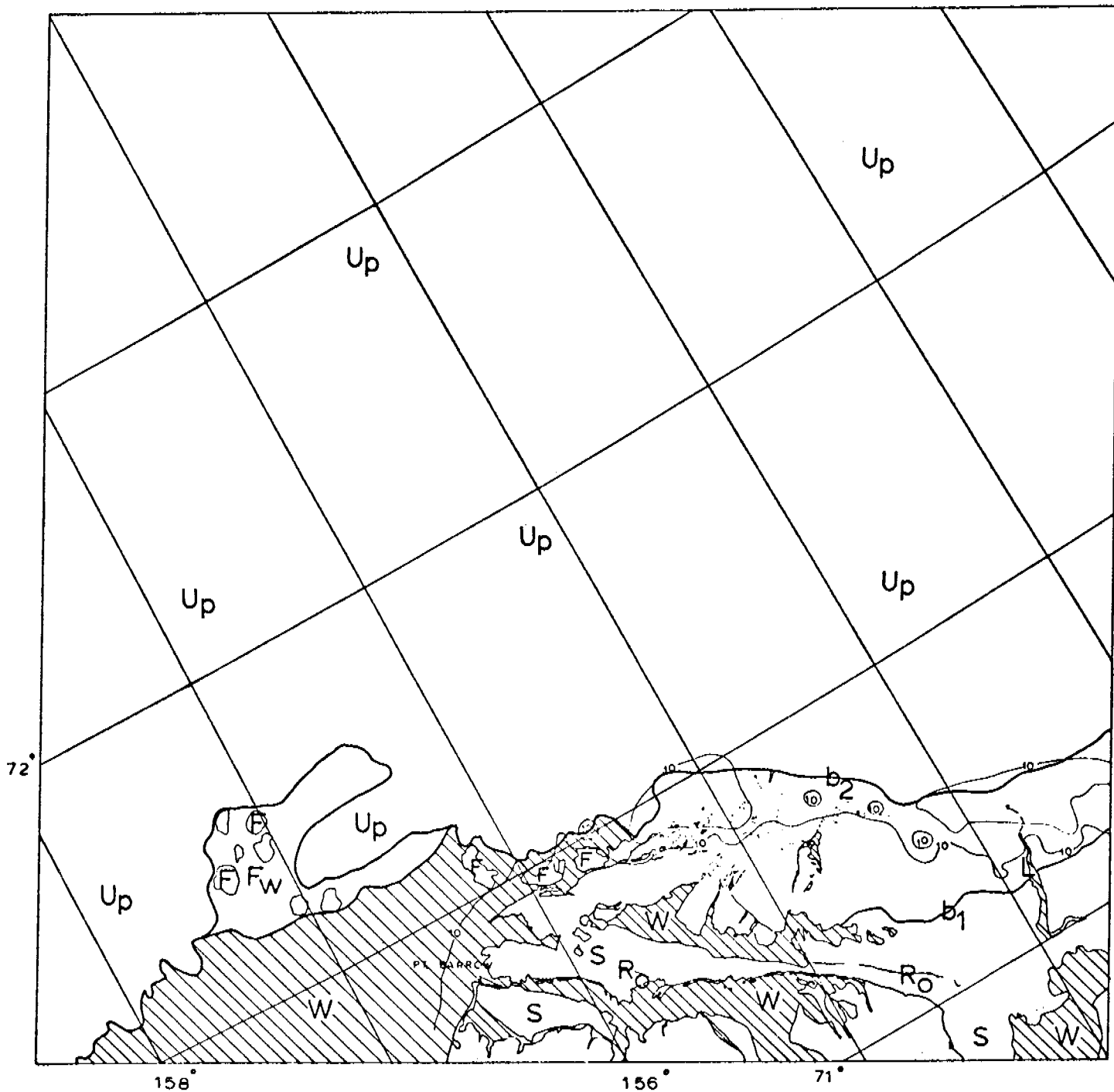
E-2-902-21173-7

E-2-902-21175-7

12 JULY 1977

Scene 2903-21231 (13 July 1977)

Substantially more breakup of the nearshore ice has occurred since the 12 July images (scenes 2902-21173 and 2902-21175) were obtained. Much more open water (W) is visible and the heavily ridged zone between boundaries b_1 and b_2 is fractured in several areas.

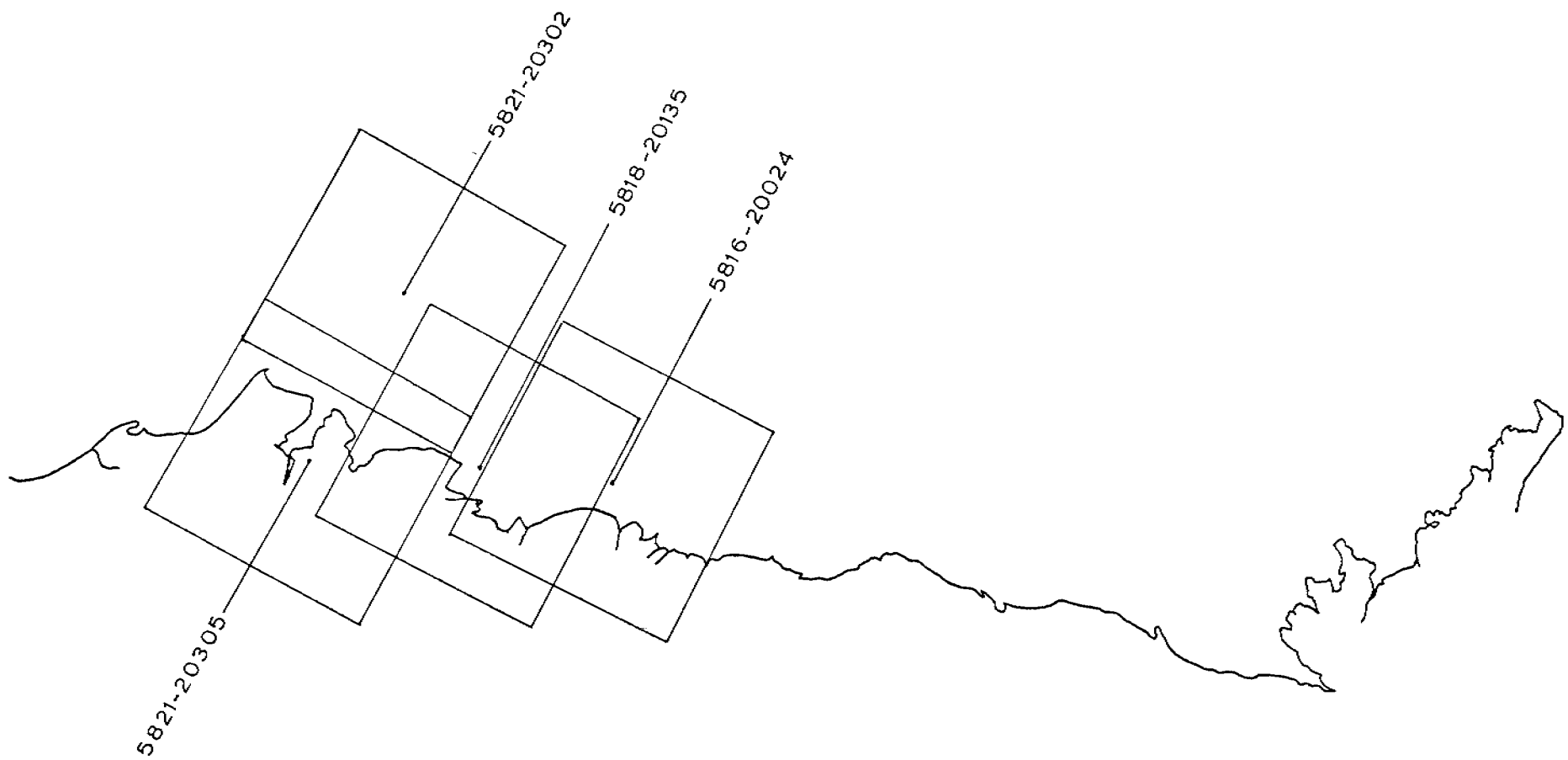


0 10 20 30 40
KILOMETERS

BEAUFORT SEA

E-2-903-21231-7
13 JULY 1977

211



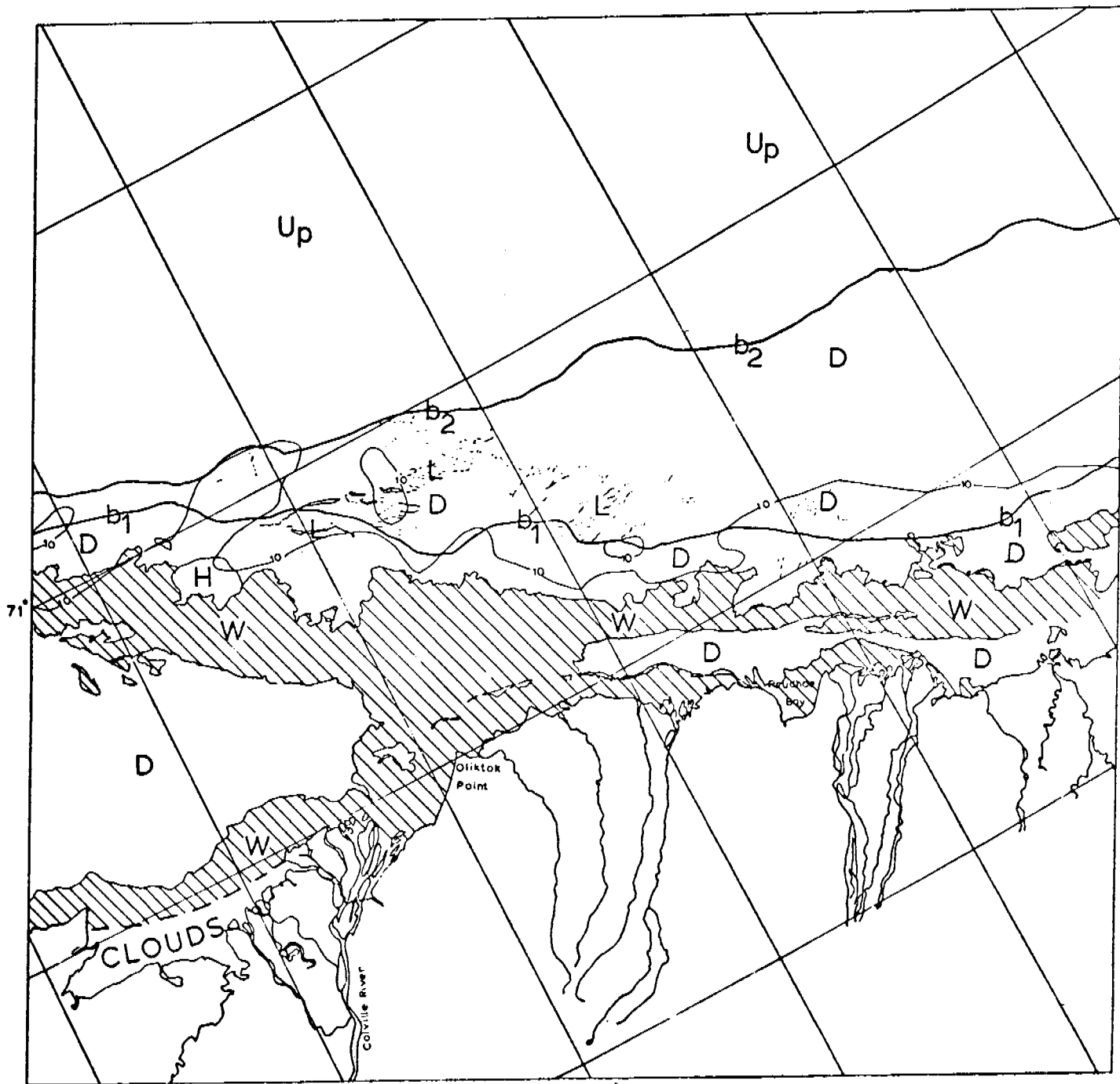
BEAUFORT SEA
1-18 JULY 1977
CYCLE 5804-5821

Scene 5816-20024 (13 July 1977)

The remaining nearshore ice is still relatively consolidated but is steadily decreasing in extent. As the ice decays, it becomes increasingly difficult to precisely locate the boundaries between the different zones. Areas of the ridged zone, north of boundary 'b₁', that are labeled 'L' are not true leads but are parallel fractures in the ice indicating left lateral motion of the ice in the area north of boundary b₁ with respect to the area south.

The hummocked area noted in earlier images north of Harrison Bay is all that remains of the large circular ridge feature (labeled 'H' in this map). There are a few small floes floating in the areas labeled open water (W).

Boundary b₂ is approximate; the edge of stationary ice is decaying such that it appears very similar to the unconsolidated pack ice.



0 10 20 30 40
KILOMETERS

BEAUFORT SEA

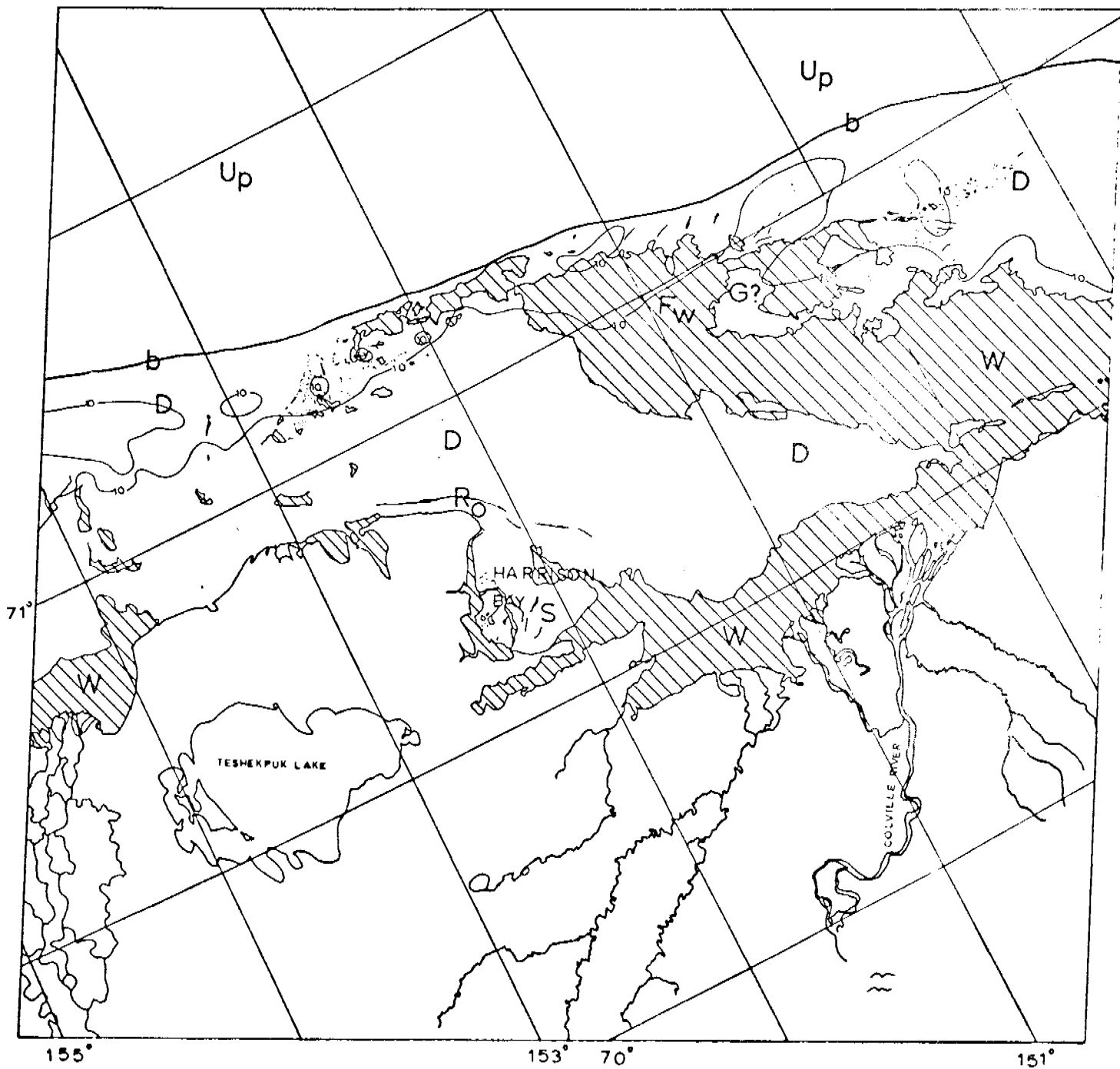
E-5-816-20024-7
13 JULY 1977

Scene 2818-20135 (15 July 1977)

The nearshore ice is very decayed in this scene of Harrison Bay. Large sections have moved; the sheet of ice in western Harrison Bay has moved towards shore as evidenced by the breakup of the old ridge labeled 'Ro'. The small sheet of smooth ice (S) has broken up. The possible remnants labeled 'G?', may or may not be grounded. These remnants appear to be unconsolidated pieces of the original feature.

The nearshore ice has decayed to the point that the boundary between it and the pack ice is very difficult to distinguish and is only located approximately (b).

The areas labeled 'W' are substantially free of floes. The area labeled 'Fw' contains approximately 5% floes by area.



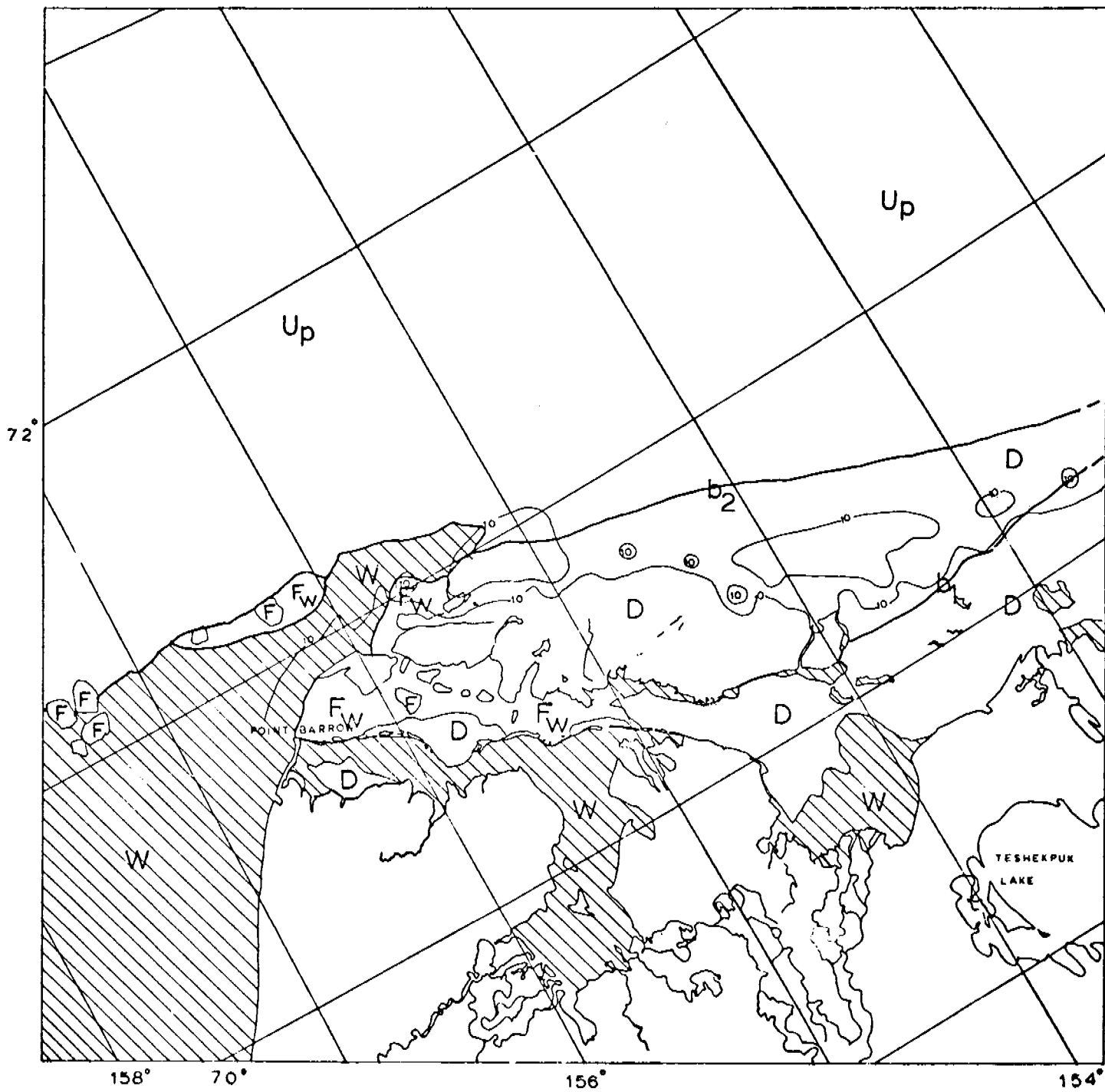
0 10 20 30 40
KILOMETERS

BEAUFORT SEA

E-5-818-20135-7
15 JULY 1977

Scenes 5821-20302 (18 July 1977)
5821-20305

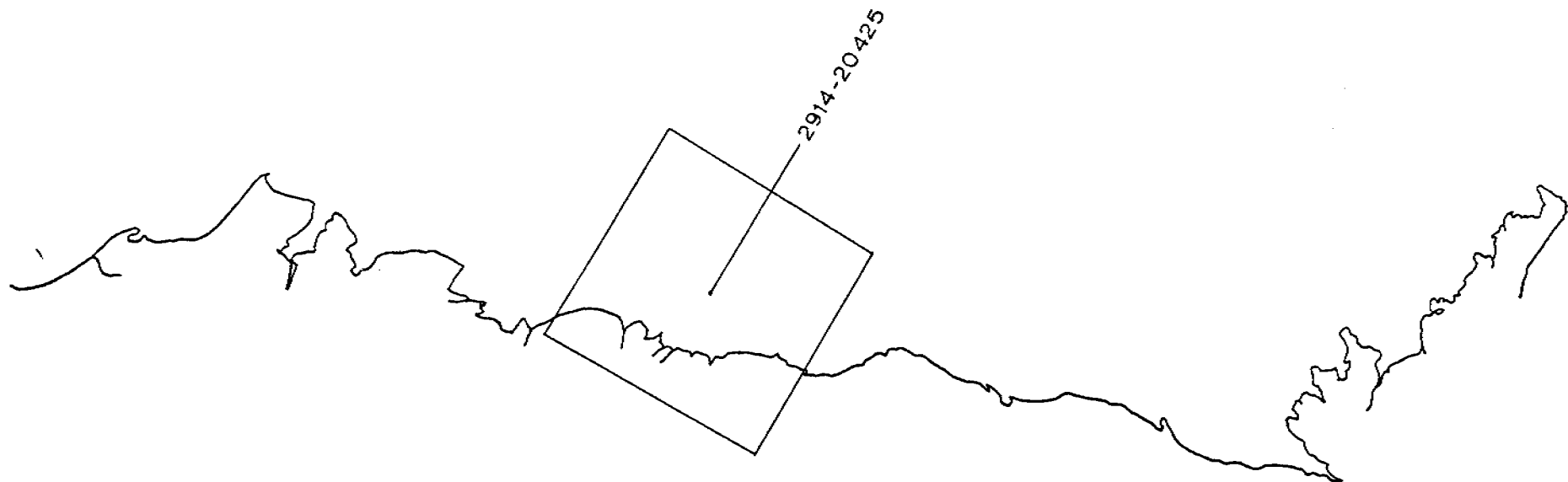
This scene is pretty much self-explanatory. Boundary b_2 is approximate. The near-shore ice appears to grade almost indistinguishably into the unconsolidated pack ice. Both zones of near-shore ice are very decayed with the 'smoother' inshore zone appearing more decayed than the 'rough' outer zone.



0 10 20 30 40
KILOMETERS

BEAUFORT SEA

E-5-821-20302-7
E-5-821-20305-7
18 JULY 1977



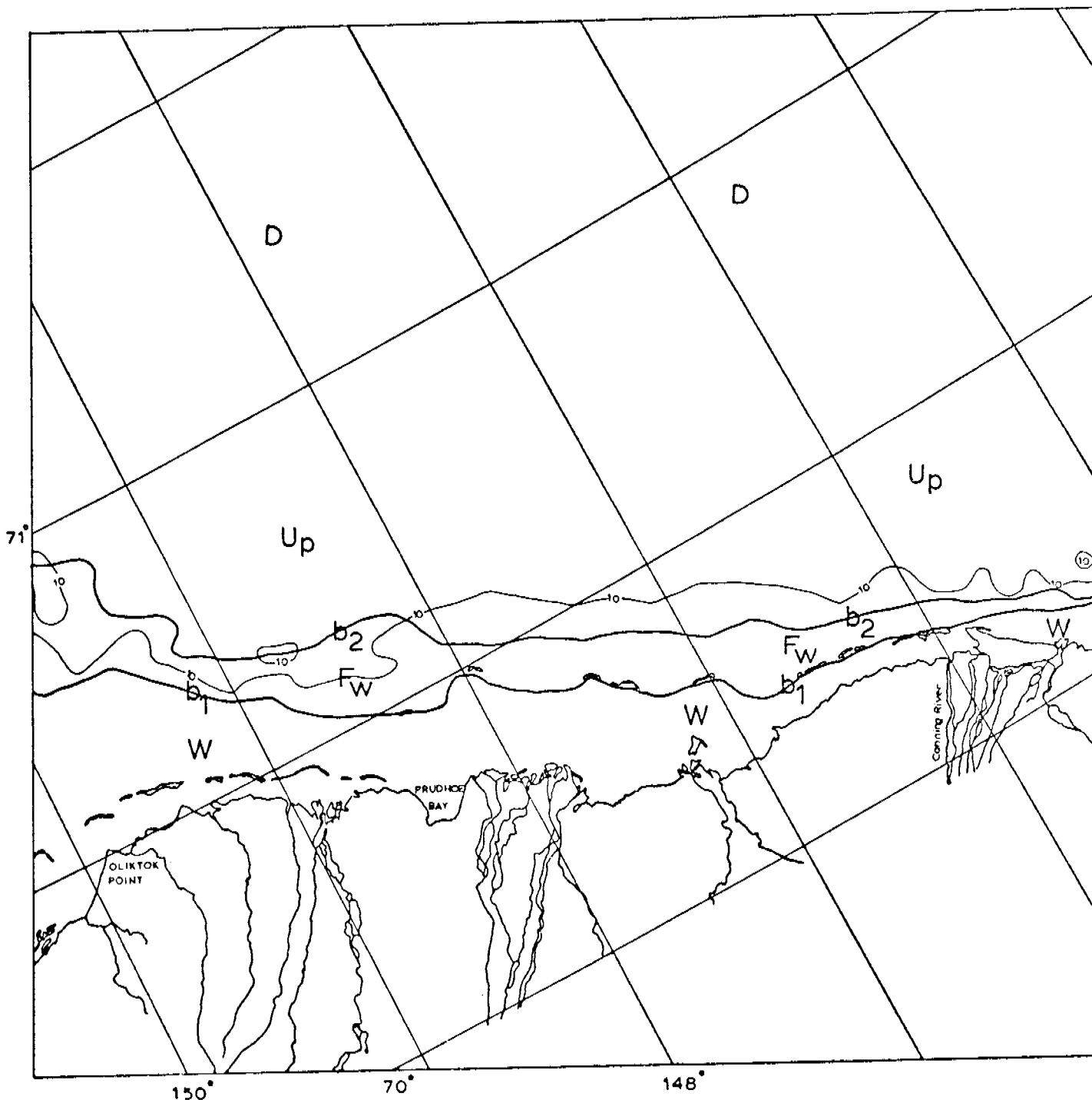
BEAUFORT SEA

13-30 JULY 1977

CYCLE 2903-2920

Scene 2914-20425 (24 July 1977)

The area between shore and b_1 is completely open water with no loose floes visible. The area between b_1 and b_2 is open water with floes and floating ice with concentrations from $\sim 10\%$ to $\sim 90\%$. The ice north of boundary b_2 is no longer stationary and is classed as pack ice (unconsolidated grading to decayed). However, some features spreviously in the stationary ice are still visible. Clouds partially obscure the pack ice.



0 10 20 30 40
KILOMETERS

BEAUFORT SEA

E-2-914-20425-7
24 JULY 1977

ANNUAL REPORT

Contract Number: 03-5-022-55

Research Unit Number: 265

Reporting Period: 1 April 1977 to 31 March 1978

Number of Pages: 39

DEVELOPMENT OF HARDWARE AND PROCEDURES
FOR IN-SITU MEASUREMENT OF CREEP IN SEA ICE

Lewis H. Shapiro

Geophysical Institute
University of Alaska
Fairbanks, Alaska 99701

Contributing Scientist:

Earl R. Hoskins

Department of Geophysics
Texas A & M University
College Station, Texas

March 31, 1978

TABLE OF CONTENTS

Page

I.	SUMMARY	
II.	INTRODUCTION	
	A. General Nature, Scope and Objectives	
	B. Relevance to Problems of Petroleum Development	
III.	CURRENT STATE OF KNOWLEDGE	
IV.	STUDY AREA	
V.	SOURCES, METHODS AND RATIONALE OF DATA COLLECTION	
VI.	RESULTS	
	A. Introduction	
	B. Viscoelastic Model for the Strength of Sea Ice	
	1. Introduction	
	2. Stress-Strain Relationship of the Four-Parameter Model	
	3. Constant Stress	
	4. Constant Stress-Rate	
	5. Constant Strain Rate	
	6. Failure	
VII.	DISCUSSION	
	A. Initial Tangent Modulus (Young's Modulus)	
	B. Fundamental Strength	
	C. Strain at Failure	
	D. Load Rate and Time Dependency of Failure Strength	
VIII.	CONCLUSION	
IX.	SUMMARY OF 4TH QUARTER OPERATIONS	
	A. Field Activities	
	B. Methods	
	C. Results	
	D. Problems Encountered	
	E. Estimate of Funds Expended	
	F. Milestone Chart	
	REFERENCES	
	FIGURE CAPTIONS	

I. SUMMARY

The objectives of this project are to develop and test the procedures and hardware required for in-situ measurement of the mechanical properties of sea ice, and to conduct a program of such measurements. The properties of primary interest are the strength, and elastic and viscoelastic constants in uniaxial and biaxial compression, but the strength in shear and tension has also been considered. In addition, the results of the extensive series of laboratory tests done by Peyton (1966) are also being reevaluated. The intention is to compare the results of the laboratory and in-situ tests in order to determine the degree with which laboratory results on small samples are representative of those from larger samples in the field.

In the last annual report of this project, the derivation of a one-dimensional, non-linear viscoelastic stress-strain law for sea ice was presented. During the past year, this study has been extended to include a failure criterion, so that the model now describes the behavior of some ideal material through the elastic and viscoelastic ranges up to failure, but not including post-yield behavior following ductile failure. The results of the law agree with the results of the preliminary analysis of Peyton's data, and with first results from the in-situ tests, but further analysis is required for verification.

A field program is currently in progress in which it is intended to test about 100 samples of ice with dimensions of 30 x 30 x 60 cm in uniaxial compression. Tests are being conducted at constant load to examine creep and creep-rupture behavior, and at constant loading rates to determine the strength. The methods used and results to date are described in the summary of 4th quarter activities below.

II. INTRODUCTION

A. General Nature, Scope and Objectives

The problem of translating results from laboratory tests to field conditions is well known in many branches of science, and forms an important aspect of studies of the mechanical properties of sea ice. It is difficult in the laboratory to simulate the effects of temperature and salinity gradients, continuous variations in grain size and ice fabric, and the presence of inhomogeneities on scales larger than laboratory samples. Further, mechanical properties of the ice can change during the processes of removal from the ice sheet, storage, and transport. Thus, a program is needed to determine the mechanical properties of the ice using large, relatively undisturbed samples, for comparison and verification of laboratory results.

The objective of this project is to develop the techniques, procedures and equipment necessary to measure as many as possible of the mechanical properties of the ice by in-situ methods; to utilize these procedures to conduct a program to obtain the relevant measurements; and to compare these results with published results of laboratory tests. In conjunction with these studies, it has also been necessary to develop the required mathematical description of the deformational properties of sea ice in order for the results of the experimental program to be interpreted.

B. Relevance to Problems of Petroleum Development

Any permanent or semi-permanent structure located off the Arctic Coast of Alaska must contend with the hazard that sea ice presents to its stability. The extent of this hazard depends on three basic parameters. First, the strength of the structure itself, with respect to its ability to withstand forces of a given magnitude. Second, the geometry of the interaction between the structure and the surrounding ice, including the state of bonding between the two and, finally, the strength of the ice, which determines the maximum force that the ice can sustain in the mode of failure which the structure is designed to induce. The first two of these parameters are determined largely by the third, the strength of the ice, and it is to this problem that the project is directed.

III. CURRENT STATE OF KNOWLEDGE

Weeks and Assur (1967) reviewed the state of knowledge regarding the mechanical properties of sea ice, and that work has been made current by Schwarz and Weeks (1977). The results of these reviews can be summarized by noting that major uncertainties of the strength of sea ice exist with respect to the effect of stress- or strain-rate, sample size, and loading direction relative to the dominant crystal orientation for all failure modes. Further, the effect of confining pressure has not been investigated, despite its importance for many applied problems.

A more complete review of previous work on the creep of sea ice has been reported in previous annual reports of this project.

IV. STUDY AREA

As in past years, the field program is being conducted in the landfast ice sheet at the Naval Arctic Research Laboratory at Barrow, Alaska.

V. SOURCES, METHODS AND RATIONALE OF DATA COLLECTION

The testing program for the current year reflects the progress made in the development of a mathematical description of the deformational properties of sea ice described below. Based upon these results, the test program was designed to provide data specifically for testing and refinement of the model. Thus, only creep, creep-rupture and constant loading rate tests in uniaxial compression are being conducted. It is anticipated that about 100 such tests will be completed during the field season.

All of the tests are being run on samples in the top 30 cm of the ice sheet, and all are oriented in the same direction with respect to the shoreline. It is hoped that this will eliminate the effects of crystal size and orientation as a variable in the test program. Future test programs will address this point.

No attempt is made to control the temperature during these tests, so that the test temperature is the naturally occurring temperature gradient at the time the test is run. Temperatures at several depths over the top 30 cm of the ice sheet are monitored continuously during the test program to provide this information. In addition, samples are collected from which salinity measurements are to be made.

VI. RESULTS

A. Introduction

In the following sections, the mathematical model referred to above is derived, and this represents the major contribution to the project during the past year. In addition, a preliminary analysis of the results of the past field season's experimental program has been completed, but these need to be re-interpreted in terms of the model, and it has not yet been possible to do this. Thus, these results will be reported at a later time. Finally, progress has been made in preparing the data from the constant load rate tests done by Peyton (1966) for additional study. This required reviewing the test series, and selecting and plotting various test results. Several hundred tests were selected to include series of tests on ice from the upper 30 cm of the ice sheet at various temperatures and orientations of the sample relative to the direction of loading. In addition, an extensive series of tests on samples from a depth of about 110 cm were also selected. These represent the most complete series of tests which Peyton ran on any ice type, and includes a wide range of temperatures and orientations.

B. Viscoelastic Model for the Strength of Sea Ice

1. Introduction

Sea ice is recognized to be viscoelastic material within the range of parameters at which most tests are conducted, and within its environment in nature. As such, its deformation characteristics are sensitive to the applied deformation rates as well as to variables of the material, such as salinity, grain size and fabric, and to the temperature. Natural events in which the ice reaches the limits of its strength occur over time scales from seconds to hours, so that the interaction of sea ice with fixed structures can be anticipated to involve times within this range. In view of the dependence of strength on deformation rates, this implies that for a stress-strain law for sea ice to have application either to natural phenomena, such as the formation of pressure ridges, or to engineering problems, it must be capable of describing the deformation of the ice under a range of loading rates, as well as for short term application of constant loads. Thus, for example, the entire creep curve is of interest, rather than just the steady-state creep stage as is the case for studies of the flow of ice in glaciers.

The approach adopted here treats the ice as a continuum, so that details of structure and deformation mechanisms are not considered. Thus, it is not the deformation of the ice which is being described by the law, but a mathematical model which "deforms" in a manner similar to the real material over some range of values of the experimental parameters which, in turn, is determined by experiments. As a result, the applicability of the law depends on the degree to which it conforms to experimental results and it is only in the most general sense that analogies between physical processes occurring in the real material and the behavior of the model can be drawn. There is an advantage to this approach, however, in that the results are not dependent upon relatively incomplete knowledge of the deformation mechanisms, but instead, depend upon experimentally determined continuum parameters of the material.

The stress-strain law derived below is based upon the one-dimensional, four-parameter spring-dashpot model which is well-known from the theory of linear viscoelasticity. Tabata (1958) derived the parameters for such a model from the results of a series of creep tests in uniaxial compression of core samples of sea ice, and from in-situ bending of cantilever sea ice beams. This suggested that a similar model would fit the creep curves obtained by Peyton (1966), but as noted in the last annual report of this project, attempts to do this gave unsatisfactory results. The reason for this is apparently that Peyton's tests were run at stresses an order of magnitude greater than those of Tabata, with a resulting magnification of the effects of the non-linear properties of the ice. Accordingly, the four-parameter model was given non-linear properties by specifying a non-linear stress-strain relationship for the dashpots of the model. A similar approach for the case of a three-parameter model is given in Krausz and Eyring (1975).

There is little data available for sea ice upon which to base the choice of a non-linear stress-strain relationship. However, attempts to fit both the power law and the hyperbolic sine law to the limited stress vs. steady-state strain-rate data from Peyton (1966) indicated that the latter gave better agreement with the experimental results. Thus, the hyperbolic sine law was adopted, with different material constants for each of the dashpots. The resulting model is shown in Figure 1. Note, however, that the derivations and calculations which follow could as easily be done for any suitable function.

The parameters of the model are taken here as constants, although their values would reflect the temperature, salinity, fabric, and other variables which determine the material properties of the sample. Thus, a different set of the constants of the model would be required for each sample and test temperature. However, the constants are considered to be independent of the stress, strain and time.

For the purpose of presenting the model, numerical values of the constants were required, and these were selected by averaging the values of the constants as determined by fitting the creep curve [equation (9) below] to the results of several of Peyton's (1966) experiments as described in the last annual report. The samples and test conditions were different for all examples used, so that the calculated results should not be considered as representative of any particular sample or test.

Spring-dashpot models provide a basis for examining the partition of energy between their elements as deformation proceeds, and analogies can be drawn from these to the behavior of the actual material. It should be emphasized that no particular deformation mechanism is necessarily associated with each element of the model. Instead, it is assumed that any model element represents the total contribution of all of the mechanisms which deform according to the law represented by that element. In that sense, it is reasonable to refer, for example, to the strain energy stored in the spring of the Voigt model, because it represents elastic strain recovered as a function of time upon removal of load, without reference to the mechanism by which this is accomplished.

The four-parameter spring-dashpot model is the simplest model which includes all the elements of a creep curve; the initial elastic response, primary creep stage and secondary or steady-state creep stage. Thus, a curve based upon such a model might be expected to apply to any material for which an experimental creep curve can be obtained over the range of parameters at

which that material will creep. Note that this should be true for loading modes other than uniaxial compression, such as bending, shear, or tension. However, some adjustment of the constants would be required for different loading geometries. A qualitative evaluation of some of the available data on the deformation of sea ice in bending indicates that this should be investigated further.

Given that some material deforms in creep in a manner such as described by the four-parameter model it is of interest to inquire as to whether other loading programs applied to the same model might also agree with experimental results. In particular, for the case of sea ice, loading programs consisting of constant stress-rates and constant strain rates have also been considered, and with satisfactory results as demonstrated below. Previous applications of this approach have been given by Krausz and Eyring (1975) and Stulen (1962).

Finally, it should be noted that taking the material parameters of the model to be independent of stress, strain and time, prevents the model from describing the behavior of the material past the peak stress in either a constant stress-rate or constant strain-rate test, or in the stage of accelerating creep in creep tests. It is argued below that these events occur in response to some significant change in the state of the test specimen, such as the introduction of cracks, or the initiation of recrystallization. In that case, the material constants of the original model no longer apply, and the correspondence between the calculated curves and experimental data fails. The point where this occurs is taken to represent the stage of an experiment at which processes leading to failure become dominant, and a means of predicting this point for the model is indicated and compared to experimental data with satisfactory results.

2. Stress-Strain Relationship of the Four-Parameter Model

The total strain in the model of Figure 1 is given as a function of time by the equation

$$\epsilon_T(t) = \epsilon_E(t) + \epsilon_D(t) + \epsilon_V(t) \quad (1)$$

where t is the time, $\epsilon_T(t)$ is the total strain and $\epsilon_E(t)$ is the strain in the spring of the Maxwell model given by

$$\epsilon_E(t) = \frac{\sigma(t)}{k_1} \quad (2)$$

$\epsilon_D(t)$, the strain in the dashpot of the Maxwell model, is found from the integral of the equation

$$\dot{\epsilon}_D(t) = B \sinh \theta \sigma(t) \quad (3)$$

in which the dot indicates the time derivative. Equilibrium requires that the stresses in the elements of the Voigt model satisfy the relationship

$$\sigma(t) = \sigma_1(t) + \sigma_2(t) \quad (4)$$

where $\sigma_1(t)$ and $\sigma_2(t)$ are the stresses across the dashpot and spring respectively. The strain-rate of the Voigt model is therefore

$$\dot{\epsilon}_V(t) = A \sinh \phi \sigma_1(t) \quad (5)$$

while the strain is given by

$$\epsilon_V(t) = \frac{\sigma_2(t)}{k_2} \quad (6)$$

Note that the partition of stress between these elements can always be calculated because, as shown below, $\epsilon_V(t)$ can be determined at any stage in the deformation. Then, substituting (4) and (6) into (5) leads to

$$\dot{\epsilon}_V(t) = A \sinh \phi (\sigma - k_2 \epsilon_V) \quad (7)$$

and introducing (2) and the integrals of (3) and (7) into (1) gives finally

$$\epsilon_T(t) = \frac{\sigma(t)}{k_1} + B \int_0^t \sinh \theta \sigma(t') dt' + A \int_0^t \sinh \phi [\sigma(t') - k_2 \epsilon_V(t')] dt' \quad (8)$$

where the primes indicate dummy variables, and the limits on the integrals imply the assumption that the material has no deformational history. Equation (8) is the general form of the stress-strain law of the model and, in principle, can be integrated for any given function of the stress.

3. Constant Stress

Two types of tests are conducted at constant stress; creep tests and creep-rupture tests. The difference between the two is in the magnitude of the applied stress. In creep tests the stress is kept sufficiently small that steady-state creep is achieved, while creep-rupture tests are intended to lead to failure. Note that the derivation assumes constant stress, rather than constant load, so that the applied load is assumed to be adjusted to compensate for changes in cross-sectional area of the specimen as the test proceeds.

For constant stress experiments, the stress can be written as

$$\sigma(t) = \sigma_c u(t)$$

where $u(t)$ is the unit step function defined by

$$u(t) = \begin{cases} 0 & t < 0 \\ 1 & t \geq 0 \end{cases}$$

and σ_c is the applied constant stress. For this case, the two integrals on the right side of the equation (8) can be evaluated, and, following rearrangement, the strain-time relationship is found to be

$$\epsilon_T(t) = \left(\frac{k_1 + k_2}{k_1 k_2} \right) \sigma_c + Bt \sinh \theta \sigma_c - \frac{2}{\phi k_2} \tanh^{-1} \left(\tanh \frac{\phi \sigma_c}{2} e^{-A\phi k_2 t} \right) \quad (9)$$

Equation (9) describes a creep curve with an instantaneous response to the applied stress given by the ratio σ_c/k_1 , the extension of the spring of the Maxwell model. The steady state strain-rate is the time derivative of the second term, the strain in the dashpot of the Maxwell model. The remaining terms describe the deformation of the Voigt model which largely defines the primary creep segment of the curve. Note that the value of this component of the total strain is asymptotic to the quantity σ_c/k_2 for large values of t .

Sample creep curves are shown in Figure 2, and partition of the strain in the elements of the model is given in Figures 3 and 4 for a "high" and a "low" stress test.

4. Constant Stress-Rate

For constant stress-rate tests, the stress as a function of time is given by

$$\sigma(t) = \bar{\sigma} t$$

where $\bar{\sigma}$ is the stress increment applied per unit of time. Substituting this expression into (4) and using (5) and (6) to find $\sigma_2(t)$ in terms of $\sigma_1(t)$ then gives

$$\bar{\sigma} t = \sigma_1(t) + Ak_2 \int_0^t \sinh \phi \sigma_1(t) dt'$$

Differentiating with respect to time and separating variables then leads to the equation

$$\int_0^t \frac{d\sigma_1'(t)}{C - \sinh \phi \sigma_1'(t)} = Ak_2 \int_0^t dt' \quad (10)$$

where the primes indicate dummy variables and the constant C has been substituted for $\bar{\sigma}/Ak_2$. Then, introducing the substitution

$$z = C - \sinh \phi \sigma_1'(t)$$

and performing the integration on the right side of (10) gives

$$-\frac{1}{\phi} \int_C^{C - \sinh \phi \sigma_1'(t)} \frac{dz}{z(z^2 - 2Cz + C^2 + 1)^{1/2}} = Ak_2 t$$

Taking note of the values of the coefficients in the denominator, the left side of this equation can be integrated (Dwight, 1947, #380.111) and rearranged to

$$\sigma_1(t) = \frac{1}{\phi} \sinh^{-1} \left[\frac{C \sinh(Dt + E) - 1}{C + \sinh(Dt + E)} \right] \quad (11)$$

in which

$$D = \phi k_2 A(1 + C^2)^{1/2}$$

and

$$E = \sinh^{-1} \frac{1}{C}$$

The stress-strain equation for the Voigt model can then be found from (4), (5) and (11), and combined with those for the elements of the Maxwell model given by (2) and the integral of (3), to give the complete stress-strain relationship of the model for constant stress-rates as

$$\epsilon(t) = \frac{k_1 + k_2}{k_1 k_2} \sigma(t) + \frac{B}{\theta \bar{\sigma}} [\cosh \theta \sigma(t) - 1] \\ - \frac{1}{\phi k_2} \sinh^{-1} \frac{C \sinh \left[D \frac{\sigma(t)}{\bar{\sigma}} + E \right] - 1}{C + \sinh \left[D \frac{\sigma(t)}{\bar{\sigma}} + E \right]} \quad (11)$$

Sample curves are given in Figure 5. Note the variation in the initial slope with changes in the stress-rate, and the rapid increase in strain at high stresses. These characteristics of the curves can be explained by examining the response of the individual elements of the model to the applied stress. This is shown in Figures 6 and 7, which are plots of the stress-strain curve for each model element, for the stress vs. total elastic strain (total strain less the strain in the dashpot of the Maxwell element) and, for the stress vs. total strain resulting from a test at a "high" stress rate and a second test at a "low" stress rate.

The latter two figures show that the initial response to the applied stress is controlled by the spring of Maxwell model, which corresponds to the true modulus of elasticity. For the model parameters chosen here, the strain in the Voigt element is then responsible for the initial non-linear portion of the curve, with the dashpot of the Maxwell model contributing to the rapid increase in strain with stress at the higher stress levels. Note that the range of stresses over which a valid measurement of Young's Modulus can be made is indicated by the range over which the curves of strain in the spring of the Maxwell model and of total elastic strain coincide in Figures 6 and 7. This range clearly increases with increasing stress rate, while the curves of individual tests at high rates also tend to coincide (Figure 5).

An obvious question exists with respect to the segmented nature of the stress-strain curves at higher stress rates. That is, whether in fact this effect is characteristic of any material (sea ice in this case), or merely a property of the model representation. Examination of Peyton's (1966) data clearly shows that these features do occur in many cases, and that numerous other curves in the data, because they consist of few data points, could be interpreted in that way. However, there are a significant number of curves which are smooth, and admit no possibility of the interpretation described above. The problem may be resolved when the examination of Peyton's data is complete. However, for the present, it is reasonable to conclude that experiments on some ice types, within some range of stress rates and temperatures do indeed produce stress-strain curves such as described by the model.

5. Constant Strain Rate

For a constant strain rate $\bar{\epsilon}$ applied to the model, the strain at time t is

$$\bar{\epsilon}t = \frac{\sigma_2(t)}{k_2} + \frac{\sigma(t)}{k_1} + B \int_0^t \sinh \theta \sigma(t) dt' \quad (12)$$

while the strain rate is

$$\bar{\epsilon} = A \sinh \phi \sigma_1(t) + \frac{\dot{\sigma}(t)}{k_1} + B \sinh \theta \sigma(t) \quad (13)$$

Solving (13) for $\sigma_1(t)$ and (12) for $\sigma_2(t)$ and substituting into (4) then gives

$$\sigma(t) = \frac{1}{\phi} \sinh^{-1} \frac{\dot{f}}{A} + k_2 f \quad (14)$$

where

$$f = \bar{\epsilon}t - \frac{\sigma(t)}{k_1} - B \int_0^t \sinh \theta \sigma(t) dt'$$

These equations have been integrated numerically, and the solution curves are given in Figure 8. In addition, the partition of strain between the model elements for "high" and "low" strain-rate tests are shown in Figures 9 and 10.

In contrast to the constant stress-rate tests, the constant strain-rate tests reach a steady state when the strain-rate in the dashpot of the Maxwell element reaches the applied strain-rate. At that time, the elastic elements of the model are no longer active. In actual experiments at sufficiently high strain rates, failure occurs before steady-state is reached. This point is discussed further below.

The curves of Figure 8 also indicate the variation of the elastic modulus with strain-rate, as was described above for the constant stress-rate tests. As above, the reasons are apparent from consideration of the strain of the individual elements of the model shown in Figures 9 and 10.

Finally, note that the comments above regarding the occurrence of segmentation of the stress-strain curves for the constant stress-rate tests also apply to the curves of Figure 8.

6. Failure

The parameters of the model have been assumed to be independent of the test variables, stress, strain and time. Thus, the calculated stress-strain and strain-time curves could be extended indefinitely, with respect to these variables without the appearance of the discontinuities or inflection points which would result from failure of the sample in actual experiments. Introduction of a damage function into the model parameters could overcome this limitation. However, at present it appears to be more useful to establish a failure criterion based upon the deformation of the model, with the recognition that this represents the limit of the range of the variables over which the model is expected to describe experimental results. Then, given a failure criterion for the model, relationships between the strength and the stress-rate, strain-rate, time to failure in creep-rupture tests, etc., can be calculated and compared with experimental data. As shown below, the results of such a comparison are in good agreement.

In real materials, failure is a process rather than an event, in the sense that a critical stress at which failure occurs is not reached throughout the entire test specimen at the same instant. Instead, the sample breaks down over a finite time interval as the stress is redistributed after each successive failure of a relatively small volume within which the critical stress has been reached. This breakdown is accompanied by a change in the material constants, such as the decrease in Young's modulus with increase in the number and length of cracks in a sample. As a result, as failure is approached in any test, at some time the stress-strain curve deviates from its projected path. The accuracy of determination of the point at which this occurs depends upon the instrumentation, and probably on the nature of the operative failure process. The important point is that experimental curves do exhibit this property, and this, in turn, results from a change in the values of the material constants as failure is approached.

To illustrate this, consider the strain-time curve of a creep-rupture test. Following application of the load and the initial elastic response, the curve progresses into the primary creep stage, with an accompanying continuous decrease in strain-rate. In a creep test, the strain-rate continues to decrease until steady-state creep is reached. However, in a creep-rupture test, the strain-rate reaches a minimum value at the time at which the inflection point, which marks the initiation of tertiary creep, appears on the strain-time curve. Subsequently, the strain increases with an accelerating rate until rupture occurs. Note that once the inflection point has been reached, rupture must eventually follow unless the stress is removed. Thus, the inflection point can be considered as indicating the initiation of processes leading to failure, with an accompanying change in the response of the sample to the

applied load. This, in turn, implies a change in the parameters which define the material properties of the sample because, without such a change, the inflection point would simply not appear on the curve. For creep-rupture tests, the fact that only the strain varies as a function of time simplifies the problem of identifying the point where this change occurs.

Thus, there are two "critical" points on curves of experiments which are taken to failure. The first is that point at which the failure process becomes the dominant mechanism of deformation, and is indicated by the deviation from the projected curve described above. The second is the actual point of failure at which the sample carries its maximum load in one of the rate tests, or at which rupture occurs in a creep-rupture test. The distance along the curve between these points then represents the breakdown of the sample, and its duration probably depends upon the failure mechanism and the loading parameters.

As noted, the model includes no provision for varying the mechanical properties with the variables of the test. Thus, any failure criterion adopted for the model can only depict the first of the critical points, the point at which the experimental curve deviates from its expected behavior.

Note that this point does not coincide with the engineering yield strength as presently defined (ASTM Standard E8-69). That is, the stress at some specified value of the permanent strain (usually taken as 0.2%). As shown below, for some tests, this value of the permanent strain, represented by the strain in the dashpot of the Maxwell model, can be exceeded before failure (in the sense of the model) occurs.

Peyton's (1966) data provides a basis for selecting a reasonable failure criterion for the model in the results of approximately 40 creep-rupture experiments on sea ice samples of a variety of fabrics, orientations and grain sizes, which were tested at several temperatures between -6°C and -21°C and at stresses from .21 MPa (30 psi) to 2.8 MPa (400 psi). For all of these tests, the strains at the points of minimum strain-rate ranged approximately from 5×10^{-3} to 2×10^{-2} . This was considered to be sufficiently narrow to imply a relationship with the strain, probably through the strain energy. Accordingly, a strain energy criterion of failure was assumed to apply to the model, and the implications and comparison of the results with available data are described below.

The approach through which this is accomplished is taken from Reiner (1960) in which the von Mises yield criterion was applied to a 3-parameter model of a linear viscoelastic substance. The extension to the 4-parameter, non-linear model considered here follows directly. Noting that the work done in deforming the dashpots of the model is assumed to be dissipated through internal friction, it is postulated that failure (in the sense described above) occurs at some critical value of that part of the distortional stress-work which is conserved as elastic strain energy in the springs of the model. This critical value is identified with the resilience, "R", the work (per unit volume) required to deform an elastic body to its elastic limit.

Assuming the model to be elastically isotropic, for a uniaxial load $\sigma^*(t)$, the second invariant of the stress deviator becomes simply

$$J_2 = \frac{1}{3} [\sigma^*(t)]^2$$

so that the distortional strain energy is

$$W_d = \frac{1}{6G} [\sigma^*(t)]^2 = \frac{1}{2G} J_2$$

where G is the shear modulus. This can be written as

$$W_d = \frac{(1 + \nu)E}{3} [\epsilon^*(t)]^2 = a E [\epsilon^*(t)]^2$$

where ν is Poisson's ratio and E is Young's modulus. Finally, following Reiner, the distortional strain energy of the model is simply the sum of the the strain energies stored in the two springs and failure occurs when this reaches, the value R . That is, when

$$R = W_d = a \left\{ k_1 [\epsilon_E(t)]^2 + k_2 [\epsilon_V(t)]^2 \right\}. \quad (15)$$

An immediate consequence of the assumption that failure of the model is dependent upon the resiliancy is that both upper and lower limits of stress can be established between which the strength of the model must fall, for any loading program in which the maximum stress is reached in a finite length of time (instantaneously applied stresses which are greater than the upper strength limit will, according to the model, cause instantaneous failure). This can be demonstrated by rewriting equation (15) in terms of the stresses and rearranging to give the equation of an ellipse in σ - σ_2 space,

$$\frac{\sigma^2}{b_1} + \frac{\sigma_2^2}{b_2} = 1$$

in which

$$b_1 = \frac{Rk_1}{a}, \quad b_2 = \frac{Rk_2}{a}$$

and the stresses are those defined in equations (2) and (6). Equilibrium across the model [equation (4)] requires that $\sigma \geq \sigma_2$, so that the possible combinations of σ and σ_2 at failure must fall on the curve shown in Figure 11. The value of σ in any such pair then represents the strength of the model. Note that the assumption that $k_1 > k_2$ was used in preparing Figure 11, but, as shown below, the same conclusion would hold for $k_2 > k_1$, in which case the long axis of the ellipse would be parallel to the σ_2 -axis.

From Figure 11, the upper limit of the strength, σ_u , occurs at $\sigma_2 = 0$ (and $\epsilon_v = 0$) which, from equation (15) gives

$$\sigma_u = \left(\frac{k_1 R}{a} \right)^{1/2}$$

This corresponds to an experiment in which the load is applied instantaneously so that no strain occurs in the Voigt model and all of the elastic strain energy required for failure is developed in the spring of the Maxwell model. Thus, σ_u represents the maximum stress that the model can sustain for loading over a finite time interval, but the minimum stress which will result in instantaneous failure.

The lower limit of the strength, σ_b , occurs when $\sigma = \sigma_2$ and, from equation (15) is given by

$$\sigma_b = \left[\frac{Rk_1 k_2}{a(k_1 + k_2)} \right]^{1/2}$$

Any loading program applied to the model which does not include a value of the stress at least equal to σ_1 will not lead to failure, irrespective of the time interval over which the stress is maintained. Thus σ_b represents the "fundamental strength" of the model.

Finally, dividing equation (17) by (18) gives

$$\frac{\sigma_u}{\sigma_b} = \left(1 + \frac{k_1}{k_2} \right)^{1/2}$$

which shows the dependence of the ratio of the strength limits on the ratio of the spring constants. Note also that $\sigma_u > \sigma_b$ for any $k_1 > 0$, irrespective of the value of k_2 , as was stated above.

The application of equation (15) to the model was accomplished by assuming some value of the strain of the spring of the Maxwell model required to cause failure for a load applied instantaneously. This was taken as $\epsilon_F = 2.5 \times 10^{-3}$. Then, assigning a value of $a = .4$ (corresponding to ν approximately .3) a value of "R" was calculated and used to define the failure of the model in a series of "experiments" calculated for the three tests described above. For each constant stress-rate calculation the stress, strain, strain-rate and test duration were determined, while for the case of constant strain-rate, the stress, strain, stress-rate and test duration were calculated. Finally, for creep-rupture tests, the strain, strain-rate and time to minimum strain-rate were determined.

The results of these calculations are presented in Figures 12 through 15, where the values of the parameters plotted are those at the instant of failure in the sense of the model. That is, at the point where equation (15) is satisfied. Note that the heavy lines in the plots indicate the fact that the resulting curves are so close together that they are within the range of values covered by the line width. This correspondence can be demonstrated to be the result of the assumption that failure occurs at a critical value of the resilience.

The value of σ_b for the model parameters chosen is indicated on Figure 12, and the curve extended to lower stresses and strain rates using equation (3), the stress-strain rate relationship for steady-state creep. This step follows the suggestion of Hawkes and Mellor (1972) who demonstrated a similar continuity based upon creep tests and constant strain-rate tests on polycrystalline fresh ice. Note that the same curve has been extended to higher stresses to indicate the nature of the transition to failure.

The total strain at failure for the three types of experiments is shown in Figure 14. Note that the value of the strain is a minimum at the stress required to cause instantaneous failure, and increases without bound as the lower limit of the strength, σ_b , is approached. The latter feature is due to the increase in the time to failure at the lower stresses as shown in Figure 13, which permits the strain in the dashpot of the Maxwell model to become large relative to the elastic strain. The point is illustrated by comparing the curve of strength vs. total strain with the curve of strength vs. elastic strain as indicated by the dashed line in Figure 14. It is also clear from this figure, that the engineering yield strength defined above, can be exceeded before equation (15) is satisfied.

The strength vs. time to failure curves of the three experiments are shown in Figure 13, and these are clearly dispersed more than those of Figures 12, 14 and 15. Note that the three curves are asymptotic to both σ_b and σ_u , with curvature at the high stresses not apparent until the time to failure is in the range of 10^{-2} minutes or less, corresponding to about 90% of σ_u . Similarly, the curvature at the lower stresses develops at stresses no more than about 10% greater than σ_b . Between these values, the curves are essentially linear on the semi-logarithmic plots used here.

VII. DISCUSSION

As described in the introduction, the model represents the deformation and failure of some ideal material, so that its utility depends upon the degree to which it can be used to predict the behavior of real materials under various loading conditions. In this section, the results of the model calculations are qualitatively compared with experimental results for both fresh and sea ice. These will show that the model does provide a framework which describes many of the observed features of experimental results for uniaxial compression tests. The fact that so many of these are included in the model indicates that it may indeed be a useful tool for analysis of such tests.

A. Initial Tangent Modulus (Young's Modulus)

Hawkes and Mellor (1972) note that reported values of Young's modulus for static tests on fresh ice are generally lower than those for dynamic tests, except at very low temperatures or high loading rates. Under the latter conditions, the modulus approaches that for dynamic tests. Results obtained from Peyton's (1966) experimental data and by Vaudrey (1977) on sea ice also indicate an increase of Young's modulus for increasing loading rates.

The stress-strain curves for constant stress-rate and constant strain-rate shown in Figures 5 and 8, include this effect. In addition, they tend to converge to give the modulus of the spring of the Maxwell model at high rates of loading. Note that a dynamic measurement of Young's modulus on the model would also measure the modulus of this spring. Thus, the model is consistent with experimental results regarding this parameter.

B. Fundamental Strength

The fundamental strength of the model is consistent with observations of the transition from creep to creep-rupture behavior in constant stress tests and from steady-state creep to failure in constant strain-rate tests. Gold (1970) described a threshold stress for constant stress tests below which steady-state creep was achieved, while above it creep-rupture always occurred. Similarly, Dillon and Andersland (1967) described constant strain-rate tests in which steady-state stress was reached for applied strain-rates below some threshold value, while failure occurred for higher rates. The model displays both these effects through the idea of fundamental strength, as described above.

C. Strain at Failure

Figure 14 shows that the range of total strain at failure is relatively narrow except at low strengths corresponding to tests at very low loading rates. This is consistent with the experimental results of Hawkes and Mellor (1972) and Peyton (1966). In addition, the former authors note unreported work by Halbrook which showed that the strain at minimum strain-rate for creep-rupture tests tends to be similar to the strain at failure in constant strain-rate tests. This observation is described by the calculations plotted in Figure 14.

D. Load Rate and Time Dependency of Failure Strength

The curves in Figures 12, 13 and 15 show the dependency of the strength on the rate of loading and the time to failure. These are clearly related for the cases of constant load-rate and constant strain-rate tests, and, as noted above, the relationship with the creep-rupture tests can also be explained in terms of the behavior of the model. Curves which are qualitatively similar to those of the above figures have been experimentally determined by Peyton (1966) for sea ice in constant stress-rate tests, by Gold (1967) for fresh ice at constant stress, and by Hawkes and Mellor (1972) for fresh ice at constant strain-rate.

Hawkes and Mellor (1972), noted that the strength of the ice tended to become asymptotic to some value at high strain rates. However, other investigators have found a peak in the strength-strain-rate curve at a rate of about 1×10^{-3} (Scharz and Weeks, 1977, Vaudrey, 1977), beyond which the strength falls with increasing strain-rate, the peak is identified with the brittle-ductile transition. Hawkes and Mellor (1972) attribute this instead to the experimental procedures, and find no such decrease. Experimental results from the in-situ tests run under this program are as yet inconclusive (see next section). However, even if real, the effect is not included in the model behavior as yet, so that at present, the model should not be extended beyond the range of ductile failure.

VIII. CONCLUSION

Conclusions regarding the applicability of the model must be taken as preliminary until quantitative evaluations can be conducted. An appropriate data set is being acquired during the present field program (see next section), and the continuing study of Peyton's (1966) experimental results will provide

additional data for this purpose. However, the results to date must be regarded as encouraging. The model provides a framework within which many previously unrelated experimental observations are shown to be consistent with a single, relatively simple, mathematical structure. As such, it provides a conceptual framework for the interpretation of appropriate experimental data. In fact, preliminary work suggests that this may extend to the cases of bending tests and biaxial loading as well.

IX. SUMMARY OF 4TH QUARTER OPERATIONS

A. Field Activities

The field program was begun as scheduled and will continue until early May. It is anticipated that about 120 tests will be conducted during this time. These will be a mixture of creep, creep-rupture and constant stress-rate tests designed to provide data to test the model described above.

The field party consists of Mr. Ronald Metzner (Geo. Inst., U. of Alaska), who is responsible for the operation of the program, and Mr. Rod March (Geo. Inst., U. of Alaska), as assistant. Dr. E. R. Hoskins (Texas A & M Univ.) was also at the site during most of the month of March to evaluate the design of the experiments and provide guidance and assistance with all aspects of the program. In addition, expeditors from NARL have been used when available to assist in the preparation of test samples. Finally, the Principal Investigator has visited the site periodically to maintain overall supervision of the project.

B. Methods

As noted above, all tests planned for this field season are to be run in uniaxial compression. Test specimens are set up by cutting blocks 36 x 36 x 60 cm from the ice sheet. The bottom of the block is then squared to a thickness of 30 cm, and the hole filled with water to that depth and allowed to freeze back. When frozen, a double layer of plastic sheeting is laid in the bottom of the hole, the block replaced, with a 30 x 30 cm flatjack at each end, and water poured into the remaining spaces to freeze the block and flatjacks into the ice sheet. Two aluminum rods are then frozen into the block on the center line 20 cm from each flatjack. These extend down into the block for up to 20 cm, with about the same length of rod projecting out of the block. The specimen is then allowed to remain in place for several days, so that it can return to thermal equilibrium with the surrounding ice sheet.

Just prior to testing, the block is cut loose from the ice sheet by chain saw cuts at least 30 cm deep, which connect holes drilled at the ends of each flatjack. The purpose of the holes is to reduce the stress concentration at the tips of the flatjacks and prevent cracks from propagating through the ice to other test specimens. When the cuts are completed, the block is left as a 30 x 30 x 60 cm prism, with a flatjack on each end, and free surfaces on three sides. The only stress on the block prior to loading is that transmitted across the base by the weight of the block. The double layer of plastic sheeting at the base of the block provides an unbonded surface which will not transmit a shear stress across the boundary.

Each block is instrumented with two linear potentiometers placed on the pegs, at heights of about 2 and 20 cm above the ice surface, to measure the change in distance between the pegs as the test proceeds. Two measurements are required in order to correct for rotation of the pegs due to bending at the surface of the block. Finally, a pressure transducer is installed on one of the flatjacks, and the two flatjacks are connected by hoses to a bottle of nitrogen gas.

The specimen is loaded by feeding gas to the flatjacks through a pressure regulator. The rate of loading is controlled by hand for constant load rate tests, or by instantaneous release of gas through a ball valve for creep and creep-rupture tests. The output is recorded either on a strip chart, oscilloscope or a Vishay Model 220 strain recording system, depending upon the type of test being run, the rate, and the type of data required.

Flatjack pressure is recorded directly from the pressure transducer. The strain, as noted, is calculated from the output of the two linear potentiometers. In addition, on some tests a strain extensometer is also frozen directly to the surface of the block, and foil strain gauges are embedded in the block. These provide a check on the accuracy of the measurements.

Several test specimens have also been installed with plastic sheeting wrapped around the flatjacks to reduce the bonding between the specimen and the flatjack. The obvious purpose is to examine the effect of such bonding on the measured strength.

Ice temperatures at 5 depths between the surface and 35 cm are recorded continuously and provide the temperature profile of the ice during each test. Samples for salinity measurements are collected from each block immediately after testing.

C. Results

To date, about 70 samples have been set up, and approximately 50 experiments have been run. No strain data was acquired during the first 30 of these tests because of problems with the instrumentation. These have been corrected, and strain data are now being taken.

A short series of creep-rupture and constant stress-rate tests was conducted early in the program to provide some indication as to whether the model described above would give reasonable results, and to check the reproducibility of the test data. This was done by first running a constant stress-rate test to failure and noting the time to failure and the strength. Then, a creep-rupture test was immediately run on another sample at the failure strength measured in the constant stress-rate test. The model predicts that the time to failure of these two tests at the same failure stress should differ by about a factor of ten, with the creep-rupture test failing in the shorter time period. This was verified by the test results, and subsequent tests of this type have continued to give this result.

A series of about 25 tests were also run at constant stress-rates ranging from approximately 31 kPa/min (4.5 psi/min) to 3.3 GPa/min (485,000 psi/min) to establish the curve of strength vs. stress-rate. The data are shown in Figure 16. Note that these are preliminary results, and are uncorrected for known timing errors which could change the higher stress rates by as much as 10%. Also, the tests were run at temperature differences of as much as 5°C and the effects of this variation have not been evaluated. However, the scatter of data points clearly shows the expected shape of the curve of Figure 15.

From Figure 16, there is an indication that the measured strengths are decreasing for tests at high rates. Further, examination of several test specimens after failure indicates that the mechanism of failure is different for high stress-rate tests. For low stress-rate tests, the blocks fail by the propagation of numerous cracks in the horizontal plane, and these are distributed throughout each specimen. At high rates, a single vertical crack formed at an angle of about 30° to the horizontal principal stress direction and horizontal cracks were entirely absent. At intermediate stress-rates, both cracks were present, with indication that the vertical crack had formed prior to at least some of the horizontal cracks. Thus, a transition in failure mechanism is indicated, and the subject requires further study.

Finally, the peak stress-rate reached may represent the limit possible with the available equipment. This rate was achieved by loading directly from a gas bottle at a pressure of 13.8 MPa (2000 psi) through a short hose. The gas was released by a ball valve, so that the limit on the loading rate is determined by the rate at which the gas can flow through the inlet nipple on the flatjack. This therefore, determines the upper limit on the loading rate which can be achieved.

D. Problems Encountered

None

E. Estimate of Funds Expended

\$35,000

F. Milestone Chart

No modification is required from the original proposal.

REFERENCES

- Dillon, H. B., and Andersland, O. B., 1967, Deformation Rates of Polycrystalline Ice, in Ōura, H., ed., Physics of Snow and Ice: Int. Conf. on Low Temp. Science, 1966, Proc., Vol. 1, Pt. 1, [Sapparo], Inst. of Low Temp. Science, Hokkaido Univ., p. 313-328.
- Dwight, H. B., 1957, Tables of Integrals and Other Mathematical Data, Macmillan Co., New York, 288 p.
- Gold, L. W., 1967, Time to Formation of First Cracks in Ice, in Ōura, H., ed., Physics of Snow and Ice: Int. Conf. in Low Temp. Science, 1966, Proc., Vol. 1, Pt. 1, [Sapporo], Inst. of Low Temp. Science, Hokkaido Univ., p. 359-370.
- Gold, L. W., 1971, The Failure of Ice, in, Int. Assoc. of Hydraulic Research, IAHR Symposium: Ice and its Action on Hydraulic Structures; Reykjavik, Iceland, 1970, paper 5.
- Hawkes, I., and Mellor, M., 1972, Deformation and fracture of ice under uniaxial stress, Jour. Glaciology, 11, 61, p. 103-131.
- Krausz, A. S., and Eyring, H., 1975, Deformation Kinetics, John Wiley and Sons, New York, 398 p.
- Peyton, H. R., 1966, Sea Ice Strength, Geophysical Institute, University of Alaska, Report UAG R-182, 273 p.
- Reiner, M., 1960, Plastic Yielding in Anelasticity, J. Mech. Phys. Solids, 8, p. 255-261.
- Schwarz, J. and Weeks, W. F., 1977, Engineering Properties of Sea Ice, Jour. Glaciology, 19, 81, p. 499-531.
- Stulen, F. B., 1962, A Model for the Mechanical Behavior of Metals, Materials-Research and Standards; ASTM, 2, 2, p. 102-109.
- Tabata, T., 1958, Studies on viscoelastic properties of sea ice, in Arctic Sea Ice, U.S. National Academy of Sciences, National Research Council, Pub. 598, p. 139-147.
- Vaudrey, K. D., 1977, Ice Engineering-Study of Related Properties of Floating Sea-Ice Sheets and Summary of Elastic and Viscoelastic Analyses, U. S. Navy Civil Engineering Lab, Technical Report R 860, 81 p.
- Weeks, W. F. and Assur, A., 1967, The mechanical properties of sea ice, CRREL Monograph II-C3, 94 p.

FIGURE CAPTIONS

- Figure 1. Four-parameter model of a viscoelastic solid showing definitions of the constants and form of the non-linear stress-strain relationship for the dashpots.
- Figure 2. Strain-time curves calculated for constant stress case.
- Figure 3. Strain-time curves for constant stress of 2.07 MPa (300 psi) showing the partition of strain between elements of the model. ϵ_T = the total strain, ϵ_L = elastic strain (sum of the strain in the spring of the Maxwell model and the Voigt model), ϵ_V = strain in the Voigt model, ϵ_D = strain in the dashpot of the Maxwell model, and ϵ_E = strain in the spring of the Maxwell model.
- Figure 4. Strain-time curves for constant stress of .69 MPa (100 psi) showing partition of strain between model elements. Symbols are the same as in Figure 3.
- Figure 5. Stress-strain curves calculated for constant stress-rate tests as indicated.
- Figure 6. Stress-strain curves showing partition of strain between model elements for a constant stress-rate test at 6.9 MPa/min (1000 psi/min). Symbols as defined in Figure 3.
- Figure 7. Stress-strain curves showing partition of strain between model elements for a constant stress-rate test at 69 kPa/min (10 psi/min). Symbols as defined in Figure 3.
- Figure 8. Stress-strain curves calculated for constant strain-rate tests as indicated.
- Figure 9. Stress-strain curves showing partition of strain between model elements for a constant strain-rate test at a strain-rate of 1×10^{-3} . Symbols as defined in Figure 3.
- Figure 10. Stress-strain curves showing partition of strain between model elements for a constant strain-rate test at a strain rate of 1×10^{-5} . Symbols as defined in Figure 3.
- Figure 11. Yield curve of the four-parameter model in $\sigma - \sigma_2$ space.
- Figure 12. Strength vs. strain-rate curve for constant stress, constant stress-rate and constant strain-rate calculations. All three curves fall within the range covered by the heavy line. Thin, solid line represents the stress vs. steady state strain-rate for $\sigma < \sigma_b$. The extension of this curve above σ_b is indicated by the dashed line. See text for further description.
- Figure 13. Strength vs. time to failure for constant stress (σ), constant stress-rate ($\dot{\sigma}$) and constant strain-rate ($\dot{\epsilon}$) calculations.

- Figure 14. Strength vs. strain at failure for constant stress, constant stress-rate and constant strain-rate calculations. All three curves fall within the range of the heavy lines. Solid line indicates the total strain at failure, and the dashed line is the elastic strain ($\epsilon_V + \epsilon_E$) only.
- Figure 15. Strength vs. stress-rate for constant stress-rate ($\bar{\sigma}$) and constant strain-rate ($\bar{\epsilon}$) calculations. Heavy line shows the range over which both curves approximately coincide. See text for discussion.
- Figure 16. Strength vs. loading rate for in-situ tests conducted in March, 1978. Compare with Figure 15.

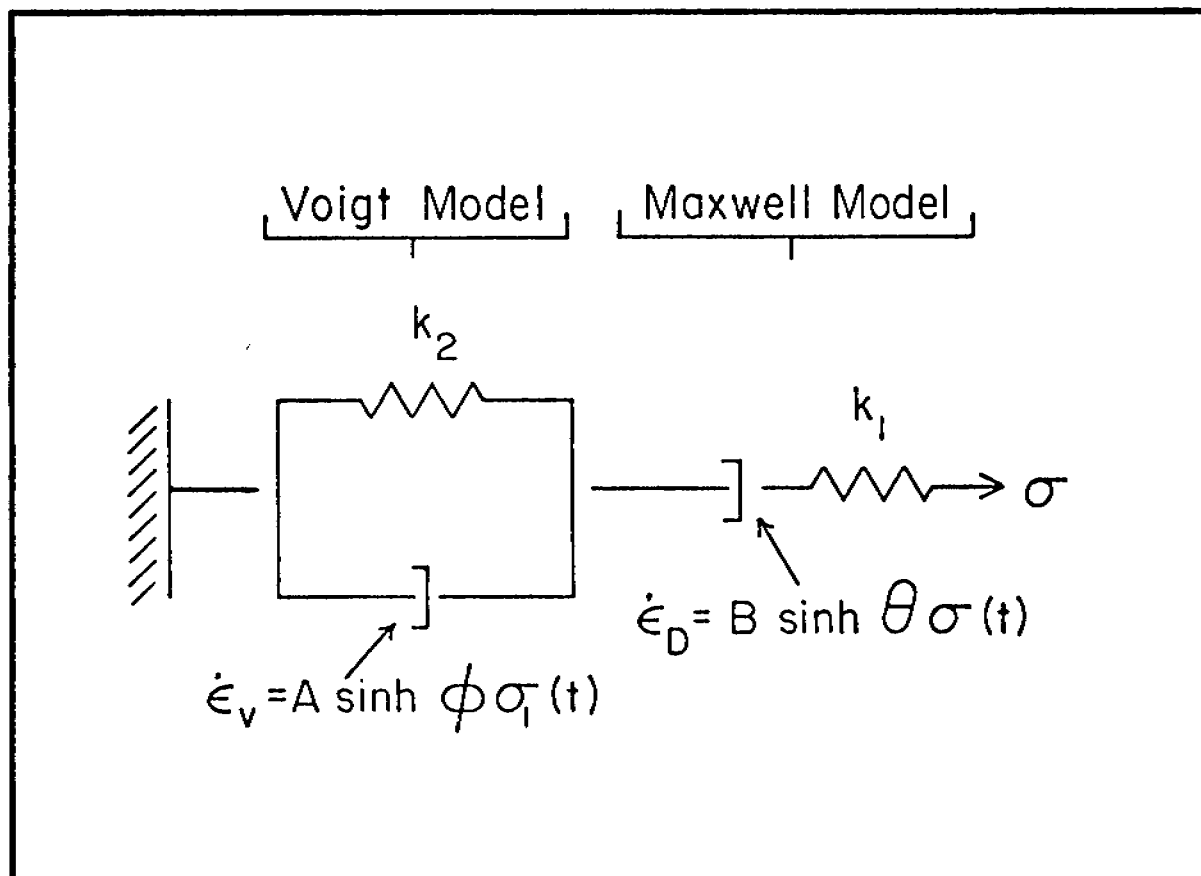


Figure 1.

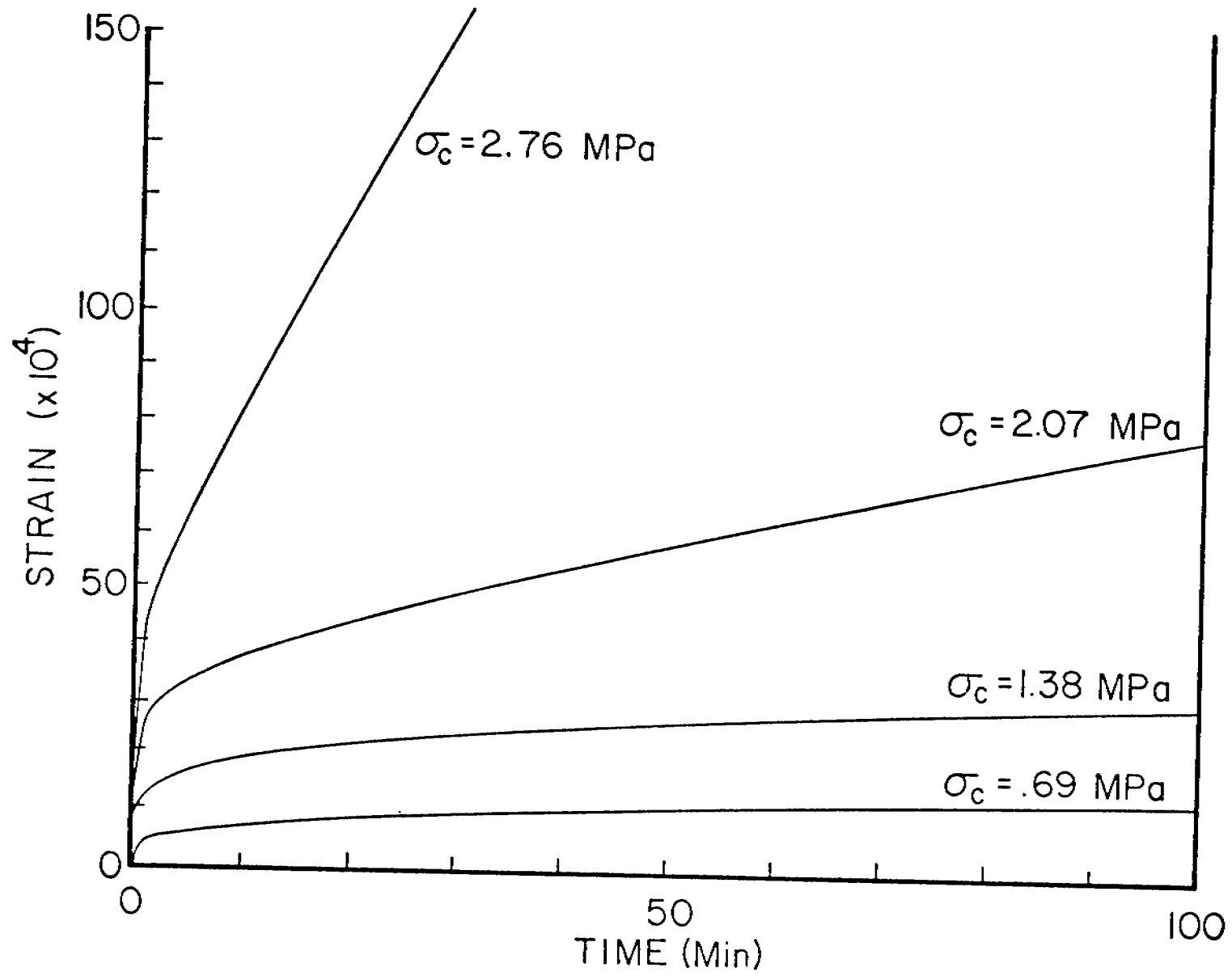


Figure 2.

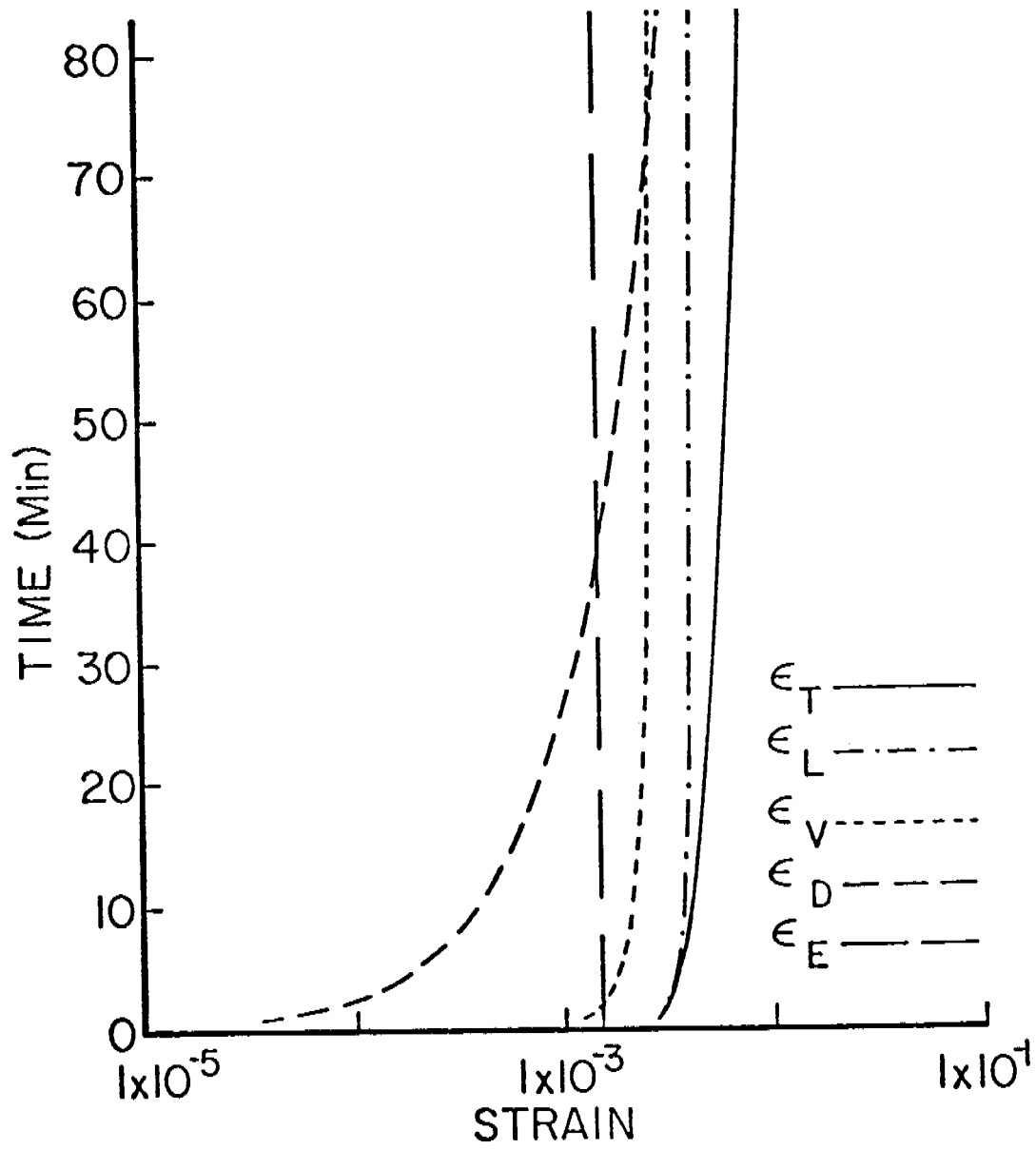


Figure 3.

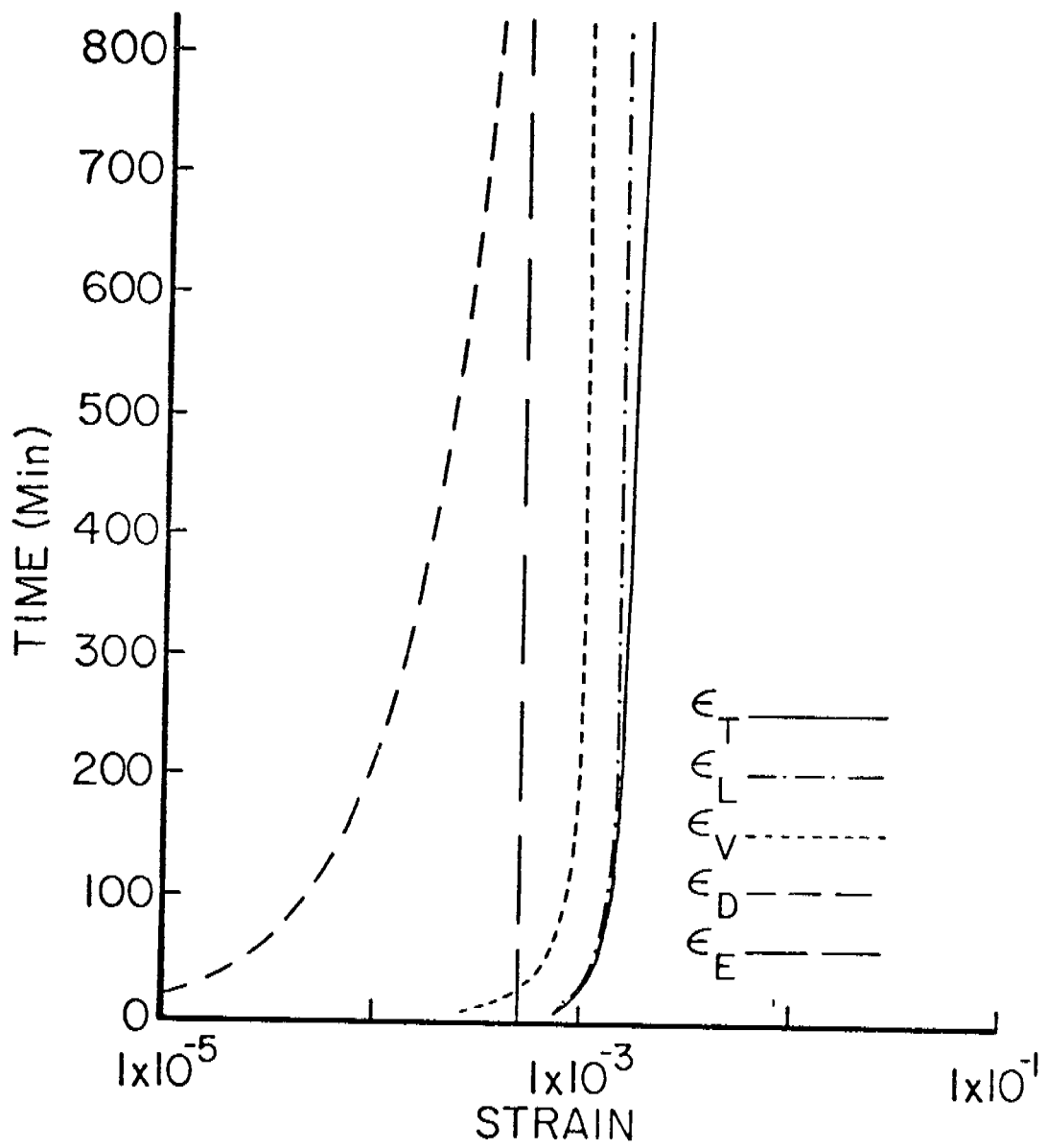


Figure 4.

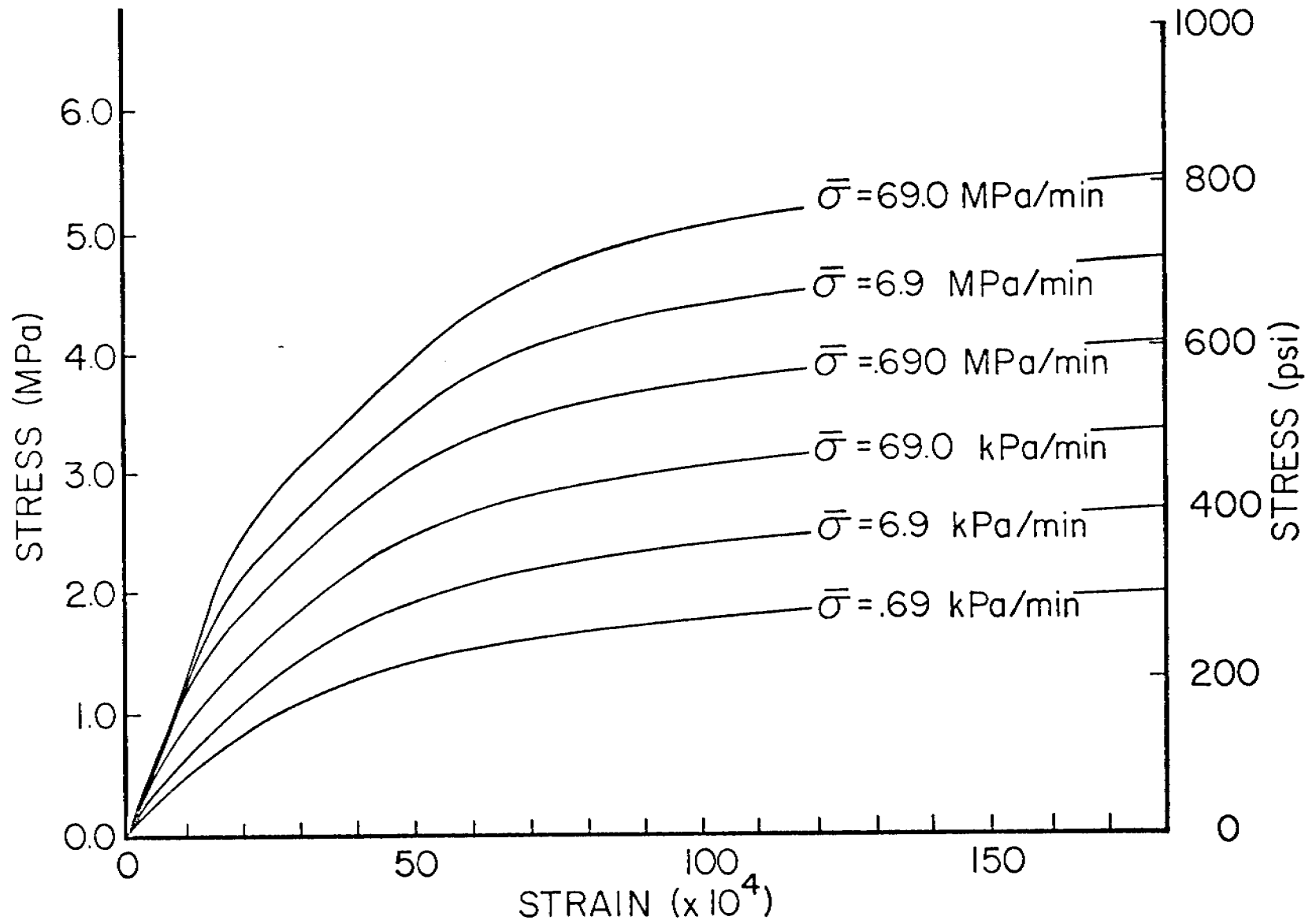


Figure 5.

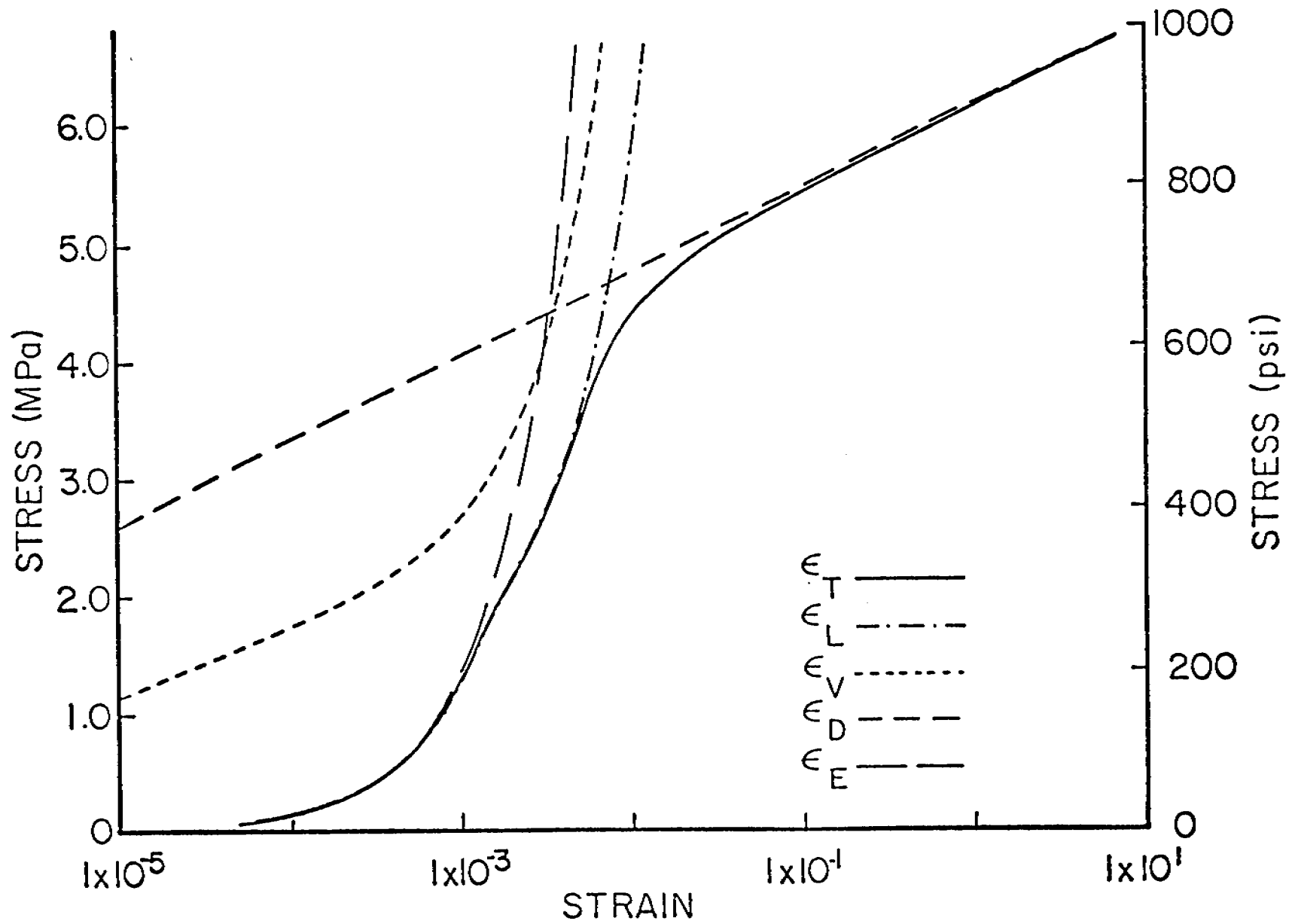


Figure 6.

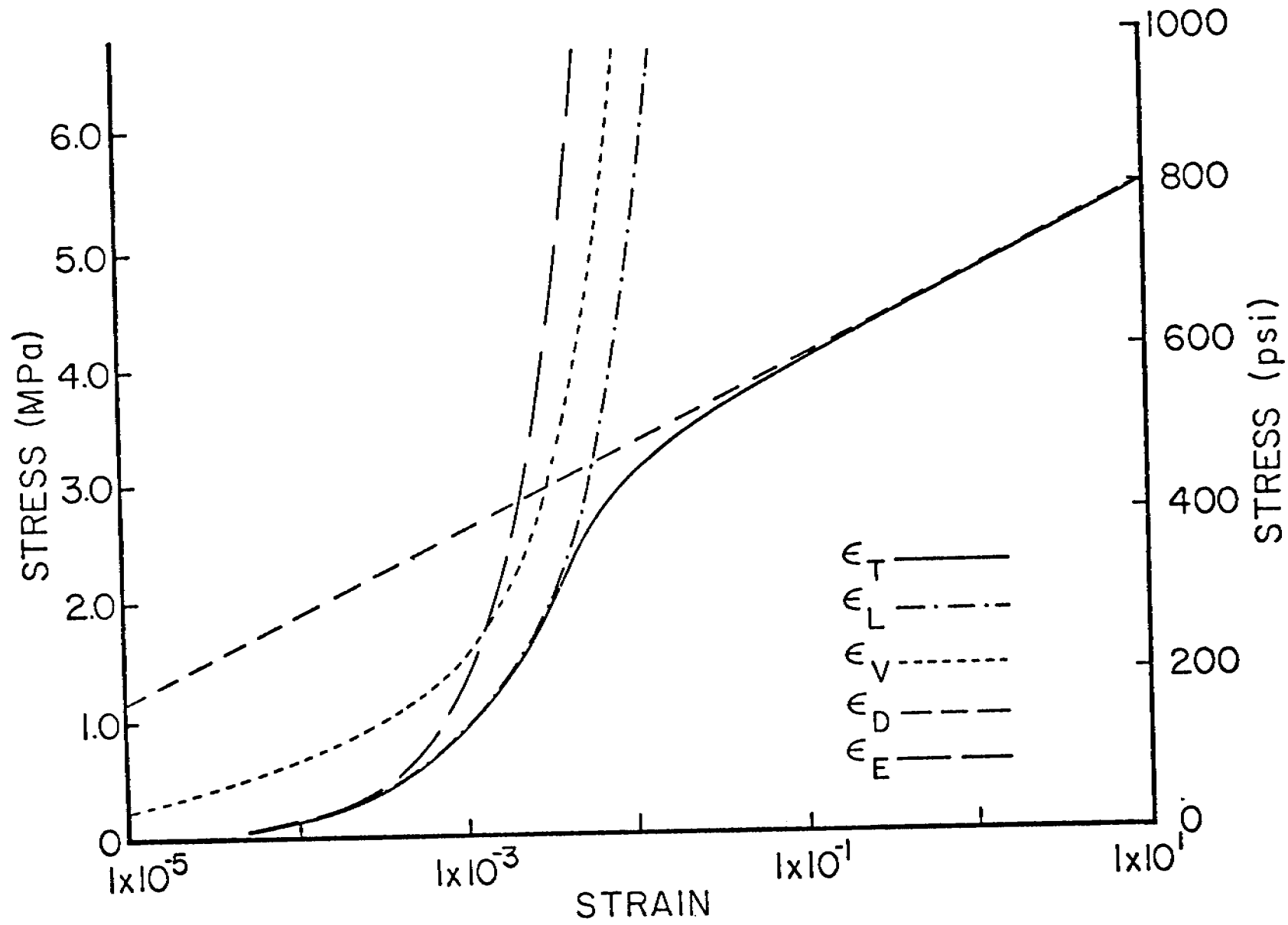


Figure 7.

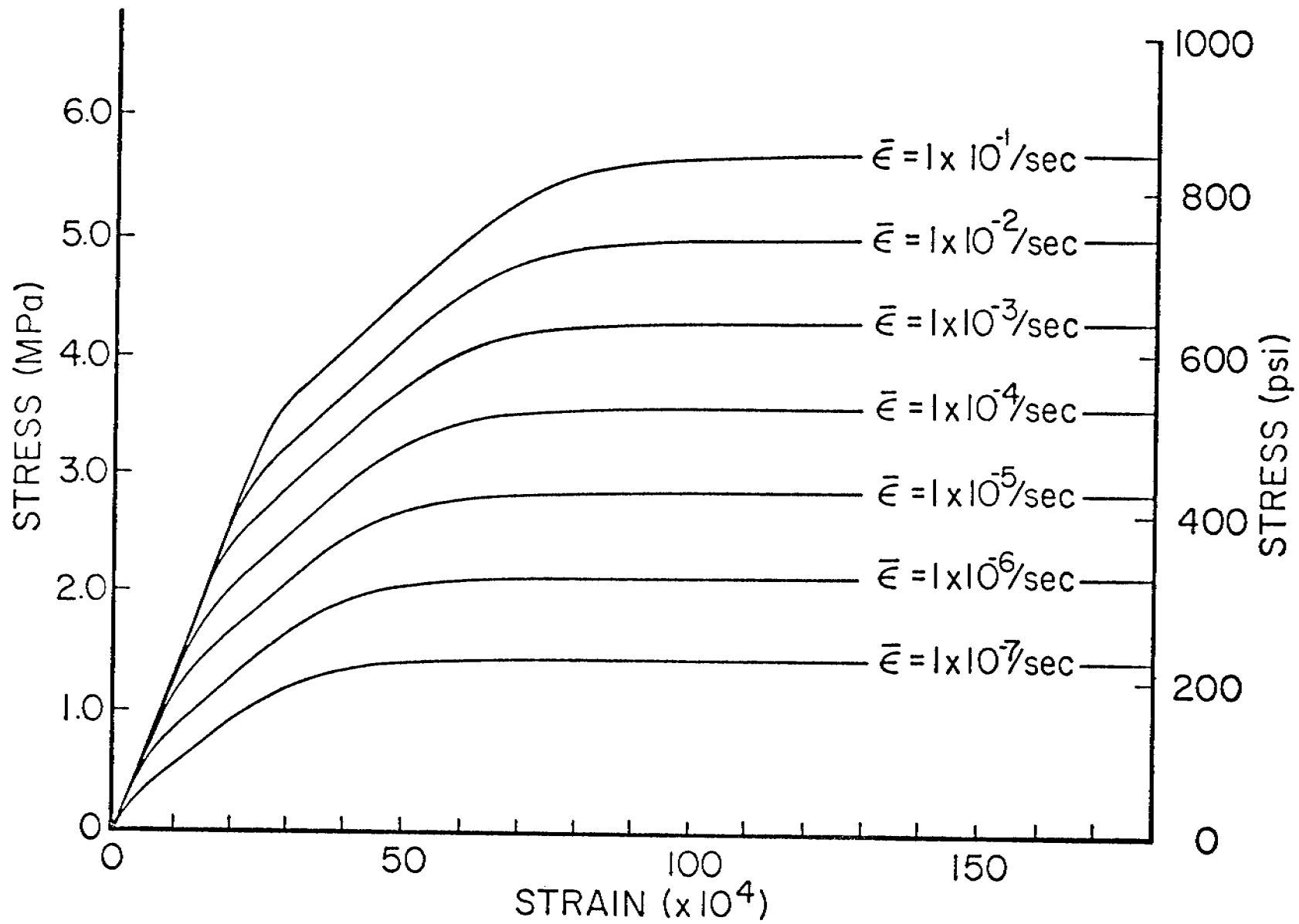


Figure 8.

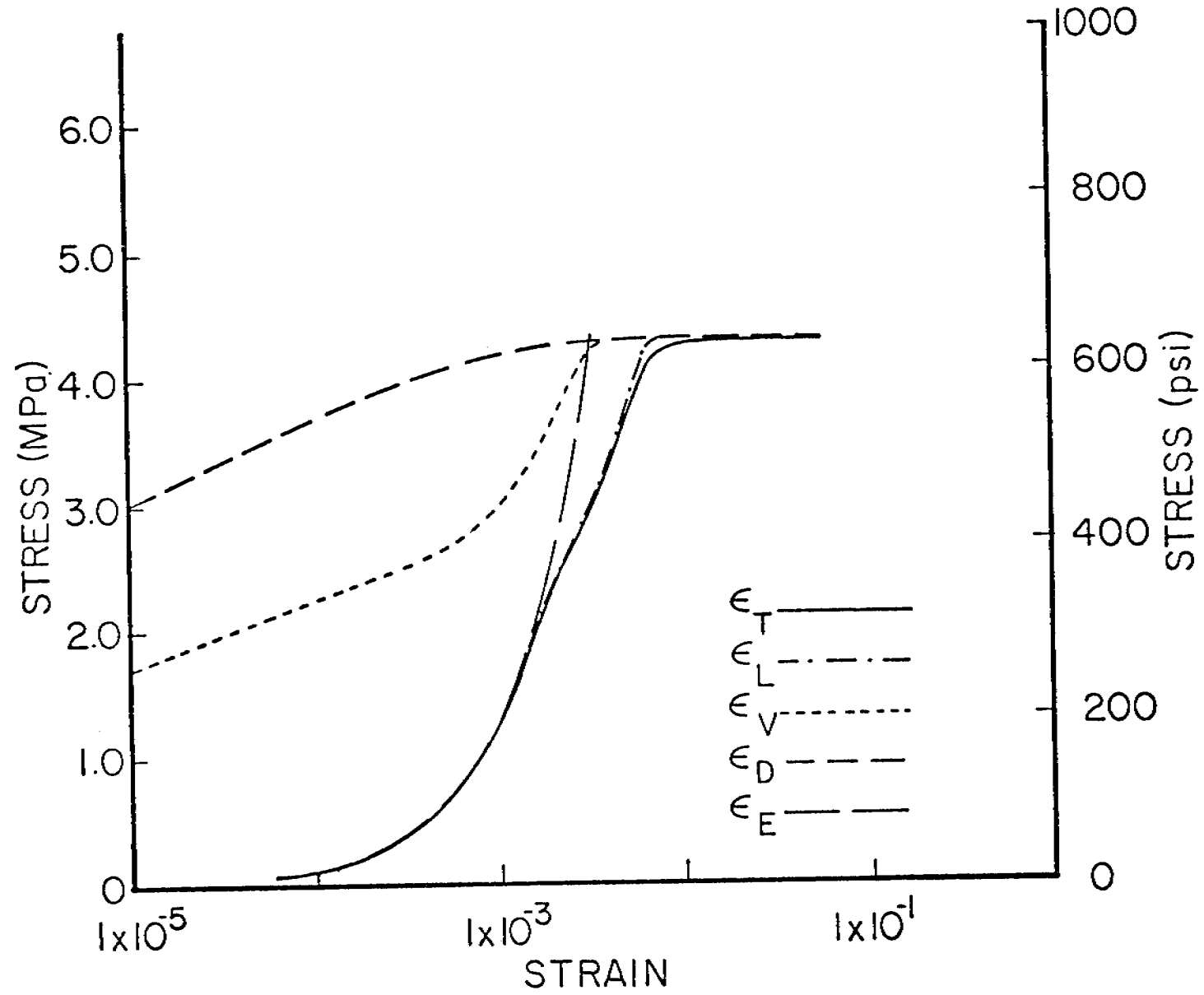


Figure 9.

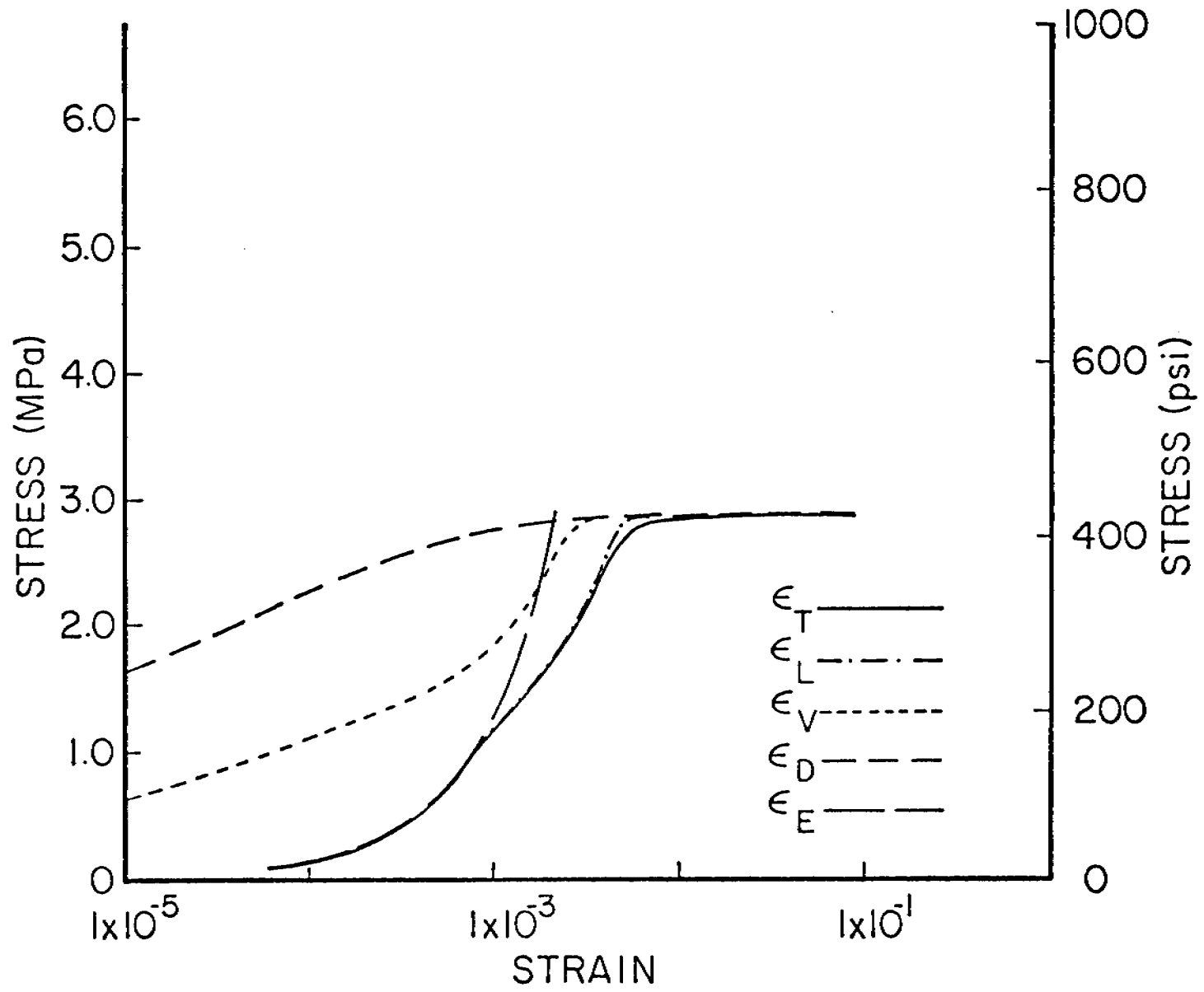


Figure 10.

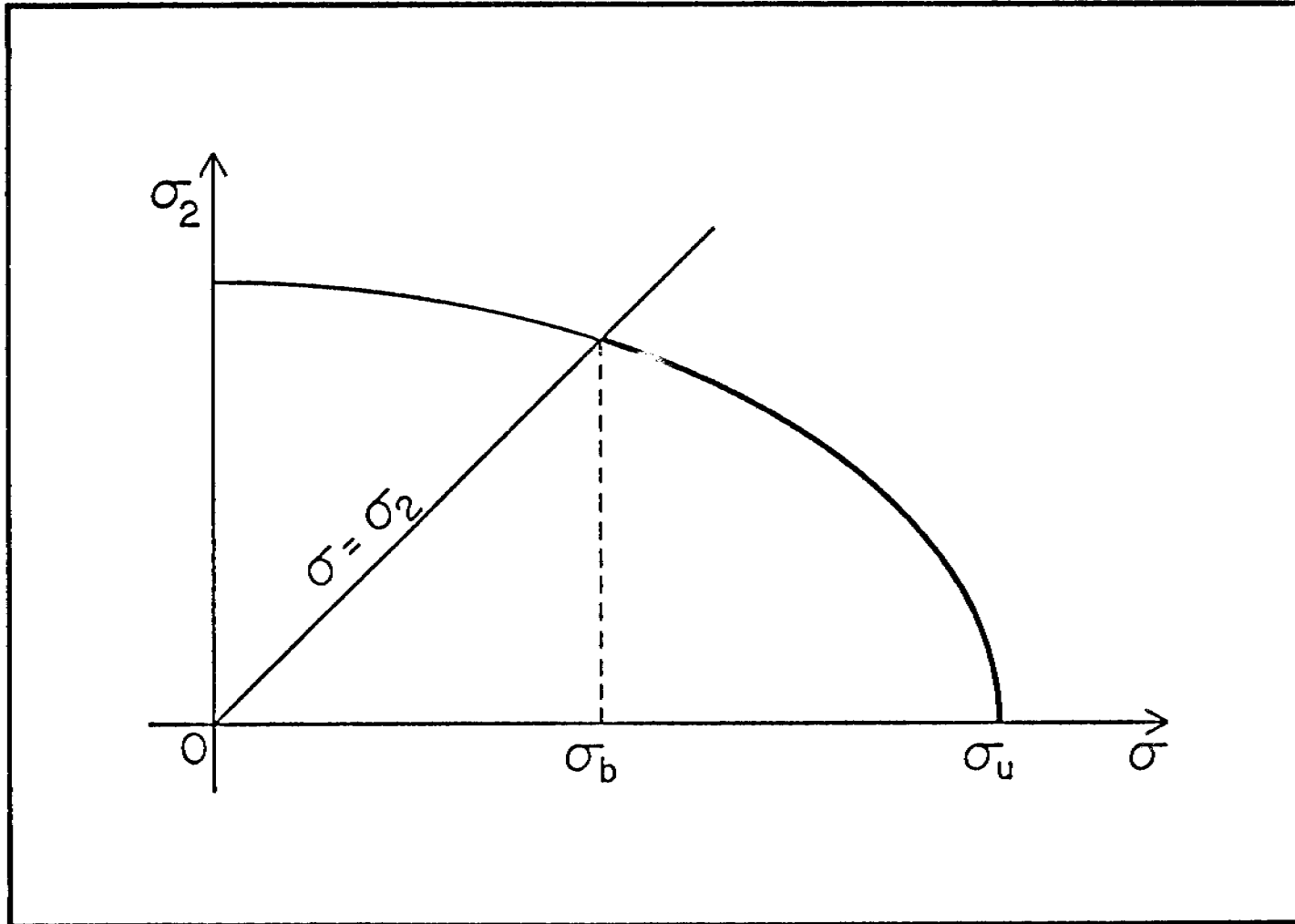


Figure 11.

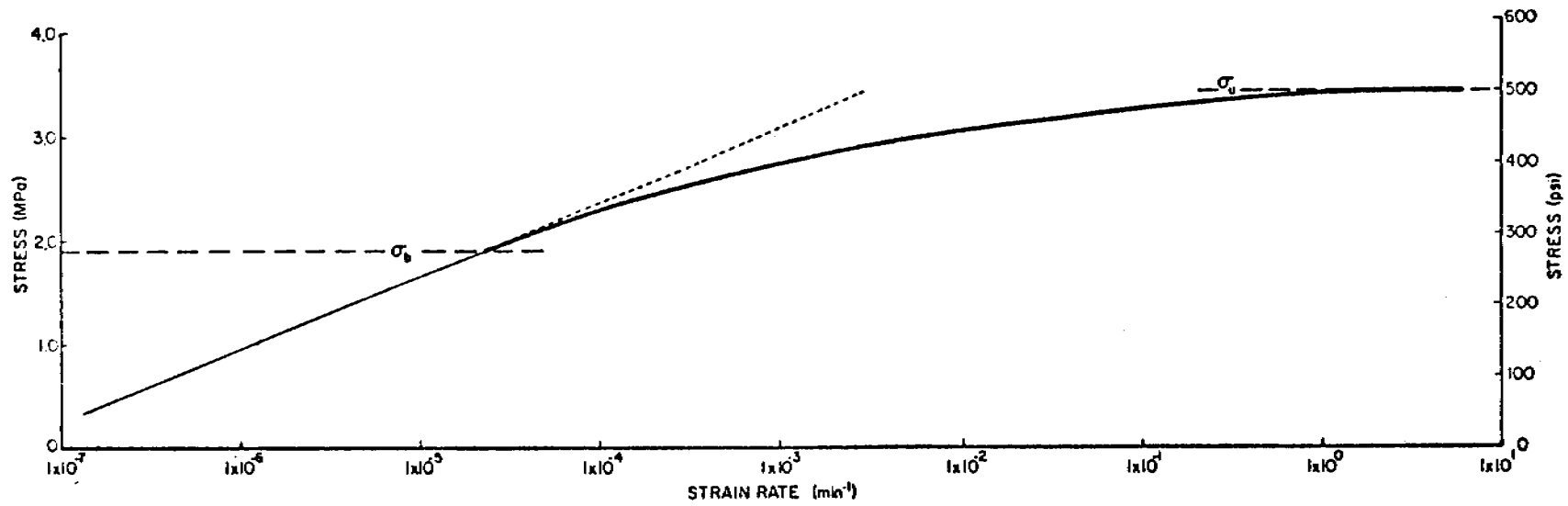


Figure 12.

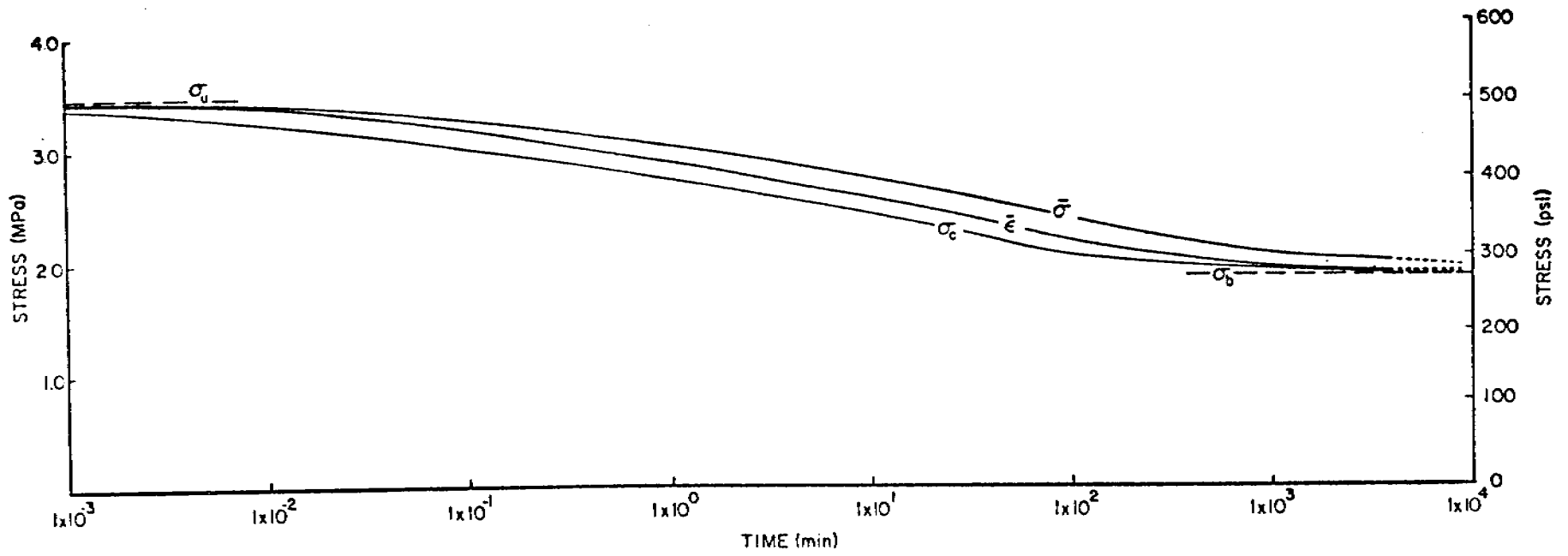
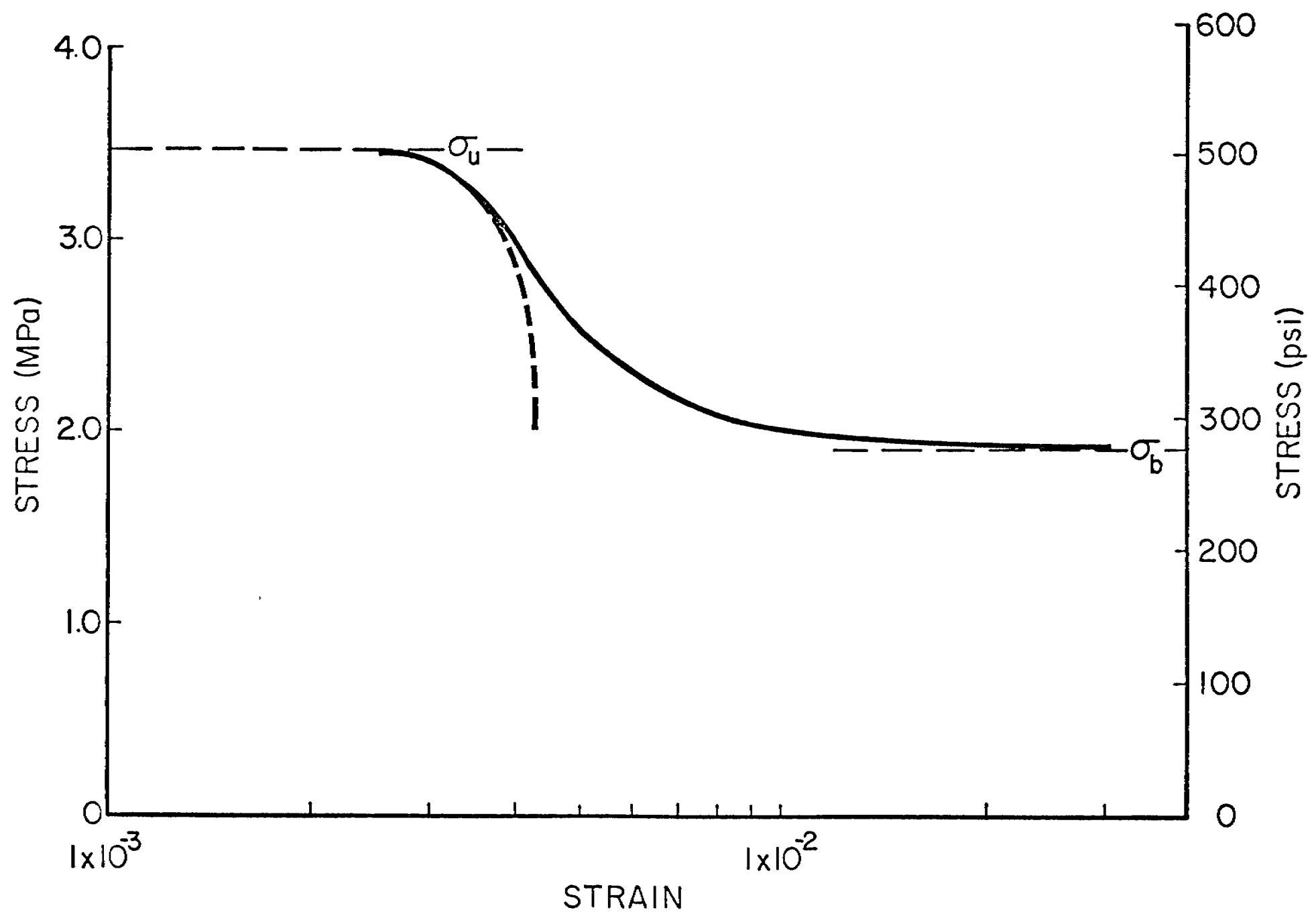


Figure 13.

257



STRAIN
Figure 14.

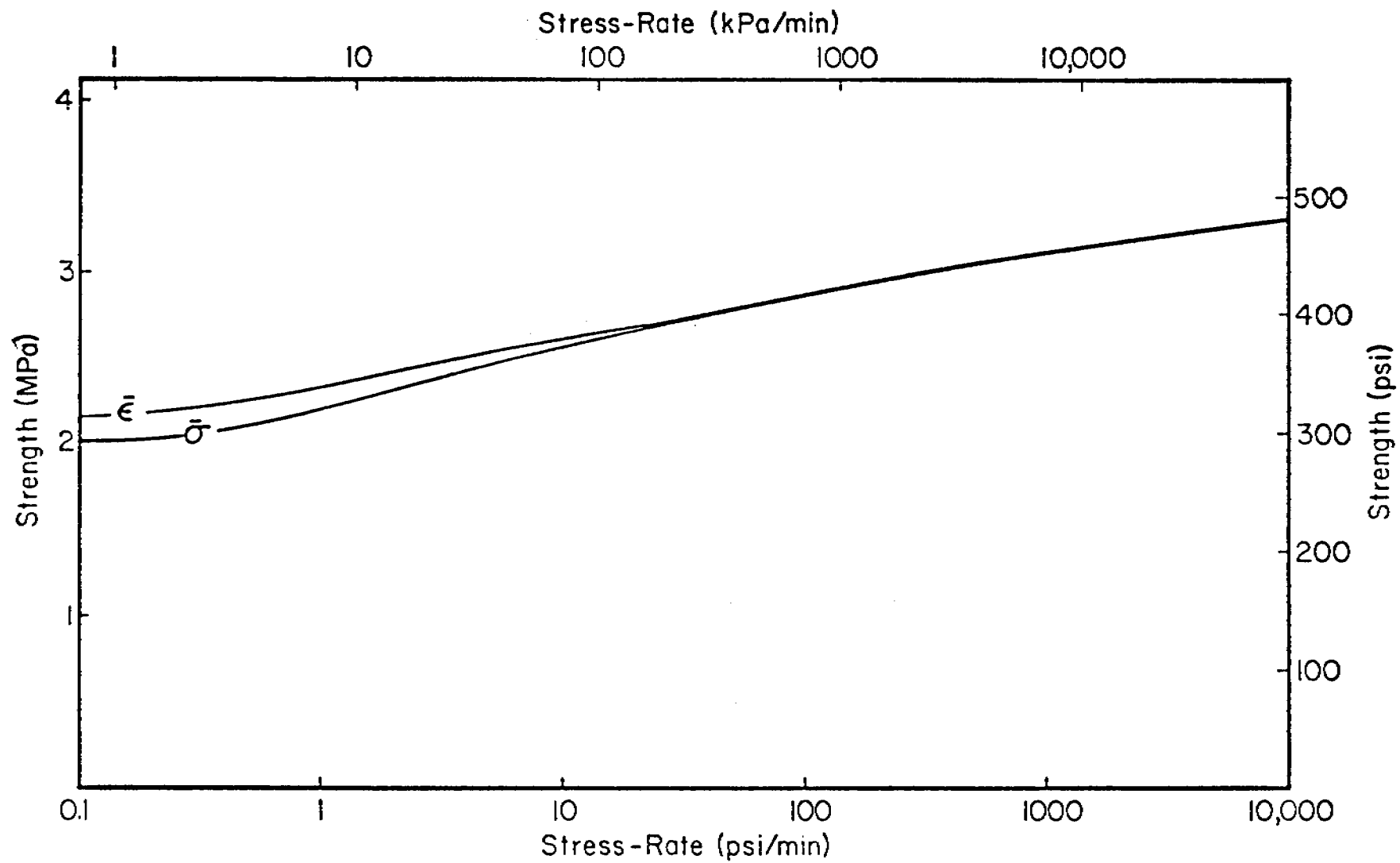


Figure 15.

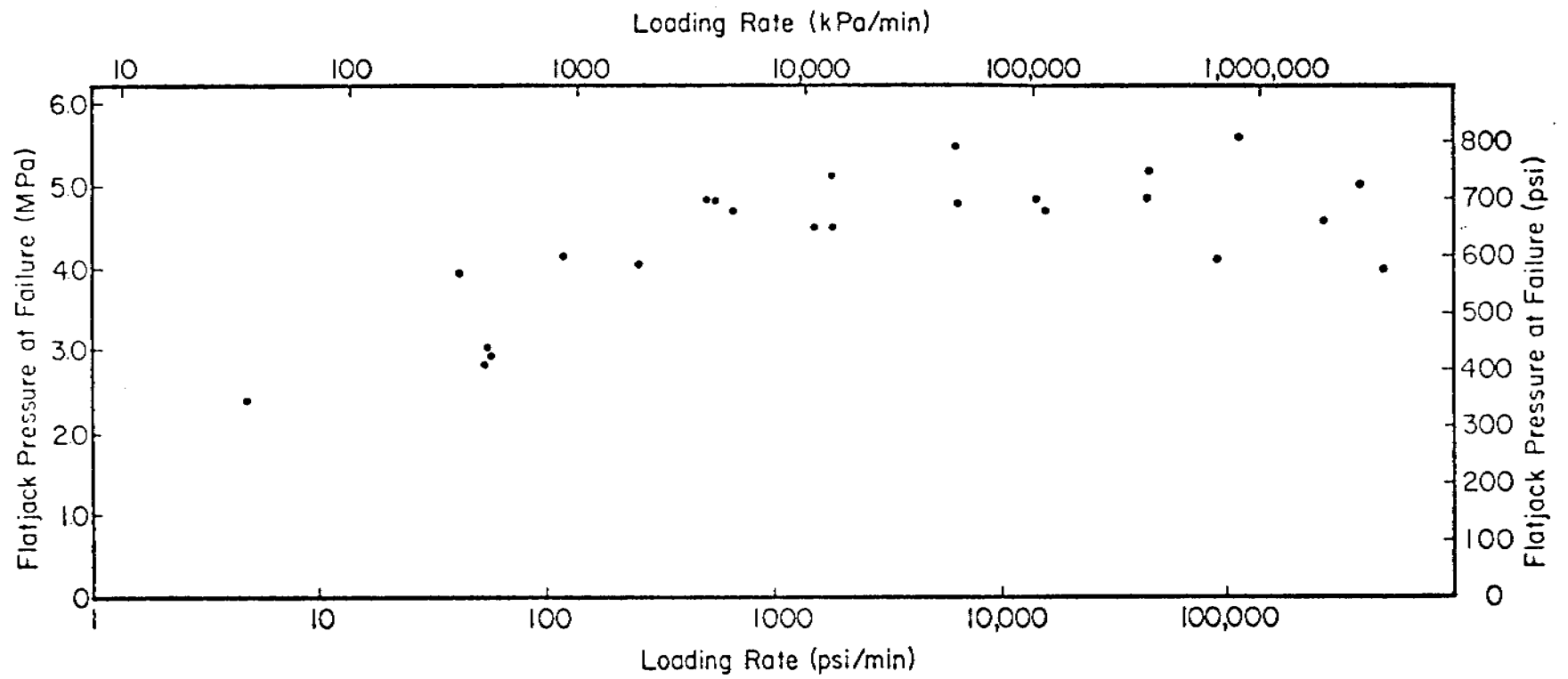


Figure 16.

ANNUAL REPORT

Contract # 03-5-022-55
Research Unit #267
Reporting Period:
April 1, 1977
to March 31, 1978
Number of pages: 30

OPERATION OF AN ALASKAN FACILITY
FOR APPLICATIONS OF REMOTE-SENSING DATA TO OCS STUDIES

Albert E. Belon
Geophysical Institute
University of Alaska

April 1, 1978

TABLE OF CONTENTS

- I SUMMARY OF OBJECTIVES
- II INTRODUCTION
 - A. General Nature and Scope of Study
 - B. Specific Objectives
 - C. Relevance to Problems of Petroleum Development
- III CURRENT STATE OF KNOWLEDGE
- IV STUDY AREA
- V SOURCES, METHODS AND RATIONALE OF DATA COLLECTION
 - A. Remote-Sensing Data Acquired for the OCS Program
 - 1. Landsat data
 - 2. NOAA satellite data
 - 3. USGS/OCS aircraft data
 - 4. NASA aircraft data
 - 5. NOS aircraft data
 - 6. Army aircraft data
 - 7. Preparation and distribution of remote-sensing data catalogs
 - B. Remote-Sensing Data Processing Facilities and Techniques
 - C. Consultation and Assistance to OCS Investigators
 - 1. General Assistance
 - 2. Individual Assistance
- VI RESULTS
 - A. Establishment of a Remote-Sensing Facility for OCS Studies
 - B. Disciplinary Results of the Applications of Remote-Sensing Data to OCS Studies
- VII & VIII DISCUSSION AND CONCLUSIONS
- IX SUMMARY OF FOURTH QUARTER OPERATIONS
 - A. Laboratory Activities During the Reporting Period
 - 1. Operation of the remote-sensing data library
 - 2. Operation of data processing facilities
 - 3. Development of data analysis and interpretation techniques
 - 4. Consultation and assistance to OCS investigators
 - B. Problems Encountered/Recommended Changes
 - C. Estimates of Funds Expended

OPERATION OF AN ALASKAN FACILITY
FOR APPLICATIONS OF REMOTE-SENSING DATA TO OCS STUDIES

1977/78 Annual Report

Principal Investigator: Albert E. Belon
Affiliation: Geophysical Institute, University of Alaska
Contract: NOAA # 03-5-022-55
Research Unit: # 267
Reporting Period: April 1, 1977 - March 31, 1978

I - SUMMARY OF OBJECTIVES

The primary objective of the project is to assemble available remote-sensing data of the Alaskan outer continental shelf and to assist OCS investigators in the analysis and interpretation of these data to provide a comprehensive assessment of the development and decay of fast ice, coastal geomorphology and ecology, sediment plumes and offshore suspended sediment patterns along the Alaskan coast from Yakutat to Demarcation Bay.

Four complementary approaches are used to achieve this objective. They are: 1) the operation of a remote-sensing data library which acquires, catalogs and disseminates satellite and aircraft remote-sensing data; 2) the operation and maintenance of remote-sensing data processing facilities; 3) the development of photographic and computer techniques for processing remote sensing data; and 4) consultation and assistance to OCS investigators in data processing and interpretation.

Thus, the project has primarily a support role for other OCS projects, and in itself does not usually generate disciplinary conclusions and implications with respect to OCS oil and gas development. Such results will be generated by the various disciplinary OCS projects, most of which are users of remote-sensing data and services provided by our project. At this time at least two dozen OCS projects are utilizing remote-sensing data routinely, six of them (RU #88, 99, 248, 249, 257, 289A) almost exclusively. In addition, the availability of near-real-time remote-sensing data (NOAA satellite) and delayed repetitive data (Landsat and aircraft) provides a continuous monitoring of environmental conditions along the Alaskan continental shelf for research and logistic support of the OCSEAP Program.

II - INTRODUCTION

A. General Nature and Scope of Study

The outer continental shelf of Alaska is so vast and so varied that conventional techniques, by themselves, are unlikely to provide the detailed and comprehensive assessment of its environmental characteristics

which is required before the development of its resources is allowed to proceed during the next few years. The utilization of remote-sensing techniques, in conjunction with conventional techniques, provides a solution to this dilemma for many disciplinary investigations. Basically the approach involves the combined analysis of ground-based (or sea-based), aircraft and satellite data by a technique known as multistage sampling. In this technique, detailed data acquired over relatively small areas by ground surveys or sea cruises are correlated with aerial and space photographs of the same areas. Then the satellite data, which extend over a much larger area and provide repetitive coverage, are used to extrapolate and update the results of the three-way correlations to the entire satellite photograph. Thus, maximum advantage is taken of the synoptic and repetitive view of the satellite to minimize the coverage and frequency of data which have to be obtained by conventional means.

B. Specific Objectives

The principal objective of the project is to make remote-sensing data, processing facilities and interpretation techniques available to the OCS investigators so that the promising applications and cost effectiveness of remote-sensing techniques can be incorporated in their disciplinary investigations. The specific objectives of the project are: 1) the acquisition, cataloging and dissemination of existing remote-sensing data obtained by aircraft and satellites over the Alaskan outer continental shelf, 2) the operation and maintenance of University of Alaska facilities for the photographic, optical and digital processing of remote-sensing data, 3) the development of photographic, optical and computer techniques for processing remote-sensing data for OCS purposes and 4) the active interaction of the project with OCS users of remote-sensing data, including consultation and assistance in disciplinary applications, data processing and data interpretation.

C. Relevance to problems of petroleum development

The acquisition of remote-sensing data, especially satellite data, has proved to be a cost-effective method of monitoring the environment on a synoptic scale. Meteorological satellites have been used for over a decade to study weather patterns and as an aid to weather forecasting. The earth resources satellite program, initiated in 1972, offers a similar promise to provide, at a higher ground resolution, synoptic information and eventually forecasts of environmental conditions which are vital to petroleum development on the continental shelf. For instance the morphology and dynamics of sea-ice which are relevant to navigation and construction of offshore structures, the patterns of sediment transport and sea-surface circulation which will aid to forecast trajectories of potential oil spills and impact on fisheries, the nature of ecosystems in the near-shore regions which can be changed by human activity, are among the critical development-related environmental parameters which can be studied, in conjunction with appropriate field measurements, and eventually routinely monitored by remote-sensing.

III - CURRENT STATE OF KNOWLEDGE

The utilization of remote-sensing techniques in environmental surveys and resource inventories has made great strides during the last few years with the development of advanced instruments carried by aircraft and satellites. The early meteorological satellites had a ground resolution of a few miles and a broad-band spectral response which made them well-suited to meteorological studies and forecasting but inadequate for environmental surveys. The ground resolution of the sensors has been gradually much improved over the years and thermal sensors were added for cloud and sea temperature measurements, but generally the relatively low ground and spectral resolution of the meteorological satellites is a limitation for environmental surveys.

The initiation of a series of Earth Resources Technology Satellites (now renamed Landsat) in July 1972 was intended to fill the need for synoptic and repetitive surveys of environmental conditions on the land and the near-shore sea. With a ground resolution of about 80 meters and sensitivity in four visible spectral bands, Landsat-1 and 2, have fulfilled that promise beyond all expectations. Landsat 3 was launched on March 5, 1978 and has achieved earth orbit. Sensor packages are still undergoing testing, but soon data should be acquired which will have higher ground resolution (40 meters for the RBV system) and a thermal spectral band which will improve capabilities enormously. The Seasat satellite, to be launched in May 1978, will have all-weather capabilities through the use of imaging radars and, as the name implies, has been specially designed for environmental surveys of the sea.

The development of techniques for analyzing and interpreting Landsat have proceeded at an even more rapid pace than the satellite hardware. While in 1972 much of the Landsat data interpretation was done by visual photointerpretation, the last four years have seen major developments in photographic, optical and, in particular, digital techniques for processing and interpreting the Landsat data. Some of these techniques, applicable to OCS studies, will be discussed in section V and VI of this report.

Through the impetus provided by the national commitment to satellite observations of the earth, the aircraft remote-sensing program has also made great strides in the last few years. While in the early 1960's airborne platforms were mostly used for aerial photography, the late 1960's saw the development of advanced multispectral scanners, thermal scanners, side-looking radars and microwave radiometers, partly for the testing of future satellite hardware and partly because the airborne observations serve for middle-altitude observations between ground and satellite measurements as part of the multistage sampling technique. Two philosophies are apparent in the airborne remote-sensing program: the first, exemplified by the NASA program as well as several universities and industrial agencies, involves relatively large aircraft and sophisticated instrumentation which produce vast quantities of data usually applied to intensive, non-repetitive surveys of relatively small areas. The second approach uses airborne remote-sensing in a truly supporting role for ground-based or satellite measurements. The aircraft are

smaller and the instrumentation usually consists of proven, simpler instruments such as aerial cameras, single-band thermal scanners, and single wavelength side-looking radars which usually generate data only in photographic format. The costs of data acquisition and data processing, while they are not small, are sufficiently low that the approach is often used for repetitive surveys of relatively large areas. In our opinion the second approach fulfills best the needs of the NOAA/OCSEAP program and we have been working very closely with the NOAA Arctic Project Office toward the implementation of such a remote-sensing program.

IV - STUDY AREA

The study area for the project includes the entire continental shelf of Alaska, except for the southeastern Alaska panhandle. This area includes the Beaufort, Chukchi and Bering Seas and the Gulf of Alaska shelves and coastal zone. Temporal coverage is year-round, although the data coverage from November 1 to February 15 is limited owing to the very low solar illumination prevailing at high latitudes during winter.

V - SOURCES, METHODS AND RATIONALE OF DATA COLLECTION

A remote-sensing data library and processing facility was established in 1972 on the Fairbanks campus of the University of Alaska as a result of a NASA-funded program entitled "An interdisciplinary feasibility study of the applications of ERTS-1 data to a survey of the Alaskan environment". This experimental program, which covered ten environmental disciplines and involved eight research institutes and academic departments of the University, terminated in 1974, but the facility which it established proved to be so useful to the statewide university and government agencies that it has continued to operate on a minimal basis with partial funding from a NASA grant and a USGS/EROS contract. In view of the large potential demand of the OCS program on these facilities, a proposal was submitted to NOAA in March 1975 for partial funding of the facility for OCS purposes. This proposal resulted in a contract from NOAA on June 12, 1975, and the work performed since that time is the basis for the present report.

As a result of the NASA-funded program, the remote-sensing data library had total cloud-free and repetitive coverage of Alaska by the ERTS - now renamed Landsat - satellite from the date of launch (July 29, 1972) to May 1974 (about 30,000 data products), 60 rolls of imagery acquired by NASA aircraft (NP3 and U-2) some of which includes coverage of the Beaufort Sea, Cook Inlet and Prince William Sound, and substantial facilities for photographic, optical and digital processing of these data. Through a NOAA-funded pilot project, which studied applications of NOAA satellite data in meteorology, hydrology, and oceanography, the remote-sensing data library also had nearly complete coverage of Alaska by the NOAA satellites since February 1974.

A. Remote-Sensing Data Acquired for the OCS Program

1) Landsat data

At the initiation of the project we performed searches of the EROS Data Center (EDC) data bank for Landsat and aircraft remote-sensing data obtained over the four areas of interest to the OCSEAP program. From the several thousand scenes so identified, we selected the scenes which we did not have in our files and which had satisfactory quality and 30% or less cloud cover. As a result of this search 566 Landsat scenes (2830 data products) were ordered from the EROS Data Center in the following data formats:

- 70mm positive transparencies of multispectral scanner (MSS) spectral bands 4, 5 and 7
- 70mm negative transparencies of MSS spectral band 5
- 9-1/2 inch print of MSS spectral band 6

During the first two years of the project, 1,106 additional cloud free scenes were acquired by the satellite and purchased from EDC.

After March 31, 1977, the EDC price for Landsat products having increased by an average of 166%, we reduced our routine purchase of selected Landsat scenes to two formats:

- 70mm positive transparency of MSS, spectral band 5
- 9 1/2 inch print of MSS, spectral band 7

Other formats are ordered on a case-by-case basis and at the request of individual OCS investigators. During the past year, 1,167 scenes were added to our files.

2) NOAA satellite data

With the termination of a NOAA pilot project, sponsored by NOAA/NESS, in October 1975, our acquisition of NOAA satellite scenes stopped after having accumulated 1320 images since February 1974. Following an interim arrangement with the National Weather Service, which turned out to be inconvenient for both parties, funding was provided by OCSEAP, starting on 1 February 1976, to purchase NOAA satellite imagery directly from the NOAA/NESS Satellite Data Acquisition Facility at Fairbanks. Under this purchase order we are receiving two NOAA scenes daily from the Bering Sea pass of the satellite (covering the Beaufort, Chukchi and Bering Seas) and one scene daily from the interior Alaska pass (covering the Gulf of Alaska) in both the visible and infrared spectral bands (6 images daily except in winter) for a total of 907 images received during the reporting period.

In addition we have made arrangements with the NOAA/NESS facility to save digital tapes of the thermal infrared data, upon request and for the cost of tape replacement, for scenes which are especially cloud-free or of high interest to OCS investigators. These tapes allow the precise mapping of sea-surface temperatures at locations and at times of special interest to OCS investigators.

3) USGS/OCS aircraft remote-sensing data

In November 1975, we started receiving the remote-sensing data acquired by USGS aircraft, under a NOAA/OCS contract, along the Alaskan arctic coast since July 1975. These data consist of six 250 ft. rolls of black and white aerial photography and 42 strips of side-looking radar imagery. This program terminated in December 1975.

4) NASA aircraft remote-sensing data

Over the last few years the NASA Earth Resources Aircraft Program has flown several missions over preselected test sites within Alaska. The program is directed primarily at testing a variety of remote-sensing instruments and techniques and to support NASA-sponsored investigations. However, black and white and color-infrared aerial photography were obtained on most missions and in particular during the May 1967, July 1972, June 1974, and October 1976 missions which include flights over portions of the Alaskan coast and coastal waters. We have acquired copies of these data from NASA.

The U-2 imagery of the Beaufort Sea obtained in June 1974 is of particular interest to OCS investigators because it was obtained during the sea-ice break-up period, it covers a large area (20x20 mi.) in a single frame with good ground resolution (10 ft), and nearly concurrent Landsat data are available. Similarly, the U-2 imagery of the northern Gulf of Alaska and Prince Williams Sound, acquired in October 1976, is of excellent quality.

During June 1977 the U-2 aircraft once again acquired photography over Alaska. New flight lines, mostly in the Prudhoe Bay area, using a 6" and 12" focal length lens were flown and copies of the data are included in our files.

5) NOS aircraft remote-sensing data

In spring 1976 we learned that the National Ocean Survey's (NOS) Buffalo aircraft was scheduled to obtain aerial photographic coverage of Shelikof during summer 1976. Knowing that this area is frequently covered by clouds, we requested NOS to acquire aerial photography of other areas of the Alaskan coastal zone on a non-interference basis with their primary mission. NOS agreed to do so for the cost of the raw film. As a result 1316 frames of color aerial photography were acquired, covering the entire coast from the Yukon delta to Cape Lisburne and several isolated areas in the Gulf of Alaska.

During July 1977 the NOS aircraft flew additional flight lines on the Chukchi and Beaufort coasts extending our coverage eastward to the mouth of the Kogu River, in Harrison Bay. This medium scale photography is of excellent quality and has been used heavily by OCS investigators.

6) Army aircraft remote-sensing data

With the termination of the USGS/OCS remote-sensing data acquisition program in December 1975, an important need developed for all-weather

remote-sensing coverage of the Beaufort and Chukchi coasts during critical periods (end of winter and end of summer). We worked closely with the OCSEAP Arctic Project Office and with a major user (Dr. Cannon, RU #99) in investigating various options culminating in a contractual arrangement with the U. S. Army remote-sensing group at Ft. Huachuca, Arizona.

Under this contract an Army Mohawk aircraft equipped with an all-weather side-looking radar (SLAR) flew two missions in Alaska in May and August 1976 resulting in complete SLAR coverage (51 flights) of the Beaufort and Chukchi shelves during the critical periods. These data have been heavily used, particularly by OCSEAP RU #88 (Weeks) and RU #99 (Cannon).

An April 1977 SLAR mission was flown which resulted in spring sea-ice coverage of the Chukchi and Beaufort coastlines as far east as Camden Bay. A section of one of these flight lines is included here showing spring activity in the area of Prudhoe Bay. (Figure 1)

7) Preparation and distribution of remote-sensing data catalogs

All the remote-sensing data available in our files for the Alaskan continental shelf have been indexed and plotted on maps. Catalogs summarizing the availability of these data and providing instructions for selecting and ordering data have been prepared and distributed to all OCS investigators as appendices to the series of Arctic Project Bulletins (Nos. 6, 9, 10, 12, 14, and 17). In addition we have developed a file of catalogs and photo indices of aerial photography obtained by federal, state and industrial agencies in Alaska, and we attempt to stay informed on plans for future aircraft photographic missions.

B. Remote-Sensing Data Processing Facilities and Techniques

The facilities and equipment commonly used for remote-sensing data processing are listed in Figure 2. Most of this equipment is not devoted exclusively to remote-sensing data processing but arrangements have been made to support the needs of the OCS investigators on a time-share and work-order basis, and to take into account the needs of the OCS program in any planned modifications or expansions.

The optical and photographic processing techniques developed for the remote-sensing program are described in the flow diagram of Figure 3.

Photographic processing probably needs no further explanation. The full range photographic laboratory of the Geophysical Institute is well adapted to the generation of custom, as distinct from production run, photographic products. However, the available equipment limits photographic enlargements to 16x20" maximum size from 8x10" originals. Electronically dodged prints or transparencies are produced by contact printing only.

Optical processing revolves around the use of specialized equipment such as the multiformat photo-interpretation station, the zoom transfer scope, the color additive viewer and the VP-8 image analyzer in addition to conventional light tables, stereoscopes and a binocular zoom magnifier.

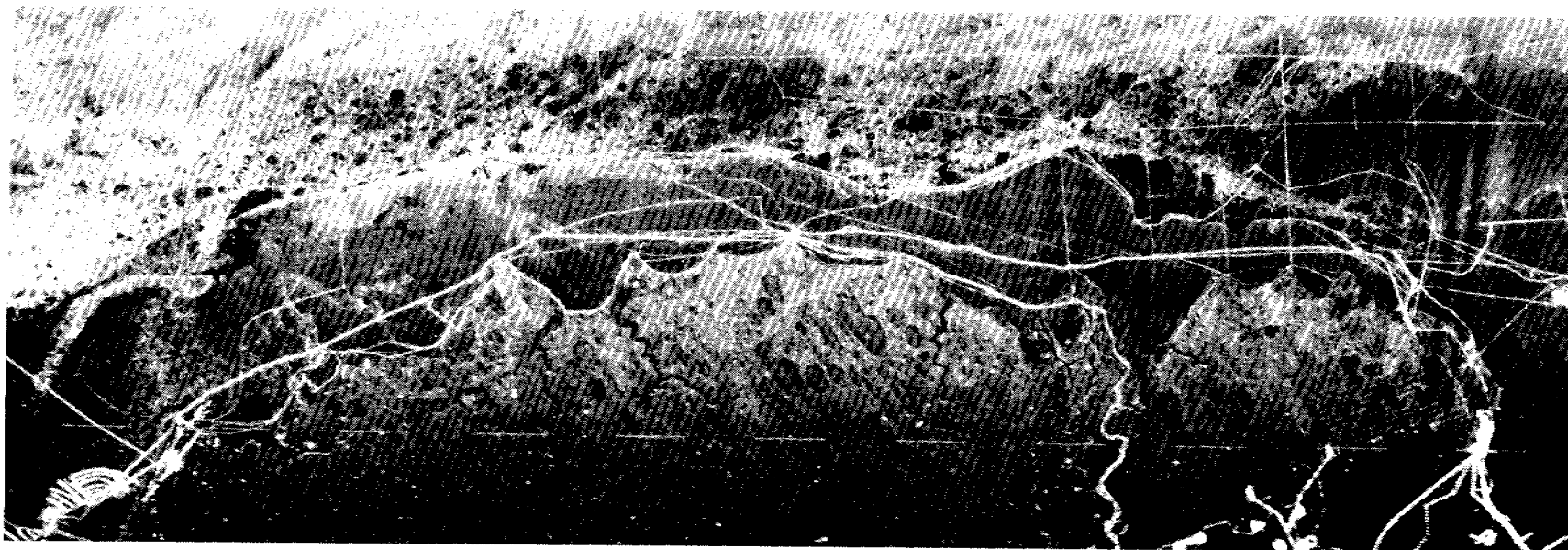
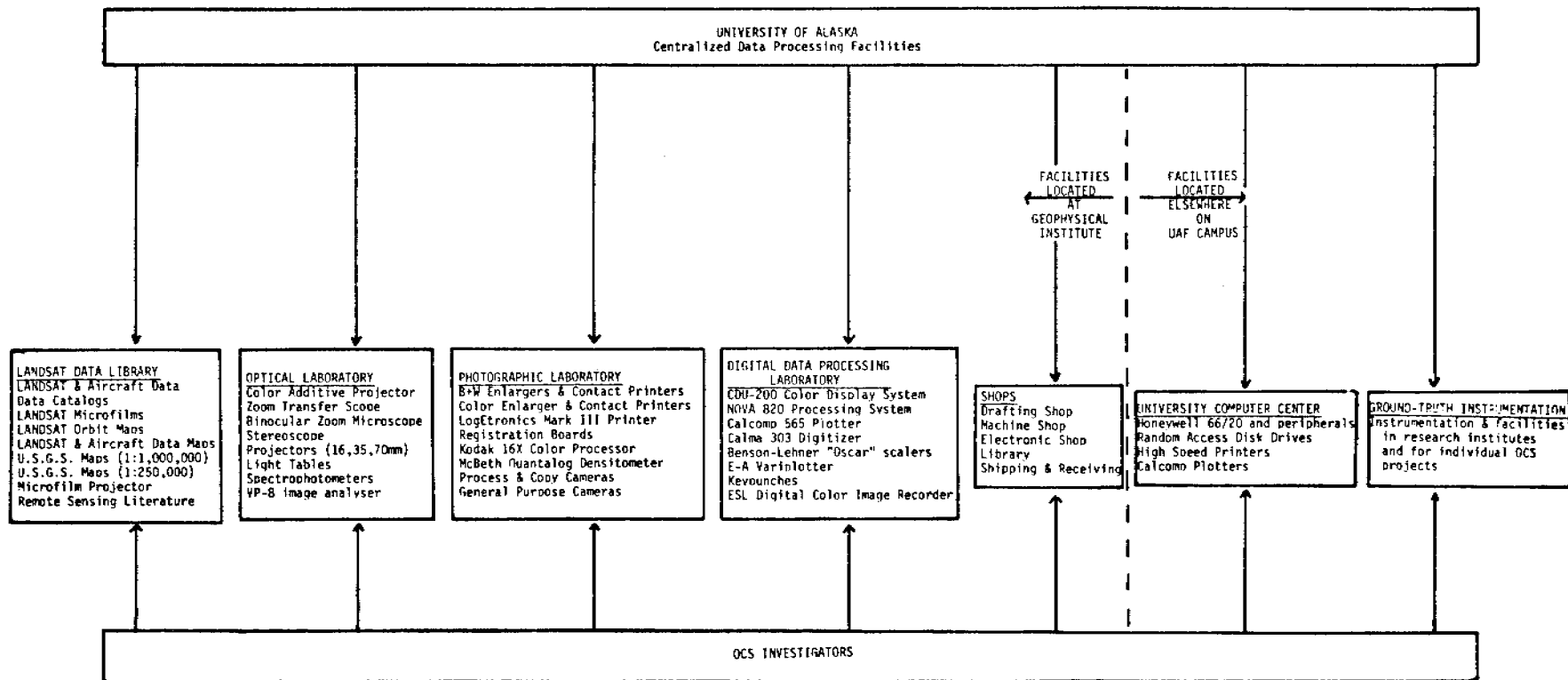


Figure 1 Side Looking Airborne Radar

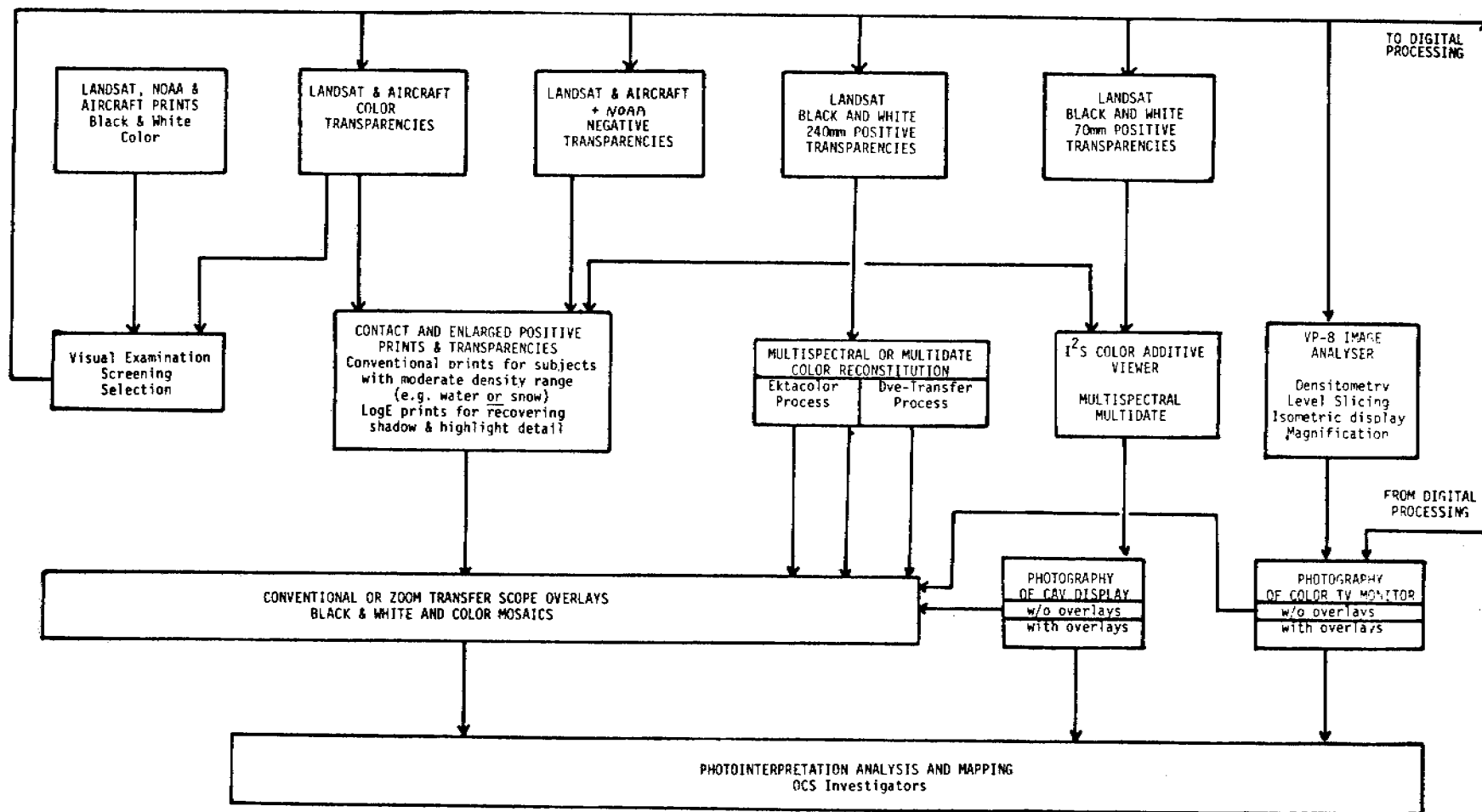
This Radar image was acquired in April 1977 over the Prudhoe Bay-Simpson Lagoon area. SLAR is particularly sensitive to surface roughness and the availability of reflecting surfaces for the 3.5 cm radar signal. Consequently ice roughness is well mapped, although the return signal tends to saturate in areas of increased roughness thereby limiting the dynamic range of the recorded information. For instance, man-made features such as ice roads give a saturated return signal while the berm on the roadside is less than a meter high. On the other hand, the texture of ice piled around smooth pans is well portrayed. This information would be extremely useful when planning field work on the ice. Note the Union Oil's Ice Island and surrounding snow fences in the extreme lower left corner of the image, Prudhoe Bay oil field facilities on the right and numerous roads and trails on the near shore ice.

OCSEAP RU 267 (Belon)



Centralized Data Processing Facilities

Figure 2



Optical and Photographic Processing

Figure 3

Multiformat Photo Interpretation Station - Analysis of aerial imagery in roll form is a cumbersome task and is likely to damage the original material even with careful handling if one uses ordinary reel holders and a light table. With stereo coverage, it is impossible to achieve stereo viewing with the frames appearing on the roll format unless one uses the photo interpretation machine. It can accommodate either 5-inch or 9-inch film formats and the film transport adjusts to permit stereo viewing with varying amounts of forward lap between frames. The viewing turret includes zoom binoculars with up to 5X magnification.

Zoom Transfer Scope - The time-consuming process of transferring information from images to maps is made considerably easier by the use of the zoom transfer scope. This table-top instrument allows the operator to view simultaneously both an image and a map of the same area. Simple controls allow the matching of differences in scales (up to 14X) and provide other optical corrections so that the image and the map appear superimposed. In particular a unique one-directional stretch capability (up to 2X) allows the matching of computer print-out "images" to a map or photograph.

Color Additive Viewer/projector/tracer - This instrument is primarily intended for the false-color recomposition of Landsat images from 70mm black and white transparencies and tracing information contained on these images at scales of 1:1,000,000 and 1:500,000. However it has proved to be very useful also for superimposing and color-coding Landsat images acquired on different dates and looking for change or movement and for viewing any other enlarged image on 70mm film format.

VP-8 Image Analysis System - The VP-8 image analysis system provides an electronic means of quantizing information contained in a photograph when the sought information can be expressed in terms of density ranges. It consists of:

- a light table having uniform brightness and a working surface of 15x22 inches
- a vidicon camera which transforms the photographic (transmittance) data to electrical signals
- an electronic image analyser which quantizes and formats the vidicon signals
- a CRT oscilloscope
- a color television monitor as an output device

The capabilities of the VP-8 image analysis system include:

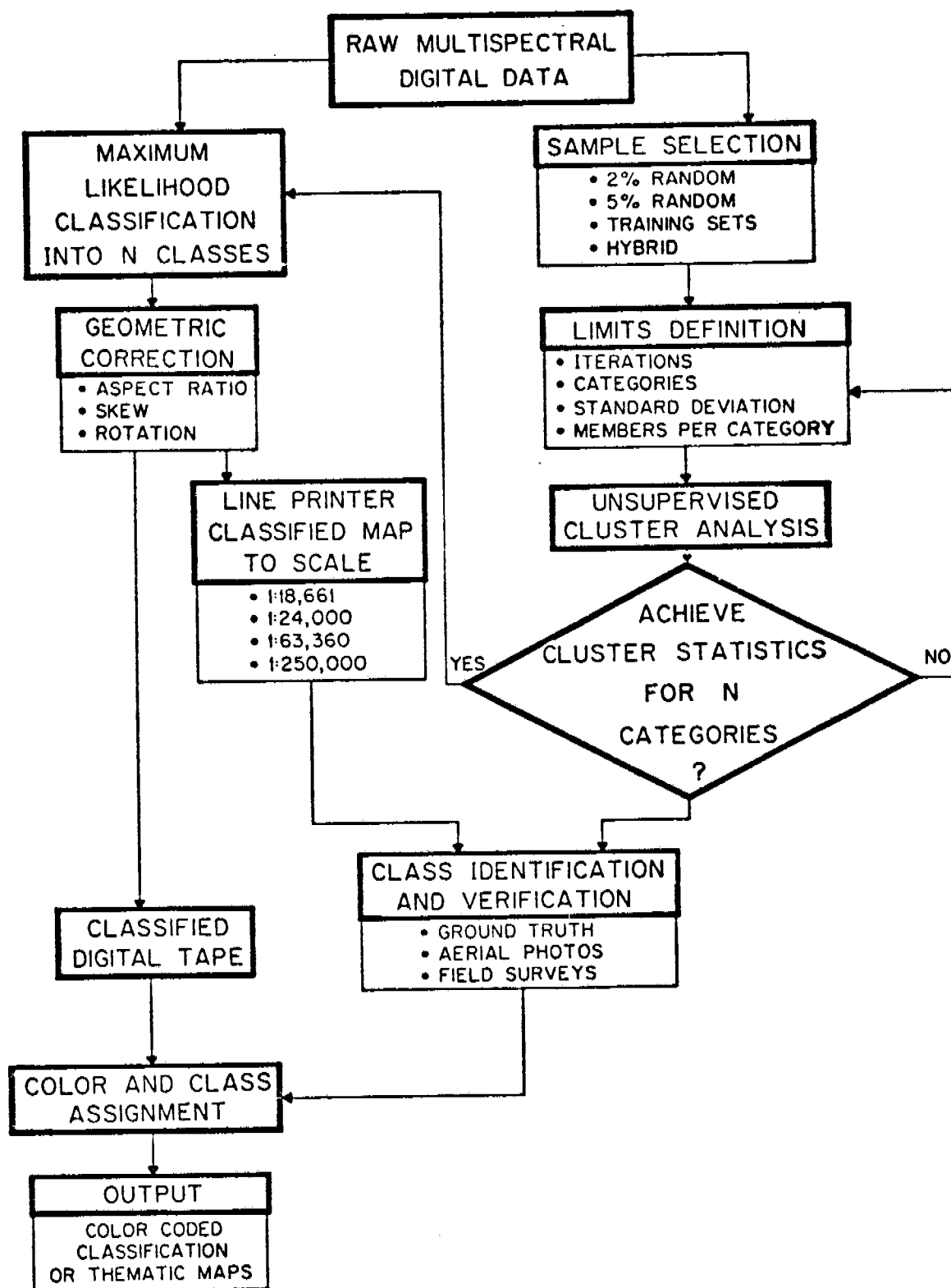
- density level slicing. This feature allows lines of uniform density on the input image to be displayed as contours. These contours form the boundaries of density bands which are displayed as up to 8 color bands on the color television monitor. The base density levels and the density range of the bands are individually as well as collectively variable. An example and illustration of the density slicing technique applied to coastal sedimentation studies was provided in the OCSEAP Arctic Project Bulletin No. 7, Appendix C, "Environmental Assessment of Resource Development in the Alaskan Coastal Zone based on Landsat Imagery" by A. E. Belon et al, University of Alaska.

- single scan line display. Any single horizontal scan line of the vidicon camera can be selected for display on the CRT oscilloscope by positioning a horizontal cross-hair on the image. This display of a single scan line is effectively a microdensitometer trace.
- digital read-out of point densities, selected by adjustable cursors or of total area of the image having a given (color-coded) density range. For instance the VP-8 image analysis system is well adapted to the area measurement of sea-ice, newly refrozen ice, and open water in any area of the Beaufort Sea imaged by Landsat.
- 3-D display. This mode of operation allows a three-dimensional presentation where the X and Y coordinates of the original image are displayed in isometric projection and intensity information is shown as a vertical deflection. Subtle features of the image, which are often lost on level-sliced displays, become obvious in 3-D displays.
- 5X magnification. This feature allows the expansion of a small part of the image on the 3-D display to full screen size.

The digital data processing equipment available to the OCS investigators include the main University computer, a Honeywell model 66/20 with 1 M bytes of core memory, which has a remote time-share terminal at the Geophysical Institute, a NOVA 820 data preprocessing computer as well as conventional line printers, plotters and digitizers. Most remote-sensing imagery in digital format is reformatted, classified or otherwise processed on offline computing systems. An overall flow diagram of digital processing of Landsat imagery is illustrated in figure 4 and discussed later in this report. Once the digital data have been processed, they are displayed on two specialized systems available at the Geophysical Institute.

The CDU-200 digital color display system is described by the simplified block diagram of figure 5. The CDU-200 performs three primary functions;

- 1) it provides a capability, similar to the VP-8 image analysis system for density slicing up to 3 bands of Landsat data in digital format. The accuracy of digital density-slicing is greater and more reproducible than with the VP-8 system because digital Landsat data have a more accurate radiometric calibration than photographic data and because up to 127 levels of intensity can be sliced (in groups of 16). Furthermore, three digital images can be stored at once on the disc of the CDU-200 system and displayed sequentially for multispectral or multi-date signature determination.
- 2) it provides a capability, similar to the color-additive viewer, for registering and combining three black and white digital images into a false-color image (displayed on the color television monitor) which has a larger scale, spatial and intensity resolution than the images displayed on the color-additive viewer.



FLOW CHART FOR GENERATING ECOSYSTEM MAPS

Figure 4 Digital Processing of Landsat Imagery

Flow chart of the unsupervised classification algorithms used for generating ecosystem maps of the Alaskan coastal zone from Landsat digital imagery.

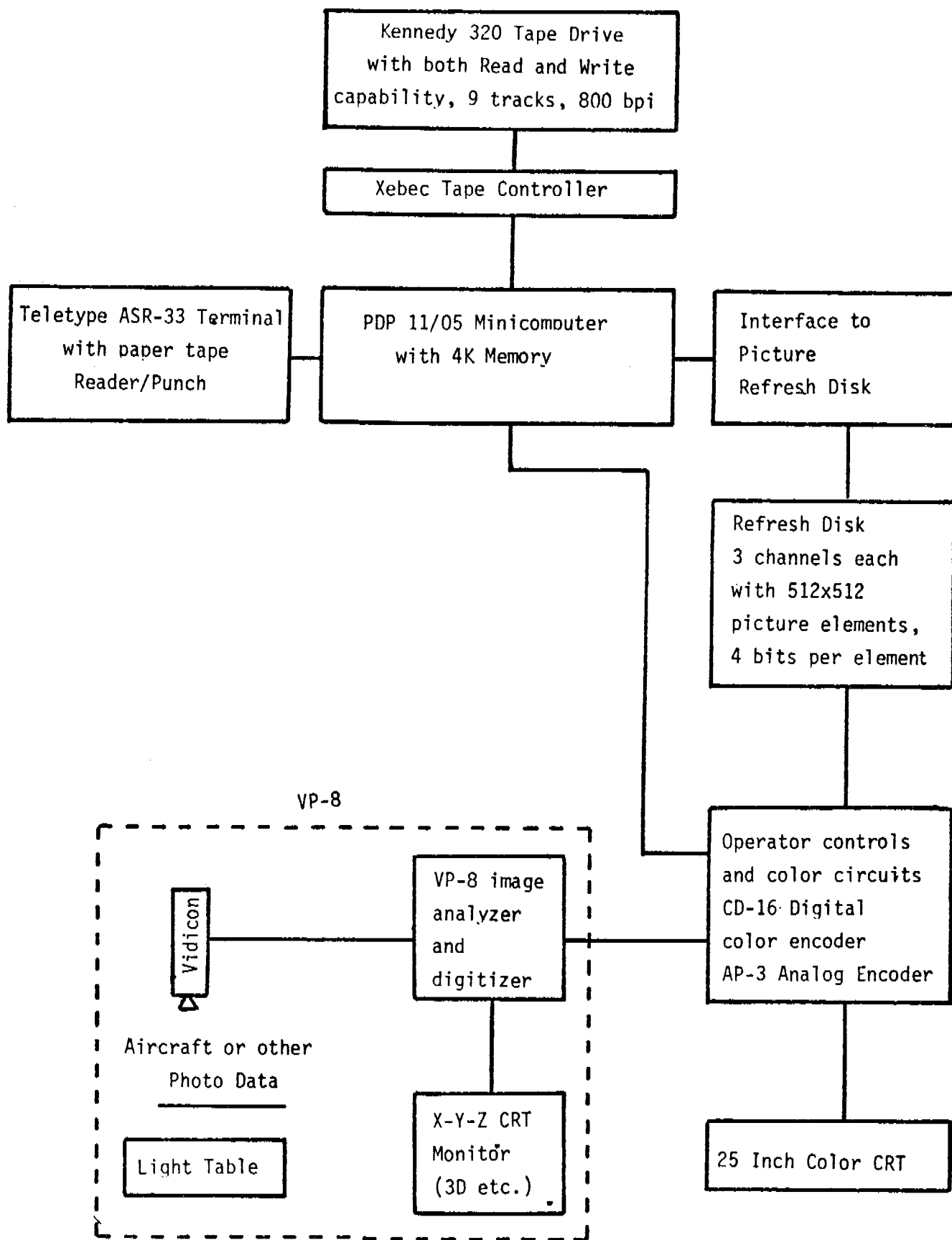


Figure 5

3) it provides a capability to generate color-coded thematic displays from the output of classification processing techniques performed by off-line computer systems. An example of the application of the CDU-200, as well as the digital color image recorder to the mapping of coastal zone ecosystems is provided in the OCSEAP Arctic Project Bulletin No. 7, Appendix C.

Digital Color Image Recorder - It often is necessary to reconstitute an image from the processed digital data in order to convey information in the most suitable form to the human mind. Also, if one deals with multi-spectral data it is impossible to convey the density of information required without the use of color. A digital image recorder with the capability of reconstituting color products was procured and installed in 1976 using State of Alaska funds appropriated to the University of Alaska Geophysical Institute. Basically it is a rotating-drum film recorder which produces four simultaneous standard images on film up to 8x10" in size. Density resolution is 255 levels of gray, and spatial resolution is 500 lines per inch. Recording rate is 1.5 lines per second. Any combination of the four negatives so produced can be registered and printed with suitable filters to produce a reconstituted color negative which can be processed and enlarged photographically.

This year the image recorder was extensively tested to improve its performance. Density levels between the four channels were adjusted to achieve precise balance for improved color discrimination. Several different color reconstitution film and processing combinations were evaluated to determine the optimum method of converting black and white positive films into color products.

Testing has been completed and it is now possible to obtain photographic images with high resolution and maximum detail from digital data products.

Remote-Sensing Data Interpretation Techniques - The basic techniques for remote-sensing data reduction and interpretation are described in flow diagram format in figure 3 (optical and photographic data processing) and figure 4 (digital data processing). The techniques for visual photointerpretation, as applied to sea-ice mapping; for density slicing, as applied to sea-surface suspended sediment mapping and transport; and for digital data processing, as applied to ecosystem thematic mapping, are described in the OCSEAP Arctic Project Bulletin No. 7, in particular its Appendix C "Environmental Assessment of Resource Development in the Alaskan Coastal Zone based on Landsat Imagery" by A. E. Belon, J. M. Miller and W. J. Stringer.

Variations of these techniques offer considerable promise of effective applications to OCS studies, but are too numerous and varied to be discussed in detail here. Usually they are developed in cooperation with individual OCS investigators for application to a specific project. Therefore we refer to the reports of other OCS investigators for detailed descriptions of applications of remote-sensing data to disciplinary studies.

C. Consultation and Assistance to OCS Investigators

This activity may be subdivided into two parts: general assistance to all OCS investigators provided through the Arctic Project Bulletins, program planning and negotiations and meetings/workshops; and individual assistance through consultation, training sessions on the use of remote-sensing data and equipment, and cooperative data analyses.

1. General Assistance

In order to familiarize OCS investigators with the available remote-sensing data, processing equipment, and interpretation techniques, we prepared seven substantial reports which were included as appendices to the OCSEAP Arctic Project Bulletins Nos. 6, 7, 9, 10, 12, 14 and 17 and distributed to all OCS investigators active in studies of the Beaufort, Chukchi and Bering Seas and the Gulf of Alaska.

The appendix to Arctic Project Bulletin No. 6 described the operation of the remote-sensing data library, provided catalogs of Landsat and aircraft data available in our files and provided instructions to OCS investigators on the selection and ordering of these data.

The appendix to Arctic Project Bulletin No. 7 described the facilities and techniques available for analyzing remote-sensing data and included a scientific report in which these facilities and techniques were used to analyse and interpret remote-sensing data in three representative investigations of the Alaskan continental shelf: sea-surface circulation and sediment transport in the Alaskan coastal waters, studies of sea-ice morphology and dynamics in the near-shore Beaufort Sea, and mapping of terrestrial ecosystems along the Alaskan coastal zone.

The appendix to Arctic Project Bulletin No. 9 provided a cumulative catalog of all available OCS remote-sensing data including Landsat and NOAA satellite data, USGS/OCS aircraft data and NASA aircraft data.

Arctic Project Bulletin No. 10 provided a catalog of the SLAR (Side-looking radar) imagery obtained by the Army Mohawk remote-sensing aircraft in May 1976.

The Appendix to Arctic Project Bulletin No. 12 provided an updated catalog of satellite and aircraft remote-sensing data acquired since the issuance of the cumulative catalog of Bulletin No. 9.

Arctic Project Bulletin No. 14 provided a catalog of the SLAR imagery obtained in May 1977 by the Army Mohawk aircraft.

Arctic Project Special Bulletin No. 17 provided an updated catalog of satellite and aircraft remote sensing data acquired through the spring and summer field season of 1977.

Although the existing remote-sensing data base is very useful in supporting OCS disciplinary projects, there is also a vital need for an airborne remote-sensing data acquisition program dedicated to OCS purposes.

To this end we have worked very closely with the NOAA Arctic Project Office in attempting to implement such a program. We participated in several meetings at the Geophysical Institute and one at Barrow in an attempt to set the USGS/OCS airborne remote-sensing data acquisition program on the right course, and took over responsibility for cataloguing, reproducing and disseminating these data. When this program failed and was terminated in January 1976, we studied alternatives and recommended several options to NOAA, one of which was a contractual arrangement with the U. S. Army remote-sensing squadron at Ft. Huachuca, Arizona. This recommendation was implemented, and two missions of the Army Mohawk remote-sensing aircraft were conducted in May and August 1976, resulting in high quality SLAR imagery of the Beaufort, Chukchi and Gulf of Alaska shelves at critical period. Another mission was conducted in April 1977. In parallel with these activities we have negotiated with NASA for the acquisition of high altitude (U-2, 65,000 ft.) aerial photography of the entire Alaskan coastal zone. This program was approved by NASA at no cost (so far) to NOAA/OCSEAP. The first attempt to acquire the requested data, in June 1975, failed because of prevailing heavy cloud cover during the 3 weeks the U-2 aircraft was in Alaska. A second attempt, unfortunately delayed until October 1976, was partially successful and acquired high quality aerial photography of the Gulf of Alaska and Prince Williams Sound. Due to excessive cloud cover very little usable U-2 imagery was acquired from the June 1977 mission; however, two flight lines in the Prudhoe Bay area were of good quality. We also participated in successful negotiations with the National Ocean Survey for acquisition of color aerial photography of the Bering and Chukchi Sea coasts during a previously scheduled mission of their Buffalo aircraft to Alaska in summer 1976. Excellent medium altitude photography was acquired from the Yukon delta to Cape Lisburne, as well as isolated areas of the Gulf of Alaska coast. In summer 1977 NOS again flew several flight lines, extending from Cape Sabine on the Chukchi Sea coast to Cape Halkett on the Beaufort Sea. This imagery is of excellent quality and is archived here for OCS investigators' use.

While the OCSEAP Arctic Project Office and our project have been fairly successful in negotiating remote-sensing data acquisition by other agencies on an irregular basis, such arrangements are not wholly satisfactory on a long-term basis because the type and format of the data vary from one mission to another and the frequency of data acquisition is insufficient to provide timely observations and good statistical information on coastal zone conditions and processes. For this reason we worked with the Arctic Project Office on a plan which would utilize a Naval Arctic Research Laboratory (NARL) C-117 aircraft, remote-sensing equipment available from several sources, and local processing of the data to provide more frequent and more relevant data on a consistent format.

OCSEAP agreed with this plan and contracted with NARL for the airborne data acquisition program and with our project (RU 267) for the processing of the data. The Cold Regions Research Laboratories (CRREL) provided a Motorola side-looking radar and a laser profilometer, as well as a qualified engineer, to NARL, and we located and secured four aerial cameras for installation in the aircraft which was subsequently modified and committed to a remote-sensing program by NARL. Our project also acquired wide-film processing and printing equipment and constructed a photographic laboratory for processing of the data acquired by the NARL aircraft.

Despite the great efforts of several individuals and agencies, the program encountered many problems and has met with little success so far, with the result that only a few flight lines of SLAR data have been acquired to-date. Furthermore the future of the program now appears uncertain because the NARL C-117 aircraft suffered serious engine failure on the last SLAR flight to Prudhoe Bay and because the U. S. Navy is likely to drastically reduce the logistic and research capabilities of NARL after September 30, 1978.

For these reasons, as well as the anticipated phasing-down of the OCSEAP, we now recommend that OCSEAP return to its previous practice of contracting for SLAR data acquisition with the U. S. Army at strategic times and on a case-by-case basis.

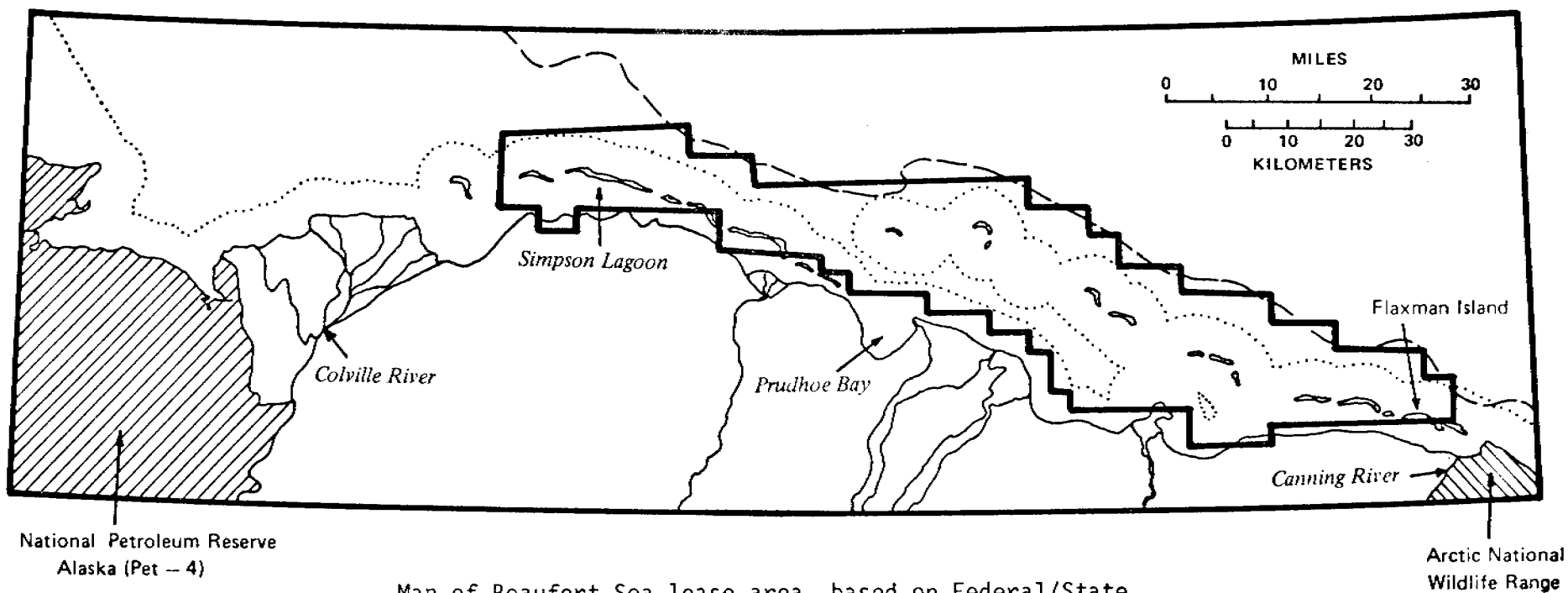
At the request of the Arctic Project Office, personnel from our project attended the Bird and Mammal Review in Fairbanks, 25-28 October, 1977. A remote-sensing display which included examples of imagery acquired during the 1977 field season was prepared for the meeting. In addition, panels showing a variety of remote sensing data applications were presented. A catalog of recent imagery was provided for the participants.

The applications specialist from our project attended the Beaufort Sea Synthesis Meeting at NARL, in Barrow on January 23-27, 1977 at the request of the Arctic Project Office. He participated in disciplinary sessions pertaining to sea ice and geology and the interdisciplinary session on gravel resources and the effects on gravel islands and causeways. A display made up of Landsat, aerial photography and side-looking radar (SLAR) imagery acquired in 1977 was previously prepared and taken to the meeting. The SLAR image (see figure 1) was of particular interest during the discussion of the Union Oil ice island project. As a result of the comments and concerns expressed during the meeting, we have located from our data files a series of four Landsat images that show the Beaufort Sea lease area during different seasons (Figures 6, 7, 8, and 9). These images, presented here at a scale of 1:1 million, show the range of conditions that occur from late winter (February) through spring (July) and into late summer (August) in the Beaufort Sea.

2. Individual Assistance

Individual assistance to OCS investigators involves consultations on the applicability of remote-sensing data to specific studies, data selection and ordering, preparation and supervision of work orders for custom photographic products and data processing, training in the use of remote-sensing data processing equipment and techniques, development of data analysis plans and sometimes participation in or performance of data analysis and interpretation.

This individual assistance has continued to increase in number and scope over the past year. 136 OCS investigators utilized our facilities during the past year, most of them for several hours, and some of them repeatedly. In addition, numerous contacts occurred by mail or telephone correspondence. Therefore, it is not possible to describe in detail



Map of Beaufort Sea lease area, based on Federal/State nomination map. This represents the maximum extent of the lease sale scheduled for December 1979; further tract deletions from within this area are possible.

..... 3-mile State of Alaska jurisdictional area
 - - - 20-meter (10 fathom) depth contour (approx.)

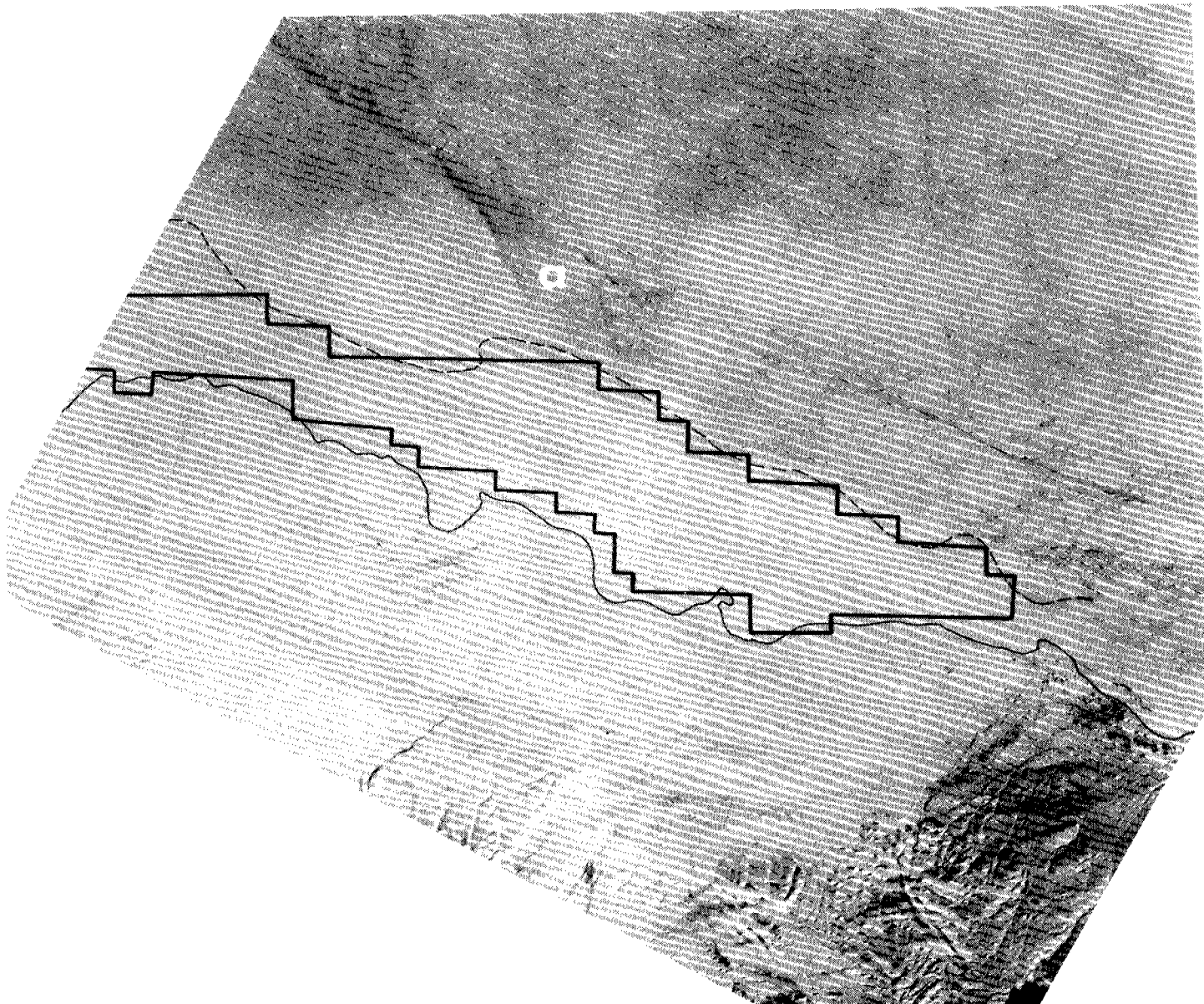


Figure 6 Beaufort Lease Area - Midwinter 1976

Landsat Scene 2392-21023 18 February 1976 This mid-winter Landsat scene shows contiguous ice extending great distances from shore. No flaw lead is visible. Near the 20-meter isobath (dashed line) along the seaward boundary of the proposed lease area large ridge systems can be seen. Condensation trails from water vapor sources in the Prudhoe Bay vicinity indicate onshore winds which could be partly responsible for the absence of open lead systems. Observations of extended contiguous ice have been documented for several years by RU 258 (Stringer), Almost every year during the winter and early spring this phenomenon occurs in the Beaufort Sea and persists for several weeks. The dark patch (a) representative of thin ice to the west of the main ridge systems indicates that in the recent past the ice had been moving leaving this area uncovered. It is likely that some of the ridges apparent on the scene were created at that time.

OCSEAP RU 267 (Belon)

Scale 1:1 Million

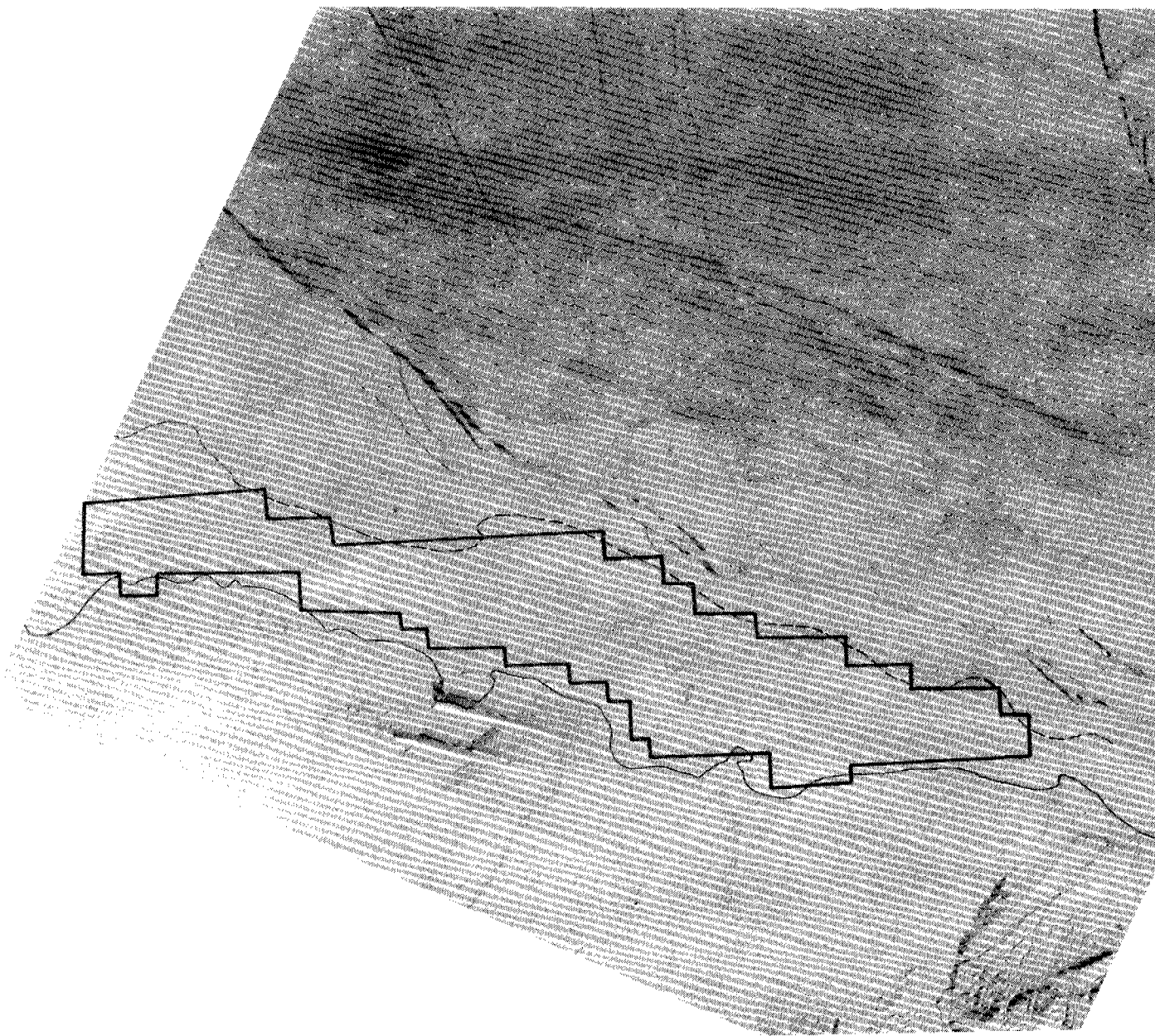


Figure 7 Beaufort Lease Area - Midwinter 1977

Landsat Scene 2752-20505 12 February 77 In contrast to Figure 6, this midwinter Landsat image shows an active shear zone a few kilometers seaward of the 20-meter isobath (dashed line). Cracks appearing to result from shear stress can be seen extending shoreward of the major fracture system. It is interesting to observe from the water vapor condensation trails that Prudhoe Bay surface winds are eastward trending while winds aloft (~ 70 meters) are bearing approximately 45° to the right, giving them a heading of nearly southeast. Clearly the surface winds at that time would not tend to hold the ice into shore as indicated for Figure 6.

OCSEAP RU 267 (Belon)

Scale 1:1 Million

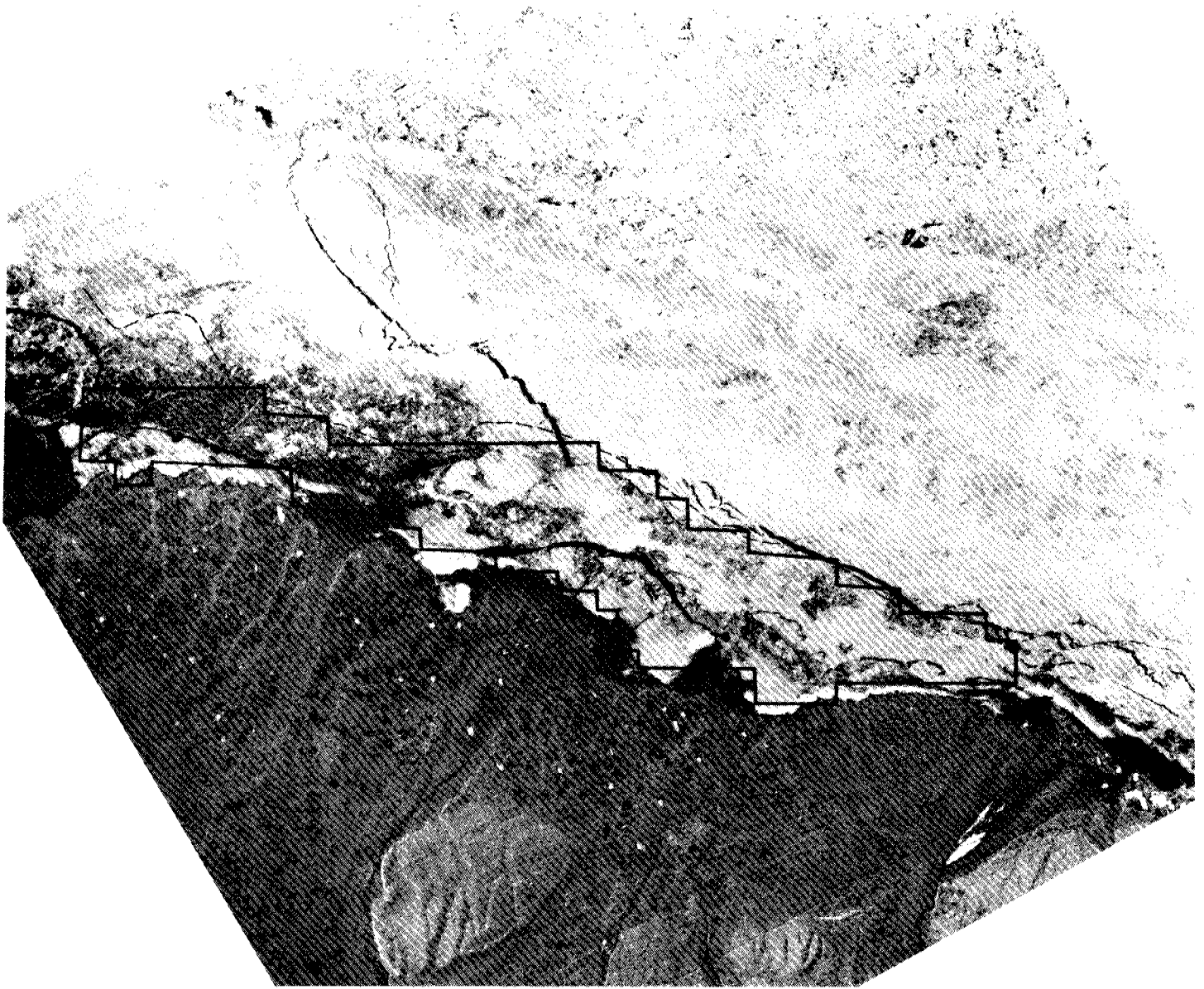


Figure 8 Beaufort Lease Area - Early Summer 1977

Landsat Scene 2898-05155 July 1977 This early summer Landsat scene shows breakup ice conditions along the Beaufort Coast. A variety of processes are at work within the lease area: Far offshore along the seaward boundary of the lease area a large lead system has opened up shifting the pack ice almost due east by a kilometer. Clearly the ice seaward of this lead is not well-grounded at this time. It is interesting to note that this lead system nearly coincides with the 20-meter isobath (dashed line). Inside the barrier islands, overflow waters from coastal rivers have helped melt the ice adjacent to shore. (This phenomena has been mapped by RU 258). Further offshore but still within the lagoons, the ice sheet is breaking into fragments free to float around the lagoons. This phenomenon indicates two interesting pieces of information: 1) The ice within the lagoons was not piled during the winter sufficiently to cause anchoring and 2) The draft of the ice sheet in the areas breaking off is now less than the water depth which, in turn when compared with bathymetric charts indicates the state of decay of the fast ice.

OCSEAP RU 267 (Belon)

Scale 1:1 Million

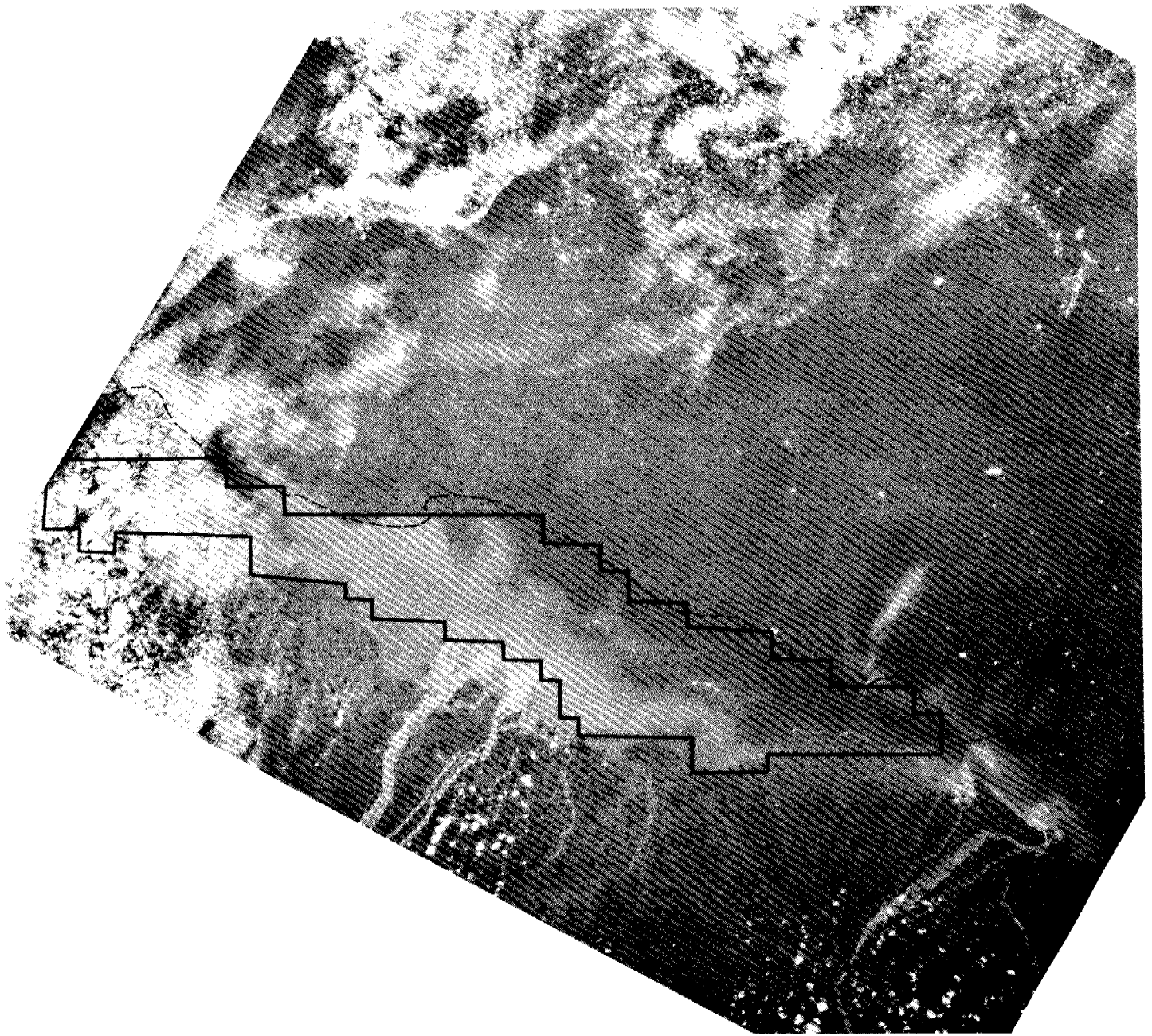


Figure 9 Beaufort Lease Area - Summer 1973

Landsat Scene 1396-21162 23 August 1973 This mid-summer scene shows sediment plumes from coastal rivers within the boundary of the proposed lease area. These sediment plumes should be useful for tracing nutrient transport resulting from erosion of nutrient-bearing soils along rivers and the coast. Information concerning potential transportation of pollutants may also be derived from circulation patterns enhanced by sediments. Farther offshore a few pieces of drift ice can be seen near the boundaries of the proposed lease area. Other mid-summer Landsat scenes show drift ice grounding within these boundaries.

OCSEAP RU 267 (Belon)

Scale 1:1 Million

these individual activities, but their scope is illustrated by listing the user projects: RU's nos. 4, 31, 34, 59, 68, 69, 83, 88, 98, 146, 149, 149, 172, 194, 196, 204, 205, 230, 244, 248, 249, 250, 251, 253, 257, 258, 259, 289, 305, 335, 337, 338, 339, 340, 341, 342, 343, 441, 458, 460, 461, 467, 470, 473, 483, 529, 530. Of these about 20 projects are using remote-sensing data routinely, and six of them (RU's no. 99, 248, 249, 257, 258, 289A) almost exclusively. The principal applications are sea-ice morphology and dynamics, coastal geomorphology and geologic hazards, sea-surface circulation and sedimentation, sea-mammals habitat, and bird habitat mapping.

VI - RESULTS

The results of the project so far can be separated into two categories: the operational results (establishment of a remote-sensing data facility) and the research results (disciplinary applications of remote-sensing data to OCS studies).

A. Establishment of a Remote-sensing Facility for OCS Studies

The principal result of the project, as specified in the work statement of the contract, is that there now exists at the University of Alaska an operational facility for applications of remote-sensing data to OCS studies. This facility and its functions have been described in detail in the previous section of the report. Briefly it consists of:

- 1) A remote-sensing data library which routinely acquires catalogs and disseminates information on Landsat and NOAA satellite imagery and aircraft imagery of the Alaskan continental shelf.
- 2) A remote-sensing data processing laboratory which provides specialized instrumentation for the photographic reproduction and optical or digital analysis of remote-sensing data of various types and formats.
- 3) A team of specialists that generates and develops techniques of remote-sensing data analysis and interpretation which appear to be particularly well-suited for OCS studies.
- 4) A staff that is continually available to OCS investigators for consultation and assistance in searching for, processing and interpreting remote-sensing data for their disciplinary investigations.

This year the data library changed location and upgraded facilities which have enhanced its utility to OCS investigators. Improvements include an increased work area, segregation of analysis equipment into independently illuminated areas, access to additional geophysical data, technical library and the OCSEAP Arctic Project Office.

As a result of the establishment of the remote-sensing facility established by our project, about twenty OCS projects are routinely using remote-sensing data, six of them almost exclusively, and many more OCS investigators are occasional users of remote-sensing data.

B. Disciplinary Results of the Applications of Remote-Sensing Data to OCS Studies

In general, the results of applications of remote-sensing data to OCS studies will be contained in the annual reports of the individual projects and need not be repeated here. However as part of our function to develop techniques of remote-sensing data analysis and interpretation, we did prepare a scientific report entitled "Environmental Assessment of Resource Development in the Alaskan Coastal Zone based on Landsat Imagery" which illustrates the applications of Landsat data to three important aspects of the OCSEAP program: studies of sea-surface circulation and sediment transport in Alaskan coastal waters, studies of sea-ice morphology and dynamics in the near-shore Beaufort Sea, and mapping of terrestrial ecosystems in the Alaskan coastal zone. This report was presented at the NASA Earth Resources Symposium, Houston, Texas, June 1975 where it was acclaimed as one of the best presentations. It was also distributed to OCS investigators as part of Arctic Project Bulletin No. 7 and is now out of print due to heavy demand in spite of the fact that 250 copies were made.

A specific effort is being made to develop a digital data processing technique in response to OCSEAP project needs. We are experimenting with digital superimposition of two Landsat scenes from different dates. This multirate product will be used to attempt a computer classification of vegetation types near Point Barrow for correlation with bird habitat. Two Landsat scenes were selected from 18 July and 6 August 1976 covering an area 24x12 km. Control points from the two scenes were selected and an eight channel magnetic tape was produced (2 scenes times 4 spectral bands for each scene). The objective of this test is to perform a computer classification of the new multirate image so that ground data can be collected this field season to determine the correlation between spectral classes and bird habitat type. If successful, this technique may be applied to larger areas on the coast along potential lease sites to help assess impact.

VII & VIII - DISCUSSION AND CONCLUSIONS

The principal objective of the contract, as specified in its work statement, has been achieved: a facility for applications of remote-sensing data to outer continental shelf studies has been established at the University of Alaska and is now fully operational.

The remote-sensing data library has acquired all available cloud-free remote-sensing imagery of the Alaskan continental shelf, catalogued it and provided information on its availability to all OCS investigators through the series of Arctic Project Bulletins.

Existing instrumentation for analysing remote-sensing data has been consolidated into a data processing laboratory and techniques for its use have been developed with particular emphasis on the needs of the OCSEAP program. New instrumentation is being acquired and new analytical techniques are continually being developed from this contract and other funding sources.

The staff of the project is interacting with a gradually increasing number of OCS investigators, providing consultation and assistance in all aspects of remote-sensing applications from data searches and ordering to advanced analyses of the data in photographic and digital format. We have also worked very closely with the OCSEAP Arctic Project Office in designing an interim remote-sensing data acquisition program using contract and aircraft missions by other agencies.

At this time about twenty OCS projects are using remote-sensing data and processing facilities routinely, some of them almost exclusively of other research activities, and many more OCS investigators are occasional users of remote-sensing data. While the number of user projects has increased over the past year, we anticipate a shift in the interest of OCS investigators. As the focus of OCSEAP changes from synoptic studies to the leasing process, requests should become more detailed and site specific in nature. Studies of processes and potential impacts on individual areas will rely heavily on historical remote sensing data and detailed interpretations on a case by case basis. It will be important to collect and archive available coverage as well as assist in the acquisition of more detailed imagery of key areas.

It is clear from the foregoing discussions and from consultations with OCS investigators, regarding their study plans for the next year, that there will be a continuing need for the research support that our project provides. We intend to submit a continuation proposal to NOAA for this purpose.

IX - SUMMARY OF FOURTH QUARTER OPERATIONS

This quarterly report covers the period January 1 to March 31, 1978.

A. Laboratory Activities During the Reporting Period

1. Operation of the remote-sensing data library.

Although we continue to search continuously for new Landsat imagery of the Alaskan coastal zone entered into the EROS Data Center (EDC) data base, during this reporting period only six new scenes have been received at a total cost of \$96. The small number of scenes ordered reflects the fact that the satellite does not acquire data of Alaska during January and early February, owing to the very low solar illumination. Another factor is the time delay in delivery of data after acquisition, normally three to five weeks.

We continued to receive three daily scenes from NOAA satellite for a total of 171 scenes at a cost of \$2,177.40. Again, owing to the low solar illumination during January and February, images in the visible spectral band were not acquired by the satellite for the first six weeks, but the thermal IR images which depend on emitted, rather than reflected radiation, were received throughout the reporting period.

No new aircraft remote-sensing data were received in the reporting period.

Seventeen OCS investigators made extensive use of our facilities during this reporting period. Their needs were varied and ranged from data searches and placement of data and work orders to utilization of data analysis equipment and cooperative studies. Data purchases by OCS investigators totaled \$340 for orders placed to EDC for Landsat products, \$121 for NOS aerial photography and \$99 for NOAA imagery. Most investigators utilized library copies of data archived in our facility.

2. Operation of data processing facilities.

Testing of the computer driven film recorder (IGOR) was completed during this reporting period and it is now fully operational (See Section V.B this report).

3. Development of data analysis and interpretation techniques.

An effort is underway to develop a technique to relate side-looking radar (SLAR) imagery of sea ice to seal distribution in the Beaufort Sea. Our applications specialist is working with Brendan Kelley (Shapiro, RU 250) to attempt a correlation between density levels from the radar imagery and seal distribution data collected from aerial survey flights. A microdensitometer and color density slicer are being used to quantify the characteristics of sea ice recorded on SLAR.

Work continues to develop the technique of multirate Landsat digital analysis to map bird habitat, as reported in Section VI B.

4. Consultation and assistance to OCS investigators

Seventeen OCS investigators requested our assistance in searching for, obtaining or analysing remote-sensing data. Some visitors to our facility are not formal OCSEAP investigators but their activities are OCSEAP-related and they are mentioned here. Users (OCS and non-OCS) this quarter included:

Erk Reimnitz and Peter Barnes, RU 205, spent several hours in our facility prior to attending the Beaufort Sea Symposium browsing through the latest data available.

Glenn Seaman, working with Burns, RU 248, looked at the most recent NOAA imagery to get an idea of current ice conditions before going out in the field.

John Harper, Louisiana State University, Coastal Studies Institute, is interested in the possibility of submerged shoals in the Peard Bay area of the Chukchi Sea and called to ask about NOS photography available of the area. Scenes were plotted on a map to delineate exact coverage and samples of products sent to him. He responded by placing an order for several images.

Peter McRoy, RU 305, requested a data search for Landsat imagery of the Prince William Sound area. A suitable scene was located and several data products ordered for him. We will assist him in analysis of the scene during the next reporting period.

Brendan Kelly, working with Shapiro, RU 250, asked our assistance in developing a technique to relate side-looking radar (SLAR) imagery of sea ice to seal distribution in the Beaufort Sea. We worked with him on this project. Progress and initial results are reported in section A.3 of this report.

Peter Reinhardt, working with RU 59, Hayes, called to ask about the availability of NOS aerial photography for Kodiak Island. Maps showing flight lines and ordering information were sent to him.

Jerry Brown, USA/CRREL, called and asked our assistance in plotting the 1977 U-2 aerial photography of Prudhoe Bay on maps giving exact image boundaries. This was done and sent to him along with ordering information.

Jan Cannon, RU 99, uses our facilities regularly to examine and analyse the latest imagery available.

Leonard Peyton, RU 458, looked at and ordered an enlargement of NOS photography of his study area.

Kristina Ahlmas, working with Royer, RU 289, is a regular user of our facility and utilizes the NOAA imagery archived here extensively.

Niren Biswas, RU 483, searched through Landsat and NOAA imagery of his study area in Kotzebue Sound, in order to relate seismic data to major episodes of ice movement.

Bill Stringer, RU 257, uses our library copies of Landsat data to determine which scenes to have enlarged for use in his ice-mapping project.

David Drake, RU 230, ordered several NOAA images which we had previously determined were suitable for his study of sediment transport in the Bering Sea.

Special assistance was provided to Dr. Juergen Kienle (RU 251) this period. On 6 February 1977 a volcanic eruption on the Alaska Peninsula was reported by the U. S. Coast Guard. The source of

the eruption was Westdahl, a historically active volcano on the east end of Unimak Island. For the week following the eruption, NOAA 5 satellite imagery was procured for Dr. Kienle on a special service basis from the NOAA/NESS facility in Fairbanks. Enlargements from two of these NOAA passes were of particular interest and are included here. Figure 10a is from the 9 February 1978 pass which records synchronous eruptions at Westdahl and Shishaldin, a volcano 50 km to the east. A later pass that day (21:29 UT figure 10b) shows a dark triangular area south of Westdahl approximately 300 km² in area, believed to be an extensive ash fall which led to the evacuation of the Scotch Cap Coast Guard Station. At the time of the evacuation, a meter of ash had accumulated at the station, 16 km south of Westdahl. Copies of the NOAA satellite imagery have been sent to the Smithsonian for inclusion in the monthly Scientific Event Alert Network Bulletin, to show the method of using remote sensing data for near-real time monitoring and hazard evaluation.

B. Problems Encountered/Recommended Changes

As mentioned in section V.C.1 of the annual report, the future of the NARL airborne remote-sensing data acquisition program is very uncertain. We will work with the OCSEAP Arctic Project Office to explore alternatives.

Owing to the major price increase effected by the EROS Data Center for remote-sensing data products, coupled with the successful launch of Landsat-3 which will generate more high quality data, it is likely that our budget for data purchases will be exhausted well before the end of the contract period. Once the needed funds have been estimated, we will request a transfer of funds from technical services (labor-currently underexpended) to material and supplies at no change in the total budget of the contract.

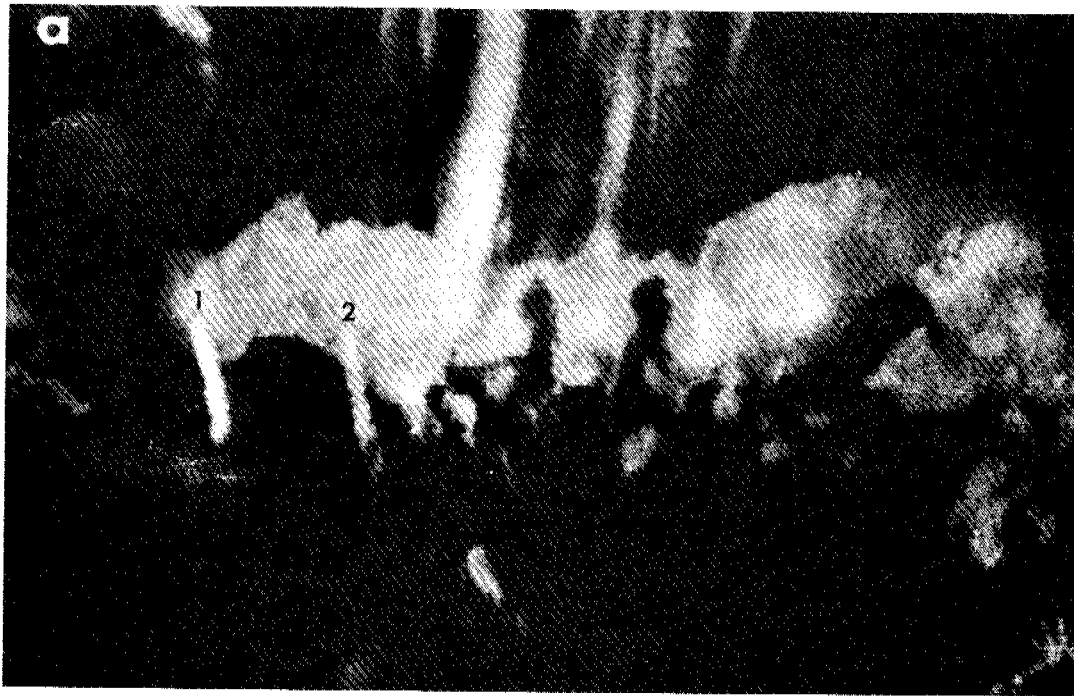


Figure 10a and 10b - Volcanic Eruptions on Unimak Island

These images are digital enlargements of NOAA-5 satellite imagery of Unimak Island on the Alaska Peninsula obtained following the eruption of Westdahl on February 5, 1977. Figure 10a shows plumes from the synchronous eruption of Westdahl (1) and Shishaldin (2) as recorded on 9 February 1977, 0535UT. On Figure 10b, 9 February 1977, 2129UT, a dark triangular area (3) is visible south of Westdahl, 300 Km² in size that is believed to be an ash fall. The plume from the volcano bisects the area and trails off to the southwest.

OCSEAP RU 267 (Belon)



ANNUAL REPORT

Contract: #03-5-022-56
Research Unit: #289
Task Order: #19
Reporting Period: 3/1/77-3/31/78
Number of Pages: 30

CIRCULATION AND WATER MASSES IN THE GULF OF ALASKA

D. Thomas C. Royer

Institute of Marine Science
University of Alaska
Fairbanks, Alaska 99701

March 1978

TABLE OF CONTENTS

I. SUMMARY

II. INTRODUCTION.

III. CURRENT STATE OF KNOWLEDGE.

IV. STUDY AREA.

V. SERVICES, METHODS, AND RATIONALE OF DATA COLLECTION

VI. RESULTS

VII. DISCUSSION.

VIII. CONCLUSIONS

IX. NEEDS FOR FURTHER STUDIES

X. SUMMARY OF FOURTH QUARTER OPERATIONS.

 Task Objectives

 Field Activities.

 Results

 Preliminary Interpretations of Results.

 Problems Encountered.

APPENDIX I - Abstracts of Papers Submitted

APPENDIX II - CTD Noise Tests During February 1978
 Discoverer Sea Trials

I. SUMMARY

The results forthcoming from this research unit's efforts reflect a maturing effort. We are now beginning to understand, we believe, some of the causes of the distributions of the observed parameters. Therefore, we can now go somewhat beyond a purely descriptive presentation that has been relied on in the past reports.

The most important result of this year's research is the separation of precipitation and wind stress effects on the coastal dynamic height, and hence the coastal circulation. We can now speculate on the effects of precipitation, both local and large scale, on coastal circulation and also on the interaction of coastal currents with the Alaska Current. The system is not entirely as straightforward as might be assumed from the above statements. There is evidence of eddies and other perturbations in the circulation that are both temporary and permanent. We know also that the wind stress effects the circulation, but are not sure as to the exact mechanism or magnitude. As our knowledge advances for this region, we are now able to ask more numerous and better questions than we could previously.

Besides the discovery of the precipitation effect, the shelf circulation appears to consist of a coastal current and a shelf break current with weak flow between them. There is some evidence for baroclinic flow into Prince William Sound. There is also evidence that fresh water runoff affects the transport in the Alaska Stream and that maybe this is a boundary between the coastal waters and oceanic waters. We have found that the geostrophic currents, as determined from CTD/STD measurements, correspond to results of the drifters. We have also constructed a numerical model which can be used to represent flow found on the shelf. Field

efforts were also begun to address the interaction of Prince William Sound circulation with the circulation in the Gulf of Alaska.

II. INTRODUCTION

The past year's work on R.U. #289 shows a change in emphasis from oceanographic field work to data analysis and interpretation. Five cruises were carried out by personnel on this project last year with about 220 CTD/STD stations occupied and two current water arrays deployed. These figures represent decreases in field activities from previous years. The numbers associated with analysis and interpretation are not as well defined as those of the data collection phase. However, a broader understanding of the processes affecting the circulation and how they operate has been achieved this year and this understanding is expected to improve as the analysis continues. For example, in last year's OCSEAP Annual Report, flow regimes were defined for the first time for the northern Gulf of Alaska. This year, we know those driving forces which probably cause these different flow regimes.

The OCSEAP mesoscale current study for the Gulf of Alaska began in 1974 with only vague ideas on the general circulation of the region. No direct current water measurements had been taken and seasonal hydrographic sections were sparse. It was known that the subarctic gyre circulation was cyclonic and transport estimates ranged from $5-15 \times 10^6 \text{ m}^3/\text{s}$. It was assumed that large scale forcing by wind stress was important in controlling circulation. Three and one-half years of data collection, confirm these initial assumptions, but add other factors which influence circulation in the Gulf of Alaska. The spatial scales of the important forces in the region range from tens of kilometers to

thousands of kilometers. They range in time from minutes to years. Practical restrictions do not allow the study of events on all of these scales. The importance of the forces which drive the circulation are evaluated from prior data and new field programs are developed to study those events of importance to the circulation. For example, it was thought, initially, that Prince William Sound would probably not be impacted by oil and gas development on the continental shelf in the northeast Gulf of Alaska. Our studies show, however, that Prince William Sound is likely to be impacted and new efforts were begun to incorporate studies of it along with the mesoscale current work.

III. CURRENT STATE OF KNOWLEDGE

In contrast to earlier emphasis in field work by this research unit, the present analysis phase has enabled a better understanding of the dynamics of the Gulf of Alaska circulation. We now have much improved estimates of magnitudes, directions, spatial dimensions and temporal changes in the currents of the region. Comparisons of our results with those of other investigators working in the region are beginning to reveal features of the circulation that a single research unit could not uncover. We have also reached the point where field measurements can be designed to verify predicted flow patterns.

IV. STUDY AREA

Field work under this research unit has ranged over the continental shelf of the southern Alaska coastline from Yakutat to Unimak Pass from the coastline to tens of kilometers beyond the shelf break. The satellite data achieved for OCSEAP by this unit covers the entire Alaskan coastline

from the Beaufort Sea to Southeast. The analysis portion of the past years work has been addressing the entire Gulf of Alaska region, whereas field work in the past year has been limited to that portion from Prince William Sound to Kodiak Island. The study area represents a combination of the NEGOA and Kodiak lease areas. This is because the two regions are connected through the shelf circulation along with the larger scale circulation of the region.

V. SERVICES, METHODS AND RATIONALE OF DATA COLLECTION

As in previous years, the primary data collection methods used by this research unit is the CTD/STD (salinity - temperature - depth) profile. Some current meter and bottom pressure gauge deployments have also been undertaken to supplement the hydrographic data. From the CTD/STD, contour maps of salinity, temperature, density and dynamic height are constructed. These contours provide information on the direction and intensity of the flow. The current meter measurements provide a means of "calibrating" the currents obtained from the density (salinity - temperature) fields. The sea level as measured at the coastline by NOS (National Ocean Survey) stations is used in conjunction with the bottom pressure data to determine changes in the slope of sea level between the two positions and hence a measure of current changes.

The CTD/STD station positions are determined by 1) a knowledge of the spatial scales of the features to be measured and 2) requirements to continue a time history of oceanographic parameters at a particular location. The objective of both of these criteria is an improved understanding of changes in the parameters, spatially and temporally.

VI. RESULTS

The most important result of the past years work under R.U. #289, is that the coastal currents in the northern Gulf of Alaska respond seasonally to precipitation and wind stress. The precipitation affects the currents through the input of fresh (low density) water at the coastline. This high rate of inflow at the coastline is due to a cross-shelf precipitation gradient (decreasing offshore), and coastal runoff. It is enhanced during most of the year by a coastal convergence of surface water due to wind stress. The evidence for this control of currents through dynamic height is presented in Figure 1. Minima in the sea level and dynamic height at all levels occurs in April. In May there is a sudden increase in these parameters reflecting the sudden spring break-up and release of snow that accumulated over the winter (generally beginning in December). June has another minimum in all parameters including precipitation. A gradual increase begins in July with the peak in the precipitation and upper layer (0-1000 db) dynamic heights occurring in September-October. The delay in the response time of the lower layer, maxima represents their response to the wind stress (upwelling index, UI) which peaks in January. The correlation matrix (Table I) demonstrates the relationships of those various parameters. It must be noted that the effect of the precipitation in the northern Gulf of Alaska is the result of longshore accumulation of fresh water from the point where the North Pacific Current splits to form the Alaska and California Currents. This means that precipitation and runoff from Washington, British Columbia and southeast Alaska are important to the coastal circulation in the northern Gulf of Alaska.

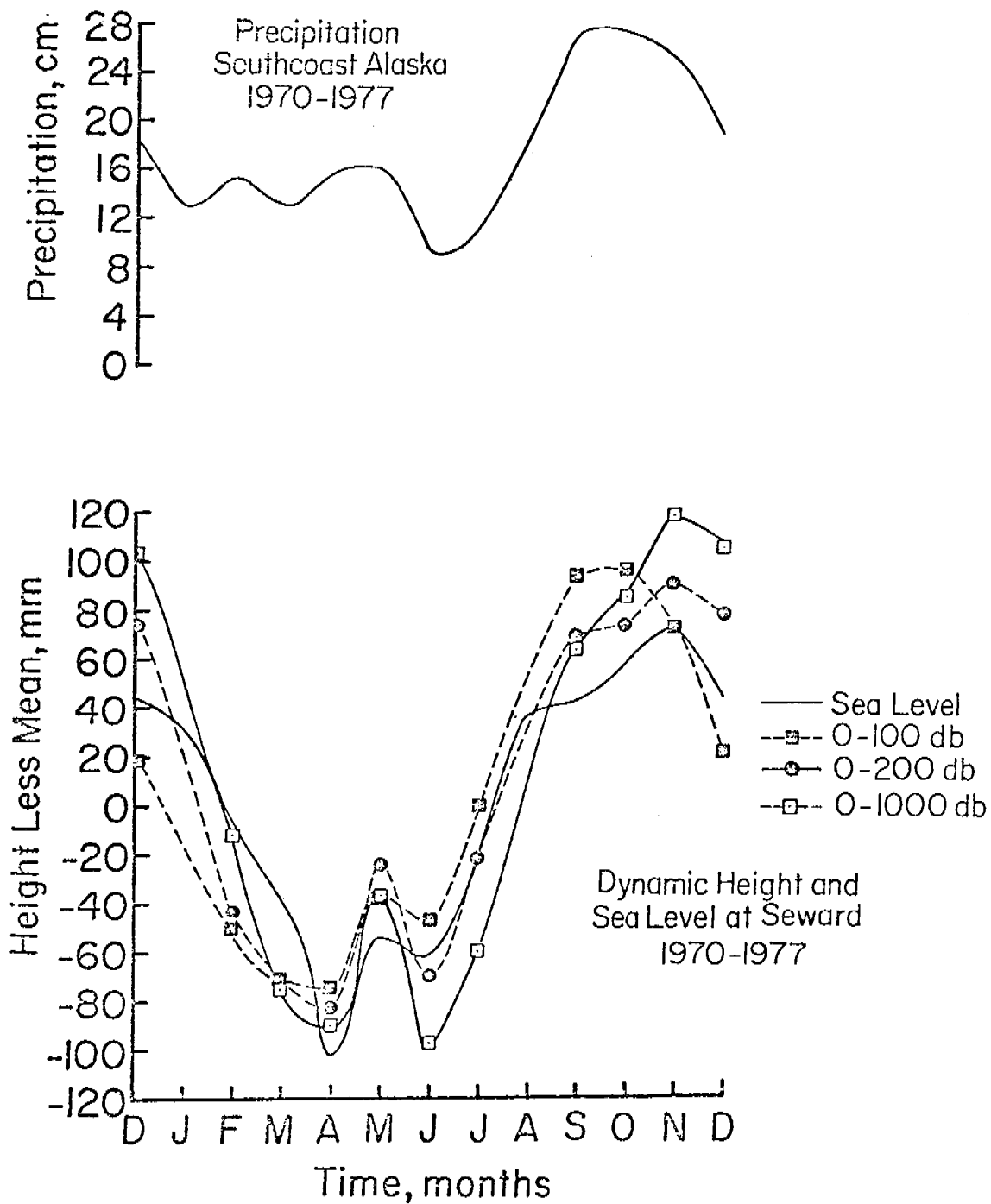


Figure 1. Sea level, dynamic height, and precipitation cycles for south coast of Alaska.

TABLE I

CORRELATION MATRIX - MONTHLY MEANS AT SEWARD

	(0-100)	(0-200)	(200-1000)	(0-1000)	UI	Precipitation	Sea Level
(0-100)	1						
(0-200)	.931	1					
(200-1000)	-.182	-.046	1				
(0-1000)	.850	.969	.221	1			
UI	.045	-.190	-.839	-.401	1		
Precipitation	.862	.835	.282	.843	-.116	1	
Sea Level	.880	.934	.132	.940	-.388	.744	1

Confidence
Level

R

99.95%	.861
99.50%	.756
97.5%	.624
95%	.544
90%	.439
80%	.298

The dominance of precipitation effects in the upper layers does not mean that wind stress is not important in these layers. Indeed, wind stress can only act directly on the surface layers and its effects must be transmitted downward through the water column. Therefore it should be emphasized that wind stress remains of great importance to the circulation of the Gulf of Alaska. The vertical density gradient is converted to a horizontal gradient through wind stress induced coastal convergence and it is these horizontal density gradients which drive the baroclinic, geostrophic currents.

We have constructed a two dimensional (actually, quasi three dimensional) numerical model which can simulate the effects of wind stress and fresh water input. The model is being applied to the section of the continental shelf off Seward. It is a finite-difference, cross-sectional model on a 16 m by 3 km grid. It is a nonlinear model which incorporates Coriolis acceleration, salt and heat diffusion, advection, variable eddy viscosity, bottom topography and stratification. It outputs the distributions of velocity (in three dimensions), temperature and salinity. The use of the hydrographic data for the Seward Line shows that the near-shore westward current is due to a combination of runoff from Prince William Sound and the Copper River and wind stress, whereas the current along the shelf break is a result of runoff from regions east of Kayak Island, including British Columbia and southeast Alaska. The model is being used in an attempt to explain the current reversal (eastward flow) at IMS 9 ($58^{\circ}41.1' N$, $148^{\circ}21.6' W$) which occurs on a seasonal basis from July through September. This reversal was reported in last years Annual Report. It is believed that the coastal and shelf break currents are the boundaries of a cyclonic current system extending between Middleton to Kodiak Islands, and

that there is a reversal throughout the year. Its position shifts seasonally, which explains why it is not always seen at IMS 9.

The bottom pressure measurements at IMS 9 reveal a long term trend in the slope between 9 and the sea level gauge at Kodiak. Unfortunately, the primary comparison was to have been done with Seward where the gauge was not operating during the deployment period. The tide data for Kodiak and 9 give no evidence of a harbor effect. That is, the tidal amplitudes and spectra are nearly identical for the two stations. This also means that there is a large tidal amplitude over the shelf.

Comparisons are being made between the dynamic topographies from the CTD/STD data and the trajectories of the drifting buoys released by D. Hansen, AOML as part of the OCSEAP work. These buoys were released in late May-early June 1976 and hydrographic sections were taken in April and September 1976. The April section has a cyclonic eddy at the shelf break off Yakataga with an anticyclonic eddy or meander to the east, adjacent to it (Figure 2). The anticyclonic eddy to the west of Kayak Island is also present in the topography. Hansen's drifter tracks for drifter numbers 1174 and 1133 correspond to this topography. This demonstrates that the drifters are closely approximating the geostrophic flow or that the flow is in geostrophic balance. The dynamic topography, also shows that there is baroclinic inflow into Prince William Sound through Hinchinbrook Entrance. This is due to the downward slope of dynamic height as one progresses into Prince William Sound.

The inflow into Prince William Sound, as first demonstrated by the drifters, and now by the dynamic topography has prompted the initiation of a field program to study this inflow in detail. Current meter arrays were installed in Hinchinbrook Entrance and Montague Strait in November

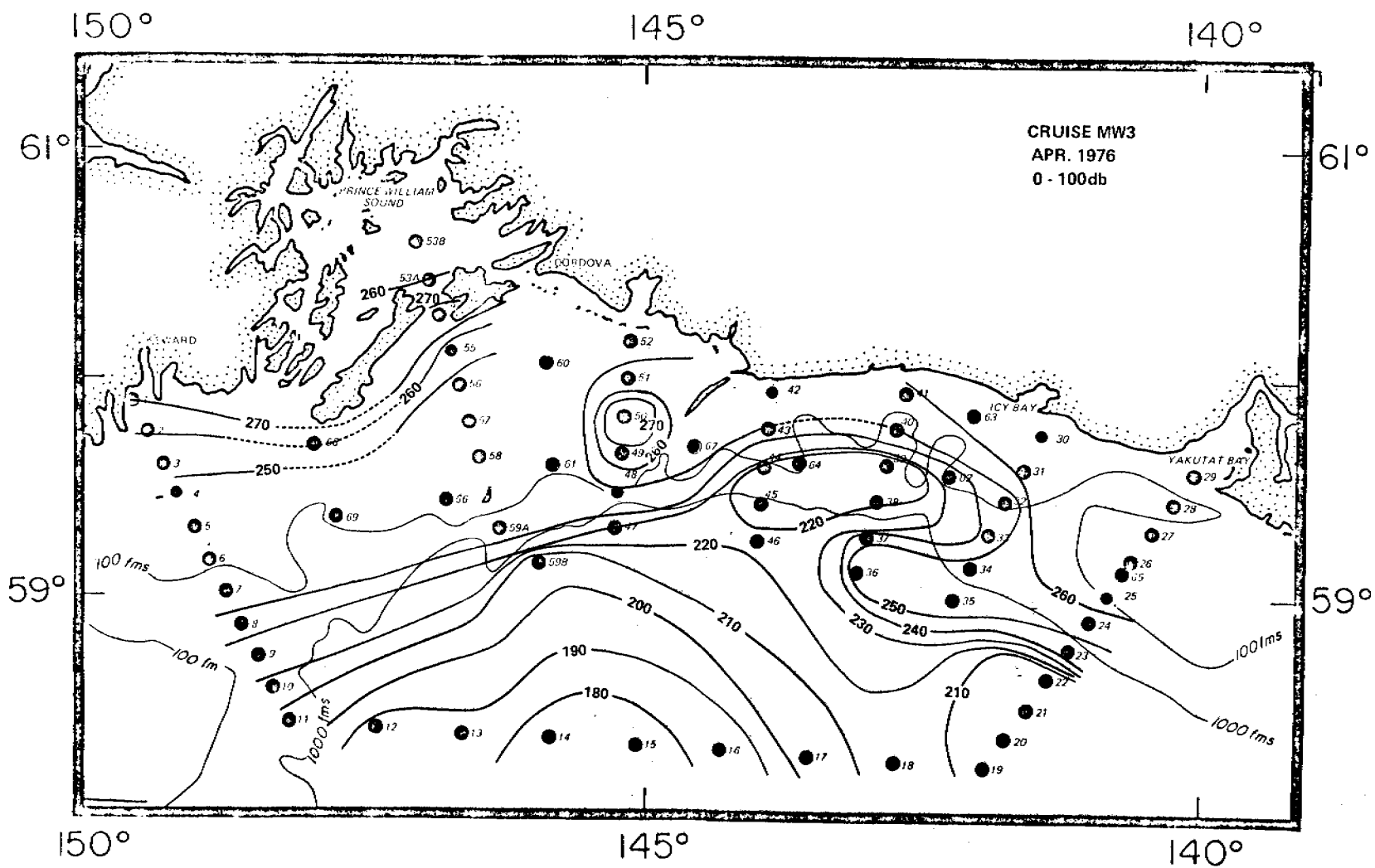


Figure 2. Dynamic topography for NEGOA, April 1976, 0-100db.

1977. Recovery is expected in April 1978. CTD/STD measurements are being carried out on a quarterly basis in Prince William Sound and the waters adjacent to it.

During the past year, it was discovered that noise problems exist with some of the CTD/STD as gathered on some ships. The symptom is that in the one meter averaged data from these ships, there are a large number of depths with no acceptable salinity or temperature values. It was found that the discrete values of temperature and salinity for these particular ships (in contrast to the one meter averages) have a considerable amount of noise in them, along with the depth parameter. The noise approached the manufacturers stated accuracy of the instrument, $\pm 0.02^\circ/\text{‰}$, $\pm 0.02^\circ\text{C}$. The spectra of this noise is depth dependent. The conclusion is that there is a mismatch in the CTD/STD deck equipment and the hydrographic cable. The impedance will be depth dependent and will force an over or underdriving of the amplifiers or filters causing erroneous signals for the various parameters. All of the ships with this noise problem are in the NOAA fleet and have a larger diameter hydrographic cable than those of the academic fleet (*Acona* and *Moana wave*). This problem was investigated on a shakedown cruise on the *Discoverer* in February 1978 and is expected to be corrected by the 1978 field season. Prior data do contain these errors, however (see attached addendum).

As in the past, the incoming NOAA-VHRR satellite data is continually monitored on a weekly basis, as the Remote Sensing Library at the Geophysical Institute receives positive transparencies of the satellite orbits covering Alaska with surrounding ocean areas. In scenes that show cloudfree areas or cloud systems of special interest, photographic prints

are made of both the visible and infrared band during the light season, infrared only during the dark, when the sun does not get high enough above the horizon. Areas showing special features of interest are enlarged. For cloudfree ocean areas grey scale enhancements are produced in the infrared range to show surface temperature structure.

Photographic prints generated by the above mentioned procedures are cataloged in ring binders that are accessible for viewing by interested investigators. Through 1977, the collection consists of 19 binders that have been cataloged (last two with the typist). Copies of the catalog index have been distributed to the Remote Sensing Library at Geophysics and PMEL in Seattle. Two new binders have been started for the 1978 imagery for (a) The Arctic Ocean - Bering Sea and (b) The Gulf of Alaska to the Aleutians.

During 1977, 1600 new prints were produced including 500 photographic enlargements and 215 infrared temperature enhancements. Twenty-one digital magnetic tapes, covering conditions of special interest were copied for permanent retention and possible future study. Of the above prints, about 250 have been submitted to other investigators (excluding Royer). As a group, the scientists at PMEL in Seattle have requested most imagery. The largest individual support has been given to Dr. George L. Hunt, Jr. of UCI, including continuous monitoring of the Pribilof Islands during the bird migration and nesting season. For one of his cruises it was possible to supply cloudfree simultaneous satellite coverage. This was beneficial to the understanding of the upwelling around the Pribilof Islands and its relationship to the bird habitation.

From time to time the satellite imagery collection has been used by IMS graduate students looking for various features of interest to

their OCS - supported supervisors, like the location of the ice edge in the Bering Sea, flow of suspended sediments and cloud movements.

The following list of cruises was completed in the past year:

Date	Ship	CTD/STD Stations	Area	Comments
Mar. 1977	<i>Miller Freeman</i>	36	Seward-Cook Inlet	
Aug. 1977	<i>Acona</i>	20	Kodiak Island Shelf	
Nov. 1977	<i>Discoverer</i>	94	Seward-Kodiak Island Shelf	
Nov. 1977	<i>Acona</i>	20	Prince William Sound-Hinchinbrook Entrance	2 current meter moorings
Feb. 1977	<i>Acona</i>	40	Prince William Sound	

VII. DISCUSSION

The investigation of the circulation in the Gulf of Alaska under this program has progressed from the point where only vague details were known, to a point where we can now provide some of the necessary details and explain why they should occur. For example, prior to this study it was known that the Alaskan Stream had a transport of $7-15 \times 10^6 \text{ m}^3 \text{ s}^{-1}$ with currents on the order of one knot. Our work shows that while the transport is correct, the width of the current is narrower than previously assumed (from 50-80 km in width) and more intense (speeds greater than 2 knots). This leads to the speculation that the Alaska Stream is a boundary between the coastal waters on the continental shelf and offshore oceanic waters.

In order to evaluate the possibility of coastal and deep ocean waters intensity to form the Alaska Stream, the horizontal density gradient (which drives the baroclinic geostrophic flow) has been separated into its salinity and temperature gradient components. In the Alaska Stream the horizontal salinity gradient contributes 2/3 of the horizontal density gradient with the temperature gradient yielding the remainder. Therefore, factors affecting the horizontal salinity gradient have twice the effect as those affecting the horizontal temperature gradient. Precipitation, by changing coastal salinity, can in turn, affect the Alaska Stream. Both temperature and salinity gradients are altered greatly by the coastal and shelf break convergence or divergence. Work is progressing on the breakdown of the contributions to the Alaska Stream transport of these two effects using OCSEAP gathered data. A similar analysis on the coastal current near the shore boundary will be attempted.

In a similar sense, the eddies discussed previously (Figure 2) appear to be temperature or salinity driven. The eddy to the northwest appears on a temperature contour map at 100 m (Figure 3) whereas the meander (or eddy) to the southeast appears on the salinity contour map (Figure 4) at 100 m. It is believed that the temperature driven cyclonic eddy was found by winter-mixing somewhere to the southwest off Kodiak and propagated to its indicated position. This forcing a meander in the Alaska Current and hence the anticyclonic, salinity-driven eddy. Similar eddies have been observed previously but further offshore. It can also be inferred from Figure 4 that the anticyclonic eddy west of Kayak Island is salinity driven. Because the drifters released in May-June 1976 saw these same eddies we know that they are not short-lived features. However, they were gone by September 1976, except for the Kayak Island eddy.

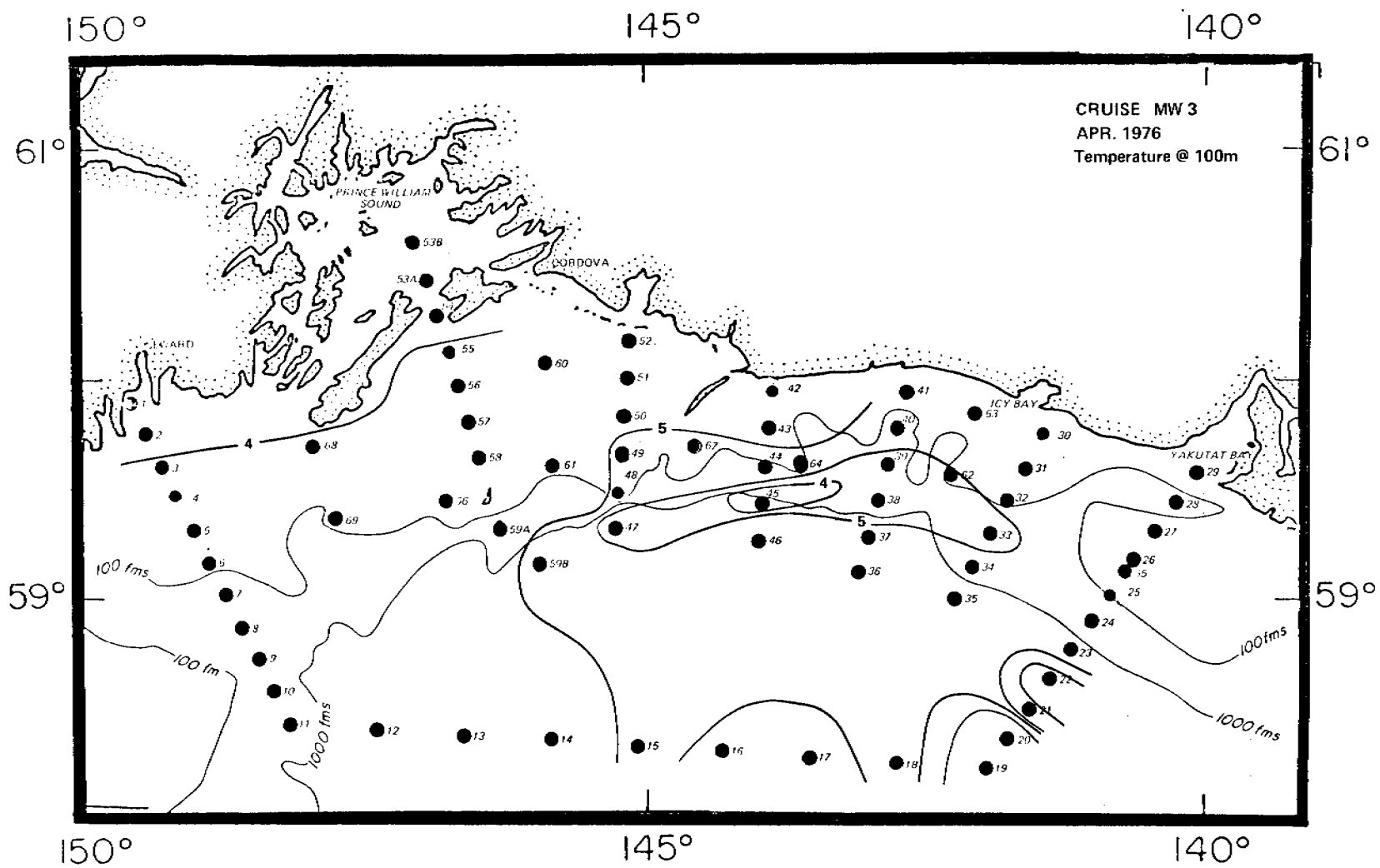


Figure 3. Temperature at 100 m, NEGOA, April 1976.

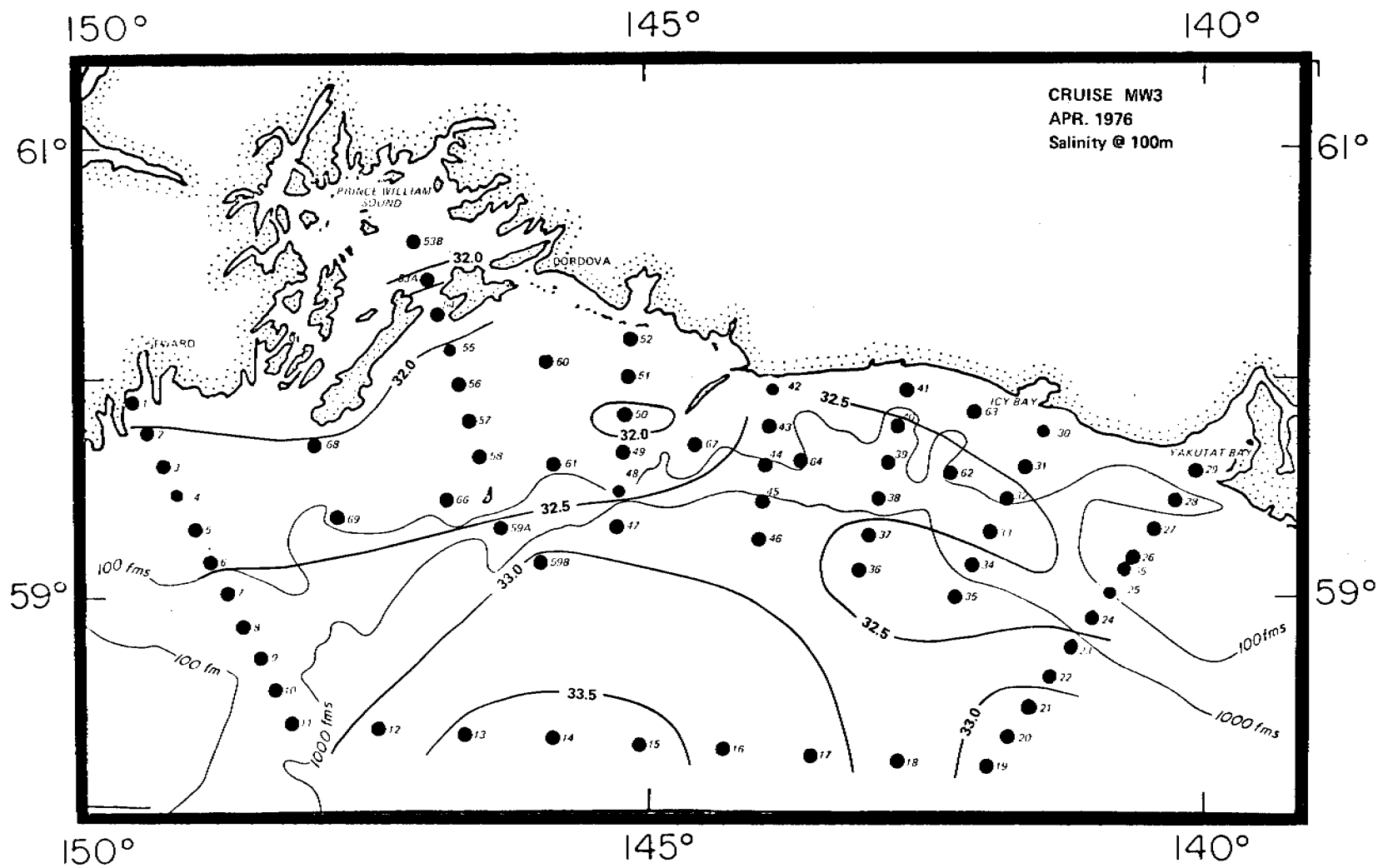


Figure 4. Salinity at 100 m, NEGOA, April 1976.

From discussions with the OCSEAP biological investigators, it has become apparent that eddies and other regions of low net flow are often areas of high biological activity. The eddies for April 1976 did not have any biological measurement made in them but the permanent eddy behind Kayak Island represents a unique biological region. Similarly, Prince William Sound has high productivity along with the low flow shelf area to the east of Kodiak Island. These low flow areas also represent areas where the entrance of pollutants would be especially harmful both from the standpoint of residence time and biological implications.

Because of the biological implications of the Kayak Island eddy and the interaction of the coastal current with Alaska Stream flow, the Kayak Island - Middleton Island region of the shelf is extremely important to the transport of pollutants on the continental shelf in the northern Gulf of Alaska. After the westward flowing coastal current impinges on Kayak Island (Figure 2), it can either enter the Alaska Stream or the Kayak Island eddy. The narrow shelf width at this position allows this transfer from the coastal current to Alaska Stream. That portion entering the stream, tends to remain at the surface, forming a low density surface layer. The difference in vertical density structure in this layer as compared with waters on either side, allows solar heating to be contained in a shallower layer. This produces a surface temperature difference which can be detected down the Alaska Stream along the Aleutian Islands, making satellite IR imagery an effective means of tracing the Alaska Stream.

That portion of the shelf circulation that does not enter the Alaska Stream is forced by the Middleton Island shoals to flow westward, north of the island. Geostrophy and bathymetry then combine to form the eddy to the west of Kayak Island. This eddy depends on the upstream longshore flow

and the Copper River outflow. The latter can create a longshore pressure gradient forcing offshore flow near its mouth. The cross-shelf pressure gradient will, in general, dominate, forcing westward flow.

The Kayak Island - Middleton Island system splits the shelf circulation into coastal boundary and shelf break components with a meandering flow between them. It makes the upstream region a place where the coastal current can interact strongly with the Alaska Stream. This type of meandering shelf flow continues on the east side of Kodiak Island. Changes from the input of fresh water out of Cook Inlet south of Kodiak might alter the shelf circulation along the Aleutians in a similar manner to that found off Yakutat.

The comments on the effects of precipitation and bathymetry should not be construed to mean that wind stress effects are not important in the Gulf of Alaska. On the contrary, wind stress and the accompanying convergence of surface waters along the coastline will tend to enhance the horizontal density gradients and intensify the cyclonic circulation. In this regard, we are evaluating the use of surface pressure charts, direct observation and Bakan's upwelling index as to their best application in examining the actual wind field over the Gulf of Alaska.

Because we now have data, both oceanographic and meteorological, that extends over several years some estimates of the year to year variation in the various parameters is now possible. For example, it is well known that the precipitation for the fall of 1977 was anomalous over the south coast of Alaska. Examination of historical weather records can yield some ideas on how common this type is and allow estimates of variance of the coastal circulation based on these data.

VIII. CONCLUSIONS

Precipitation and wind stress are now known to cause an annual change in the circulation on the continental shelf in the Gulf of Alaska. The narrow, intense Alaska Stream could also be responding to these effects. The precipitation effect, and possibly the wind stress are larger scale phenomenon than were previously assumed. For example, flow into or out of Prince William Sound depends not only on the oceanographic and meteorological conditions within the sound, but on the meteorological conditions in the Copper River Valley which control the river flow and precipitation along the southeast and British Columbia coasts. Therefore, the oceanographic conditions in the NEGOA area are responding to larger scale forcing. We have a knowledge of those forces which affect the shelf circulation and some idea of their relative importance. Further analysis is required to substantiate these initial conclusions and additional studies are required in areas particularly sensitive to oil pollution.

IX. NEEDS FOR FURTHER STUDIES

Additional field work should investigate the circulation on the inner (coastal) and outer (shelf break) boundaries. The mid-shelf area should continue to be monitored for any changes, but probably does not require an intensive sampling program. The inner boundary includes the coastal current and Prince William Sound studies. A study from Kayak Island to Seward including Prince William Sound is presently underway and the sampling should continue into at least next years work. The questions to be answered by such a study are what is the nature of the inflow and outflow in Prince William Sound; is it seasonally dependent; does it depend on wind stress, Copper River outflow, precipitation/runoff

within Prince William Sound; perturbations in the Alaska Stream and; what is its variation with depth? Numerical models of the Copper River shelf region and Prince William Sound should be carried out.

Additional work on estimating precipitation and runoff in the Alaskan coastal regions as well as British Columbia is required. Using precipitation measurements from drilling platforms, estimates of offshore precipitation and its gradient must be carried out in order to further evaluate the effect of precipitation on the ocean circulation. Satellite imagery is important to the precipitation studies in order to determine the width scale of the coastal current which is necessary to estimate the velocity of the coastal flow.

Attention should be directed to a detailed investigation of the shelf break current, the Alaska Stream. This should include an evaluation of the forces which drive the stream, its seasonal and interannual variations and its interaction with the coastal current. Satellite imagery are useful in this respect for they can be used to determine the position and possibly the width of the stream. The SEASAT-A satellite data should be used to track the stream through dynamic topography, salinity and/or temperature information. The capability of this satellite system to measure cloud obscured sea surface temperatures would allow short term variations in sea surface temperatures to be analyzed. This is in contrast with the NOAA satellites now in operation which cannot see through cloud cover, making most passes over the Gulf of Alaska useless for sea surface temperature measurements. Attempts should be made to place the satellite tracked drifters (R.U. #217) into the Alaska Stream.

Further analysis should be done on the existing OCSEAP data. Seasonal and interannual fluctuations should continue to be described. A

detailed evaluation of hydrographic, current meter and bottom pressure data for the Seward line is now underway and the monitoring of the hydrographic conditions along this line is an effective way of determining anomalous oceanographic conditions for the region since this line has a long history of observations.

The transport in the upper twenty meters (above the depth of the highest current meter in an array and above the drogue depth of the drifting buoys) still is a problem. In the open ocean there is evidence that some satellite-tracked drifters behave the same with or without their drogues. In coastal areas with large vertical density gradients this might not be true. A perplexing result of the drifter study in NEGOA was that the drifters tended to cross the dynamic topography though most flow was along the contours. This slight cross-topography flow could be the result of return flow beneath the outward flowing fresh water lens. In any case, it is dangerous to assume that the drifting buoys are describing the path that an oil spill might take. Studies of the transport in the upper 20 meters would solve this dilemma.

X. SUMMARY OF FOURTH QUARTER OPERATIONS

Task Objectives

To gather and analyze hydrographic and current meter data in the northern Gulf of Alaska for the purpose of describing possible flow trajectories. To describe the physical environment and to understand its driving mechanisms. To continue to monitor NOAA satellite data for use by this project and other OCSEAP investigators.

Field Activities

- 1) Cruise - 15-24 February 1978, R/V *Acona*
- 2) Scientific Party
 - J. Niebauer
 - F. Waite
 - W. Kopplin
 - D. Livingstone
- 3) Methods - STD sampling
- 4) Sample Locations - Prince William Sound and adjacent continental shelf
- 5) Data Collected - 40 STD stations

Results

The cruise studying Prince William Sound and the continental shelf adjacent to the sound was completed. High winds and seas limited the field activities with few stations being occupied outside the sound itself. The current meter arrays were interrogated and found to be in place. Recovery is planned for April.

Analysis has begun on an investigation of the dynamics which control the coastal current and the Alaska Current. This study will center on a breakdown of horizontal density gradients into their horizontal temperature and salinity gradients. Preliminary results indicate that the salinity gradient is most important to depths in excess of 500 m.

A comparison of dynamic topography and the tracks of the satellite tracked drifters (R.U. #217) is being carried out. Results show that, in general, the two data sets agree. Both give evidence of meanders, eddies and flow into Prince William Sound from April-June 1976.

Precipitation measurements from the Alaskan Star, a drilling platform located about 40 km south of Yakataga, from April 1977 through February 1978 have been made available to this unit by M. Crane. These

data show that there is little similarity between the coastal and offshore rainfall. Further analysis will be made to determine seasonal variations to this pattern.

Preliminary Interpretations of Results

The dependence of the deep sections (> 500 m) of the Alaska Stream on the horizontal gradient of salinity are surprising. We have assumed that the upper layers were salinity dependent, but coastal convergence must operate in a manner to allow this effect to reach great depths. There is a possibility that recirculation might occur in the Gulf of Alaska with two or more separate subarctic gyres.

The good comparison of the drifter and dynamic topography charts means that geostrophy is observed to a large degree in the Gulf of Alaska coastal waters. There is some cross-isopleth flow by the drifters shoreward, which can be explained by using an argument of return flow beneath the upper layer fresh water outflow. An important conclusion is that there is long term persistence of eddies and meanders here. By long term, time scales of the order of weeks to months are implied. These features will effect the current meter measurements taken within them.

The large decrease in precipitation offshore, in excess of 2 cm/km for a given month, will produce longshore, baroclinic geostrophic currents of the order of tens of centimeters per second. The very small seasonal signal of offshore precipitation is also surprising in light of the large signal of the nearly coastal stations. The horizontal gradient of fresh water input depends on this horizontal gradient of precipitation and the amount of precipitation received at the coastline, the runoff area and the width of the coastal current. All of those factors must be considered in order to evaluate the strength of the coastal current.

Problems Encountered

Efforts to obtain coastal precipitation data for the British Columbia coast and Ocean Station P have not been successful as of this date. A request has been made to the Canadian government.

The work by M. Crane required to get the precipitation data from the Alaskan Star is appreciated. It would be helpful to obtain other meteorological parameters from this rig and others operating in the lease areas. Requirements in the lease regulations by BLM or USGS for the collection of these data should be considered.

We are encountering difficulties in obtaining necessary acoustic releases to deploy current meters on the continental shelf area adjacent to Prince William Sound in support of the numerical modelling efforts of R.U. #140. It is unknown at this time if we can deploy these arrays on our upcoming April cruise.

APPENDIX I

ABSTRACTS OF PAPERS SUBMITTED

ON THE EFFECTS OF PRECIPITATION ON COASTAL CIRCULATION
IN THE GULF OF ALASKA, THOMAS C. ROYER, SUBMITTED TO
THE *JOURNAL OF PHYSICAL OCEANOGRAPHY*

ABSTRACT

Surface waters in the Gulf of Alaska undergo a net dilution throughout the year since precipitation always exceeds evaporation there. Recent hydrographic data gives evidence that seasonal dynamic height fluctuations in the upper layers (< 100 m) are well-correlated with the seasonal changes in precipitation. The precipitation effect is enhanced by coastal mountain ranges which add to a general offshore decrease in rainfall and contribute fresh water at the coast through runoff. Additionally, previous estimates of the precipitation gradient offshore appear to be in error. Precipitation alters the dynamic height through salinity changes. This dependence of dynamic height on salinity is possible here because of the high precipitation (> 130 cm yr⁻¹), the longshore have accumulation of fresh water around the gyre, and the low water temperatures.

The coastal sea level is also found to be well-correlated with the local dynamic height, though not in phase with heating and cooling. Sea levels here contain information on the local steric properties and regional offshelf circulation effects on them are minimal. The barotropic effects on sea level are small here.

Since the precipitation and cross-shelf gradient of dynamic height are well-correlated, coastal precipitation can be successfully used to estimate longshore currents. The dynamic height beneath 100 m responds to wind stress changes through Ekman pumping and coastal divergences and convergences. Thus, precipitation and wind stress are important forces in the subarctic gyre circulation.

CURRENT GYRES ON THE CONTINENTAL SHELF OF THE GULF OF ALASKA,
STEVEN WORLEY AND THOMAS C. ROYER, SUBMITTED TO *JOURNAL OF*
GEOPHYSICAL RESEARCH

ABSTRACT

An oceanographic study of coastal waters in the Gulf of Alaska has revealed forced current responses that are not explained by Ekman dynamics. Regional gyres are the cause for this atypical response. The existence of these gyres is supported by current meter observations, a numerical model, satellite imagery and Lagrangian drifters. Currents resulting from nearshore dilution by freshwater discharge are a primary forcing mechanism within the gyre system.

APPENDIX II

CTD NOISE TESTS DURING FEBRUARY 1978
DISCOVERER SEA TRIALS

UNIVERSITY OF ALASKA

MEMORANDUM

TO: Cmdr. Joe Sower, PMC Electronics Division
FROM: D. L. Nebert and R. L. Seitz, IMS
DATE: 7 March 1978
SUBJECT: Recent CTD Noise Tests During the February 1978 *Discoverer*
Sea Trials

It has been established that a noise problem existed for certain cruises aboard the NOAA vessels *Surveyor*, *Miller Freeman* and the *Discoverer* (see attachments). This noise problem is such that it is undetectable from the analog trace and can easily go unnoticed unless a special effort is made to examine the signal or raw data. Once processing begins, the problem may become apparent, especially if an attempt is made to correct for the thermal mass of the temperature sensor.

The simplest way to eliminate the observed noise problems is to average or filter the data - an approach suggested by several people. This approach will eliminate the noise, but also will limit resolution for S, T and D. Fine structure, on the order of 2 to 5 meters, is now being investigated by scientists at several institutions. Standard CTD/STD casts will provide this resolution if care is taken to reduce signal noise. Thus, we believe that the signal should be of the best quality possible before processing commences.

Through the efforts of George LaPiene, Lt. Cmdr. Wood and others, arrangements were made to examine the noise problem during the February 1978 sea trials for the *Discoverer*. The objective was to bring all interested parties together to evaluate causes and possible cures for this problem.

In general, it is believed that the "subliminal" noise is caused by over-driving the distribution amplifier. However, there may be other causes which have not yet been identified. The following four items can cause signal deterioration:

1. significant alteration of cable length (shortening),
2. switching winches (different cable length),
3. addition or removal of a sensor from the fourth channel,
4. changing "fish".

After any major change in the system, it would be prudent to examine signal quality.

From outside of the NOAA organization, it appears that your office should take the lead in establishing procedures that will insure high quality CTD/STD data. It is with this in mind that we make the following suggestions:

1. A routine procedure should be established to check signal quality. Checks should be made several times per cruise and certainly after any significant change in the CTD system. This routine check should include a check of the composite signal amplitude and a check of each individual channel square wave for "jitter". Corrective action should also be included.
2. An occasional full-systems check with an oscilloscope and spectrum analyzer should be conducted to monitor the signal throughout a cast. This is necessary because the CTD signal will vary in amplitude with a change in parameter values. During the *Discoverer* sea trials, it was noticed that noise components (as viewed on the spectrum analyzer) varied during a 200 m cast. It would be ideal if each ship was equipped with an audiospectrum analyzer for continuous monitoring of signal to noise ratios. This would allow the detection of many problems long before they became serious. Of course, it would be necessary to document the procedure so that ship's personnel can conduct this monitoring. It is recommended that both Plessey (Environmental Systems) and Larry Murdock of NRCC be encouraged to provide input for the procedure to check the CTD system. Both Plessey and Murdock have an interest in seeing the systems work properly.
3. It is recommended that a training program be initiated for familiarization with CTD instrumentation, operations, and use of the CTD data. This should include officers, electronic technicians, and survey technicians. NRCC has offered to hold such classes for familiarization with oceanographic equipment. It would be highly desirable if this could be worked into the in-port schedule. Another opportunity for familiarization would be to encourage scientists participating on cruises to explain in detail just what they intend to do with the data. After several seminars of this sort, ships personnel should be able to interact more actively with visiting scientists and become an even more effective part of the team. (This should not be restricted to CTD procedures.)
4. Communication channels must be enhanced between Operations Officers, Oceanographic Officers, Survey Technicians, Shipboard Electronic Technicians, the PMC Electronics Group at Lake Union, the CTD group at Sand Point and scientific users (to include NOAA in Juneau). Perhaps communications are too formal or there are rivalries; the net effect is detrimental to the overall operation. Any group within the system should be able to suggest and/or recommend. From our standpoint as users of the data, we have found it extremely frustrating that we have had such minimal and indirect control over how data has been collected and how data quality has been assured.

In closing, we wish to express our appreciation for the opportunity to meet with other interested parties aboard the *Discoverer* during sea trials. We hope this sort of cooperative interaction continues and sincerely hope that all participants in such exchanges (including the scientists) will leave with a better understanding of data collection needs and the problems inherent in meeting those needs.

Attachments: Memos to T. C. Royer

ANNUAL REPORT

Contract #R7120848
Research Unit: 367
Reporting Period:
April 1, 1977 -
April 1, 1978
No. of Pages:--plus Appendices

NEAR-SHORE METEOROLOGY

R. Michael Reynolds

Pacific Marine Environmental Laboratory
National Oceanic and Atmospheric Administration
3711 - 15th Ave., N.E.
Seattle, WA 98105

April 1, 1978

CONTENTS

PAGE

1. Summary of Objectives
2. Introduction
 - A. General Nature and Scope of Study
 - B. Specific Objectives
 - C. Relevance to Problems of Petroleum Development
3. Current State of the Knowledge
4. Study Area
5. Rationale, Sources, and Methods of Data Collection
6. Results - Appendices
 - A. Coastal Meteorology in the Gulf of Alaska,
Icy Bay to Yakutat
 - B. A Look at Wind Conditions in Lower Cook Inlet
B-1 NWS Reports of Empiracle Procedures
 - C. Summary of Activities and Preliminary Report:
Near Shore Meteorology Program--Ship Surveyor
 - D. Cruise Report Covering Meteorological
Activities in Lower Cook Inlet and the
Western Gulf of Alaska

1. SUMMARY OF OBJECTIVES

1. To characterize the regional wind field in three areas: Albatross Banks, Lower Cook Inlet, and Hinchinbrook Entrance. Characterization includes mean seasonal circulations as well as synoptic and diurnal patterns. Priority will be placed on Lower Cook Inlet.
2. To estimate the ability of present forecasting techniques to predict winds in the above regions. To delineate those regions which are not easily forecasted and if possible to recommend what steps are necessary to make these regions more predictable.
3. To relate observed over-water winds to winds predicted by the PMEL meteorological mesoscale model. To produce techniques with which to assess the ability of the model to predict winds in the above areas.

2. INTRODUCTION

A. General Nature and Scope of Study

Many near-surface meteorological processes act to modify the surface winds in the coastal regions of Alaska, often enough to seriously affect any attempts at relating synoptic weather maps to surface conditions. A typical example is the case of a predicted mild wind which, in actuality, is strong and offshore near the coast, principally due to drainage from the interior. Further from shore, the lower continental air becomes modified by both the warmer seas and upper-level entrainment of the air above, thus altering its speed and direction. A thorough knowledge of coastal wind conditions is an important consideration in offshore industrial development through its effects both on the mean water flow and the trajectory of surface contaminants.

The work under R.U. 367 is designed to define which processes are acting to modify the wind field along the coast of Alaska, how prevalent they are, and how far off shore they act. Shipboard measurements, remote stations, and all available meteorological data are to be utilized in as complete a description as possible of three regions: Lower Cook Inlet, Albatross Banks, and Prince William Sound (see Figure 1).

The work is principally a comparison of the observed flow field and larger scale forcing, with some consideration to the energetics of the planetary boundary layer in these

regions. Both ends of the spectrum are important in such a study due to the juxtaposition of the different modifying processes. However, due to the complicated terrain, especially in the Lower Cook Inlet region, a thorough descriptive summary of the region is of foremost importance.

There appears to be three main processes which can modify the wind field along the coast. At various times any of these can be significant. First, the mountainous terrain produces a complex wind field which is evident on land and which often extends a significant distance offshore. A study of coastal processes in the vicinity of Icy Bay shows that the mountain effect is seen 100 km offshore (Appendix A). Second, slope winds (katabatic flow), the downhill movement of a stable boundary layer, can cause significant winds along the Alaskan coast, especially in estuaries such as Lower Cook Inlet. Third, a strong land-sea difference in air temperature in the boundary layer produces a force capable of modifying surface winds from prediction based on pressure and friction effects. This baroclinic shear (thermal wind) acts to enhance the westerly component of the mixed layer in a rather complicated way; one manifestation of this force is the sea breeze circulation.

This study will concentrate on the Lower Cook Inlet (LCI) region as this region is the most complicated, unpredictable, and most vulnerable to industrial development. As is always the case with these regions, data is sparse and

intermittant. For example, the entire western coast of LCI is without a single village, not to mention an airport or weather facility. Hence, if some comparison of actual versus predicted winds is to include this important area, remote meteorological stations must be erected (Station 22 in Figure 2). Aside from these stations, met data will be collected from all available sources which can be considered representative. Since over-the-water winds are desired, not all meteorological stations are appropriate. One of the outcomes of this study will be to indicate the errors involved in trying to predict offshore winds based on various coastal stations. Over-the-water winds will be measured by NDBO data buoys, and if possible on various oil exploration rigs. In addition, all measurements made by research ships as well as others making regular trips in these waters will be included in the data set.

B. Specific Objectives

The specific objective of this study is to synthesize all possible data sources into a succinct set of highly understandable products which will allow one to assess the following:

1. Seasonal wind fields, the most probable winds and pressure patterns based on historical data.
2. Applicability of shore stations to over water wind estimates.
3. Predictability of local winds in various remote regions from NWS analysis, NWS prognoses, and a

variety of empirically derived predictive algorithms such as those described in Appendix B.

The concept of coordinating such a wide variety of data sources into a single regional description is relatively new. Most importantly, the resulting products from such an analysis need to be easily assimilated by a casual study. The development of a satisfying product is one of the prime goals of the study. The techniques learned can be applied to other areas of interest.

As local wind fields are delineated, almost immediately patterns begin to emerge which distinguish specific physical processes (e.g., the effects of katabatic drainage in the vicinity of Homer in the winter is easily seen in the average wind summary, see Appendix B).

C. Relevance to Problems of Petroleum Development

Lower Cook Inlet has just endured a major lease sale in which oil companies promised record breaking sums for the opportunity to drill. In the near future, there will be as many as eight exploratory drilling platforms in operation, and if oil is indeed discovered, many more operations will be initiated with the concomitant increased probability of an accident. Furthermore, research into the oceanic circulations in this enclosed region, reveals a chaotic unpredictable pattern, to a large extent controlled by the wind stress history over the water. This ability of the wind to control the current field, especially the near surface currents, coupled with

the direct frictional coupling of the wind to the surface oil, confirms the importance of a knowledge of the wind field.

In addition, knowledge of the predictability of the winds in various regions is important for any shipping, platform service operations, or aircraft operations, not to mention oil spill trajectory predictions. Thus, any areas which do not yield to existing forecast procedures, must be delineated. Either new forecasting techniques need to be developed, or direct telemeterins measurements must be made to properly specify the winds in these regions.

3. CURRENT STATE OF THE KNOWLEDGE

A thorough survey of all available sources of information on the coastal climatology of the Gulf of Alaska, is presented in the Appendix. Appendix A is a summary of research in the coastal winds in the vicinity of Icy Bay. As a part of that report, a summary of the large scale synoptic patterns in the Gulf of Alaska is presented. That summary is equally applicable to the more Western regions such as LCI and Albatross Banks.

The local winds in the LCI region have been summarized in Appendix B, a preliminary study of historical data with the addition of some recent direct measurements by data buoy EB-39 before it failed. That report covers all known sources of information on the winds in LCI, and includes a summary of empirical procedures regularly used by the NWS office to forecast surface winds in such regions as the Barren Islands, Valdez, and Hichinbrook Entrance.

4. STUDY AREA

A map of the study area is shown in Figure 1, taken from an aeronautical map for this region. Also shown on the map are the locations of the various sources of data for the research, to be discussed later. In the area of Lower Cook Inlet, mountains dominate the nearly parallel coastline. Based on the studies of mountain steering in the Icy Bay region one would expect the winds in the upper region of LCI to be almost always either up or down the channel, a fact which is confirmed by the wind study in Appendix B. However, south of the forelands, the general broadening of the channel separation results in a reduction of the wind speeds in LCI compared to those in the Upper Cook Inlet. Further south the mountain trend is broken on each side; to the west by the Kamishak Gap, and by Kennedy Entrance to the east. The presence of these gaps produces a tendency for winds in the area of Augustine Island to be either easterly or westerly. Westerly winds are especially strong in the winter when a pronounced low occupies the Gulf of Alaska to the east of LCI. Then winds flow down gradient, funneling through the Kamishak Gap and spreading across the open water. Exactly how often this occurs, and what the seaward extent of it is, is one of the prime objects of this study.

A region of lesser importance is the region to the east of Kodiak Island, in the vicinity of the Albatross Banks. This region is less complicated than the LCI region, as it

faces the open sea and hence is similar, general features, to the Icy Bay region. In such areas, we expect to see katabatic funneling near the mouths of the estuaries producing offshore flow components extending out some 20 km, and some mountain steerage further offshore. The extent of the mountain steerage can be of the order of 100 km, and analysis of the data from data buoy EB-72 will help refine this estimate.

Finally, the region of Hichinbrook Entrance is of importance, and a data buoy has been placed there. As discussed above, and elaborated on below, measured winds in this region will be compared to those predicted by a variety of sources to establish some measure of the predictability of those winds.

5. RATIONALE, SOURCES, AND METHODS OF DATA COLLECTION

As any experienced field scientist knows, direct measurement of over the water winds is very difficult, and reasonably expensive. Thus, any direct measurements of the winds over the water are terribly important, and every means possible to gain such measurements is being sought. Any meteorological measurements made over land are suspect as being non-representative of the winds even a few kilometers out to sea. For instance, most NWS stations are located at airports, whose site is selected specifically because the winds are consistent in direction and weak. Even exposed beaches provide poor comparisons to wind conditions offshore. In the study of the Icy Bay area (Appendix A), the effects of mountain blockage extend more than 100 km offshore, which is more than enough to completely cover an enclosed region such as Lower Cook Inlet, and closer to shore, winds which are generated by thermal effects are apparent; katabatic flows and sea breeze winds are seen to 20 km offshore. Hence, some compromise must be reached which will help resolve the questions with which R.U. 367 deals, yet is within the bounds of the budgeted money.

The approach to be taken is to consider individual regions of the scale of 10 km within the study area, those from which reasonably frequent meteorological observations are available. Some of these regions are over water, some are along coastlines. Figure 2 is a map showing all possible

sources of meteorological observations which report regularly. Table 1 is a key to the map, and lists the sources of this data, while Table 2 is a description of the NWS stations, the most reliable and frequently reporting stations. There are several sources of data shown on the map, which report infrequently or sporadically and it is one of the goals of the particular approach to make use of these sporadic sources. Two of the main sporadic sources are the Alaskan State Ferry TUSTUMENA whose route is shown in the figure as a dashed line, and the research ships from NOAA. The plan is that whenever a measurement from any source falls into a designated area, it can be included in the statistical description of that area. This concept is similar to the meteorological atlases which are available from the Navy and NWS covering the open ocean on a large scale. In the same fashion, climatic summaries of the regions from which data is available will be made. The summaries will be in the form of wind fabric diagrams as described in Appendices A and B.

However, with the goals of providing a mesoscale descriptive summary and a predictive tool which can be used in the event of an oil spill, we will also stress the predictability of the winds in each region. Thus, the winds in an area will be compared with winds which have been predicted by any of several techniques; generally some synoptic analysis or prediction from which geostrophic winds have been derived. Hopefully, empirical predictive mechanisms which are routinely

used by the NWS and described in Appendix B, can be expanded and simplified for any regions from which data exist.

Direct measurements will be compared against several synoptic bases to establish which base is the most effective in predicting winds. The most ideal candidates for selection are the NWS derived prognoses from the Limited Area Fine-Mesh model (LFM). The study underway will at least designate those local regions which cannot be predicted with this or any other synoptic base and thus require direct wind measurement. The relative skill of the prognosis and final analysis for the same period will also be established. Often, the analysis which is developed after the fact and based on measured data as well as physical equations, will not agree with the prog which was issued earlier for the same time. The extent of this disagreement will be established.

As part of the AIDJEX experiments in the Arctic, a mesoscale pressure array was employed as a means of deriving the geostrophic winds in a region with limited coverage by NWS. It was found that often large differences existed between the winds derived by the pressure array and those derived by NWS analysis. Direct wind measurements confirmed that the pressure net was necessary to accurately determine geostrophic winds. The mesoscale pressure array concept will be employed in this study as an alternate form of synoptic base. The NWS coverage along the southern coast is much superior to that in the north, but there are reasons to expect

differences between the NWS analysis and a mesoscale pressure net; principally, the pressure field developed by the NWS LFM is based on a global model which smoothes the isobar contours over a length scale of several hundred kilometers. Figure 3 shows the grid points on which the LFM operates. It is entirely feasible that smaller orographically or thermally derived pressure differences exist in a limited region. In fact, during winter when strong land-water temperature differences exist in confined regions, this could very well dominate the pressure field in the boundary layer.

Figure 4 is a map of the proposed grid scale for the mesoscale pressure array derived winds. Most of the NWS pressure stations shown in Figure 2 will be used in deriving a fifth order polynomial fit to the isobaric pattern. The LFM pressure points shown in Figure 3 will be used to tie down the boundary pressure of the region. If it is determined that a pressure array is necessary to properly now-cast the local winds, then a necessary recommendation for any spill response activities would be the initiation of a real time reporting network, which could feed data to NWS-Anchorage for near-real computation of the winds over any selected region.

An important consideration in a study such as this is to arrive at a set of products which can be easily assimilated and used by an observer. At present, we are working on several ideas, and will be in contact with other researchers in the OCSEA Program to arrive at a meaningful end. At this

time, one promising alternative is a variation of the fabric diagram discussed in the Appendices. Such parameters as surface-to-geostrophic wind veer, reduction, and variability can be contoured against the geostrophic wind vector as computed from any of the synoptic bases.

The above statistical mesoscale summary is an ambitious project, but has a great deal of potential. The programs developed are easily applied to other mesoscale regions such as the vicinity of Norton Sound or the Bering Sea. In any mesoscale region, as more data is collected, more of the subgrids such as shown in Figure 4 can be described. It is felt that the complete analysis will take on the order of two years to fully implement. Thus, each future progress reports will discuss one or more of the aspects of this plan.

As regards the confirmation and appraisal of any mesoscale model, this statistical summary provides a reasonable tool to that end. While an airplane study can provide a high quality data set with which to compare model performance in one particular instance, a statistical compilation such as described here with fabric diagram presentation can appraise the model performance in a general context. The present model in use for the Alaska region, the modified Lavoie model, is much more capable of describing the general regional picture rather than any specific situation, hence is more amenable to appraisal by a statistical study such as the one described above.

6. RESULTS

The results of research thus far are summarized in four appendices to this report. The first appendix is a summary of the work done in the vicinity of the Malaspina Glacier and Icy Bay. Included in this report is a discussion of the synoptic conditions expected in the entire Gulf of Alaska, and hence is applicable to the region under study in this report. The second appendix is a summary of existing data in the region of Lower Cook Inlet. This report represents a starting place for continuing research as it contains certain postulates which will need to be confirmed by future research. The next two appendices are reports of two recent field expeditions to the Alaskan coast. The former trip to the Bering Sea was to field test a new boundary layer sounding system, and to appraise the mesometeorological conditions of the ice edge. The latter appendix covers a trip to the Lower Cook Inlet and the western Gulf of Alaska. Meteorological conditions were observed, the data buoy was intercompared with ship data, and the Airsonde system was further evaluated. As this cruise was made in March, a detailed and specific report could not be generated in time for this report, and the cruise report for that trip has been included for completeness.

TABLE 1. List of Meteorological Stations Shown in Figure 2.

1.	Anchorage	NWS
2.	King Salmon	NWS
3.	Kodiak	NWS
4.	Homer	NWS
5.	Kenai	NWS
6.	Iliamna	NWS (part time AMOS)
7.	Whittier	NWS
8.	Seward	NWS
9.	Valdez	NWS
10.	Cordova	NWS
11.	Johnston Point	NWS (Air Force)
12.	Big River Lake	NWS (contract)
13.	Dolly Varden	Oil Rig
14.	Phillips	Oil Rig
15.	Shuyak	NWS (remote wind)
16.	Cape Hinchinbrook	NWS (AMOS)
17.	Middleton Island	NWS (AMOS)
18.	EB-39	NDBO
19.	EB-72	NDBO
20.	EB-	NDBO
21.	Tustumena	Alaskan Ferry
22.	Contact Point	PMEL
23.	Augustine Island	PMEL

TABLE 2. NWS data sources and brief description of each.

STATION	PRESS (INS)	S.L. PRESS (MB)	ALTIM (INS)	TDRY (F)	TWET (F)	TDEN (F)	WIND		OBSERVATION SCHEDULE
							DIR 00-36	SPEED (KTS)	
Anchorage	x	x		x	x		x	x	hourly
King Salmon	x	x		x	x		x	x	"
Kodiak	x	x		x	x		x	x	"
Valdez	x	x		x	x	x	x	x	"
Homer	x	x		x	x	x	x	x	" , generally
Cordova	x	x		x		x	x	x	"
Kenai	x	x		x		x	x	x	"
Whittier			x	x	x	x	x	x	"
Seward	x	x		x	x	x	x	x	Generally 12/day, not on GMT.
Illiamna	x	x		x	x	x	x	x	08-15 hourly, Tues-Fri. 06-21 hourly, Sat-Mon.
Big River Lake			x (bkn)	x	x	x	x	x	07-20 hourly
Johnstone Point			x	x	x	x	x	x	02z,18Z,22Z
Phillips Oil Rig				x			x (quad)	x	sporadic, about 4/day
Dolly Varden Oil Rig	x			x			x	x	sporadic, about 4/day

Note: When TWET is available, TDRY and TWET are reported to tenths of degree. If only TDEW and TDRY are available, they are only reported to the nearest degree.

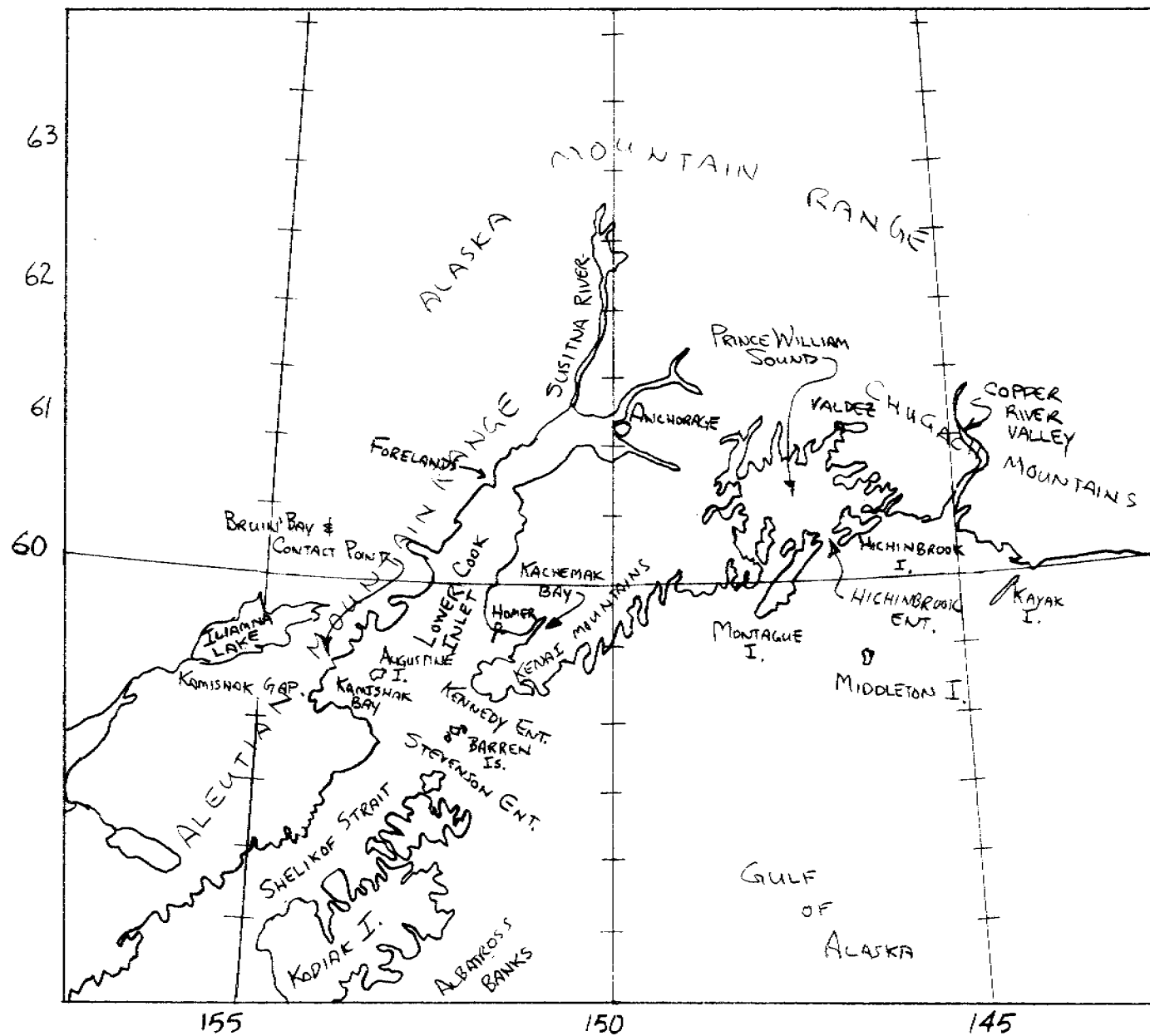


Figure 1. Map of the study area showing main topographical features.

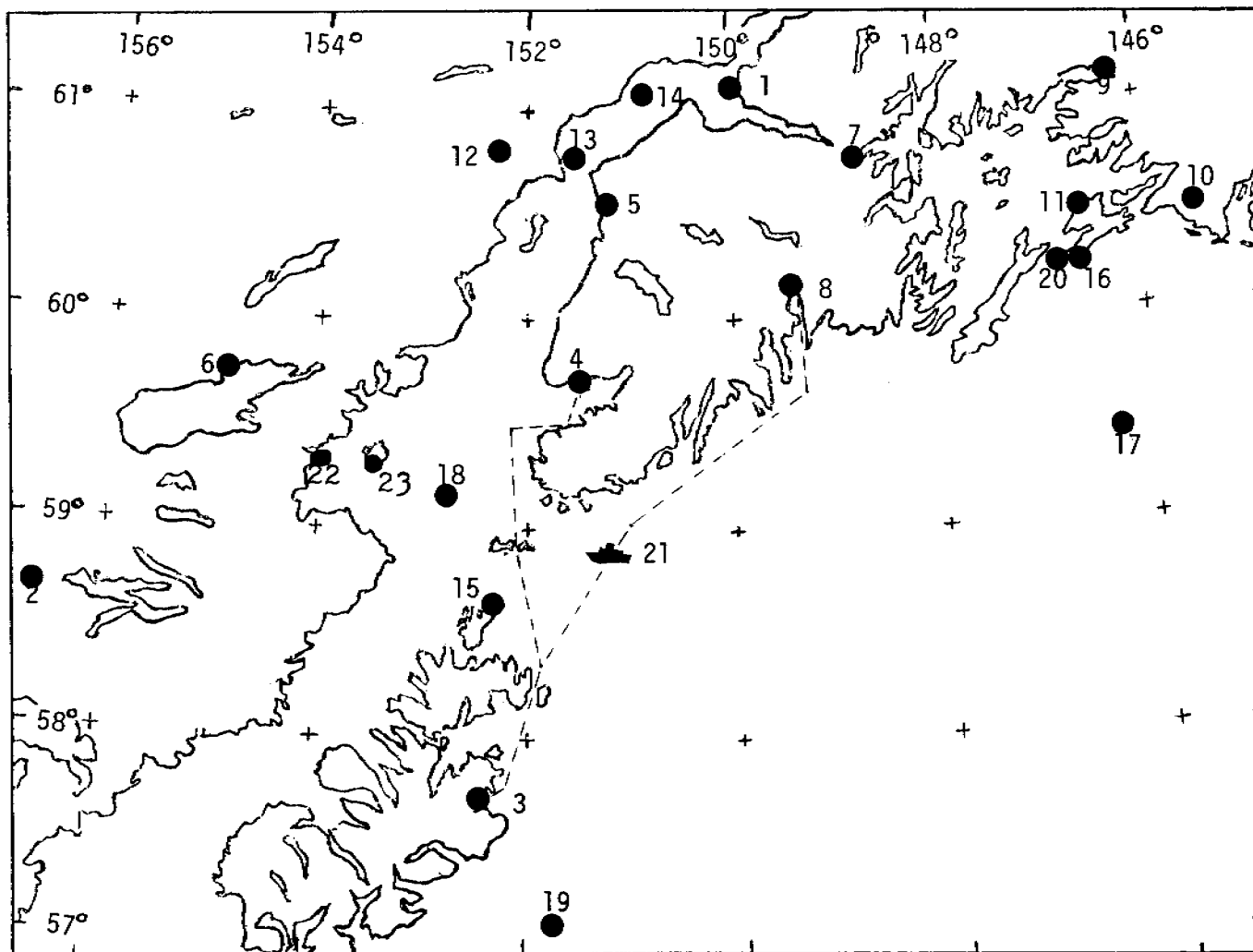


Figure 2. Map of the study area showing sources of data which will be included in this study.

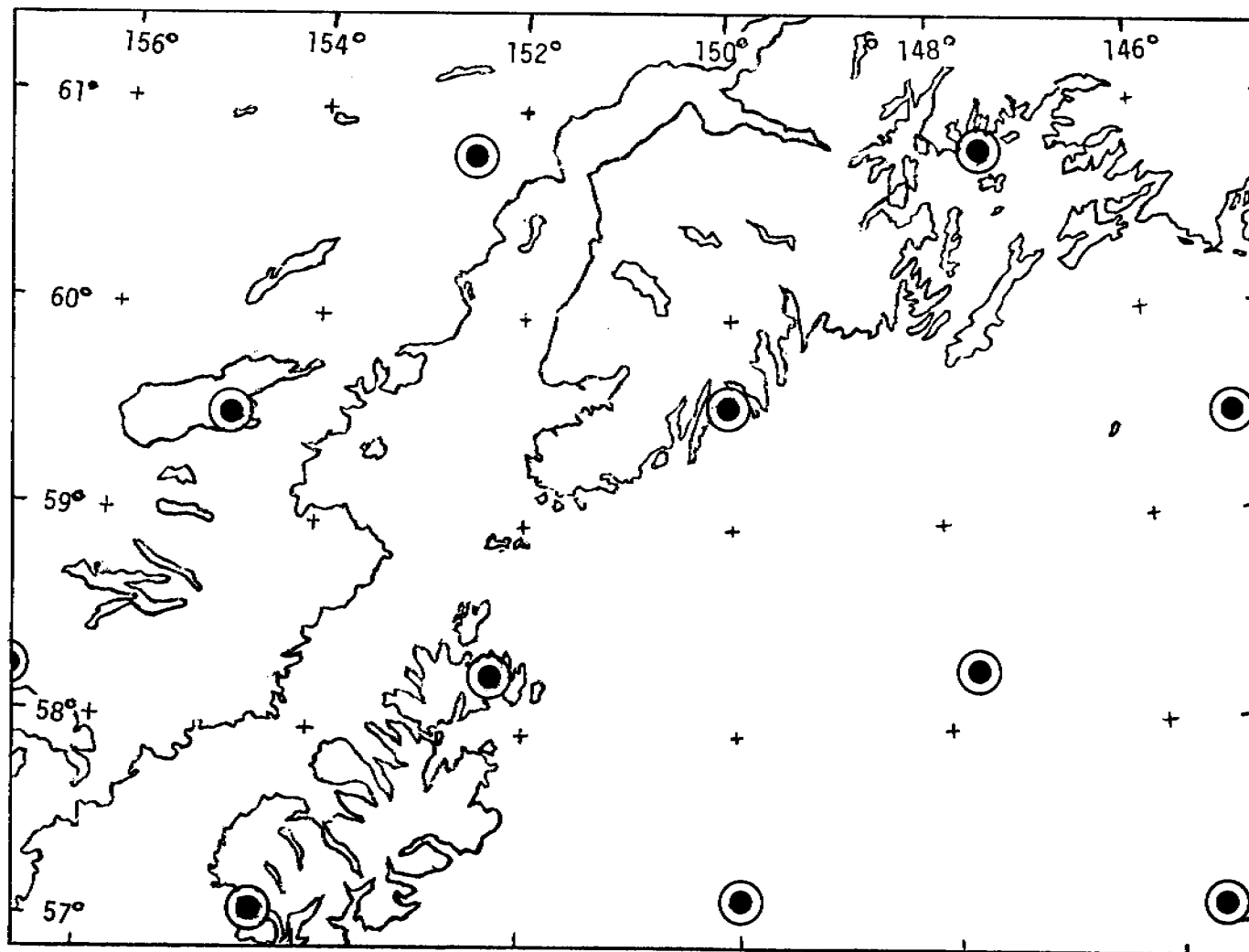


Figure 3. Map showing the position of the LFM grid points for the study area. Note that five of the points are very near the boundaries of the region, and will be used for securing the boundary pressure in the mesoscale pressure net.

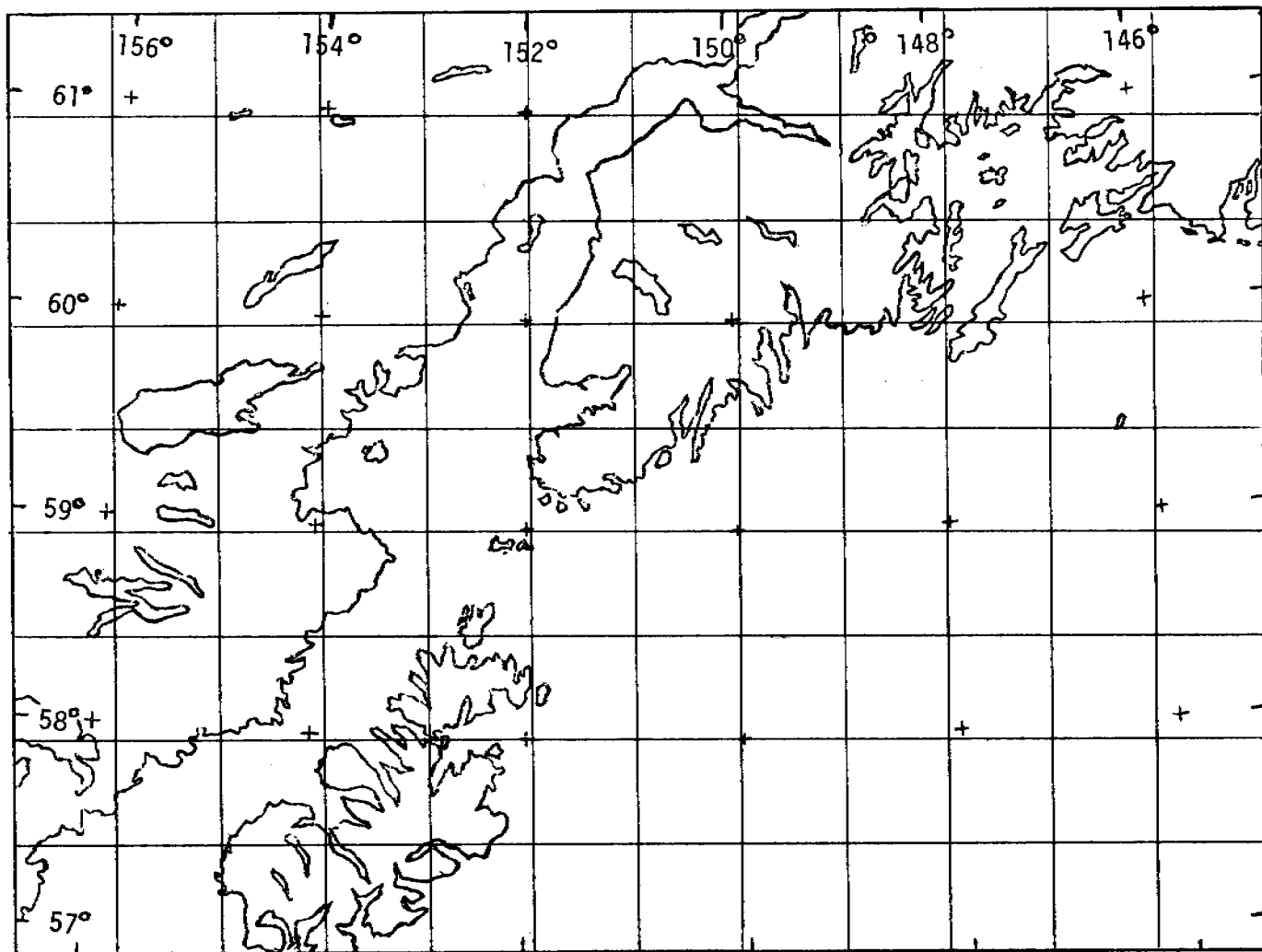


Figure 4. Proposed grid for the mesoscale pressure field. Geostrophic wind will be computed for each grid point.

APPENDIX A
COASTAL METEOROLOGY IN THE GULF OF ALASKA
ICY BAY TO YAKUTAT

TABLE OF CONTENTS

PAGE

Abstract

1. Introduction
2. Synoptic Scale Weather Patterns
3. Analysis of a Mesoscale Array
4. Shipboard Measurements
5. Aircraft Measurements
6. Conclusion

ABSTRACT

Studies of coastal meteorology in the vicinity of the Malaspina Glacier, between Icy Bay and Yakutat Bay, identify several physical processes which contribute to the coastal wind field. The coastal mountain range impedes synoptic scale systems and locally distorts the wind field yielding a predominantly bimodal wind direction along the coast. During the winter, and at night during the summer, stable boundary layers drain down the mountains and glaciers forming katabatic winds. Focusing of these winds into the many estuaries often produces katabatic jets. Rapid exchange of heat and momentum between the ocean and atmosphere act to dissipate the katabatic effect offshore. Analysis of a mesoscale array of wind sensors suggests that the coastal mountain affects appear offshore for distances approaching 200 km while katabatic flows are present only to about 25 km.

Measurements of specific cases have been taken by ship and aircraft. These studies generally concur with the above observations. In addition, these case studies reveal details of the internal structure of the boundary layer.

COASTAL METEOROLOGY IN THE GULF OF ALASKA
ICY BAY TO YAKUTAT BAY

R. Michael Reynolds

Thomas R. Hiester

S. A. Macklin

1. INTRODUCTION

During the past two years, a variety of studies of Gulf of Alaska coastal meteorology have been undertaken as part of the Outer Continental Shelf Environmental Assessment Program (OCSEAP). These studies have been concentrated in the vicinity of the Malaspina Glacier between Icy Bay and Yakutat Bay (Figure 1). The topography of this region as shown in Figure 2 is broad semicircular glacier surrounded by a dramatic coastal mountain range, the St. Elias Mountains (for example, Mt. St. Elias rises to 5.49 km altitude only 50 km from the mouth of Icy Bay).

In section 2 of this report, the general synoptic scale weather conditions for the Gulf of Alaska are summarized. Synoptic weather summaries for the Gulf of Alaska are treated in several publications (Dept. of Commerce, 1961; U.S. Navy, 1944; Putnins, 1966; Bilello, 1974), but anomolous interaction of the synoptic scale flow with the mountain barrier is only briefly treated by these publications.

Coastal winds, within 100 km of the coastline, are much less understood. Searby (1969) attempted to collect as

much information as possible on the observed coastal weather in the Gulf of Alaska; mountain blockage and katabatic winds are briefly mentioned. However, the bulk of the information is restricted to a compilation of synoptic summaries. Such important questions as frequency and predictability of these coastal occurrences are yet to be addressed. From the discussion of a simple mesoscale array which was deployed in the study area (section 3), it is apparent that an understanding of the active processes are crucial to predicting coastal mesoscale weather, especially wind fields.

A detailed description of the coastal mesoscale wind field during a variety of weather conditions was obtained by ship and instrumented aircraft studies. Section 4 discusses shipboard measurements of the offshore boundary layer structure while section 5 is a thorough summary of aircraft flights. The wind fields revealed by these studies agree well with the deductions made by analysis of the mesoscale array.

2. SUMMARY OF SYNOPTIC SCALE METEOROLOGY

The Gulf of Alaska is a region of prodigious barometric activity, especially in the winter. Three main features of the mean barometric pressure field (Figure 3) are the Aleutian Low which dominates the North Pacific in the winter, the North Pacific High which is displaced south in the winter but spreads northward in the summer, and the continental high of winter which covers the main land masses of Siberia, Alaska, and British Columbia.

In summer, increased heating over land produces a relative low pressure which weakens the Aleutian Low while in winter excess cooling results in the continental high and the low develops. The trough of the Aleutian Low controls the passage of an endless stream of cyclonic disturbances traveling eastward across the North Pacific. Figure 3 also shows average storm tracks for various times of the year wherein the effect of the Aleutian Low is evident. Often in this area, disturbances originate either spontaneously or by amoeboid fission.

It must be stressed that the mean pressure field exhibited in Figure 3 bears little resemblance to the actual distribution at any time. In an attempt to statistically treat daily weather patterns for the Alaskan region, Putnins (1966) analyzed over 18 years of surface and 500 mb weather maps. After developing a classification scheme which established 22 synoptic patterns, he determined the frequency of these patterns for each month of the year. Figure 4a-4b is a sample of his results, the six most common weather types for four months, representing each season. These are real maps selected as typical for the classification type. The statistical nature of the three main features of the pressure field is apparent in these maps, especially the Aleutian Low. The convergence of cyclonic disturbances into the Gulf of Alaska is also apparent.

The coastal mountains of British Columbia and Alaska

present a barrier to the movement of disturbances with the result that many of them stagnate in the Gulf of Alaska for several days, especially with an inland high pressure. Occasionally, if unable to move forward, these cyclones make a retrograde course toward the northwest.

The air mass north of a front is very stable in the lower levels. . . . Once the arctic front has moved against the mountain range, only a vigorous circulation aloft can cause it to move further. With moderate southerly winds, maritime air moves quite freely into the Cook Inlet-Susitna Valley area, and less easily into the Copper River Valley, and the front then has a tendency to become stationary along the Alaska Range. . . . Strong southwesterly winds, however, occasionally force the front up the Kuskowim and Nushagak Valleys. At this point there is no definite physical barrier to impede further movement of the front so it can now readily penetrate to the interior of the state and influence the weather accordingly. Nevertheless, exactly how far inland the front moves is dependent almost entirely upon the strength and persistence of the steering level winds. (Bilello, 1974)

As the marine air crosses the Alaska range a great deal of orographically-induced precipitation occurs as evidenced in the climatic summary given in Figure 5. An annual rainfall of 1.47 m at Middleton Island can be compared with 2.62 m at Cape St. Elias or 3.36 m at Yakutat.

3. ANALYSIS OF A MESOSCALE ARRAY

In order to ascertain the effects of the coastal mountain range on the coastal wind field, an array of meteorological surface stations has been examined. Figure 6 is a map of the study area which shows the locations of array elements. Data buoys EB-33 (58.5°N , 141.0°W), EB-70 (59.5°N ,

142.2°W), and EB-43 (59.8°N, 142°W), two shore-based remote stations at Pt. Riou (59°55'N, 141°32'W) and Pt. Manby (59°41'N, 140°17'W), and the National Weather Service (NWS) Facility at Yakutat were utilized in this analysis.

The data buoys were deployed by the NOAA Data Buoy Office (NDBO) who received the data by satellite link, then edited and reduced the data into a standard archival format in which wind speed is given to the nearest mile/hr and direction to the nearest ten degrees. The remote stations are made by Climatronics, Inc. and record on a 30-day strip chart with accuracy roughly equivalent to the data buoys. The NWS Facility provides both hourly surface operations and twice daily upper air soundings.

In order to have a measure of the synoptically-deduced wind field, surface winds derived from the Navy Fleet Numerical Weather Center (FNWC) were used. These winds are computed by the FNWC for a position of 59°39.9'N, 142°10.5'W (Bakun, 1973) by geostrophic assumption in which a simple computation of pressure gradient is made using a 5 point centered array with the FNWC Hemispheric 6° mesh model. Surface winds were then derived by a simple reduction by 30% and rotation by 15°.

Two periods of time are selected for study, 6 March to 3 April 1977, and 6 May to 1 June 1977. These two periods, representative of late winter and early summer, were periods when all elements of the array appeared to be functioning properly.

The results of the FNWC analysis are shown in Figure 7. The two time series of winds exhibit similar properties in that direction is indicative of the passage of cyclonic disturbances to the south. The mean wind speed for each period is about 3.5 to 4 m/s but the variance in the winter case is somewhat greater.

A modified version of the wind fabric diagram of Davis, et al. (1977), provides an informative display of wind statistics. The wind fabric diagram is essentially a contoured map of the wind velocity probability distribution given in per cent of the total observations per 1% area of the diagram. Wind direction is plotted according to meteorological tradition--the compass direction from which the wind is blowing. Although calculations can be made from any similar frequency distribution maps, qualitative interpretation is difficult unless one knows that contours enclosing equal areas at any given region of the diagram do in fact contain the same number of observations and therefore represent areas of equally probable wind occurrences. This can only be done if the velocity is mapped onto the diagram proportional to the square of the radius in order to compensate for the spreading of radial line segments. From the contoured map one can easily calculate the probability of observing the wind in any direction and velocity sector, and perform statistical significance tests for features seen on the diagram.

A wind fabric diagram of the FNWC-derived surface winds

is given in Figure 8. The diagram indicates that winds tend to be fairly uniformly distributed for both periods of time. The more frequent SE winds in the May record is a result of the long period of SE winds during the first part of that period. With only a single month's data, it is difficult to assess whether this prolonged period is typical.

Time series for EB-70, EB-43, Pt. Riou, and Pt. Manby are given in figures 9 and 10. It is with these measurements that the importance of coastal proximity is seen. The wind speed signals show distinct similarities with the FNWC winds. Both data buoy records exhibit wind events which are seen on the FNWC record. The land stations also show wind events, but with a much reduced amplitude. While there is a slight reduction in wind speed between EB-70 and EB-43 which was closer to shore, inexplicably, the wind speed of FNWC more closely agrees with EB-43. Overall, wind speed correlation coefficients between the data buoys and FNWC are approximately .70 to .85.

However, comparisons of the direction of the winds are a different matter as evidenced by wind fabric diagrams for the records (Figures 11 and 12). While the FNWC winds exhibited no special preference for direction, the measured winds showed distinct influence of the coastline. EB-70 has an almost symmetrical bimodal character with the most common wind directions being approximately 115° and 270° . EB-43 shows a bimodal character also, but during the winter the winds are

much more common from the east, probably an offshore manifestation of the winter drainage winds from Malispina Glacier. During summer, winds at this location are much more symmetrically bimodal. Coastal winds measured at Pt. Riou and Pt. Manby shows much orographic control. During winter at Pt. Riou, the combined katabatic drainage winds and mountain blocking result in winds which almost continuously blow from the NE, down the glacier. Hence in addition to orographic control, diurnal forcing is apparent in the record, both in March and May; during the coldest period of the day, drainage flow down the glacier from the north dominates, while during daylight hours the flow is more from the NE and E (see Figures 9d and 10d).

Additional detail of the flow distribution can be obtained by use of correlation plots where wind direction from two different sources are plotted on the same graph. Well-coorelated direction would be represented by points which cluster about a 45° line. Figure 13a to 13d is a comparison of winds from each coastal station to the FNWC winds for the March period; Figure 14a to 14d covers the May period. The lack of correlation with FNWC is apparent as is the coastal effect. When data from EB-70 is compared to EB-43 (Figures 13e and 14e), an interesting feature is observed. In general, even though buoy winds favor an E-W direction, a cluster of points in the upper left-hand corner of the plot indicates occurrences of wind reversal when EB-43 records easterly winds

while EB-70 has westerlies. The density of the cluster in Figure 13e suggests this is not a rare wintertime occurrence, and the symbol code suggests it happens for a variety of wind speeds.

Examination of the data in greater detail was undertaken to ascertain if it was possible, with this limited data set, to pinpoint a scheme which would allow a forecast of these occurrences with synoptic maps. The time series, Figure 9a and 9b, shows that while both EB-70 and EB-43 switch directions quite rapidly, EB-43 tends to persist with an easterly flow after EB-70 has reversed. Figure 15 is a plot of the directions measured by EB-70 and EB-43 for the March period. The encircled capital letters A through D in the figure are four cases where the flow reversal is apparent. A dashed line indicates the direction calculated by FNWC. Because of poor synoptic coverage in this area, there was no readily apparent consistency in the synoptic analysis. The presence of fronts and short waves cannot readily be predicted from the analysis. The suddenness of the wind switches and the great variation on such small scales, along with the poor agreement with FNWC suggests mesoscale events within the synoptic scale. During the aircraft study, a small frontal discontinuity which showed such a wind reversal was detected. It cannot be said that katabatic flow is not a significant factor. The reversals occur in late afternoon with sharp transitions to easterly flow. This behavior is indicative of an offshore katabatic tongue

has been observed from shipboard measurements and is discussed in section 4.

4. SHIPBOARD MEASUREMENTS

During a cruise aboard the NOAA ship Oceanographer in early February 1975, a set of radiosondes was released on a trackline orthogonal to the coastline. Figure 16 summarizes the surface meteorological observations made by the ship at the time of the balloon ascents 6 through 11. The synoptic pressure pattern was dominated by an inland high cell such that the geostrophic wind was northerly, indicating advection of the arctic continental air mass offshore. During the period of measurement, the weather was generally clear with light northerly winds (see Putnins' weather type D, Figure 4d). EB-33, a nearby data buoy, confirms the flow extends offshore for some distance. In this case a general warming of the atmospheric boundary layer is observed. Katabatic drainage winds are superimposed on the offshore flow as evidenced by measured winds at stations 6, 7, and partially 8. These winds indicate flow down the glacier extends to 20-30 km offshore. Figure 17 is a comparison of near simultaneous profiles from the NWS station at Yakutat and a shipboard ascent at station 8, 33 km offshore. A strong ground-based inversion at Yakutat is mixed offshore to an altitude of about 500 m. Humidity proves to be an excellent indication of inversion height as it reflects a sharp cutoff to dryer air above.

During another cruise, in March 1976, a more extensive set of measurements was made in the same area. Surface data and vertical profiles were made at 35 stations, however, only one line of nine stations will be considered here. This line was taken during a period when synoptic conditions were nearly stationary. Figure 18 summarizes the surface observations during this section. Again, a clear progression in surface air temperature is evident over the line. The winds, however, make a distinct westerly shift between stations 9 and 10, which will be discussed below. It must be noted here that these data are contaminated somewhat by diurnal heating occurring over the time period of the measurements. This is one of the serious disadvantages of making shipboard measurements of this type.

A surface pressure analysis for 1200Z 9 March 1976 is shown in Figure 19. Observed wind vectors indicate the air mass observed at EB-33 was modified by passage over the Gulf of Alaska. Yakutat measurements indicate an offshore flow of cold air. Coincident vertical profiles of potential temperature and mixing ratio for Yakutat and station 7, 8.5 km offshore, are shown in Figure 20. Although each temperature profile is quite neutral aloft, the mixing ratio profiles indicate that a mixed layer extending to about 1000 m caps a katabatic layer of strong temperature inversion especially evident in the Yakutat sounding. In the 8.5 km passage from the coastline to the position of ascent, a surface mixed layer

has developed. The profiles reflect an eastward temperature gradient consistent with the synoptic pattern. A humidity maximum is also apparent at about 700 m.

The data indicate a low katabatic flow offshore which is rapidly modified by convective surface heat transfer until it is the same temperature as the air above. At this point mixing occurs throughout the deeper mixed layer, up to about 1000 m. The wind arrows in Figure 18 imply this occurs at about 24 km offshore when the winds makes an abrupt direction change from directly offshore to near geostrophic. A contour plot of the potential temperature profiles (Figure 21) shows many interesting characteristics of the offshore modification. Katabatic flow is seen to be a tongue of cold air extending offshore. The overriding mixed layer has a height of about 900 m at 10 km from the coast growing to about 1500 m at 60 km offshore. The flow of the upper layer is into the page, but temperature and inversion height increase offshore. This is partially explained by Figure 19; since the flow direction is oblique to the coast, air farther offshore has been over water a longer time.

Also evident in the cross section is a cold air core located at 1000 m approximately 30 km offshore. Careful examination of the data indicates this is a real excursion, but at the time of this writing, no firm explanation of this core is available.

Figure 22 is a cross section of mixing ratio. Although

there is some scatter, a weak humidity maximum is evident in the mixed layer. The height of the maximum varies from 240 m at the coast to 580 m at 60 km offshore. A rapid transition to dryer air marks the the top of the mixed layer at about 1000 m. Details of the structure of the katabatic tongue are evident in a profile taken by tethered balloon boundary layer profiler (BLP) at station 6, about 6 km offshore. The BLP sonde measures temperature, wet-bulb temperature, wind speed, wind direction, and pressure. Although the pressure sensor malfunctioned, reasonable height estimates could be made in the following way: ascent and descent were scaled by matching the heights at which a sharp transition in wind direction occurred. Constant rates of ascent and descent were assumed. The vertical height was assigned by letting the temperatures at maximum height equal that of the radiosonde released just prior to flight. The resulting profile is given in Figure 23.

Figure 23 shows a convective mixed layer extending from the surface to about 30 m. This is capped by a very stable katabatic layer to about 250 m. At this point the low-level northerly katabatic flow abruptly gives way to the westerly synoptic wind field. There is some indication of overshoot, typical of nocturnal jet phenomena observed above stable ground-based inversions.

The wind speed reaches a near-zero minimum above 250 m, and the stability begins decreasing toward the neutral values seen aloft in Figure 20. Somewhere between stations 9 and 10

(between 20 and 28 km offshore) the surface convective layer must penetrate the katabatic "lid" designated by the level of abrupt wind shear, thereby allowing a downward mix of westerly momentum with resulting surface westerlies.

5. WIND FIELDS BY AIRCRAFT MEASUREMENTS

5.1 Instrumentation and Objectives

Previous field investigations attempting to examine the detailed spatial structure of the coastal meteorological processes in the Yakutat area have been handicapped by the time necessary for a ship to move between stations. Any temporal changes occurring during transit interfered with the interpretation of the spatial structure. To alleviate this problem, an instrumented aircraft was used during an intensive observation period from 21 February 1977 to 4 March 1977.

The aircraft used was a twin engine Beechcraft Queen Air, which is operated by the National Center for Atmospheric Research (NCAR), Boulder, Colorado. Figure 24 is a photograph of the Queen Air with its specially instrumented gust probe. By combining exceptionally high quality instrumentation, a high speed data logger, and a precision inertial navigation system (INS), data collection sufficient to describe the turbulent behavior of the boundary layer is possible (Lenschow, 1972). Up to 64 data words are recorded at a rate of 8 Hz. The three dimensional wind field, temperature, humidity, and sea surface temperature are among the many measured quantities.

At an airspeed of 140 knots, the Queen Air can easily cover the Yakutat-Icy Bay area in $3\frac{1}{2}$ hours, weather permitting. A typical flight plan with two primary objectives is shown in Figure 25 and is summarized in Table 1.

The first objective of the aircraft study was to obtain a survey of the surface wind velocity field from a height of 60 m and roughly 10 km offshore. The longshore wind distribution was measured twice, once flying each direction along the coast in order to provide redundancy in sampling and to provide measurements of opposite headings. The latter point is valuable in the determination and elimination of possible instrumental biases in the gust probe system. The flight directly over EB-43 provides a geographical check on any drift present in the INS.

The second objective was to obtain a complete picture of the planetary boundary layer structure from the coast to 60 km offshore. Such a picture provides boundary conditions in the case of onshore flow, reveals the effects of air modification upon the wind velocity field in the case of offshore flow, or reveals the distance seaward that coastal effects are present in the case of longshore flow. Offshore legs flown at several levels along the vertical soundings at each end of the track satisfy this objective.

5.2 Data Analysis

Before any computations were undertaken, a thorough search of time series plots of all variables were made. The

TABLE 1. Summary of Flight Plan shown in Figure 5.3

Way Points	Altitude Meters	Remarks
1-2-3	60	Longshore wind distribution.
6-7	15-180	Vertical sounding at coast- lower level
7-6	180-900	Vertical sounding at coast- upper level.
8-9	30	
9-8	100	Offshore wind distribution and vertical structure including
8-9	200	upper level (environment) conditions.
9-8	400	
8-9	900-1350	
9-8	60	
3-4	60	Longshore variation
4-5	60	Check INS with EB-43 position comparison
5-3-2-1	60	Return home, repeat measure- ments allow improved error analysis.

data set had very few "glitches" and in all cases the bad data could be avoided entirely rather than requiring any de-spiking or replacement of bad data. Continuous intervals of level flight and uniform heading were selected from the time series for further processing.

Errors in the wind measurements arise from a multitude of complexities in the inertial navigation gust probe system. Very broadly, there are three types of errors: random, bias, and non-random time-dependent. Although a substantial amount of effort has gone into the analysis, understanding, and compensation of these errors, there has never been a complete error analysis of the INS-gust probe system in meteorological applications.

Analysis of the accuracy of the sensors that measure the air velocity relative to the aircraft (Lenschow, 1972) shows that the primary limitation on the accuracy of these sensors is due to the limited knowledge of the upstream effects of the airplane on the airflow. Fluctuations about the mean velocity may be measured to within 0.1 m/sec and (after compensation of certain non-random errors) the absolute wind velocity measured to better than 1 m/sec. Telford, et al. (1977) estimate this latter figure may be reduced to 0.3 m/sec with appropriate data collection and processing methods.

Bias errors are evident when flights along different headings yield differing wind measurements. Differences of 4 m/sec for opposite headings are not impossible. Consistent

biases are easy to remove once they have been determined. Under horizontally homogeneous conditions biases can be determined whenever the airplane changes course significantly. In the Yakutat coastal area, conditions are far from horizontally homogeneous, in fact it was the coastally-induced inhomogeneities that were to be measured. Hence only by backtracking over the same region, and then only under stationary conditions, could biases be determined. In all cases tested, bias errors were found to be negligible.

The wind vector is obtained from the difference between the aircraft motion relative to the air and its motion relative to the ground. The aircraft motion relative to the ground is determined from the INS. Two electronic integrations of accelerometer outputs give the aircraft position (relative to its starting position) which is then digitized and stored on tape. Later differentiation of this position information yields the aircraft's velocity. Minor errors in the position (by commercial navigation standards) become large errors in the wind measurement. Accelerometer bias or initial misalignment of the gyroscopically stabilized platform and any subsequent drift errors of the accelerometers or gyros lead to a non-random, oscillating velocity error with a period of 84 minutes known as the Schuller period. The amplitude of the Schuller oscillation can be as large as 2 m/sec.

If during a flight the airplane crosses several known geographical checkpoints, the position error can be determined

and velocity errors due to the Schuller oscillation or even spurious velocity errors can be compensated. In these flights the position errors noted upon passing the environmental data buoy EB-43, certain beach crossings, and the Yakutat airport upon landing can be used to reduce error. In the data presentations that follow, no compensation for the Schuller oscillation has been made. This implies that the absolute wind speed is typically only known to within 2 m/sec or 4 knots and direction within 10 degrees. Since the magnitude of these errors is time dependent with a period of 84 minutes, relative differences between adjacent measurements can generally be trusted at the 0.1 m/sec level.

In the following subsection, three presentations of the aircraft data are used. In the preparation of the vertical soundings, 1 sample/sec data were block averaged in groups of 3 samples, and the resulting series was filtered with a 3 point equally weighted running mean filter. Profiles taken at the beach at waypoint 8 are plotted as a solid curve, soundings over the ocean at waypoint 9 are plotted as a dotted line, and for comparison the Yakutat radiosonde profiles are plotted as a dashed curve.

Measurements of the offshore distribution of winds, temperature, mixing ratio (grams of water vapor per kg of dry air), and sea surface temperature were prepared using the same routine that was used for the soundings. An area distribution of those quantities at a height of 60 m is also presented

using wind barbs (c.f. Figure 28). One full barb represents 10 knots, $\frac{1}{2}$ barb = 5 knots. In some cases a vector with a dot at the origin and no barb at the tail represents winds of under $2\frac{1}{2}$ knots. Plotted numerically from a position usually just northwest of the origin of each vector and proceeding clockwise about the origin are the temperature, mixing ratio, and sea surface temperature. In the area distribution, each measurement is typically an average of 3 minutes flight or 11 km of air sampled. The longshore distributions were fairly consistent for each direction of travel, so only the measurements made during the flight from Yakutat to Icy Bay are plotted in every case except for 28 February. In that case the longshore distribution represents the return flight to Yakutat.

5.3 Results of the Aircraft Measurements

The NCAR Queen Air was available for research in Yakutat between 21 February and 3 March 1977. During that time seven flights were accomplished although due to inclement weather a full research flight pattern (Figure 25) was executed only three times.

During much of the experimental period the 500 mb flow was dominated by the same large amplitude wave that caused unseasonal winter weather over most of the U.S. and Canada. A low pressure in the Bering Sea and a ridge line along western North America cooperated to drive most storms onshore in southeast Alaska. The 500 mb geostrophic winds were, on the

average, southwesterlies. At the surface, low pressure systems in the Gulf of Alaska and north central Pacific persistently moved northeastward causing south or southeast geostrophic flow in the Yakutat area. As low pressure centers approached the coast the pressure gradient offshore increased. Putnins (1966) showed that conditions of a high pressure center and a large pressure gradient inland, occurred about 26% of the time in February. However, such conditions did not occur during these experiments. Consequently, the meteorological situation was not conducive to the development of cold drainage winds from the interior. Post frontal weather usually consisted of continued southerly winds bringing stratocumulus clouds and light rain or snow showers. Taken all together, these conditions gave Yakutat an unseasonably warm and wet year with very little snowfall.

1) Flight #1 - 22 February 1977

Flight #1 was made on 22 February 1977 between 1000 and 1230 Yukon time (YT) or 1900-2300Z. Within the study area the cloud cover was 100% stratus with cloud base between 60 and 100 m, and with another layer of stratocumulus above with cloud base at about 1.5 km. Mixed rain and snow showers separated by about 15 km intervals were encountered along the flight. The low ceiling and the tendency for light icing on the airplane and instruments made the full flight pattern infeasible, therefore just a longshore field distribution was measured.

The 500 mb and surface synoptic analyses of 00Z, 23 February are shown in Figure 26. The 500 mb low center is positioned above the surface low indicating that the storm was no longer intensifying but had previously matured. The surface low had been filling and weakening for twelve hours, however the pressure gradient near the study area increased as the low center approached the coast. Consequently the surface geostrophic winds were backing with time. Note also the weak pressure gradient just northwest of the Yakutat area.

The Yakutat rawinsonde profiles are shown in Figure 27. The large veering of the wind with height from an ENE wind at the surface along with the stable potential temperature profile suggest cool winds draining downslope near the surface. There is little indication of a well mixed layer in these profiles, but it should be recognized that the stability implied by the potential temperature profile is exaggerated under saturated in-cloud conditions since vertical displacements follow the moist adiabatic process. The wind, temperature, mixing ratio, and sea surface temperature fields measured from the aircraft are shown in the area distribution in Figure 28. The sea surface temperature has a pronounced gradient along the track. The wind, temperature, and humidity fields all show small and somewhat inconsistent changes along the track. It is likely that the sporadic regions of precipitation are at least partially responsible for these variations.

2) Flight #2 - 24 February 1977

Flight #2 was made on 24 February between 1200 and 1400 YT or 2100-2300Z. The 500 mb low center of the previous flight was pushed inland by a slight ridge approaching from the south. The region of weak pressure gradient northwest of Yakutat developed into a slight high pressure center giving Yakutat 5 knot easterlies aloft at 12Z on 24 February. The weakening low of the previous flight had moved eastward against the coast and stagnated there as it continued to fill. The slight offshore flow due to this decaying low to the south and the weak pressure aloft provided clear pre-dawn skies over Yakutat. Preparations for a flight were begun. By the time all preparations were made (longer than anticipated due to instrument warmup difficulties) a frontal system had moved in from the southwest and completely obliterated the remnant surface low. Immediately after takeoff, snow showers began in Yakutat but the shower activity was somewhat less intense in the study area. The 00Z, 25 February 500 mb analysis and the 18Z, 24 February surface analysis are shown in Figure 29.

The Yakutat sounding along with the aircraft sounding at waypoint 8 (beach) are shown in Figure 30. The aircraft sounding shows much more clearly than does the Yakutat sounding, the presence of a mixed layer. Over the beach this mixed layer depth appears to be about 500 m. The profiles are in general agreement above the mixed layer. Within the mixed layer the air at the beach is drier and appears to come from a

more northeasterly direction, whereas the Yakutat air is moister and from the ESE except near the surface where it also shows northeast winds.

The offshore distribution of winds, temperature, mixing ratio and sea surface temperature is shown in Figure 31. There is a decrease in wind speed by 8 knots over a distance of 5-6 km but this event does not seem to be correlated with other variables. The wind veers offshore at a rate of 1.5° per km from 65° at the beach to 120° about 40 km offshore where the wind direction holds nearly constant and agrees well with a geostrophic approximation. The mixing ratio increases from 3 g/kg at a rate of 0.06 g/kg per km for about 20 km, and then settles to about 4.5 g/kg. The air-sea temperature difference is everywhere about -3.5°C .

The area distribution is shown in Figure 32. The winds are stronger than those of flight #1 and the consistency in speed and direction indicates that the effects of the small scale topography nearby are not large. However, from the increase in wind speed observable across Yakutat Bay to the southern extremity of the Malaspina Glacier, and from the increase in wind speed offshore along with the offshore veering of the wind seen in Figure 31, it may be inferred that there is confluence of air blowing across the mouth of Yakutat Bay and air blowing across and out of Yakutat Bay along its western shore. This is further supported by the increase in temperature in the confluent region reflecting the longer time that

air has spent over the water of Yakutat Bay compared to the shorter time air on either side of the southern extremity of the glacier has spent over water. The Yakutat surface report shows wind blowing offshore. Likewise in the longshore distribution along the western third of the glacier, we see lower momentum air of lower temperature with a slight northerly component indicative of some transit time over the Malaspina Glacier.

It can be inferred then that over the land areas of the Malaspina Glacier and over the Yakutat foreland there is a larger northerly component to the flow than exists over the coastal waters. Downslope katabatic flow is suggested as a cause of this phenomenon. However, the moisture field is quite homogeneous and fairly close to saturation indicating that the air is of maritime origin. It is unlikely that there is significant drainage flow from the high mountains on this day and any downslope forcing is in response to maritime air piling up against the mountains. It should be noted that all of these subtle flow features described for this day could be due to variations in the surface drag as air blows across Yakutat foreland, Yakutat Bay, and the Malaspina Glacier.

3) Flight #3 - 25 February

Flight #3 was made on 25 February between 1000 and 1400 YT or 1900-2300Z. The 12Z, 25 February 500 mb and 18Z surface analyses are shown in Figure 33. The 500 mb trough south of

Yakutat on the previous day has turned into a small low center. Elsewhere the pressure gradient is very weak. Yakutat shows 20 knot winds from the southwest at 500 mb. At the surface the front from the previous day had dissipated with mostly clearer air moving in behind. Another low center moved into the region from the south. As this center moved north and inland around Prince Rupert, the isobars largely followed the coastline causing a poorly defined pressure gradient in the study area. The pressure gradient (as told by this analysis) is stronger inland than offshore.

The skies on this day in the study area were clear except for some small cumulus activity about 25 km offshore of the Malaspina Glacier. A satellite photo shows these clouds clearly as a very thin fingerlike protrusion spiralling into a small broken cumulus center about 100 km SSW of Icy Bay. This barely discernible cloudy patch is associated with, as will be seen, dramatic changes in the wind field on this day.

Aircraft soundings at the beach and at waypoint 9 along with the Yakutat sounding are shown in Figure 34. The aircraft sounding over the ocean shows a very well-mixed layer 500 m deep. The same upper level temperature structure is seen in the beach sounding, but the lowest 400 m show a stable profile. As is clearly seen in the wind profile of the beach sounding, the cooler and drier air is coming from 30-70° over the glacier and indicates some drainage from the valleys to the north.

The startling difference in the wind directions observed in the two aircraft soundings of Figure 34 is better seen in the offshore distributions shown in Figure 35. Within an interval of a few hundred meters the wind speed drops from 5 m/sec to 1 m/sec. The temperature trace shows a sharp but slight increase and the humidity shows similar behavior but of the opposite sense. The wind direction is much slower to respond, taking 10 to 15 km to shift to a nearly steady direction. An observer aboard the aircraft noted an increase in the turbulence intensity as this "front" was penetrated. This was not a spurious event recorded on one pass of the aircraft. Subsequent passes at higher levels showed the same event persisted at least throughout the mixed layer, although the changes through this front weakened with height. This is the event apparently related to the mesoscale patch of cloudiness mentioned above. Careful analysis of the vertical structure of this event has not yet been attempted. It is worthwhile noting that although this structure was the most dramatic and best sampled phenomenon of its kind in the Yakutat area, we have seen others. Therefore, while such happenings may not be commonplace, they are certainly not exceptions in these coastal regions.

The area distribution over the study area is shown in Figure 36, which shows wind flowing out of Yakutat Bay, warming and moistening as the cool drainage air passes over the warmer sea surface. Again we see a relative wind maximum off-shore of the southern extremity of the Malaspina Glacier.

It is not clear what processes are active in the Icy Bay region where the winds are warm, dry, very light easterlies. The full impact of the wind direction reversal does not show in this figure since each vector is an average over 11 km.

4) Flight #4 - 26 February

Flight #4 was made on 26 February at 1300-1600 YT or 2200-0100Z, 27 February. The 500 mb flow shown in Figure 37 is southerly south of Yakutat and is turning onshore at Yakutat. The pressure gradient is strengthening but is still weak over the central Gulf of Alaska. Yakutat reports winds of 30 knots at 210° for that level. At the surface, a low pressure center had developed along a long front emanating from the Aleutian Low. This storm moved to the east with 500 mb flow and then turned north toward Yakutat by the time of the 00Z map of Figure 37. The pressure gradient is large around Sitka but still weak and poorly defined in the study area. The NWS analysis shows a slight low center north of Icy Bay. Yakutat was generally overcast with a ceiling of 2 km. There were no clouds over the Malaspina Glacier or the mountains but there were some offshore cumulus clouds 200-450 m thick.

The aircraft beach sounding and the Yakutat rawinsonde sounding are shown in Figure 38. There is not particularly good agreement between the two. The largest differences are in the mixing ratio and wind direction profiles. The beach air is drier than the Yakutat air and the beach winds are ENE throughout the mixed layer whereas the Yakutat sounding shows

northeast winds at the surface becoming southeast winds at 700 m. Judging from the aircraft sounding, the mixed layer is 500 m deep.

The offshore distributions are shown in Figure 39. This figure shows very little horizontal temperature gradient at 30 m which is at some discrepancy with the average at 60 m plotted in Figure 40. The mixing ratio increases slightly offshore and shows more variance in the first 20 km than in the last 30 km offshore. The wind direction is roughly 70° along the track but also shows more variance in the first 20 km. There appears to be some correlation between these two signals in the 20 km nearest the coast. The wind speed increases steadily offshore by 5 m/sec in 50 km which correlates with the increased pressure gradient offshore (Figure 37).

Similar to 25 February, Figure 40 shows air flowing out of Yakutat Bay and near the coast, turning to follow the coast. Also similar, the air offshore of the western half of the Malaspina Glacier and Icy Bay is a little warmer and drier than the air nearer Yakutat.

5) Flight #5 - 28 February

Flight #5 was made on 28 February between 1200 and 1600 YT or 2100-0100Z. The weather on this day was generally clear but with several large, isolated, precipitating cumuli with anvil tops. The 00Z, 1 March 500 mb analysis was unavailable so the 12Z, 28 February map is shown in Figure 41. The trough that deepens in the southerly direction is the remnant of a low

pressure region that had almost formed a closed center. Observations made from the aircraft of a wave cloud over Mt. St. Elias and the trajectories of the precipitating cumuli, from the Yakutat sounding, and from an interpolation of the 12Z 500 mb analysis of 28 February and 1 March, reveal the flow aloft was from 270° - 290° . Therefore, the study area was probably just ahead of the crest of a ridge. The surface analysis for 00Z, 1 March is also shown in Figure 41. There is a stationary front north of the study area and a warm front approaching from the southwest. The strong inversion that caused the anvil tops on the cumulus was the upper level warm front. A ridge pushing northward ahead of the warm front has separated into two lobes what was previously one region of low pressure. The soundings at Yakutat show that the lowest 3 km had been drying, cooling, and becoming less stable, possibly indicating that some of the low level air had been squeezed southward out of the region of the stationary front. Note that the study area is near a col in the flow pattern. Bringing all of these considerations together, an intermediate contour of 1014 mb (dashed line) has been drawn in.

The aircraft and Yakutat soundings are plotted in Figure 42. The agreement in wind direction although interesting when compared to the lesser agreement of other quantities, is probably fortuitous. Yakutat had not yet experienced any showers, the beach sounding was made while precipitating cumulus clouds were within 50 km, and the offshore sounding

was made in air modified (and apparently mixed) by the previous passage of a shower.

The effects of a nearby shower on the adjacent territory is evident in the signature of the offshore distributions shown in Figure 43. The aircraft passed a few km to the east of the eastward moving shower about 34-45 km from shore. The cool gust-front leading the shower shows up clearly.

Figure 44 is chaotic in both the wind and thermodynamic fields. The nearest precipitating showers were located southeast of EB-43 and south of Icy Bay, east of the southern two measurements of the offshore trackline (same shower noted in Figure 43 but it had moved across the trackline so the measurements of this figure were made behind the storm), and 50 km SSE of Yakutat. Many other showers were visible outside the perimeter of Figure 44.

6) Flight #6 - 1 March

Flight #6 was made on 1 March between 1400 and 1700 YT or between 2300Z and 0200Z, 2 March. The 2 March 00Z analyses are drawn in Figure 45. The slight depression of the 500 mb surface above the surface low pressure indicate that the storm was at its maximum intensity and would soon decay, as it quickly did. The storm shown on the surface analysis is that which was approaching Yakutat on 28 February. The winds were very strong ahead of the occluded front and fairly light behind. Only a trace of precipitation was observed at the NOAA ship SURVEYOR stationed off the coast of the Malaspina

Glacier. There was 100% overcast with cloud base at 300-350 m.

The soundings are plotted in Figure 46. The agreement between the Yakutat and aircraft soundings is good except for the previously observed tendency for the vertically averaged beach winds to be more northerly and a little stronger than the Yakutat winds.

The offshore distributions plotted in Figure 47 are again similar to the previous flights with a southeast geostrophic wind. There is a slight drying trend as the shore is approached and the winds veer slightly offshore. The relative wind maximum 10-15 km offshore which has been hinted at in previous flights, is visible again. The offshore veering is apparent in the area distribution of fields in Figure 48. Similar to 26 February the flow west of icy Bay shifts from northeasterly to easterly.

7) Flight #7 - 3 March

The final flight was carried out on March 3, 1977 between 1300 and 1600 YF or 2200Z and 0100Z, 4 March, Figure 49 shows the 00Z, 4 March 500 mb and surface analyses. Twelve hours earlier at 500 mb, a low centered near 57°N , 157°W had been giving Yakutat southwesterly flow becoming westerly over the Yukon. By the time of Figure 49 a slight ridge had formed between that low and Yakutat, and upon moving eastward was creating westerly anticyclonic flow over Yakutat. Correspondingly, the surface had been dominated by nearly parallel isobars and an elongated low pressure region spanning much of

the Gulf of Alaska. Yakutat had strong southwesterlies and high seas. Also by the time of Figure 49, the low center had closed up considerably. A ridge developed giving Yakutat westerly or southwesterly winds. The cloudcover was 70% altocumulus and altostratus. Due to heavy seas the SURVEYOR occupied a station at the mouth of Icy Bay, so offshore legs were flown from there. No 30 m offshore leg was flown.

No aircraft sounding was made but the SURVEYOR launched a radiosonde which is compared with the Yakutat rawinsonde in Figure 50. The two soundings compare well except Yakutat shows a slightly more stable potential temperature profile and a slightly more moist mixing ratio profile.

The area distribution, Figure 51, shows that for strong winds, impinging directly on the coast, the wind field is not perturbed by local coastal effects. As Icy Bay is approached from offshore the air is clearly being warmed by the warmer ocean surface below. In this figure a consistent veering from surface winds, measured by EB-70, EB-43 and Yakutat, to the aircraft measurements at 60 m indicates that Ekman turning is still a significant consideration even in apparently unstable boundary layers.

6. CONCLUSIONS

The St. Elias Mountain range, presenting a rather abrupt coastal demarcation, has a noticeable effect on the movement and development of cyclonic disturbances in the Gulf of Alaska. Most noticeably, there is an observed retardation in

isobars on the coastal side of the cell.

The mesoscale wind field in the vicinity of the Malaspina Glacier shows local orographic control sufficient to invalidate synoptic analysis. Coastal winds show a pronounced east-west bimodal character (the general trend of the mountain range) which tends toward a synoptic fit, but is evident at least 100 km offshore.

As the coast is approached, katabatic drainage winds contribute an offshore component to the flow field. This flow, the result of downhill drainage of dense surface air, is an almost permanent winter feature, but seems to occur mainly at night during the summer. At the coast, these winds will dominate all other processes yielding flow directly offshore. The katabatic winds are quickly modified over the ocean however, and are seldom seen further than 20 km offshore.

Analysis of data buoys EB-43 and EB-70, 20 and 60 km offshore, show occasions of easterlies at EB-43 but westerlies further offshore at EB-70. An explanation of these occurrences could be provided by two other processes, more erratic occurrences which have been observed to strongly modify the coastal wind field in a somewhat sporadic manner. Instrumented aircraft measurements have detected sharp, horizontal, mesoscale discontinuities in the atmospheric boundary layer and regions of horizontal convergence. This discontinuity was confirmed in one instance by a satellite photograph showing a thin cloud streak which agrees with the aircraft observation

of the discontinuity as a region of a strong convergence between NE offshore coastal winds and SW winds offshore. It appears that such regions of discontinuity are not unusual especially during the winter.

A second erratic occurrence in the coastal wind field is a local confluence between drainage winds directly off the glacier and winds from adjoining Yakutat Bay. This confluence manifests itself as a coastal jet, approximately longshore of the SE coast of the glacier.

A comparison between data buoy and aircraft measurements showed consistent veer of about 10° over a 60 m height, an unexpected result for a convective "mixed" layer.

A mountainous coastline with strong thermal forcing and katabatic flow produces a highly chaotic wind field for large distances offshore. It is doubtful if a numerical model equipped with sophisticated parameterization techniques could resolve such chaos in much more than a rudimentary fashion. To better understand the physical processes contributing to the wind field, the principle mechanisms need to be isolated. Thus future studies of coastal atmospheric physics (aside from descriptive studies such as this report) should be aimed at specific regions which provide such isolation. One example is the Arctic ice edge, where topographic and frictional differences are minimized.

REFERENCES

- Bakun, A., 1973: Coastal Upwelling Indices, West Coast of North America, 1946-71, NOAA Tech Rept. NMFS SSRF-671, 103 p.
- Bilello, M. S., (1974): Air Masses, fronts and Winter Precipitation in Central Alaska. Cold Regions and Engineering Laboratory.
- Climatological and Oceanographic Atlas for Mariners, Volume II, North Pacific Ocean (1961). Prepared by Office of Climatology and Oceanographic Analysis Division, Dept. of Commerce.
- Davis, B. L., and M. W. Ekern, 1977: Wind Fabric Diagrams and Their Application to Wind Energy Analysis. J. Appl. Meteor. 16, 522-531.
- Lenschow, D. H. (1972): The measurement of air velocity and temperature using the NCAR Buffalo Aircraft Measuring System. NCAR Technical Notes, NCAR-TN/EDD-74, National Center for Atmospheric Research, Boulder, 39 p.
- Putnins, P. (1956). Studies on the Meteorology of Alaska, Environmental Data Services, Silver Springs, MD., 90 p.
- Searby, H. W. (1969). Coastal weather and marine data summary for the Gulf of Alaska, Cape Spencer westward to Kodiak Island. ESSA Tech. Memo. EDSTM8, 30 p.
- Telford, J. W., P. B. Wagner, and A. Vazini, 1977: The Measurement of Air Motion from Aircraft. J. APPL. METEOR. 16, 156-166.
- U.S. Navy Hydrographic Office (1944). Weather Summary - Alaska Area. Pub. No. 526, 279 p.

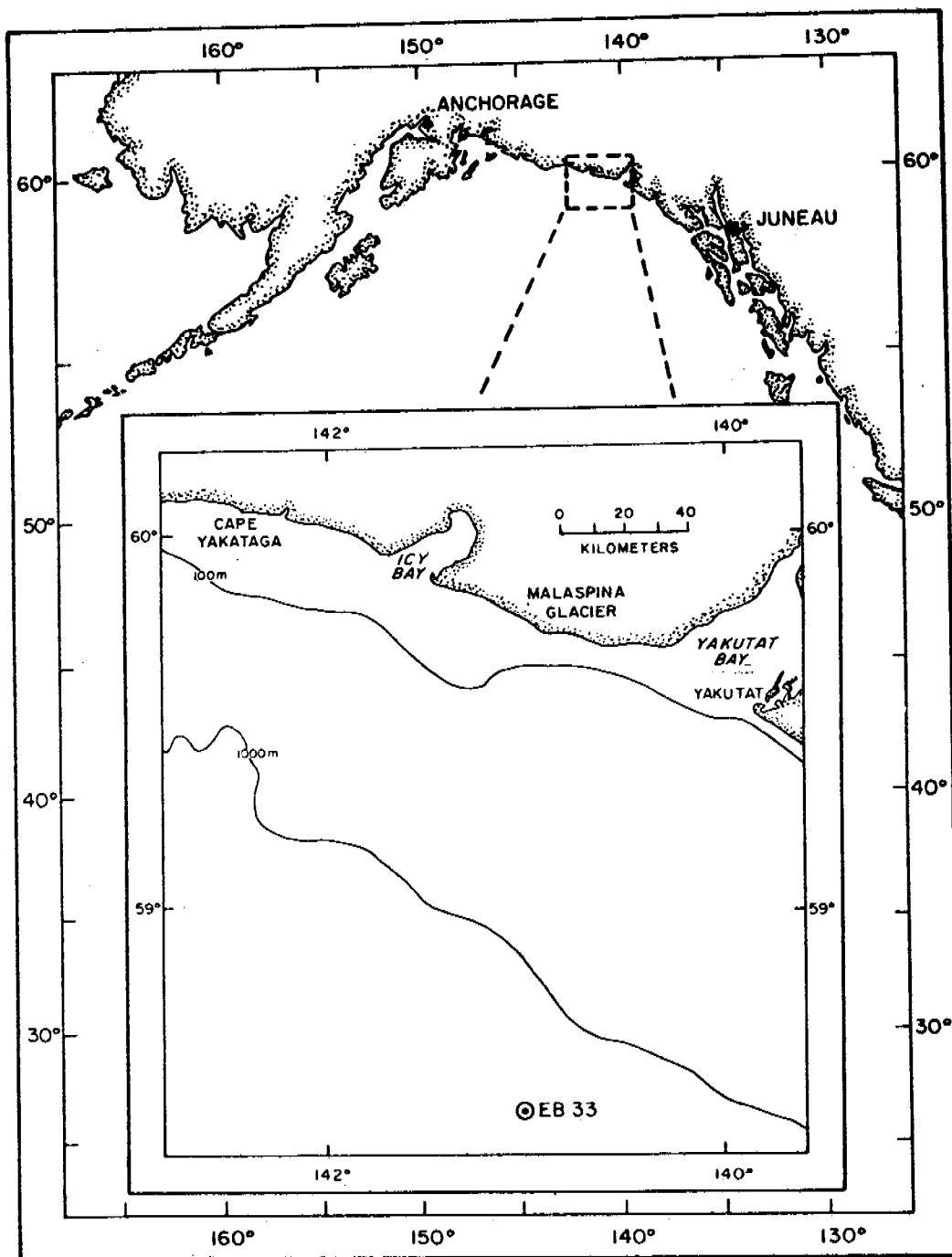
FIGURE CAPTIONS

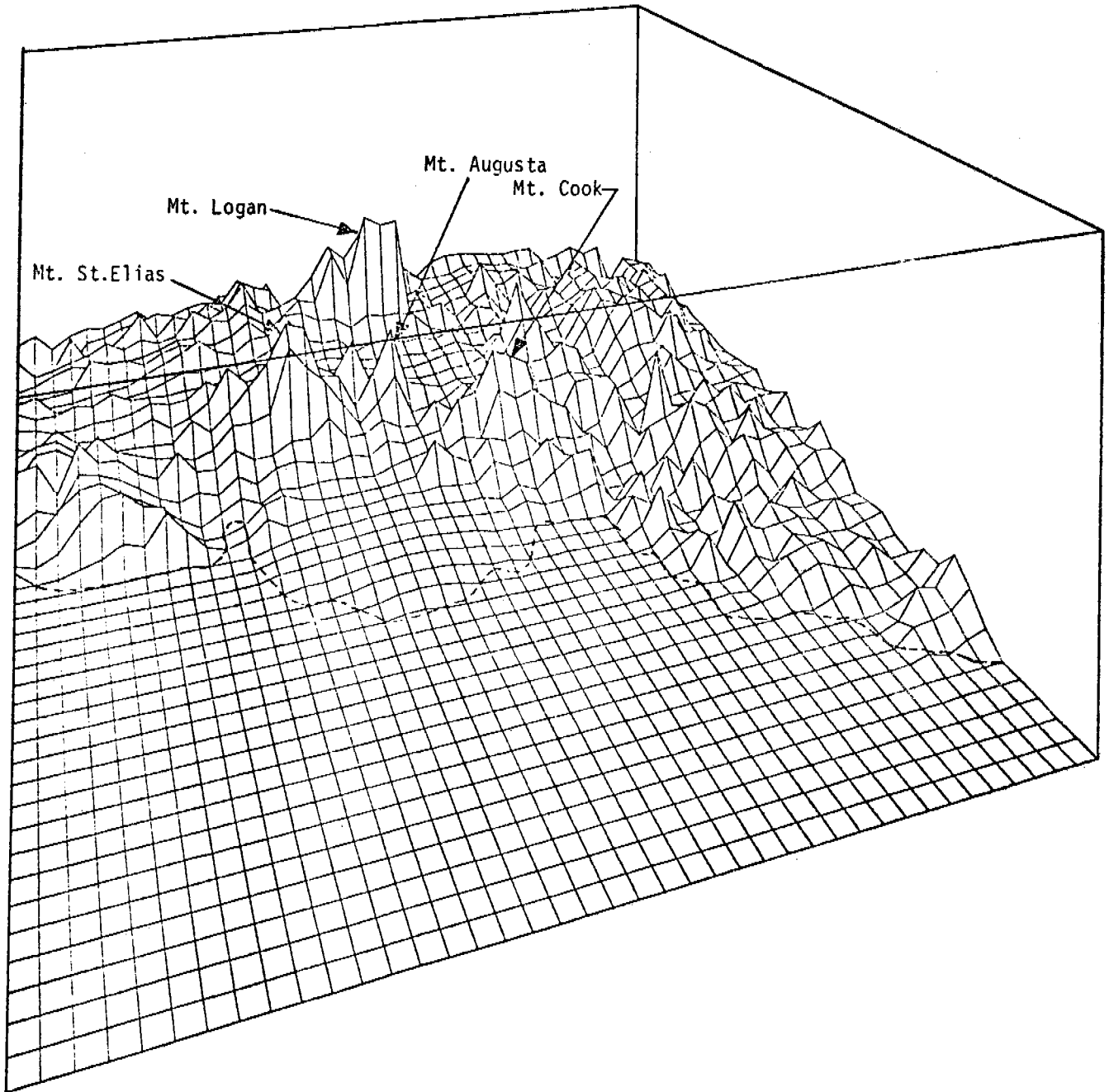
- Figure 1. Map of the study area showing the Malaspina Glacier and offshore environmental data buoy EB-33.
- Figure 2. Isometric contour map of the study area. Each grid is a 5 km x 5 km square.
- Figure 3. Average meteorological conditions in the Gulf of Alaska for various months of the year. Solid arrows are principle storm tracks, dashed lines are secondary tracks. (From Searby, 1969).
- Figure 4. Most common synoptic types as classified by Putnins (1966). Classification symbol and percentage of occurrence are shown in upper right hand corners: a) May, b) August, c) November, d) February.
- Figure 5. A summary of climatic conditions in the Gulf of Alaska (Searby, 1969).
- Figure 6. Map showing location of meteorological sensors.
- Figure 7. Time series of surface winds derived by the U.S. Navy Fleet Numerical Weather Center, FNWC, for two study periods: a) 6 March to 3 April, b) 6 May to 1 June.
- Figure 8. Wind fabric diagrams of winds derived by FNWC for two study periods: a) 6 March to 3 April, b) 6 May to 1 June.
- Figure 9. Time series of surface winds and temperature for coastal stations for 6 March to 3 April period: a) EB-70, b) EB-43, c) Pt. Riou, d) Pt. Manby.
- Figure 10. Time series of surface winds and temperature for coastal stations for 6 May to 1 June period: a) EB-70, b) EB-43, c) Pt. Riou, d) Pt. Manby.
- Figure 11. Wind fabric diagrams for coastal stations for 6 March to 3 April period: a) EB-70, b) EB-43, c) Pt. Riou, d) Pt. Manby.
- Figure 12. Wind fabric diagrams for coastal stations for 6 May to 1 June period: a) EB-70, b) EB-43, c) Pt. Riou, d) Pt. Manby.

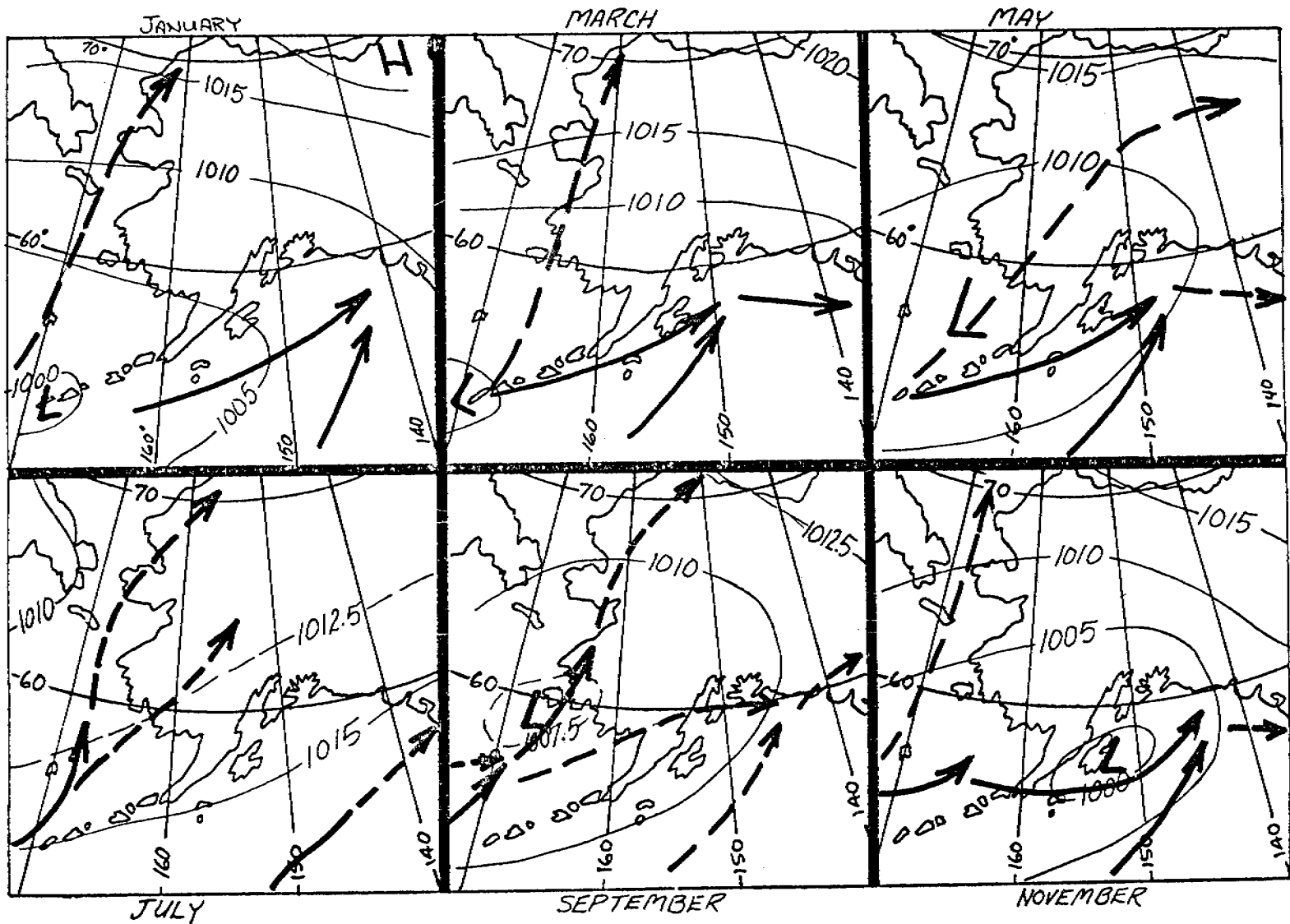
- Figure 13. Correlation plots of wind direction for 6 March to 3 April period: a) EB-70 vs. FNWC, b) EB-43 vs. FNWC, c) Pt. Riou vs. FNWC, d) Pt. Manby vs. FNWC, e) EB-43 vs. EB-70.
- Figure 14. Correlation plots of wind direction for 6 May to 1 June period: a) EB-70 vs. FNWC, b) EB-43 vs. FNWC, c) Pt. Riou vs. FNWC, d) Pt. Manby vs. FNWC, e) EB-43 vs. EB-70.
- Figure 15. Comparison of wind directions monitored by EB-43 and EB-70. The dashed line is the wind direction indicated by FNWC. Letters A, B, C, D indicate wind reversal events.
- Figure 16. Surface observations of wind and temperature for 3 February 1975 at stations 6 through 11 (wind barb = 5 knots, temperature in °C).
- Figure 17. Comparison of radiosonde ascent #8 with NWS ascent from Yakutat at the same time (1200Z, 3 February 1975).
- Figure 18. Surface observations for the March 1976 study. Open circles indicate clear skies; wind barbs represent 10 knots; temperature (°C), coded pressure (mb), and dewpoint temperature (°C) are shown in clockwise order beginning from a point roughly NW on the station symbol.
- Figure 19. Weather map for Gulf of Alaska - 1200Z, 9 March 1976. Temperature and dewpoint are in °F.
- Figure 20. Comparison of radiosonde ascent #7 with NWS ascent from Yakutat at the same time (1200Z, 9 March 1976).
- Figure 21. Contour plot of potential temperature vs. distance offshore. Of note are the katabatic cold wedge and cold core at 1000 m.
- Figure 22. Contour plot of mixing ratio vs. distance offshore. A prevailing maximum slowly increases in height offshore.
- Figure 23. Profiles of temperature and winds from radiosonde (x), tethered balloon ascent (solid line), and descent (dotted line) taken at station 6, about 6 km offshore. Wind direction indicates a sharp transition at 250 m. There is evidence of a shallow mixed layer at 30 m.

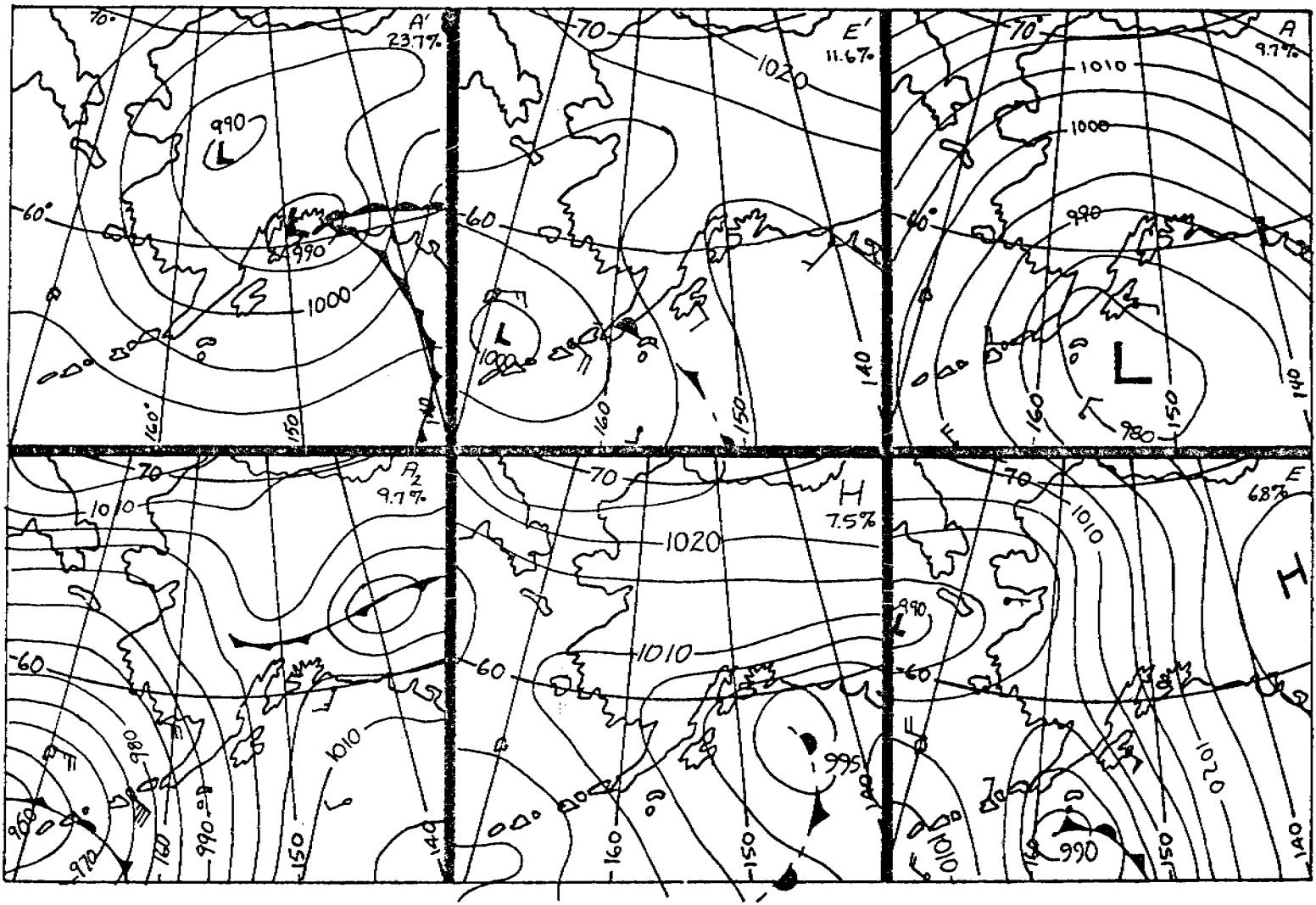
- Figure 24. Photograph of the NCAR Queen Air N3040 (foreground) used during the intensive study.
- Figure 25. Typical flight plan for the NCAR Queen Air study of the Yakutat coastline.
- Figure 26. 500 mb (upper) and surface (lower) analyses for 00Z, 23 February 1977.
- Figure 27. 00Z, 23 February Yakutat rawinsonde profiles.
- Figure 28. Area distribution during flight #1, 22 February of wind, temperature, mixing ratio and sea surface temperature at 60 m. 1 full barb = 10 knots, 1/2 barb = 5 knots. Temperature ($^{\circ}\text{C}$), mixing ratio (g/kg) and sea surface temperature ($^{\circ}\text{C}$) are plotted in clockwise order beginning from a point roughly NW on the station symbol.
- Figure 29. 00Z, 25 February 500 mb (upper) and 18Z, 24 February surface (lower) analyses.
- Figure 30. 00Z, 25 February Yakutat rawinsonde (dashed) and aircraft waypoint 8 (solid) profiles.
- Figure 31. Offshore distribution of temperature, sea surface temperature, mixing ratio, wind speed, and wind direction at 30 m for 24 February, flight #2.
- Figure 32. Area distribution of meteorological parameters for flight #2, 24 February.
- Figure 33. 12Z, 25 February 500 mb (upper) and 18Z surface (lower) analyses.
- Figure 34. 00Z, 26 February Yakutat rawinsonde (dashed), aircraft waypoint 8 (solid), and aircraft waypoint 9 (dotted) vertical profiles.
- Figure 35. Offshore distribution of meteorological parameters for flight #3, 25 February.
- Figure 36. Area distribution of meteorological parameters for flight #3, 25 February
- Figure 37. 00Z, 27 February 500 mb (upper) and surface (lower) analyses.
- Figure 38. 00Z, 27 February Yakutat rawinsonde (dashed) and aircraft waypoint 8 (solid) profiles.
- Figure 39. Offshore distribution of meteorological parameters for flight #4, 26 February.

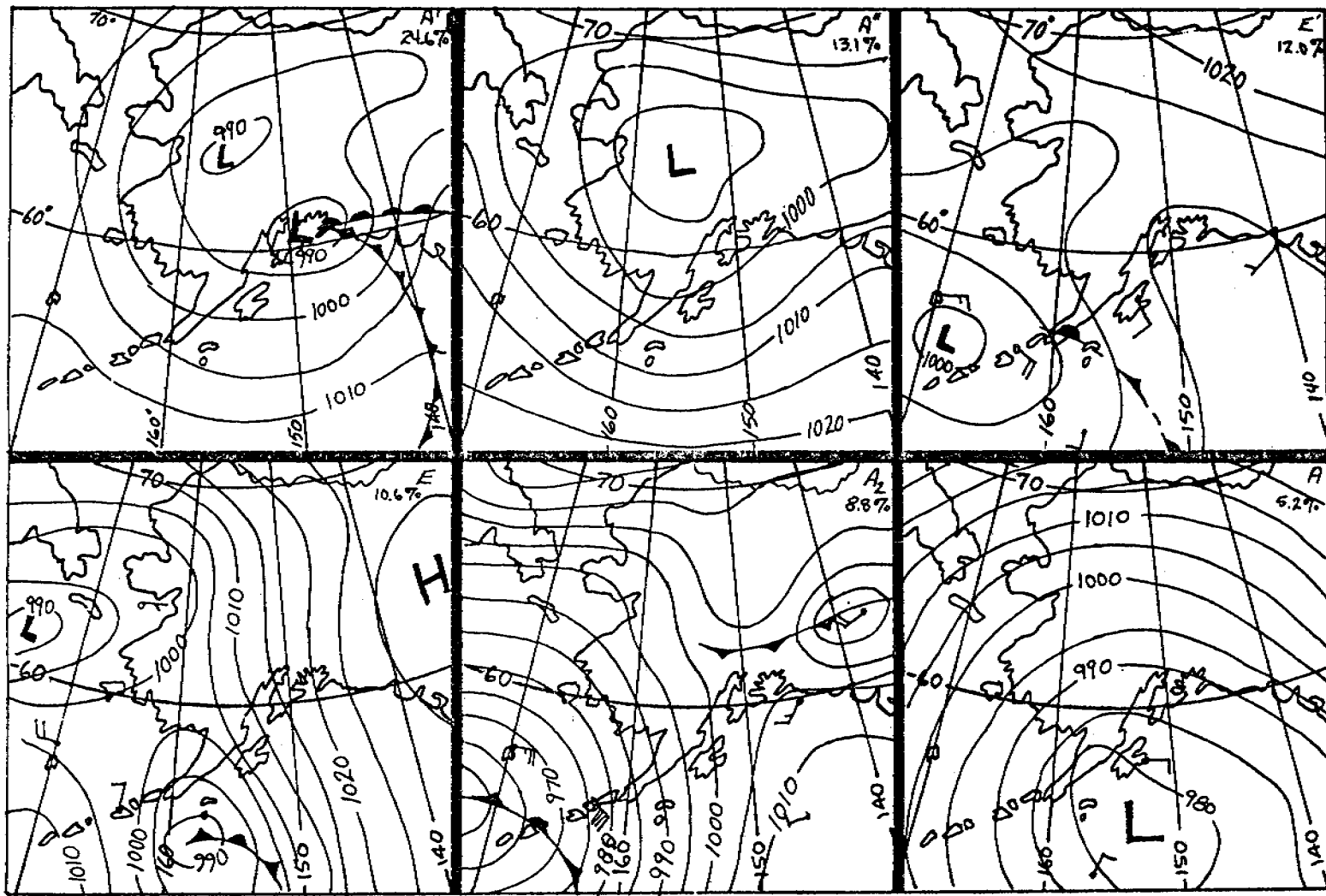
- Figure 40. Area distribution of meteorological parameters for flight #4, 26 February.
- Figure 41. 12Z, 28 February 500 mb (upper) and 00Z, 1 March surface (lower) analyses.
- Figure 42. 00Z, 1 March Yakutat rawinsonde (dashed), aircraft waypoint 8 (solid), and aircraft waypoint 9 (dotted) vertical profiles.
- Figure 43. Offshore distribution of meteorological parameters for flight #5, 28 February.
- Figure 44. Area distribution of meteorological parameters for flight #5, 28 February.
- Figure 45. 00Z, 2 March 500 mb (upper) and surface (lower) analyses.
- Figure 46. 00Z, 2 March Yakutat rawinsonde (dashed) and aircraft waypoint 8 (solid) profiles.
- Figure 47. Offshore distribution of meteorological parameters for flight #6, 1 March.
- Figure 48. Area distribution of meteorological parameters for flight #6, 1 March.
- Figure 49. 00Z, 4 March 500 mb (upper) and surface (lower) analyses.
- Figure 50. Yakutat rawinsonde and SURVEYOR radiosonde vertical profiles for 00Z, 4 March.
- Figure 51. Area distribution of meteorological parameters for flight #7, 3 March.

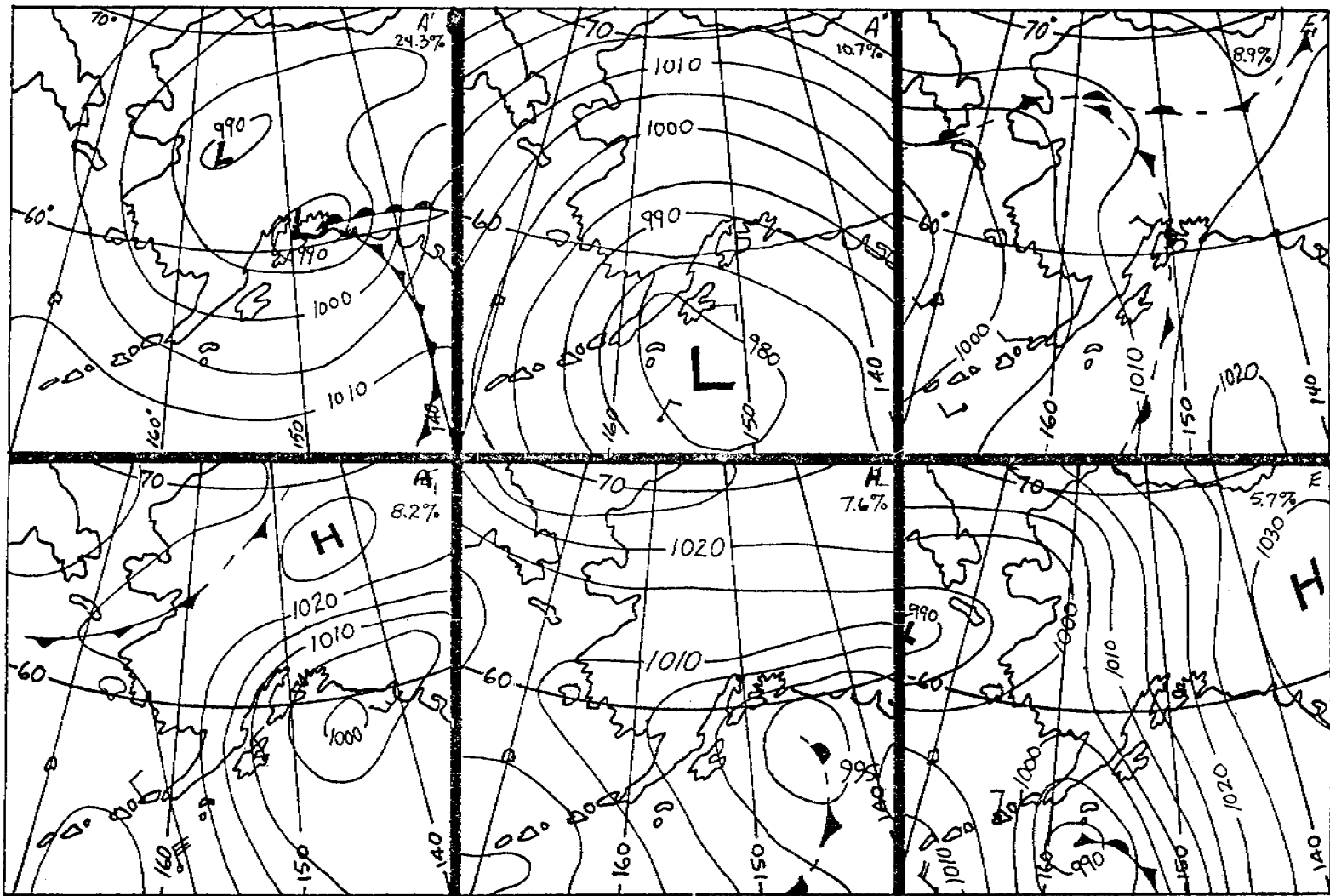


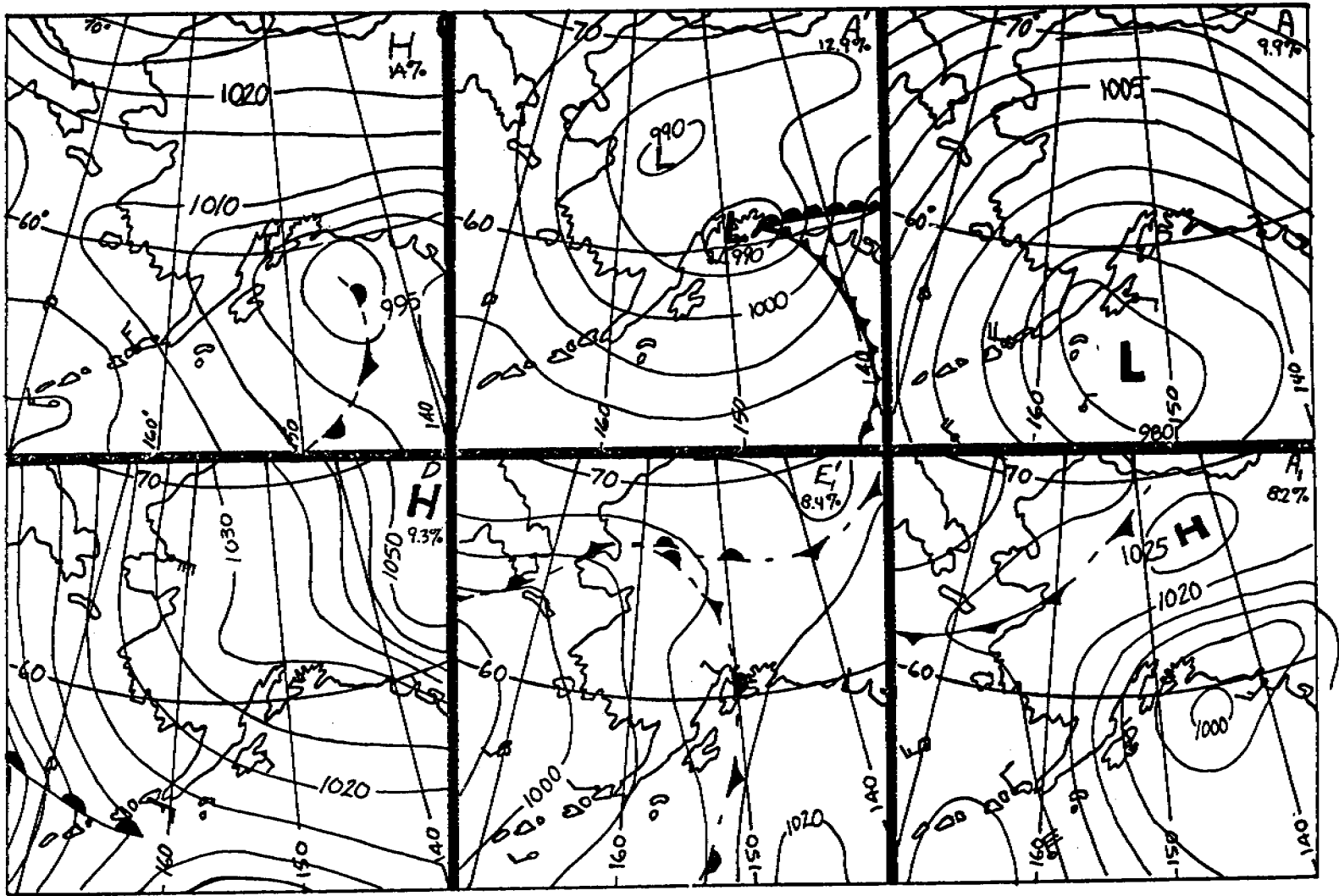


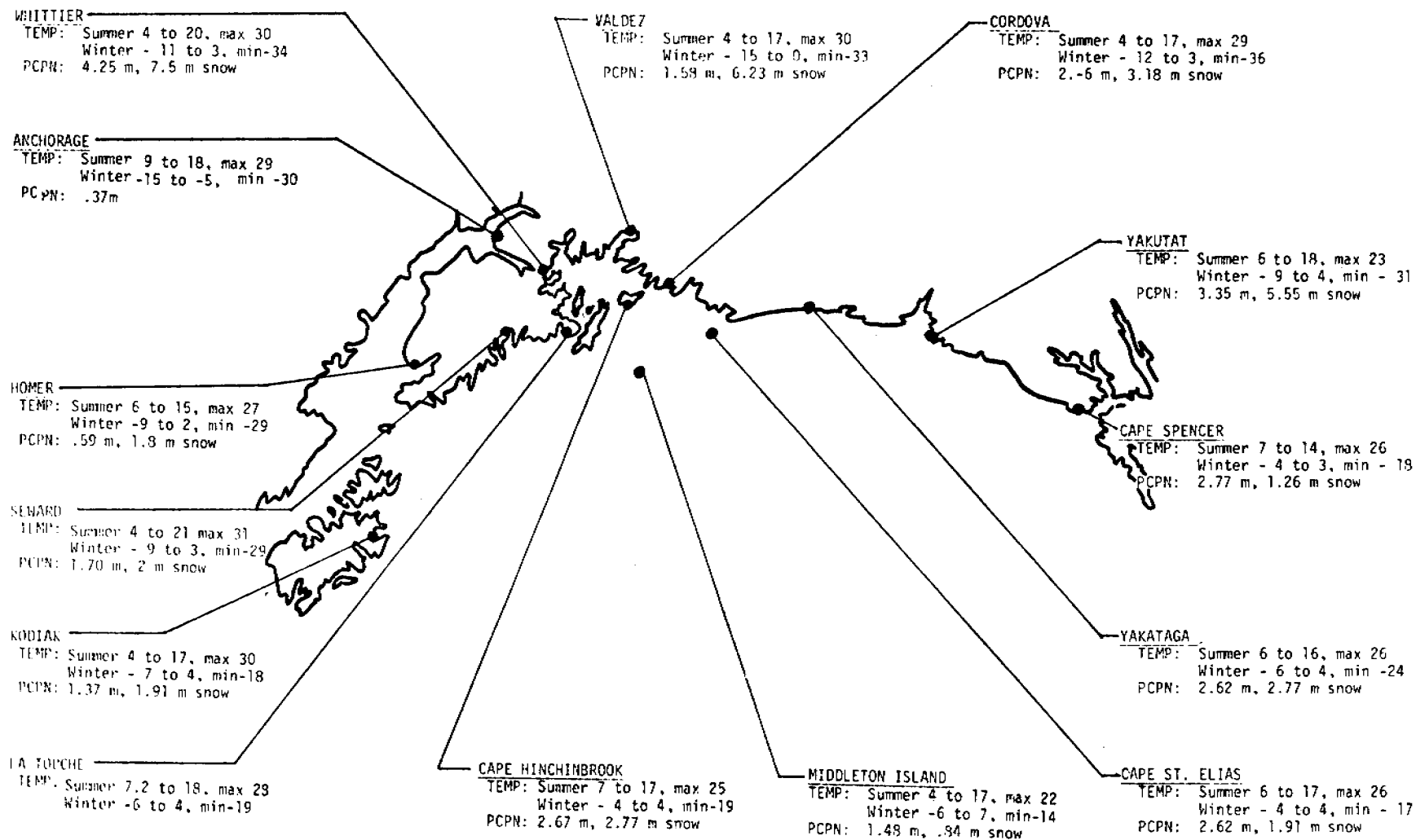


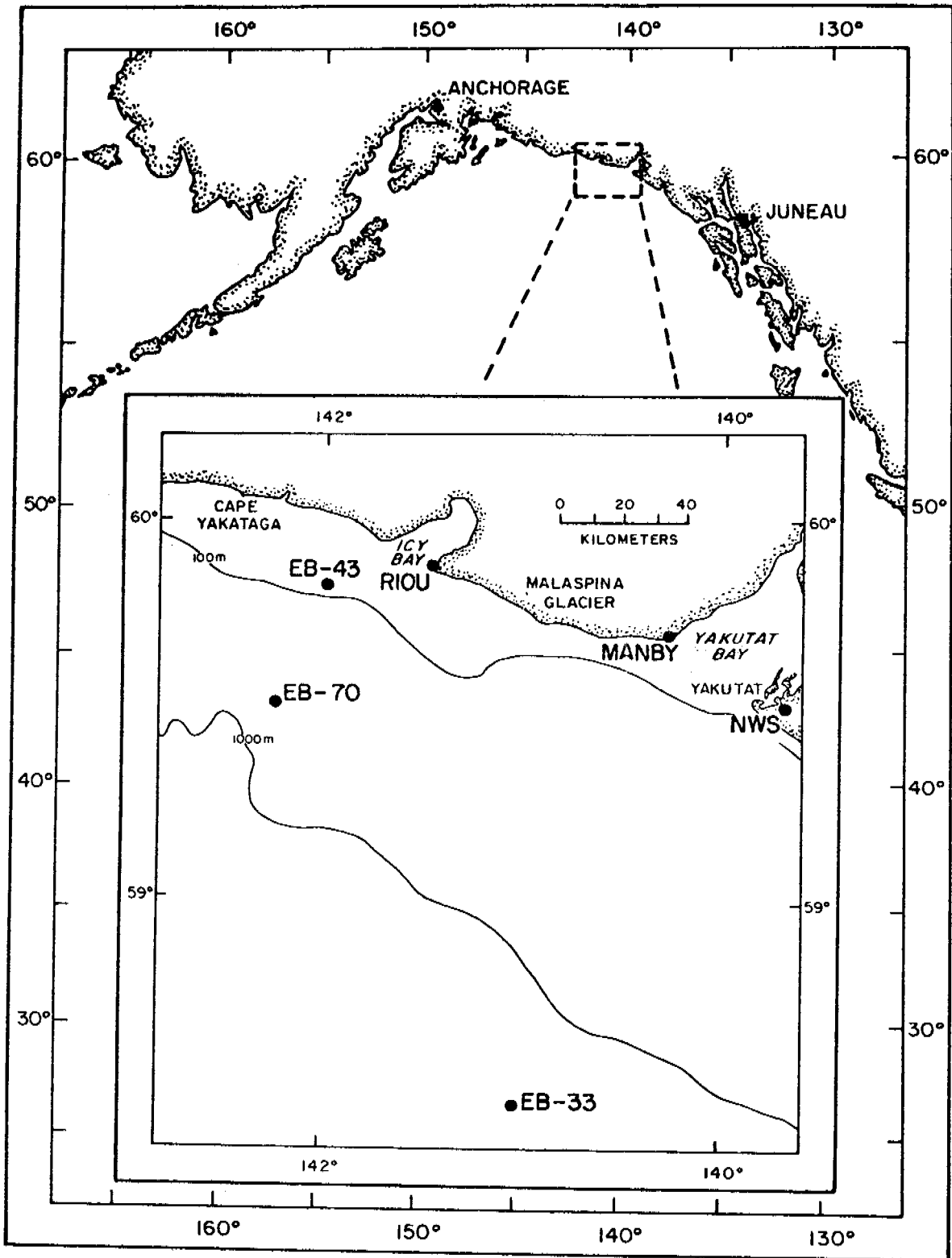








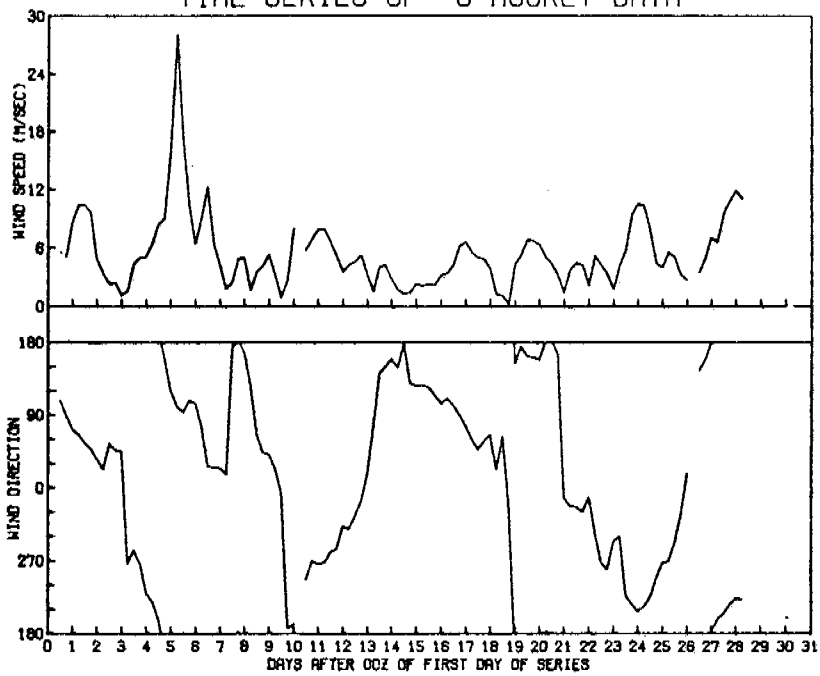




FNWC

6 MAR THROUGH 3 APR 1977

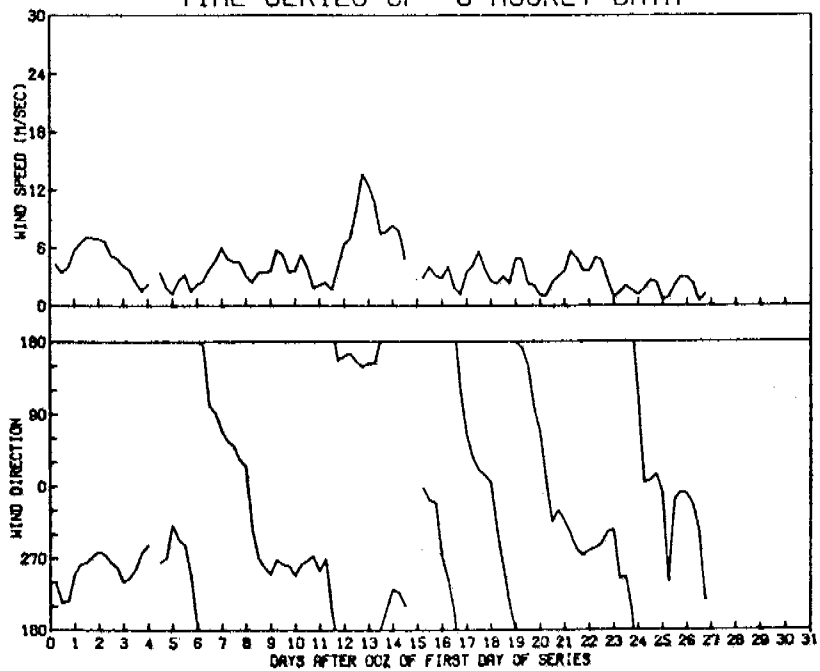
TIME SERIES OF 6 HOURLY DATA

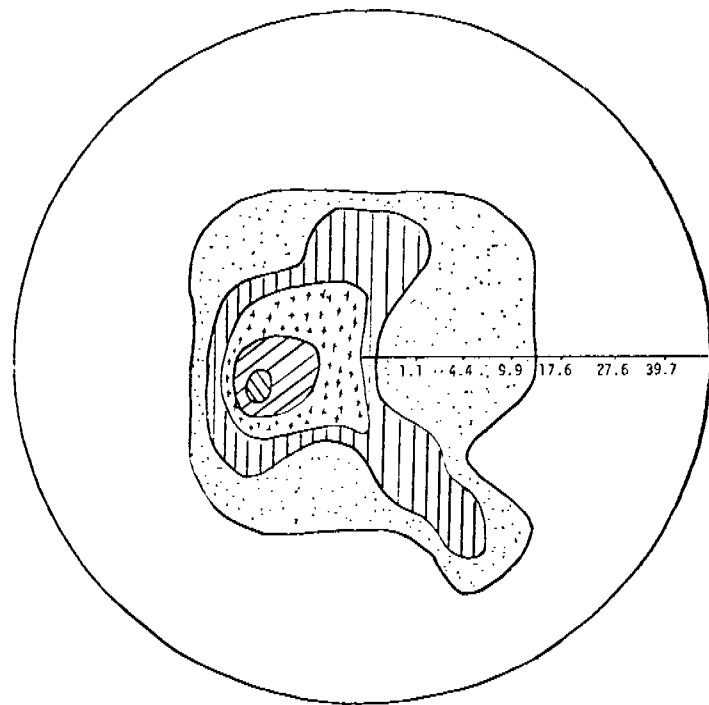
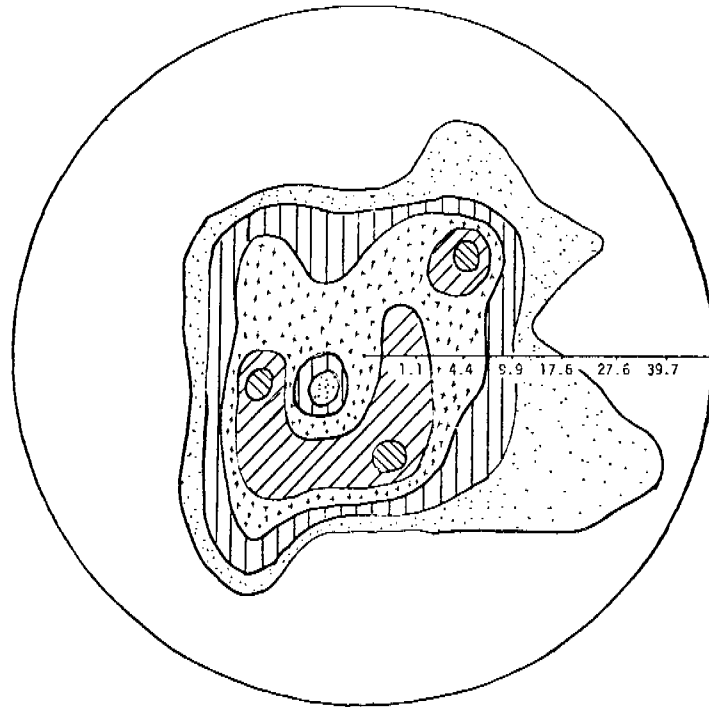


FNWC

6 MAY THROUGH 1 JUN 1977

TIME SERIES OF 6 HOURLY DATA

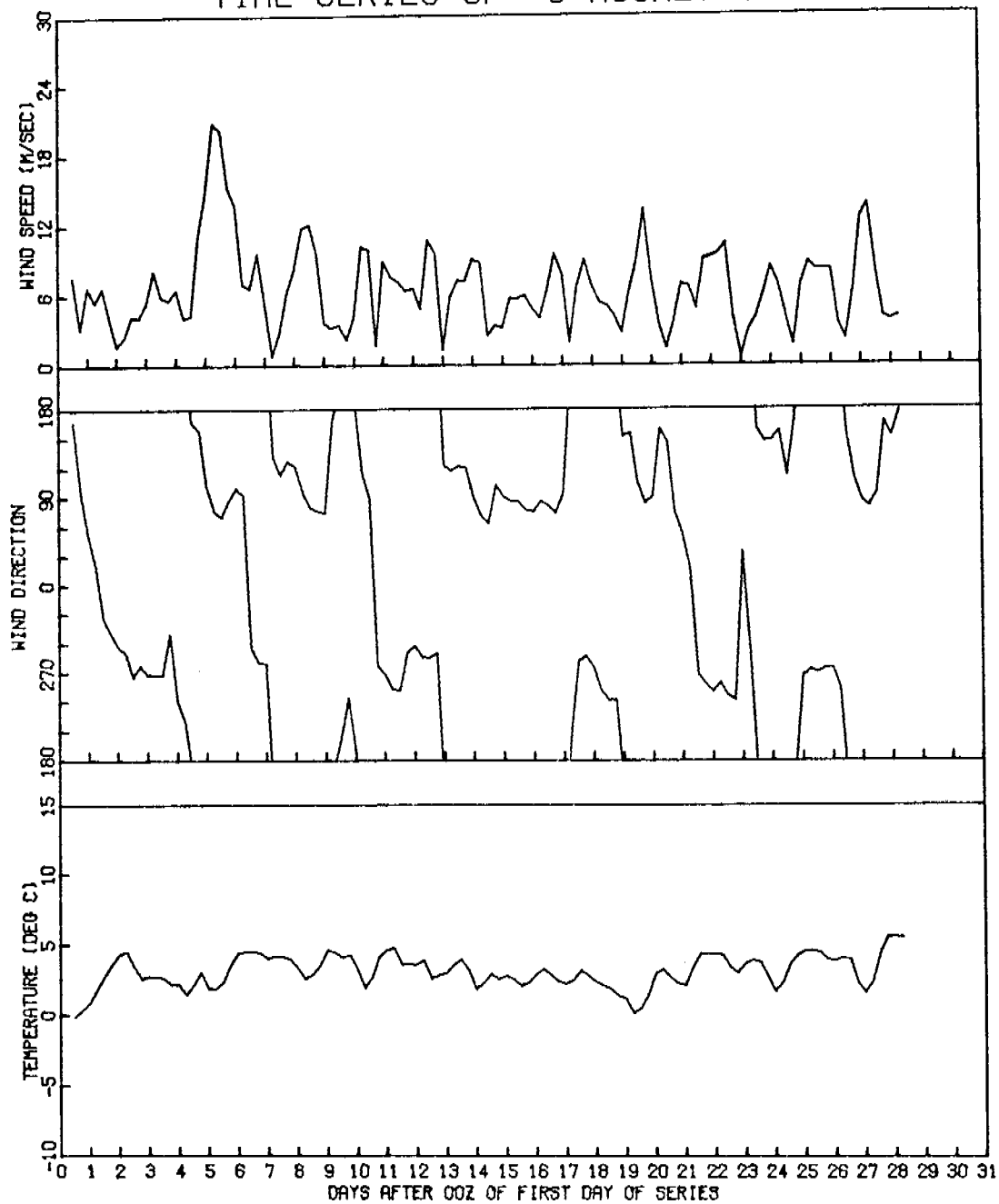




EB-70

6 MAR THROUGH 3 APR 1977

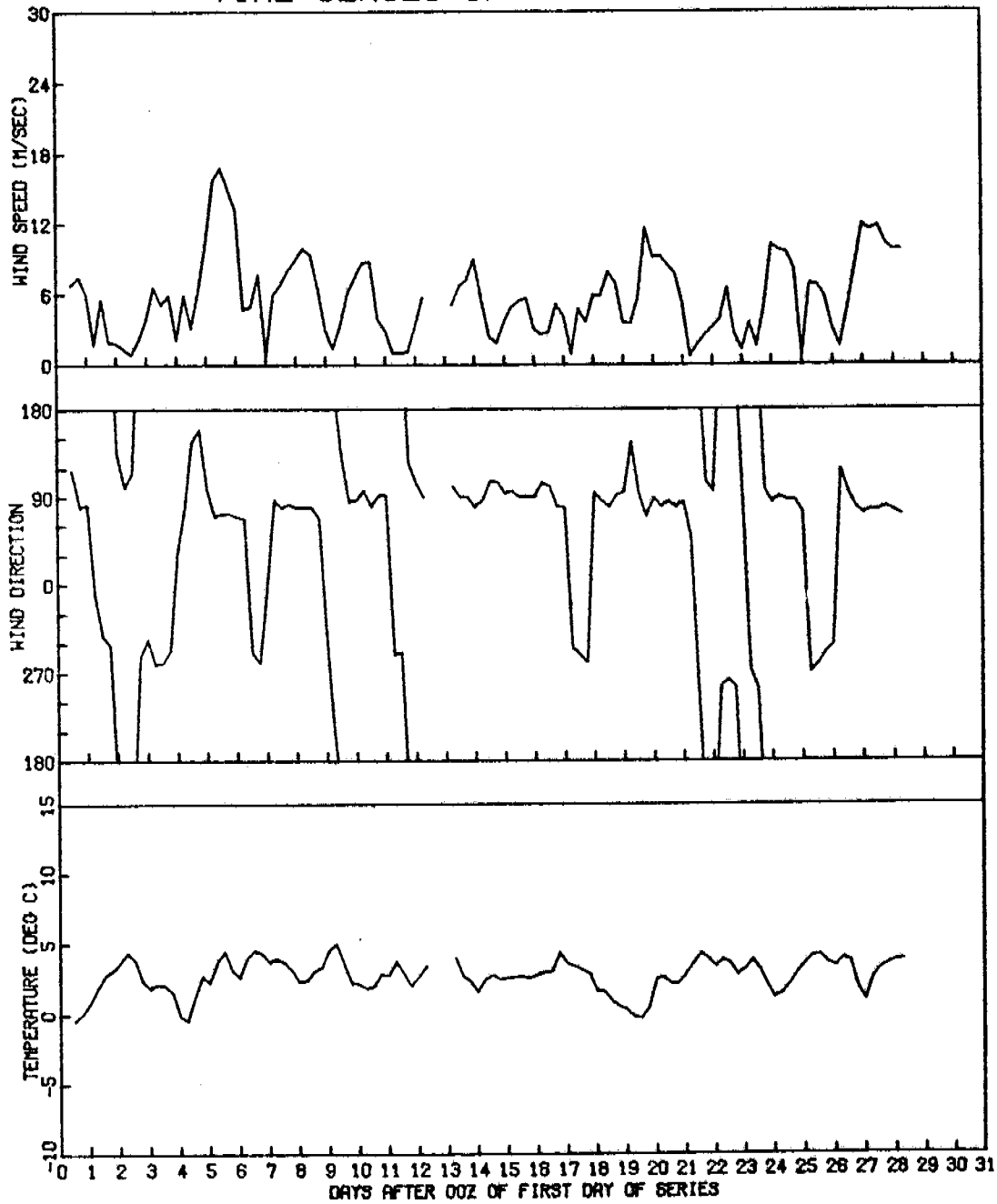
TIME SERIES OF 6 HOURLY DATA



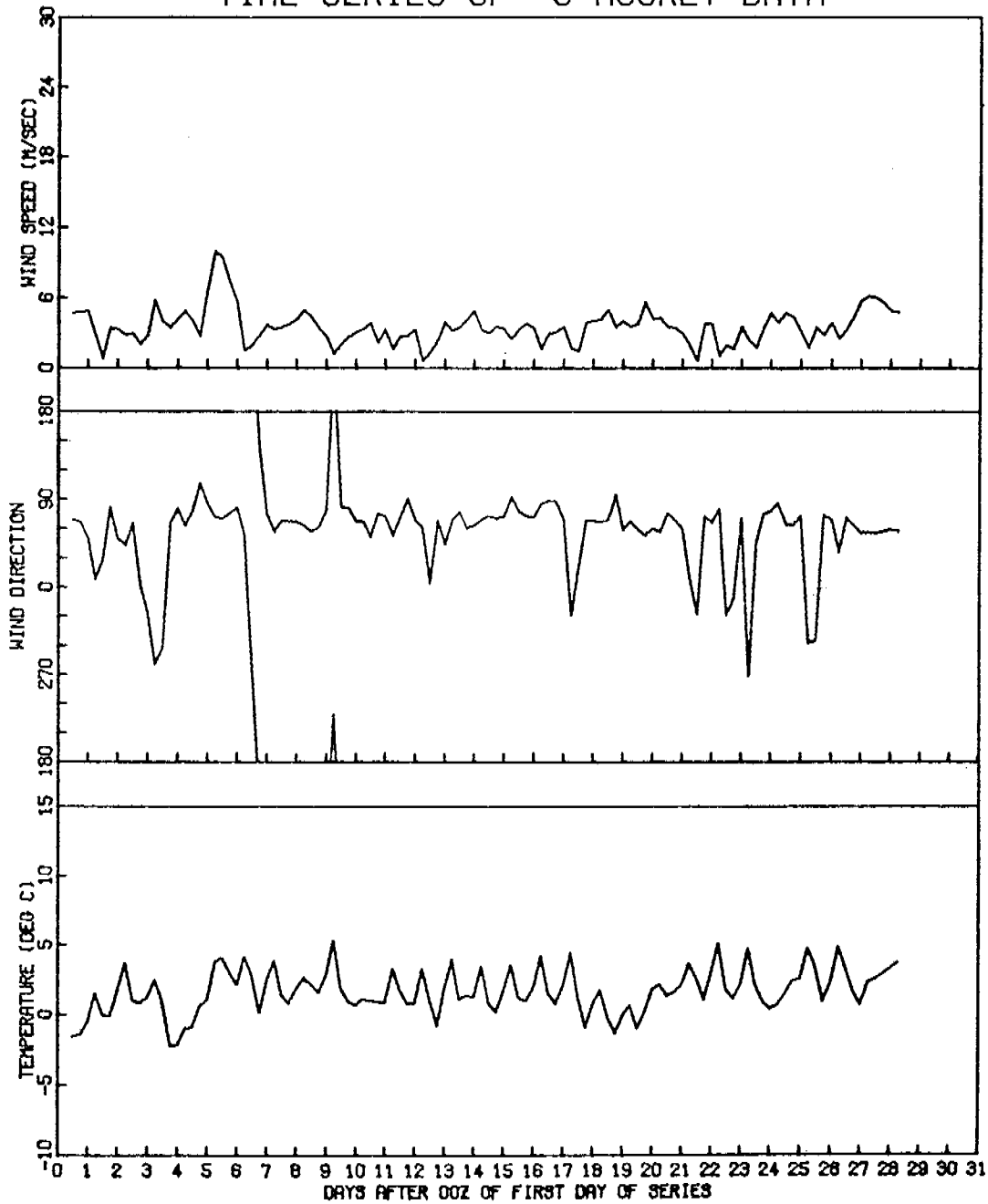
EB-43

6 MAR THROUGH 3 APR 1977

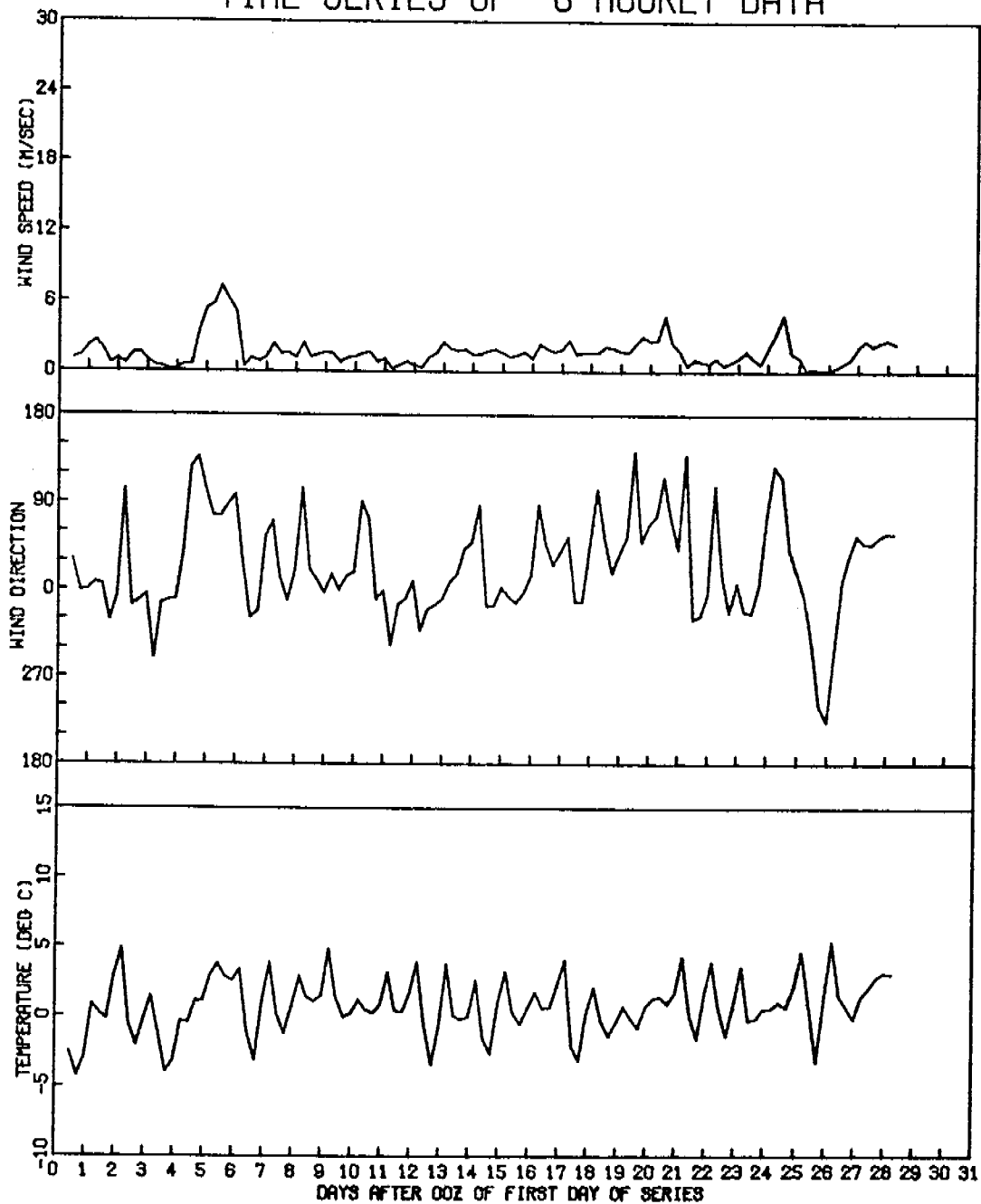
TIME SERIES OF 6 HOURLY DATA



PT. RIOU 6 MAR THROUGH 3 APR 1977
TIME SERIES OF 6 HOURLY DATA



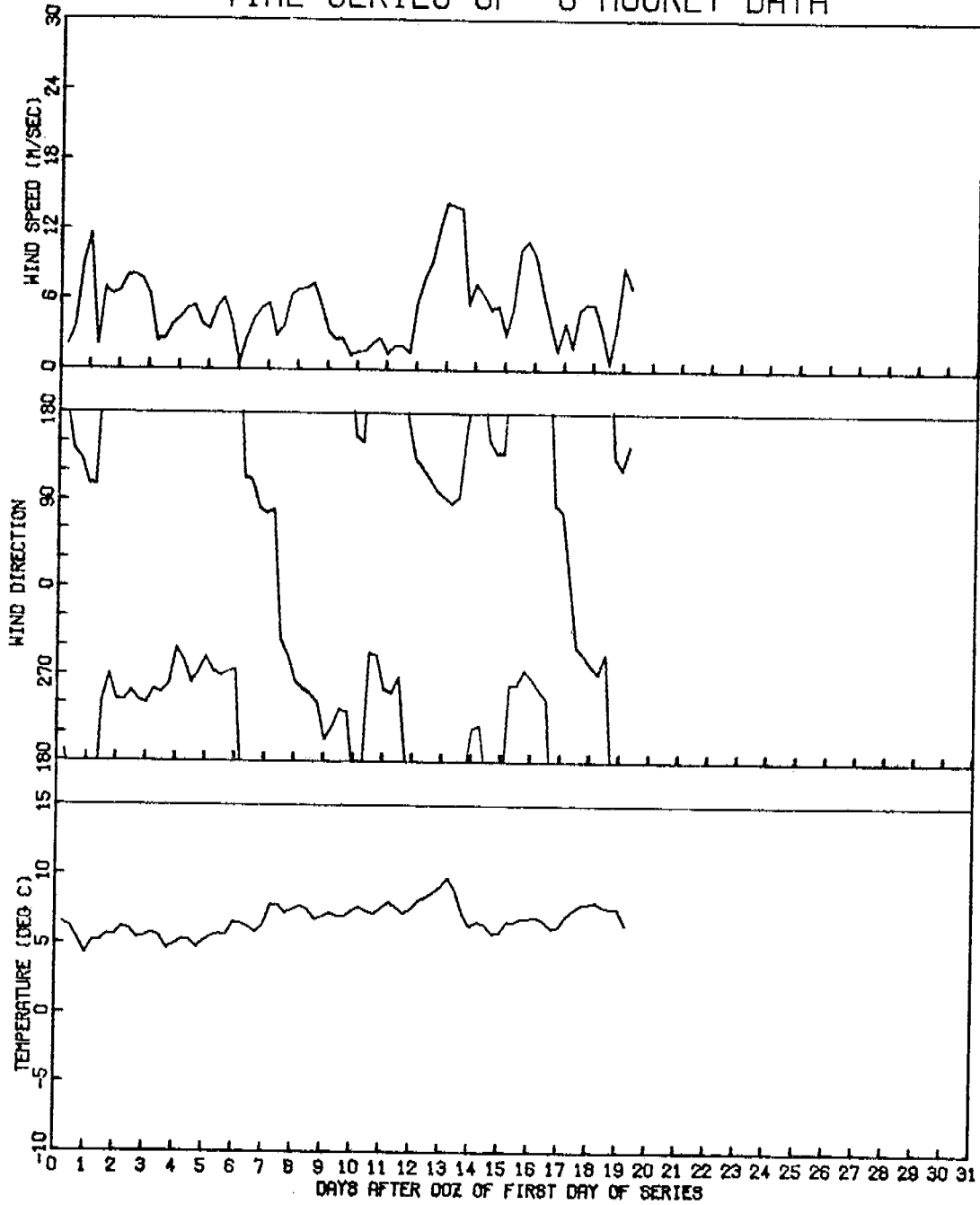
PT. MANBY 6 MAR THROUGH 3 APR 1977
TIME SERIES OF 6 HOURLY DATA

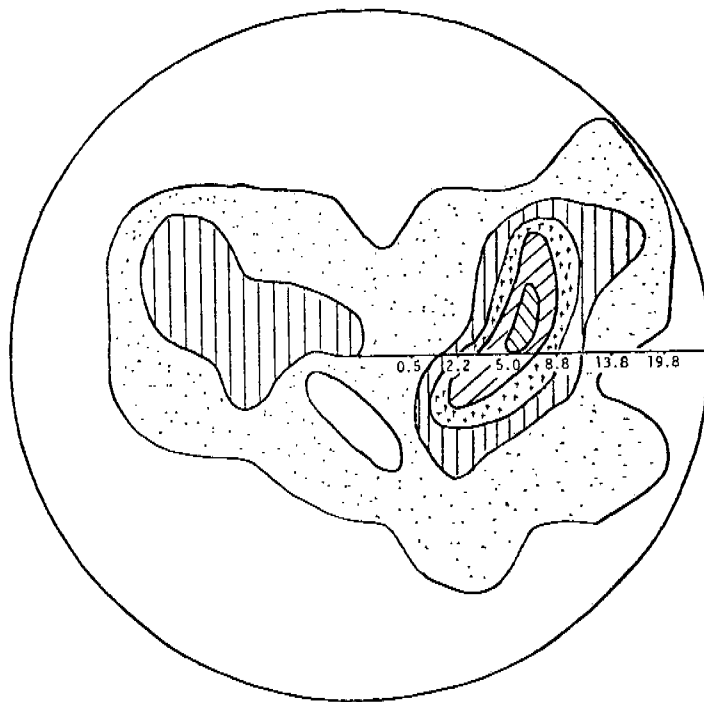
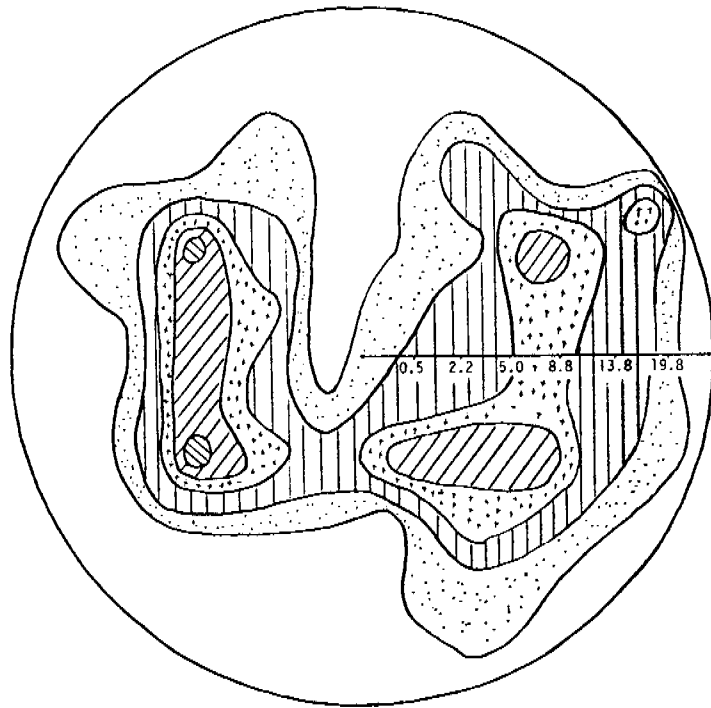


EB-70

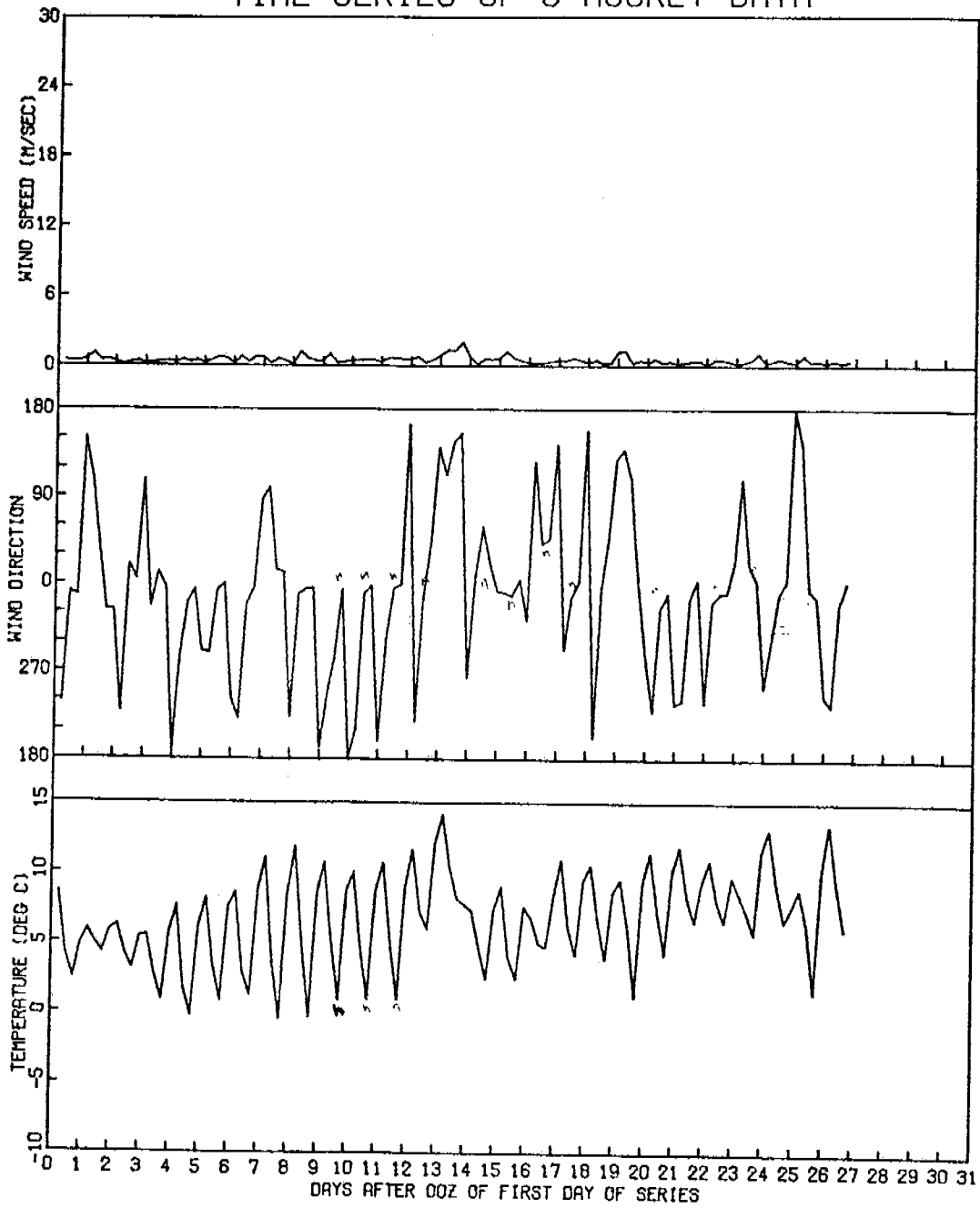
6 MAY THROUGH 1 JUN 1977

TIME SERIES OF 6 HOURLY DATA

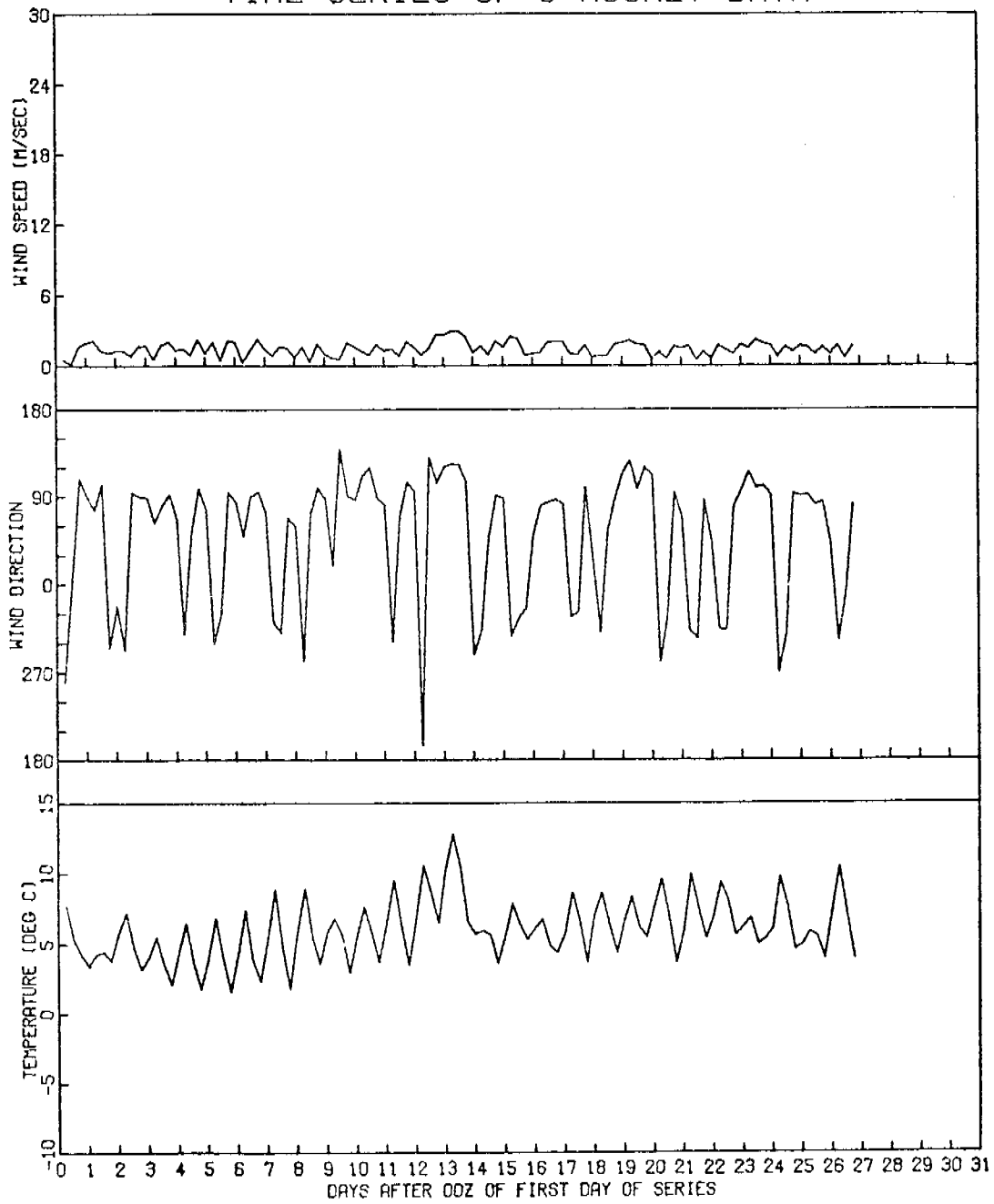




PT. MANBY 6 MAY TO 1 JUNE 1977
TIME SERIES OF 6 HOURLY DATA



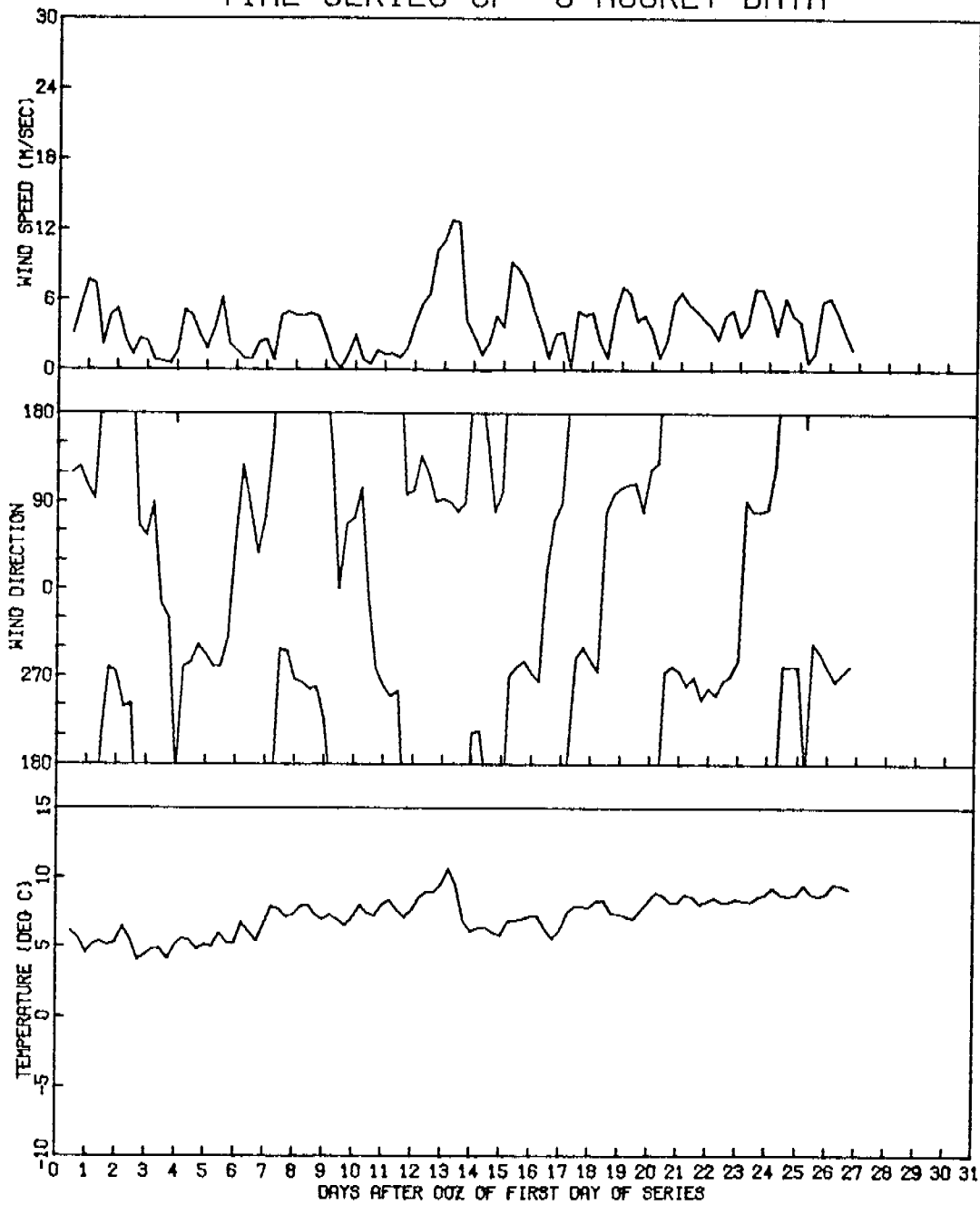
PT. RIOU 6 MAY TO 1 JUNE 1977
TIME SERIES OF 6 HOURLY DATA

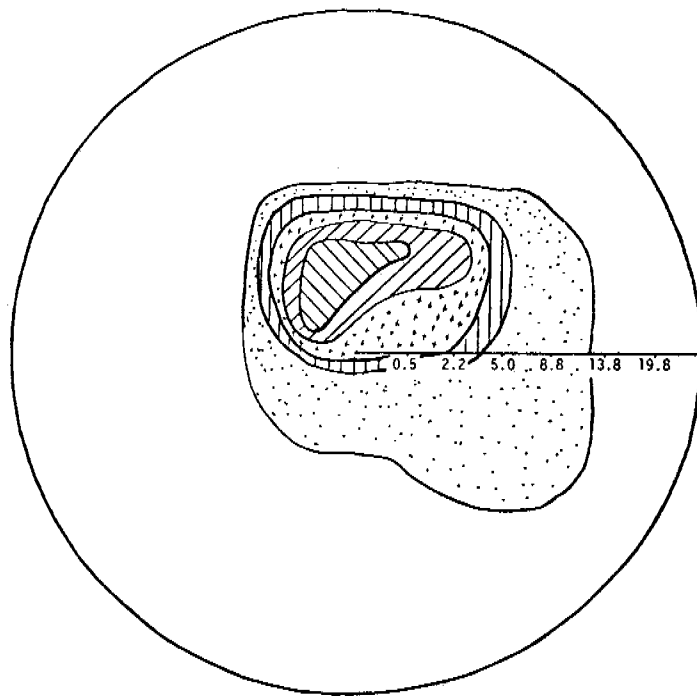
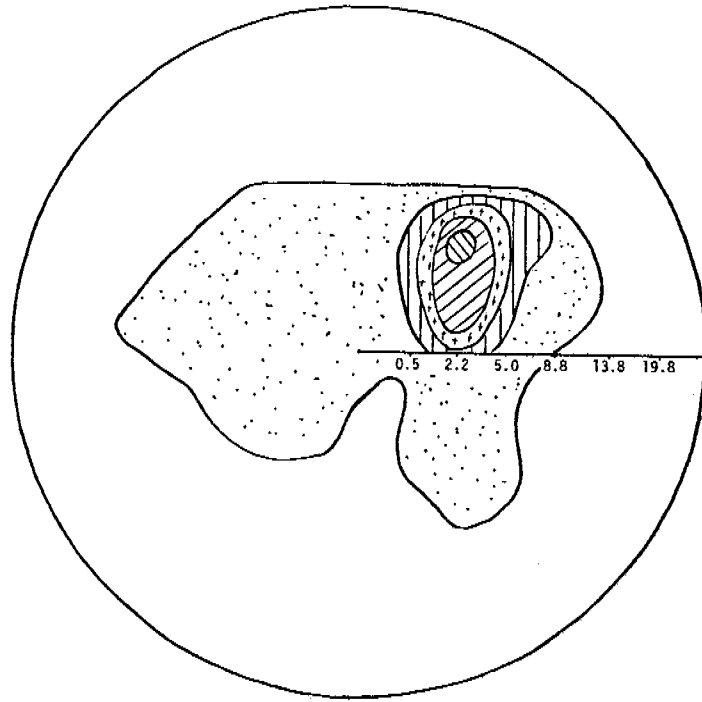


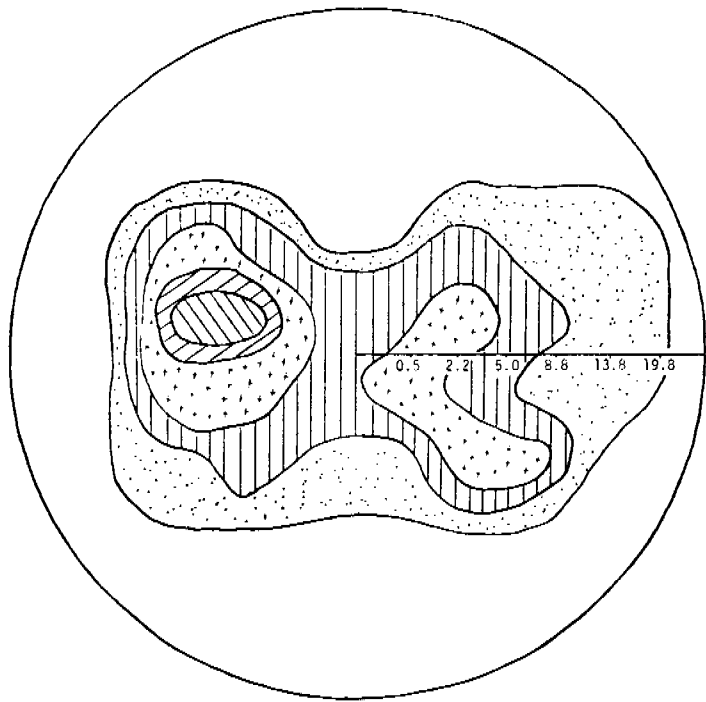
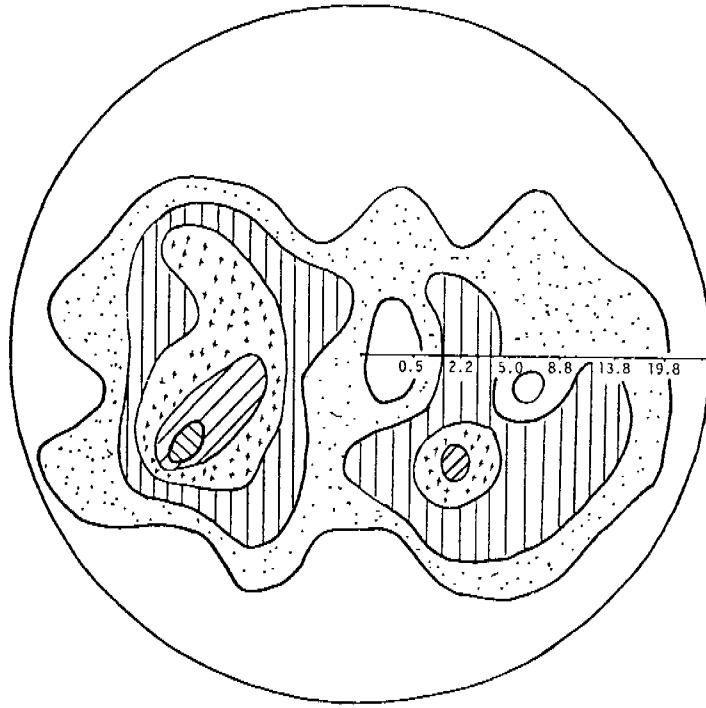
EB-43

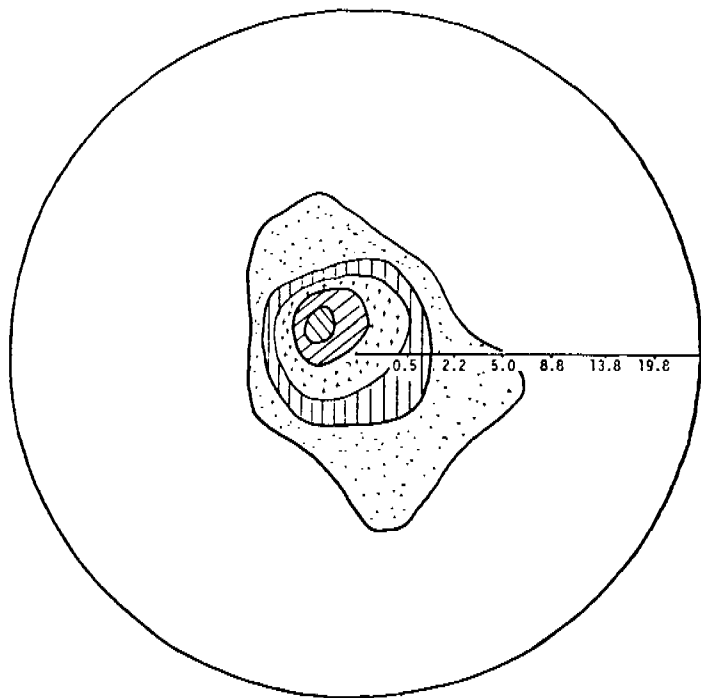
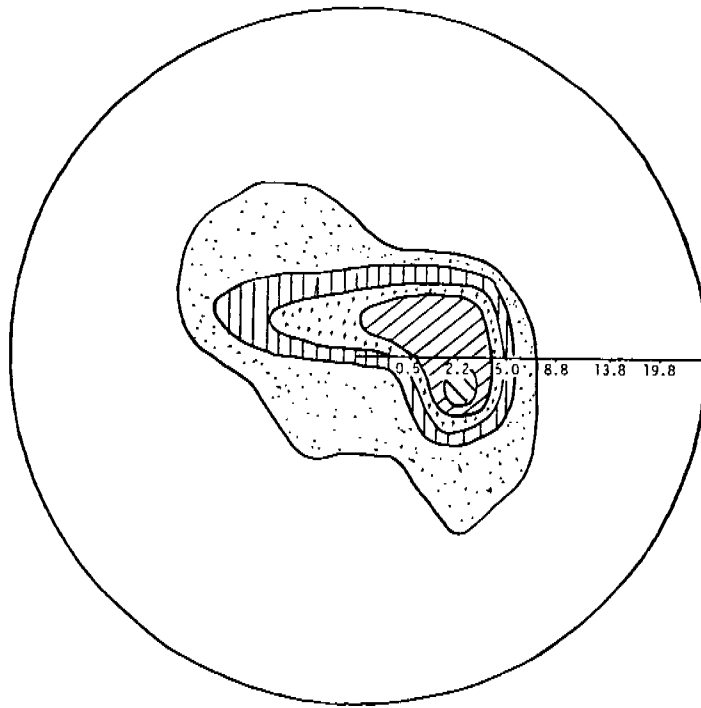
6 MAY THROUGH 1 JUN 1977

TIME SERIES OF 6 HOURLY DATA

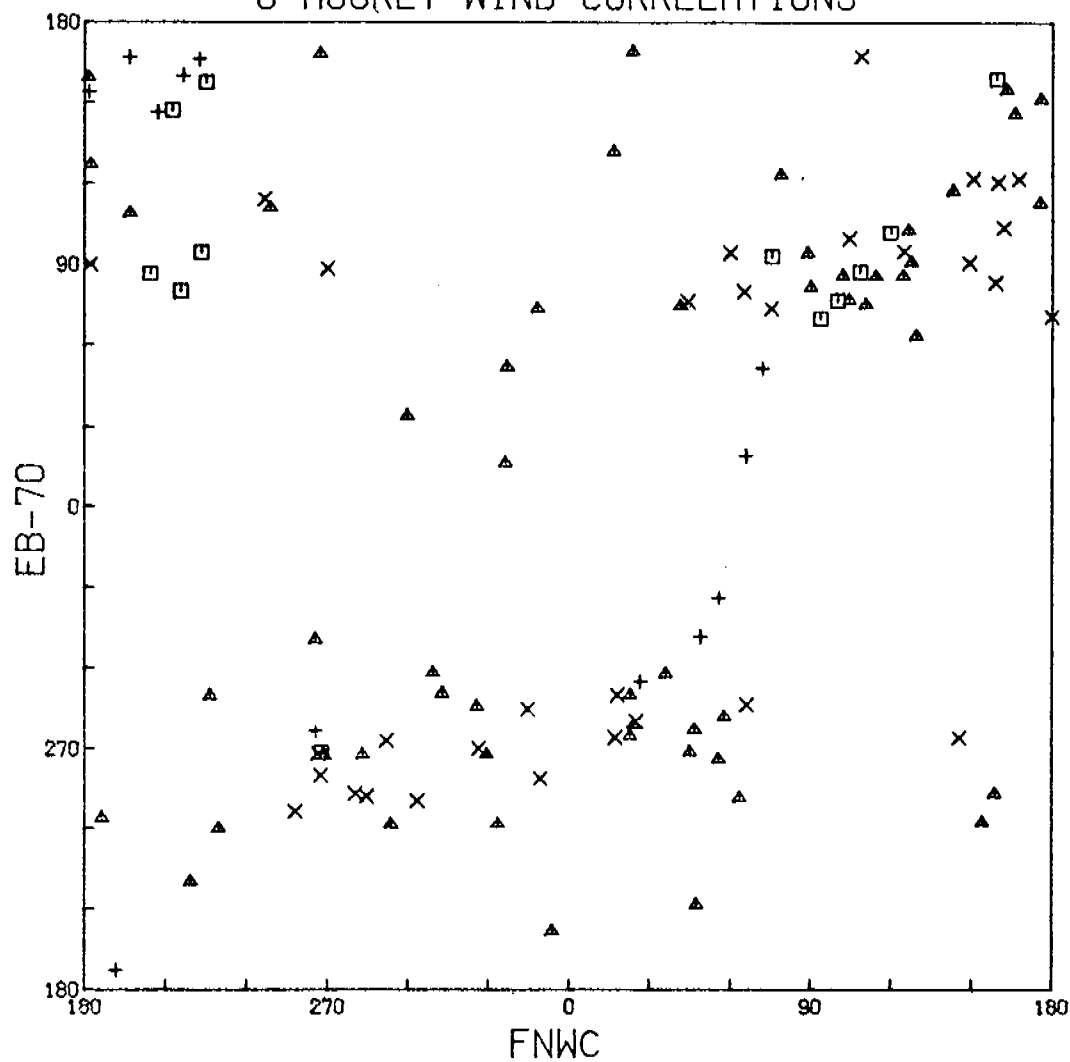






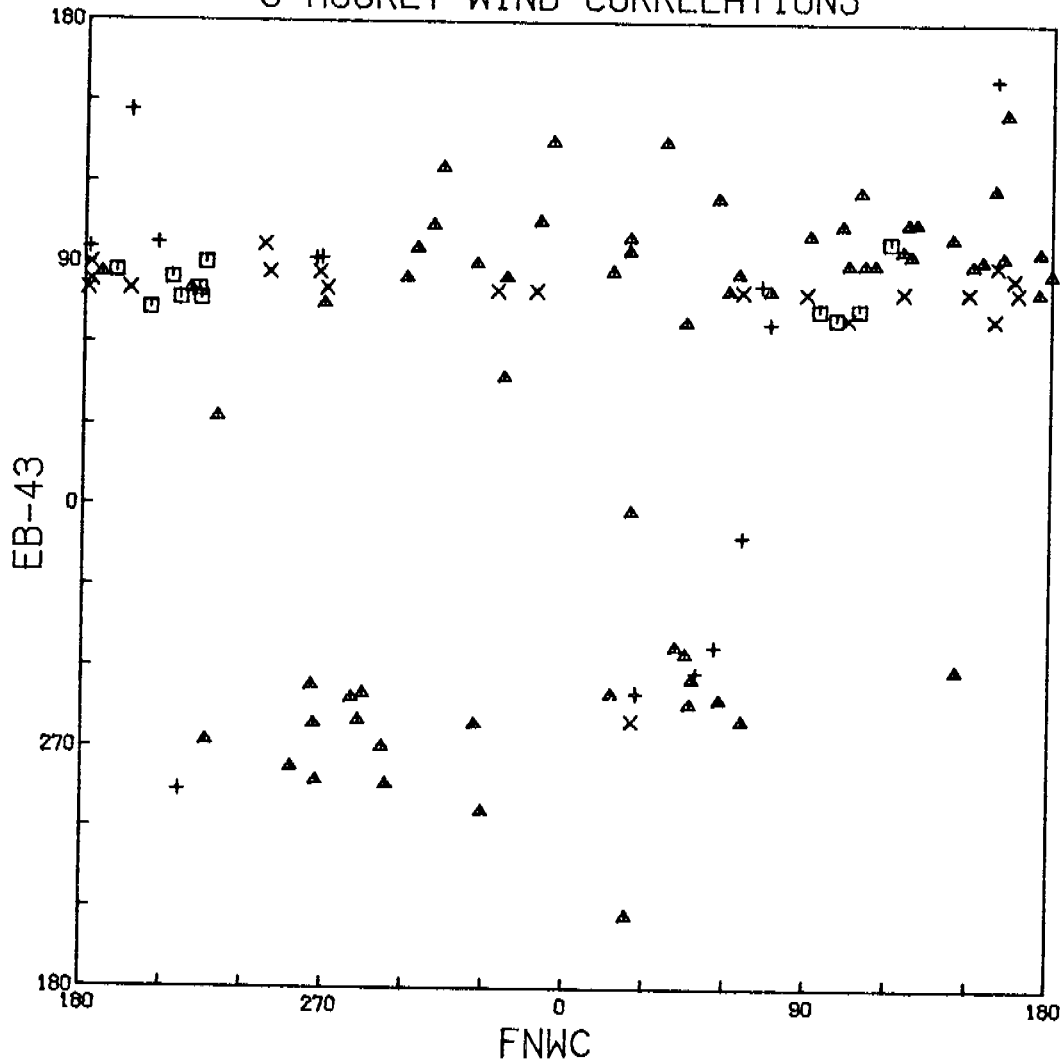


6 MARCH TO 3 APRIL 1977
6 HOURLY WIND CORRELATIONS



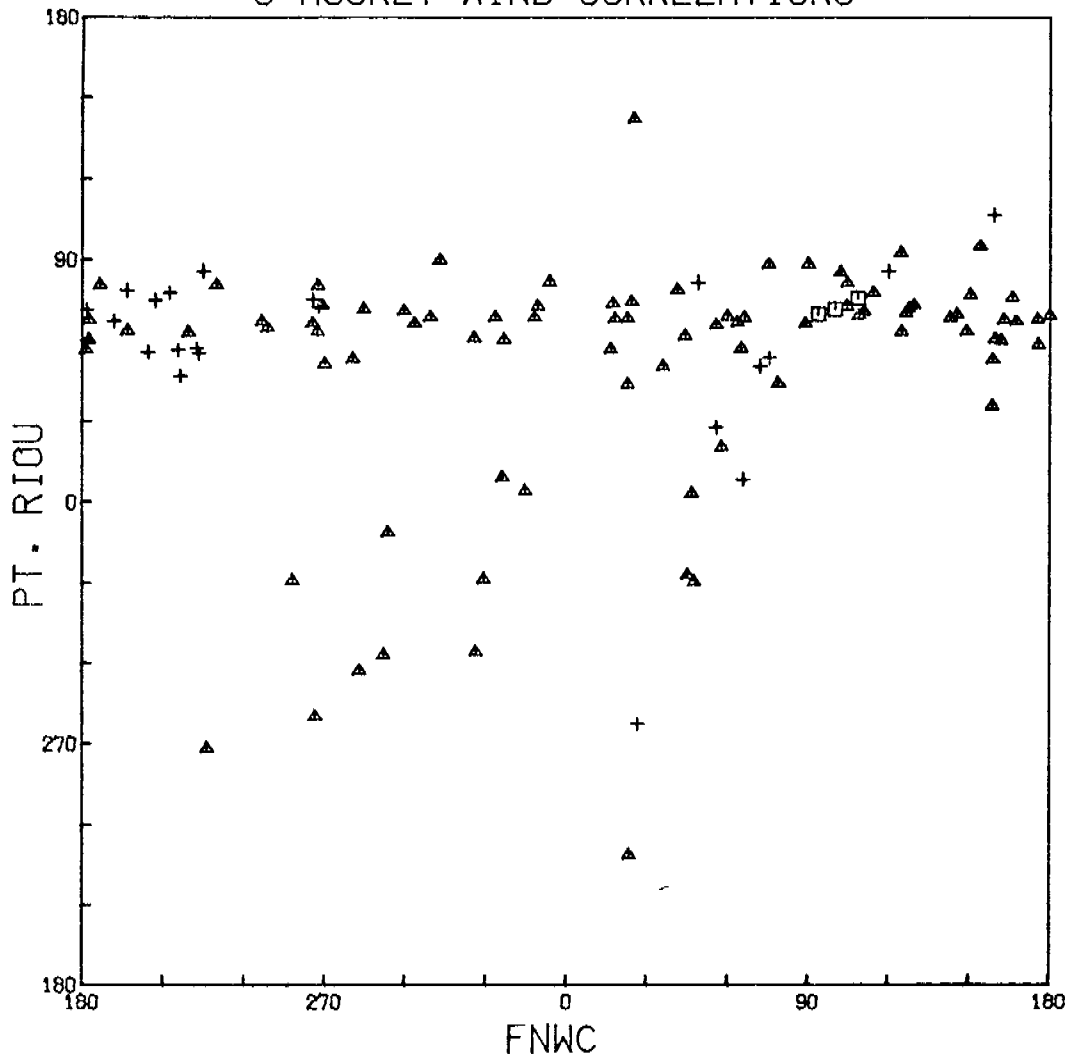
- = BOTH WINDS GREATER THAN 7 M/SEC
- △ = NEITHER WIND GREATER THAN 7 M/SEC
- × = ORDINATE WIND ONLY GREATER THAN 7 M/SEC
- + = ABSCISSA WIND ONLY GREATER THAN 7 M/SEC

6 MARCH TO 3 APRIL 1977
6 HOURLY WIND CORRELATIONS



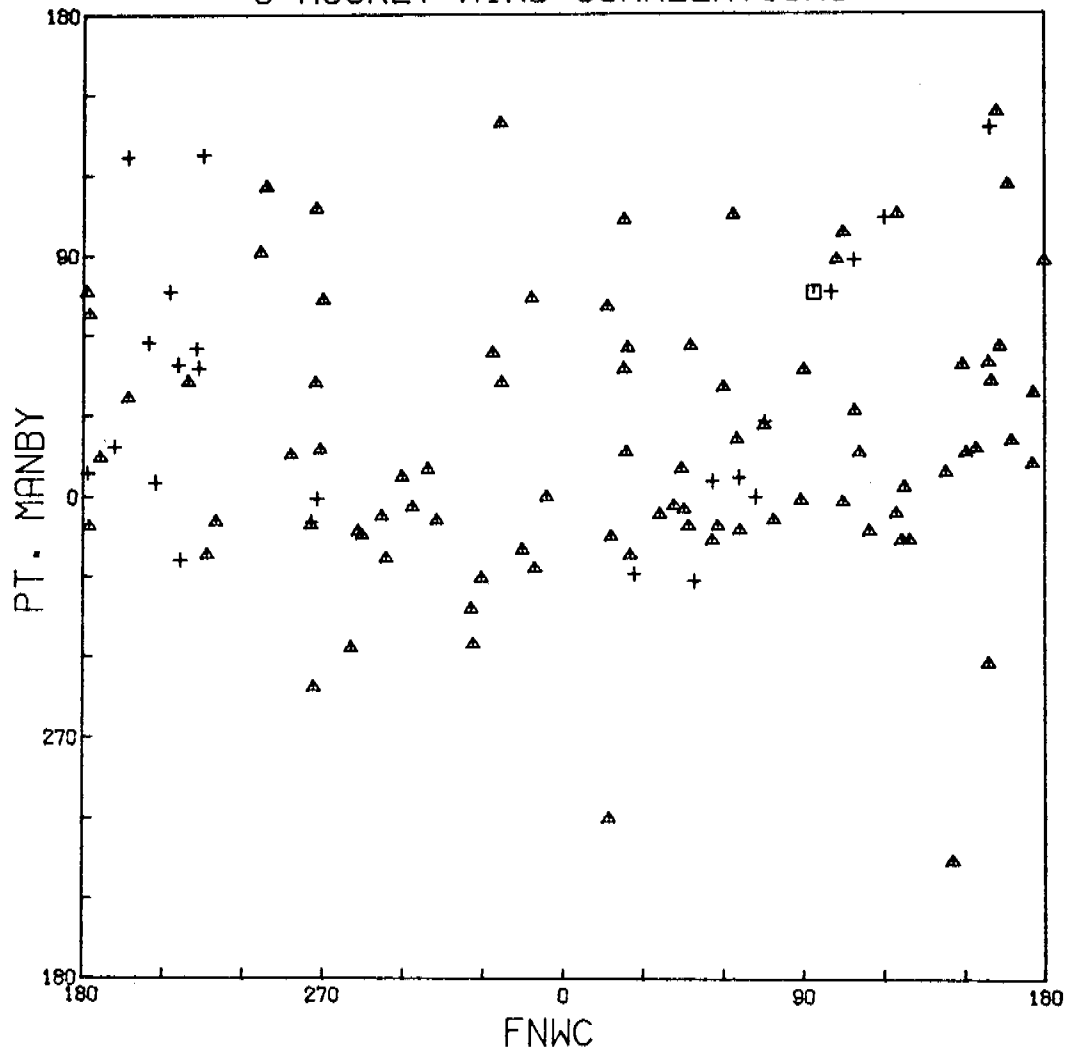
- = BOTH WINDS GREATER THAN 7 M/SEC
- ▲ = NEITHER WIND GREATER THAN 7 M/SEC
- × = ORDINATE WIND ONLY GREATER THAN 7 M/SEC
- + = ABSCISSA WIND ONLY GREATER THAN 7 M/SEC

6 MARCH TO 3 APRIL 1977
6 HOURLY WIND CORRELATIONS



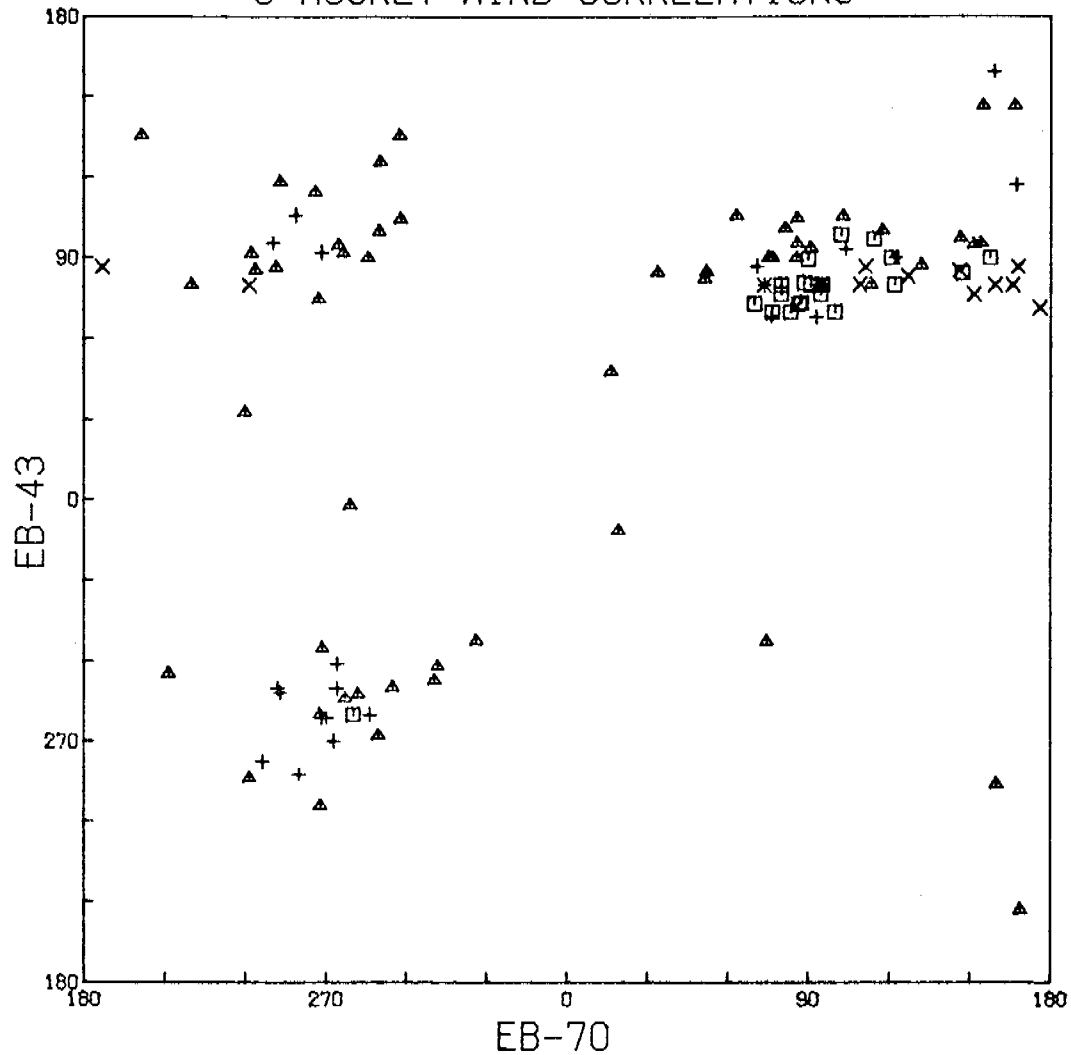
\square = BOTH WINDS GREATER THAN 7 M/SEC
 \triangle = NEITHER WIND GREATER THAN 7 M/SEC
 \times = ORDINATE WIND ONLY GREATER THAN 7 M/SEC
 $+$ = ABSCISSA WIND ONLY GREATER THAN 7 M/SEC

6 MARCH TO 3 APRIL 1977
6 HOURLY WIND CORRELATIONS



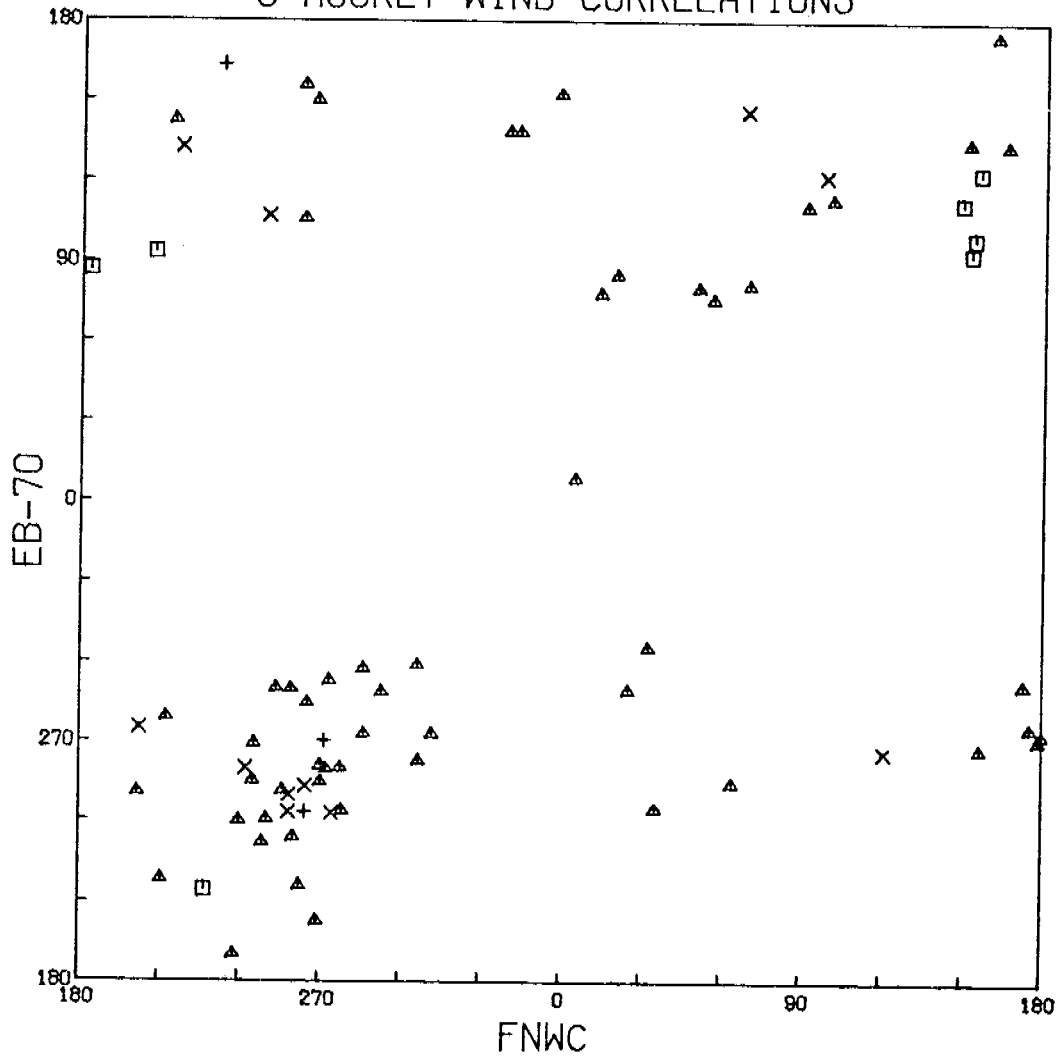
- = BOTH WINDS GREATER THAN 7 M/SEC
- ▲ = NEITHER WIND GREATER THAN 7 M/SEC
- × = ORDINATE WIND ONLY GREATER THAN 7 M/SEC
- + = ABSCISSA WIND ONLY GREATER THAN 7 M/SEC

6 MARCH TO 3 APRIL 1977
6 HOURLY WIND CORRELATIONS



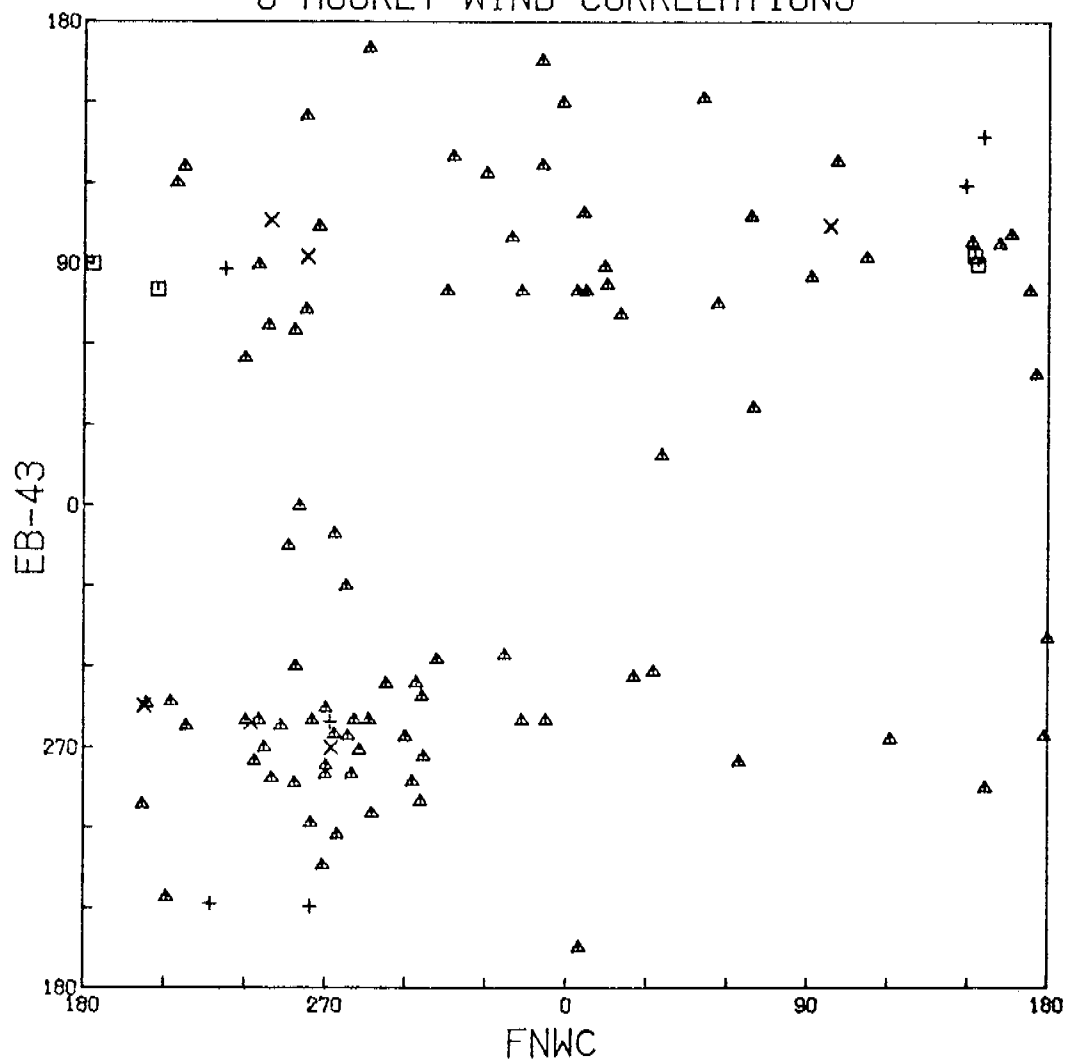
- = BOTH WINDS GREATER THAN 7 M/SEC
- △ = NEITHER WIND GREATER THAN 7 M/SEC
- × = ORDINATE WIND ONLY GREATER THAN 7 M/SEC
- + = ABSCISSA WIND ONLY GREATER THAN 7 M/SEC

6 MAY TO 1 JUNE 1977
6 HOURLY WIND CORRELATIONS



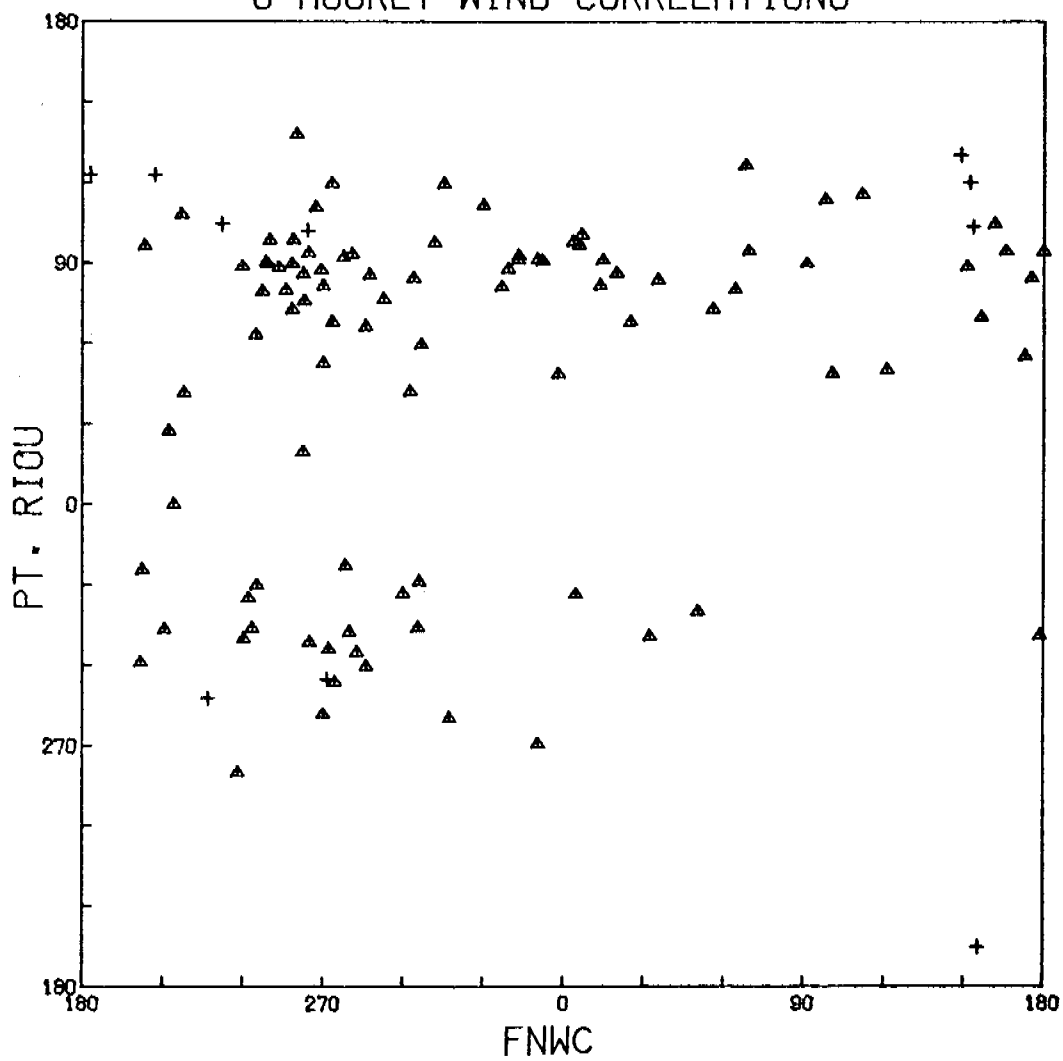
- = BOTH WINDS GREATER THAN 7 M/SEC
- △ = NEITHER WIND GREATER THAN 7 M/SEC
- × = ORDINATE WIND ONLY GREATER THAN 7 M/SEC
- + = ABSCISSA WIND ONLY GREATER THAN 7 M/SEC

6 MAY TO 1 JUNE 1977
6 HOURLY WIND CORRELATIONS



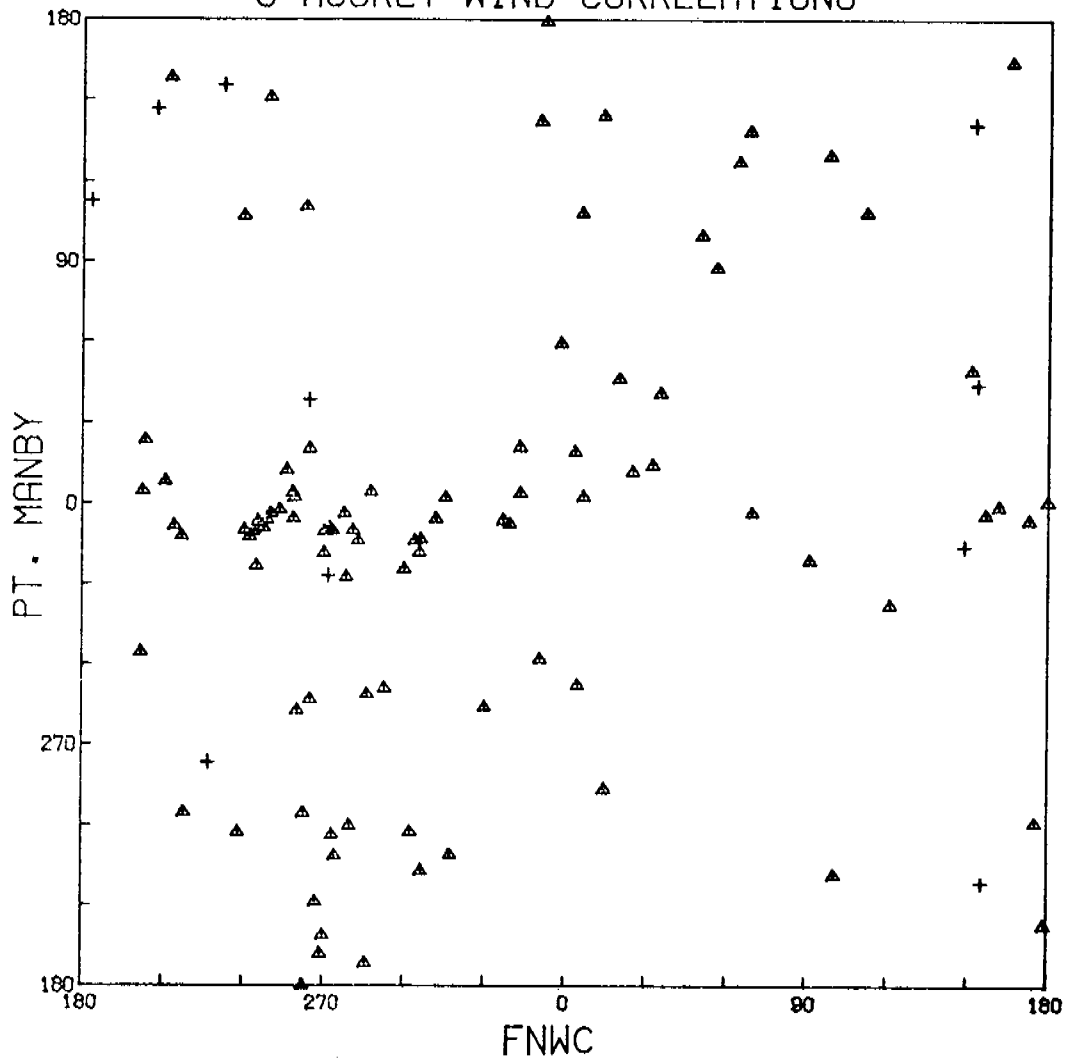
- = BOTH WINDS GREATER THAN 7 M/SEC
- △ = NEITHER WIND GREATER THAN 7 M/SEC
- × = ORDINATE WIND ONLY GREATER THAN 7 M/SEC
- + = ABSCISSA WIND ONLY GREATER THAN 7 M/SEC

6 MAY TO 1 JUNE 1977
6 HOURLY WIND CORRELATIONS



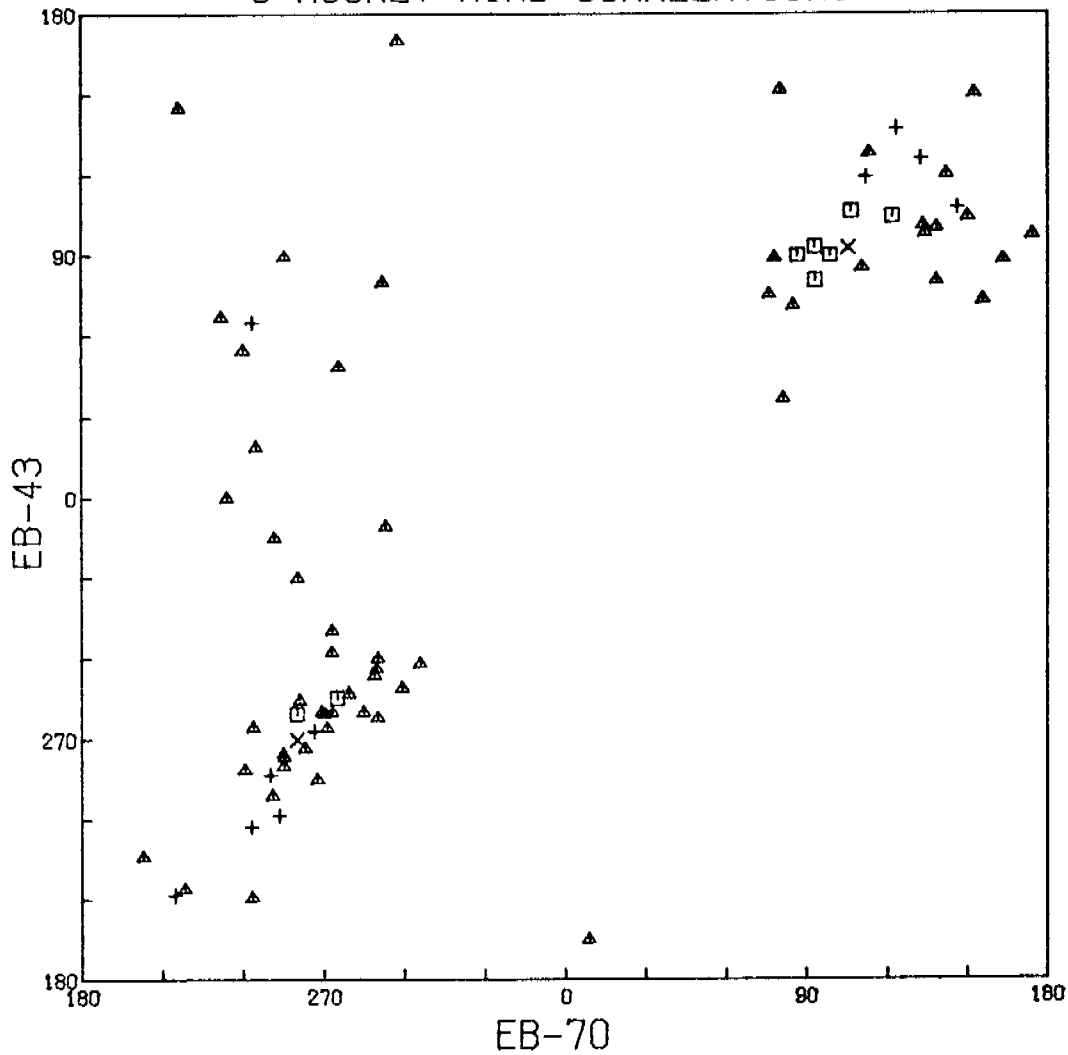
- = BOTH WINDS GREATER THAN 7 M/SEC
- △ = NEITHER WIND GREATER THAN 7 M/SEC
- × = ORDINATE WIND ONLY GREATER THAN 7 M/SEC
- + = ABSCISSA WIND ONLY GREATER THAN 7 M/SEC

6 MAY TO 1 JUNE 1977
6 HOURLY WIND CORRELATIONS

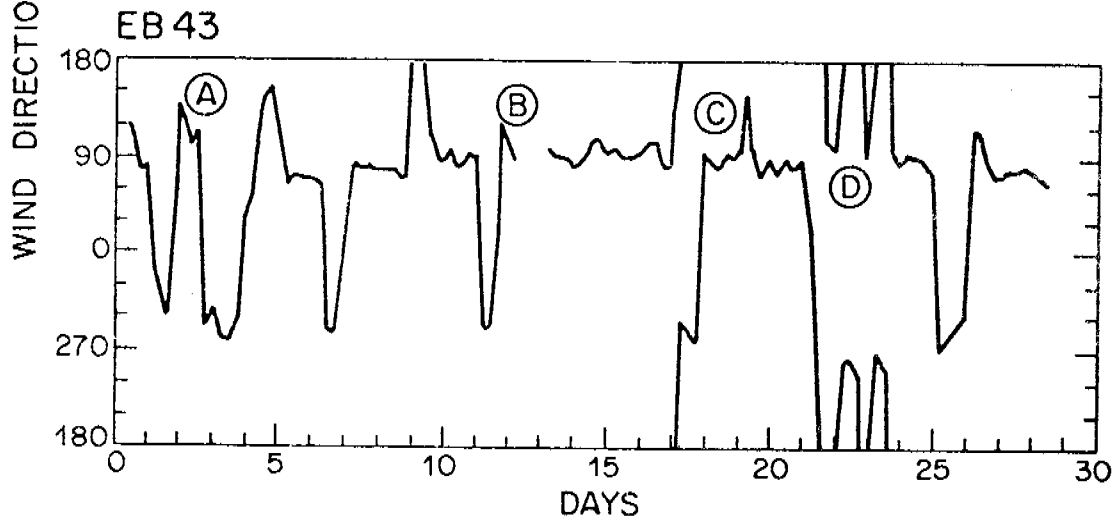
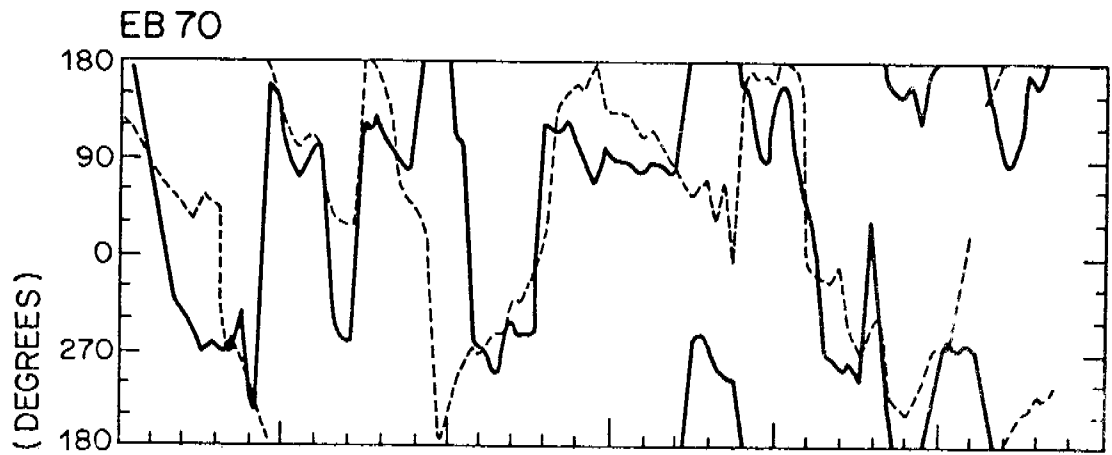


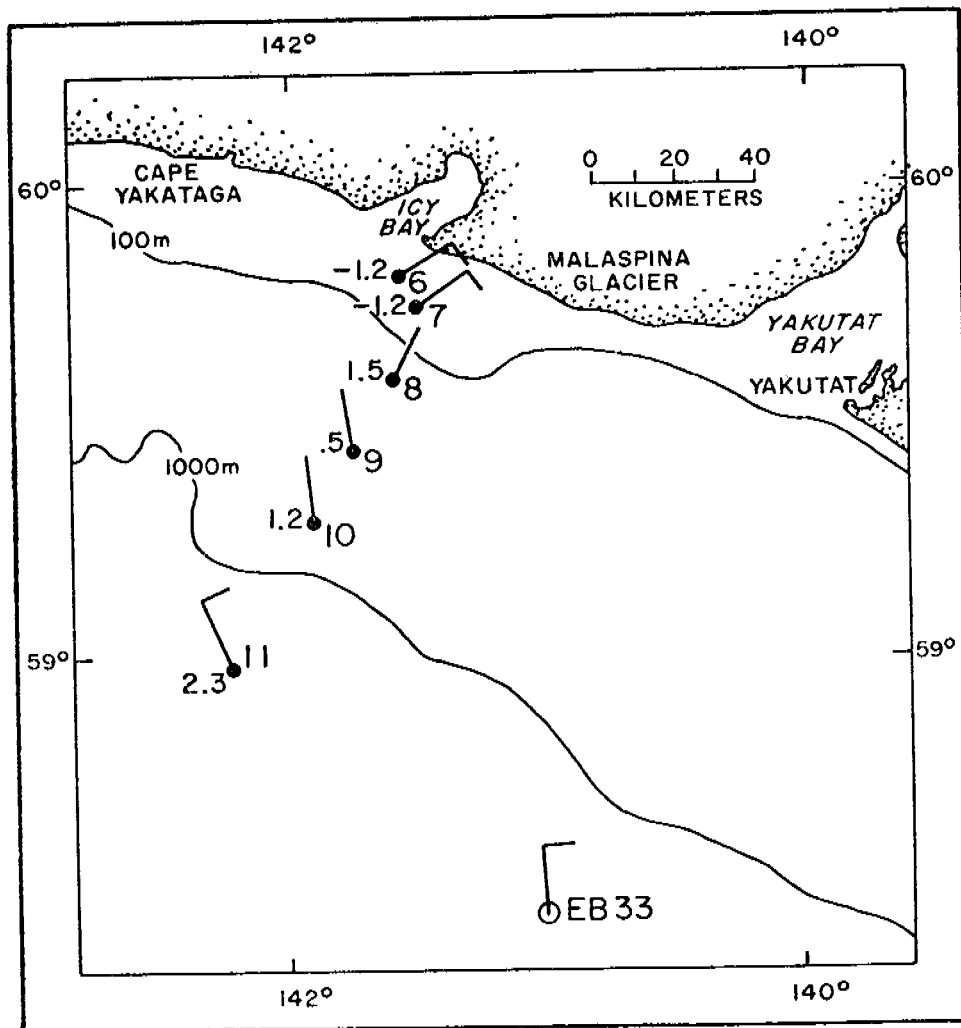
- = BOTH WINDS GREATER THAN 7 M/SEC
- △ = NEITHER WIND GREATER THAN 7 M/SEC
- × = ORDINATE WIND ONLY GREATER THAN 7 M/SEC
- + = ABSCISSA WIND ONLY GREATER THAN 7 M/SEC

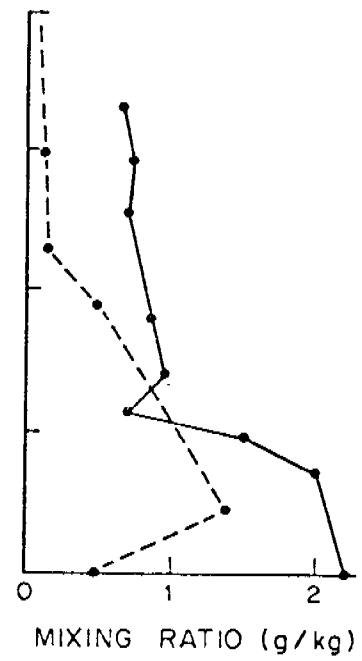
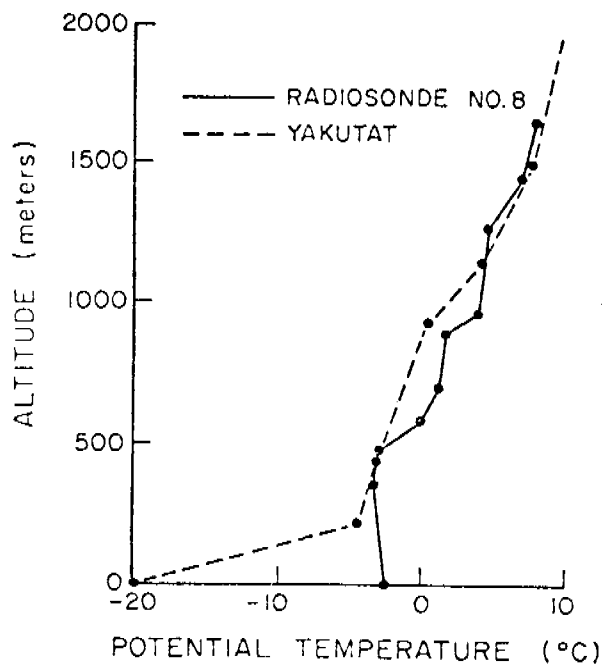
6 MAY TO 1 JUNE 1977
6 HOURLY WIND CORRELATIONS

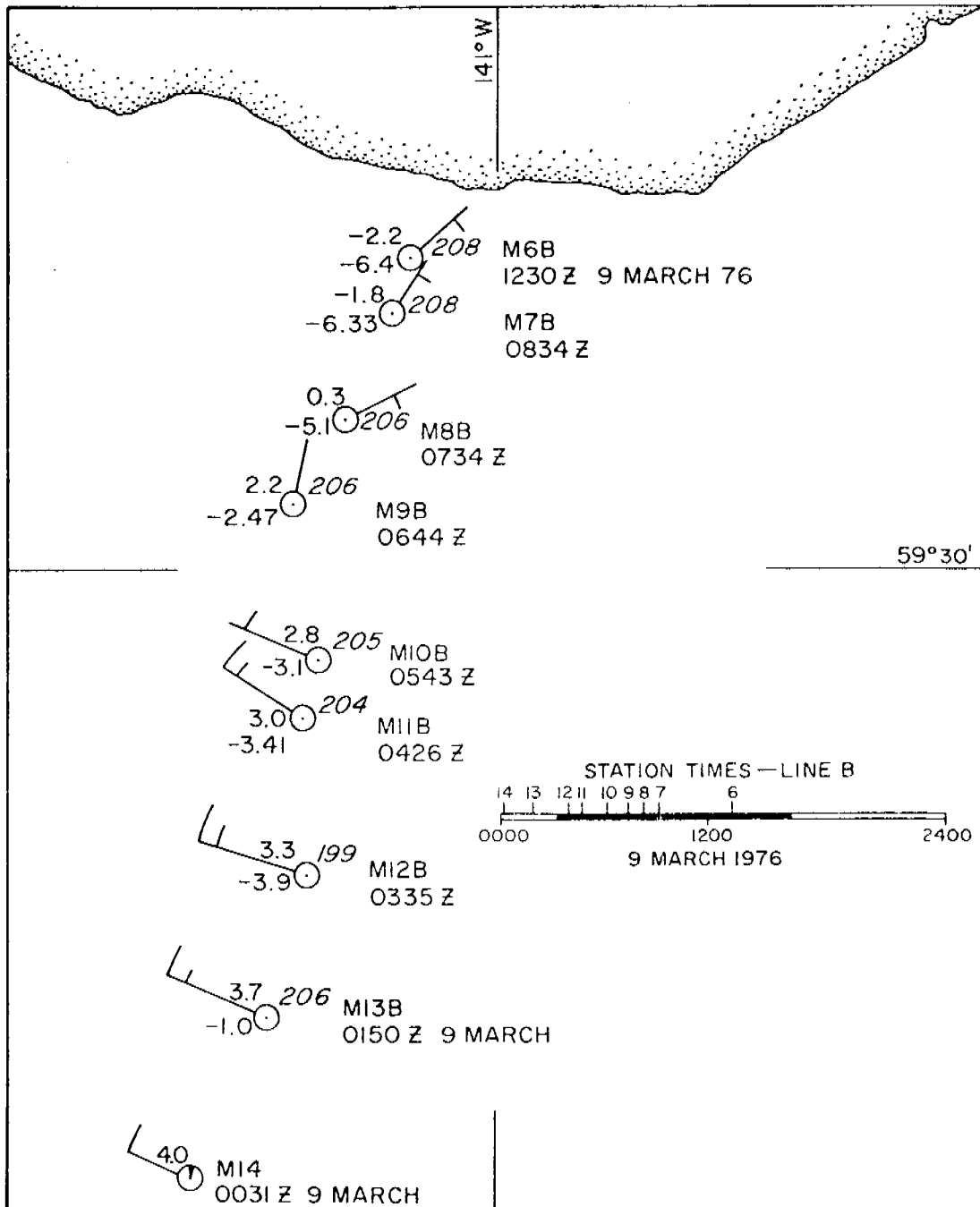


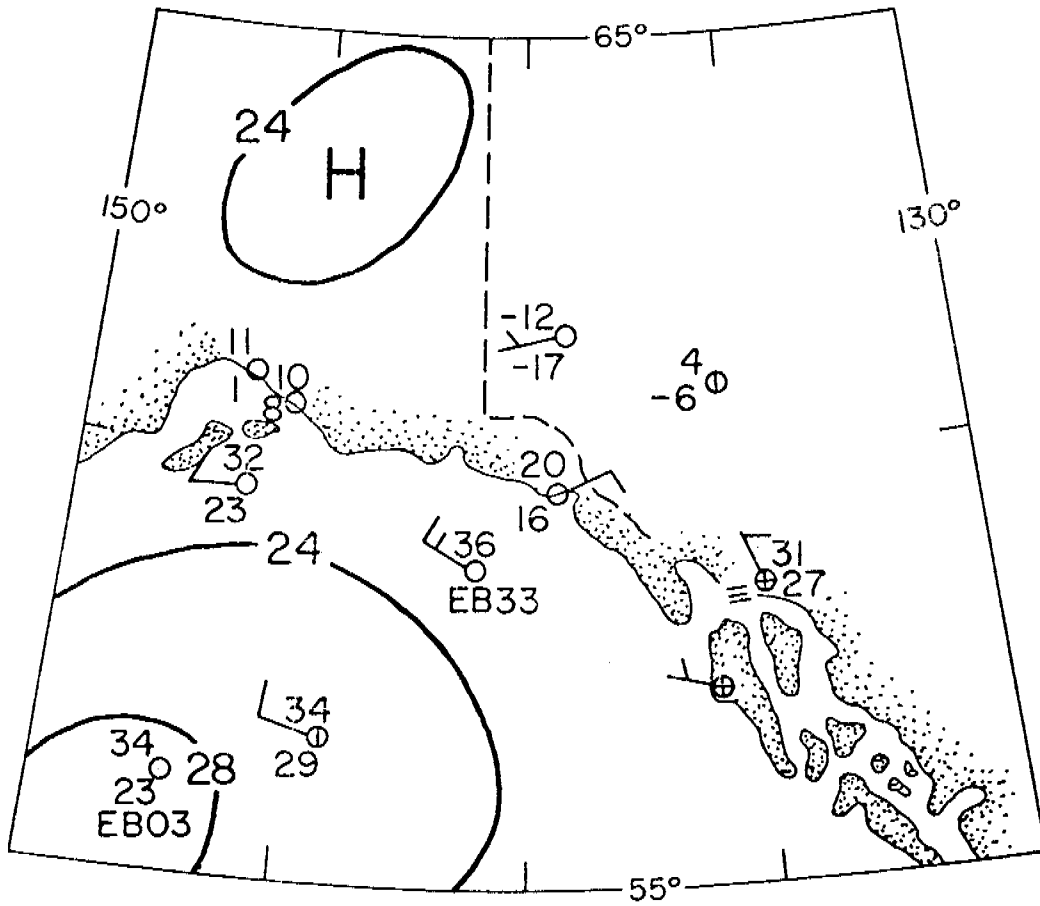
\square = BOTH WINDS GREATER THAN 7 M/SEC
 \triangle = NEITHER WIND GREATER THAN 7 M/SEC
 \times = ORDINATE WIND ONLY GREATER THAN 7 M/SEC
 $+$ = ABSCISSA WIND ONLY GREATER THAN 7 M/SEC

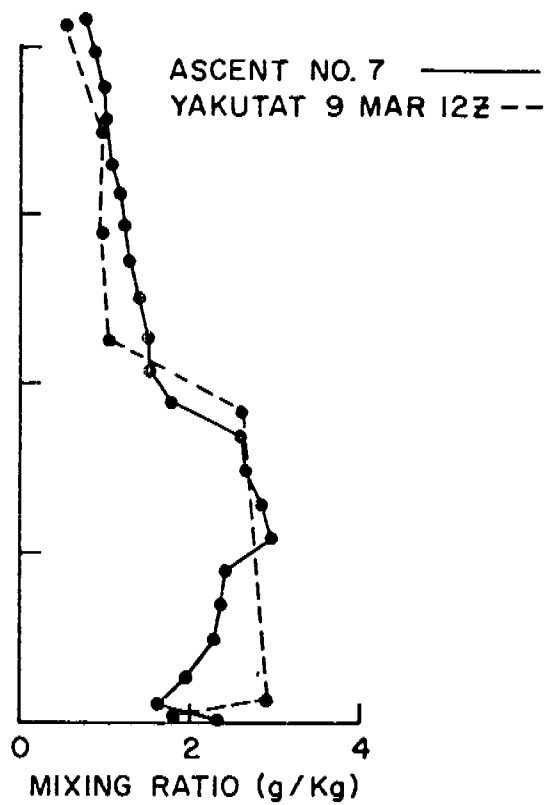
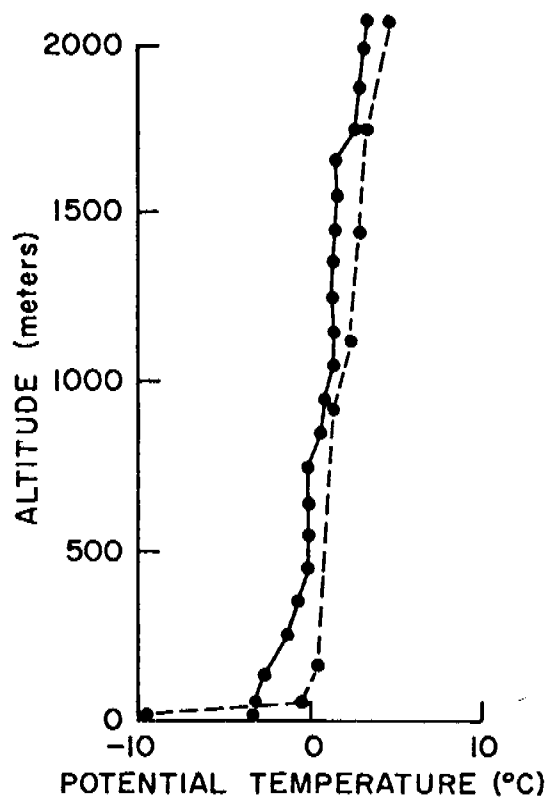


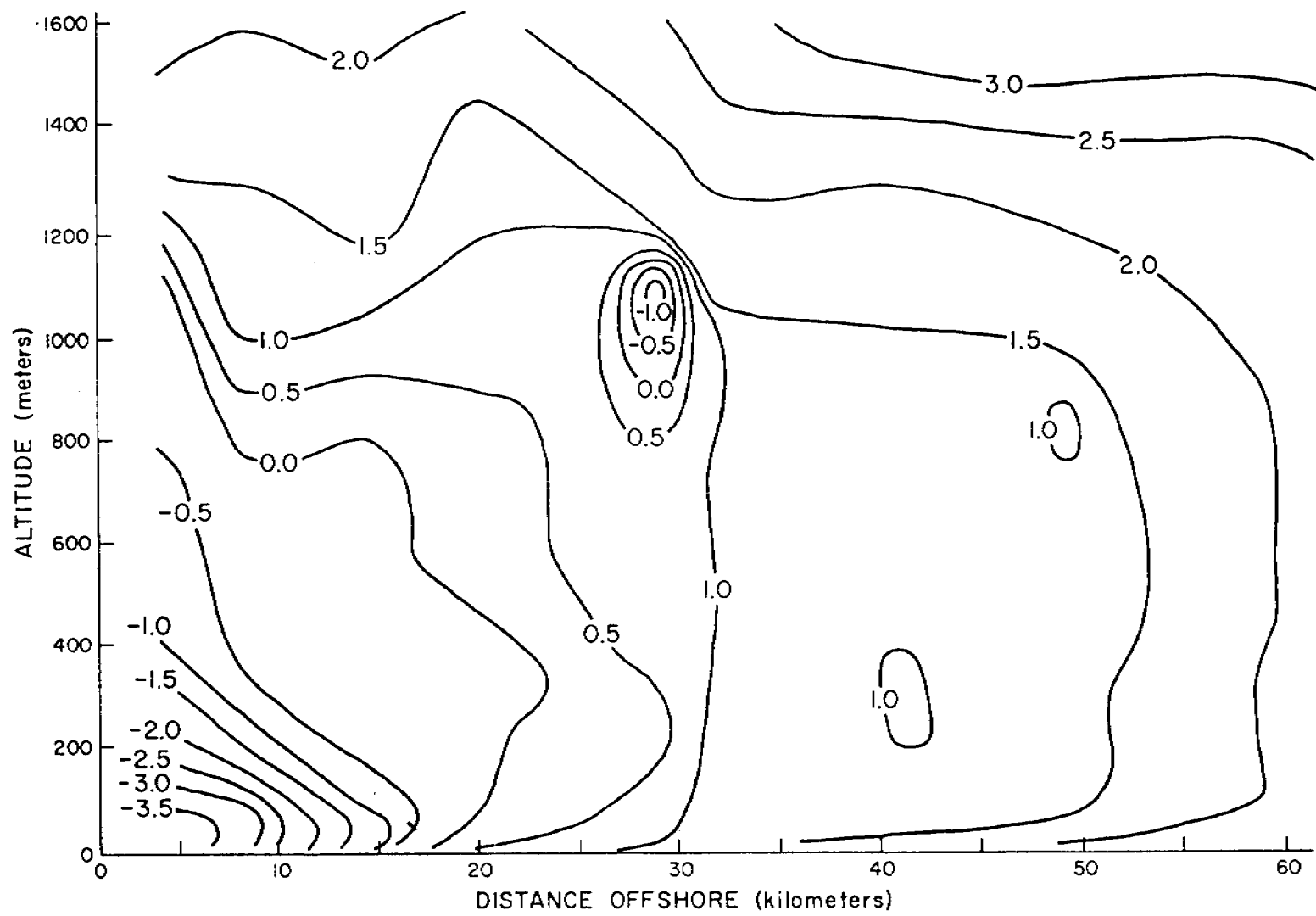


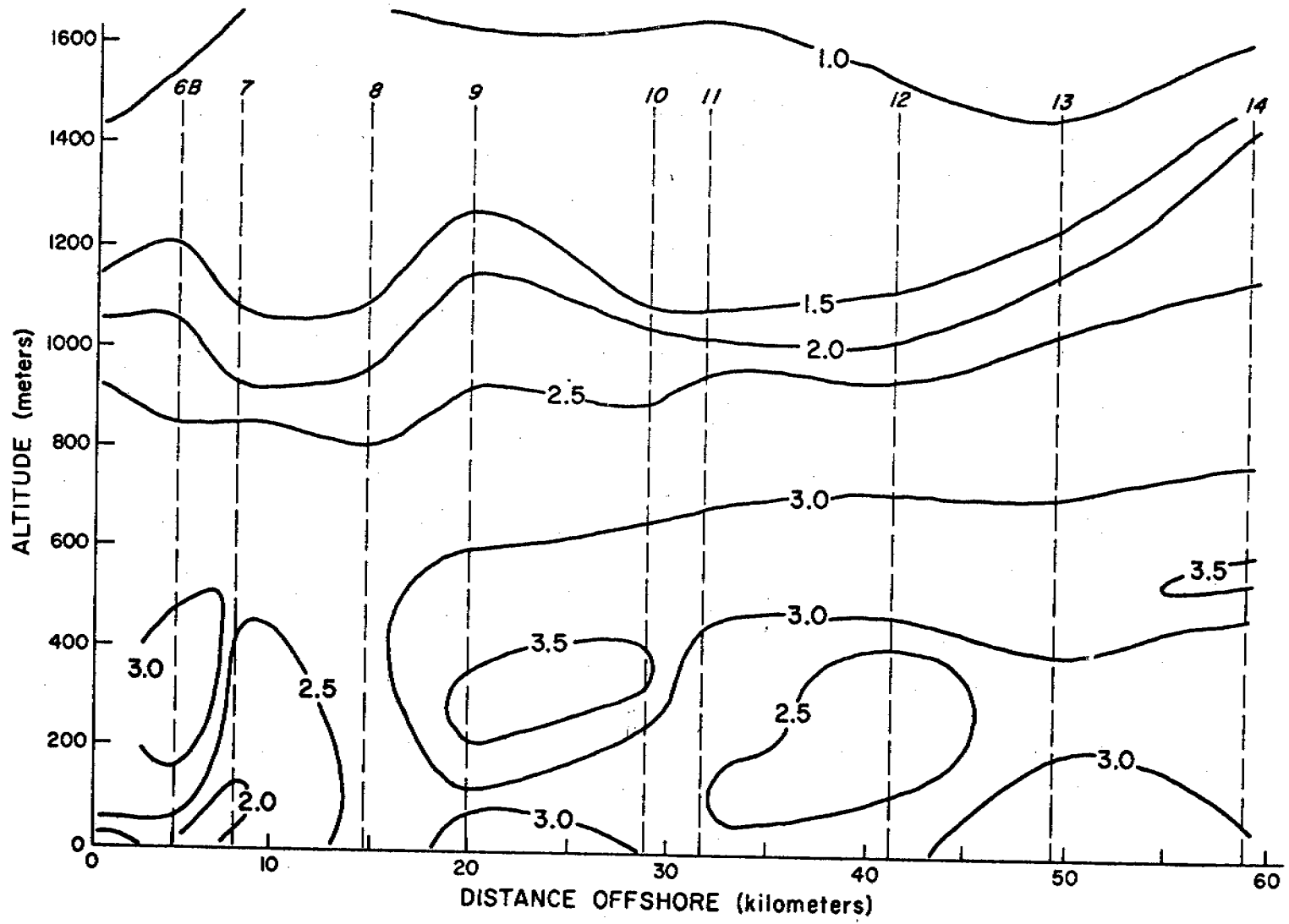


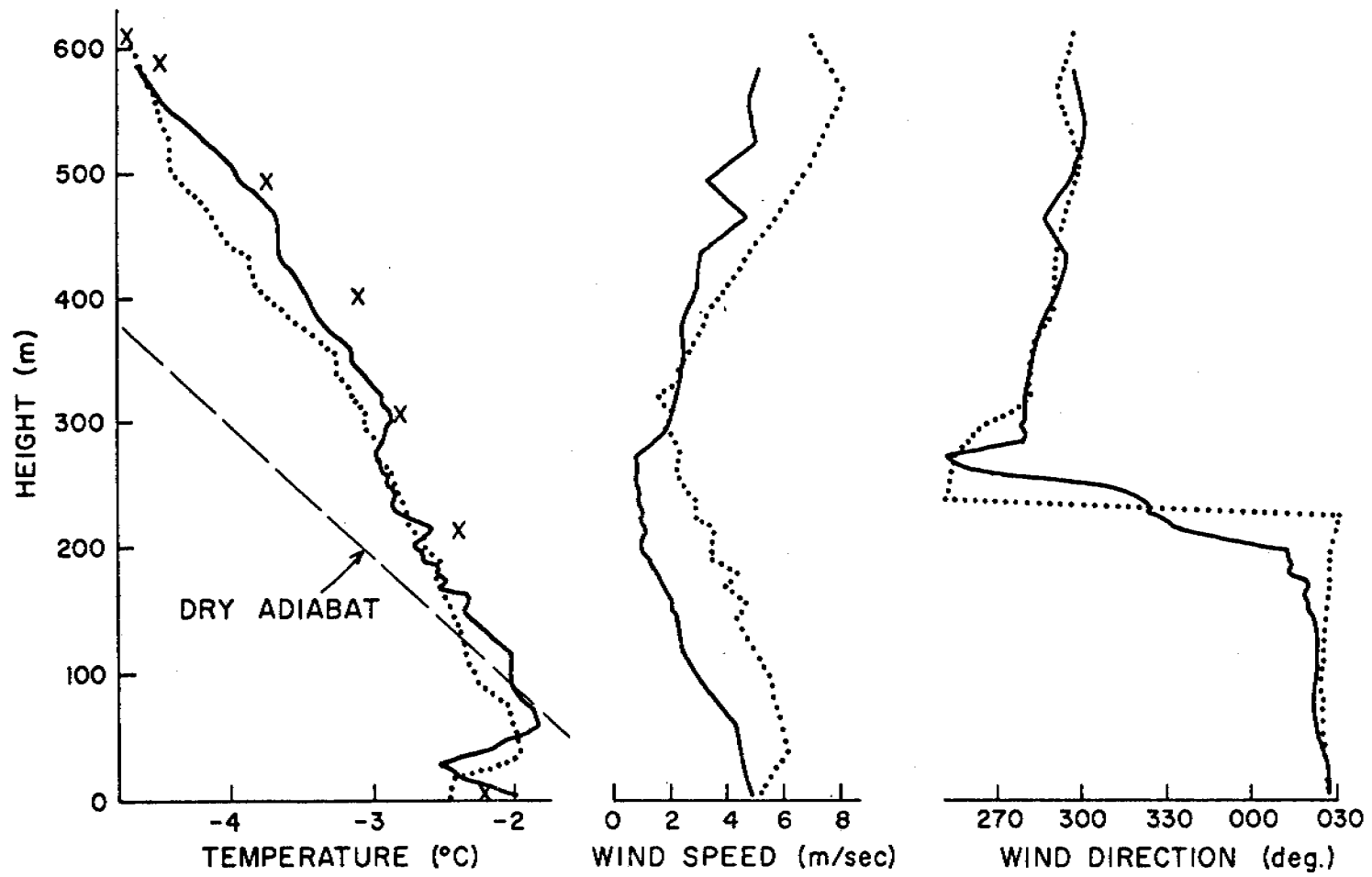




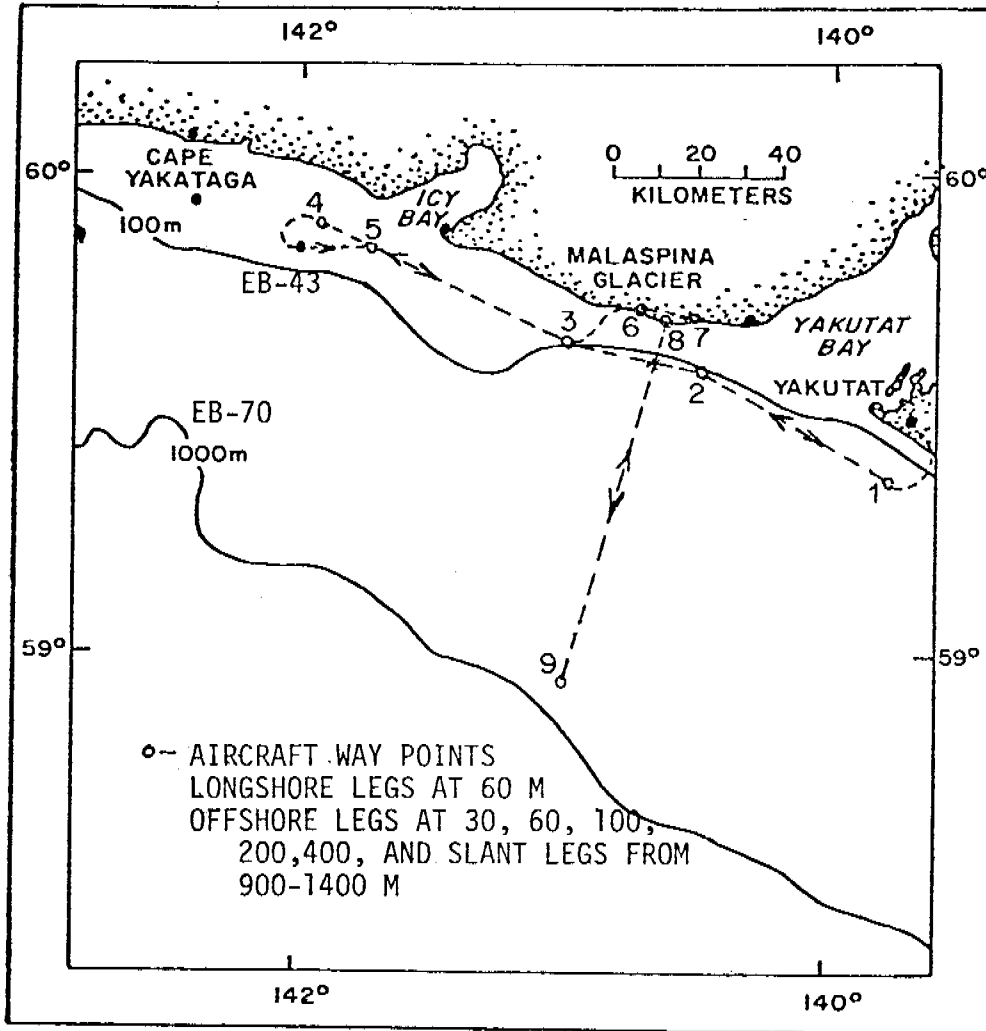


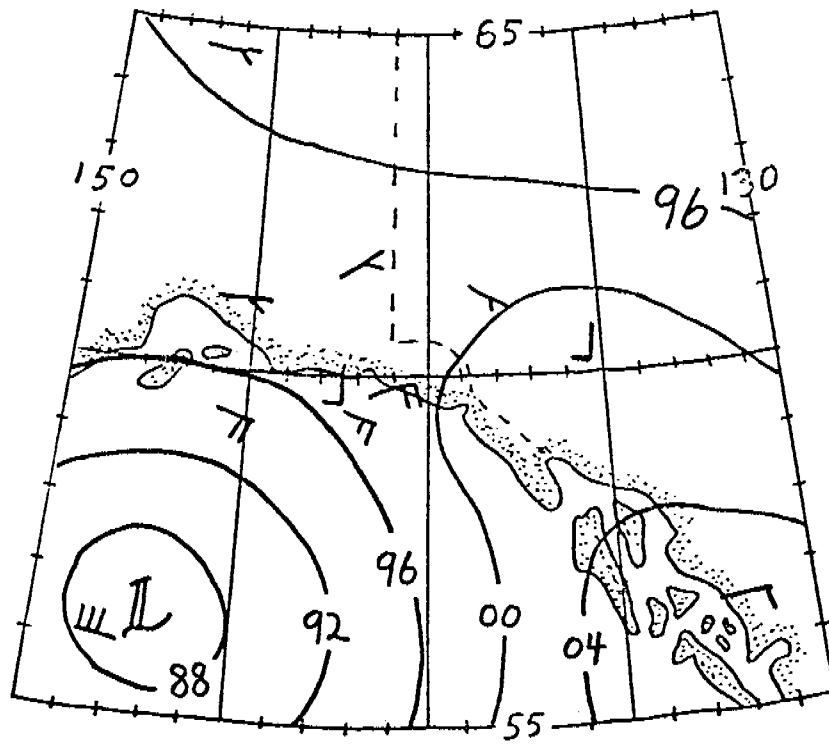
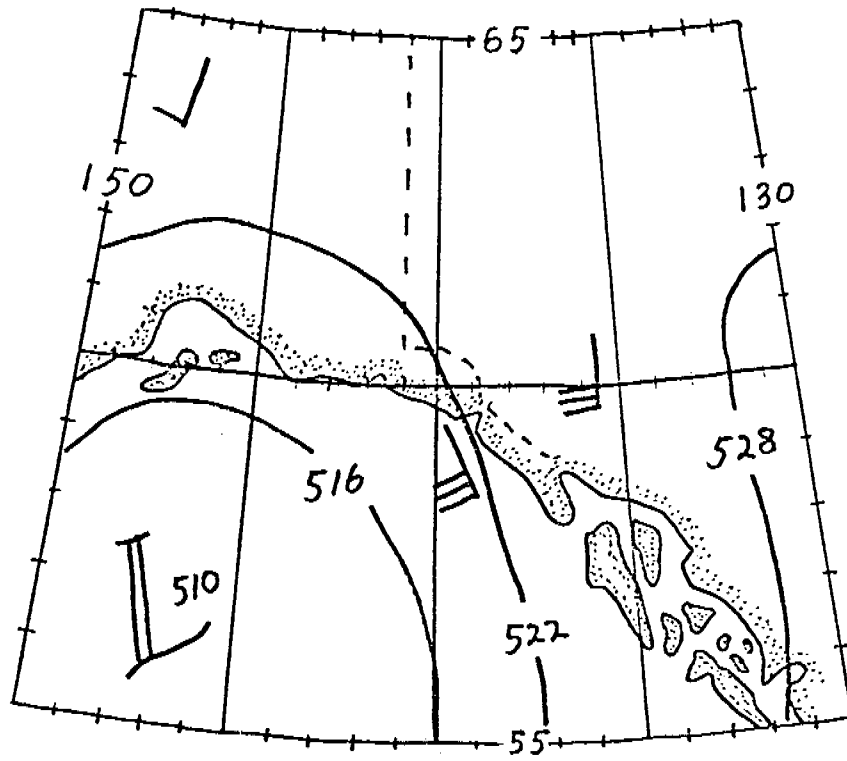


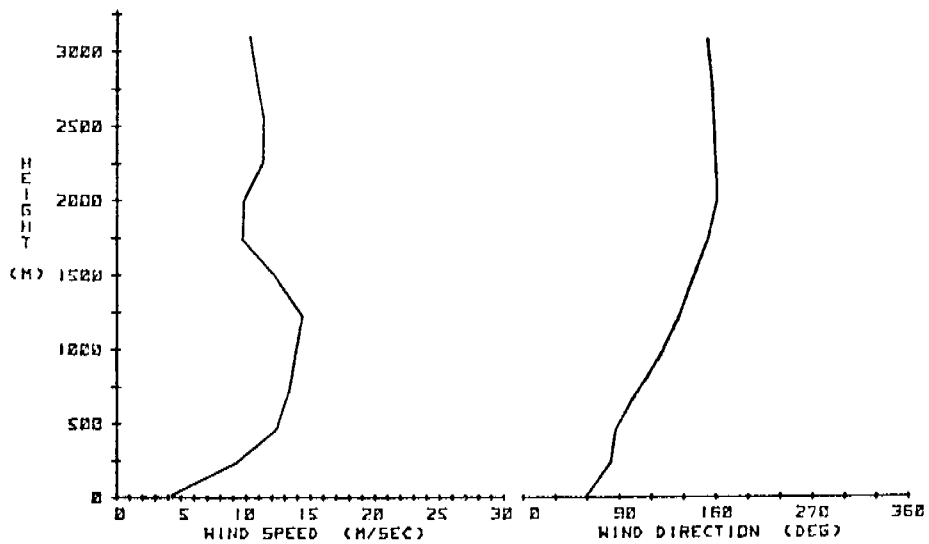
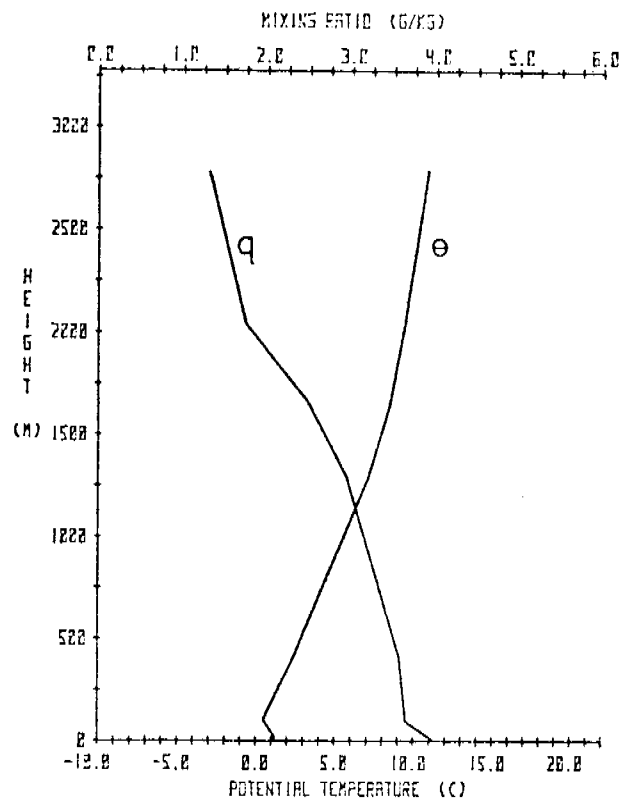


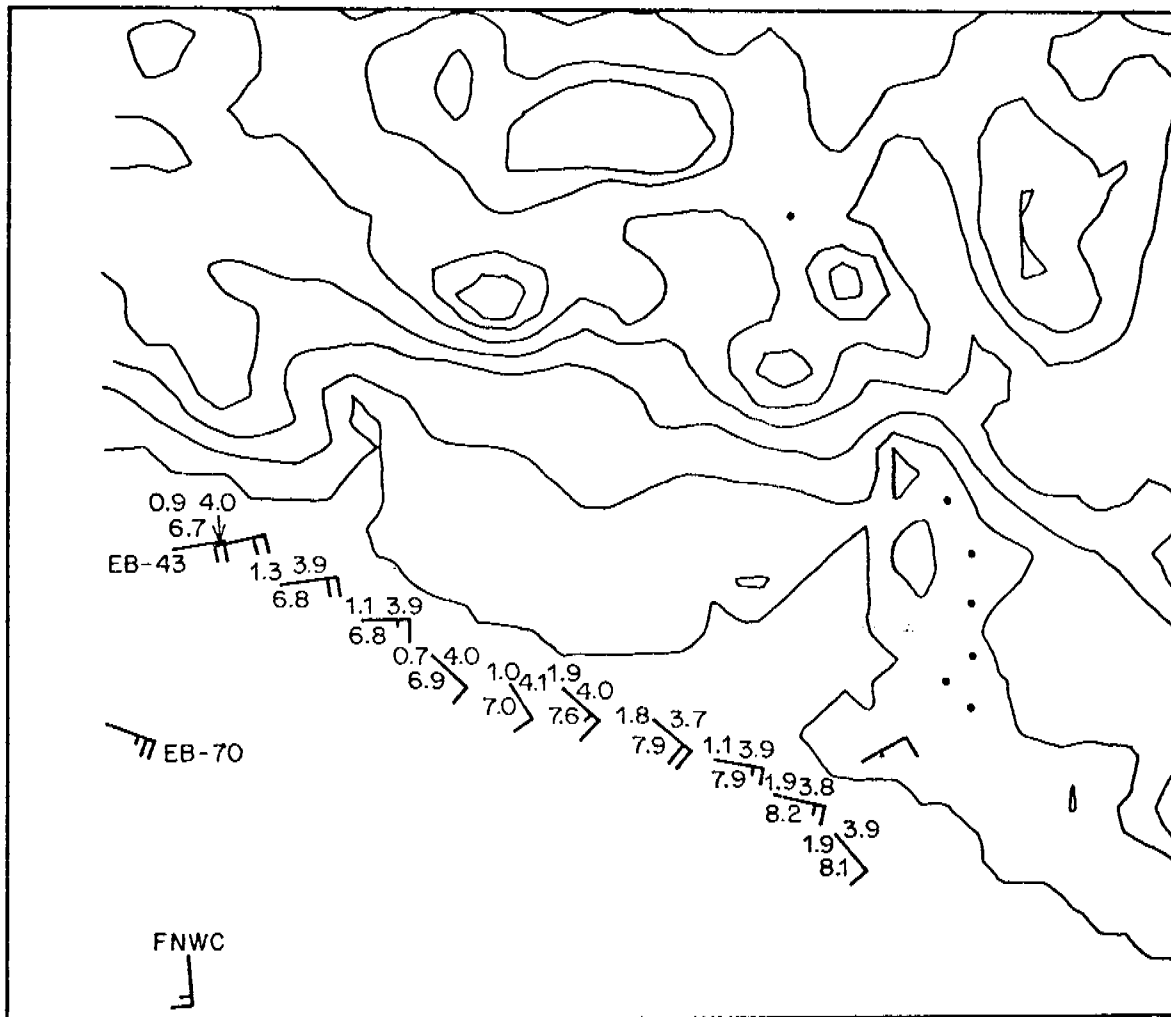


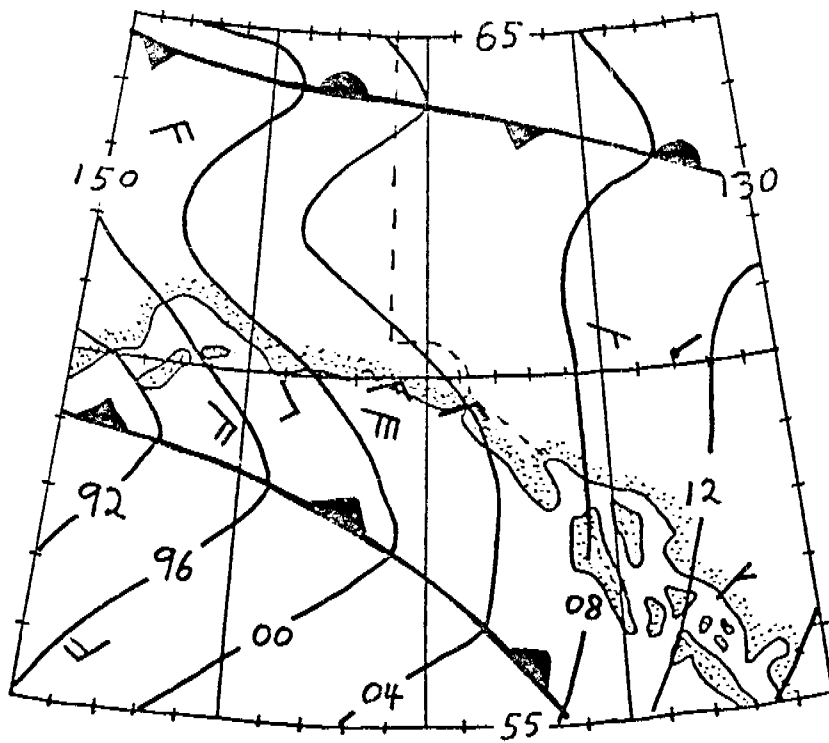
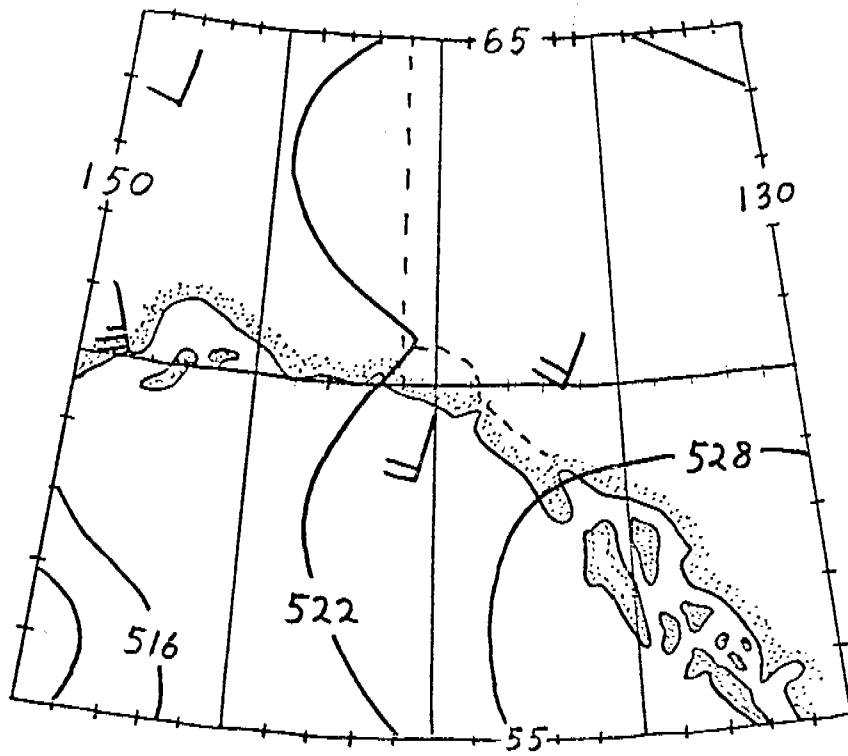


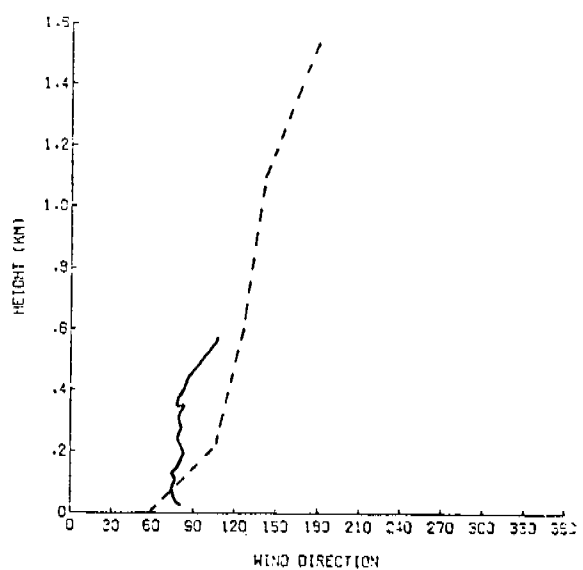
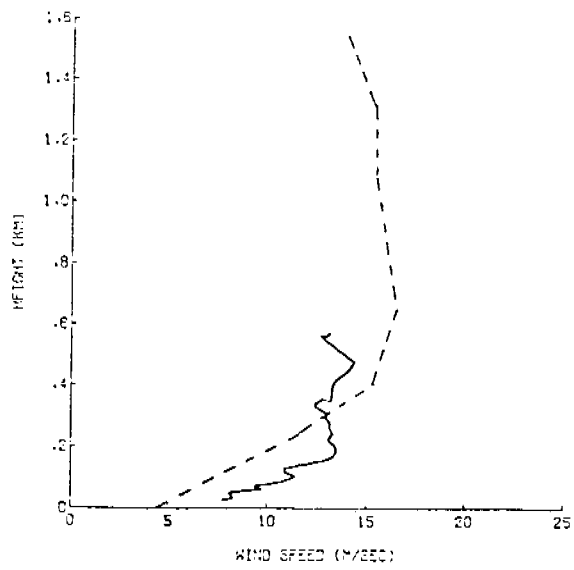
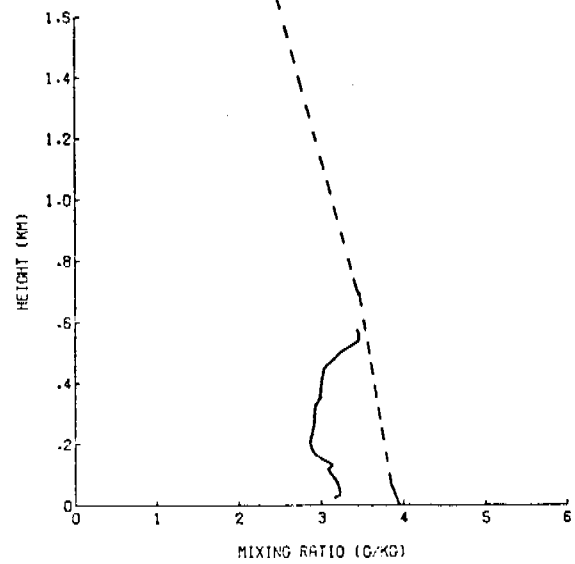
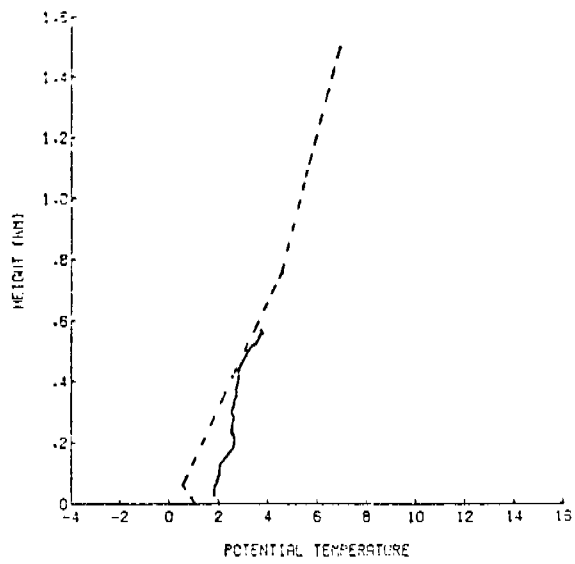


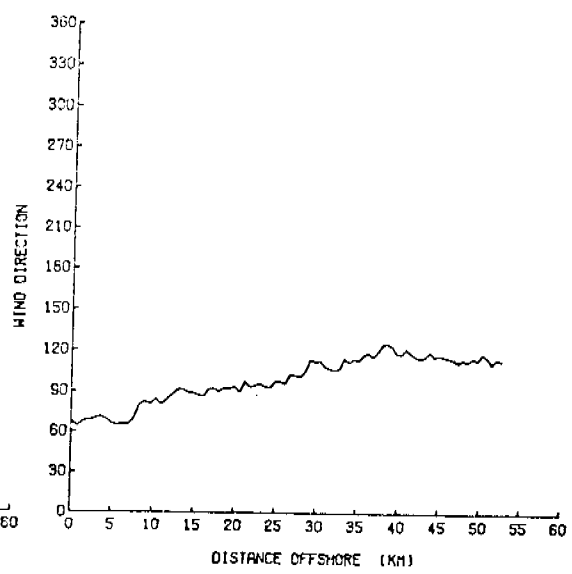
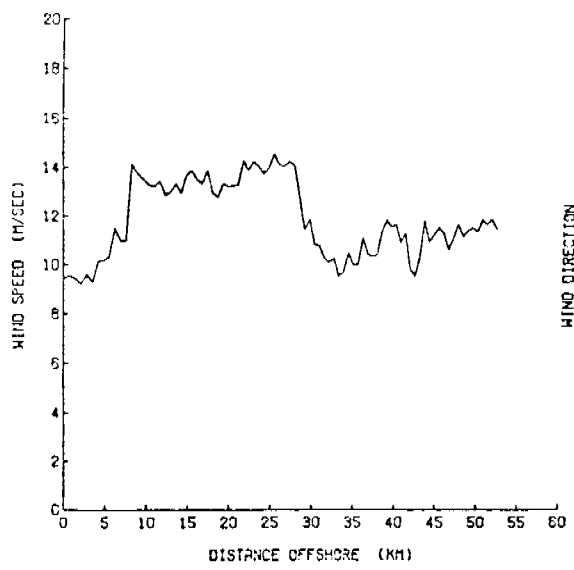
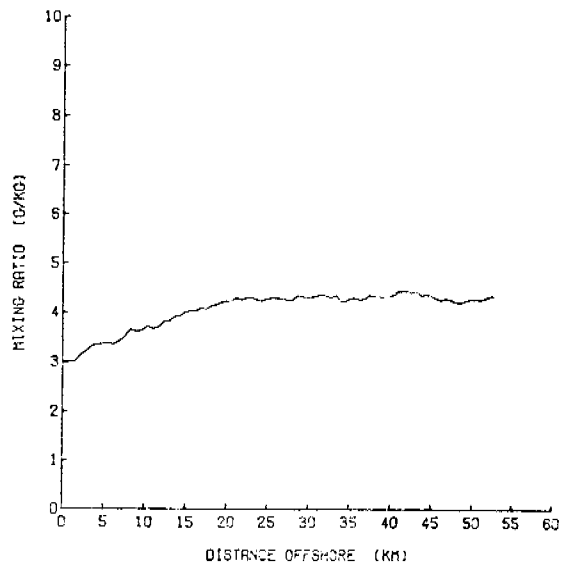
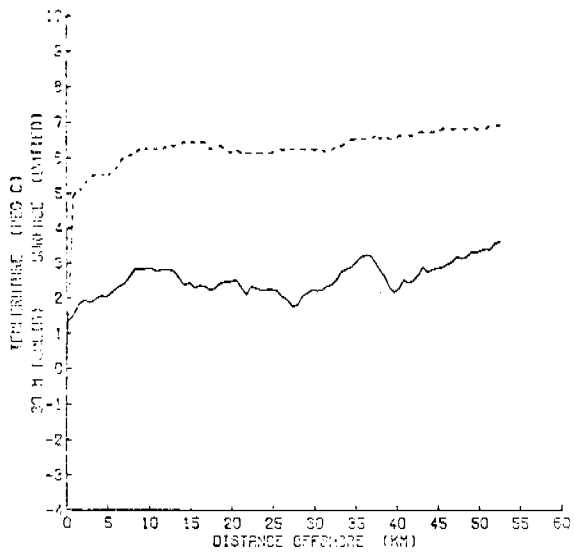


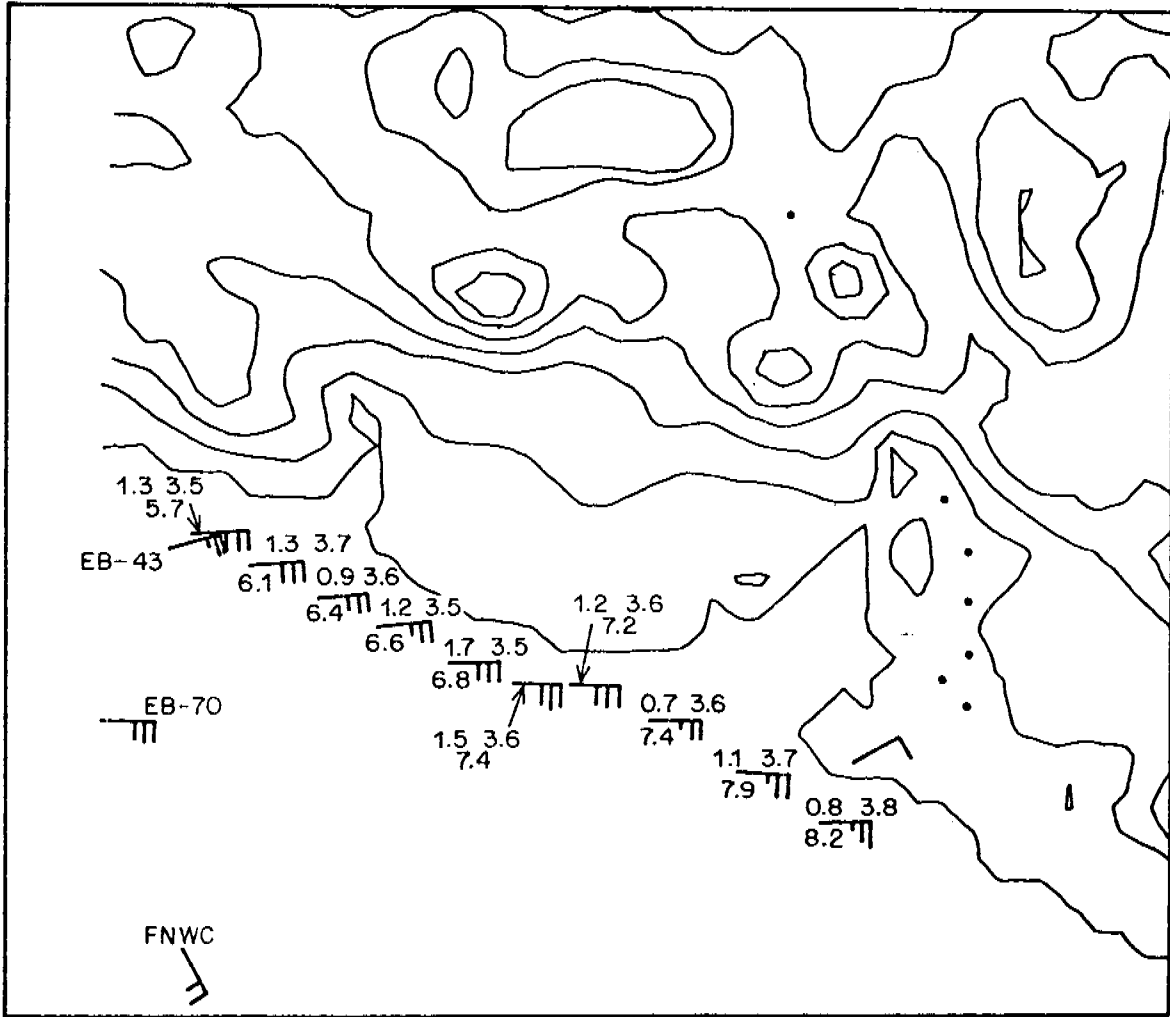


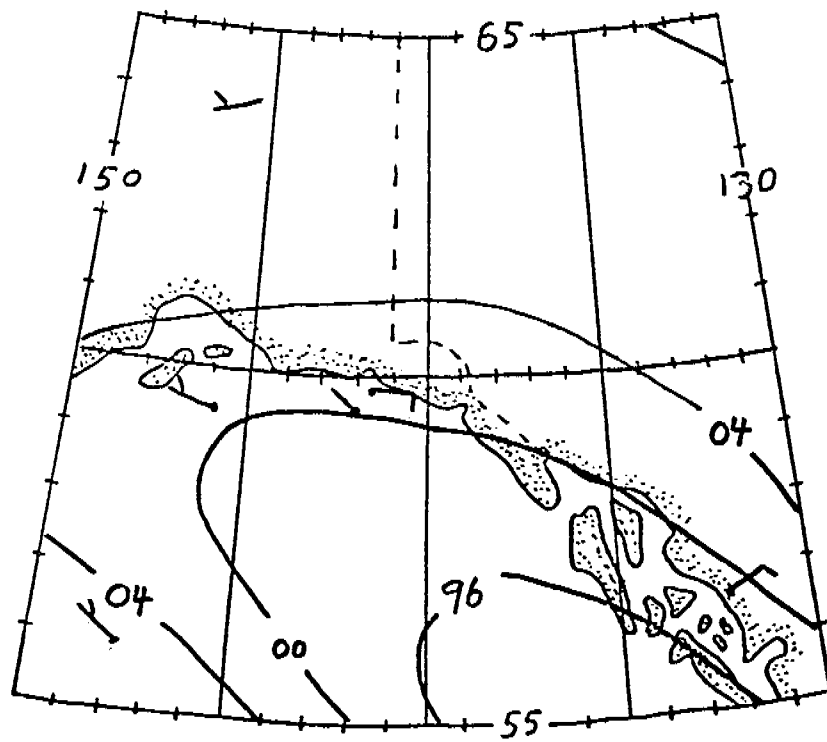
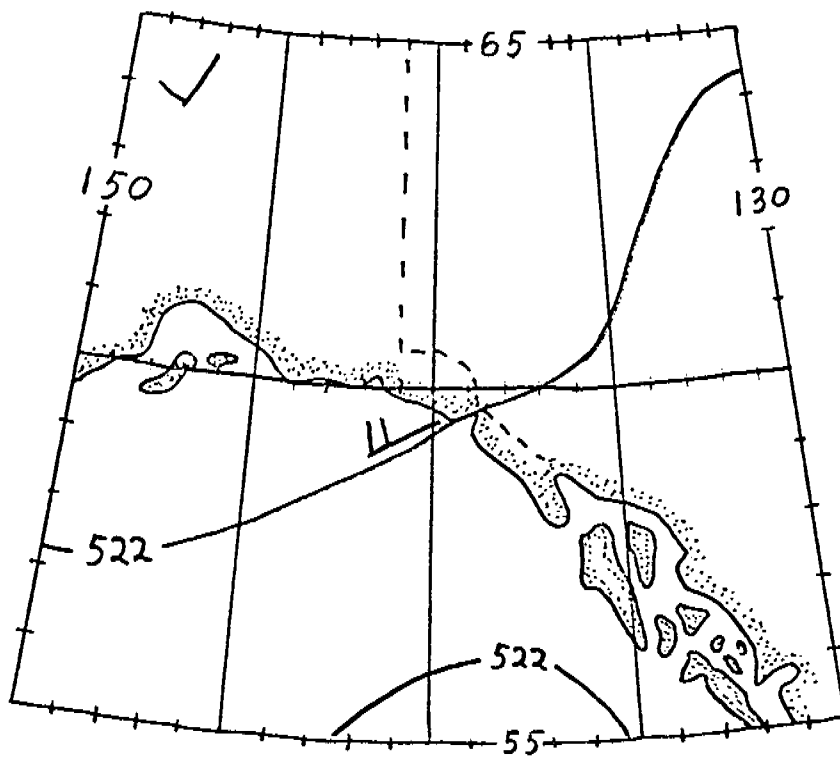


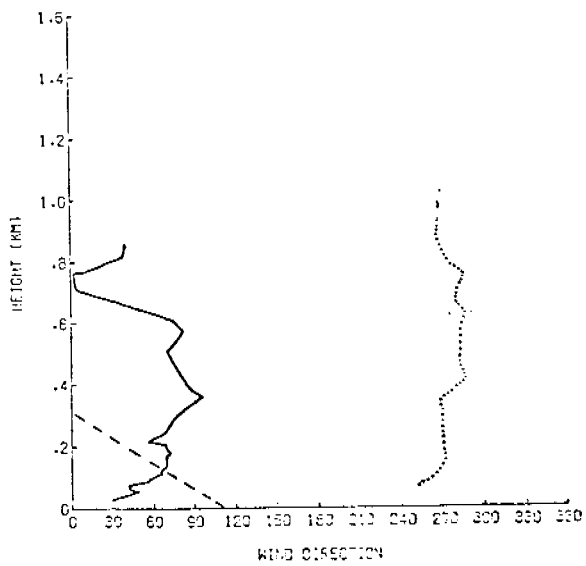
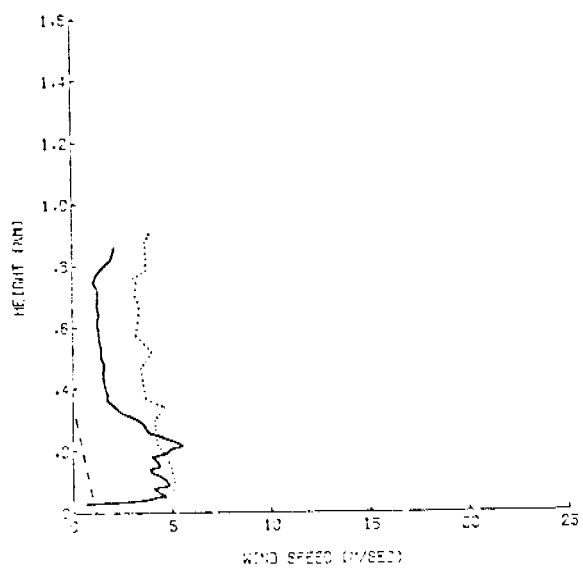
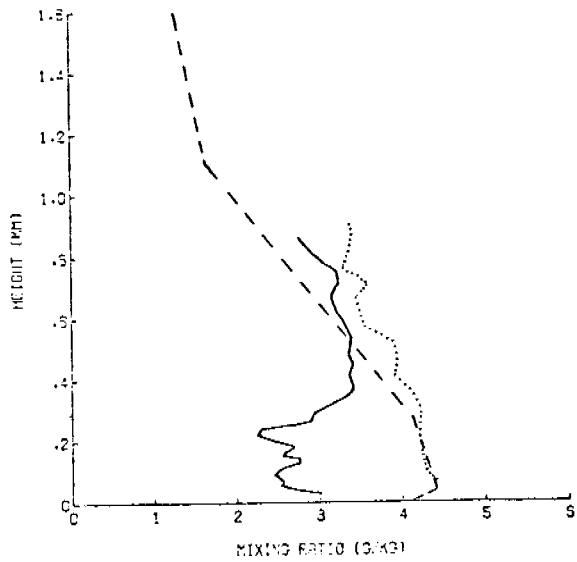
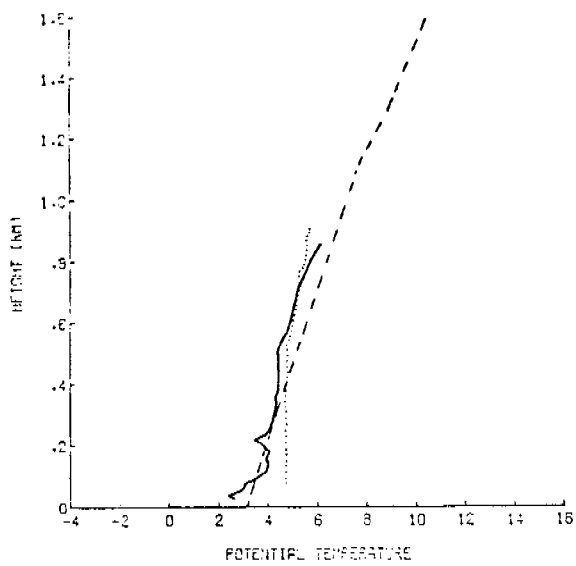


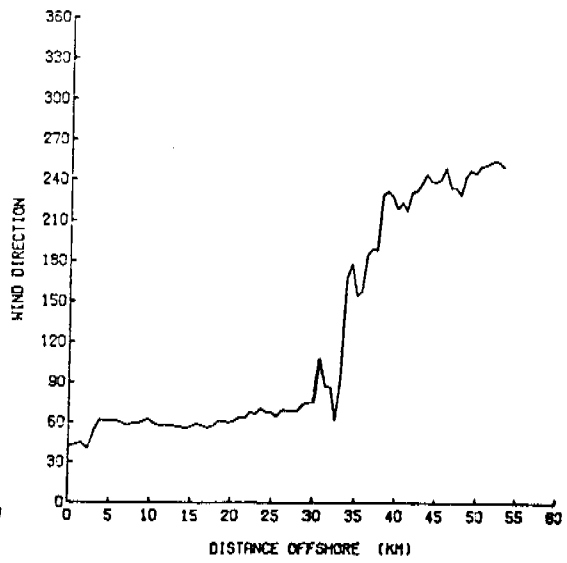
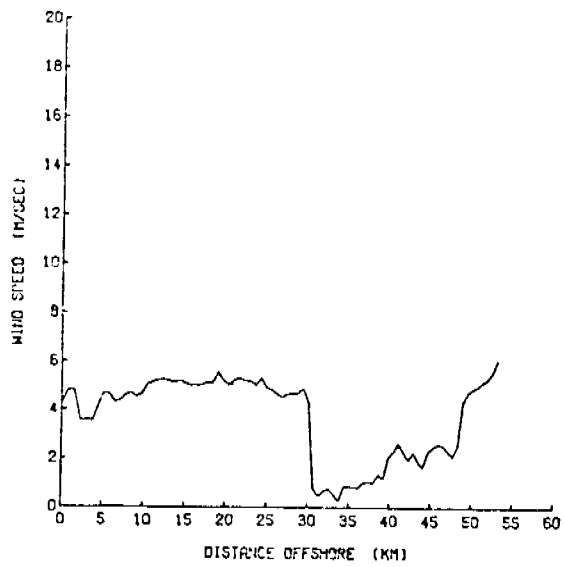
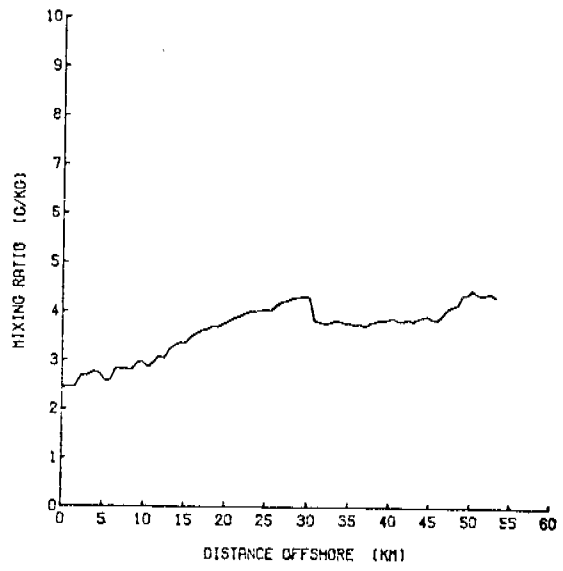
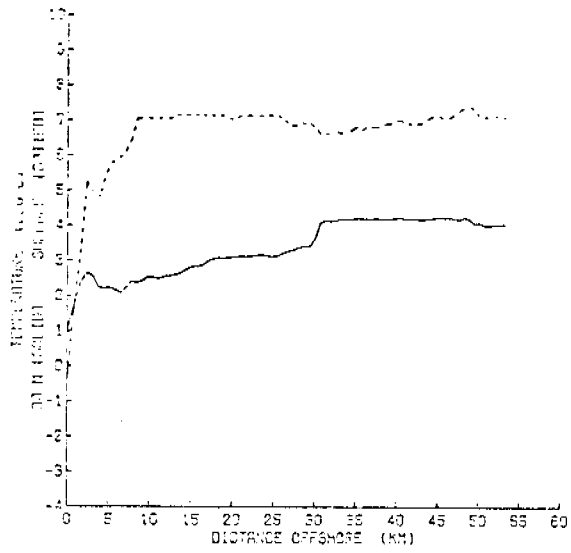


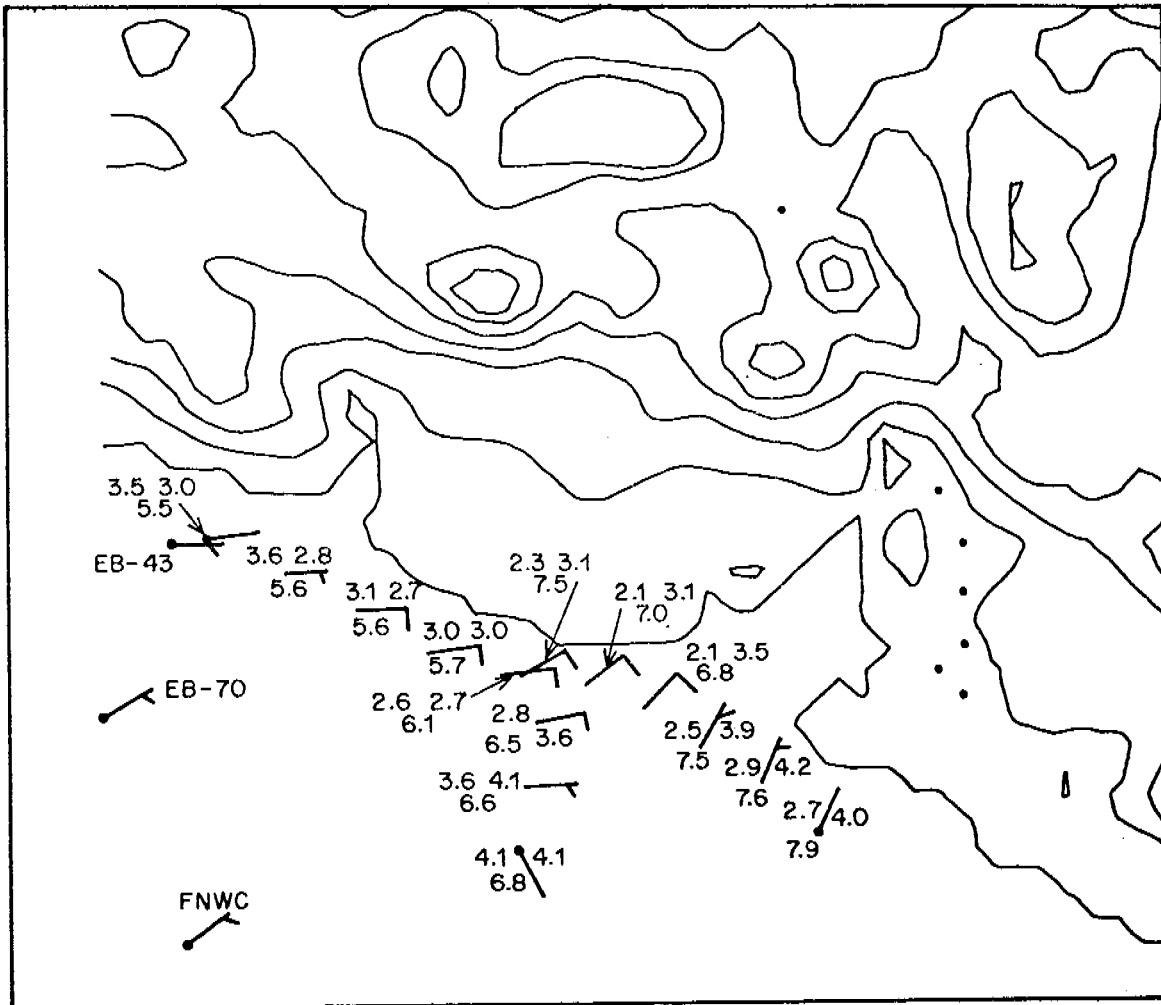


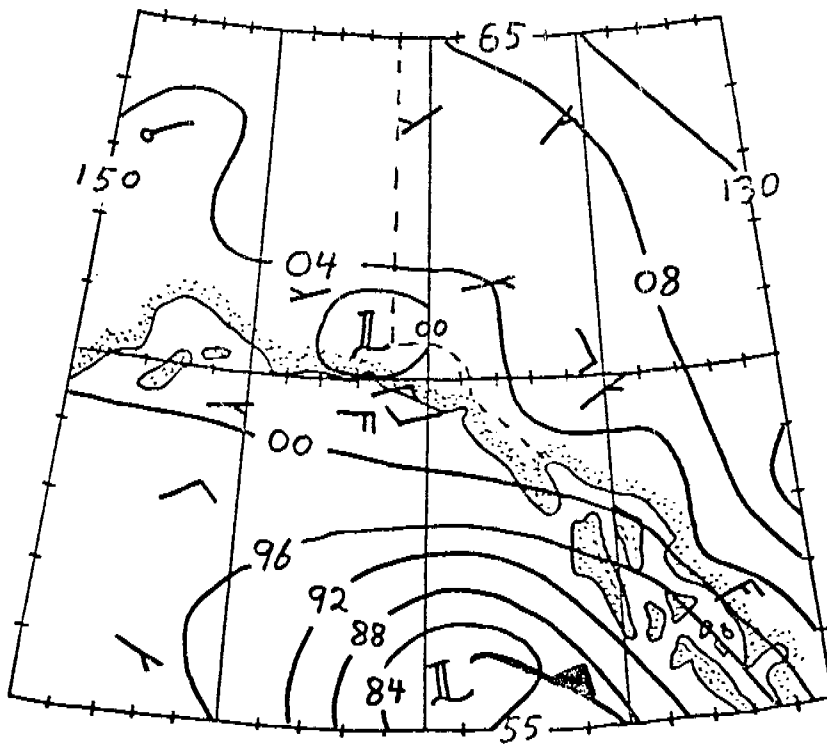
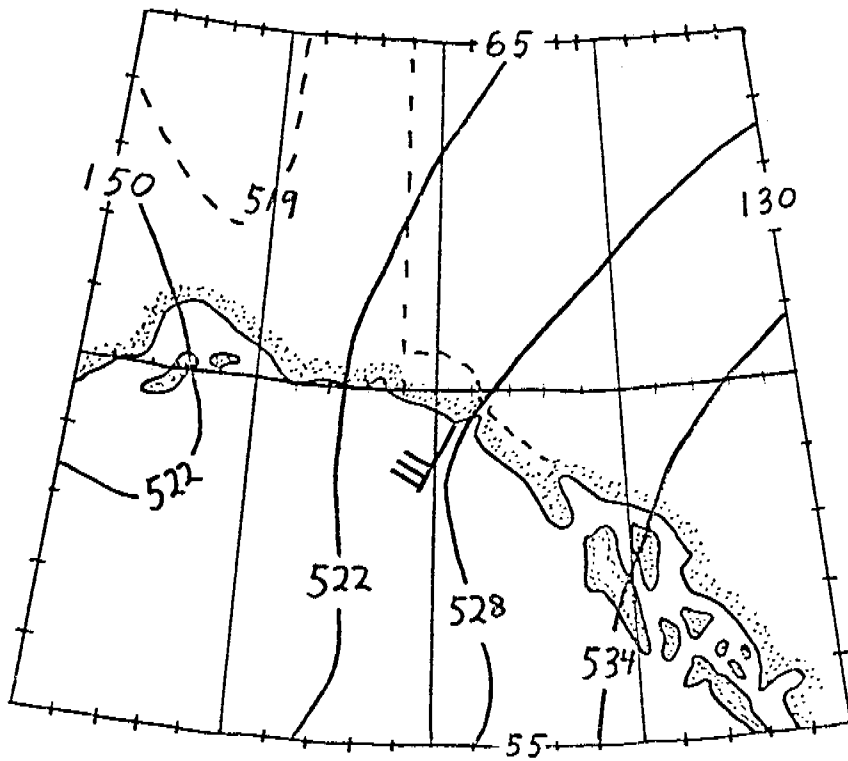


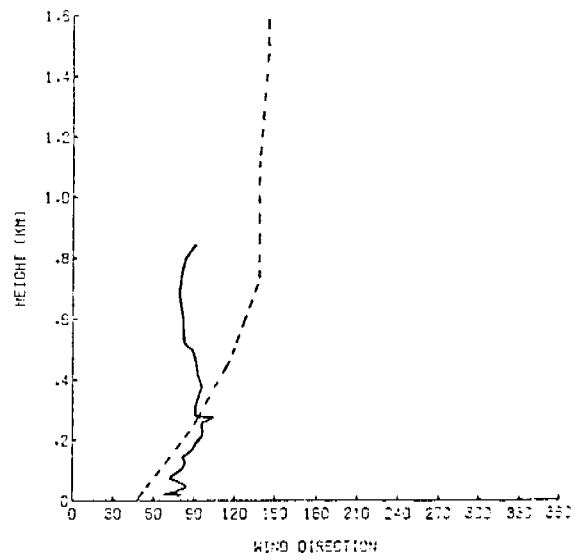
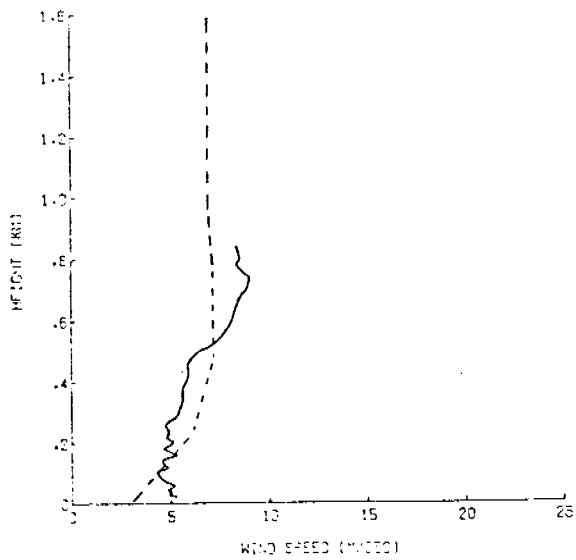
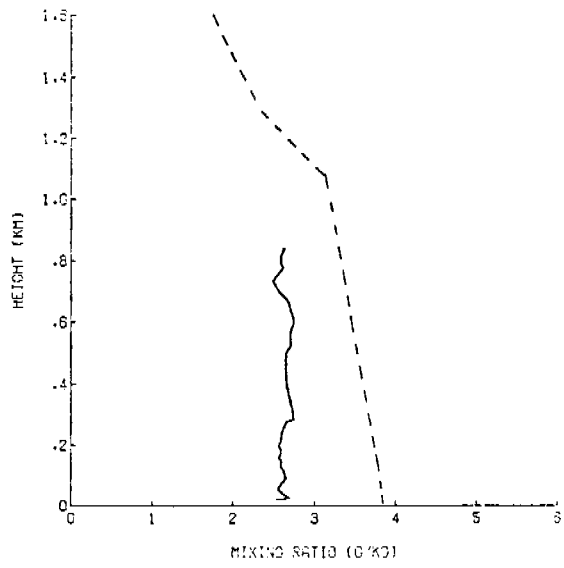
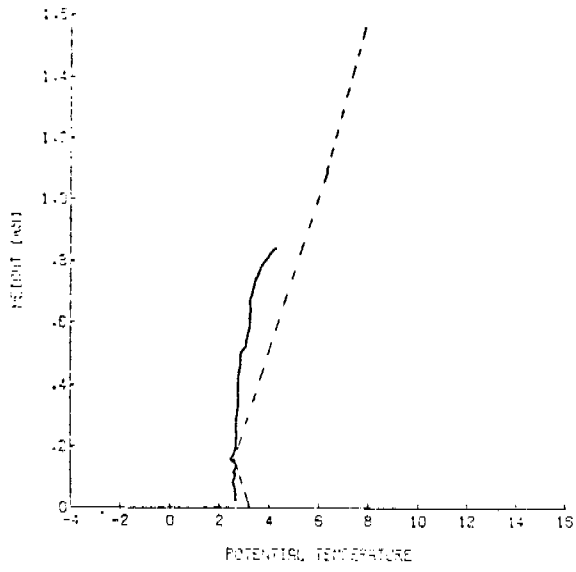


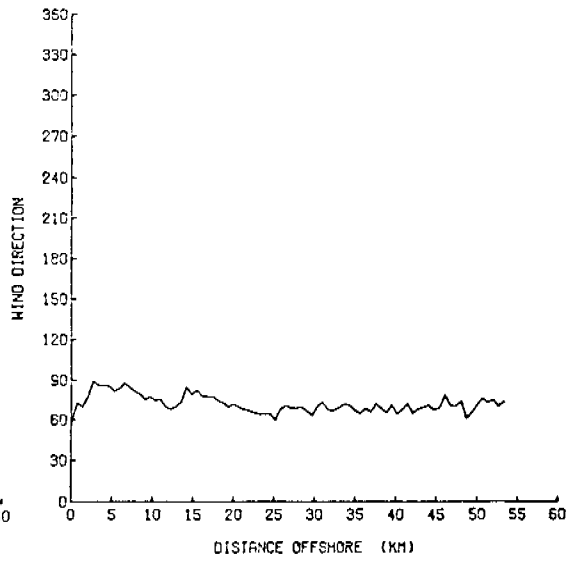
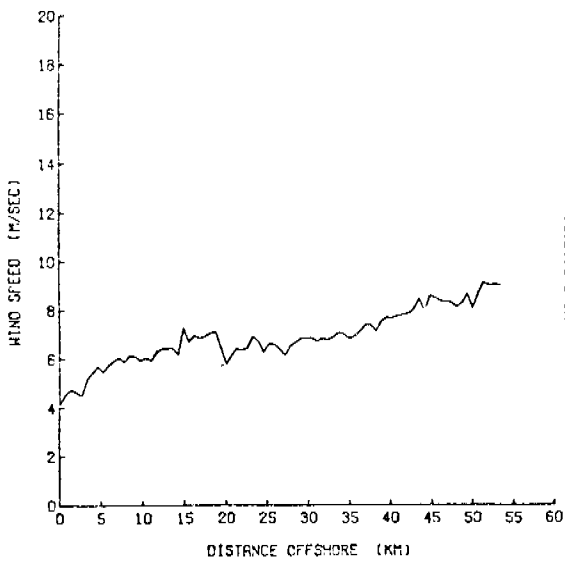
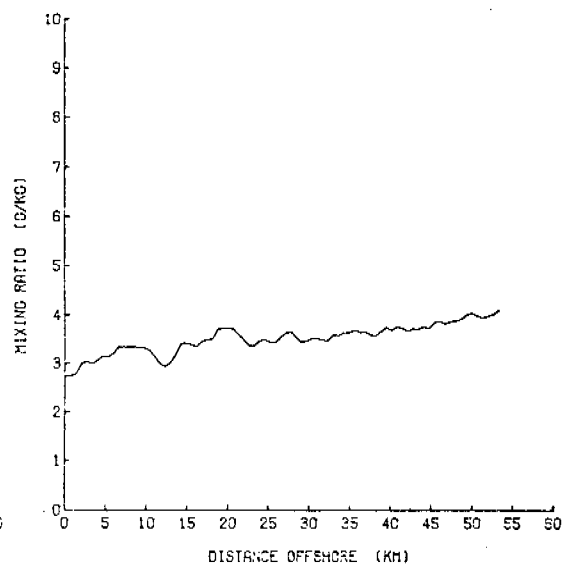
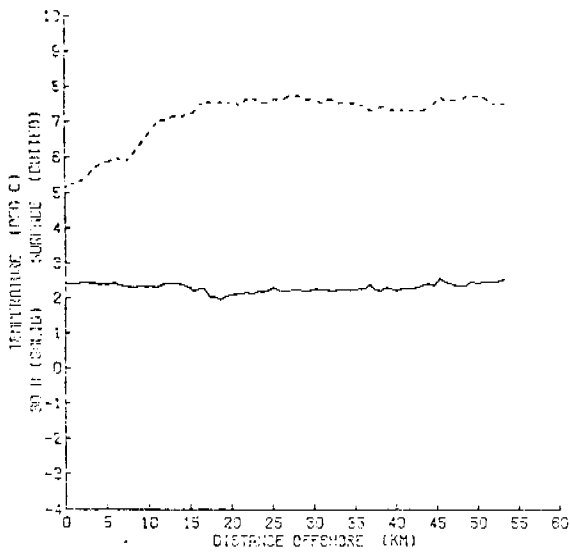


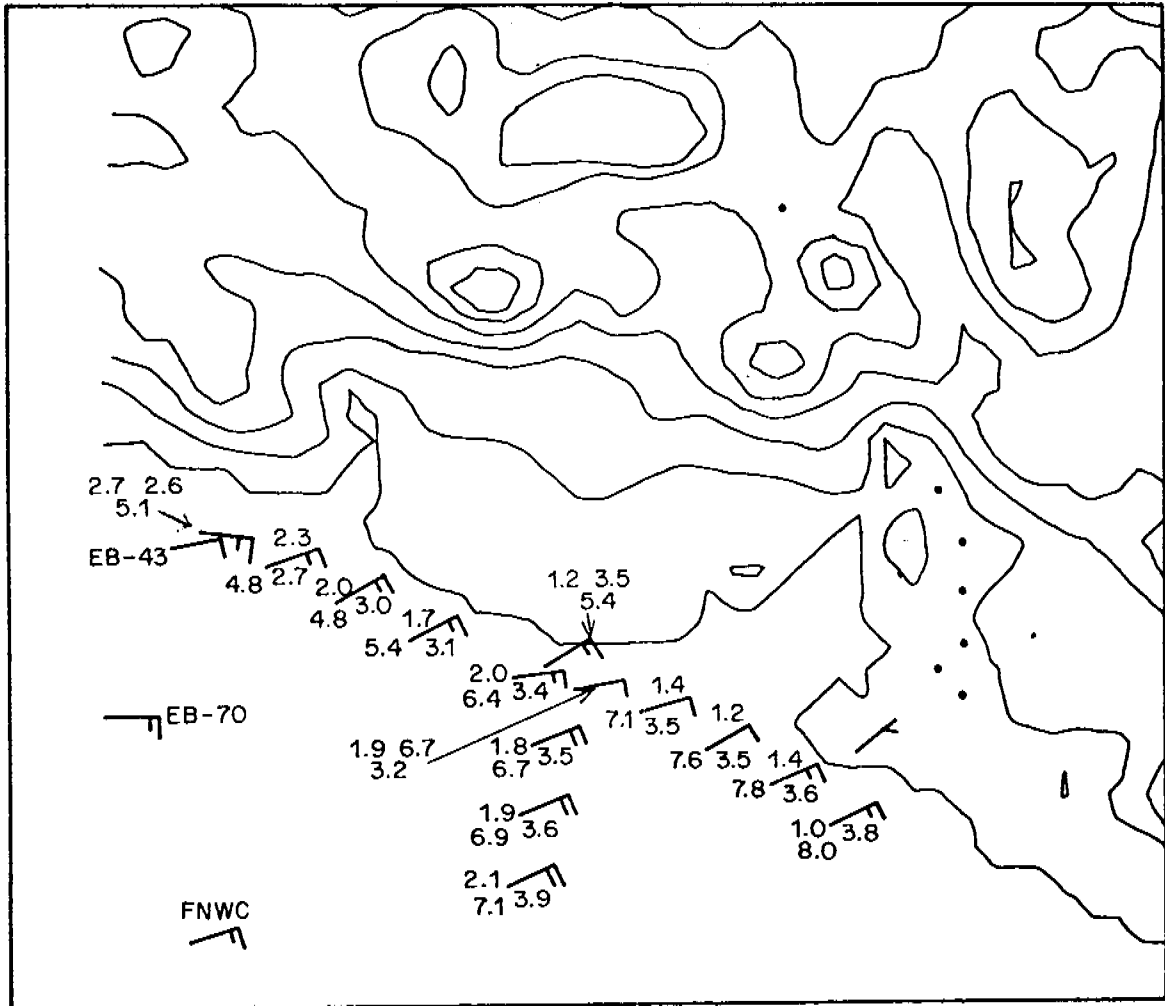


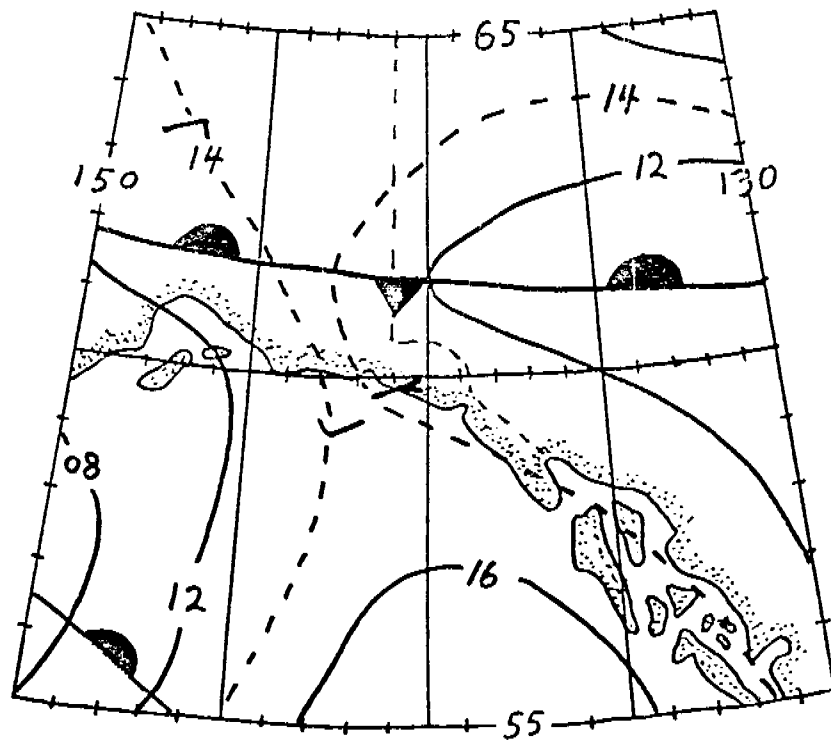
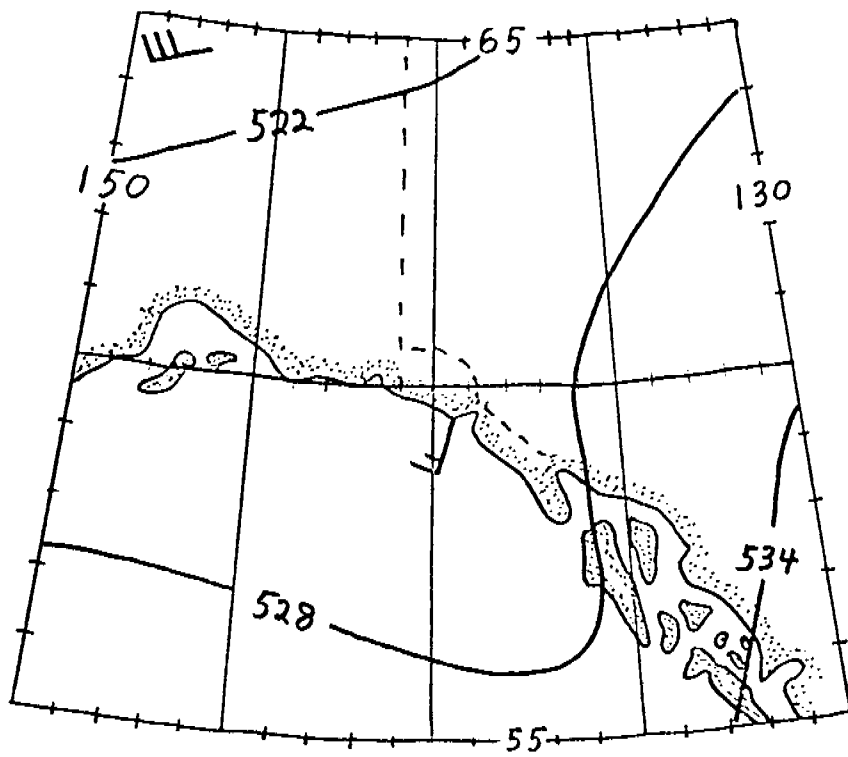


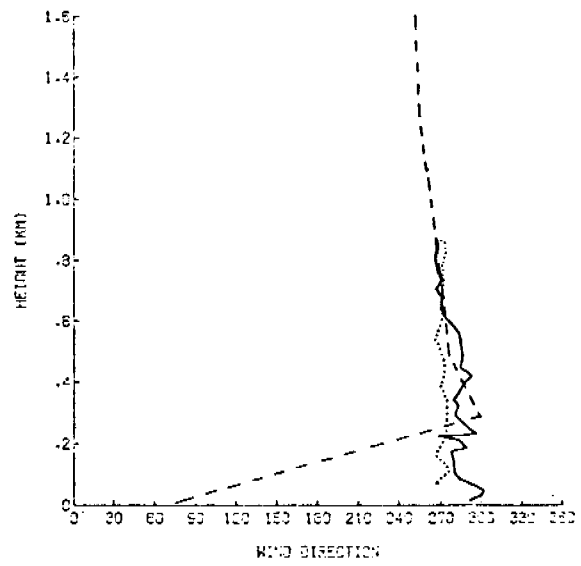
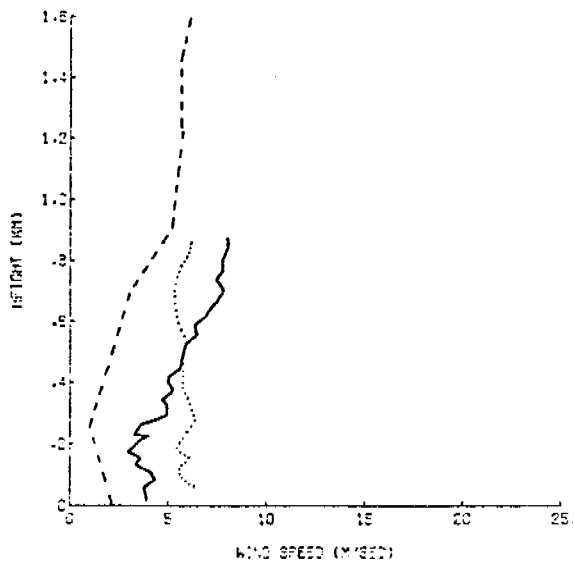
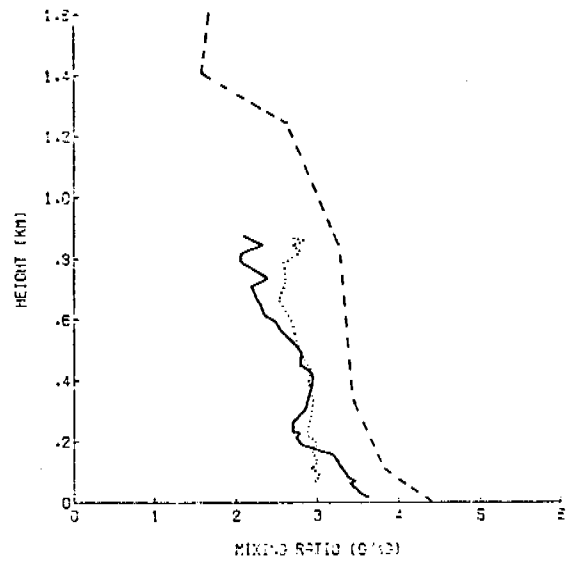
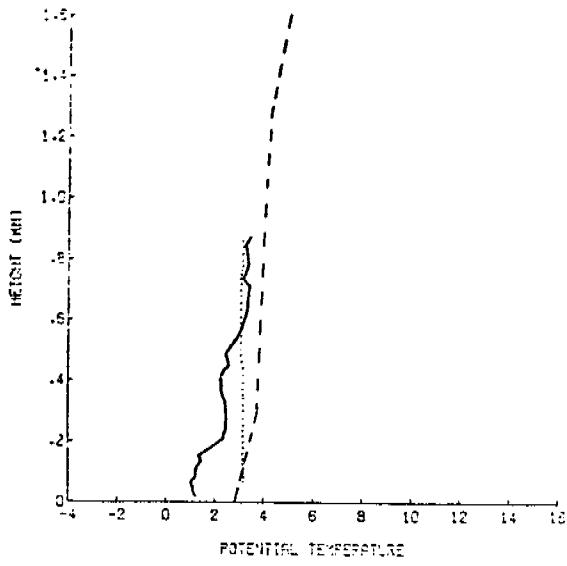


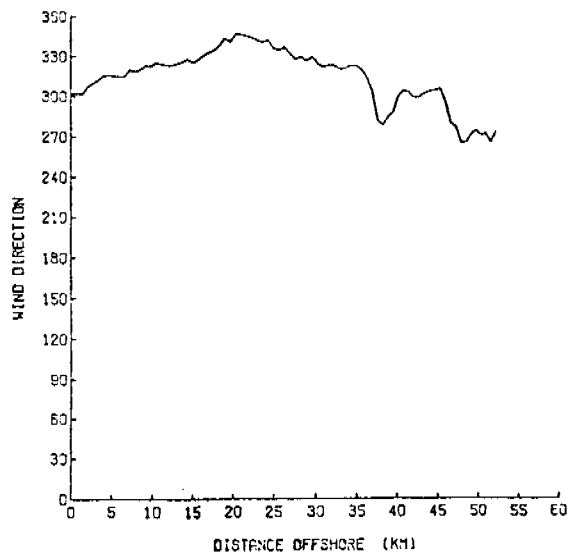
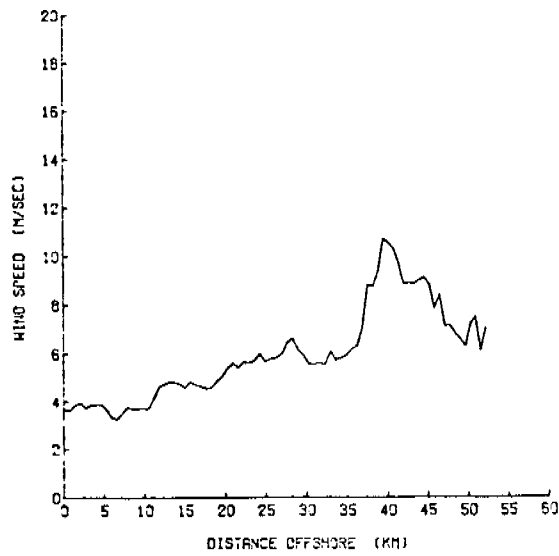
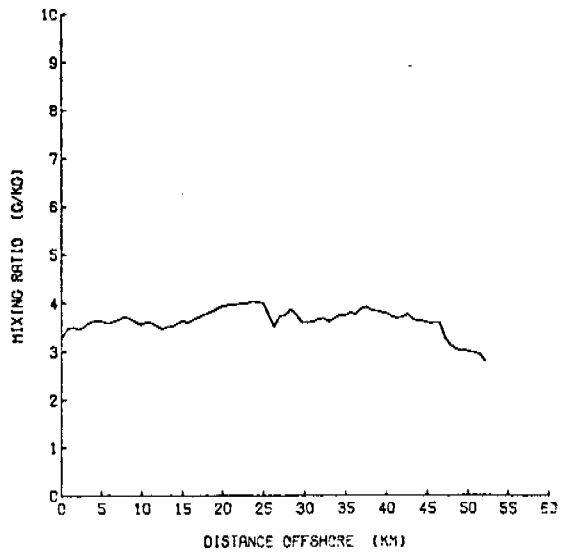
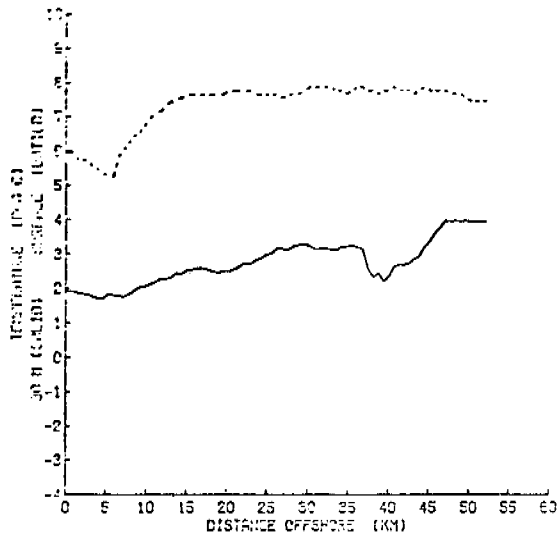


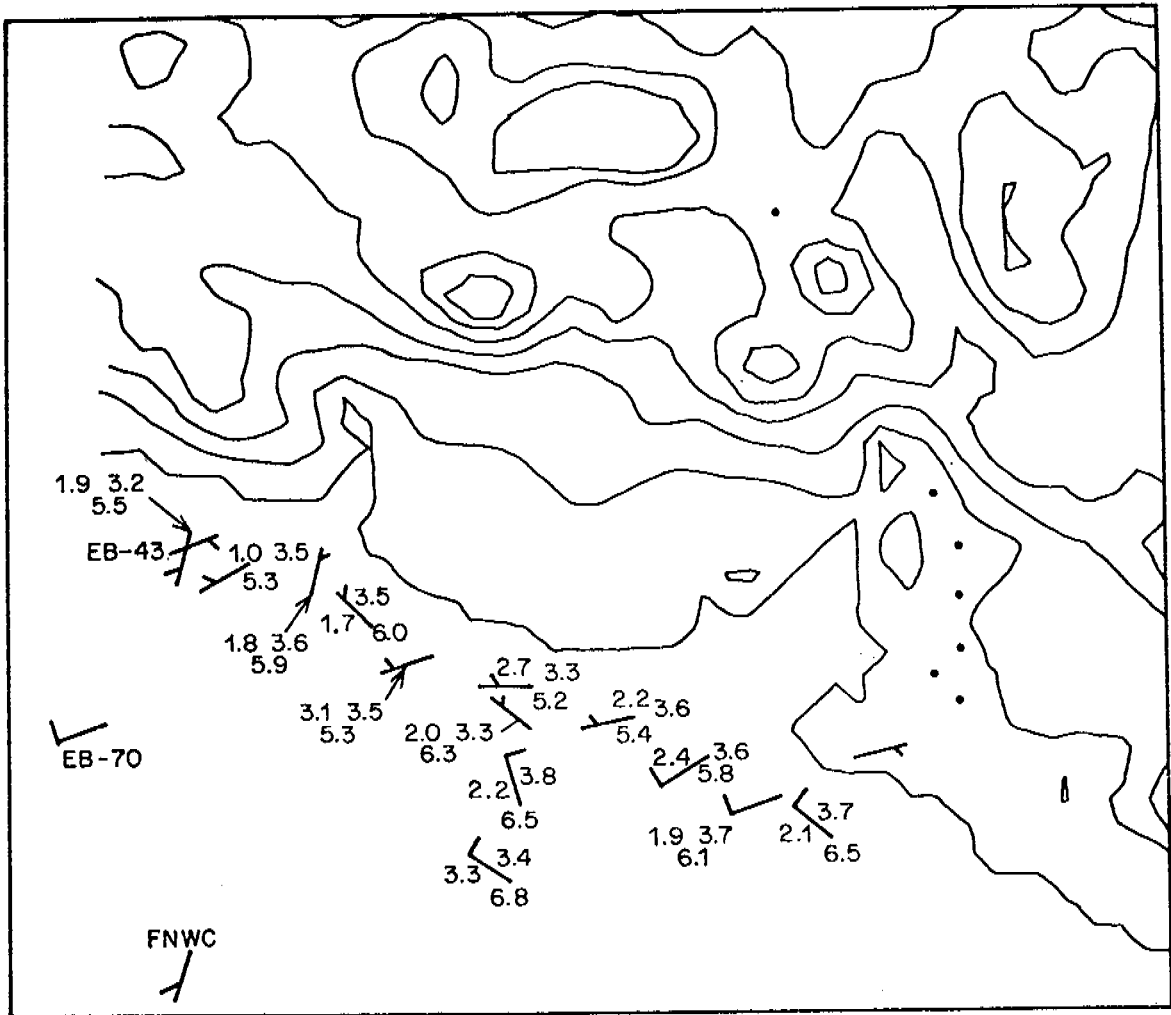


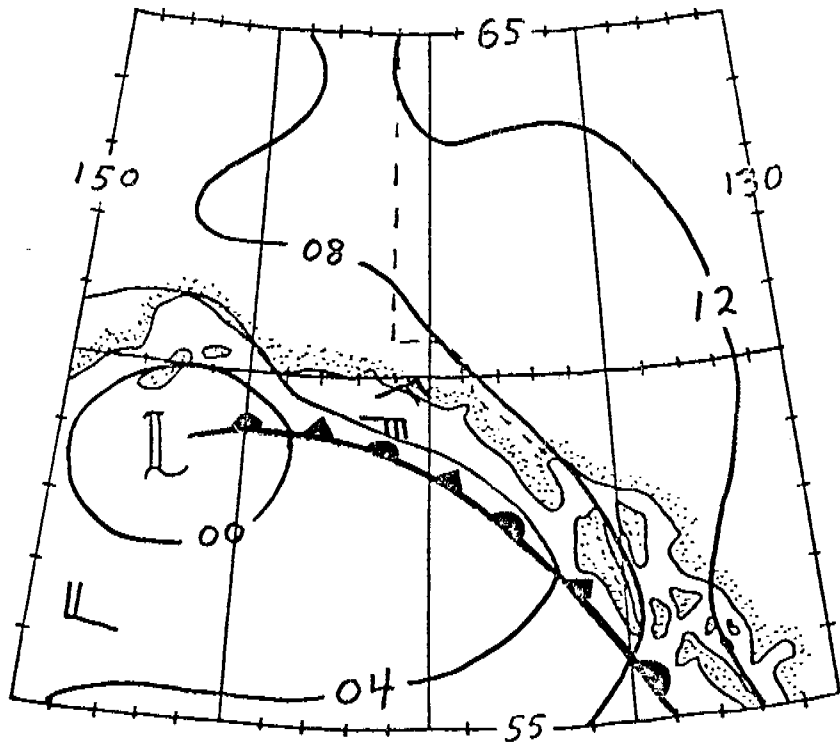
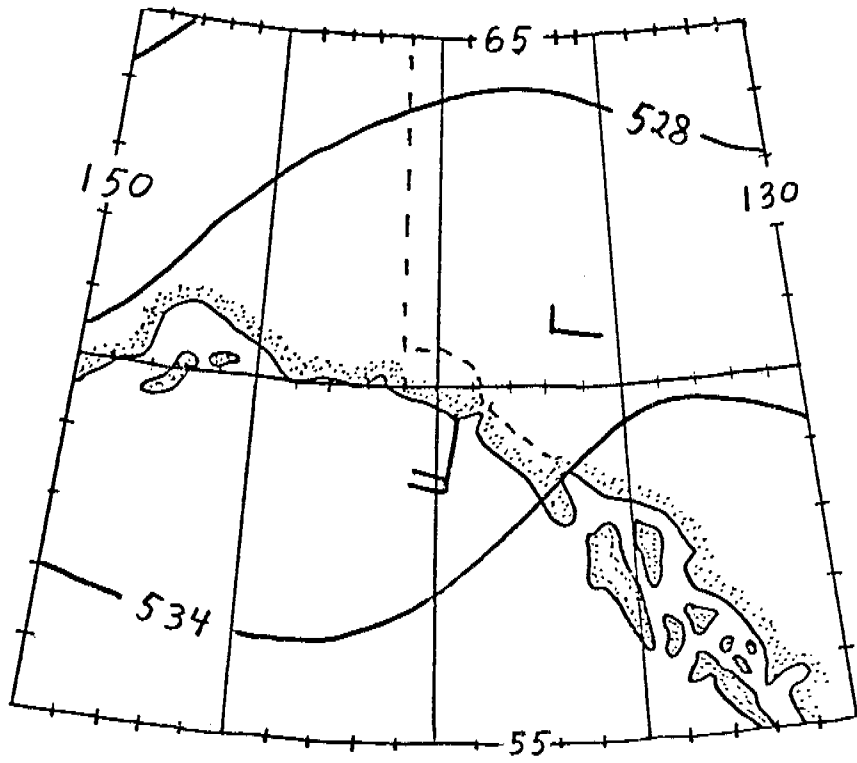


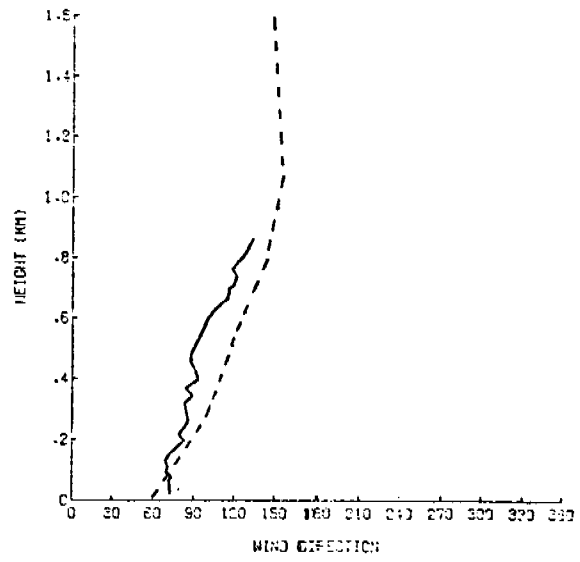
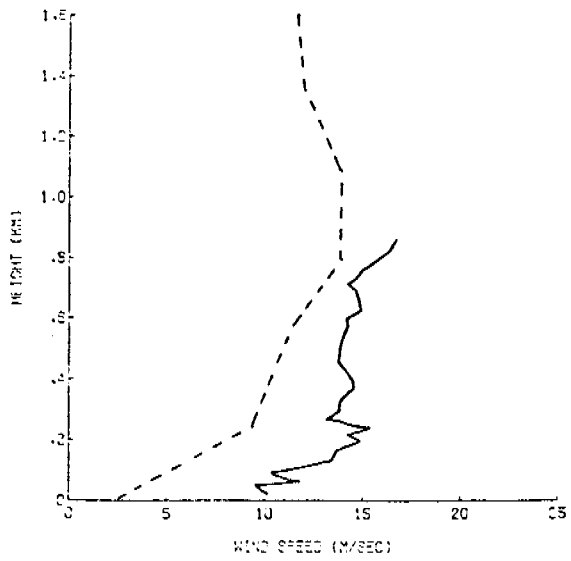
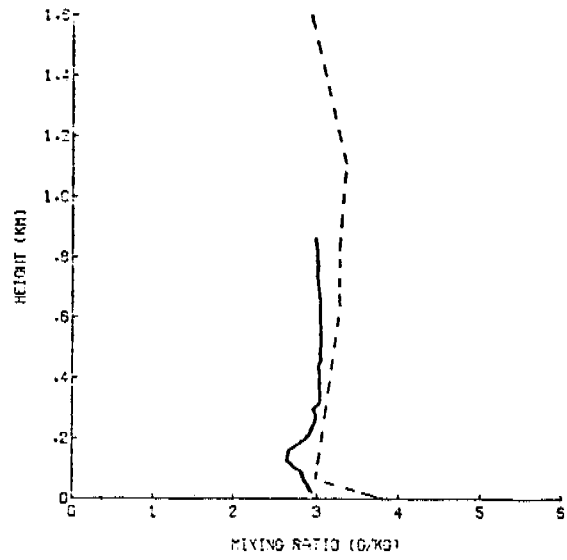
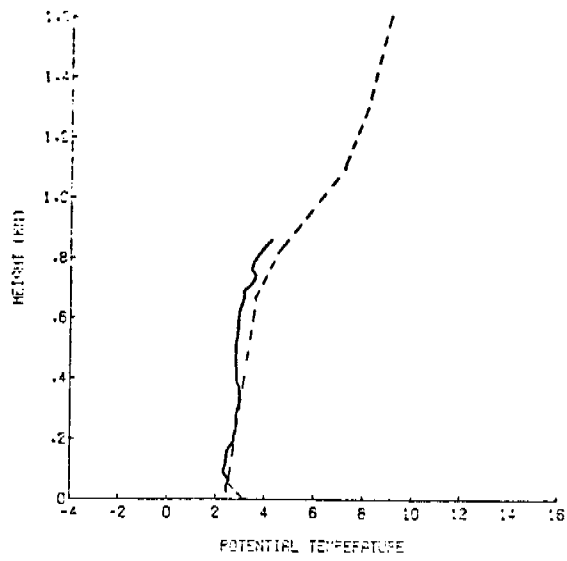


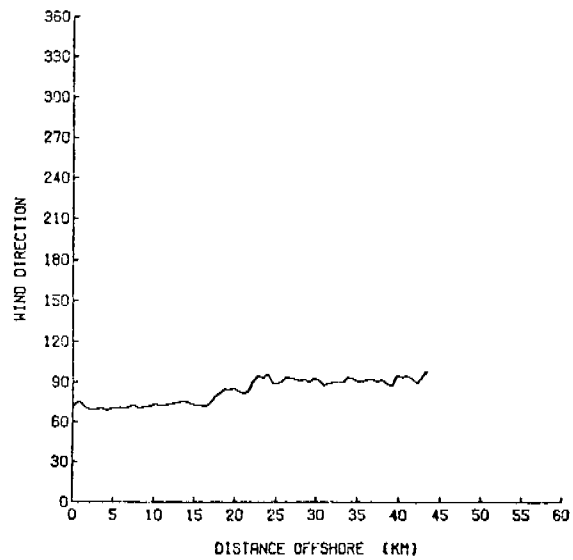
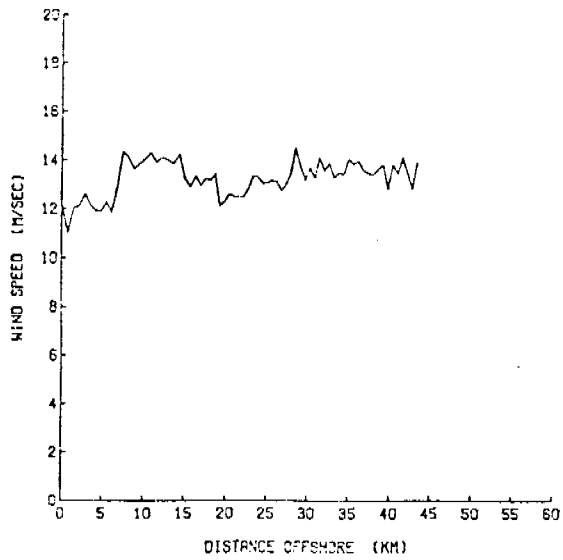
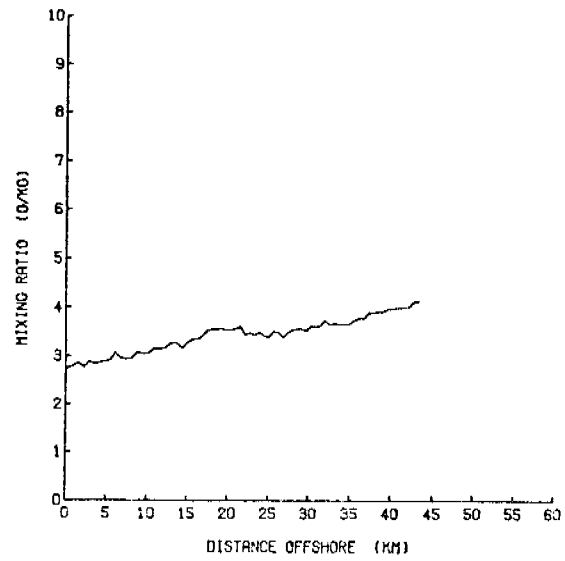
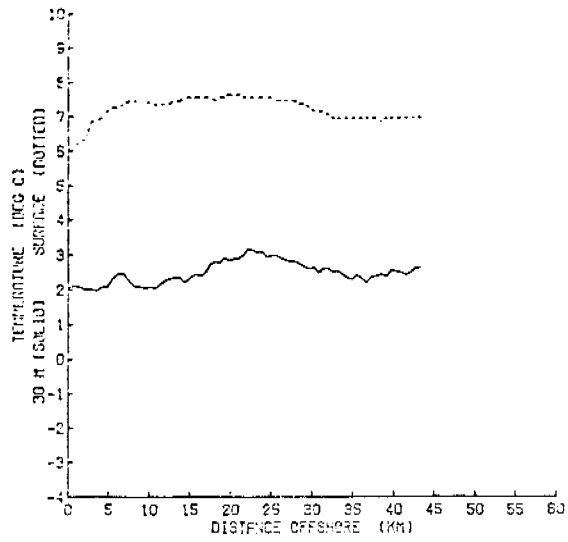


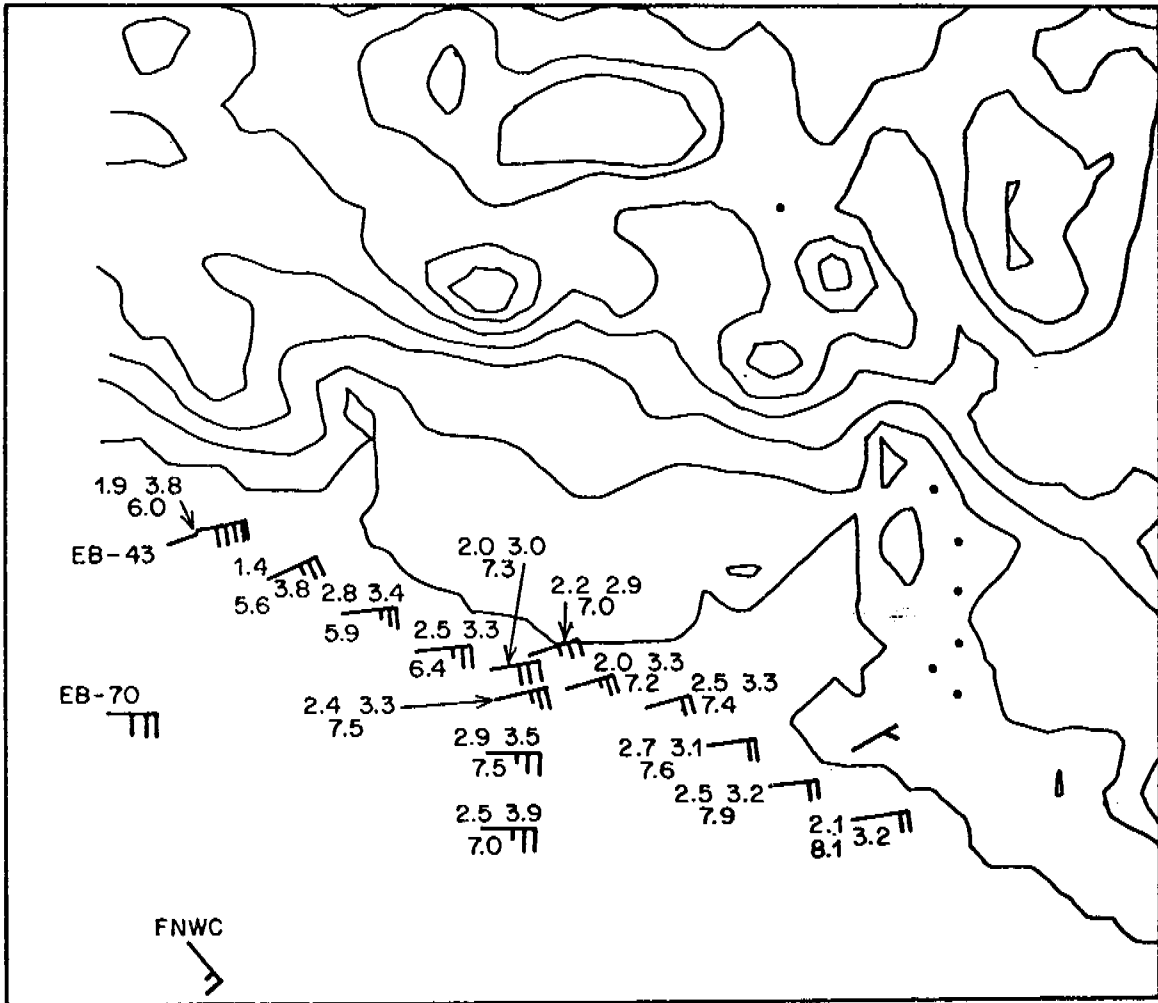


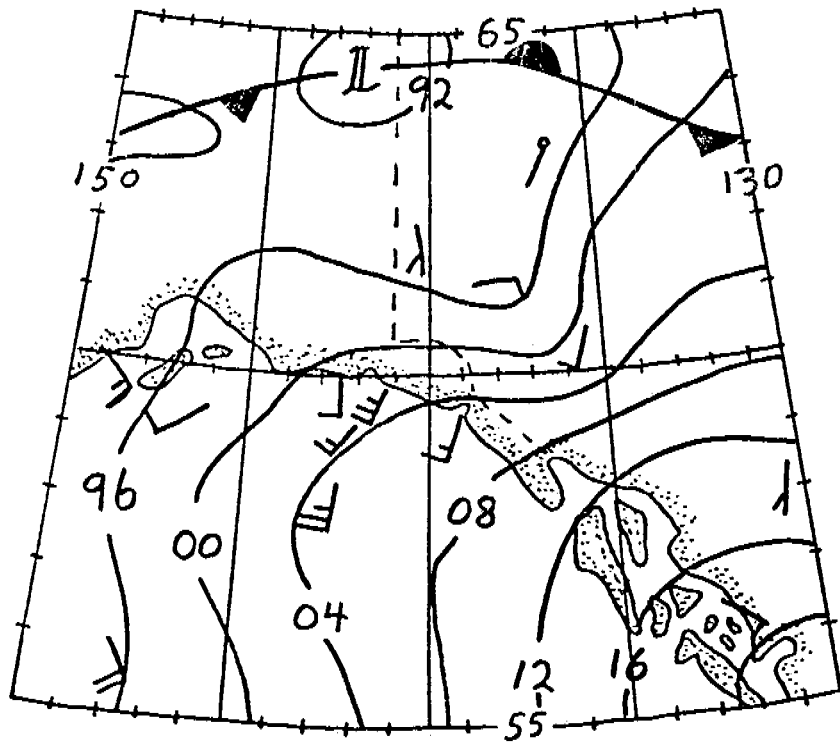
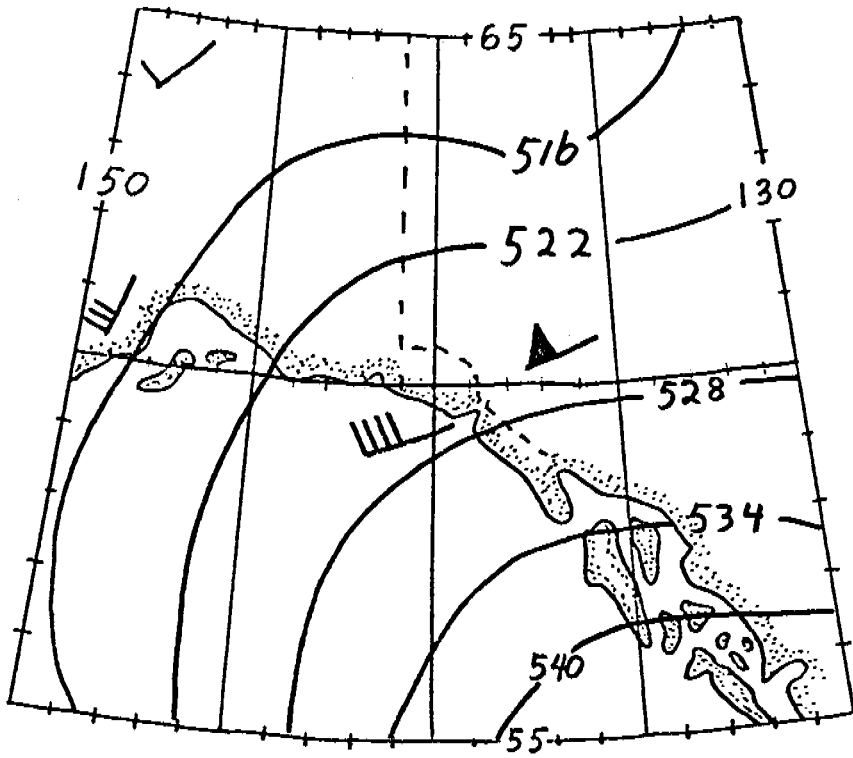




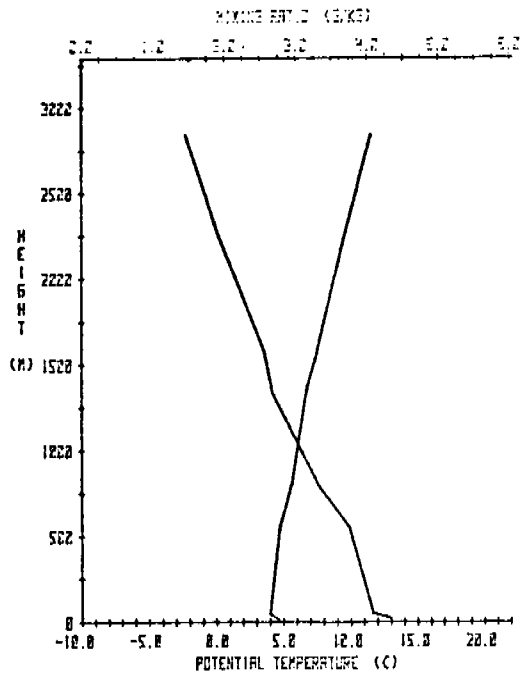




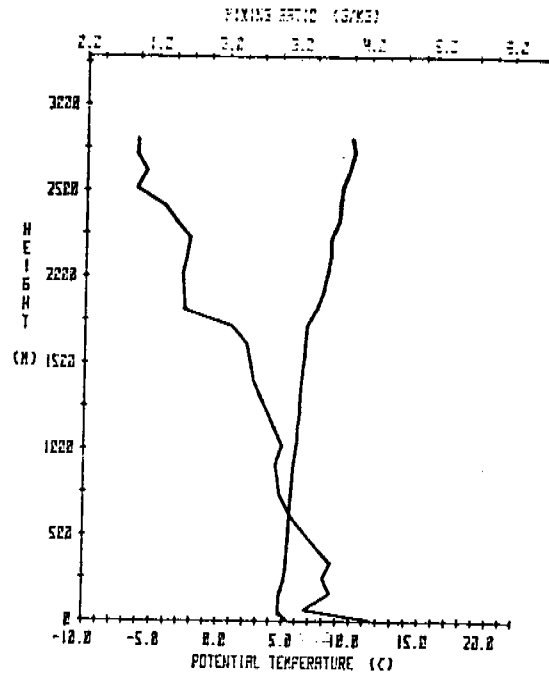




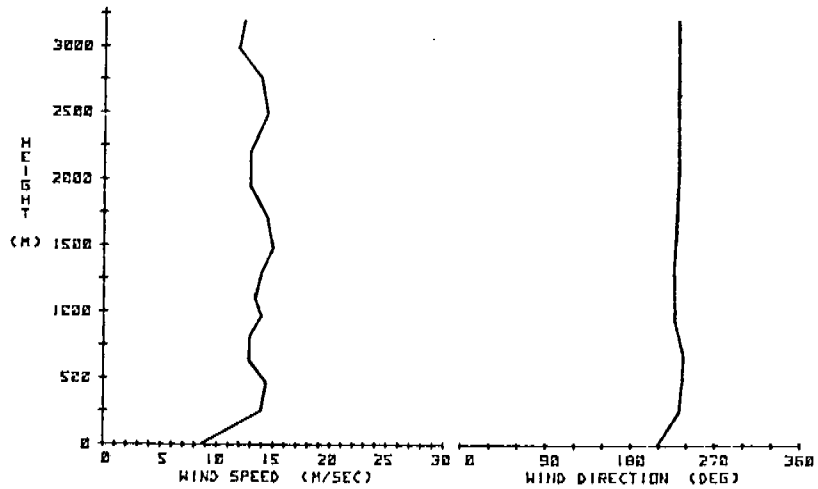
AKMETS YAK 772303231523593:0201334220212172

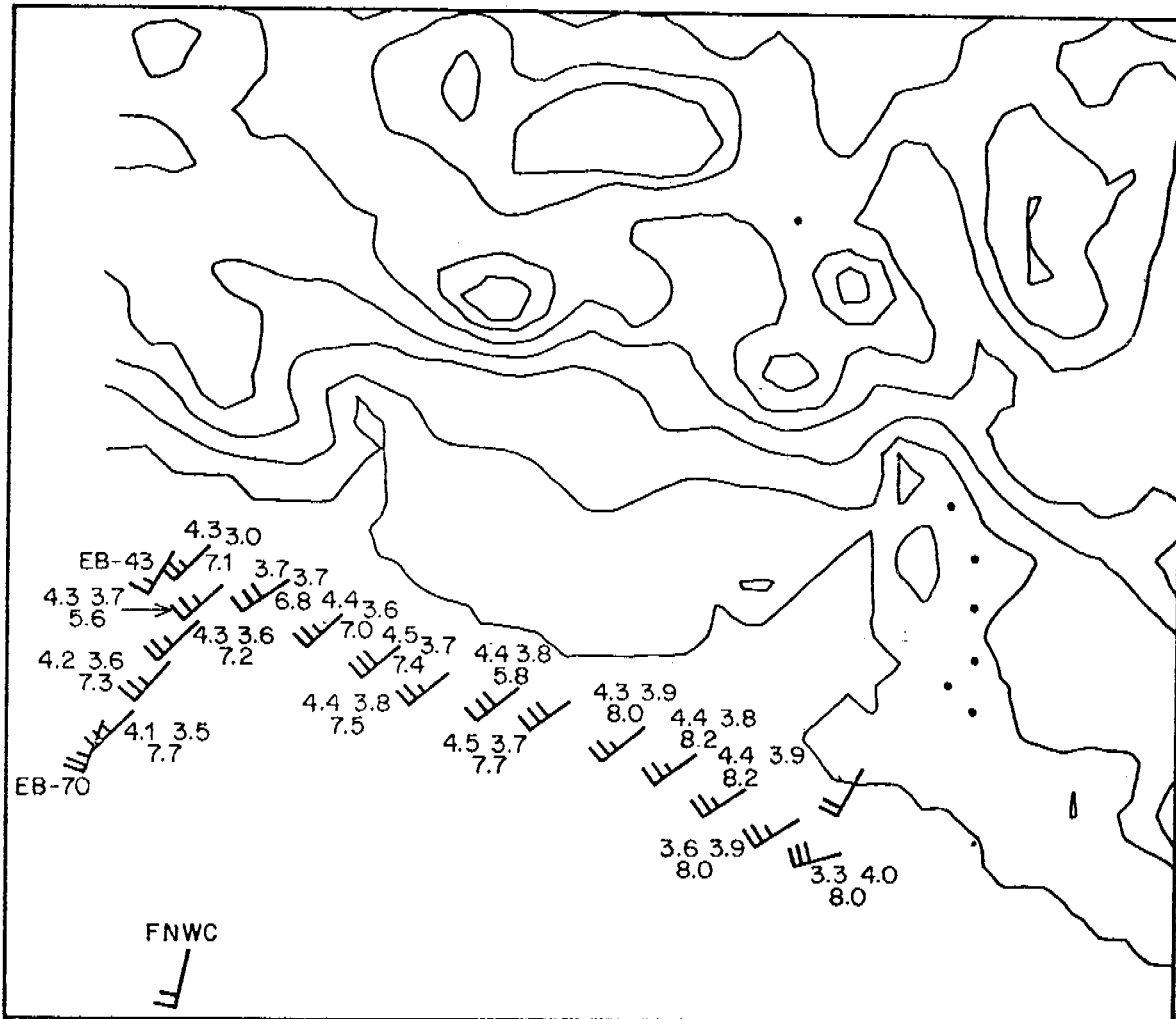


AKMETS N-2 03/03/77 2323Z 59 58.1 N 141 44.8 W



AKMETS YAK 03/03/77 2315Z 59 31.0 N 139 40.0 W





APPENDIX B
A LOOK AT WIND CONDITIONS IN
LOWER COOK INLET

A LOOK AT WIND CONDITIONS IN LOWER

COOK INLET

1. Introduction

An understanding of the dynamics of the air and the water circulations in lower Cook Inlet (LCI) is crucial if the potential hazards of oil development are to be accurately assessed. The weather affects the water circulation of L.C.I. via a number of mechanisms operating through a variety of time and space scales. The cloud cover, which prevents insolation during daytime and retards the passage of infrared radiation to space at night, influences the heat budget and structure of the near surface waters. Precipitation and subsequent runoff determine the fresh water input to L.C.I. Temperature trends on the order of months in duration influence the development and breakup of ice in L.C.I. Winds, of course, directly force the circulation on a broad range of timescales, although it is the high wind speed events that have the most dramatic effect and could cause the most serious problems in the event of an oil spill.

This report deals only with the wind field in and around L.C.I., questioning three basic points:

1. Do conditions change substantially from year to year?
2. Can the local winds in L.C.I. be characterized in terms of the synoptic scale flow?
3. What are the extremes from normal behavior?

Using the limited data that is available combined with information gained from pilots who have first-hand experience with the winds of Cook Inlet, conjectures can be made in answer to the above questions. The data needs that must be filled to verify these conjectures will be obvious.

2. Annual Variability of Winds in Cook Inlet

Figure 1 is a map of the Cook Inlet region showing topographical features referred to below. Figures 2, 3, and 4 were constructed from 4½ years of climatological data for Anchorage. Figure 2 shows the direction of the resultant wind vector created from all observations for each month of the 4½ year sample. It is plain that there are very consistent summer and winter regimes. The behavior of the transition seasons of spring and fall follow similar behavior from year to year, but the onset of these transitions can differ by about one month. The summer and winter average winds differ in direction by 180 degrees. The orientation of these averaged winds, N to NNE in winter and S to SSW in summer is closely aligned with the 3000 foot elevation contour, whereas the orientation of the crest of the Kenai Mountains is more NE to SW, as also is the orientation of northern Cook Inlet. This indicates strong topographical control of the planetary boundary layer which is typically 600-900 m deep.

Figure 3 shows the average wind speeds of this sample. It is evident that on an annual basis, the average summer wind speeds are higher than the average winter speeds, contrary to what one would expect in the light of the increased vigor of winter storms. This difference in speeds is probably due to the nonhomogeneous and unrepresentative location of the Anchorage airport. The summer winds, as Figure 2 shows, tend to come from the south over the smooth water surface where less drag is felt by the wind, than over the rougher land surface that the northerly winter winds must cross.

Figure 4 is a plot of the resultant vector wind speed divided by the average wind speed for each month expressed in percent. (Note that meteorologists refer to the resultant vector as the vector sum of all observations divided by the number of observations while strictly speaking the resultant wind vector is simply the vector sum.) This ratio is a crude measure of the variability of the winds within the given month; a high value indicates a more consistent wind direction than a low value. We see that in summer the winds are more consistent in direction than at other times of the year. The spring and early fall transitions are somewhat less consistent in wind direction. This crude measure of the variability of the wind direction within a given month shows no firm year to year behavior in late fall and winter.

From this quick study of a few years of Anchorage climatological data, it can be assumed that the dynamics of the Cook Inlet environment behave normally. That is, a sufficiently detailed study in any given year will point out the basic wind field patterns and responsible physical mechanisms with confidence, although the annual variations reveal that many years must be studied to determine with confidence the frequency of extreme wind behavior.

3. Synoptic Scale Flow Climatology and the Winds of Lower Cook Inlet

The most complete and authoritative summary of synoptic flow patterns and associated weather in Alaska is that of Putnins (1966). Readers of this report are probably familiar with that work but since it was used heavily in the preparation of this report, it will be briefly summarized here.

Putnins determined 22 surface flow patterns with some upper level characteristics that he felt descriptive of any Alaskan weather situation. For each day during the period 1 January 1945 to 31 March 1963 he determined which of the 22 flow types characterized that day's weather, then statistically summarized each month in terms of the frequency of occurrence of each flow type and the average weather associated with that type for selected stations. The 22 patterns and geostrophic winds over LCI are very briefly described in Table I. Table II shows the first, second, third, fourth, fifth, sixth, seventh, and eighth most commonly observed flow types for each month. For example, the third most common flow type observed in November, the eleventh month, is Type E₁'. Examples of the six most commonly observed pressure patterns and the percentage of occurrence for May, August, November, and February are shown in Figure 5.

The outstanding feature of Table II is the dominance of flow Type A' throughout the year, even in summer. As Table I and Figure 5 indicate, one would expect from type A' cyclonic flow in the Gulf of Alaska, a poorly defined pressure gradient over Cook Inlet with surface winds probably northerly to westerly.

To compare Tables I and II with observations at Homer and Kenai for January through November of 1970, "wind fabric" diagrams were prepared. The wind fabric diagram is essentially a contoured map of the wind velocity probability distribution given in percent of the total observations per 1% area of the diagram. Wind direction is plotted according to meteorological tradition--the compass direction from which the wind is blowing. Although calculations can be made from many similar frequency distribution maps, qualitative interpretation is difficult unless one knows that contours enclosing equal areas at any given region of the diagram do in fact contain the same number of observations and therefore represent areas of equally probable wind occurrences. This can only be done if the velocity is mapped onto the diagram proportional to the square of the radius in order to compensate for the spreading of radial line segments. From the contoured map one can easily calculate the probability of observing the wind in any direction and velocity sector, and perform statistical significance tests for features seen on the diagram.

Figures 6 and 7 each show four diagrams corresponding to January through March, April through June, July through September, and October through November. Figure 8 shows the orientation of certain geographical features for easy interpretation. The first fact clearly visible for both Kenai and Homer is that the winds are mostly along the axis of the mountains or inlet. The broadening of the northerly to northeasterly lobe in the Homer diagram is no doubt caused in part by weak winds draining down the slope of a 2800 foot summit to the north, and may reflect some influence of Kachemak Bay. Northeasterly winds dominate the flow in winter while southwesterly winds prevail (or almost do so) in summer. The apparent greater speed in summer is once again probably an artifact of the southern exposure over water and northern exposure over land. Therefore, the Kenai and Homer wind behavior is similar to the behavior of the winds at Anchorage as revealed in the previously shown climatological data.

Returning now to Putnins' summary, the prevalence of northeasterly winter winds at Anchorage, Kenai and Homer may be explained in terms of orographic channeling of the flow driven by the synoptic scale pressure pattern and in large part also to the southward drainage and channeling of cold air north of Anchorage. The presence of southwesterly winds in summertime is more challenging since Putnins' collection of typical pressure patterns imply that there are few cases of southwest winds over L.C.I. The observed southwesterlies must then be part of a solenoidal circulation caused by the heating of the Alaskan interior, and funneling of the winds by the mountains. Diemer* informs us that the funneling of winds in the upper arm of Cook Inlet is not strongly affected by synoptic disturbances. These

*Chief forecaster, NWS, Anchorage, personal communication.

data suggest that even Homer is screened from the effects of synoptic disturbances.

At the time of this writing, the only available data from within LCI was from EB-39 from 1 July 1977 to its failure in mid September. A time series of those data is shown in Figures 9a-c. The wind fabric of these data is plotted in Figure 10a. Contrary to the July through September period wind fabrics for Kenai and Homer, this diagram shows a pronounced two lobe structure oriented along a NW-SE line. Figure 8 reveals that the winds tend to blow in through Kennedy Entrance or through Kamishak Gap. Figure 10b is called an energy diagram since what is plotted are contours of percentages of the total sum of the velocity squared per 1% area of the diagram. For comparison of energy features with the wind fabric features the axis of the energy diagram is labelled the same as in the wind fabric diagram. The velocity squared is of interest since the surface stress which will drive the currents is proportional to the square of the speed. Figure 10b shows that although there are relatively few measurements of relatively large ENE winds, because they are large they contribute significantly to the surface stress.

Attempts at detailed comparison between winds derived from Putnins and coastal wind stations are probably futile and meaningless. Perhaps comparisons with EB-39 over open water are less so. Figure 11 is a wind fabric created subjectively from Putnins' work and should be accepted only for gross features. A pressure gradient was selected from Putnins' "model types" over LCI, converted to a geostrophic wind vector which was reduced by 20% and rotated 10-30 degrees across the isobars toward low pressure to account for surface drag. The frequency of occurrence for each type was the average of that found in Putnins for July through September. The resulting plot on the wind fabric was of course very spiked having at most 22 points plotted. A simple numerical smoother was used to finally produce Figure 11. The resulting plot shows the SE winds through Kennedy Entrance, the NE winds similar to those seen at Homer and Kenai, and a hint at some westerly winds. While winds derived from Putnins in this way do not accurately reproduce features actually observed at any given point (it could not be expected to) they do seem to include general features that characterize several regions of the LCI flow. Therefore, a Putnins-type approach narrowed down to LCI, using the pressure field in the vicinity of Cook Inlet may prove fruitful. The mesoscale pressure field could similarly be categorized and used as an input into a mesoscale model.

4. Extreme Wind Events in Lower Cook Inlet

No individual is more acutely aware of severe winds than is the pilot of an airplane. Skilled pilots can make reasonable estimates of the wind speeds and directions of the currents they are in. During a recent trip to Alaska, one of the authors consulted several knowledgeable pilots. The following is a composite of their comments:

Winter drainage winds (williwaws) pouring out of Knik and Turnagain Arms diminish south of the Forelands. Drainage winds often flow from upper Kachemak Bay and from Douglas Glacier on the west side. Drainage winds also flow from the deeper valleys of the Kenai Peninsula, especially that above Tustumena Lake. Once in late

October due to the strength of those winds a commercial flight from Homer to Kenai was forced to fly around Anchor Point and up the coast rather than take the usual inland route at 2500 feet. It was observed that the resulting surface water waves and transport were westward across the inlet.

During the late summer and early fall there is often a strong westerly wind flowing through the Kamishak Gap between the Aleutian Range and the Chigmit Mountains. On occasion 100 knot winds have been observed at Bruin Bay. This flow is often accompanied by water spout formation along the cliffs south of Contact Point and at Pedro Bay on Iliamna Lake and at Iniskin Bay north of Augustine Island. These winds apparently achieve their strong velocities from orographic channeling as they are observed to dissipate quickly after diverging into Cook Inlet, although they are still noticeable at Augustine Island. Augustine Volcano itself generates fairly frequent katabatic winds and lee wake effects.

Throughout the region (including Shelikof Strait) the most unpredictable and damaging winds by far are the westerlies. The Barren Islands are particularly notorious for local violent winds.

To gain some insight into the causes of maximum wind events one might turn again to Putnins. For each month and type, Putnins lists the maximum wind speed observed. Table III lists the month and type of flow in which the first, second, and third highest wind speeds during Putnins study period occurred. For example, the second highest wind speed ever encountered (during Putnins' study period) in a January occurred during a type H flow pattern. Maximum winds at Anchorage are about 45 to 55 knots. Note that type A' flow is once again prominent, perhaps just a reflection of the amount of time that type A' flow is observed. However, since A' reflects weak and poorly developed low pressure centers over the Anchorage area, high wind speeds must come from drainage winds. Similarly flow type D shows up prominently in the winter as a source of high wind velocities, although Table II shows type D is generally not the dominant synoptic pattern. Type D flow has a high pressure over Alaska with anticyclonic flow at 500 mb. Precipitation is rare and cloud cover averages 30-40% compared with 60% for most other patterns. Type D tends to set in and last longer (2 to 3.3 days) than most other patterns (1 to 2 days). The long period of clear skies, and a strong north-south pressure gradient clearly mark these winds as drainage winds similar to the Taku winds of southeast Alaska.

5. Coastal Wind Forecasting Techniques

In the last few decades a marked degree of expertise has been developed by the National Weather Service towards prediction of coastal winds along the south Alaska coast. Increased network instrumentation and weather reporting coupled with the immense growth in nautical and aeronautical traffic have enabled several empirical techniques to be verified and constantly upgraded. These forecast techniques range from simple

pressure-differencing schemes to more sophisticated balances between pressure forcing, drainage and spill-over winds, and solenoidal circulations. In general these techniques may be applied with limited success by a novice, but the subjective modifications which only a skilled meteorologist with a "feel" for Alaskan winds is capable of making are deemed necessary for accurate forecasting.

This report section will deal with pressure differencing techniques for the Barren Islands, lower Cook Inlet, Resurrection Bay, Whittier, Copper River Delta, Lynn Canal and Sitka; with resultant wind forecasting for Valdez from wind components due to several forcing factors; and with surface wind-geostrophic wind relations for some Alaskan coastal passes. Special thanks are rendered to Ed Diemer and Francis Poole of the NWS Alaska Region for supplying forecast documents and elucidating forecast techniques.

Figure 12 shows the work sheet used by the NWS for 24 hourly wind forecasts for the locations shown across the bottom of the figure. These predictions are derived from multiplication of the pressure difference in millibars between reporting stations listed at the top of the columns (AKN = King Salmon, ADQ = Kodiak, CDV = Cordova, ANC = Anchorage, ENA = Kenai, GKN = Gulkana, XY = Whitehorse, YAK = Yakutat, JNU = Juneau, DL = Dease Lake, SIT = Sitka, FAI = Fairbanks, TKA = Talkeetna, MCG = McGrath) by an empirical constant derived from correlation of observed pressure differences with observed winds. This constant is also listed at the top of each column. Then a subjective modification is made dependent on the winds aloft and rate of pressure change. Some additions to the figure (but not shown) are: A lower Cook Inlet surface wind prediction from the Homer-King Salmon pressure difference times 6.5, and revision of the Barren Island constant to at least 6. Wind direction is considered parallel to the isobars following the Buys-Ballot Law (with the wind at the back, low pressure is to the left) unless orographic channeling of the surface flow is apparent.

For example, assume a low in the Gulf of Alaska with a pressure at King Salmon of 990.2 mb and at Kodiak 985.1 mb, holding steady at each location. The surface wind prognostication for the Barren Island is then $(990.2-985.1) \times 6 = 31$ kts. If King Salmon pressure is rising at a rate of 2 mb/hour while Kodiak is steady, then the pressure difference is increased by 2.4 times the pressure tendency according to the isallobaric rule at the top of the worksheet. In this case the Barren Island surface wind is $(990.2 + 2.4 \times 2 - 985.1) \times 6 = 59$ kts.

Figure 13 illustrates the worksheet used in determination of Resurrection Bay surface winds. This procedure derived by Ruben Schulz again is a pressure-differencing technique although in this case based on two nearly orthogonal pressure gradients: Anchorage-Cordova and Gulkana-Kenai. The pressure difference factor is multiplied by 8 and 12 to determine the wind speed range, and by 16 to account for gusts if the winds aloft are northerly. According to Schulz, the method is 95% effective, failing when a micro-pressure gradient is established between Anchorage and Seward, and Kenai and Seward. In this case, wind trajectories align themselves with the nearby glacier field and Resurrection Bay surface winds are "squirrely" (katabatic). Using Figure 13, if ANC-CDV = -10 mb and GKN-ENA = 6 mb then the surface wind prediction is from the south at 10 to 15 kts with gusts to 20 kts. A similar method will soon be published for Whittier-Passage Canal.

Such simple pressure-differencing techniques have worked quite successfully along the Alaskan coast as evidenced by the broad area over which this scheme is used. It must be pointed out, however, that this method is only valid when pressure gradients are significantly large and completely dominate the wind-producing balance of physical forces.

A more sophisticated surface wind forecasting measure is in use in the Valdez region. This procedure was formulated by Knowles and is completely described in the NOAA/NWS Alaska Region Technical Procedures Bulletin No. 3 appended to this report. It is essentially a resultant wind vector derived from summation of four component winds.

The pressure-gradient wind results from the orographic channeling of wind produced by the overall synoptic pressure pattern. This wind component is calculated by multiplying one half the geostrophic wind speed by a wind direction dependent factor varying from 0.2 to 0.7. Wind direction is determined by subtracting 50° from geostrophic and modifying by $\pm 10^\circ$ to 20° dependent again on wind direction.

Drainage wind or katabatic wind is a gravity-driven downslope density wind occurring over sloping snow and ice surfaces. The magnitude for the Valdez forecast is dependent on sky cover and season of the year. Flow direction is always from 080° down Valdez Glacier. If skies are forecast to be clear then in winter the drainage wind speed is 7 kts, in spring 5 kts, and in fall 4 kts. In summer, or if the sky is obscured, wind speed is always 2 kts.

Spill-over winds are the result of cold air from the Copper River Basin attaining a depth great enough to push southward through the passes of the Chugach Mountains. This cold air then flows seaward down the many tributary valleys and drains into Port Valdez. This wind exists only when Copper River Basin air is denser than that at Valdez, that is when the 1000-500 mb thickness is lower in the Copper River Basin. In this case the spillover component flows at a direction equal to the geostrophic direction and at speed equal to one-fourth geostrophic times a wind-direction dependent factor varying from 0 to 1.

The sea breeze is a solenoidal circulation resulting from differential diurnal heating of air masses over land and sea. During the day (providing the land is devoid of radiation-sinking snow and ice) there exists a landward wind component. In Valdez the peak speed is calculated as one half the expected diurnal temperature range in Fahrenheit degrees; the sea-breeze direction is from 180° at onset (9-10 AM), from 220° at peak flow (2-3 PM), and from 300° at its ending (9-10 PM). The final Valdez surface wind prediction is derived by vectorially summing the component winds. An example and further hints are also contained in the Bulletin appended.

A relation between surface winds in coastal passes and isobaric spacing and orientation was worked out by Philip Weber of the old Weather Bureau from oil company data taken in Bear Creek Pass in the Alaska Peninsula in 1959. Examination of winds at stations near the mouths of other coastal mountain passes indicate similar results to the pilot study. A most interesting feature is the information on geostrophic departure. This work is still used in coastal wind predictions, and is appended to this report (Surface Winds in some Alaskan Coastal Passes).

It is felt that these methods of predicting coastal winds in Alaska will be of value to the OCSEAP endeavor, especially if numerical modeling

attempts are shortcoming. Although often simple in their physical approach to prognostication, the success which these techniques have enjoyed is indicative of continued development. Toward this end, PMEL researchers will share pertinent results learned from Alaskan fieldwork with the forecasting group at NWS, Anchorage. In turn, NWS Anchorage will appraise PMEL of modifications to coastal wind forecasting techniques.

6. Generalizations and Suggestions for Future Research

Flow in northern Cook Inlet is orographically channelled with winds being almost independent of the synoptic scale pressure pattern. Winter winds predominantly blow down the inlet while summer winds are predominantly up the inlet. The very brief record from EB-39 shows that lower Cook Inlet winds more closely resemble the synoptic scale flow inferred from Putnins work; that is the blow primarily along a NW-SE axis. However, since this axis coincides with the axis that passes through Kamishak Gap and Kennedy Entrance, the LCI winds are also strongly influenced by orography.

The two nearly orthogonal flow axes of lower and northern Cook Inlet intersect somewhere in LCI. With westerly flow through Kamishak Gap and northerly flow down northern Cook Inlet there is convergence in LCI with strong winds exiting the region over the Barren Islands. In the summer LCI can become an area of divergence. The precise location of the center of these converging/diverging regions is unknown and no doubt varies significantly. Therefore LCI is strongly nonhomogeneous in wind direction, and, probably speed.

As a useful "first guess guideline," the report made by Dames and Moore (reported in the Final Environmental Statement of the Proposed 1976 Outer Continental Shelf Oil and Gas Lease Sale, Lower Cook Inlet) is useful. Dames and Moore reduced Putnins' 22 flow regimes to 5 basic synoptic scale flow directions for Cook Inlet. Then, based on evidence presumably similar to that presented in this report, they prepared wind direction and isotach maps. The isotachs they showed were the best estimates of the mean wind speeds. To account for light and extreme wind speeds, they proposed a probability distribution for wind speed with which one could estimate the frequency of occurrence of different wind speeds for a given flow pattern.

Because they serve as a useful guideline, the five basic patterns with the suggested mean isotachs from the Dames and Moore report have been adapted and are shown in Figures 14a to e. According to Dames and Moore, speeds in the range of 0.5 to 1.5 times the mean wind speed occur 60% of the time for a given pattern. They suggest high wind speeds (1.5-2.5 times mean speed) occur 20% of the time, very high winds 5% of the time and light winds 15% of the time. In Figure 14 the frequencies of occurrence of the normal wind speed regime of the pattern shown for four months of the year are listed.

The gross features of the winds at Homer, Kenai, and perhaps the small sample at EB-39 are reproduced in these figures. Because of the success of these figures at certain locations (locations that no doubt were the major inputs to the calculations) it is tempting to regard the entire set of figures as pat. In terms of predicting oil spill trajectories in LCI this would be a grave error. These figures are simply interpolations and extrapolations to the data-deficient western side of Cook Inlet. The actual

wind speeds and directions at given locations for two similar synoptic scale pressure patterns (i.e. same Putnins type) may differ significantly from each other and from the archetypes of Dames and Moore.

As one example, recall from section 5 that the isallobasic wind component, that component of the flow out of balance with other forces due to pressure tendencies, can nearly double the wind speed (according to NWS forecasting techniques which also need further verification). A straight Putnins-type approach which pays no attention to the pressure pattern history cannot reveal the mesoscale effects of the isallobasic wind. The mesoscale pressure network study to be undertaken by PMEL will reveal what areas of LCI are most affected by the isallobasic wind component and to what degree. It will also be determined whether a Putnins or mode approach is useful on a small regional scale, and whether more forecasting algorithms for specific locations (say EB-39) can be devised.

Another area in which the Dames and Moore archetype approach fails is in showing the severe gusty winds that pilots report such as those flowing out of Kamishak Gap and then diverging in the vicinity of Augustine Island. The two remote weather stations to be placed on Augustine Island and in Bruin Bay will add substantially to the knowledge of western shore processes.

Lower Cook Inlet is meteorologically complex. The analysis of the mesoscale pressure network along with data from EB-39, two remote weather stations, and scattered ship reports may fail to adequately resolve the complexities sufficiently enough to make meaningful improvements to the Dames and Moore work. At worst some estimate of the feasibility of their approach and the magnitude of the errors associated with using it will be determined. Thorough solution of the lower Cook Inlet meteorological problems may come only with the use of more instrument platforms in the inlet itself (buoys, oil rigs) or with an instrumented aircraft free to probe the entire region.

LIST OF TABLES

- I. A brief summary of Putnins' flow types in the vicinity of Cook Inlet
- II. Month, Putnins' flow type, and rank of occurrence
- III. Month, Putnins' flow type, and rank of maximum speeds observed at Anchorage

TABLE I

Brief Summary of Putnins' Flow Types in the Vicinity of Cook Inlet

TYPE	GEOSTROPHIC WIND DIRECTION	COMMENTS
A,Ac	ESE	Low in Gulf of Alaska (GOA)
A'	N-NW	Cyclonic flow in GOA, weak and spotted low centers over Cook Inlet (CI)
A''	W	Low center in Alaska, strong westerlies over CI
A'''	SSW	High in GOA, strong winds
A ₁	N	Low in GOA, strong winds
A ₂	SSE	Low in Aleutians, strong winds in Kennedy Entrance
A ₃	W	Weak pressure gradient
B	W	Low in North Pacific, weak and poorly defined pressure gradient
C	ENE	Weak low in GOA, easterlies in Kennedy Entrance
D	E	High over Yukon
D'	NNE	High over Bering Sea and Alaska, Lows in North Pacific
D ₁	ENE	Broad band of easterlies into Kennedy Entrance
E	SE	Low in North Pacific, High over Yukon
E'	SE	Weak low over Aleutians
E''	NE-SE	Deep low over Kamchatka, high over Yukon, low near Queen Charlotte Islands
E ₁ ,	SE	Low over Aleutians
E ₁	S	Low over Aleutians, southerly winds diverging over CI
F	W	Cold front in vicinity of CI
F ₁	ENE	Long band of ENE winds
G ₁	NNW	Low in GOA
H	NNE	Low in GOA

TABLE II

Month, Putnins' Flow Type, and Rank of Occurrence

DECREASING ORDER OF PERCENTAGE OF OCCURRENCE

TYPE	I	II	III	IV	V	VI	VII	VIII
A		11	1,2,5	3,9,10,12	4,6	8		
A _c	10						11,12	3,9
A'	3,4,5,6, 8,9,10,11, 12	1,2,7						
A''		8	7	6		9	10	
A'''						7	8	
A ₁		12	3,4	11		1,2,10	6,9	
A ₂			6	5,7	8,9			
A ₃								
B								
C								
D	1			2,4	3	12	7	11
D'								6,7
D ₁					12	3		1,2,5
E		9		8	7,10	4,5,6,11	1	
E'	7	5,6	8,9				2,4	
E''								
E ₁								
E' ₁			11		1,2		3,5	4,8,10,12
F								
F ₁								
G								
H	2	3,4	10,12	1	5,11			

TABLE III

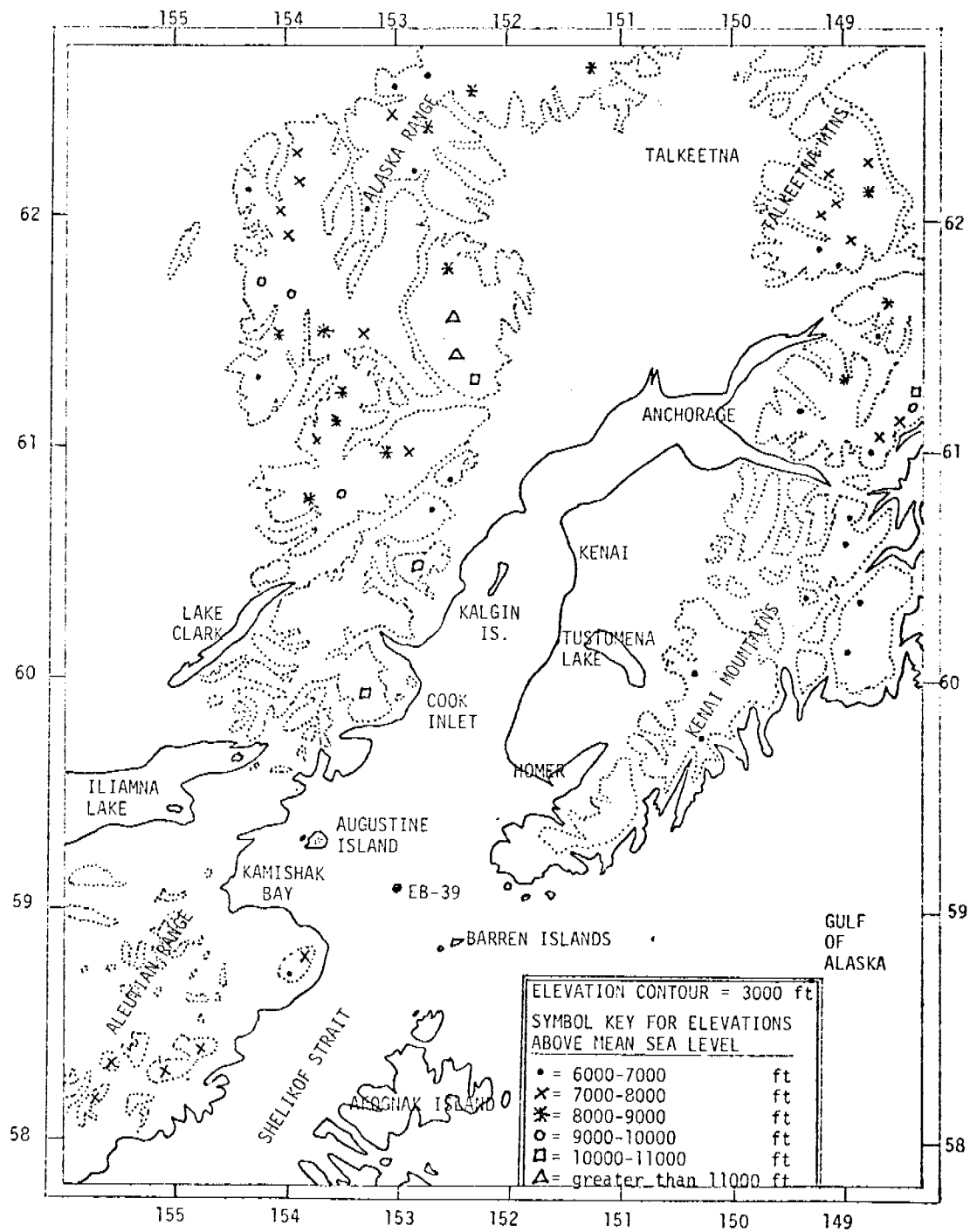
Month, Putnins' Flow Type, and Rank of Maximum Speeds Observed at Anchorage

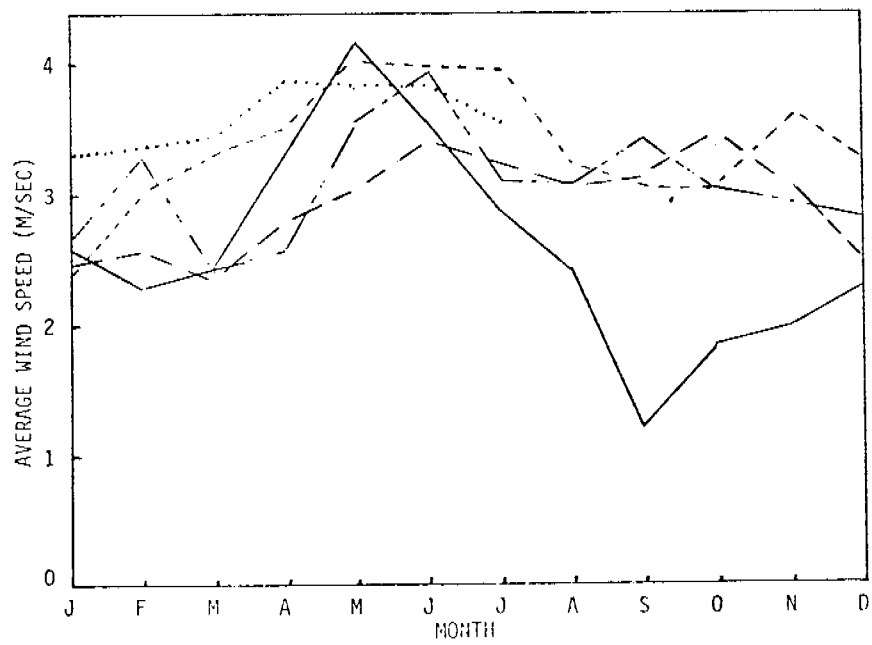
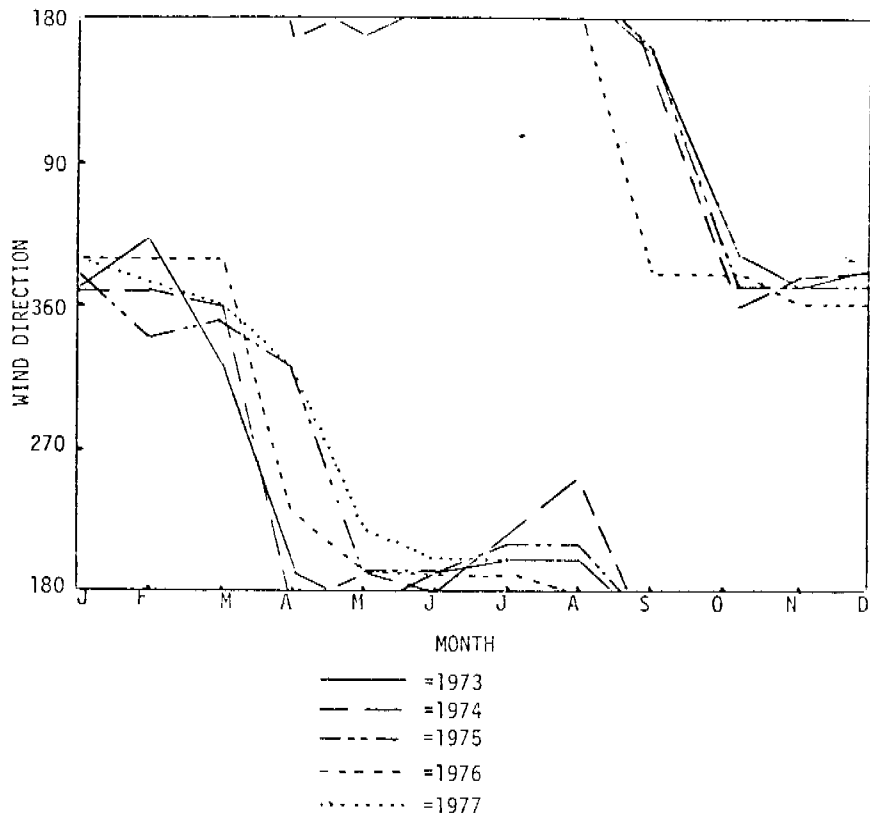
DECREASING ORDER OF MAXIMUM SPEED

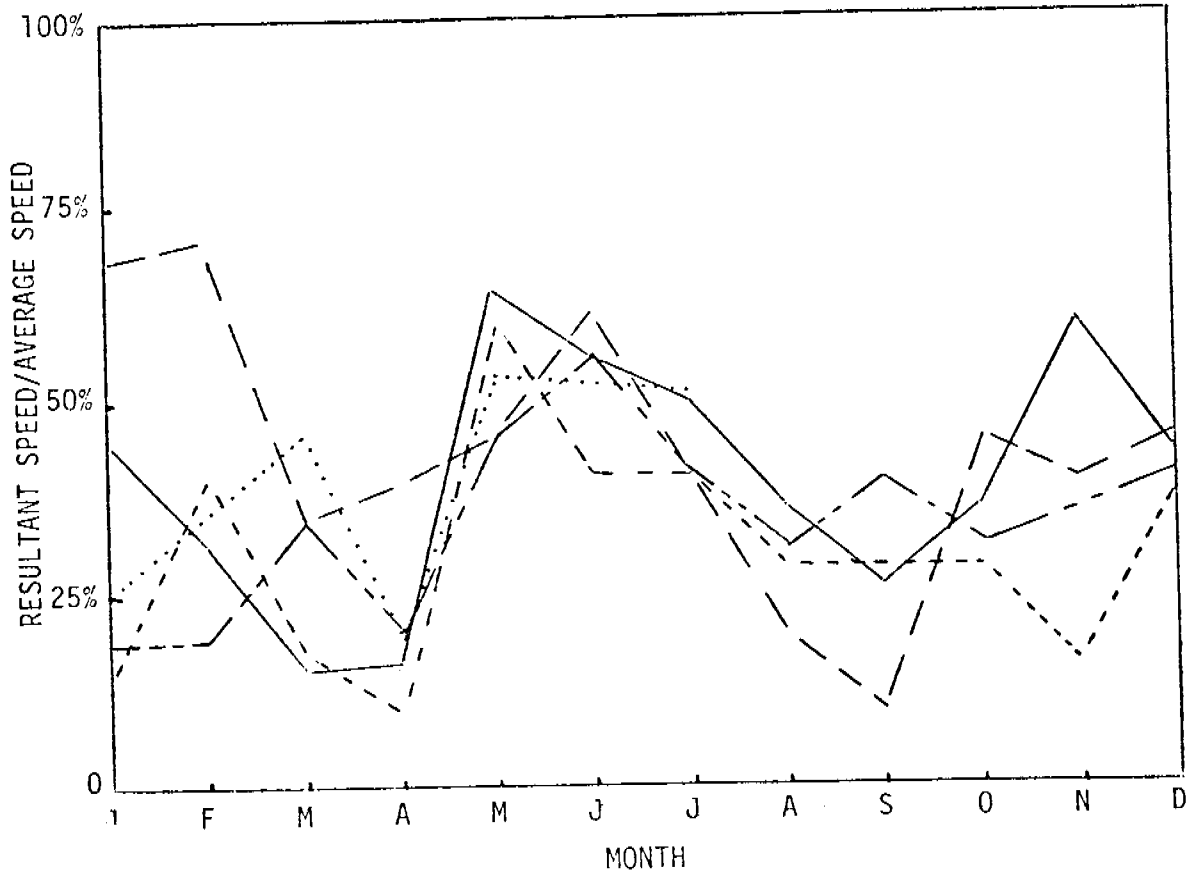
TYPE	I	II	III
A	10	2,5	9
A _C			3,12
A'	5,9	3,4,7,10,12	8,11
A''	8		6
A'''	6		
A ₁	4	11	2
A ₂	1	6	7,10
A ₃			
B			
C			4
D			5
D'	2,3,11,12		
D ₁			
E			
E'	7		
E''			
E ₁		8	1
E ₁ '			
F			
F ₁			
G		9	
H		1	

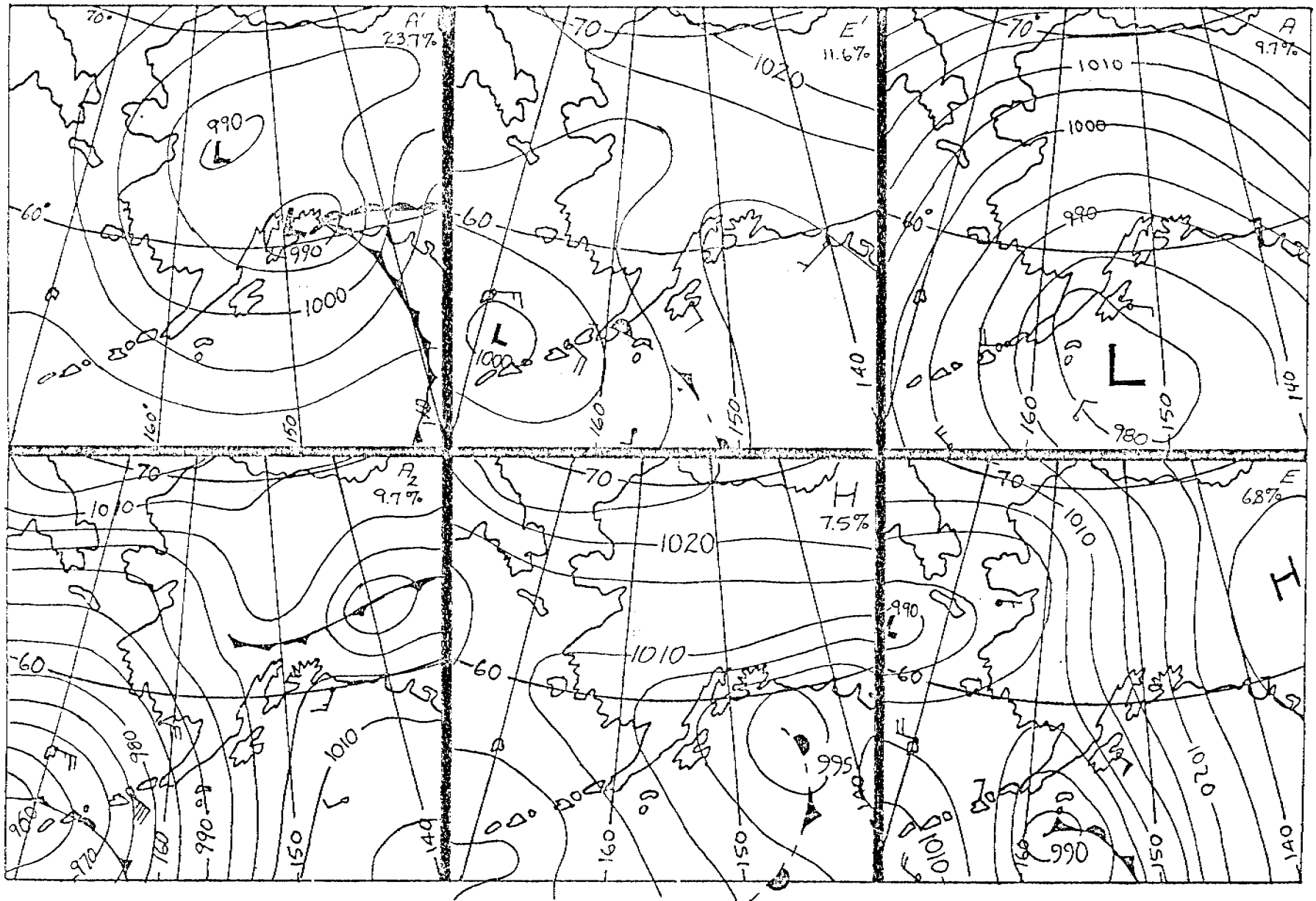
LIST OF FIGURES

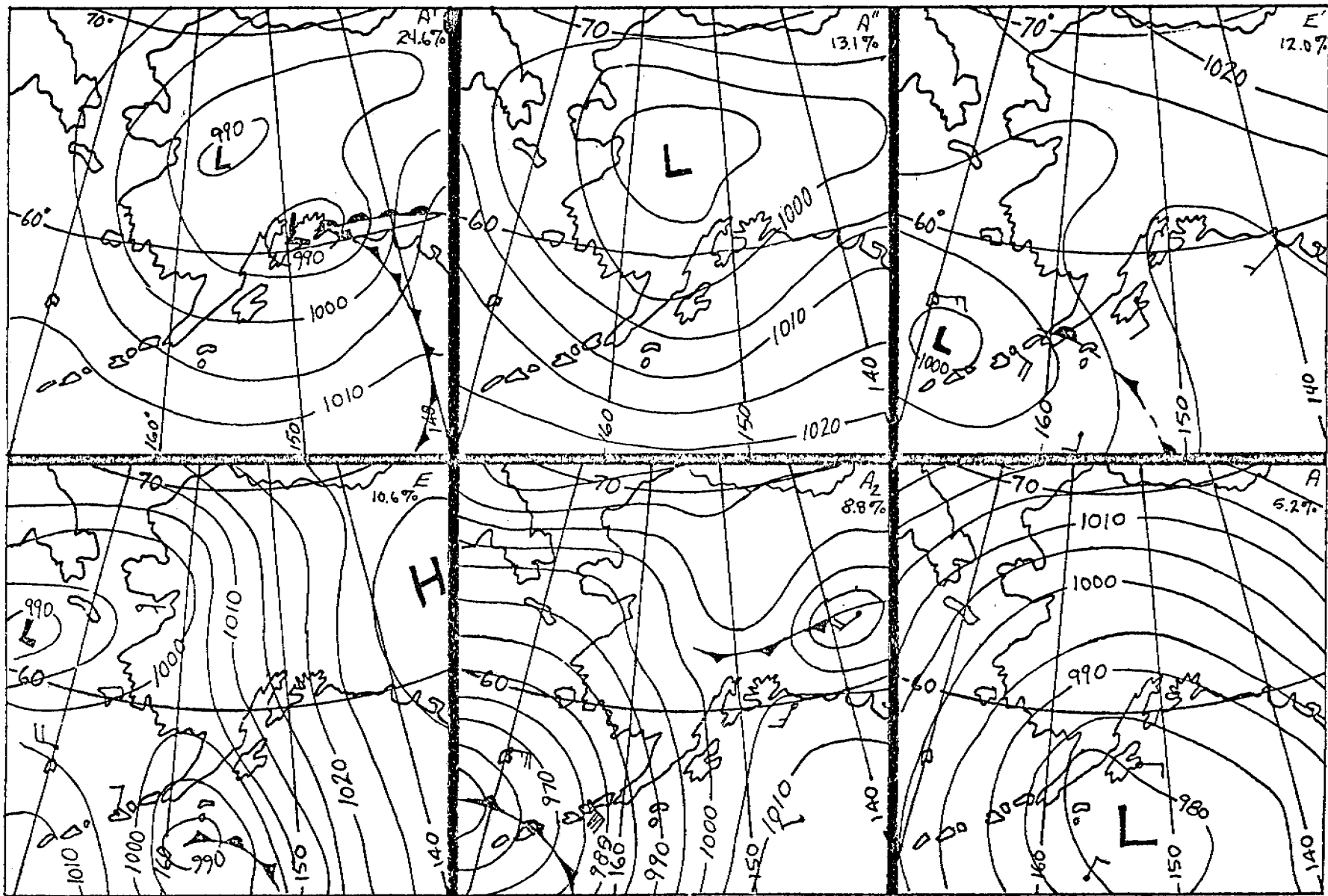
Figure	Caption
1	Topography in the Cook Inlet area
2	Monthly resultant wind direction from 4½ years of Anchorage (airport) data
3	Monthly average wind speed at Anchorage
4	Monthly resultant wind speed divided by monthly average wind speed at Anchorage
5	Most common synoptic types as classified by Putnins (1966). Classification symbol and percentage of occurrence are shown in upper right hand corners: a) May, b) August, c) November, d) February
6	Wind fabric diagrams for Homer, constructed from 1970 three hourly data
7	Wind fabric diagrams for Kenai, constructed from 1970 three hourly data
8	Orientation of geographical features near lower Cook Inlet for interpretation of wind fabric diagrams
9	Time series of wind speed, direction and temperatures from EB-39. Blank spaces are bad or missing data: a) July, b) August, c) September
10	Wind fabric diagram (a) and energy diagram (b) of the EB-39 data shown in Figure 9.
11	Wind fabric diagram approximation for lower Cook Inlet, July through September, constructed using Putnins (1966).
12	NWS worksheet used for wind forecasting at selected locations
13	Wind forecasting worksheet for Resurrection Bay
14	Mean wind speeds and directions in lower Cook Inlet as suggested by Dames and Moore; a) northerly geostrophic wind b) southeasterly geostrophic wind, c) easterly geostrophic wind, d) northwesterly geostrophic wind, e) southwesterly geostrophic wind.

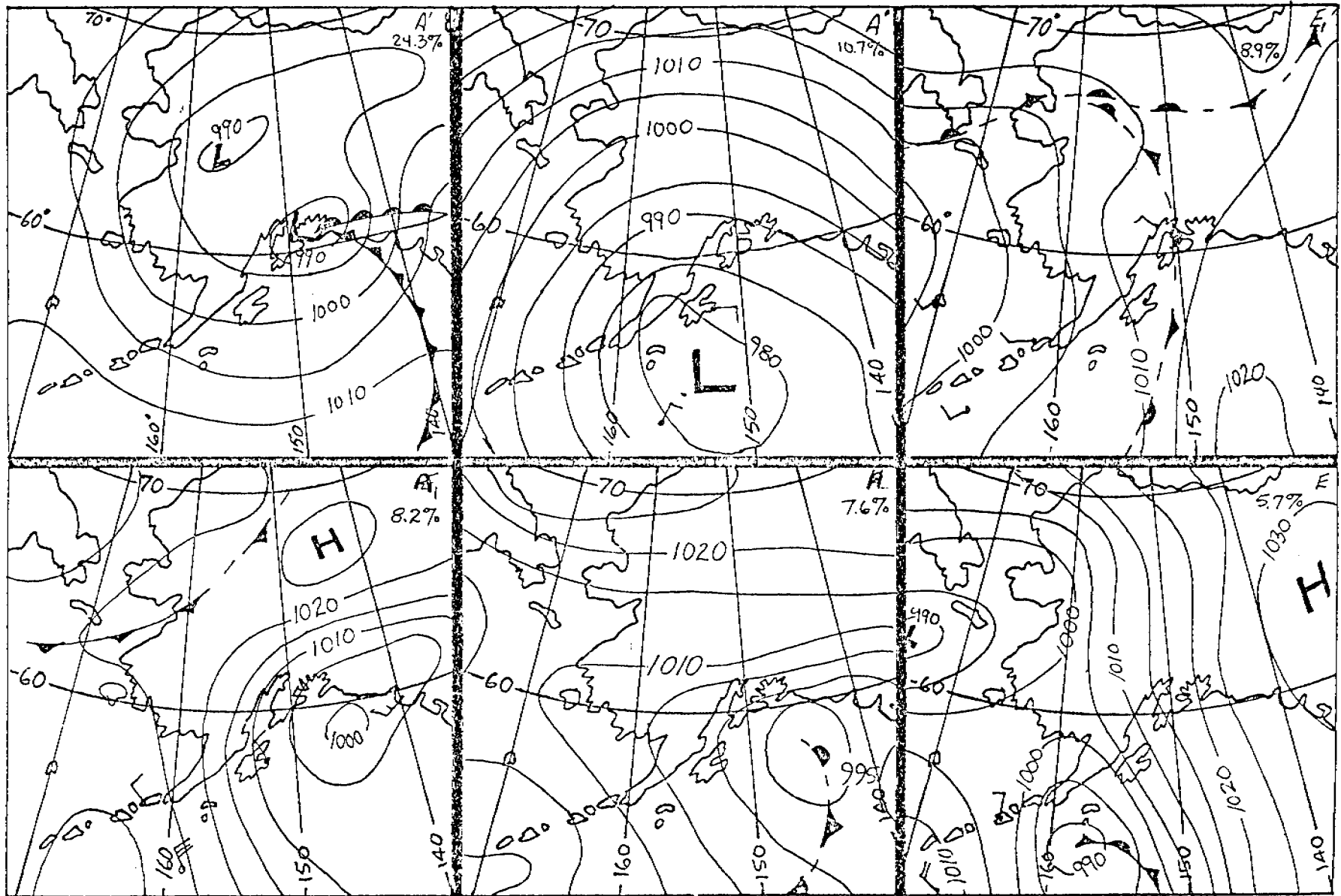


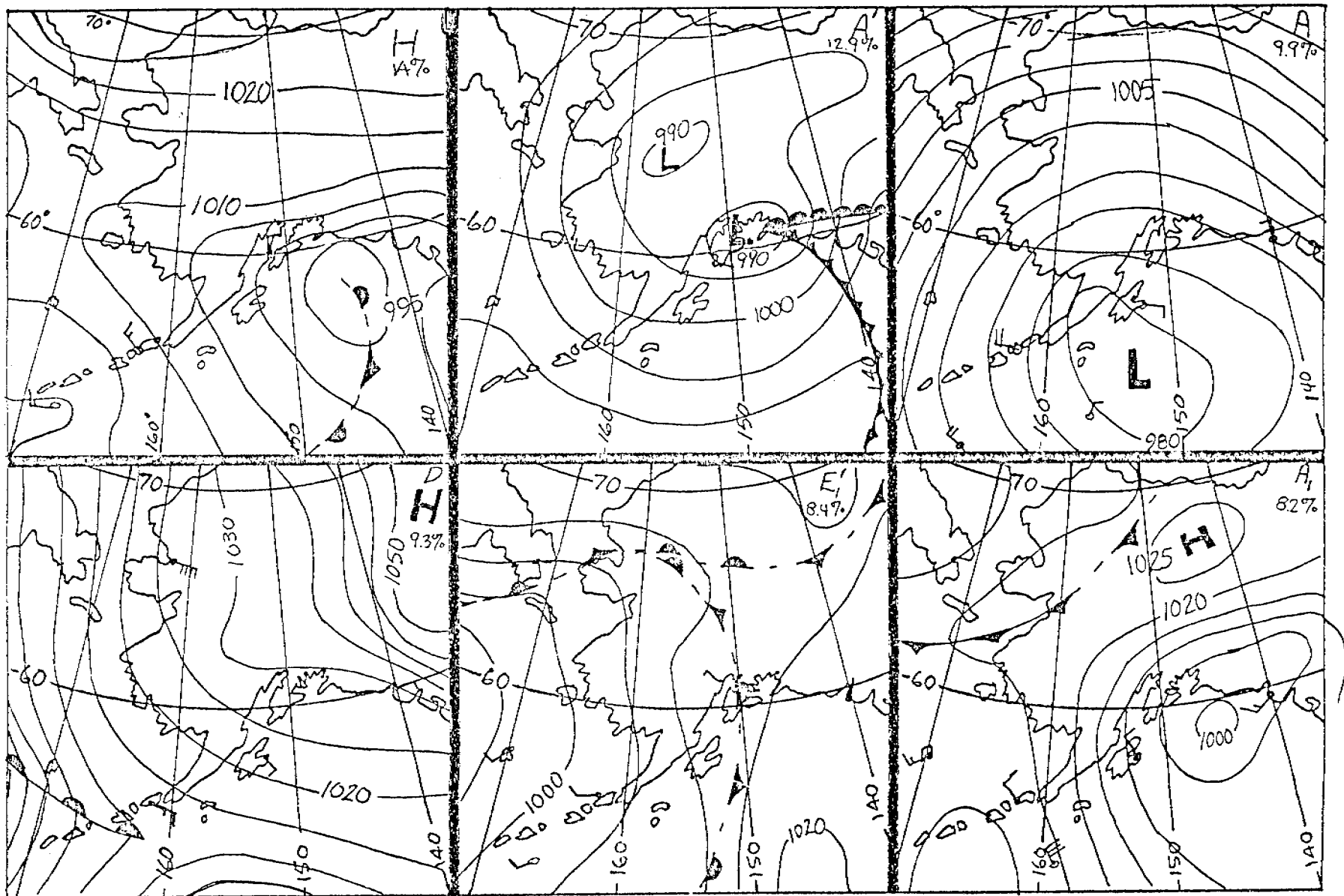


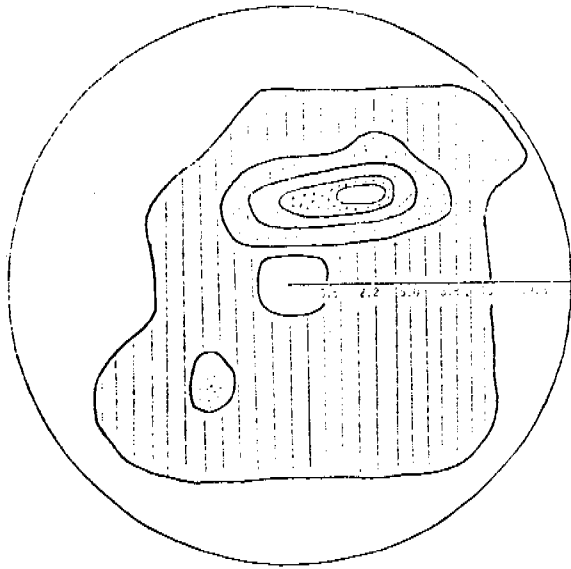




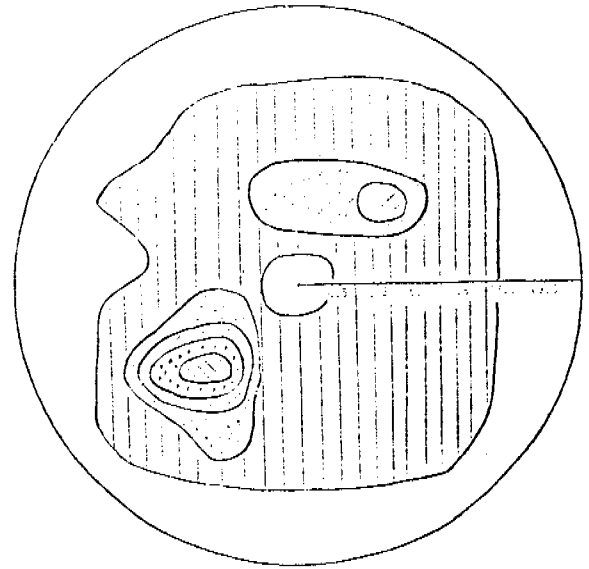




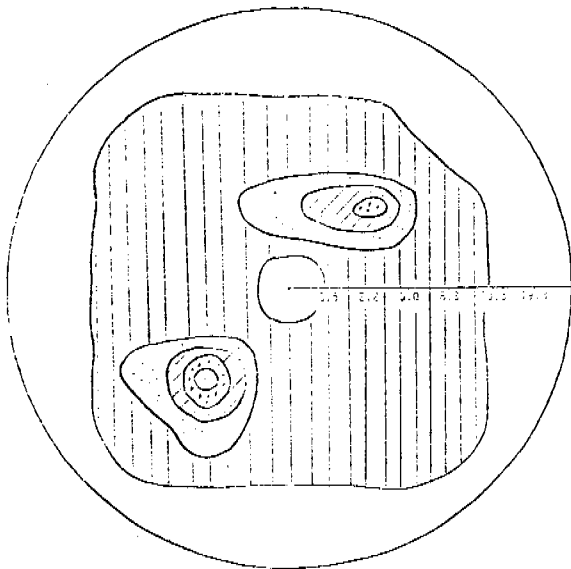




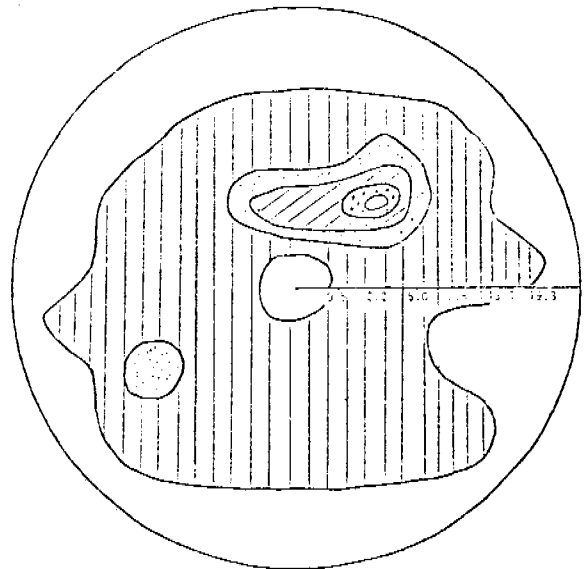
JANUARY-MARCH



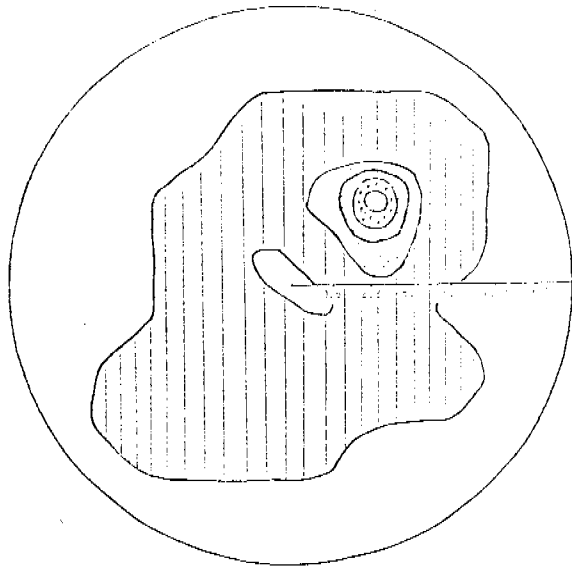
APRIL-JUNE



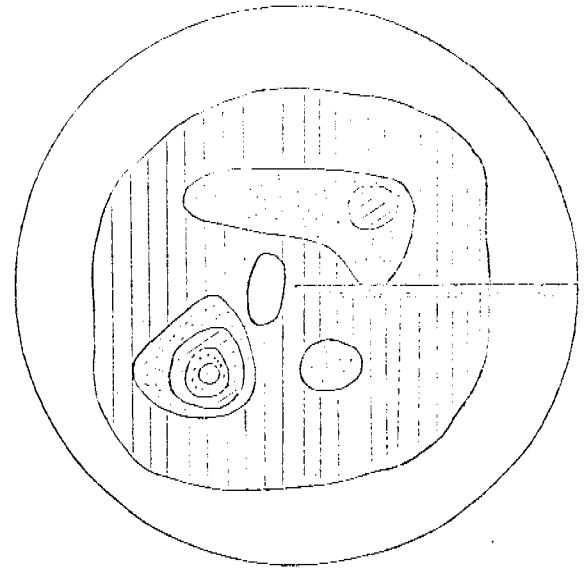
JULY-SEPTEMBER



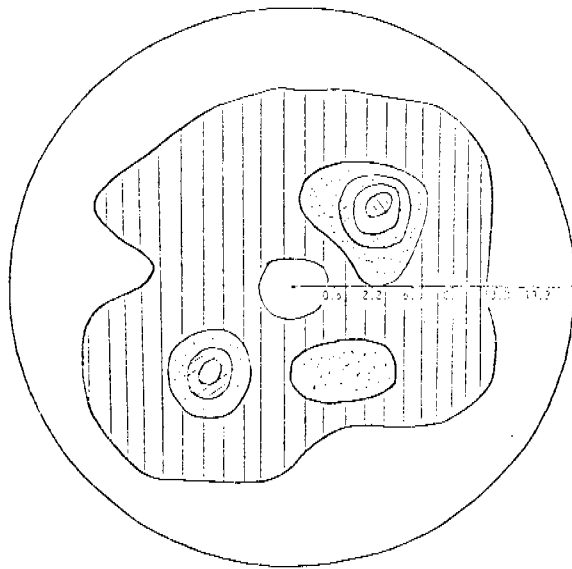
OCTOBER-NOVEMBER



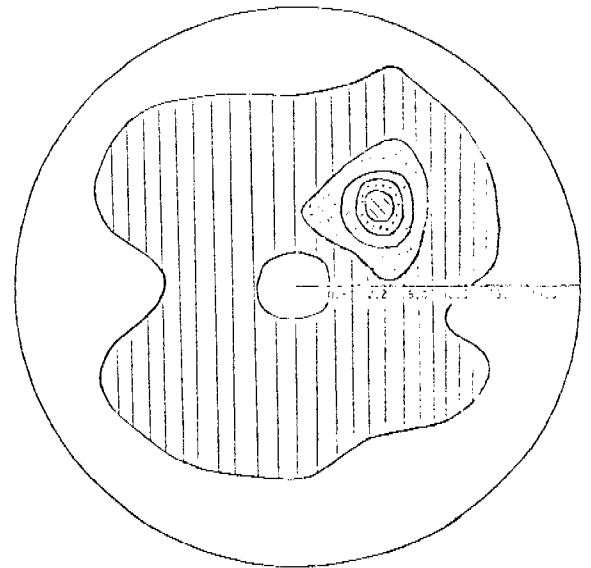
JANUARY-MARCH



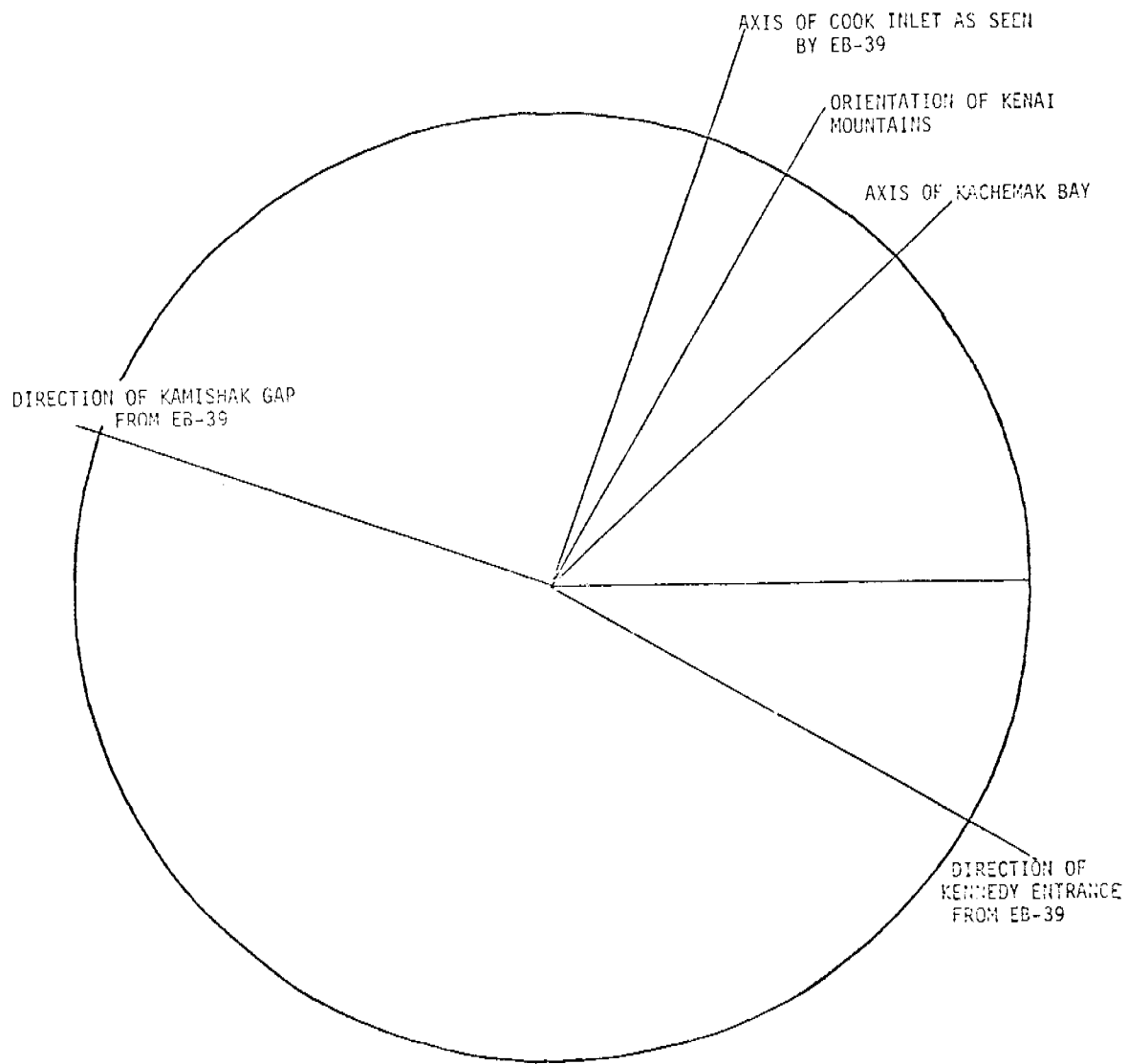
APRIL-JUNE



JULY-SEPTEMBER



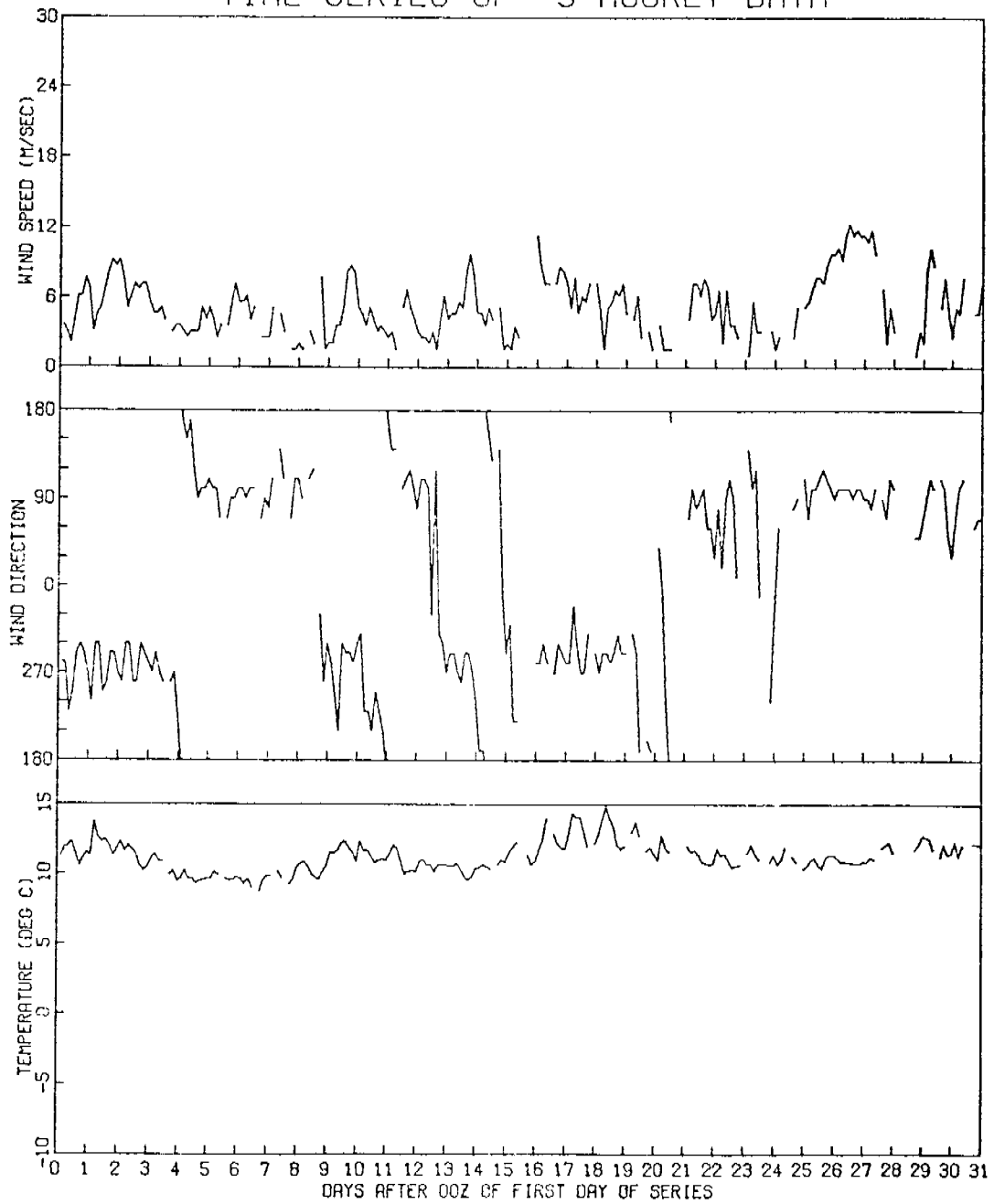
OCTOBER-NOVEMBER



EB39

1 JUL THROUGH 31 JUL 1977

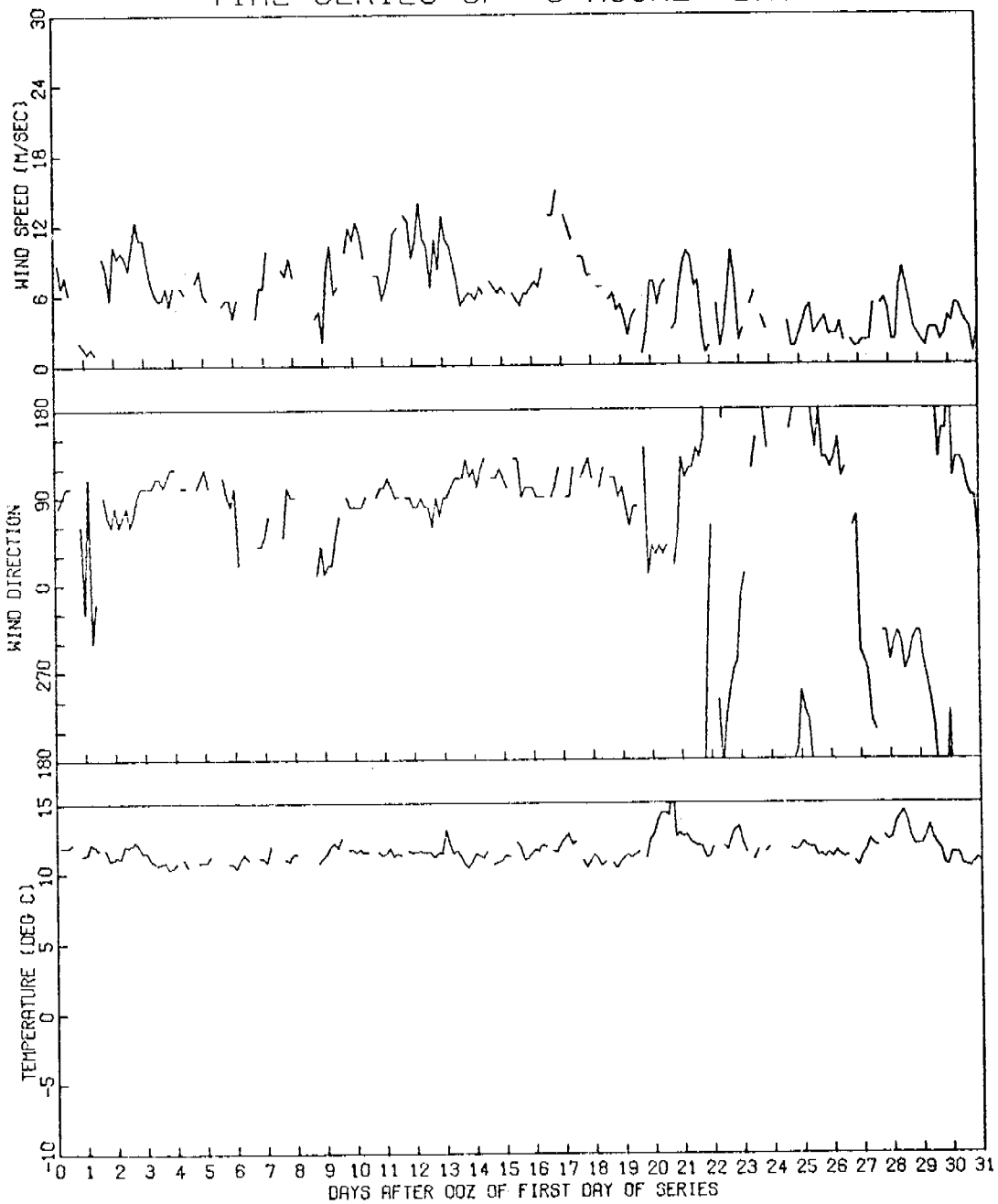
TIME SERIES OF 3 HOURLY DATA



EB39

1 AUG THROUGH 31 AUG 1977

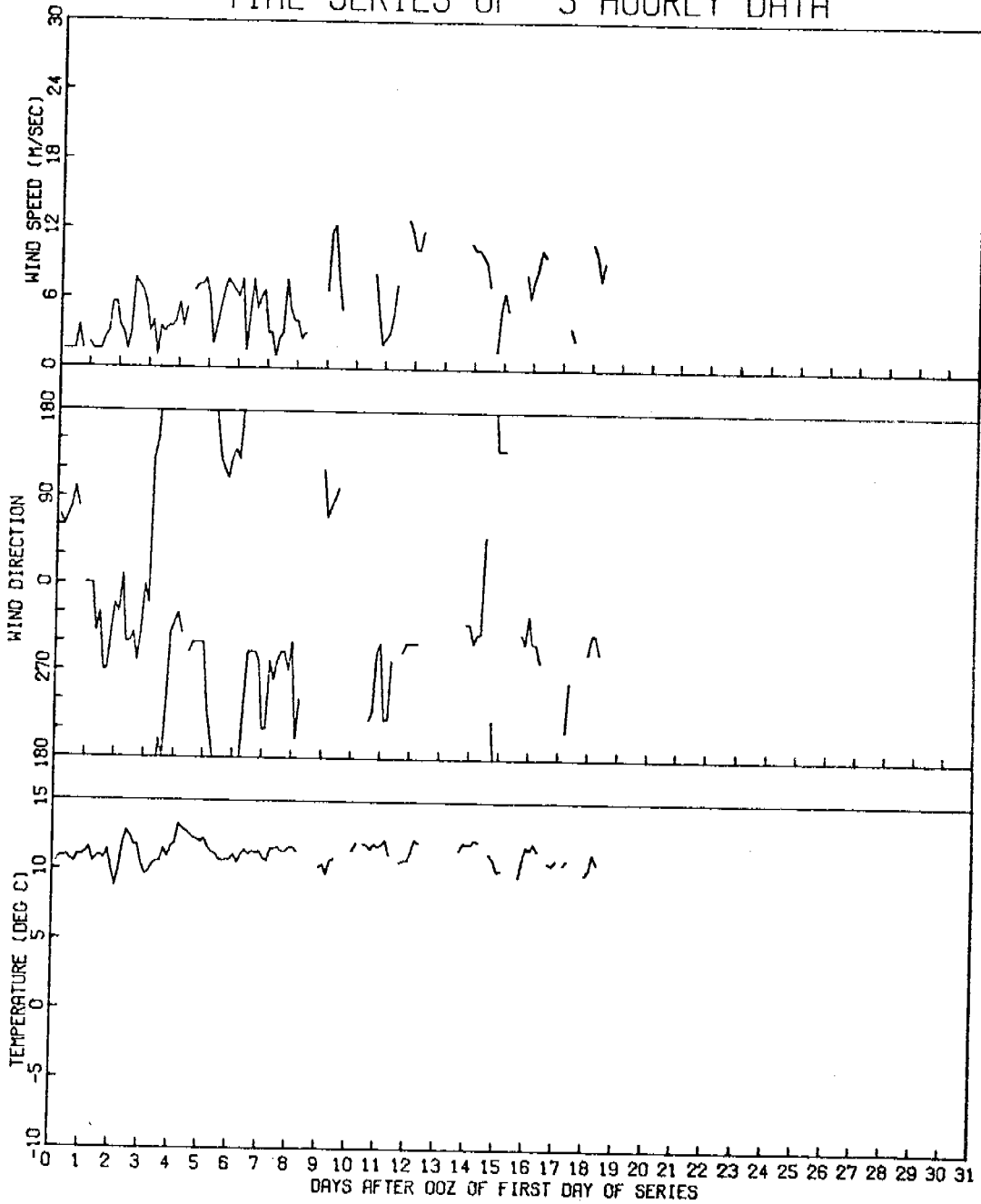
TIME SERIES OF 3 HOURLY DATA

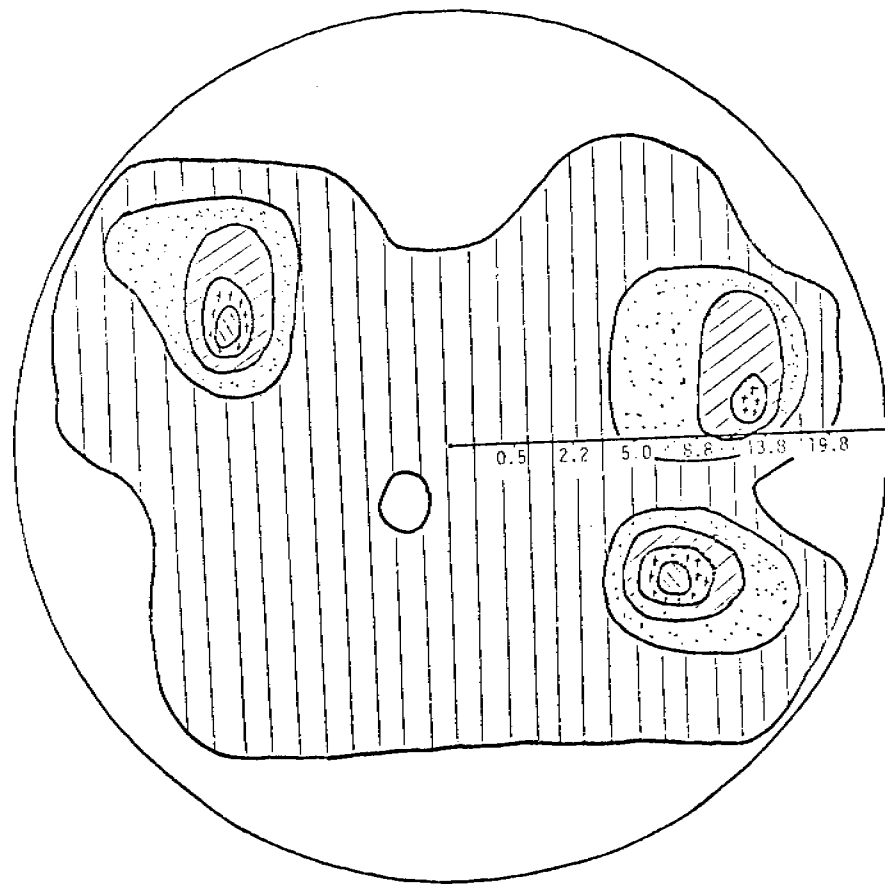
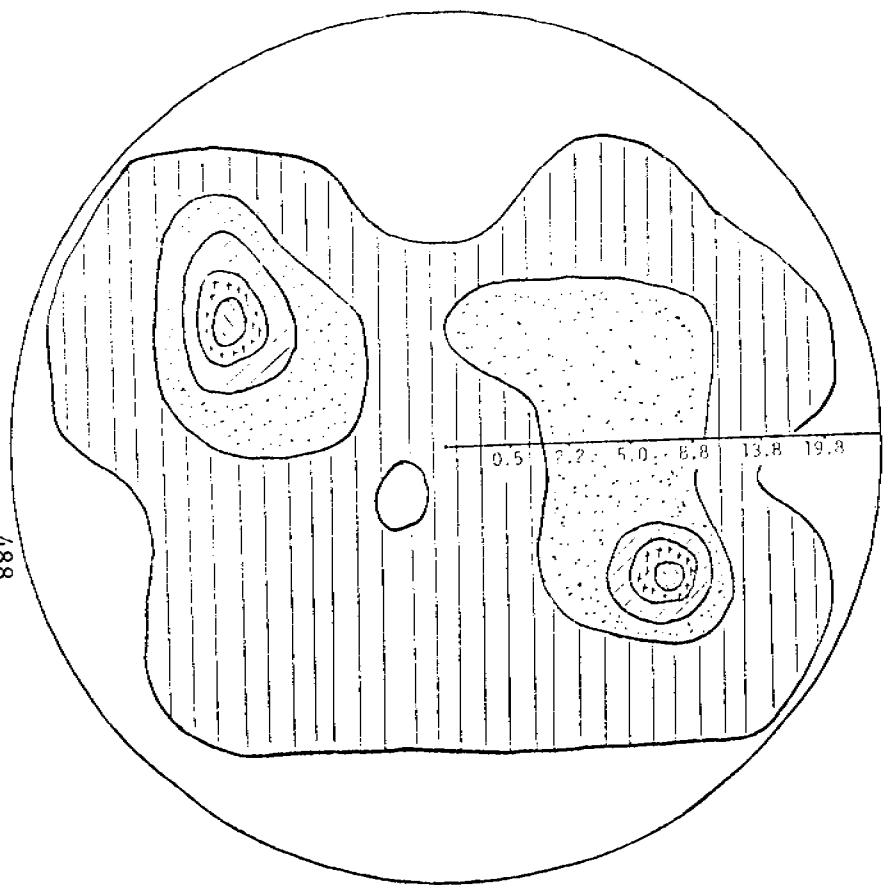


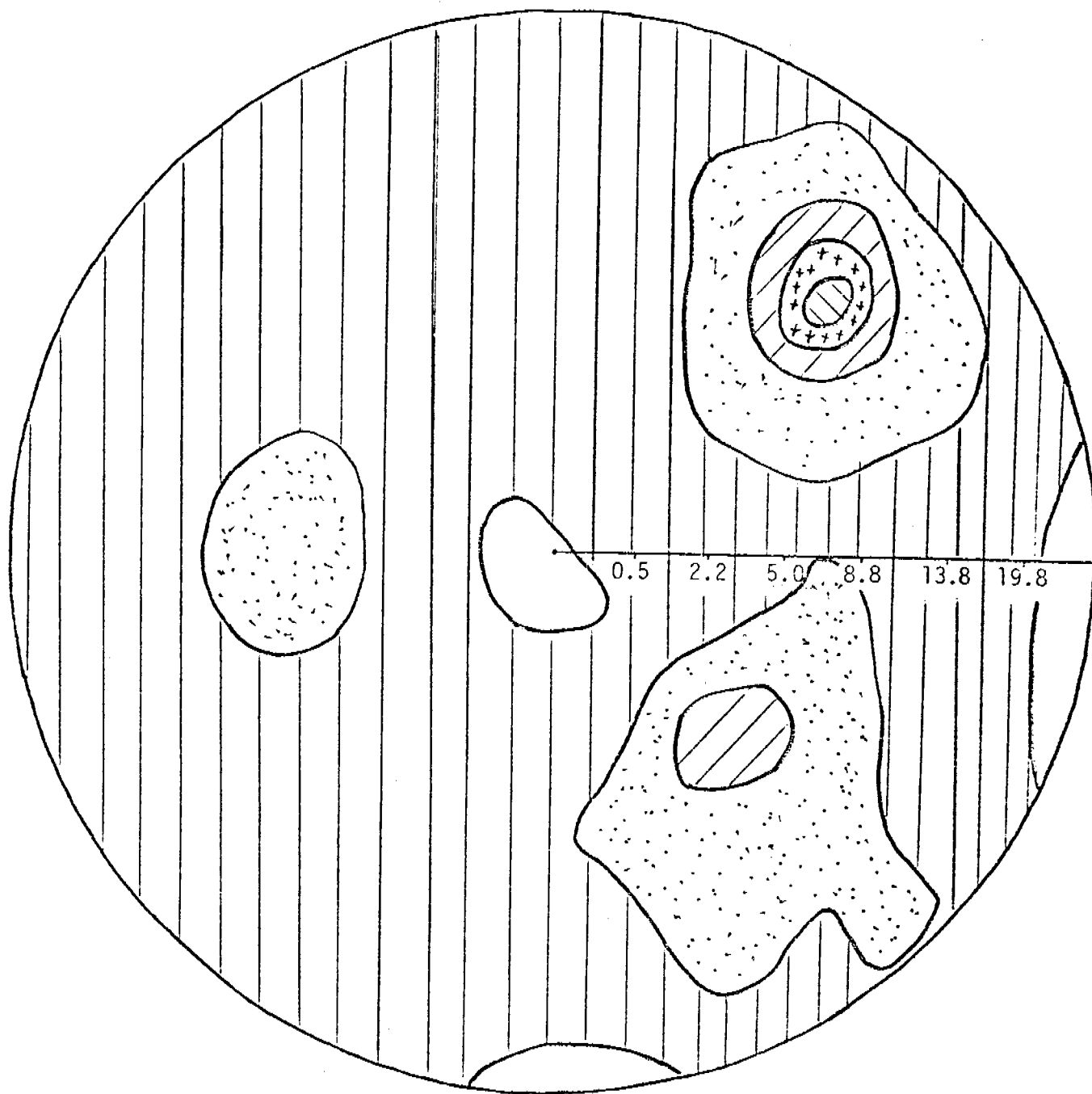
EB39

1 SEP THROUGH 30 SEP 1977

TIME SERIES OF 3 HOURLY DATA







DELTA P

(Date GMT) _____

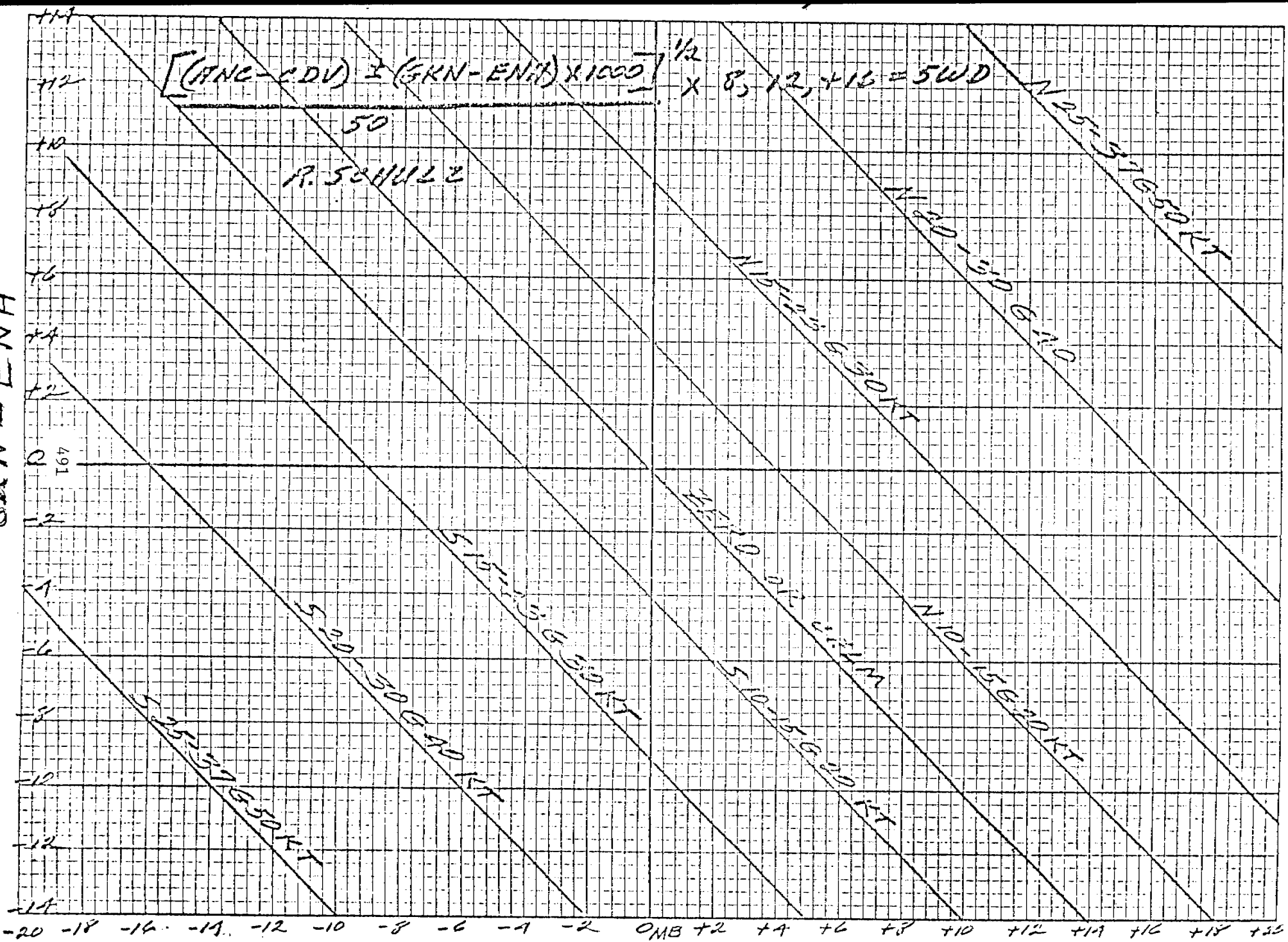
Correction factor due acceleration at 6GN is 2.4 times the pressure change per hour.

WIRE No	ADQ-ADQ 4-5X	ANC-ANC 6X	CDV-CDV 5X	IRK-IRK 4X	JNU-JNU 3X	SIT-SIT 2X	CDV-CDV	IRA-IRA	ANC-ANC	MOG- CDV
00										
01										
02										
03										
04										
05										
06										
07										
08										
09										
10										
11										
12										
13										
14										
15										
16										
17										
18										
19										
20										
21										
22										
23										
	barren islands	turnagain arm and Whittier	copper rvr delta	dry bay	lynn canal 490	max gst sitka	PAQ wnd study		ANC wnd study dsipt fog 1.3+ N wnd 3.0+	

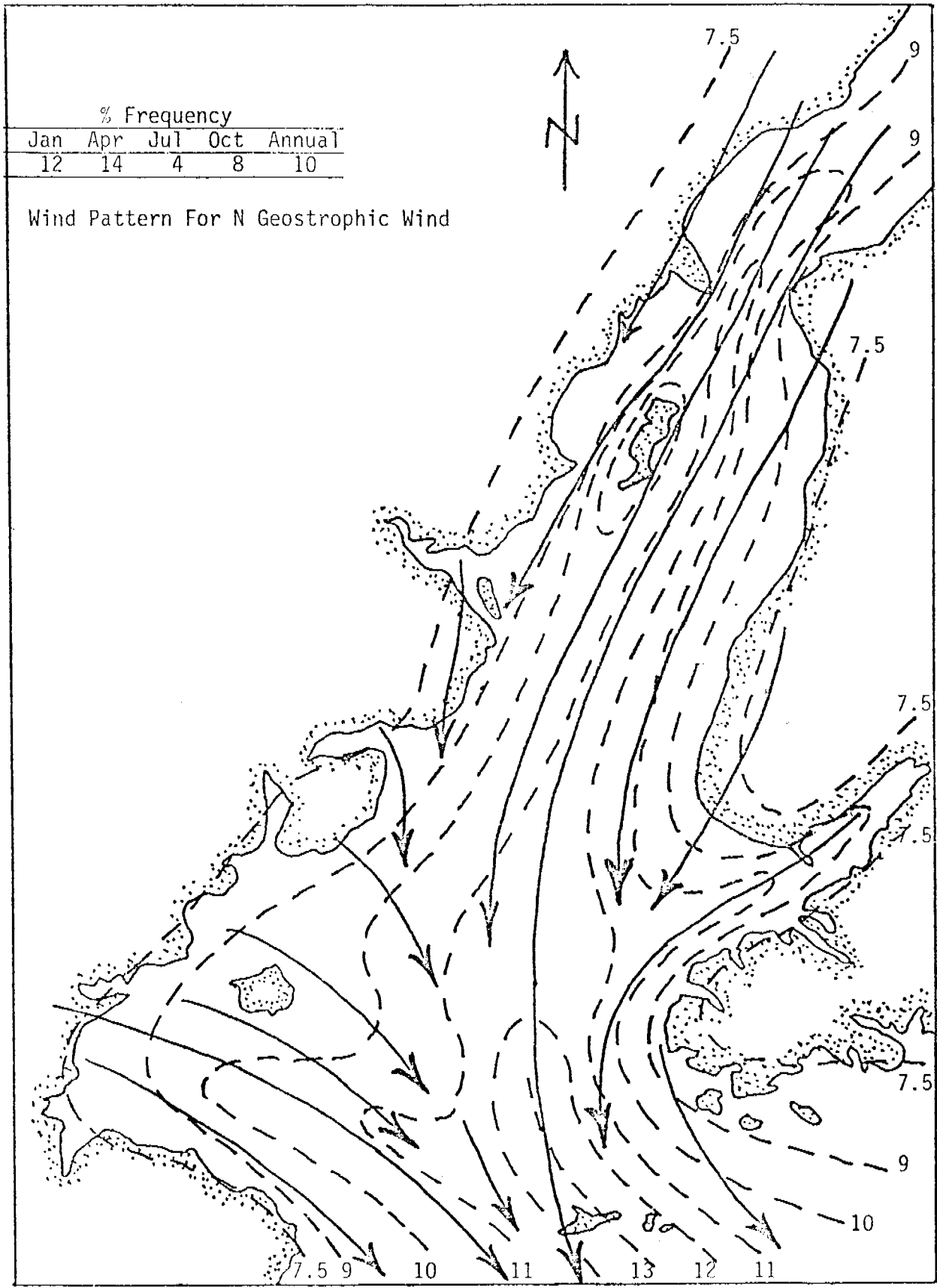
GKN - ENA

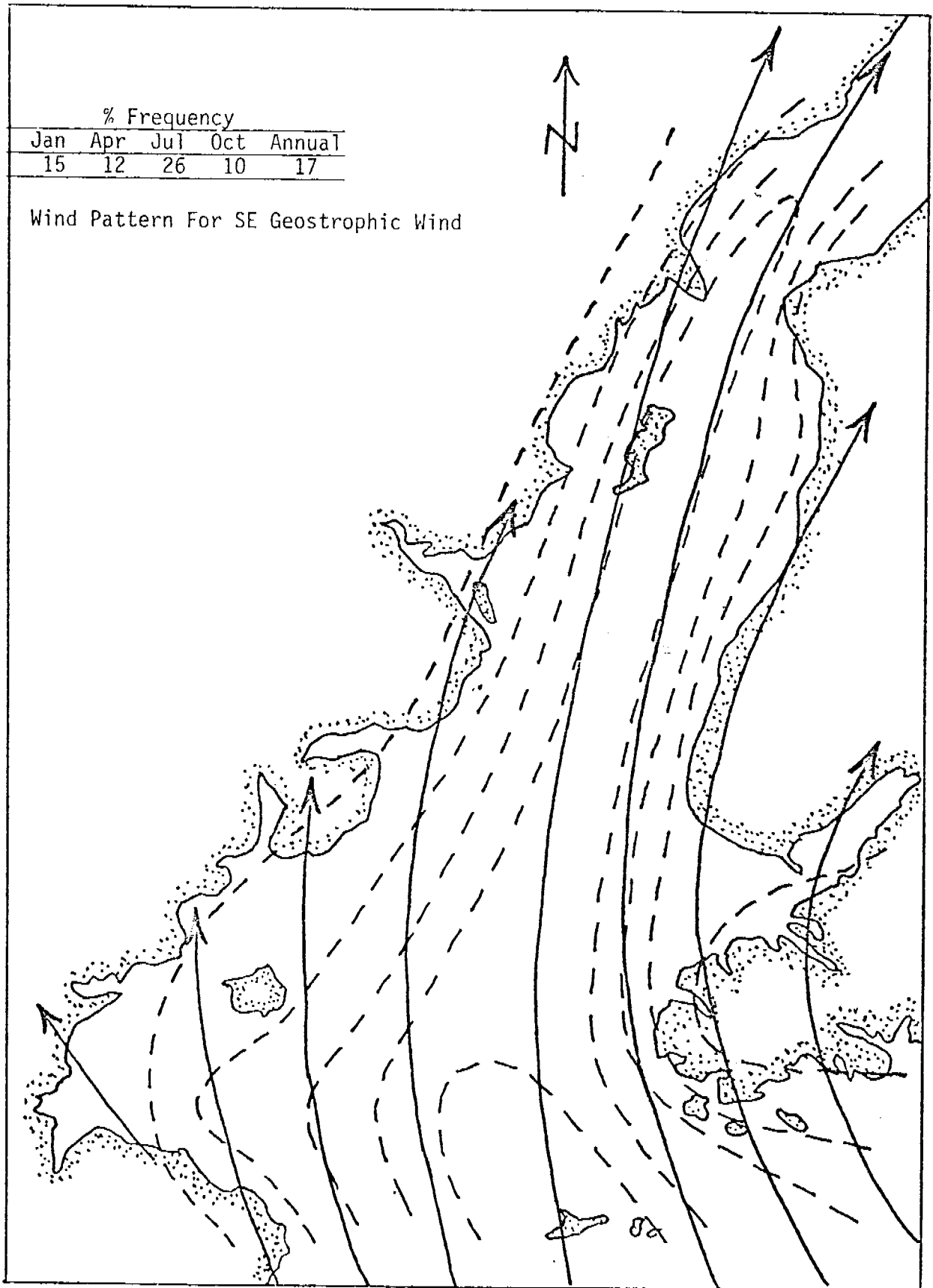
$$\left[\frac{(FNE - CDV) \pm (GKN - ENA) \times 1000}{1/2} \right] \times 8, 12, +16 = 5WD$$

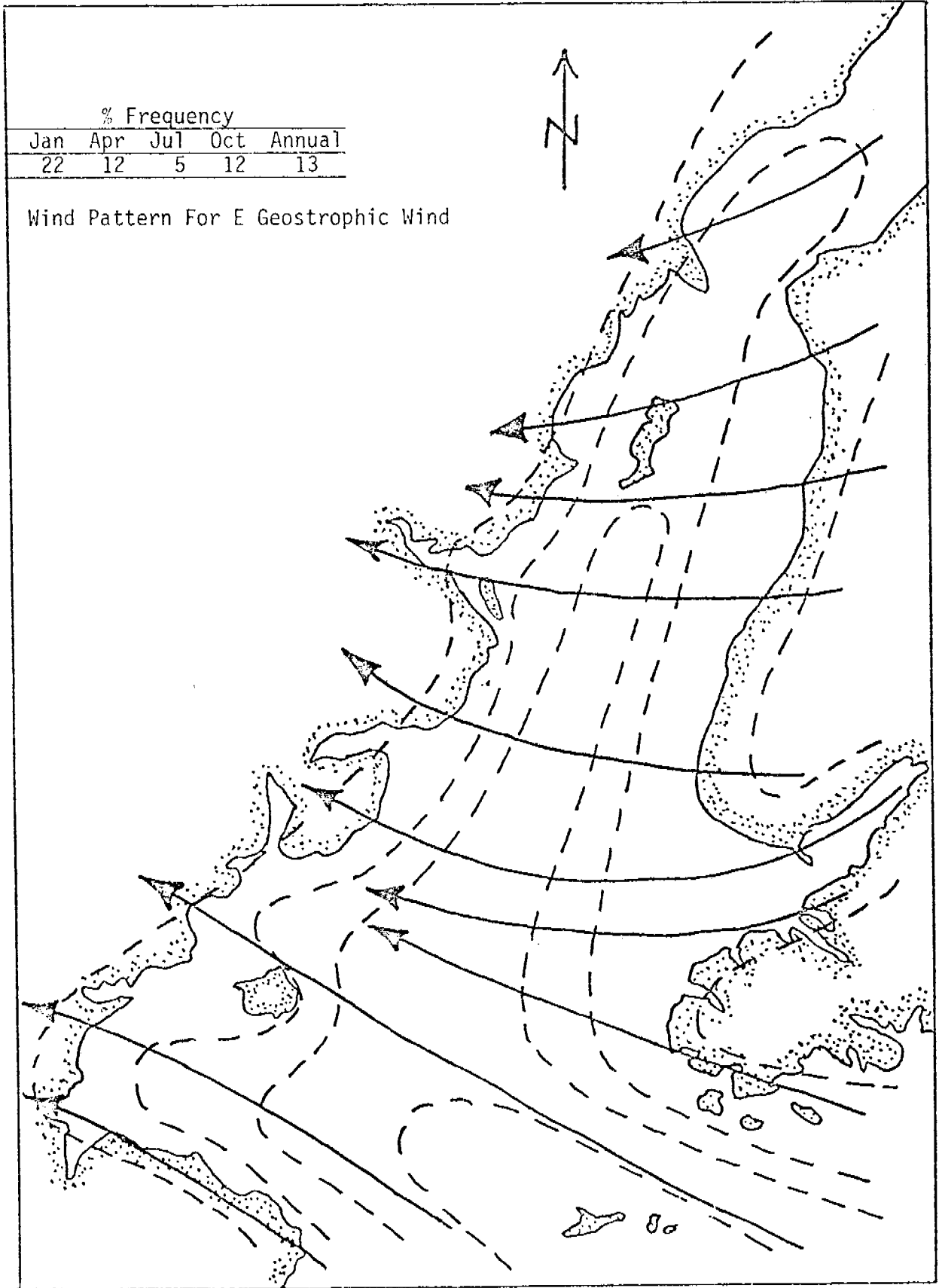
50
R. SCHULZ

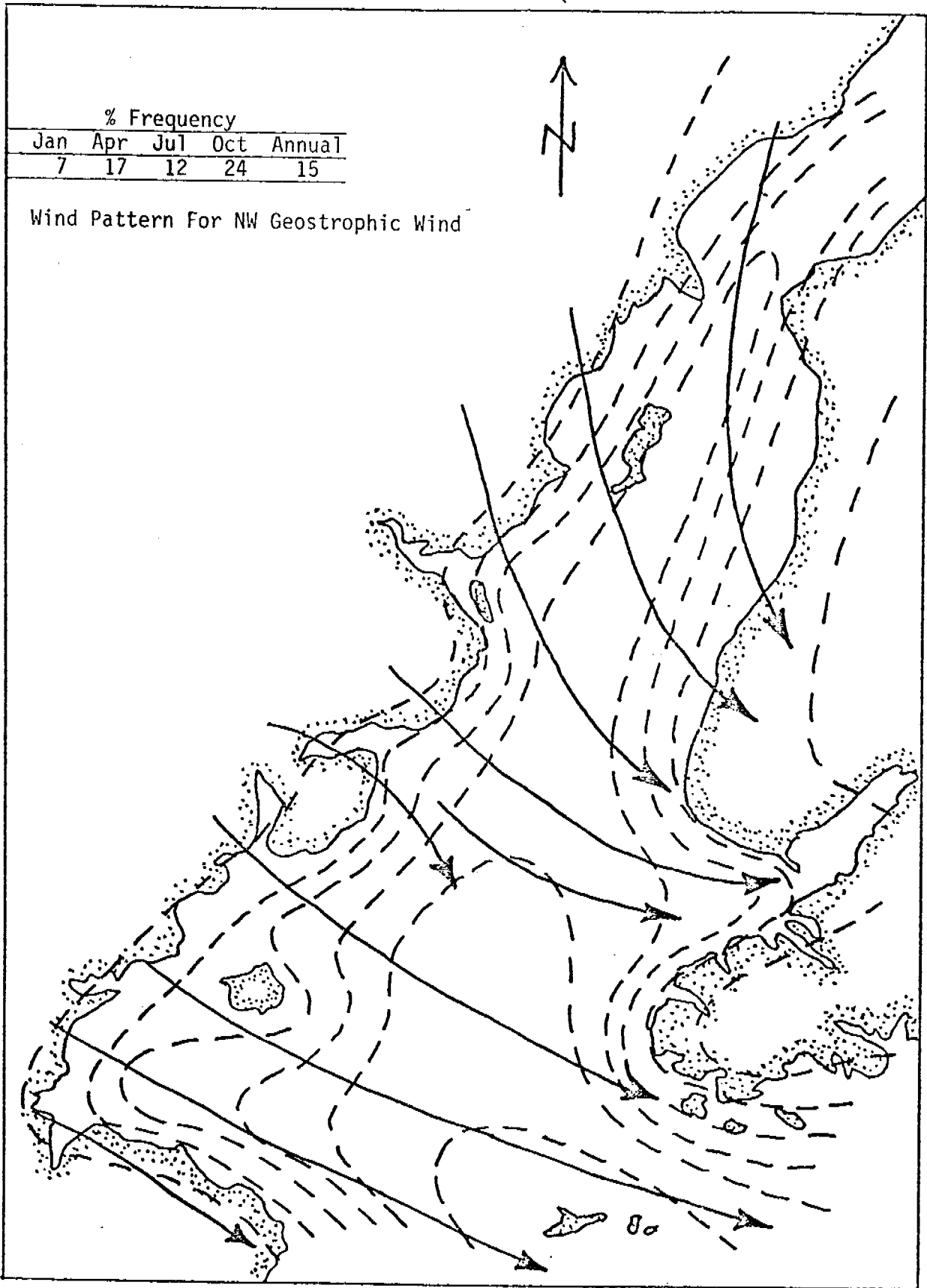


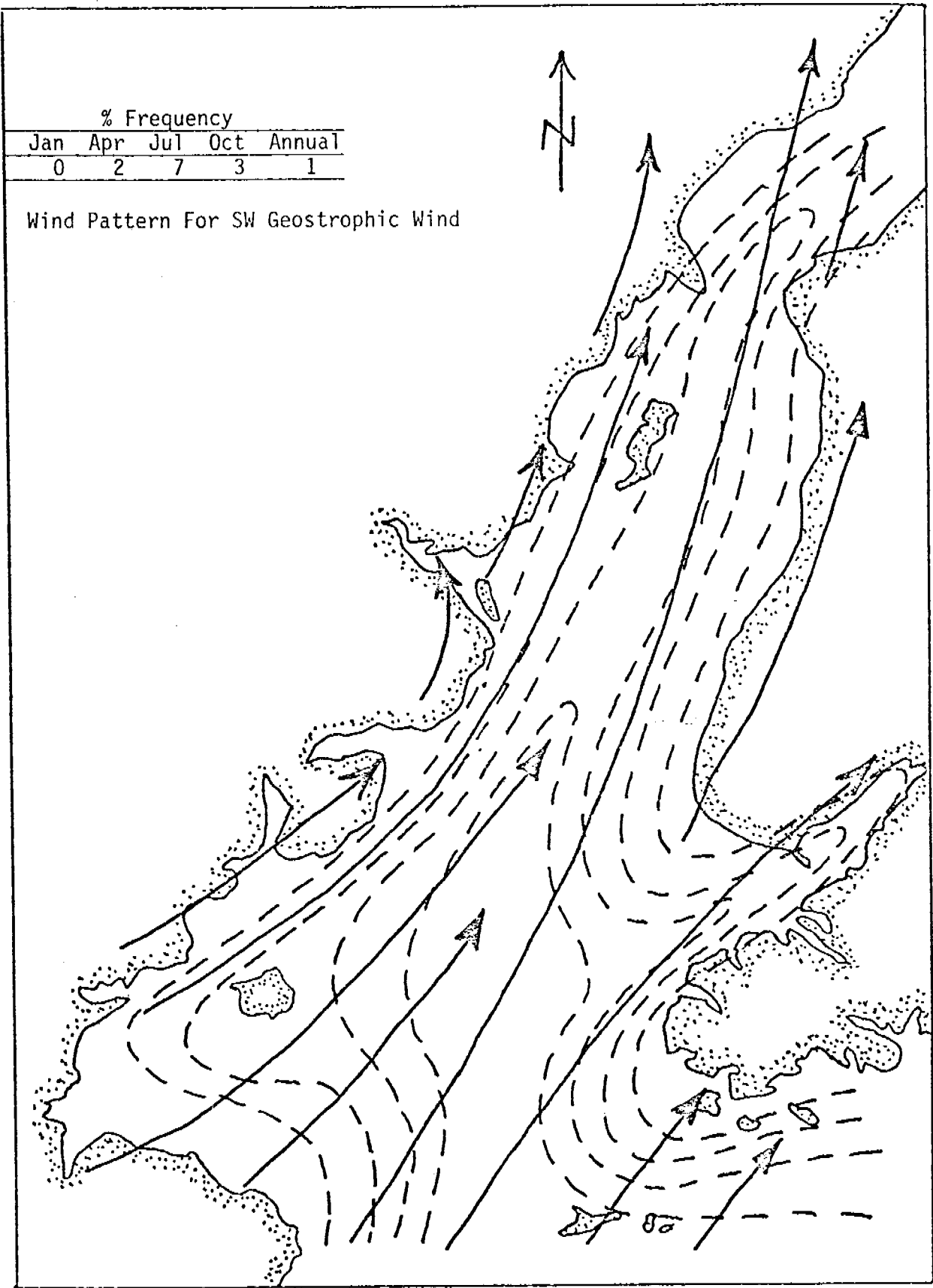
FNE - CDV











Appendix B-1

NWS Reports of Empiracle Procedures

Surface Winds in Some
Alaskan Coastal Passes

G. Philip Weber

Weather Bureau Airport Station
Anchorage, Alaska

Abstract

Estimated geostrophic winds from surface isobar spacing and orientation are compared with the winds actually encountered at Bear Creek, Alaska during the months January to March, 1959. The isobaric orientation (or direction) at which the flow through the pass reverses direction is noted.

One interesting result was that the wind through the pass reversed direction before the surface isobaric analysis indicated the pressure was higher on the upwind end of the pass. This apparently resulted from a piling up of the air on the upwind side of the mountain range resulting in higher pressures than would be estimated from the surface chart and from a dearth of air (and lower than expected surface pressure) on the downwind side of the range. The same effect was later noted at Seward, Alaska. Wind speeds through Bear Creek Pass averaged near or slightly above the geostrophic indication, but maximum daily speeds were always higher than the geostrophic. Extreme daily maximum wind gusts exceeded the geostrophic estimation by 50 knots in a few cases.

Examination of winds at stations near the mouths of other coastal mountain passes gave speeds roughly one-half of the geostrophic indication, suggesting (in view of the smaller pass area above the mouth) that the speeds in the passes are roughly comparable to those found at Bear Creek.

INTRODUCTION Because of the strong winds and poor weather encountered in a mountain pass, such a locale is not often used as a site for a weather observing station. From a meteorological point of view, it was particularly fortuitous when Humble Oil Company decided to investigate a promising oil structure in the Bear Creek area of the Alaska Peninsula (see Figure 1). In addition to maximum and minimum thermometers, the oil well drilling site was equipped with a company owned wind recorder which provided continuous records of wind direction and speed. The recorder sheets were not available for this study, but daily observations of wind direction and speed telephoned to the Anchorage Weather Bureau Airport Station each morning at approximately 0800 Alaska Standard Time were available; in addition to the current wind, the observer also read from the recorder the maximum wind speed and direction during the preceding 24 hours.

The floor of the northwest-to-southeast pass is at an elevation of 200 to 400 feet mean sea level for most of its 10-mile length, which extends from Lake Becharof on the northwest to Jute Bay on the southeast side of the Peninsula (see Figure 2). The observing site was less than $\frac{1}{2}$ mile north of the center line of the pass and at an elevation of about 900 feet (approximately 500 feet higher than the floor level). The width of the pass between the 1,000 foot contours is slightly less than $1\frac{1}{2}$ miles at the site location, which is 135 miles due west of Kodiak Naval Base. Some of the most severe winter storms in the Northern Hemisphere occur in the eastern Aleutians and the Gulf of Alaska, so very strong wind flow both from the southeast and from the northwest occurs through Bear Creek Pass each winter. The strongest wind reported to the Anchorage Weather Bureau was 156 miles per hour (135 knots) from the east in November, 1958; the strongest west-northwest wind of 120 miles per hour (104 knots) occurred in late September 1958. Table I shows the frequency of occurrence of maximum daily wind speeds for selected speed ranges and for the months October through March.

It is interesting that approximately 40% of the maximum daily gusts exceed 60 knots from both directions and though the strongest reported wind of 135 knots was from the east, only 13% of the east-southeast winds exceeded 80 knots while 20% of the west-northwest winds exceeded that value. A larger sample might even this out a bit, but it seems reasonable that the greater frequency of intense lows in the Gulf of Alaska as compared to the eastern Bering Sea, and portrayed in Weather Bureau Research Paper No. 40 (1), is responsible for the greater frequency of strong west-northwest winds.

Since the wind flow through Bear Creek Pass is believed to be roughly representative of the flow through many of our coastal passes, it seemed wise to utilize some of the wind data and relate it to the surface isobar orientation and spacing so the practicing meteorologist can have the benefit of this knowledge in preparing wind forecasts through and opposite mountain passes.

Table I
 Frequency of Maximum Daily Wind Speeds
 during Winter at Bear Creek, Alaska

	<u>East-southeast Winds</u>	<u>West-northwest Winds</u>
	(105 cases)	(95 cases)
less than 40 knots	29%	27%
40 - 60 knots	32%	34%
61 - 80 knots	26%	19%
81 - 100 knots	12%	16%
more than 100 knots	1%	4%

PROCEDURE In relating the actual wind flow through the pass to the isobaric orientation and spacing, data for the three months January through March, 1959 were studied in detail; in addition, selected strong wind cases which occurred in January and February, 1958 were included to increase the number of cases considered. Since surface charts were not available for 1958, it was necessary to plot and analyze these additional charts. To be consistent with the work charts used for 1959, surface isobars were drawn as if the Aleutian Mountain Range did not exist; no provision was made for the higher surface pressures which would prevail on the windward side and the lower pressures which would be expected to prevail on the leeward side of the range. A total of 67 surface charts were used in preparing Figure 3.

Figure 3 shows the average wind speed for each direction as a percentage of the geostrophic speed (based on the spacing of surface isobars without correction for curvature); wind directions were computed to the nearest 10 degrees and because of the small number of cases with some directions, the values for each direction are actually a smoothed value based on three adjacent 10-degree wind directions. Even then, some of the values are based on as few as two or three cases; nevertheless, the logic of the pattern lends support to the belief that the values obtained are of a reasonably correct order to fulfill the purpose of the study. As would be expected, there are two distinct lobes on the diagram - one associated with isobaric orientations which give a northwesterly flow, and the other with surface isobaric orientations which produce a southeasterly air

flow through the pass. The wind direction reverses and the speed is very light when the surface isobars indicate a gradient wind direction of 050-060° or 230-240°; an isobar with an orientation of 055 to 235° is almost parallel to the Aleutian Mountain Range in the Bear Creek area which is roughly on a line from 220-040° true direction. The 10-20° clockwise deviation from the parallel with the Range is believed to result from frictional effects; in fact, a study of the flow through other passes suggests that this deviation is probably nearer to 20-30° than the 10-20° obtained at Bear Creek. The diagram shows clearly that as soon as the isobaric orientation reaches an angle of about 40° with the parallel to the mountain range, the wind component across the Range becomes sufficient to establish a substantial flow through pass. Figure 3 is based on the actual flow at 0800 AST and average speeds equivalent to 125 to 150% of the geostrophic wind speed are evident from several directions. The decrease in wind with directions 140 to 160° is interesting and probably results from local terrain effects in this particular pass. Figure 3 includes all cases without regard to the geostrophic wind speed, considering only the direction of the surface isobaric orientation across the area.

In Figure 4, the geostrophic wind speed has been related to the ratio of the actual surface wind speed to the geostrophic wind speed; curve A is for the observed 0800 AST wind speed and curve B is for the maximum daily wind gust observed during the 24-hour period preceding the surface chart; individual cases are shown to furnish an idea of the variance experienced. The average speed of the 0800 AST winds used for curve A was 43 knots and the average error on the dependent data was 7 knots. The average speed of the observed daily maximum wind gusts used for curve B was 74 knots and the average error of the dependent data was 9 knots. These average errors of 12-15% are within the limits required in forecasting. In addition to the selected data for January through March, 1959, some additional cases from late September, October, and November, 1958 were utilized to construct the curves of Figure 4.

The results from Figures 4 have been combined on Figure 5 which can be used, along with Figure 3, in estimating wind speeds through Bear Creek Pass. Observations are no longer available from Bear Creek Pass. In forecasting, the first step is to line up the mountain range on Figure 3 parallel to the actual range; if the direction of flow (indicated by surface isobars) across the range lies

within one of the two large lobes on Figure 3, the forecaster can use Figure 5 to estimate the wind speed through the pass; should the direction of flow across the range lie within one of the two minimums shown on Figure 3, the flow will be considerably less than shown by Figure 5 and the forecaster should be guided accordingly. Three curves have been entered on Figure 5. Curves A and B are taken from Figure 4. Curve A refers to the 0800 AST observed wind speed while curve B refers to the maximum observed wind gust during a 24-hour period.

The final curve on Figure 5 (curve C) shows the relationship found by Taylor (2) over relatively smooth ground and reproduced by Petterssen (3). Petterssen felt that the ratio of the observed wind to the geostrophic wind probably approximated 0.5 for wind speeds stronger than those studied by Taylor; this value has been assigned to a geostrophic wind speed of 80 knots on curve C and Taylor's results have been extrapolated by the dashed line to this postulated value for comparison with the curves found for Bear Creek. As would be expected, the wind speeds through Bear Creek Pass are considerably stronger than those measured by Taylor over open, relatively smooth ground. The maximum daily gust is about three times as strong as Taylor's results for geostrophic wind speeds less than 50 knots and roughly two-and-a-half times as strong for geostrophic speeds of 80 knots. For very strong speeds, such as a geostrophic speed of 120 knots, the strongest daily gust is about twice the speed expected over open, relatively smooth ground.

SEWARD, ALASKA AIRPORT WIND The airport at Seward is located near the middle of a valley approximately four miles wide. During north wind conditions, air feeds into this valley from the north (through Moose Pass and the Kenai Lake Pass) and from the northwest (through Resurrection River Pass.) Contour maps suggest that the area of the passes as they approach Seward is about $\frac{2}{3}$ that of the airport valley. Applying the results from Bear Creek for the 0800 AST wind speed and using $\frac{2}{3}$ of this value, one would expect a geostrophic wind of 20 knots to result in a wind at Seward Airport of 19 knots, a geostrophic wind of 40 knots to result in a wind of 26 knots, a geostrophic wind of 60 knots in a wind of 34 knots, and a geostrophic wind of 80 knots in a wind of 35 knots. The actual results were 14 knots, 20 knots, 26 knots and 33 knots respectively; for the weaker gradients, the actual winds were only about 70-80% of those expected, but the actual value for the 80 knot geostrophic

wind was very close. The data used for Seward Airport included 40 cases from year 1953 and 7 cases from 1954.

Of these 47 cases, 30 had north to northeast geostrophic winds and 7 had south-southwest to east-southeast geostrophic winds; the former were always associated with northerly flow and the latter with southerly flow. To measure the effect of the surface pressure increase on the windward side of the range and decrease on the leeward side, analysis of the 37 surface charts was accomplished without reference to the Seward surface pressure, then the deviation of the actual pressure from that derived from the analyzed charts was determined. The results are summarized on Table II.

Table II

Deviation of Actual Surface Pressures at Seward,
Alaska from Pressures Estimated from Surface Charts

(37 cases from 1953, 1954 data)

<u>Pressure Deviation</u>	<u>Windward Cases</u>	<u>Leeward Cases</u>
+2.1 to 3.0 mb.	1	
+1.1 to 2.0	2	
0.0 to 1.0	4	1
0.0 to -1.0		11
-1.1 to -2.0		10
-2.1 to -3.0		6
-3.1 to -4.0		1
-4.1 to -5.0		1
Average Error	+1.0 mb.	-1.4 mb.

LYNN CANAL. This inlet, located in extreme northern Southeast Alaska, is about 8 miles in width and is rimmed on each side by mountains rising rather abruptly from the water's edge to elevations of 5,000 to 7,000 feet; during winter, air from the Yukon Territory and extreme northwestern British Columbia streams southward through mountain passes of the Coastal Range down Lynn Canal toward the normally lower pressures in the Gulf of Alaska. Again, using topographic maps of the U. S. Geological Survey (4), the area of Lynn Canal is approximately twice that of the passes to the north which feed air into

the Canal. On the average, the wind speeds at a well-exposed observing site (Eldred Rock) are fairly close to 60% of the geostrophic wind speed. There is some indication that Lynn Canal begins to act like a mountain pass under strong gradient conditions - that is, the wind speeds attained are fairly close to those indicated by the curve for 0800 AST wind speed shown in Figure 4 for Bear Creek; however, the sample is too small to draw a definite conclusion. Furthermore, some of the strongest surface gradients are with isobar orientations fairly close to parallel with the mountain range; this no doubt results in decreasing the wind flow through the Canal. Strong geostrophic wind speeds from the east-northeast (normal to the Coastal Range) tend to give considerably stronger northerly winds through Lynn Canal than the more usual orientation of isobars nearly parallel with the Range.

SUMMARY. The surface wind flow through a mountain pass has been related to the geostrophic wind direction and speed. Excluding those geostrophic wind directions when the flow through the pass diminishes because of flow parallel with rather than across the mountain range, it was found that the average speed of the surface wind through the pass is stronger than the geostrophic wind speed on the average, but is less than the geostrophic speed with the stronger gradients. However, wind gusts considerably stronger than the geostrophic occur and the speed of these gusts exceeds the geostrophic indication even at very strong speeds. In forecasting winds through passes similar to Bear Creek, the meteorologist can furnish a rough estimate of average wind speeds from curve A of Figure 4, but he should amplify his forecast by indicating wind gusts to at least the values shown on curve B of Figure 4.

It was found at Seward, Alaska that pressures on the windward side of a mountain range will average about one millibar higher, and on the leeward side one to two millibars lower than the analyst would expect in the absence of observational data.

Wind speeds observed at both Seward Airport and through Lynn Canal suggest that wind speeds through the passes feeding these observing sites are probably of the same order as those encountered in Bear Creek under similar conditions. However, this is only a rough estimate; certainly, the width of the pass and the height to which the mountains rise, as well as the sharpness of the rise, on each side of the pass are important considerations. While little quantitative data is available, it is a reasonably well-established fact that wind flow from the southeast

rough Portage Pass, located a short distance southeast of Anchorage is stronger, under similar isobaric conditions, than the flow through Bear Creek. Portage Pass is narrower and the confining mountains are higher. Therefore, the results of this study, while perhaps serving as a rough guide for other mountain passes, should be considered reliable only for Bear Creek Pass; the fact that the observing site was not in the middle of the pass no doubt biased the results toward lower speeds than one would actually encounter in the center of the pass.

FIG. 1 LOCATION OF OBSERVATION SITES

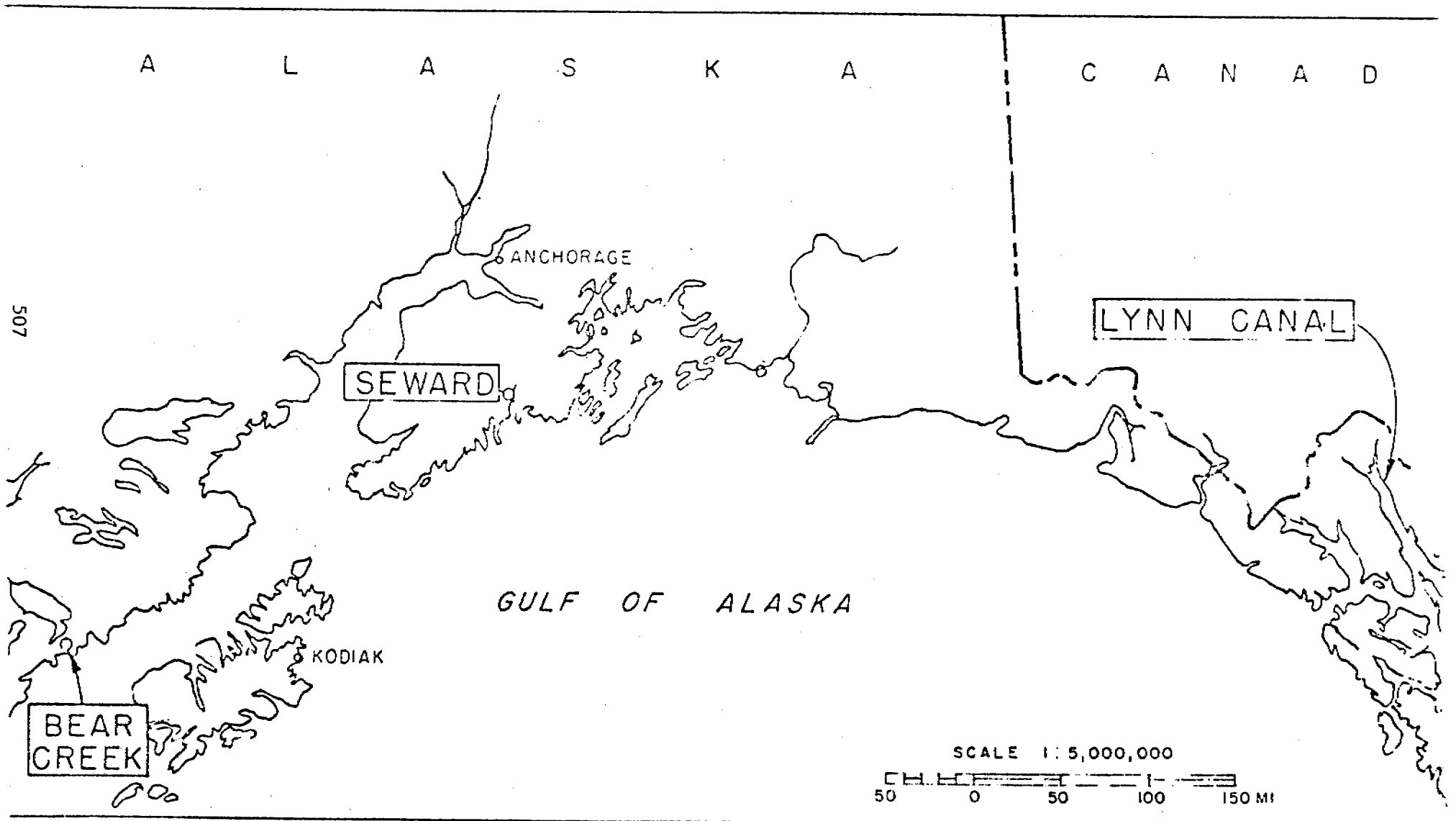


FIG. 2 - TOPOGRAPHY OF THE BEAR CREEK,
ALASKA AREA

NOTE CONTOURS IN HUNDREDS OF FEET

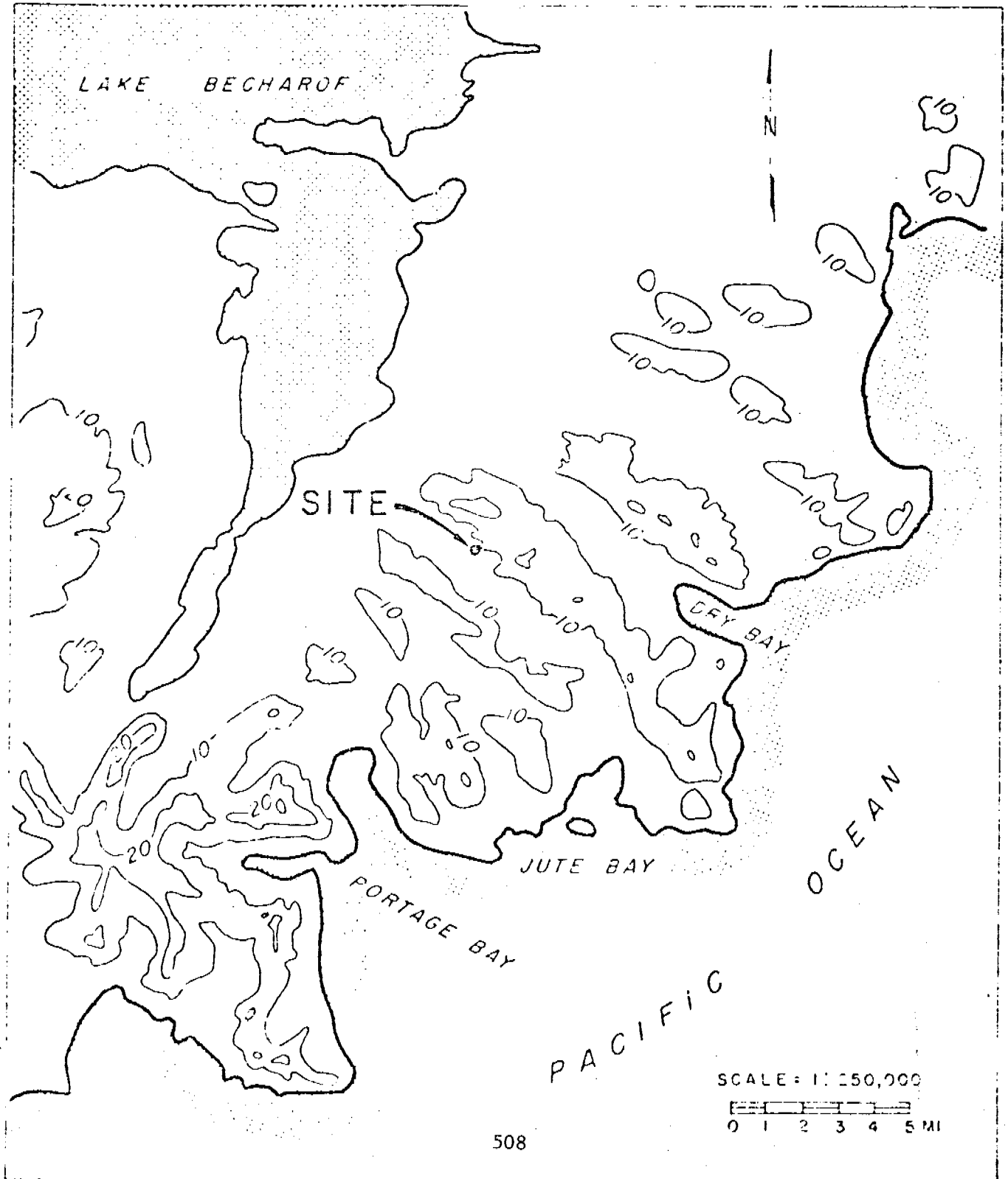


FIG. 3 - ACTUAL WIND SPEED AS A PERCENT OF THE GEOSTROPHIC WIND SPEED FOR EACH GEOSTROPHIC WIND DIRECTION

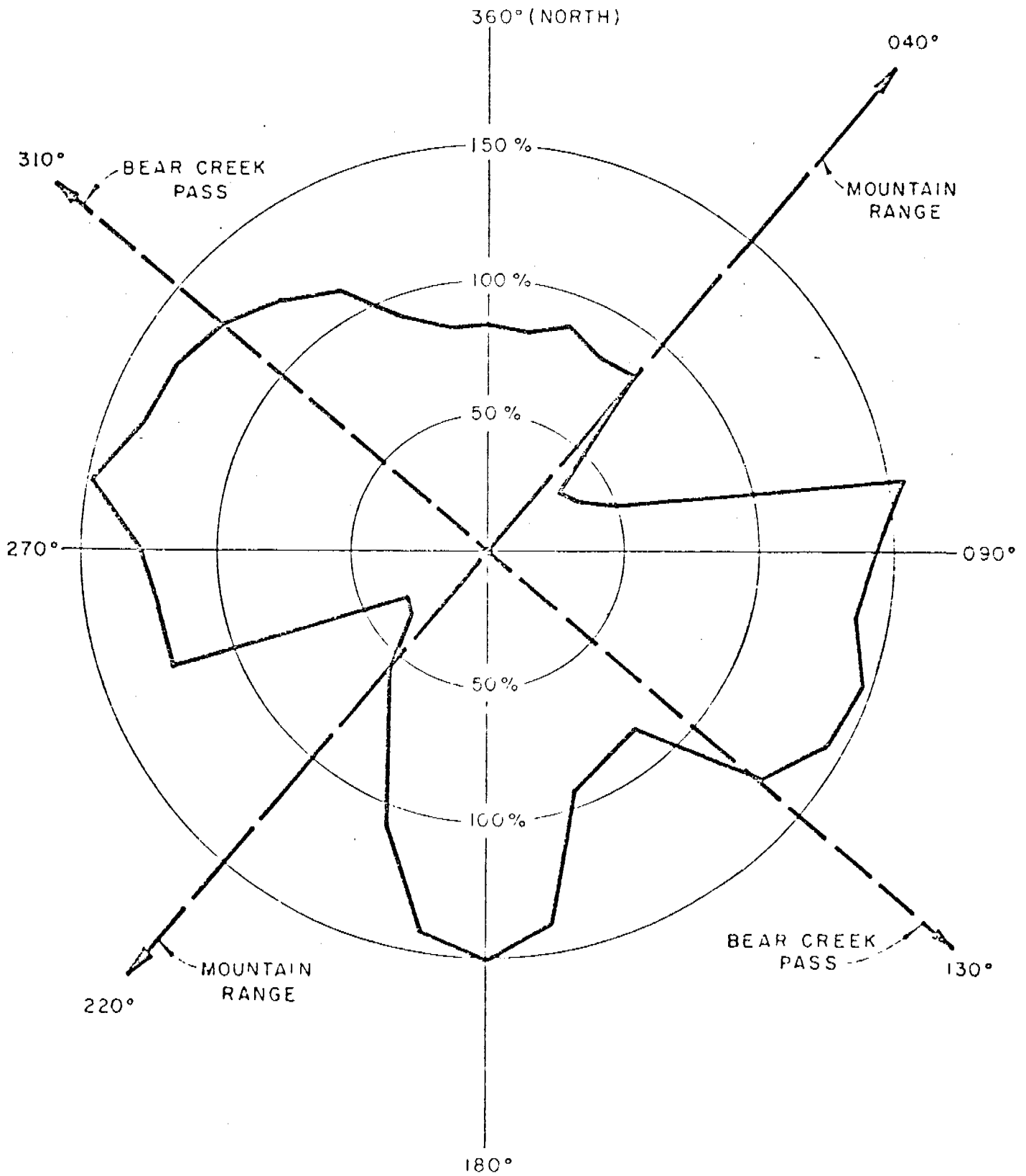


FIG 4 - RELATION BETWEEN THE OBSERVED WIND SPEED AND THE GEOSTROPHIC SPEED.

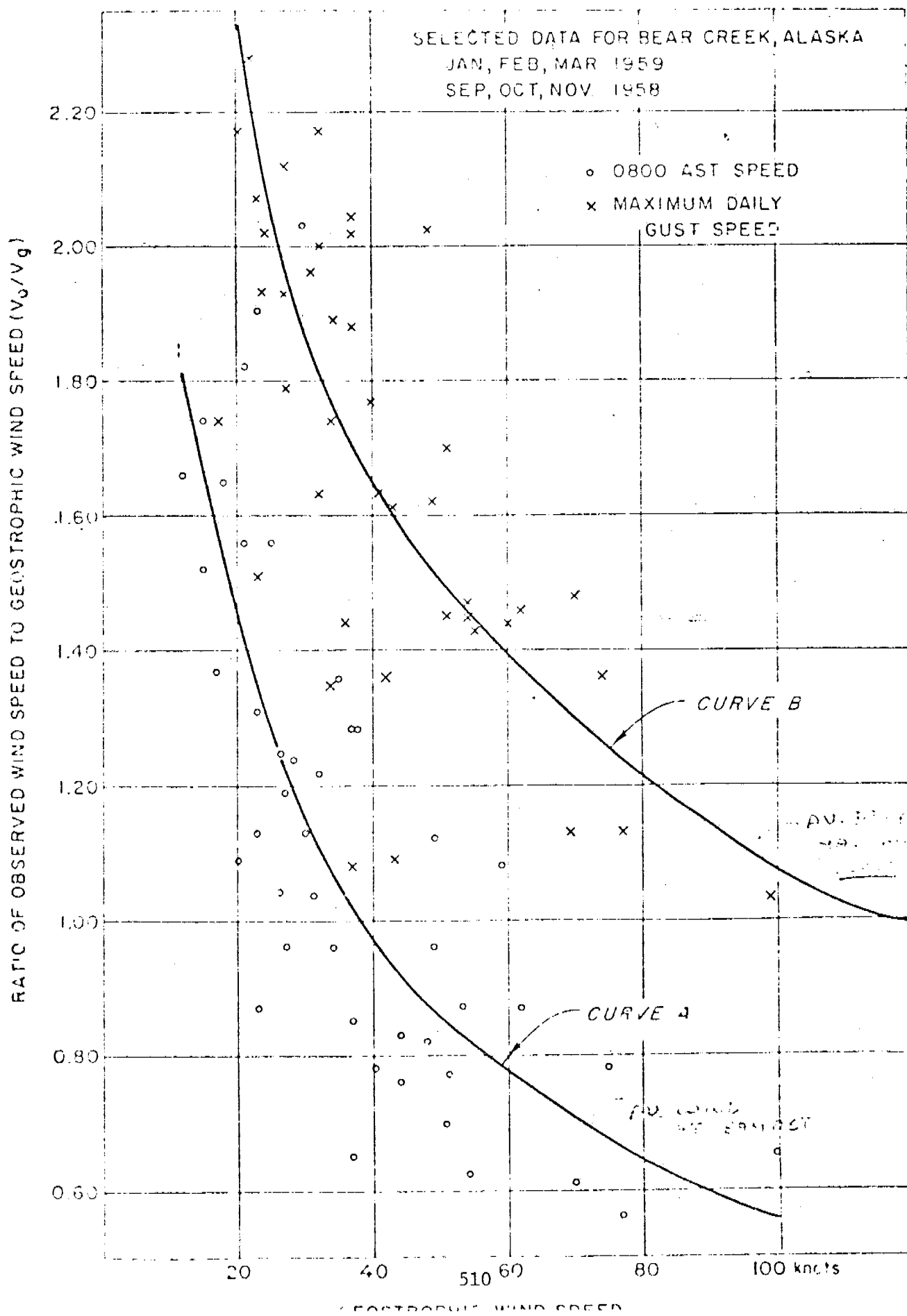
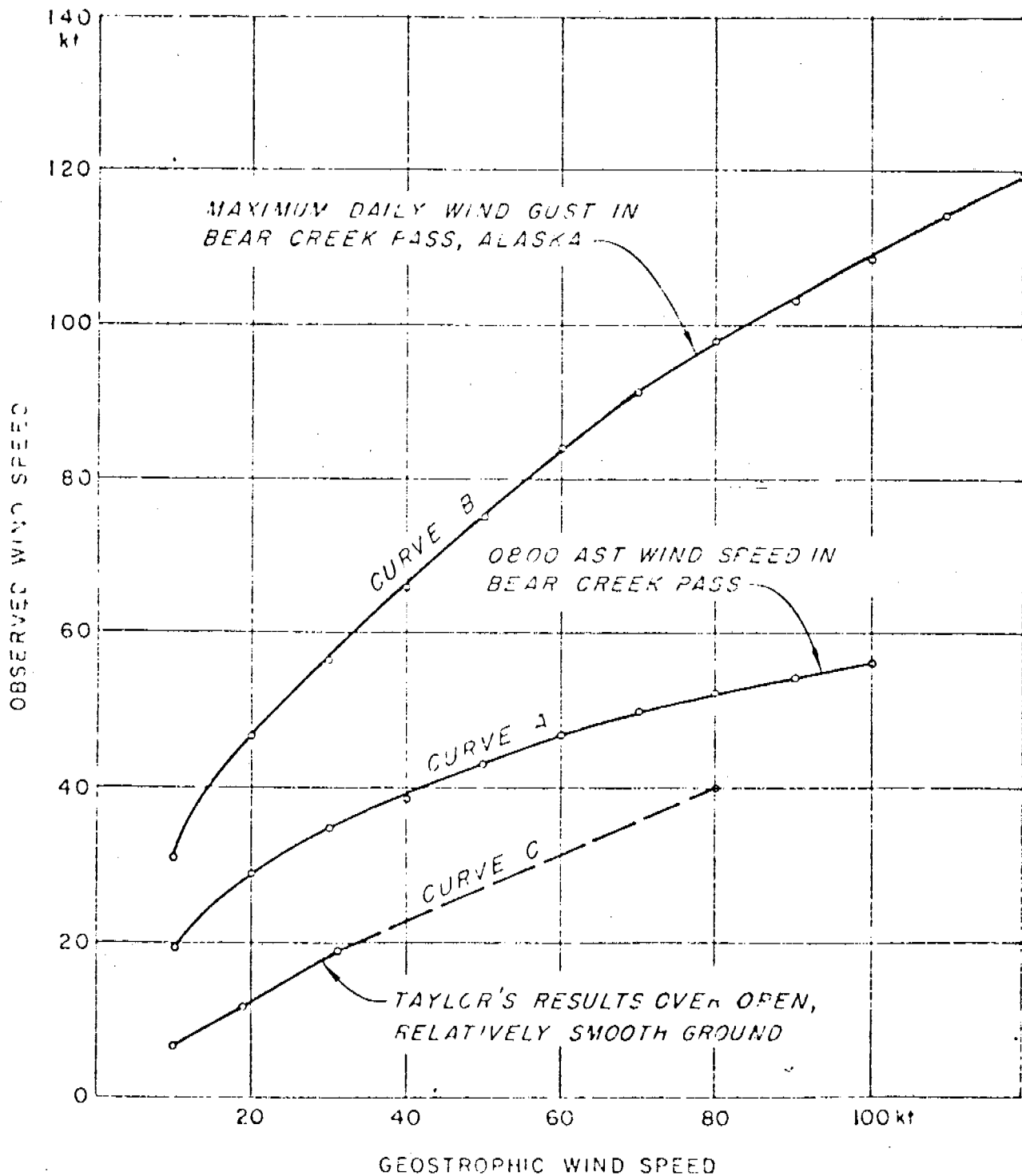


FIG. 5. - RELATION BETWEEN THE OBSERVED WIND SPEED AND THE GEOSTROPHIC SPEED IN A MOUNTAIN PASS



References

- (1) U. S. Weather Bureau, "Principal Tracks and Mean Frequencies of Cyclones and Anticyclones in the Northern Hemisphere", 1957
- (2) G. I. Taylor, Trans. Roy. Soc. (London) A, Vol. 215, 1915
- (3) Book: S. Petterssen, Weather Analysis and Forecasting, Second Edition, Vol. I, 1956
- (4) Maps: U. S. Geological Survey Topographic Maps, 1:250,000, 1951

ALASKA REGION

TECHNICAL PROCEDURES BULLETIN NO. 3

SUBJECT: VALDEZ WIND FORECAST PROCEDURE

AREA: VALDEZ, ALASKA

AUTHOR: HERSCHEL T. KNOWLES

DATE: APRIL 1977

ABSTRACT. *This bulletin describes a forecast procedure for predicting surface winds at Valdez, Alaska. The procedure considers wind components caused by several factors and combines them to produce a local (resultant) wind.*

NOAA / NATIONAL WEATHER SERVICE



VALDEZ WIND FORECAST PROCEDURE

INTRODUCTION

This bulletin describes a procedure to predict surface winds at Valdez, Alaska. The approach taken assumes that the resultant wind at Valdez is made up of components produced by several physical processes. Four primary components are computed independently and added vectorially to find the resultant wind. These component winds and their causes are briefly described below.

1) The pressure gradient wind is a result of the synoptic scale pressure pattern as well as the sheltering and diverting effects of terrain.

2) The sea breeze is primarily a result of land and sea surface temperature differences.

3) Drainage winds are caused by gravity acting on the relatively dense air overlying the sloped surfaces of glaciers, snow covered ground or other cold terrain. The ensuing flow of air drains through the numerous river valleys that feed into Valdez Basin.

4) Spill-over winds are the result of cold air from the Copper River Basin attaining a depth great enough to push southward through the passes of the Chugach Mountains. Once again, gravity does its thing and air rushes seaward down the tributary valleys draining into Port Valdez.

To compute wind components, forecast values of the pressure gradient over Valdez, the 500-1000 MB thickness, cloud cover and temperature have to be known. (We suggest using the LFM prog series for pressure gradient and thickness, but any good surface prog is acceptable.)

Follow the procedure given below using the 12-hour LFM prog first, repeat, using the 24-hour prog, the 36-hour prog, etc. In doing so, you derive a wind forecast at 12-hour intervals. Interpolate for winds between map time.

FORECAST PROCEDURE FOR VWS

A. Determine the pressure gradient wind.

1. With dividers measure the minimum distance between isobars covering a 4MB interval over Valdez. Go to the geostrophic wind scale (Figure 1.) to find the geostrophic wind speed.

2. Determine the geostrophic direction of the wind in degrees (wind parallel to the isobars).
3. Multiply the wind speed in 1) by 1/2.
4. Subtract 50° from the wind direction in 2).
5. Multiply the wind speed in 3) by the factor shown in Table 1.
6. Alter the wind direction in 4) by the amount shown in Table 1.
7. Wind speed and direction in 5) and 6) is the computed pressure gradient wind.

Pressure Gradient Wind _____

B. Determine the drainage winds.

1. Will skies be clear (3/10 or less cloud cover) at map time?

Yes. Use the following for drainage winds in specified month.

Dec	Jan	Feb	0807
Mar	Apr	May	0805
Jun	Jul	Aug	0802
Sep	Oct	Nov	0804

No. Use 0802 all months.

Drainage Wind _____

C. Determine Spill-over winds.

1. Are 1000-500 MB thickness values lower in Copper River Basin than in Valdez? (Look at dashed lines on LFM surface prog.)

No. a) No spill-over winds.

- Yes.
- a) Multiply wind speed in A1) by 1/4.
 - b) Multiply wind speed in a) by factor shown in Table 2.
 - c) Use wind direction in A2) for spill-over wind direction.
 - d) b) and c) are spill-over wind speed and direction.

Spill-over Wind _____

D. Determine the sea breeze.

1. Compute the sea breeze in the warm season only (from the time snow cover disappears in the spring until first significant snow in the fall).
2. Make an estimate of the temperature range expected for the day. (The afternoon high minus the early morning low.)
3. Multiply 2) by 1/2. This value expressed in knots approximates the speed of the sea breeze during its peak period in the afternoon.

(The onset of the sea breeze usually occurs about 9-10 AM, peaks at 2-3 PM and ends at 9-10 PM. However the larger the temperature range, the earlier the onset and later the ending time. Conversely, the smaller the temperature range, the later the onset and earlier the ending time.)

4. Sea breeze direction. At onset use 180°, at peak use 220°, and at ending use 300°.

E. Add the pressure gradient, drainage, spill-over and sea breeze winds by vector addition to find the total wind at VWS. (See appendix for instructions on vector addition.)

F. Forecast gustiness with winds greater than 10 knots. Gusts are approximately 1.7 times the computed wind.

G. Repeat procedure for subsequent prog charts.

H. Make necessary adjustments for hours between map valid time.

OTHER FORECAST GUIDELINES

A. With strong north or northwesterly flow at 500 MB, especially with cold advection, increase the magnitude of gusts.

B. Wind direction is extremely variable at Valdez, especially when spill-over winds are significant. Reflect this fact in the wording of the forecast.

C. For areas on the western side of Valdez, Mineral Creek has a pronounced influence. To get an estimate of the winds in that area, increase the drainage winds by 50% and also the spillover winds by 50%. In both cases, use 010° for the direction of the winds. Sea breeze and pressure gradient winds remain unchanged. Use vector addition to find total wind just as before.

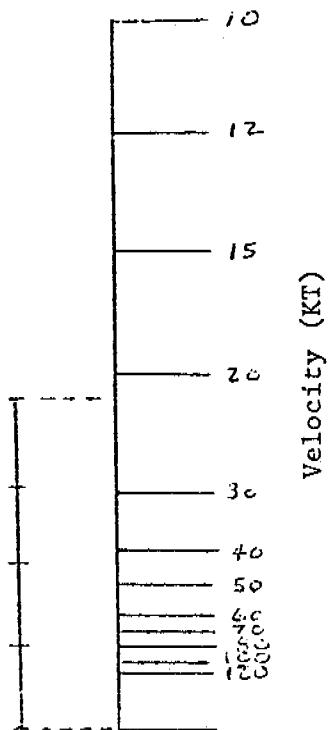
Similarly, winds from Valdez Glacier have a large impact on the airport (VDZ). Increase drainage and spill-over wind speeds by 25%. Use 080°

for direction. Sea breeze and pressure gradient winds are the same as at VWS.

D. If it's apparent that the LFM is in error, use your own judgment to determine what the pressure gradient and other parameters should be in order to make your wind computation.

E. When winds are computed to be 6 knots or less, they are frequently calm. "Light and variable" would be a proper forecast under these conditions.

GEOSTROPHIC WIND SCALE



ADJUSTMENTS TO MAP SCALE

If using Alaska surface analysis, take twice the distance measured.

If using LFM prog charts (larger ones) A138 or A045B, take 4 times the distance measured.

If using LFM prog charts (smaller ones) A142N, A112N, A147N, A158N, A039N, A036N, A044N, or A060N, take 8 times the distance measured.

Figure 1.

Example: The 4MB interval measured on LFM chart A138 was . Marking off 4 times that distance, as above, we find that the geostrophic wind speed is 22kt.

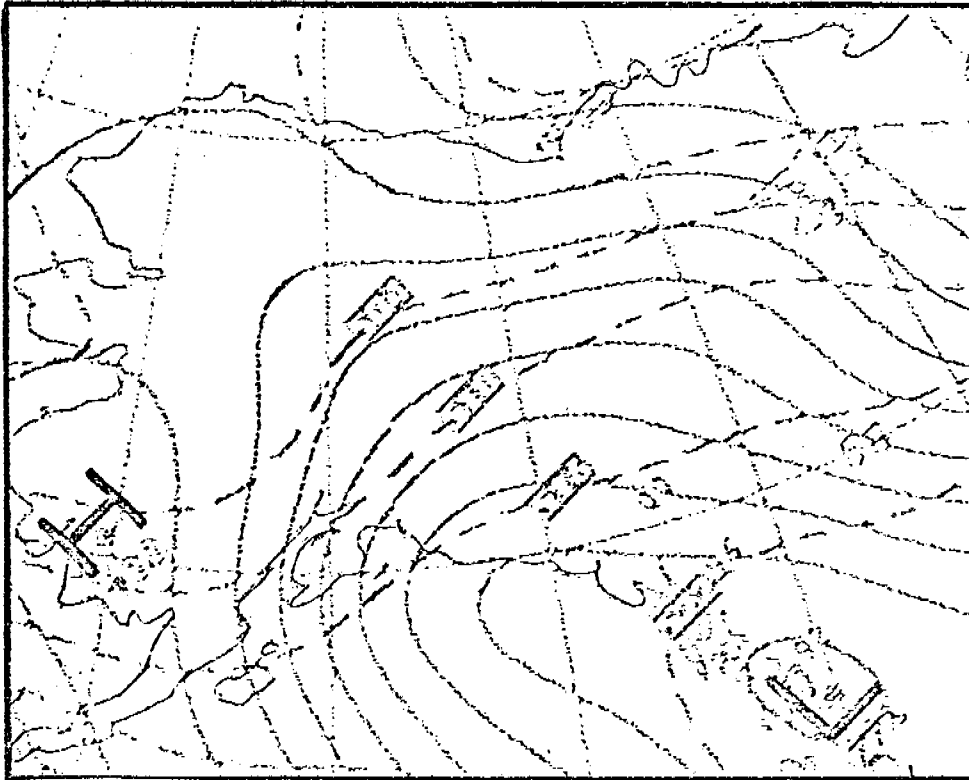


Figure 2. LFM A133..12HR FCST SFC/1000-500 Thickness
Valid 00Z Thu 24 Mar 1977.

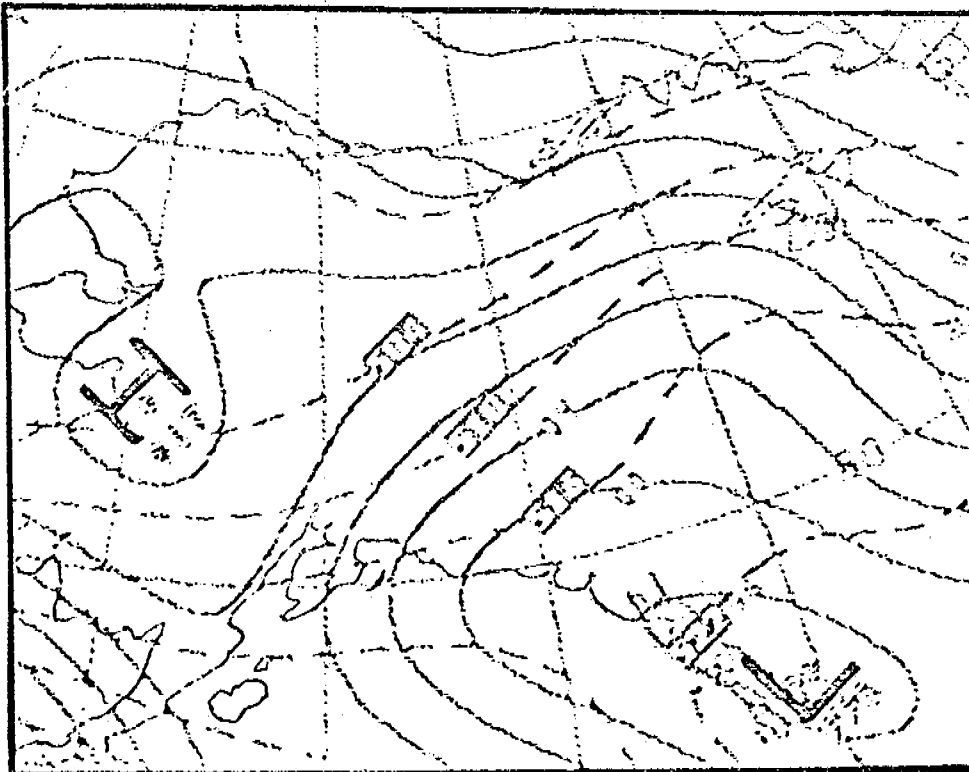


Figure 3. LFM A133..24HR FCST SFC/1000-500 Thickness
Valid 12Z Thu 24 Mar 1977.

TABLE 1.

Wind Direction (in A4)	Multiply Wind Speed by	Alter Wind Direction by
001-030	.2	+10 Deg.
031-060	.2	+20
061-090	.3	+10
091-120	.5	-10
121-150	.4	-20
151-180	.5	-10
181-210	.4	+10
211-240	.5	+20
241-270	.7	+10
271-300	.4	-10
301-330	.2	-20
331-360	.2	-10

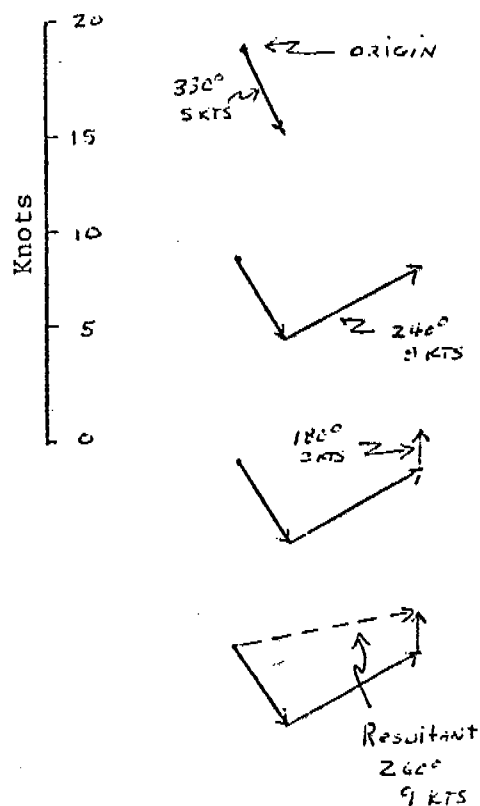
TABLE 2.

If Geostrophic Wind Direction is	Multiply by
040	1
030 or 050	1
020 or 060	.9
010 or 070	.9
360 or 080	.8
350 or 090	.6
340 or 100	.5
330 or 110	.3
320 or 120	.2
130-310	0

APPENDIX A

Vector Addition

- 1) Plot vector representing first wind component. The length of the vector represents the wind speed. Lay out vector in direction wind is blowing.
- 2) Plot second wind component as in 1), but place tail of second vector at head of first. Use same scale to determine length of vector.
- 3) Subsequent wind components are plotted as in 2) tail to head.
- 4) Resultant wind is vector extending from origin to head of last wind component. Length of resultant vector is wind speed. The direction is that from which vector is pointing.



APPENDIX B

Sample Wind Forecast Computation

It is 7:30 AM 23 March 1977. We want to make a wind forecast for today, tonight, and tomorrow. The LFM package (chart A138) has just cleared the facsimile. The surface prog verifying 24 March 00Z and 12Z are shown in Figures 2 and 3.

First, we will compute a wind based on the 00Z map which should be representative of this afternoon's winds. Then we'll repeat the process using the 12Z map and then the 00Z map for the following day (not shown).

A. Determine the pressure gradient wind.

- | | |
|--------------------------------------------------------------------------------|-----------------|
| 1. Measure pressure gradient and determine wind speed using geostrophic scale. | <u>38 knots</u> |
| 2. Wind direction. | <u>040°</u> |
| 3. Multiply 1) by 1/2 | <u>19 knots</u> |
| 4. Subtract 50° from 2) | <u>350°</u> |
| 5. Multiply 3) by factor in Table 1.
.2 x 19 = 3.8 | <u>4 knots</u> |
| 6. Alter 4) by amount in Table 1.
350° - 10° = 340° | <u>340°</u> |
| Pressure Gradient Wind | <u>3404</u> |

B. Determine the drainage wind. From available sources we determine that skies will be clear today, tonight, and tomorrow.

1. Will skies be clear?
Yes. So we use wind for March - 0805

Drainage Wind	<u>0805</u>
---------------	-------------

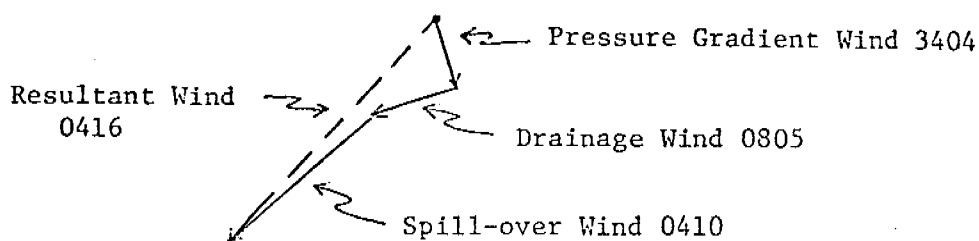
C. Determine the spill-over wind.

1. Are thickness values lower in the Copper River Basin than at Valdez? An examination of the 12 hour prog indicates that they are.
- a) Multiply A1) by 1/4. $38 \times 1/4 = 9.5$ 10 knots

b) Multiply a) by factor in Table 2.	$1 \times 10 = 10$	<u>10 knots</u>
c) Use A2) for direction		<u>040°</u>
	Spill-over wind	<u>0410</u>

D. Determine the sea breeze. There is still a deep snow cover over the area - no sea breeze.

E. Add components to find resultant wind.



The resultant of total wind at Valdez should be from 040° at 16 knots this afternoon.

F. Gustiness. Since the winds are computed to be greater than 10 knots, we can estimate gusts to $(16 \times 1.7 = 27.2)$ 27 knots.

G. Repeating the process using the map verifying tomorrow morning at 12Z, we find that winds should be from 040° at 13 knots with gusts to 22 knots.

Although not shown, the map verifying tomorrow afternoon was used to determine a wind at that time from 080° at 6 knots.

With this information we would make a wind forecast something like this:

"Northeasterly winds 15 to 20 mph and gusty today and tonight becoming light and variable (or light easterly) tomorrow afternoon."

APPENDIX C
SUMMARY OF ACTIVITIES AND PRELIMINARY REPORT
NEAR SHORE METEOROLOGY PROGRAM
SHIP SURVEYOR 13 Feb. to 1 March 1978

SUMMARY OF ACTIVITIES AND PRELIMINARY
REPORT

NEAR SHORE METEOROLOGY PROGRAM

NOAA SHIP SURVEYOR

LEG I - BERING SEA - 13 FEB - 1 MAR 1978

6 MARCH 1978

THOMAS R. HIESTER

SUMMARY OF ACTIVITIES AND PRELIMINARY

REPORT

1. Objectives

The goals of the meteorology study on this cruise may be summarized as (discussed further below):

- 1) measure, weather permitting, air mass transformation process
- 2) determine problems and characteristics of the "airsonde" as used aboard ship
- 3) observe the character of the arctic ice edge.

The primary objective of the Near Shore Meteorology Program on Leg I was to study, weather permitting, the air mass modification process as cold, dry, arctic air blows south across the edge of the arctic ice over the warmer Bering Sea. In such an outbreak of cold air, beginning at the edge of the ice and continuing downwind, heat from the ocean is picked up by the cold air thereby increasing the turbulent kinetic energy of the planetary boundary layer (PBL). The top of the PBL in cases such as these is marked by a strong temperature inversion where increased static stability suppresses turbulence. The increased turbulence within the boundary layer causes entrainment of air from above the temperature inversion into the mixed layer below. Hence, as one moves downwind of the ice edge the depth of the mixed layer is expected to increase at a rate that depends primarily on the air--sea temperature difference and the temperature structure above the mixed layer. The rates of warming, moistening, and growth of the PBL in a downwind section are the parameters we intended to measure.

To accomplish these measurements we intended to use the "airsonde" manufactured by Atmospheric Research Company. The airsonde is considerably easier to prepare for launch than the conventional radiosonde (calibrations have been performed by the manufacturer), is lighter (requiring substantially less helium), and provides an increased vertical resolution (making it ideal for detailed boundary layer research). The airsonde is however a new instrument and has never before been used aboard ship. It was a fact finding objective of this leg to determine the characteristics of and problems with using airsondes on a ship.

The third objective was to observe the character of the arctic ice edge. The simplest approach to modelling the ice edge is as a straight knife edge. Some insight into the sacrifices made when using this assumption can be gained through direct observation.

2. Activities

The SURVEYOR departed from the Seattle area for the Bering Sea at about 0300 Z 14 February 1978. As this was an oceanographic cruise, Table 1 and Figure 1 and 2 which list and show the CTD stations occupied during the cruise provide a convenient Bering Sea itinerary. Figure 3 depicts surface

pressure patterns during the cruise. These are taken from Fleet Numerical Weather Central 12 hour prognoses received on board the SURVEYOR. While not being true analyses they do closely represent actual conditions. In addition, Table 2 is a copy of the weather observation sheet of the SURVEYOR Deck Log.

Partially due to persistently uninteresting weather conditions and partially due to telemetry difficulties with the airsondes, only seven airsondes were launched during Leg I. These launches are summarized in Table 3. Discussion of each launch appears in the next section.

Qualitative ice observations with supporting photographs were made and are discussed in the next section. Ms. Jane Bauer, a graduate student from the University of Washington, was aboard as an ice observer. No doubt, a more comprehensive report will be available through her.

3. Discussion

3.1 Airsonde flights

The airsonde is a new instrument that should be able to provide great detail for boundary layer measurements. However it is new and has never before been used on a ship. It was expected that several airsondes would be launched to gain familiarity with their performance at sea.

Launch #1 was a trial launch in the Gulf of Alaska. The combination of underinflation of the balloon with the balloons being caught in a down-draft in the lee side eddy induced by the ship resulted in the airsonde making contact with the sea surface before limping upward at a slow ascent rate. One styrofoam wing of the airsonde was seen to have been damaged. The sonde continued to transmit but the signal was noticeably garbled.

Launch #2, also in the Gulf of Alaska was also a failure due to launch technique. A yank of the line (connecting the balloon to the airsonde) by the balloon broke the styrofoam flange where the line is tied to the airsonde. The airsonde plunged into the water and ceased to transmit. Although this appears to be a weak point in the airsonde construction, it was found that perfection of launch technique could prevent this problem. Additionally, the next generation of airsondes will be molded styrofoam rather than the carved and glued airsondes currently available. It was at a glued junction that the break occurred.

Flight #3 was a successful lift-off but data collection was largely unsuccessful. Telemetry was good for only about 50 meters. The antenna setup being used was not that provided by AIRCO and it was believed that there may have been substantial signal loss through that setup. Several minutes after the signal had been lost, the AIRCO antenna was plugged in using a 2 m length of RG 58 coaxial cable. The signal strength was enhanced enabling the ground station to lock in on the signal. However, only about 30% of the temperature and pressure data were received due to excessive noise. The highest "accurate" pressure datum was 750 mb (surface pressure was 975 mb). Reception using the shorter antenna cable was somewhat fortuitous in that there was line of sight contact with the aft laboratory on the ship. More generally antennas need to be mounted in an exposed location such as on the SURVEYOR helicopter pad, or not use the laboratory. The latter choice is hardly feasible in inclement weather.

Flight #4 used a 9 meter RG 58 antenna cable and the AIRCO antenna mounted on the helicopter pad. Reception of the signal was good up to about 1200 m. Loss of the signal occurred as the ship changed course (there was no interruption of the line of sight). Whether this was coincidental is unknown.

That afternoon there were snowshowers visible in all directions and within 15 km. It is likely that the clear air sampled by airsonde #4 had recently been modified by the shower activity. A preliminary look at the potential temperature profile would support this notion. Figure 4a shows a mixed layer of 100 m thickness beneath a stable layer presumably established by the aftermath of precipitating convection. A mixed layer is reestablishing itself and the very shallow mixed layer (for open ocean) seen in Figure 4 indicates the modification due to the precipitation and convection occurred just shortly before the measurements were made. This was in fact the case. A shower was observed to cross the course of the ship at a distance of about 10 nautical miles about 45 minutes prior to the launch of the airsonde.

Although the data of Figure 4a look internally consistent, the ground value is several degrees higher than the simultaneous ships hourly observation. A high quality surface measurement was not made due to an oversight, nevertheless, the quartermasters measurement is believed to be nearly correct. Since the bias is consistent with height as judged by the interpretation of the features of the sounding, the problem cannot be one of inadequate aspiration before launch. This is the only flight where such a large bias was observed.

As the pressure patterns in Figure 3 show, winds in the vicinity of the ice edge in the eastern portion of the Bering Sea were off the ice during the transit of the Gulf of Alaska, but were generally onto the ice during SURVEYOR's time in the Bering Sea. For much of 22 February (GMT) the ship reported NNE winds. The cloud cover was 95% stratocumulus, low ceiling, and blue sky above; symptoms of a possible air modification case. The prognosis didn't look promising but it was decided to launch a series of airsondes at the CTD locations as the ship approached the ice. If by the time the ship got to the ice the winds were indeed (still) off the ice, the ship would turn around and steam downwind as planned.

Flight #5 was made at CTD grid #22. A potential temperature profile is shown in Figure 4b. The two higher temperatures near the surface are probably an artifact of inadequate aspiration of the sonde before lift off. Although the sonde was hung out in the open air for 10 minutes prior to launch, it was not done in a way in which it would spin thereby forcefully aspirating the thermistors. The mixed layer potential temperatures higher up agree exactly with that of the quality surface measurement obtained with the Assman hygrometer thermometer.

The observer estimated that the balloon entered the base of the cloud deck at about 300 m. The potential temperature profile shows an increase in θ at about 300 m at a rate of about $4^\circ/\text{km}$. The temperature lapse rate is then the moist adiabatic and the top of the boundary layer would then be marked by temperature inversion above the moist adiabatic layer. Such an inversion is not seen in this profile; the sonde did not get out of the boundary layer before data reception was lost.

Flight #6 was made when the SURVEYOR had penetrated 6 km into the broken, slushy edge of the arctic ice. Actual hardpack ice was still 25 to 35 km farther north. As the ice was approached (Cf. Table 2) the winds at the surface shifted from near southerly to east northeasterly. As the balloon ascended the observer noted that the winds abruptly changed from ENE to SE or SSE somewhere around 150 m up. The potential temperature sounding is shown in Figure 4c. Note that there is a shallow mixed layer about 100 m thick beneath a strong temperature inversion followed by a slightly stable layer.

This will be a very complex and interesting sounding for further analysis. The following is a plausible suggestion of the events occurring near the ice edge. There is a southerly on ice flow that is not disturbed greatly by the ice above a few hundred meters. As the air at the surface blows over the ice it cools but there is enough wind shear to sustain a downward turbulent heat flux in the 100 m deep mixed layer. Since the surface air is cooling the surface pressure increases to the north. This leads to the more easterly geostrophic wind at the surface. A quick look at the mixing ratio shows a fairly constant value of about 3.5 g/kg at least through the inversion. This supports the hypothesis that the near surface air is oceanic air being cooled rather than colder (and probably drier) air slipping down the pressure gradient and being warmed. Whether the winds are in a thermal wind balance, i.e., if the surface wind is simply in geostrophic plus friction balance, or if there is an ageostrophic component to the flow is not yet clear. It is clear that this is an interesting case involving interaction of scales of motion and is worthy of further consideration.

Flight #7 was also made several kilometers into the ice. The potential temperature profile is shown in Figure 4d. The data gap was from bad telemetry but it appears that the gap was within the mixed layer. The winds were from the SE, definitely from the sea, and the surface cooling is again evident. The motivation for Flight #7 came from the observation of breaking Kelvin-Helmholtz waves in a low level cloud layer about 30 minutes prior to launch. Cloud base was estimated to be at about 1 km with the wave crests some 500 m higher. Due to the bad telemetry link data was only obtained for the mixed layer and some of the stable layer. The pressure versus time signal does show, if believable, that the airsonde was caught in downdrafts within the stable layer, indicative of strong gravity waves. No directional shear could be seen.

3.2 The Ice "Edge"

The SURVEYOR only penetrated some 6-8 km into the edge of the ice. However pictures and descriptions from helicopter CTD operations out of Nunivak help complete a rough picture suitable for this report.

For PBL modelling of the ice edge the critical question is, how closely does the edge behave as a discontinuity in heat and momentum fluxes? Having visited the ice edge it is clear that the answer is not straightforward but is very dependent on the past history of the ice for a time scale of, say, 2 weeks. Consider the changes occurring in the following scenario.

There is a long period of clear skies and light northerly winds bearing very cold air. Ice forms at the southern extremity of the existing ice. Let's just say that a definite edge is formed. Now a storm in the Bering Sea whips up a spectrum of swell that propagates into the ice edge. The new ice at the ice edge is very soft and breaks easily when stressed. The short wavelength swell is attenuated quickly, breaks the ice into elements whose horizontal scales are roughly the same as the wavelength of the swell. The longer wavelength swell move further into the ice, and the characteristic ice tablets become correspondingly larger. Far enough into the ice, the energy in the swell is small, the ice is stronger, and this method of breaking the ice no longer works. I do not know precisely what this distance might be but it is at least 20 km.

Now let the storm move northward giving strong southwesterly winds. All the broken blocks compact into one another. Differential wind stress creates pressure ridges and leads in the pack ice to the north.

A storm spins up in the Gulf of Alaska causing northeast winds over the ice edge, but not very cold winds. The momentum flux begins moving the ice blocks, which were compacted together, southward. The smaller blocks (which were nearest the edge) lead the procession. Some of them cluster together and in their colliding and mutual interference they move as a group more slowly than individuals either out ahead or to the rear. Consequently there forms a band of clustered ice blocks. There may be several bands parallel to the ice edge that are several km wide and ten times that long, with several km of open water between each band. The amount of exposed water in each band is highly variable as is the heat flux.

This is far enough to make the point that the conditions at the ice edge are quite variable and depend substantially on the history of the ice.

4. Conclusions

The airsonde system must be improved for the conditions encountered on ships. New electronics were provided for the ground station in Leg II of the SURVEYOR cruise that have a less sensitive threshold for discriminating between bad signal (which is discarded) and good data. Of course, obtaining data with the second version of the ground station electronics (if it works better) that would have been discarded with the first version may come at some expense in accuracy.

The border region along the ice edge consists of a mixture of ice, slush, water, and open leads, and is at least 20 times as wide as the PBL is deep. Therefore the ice edge is not an ideal location for PBL air modification studies. Certainly a ship is too slow and inflexible to measure the spatial variations of the fluxes. The Bering Sea is however an ideal location for larger scale air modification studies that emphasize the communication of the lower level transformation process through the cloud layer to the upper troposphere. In this kind of study the downwind length scale would be 50 to 100 times the width of the ice edge border.

The soundings gathered on this cruise do show the ice edge to be an area worthy of PBL studies. The boundary layer is highly baroclinic but uncomplicated by topography. Flows from either on or off the ice are of interest. To adequately sample the PBL an airplane instrumented to make

visual and infrared mapping of the surface and turbulent flux measurements would be required. The aircraft would have to have a long range, partly due to long ferry times required and partly due to the length scales to be sampled. The NOAA P-3 aircraft are ideal.

TABLE I

LIST OF CTD STATIONS
BERING SEA 1978

B-BOP GRID #	TIME (GMT)	DATE	LATITUDE (N)	LONGITUDE (W)	DEPTH (M)	
1	9	0609	20 FEB	54 44.4	167 54.3	1500
2	10	0926		54 57.1	168 19.6	1730
3	3	1406		54 33.5	168 58.8	1500
4	2	1753		54 10.6	168 30.6	2500
5	2.1	2152		53 56.1	169 13.6	1760
6	3.1	0137	21 FEB	54 18.5	169 35.5	2080
7	4.2	0630		54 22.9	170 47.7	2100
8	4.1	1024		54 41.1	170 05.6	1820
9	4	1358		54 55.1	169 26.2	2820
10	11	1745		55 11.2	168 41.6	1995
11	19	2222		55 19.7	167 56.1	270
12	20	0030	22 FEB	55 30.9	168 23.1	282
13	21	0228		55 40.2	168 50.9	349
14	12	0505		55 26.6	169 15.8	2270
15	5	0847		55 15.8	170 00.6	2500
16	5.1	1230		55 02.2	170 48.0	3150
17	6	1655		55 33.5	170 40.2	3146
18	13	2228		55 43.7	169 57.2	2415
19	22	0302	23 FEB	55 50.0	169 20.3	1610
20	32	0609		55 58.1	168 48.1	585
21	42	0822		56 08.0	168 17.3	162
22	52	1102		56 20.1	167 44.1	128
23	64	1404		56 35.1	166 57.1	97
24	64.1	1628		56 50.6	166 22.4	76
25	85.1	1841		57 07.0	165 49.4	71
26	85	2050		57 21.5	165 20.3	68
27	96.1	0131	24 FEB	57 50.0	165 25.9	55
28	96.1	0228		57 51.7	165 27.3	55
29	96.2	0445		57 49.5	165 29.2	58
30	96.3	0559		57 46.4	165 35.2	60
31	96.4	0716		57 44.0	165 40.7	62
32	96.5	0838		57 37.5	165 45.2	64
33	85.2	1029		57 30.0	165 32.8	62
34	85	1205		57 21.9	165 19.6	64
35	85.3	1337		57 14.1	165 06.9	64
36	84.1	1453		57 07.5	164 55.5	68
37	84	1611		57 01.8	164 44.7	68
38	84.2	1736		57 08.5	164 28.3	67
39	94.1	1917		57 17.5	164 07.7	64
40	94	2040		57 24.4	163 49.3	57
41	95.1	2247		57 35.5	164 17.7	55
42	95	0035	25 FEB	57 44.6	164 43.2	51
43	95.2	0223		58 00.4	164 56.7	43
44	106.1	0356		58 13.0	165 06.5	42

TABLE I (continued)

E-BOP GRID #	TIME (GMT)	DATE	LATITUDE (N)	LONGITUDE (W)	DEPTH (M)
45	106.1	0528	25 FEB 58 14.8	165 07.4	43
46	106.2	0715	58 08.6	165 07.6	48
47	106.3	0814	58 02.7	165 07.2	49
48	106.4	0923	57 55.8	165 08.4	49
49	106.5	1025	57 49.8	165 06.0	51
50	106.6	1127	57 44.9	165 05.8	58
51	106.7	1227	57 39.0	165 05.0	59
52	996.1	1920	58 10.9	165 17.4	46
53	996.2	2001	58 12.2	165 17.5	46
54	996.3	2124	58 14.1	165 18.3	46
55	996.4	2310	58 17.2	165 21.4	46
56	996.5	0246	26 FEB 58 11.4	165 21.7	44
57	105	0756	58 07.7	164 13.6	47
58	104.1	2225	57 37.6	163 10.4	47
59	104.2	2322	57 31.1	163 12.2	45
60	104.3	0020	27 FEB 57 24.4	163 12.1	49
61	104.4	0114	57 19.2	163 14.0	53
62	104.5	0203	57 13.6	163 14.0	53
63	104.6	0317	57 06.6	163 11.3	60
64	000.0	2016	54 19.0	164 51.5	55

TABLE II
DECK LOG - WEATHER OBSERVATION SHEET

SUNDAY

NOAA SHIP											DATE	
SURVEYOR S-132											19 FEBRUARY 1978	
HOUR	PRESENT WEATHER	VISI-BILITY (N.M.)	WIND		STATE OF SEA			SEA WATER TEMP. (F/C)	AIR TEMP. (F/C)		PRES-SURE (IN)	REMARKS
			DIR.	SPEED (kts)	WAVE HT. (ft)	SWELL			WET BULB	DRY BULB		
						DIR.	HT. (ft)					
0100	CL	10	245	11	2	050	4	2.8	2.2	3.3	28.91	
0200	CL	10	250	17	2	050	4	2.8	2.2	3.3	28.90	
0300	CL	15	270	16	3	050	5	2.8	1.7	2.2	28.90	CL
0400	CL	15	255	19	3	050	5	2.8	0.6	2.2	28.91	
0500	CL	15	255	19	2	050	5	2.2	0.0	2.2	28.92	
0600	PC	20	235	15	2	050	5	2.2	0.0	2.2	28.91	
0700	PC	20	242	17	1	050	4	2.2	0.6	2.2	28.90	JA
0800	CL	20	234	16	1	250	3	2.2	2.1	2.3	28.90	
0900	CL	20	227	15	2	240	4	2.2	2.2	3.1	28.91	
1000	F-L	2	220	15.5	2	240	3	2.2	2.2	2.2	28.90	entering Unimak
1100	SW	2	240	16	2	290	6	1.1	1.5	1.5	28.91	IN BEHIND SEB
1200	S	3	245	11	2	290	6	2.2 1.7	1.7	1.7	28.90	
1300	L	4	275	8	2	290	6	2.2	1.7	1.7	28.90	
1400	S	4	275	8	2	290	6	2.2	1.7	1.7	28.90	
1500	L	5	335	9	2	290	6	2.2	1.1	1.1	28.92	CL
1600	CL SW	3	040	2	1	310	4	2.2	0.0	1.1	28.93	
1700	CL	4	CALM	0	0	320	3	2.2	0.6	1.0	28.93	
1800	CL	6	150	4	1	310	3	2.2	0.3	1.1	28.94	
1900	CL SW	4	155	4	1	310	3	2.2	0.3	1.1	28.94	J
2000	CL	5	255	4	0	350	3	3.8	0.8	1.9	28.96	CLOUDS ARE DISSIPAT
2100	CL	10	240	4	0	350	3	3.8	0.8	1.3	28.98	
2200	CL	10	246	4	0	350	3	3.8	0.8	1.2	28.98	
2300	CL	5	070	4	^	350	3	3.6	0.3	0.5	29.00	
2400	CL	5	110	02	U	350	3	3.6	0.0	1.1	29.00	N

GMT =

534

DECK LOG - WEATHER OBSERVATION SHEET

NOAA SHIP

SURVEYOR S-132

MONDAY

DATE

20 FEBRUARY 1976

GMT=

HOUR	PRESENT WEATHER	VISI-BILITY (N.M.)	WIND		STATE OF SEA			SEA WATER TEMP. (F/C)	AIR TEMP. (F/C)		PRES-SURE (IN)	REMARKS
			DIR.	SPEED (kts)	WAVE HT. (ft)	SWELL			WET BULB	DRY BULB		
						DIR.	HT. (ft)					
+10												
0100	PC	10	205	03	0	350	3	03.6	-0.6	+1.1	29.00	
0200	PC	10	220	04	0	350	3	03.6	-0.6	+1.1	29.00	
0300	CL-S	07	220	04	0	350	3	03.6	-0.6	+1.1	29.00	gsm
0400	CL	10	215	6	0	350	3	3.5	0.0	2.3	29.01	
0500	CL	10	200	9	0	350	3	3.5	0.6	1.7	29.03	
0600	CL	15	195	13	1	350	3	2.8	0.2	2.2	29.02	
0700	CL	15	190	16	2	350	4	2.2	-0.3	1.7	29.04	1/4
0800	CL	12	170	15	1	350	4	3.5	0.2	1.8	29.07	
0900	CL	12	187	5	0	350	4	3.5	0.0	0.8	29.08	snow showers in the vicinity
1000	CL	15	175	15	1	350	4	3.5	0.2	2.0	29.09	
1100	CL	15	170	20	1	350	4	3.5	0.0	2.2	29.09	
1200	CL	15	175	18	3	350	4	3.5	-0.6	2.2	29.10	
1300	CL	15	175	20	3	350	4	2.2	-0.6	2.2	29.10	
1400	CL	15	175	21	3	350	4	2.2	2.8	6.1	29.10	
1500	CL	15	165	20	2	340	4	2.2	0.0	2.2	29.10	gsm
1600	CL	20	160	16	2	340	5	2.2	0.0	2.3	29.11	
1700	CL	20	152	16	2	340	5	2.2	0.1	2.3	29.12	
1800	CL	15	135	16	2	330	5	2.2	1.1	3.3	29.12	
1900	CL	10	148	18	2	330	5	2.8	0.0	2.2	29.12	1/2
2000	CL	12	146	20	2	330	5	2.9	1.0	2.0	29.12	
2100	CL	12	155	17	2	140	4	2.9	0.6	1.6	29.14	
2200	CL	12	184	135	1	140	4	2.9	0.2	1.2	29.16	4/8 cu
2300	CL	12	142	12	1	535	4	2.9	0.3	1.2	29.18	" "
2400	PC	12	130	15	1	140	4	2.9	-0.6	1.2	29.18	

TABLE II (continued)
DECK LOG - WEATHER OBSERVATION SHEET

TUESDAY

NOAA SHIP												DATE	
SURVEYOR 5-132												21 FEBRUARY 1978	
HOUR	PRESENT WEATHER	VISI-BILITY (N.M.)	WIND		STATE OF SEA			SEA WATER TEMP. (F/C)	AIR TEMP. (F/C)		PRES-SURE (IN)	REMARKS	
			DIR.	SPEED (Kts)	WAVE HT. (ft)	SWELL			WET BULB	DRY BULB			
						DIR.	HT. (ft)						
0100	PC	12	140	12	1	140	03	03.1	-0.8	+1.7	29.19		
0200	PC	12	140	12	1	140	03	3.1	-0.8	+1.7	29.20		
0300	PC	12	070	06	1	140	03	3.1	-0.6	+1.9	29.20	sun	
0400	CL	12	055	5	1	200	03	2.8	-0.5	2.3	29.20		
0500	CL	15	020	5	1	200	3	2.2	-0.6	1.7	29.20		
0600	CL-SW	6	016	12	1	200	3	2.8	0.0	2.2	29.16		
0700	F-SW	2	332	19	1	340	3	3.3	0.6	+1.7	29.14	J	
0800	SW	2	035	15	1	340	3	3.6	1.3	1.3	29.12		
0900	SW	2	025	17	1	340	3	3.6	1.5	1.5	29.11		
1000	SW	3	030	17	2	050	3	3.6	1.8	2.0	29.09		
1100	SW	4	050	18	2	050	4	3.6	1.5	1.5	29.06	J	
1200	SW	5	048	18	2	050	4	2.2	1.1	2.2	29.06		
1300	CL	5	050	15	2	050	4	2.2	1.0	2.1	29.06		
1400	CL	7	040	21	2	050	4	2.2	1.0	2.1	29.04		
1500	CL	7	040	21	2	050	4	2.2	1.1	2.1	29.04	sun	
1600	S CL	3	040	22	2	045	5	2.7	0.8	1.9	29.04		
1700	S CL	3	040	25	2	050	5	2.2	0.6	1.7	29.04		
1800	CL &	4	040	25	2	055	5	2.2	0.6	1.7	29.04		
1900	CL &	4	040	23	2	055	5	2.8	0.0	1.7	29.02	J	
2000	CL-SW	3	030	22	2	055	6	3.6	0.1	1.8	29.03		
2100	L	5	040	20.5	2	055	6	3.6	1.0	1.3	29.03		
2200	L	9	040	21	2	055	6	3.6	1.0	1.2	29.03		
2300	L	9	025	22	2	055	6	3.4	1.0	1.4	29.03	J	
2400	L	7	030	18	2	055	6	3.4	1.3	1.8	29.03		

GMT =

TABLE II (continued)

DECK LOG - WEATHER OBSERVATION SHEET

NOAA SHIP												DATE	
SURVEYOR S-132												WEDNESDAY	
HOUR	PRESENT WEATHER	VISI-BILITY (N.M.)	WIND		STATE OF SEA			SEA WATER TEMP. (F/C)	AIR TEMP. (F/C)		PRES-SURE (IN)	REMARKS	
			DIR.	SPEED (kts)	WAVE HT. (ft)	Swell			WET BULB	DRY BULB			
						DIR.	HT. (ft)						
0100	CL	7	030	20	1	055	04	2.2	0.6	11.8	29.06		
0200	CL	7	030	20	1	055	06	2.2	0.6	11.7	29.06		
0300	CL	7	020	20	1	055	06	3.9	0.3	11.6	29.06	sm	
0400	CL SW	4	027	15	1	050	6	2.2	0.6	1.7	29.04		
0500	CL	6	023	17	2	050	7	2.2	0.6	1.7	29.04		
0600	cl	6	027	17	2	040	8	2.2	0.6	1.7	29.02		
0700	cl &	5	020	17	2	070	7	2.2	0.6	1.7	29.02	JS	
0800	CL	5	010	19	2	060	8	2.9	1.0	1.3	28.97		
0900	CL	5	010	19	2	060	8	2.9	1.2	1.9	28.99		
1000	SW	5	010	19	2	060	8	2.9	1.2	1.9	28.98		
1100	CL	10	015	19	2	060	8	2.9	1.3	1.8	28.98	tyc	
1200	CL	10	015	17	2	050	8	2.2	1.0	2.2	28.98		
1300	S	7	010	15	2	050	8	2.2	1.3	1.8	28.95		
1400	S	7	005	12	2	040	8	2.2	0.4	1.7	28.94		
1500	S	7	005	12	2	040	8	2.2	0.1	1.2	28.93	sm	
1600	SW CL	3	020	6	1	050	6	Bucket 5.5	0.0	1.7	28.90		
1700	cl	6	060	5	1	040	6	Bucket 3.5	0.6	1.7	28.89		
1800	cl	7	075	5	1	050	5	2.2	0.8	1.9	28.89		
1900	cl	12	125	6	1	060	5	2.2	1.0	1.9	28.88	JS	
2000	CL	10	100	10	1	060	5	3.0	1.8	1.9	28.89		
2100	L	10	110	11	1	060	5	3.0	1.5	1.5	28.89		
2200	CL	10	114	11	1	060	5	2.8	1.0	1.5	28.90	PARTIAL CLEARING 7/8 CUMULUS	
2300	CL	10	105	12.5	1	060	4	2.8	1.0	1.5	28.92	tyc	
2400	CL	10	130	14	1	060	4	2.8	0.6	1.9	28.94		

GMT=

TABLE II (continued)
DECK LOG - WEATHER OBSERVATION SHEET

THURSDAY

NOAA SHIP											DATE	
SURVEYOR 5132											23 FEBRUARY 1978	
HOUR	PRESENT WEATHER	VISI-BILITY (N.M.)	WIND		STATE OF SEA			SEA WATER TEMP. (F/C)	AIR TEMP. (F/C)		PRES-SURE (IN)	REMARKS
			DIR.	SPEED (kts)	HT. (ft)	DIR.	HT. (ft)		WET BULB	DRY BULB		
0100	CL	10	135	10	1	060	4	2.5	0.0	1.7	28.96	
0200	CL	10	145	17	1	060	4	2.5	1.2	1.8	28.96	
0300	CL	10	155	17	1	060	4	1.7	0.0	2.1	28.98	Dr
0400	CL	12	155	10	1	060	4	2.5	0.6	2.2	28.98	
0500	CL	12	170	14	1	060	3	2.2	0.8	2.2	29.00	
0600	CL	12	175	15	1	060	2	1.9	0.6	2.2	29.03	LIGHT SNOW Showers
0700	CL	12	169	16	1	150	2	1.7	0.6	2.2	29.08	RAIN & SNOW: 1/2 Showers IN AREA
0800	CL	12	152	18	1	165	3	1.3	0.5	2.0	29.12	
0900	CL	12	165	12.5	1	165	3	1.3	0.9	1.5	29.15	
1000	CL	12	128	16	1	165	3	0.9	1.2	2.0	29.16	
1100	CL	12	130	14	1	165	3	0.5	1.0	1.5	29.18	Dr
1200	CL	12	095	16	1	165	3	-2.2	-0.1	+1.1	29.20	
1300	CL	7	140	08	1	165	3	-2.2	-1.1	+0.6	29.20	
1400	CL	10	080	14	0	170	2	-2.2	-1.1	+0.6	29.20	
1500	CL	10	095	15	0	170	3	-2.2	-0.6	+1.1	29.18	Dr
1600	CL	4	090	15	0	170	3	-1.7	-0.9	+0.6	29.18	
1700	CL	5	110	12	0	190	3	-1.7	-0.6	1.0	29.18	
1800	CL SW	4	107	17	0	190	4	-1.6	-0.2	1.1	29.18	AT THE OUTER ICE EDGE
1900	CL	4	095	13	0	180	3	-1.6	-1.1	+0.6	29.17	Dr
2000	CL	4	080	15	0	180	3	+0.9	0.3	0.2	29.16	
2100	CL	4	080	15	0.5	180	3	0.1	0.5	0.0	29.14	
2200	CL	4	070	13	0.5	180	3	0.1	0.2	0.0	29.12	
2300	CL-SW	4	070	13	0.5	180	3	0.1	0.0	0.0	29.10	Dr
2400	CL-SW	5	070	06	0	180	3	0.0	-0.9	+0.1	29.06	Dr

GMT =

TABLE II (continued)
DECK LOG - WEATHER OBSERVATION SHEET

NOAA SHIP

SURVEYOR 5-132

FRIDAY

DATE

24 FEBRUARY 1978

GMT =

HOUR	PRESENT WEATHER	VISI-BILITY (N.M.)	WIND		STATE OF SEA				SEA WATER TEMP. (F/C)	AIR TEMP. (F/C)		PRES-SURE (IN)	REMARKS
			DIR.	SPEED (kts)	WAVE HT. (ft)	SWELL		WET BULB		DRY BULB			
						DIR.	HT. (ft)						
0100	CL-SW	4	050	05	0	180	3	0.0	-0.9	+1.1	29.06		
0200	CL-SW	4	CALM		0	180	3	0.0	-0.9	+1.1	29.04		
0300	CL	5	090	05	0	180	3	+0.5	0.0	+0.8	29.04	sm	
0400	cl	8	220	8	0	160	2	0.9	0.0	1.1	29.04		
0500	cl &	7	185	9	0	150	2	1.0	10.9	2.2	29.05		
0600	cl	10	160	9	0	120	3	1.4	1.1	2.2	29.06		
0700	cl	12	157	12	0	090	3	0.7	1.1	2.2	29.08	js	
0800	CL	12	160	12	0	090	5	0.8	1.3	1.5	29.11		
0900	CL	12	155	12	0	090	5	0.0	1.3	1.5	29.13		
1000	CL	12	130	16	0	090	5	0.0	1.0	1.2	29.14		
1100	CL	12	130	14	0.5	090	5	0.2	1.0	1.8	29.16	TJC	
1200	CL	12	135	17	0.5	090	4	-1.2	4.1	2.5	29.16		
1300	CL	12	130	16	0.5	090	4	-1.2	+1.1	2.5	29.16		
1400	CL	12	120	16	0.5	090	4	-1.7	+0.1	-1.7	29.14		
1500	PC	15	120	15	1	090	4	-1.7	0.0	+1.7	29.14	sm	
1600	cl	13	118	13	1	100	4	-1.4	4.1	0.6	29.14		
1700	cl	13	107	12	1	105	3	-1.5	-1.1	0.0	29.14		
1800	cl	13	130	9	0	110	3	-1.6	-1.1	0.0	29.14		
1900	cl	12	080	6	0	110	2	-1.6	-1.1	0.0	29.14	js	
2000	cl	12	085	8	0	110	2	-1.6	-1.0	0.0	29.16		
2100	SW-CL	12	085	8	0	110	2	0.8	0.5	0.5	29.17		
2200	CL	12	075	6.5	0	110	2	0.8	-1.0	-1.0	29.18		
2300	CL	7	110	4	0	110	2	-1.3	-1.0	0.7	29.19	TJC	
2400	CL	7	115	4	0	110	2	-1.4	-1.4	-0.1	29.20		

TABLE II (continued)
DECK LOG - WEATHER OBSERVATION SHEET

SATURDAY

NOAA SHIP												DATE		
SURVEYOR 5-132												25 FEBRUARY 1978		
HOUR	PRESENT WEATHER	VISI-BILITY (N.M.)	WIND		STATE OF SEA			SEA WATER TEMP. (F/C)	AIR TEMP. (F/C)		PRES-SURE (IN)	REMARKS		
			DIR.	SPEED (kts)	HT. (ft)	DIR.	HT. (ft)		WAVE	SWELL			WET BULB	DRY BULB
0100	CL-SW	5	195	06	0	110	2	-1.5	-1.4	0.0	29.22			
0200	CL	7	235	06	0	110	2	-1.7	-1.1	0.0	29.25			
0300	CL-SW	10	240	08	0	110	2	-1.5	-0.8	+0.6	29.32	sm		
0400	CL	10	220	12	0	110	2	-1.1	0.0	0.0	29.32			
0500	CL	10	210	13	0	110	2	-1.1	-0.5	0.0	29.34			
0600	S	0.5	220	9	0	110	2	-1.1	-0.2	0.0	29.39	SNOW		
0700	C	5	220	6	0	110	2	-2.2	-0.2	0.0	29.42	gpc		
0800	CL	4	CALM		0	120	2	2.0	0.6	0.0	29.45			
0900	SW	3	150	10	0	140	2	2.0	0.5	0.5	29.50			
1000	CL	7	150	10	0	/	2	7.8	0.0	0.5	29.54			
1100	CL	7	130	8	0	/	2	7.8	0.0	0.4	29.56	gpc		
1200	PC	10	115	8	0	/	2	2.0	-0.6	-1.1	29.54			
1300	CL	10	110	12	0	/	2	2.0	-1.1	+0.6	29.57			
1400	CL	10	120	15	0	/	2	-2.2	-1.1	+0.6	29.58			
1500	CL	10	210	18	0	/	1	-2.2	-1.1	+1.0	29.55	gpc		
1600	CL	10	215 050	21	0	/	1	BUCKET -1.8	-1.0	0.0	29.53			
1700	CL	10	050	30	1	120	3	BUCKET -1.8	-0.5	0.5	29.51			
1800	CL	10	100	31	2	110	3	INTAKE 2.2	-0.5	0.5	29.44			
1900	CL	10	100	31	2	110	3	INTAKE 2.2	-0.5	0.0	29.45	gpc		
2000	CL	10	090	33	2	110	3	2.8	0.5	0.0	29.43			
2100	CL	10	090	32	2	110	5	2.8	0.0	0.9	29.46			
2200	CL	10	100	35	2	110	5	1.8	0.2	1.8	29.43			
2300	CL	10	105	37	2	110	6	1.8	0.2	1.5	29.40	gpc		
2400	CL	10	105	35	3 ⁵⁴⁰	110	8	-1.8	-0.6	1.3	29.40			

TABLE II (continued)
DECK LOG - WEATHER OBSERVATION SHEET

NOAA SHIP <i>SURVEYOR S-132</i>												DATE <i>SUNDAY</i> <i>26 FEBRUARY 1978</i>	
HOUR	PRESENT WEATHER	VISI- BILITY (N.M.)	WIND		STATE OF SEA			SEA WATER TEMP. (F/C)	AIR TEMP. (F/C)		PRES- SURE (IN)	REMARKS	
			DIR.	SPEED (Kts)	HT. (ft)	DIR.	HT. (ft)		WET BULB	DRY BULB			
													WAVE
0100	CL	10	105	38	4	110	12	-2.2	-0.1	+1.7	29.36		
0200	CL	10	105	38	4	110	12	-2.2	0.0	+1.7	29.36		
0300	CL-R	10	105	36	4	110	10	-2.2	0.0	+1.1	29.35	<i>sm</i>	
0400	CL R	5	095	34	4	110	8	-2.2	0.5	1.0	29.35		
0500	CL R	5	105	35	4	110	8	-2.2	1.0	1.5	29.33		
0600	CL R	5	110	38	5	110	10	-2.2	1.0	1.5	29.33		
0700	CL	8	110	36	5	110	10	-2.2	1.0	2.0	29.34	<i>PSC</i>	
0800	R	5	110	35	3	110	10	-1.4	1.2	1.6	29.34		
0900	R	5	110	35	3	110	10	-1.4	1.2	1.6	29.34		
1000	L	4	110	35	3	110	10	-1.4	1.5	2.3	29.35		
1100	L	4	095	30	3	110	10	-1.4	1.2	2.0	29.36	<i>TJC</i>	
1200	L	5	110	30	3	110	10	-1.3	0.0	+1.1	29.36		
1300	CL	7	110	44	3	110	10	-1.3	+1.1	+2.2	29.34		
1400	CL	7	110	42	3	110	10	-2.2	+0.6	+1.2	29.32		
1500	CL	10	105	35	3	110	10	-1.2	+0.6	+1.7	29.31	<i>sm</i>	
1600	CL	10	100	34	3	110	10	-2.1	1.2	2.0	29.32		
1700	CL	8	100	32	3	110	10	0.6	1.2	2.0	29.29		
1800	CL	8	095	30	3	085	10	0.6	1.0	1.5	29.30		
1900	CL	8	110	24	3	085	10	0.0	0.5	1.0	29.28	<i>PSC</i>	
2000	CL-L	8	106	24	3	085	10	0.0	2.2	2.2	29.26		
2100	CL	8	123	25	3	085	10	0.0	2.2	2.2	29.22		
2200	CL	15	127	18	2	085	8	0.9	2.3	2.5	29.26		
2300	PC	15	145	26	2	085	8	1.7	2.3	3.0	29.25	<i>TJC</i>	
2400	PC	15	143	28	2	085	8	1.7	1.1	2.8	29.26		

GAT =

H10

TABLE III

Airsonde Launches--Bering Sea 1978

NO	DATE	TIME GMT	LAT N	LONG W	
1	17 Feb	0000	Northwest Gulf of Alaska		Under inflated balloon--Sonde immersed in ocean before struggling ascent
2	19 Feb	0016	54 12.1	157 22.8	Poor launch technique--Sonde broke and fell into Pacific
3	19 Feb	0038	54 11.9	157 32.5	Successful launch--Poor telemetry Using large antenna
4	21 Feb	0100	54 18.5	169 35.5	Using small antenna on 9 m cable; received up to 1200 m. Recent snow showers in vicinity
5	23 Feb	0340	55 50.0	169 20.3	Small antenna on 9 m cable; received to 950 m. Stratus cloud base at 300 m.
6	24 Feb	0209	57 51.6	165 27.2	Small antenna on 2 m cable; received up to 800 m. Directional wind shear at 150-200 m. 6 km into ice
7	25 Feb	2043	58 13.4	165 17.7	Small antenna on 9 m cable; received signal up to 1.2 km but with large data gaps. Kelvin Helmholtz waves noted in low clouds. About 6 km into ice.

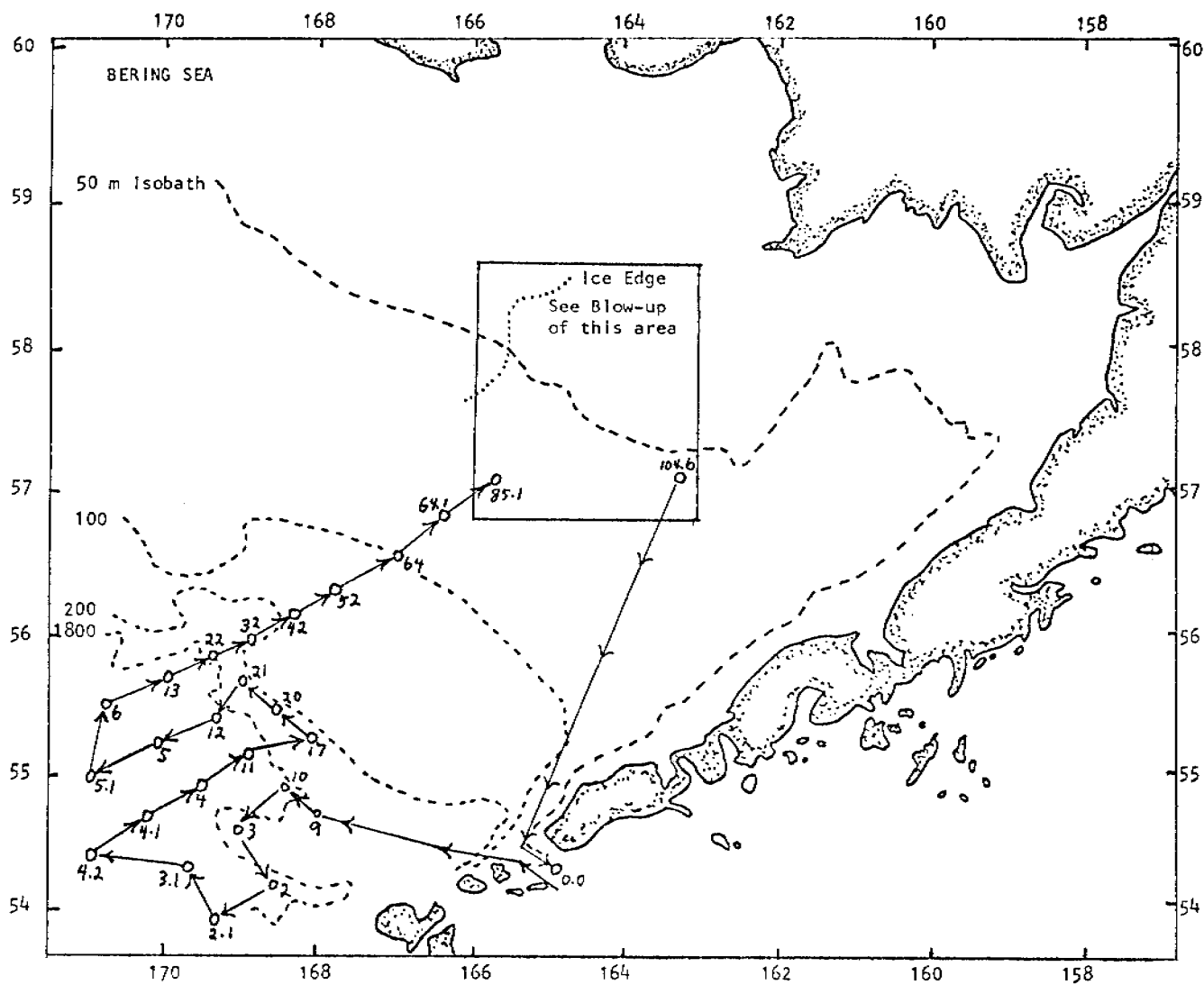


Figure 1. CTD stations occupied during Bering Sea SURVEYOR cruise

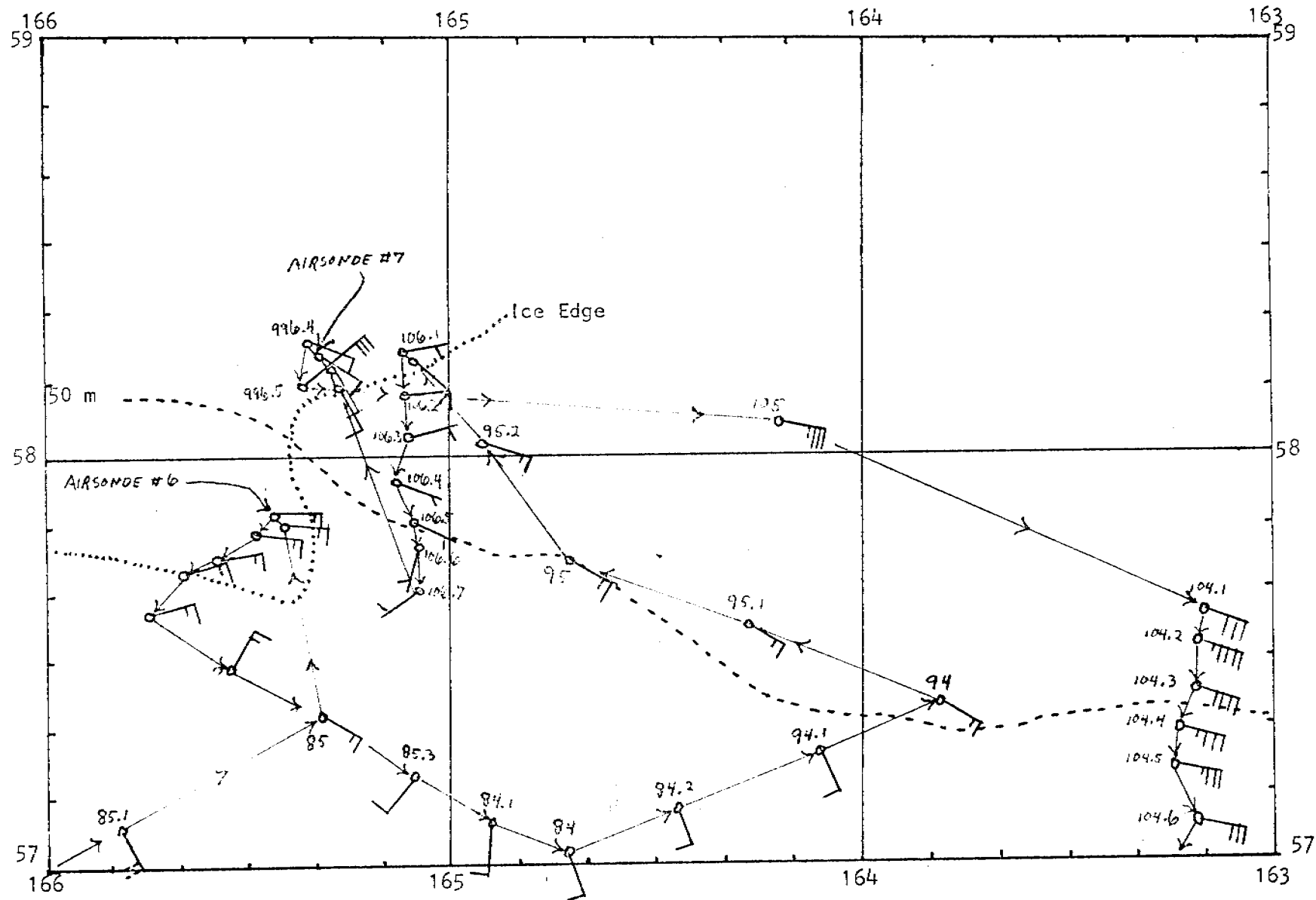
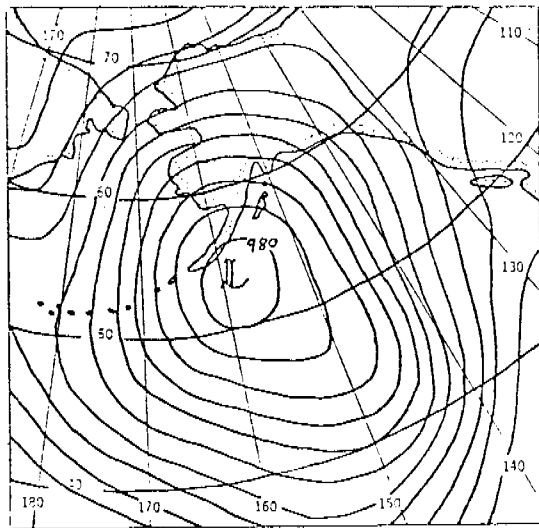
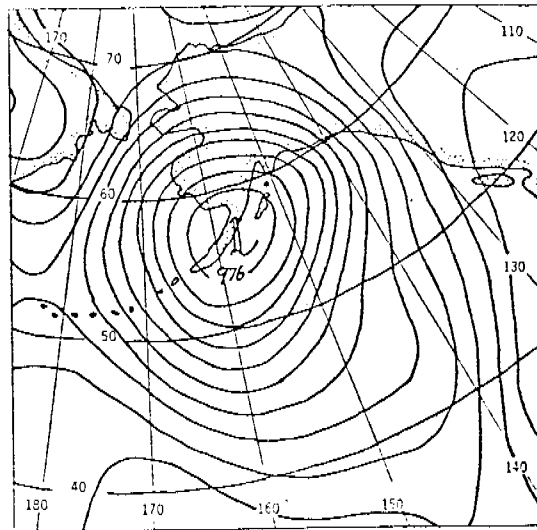


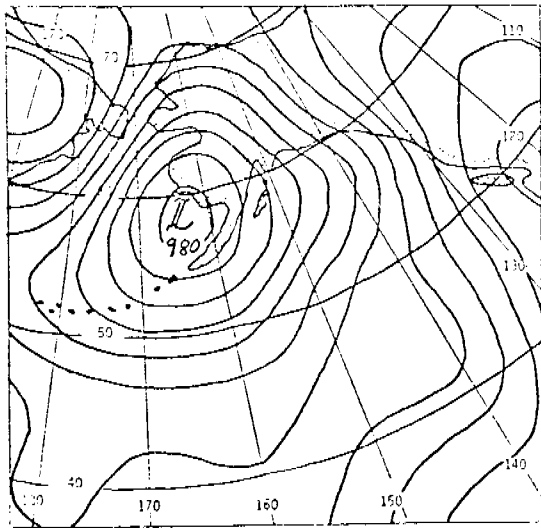
Figure 2. Inset of Figure 1 showing CTD stations and ship wind measurements. One barb = 10 knots. Also shown are the locations of airsonde flights 6 and 7.



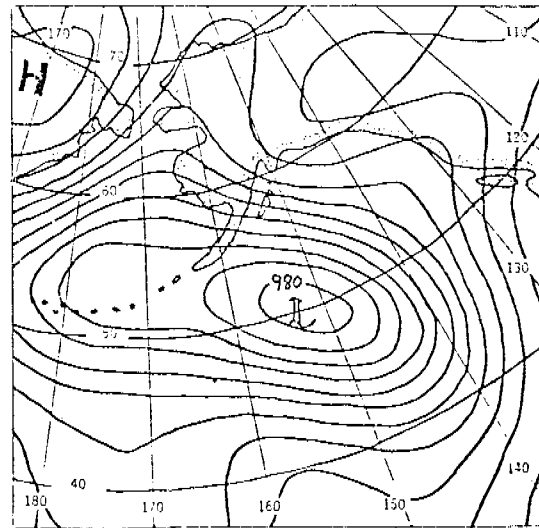
00Z 18 February 1978



00Z 19 February 1978

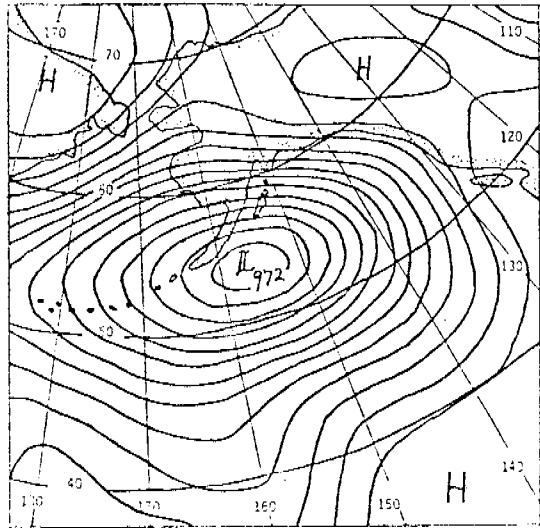


00Z 20 February 1978

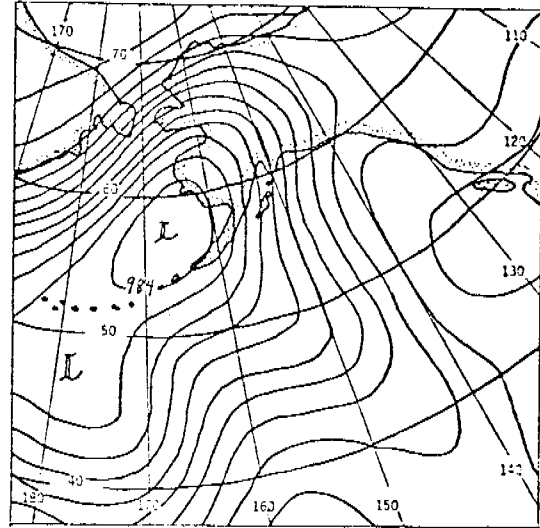


12Z 21 February 1978

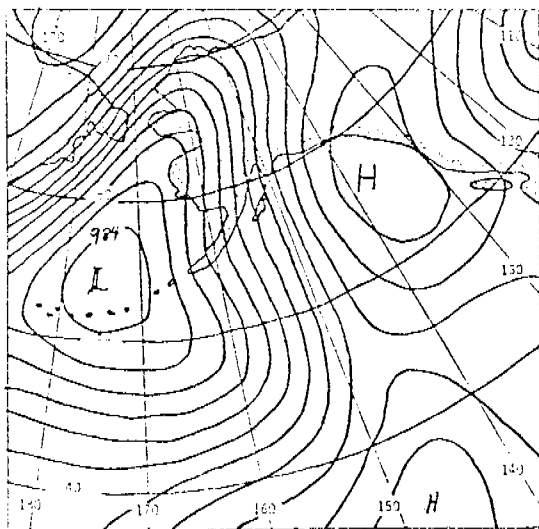
Figure 3. Surface pressure 12 hour prognoses valid for the times shown. Obtained from FNWC broadcasts received onboard the SURVEYOR. Contour interval is 4 mb.



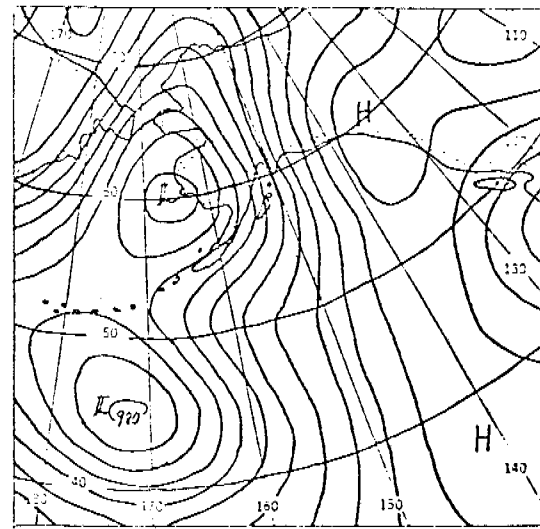
00Z 22 February 1978



00Z 23 February 1978



00Z 24 February 1978



12Z 25 February 1978

Figure 3. continued

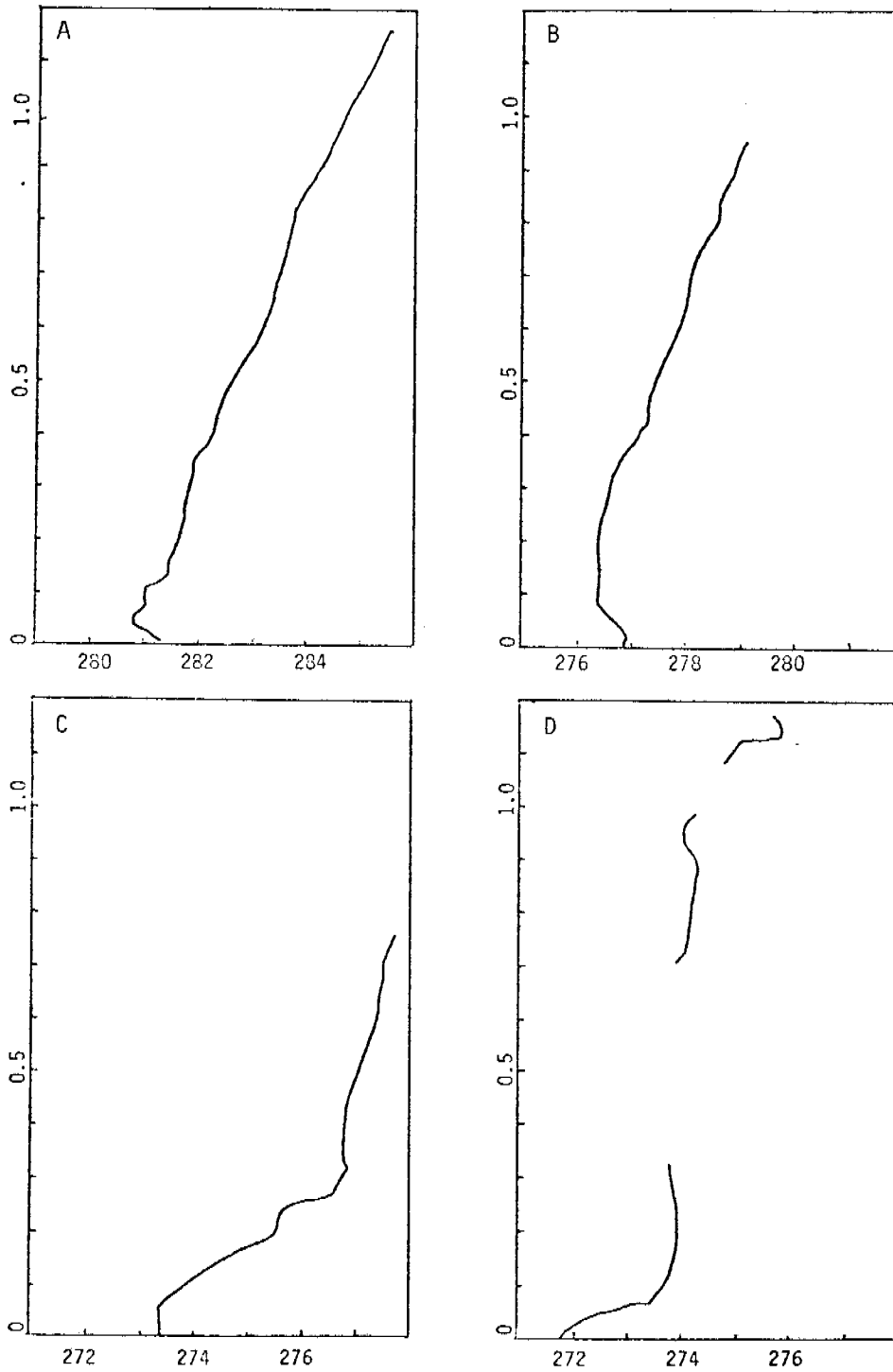


Figure 4. Potential temperature in Kelvins vs. height in km.
 A=Airsonde #4
 B=Airsonde #5
 C=Airsonde #6
 D=Airsonde #7

APPENDIX D
CRUISE REPORT COVERING METEOROLOGICAL ACTIVITIES IN LOWER
COOK INLET AND THE WESTERN GULF OF ALASKA

CRUISE REPORT

Surveyor Cruise RP-4-SU-78A, leg II

Chief Scientist: Robin D. Muench
Research Oceanographer
NOAA/PMEL

Other Scientific Personnel: Stewart A. Macklin
Meteorologist
NOAA/PMEL

Brad Eckert
Electronic Technician
NOAA/NOS

Introduction:

The Coastal Physics Group, Pacific Marine Environmental Laboratory (PMEL), Seattle, Washington has for the past three years been actively participating in the Outer Continental Shelf Environmental Assessment (OCSEA) program. This cruise was carried out in support of the OCSEA program, which has as its general objectives: (1) provide comprehensive environmental data and information on the Alaskan continental shelf lease areas; (2) define the probable ecological impact of oil exploration, production, storage and transshipment on the continental shelf; (3) refine our understanding of key ecological dynamic processes; and (4) provide a basis for predictive or diagnostic models of the ecosystem response to contamination by petroleum and its by-products.

In response to these general objectives, PMEL has been carrying out field programs designed to measure water temperature, salinity and density fields and their associated circulation patterns, and to survey coastal weather phenomena. Major goals have been to define critical circulation and mixing parameters in the water and to offer means of prediction of mesoscale coastal wind features too small to be delineated by the synoptic network of the National Weather Service (NWS), NOAA. Towards this end, field studies have been carried out throughout the Alaskan continental shelf from Norton Sound to the Yakutat Bay region. With the 1978 fiscal year, two new areas have been selected for intensive study: (1) the shelf region surrounding Kodiak Island, with particular emphasis on Albatross and Portlock banks; and (2) lower Cook Inlet and Shelikof Strait.

Cruise Objectives:

This cruise supported that portion of the OCSEA program addressing physical oceanographic and meteorological problems in the northwest Gulf of Alaska and lower Cook Inlet regions. Oceanographically, its purpose was to utilize a profiling conductivity/temperature/depth (CTD) system to determine mid-winter temperature, salinity and density fields. Drift cards (surface drifters) were deployed at selected locations to provide later information on surface water motions. Specific scientific problems

were: (1) circulation and mixing processes in the Portlock and Albatross banks region, particularly bifurcation of the mid-depth (200-250 m) westward-flowing warm core of the Alaska Current east of Portlock Bank; (2) structure and dynamics of the Alaska Current, a major westward-flowing boundary current which coincides roughly with the continental shelf break, from about 148°W to 158°W; (3) shelf circulation and mixing processes southwest of Kodiak Island to Mitrofanina Island; (4) circulation through Shelikof Strait; and (5) circulation and mixing processes in lower Cook Inlet south of roughly the latitude of Anchor Point.

Meteorologically, the objectives of this cruise were three-fold: (1) to test and evaluate new atmospheric profiling equipment; (2) to obtain quality surface meteorological comparison measurements between the Surveyor and environmental data buoys in lower Cook Inlet and on Albatross Bank; and (3) to identify and cross-section expected mesoscale atmospheric flows in lower Cook Inlet.

Methods:

Overall program objectives for the northwest Gulf of Alaska during this period were addressed via a two-vessel operation using the NOAA vessels Surveyor and Discoverer. Operations of the two vessels were closely coordinated via daily radio contact between the Chief Scientists, in addition to detailed pre-cruise discussion. This report is concerned with the work undertaken by the Surveyor.

Oceanographic objectives of this cruise were addressed by occupying section lines of CTD stations in a generally northwest-southeast direction across Portlock and Albatross banks east and south of Kodiak Island. An especially high station spatial density in the Portlock-eastern Albatross banks region was intended to allow resolution of the bifurcating core of warm, subsurface water and of vertical mixing on shoal areas of these banks. These closely-spaced stations addressed the first of the five oceanographic problems outlined above. These CTD data will be supplemented with data from five current meter moorings which were recovered from central Albatross Bank early during this cruise, by the Discoverer.

The second oceanographic problem, structure and dynamics of the Alaska Current, was approached by extending all CTD sections from the banks well out over the shelf break (200 m) into the current core. Two sections, one over Portlock Bank and one running south from the Trinity Islands, were extended seaward to completely traverse the current. All sections extending off the shelf break will be used to define temperature and salinity structure in the current. The two extended sections will be used, in addition, to compute baroclinic volume transport of water by the current. Ship drifts during occupation of CTD stations in the current were specifically monitored to provide estimates of surface water motion (allowing for wind effects).

The third oceanographic objective, circulation and mixing processes southwest of Kodiak Island, was addressed by the Discoverer concurrently with this cruise. They occupied CTD stations and recovered current meter moorings which had been deployed in October 1977.

The fourth objective, circulation through Shelikof Strait, was approached jointly by this cruise and the Discoverer. We occupied a closely-spaced section of CTD stations across southwestern Shelikof Strait, while Discoverer occupied stations axially up the Strait and close-spaced sections across the northeastern end. These data will be used to compute baroclinic current speeds and to examine temperature-salinity distributions for evidence of mixing and flow processes. Toward this end, a moored current meter array containing three meters in the northeastern end of the Strait was recovered by Discoverer; this array was deployed in October 1977.

The final oceanographic problem, that concerned with circulation and mixing in lower Cook Inlet, was addressed entirely by Discoverer, with CTD sections and recovery of moored current meters and pressure gauges.

Overall study of surface water circulation on Portlock and Albatross banks was supplemented, in addition to the CTD casts, by deployment of drift cards at selected locations on the banks (cf. Appendix B). These cards, marked with three languages (English, Russian and Japanese) with instructions for return of information on their recovery and promises of a \$1 US reward, are designed to float at the water's surface. Their eventual recovery, from beaches and by fishing vessels, will allow reconstruction of approximate pathways for surface water motion (trajectories).

To ensure quality control of the CTD data, temperature and salinity calibration samples were taken with a Nansen bottle every other cast. In addition, 5-sample temperature and salinity calibration casts were taken on the first ~~and final~~ stations of the cruise. Data tapes from the DDL were replaced with fresh tapes and replayed about once each day and a half (whenever the 7" reels were filled) to verify proper functioning of the CTD system. In addition, analog charts were routinely taken at each cast. Some variation in lowering rates was attempted in order to better define temperature and salinity through high gradient regions. Decrease of the lowering rate from 30 to 10-20 m/min through the upper 300 m of the water column did not markedly improve the quality of data (as determined by the salinity spiking). It was, moreover, impossible to accurately control lowering rate at these low speeds. In view of these facts, coupled with the considerable additional time required for the slower lowering rate (20 min/cast for casts deeper than 300 m), it was decided to retain the 30 m/min lowering rate. Below 300 m, the lowering rate remained at 60 m/min.

Some use was made of the Surveyor PDP8/E computer's capability to plot vertical temperature, salinity and density profiles using the DDL tapes, particularly when trouble-shooting. In view of the appreciable time required for these plots, coupled with lack of calibration and lowering rate/response time corrections for the data, it was decided not to use this plotting capability on a routine basis. The analog temperature and salinity plots from the CTD system were adequate for monitoring system performance cast by cast and for observing features in the water column.

The first two meteorological objectives were achieved in "piggyback" fashion concurrent with the CTD measurements. The initial CTD transects allowed adequate time for familiarization with and evaluation of the newly acquired Airsonde atmospheric profiling system. Weather permitting, sondes

were launched at 1115 and 2315 UT (standard NWS radiosonde ascent times). This scheme was selected because it allows comparison of Airsonde data with simultaneous NWS-derived profiles from selected south Alaska stations.

Close proximity of EB-72 to the CTD stations on Albatross Bank allowed pursuit of the second meteorological objective with minimal disruption of the oceanographic operation. In order to verify operation of the environmental data buoy and to obtain at least a crude calibration with PMEL standard instrumentation, Surveyor conducted three routine hourly deck weather observations while positioned within one mile of EB-72. The ship was stationed such that no flow interference patterns were generated over either platform. ~~Due to in-cruise scheduling, it was necessary to assign verification/calibration of the lower Cook Inlet environmental buoy, EB-39, to the Discoverer.~~

The third meteorological objective, identification of lower Cook Inlet wind patterns, was also originally scheduled as a piggyback operation. This has been redesigned as a primary endeavor and is discussed in a separate section appended to this report (Appendix C).

Low level profiles through the atmospheric boundary layer were acquired using an expendable AS-1C Airsonde and associated TS-2AR ground station, all manufactured by the Atmospheric Instrumentation Research Company, Boulder, Colorado. The Airsonde is an aerodynamically-shaped styrofoam package containing wet and dry bulb thermistors for temperature measurement, a capacitance-interfaced aneroid cell for pressure sensing, switching circuitry and a 403 MHz transmitter with antenna. The shape of the sonde allows it to spin about a central vertical axis thus aspirating the thermistors as the sonde is carried aloft by a 30 gram sounding balloon inflated to 350 grams static lift. The sonde is powered by a 9V transistor battery, is precalibrated and transmits its A data frame (wet and dry bulb temperatures, pressure) every 6-8 seconds.

The TS-2AR ground station is a receiver and micro-processor which decodes the incoming signal, converts to physical units and reencodes the data for relay to any of three peripheral devices: strip-chart recorder, cassette recorder or Hewlett-Packard Model 97 printing calculator. This complete ground package is encased in an aluminum suitcase suitable for shipping.

Preliminary Results:

This cruise consisted of two phases. The first phase lasted from 3-17 March and consisted primarily of occupation of 182 consecutive CTD casts along NW-SE section lines traversing Portlock and Albatross banks (Appendix A). Occupation of these sections commenced at the NE end of the study region and worked southwestward to the Trinity Islands region. The Surveyor then proceeded north around the Trinity Islands and occupied the final CTD section of the cruise across southwestern Shelikof Strait. During this first phase, drift cards were deployed at 13 locations over the banks (Appendix B), eleven airsondes were launched (cf Table 1 and

discussion below) and a three-hour set of surface meteorological observations were obtained adjacent to data buoy EB-72 for later comparison with data from the buoy.

On 17 March Surveyor proceeded north to lower Cook Inlet and carried out the second phase of the cruise. This was a survey of surface and upper-air meteorology of lower Cook Inlet designed to study local winds. On 19 March, Surveyor returned to Kodiak and the cruise was terminated on schedule.

Rigorous analysis of temperature and salinity data from the CTD must await final processing at PMEL. This processing includes calibration and corrections for error due to lowering rate in conjunction with vertical temperature gradients. Monitoring of the analog output from the CTD, and of digital printout derived from the DDL tapes, allows however some observations of a preliminary nature.

- 1) The warm subsurface core of the Alaska Current was readily apparent along the shelf break and to seaward. This core occurred at depths of approximately 100-200 m and attained maximum temperatures of the order of 6°C.
- 2) The upper portion of the warm core was characterized by considerable vertical temperature and salinity structure having scale lengths of the order of tens of meters and sharp vertical gradients. There was negligible correlation between details of this structure at adjacent stations, and in one case the structure had changed appreciably between a down- and upcast at the same station. These small features appear to be transient, and may be related to lateral interfingering of the cold, vertically uniform water on the banks with the warmer water of the Alaska Current.
- 3) Water on the banks off Kodiak Island was vertically well-mixed, as anticipated. Horizontal gradients in both temperature and salinity were apparent in the vertically mixed regions.
- 4) There was evidence of the warm subsurface layer from the Alaska Current near-bottom east of Kennedy Entrance. This supports the prior concept of westward flow of water from the Alaska Current through Kennedy Entrance.

In addition to the CTD observations, ship drift clearly located the high-speed core of the Alaska Current. At one deep off-shelf station, for example, drift was about 10 km to the southwest during the 90-minute duration of the station. Winds were from the northwest, and the ship held into the wind and was near-motionless with respect to the surface water. This suggests a surface current of about 3.6 knots to the southwest. Previous estimates of baroclinic current speed in the Alaska Current are on the order of 2 knots at the surface, so this estimate of total speed is in rough agreement. Extreme wire angles for the CTD, despite little ship motion relative to the water, suggested that a strong vertical shear was present. This is in agreement with the concept of a baroclinic current, with speeds decreasing with depth.

Eleven Airsondes were launched over the period 2-16 March 1978. Time and position of launch, pertinent surface meteorological data and ceiling of usable information obtained are given in Table 1. A favorable launch routine was established whereby a single person can prepare and launch a sonde in 10-15 minutes. Ascent to 3000 m then requires an additional 15-20 minutes. Data acquired can be replayed through the system, generating a finished data product in an additional 60-90 minutes. Two major drawbacks (both correctible by the manufacturer) were discovered and are detailed below.

The Airsonde system is clearly superior to the radiosonde system which it replaces. The lightness of the sonde allows launch using a much smaller balloon, a critical factor in working from a vessel. Its precalibration cuts preparation time in half. Real-time printout of physical units permits the researcher to immediately discern atmospheric structure, allowing more prudent use of scientific resources. Most important, automatic processing of the data removes the element of human error and generates a finished product in a much shorter time. The data density allows definition of fine-scale atmospheric structure undiscernable with radiosondes.

As alluded to above, this shipment of prototype Airsondes was plagued with two difficulties. Poor signal-to-noise ratio at intermediate altitudes (1500-2000 m) prevented proper operation of the micro-processor with subsequent loss of usable data. It is felt that this is a unique problem of the marine environment, as land-based flights have been made routinely to altitudes of 10,000 m. Increasing transmitter power and/or preamplifying and filtering the reception would cure this problem. Secondly, the wet-bulb thermistor malfunctioned occasionally, its indicated temperature suddenly becoming higher than that of the dry-bulb thermistor, a physical impossibility. This phenomenon was often observed to occur during penetration of a cloud layer and is probably caused a mis-design of the wicking and reservoir.

In the early morning hours of March 14, Surveyor made three passes within one mile of EB-72 on Albatross Bank. The exact times and positions as well as the meteorological data recorded for later comparison with buoy tapes are listed in Table 2. ~~A similar program was carried out by the NOAA ship Discoverer at EB-39 in lower Cook Inlet.~~

All objectives of the lower Cook Inlet meteorological program, as detailed in Appendix C, were attained except the Discoverer-Tustumena surface meteorological data intercomparison. This objective could not be completed in the short time span dictated by the Tustumena's schedule; future experimental plans will include this objective.

The Surveyor began the lower Cook Inlet meteorological survey on 17 March 1978 at 1900 UT just north of Shuyak Island, then cruised northwest to Cape Douglas, Kamishak Bay and on to the other locations detailed in Appendix C. She finally arrived at data buoy EB-39 at 1500 UT, 18 March 1978. Airsondes were released at all stations, including the Barren Islands station occupied after the EB-39 time series. Surveyor maintained station at EB-39 until 0700 UT on 19 March. Routine meteorological

Table 1: Airsonde ascents for evaluation period

Airsonde Designation	Date/Time (UT)	Position Lat (n)/Long (W)	Surface Meteorological Conditions					Height Attained (m)
			Pressure (mb)	Wind (dir/kts)	Temp (°C)	Wet bulb (°C)	Sea sfc (°C)	
LC1	03-02-78 2254	57-43.6 152-30.9	1017.3	calm	4.8	3.0	---	4217
LC2	03-04-78 2339	58-21.2 148-18.4	1002.8	240/15	2.0	-0.3	4.9	3008
LC3	03-05-78 1115	58-51.5 149-45.8	996.4	265/06	2.0	-0.3	4.6	1121
LC4	03-05-78 2320	59-05.2 150-39.0	996.8	100/05	1.5	-0.6	4.6	1730
LC5	03-06-78 1112	58-31.8 150-45.0	996.1	080/03	0.9	-1.1	4.4	1710
LC6	03-07-78 0010	57-57.9 148-47.0	985.3	345/18	2.6	0.9	4.7	710
LC7	03-09-78 2317	58-54.8 151-47.7	999.2	308/09	3.3	2.4	4.4	2077
LC8	03-10-78 1125	58-21.3 151-07.0	1010.6	290/06	1.7	-0.5	4.3	2755
LC9	03-10-78 2344	57-31.2 149-48.5	1014.8	100/12	3.1	2.0	4.9	1561
LC10	03-11-78 1100	57-04.4 149-49.2	1017.6	107/12	3.3	2.4	4.6	1390
LC11	03-16-78 2318	56-46.6 155-00.5	1012.0	300/05	-0.1	-2.1	3.3	3419

Table 2: Positions and surface data from EB-72 comparison.

Date	Time (UT)	Position Lat/Long	T(°C) T _w (°C)	Wind spd. Wind dir.	T _{sea} (°C) Vis (mi)	Swell (m) Dir(°T)	Wave (m) P("Hg)
3-14-78	1359	57-07.0 151-44.9	3.3 2.2	26 kts. 065°T	3.9 3	2 075	1 29.35
3-14-78	1455	57-08.2 151-45.4	2.2 1.7	28 kts. 056°T	3.3 3	7 075	1 29.36
3-14-78	1555	57-08.1 151-44.7	2.2 2.2	18 kts. 076°T	3.3 3	7 075	1 29.33

observations were conducted hourly, and airsondes were released at two-hourly intervals commencing at 1800 UT, 18 March. A summary of lower Cook Inlet Airsonde activity is contained in Table 3.

Between the 1900 and 2000 hourly surface observations on 18 March at EB-39, Surveyor and Discoverer made two meteorological intercomparison passes. Temperature measurements were made with a sling psychrometer on the weather side bridge wing. Surveyor reported winds from both the port and starboard anemometers. At times of observation, the ships were within $\frac{1}{4}$ mile of each other, steaming parallel courses into the wind and travelling at the same rate of speed. Results from this intercomparison are presented in Table 4.

Summary and Acknowledgments:

This cruise was an extremely successful one from a scientific viewpoint. We've obtained a more complete set of environmental data than ever before from this region at this time of year; this will be invaluable in defining the complex regional oceanographic and meteorological regimes. This success has been due to extremely efficient and trouble-free operations on the part of Surveyor and her personnel, aided by a period of abnormally mild weather. Since all personnel involved have functioned as a team, individual names will not be mentioned. Especial thanks are due, however, to the ship survey crew whose care and attentiveness during scientific operations ensured data quality under often less-than-ideal conditions. They and they alone are responsible for the consistently high quality data obtained. We acknowledge, also, the efforts made by Captain Grunwell, the officers and men of Surveyor in carrying out this operation in a trouble-free and professional manner.

This cruise was carried out under the auspices of the BLM-sponsored Outer Continental Shelf Environmental Assessment Program.

Problems Encountered and Suggestions:

Problems encountered during this cruise were minimal. The DDL of the CTD unit malfunctioned and had to be replaced with another unit, which caused the loss of digital data from one station. On another occasion, the underwater unit failed and a minor repair cured the problem with no loss of data. On deep (1500 m) casts in regions of high current shear, the CTD underwater unit tended to stream away from the ship with consequent large wire angles, erratic lowering rates and some decrease in data quality. Addition of more weight to the unit did not cure the problem completely, but eased it considerably. This would not be a common problem, as few locations in the normal operating areas have current shears as high as those encountered in the Alaska Current off Kodiak Island.

It was felt by us that the ship survey technicians are capable of carrying out more complex and responsible tasks than are presently assigned to them. While this particular cruise was limited in scope,

Table 3: Airsonde ascents for lower Cook Inlet

Airsonde Designation	Date/Time (UT)	Position Lat (N)/Long (W)	Surface Meteorological Conditions					Height Attained (mb)
			Pressure (mb)	Wind (dir/kts)	Temp (°C)	Wet bulb (°C)	Sea sfc (°C)	
LC12	03-17-78 1920	58-41.7 152-18.7	1006.7	352/09	0.5	-1.0	4.4	762
LC13	03-17-78 2104	58-50.2 152-47.5	1007.6	017/14	0.1	-1.6	4.4	729
LC14	03-17-78 2241	58-59.6 153-14.5	1008.2	297/11	0.9	-0.5	2.7	565
LC15	03-18-78 0130	59-17.8 153-37.3	1008.9	045/01	-0.8	-2.9	1.5	625
LC16	03-18-78 0349	59-21.7 153-16.3	1008.9	031/09	0.1	-2.5	1.8	700
LC17	03-18-78 0540	59-33.9 153-00.0	1009.5	033/08	0.1	-2.1	2.7	600
LC18	03-18-78 0817	59-33.4 152-16.5	1009.3	020/17	0.2	-1.2	4.0	469
LC19	03-18-78 1005	59-32.4 151-41.5	1009.1	063/08	0.0	-1.3	3.9	747
LC20	03-18-78 1735	59-08.9 152-47.1	1008.0	020/17	0.6	-0.7	4.3	(5m)
LC21	03-18-78 1753	59-09.1 152-47.3	1007.9	020/14	0.6	-0.7	4.3	929
LC22	03-18-78 2013	59-10.6 152-47.9	1006.9	020/22	0.5	-0.6	4.3	800
LC23	03-18-78 2212	59-09.3 152-46.2	1005.3	027/20	0.7	-0.5	4.2	783
LC24	03-19-78 0004	59-09.5 152-45.8	1003.3	036/21	1.1	-0.4	4.2	724
LC25	03-19-78 0205	59-09.4 152-45.4	1001.2	045/18	1.7	0.2	4.2	633
LC26	03-19-78 0401	59-09.9 152-48.9	998.9	055/22	1.3	0.5	4.3	806
LC27	03-19-78 0700		995.1	075/14	3.1	2.2	4.5	845

Table 4: Surveyor-Discoverer meteorological intercomparison.

Date/ Hour(UT)	Present Weather	Vis. (n.m.)	Wind/ Dir.	Wave/ Swell	T _{sea} (°C)	T(°C)/ T _w (°C)	P(mb)	Ship
3-18-78 0927	Cloudy	25	26(p) 24(s)/ 020	1'/ 0	3.3(int) 4.3(B)	0.8/ -0.5	1007.3	<u>Surv.</u>
			26/ 020		4.1	0.2/ -1.0	1007.5	<u>Disco.</u>
3-18-78/ 0935	Cloudy	35	22(p) 24(s)/ 020	1'/ 0	4.3	0.8/ -0.5	1007.3	<u>Surv.</u>
			22/ 020			0.0/ -1.2	1006.9	<u>Disco.</u>

At time of observations, Surveyor speed = 7 knots, course 020°T.

Position of <u>Surveyor</u> :	<u>1st pass</u>	<u>2nd pass</u>
	59-10.6	59-11.5
	152-46.3	152-45.7

consisting primarily of CTD work, some cases in point come to mind.

- 1) Use of the UGR is essential in defining distance between the CTD unit and the bottom, yet the survey techs have apparently not been trained in making appropriate adjustments to this unit. Misinterpretation of the UGR trace (the machine's fault) in one instance necessitated repeating a cast; adjustment of the unit would have eliminated the problem. We feel that anyone using a piece of gear should understand its operation and be capable of adjusting it to obtain maximum information.
- 2) The PDP8/E computer has considerable capabilities. Given the appropriate software (much of which is available), the survey techs could be taught to run relatively complex routines on data. Since the calibration samples are run aboard ship, there is no reason why the CTD data could not be run through the mill and the Chief Scientist provided with a final, corrected product. Going a step further, this could then be used to generate vertical sections, profiles, etc. and allow data analysis to commence aboard ship. (The research vessel Thompson has such a capability.)
- 3) Smooth plotting should be done on the computer. This would be faster, more accurate than hand plotting. Admittedly, this can't be implemented overnight. If done, however, it would free the survey techs to pursue item 2 above. It seems to me that these personnel, several of whom have had considerable training, could be better used than for plotting.

These comments are intended as constructive. Surveyor, with its heavy weather capabilities, computer and ample complement of personnel, is capable of doing better than its already better-than adequate best.

APPENDIX A

CTD Casts taken during Surveyor cruise RP-4-SU-78A, Leg II.

PORTLOCK-ALBATROSS BANK REGION						
<u>CAST NO.</u>	<u>STA. NO.</u>	<u>JD</u> *	<u>HR</u> *	<u>LATITUDE</u>	<u>LONGITUDE</u>	<u>DEPTH(m)</u>
001	519	63	1652	58-09.2	147-43.5	2195
002	518	63	1948	58-14.5	147-57.3	2048
003	517	63	2135	58-18.2	148-07.4	1400
004	516	63	2326	58-21.6	148-18.7	1170
005	515	64	0113	58-23.7	148-27.1	640
006	514	64	0303	58-28.6	148-38.2	122
007	513	64	0409	58-31.4	148-48.5	114
008	512	64	0509	58-34.5	148-58.0	110
009	511	64	0610	58-38.1	149-07.3	130
010	510	64	0721	58-41.4	149-16.6	142
011	509	64	0819	58-45.2	149-27.6	185
012	508	64	0939	58-47.9	149-36.8	215
013	507	64	1046	58-51.7	149-46.4	240
014	506	64	1306	58-54.0	149-55.4	232
015	505	64	1507	59-00.1	149-56.7	205
016	504	64	1602	59-05.3	149-59.6	180
017	503	64	1653	59-11.5	150-02.0	132
018	502	64	1736	59-15.6	150-03.1	195
019	501	64	1827	59-21.6	150-06.4	170
020	520	64	1925	59-16.7	150-07.0	182
021	521	64	2012	59-13.1	150-11.8	117
022	522	64	2102	59-11.8	150-21.8	177
023	523	64	2154	59-08.1	150-29.8	111
024	524	64	2251	59-04.6	150-39.4	108
025	525	65	0024	59-01.4	150-45.3	165
026	528	65	0125	59-02.3	150-56.1	152
027	527	65	0211	59-06.0	150-57.4	177
028	526	65	0313	59-10.0	150-58.7	62
029	549	65	0359	59-07.4	151-06.0	97
030	550	65	0445	59-03.8	151-06.3	100
031	551	65	0535	58-59.7	151-05.6	157
032	529	65	0633	58-57.7	150-55.0	140
033	530	65	0750	58-51.4	150-52.9	160
034	531	65	0852	58-44.6	150-50.2	180
035	532	65	1002	58-38.6	150-47.2	200
036	533	65	1101	58-31.9	150-45.0	132
037	534	65	1204	58-27.8	150-33.5	73
038	535	65	1259	58-25.1	150-22.4	71
039	536	65	1358	58-21.1	150-11.1	50
040	537	65	1442	58-18.6	150-03.2	46
041	538	65	1546	58-16.2	149-52.0	60
042	539	65	1643	58-13.4	149-43.2	59
043	540	65	1755	58-10.3	149-19.6	100
044	541	65	1842	58-07.9	149-23.1	125
045	542	65	1954	58-03.7	149-10.2	108
046	543	65	2050	58-01.7	149-02.4	119
047	544	65	2156	57-59.0	148-52.3	575
048	545	66	0010	57-57.9	148-47.0	807

*All dates and times are UT.

APPENDIX A (cont'd)

<u>CAST NO.</u>	<u>STA. NO.</u>	<u>JD*</u>	<u>HOURL*</u>	<u>LATITUDE</u>	<u>LONGITUDE</u>	<u>DEPTH(m)</u>
049	546	66	0143	57-55.7	148-39.9	450
050-51	547	66	0325	57-51.8	148-33.1	1756
052	548	66	0600	57-51.2	148-25.6	1830
053	772	66	1157	56-52.7	148-12.2	4389
054	771	66	1445	57-00.5	148-23.4	4680
055	770	66	1726	57-08.1	148-38.6	4930
056	769	66	2013	57-15.2	148-49.6	3475
057	768	66	2228	57-22.6	149-01.1	2516
058	767	67	0043	57-30.7	149-13.3	2560
059	572	67	0219	57-32.6	149-17.3	1950
060-61	571	67	0521	57-36.1	149-20.7	1463
062	570	67	0753	57-40.4	149-28.4	970
063	569	67	0921	57-44.4	149-34.1	505
064	568	67	1046	57-48.2	149-39.6	278
065	567	67	1159	57-53.0	149-46.1	240
066	566	67	1314	57-56.5	149-53.3	261
067-68	565	67	1416	57-59.9	149-57.6	280
069	564	67	1546	58-04.1	150-06.5	320
070	563	67	1652	58-06.8	150-16.8	250
071	562	67	1735	58-08.9	150-20.1	170
072	561	67	1836	58-12.3	150-27.7	993
073	560	67	1942	58-18.5	150-38.6	61
074	559	67	2037	58-24.9	150-48.9	75
075	558	67	2147	58-31.4	151-01.5	155
076	557	67	2226	58-33.7	151-07.1	174
077	556	67	2357	58-40.0	151-06.5	170
078	555	68	0050	58-44.1	151-04.9	165
079	554	68	0157	58-48.7	151-04.0	139
080	553	68	0252	58-53.9	151-03.5	168
081	552	68	1511	58-56.7	151-06.3	161
082	573	68	1655	58-57.8	151-16.0	152
083	574	68	1813	59-00.3	151-25.6	131
084	575	68	1909	59-02.3	151-37.6	142
085	576	68	2000	59-04.3	151-45.7	100
086	577	68	2038	59-03.9	151-55.2	192
087	578	68	2206	59-00.3	151-46.6	128
088	579	68	2307	58-54.6	151-47.2	110
089	580	69	0027	58-49.9	151-38.9	137
090	581	69	0126	58-46.2	151-45.4	210
091	582	69	0234	58-40.8	151-47.0	132
092	583	69	0335	58-36.0	151-44.0	159
093	584	69	0424	58-32.2	151-46.6	177
094	585	69	0518	58-27.6	151-50.0	104
095	586	69	0610	58-27.6	151-46.5	195
096	587	69	0714	58-25.5	151-36.8	174
097	588	69	0843	58-24.2	151-28.5	170
098	589	69	0956	58-23.4	151-19.0	120
099	589	69	1002	58-23.4	151-19.1	120
100	590	69	1116	58-21.3	151-07.0	117

*All dates and times are UT.

APPENDIX A (cont'd)

<u>CAST NO.</u>	<u>STA. NO.</u>	<u>JD*</u>	<u>HOUR*</u>	<u>LATITUDE</u>	<u>LONGITUDE</u>	<u>DEPTH(m)</u>
101	591	69	1200	58-18.1	151-02.7	145
102	592	69	1338	58-12.0	150-59.6	105
103	600	69	1435	58-05.7	150-57.2	143
104	601	69	1533	58-02.5	150-49.9	148
105	602	69	1619	57-58.2	150-44.6	119
106	603	69	1711	57-55.3	150-37.0	121
107	604	69	1759	57-51.9	150-28.7	95
108	605	69	1846	57-49.2	150-22.4	100
109	606	69	1930	57-47.0	150-15.5	115
110	607	69	2033	57-42.9	150-06.9	177
111	608	69	2125	57-40.7	149-59.4	225
112	609	69	2242	57-35.0	149-51.0	236
113	610	69	2344	57-31.2	149-48.5	1030
114	611	70	0132	57-27.2	149-42.9	1600
115	612	70	0321	57-23.2	149-39.2	1830
116	613	70	0515	57-18.9	149-32.8	2100
117	626	70	0816	56-59.9	149-40.8	3500
118	625	70	1006	57-03.8	149-48.1	2340
119	624	70	1155	57-08.5	149-55.7	1617
120	623	70	1329	57-12.6	149-59.5	1700
121	622	70	1532	57-16.5	150-05.7	1520
122	621	70	1733	57-21.8	150-10.7	669
123	593	71	2239	57-59.9	152-05.0	180
124	628	71	2340	57-55.1	152-01.6	198
125	629	72	0038	57-50.1	152-03.7	113
126	630	72	0153	57-44.6	152-00.6	110
127	631	72	0317	57-36.9	151-53.1	146
128	644	72	0436	57-29.8	151-55.8	86
129	632	72	0549	57-33.8	151-41.0	120
130	633	72	0646	57-31.4	151-33.4	145
131	634	72	0750	57-26.5	151-26.3	165
132	635	72	0852	57-21.4	151-23.1	150
133	636	72	0955	57-16.2	151-18.3	155
134	637	72	1101	57-11.3	151-15.0	143
135	638	72	1212	57-05.7	151-06.5	430
136	639	72	1327	57-01.8	151-02.7	578
137	640	72	1454	56-55.4	150-58.7	1200
138	641	72	1627	56-51.7	150-55.1	1700
139	642	72	1823	56-45.9	150-46.9	2100
140	643	72	2018	56-39.3	150-44.9	2926
141	654	72	2322	56-21.5	150-54.5	5415
142	653	73	0208	56-29.8	151-01.2	3100
143	652	73	0440	56-39.7	151-08.6	2200
144	651	73	0624	56-43.5	151-10.0	1465
145	650	73	0807	56-48.5	151-15.7	955
146	649	73	0932	56-53.2	151-20.1	900
147	648	73	1058	56-58.3	151-24.8	677
148	647	73	1225	57-04.1	151-29.6	165
149	646	73	1309	57-06.7	151-35.3	115

*All dates and times are UT.

APPENDIX A (cont'd)

<u>CAST NO.</u>	<u>STA. NO.</u>	<u>JD*</u>	<u>HOURL*</u>	<u>LATITUDE</u>	<u>LONGITUDE</u>	<u>DEPTH</u>
150	645	73	1712	57-16.3	151-42.3	55
151	656	73	1926	57-10.3	152-20.3	80
152	657	73	2106	57-03.1	152-07.8	75
153	667	73	2320	57-03.7	152-50.4	86
154	668	74	0021	56-59.7	152-42.1	145
155	669	74	0112	56-56.0	152-36.9	145
156	670	74	0206	56-53.7	152-33.9	154
157	671	74	0312	56-48.7	152-29.5	159
158	672	74	0508	56-42.6	152-29.7	163
159	673	74	0608	56-38.2	152-28.6	160
160	674	74	0726	56-32.2	152-29.3	265
161	675	74	0859	56-25.1	152-24.3	295
162	676	74	1010	56-22.0	152-20.2	540
163	677	74	1135	56-18.0	152-16.8	2000
164	678	74	1432	56-13.3	152-09.0	3880
165	776	74	2121	55-13.0	152-47.7	3475
166	775	74	2309	55-19.5	152-56.4	4950
167	774	75	0146	55-28.0	153-09.2	5267
168	773	75	0358	55-36.6	153-20.8	4050
169	700	75	0559	55-42.7	153-24.3	3000
170	699	75	0829	55-45.8	153-29.6	1355
171	698	75	1053	55-49.8	153-36.1	990
172	697	75	1259	55-54.3	153-41.0	270
173	696	75	1400	55-58.9	153-44.8	105
174	695	75	1525	56-07.5	153-56.3	185
175	694	75	1646	56-14.5	154-06.6	145
176	693	75	1808	56-23.7	154-15.6	40

SHELIKOF STRAIT

177	330	76	0205	57-20.6	154-56.0	159
178	329	76	0306	57-24.0	154-01.3	236
179	328	76	0402	57-26.7	155-07.3	238
180	327	76	0500	57-29.8	155-14.3	247
181	326	76	0604	57-33.0	155-20.5	285
182	325	76	0702	57-36.1	155-26.6	220

*All dates and times are UT.

APPENDIX B

Data on drift card deployments over Portlock
and Albatross banks

3-20 March 1978

<u>CARD NO's</u>	<u>JD</u> *	<u>HOUR</u> *	<u>LATITUDE</u>	<u>LONGITUDE</u>
101-200				
(exc. 165)	64	2250	59-04.6	150-39.4
201-300	65	1115	58-31.8	150-45.0
301-400	65	1546	58-16.2	149-52.0
401-500	65	2001	58-03.6	149-10.3
1401-1500	69	0036	58-50.0	151-39.0
501-600				
(exc. 513)	69	0505	58-27.6	151-50.0
901-1000	69	1133	58-21.4	151-06.9
601-700	69	1617	57-58.3	150-44.6
701-800	72	0806	57-25.8	151-25.8
801-900	73	1718	57-16.3	151-42.2
1001-1100	73	2106	57-03.1	152-07.8
1101-1300				
(exc. 1207)	74	0201	56-53.6	152-33.9
1301-1400	75	1522	56-07.5	153-56.2

*All dates and times are UT.



APPENDIX C

LOWER COOK INLET

METEOROLOGICAL EXPERIMENT

OBJECTIVES:

1) Survey of lower Cook Inlet (see figure) with stops at:

- a) Shuyak Island 58° 41.0' N
 152° 19.0' W
- b) Cape Douglas 58° 58.5' N
 153° 19.5' W
- c) Kamishak Bay 59° 17.7' N
 153° 37.0' W
- d) Augustine Island 59° 21.3' N
 153° 16.2' W
- e) Chinitna Point 59° 34.1' N
 153° 00.0' W
- f) Kachemak Bay 59° 32.3' N
 151° 41.0' W
- g) EB-39 59° 10.1' N
 152° 45.2' N
- h) Barren Islands 58° 56.0' N
 152° 07.0' W

2) Surface meteorological intercomparison with NOAA Ship DISCOVERER, Alaska State Ferry TUSTUMENA, EB-39.

3) 12-hour time series at EB-39.

METHODS:

1) Surface meteorological data are collected routinely by the Quartermaster. In addition, strip chart provides constant analog trace of surface winds. Airsonde ascent at each station plus an additional ascent on Shuyak - Douglas leg and Chinitna - Kachemak leg.

TOTAL: 8 Stations
 10 Airsondes

2) To be arranged with DISCOVERER, TUSTUMENA, if possible at least one comparison measurement of surface meteorological parameters will be executed. Ships should attempt to steam parallel to each other into the wind as close as safety permits. DISCOVERER will intercompare with TUSTUMENA, SURVEYOR with DISCOVERER, if possible.

3) Time permitting, the EB-39 station is extended by 12-hours. Airsondes are released every two-hours, plus routine deck weather measurements.

TOTAL: 7 Airsondes



(Continued)



SCHEDULING:

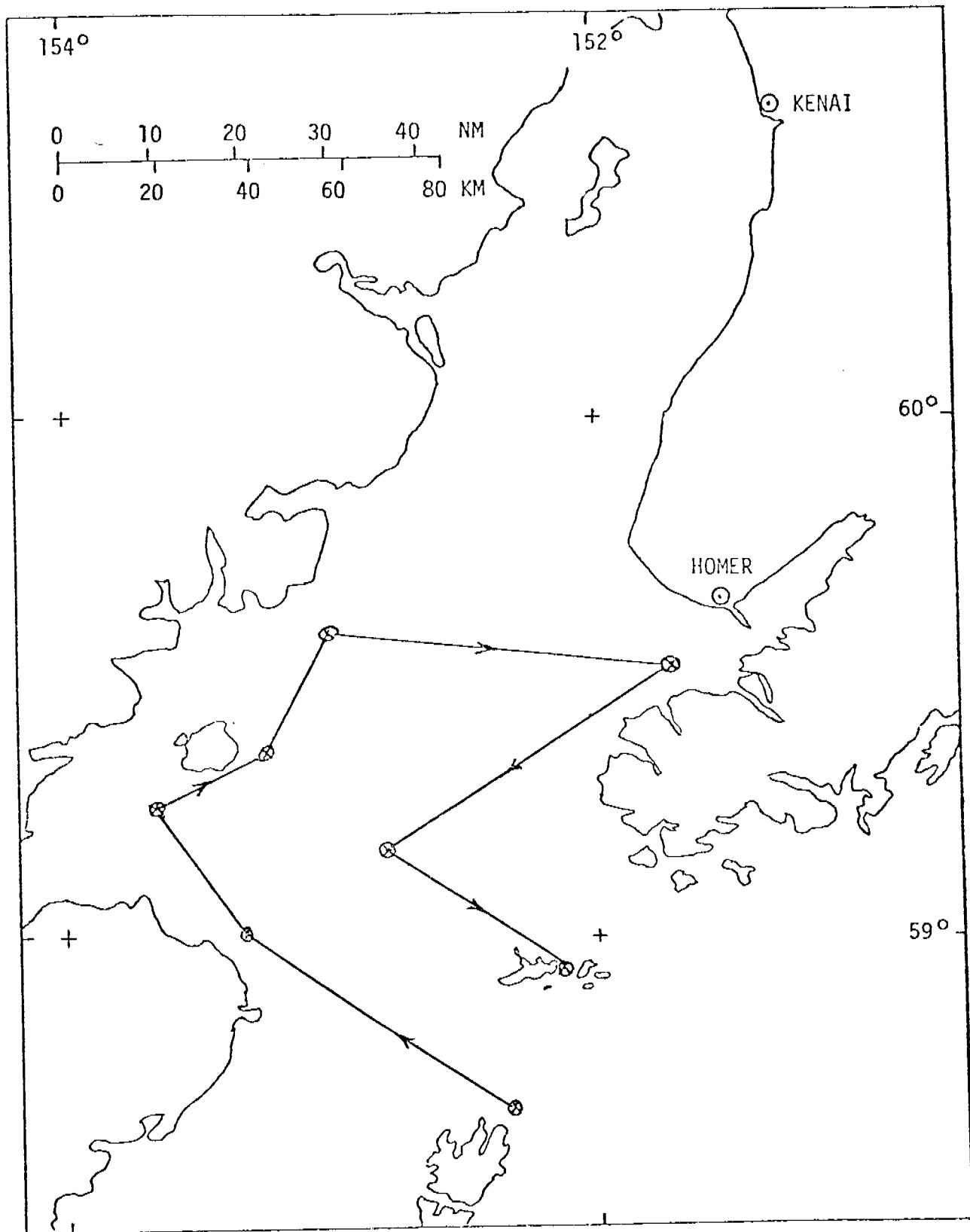
- 1) This experiment requires 41-hours to complete (28-hours without EB-39 time series).
- 2) Approximate distance between stations:

Shuyak - Douglas	36 NM
Douglas - Kamishak	21 NM
Kamishak - Augustine	12 NM
Augustine - Chinitna	16 NM
Chinitna - Kachemak	40 NM
Kachemak - EB-39	40 NM
EB-39 - Barren Island	27 NM

- 3) Tentative Schedule * (local time):

		<u>With Time Series</u>		<u>Without Time Series</u>
Arr: Shuyak	3/17	1415	3/18	0215
Dep: Shuyak		1445		0245
Arr: Douglas		1845		0645
Dep: Douglas		1915		0715
Arr: Kamishak		2130		0930
Dep: Kamishak		2200		1000
Arr: Augustine		2330		1130
Dep: Augustine	3/18	0000		1200
Arr: Chinitna		0200		1400
Dep: Chinitna		0230		1430
Arr: Kachemak		0630		1830
Dep: Kachemak		0700		1900
Arr: EB-39		1100		2300
Dep: EB-39	3/19	0015	3/19	0015
Arr: Barren Islands		0100		0100
Dep: Barren Islands		0130		0130

* Time schedule assumes ship averages
10 knots between stations.



ADMINISTRATIVE REPORT

AR-1855-NOAA
MARCH 1978

Research Unit #435

ANNUAL REPORT
1 April 1977 - 31 March 1978

Prepared for: DEPARTMENT OF COMMERCE
(National Oceanic and Atmospheric Administration)

Contract No.: 03-6-022-35249



Progress Report

MODELING OF TIDES AND CIRCULATIONS OF THE BERING SEA (RU 435) National Oceanic and Atmospheric Administration

April 1, 1977 - March 31, 1978

Jan J. Leendertse and Shiao-Kung Liu

INTRODUCTION

In the initial phase of the study, two three-dimensional models were set up--namely, a Bristol Bay model and a Norton Sound model. During that period several preliminary tests were made with the models using the estimated tidal regime at the models' open boundaries. Both models use fixed diffusion coefficients for the vertical and horizontal exchanges of momentum and constituent transport. During this reporting period (April 1977 to the present), substantial improvement has been made in both the computational scheme and the graphical system for the modeling of these two areas. The particular emphasis of the last quarter (January-March 1978) has been on the adjustment of density fields of the modeled areas. Major progress made during the reporting period is as follows:

I. MODEL EXTENSION

Both models have been converted to use our most recent computational method developed under the sponsorship of the Office of Water Research and Technology, Department of the Interior. This new model has the advantage that it considers the intensity and transport of the subgrid-scale (turbulent) energy in a system. The vertical exchange computation is computed from the local turbulent energy intensities, a length scale and a density gradient in an implicit fashion, in contrast to the explicit scheme employed in the earlier version, thus removing the most critical stability conditions associated with the computational scheme. In the horizontal direction, the diffusion coefficient contains two parts. The first part represents the local subgridscale horizontal mixing which cannot be resolved by the computational grid as advective terms. This part is estimated considering the characteristic length scale (grid dimension). The second part is calculated as a function of the deformation of the local velocity field. With the new scheme, requirements for field diffusion experiments are minimized.

Recently, another major improvement in the computation method has been made. The new scheme gives an accurate account of the arbitrary bathymetry at each spatial grid location, thus allowing for more precise computation of wave propagation in the model. In the meantime, the accuracy of the calculated currents in the lower layers is expected to be improved.

At the present time, this latest version of the model is being implemented in both the Bristol Bay and the Norton Sound models.

II. MODEL SYSTEM

In the graphical system, the facility for vertical plots is extended to all variables. Computed time histories at selected depths up to six series can now be plotted on a single frame. To reduce compiling and storage costs, the graphic system consists of a fixed and a variable part, thus improving the efficiency of the storage usage. Computational sub-routines in the program are independent of the model's dimensions and need not be recompiled for each case. We are at present developing a graphical system for analyzing tidal constituents in the modeled area determined from the computed water level data by means of Fourier transformation for each frequency considered in the model. This involves extensive programming and is expected to continue into the next quarter.

III. MODEL SETUP

The Bristol Bay model has been re-schematized to incorporate the field data collection program scheduled for this fiscal year (see Fig. 1). The model realignment will also allow us to take full advantage of data obtained previously from the range of pressure gauges and current meter deployments. The new arrangement will allow us to obtain better vertical resolution (i.e., from 7 to 15 layers) to incorporate the recently obtained field data on the vertical nonuniformity of the bay current and density system without sacrificing too much horizontal resolution. The new setup will also make the time integration procedure twice as efficient as compared with the previous version.

A series of simulations has been made using the new model of Bristol Bay for the adjustment of the density field and the impact of wind on the tidal propagation in the bay system. Figures 2 and 3 illustrate the computed distributions of surface tidal currents and water levels and the rise and fall of the water surface during flood and ebb tide. Figures 4 and 5 show the computed surface currents and water level during flood and ebb tide under the influence of a 20-knot south-southwestern wind. Figures 6 and 7 show the distribution of salinity and temperature in the surface layer 37 hrs after the beginning of the simulation. Figures 8 and 9 give the vertical profiles of salinity and temperature through a particular cross-section of the modeled area. Figures 10 and 11 give a comparison of the vertical distribution of the subgridscale turbulent energy densities (ergs/unit mass) with and without the surface energy input from the wind. Of particular interest is the low turbulent energy level near the sharp salinity and temperature gradient where local turbulences are suppressed. This effect is also shown in Fig. 12 for a location near station BC-5. Pronounced velocity differences near the sharp density gradient illustrate the characteristics of a two-layer system. Figures 13 through 16 are the water level variations and vertical distributions of tidal currents (without wind) for six selected levels at the same station, where both the diurnal and the semi-diurnal tidal components are significant.

Schematization of the Norton Sound model is shown in Fig. 17. This model has a horizontal grid dimension of 39×43 with 7 layers. Horizontal and vertical distributions of salinity and temperature data are now being inserted in this model. Because the scheduled tidal data collection

program will be conducted in September of this year, historical data are being used to drive the Norton Sound model. Figure 18 illustrates a typical computed output from the model showing isocontours of water levels, rise and fall of the water surface and tidal currents in the top layer at a particular time in a simulation.

IV. INTERACTION WITH OTHER RESEARCH UNITS

During the reporting period both investigators participated in the Physical Oceanography Workshops taking place in May and in November 1977. At those meetings results of this study were presented. Aspects of investigator-data management interaction were discussed.

On October 13, 1977 a meeting between the Project Officer, Mr. M. Pelto of OCSEAP in Juneau, and Dr. R. Charnell of the Pacific Marine Environmental Laboratory in Seattle and Rand's investigators was held in Santa Monica. At that meeting an overview of the progress of our investigation was presented and we discussed extensively our data requirements.

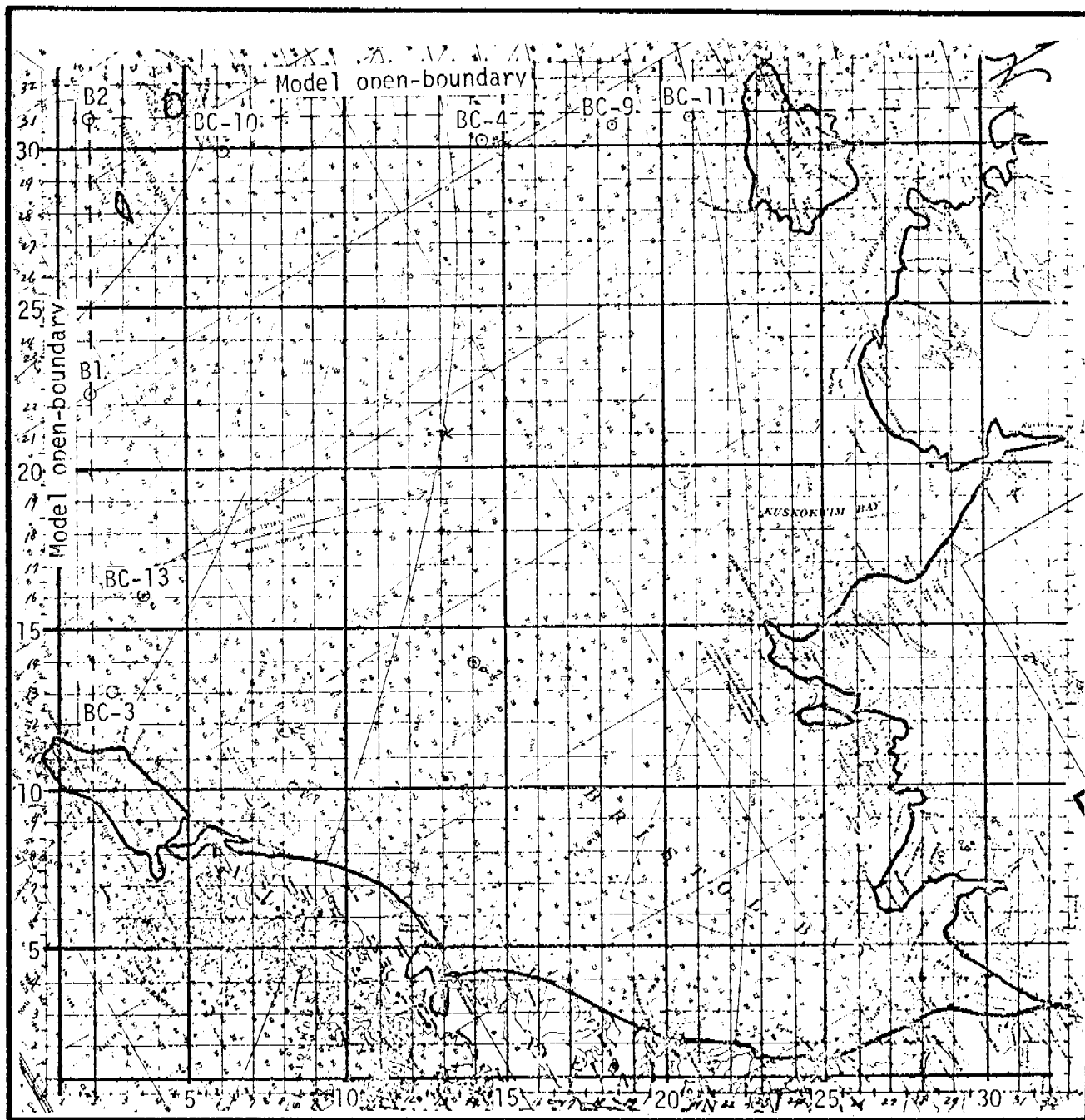
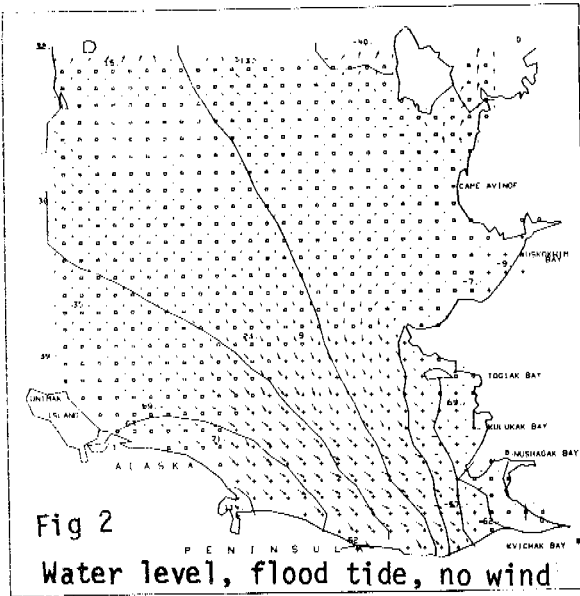
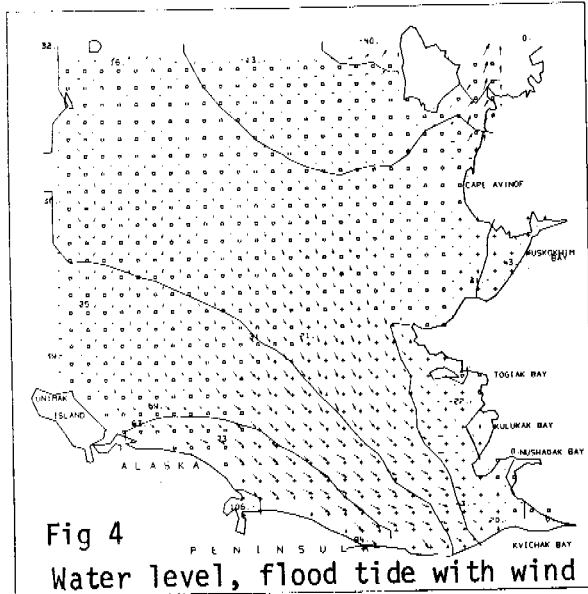


Fig. 1--Realigned three-dimensional model of Bristol Bay, showing horizontal schematization and locations of the model's open boundaries



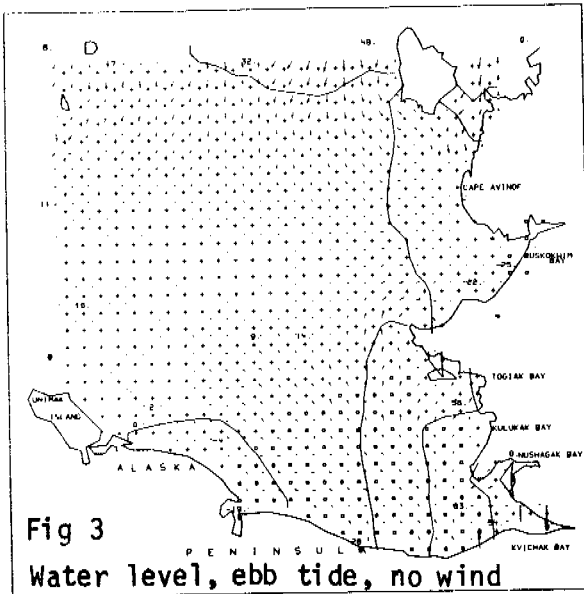
WATER LEVEL
Grid size = 21875 m
Velocity vector - grid size = 75.0 cm/sec
Isolines at 0 120K10+05 0 900K10+02 0 600K10+02
0 300K10+02 0 100K10+02 0 0K10+02
0 500K10+02 0 900K10+02 0 120K10+05
FROM DATA SET GENERATED 78/03/09
03/15/78 15.01.45
Contour values can be determined from the order indicated above, counting inward from land boundaries.

00:48 Z 0-0
BRISTOL BAY STEP - 498



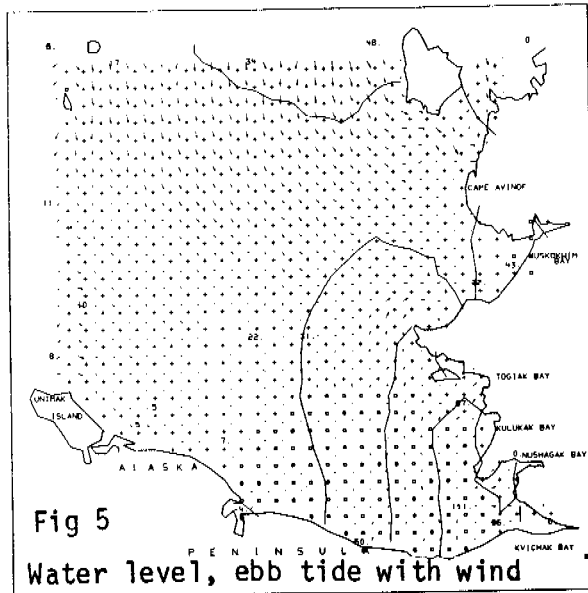
WATER LEVEL
Grid size = 21875 m
Velocity vector - grid size = 75.0 cm/sec
Isolines at 0 120K10+05 0 900K10+02 0 600K10+02
0 300K10+02 0 100K10+02 0 0K10+02
0 500K10+02 0 900K10+02 0 120K10+05
FROM DATA SET GENERATED 78/03/12
02/13/78 15.43.17
Contour values can be determined from the order indicated above, counting inward from land boundaries.

00:48 Z 0-0
BRISTOL BAY STEP - 498



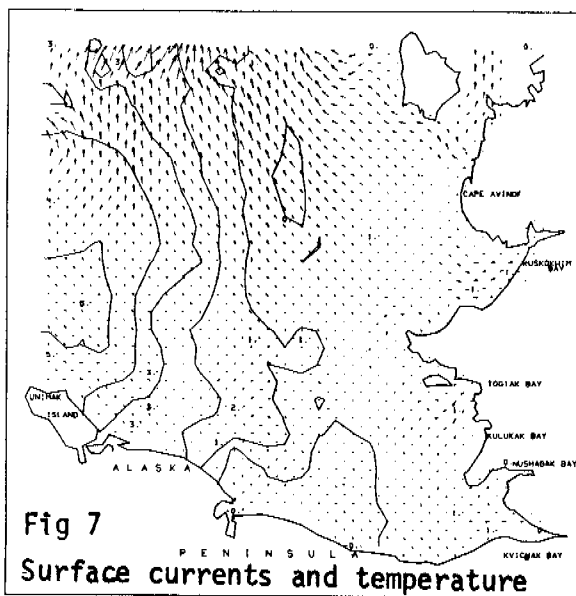
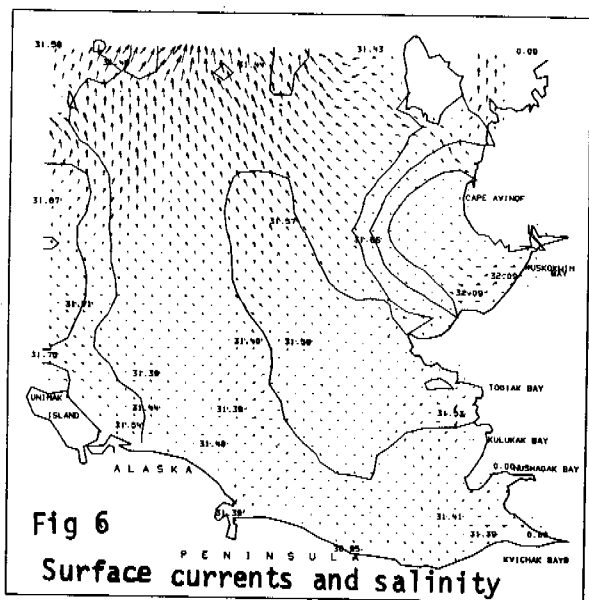
WATER LEVEL
Grid size = 21875 m
Velocity vector - grid size = 75.0 cm/sec
Isolines at 0 120K10+05 0 900K10+02 0 600K10+02
0 300K10+02 0 100K10+02 0 0K10+02
0 500K10+02 0 900K10+02 0 120K10+05
FROM DATA SET GENERATED 78/03/09
03/15/78 15.01.45
Contour values can be determined from the order indicated above, counting inward from land boundaries.

07:00 Z 0-0
BRISTOL BAY STEP - 620



WATER LEVEL
Grid size = 21875 m
Velocity vector - grid size = 75.0 cm/sec
Isolines at 0 120K10+05 0 900K10+02 0 600K10+02
0 300K10+02 0 100K10+02 0 0K10+02
0 500K10+02 0 900K10+02 0 120K10+05
FROM DATA SET GENERATED 78/03/12
02/13/78 15.43.17
Contour values can be determined from the order indicated above, counting inward from land boundaries.

07:00 Z 0-0
BRISTOL BAY STEP - 620



13:12 Z-0-0
BRISTOL BAY STEP = 7%

SALINITIES AT 3.0 M
Grid size = 21825 m
Velocity vector grid size = 75.0 m/sec
Isolines at 0.315x10⁻⁰², 0.317x10⁻⁰², 0.320x10⁻⁰², 0.325x10⁻⁰², 0.327x10⁻⁰², 0.329x10⁻⁰², 0.332x10⁻⁰², 0.332x10⁻⁰²
FROM DATA SET GENERATED 70/03/89
03/15/78 15.01.40
Contour values can be determined from the order indicated above, counting inward from land boundaries.

13:12 Z-0-0
BRISTOL BAY STEP = 7%

TEMPERATURE AT 3.0 M
Grid size = 21825 m
Velocity vector grid size = 75.0 surface
Isolines at -0.200x10⁻⁰¹, 0.000x10⁻⁰¹, 0.100x10⁻⁰¹, 0.100x10⁻⁰¹, 0.200x10⁻⁰¹, 0.300x10⁻⁰¹, 0.400x10⁻⁰¹, 0.500x10⁻⁰¹, 0.600x10⁻⁰¹
FROM DATA SET GENERATED 70/03/89
03/15/78 15.01.40
Contour values can be determined from the order indicated above, counting inward from land boundaries.

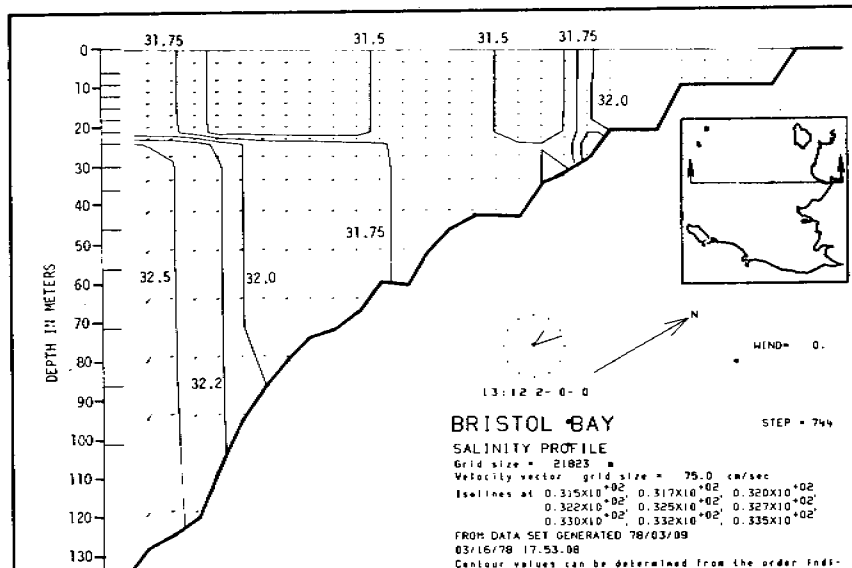


Fig 8 Salinity and current profile

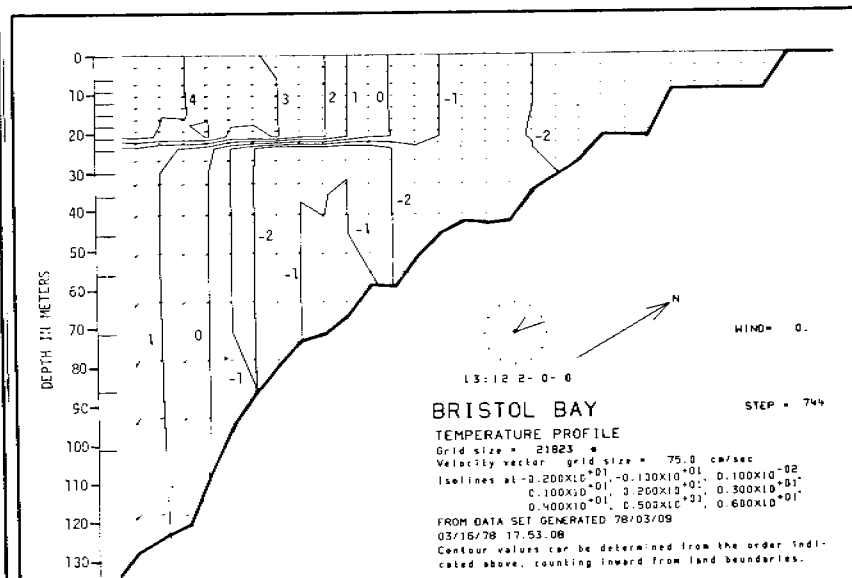


Fig 9 Temperature and current profile

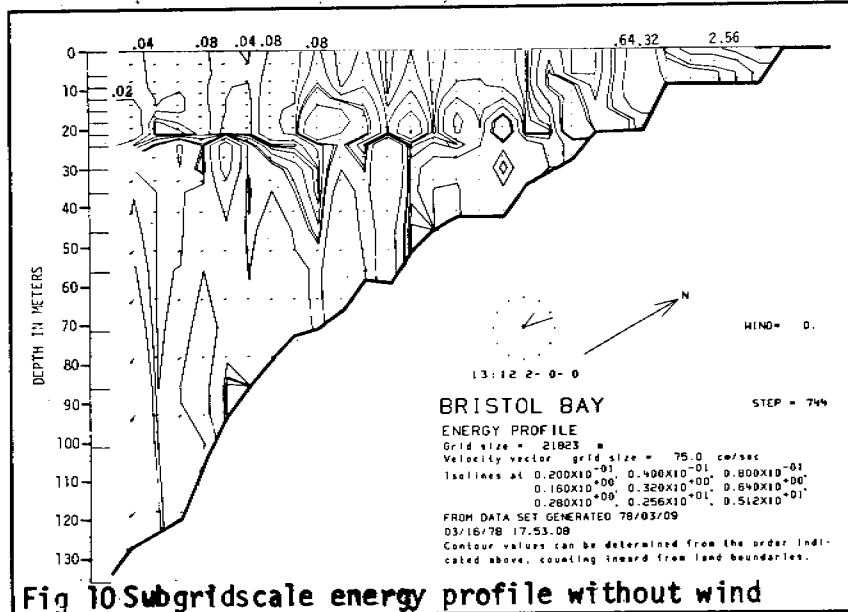


Fig 10 Subgridscale energy profile without wind

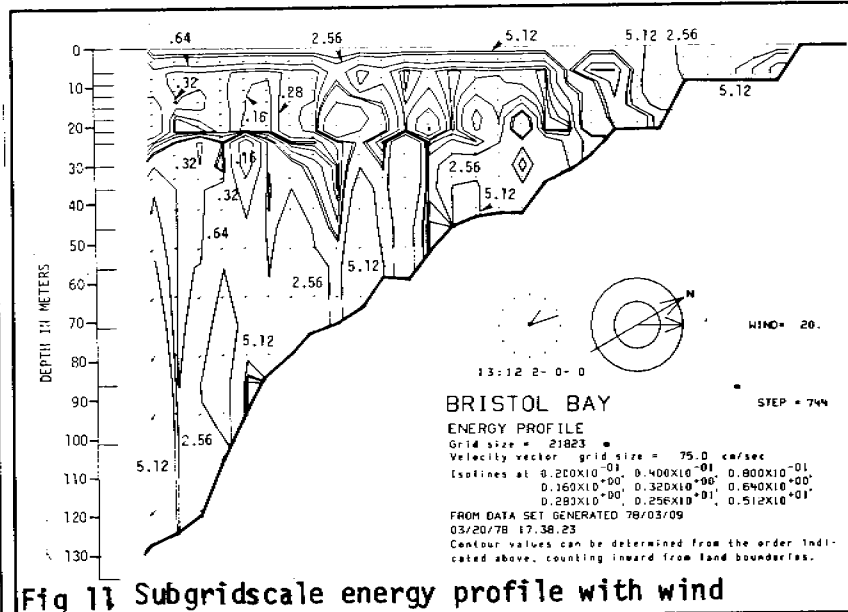


Fig 11 Subgridscale energy profile with wind

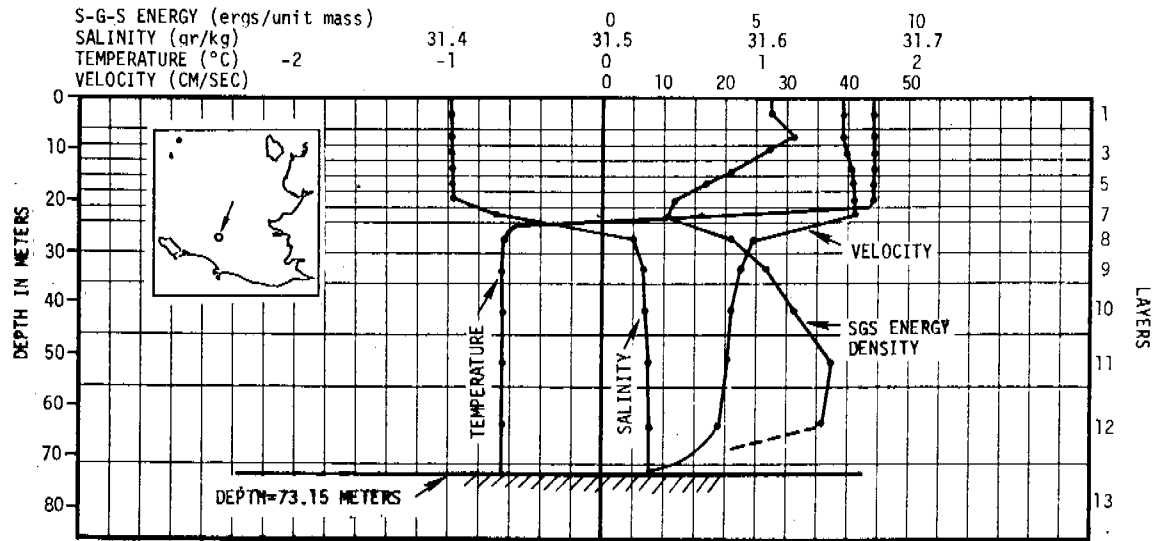


Fig 12 Computed vertical profiles of current velocity, salinity, temperature and subgridscale energy during flood tide with wind

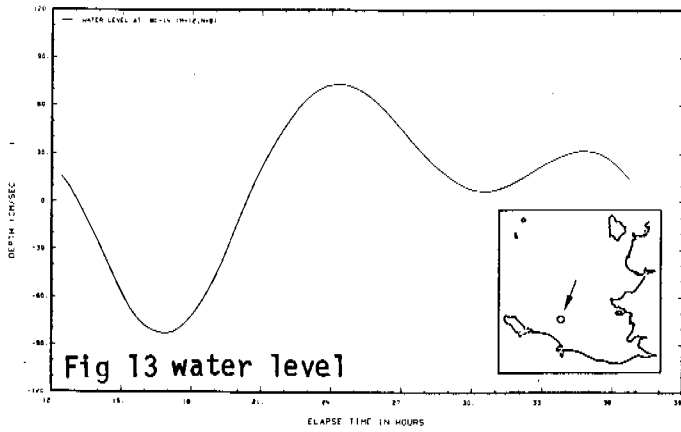


Fig 13 water level

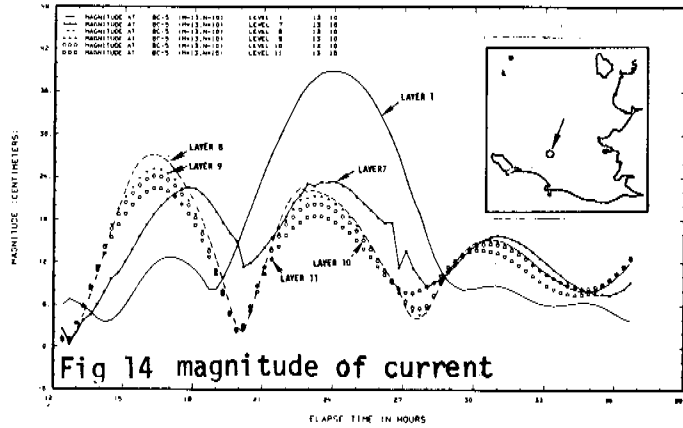


Fig 14 magnitude of current

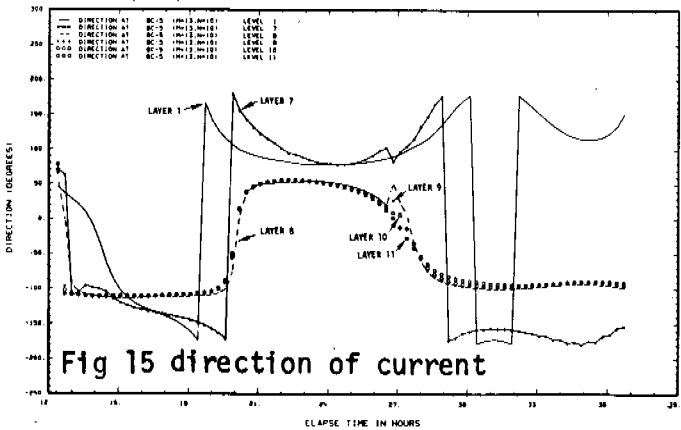


Fig 15 direction of current

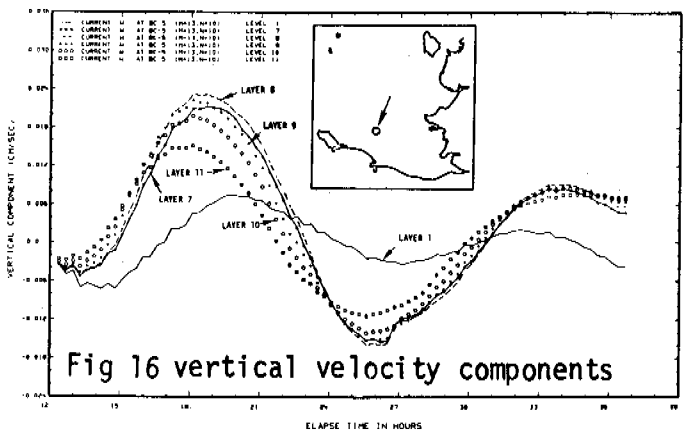


Fig 16 vertical velocity components

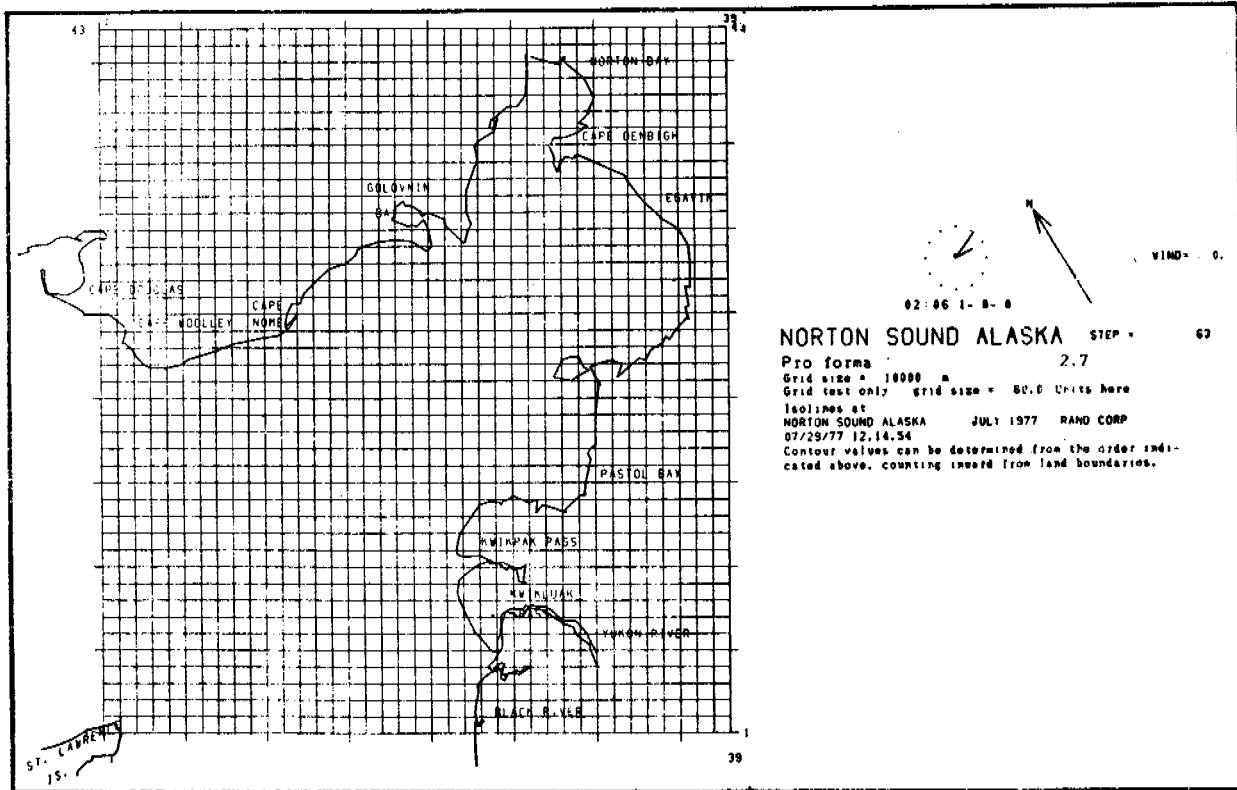


Fig 17 Schematization of Norton Sound model

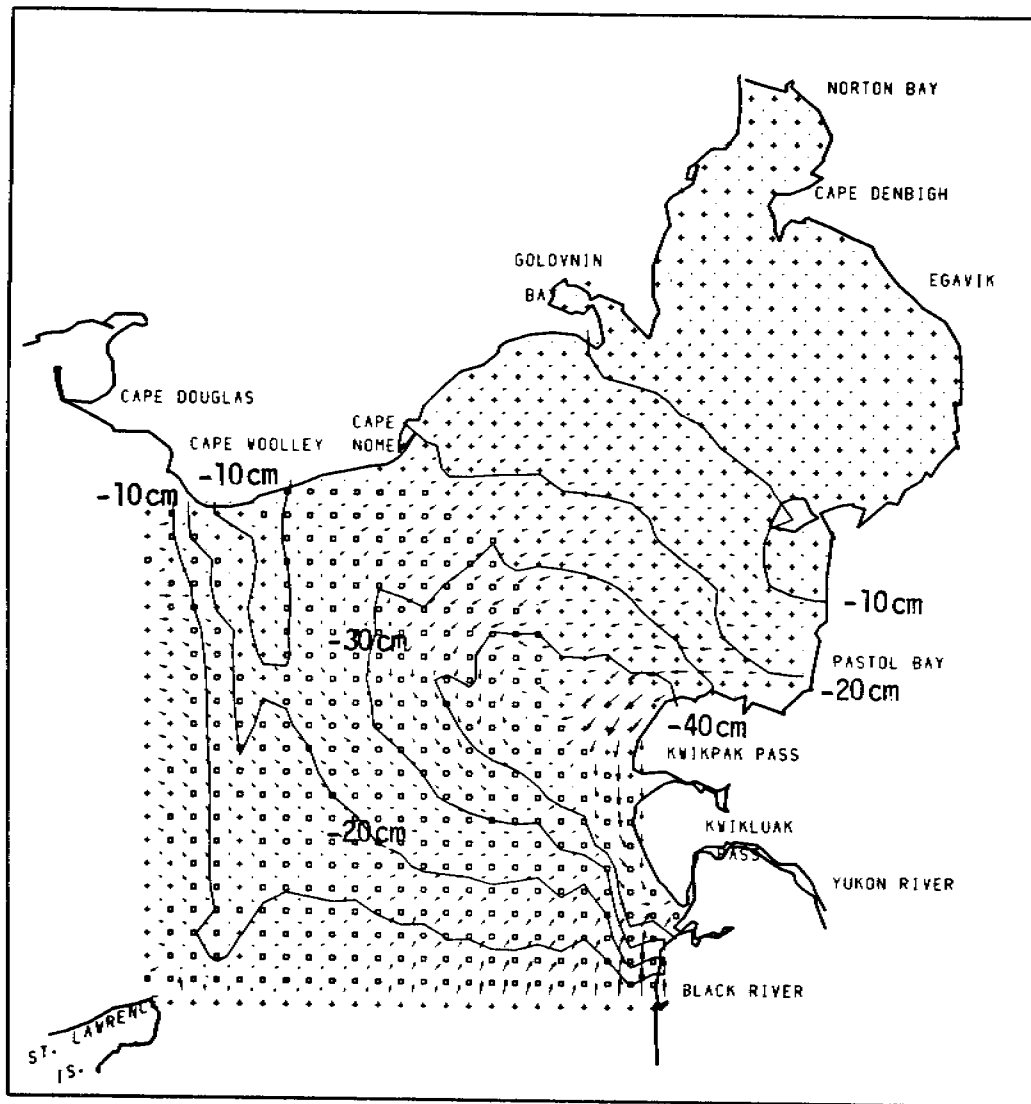
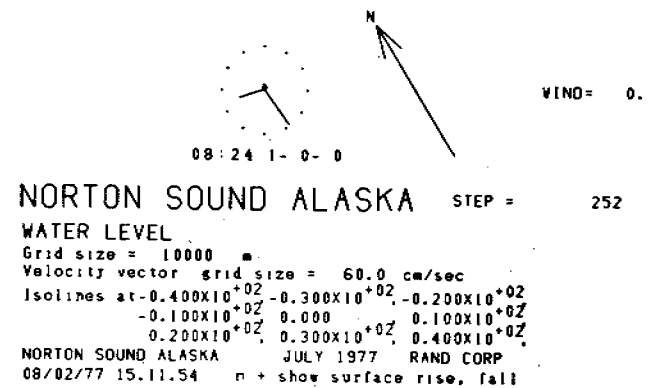


Fig 18 Graphical output of the Norton Sound model showing isocontours of water levels, rise and fall of the water surface and currents in the top layer at a particular time in a simulation



ANNUAL REPORT

Contract: 03-5-022-67 TO 13
Research Unit: 519
Reporting Period: 1 Apr 77 - 31 Mar 78
Number of Pages: 26

COASTAL METEOROLOGY OF THE ALASKAN ARCTIC COAST

Eric Leavitt
Research Scientist

Polar Science Center
Division of Marine Resources
University of Washington
Seattle, Washington 98195

1 April 1978

CONTENTS

	Page
I. Summary	1
II. Introduction	1
III. Current State of Knowledge	1
IV. Study Area	2
V. Sources, Methods and Rationale of Data Collection	2
VI. Results	3
VII. Discussion	3
VIII. Conclusions	4
IX. Summary of Fourth Quarter Operations	4
References	5
Figures	6-10
Appendix: Progress on the sea breeze study of the Alaskan Arctic coast by Tom Kozo	11
References	16
Tables	17-19
Figures	20-25

I. Summary

The objectives of this program are to measure and model mesoscale processes in the surface winds of the Beaufort Sea Coast. The two mesoscale phenomena being studied are sea breeze forcing and mountain barrier baroclinity. Any attempt to understand oceanic circulation and resultant pollutant trajectories must include a description of the surface winds. The strong correlation between surface winds measured at widely separated points on the coast suggest that only a few measurement points would be needed to provide a data set for current trajectory studies near the coast.

II. Introduction

A. General Nature of the Study

This study was designed to measure actual winds and air pressures in the Prudhoe Bay area and to model local or mesoscale phenomena which create departures from synoptic forcing. This work extended the modeling of sea-breeze and mountain effect winds begun under RU 519 (Carsey, 1977). In particular, the measurements made during the 1977 field season provide meteorological input for the Simpson Lagoon studies of Mathews (RU 526) and Mungall (RU 531).

B. Specific Objectives

1. Measurement of surface winds and atmospheric pressures in the Prudhoe Bay area during seasons of interest.
2. Develop a sea-breeze model and test it with data gathered in the 1976 and 1977 field seasons to estimate likelihood of occurrence and scales and magnitudes for sea-breeze cells along the Beaufort Sea coast.
3. Determine the influence of orographic baroclinity on the surface winds measured in the Prudhoe Bay area.

C. Relevance to Problems of Petroleum Development

Since winds are the principal driving force for surface currents, any attempt to predict current trajectories must include a prediction of the surface wind field. The potential effect of spills or other accidents will be strongly influenced by the wind regime. Limitations on development in particular areas depend on how much damage over how wide an area could result from a given accident. Demands made for containment and/or clean-up will also depend on the potential effect of a particular accident. Setting these limits will require at least basic information on the likely wind field.

III. Current State of Knowledge

Except for the few NWS stations, wind information for the coastal and offshore regions of the Beaufort Sea is sparse. The traditional method of

obtaining surface winds from geostrophic winds computed from the surface pressure field is also hampered by a lack of data both inland from the coast and offshore. Carsey (1977) illustrated the increased detail in the pressure field when data from OCS buoys and additional land pressure measuring sites were added to the NWS data set. Geostrophic wind directions differed as much as 60° between the two analyses.

Calculation of surface winds from the synoptic pressure field is further complicated by the possible existence of a sea breeze circulation in the summer and mountain barrier baroclinity (Schwerdtfeger, 1974). The latter has its strongest influence in winter, but could be important at times in the summer. The sea breeze circulation is generated by the land-sea temperature gradient caused by unequal heating of the surfaces by solar radiation and can result in an alongshore component (approximately SSE) in the surface wind at the coast. Previous work, reported in Carsey (1977), suggests that the sea breeze occurs about 1/3 of the time in the summer. Its scale and magnitude is currently being investigated by T. Kozo and should be completed by fall, 1978. Further detail on this study is given in Appendix A.

Mountain barrier baroclinity, as postulated by Schwerdtfeger, results from the piling up of cold air against the Brooks Range and is evidenced by a west wind parallel to the mountain range. He suggests that this explains why in winter west winds are more common at Umiat and at Barter Island than at Barrow.

IV. Study Area

The area of study is from east Harrison Bay (151°W) to west Camden Bay (145°). Data collection was undertaken during two periods of the 1977 field season. In the spring period, April 25 to June 1, measurements were concentrated at coastal points from Flaxman Island to the Colville Delta. The summer period, July 20 to September 1, focused on measurements in the Simpson Lagoon area.

V. Sources, Methods and Rationale of Data Collection

Spring 1977

During the spring period, Meteorology Research, Inc. (MRI) mechanical weather stations measured wind speed and direction, and temperature at Brownlow Point, Cottle Island, and Tolaktovut Point. Presence of a generator at Oliktok Point permitted use of a Climet wind measurement system to record wind speed and direction, and an EG&G hygrometer to record temperature and dew point, both were borrowed from AIDJEX. Stations recording atmospheric pressure on Weather-measure and Belfort microbarographs were serviced and calibrated weekly with two Negretti and Zambra precision digital barometers. The pressure measurement locations were Deadhorse, Oliktok, Umiat, Happy Valley, and Narwhal Island. The NOAA Bell 205 helicopter was used to reach the coastal points from the OCS billet at Deadhorse. Circuits to service the pressure sensors were usually flown in Cessna 180's.

Summer 1977

The MRI weather stations, during the summer period, recorded wind speed and direction, and temperature at Cross and Cottle Islands. The Climet and EG&G

system and a microbarograph were operated throughout August at the manned camp on Pingok Island. In addition, an intensive series of radiosondes and double-theodolite pibal observations was carried out at Pingok to determine vertical wind shear and temperature profiles. Finally, a mesoscale pressure triangle was maintained with microbarographs at Deadhorse, Umiat, and Oliktok. Aircraft from ERA and Trans-Alaska Helicopter Companies were used to visit the MRI stations until the NOAA Bell 206 helicopter became available in mid-August. Either a NARL Cessna 206 or Jim Helmrich's Cessna 206 was used to service the pressure triangle weekly.

VI. Results

Data measured by the Climet and EG& G sensors was recorded every 10 or 20 minutes on grocery tape by a Digitec digital data logger. One minute averages of wind speed and direction, temperature, and dew point were then selected at 00, 03, 06, 09, 12, 15, 18, and 21 hours GMT. The MRI weather stations record average direction, wind run, and temperature on a small strip chart. One hour averages of these variables were selected for the same three-hourly intervals as above. Pressure was also picked from the microbarograph charts at three-hourly intervals. The pressures were calibrated using the Negretti and Zambra precision barometers as transfer standards and then were reduced to equivalent sea level pressure using the hypsometric equation, station altitude and mean air temperature. This data will be submitted to the OCS data bank on schedule. Plots of wind and temperatures are presented in section VII.

Data for May 1977 have been reduced and analyzed to study the barrier effect of the Brooks Range to winds between Deadhorse and Barter Island. The investigation has been completed, and a final report on this work is being prepared by F. Carsey and will be submitted in April 1978.

A sea-breeze model has been successfully run on the University of Washington computer. A discussion of some preliminary results is presented in Appendix A.

VII. Discussion

Wind speeds and directions for May 1977 from Narwhal Island, Brownlow Point and Barter Island are shown in Figure 1. There is a striking correlation in speeds and directions among the stations, especially considering the large distances between the stations; Brownlow is approximately 75 km to the east of Narwhal and Barter is about 90 km to the east of Brownlow. The mean wind speed is approximately 7 m/s and the wind directions are between 60°-90° nearly two-thirds of the time; the second most common wind direction is about 270°.

Pingok Island, Cottle Island and Cross Island wind data for August 1977 are plotted in Figure 2. Temperature data recorded in May and August from the 6 sites are also shown in Figure 3. Again there is good agreement in wind speed and direction between stations, although this is not as surprising since Pingok and Cottle Island are only 20 km apart. Cross Island is another 40 km to the east of Cottle Island and is also 20 km seaward. Unfortunately the Cross Island data for the wind event of August 9-14 is missing. The average wind speed is

about 6 or 7 m/s and the most common wind directions are 70°-90° just as in May.

For comparison, wind data collected in August 1976 at Tolaktovut, Cottle Island and Narwhal are plotted in Figure 4. Temperature data from these stations are shown in Figure 5. Again the correlation between the three stations is large, with similar wind speeds and directions to the 1976 data. However, the 1976 August 17-20 wind speed and to a lesser extent direction data at Tolaktovut appear to show a strong diurnal variation that is absent from the Islands data.

We should add one caution on accepting this data as the norm. The wind regime in the two August periods shown were very similar to one another. But, in 1975 the winds during late July and August were much different, blowing more often from the west and north-west and keeping the ice up against the coast.

VIII. Conclusions

Given the strong correlation between winds measured at wide separations along the coast, it would be possible to provide winds for predicting coastal current trajectories with only a few measurement points. This would be more accurate than calculating the surface wind from the geostrophic wind; especially given the possibility of mesoscale phenomena such as the sea breeze and the necessity for simultaneously measuring boundary layer stratification. However, this must be qualified if winds are required further than 20 or 30 km offshore or inland from the coast. The relative ease with which pressure sensor equipped data buoys can be set out on the ice, or for that matter inland from the coast, suggest their use in the latter case. The wind measurements along the coast could then serve as input to the calculation of surface winds from the pressure field. Such a combination of wind and pressure measurement stations could be set up and maintained for a relatively small expenditure, providing an excellent data base for studies of current (or oil spill) trajectories.

IX. Summary of Fourth Quarter Operations

A. Ship or Laboratory Activities

1. Field trip schedule: None undertaken during period

2. Scientific party:

E. Leavitt, University of Washington, New Principal Investigator

F. D. Carsey, University of Washington, Former Principal Investigator

T. L. Kozo, University of Washington, Graduate Student, Numerical Modeler

R. H. Andersen, University of Washington, Computer Programmer and Data Analyst

3. Methods

Numerical modeling of sea breeze system in Simpson Lagoon area.

Analysis of Spring 1977 data to examine barrier effect of Brooks Range coastal winds.

Reduction and calibration of data taken during 1977 field season.

4. Sample localities:

Spring 1977 (April 25 - June 1)

Recording weather stations at Brownlow Point, Narwhal Island, Island and Tolaktuvut Point.

Microbarographs at Deadhorse, Oliktok, Umiat, Happy Valley, and Narwhal Island.

Summer 1977 (July 20 - September 1)

Radiosondes and double theodolite pibals at Pingok Island.

Recording weather stations at Pingok Island, Cottle Island, and Cross Island.

Microbarographs at Deadhorse, Umiat, Oliktok, and Pingok Island.

5. Data analyzed:

Continuous record of wind speed, wind direction, and temperature at weather station sites.

Continuous record of atmospheric pressure at microbarograph sites.

Discrete observations of vertical wind shear and turning and temperature profiles at balloon launchings.

6. Milestone chart and data submission schedules:

Data from the 1978 field year will be forwarded to OCSEAP by 1 December 1978. Processing of 1977 data is nearly complete. Personnel change transition has resulted in some delays.

B. Problems Encountered/Recommended Changes

None

C. Estimate of Funds Expended, as of 31 March 1978: \$62,666.51

References

Carsey, F. 1977. Coastal meteorology of the Alaskan arctic coast. Annual Report RU 519 OCSEAP Arctic Project.

Schwerdtfeger, W. 1974. Mountain barrier effect on the flow of stable air north of the Brooks Range. Climate of the Arctic, Conference Publication of the Geophysical Institute, University of Alaska, Fairbanks, pp. 204-208.

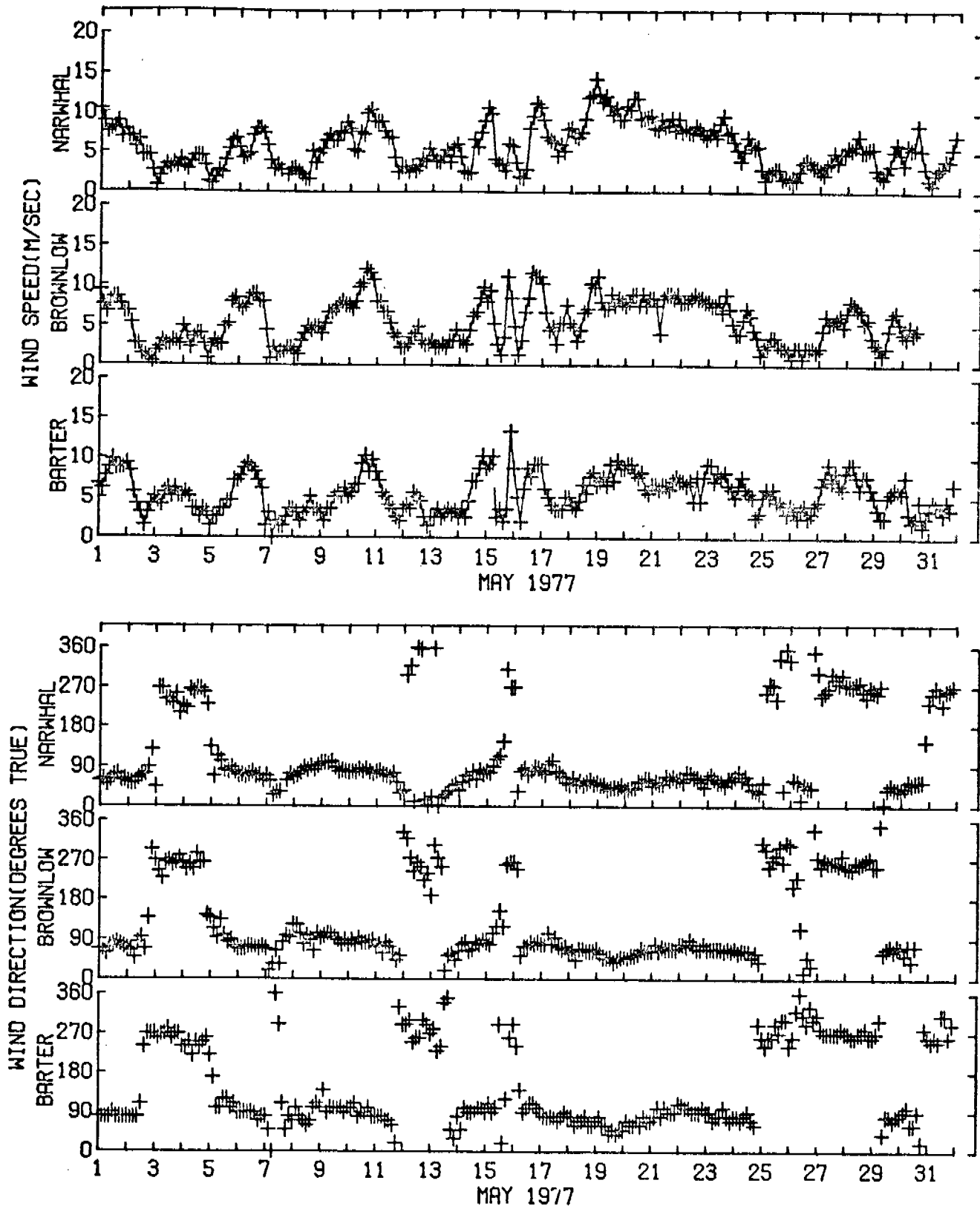


Figure 1: Wind speed and direction at Barter Island, Brownlow Point, and Narwhal Island during May 1977.

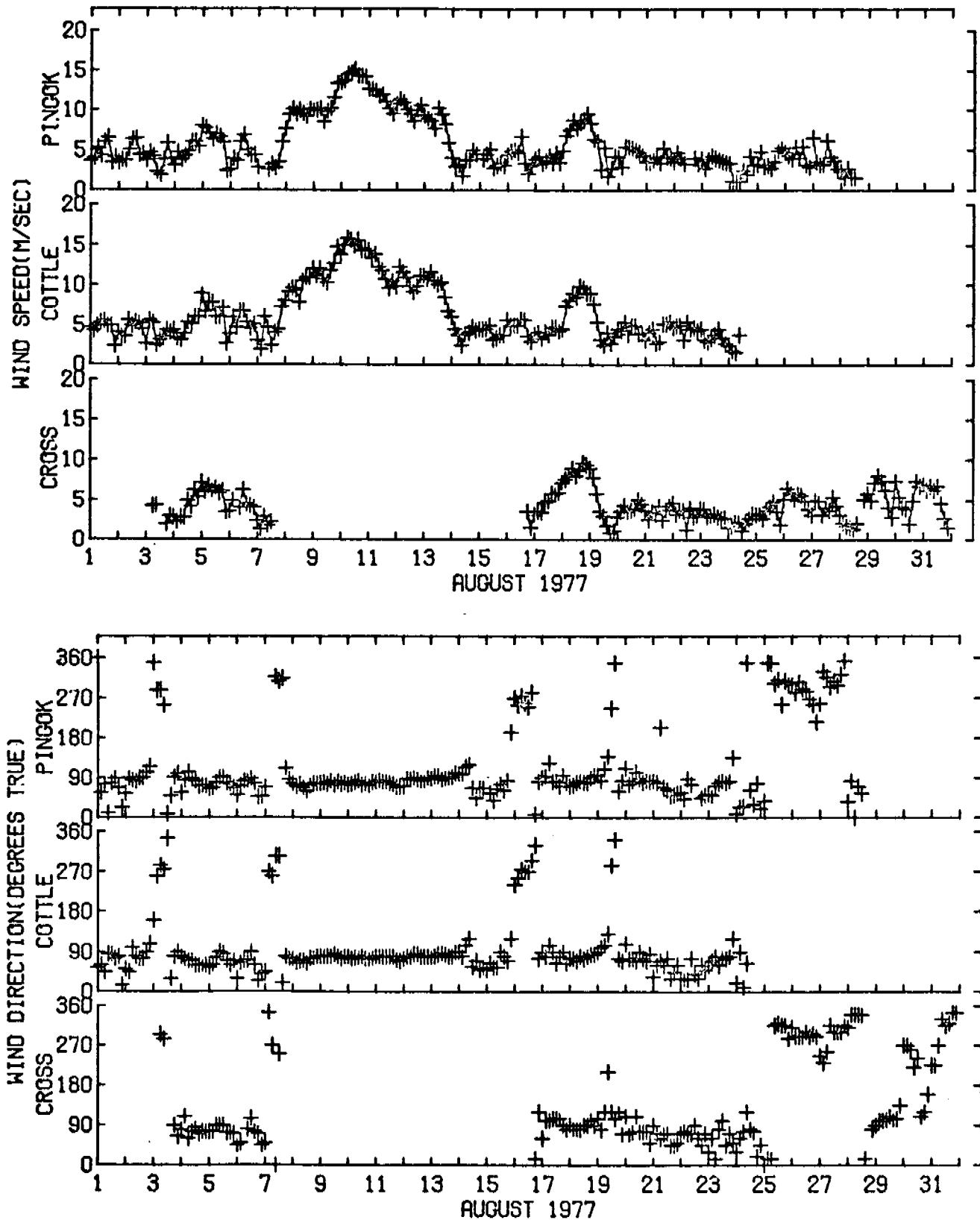


Figure 2: Wind speed and direction at Cross Island, Cottle Island, and Pingok Island during August 1977.

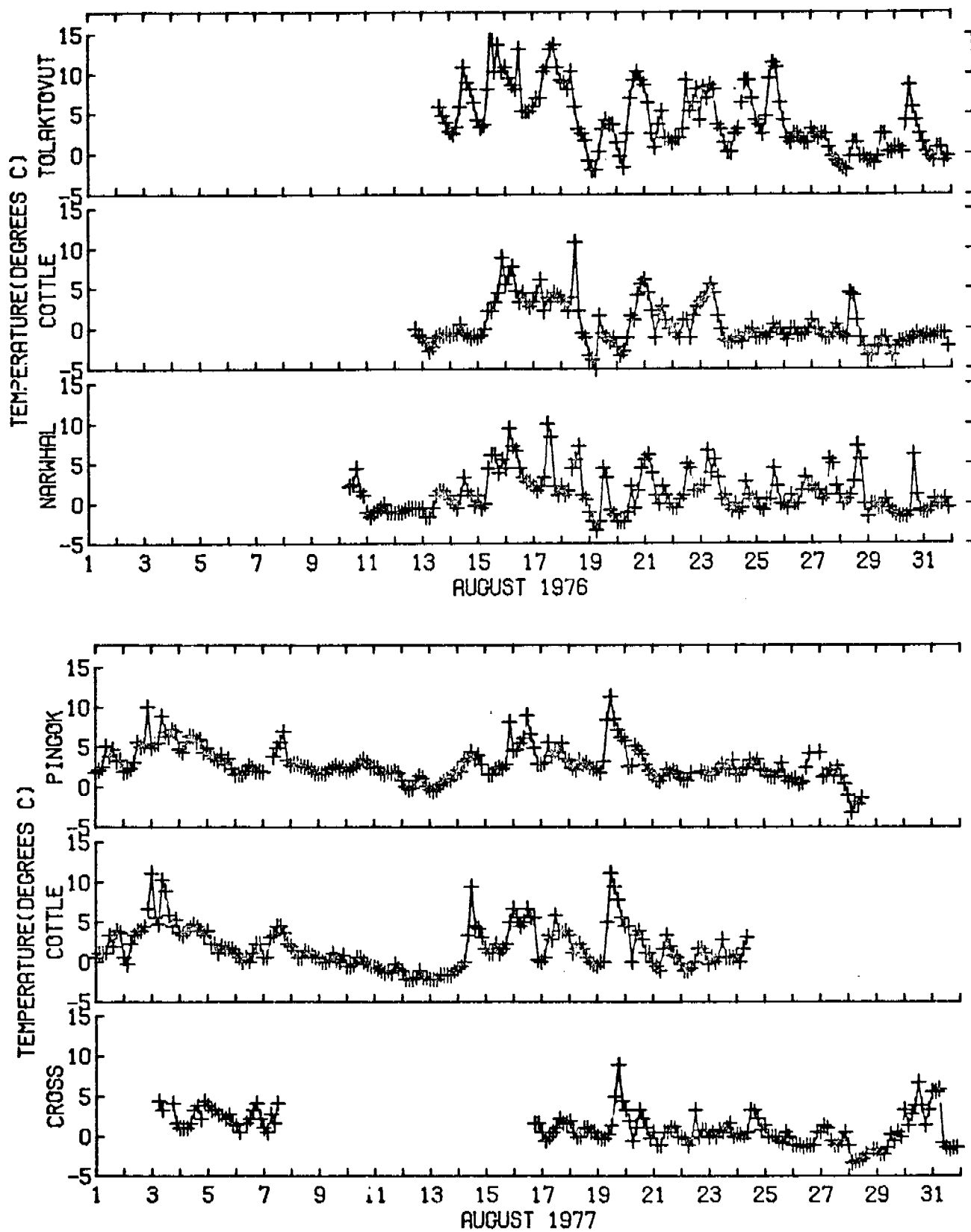


Figure 3: Temperature at Narwhal Island, Cottle Island, and Tolaktovut Point during August 1976, and at Cross Island, Cottle Island, and Pingok Island during August 1977.

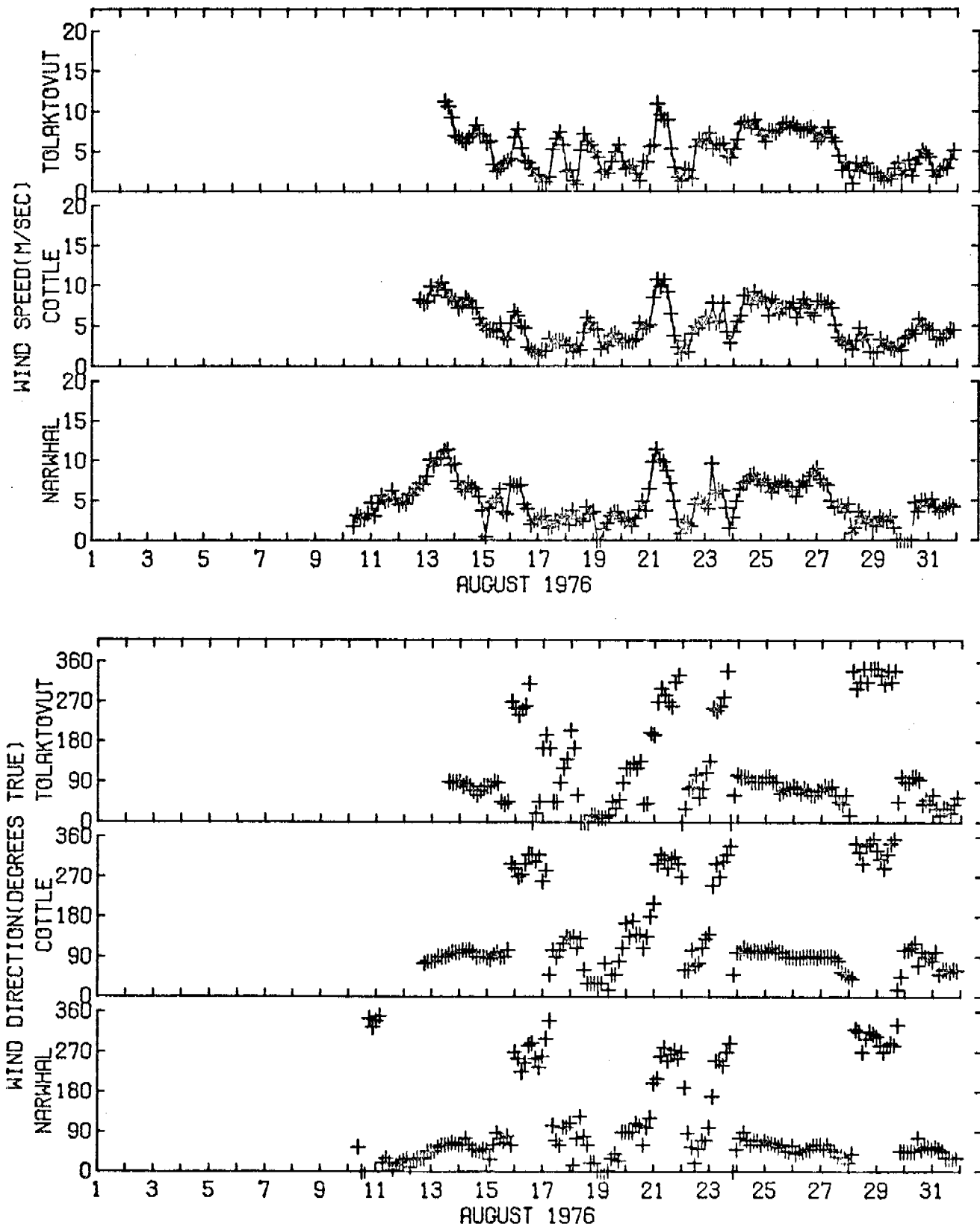


Figure 4: Wind speed and direction at Narwhal Island, Cottle Island, and Tolaktovut Point during August 1976.

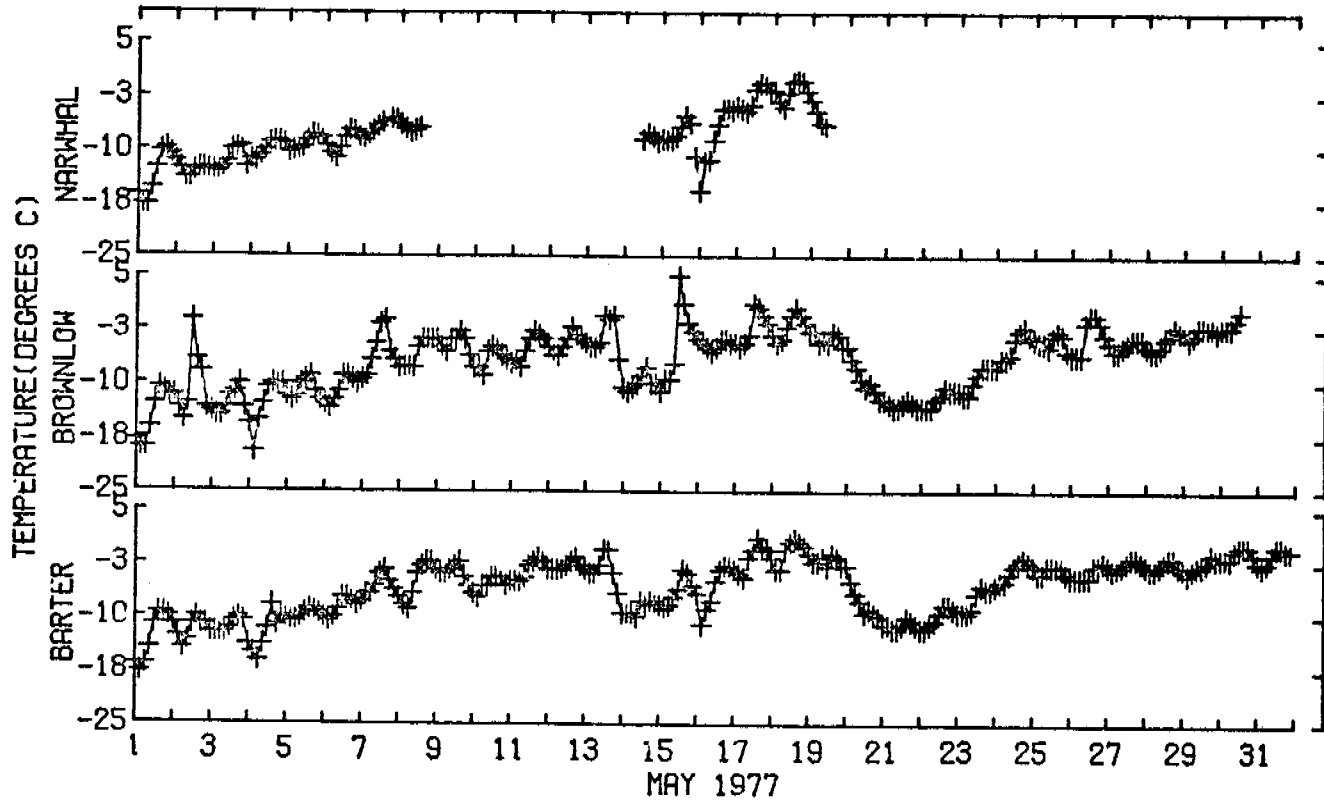


Figure 5: Temperature at Barter Island, Brownlow Point, and Narwhal Island during May 1977.

APPENDIX

PROGRESS ON THE SEA BREEZE STUDY OF THE ALASKAN ARCTIC COAST

by
Tom Kozo

The sea breeze (Defant, 1951) in general is a mesoscale response to horizontal gradients in surface heating. The sea breeze cell is usually contained in the atmospheric boundary layer (typically the lowest 1 km of the atmosphere), but its horizontal extent is large enough that the effect of the earth's rotation and the synoptic pressure gradient cannot be ignored (e.g., Walsh, 1974).

Previous investigators (Cotton, et al., 1976) have found that the synoptic (large scale) environment is altered by the sea breeze through 1) perturbing the vertical thermodynamic profile, 2) increasing the depth of the planetary boundary layer, 3) inducing greater surface fluxes of momentum, heat, and moisture, 4) changing the vertical shear of the horizontal wind in the lower levels of the atmosphere, and 5) developing regions of intense horizontal convergence of heat, moisture and momentum.

There is evidence from meteorological observations that mesoscale forcing exists along the north coast of Alaska. This forcing should not be neglected in nearshore air-sea interaction studies.

Rawinsonde data from Barter Island, Alaska, which has similar wind conditions to that of Prudhoe Bay, showed that the percentage of days per month where the vertical shear of the horizontal wind is altered beyond that found in normal boundary layers was approximately 25% for both 1976 and 1977 (months of July-September). Table I shows some examples of the change in wind direction and speed from the surface to the height of the 950 mb pressure level.

Moritz (1977) found that computed surface geostrophic wind speeds decreased 40% from January to July, but the measured surface winds showed only a 4% decrease. Also, for the same magnitude of calculated geostrophic wind, July surface east winds are stronger and more frequent than July surface west winds.

Large discrepancies between computed geostrophic wind and observed surface winds can be seen in Table II from our 1976 data. Geostrophic winds were calculated using a two-dimensional least squares fit to pressure data (Kozo, 1977). The days where large discrepancies exist (indicated by a *) can be attributed to a large horizontal temperature gradient (ΔT) existing between Prudhoe airport and the ocean (assumed $\approx 0^\circ\text{C}$) and/or a similarly large ΔT between Prudhoe airport and Happy Valley (pipeline camp ≈ 130 km inland). However, days with a large ΔT that had shoreward gradient winds above 5 m/s did not exhibit these large differences. Walsh (1977) states that onshore synoptic flow will inhibit a local thermal circulation.

Because the sea breeze transfers mass aloft from land to sea, the surface pressure should increase at sea relative to land. Data collected

on August 19, 1977, at Pingok Island and Oliktok (Table III) illustrate this effect. The net difference in the pressure change is 0.72 mb, in the correct direction. This is the first reported observation of this effect on the Alaskan arctic coast.

The arctic sea breeze is expected to exhibit some unique features as compared to those of mid-latitudes. Though the surface land temperature may drop 15°C over the relatively short arctic summer twilight, our observations show that typically it never falls below the sea surface temperature (see Table III). Therefore, the nighttime land breeze which alternates with the sea breeze in mid-latitudes will be absent.

The tundra-ocean thermal contrast should produce an onshore acceleration component from the sea breeze but turning due to the Coriolis force results in an alongshore component. Partly because of the larger Coriolis force, this turning occurs more quickly than it does in mid-latitudes.

In order to study the arctic sea breeze with its unique properties, a non-linear two-dimensional model (Estoque, 1961) was chosen which can be altered to simulate the experimental data. This model allows for imposition of prevailing synoptic conditions (Estoque, 1963) and has been adapted for lake breeze studies (Sheih and Moroz, 1974). The model equations are reproduced below.

EQUATIONS: CONSTANT FLUX SUBLAYER $0 \leq h \leq 50$ m

$$(1) \quad \frac{\partial}{\partial z} \left(K \frac{\partial u}{\partial z} \right) = 0 \quad \text{Vertical fluxes}$$

$$(2) \quad \frac{\partial}{\partial z} \left(K \frac{\partial \theta}{\partial z} \right) = 0 \quad \text{of}$$

$$(2) \text{ Heat and Momentum (1)}$$

$$\text{Mixing Coeff. } \left\{ \begin{array}{l} K_o = K_u \\ K = \left[k_o(z + z_o)(1 + \alpha k_1) \right]^2 \\ K = \lambda(z + z_o)^2 \left(\frac{g}{1} \left| \frac{\partial \theta}{\partial z} \right| \right)^{1/2} \end{array} \right. \quad \begin{array}{l} R_i \geq (R_i)_c = .03 \text{ Forced convection} \\ R_i < (R_i)_c \quad \text{Free convection} \end{array}$$

$$\text{where } \alpha = -3 \quad \lambda \approx .9$$

$R_i \equiv$ Richardson number

$K \equiv$ mixing coefficient

K_θ (temperature) = K_u (velocity)

$k_o =$ von Karman's Constant

$z_o =$ roughness parameter

UPPER SUBLAYER: $h \leq z \leq H \approx 2$ km

$$\frac{d\vec{v}}{dt} = \frac{-RT}{p} \vec{v}_p - \vec{F}kx\vec{v} + \frac{\partial}{\partial z} \left(K \frac{\partial \vec{v}}{\partial z} \right)$$

$$\frac{d\theta}{dt} = \frac{\partial}{\partial z} \left(K \frac{\partial \theta}{\partial z} \right) \quad \frac{\partial p}{\partial z} = \frac{-p g}{RT}$$

$$\frac{1}{p} \frac{dp}{dt} = -\nabla \cdot \vec{V} - \frac{\partial w}{\partial z}$$

here $V = iv + jv \equiv$ horizontal wind vector

$$\nabla = i \frac{\partial}{\partial x} + j \frac{\partial}{\partial y}$$

K is linearly decreasing with height from K_h at $z = 50$ m to 0 at $z = 2000$ m.

$$V = V_L + U', \quad \theta = \theta_L + \theta', \quad \text{where } \left\{ \begin{array}{l} L \text{ represents synoptic component} \\ ' \text{ represents the disturbance} \end{array} \right\}$$

LARGE SCALE:

$$\frac{\partial V_L}{\partial t} + V_L \cdot \nabla V_L + w_L \frac{\partial V_L}{\partial z} = -\frac{RT_L}{p_L} \nabla p_L - f k \times V_L$$

$$\frac{\partial \theta_L}{\partial t} + V_L \cdot \nabla \theta_L + w_L \frac{\partial \theta_L}{\partial z} = 0$$

$$\nabla \cdot V_L + \frac{\partial w_L}{\partial z} = 0$$

$$\frac{\partial p_L}{\partial z} = -\frac{p_L g}{RT_L}$$

Subtract the large scale from the upper sublayer equations. Note:

keep terms to 1st order in disturbance.

$$(I) \quad \frac{\partial V'}{\partial t} = -V' \cdot \nabla V_L - V_L \cdot \nabla V' - w' \frac{\partial V_L}{\partial z} - w_L \frac{\partial V'}{\partial z} - \frac{RT}{p} \nabla p' - f k \times V' + \frac{\partial}{\partial z} \left(K \frac{\partial \theta'}{\partial z} \right)$$

$$(II) \quad \frac{\partial \theta'}{\partial t} = -V' \cdot \nabla \theta_L - V_L \cdot \nabla \theta' - w' \frac{\partial \theta_L}{\partial z} - w_L \frac{\partial \theta'}{\partial z} + \frac{\partial}{\partial z} \left(K \frac{\partial \theta'}{\partial z} \right)$$

$$(III) \quad \frac{\partial p'}{\partial z} = -\frac{p' g}{RT} + \frac{g p_L}{RT_L}$$

Differentiate the continuity equation with respect to z and

assume the compressibility term is negligible.

$$(IV) \quad \frac{\partial^2 w}{\partial z^2} + \frac{\partial}{\partial z} (\nabla \cdot v) = - \frac{\partial}{\partial z} \left(\frac{1}{p} \frac{d}{dt} \right) \approx 0$$

Subtract large scale: remember $\frac{\partial}{\partial y} = 0$

$$\frac{\partial^2 w'}{\partial z^2} = - \frac{\partial}{\partial z} \left(\frac{\partial u'}{\partial x} \right)$$

external boundary conditions:

$$\text{at } x = \pm D: \quad \frac{\partial}{\partial x} (v', p', \theta') = w' = 0$$

$$\text{at } z = H: \quad p' = w' = v' = T' = \theta' = 0$$

$$\text{at } z = 0 \quad v = w = 0, \quad \theta = \theta(x, t)$$

The heating function for midlatitude ($\theta = 45^\circ N$) conditions is

$$\text{at } z = 0 \quad \begin{cases} T = 283 + 10 \sin(15t + 240^\circ) & \text{land } x < 0 \\ T = 283 & \text{water } x > 0 \\ T = 1/2[T(x > 0) + T(x < 0)] & x = 0 \end{cases}$$

t is the number of hours after midnight. Initial conditions: at $t = 8$,

$$u', v', T' = 0. \quad \text{For this model first run } v_L(x, z, t) = 0$$

$$T_L(x, z, t) = 283 - .008z. \quad z \text{ is in meters, } .008 \equiv \text{lapse rate } (8^\circ/\text{km}).$$

The heating function for the arctic conditions is:

$$\text{at } z = 0 \quad \begin{cases} T = 273 + 15 [\sin(15t + 240)]^2 & \text{land } x < 0 \\ \quad = 273 + 15 [.33]^2 + 540 < 15 + 240 < 720 \\ T = 273 & \text{water } x > 0 \\ T = 1/2[T(x > 0) + T(x < 0)] & x = 0 \end{cases}$$

$$T_L = \begin{cases} (x, 50, 0) = 275 \\ (x, 150, 0) = 279 \\ (x, 250, 0) = 283 \end{cases} \quad \begin{array}{l} \text{(Inversion assumed over} \\ \text{land and water)} \end{array}$$

350 meters on up

$$T_L = 283 - .008z$$

This model has now been run with modifications appropriate for the arctic, including: the heating function described above, initial land-sea temperature gradient of 15°C , a steep initial surface-based inversion and a value of f for latitude 71°N .

An example of the turning with time of the velocity vector for the model mid-latitude sea breeze versus the model arctic sea breeze can be seen in Figure 1. The morning arctic inversion inhibits initial convection cell formation which triggers the sea breeze perturbation. As a result, the arctic sea breeze direction and magnitude start out behind the mid-latitude vector. However, it can be seen that the arctic vector catches up by late afternoon.

Figures 2 through 9 show isotachs of the model output for the u velocity (perpendicular to the coast, negative sense toward land), v velocity (parallel to the coast, positive sense out of the paper), w velocity (positive upwards) and temperature contours. The spacing between horizontal grid points is variable, with 5 km spacing near the coastline for higher resolution. The vertical grid spacing is 100 meters. Wind velocities less than 1 meter/sec in magnitude are not shown on these figures.

Figures 2 through 5 represent output at 1400 LDST (time of the maximum value of the heating function). The model started at 0800 LDST and took 6 hrs. to build a wind regime of enough magnitude for contouring. This is due to the time required to offset the steep inversion and form an initial convective cell. Note in Figure 3, the v component is largest at the coast and of limited vertical extent. The w component in figure 4 shows a well-developed convective cell. The effect of the mesoscale perturbation on the temperature field is limited to a height of 650 meters (Figure 5).

Figures 6 through 9 are output at 1600 LDST. Comparison of Figure 6 with Figure 2 shows that the sea breeze front has moved both seaward and landward about 20 km. Figure 7 shows a well-developed v component with return flow (into paper) of -2 m/s aloft. A confused convective cell has developed in Figure 8 showing vertical convergence aloft with some landward cell motion. Figure 9 is similar to 5 with some cooling depicted near the surface.

The predominance of the v velocity appears to be due to absence of an appreciable mesoscale pressure gradient parallel to the coast, a reduced K due to the formation of a surface inversion with resultant damping of turbulence, and the greater Coriolis force. An example of pibal (pilot balloon tracked by theodolite) data (Figure 10) taken on Pingok shows a wind velocity profile late in the afternoon which seems to fit the model output.

Future model calculations will concentrate on reproducing the sea-breeze circulation observed in our coastal meteorology study. Pressure data from buoys (ADRAMS) deployed on the pack ice, National Weather Service stations at Barrow and Barter Island, DEW Line sites, pipeline camps and additional coastal stations (see text) will be used to model the synoptic

wind field. The value of the surface roughness (z_0) will be changed to representative values for tundra, ocean and possibly ice. A mixing ratio equation will be added to include the effect of humidity on the model results. Plus, the horizontal diffusion term will be kept because it is potentially important in the vicinity of the sea-breeze front. This work should be completed in late 1978.

REFERENCES

- Cotton, W. R., R. A. Pielke, and P. T. Gannon. 1976. Numerical experiments on the influence of the mesoscale circulation on the cumulus scale. *J. Atmos. Sci.*, 33, pp. 252-261.
- Defant, A. 1960. *Physical Oceanography, Vol. II*. Pergamon Press, New York. 598 pp.
- Estoque, M. A. 1961. A theoretical investigation of the sea breeze. *Quart. J. R. Meteor. Soc.*, 87, pp. 136-146.
- Estoque, M. A. 1963. The sea breeze as a function of the prevailing synoptic situation. *J. Atmos. Sci.*, 19, pp. 244-250.
- Kelley, J., and D. Weaver. 1969. Physical processes at the surface of the Arctic tundra. *Arctic*, 22, pp. 425-437.
- Kozo, T. L. 1977. Coastal meteorology of the Alaskan arctic coast. OCS Contract 3 03-5-022-671011.
- Moritz, R. E. 1977. On a possible sea breeze circulation near Barrow, Alaska. *Arctic Alp. Res.*, 9, pp. 427-431.
- Sheih, C. M., and Moroz, W. J. 1975. Mathematical modelling of lake breeze. *Atmos. Envir.*, 9, pp. 575-586.
- Walsh, J. E. 1974. Sea breeze theory and applications. *J. Atmos. Sci.*, 31, pp. 2012-2026.
- Walsh, J. E. 1977. Measurements of the temperature, wind and moisture distribution across the northern coast of Alaska. *Arctic Alp. Res.*, 9, pp. 175-182.

TABLE I
Barter Island
1976

<u>Month</u>	<u>Day</u>	<u>Height</u>	<u>Dir.</u>	<u>W.S.</u> <u>(m/s)</u>	<u>(GMT)</u> <u>Time</u>
8	1	SFC	090	2	000
		651	270	6	
	7	SFC	030	6	000
		532	270	7	
	11	SFC	070	3	000
		506	166	3	
23	SFC	050	3	000	
	582	273	4		
<u>1977</u>					
8	20	SFC	090	4	000
		618	269	9	
	24	SFC	320	2	000
		496	065	2	
29	SFC	012	3	000	
	553	109	5		
9	2	SFC	090	4	000
		607	276	6	

Examples of the change in wind direction and speed from the surface to the height of the 950 mb level. These were extracted from Barter Island, Alaska rawinsonde data.

TABLE II

Comparison of computed average geostrophic winds (\bar{V}_{geo}) with observed average surface winds (\bar{V}_{10}). The times are in Greenwich Mean Time, and can be converted to L.D.S.T. by subtracting 9 hours.

1976	TIME	(CALC.) \bar{V}_{geo} (O-D)	(MEAS.) \bar{V}_{10} (C-T)	SURFACE WIND DIRECTION	$\Delta T/10$ km (P-S)	$\Delta T/120$ km (P-H)
Aug. 15	0000Z	7.66	7.15	090	8.9	11.7
	*1200Z	2.66	5.26	085	2.8	6.6
Aug. 16	*0000Z	.55	4.10	090	17.8	4.4
	1200Z	7.18	6.71	270	10.0	-1.6
Aug. 17	0000Z	4.63	2.97	320	7.8	3.9
	1200Z	2.59	1.54	285	6.7	1.1
Aug. 18	*0000Z	1.99	4.83	105	10.6	2.7
	*1200Z	2.28	2.68	135	6.1	-1.5
Aug. 19	0000Z	6.42	5.66	030	11.1	0.0
	1200Z	5.39	4.36	030	.6	.5
Aug. 20	0000Z	4.57	3.74	050	4.4	1.7
Aug. 21	0000Z	4.49	3.36	110	7.0	6.9
	1200Z	8.09	7.15	300	6.1	2.8
Aug. 22	*0000Z	7.72	9.04	310	6.1	-1.5
	1200Z	5.73	1.45	060	2.8	.5
Aug. 23	0000Z	6.35	5.26	075	6.7	6.1
	1200Z	7.70	6.33	250	8.9	-1.1
Aug. 24	*0000Z	3.02	6.93	105	7.8	6.6
	*1200Z	5.85	5.99	100	2.2	.6
Aug. 31	*0000Z	4.41	5.03	100	7.8	9.4
	*1200Z	3.39	3.58	100	2.2	6.7
Sept. 2	*0000Z	1.82	2.53	040	2.8	10.0
Sept. 3	*0000Z	3.52	5.32	105	2.2	11.7
	1200Z	2.18	1.50	070	1.1	3.9
Sept. 4	0000Z	7.98	4.03	075	2.8	1.6
	*1200Z	4.66	6.64	255	1.1	-2.2

O-D \equiv Oliktok-Deadhorse; C-T \equiv Cottle Island-Tolaktovut Point;
P-S \equiv Prudhoe Airport-Sea; P-H \equiv Prudhoe Airport-Happy Valley
 ΔT \equiv Temperature Difference ($^{\circ}\text{C}$); * \equiv indicates discrepancy where
surface wind exceeds geostrophic value.

TABLE III

August 19, 1977

<u>L.D.S.T.</u> <u>Time</u>	<u>P(mb)</u> <u>SEA-PI</u>	<u>(mb)</u> <u>ΔP</u>	<u>P(mb)</u> <u>LAND-OLI</u>
0900	1020.25	.33	1019.92
1200	1022.25	.32	1021.93
1500	1023.95	.42	1023.53
1800	1025.15	.72	1024.43
2100	1026.45	.72	1025.73

Change in measured sea level atmospheric pressure at Oliktok Dew Line site compared with that at Pingok Island (skm from coast)

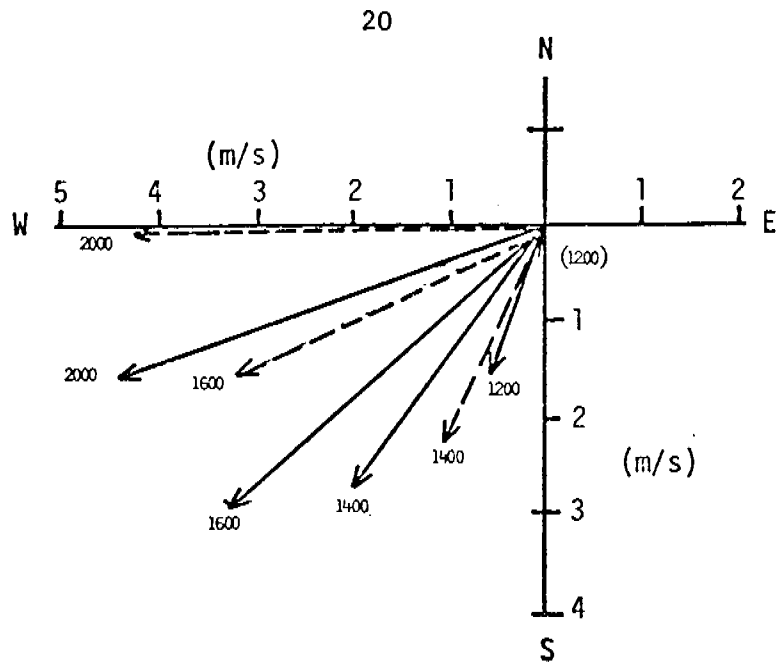


Figure 1. Comparison of modeled velocity vectors. Mid-latitude (solid line), Arctic (dashed line). Local time is used.

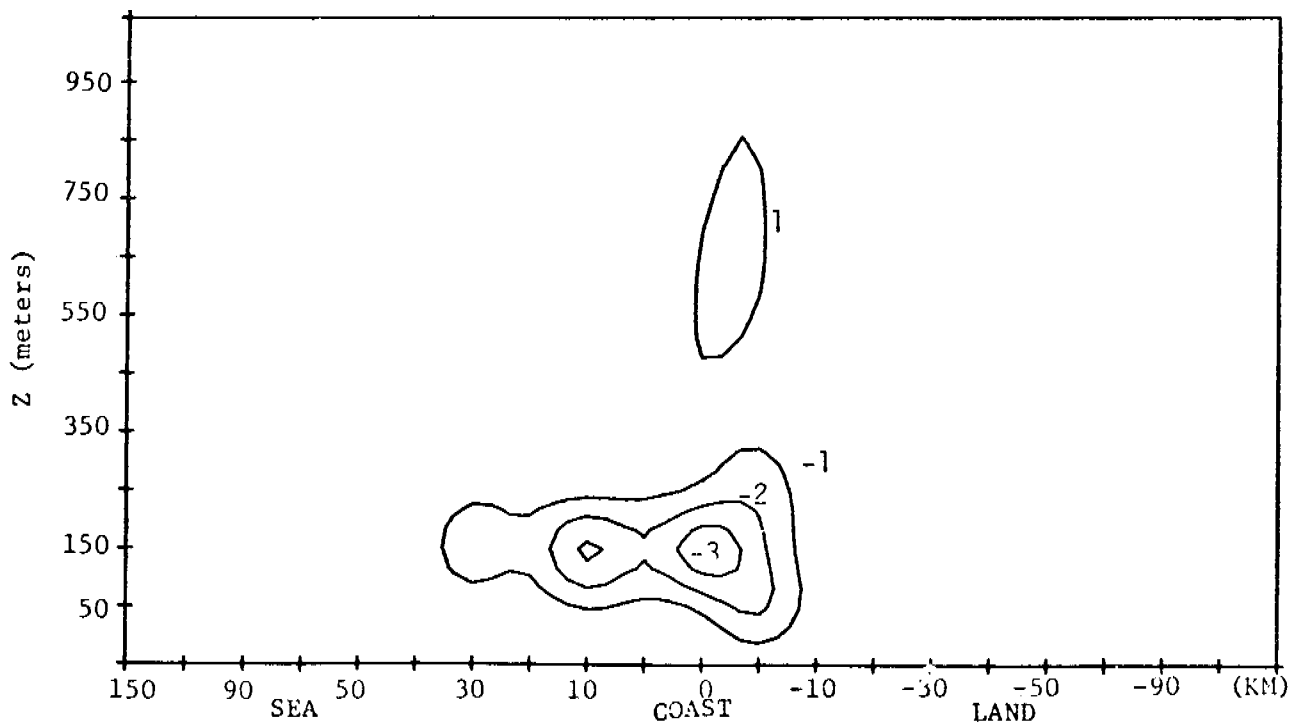


Figure 2. U - velocity contours in m/s with negative values toward land, at 1400 LDST.

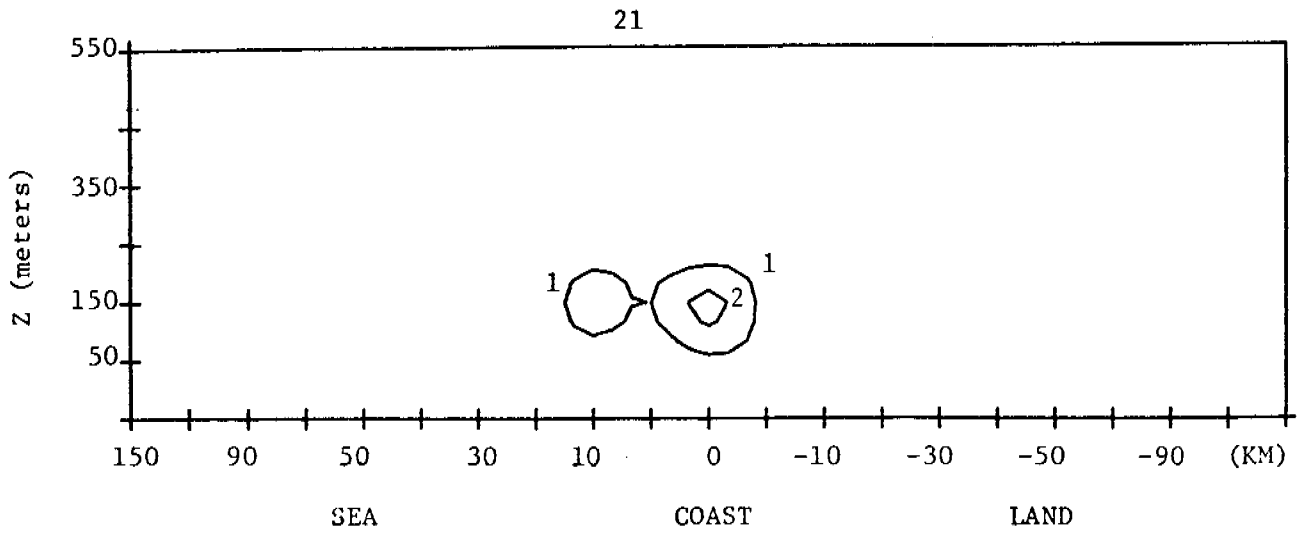


Figure 3. V - velocity component contours in m/s, at 1400 LDST. Positive values out of paper.

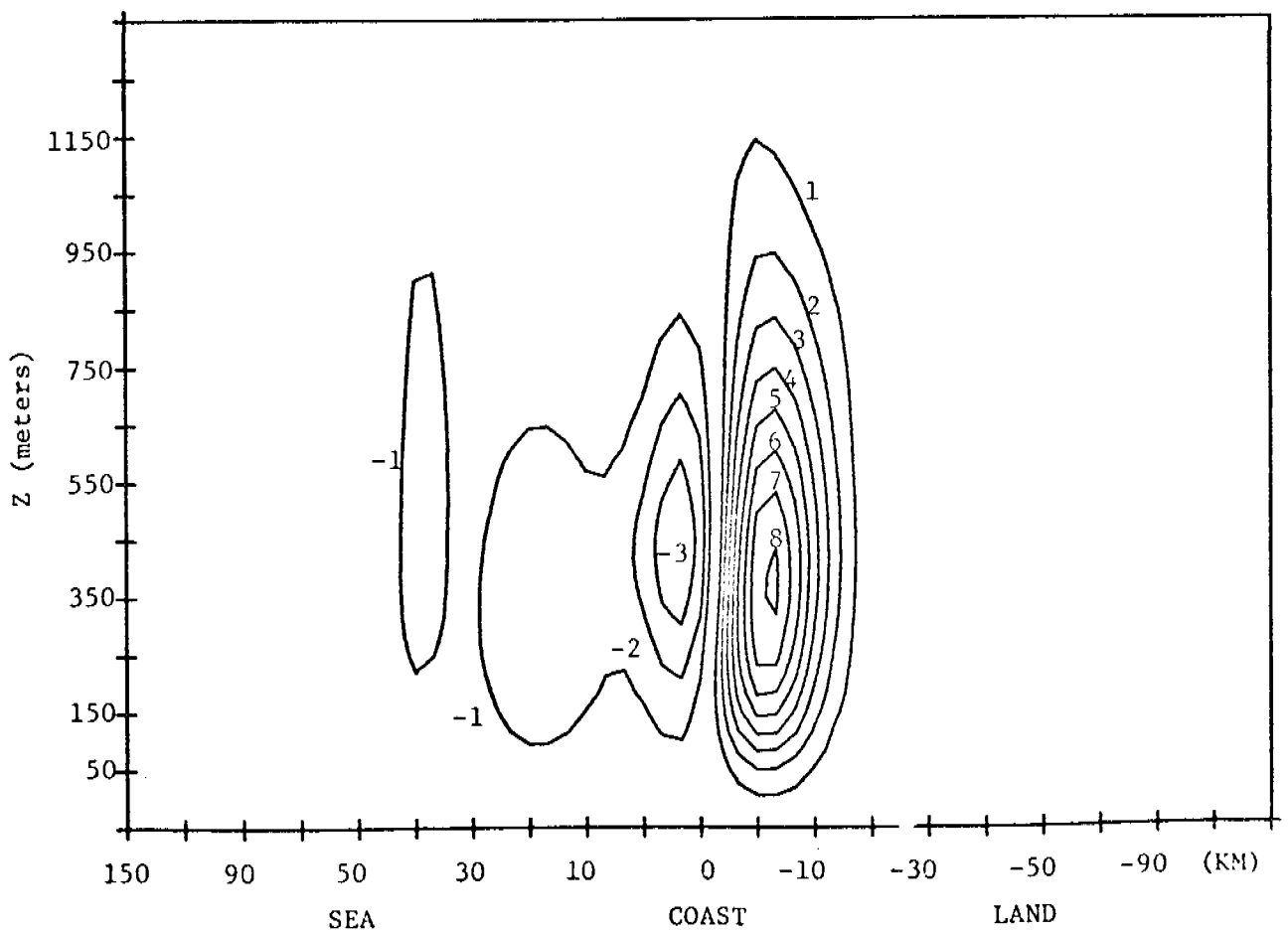


Figure 4. Vertical velocity component (w) contours in cm/s at 1400 LDST. Positive values are upward velocities.

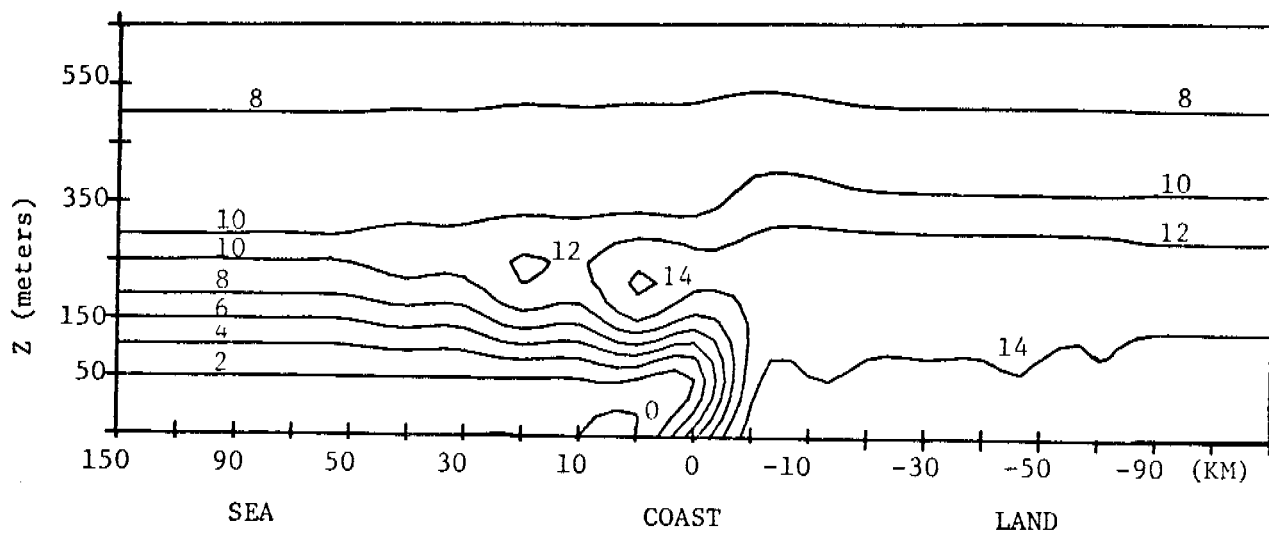


Figure 5. Temperature contours in degrees centigrade at 1400 LDST.

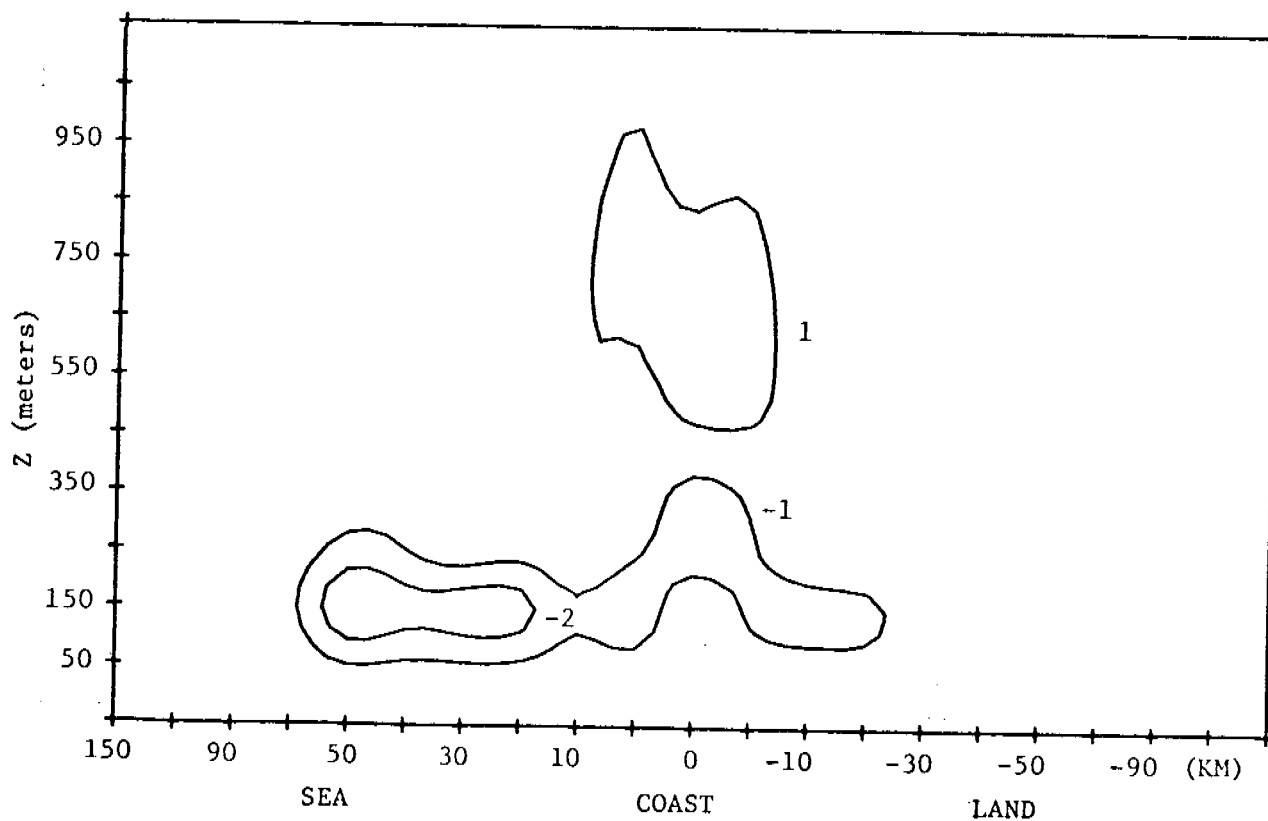


Figure 6. U - velocity contours as in figure 2 except for 1600 LDST.

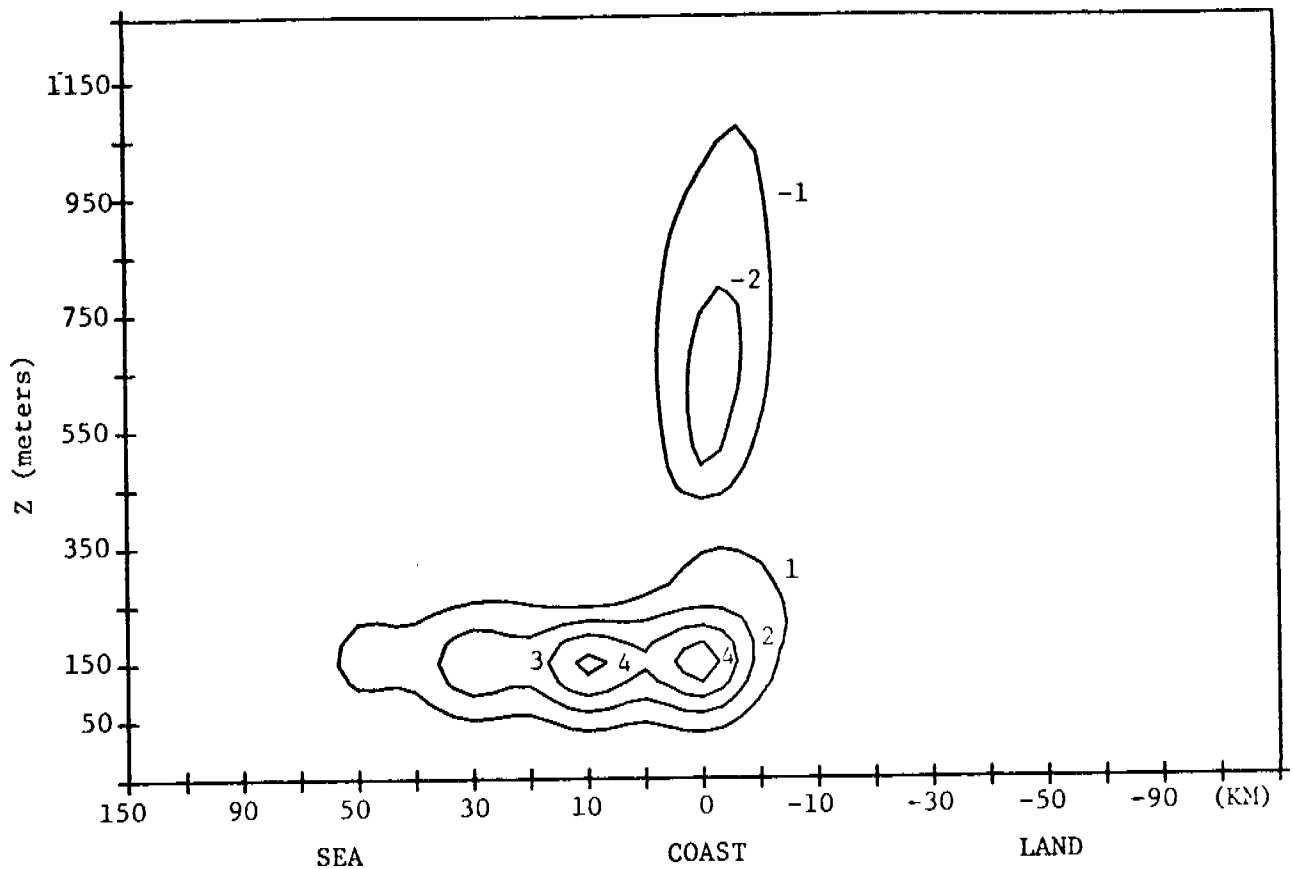


Figure 7. V - velocity contours as in figure 3, except for 1900 LDST.

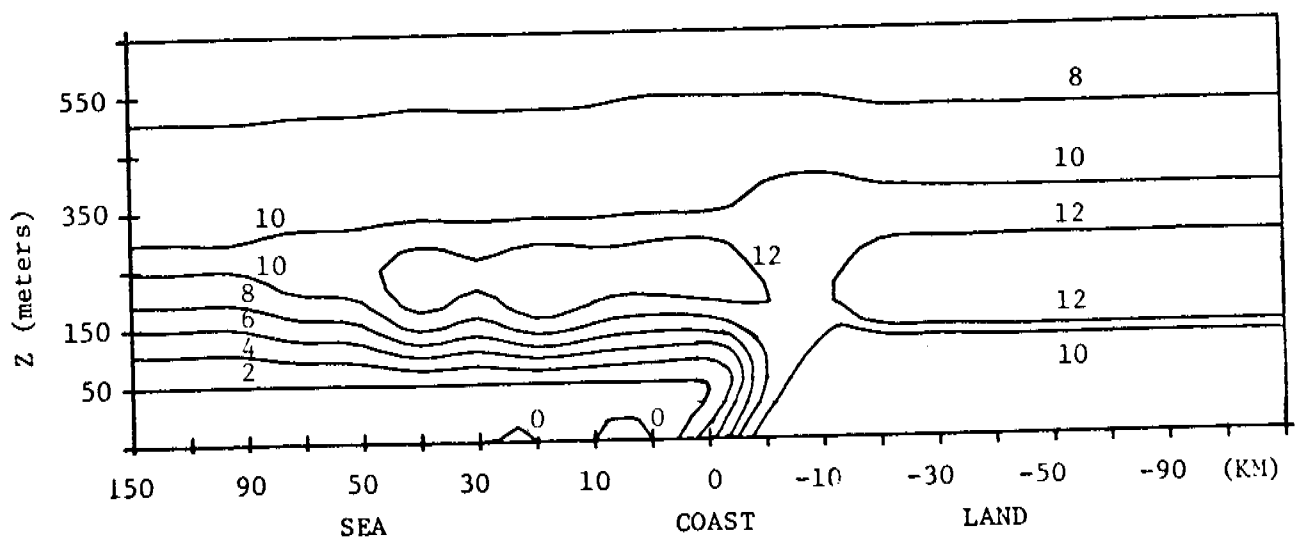


Figure 8. Temperature contours as in figure 5, except for 1600 LDST.

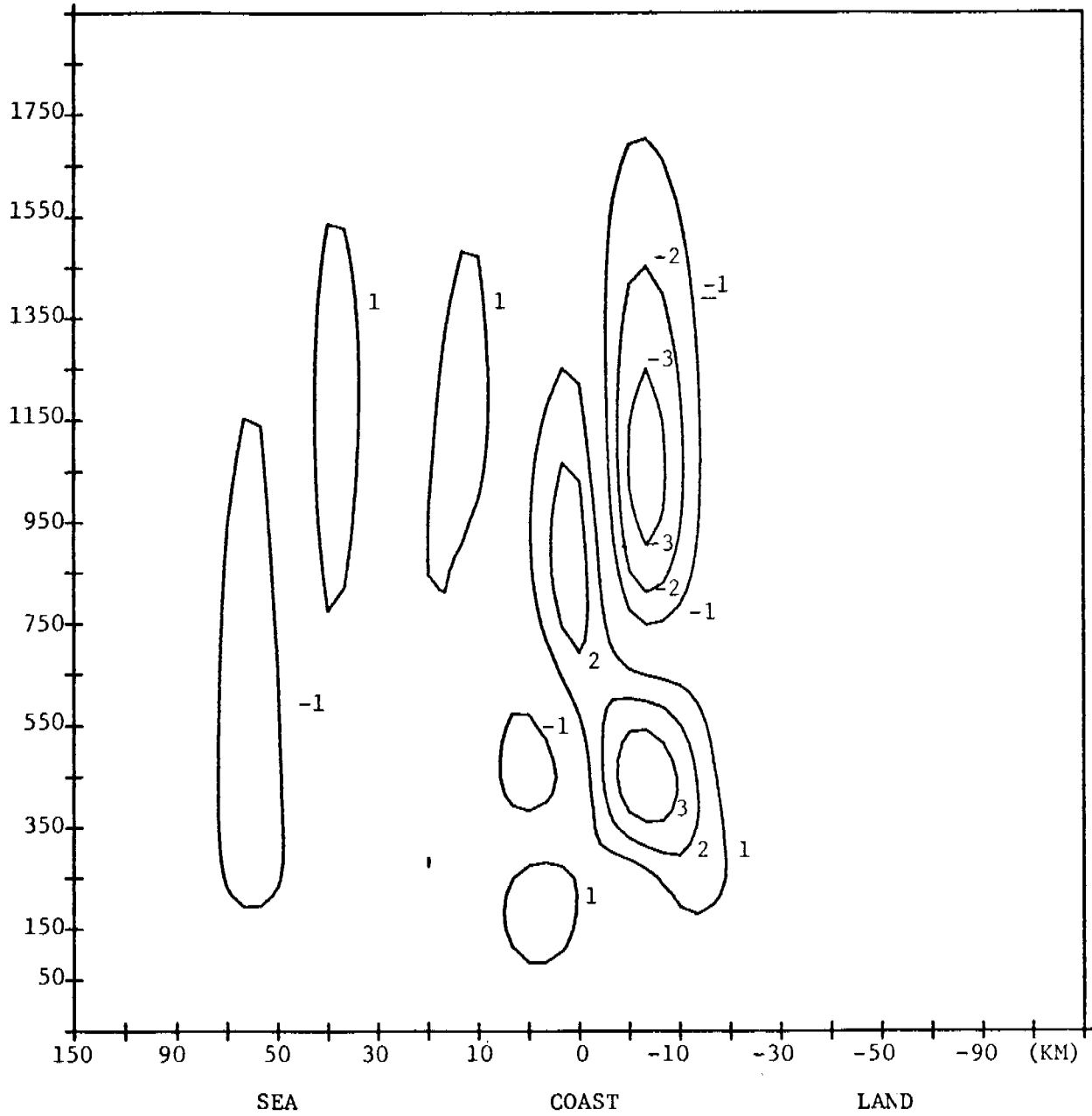


Figure 9. W - velocity contours as in figure 4, except for 1600 LDST.

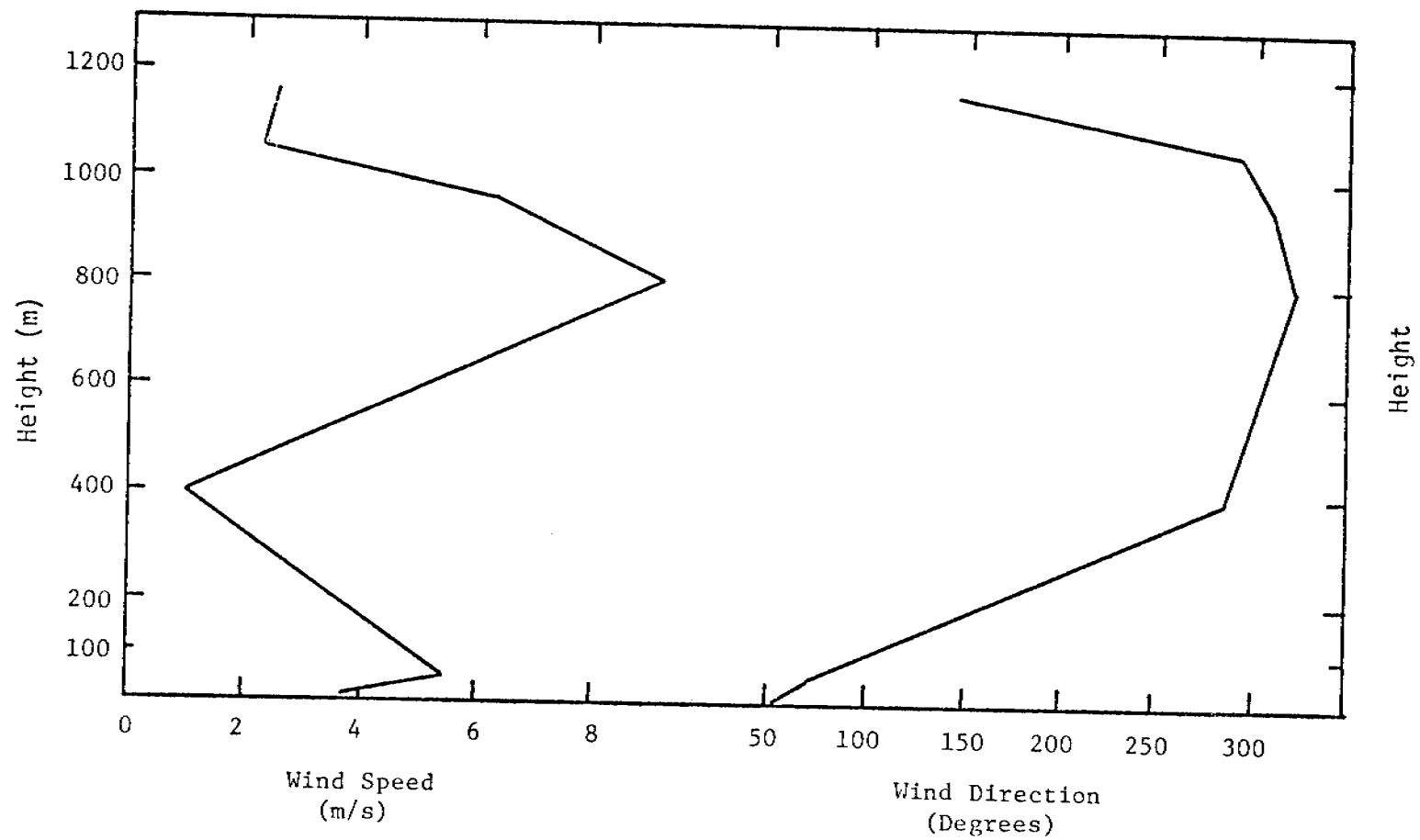


Figure 10. Variation of wind speed and direction with height at Pingok Island, 6 August 1977 at 2237 LDST. Data was obtained by-dual theodolite tracking of a pilot balloon.

ANNUAL REPORT

Contract Number: 03-5-022-56

Research Unit Number: 526-77

Task Order Number: 13

Reporting Period: 1 April 1977 to 31 March 1978

Number of Pages:

CHARACTERIZATION OF THE NEARSHORE HYDRODYNAMICS
OF AN ARCTIC BARRIER ISLAND - LAGOON SYSTEM

J. B. Matthews

Geophysical Institute
University of Alaska
Fairbanks, Alaska 99701

March 31, 1978

TABLE OF CONTENTS

- I. SUMMARY
- II. INTRODUCTION
 - A. General Nature & Scope of Study
 - B. Specific Objectives
 - C. Relevance to Problems of Petroleum Development
- III. CURRENT STATE OF KNOWLEDGE
- IV. STUDY AREA
- V. SOURCES, METHODS AND RATIONALE OF DATA COLLECTION
- VI. RESULTS
- VII. DISCUSSION
- VIII. CONCLUSIONS
- REFERENCES
- IX. SUMMARY OF 4TH QUARTER OPERATIONS
 - A. Ship or Laboratory Activities
 - B. Problems Encountered/Recommended Changes
 - C. Estimate of Funds Expended

I. SUMMARY

The objectives are to provide understanding of the physical processes occurring in a typical barrier-island lagoon system along the Beaufort Sea coast as part of the input to an ecological process study. Preliminary conclusions from the first year's work are that the system is primarily driven in the open water season by meteorological events, water from the rivers appears to stay nearshore and move in a generally westward direction. Causeways and other solid structures appear to modify the longshore flow. More data are needed to ascertain the pumping process of water masses between the barrier islands in response to meteorological events as well as data on flow and water quality before and during ice breakup. Flushing times during strong winds and storms could be of the order of a few days and surface drifters reached Point Barrow from Prudhoe Bay in less than a week.

Implications for oil and gas developments are that, during the open water season, spilled oil could be distributed over the whole coastline in about one week if it coincided with the frequent storm conditions. Preliminary results suggest that islands, causeways and other obstructions to longshore flow need to be designed with consideration for allowing free passage of the brackish river waters near the mainland shores.

II. INTRODUCTION

A. General nature and scope of study

The work in this project is an integral part of the larger study entitled "Beaufort Sea Barrier Island-Lagoon Ecological Process Studies" under research unit number 467. As such, its major aim is somewhat different from other physical oceanographic projects in that its general nature and scope are determined by the needs of RU 467 as determined by the other investigators in conjunction with the results of the numerical model of the ecosystem processes.

The basic purpose of RU 467 is to provide answers to questions of impact upon ecosystem processes in a marine system typical of the Beaufort Sea coast. The basic objective of this project is to support these goals with emphasis on the physical processes occurring in the region of the Simpson Lagoon which was chosen as the typical area. The physical process study work is further subdivided between this project and RU's 531 (Mungall, Texas A & M) and 519 (Carsey, U. of Washington). This project is reviewing estuarine lagoon hydrodynamics as they relate to Simpson lagoon, performing limited numerical modeling work to determine key locations for field experiments and carrying out experiments to measure the tide and surge levels and water currents, temperatures and salinities around Simpson Lagoon.

B. Specific objectives

The specific tasks of this program are as follows:

1. To review estuarine lagoon dynamics as they relate to Simpson Lagoon.
2. To obtain current meter measurements of the flow into and out of Simpson Lagoon and relate these data to prevailing conditions aided by numerical modeling techniques.

3. To obtain sea level data around Simpson Lagoon and relate these data to prevailing conditions to separate tidal events from storm surges.
4. To obtain water temperature and salinity data around Simpson Lagoon and use these data in conjunction with other measured data on weather, currents and sea levels and, aided by numerical models, to characterize the circulation and flushing of Simpson Lagoon.

Data from these activities will be used to provide a better understanding of the nearshore dynamics in the Beaufort Sea. Throughout the course of the work as new information and insights are gained into the physical processes, the knowledge is shared with other investigators involved with the work. This latter activity provides a powerful interdisciplinary insight to the nearshore processes and continually re-directs the project towards the important and relevant measurements. It also places an additional burden on the principal investigator in that he has many synthesis meetings and workshops for which to prepare reports in addition to the normal load.

C. Relevance to problems of petroleum development

Physical circulation and processes occurring in the nearshore regions of the Beaufort Sea have a primary influence on the biological processes. Currents and water temperature, salinity and turbulence have a direct effect on organisms at the base of the food chain. These in turn affect the higher organisms such as fish and birds which are vulnerable to oil related impacts along the Alaskan north slope coast.

These applications are in addition to the obvious applications of physical circulation in transporting spilled oil and other hazardous materials related to the petroleum development. We have also examined the currents and water quality near an existing causeway built to aid petroleum development. This work could assist in the improvement of similar structures built in the future.

The relationship of this work to petroleum development-related hazards is unusually well-defined because the work in the overall ecosystem process study (RU 467) has been narrowed to look only at those processes likely to be impacted by such development. Thus, all the work is directly related to problems of petroleum development.

III. CURRENT STATE OF KNOWLEDGE

There have been very few studies of the nearshore circulation in the Beaufort Sea prior to this one. Simpson Lagoon was chosen as the site for the work because it was the best studied barrier island-lagoon system and so that we might build on the earlier work.

The study of Kinney et al. (1972) established a data baseline for the Colville Delta region and west end of Simpson Lagoon. The sea level measurements of Matthews (1970) in conjunction with the observations of Kinney and his co-workers clearly indicated that the shallow nearshore waters were dominantly wind-driven during the open-water season. Subsequent work by Wiseman et al. (1973) confirmed that coastal processes are dominated by storm-related events for lagoon-barrier island systems in both the Chukchi and Beaufort Seas. Wiseman and his co-workers based their conclusions on work on Kasegeluk Lagoon

at Point Lay and on Simpson Lagoon at Pingok Island. These and other studies were summarized in Reed and Sater (1974) and the work initiated by Kinney et al. (1972) was reported in final form in Alexander et al. (1975) immediately prior to the initiation of the OCS studies.

Except for the work of Barnes et al. (1972 and 1977) dealing principally with nearshore geological processes, and Callaway (1976), concerned with tidal numerical modelling, the OCS work was initially concerned with the circulation on the outer shelf seaward of the LOM isobath. Barnes et al. made some very interesting observations of nearshore temperature, salinity, sea level currents west of Prudhoe Bay in Stefansson found and interpreted these results as showing a westerly flow associated with strong northeasterly winds, lowered sea levels, low temperatures and high salinities. Unfortunately, Callaway's modeled results were not verified by field observations. Barnes and Garlon (1972) showed a maximum westward surface drift of 38 cm/sec from draft card releases.

The work of Aagaard and Haugen (1977) revealed the current structure on the outer shelf on a seasonal basis and was complemented by water structure studies in the same area (Aagaard, 1977). Between the 20M and 100M isobaths winter currents were generally less than 5 cm/sec whereas tidal currents were generally less than 1 cm/sec. Between the 100M and 200M isobaths currents of over 55 cm/sec were observed between May and September. The structure of circulation inshore of the 20M isobath was not investigated by Aagaard and his co-workers. Their work, however, does provide a larger framework in which to relate the nearshore circulation.

Prior to the present work there has only been one attempt to make current measurements in Simpson Lagoon (see Dygas in Alexander et al. 1975) using moored digital recording instruments. Records of 7 and 38 days were obtained during the summers of 1971 and 1972 respectively. The current meter was located in mid-lagoon between Oliktok Point and Spy Island in an effort to measure the flow through the lagoon parallel to shore. It was 1M above the bottom in a total water depth of 2.5M and yielded useful records for the periods 25 August to 1 September 1971 and 11 August to 18 September 1972.

IV. STUDY AREA

The study area is Simpson Lagoon as shown in Figure 1. Although the associated biological studies were carried out in Simpson Lagoon only, for physical oceanographic work it is necessary to consider the barrier island-lagoon system as a whole. Thus, our study area extends from Prudhoe Bay in the east to Harrison Bay in the west.

V. SOURCES, METHODS AND RATIONALE OF DATA COLLECTION

Written approval of the contract being received in June 1977, an extensive field program was not planned for summer 1977. It was decided to attempt to deploy three current meters and a tide gauge in strategic locations around Simpson Lagoon since data from such instruments could furnish the much-needed data on flushing rates and surge-related water movement. A tide gauge was operated by the National Ocean Survey at Prudhoe Bay to supplement data from our lone instrument.

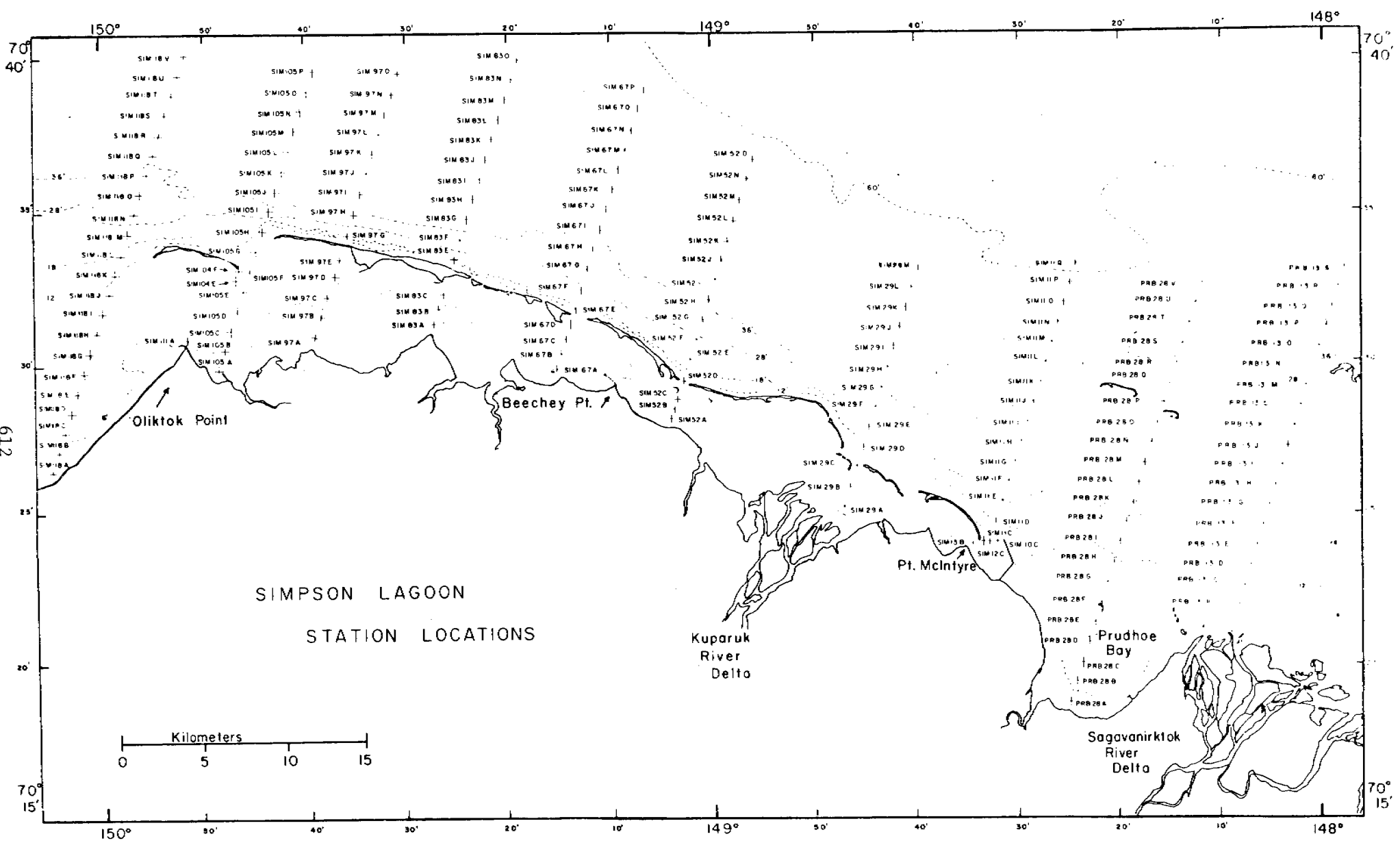


Figure 1. Simpson Lagoon showing station locations.

Mungall (RU 531) provided limited spot readings of current speed and direction, temperature and salinity at the east end of the lagoon near the ARCO causeway. Carsey (RU 519) provided wind speed and direction and barometric pressure reduced to sea level for sites at Pingok Island, Cross Island, Cottle Island, Oliktok Point, Deadhorse and Umiat. Craig (RU 467) provided sea surface temperatures and salinities at sites near Pingok Island.

Considerable thought was given to methods of current measurement in water 2 to 3M deep. There had been a number of reports of data aliasing from current measurements taken near the surface in the zone of direct wave influence (Pollard, 1973; Halpern et al., 1974; Saunders, 1976). These studies, however, referred to waters of somewhat greater depth than 3M and not to the Arctic Ocean. Because of the damping effect of the ice cover and the limited fetch, wave energy in the arctic is concentrated at the longer wave lengths (Hunkins, 1962 and 1965). Sea and swell are usually negligible except during storms (see Dygas in Alexander et al. 1975 and Wiseman et al. 1973). Thus, if a reasonably sheltered location were selected in relatively deep water, we could reasonably expect to avoid aliasing due to wave motion. Also, if a rigid mount for the instruments could be designed we could hope to avoid aliasing due to thrumming in the mooring line.

We chose to use Aanderaa current meters and tide gauge because they have been thoroughly tested under arctic conditions, are light, small and easy to handle and data reduction techniques are readily available. The Institute of Marine Science at the University of Alaska has developed maintenance expertise with these instruments and it was a logical decision to build on this experience. To mount the instruments rigidly in 2-3M water depths, we designed a box framework of 1/2" diameter iron pipe which rested on the sea floor. The current meter mounting rod was bolted vertically to the top and bottom cross-pieces of the box frame. The pipe work extended in four directions horizontally from the mounting rod a distance of four feet to allow the meter vane to swing freely. A tide gauge was clamped to one of the box frame members. Polypropylene lines with surface floats were used to mark the deployment and also for the placement work. A stainless steel line about 50M in length and anchor completed the assembly.

It was decided to locate the instruments in major channels of the Simpson Lagoon complex to be able to get estimates of tide and weather-induced flushing. The R/V Alumiak, a shallow draft vessel with bow A-frame, was the ideal vehicle from which to deploy the instrument arrays. Problems with the vessel have been discussed in quarterly reports. Suffice it to say that the arrays were recovered from a boston whaler. Two of the three arrays were recovered. Navigation from a boston whaler in the fog-shrouded, low topography arctic coast made it difficult to relocate the deployment sites with any certainty.

It was also planned to attempt surface drifter releases. Since the arctic shores are not walked by beach combers except for scientists, it was decided to use numbered drifters but without the reward message usually used. It was hoped to release drifters during both westerly and the prevailing easterly winds in the hope of getting more detail on the extent of the surface currents and their dependence on winds. Foggy weather precluded more than one deployment but clusters of 10 drifters were released on the line from Oliktok Point to the west end of Spy Island between 1500 hours ADT and 1700 hours ADT on 7 August 1977.

VI. RESULTS

Despite the late start in the contract (June, 1977), we were able, with assistance from the project office, to order and deploy three Aanderaa recording current meters and one tide gauge. Aanderaa tide gauge 196 and Aanderaa current meter 2169 were set at Station SIM 104F (fig. 1) at 0315 hours G.M.T. on 8 August 1977. Water depth was measured at 3.96M. The site chosen was at the southeast tip of Spy Island in the center of the Spy Island channel. Conditions were calm after a westerly wind had been blowing.

We attempted to take a line of stations SIM 118 (fig. 1) the following day. Stations B, D, F and H were taken with an RS5 salinometer. The conductivity cell never worked but we took temperature profiles and a Nansen bottle cast. Currents were read using a Hydro Products profiling current meter. The RS5A was borrowed from the Institute of Marine Science, University of Alaska; the profiling current meter from Texas A&M Foundation.

At station SIM 118H the R/V Alumiak lost engine power and steering way. Since ENE winds were freshening to 20 knots, the skipper decided to anchor and ride out the storm. By drifting down wind at anchor for several 100M., current meter number 2211 was deployed at station SIM 118H at 2315 hours G.M.T. on 9 August 1977.

The storm lasted some four days and the R/V Alumiak continued to have problems. We deployed meter 2257 at 1320 hours G.M.T. on 13 August 1977 in a measured depth of 1.31M water at station SIM 11C (fig. 1).

Meters 2257 and 2169 and tide gauge 196 were recovered on 21 September from a Boston whaler through fresh pancake ice. All the tapes had been used.

The tide gauge record was good with samples at 3.75 minute-intervals from 0418 hours G.M.T. on 8 August 1977 to 0937 hours G.M.T. on 16 September 1977 (39 days). Current meter 2169 from the same site (SIM 104F) in Spy Island channel had records from 0420 hours G.M.T. on 8 August 1977 to 0115 hours G.M.T. on 12 September 1977 (34 days). Unfortunately, the current speed sensor stopped after five hours. After two days large amounts of bad data were recorded. These data have required a large amount of time and effort to remove the bad records.

Current meter 2257 in the channel between Stump Island and the ARCO causeway yielded good data for the period from 1345 hours G.M.T. 13 August 1977 to 0515 hours G.M.T. 16 September 1977 (34 days). The only problem with these data was a digitizer malfunction at 12-sample intervals. Current meter 2211 was not recovered.

VII. DISCUSSION

Data analysis is still in progress. Unfortunately, the available computer programs at the University of Alaska were inadequate for our needs and have had to be up-dated and new ones written. Preliminary results only are presented with findings to date. Figure 2 shows temperature and salinity profiles for August and September 1977 and barometric pressure for Deadhorse Airport for August. Note that the salinity is between 29 and 31 ppt for much of August with excursions to less than 28 ppt lasting for periods over a day. These low

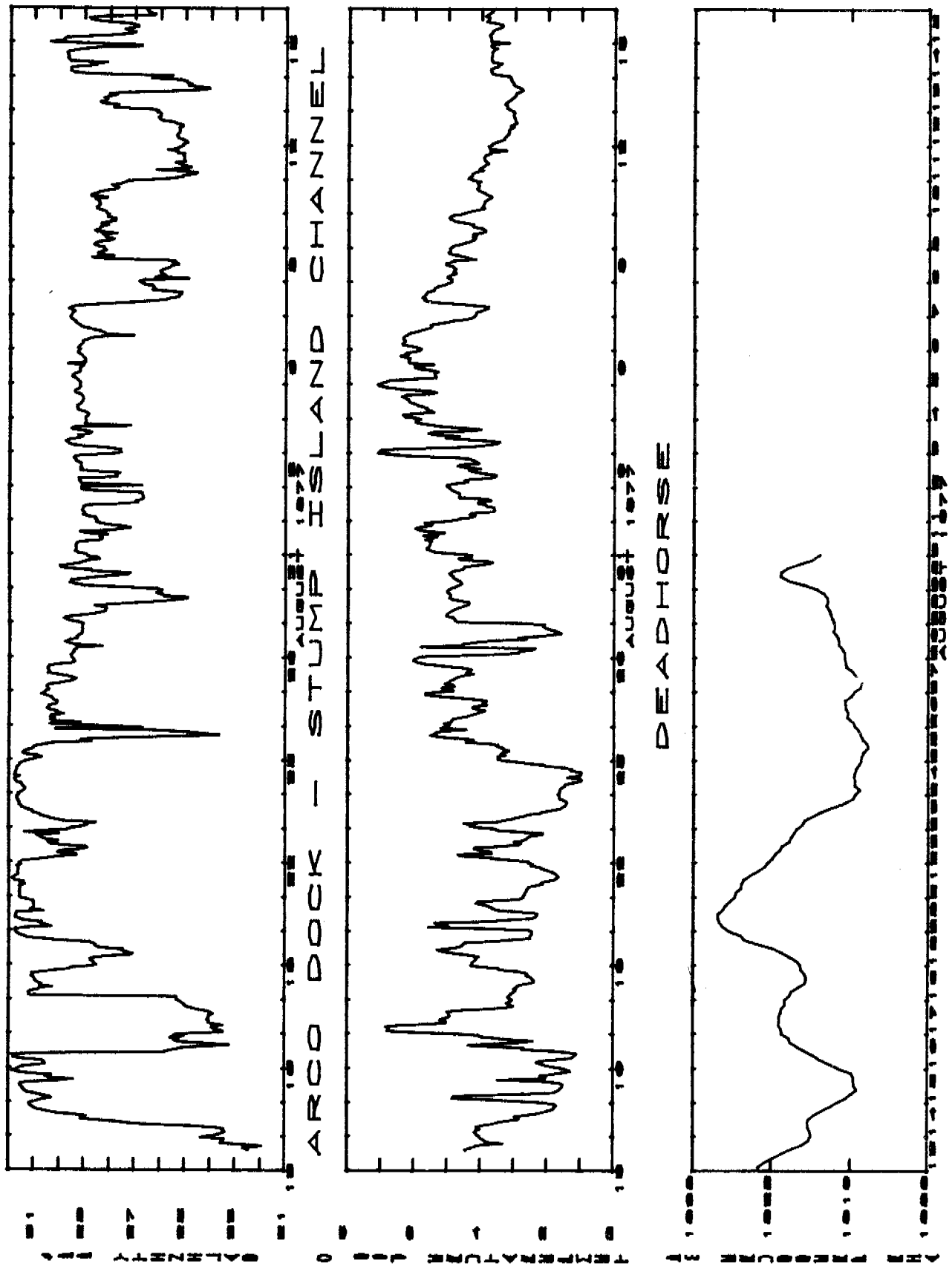


Figure 2. Temperature, salinity and pressure plots, August and September 1977.

salinity waters are associated with higher temperature (up to 5°C) water. It suggests that pulses of warm (5°C) brackish (~24 ppt) water are alternating with generally cold (<2°C) saline (>30 ppt) water. The latter must be oceanic shelf waters and the former must derive from freshwater input such as river runoff or meltwater.

Figure 3 is a stick diagram showing the currents in August and September through the Stump Island channel. Since the instrument location represents a channel with north-south axis, Cross Channel (east-west) flows are relatively unimportant. The figures are drawn with the east-west components reduced by a factor of 10. Note that currents generally flow southwards (into the lagoon) except during times when they are small. At those times, tidal motion is observed. The brackish waters seen between 16 and 18 August are associated with southward flow. This suggests that brackish water enters the lagoon between Stump Island and the ARCO causeway.

The period 13-14 August shows a similar low salinity high temperature period coming to an end. Between the 14 and 16 August; note that high salinity and low temperatures prevail. There are small deviations of of -1 or -2 ppt and +2 or +3°C which occur with outflowing (northward) currents. This suggests that slightly less brackish water is flowing from the lagoon.

These results would seem to imply that when brackish water flows into the lagoon it has a much higher freshwater component than when the brackish water flows out of the lagoon. This is interesting because it suggests that brackish water is flowing from the east, presumably from the Sagavanirktok River, and maintains its identity over a distance of about 15 km. The brackish water leaving the lagoon flows only for short periods which are probably not sufficient for large volumes of water from the Kuparuk River 9 km to the west to flow eastwards.

Data taken by Mungall (RU 531) support the hypothesis that the predominantly westward flowing waters bring brackish waters from the Sagavanirktok River into the lagoon. Figure 4 is a plot of spot samples of temperature and salinity taken throughout the lagoon on 15th August 1977. (See RU 531 report for full details). Note that near the islands, temperatures are generally lower and salinities higher than along the mainland shore. Especially noteworthy is the temperature difference (4.5°C) and salinity difference (16.3 ppt) from the east to the west side of the ARCO causeway. This was observed at 2000 hours G.M.T. on 15 August. The brackish water reached the current meter number 2257 in the Stump Island channel at 0945 hours G.M.T. on 16 August when the salinity fell from 31.83 ppt to 26.12 ppt over a 5-minute interval. Mungall's next observation west of the causeway was at 0516 hours G.M.T. on 17 August showing a salinity lowered to 28.28 ppt. The salinity at the current meter had by this time steadily fallen to 23.36 ppt. This lag between Mungall's station just west of the causeway and the current meter in mid-channel suggests that the causeway has a sheltering effect which retards brackish water from flushing near the westward causeway shore.

The return of the saline cold water occurred at the current meter at 0200 hours G.M.T. on 18 August when salinity rose from 25.44 ppt to 31.09 ppt over a 5-minute interval. By 0410 hours it had risen to 31.25 ppt at the current meter and at Mungall's west causeway site was up to 30.63 ppt.

CURRENT SPEED AND DIRECTION

20 CM/S EAST



AUGUST 1977

ARCO DOCK - STUMP ISLAND CHANNEL

CURRENT SPEED AND DIRECTION

40 CM/S EAST



SEPTEMBER 1977

Figure 3. North-south current vectors with east-west components suppressed by an order of magnitude.

SIMPSON LAGOON, ALASKA
 OCSEAP R.U. #531

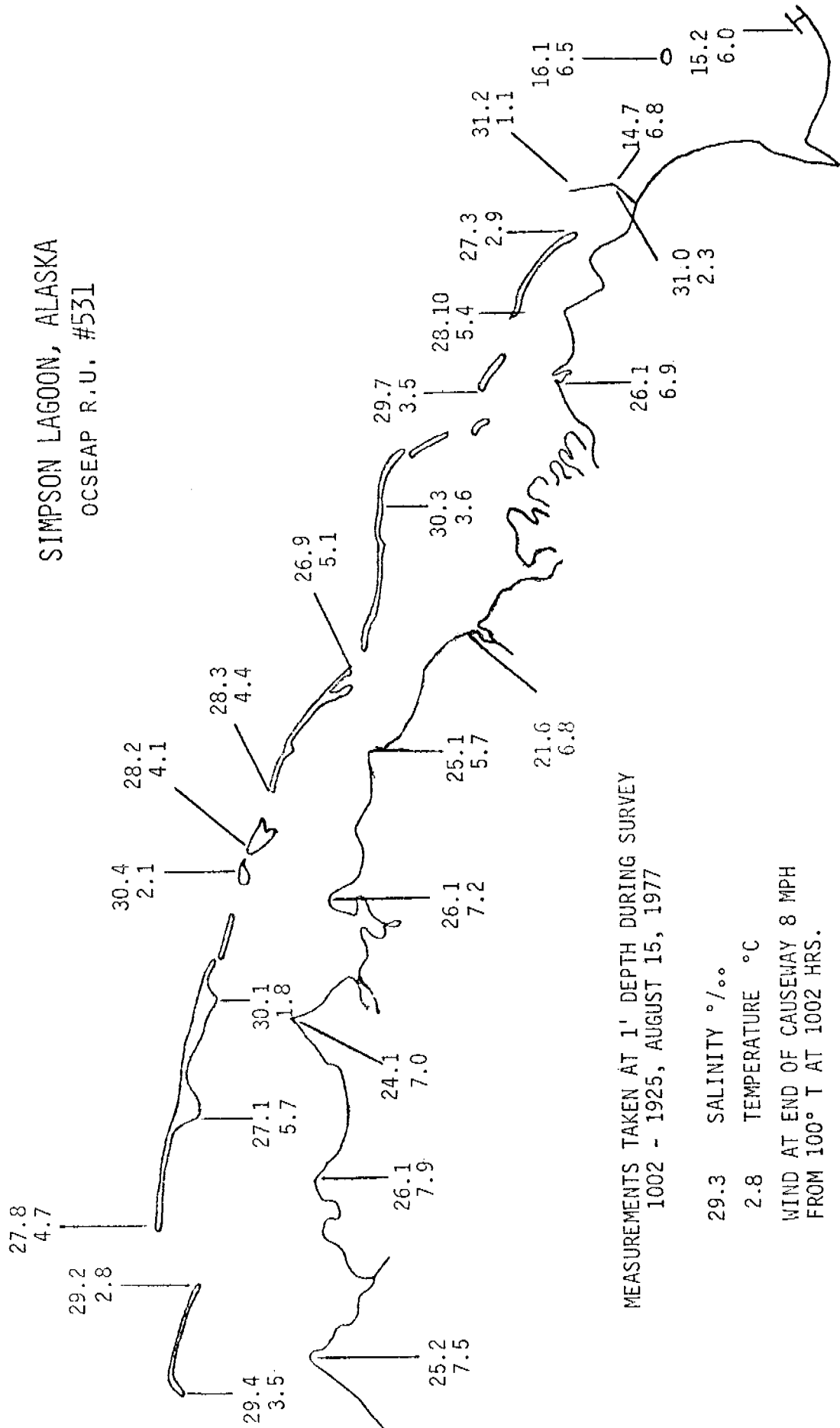


Figure 4. Salinity and temperature values taken by C. Mungall (RU 531).

By looking in detail at this one occurrence we can see that rapid changes in salinity can occur, suggesting that pulses of water move along the coast. These systems can be likened to passing saline frontal systems with a very sharp boundary between water masses.

Further confirmation of low salinity high temperature water lying near the coast was obtained from NOAA satellite infra-red imagery. Figure 5 is an infra-red picture using two scales from white to black 38°F to 44°F and 45°F to 60°F (-2.2°C to 6.7°C and 7.2°C to 15.6°C). Thus on this picture land warmer than 15.6°C shows black as does water at 6.7°C . Water or land near 7°C however shows as white. The white band hugging the coast from the east near Herschel Island is interpreted as being warm, brackish water. The band is particularly wide in Prudhoe Bay and west Simpson Lagoon. The image was taken at 2045 hours G.M.T. on 14 August 1977. The current meter temperature record shows a steady rise from 1.74°C at 2200 hours G.M.T. on 14 August to 4.04° at 0230 hours G.M.T. on 15 August. This strongly suggests that the water seen in Prudhoe Bay by the satellite passed into Simpson Lagoon through the Stump Island-ARCO causeway channel only a few hours later.

Fluctuations in the temperature and salinity values appear to be larger in early August and decrease towards mid-September (Figures 2 and 6). At Stump Island (Figure 2) temperatures show an steady decline from 6th September at about 8°C to the end of the record on 16th September when it had fallen to less than 4°C . At the Spy Island channel where larger variations in temperature were observed temperatures were less than 3°C during the September record. This is consistent with the rapid cooling occurring from about 1st September.

The salinity at the Stump Island channel (Figure 2) also shows pockets of low salinity water having progressively higher salinity throughout the record the peak runoff occur in two peaks for the Sagavaniktok River on about 1st June and 15 August with flow rates of 2.5×10^7 and 2.7×10^7 M^3/day (Carlson, 1977). The Kuparuk peaks on 1 June with 2.4×10^7 M^3/day but its record peak about 10 September reaches to only about 0.7×10^7 M^3/day . This suggests that observed salinity fluctuations probably relate to the river runoff. Unfortunately the current meter records cover only the season of the second peak runoff. These records are still being analysed for details but biologists associated with the study have indicated the need for observations earlier in the season especially during the spring breakup when productivity in the lagoon appears to be high.

Currents average about 6 cm/sec into the lagoon but at peak periods during strong ENE winds can reach average velocities of 18 cm/sec. This represents volume flows averaged over the 260 M^2 cross-section of the channel of $16 \text{ M}^3/\text{sec}$ and $347 \text{ M}^3/\text{sec}$. Computed flushing times for this entrance alone over the 0.31 km^3 volume from the ARCO entrance to Pingok Island are about 225 days and 76 days, respectively. It should be noted, however, that the Stump Island channel is not the only or deepest entrance from the east to Simpson Lagoon. The Egg Island channel is 7.5M deep at its deepest point and another very narrow channel at the east end of Long Island is 6M deep and the channel between Cottle and Long Island is at least 3.5M deep (E. Reimnitz, personal communication). The flushing rates including these deep channels might be expected to be reduced by as much as an order of magnitude.

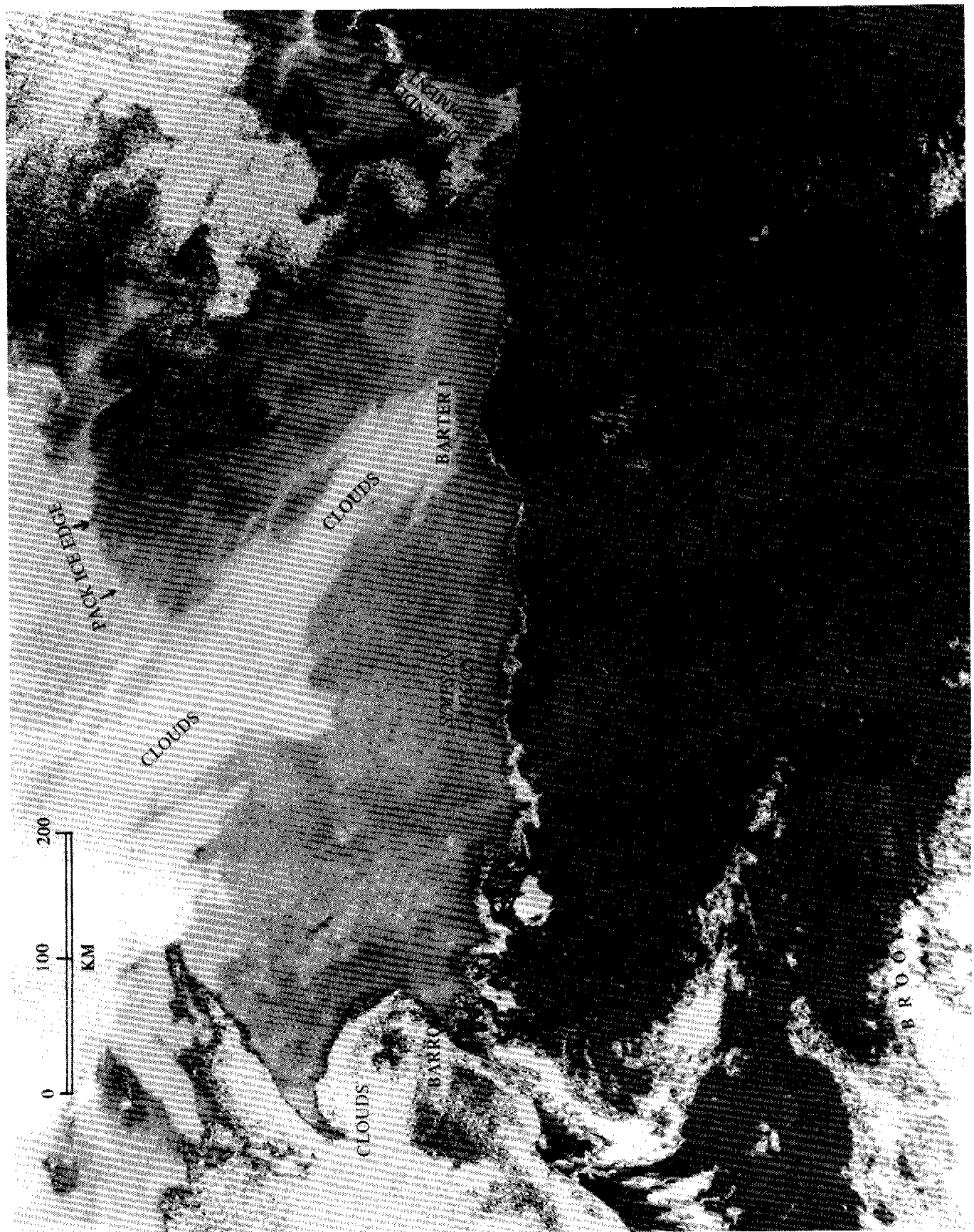


Figure 5. Infra-red satellite picture of north slope on 14 August 1977 with temperature ranges 28-44°F and 45-60°F.

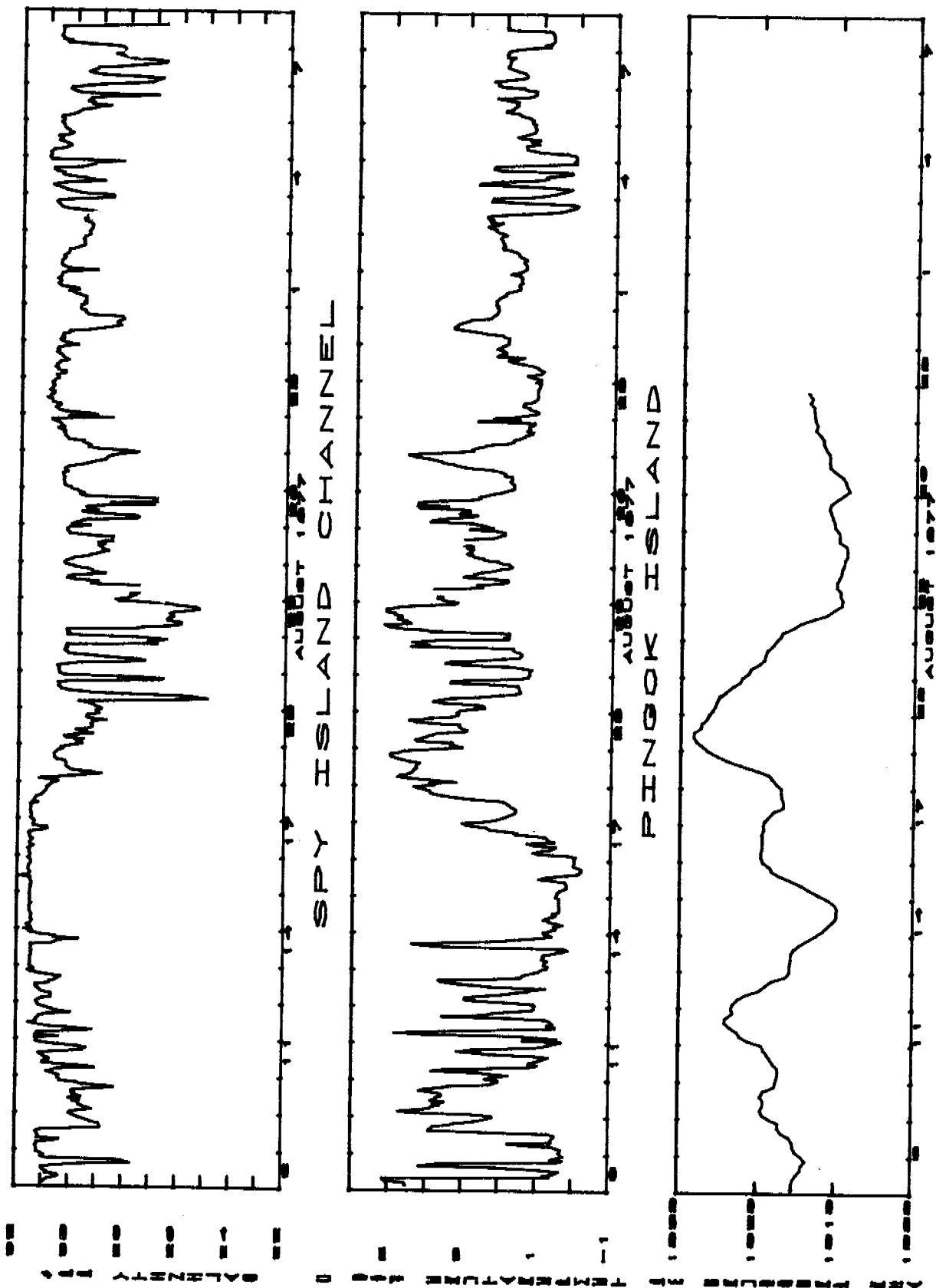


Figure 6. Temperature, salinity and barometric pressure for Spy Island channel and Pingok Island.

Analysis of the data from Spy Island channel has been complicated by the poor quality of much of the record. Figure 6 shows preliminary temperature and salinity data for Spy Island channel and barometric pressure for Pingok Island. Pressure data were kindly provided by Dr. Carsey (RU 519). The record shows generally saline (30-32 ppt) cold (1°C) water at the beginning of the record with an intrusion of warmer (up to 4°C), fresher (<29 ppt) appearing in pulses over a few days. Unfortunately, the current speed sensor was not operating but the prevailing weather at this time shows strong ENE winds with a maximum of 15 M/S on 10 August (fig. 7). It is unlikely to be Colville River water although such water can easily reach this channel. It seems more likely that the water comes from the east either from the Kuparuk or Sagavanirktok Rivers or a combination of both. This would account for the higher salinities than those observed at the ARCO causeway channel. It is also consistent with the lower salinities observed about 22 August when lower sea level, associated with higher barometric pressure, would be expected to push the lagoon waters towards the Spy Island channel. It is indeed unfortunate that the current data are not available to confirm this hypothesis.

Preliminary results for the drifters indicate a maximum recovery at 225 km distance over 5 days indicating a speed of about 50 cm/sec. This occurred during a period of winds up to 15 M/S. It is consistent with Barnes and Garlow's (1972) observation and suggests that spilled oil could spread along the north slope coast in as little as 3 to 5 days. These data apply to surface currents. It is believed that bottom currents are similar in magnitude. Since bottom currents are important to the movements of detritus, an attempt to measure these currents using bottom drifters will be made during the next field season.

VIII. CONCLUSIONS

It is reasonably well established that the lagoon waters are wind-driven and surge-driven. The preliminary conclusion can also be drawn that brackish, warm river water travels along the mainland coast in a generally westerly direction during the open-water season from August 1 to September 15. Obstructions such as the ARCO causeway are believed to impede this flow. Preliminary examination of data from a deeper channel between barrier islands suggests that the channel is important for passage of water into and out of the lagoon in response to surges. Surface drifters released before a storm suggest that oil spilled near Prudhoe Bay could reach the whole Beaufort Sea coast in less than one week.

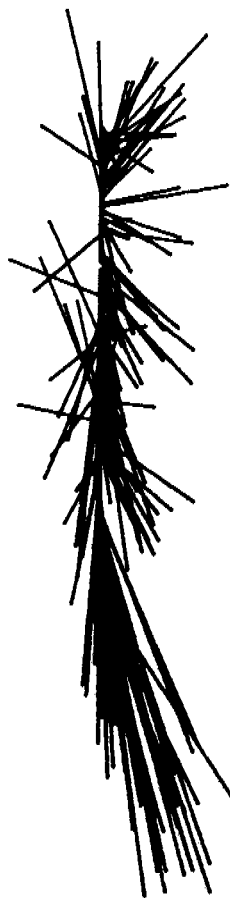
Data on flow through all major channels to Simpson Lagoon are needed to draw conclusions on flushing rates and surge-pumping of water through the lagoon. Data before and during the spring breakup in one or more major channels of the lagoon is very important to biological productivity. Attempts should be made to attain these data wherever possible.

The methods of data collection were generally successful. However, a reliable research vessel or platform will be required for deployment and recovery. The use of such a vessel is imperative if a larger field program, as we propose to launch, is to be successful. All the channels of the lagoon system need to be monitored during the field season. The instrument packages will be marked with pingers to aid in their recovery from a small boat.

PINGOK ISLAND

WIND SPEED AND DIRECTION

8 M/S



8 17 25 4

AUGUST 1977

Figure 7. Wind sock directions for Pingok Island.

The experimental design for the first season can be construed as successful. The instruments chosen yielded very useful data. Pingers and directional receivers should be used with future deployments to aid in relocation and recovery. The use of divers would further aid in instrument recovery and are essential for under-ice emplacement and recovery.

Tentative results from data analysis confirms the observation that the lagoon waters are wind and surge driven. Nearshore water appears to be generally warmer (up to 7°C) and fresher (<23 ppt) than the oceanic waters. The nearshore water appears to travel in a generally westerly direction. Surface drifters can average about 50 cm/sec. and cover the Beaufort Sea coastline in less than one week under strong easterly winds.

Preliminary analysis confirms model predictions that flushing times of the lagoons can be as small as a few days under strong winds. However more data from major channels are required to confirm this suggestion. Conditions during the ice breakup and peak runoff season are important for Geological processes and attempts to make measurements should be made.

It has been reasonably firmly established that physical oceanographic field work and modelling can form part of an ecological process study to the mutual benefit of all participants. This type of integrated study is both more rewarding and more demanding than traditional work performed along disciplinary lines.

REFERENCES

- Aagaard, K. 1977. "STD measurements in possible dispersal regions of the Beaufort Sea". Environmental Assessment of the Alaskan Continental Shelf, Annual Reports of Principal Investigators for the year ending March 1977, NOAA/ERL, Boulder, CO. Vol. XIV Transport, pp. 473-507.
- Aagaard, K. and Haugen, D. 1977. "Current measurements in possible dispersal regions of the Beaufort Sea". Environmental Assessment of the Alaskan Continental Shelf, Annual Reports of Principal Investigators for the year ending March 1977, NOAA/ERL, Boulder, CO. Vol. XIV, pp. 39-95.
- Alexander, V, Burrell, D.C., Chang, J, Cooney, R.T., Coulon, C., Crane, J.J., Dygas, J.A., Hall, G.E., Kogl, D., Mowatt, T.C., Naidu, A.S., Osterkamp, T.E., Schell, D.M., Seifert, R.D., Tucker, R.W., "Environmental studies of an arctic estuarine system". Final Report, EPA-66013-75-026, Environmental Protection Agency, Corvallis, OR. 536 pp.
- Barnes, P and Garlow, R. 1972. "Surface current observations - Beaufort Sea 1972". Open File Report 75-619, U. S. Geological Survey, Menlo Park, CA., 8 pp. plus map.
- Barnes, P., Reimnitz, E., Drake, D., Toimil, L., 1977. "Miscellaneous hydrologic and geologic observations on the inner Beaufort Sea shelf, Alaska". Open File Report 77-477, U.S. Geological Survey, Menlo Park, CA., 100 pp.
- Callaway, R.J. 1976. "Transport of pollutants in the vicinity of Prudhoe Bay". Environmental Assessment of the Alaskan Continental Shelf, Annual Reports of Principal Investigators for the year ending March 1976, NOAA/ERL, Boulder, CO. Vol. XI, pp 427-756.
- Carlson, R., Effects of seasonability and variability of stream flow on nearshore coastal areas. Environmental Assessment of the Alaskan Continental Shelf, Annual Reports of the Investigators for the year ending March 1977, NOAA/ERL, Boulder, Colorado, Vol. XIV, p. 96-250.
- Halpern, D., Pillsbury, R.D., Smith, R.L., 1974. "An intercomparison of three current meters operated in shall water". Deep-sea Research 21, pp. 489-497.
- Hunkins, K.H. 1962. "Waves on the arctic ocean". J. Geophysical Research 67(b), pp. 2477-2489.
- Hunkins, D.H. 1965. "Tide and storm surge observations in the Chukchi Sea". Limnol. and Oceanography 10(1), pp. 29-39.
- Kinney, P.J., Schell, D.M., Alexander, V.A., Burrell, D.C., Cooney, R.T., and Naidu, A.S., 1972. "Baseline data study of an Alaskan arctic aquatic environment". Report R72-3, Inst. of Marine Science, Univ. of Alaska, 275 pp.

- Matthews, J.B. 1970. "The tides at Point Barrow". Northern Engineer 2(2), pp. 12-13.
- Pollard, R.T. 1973. "Interpretation of near-surface current meter observations". Deep-sea Research 20, pp. 261-268.
- Reed, J.C. and Sater, J.E. (Eds). 1974. "The coast and shelf of the Beaufort Sea". Arctic Institute of North America, Arlington, VA, 750 pp.
- Saunders, P.M. 1976. "Near surface current measurements". Deep-sea Research 23, pp. 249-257.
- Wiseman, W.J., Jr., Coleman, J.M., Gregory, A., Hsu, S.A., Short, A.D., Suhayda, J.N., Walters, D.C., Jr., Wright, L.D. 1973. "Alaskan arctic coastal processes and morphology". Coastal Studies Inst.,

IX. SUMMARY OF 4TH QUARTER OPERATIONS

A. Ship or Laboratory Activities

1. No field activities.
5. Data analysis

Presentations of data from this study were prepared and made available at the Arctic Synthesis meeting at the Naval Arctic Research Laboratory 24-27 January, 1978.

Data were further prepared for review of the overall project (RU 467) at the BLM office in Anchorage, 7th March, 1978. A summary of probable impacts from pollution along the Arctic coast was prepared for the NOAA national pollution agency meeting in Anchorage 12-14 March, 1978.

Two current meter records have been given preliminary editing. Computer programs to accomplish this have been written or updated. Software for use on a Teletronix F051 is being developed to analyse these data. Plot routines for the Teletronix system are being assembled and tested. These have yield preliminary plots which are contained in the annual report. Tidal data are being edited and analysed. Software for data analysis is being prepared.

6. a. Editing of current meter data should be completed by the end of the next quarter. Poor record quality necessitated major revision of editing programs. Data presentation required the generation of a whole suite of software routines.

Plans are being finalized for the next field season. Additional instruments have been ordered to allow monitoring of all major channels to the lagoon. Long-life and long-range pingers and a directional receiver will be used to aid recovery of instruments without navigation aids from small vessels.

Because the flow through the channels to the lagoon under the ice during breakup is important to biological processes, it is planned to place an instrument array under the ice. This will involve cooperation with another project for logistics and the purchase of a limited amount of additional equipment. It is planned to recover data tapes after about one month's observations and just before the ice becomes unsafe to ensure that at least part of the critical season is covered. The instruments will be reset and recovered after breakup.

B. Problems Encountered/Recommended Changes

It is proposed to add a field program to attempt to recover water characteristics data from a major channel during the ice breakup and peak runoff season. These data are very valuable to other programs but have never been successfully recovered to data. Every effort will be made to maximize success. This work will utilize divers for instrument recovery and emplacement. The project will be carried out in conjunction with another OCSEAP project to aid in the logistics. The divers and equipment will be extremely useful in the recovery of other equipment later in the season.

Problems encountered during the previous field season have been addressed and steps taken to avoid similar problems during the coming field season.

ANNUAL REPORT

Contract: #03-5-022-56
Research Unit: #529
Task Order: #33
Reporting Period: 7/1/77 - 30/3/78
Number of Pages: 55

SEDIMENT CHARACTERISTICS, STABILITY, AND ORIGIN
OF THE BARRIER ISLAND-LAGOON COMPLEX,
NORTH ARCTIC ALASKA

A. S. Naidu
Principal Investigator
Assistant Professor in Marine Science

Institute of Marine Science
University of Alaska
Fairbanks, Alaska 99701

March 1978

TABLE OF CONTENTS

LIST OF TABLES

LIST OF FIGURES.

I. SUMMARY OF OBJECTIVES, CONCLUSIONS AND IMPLICATIONS WITH
RESPECT TO OCS OIL AND GAS DEVELOPMENT

II. INTRODUCTION
General Nature and Scope of Study.
Specific Objectives.
Relevance to Problems of Petroleum Development

III. CURRENT STATE OF KNOWLEDGE

IV. STUDY AREA

V. SOURCES, METHODS AND RATIONALE OF DATA COLLECTION.
Sediment Sample Collection
Samples and Sample Location During Phase I of Field Work
Samples and Sample Locations During Phase II of Field Work
Analytical Methods

VI. RESULTS.
Organic Carbon, Nitrogen and Carbonate Contents in
Sediments.
Heavy Metal Chemistry on Sediment Extracts
Radiocarbon Date on Pingok Island Peat
Coarse-Fraction Studies on Core Sections

VII. DISCUSSION
Simpson Lagoon Substrate Habitats.
Source and Depositional Sites of Fine-Grained Particles
in Simpson Lagoon.
Sediment Chemistry
Vanadium
Organic carbon, nitrogen and C/N ratios.
Stability and Growth Rate of the Pingok Island Barrier Spit.
Evolution of the Barrier Islands

VIII. CONCLUSIONS.

IX. NEEDS FOR FURTHER STUDY.

X. SUMMARY OF 4TH QUARTER OPERATIONS.
Ship or Laboratory Activities.

REFERENCES

LIST OF TABLES

- Table I. Locations of stations occupied during the Phase III 1977 Cruise of the USCGC *Glacier* in the Beaufort Sea. . .
- Table II. Locations of vibrocore sediment samples, provided by Drs. P. W. Barnes and E. Reimnitz of the U.S. Geological Survey.
- Table III. Statistical grain size parameters of the Simpson Lagoon bottom sediments.
- Table IV. Gravel-sand, silt and clay percents in Beaufort Sea sediments that were collected in summer 1977 onboard USCGC *Glacier*
- Table V. Weight percentages of gravel-sand, silt and clay in vibrocore samples collected from the Beaufort Sea coastal region.
- Table VI. Weighted peak area percentages of clay minerals in the less than two micron fraction of Simpson Lagoon sediments
- Table VII. Weight percent of carbonate, organic carbon, and nitrogen, and C/N ratios of surficial sediments of the Simpson Lagoon, Harrison Bay, Continental Shelf and deep-sea regions of the Beaufort Sea
- Table VIII. Average contents of organic carbon and nitrogen, and average C/N ratios of coastal tundra peat, and surficial sediments of the Simpson Lagoon, Harrison Bay, Beaufort Sea Continental Shelf and Canada Basin.
- Table IX. Vanadium concentrations in acetic acid - Hydroxylamine hydrochloride extracts of Simpson Lagoon sediments. . . .

LIST OF FIGURES

- Figure 1. Sample locations in Simpson Lagoon.
- Figure 2. Locations of stations occupied by USCGC *Glacier* in summer 1977 in the Beaufort Sea
- Figure 3. Locations of vibrocore sediment samples that have been collected by Drs. P. W. Barnes and E. Reimntz of the U.S. Geological Survey in 1976 and 1977
- Figure 4. Characteristics of substrate lithology in Simpson Lagoon.
- Figure 5. Sources of fine-grained (mud fraction) fluvial sediments based on detained clay mineral analysis . . .
- Figure 6. Organic carbon contents (dry weight percent) in substrate sediments in Simpson Lagoon

I. SUMMARY OF OBJECTIVES, CONCLUSIONS AND IMPLICATIONS
WITH RESPECT TO OCS OIL AND GAS DEVELOPMENT

The primary objective of this program is to understand sediment dynamics, to characterize benthic substrate habitats, and collect geochemical data on certain biologically "critical" chemical attributes of sediments (e.g. C, N and P) of the barrier island-lagoon complex of north arctic Alaska. Research will also be directed to assess the long-term directions and net volumes of alongshore transport of sandy sediments, as well as the stability and origin of the barrier islands along the Beaufort Sea coast. The additional objective of this program is to collect lithological and chemical baseline data from the contiguous area of the continental shelf of the Beaufort Sea. The chief purpose of this latter effort will be to fill in the data gaps relating to sediment dynamics and chemical baselines that exist on shelf sediments, principally between Barter Island and Demarcation Point.

In conclusion, the Simpson Lagoon may be delineated into two major substrate habitats. The narrow regions adjacent to the barrier islands and the mainland coastal plain are relatively sandy (>50% sand) than the central lagoon (>50% mud). These changes in lithology are presumably related to decrease in water turbulence toward the central lagoon. Detailed clay mineral studies substantiate our earlier interpretations that the net alongshore drift of clay-sized particles in the Alaskan Beaufort Sea coast is towards the west, and that the Simpson Lagoon is predominantly influenced by sediments from the Kuparuk River. A progressive decrease northward in the organic carbon contents in sediments have been observed in the Simpson Lagoon, and is attributed to a progressive northward decrease in the supply of organic matter from the mainland coastal plain.

Based on a Radiocarbon Date of a basal peat, the net long-term longitudinal and volumetric growth rates of the barrier spit associated with the west Pingok Island have been estimated to be 2 m/yr and 280 m³/yr, respectively. These rates are notably lower than those reported by earlier workers on the above spit on a one-season basis of their study. Further investigations are called for to check more precisely the spit growth rates on long-term and short-term basis.

Investigations on the stability and evolution of the barrier chain on the North Slope have been initiated. It would seem that there are two types of barrier islands. The tundra blanketed islands are most probably Pleistocene coastal highland remnants. In contrast, the sandy gravel islands as well as barrier spits associated with tundra islands most likely are resultants of contemporary wave/current constructive processes. Stratigraphic studies of short vibrocore samples from lagoons and islands, and sections of coastal bluffs presumably will offer us with clues on the paleogeographic history of the North Slope continental margin and, by implication, the series of geologic events that have led to the island evolution. On the basis of the knowledge thus gained we should be able to establish criteria that would help to predict impacts of oil-related activities on the stability of the North Slope barrier chain as well as the associated lagoon ecosystem. It is believed that the stability of the barrier island-lagoon ecosystem would be perturbed to some degree by altering sediment budgets in the Beaufort Sea coastal region from anthropogenic activities such as dredging, causeway construction, gravel and sand exploitation and building of artificial islands.

II. INTRODUCTION

General Nature and Scope of Study

This program (Research Unit 529) concerning sedimentological studies is part of a larger interdisciplinary research effort (RU 467), to study the physicochemical and biological processes operative in the barrier island-lagoon ecosystem of the Continental margin of the Alaskan Beaufort Sea. Additionally, the general scope of the overall program entails establishment of an ecosystem model which can be put to use in predicting possible impacts resulting from both petroleum exploration and exploitation activities in the barrier island-lagoon complex of the Beaufort Sea coast. Further details on the nature and scope of this study (RU 529) and associated investigations have been enumerated in the original proposal submitted by LGL Ltd-US, Inc. to the OCSEAP office in August 1977. Briefly, the scope of the sedimentological studies (RU 529) includes understanding of the sediment dynamics, delineating critical substrate habitats, monitoring the C, N and P contents in the substrate and suspensate sediments, alongshore sediment transport directions and evolution of the barrier island-lagoon complex.

Specific Objectives

The objectives of sedimentological research under RU 529 for FY 1978 has been enumerated in the original proposal, and are being repeated in this report for completeness purpose. The specific objectives are:

1. To continue gathering basic data on the grain size distributions of substrate sediments of the continental margin of the North Slope of Alaska, for the purpose of delineating critical benthic habitats and

understanding sediment dynamics. The area of study laterally extends between Harrison Bay in the west to Prudhoe Bay in the east, although more intense sampling of sediments will be confined to the Simpson Lagoon. Such regional extension will help establish a wider sampling base for a better understanding of sediment dynamics in the North Slope coastal region.

2. To complete background data collection on the contents of organic carbon and partitioning patterns of a selected group of biologically "critical" heavy metals (e.g. Fe, Mn, Cu, Ni, Zn, V, Cr and Co) in the lithogenous (crystal lattice-held) and nonlithogenous (readily mobilized phase) fractions of sediment samples from the lagoon and adjacent shelf region. In addition, Ba background concentrations in sediments will be analyzed, considering the importance of this element in the detection of pollution relating to discharge of drilling muds. This aspect of the study will fill in the small data gaps that exist on heavy metal backgrounds that have been collected by Dr. A. S. Naidu for the last 8 years in the Beaufort Sea and which could not be continued under an ongoing OCSEAP heavy metal program (RU 162). This portion of the study will be a complementary counterpart of the heavy metal geochemical investigations that are being pursued by Dr. Naidu's graduate student Mike Sweeney.
3. To monitor the concentrations of suspended particles in the Simpson lagoon. Additionally, the task calls for analyzing the concentrations of carbon and nitrogen in these particles as well as substrate sediments, for assessing the role of terrigenous particles as a source of nutrients to the biological community of the lagoon.

4. To define the net, long-term alongshore transport directions of gravel and sand-sized sediment particles, and to assess the volume of this alongshore drift on a long-term basis on the barrier islands.
 5. To define the mineral characteristics, source, migratory pathways, and depositional sites of clay-sized particles in the deltaic-continental shelf complex of the Alaskan Beaufort Sea.
 6. To elucidate the evolution and stability of the barrier islands in north arctic Alaska, via paleogeographic and geomorphic studies.
- The latter aspect of the investigation will be a complementary counterpart of Dr. Jan Cannon's geomorphological studies under the current OCSEAP RU 530.

Relevance to Problems of Petroleum Development

The exploitation of the petroleum reserves in the North Slope of Alaska has commenced with the recent flow of oil through the trans-Alaska pipeline. The present trend is towards exploration in the adjacent continental shelf of the Beaufort Sea. As a consequence of the OCS petroleum and gas development activities, the nearshore and the open shelf ecosystem of the Beaufort Sea is bound to be subjected to some degree of anthropogenic perturbations. The industrial activities which most likely will be introduced in this area include the construction of artificial islands and causeways for the use of drilling operations and docking facilities, dredging for maintaining navigation, and the exploitation of gravel and sand deposits from several possible sources as construction and fill materials. The impact of these activities, as well as others such as a blow-out, inadvertent discharge of cuttings and muds from drilling operations, and accidental oil

spills on the nearshore ecosystem are unknown. However, several attempts have been made postulating the possible socio-economic scenario and environmental perturbations that might result during the exploration and exploitation of petroleum reserves from the OCS lease areas of the Beaufort Sea (Arnold, 1975; Weller *et al.*, 1977). It is of interest to note that significant changes in the size distributions, benthic and chemical attributes of bottom sediments, as well as on the nearshore bathymetry have already been recognized in the vicinity of Prudhoe Bay, consequent to the building of the new ARCO causeway (Feder *et al.*, 1976; Barnes *et al.*, 1977; Grider *et al.*, 1977).

If the response of the physical environment and biological resources of the area to such changes can be properly assessed, or even predicted, it is quite possible that effective measures can be developed to protect or enhance existing resources. Few environmental studies of arctic barrier islands, lagoons, and the contiguous shallow marine regime of north arctic Alaska have been carried out, and none of these in detail. The existing data gaps for this area were identified in two OCSEAP meetings held at Barrow to synthesize the current state of knowledge on the Beaufort Sea. A few of the questions that were raised numerous times at these meetings related to the composition, stability and origin of the barrier island-lagoon complex, and the directions and amounts of sediment transport along the shore of north arctic Alaska. It was the unanimous opinion of the meeting participants that unless satisfactory answers are available to the above questions, it would not be possible to quantitatively assess - or even speculate - the possible impacts of industrial development on the Beaufort Sea nearshore ecosystem.

The aim of the sedimentological studies as embodied in RU 529 is to address to the data gaps enumerated above, and to understand contemporary sediment dynamics of the nearshore area of the Alaskan Beaufort Sea with special reference to the Barrier island-lagoon ecosystem of this coastal regime.

III. CURRENT STATE OF KNOWLEDGE

Within the past eight years or so, considerable research has been accomplished on the processes and products of sedimentation in the continental margin area of the North Slope of Alaska and the adjacent continental shelf of the Alaskan Beaufort Sea. A major portion of this research has been accomplished by scientists from three institutions, namely the University of Alaska (Institute of Marine Science), the U.S. Geological Survey (Marine Geology Branch, Menlo Park) and the Louisiana State University (Coastal Studies Institute). In a recent OCSEAP report, Naidu (in Burrell, 1977) has compiled an exhaustive bibliography of sedimentological and related investigations that have been carried out in the Alaskan Beaufort Sea shelf and coastal area. Barnes *et al.* (1977) have summarized miscellaneous hydrologic and geologic observations made by them on the inner Beaufort Sea shelf. The arctic coastal processes and morphology, as studied by the LSU Group, have been condensed in a report by Wiseman *et al.* (1973). More recent investigations supported by the BLM-NOAA environmental program in the Beaufort Sea coastal and shelf areas have been compiled in the 1977 OCSEAP Annual Report Volume.

IV. STUDY AREA

The region of our investigations is confined to the continental margin as well as the adjacent shallow continental shelf of the Alaskan Beaufort Sea. However, more intensive study, for barrier island-lagoon ecosystem modeling purpose, has been confined to the Simpson Lagoon area (Fig. 1). The latter region appears to be an adequately representative type area for ecosystem studies of island-lagoon complex along the Alaskan Beaufort Sea coast. In order to obtain a much wider data base and to assess terrigenous sources and transport directions of sediments along the Beaufort Sea coast, it has been imperative to extend sedimentological work to all the major river systems of the North Slope and to the entire barrier island chain extending from Point Barrow to Demarcation Point.

V. SOURCES, METHODS AND RATIONALE OF DATA COLLECTION

Sediment Sample Collection

To achieve the objectives of this study all sedimentological data already available for the Beaufort Sea shelf and the North Slope coastal area will be considered. Any new data on sediment samples that have been collected since the initiation of this project will be of additional use to us to fill in the data gaps and establishing broad data base for better understanding of sediment dynamics. The tasks accomplished by us during the 1977 field season were reported earlier (see Dr. Naidu's Field & Cruise report - Summer 1977), and are being repeated here for completeness.

The 1977 field season was started on 1 August, and came to a close on 6 September. Dr. A. S. Naidu and his graduate student Mr. Michael D. Sweeney spent between August 1 and 17 in the Simpson Lagoon area. The

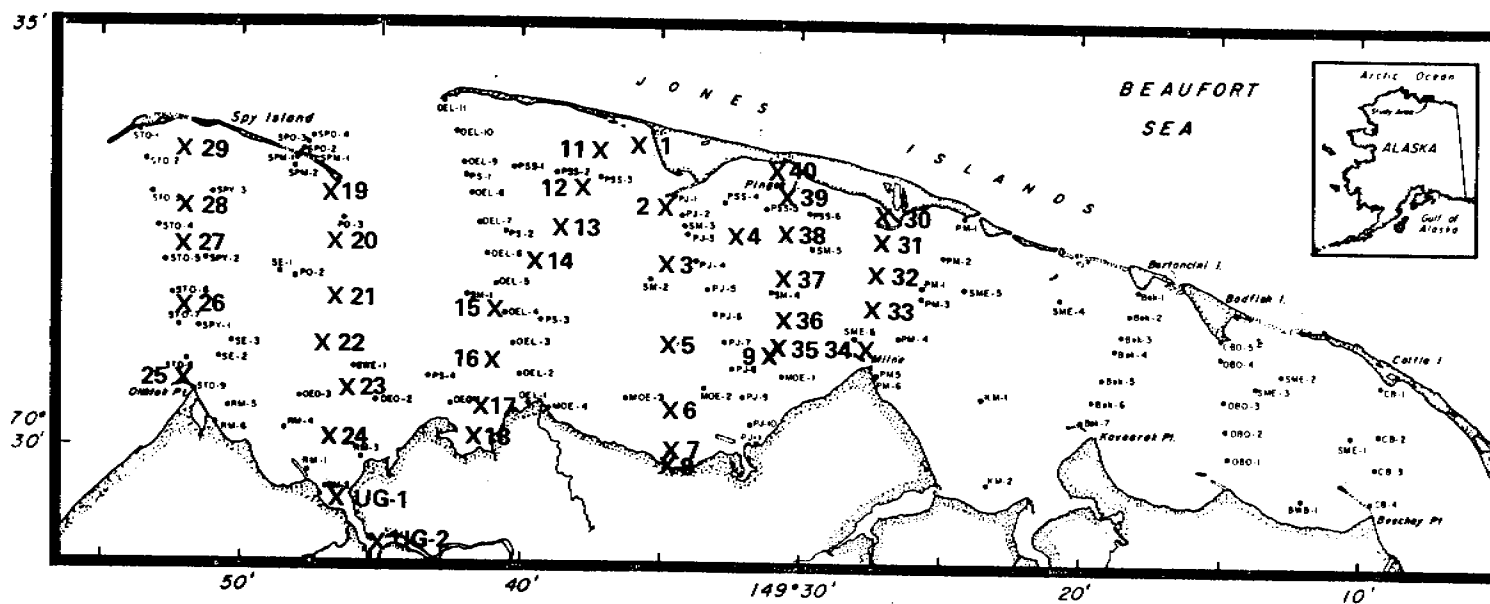


Figure 1. Sample locations in Simpson Lagoon. Locations depicted by heavy crosses indicate samples collected in Summer 1977. The remaining samples were collected by Tucker (1975) and size analysis data on them are already available.

primary task of undertaking this first phase of the 1977 summer field trip was to collect surficial sediment samples from the Simpson Lagoon and, using the Pingok Island as a base, to retrieve surficial sediment samples from all the large barrier islands of the North Slope of Alaska.

Between 17 August and 6 September (i.e., second phase of the 1977 summer field trip) both Dr. Naidu and Mr. Sweeney participated in the ice-breaker cruise of the USCGC *Glacier* in the Beaufort Sea, chiefly to fill in the sediment sample gaps existing in the shelf area extending between the Barter Island and the Demarcation Point.

Samples and Sample Location During Phase I of Field Work

Surficial sediment samples from bottom of the Simpson Lagoon were retrieved from 39 stations, stretching between the Oliktok Point and Milne Point. An Ekman grab sampler was used from a Zodiac to obtain these sediments. The sample locations were established along several N-S oriented transects (Fig. 1). In order to check precision of the sample collection, replicate (4 to 5) sediment samples were collected at several randomly situated stations in the Simpson Lagoon.

Using the NOAA helicopter, representative surficial gravel and sand samples were collected from the major barrier island beaches of the North Slope of Alaska. The islands sampled are the Thetis, Spy, Leavitt, Pingok, Bertoncini, Bodfish, Cottle, Long Island, Egg, Stump, Gull, Reindeer, Argo, Narwhal, Flaxman, Maguire, and Stockton. In addition to these samples, surficial deposits were also collected from the mainland beaches at six points between the Oliktok Point and the Point McIntyre. Also, fluvial bed load samples were obtained from the lower reaches of the

Ugnuravik, Sakonowyak, Putuligayuk, Kadleroshilik, Shaviovik and Canning rivers.

Samples and Sample Locations During Phase II of Field Work
(i.e., USCGC *Glacier* Cruise)

Our participation in the USCGC *Glacier* cruise was restricted to the third phase, which extended in the Beaufort Sea between 17 August and 6 September 1977. Prior to our joining the ship, 17 stations were already occupied. Splits of Smith-McIntyre grab sediment samples retrieved from 12 of these latter 17 stations by Mr. Gene Ruff of Oregon State University have been forwarded to us.

A total of 41 stations were occupied during the third phase of the cruise. Smith-McIntyre grab samples and short (5 to 112 cm long) gravity core samples were retrieved from 32 and 27 stations, respectively. In Table 1 are presented the locations from which the sediment and other samples were collected, and in Figure 2 are shown the locations of the sediment samples collected in the summer of 1977.

Onboard the *Glacier* interstitial water samples were expressed out from various representative horizons of five core samples. Rock gravel samples, recovered from whashing of fine sediments by Mr. Gene Ruff, were saved for our investigations.

The helicopters onboard the *Glacier* were used with great advantage for retrieving additional bed-load samples from the unsampled distributaries of the Canning and the Colville rivers. A LaFond-Dietz type snapper was hooked to the cable hoisting unit of the helicopter. Bed-loads from 4 stations of each of the two rivers were sampled. In addition water samples from two stations each from the Canning and Colville rivers

TABLE I

LOCATIONS OF STATIONS OCCUPIED DURING THE PHASE III 1977 CRUISE
OF USCGC *GLACIER* IN THE BEAUFORT SEA

Sediment samples are available from these stations

Station	Latitude N	Longitude W	Water Depth (m)
GLA 77-1	70°32'	147°29'	30
2	70°24'	146°32'	28
3	70°24'	146°32'	28
4	70°54'	146°30'	3841
5	72°56'	146°36'	3593
6	72°46'	146°22'	3566
7	72°54'	142°05'	3566
8	70°51'	141°43'	2048
9	70°42'	141°39'	640
10	78°40'	141°27'	678
11	70°31'	141°35'	406
12	69°50'	141°29'	22
13	70°05'	142°15'	35
14	70°35'	141°58'	35
15	70°11'	141°33'	54
16	70°28'	141°37'	118
17	70°19'	142°33'	51
18	70°37'	142°30'	80
19	70°38'	143°57'	146
20	70°32'	143°56'	57
21	70°21'	143°29'	41
22	70°14'	144°28'	32
23	70°45'	145°02'	109
24	70°36'	145°13'	51
25	70°23'	144°58'	38
26	70°10'	145°33'	20
27	70°38'	145°32'	54
28	70°49'	145°29'	101
29	71°02'	145°26'	521
30	71°12'	145°35'	1829
31	70°23'	146°26'	28
32	70°41'	146°31'	42
33	70°55'	146°35'	66
34	71°03'	146°19'	1646
35	70°54'	149°20'	30
36	70°44'	148°57'	22
37	71°04'	149°59'	28
38	71°06'	150°50'	19
39	71°10'	151°17'	19
40	71°10'	152°09'	24
41	71°11'	153°04'	19

Phase Three Oceanographic Stations

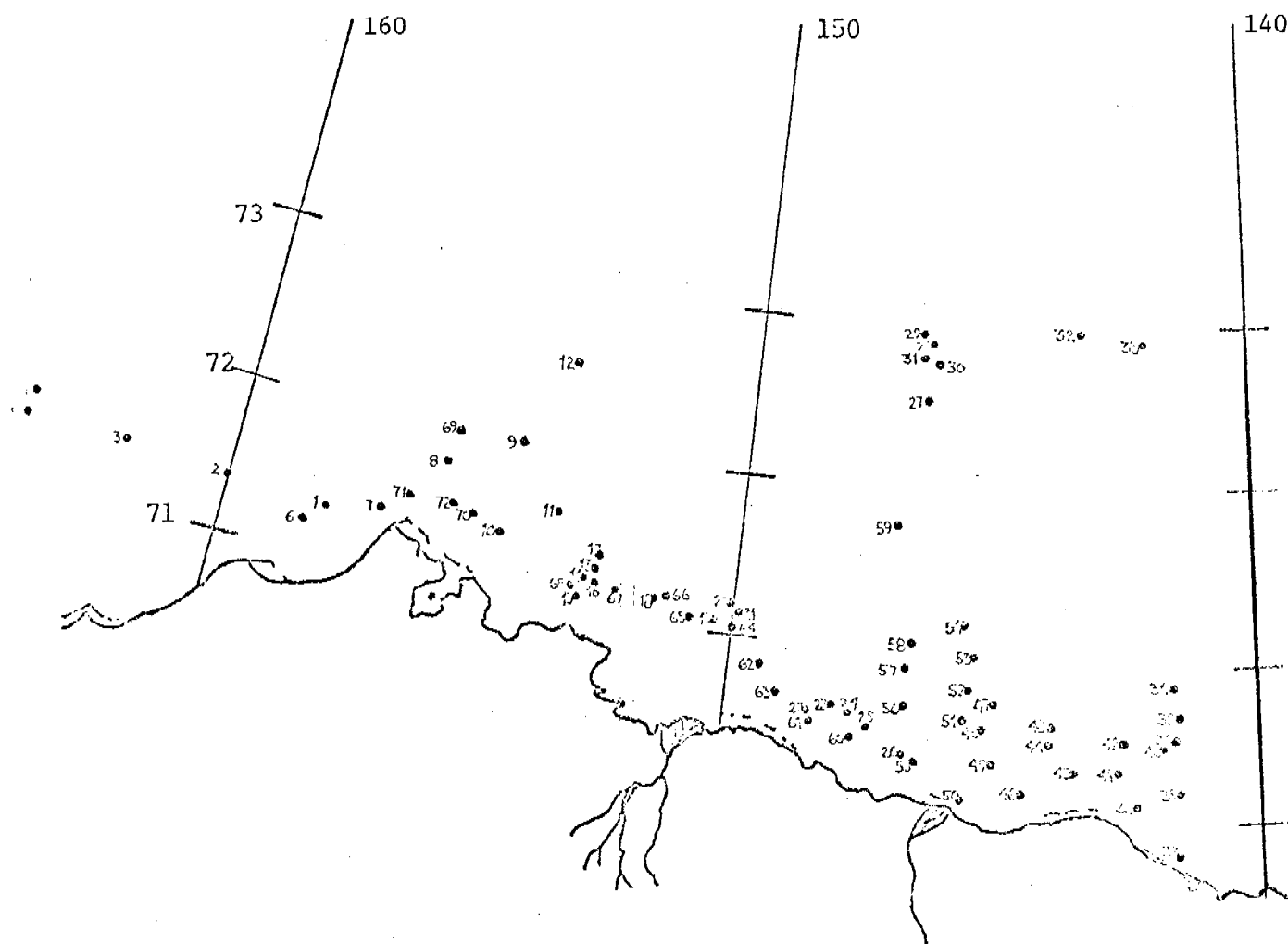


Figure 2. Locations of stations occupied by USCGC *Glacier* in Summer 1977 in the Beaufort Sea. The station location numbers correspond to those documented in the ship log book and are not the same as in Table I.

were collected for Dr. H. V. Weiss of the Naval Ocean System Center (San Diego) for Hg analysis.

About 80% of the field work originally projected by us for summer 1977 was successfully accomplished. A suite of sediment samples from an additional 20 stations along the continental margin area of the Alaskan Beaufort Sea were forwarded to us by Dr. D. G. Shaw for our studies.

To establish reliable basis for predicting impacts of oil-related activities on the stability of the barrier islands (and by implication the associated lagoon ecosystem), it would be necessary to understand the geological as well as hydrodynamic processes that have governed in the evolution of the islands. There are possibly more than one approach to elucidate the origin of the barrier islands. However, we have adopted the geological approach which includes recapitulation of the paleogeographic history of the barrier island-lagoon area, via stratigraphic studies of unconsolidated sediment core samples. To achieve this purpose, splits of core section from 17 vibrocore samples (of 2 m maximum length) were obtained from Drs. Peter W. Barnes and Erk Reimnitz of the U.S. Geological Survey (Menlo Park). Dr. Naidu and graduate student Mike Sweeney assisted in the description and splitting of the cores. Table II provides the locations of the cores and the depth of water at which they were collected. Nine of the cores were retrieved from the marine facies of the Colville Delta, 5 from the Simpson Lagoon and Gwydyr Bay area, whereas the rest of the three were sampled from the Prudhoe Bay-Stefannson Sound region (Fig. 3).

Analytical Methods

The laboratory methods that have been adopted to analyze sediment

TABLE II

LOCATIONS OF VIBROCORE SEDIMENT SAMPLES, PROVIDED BY
 DRS. P. W. BARNES AND E. REIMNITZ OF THE U.S.
 GEOLOGICAL SURVEY, FOR OUR STRATIGRAPHIC STUDIES

Vibrocore #	Latitude N	Longitude W	Water Depth (m)
PWB 75-1	70°19.0'	148°22.0'	3.0
PWB 75-3	70°24.0'	148°33.2'	1.5
PWB 75-9	70°20.1'	147°31.1'	6.5
PWB 75-13	70°44.8'	150°28.1'	19.0
PWB 75-14	70°41.5'	150°27.7'	15.0
PWB 75-15	70°37.0'	150°27.0'	12.5
PWB 75-16	70°36.3'	150°28.2'	11.5
PWB 75-17	70°34.0'	150°28.2'	8.5
PWB 75-18	70°33.3'	150°27.9'	3.3
PWB 75-19	70°33.6'	150°28.1'	2.0
PWB 75-20	70°32.7'	150°27.5'	1.5
PWB 75-23	70°29.5'	150°59.5'	1.0
PWB 75-24	70°33.2'	149°11.2'	7.5
VC 77-47	70°26.7'	148°57.0'	2.0
VC 77-48	70°30.42'	149°14.1'	2.5
VC 77-49	70°32.44'	149°30.7'	3.0
VC 77-50	70°30.7'	149°26.8'	14.0

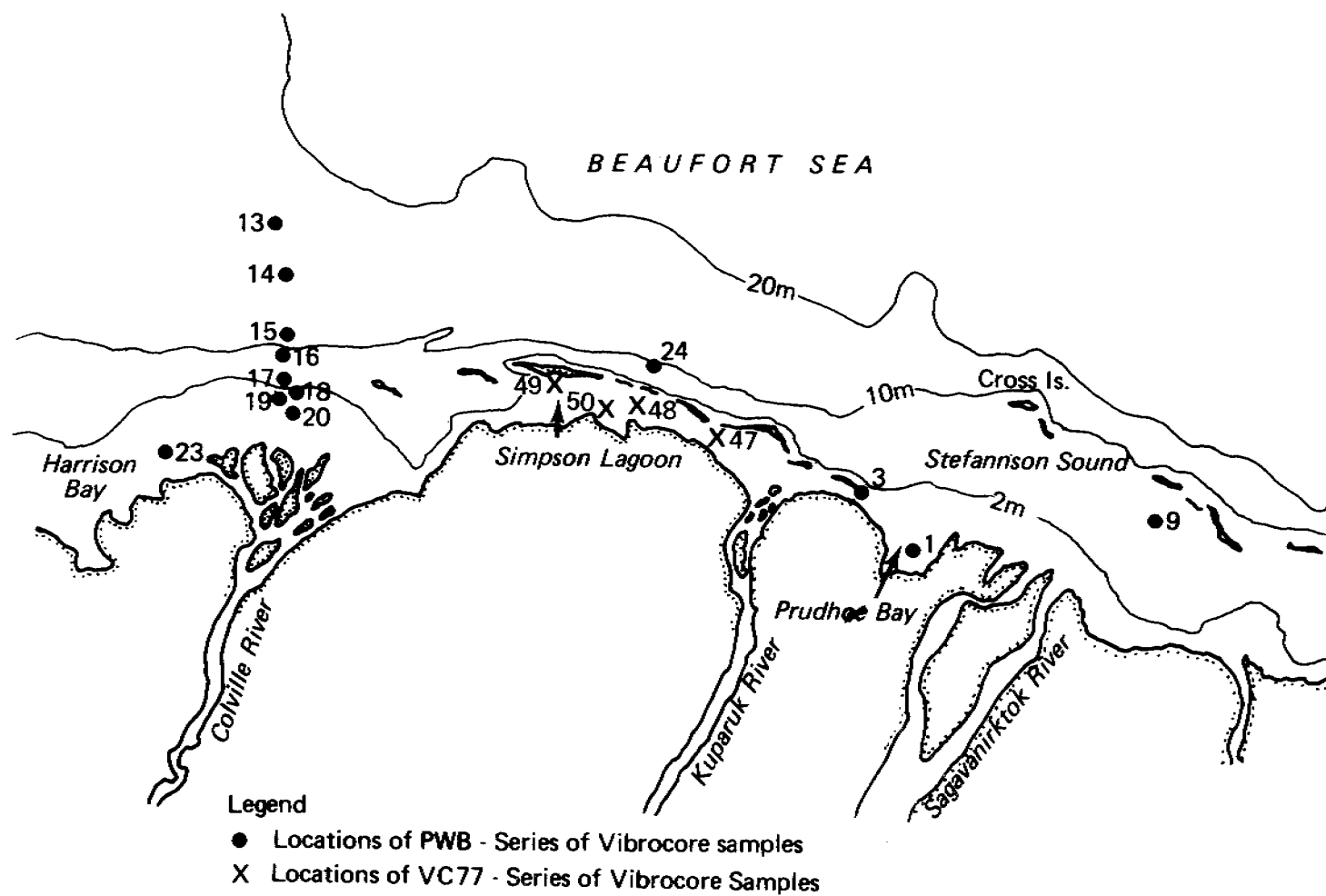


Figure 3. Locations of vibrocore sediment samples that have been collected by Drs. P. W. Barnes and E. Reimntz of the U.S. Geological Survey in 1976 and 1977. Splits of core samples from locations depicted by heavy dots have been provided to us for study.

samples have been elaborately described in the original proposal (OCSEAP RU 529-77). Briefly, the sediment size distribution analysis of the grab and core sections was performed by the usual sieve-pipetting method. Calculation of the conventional statistical grain size parameters was after Folk and Ward (1957), employing the University of Washington (Seattle) SEDAN program for Honeywell 66/40 computer system.

The clay mineral analysis of the $<2 \mu\text{m}$ of sediments was accomplished according to the methods elaborated by Naidu *et al.* (1971) and Naidu and Mowatt (1974) using X-ray diffraction technique. A variety of chemical and heat treatments was adopted to assist in the clay mineral identification. For heavy mineral studies, coarse, medium, and fine size grades of sands were considered. The heavy mineral crops in each of the size grades were separated in bromoform (sp. gr. 2.89). Coarse-fraction analyses (Shepard and Moore, 1954) on sections of vibrocore sediments are being conducted under a binocular microscope.

Sediment samples stored in a frozen state were thawed, dried, and two splits of them were taken; one for coarse and another for fine powdering. The coarse powder was subjected to Acetic acid-Hydroxylamine hydrochloride extraction (Chester and Hughes, 1967). Vanadium concentrations in these extracts were measured by neutron activation analysis, using the isotope dilution technique. The latter technique is a slightly modified version of the one developed by Weiss *et al.* (1977). The TRIGA nuclear reactor at the University of California, Irvine, was used for irradiation purpose. Dr. Naidu and Mike Sweeney participated in the analysis with technical help provided by Dr. H. V. Weiss of NOSC (San Diego).

Portions of the fine-ground gross sediment powders were taken for

analysis of organic carbon, total carbon and nitrogen contents. Organic carbon was calculated from the difference between total carbon and carbonate carbon. The total carbon was analyzed in a LECO, TC-12 automatic carbon determinator, whereas the carbonate carbon was determined manometrically (Hülsemann, 1969). Total nitrogen in the sediments were measured in a Coleman Model 29B nitrogen analyzer. Replicate analyses of nitrogen gave excellent precision.

In attempting to assess the longitudinal growth rate of the gravelly-sand barrier spit on the western Pingok Island, a basal peat formation lying under 84 cm of sand-gravel layer, at the proximal end of the spit, was sent to the Teledyne Isotopes, New Jersey for Radiocarbon Age determination.

VI. RESULTS

In Table III are included the statistical grain size parameters of the Simpson Lagoon bottom sediments. It would seem that most of the Simpson Lagoon sediments analyzed by us are constituted of poorly-sorted muddy sands or sandy muds with occasional gravel. Although there is a general covariance between the content of mud, water depth and distance from the shore, two narrow zones predominated by sand grade particles (>50% sands) can be delineated in the southern and northern portions of the Simpson Lagoon (Fig. 4). The entire lagoon width between the Oliktok Point and the western Spy Island is blanketed predominantly with mud.

In Table IV are included the percentages by weight of gravel-sand, silt and clay in the Beaufort Sea sediments collected between Barter Island and Demarcation Point. The Cambden Bay, the entire shelf region north of

TABLE III


STATISTICAL GRAIN SIZE PARAMETERS [AFTER FOLK AND WARD (1957)]
OF THE SIMPSON LAGOON BOTTOM SEDIMENTS


Sample #	Depth (m)	Gravel %	Sand %	Silt %	Clay %	Md	Mz	δ_I	Sk _I	K _G
SL877-1	1.5	7.28	89.05	3.21	0.47	1.78	1.50	1.62	-0.46	2.43
1A	1.5	0.0	83.21	15.95	1.84	2.25	2.73	1.21	0.63	2.85
1B	1.5	0.0	91.73	6.79	1.48	2.22	2.21	0.74	0.24	2.73
1C	1.5	0.0	89.77	8.44	1.79	2.26	2.27	0.89	0.31	3.19
1D	1.5	0.0	87.68	10.70	1.62	2.29	2.29	0.99	0.33	3.77
1E	1.5	0.0	86.34	12.54	1.12	2.28	2.33	0.91	0.34	2.99
2	1.8	0.0	95.79	3.44	0.78	1.74	1.72	0.62	-0.06	1.26
3	2.6	0.0	40.48	48.81	10.72	4.33	4.56	2.62	0.16	0.88
4	2.1	0.0	22.11	64.34	13.55	5.14	5.38	2.22	0.13	1.06
5A	1.8	0.0	34.35	60.38	5.27	4.25	4.52	1.57	0.35	1.09
5B	1.8	0.0	54.07	41.06	4.87	3.87	4.24	1.72	0.33	1.27
5C	1.8	0.0	48.60	45.91	5.49	4.04	4.44	1.70	0.38	1.20
5D	1.8	0.0	53.21	41.97	4.81	3.95	4.27	1.67	0.31	1.23
6	2.0	0.0	34.42	55.13	10.45	4.41	4.73	2.30	0.19	1.05
7	0.91	13.69	81.31	3.81	1.19	2.06	1.31	2.27	-0.52	2.08
8	0.3	3.46	75.52	18.47	2.56	2.54	2.63	2.17	-0.00	2.21
9	1.5	0.0	28.39	63.07	8.54	5.17	5.07	1.97	-0.00	0.92
11	2.1	0.0	17.78	74.50	7.72	4.51	5.02	1.83	0.33	1.46
12	2.1	0.0	34.44	59.22	6.34	4.22	4.58	1.82	0.28	1.59
13	2.4	0.0	8.25	85.82	5.93	4.71	5.08	1.32	0.44	1.58
14	2.3	0.0	41.05	51.03	7.92	4.25	4.41	2.16	0.15	1.11
15	1.8	2.39	79.31	14.14	4.16	2.17	2.77	2.24	0.39	2.83
17	0.6	9.25	71.17	15.96	3.63	2.05	2.14	2.73	0.00	2.57
18	0.5	0.0	59.91	33.95	6.13	3.32	4.04	1.99	0.52	1.02
19	3.2	0.0	71.59	24.84	3.57	2.63	3.16	1.34	0.76	1.23
20	2.6	0.0	88.77	9.32	1.91	2.53	2.60	0.75	0.60	5.01
21A	2.9	0.0	19.51	68.19	12.30	5.20	5.42	2.06	0.17	1.16
21B	2.9	0.0	18.53	69.62	11.85	5.27	5.40	2.04	0.13	1.10
21D	2.9	0.0	20.08	70.11	9.81	5.00	5.20	2.06	0.15	1.23
22	2.4	0.0	11.89	81.63	6.48	4.67	5.10	1.36	0.50	1.41

TABLE III. Continued

Sample #	Depth (m)	Gravel %	Sand %	Silt %	Clay %	Md	Mz	δ_I	Sk _I	K _G
SL877-23	2.4	0.0	27.00	66.73	6.27	4.81	4.61	2.09	-0.08	1.10
24	1.5	0.0	77.13	18.89	3.98	2.64	2.85	1.89	0.28	1.65
25A	2.6	0.0	67.93	27.84	4.23	2.32	3.29	2.10	0.65	1.03
25B	2.6	0.0	71.52	26.53	1.95	2.25	3.10	1.94	0.63	0.96
25C	2.6	0.0	66.19	28.96	4.85	2.46	3.39	2.14	0.63	0.88
26	3.0	0.0	21.95	72.18	5.88	4.37	4.96	1.51	0.52	1.40
27	3.0	0.0	22.06	71.43	6.51	4.38	4.77	1.64	0.41	1.32
28	2.7	0.0	16.20	73.48	10.32	4.84	5.38	1.68	0.45	1.00
29	2.4	0.0	25.22	64.85	9.93	4.66	4.96	2.22	0.17	1.17
30	1.1	0.0	80.40	18.60	0.99	1.92	2.41	1.47	0.41	1.28
31	2.6	0.0	12.17	74.30	13.52	5.62	5.85	1.86	0.15	0.99
32A	2.3	0.0	35.80	53.07	11.14	4.87	4.87	2.41	0.06	0.72
32B	2.3	0.0	18.58	66.01	15.41	6.19	5.67	2.40	-0.23	1.05
32C	2.3	0.0	29.51	60.20	10.29	5.15	5.09	2.33	-0.03	0.74
32D	2.3	0.0	36.73	53.07	10.20	4.90	4.82	2.38	0.04	0.69
33	2.1	0.0	54.33	37.55	8.11	2.73	3.92	2.34	0.68	0.66
34	1.5	0.0	98.95	0.76	0.30	1.96	2.01	0.60	0.12	1.00
35	2.0	0.0	48.46	43.19	8.35	4.15	4.40	1.96	0.28	0.78
36	2.1	0.0	42.71	47.80	9.49	4.40	4.63	2.27	0.22	0.77
37	2.3	0.0	40.88	51.69	7.43	4.35	4.43	2.10	0.15	0.85
38	2.3	0.0	28.98	59.63	11.39	4.74	4.83	2.45	0.09	0.93
39	2.0	0.0	39.80	48.30	11.89	4.39	4.51	2.75	0.06	0.85
40	1.5	0.0	76.98	19.22	3.80	2.44	2.84	1.79	0.41	2.03
UG1	0.8	0.0	62.75	31.74	5.51	3.25	3.56	1.98	0.31	1.52

Legend

 > 50% Sand

 > 50% Mud

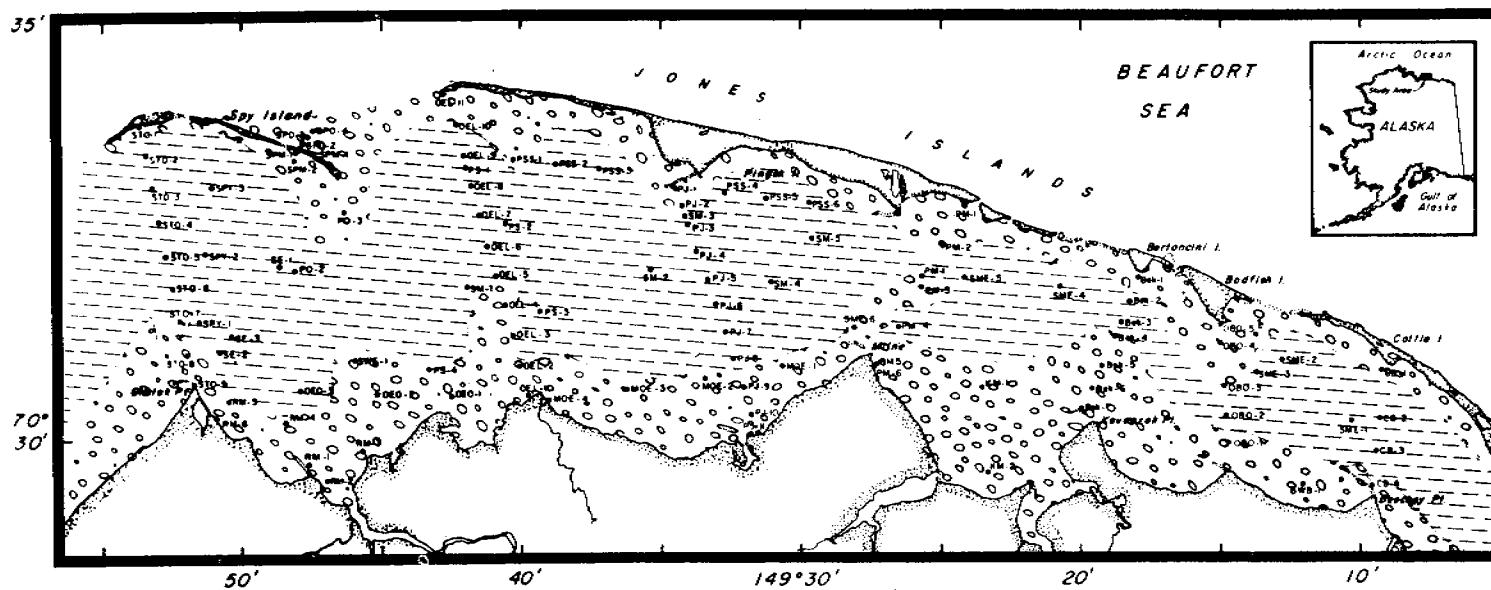


Figure 4. Characteristics of substrate lithology in Simpson Lagoon.

TABLE IV

GRAVEL-SAND, SILT AND CLAY PERCENTS IN BEAUFORT SEA SEDIMENTS THAT
WERE COLLECTED IN SUMMER 1977 ONBOARD USCGC *GLACIER*

Refer to Figure 2 and Table I for location of stations



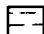
Station	Gravel-Sand	Silt	Clay
GLA77-5	-	30.39	65.83
6	0.25	18.07	81.67
7	0.08	16.79	83.13
8	1.15	23.06	75.78
9	1.65	26.91	71.43
10	0.81	43.40	55.80
11	1.48	33.31	65.20
12	34.26	34.56	31.18
15	13.75	21.99	64.26
16	11.73	46.94	41.30
18	54.24	16.57	29.19
19	12.23	32.92	54.86
20	55.28	16.64	28.08
21	1.30	34.45	64.25
23	18.97	30.56	50.47
24	52.63	18.35	29.02
25	34.41	27.98	37.61
26	52.47	27.44	20.09
27	42.28	20.46	37.26
28	30.06	27.05	42.89
29	2.05	28.46	69.49
31	23.93	41.19	34.88
35	12.18	36.40	51.42
40	6.30	54.37	39.34
42	8.81	38.77	52.42

Barter Island and the inner shelf east of the island at least up to the Demarcation Point are blanketed with sands and significant amount of gravel.

Results of our preliminary analysis of several sediment samples from the outer shelf region between Barter Island and Demarcation Point suggest that the bottom of that region is constituted predominantly of muddy deposits with relatively little sand and occasional gravel. Table V shows the gravel-sand, silt and clay percents of various continuous core sections from 8 vibrocores samples that have been analyzed to-date. The statistical grain size parameters on these core sections, as in case of the sediment grab samples collected between Barter Island and Demarcation Point, are in the process of being computed.

The clay mineral compositions in the less than 2 μm size of the Simpson Lagoon are included in Table VI. Results of the analysis on two Canning River samples show that the clay mineral assemblage consists predominantly of illite (82 and 84%) with lesser amounts of chlorite (13 to 15%), traces of kaolinite (3%) and no expandable phases. The Ugnuravik River clays have about 10% expandable components with 59% of illite, 20% of chlorite and 11% kaolinite. It would seem that in the Simpson Lagoon two broad clay mineral assemblages can be delineated. The western-most region of the Simpson Lagoon is characterized by relatively higher contents of expandable clay mineral components than the rest of the lagoon (Fig. 5). By way of comparison the adjacent Harrison Bay has significantly higher expandable phases (Naidu and Mowatt, 1974), than the Simpson Lagoon (Table VI). At this point in time the nature of the expandable phases - whether they are smectites or degraded illites - has not been resolved for all the clays analyzed.

LEGEND

-  Colville Influx, Almost Entirely (90%)
-  Predominantly Colville (85%); with minor influx of Kuparuk (10%) & Sagavanirktok Rivers (5%)
-  Predominantly Kuparuk River (80%) with minor Sagavanirktok River Influx (15%) & Colville River (5% or less).

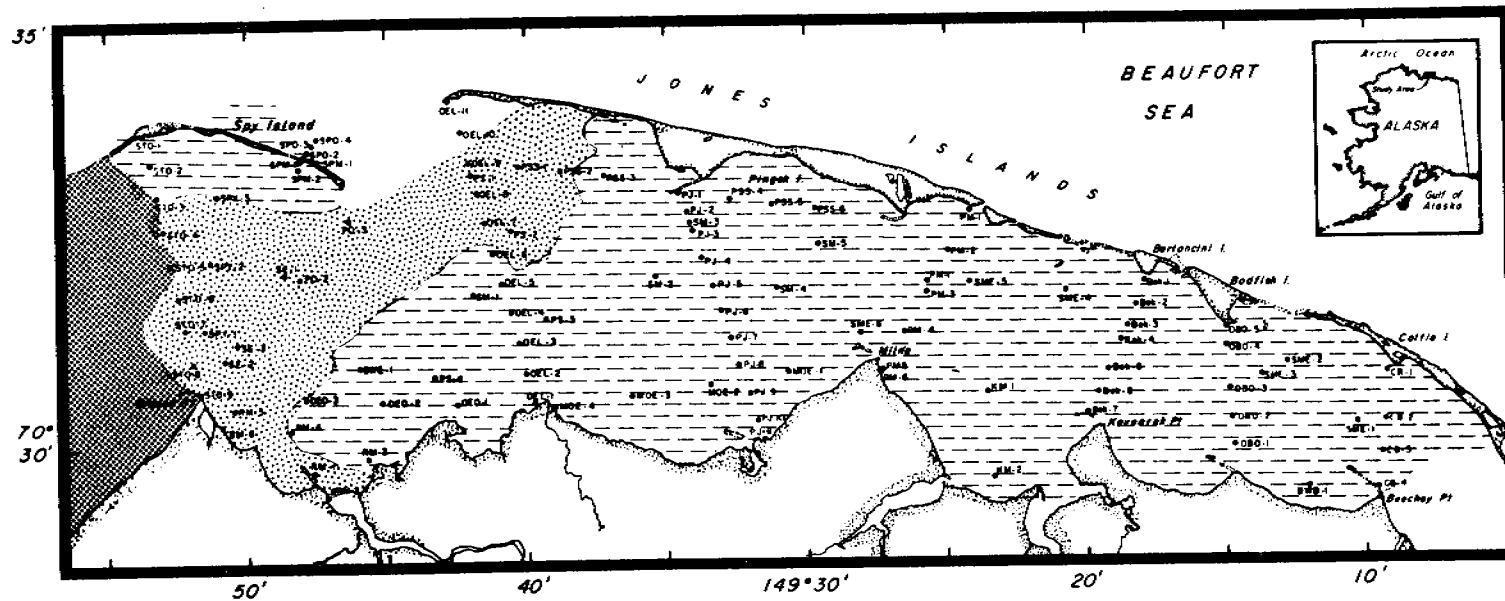


Figure 5. Sources of fine-grained (mud fraction) fluvial sediments* based on detailed clay mineral analysis.

* Sources of mud from coastal bluffs and barriers not considered.

TABLE V

WEIGHT PERCENTAGES OF GRAVEL-SAND, SILT AND CLAY IN VIBROCORE
SAMPLES COLLECTED FROM THE BEAUFORT SEA COASTAL REGION

Refer to Table II and Figure 3 for core locations.
For sections left blank, no data were available
at the time this report was prepared

Vibrocore #	Core Section (cm)	Gravel + Sand	Silt	Clay
PWB 75-1	0-10			
	10-20	2.8	69.8	27.4
	20-30			
	30-40			
	40-50			
	50-60	2.3	71.0	26.7
	60-70	2.3	73.1	24.6
	70-80	1.5	76.3	22.2
	80-90			
	90-100			
	100-107	2.6	76.4	21.0
PWB 75-13	0-10	67.5	13.4	19.1
	10-20	80.5	8.9	10.6
	20-30			
	30-40	5.5	36.6	57.9
	40-50	20.8	39.8	39.4
	50-60	47.8	22.5	29.7
	60-65	54.0	20.1	25.9
PWB 75-14	0-10			
	10-20			
	20-30			
	30-40			
	40-50	1.1	44.3	54.6
	50-60			
	60-65	0.5	45.4	54.1
PWB 75-16	0-10	23.4	43.8	32.8
	10-20	16.3	52.1	31.6
	20-30	10.0	46.7	43.3
	30-40	14.2	46.3	39.5
	40-50	15.1	47.9	37.0
	50-60	34.9	39.1	26.0
	60-70	14.8	48.2	37.0
	70-80	13.3	51.7	35.0
	80-90	15.3	43.7	41.0
	90-100	24.2	42.2	33.6
	100-103	22.3	45.5	32.2

TABLE V. Continued

Vibrocore #	Core Section (cm)	Gravel + Sand	Silt	Clay
PWB 75-18	0-10	27.4	50.4	22.2
	10-20	64.8	24.4	10.8
	20-30	14.0	65.0	21.0
	30-40	38.5	40.0	21.5
	40-50	50.1	32.1	17.8
	50-60	27.9	52.4	17.9
	60-70	8.1	66.9	25.0
	70-80	20.4	57.9	21.7
	80-90	2.6	61.6	35.8
	90-100	13.0	51.3	35.7
	100-110	13.5	60.3	26.2
	110-120	16.7	58.0	25.3
	120-130	43.1	43.1	13.8
	130-140	21.9	58.6	19.5
	140-150	6.1	61.7	32.2
	150-160	7.8	63.2	29.0
	160-170	11.0	61.0	28.0
170-180	8.3	64.6	27.1	
180-190	4.4	67.0	28.6	
PWB 75-19	0-10	70.9	19.7	9.4
	10-20	89.8	5.3	4.9
	20-30	85.7	8.3	6.0
	30-40	67.2	23.2	9.6
	40-50	35.5	42.9	21.6
	50-60	72.1	20.5	7.4
	60-70	63.3	27.8	8.9
	70-80	64.4	26.5	9.1
	80-90	13.7	69.4	16.9
	90-100	74.1	16.4	9.5
	100-105	81.3	12.5	6.2
PWB 75-20	0-5	76.0	16.4	7.6
	5-10	66.8	26.3	6.9
	10-15	75.8	17.1	7.1
	15-20	33.2	51.6	15.2
	20-25	51.8	34.8	13.4
	25-30	16.9	63.9	19.2
	30-35	21.9	59.4	18.7
	35-40	52.3	34.7	13.0
	40-45	52.1	33.4	14.5
	45-50	33.0	50.6	16.4
	50-55	32.0	50.0	18.0
	55-60	16.2	68.6	15.2
	60-65	70.9	19.8	9.3

TABLE V. Continued

Vibrocore #	Core Section (cm)	Gravel + Sand	Silt	Clay
PWB 75-20 (cont'd)	65-70	35.2	41.9	22.9
	70-75	46.1	35.1	18.8
	75-80	60.6	26.3	13.1
	80-85	51.7	35.0	13.4
	85-90	46.6	38.6	14.8
	90-95	53.1	34.9	12.0
	95-100	26.8	53.3	19.9
	100-105	19.4	57.6	23.0
	105-110	33.2	47.9	18.8
	110-115	47.0	36.6	16.4
	115-120	45.4	43.7	10.9
	120-125	65.8	24.0	10.2
	PWB 75-23	0-10	32.9	47.1
10-20				
20-30		18.2	56.7	25.1
30-40		59.4	28.2	12.4
40-50		18.8	59.1	22.1
50-60				
60-70				
70-80		38.4	38.7	22.9
80-90				
90-100				
100-110		15.5	58.4	26.1
110-120				
120-130		28.2	51.3	20.5
130-140				
140-150	27.3	43.1	29.6	

TABLE VI

WEIGHTED PEAK AREA PERCENTAGES (AFTER BISCAYE, 1965) OF CLAY
MINERALS IN THE LESS THAN 2 MICRON FRACTION OF SIMPSON LAGOON SEDIMENTS

Sample No.	Expandable	Illite	Kaolinite	Chlorite
SL877-1	trace	71	10	19
SL877-2	5	67	11	17
SL877-3	9	55	NR	NR
SL877-4	4	65	9	21
SL877-5	5	66	11	18
SL877-6	8	59	10	23
SL877-7	2	71	10	17
SL877-8	2	64	12	22
SL877-9	4	63	12	21
SL877-11	10	59	12	19
SL877-12	7	63	10	20
SL877-13	14	54	10	22
SL877-14	3	66	12	19
SL877-15	5	62	12	20
SL877-17	2	65	14	19
SL977-19	6	64	10	20
SL877-20	10	57	12	21
SL877-21	13	56	9	22
SL877-22	10	60	NR	NR
SL877-23	3	66	11	20
SL877-24	6	63	11	20
SL877-25	11	60	NR	NR
SL877-26	13	54	12	21
SL877-27	14	53	12	21
SL877-28	7	57	13	23
SL877-29	5	68	11	16
SL877-31	8	59	10	23
SL877-32	4	70	7	19
SL877-33	3	62	12	23
SL877-34	trace	64	13	23
SL877-35	12	56	11	21
SL877-36	10	54	12	24
SL877-38	9	56	12	23

NR = The kaolinite and chlorite percents have not been resolved as yet.

The group of sediments collected from the open marine region between Barter Island and Demarcation Point (Table I) have been prepared for X-ray diffraction analyses. Clay (<2 μm) from a sample of mud collected over a grounded iceberg situated off the Sagavanirktok River and at 70°32'N and 147°46'W, was subjected to clay mineral analysis. This ice-rafted clay was composed of 70% illite, 11% kaolinite, 20% chlorite and traces (<2%) of expandable components.

Heavy and light minerals from various size grades of sands of a number of barrier islands and North Slope rivers have been separated in bromoform and are in the process of being weighed and percentages computed.

Organic Carbon, Nitrogen and Carbonate Contents in Sediments

In Table VII are shown the percentages on dry weight basis of organic carbon, total nitrogen and carbonate contents, as well as the organic carbon/nitrogen ratios (C/N) in gross sediments of the Simpson Lagoon. For comparison purposes, above values for the Harrison Bay, continental shelf and abyssal region of the Beaufort Sea are also included in Table VII. The averages of organic carbon, nitrogen, carbonate contents and organic carbon/nitrogen ratios for the above environments and tundra peat of North Slope coastal bluffs are summarized in Table VIII. The organic carbon contents of sediments when plotted on a map of the Simpson Lagoon (Fig. 6), show three broad distributional patterns. In the southern portion of the lagoon and spreading across the lagoon off the Milne Point, the organic carbon is relatively higher (>2%) than in the central lagoon (1-2%) and the northern lagoon (<1%). In contrast to the above, neither

Organic Carbon Contents (wt. %)

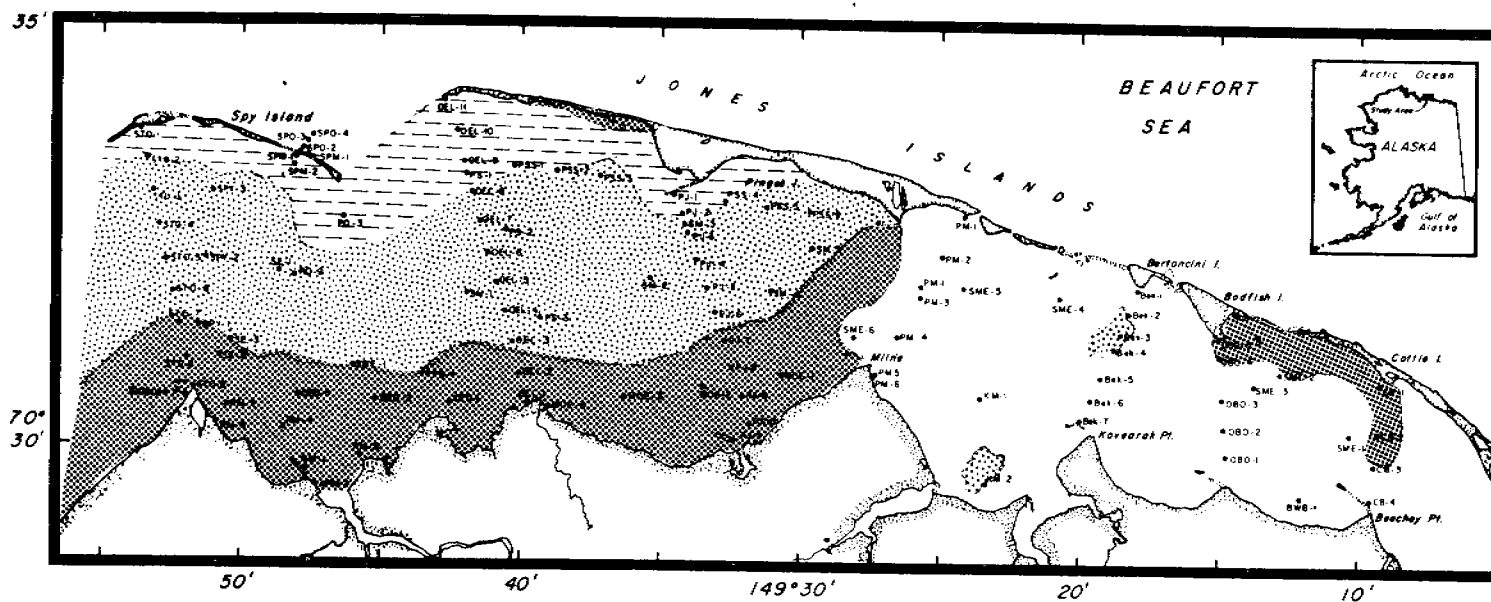
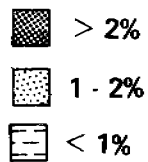


Figure 6. Organic carbon contents (dry weight percent) in substrate sediments in Simpson Lagoon.

TABLE VII

WEIGHT % OF CARBONATE, ORGANIC CARBON, AND NITROGEN, AND C/N RATIOS OF SURFICIAL SEDIMENTS OF THE SIMPSON LAGOON, HARRISON BAY, CONTINENTAL SHELF AND DEEP-SEA REGIONS OF THE BEAUFORT SEA

Sample No.	Depositional Environment	Depth (m)	CO ₃ ⁼	Corg.	N	C/N
AJT71-38	Lagoon	1.5	10.0	1.51	0.129	12
AJT71-39	Lagoon	2.1	8.5	0.53	0.059	9
SL877-1	Lagoon	1.5	1.95	0.45	NA	-
SL877-2	Lagoon	1.8	1.33	0.16	0.025	6
SL877-3	Lagoon	2.6	9.49	1.13	0.114	10
SL877-4	Lagoon	2.1	8.35	1.74	0.127	14
SL877-5	Lagoon	1.8	9.67	0.89	0.055	16
SL877-6	Lagoon	2.0	9.02	2.69	0.156	17
SL877-7	Lagoon	0.9	5.84	0.27	0.019	14
SL877-8	Lagoon	0.3	5.34	1.83	0.094	20
SL877-9	Lagoon	1.5	9.17	2.19	0.156	14
SL877-11	Lagoon	2.1	10.84	0.45	0.100	5
SL877-12	Lagoon	2.1	9.76	1.65	0.094	18
SL877-13	Lagoon	2.4	10.62	1.10	0.088	13
SL877-14	Lagoon	2.3	7.82	1.40	0.089	16
SL877-15	Lagoon	1.8	2.64	0.30	0.0835	4
SL877-17	Lagoon	0.6	7.35	0.59	0.098	6
SL877-18	Lagoon	0.46	3.82	3.12	0.201	16
SL877-19	Lagoon	3.2	5.98	0.42	0.023	18
SL877-20	Lagoon	2.6	1.91	0.35	0.026	13
SL877-21	Lagoon	2.9	9.63	1.47	0.103	14
SL877-22	Lagoon	2.4	10.64	1.59	0.090	18
SL877-23	Lagoon	2.4	9.24	2.18	0.125	17
SL877-24	Lagoon	1.5	4.53	0.83	0.063	13
SL877-25	Lagoon	2.6	4.77	1.99	0.093	21
SL877-26	Lagoon	2.9	9.56	1.14	0.097	12
SL877-27	Lagoon	3.04	10.47	1.13	NS	-
SL877-28	Lagoon	2.7	11.24	1.23	0.089	14
SL877-29	Lagoon	2.4	10.45	0.70	0.093	8
SL877-30	Lagoon	1.0	3.14	0.32	0.025	13
SL877-31	Lagoon	2.6	11.49	1.65	NA	-
SL877-32	Lagoon	2.3	12.07	1.56	0.091	17
SL877-33	Lagoon	2.1	7.25	1.12	NA	-
SL877-34	Lagoon	1.5	3.23	0.09	0.013	7
SL877-35	Lagoon	2.0	9.72	1.66	NA	-
SL877-36	Lagoon	2.1	8.69	1.47	0.087	12
SL877-37	Lagoon	2.3	8.44	1.11	NA	-
SL877-38	Lagoon	2.3	8.93	1.00	0.100	10
SL877-39	Lagoon	2.0	8.02	1.36	NA	-
SL877-40	Lagoon	1.5	3.64	0.46	0.044	11
HB-1	Bay	3.2	2.4	1.13	0.091	12
HB-3	Bay	3.0	0.9	0.17	0.014	12
HB-4	Bay	3.0	2.4	1.40	0.127	11
HB-5	Bay	3.0	1.2	0.15	0.067	17
HB-6	Bay	2.8	3.1	1.15	0.067	17

TABLE VII. Continued

Sample No.	Depositional Environment	Depth (m)	CO ₃ ⁼	Corg.	N	C/N
HB-7	Bay	2.3	9.6	0.80	0.074	11
UG-1	Fluvial	0.8	4.13	4.40	0.238	19
POND-1	Pond	-	3.36	NA	1.150	-
BSS-88	Shelf	30	1.75	0.80	0.091	9
BSS-83	Shelf	50	3.60	0.96	0.119	8
BSS-62	Shelf	44	8.75	0.63	0.076	8
GLA71-1	Shelf	26	5.29	0.89	0.080	11
GLA71-3	Shelf	45	6.60	0.98	0.062	16
GLA71-12	Shelf	26	6.29	0.64	0.085	8
GLA71-23	Shelf	27	10.56	NA	0.078	-
GLA71-25	Shelf	26	9.81	NA	0.093	-
GLA71-27	Shelf	47	7.74	NA	0.048	-
GLA71-44	Shelf	48	7.60	NA	0.071	-
GLA71-63	Shelf	26	6.49	NA	0.090	-
GLA71-71	Shelf	21	6.61	0.81	0.073	11
GLA71-72	Shelf	47	2.98	0.87	0.1094	9
GLA71-78	Shelf	29	3.36	1.12	0.132	9
GLA71-80	Shelf	33	2.54	0.91	0.100	9
T3-1	Abyss	3637	4.2	0.74	0.130	6
T3-2	Abyss	3650	3.1	0.71	0.108	7
T3-3	Abyss	3795	0.6	0.73	0.218	3
T3-4	Abyss	3792	2.9	0.74	0.240	3
T3-5	Abyss	3761	1.2	0.75	NA	-
T3-6	Abyss	3827	1.1	0.79	0.346	2
T3-7	Abyss	3830	0.9	0.77	0.347	2
T3-8	Abyss	3833	1.2	1.16	0.347	1
T3-9	Abyss	3860	5.3	0.39	0.152	3
T3-10	Abyss	1705	8.0	0.39	0.111	4
T3-11	Abyss	1106	4.1	0.47	0.096	5
T3-12	Abyss	3835	0.8	0.79	0.087	9

NA=Not analyzed as yet

TABLE VIII

AVERAGE CONTENTS (BY DRY WT. %) OF ORGANIC CARBON AND NITROGEN,
AND AVERAGE C/N RATIOS OF COASTAL TUNDRA PEAT, AND
SURFICIAL SEDIMENTS OF THE SIMPSON LAGOON,
HARRISON BAY, BEAUFORT SEA CONTINENTAL SHELF
AND CANADA BASIN

<u>Environment</u>	<u>Organic Carbon</u>	<u>Nitrogen</u>	<u>C/N Ratios</u>
Harrison Bay	0.80	0.06	13
Simpson Lagoon	1.17	0.08	15
Beaufort Sea Shelf (21 m to 50 m)	0.86	0.09	10
Canada Basin (1160 to 3835 m)	0.70	0.19	4
Coastal Tundra Peat	-	-	19*

*Average of C/N ratios of several samples provided by Dr. D. Schell
(personal communication).

neither nitrogen contents nor C/N ratios show any definite areal distributional pattern in the lagoon. It is of interest to note that more than two thirds of the analyzed lagoonal sediments have relatively higher C/N ratios (Tables VII and VIII) than the C/N ratios (i.e. between 8 and 12) generally reported for deltaic and shallow marine sediments of the world. As suggested by the data summarized in Table VIII there seem to be a progressive decrease in the C/N ratios of sediments away from the north Alaskan continent and towards deeper waters. Further, the C/N ratios of a number of sediment samples in the Simpson Lagoon do not markedly differ from those of the tundra peat in the adjacent coastal bluffs (Table VIII), although the averages of the C/N ratios are significantly different.

Heavy Metal Chemistry on Sediment Extracts

At this point in time only vanadium concentrations have been analyzed on the Acetic acid-Hydroxylamine hydrochloride extracts of the Simpson Lagoon sediments. Table IX shows the concentrations of vanadium in the extracts. On an average the content of vanadium in the acid extracts of lagoon sediments is 5 $\mu\text{g/g}$ which is quite comparative to the average of 8 $\mu\text{g/g}$ of vanadium obtained in similar extracts on adjacent continental shelf sediments of the Beaufort Sea by Naidu (in Burrell, 1977).

Radiocarbon Date on Pingok Island Peat

A preliminary radiocarbon date on a sample of basal peat, which was gathered from under 84 cm of sand-gravel overburden on the proximal end of the barrier spit in the western end of the Pingok Island, is 2600 \pm 10% years B.P.

TABLE IX

VANADIUM CONCENTRATIONS ($\mu\text{g/g}$) IN ACETIC ACID - HYDROXYLAMINE
 HYDROCHLORIDE EXTRACTS (CHESTER AND HUGHES, 1967) OF SIMPSON LAGOON SEDIMENTS

<u>Sample No.</u>	<u>Vanadium ($\mu\text{g/g}$)</u>	<u>Sample No.</u>	<u>Vanadium ($\mu\text{g/g}$)</u>
SL877-1D	3.1	SL877-18	7.5
SL877-2	3.2	SL877-19 (1)	1.9
SL877-3	6.1	SL877-19 (2)	1.9
SL877-4	7.2	SL877-21D	7.0
SL877-4A	7.8	SL877-22	5.4
SL877-5A	4.9	SL877-24	4.0
SL877-5B	4.5	SL877-25C	4.3
SL877-5C	5.1	SL877-27	6.3
SL877-6	6.2	SL877-28	6.3
SL877-8	2.6	SL877-29	7.4
SL877-8A	2.4	SL877-30	1.8
SL877-9	5.1	SL877-31	7.5
SL877-11	6.5	SL877-32B	4.8
SL877-11A	6.1	SL877-33	4.3
SL877-13	5.7	SL877-37	5.1
SL877-14(1)	5.8	SL877-38	9.0
SL877-14(a)	4.9	SL877-40	3.6
SL877-14(3)	4.3	SL877-40(2)	2.5
SL877-15	5.0	Ugnuravik R.	3.8
SL877-17	4.0		

Coarse-Fraction Studies on Core Sections

Coarse-fractions (>0.062 mm size grade) from about 60-70 sections of 8 vibrocores have been separated for detailed study under the binocular microscope. Results of these studies will provide with criteria to recapitulate the recent paleogeography of the North Slope continental margin and by implication evolution of the barrier island. A preliminary study of the coarse fraction in a basal 25-cm thick basal peaty layer (under 125 cm of overburden) in Vibrocore sample No. VC-49 (see Table II and Fig. 3 for core location) has been accomplished. It is interesting to note that both fresh-water and marine faunal components have been identified in the above sample. However, the fresh-water components - represented generally by the snail *Valvata* sp. and bivalve *Pisidium* sp. - are overwhelmed by marine populations constituted of numerous foraminiferas and ostracods, and two cyrtodaria kurriana. Almost all of the snails were either fragmented or extremely friable; one of the cyrtodarias was in a perfect state of preservation.

The structure and lithology of the more intensively studied vibrocore (VC77-49) show notable stratigraphic variations, as exhibited in the sectioned core length, particularly in the resin-mounted half. The top 40-cm of the core consists of laminated mud, 40-70 section of partly bioturbated sandy mud, 70-95 cm of clean (oxidized ?) cross-bedded sand, 95-125 cm of greyish-black (reduced ?) cross-bedded sand, and a basal 25-cm of cross-bedded (?) peat. Unlike a residual peat deposit formed *in situ* from standing tundra, the basal peat of vibrocore-49 was friable and did not occur as a coherent, stringy peat mesh. Therefore, the peat is most likely of "detrital" origin. Study of the structures and stratigraphic variations

in lithology of other vibrocores have not been completed as yet. However, it will suffice to state at this point in time that wide stratigraphic variations in structure and lithology have been noticed between the different cores within the relatively small area of the Simpson Lagoon.

VII. DISCUSSION

Simpson Lagoon Substrate Habitats

On the basis of observed patterns of areal variations in lithology, it would seem to justify that two types of substrate habitats can be distinctly delineated in the Simpson Lagoon. The chief textural basis of such a habitat classification is the contents of silt plus clay (e.g. mud) in 127 representative sediment samples that were collected from the Simpson Lagoon and analyzed by Tucker (1973) and by us (Table III). As mentioned earlier, the central lagoon substrate is characterized by sandy muds (>50% mud), whereas the substrate of the narrow lagoon regions adjacent to the Jones Islands and the mainland coastal plain are constituted of muddy sands (>50% sand). These areal variations in substrate lithology most likely reflect the relatively higher turbulence in shallow waters adjacent to the lands, and deposition of larger amounts of finer particles in the deeper, relatively tranquil central lagoon basin. It is noteworthy to mention here that lateral displacement of water masses along the Simpson Lagoon as well as along the contiguous coastal regime up to Prudhoe Bay, is generally confined to the narrow region adjacent to the mainland coastal plain. Presumably, relatively higher turbulence also exists along this region, which winnows out larger amounts of silt and clay-sized particles from the substrate. The predominance of mud across the lagoon width in the western end - between Oliktok Point and west Spy Island - most probably is

attributable to local supply and deposition of large amounts of fine-sized particles from the Colville outflow.

Source and Depositional Sites of Fine-Grained Particles in Simpson Lagoon

Our continued detailed studies of the less than 2 μm fraction of sediments have led us to believe that the clay mineral assemblages of the Canning, Sagavanirktok, Kuparuk, and Colville rivers can be quite effectively discriminated. Analysis of the Canning River clays shows that those clays have no expandable minerals and have only traces of kaolinite. In contrast to this the clays of the Colville, Kuparuk, and Sagavanirktok Rivers have significant amounts of expandable clay minerals as well as kaolinite. Further, the Canning River clays (<2 μm) characteristically have considerable amounts of calcite associated with the clay minerals. The only other fluvial clay from the North Slope which does have a little calcite is that from the Sagavanirktok River. Additionally, the 17 Å basal 'd' dimensions of the expandable clay mineral components in the Sagavanirktok and Kuparuk Rivers, upon 1N KCl solution saturation and subsequent glycolation (and not subsequent to 1N MgCl_2 saturation and glycolation) collapse to a 'd' dimension of 10 Å. Therefore, it would seem that the expandable components in the latter two fluvial clays are most likely degraded (depotassicated) illites rather than true smectites or mixed-layered minerals with smectitic phases. In contrast to the Sagavanirktok and Kuparuk clays, we have shown earlier (Mowatt *et al.*, 1974) that the expandable phases of the Colville clays either do not collapse or collapse very little subsequent to saturation with 1N KCl and MgCl_2 solutions, followed by glycolation. The latter detailed studies suggest that the Colville clays have well-defined discrete smectite and/or mixed-layered smectitic phases in them.

Based on our ability to fingerprint various fluvial clays of the North Slope, it would seem that clay mineral compositions of the $<2 \mu\text{m}$ fractions of sediments can be used as natural tracers to elucidate the terrigenous sources, transport pathways and depositional sites of fine-grained sediment particles in the continental margin area of the Beaufort Sea.

On the basis of our knowledge of clay mineral assemblages of the major rivers of the North Slope and the Simpson Lagoon, it is evident that presently the lagoon is predominantly impacted by fine sediments from the Kuparuk River (Fig. 6). The only portion of the lagoon which receives large influxes of Colville River clay is the area on the western end of the lagoon, between Oliktok and Spy Island (Fig. 6). There are evidences to suggest that occasionally significant amounts of fine clays from the Sagavanirktok River are dispersed and locally deposited in the eastern Simpson Lagoon. These conclusions, therefore, substantiate our earlier inferences, based on reconnaissance surveys (Naidu and Mowatt, 1974), that the net alongshore drift of fine-sized particles in the North Slope coastal region is generally toward the west. The latter conclusion is well substantiated by the observed turbid plume structure (Barnes and Reimnitz, 1974) and the current flow pattern for the above coastal regime (Wiseman *et al.*, 1973; Dygas, 1974; Barnes *et al.*, 1977; Mathews, personal communication).

Sediment Chemistry

Vanadium

At this point in time all heavy metal data have not been gathered. Vanadium concentrations in sediment extracts (Chester and Hughes, 1967) is

relatively higher in the central Simpson Lagoon. This is not surprising considering the larger amounts of mud that are deposited in the central lagoon region and, by implication, the larger capacity of clay-sized particles to fix by adsorption/exchange "readily mobilized" vanadium. It would be of interest to check if there are relatively large populations of tunicates in the central Simpson Lagoon, because the latter organisms tend to preferentially concentrate vanadium in their tissues.

Organic carbon, nitrogen and C/N ratios

Comparison of Figures 4 and 6, showing patterns of organic carbon and substrate lithologic variations in the Simpson Lagoon brings to light some 'unusual' correlations. The southern region with relatively high organic carbon contents in sediments is generally characterized by relatively coarser substrate. In contrast to this trend in the northern marginal region of the Simpson Lagoon, where the substrate is likewise coarser than in the central lagoon, the organic content is generally the lowest. In most depositional milieu it is commonly observed that organic particles tend to codeposit with clay- and silt-sized particles chiefly because of their similar hydraulic equivalents. Therefore, the association of relatively larger amounts of organic carbon (and by implication organic matter) with the coarser substrate of the southern marginal region of the Simpson Lagoon seems quite atypical. It is our belief that the unusually higher contents of organic carbon in the latter region are attributable to a ready local source of organic matter from the erosion of adjacent coastal tundra bluffs, and that bulk of this organic detritus is most likely in the form of small consolidated tundra mats or shreds. Consequently the organic

matter in the southern Simpson Lagoon is not quite prone to normal hydraulic sorting action as one would expect in case of discrete organic particles. The latter conclusion seems reasonable in light of the earlier observations that the southern lagoon is probably subjected to relatively higher turbulence.

We have not understood all the factors that control the contents of nitrogen in the lagoon sediments, which as mentioned earlier do not exhibit any particular areal distributional trend. One would normally have expected a close covariance in distributional pattern between organic carbon and total nitrogen, because bulk of the latter and all of the carbon would be ascribed to organic matter. The lack of such a close covariance is difficult to explain at this stage of our study, but may be related to different degrees of bacterial decomposition of the terrigenous organic debris and disparate stages of nitrification attained over various regions of the lagoon.

It is noteworthy to have documented significant variations in the C/N ratios of surficial sediments of the North Slope coastal region (Simpson Lagoon and Harrison Bay), continental shelf of the adjacent Beaufort Sea and the abyssal region of the Canada Basin (Table VII). Most probably these progressive marineward changes in the C/N ratios reflect the relative nature of organic debris that is being supplied to and getting intercalated with the bottom sediments of the various regions. The most likely ready and abundant source of the organic matter to sediments in the North Slope coastal environment, as mentioned earlier, is the terrigenous tundra peat which on an average has a C/N ratio of 19 (Schell, personal communication). Therefore, the significant decrease in the C/N ratios in the Simpson Lagoon and Harrison Bay sediments suggests that the depositing

peat undergoes quite rapid bacterial degradation, and that nitrification is enforced in the lagoon and bay. The progressive decrease in the C/N ratio from the coastal to the deep-sea area most likely reflects a progressive marineward increased influx of local faunal relative to terrigenous plant debris to the bottom sediment organic matter. For lagoon ecosystem modeling study in the north Beaufort Sea, it would be of primary interest to extend our present studies - in conjunction with nutrient biologist (Dr. D. Schell, RU 537) - to trace the physicochemical and biological processes that modify the organic carbon and nitrogen contents, and C/N ratios of particulate matter during its traverse from the original terrigenous source to the depositional sites in the lagoon. The role of bacteria in the above processes, of course, will be of prime importance and should be assessed.

Stability and Growth Rate of the Pingok Island Barrier Spit

It is now reasonably well documented that almost all barrier islands along the Alaskan Beaufort Sea coast have undergone some degree of temporal geomorphic changes, irrespective of the nature of the islands whether they are tundra blanketed or not. The temporal changes in the configuration of some of the islands over a few decades (from 1906 to 1974) have been assessed by Wiseman *et al.* (1973), Barnes *et al.* (1977), and Lewellen (see Hopkins *et al.*, 1977). The relatively short-term changes within one summer season for the Pingok-Leavitt island have been documented by Wiseman *et al.* (1973) and Dygas *et al.* (1972). A review of the above literature shows that the lateral growth rates of the barrier spits of the various islands are significantly different, and within any one summer season great fluctuations in the above rate can be noted. However, there is a general consensus

among most geologists working in the Beaufort Sea coast that the net alongshore drift of sediments along that coast is toward the west.

One of our research objectives, embodied in RU 529, is to assess the long-term net alongshore sediment transport direction, as well as to estimate the long-term growth rate of barrier spits along the Alaskan Beaufort Sea coast. In attempting to fulfill the latter objective we conducted field surveys on Pingok Island. During the course of this survey we encountered a peat formation on the seaward beach at the proximal end of the sand-gravel barrier spit extending to the west of the Pingok Island (e.g. the Leavitt Island). Evidently the peat deposit is not a remnant of an old collapsed coastal bluff, because it is quite an extensive contiguous formation. At the high-tide mark where a vertical section of the north spit shore is exposed, the peat is observed to lie under an overburden of 84 cm of sand and gravel. Apparently the same peat layer extends widely under the barrier spit, as suggested by the detection of a peat deposit under 79 cm of sand-gravel overburden in a trench in the center of the barrier spit. It is believed that a radiocarbon date of a sample of the upper layer of the peat would provide us with the geologic age when the sandy-gravel barrier spit most likely started to grow westward from the Pingok Island*. Therefore, the 2600 years B.P. radiocarbon date of the peat suggests that the barrier spit is geologically quite a young formation. Additionally, on the basis of this date and the approximate 5.5 km length of the spit (includes the Leavitt Island) it would seem that the average long-term growth rate of the spit on a steady state basis is

* This contention assumes that the upper portion of the peat and the sand-gravel unit lying over it are more or less contemporary deposits.

around 2 m/year. Further, assuming that the average thickness and width of the spit to be 1 m and 140 m respectively, it would seem that the long-term depositional rate of the spit volume is in the order of approximately $280 \text{ m}^3/\text{year}$.

It is interesting to compare the growth rates for the western Pingok Island spit that we have estimated on long-term basis and those reported earlier by Wiseman *et al.* (1973). The latter estimated the spit growth rate estimates in summer 1972 via field studies, as well as taking into consideration data from Dygas *et al.* (1972).

The linear growth rate of the barrier spit, as cited by Wiseman *et al.* (1973) is 6 m/year while the volumetric increase is about $7.1 \times 10^3/\text{summer}$. These accretion rates of the barrier spit in question are considerably higher than our figures. It would be of interest to check what portions of the total length and volume of the spit accretion in summer could be ascribed to catastrophic storm action and what portions to normal current/wave action. It would also be of importance to estimate the decrease in the spit areal size consequent to ice bulldozing during the ice stress season. As observed by us as well as several others, occasional storm surges can bring about large-scale degradation (e.g. in the order of 10-15 m) along some beach stretches, with almost concomitant progradation at other beach sites along the Beaufort Sea barriers. The sum total resultant of the storm and ice-ploughed actions on the sediment "budget" of the spit is unknown presently, but is conceivable that the two counteracting processes will eventually amount to net spit growth rates which are relatively much lower than the estimates that have been provided by Wiseman *et al.* (1973) on a seasonal basis. It is, therefore, no wonder that Wiseman *et al.*

(1973) have observed only a modest change in the spit length west of Pingok (tundra) Island between 1908 and 1972 (e.g. 64 years). Presently it would seem imperative that additional long-term data must be gathered before we can give more precise estimates of the barrier spit growth rate on the Pingok Island.

Evolution of the Barrier Islands

Our studies relating to the evolution of the barrier islands along the Alaskan Beaufort Sea coast is still in the preliminary stage. At this point in time we have rudimentary knowledge of the alongshore net mass sand transport direction, which is based largely on the morphology of the barrier spits and long-term migration patterns of barrier islands. We have just extended studies on the stratigraphy of vibrocore samples and into heavy minerals and gravel compositions. Without adequate knowledge of the paleogeographic history, wave refraction patterns (to be provided by physical oceanographers), sources and transport pathways of sand-sized particles, and submarine bottom profiles off the islands, it would be difficult for us to elucidate the barrier island evolution.

Field observations would seem to suggest that the Pingok, Bertoncini, Bodfish, Flaxman and other tundra blanketed islands are Pleistocene relict coastal highlands, and that the lagoon associated with them presumably have formed by transgression of the sea into low lying coastal plain region where lakes coalesced to form large water bodies. The source and origin of the boulders associated with the above-named tundra islands have not been resolved satisfactorily. They could be paleomorainic debris associated with pre-Wisconsinian glaciation in the North Slope, or they could be paleo

ice-rafted deposit (Naidu and Mowatt, 1974). Detailed petrographic studies of these gravels in relation to some of their possible sources may be helpful to resolve their origin.

In contrast to the above, islands with sand and/or gravel substrates, which are more abundant along the Beaufort Sea coast, are most probably resultants of contemporary marine constructive processes. By conventional definition* they are to be considered modern, notwithstanding that the gravel and sand constituting them may have been reworked from older residual deposit (e.g. deposit left from erosion of ancient tundra islands and/or coastal bluffs). The detection by us of several bars, hundreds of meters long and elongated parallel to the Beaufort Sea coast, suggest that at least some of the barriers might have subaerially grown from bars as a result of progressive sediment accretion via alongshore drift. Incidentally, Wiseman *et al.* (1973) have pointed out the formation of several bars in the Beaufort Sea inshore as a result of wave and current action. Although evolution of the barriers can be addressed from several stand points, our approach will be chiefly restricted to gathering geological evidences. We hope to pursue this approach in further detail in the next year.

Earlier it was our feeling that the interpretation of the stratigraphic changes in both lithology and structure of the Simpson Lagoon cores would be a straight-forward simple effort, and that the recapitulation of the Holocene paleogeography of the North Slope continental margin area and thus the origin of the barrier islands would not be too difficult to follow.

* For conventional definitions of relict, contemporary (or modern) and palimpsest deposits, refer to Swift *et al.* (1971).

However, it would seem that the recent paleogeographic history of the Simpson Lagoon area has been quite complex. This is indicated by the stratigraphic dissimilarities observed between the four cores that were collected from not too widely apart locations within the lagoon, the complex nature of depositional units in each core and the presence of both marine and freshwater faunal components in a peaty layer. Perhaps, the ultimate key to our understanding of the paleogeography of the area would depend on our ability to document precisely the processes and products of sedimentation in contemporary depositional environments of the arctic. A simple extrapolation of depositional models, based on studies on nonpolar deltas, appear to have limited paleogeographic use in the arctic. We have initiated some studies on modern deltaic sediments of the Alaskan arctic (Naidu and Mowatt, 1975), and would like to see how well the hypothesis "the present is the key to the past" can be applied to understand the recent depositional history of the North Slope coastal region.

VIII. CONCLUSIONS

At this point in time some tentative conclusions can be made and they are:

- (i) Textural attributes of sediments permit delineation of two substrate habitats in the Simpson Lagoon. The central Lagoon substrate is characterized by sandy muds, whereas the substrate of the two narrow regions adjacent to the barrier islands and the mainland coast are constituted of muddy sands. These areal variations in lithology most likely reflect the relatively higher turbulence in shallow

waters adjacent to land; the central lagoon basin acts as a depositional trap. The predominance of mud across the lagoon bottom between Oliktok Point and Spy Island is attributable to higher influx locally of fine grained particles from the Colville outflow.

- (ii) Detailed clay mineral studies of bottom sediments suggest that the Simpson Lagoon is impacted by sediments from the Kuparuk River. The area receiving significant amounts of fine sediments from the Colville River on a local scale is restricted to the western end of the Simpson Lagoon. This year's studies substantiate our earlier conclusions that the net alongshore transport of clay sized particles is toward the west between Prudhoe Bay and the Colville Delta.
- (iii) Vanadium contents in acid extracts of sediments are quite low (e.g. 5 $\mu\text{g/g}$). The higher contents of V in the central Simpson Lagoon are most probably related to larger fixation of V by adsorption/exchange in the relatively clayey sediments of that region.
- (iv) Organic carbon contents in bottom sediments show a progressive northward decrease across the lagoon width. A negative correlation between sediment types and organic carbon contents are observed on a broad regional scale. The presence of higher organic carbon contents in the relatively coarser sediments of the lagoon adjacent to the mainland coast is most likely related to larger influx of detrital peat from coastal erosion. The organic matter initially being in the form of tundra mats is not quite prone to the usual sorting and winnowing action by turbulent waters present here. Therefore, the organic mats tend to lie as residual lag deposits adjacent to the

coast. It would seem that on the basis of the nature of sediment substrate, carbon contents, as well as water mass characteristics (Dr. Mathews, personal communication) the southern portion of the Simpson Lagoon probably constitutes a distinct biological habitat as compared to the central and northern thirds of the lagoon. It would be of further interest to check if correlations exist between epibenthos populations and diversity, and these three lagoon habitats.

No significant areal trends have been noticed either in the contents of nitrogen or C/N ratios of sediments in the Simpson Lagoon. Surprisingly no parallel distributional (areal) pattern was observed between sediment carbon and nitrogen contents in the lagoon. Bulk of the organic matter in the lagoon sediments appear to have their predominant source in terrigenous peat detritus. The lower C/N ratios of the lagoon sediments (e.g. 13) relative to those of the coastal bluff peat (e.g. 19) suggests significant bacterial degradation of the latter within the lagoon and enforcement of nitrification. For purpose of lagoon ecosystem modeling along the Alaskan Beaufort Sea coast, it would be of primary concern to trace the physicochemical (pH, Eh, water turbulence, sedimentation and influx rates, etc.) and biological factors that modify the organic carbon and nitrogen contents of terrigenous particles, from North Slope rivers and coastal bluffs to their depositional sites in the lagoon.

- (v) We believe that barrier islands along the Beaufort Sea coast have evolved in two different ways. The barriers with well-defined thick tundra blanket are most probably relict Pleistocene coastal features. The rest of the barrier islands, as well as the barrier spits, are

most likely contemporary products of constructive wave/current action. The successive geologic events which have led to the latter island formation are difficult to recapitulate without further knowledge of the regional paleogeography, several physical oceanographic parameters, and present sediment dynamics.

All available evidences indicate that the barrier islands and spits are migrating (or growing) westward. The net longitudinal and volumetric accretion rate on a long-term steady-state basis is about 2 m/year and 280 m³/year, respectively. The latter rates have been estimated on the basis of a radiocarbon date of a basal peat that was discovered under sand-gravel overburden at the distal end of the barrier spit, west of the tundra blanketed Pingok Island. The above spit growth rates, as estimated by us are relatively lower than the estimates made on a short-term basis by Wiseman *et al.* (1973). Further studies are called for to establish on a more firm basis the short-term and long-term spit growth rates.

- (vi) Understanding of the origin of the boulders that are associated commonly with tundra blanketed barrier islands, presumably has implication in elucidation of the island evolution. However, no conclusive evidences have been gathered by us as yet to decide whether the boulders are paleo ice-rafted debris (Naidu and Mowatt, 1974), or they are moraines deposited by pre-Wisconsinian glaciation in the North Slope.

IX. NEEDS FOR FURTHER STUDY

It is to be kept in mind that the data presented in this "Annual Report" includes results of our field and laboratory investigations during the last 10 months. The funding for this project finally came through in June 1977, while the sample collection did not begin before August 1977. As the project has been funded initially up to September 1978, we will be continuing to work to fulfill our research objectives during the forthcoming months. Further investigations will include the following:

- (a) Detailed heavy mineral studies under the microscope will be conducted on sands of the North Slope rivers, the barrier islands, lagoon and adjacent shallow-water regions (<10 fm) of the Alaskan Beaufort Sea. The objective of this study will be to trace sources and net along-shore transport directions of sand-sized particles along the Beaufort Sea coast.
- (b) Petrographic studies of thin sections of gravels from the barrier islands will be conducted, and sources of the coastal boulders will be ascertained. Published data on gravels collected from ice islands will be taken into consideration in these studies.
- (c) Heavy metals in Simpson Lagoon and Beaufort Sea shelf sediment will be analyzed in the lithogenous and non-lithogenous fractions for establishment of baseline chemical data. This effort will be undertaken primarily to fill in small data gaps existing on heavy metals in the region between Barter Island and the Demarcation Point, and will be carried out in conjunction with a modest program funded by the USGS to us.

- (d) Detailed clay mineral studies will be continued on continental shelf sediment samples that were collected last summer to fill in existing data gaps between Barter Island and the Demarcation Point. Sources, transport pathways and depositional sites of Beaufort Sea fine-grained sediments will be elucidated via the above detailed clay mineral studies.
- (e) Statistical analysis of all available data on size distribution, clay minerals and chemical parameters for the Beaufort Sea will be conducted and a comprehensive report will be prepared on the sources and dynamics of sediments of the Beaufort Sea. Various sediment data will be transferred to the standard OCSEAP maps of the Beaufort Sea.
- (f) Additional sediment samples will be collected from the lagoon region between Milne Point and Beechey Point. Analysis of the grain size distribution of these sediments will be helpful in delineating benthic habitats and better understanding of sediment dynamics in the North Slope lagoons.
- (g) Samples of various depositional units from vertical sections of coastal bluffs will be collected next summer at several locations along the North Slope. Organic carbon and nitrogen contents of the above samples as well as of suspensate samples from the Colville and Kuparuk Rivers will be analyzed to estimate the output of nutrients, via terrigenous particles, to the Simpson Lagoon. It is also planned to analyze organic carbon and nitrogen contents of substrate sediments and suspensates of the Simpson Lagoon during calm and turbulent conditions. All these data will be of use to biologists in the understanding of nutrient

'budget' in the Simpson Lagoon, and eventually in modeling of the lagoon ecosystem.

- (h) Stratigraphic analysis of texture, coarse fraction, and minerals will be continued on the vibrocore samples from the Colville Delta, Simpson Lagoon and Prudhoe Bay area to recapitulate the paleogeography of the Beaufort Sea coastal area. This study and any additional data gathered on recent sediments would be applied to elucidate the evolution of the barrier islands.
- (i) In summer (1978) beach stakes will be established on the Pingok and Stump Islands to monitor short-term growth rate of these islands on the western end. In addition, trenches will be dug on a few sandy gravel barrier islands to check the nature of sediments underneath. We would look for some organic debris (e.g. peat, driftwood, shells, etc.) under the barrier gravels for purpose of radiocarbon dating and thus estimating growth rates of barriers.

X. SUMMARY OF 4TH QUARTER OPERATIONS

Ship or Laboratory Activities

1. None scheduled
2. Not applicable
3. Methods: Refer to Section V for details
4. Not applicable
5. Refer to Section V for details

REFERENCES

- Arnold, K. 1976. Data for State of Alaska socio-economic impact assessment of leasing in the Beaufort Sea. Submitted to the Dept. of Community and Regional Affairs, State of Alaska, Juneau. 1-24 p.
- Barnes, P., E. Reimnitz, D. Drake and L. Toimal. 1977. Miscellaneous hydrologic and geologic observations on the inner Beaufort Sea shelf, Alaska. U.S. Geol. Survey Open File Rept. 77-477 pp.
- Biscaye, P. E. 1965. Mineralogy and sedimentation of recent deep-sea clay in the Atlantic Ocean and adjacent seas and oceans. *Geol. Soc. America Bull.* 76:803-832.
- Burrell, D. C. 1977. Natural distribution of trace heavy metals and environmental background in Alaskan shelf and estuarine areas. Annual Rept. to BLM-OCSEAP Office, Boulder. Inst. Mar. Sci., Univ. Alaska, Fairbanks. 204 p.
- Chester, R. and M. J. Hughes. 1967. A chemical technique for the separation of ferro-manganese minerals, carbonate minerals and adsorbed trace elements from pelagic sediments. *Chem. Geol.* 2:249-262.
- Dygas, J. A., R. Tucker and D. C. Burrell. 1972. Geological report on the heavy minerals, sediment transport, and shoreline changes of the barrier islands and coast between Oliktok Point and Beechy Point. In: *Baseline data study of the Alaskan Arctic Aquatic Environment*, P. J. Kinney *et al.* (eds.). Inst. Mar. Sci. Rept. R-72-3, Univ. Alaska, Fairbanks. pp. 61-121.
- Feder, H. M., A. S. Naidu, D. Schammel, D. G. Shaw, E. R. Smith and G. W. Smith. 1976. The arctic coastal environment of Alaska, Vol. III. The nearshore marine environment in Prudhoe Bay, Alaska. Rept. R76-7, Inst. Mar. Sci., Univ Alaska, Fairbanks. 153 p.
- Folk, R. L. and W. C. Ward. 1957. Brazos River bar - a study in the significance of grain size parameters. *J. Sedimentary Petrology* 27:3-26.
- Grider, G. W., Jr., G. A. Robbiliard, and R. W. Firth, Jr. 1977. Final Report on Environmental Studies Associated with the Prudhoe Bay Dock: Coastal Processes and Marine Benthos. Woodward-Clyde Consultants, Anchorage, Alaska. IV85.
- Hülsemann, J. 1966. On the routine analysis of carbonates in unconsolidated sediments. *J. Sedimentary Petrology* 36:622-625.
- Mowatt, T. C., A. S. Naidu and N. Veach. 1974. Detailed clay mineralogy of the Colville River and Delta, northern Arctic Alaska: Alaskan Div. of Geol. and Geophys. Survey's Open File Report, Fairbanks. Rept. 45. 36 pp.

- Naidu, A. S., D. C. Burrell and D. W. Hood. 1971. Clay mineral composition and geologic significance of some Beaufort Sea sediments. *J. Sedimentary Petroleum* 41:691-694.
- Naidu, A. S. and D. W. Hood. 1972. Chemical composition of bottom sediments of the Beaufort Sea, Arctic Ocean. Proc. 25th Int. Geol. Congress, Montreal, Canada 10:307-317.
- Naidu, A. S. and T. C. Mowatt. 1974. Aspects of size distributions, mineralogy, and geochemistry of deltaic and adjacent shallow marine sediments, north arctic Alaska. In: *An Ecological Survey in the Beaufort Sea*. U.S. Coast Guard Ocng. Unit, Washington, D.C. Ocng. Rept. CG373-64:238-262.
- Naidu, A. S. and T. C. Mowatt. 1975. Depositional environments and sediment characteristics of the Colville and adjacent deltas, northern arctic Alaska. In M. L. S. Broussard (ed.), *Deltas: Models for Sub-surface Exploration*. Houston Geol. Soc., Houston, Texas. pp. 284-309.
- Shepard, F. P. and D. G. Moore. 1954. Sedimentary environments differentiated by coarse-fraction studies. *Bull. Amer. Assoc. of Petroleum Geologists* 38:1792-1802.
- Swift, D. J. P., D. J. Stanley and J. R. Curray. 1971. Relict sediments on continental shelves: a reconsideration. *J. Geol.* 79:322-346.
- Tucker, R. W. 1973. Sedimentary environment of an arctic lagoon. M.S. Thesis, Univ. Alaska, Univ. Microfilms, Ann Arbor, Michigan. 96 pp.
- Weiss, H. V., M. A. Guttman, J. Korkisch and I. Steffan. 1977. Comparison of methods for the determination of vanadium in sea water. *Talanta* 24:509-511.
- Weller, G., D. Norton and T. Johnson. 1977. Environmental impacts of OCS development in northern Alaska. Beaufort Sea Synthesis Report (draft). Special Bull. #15, Arctic Project Office, Univ. Alaska, Fairbanks. 219 p.
- Wiseman, Wm. J., *et al.* 1973. Alaskan arctic coastal processes and morphology. Tech. Rept. No. 149, Coastal Studies Inst., Louisiana State Univ., Baton Rouge. 171 p.

ANNUAL REPORT

Contract #03-5-022-56
Research Unit #530
Reporting Period 4/1/77 - 3/31/78
Task Order #34
Number of Pages 25
Maps Attached 5

THE ENVIRONMENTAL GEOLOGY AND GEOMORPHOLGY
OF THE BARRIER ISLAND - LAGOON SYSTEM ALONG
THE BEAUFORT SEA COASTAL PLAIN FROM PRUDHOE
BAY TO THE COLVILLE RIVER

Principal Investigator:

Dr. P. Jan Cannon
Assistant Professor of Geology
Department of Geology
University of Alaska
Fairbanks, Alaska 99701

Senior Research Assistant:

Stuart E. Rawlinson

Deputy Research Assistants:

Michael G. Moore
June Reuben

March 31, 1978

ABSTRACT

Approximately 96 kilometers of tundra capped bluffs border Simpson Lagoon. Tundra erosion rates along the mainland coast average 1.2 meters per year and are slightly higher on the islands, averaging 1.6 meters per year. Seaward facing bluffs on the islands erode slower than lagoon facing bluffs.

Expected duration from the present of the tundra covers on the offshore islands range from 40 years on Cottle Island to 270 years on Pingok Island.

Detritus input into the barrier island-lagoon system is primarily from two sources, erosion of the coast and introduction from rivers. The total detritus input, inorganic and organic, from coastal erosion is $2.5 \times 10^5 \text{ m}^3/\text{year}$, approximately $4.4 \times 10^8 \text{ kg/year}$. The Kuparuk River contributes about $1.1 \times 10^6 \text{ m}^3/\text{year}$, approximately $2.1 \times 10^9 \text{ kg/year}$. Other major rivers contribute relatively little detritus to the system.

Storm surge may completely inundate the gravel islands, and on the inland coast, may extend as much as one kilometer inland in low-lying areas.

Most of the coarse clastic materials composing the islands are lag deposits from erosion of tundra covered areas. Ice shove and wave impact constantly change the distribution of the clastics.

The Arctic coastal plain, in part, may represent a pre-Wisconsin ground moraine that in the past extended beyond the present coastline. The offshore tundra islands are remnant features, isolated from the main-

land by communication of inland lakes or low-lying areas with the ocean through inundation by erosion. The gravel islands represent the accumulation of lag clastics. Coarse clastics are not being renewed to the islands from other than local sources. These islands probably receive sand size clastics eroded from local tundra covered areas and major rivers.

TABLE OF CONTENTS

ABSTRACT. ii

INTRODUCTION. 1

GENERAL DESCRIPTION OF THE AREA 2

METHODS OF INVESTIGATION. 7

PERTINENT RESULTS OF INVESTIGATION. 8

 Coastal Exposure and Erosion Rates. 8

 Approximate Duration of the Tundra Islands. 10

 Erosional Detritus Input into the Barrier Island-Lagoon System. 11

 River Detritus Input into the Barrier Island-Lagoon System. . . 13

 Storm Surge 16

 Source of Material. 16

 Origin and Evolution of the Barrier Islands and
 Coastal Lagoons 16

REFERENCES CITED. 21

GLOSSARY. 23

LIST OF ILLUSTRATIONS

Figures

Figure 1 - Map showing the location of the investigation area	3
Figure 2 - Multiple spit development on the west end of Spy Island.	6
Figure 3 - Spit development on the east end of Cottle Island. . . .	6
Figure 4 - Strudle hole in the sea ice near the Colville River. . . .	14
Figure 5 - Lake bed being inundated along the Arctic coast.	19
Figure 6 - Idealized development of an offshore remnant island by coalescence of lakes.	20

Tables

Table 1 - Exposure and average erosion rates in the Simpson Lagoon area	9
Table 2 - Tundra duration time on the offshore islands	11
Table 3 - Volume of detritus input into Simpson Lagoon from coastal erosion	12
Table 4 - Mass of detritus input into Simpson Lagoon from coastal erosion	12
Table 5 - Detritus input into Simpson Lagoon from the Kuparuk River spring runoff	15

Maps

Map 1 - Erosion rates: Pingok Island.	in pocket
Map 2 - Erosion rates: Unnamed Island, Bertoncini Island, Bodfish Island.	in pocket
Map 3 - Erosion rates: Cottle Island.	in pocket

Map 4 - Extent of over ice detritus flow from the
major rivers in pocket

Map 5 - Areas of possible inundation by storm surge in pocket

INTRODUCTION

The purpose of this study is to provide quantitative and qualitative data for assessing the environmental impact of development within the Simpson Lagoon area. Before environmental impact assessment is possible, however, past and present natural processes and conditions of the barrier island-lagoon system must be determined. This is being done in part through computer modeling by a multidisciplinary group. More directly, observation and documentation of existing natural conditions and processes aid in defining the system.

Specific modeling requirements from the geomorphology subgroup are the volume and mass of detrital material introduced into Simpson Lagoon by shoreline erosion and from fluvial injection. Further objectives are:

1. To determine the origin and evolution (geomorphic history) of the barrier islands and coastal lagoons. Projections of future duration of the barrier islands and of the changes in coastal morphology are part of this objective.
2. To determine the source(s) of the gravel size materials that compose the barrier islands.
3. To determine the stability of the barrier island-lagoon system in respect to natural processes and man-induced effects.
4. To determine the magnitude of the geomorphological relationships between the barrier island-lagoon system and the landforms of the coastal plain.

5. To construct a spatial and temporal model of the environmental geology of the region.

Natural geological conditions and processes (the environmental geology) are best indicated by the individual landforms and/or the landform assemblages (the geomorphology) of the area. Recognition of these landforms and knowledge of the geomorphic processes by which they formed, enables the prediction of future changes, both natural and man-induced.

Results of this investigation to date are presented in this report. Refinement or modification of these results is expected during the 1978 calendar year.

GENERAL DESCRIPTION OF THE AREA

The project area extends east from the Colville River along the mainland coast to Prudhoe Bay; it includes Simpson Lagoon and the offshore islands of the Jones and Return Groups (Figure 1). The barrier island-lagoon system covers an area of roughly 240 square kilometers, about 60 kilometers in length by about 4 kilometers in width. The lagoon is very shallow, generally less than 1 meter (Tucker and Burrell, 1977).

The offshore islands are of two types, those with a thick tundra mat overlying unconsolidated clastics and ice, and those without tundra mat covers, consisting mainly of sand and gravel. The tundra covered islands, although linear in overall morphology, tend to have long straight beaches that intersect at acute angles. The gravel islands are curvilinear, long and narrow.

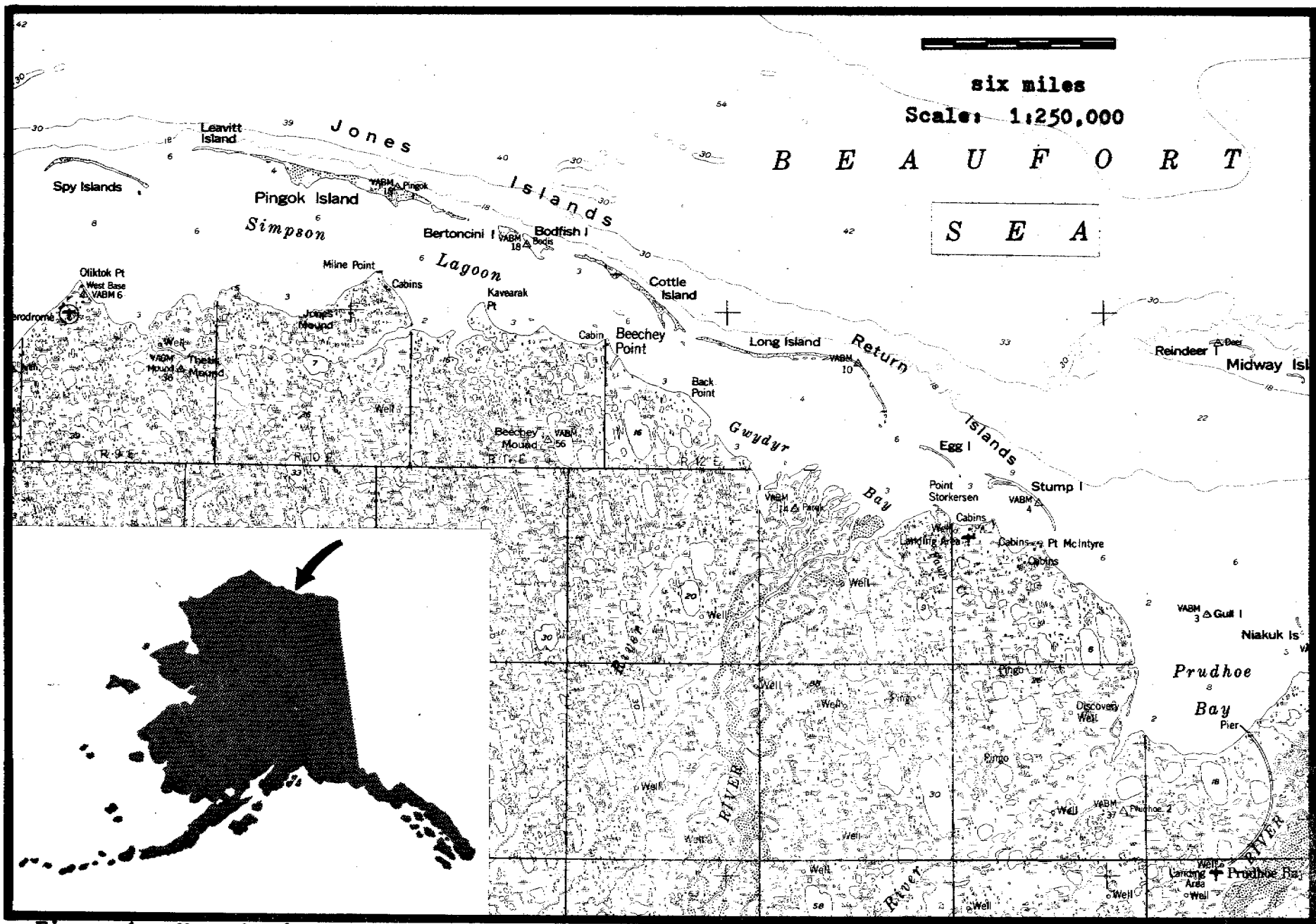


Figure 1- Map showing the location of the investigation area.

The relief of the islands and the inland coastal plain, as classified by Hartwell (1973), are low (less than 2 meters) and moderate (from 2 to 5 meters). Pingos occur on the coastal plain in limited numbers near the study area and are the only natural landform which break the otherwise flat landscape. The mainland coast and the tundra covered islands terminate abruptly at the lagoon as a steep bluff with unconsolidated talus (Hartwell, 1973) and slumped tundra mat lying on a generally narrow beach. Often, in areas of moderate relief, clear ice is visible in the bluff, underlying the sediments or tundra mat.

On the seaward side of the offshore tundra islands there is generally wide beach development. These beaches, consisting predominately of sand and gravel, slow erosion of the tundra capped bluff by dissipating the wave energy across their width before impact. The beaches are also a source of sand size clastics which accumulate as eolian deposits, against and on top of the bluff, further slowing erosion. The sand size clastics on top of the bluff form a linear dune ridge which parallels the beach. The width of the dune ridge is roughly proportional to the width of the beach. Both the gravel and tundra islands have gently sloping beaches on their lagoon sides, while seaward facing beaches are irregular as a result of ice shove. Ice shove ridges form primarily in October and November, lasting throughout the winter and into the summer until they are obliterated by storm waves.

Spit development is common on both the gravel and tundra islands. Spits forming off the western ends of the tundra covered islands are generally straight and often develop connective bars between the islands. Spits forming on the more isolated islands tend to be recurved

and occur as multiples, most often pointing westward. Multiple recurved spits have formed on the western ends Stump, Spy, and Thetis Islands (Short et al., 1974). Figure 2 shows multiple recurved spits on the western end of Spy Island. Several tundra covered islands such as Bodfish and Cottle have spits formed on their eastern ends (Figure 3).

Polygonal ground patterns are common on the tundra covered islands and the coastal plain. Talik lakes occur in the depressions between the ice wedge polygons, often enlarging by coalescence. The lakes, numbering in the thousands, tend to be elongate and oriented in a northwest - southeast direction. Lengths range from a few meters to as much as 14 kilometers; common length to width ratios are 3:1 or 4:1 (Carson and Hussey, 1959). Maximum lengths of the coastal plain lakes near the study area are about 4 kilometers. Depths are usually a meter or less, but may exceed 6 meters (Black and Barksdale, 1949).

Two major rivers, the Sagavanirktok on the east and the Colville on the west, bound the area inland from the barrier island-lagoon system. The Kuparuk is the only large river that empties directly into Simpson Lagoon. All three of the major rivers are braided and have delta systems.

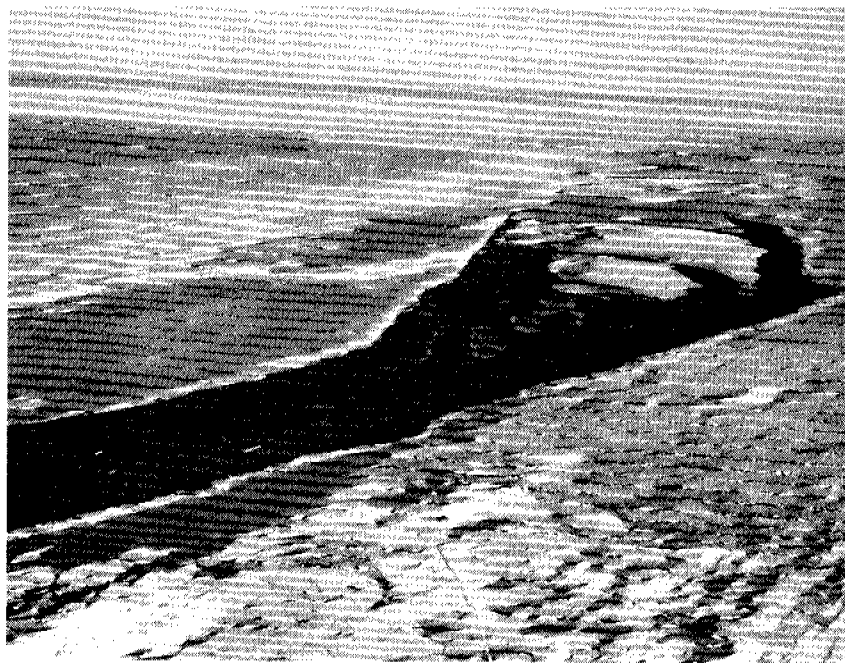


Figure 2 - Multiple recurved spit development on the west end of Spy Island. (Photograph by P. Jan Cannon)



Figure 3 - Spit development on the east end of Cottle Island. (Photograph by S. E. Rawlinson)

METHODS OF INVESTIGATION

United States Geological Survey topographic maps covering the area at scales of 1:63,360 and 1:250,000 and United States Coast and Geodetic Survey hydrographic charts at a scale of 1:50,000 were acquired to develop as well as record data. Sequential vertical photographic coverage at three different scales was also acquired for geomorphic interpretation and for measurement of erosion rates within the investigation area. An intensive literature search was conducted to provide pertinent references required for the study.

A series of low altitude reconnaissance flights were flown at different times of the year to observe and document landforms, coastal processes and changes, and to field truth remote sensing data interpretation. The flight dates were as follows:

1. June 14, 1977 (ice breakup)
2. July 27, 1977 (mid summer)
3. August 14, 1977 (mid summer)
4. October 1, 1977 (ice freezeup)
5. November 22, 1977 (post freezeup)

The mid summer flights were followed by periods of ground reconnaissance for observing and documenting geologic and geomorphic occurrences and features, i.e. stratigraphy, lithologies, landforms, and depositional and erosional processes.

Input volumes of erosional detritus were determined using the measured erosion rate values and data taken from the above mentioned maps. Average vertical dimensions used were those observed during the two

periods of ground reconnaissance during the summer.

Identification of the sources of river detritus input during spring thaw, and calculation of the area and volume of this detritus was accomplished by examination of LANDSAT imagery. Bands 4 and 7 were enlarged to 1:250,000 and simultaneously enhanced using International Imagery System equipment. Over ice detritus was mapped directly from the enhancing equipment. Verification of the extent of the coverage was done during the June overflight.

PERTINENT RESULTS OF INVESTIGATION

Coastal Exposure and Erosion Rates

The east and west boundaries of Simpson Lagoon, for the purpose of quantifying data for model input, are the ARCO causeway and Oliktok Point respectively. Within this area of approximately 240 square kilometers, 96 kilometers of tundra capped bluffs border the lagoon. From maps and sequential vertical photography these 96 kilometers of exposure on the coast and islands were differentiated into high and low topographic areas; erosion rates were then determined and averaged for both types. Deltas and estuaries were excluded from the calculations. Maps 1 through 3 show erosion rates for the tundra islands.

Following verification, data points cited by Lewellen (1976) for the coastline between Oliktok Point and Beechey Point were included in the calculations. Exposure and erosion rates are given in Table 1.

Table 1 - Exposure and Average Erosion Rates in the Simpson Lagoon Area.

	<u>High Topography</u>	<u>Low Topography</u>
Coast	47 km, 1.1 m/yr	35 km, 1.3 m/yr
Island	10 km, 1.4 m/yr	4 km, 2.0 m/yr

High topographic areas are considered to average an aggregate thickness of 2.5 meters, 0.5 meter of tundra peat capping 2.0 meters of silt, sand, gravel, and ice. Low topographic areas are considered to average an aggregate thickness of 1.5 meters, 0.5 meters of tundra peat capping 1.0 meter of silt, sand, gravel, and lesser amounts of ice.

Erosion of the Beaufort Sea coast is due to a combination of thermal and mechanical agents. Thermal erosion occurs during the summer months and has its greatest effect on the coastal bluffs. As interstitial ice and permafrost thaw, the bluffs are more susceptible to slumping and thus wave impact. Erosion of the coast and islands is most active during storm periods and seems to be structurally directed.

Variations in coastal erosion rates tend to be more a function of high versus low topography rather than protected versus unprotected coastline. High topographic areas are underlain with clear ice which retards erosion. Erosion rates in these areas are slowed by large blocks of tundra mat which slump over the bluff, protecting it from erosion.

Island erosion rates tend to be higher than mainland rates due primarily to the islands' two sides of attack. The average erosion rate (determined from 89 points on Pingok Island) in the Simpson Lagoon area

is 1.6 meters per year. The seaward side of the islands tend to erode at a slower rate than the lagoon side because of wide beach development and a stabilizing dune ridge. The wide beach dissipates the wave energy across its width before impact; the dune ridge not only acts as a physical barrier to degradation processes, but also insulates the bluff from thermal degradation. Another consideration may be that a higher degree of solar radiation strikes south facing bluffs (island-lagoon) on any given summer day.

Approximate Duration of the Tundra Islands

Expected tundra duration on the offshore islands were determined using double the average erosion rate of 1.6 meters per year, with the measured distance to be eroded. The duration was maximized by using the greatest measured distance across an island perpendicular to the eroding fronts. Two tundra islands are expected to result as the narrow portion near the center of Pingok Island erodes. For greater precision, the duration of this part of Pingok Island was determined using two spot erosion rate measurements rather than the average erosion rate.

Without tundra covers the islands will probably remain as lag deposits left from the erosion of the tundra. Coarse clastics are not presently being transported in major river systems as indicated by their sediment-choked, braided nature. Introduction of coarse clastics to the islands is unlikely over a geologically short period of time; this material is therefore nonrenewable. The introduction of sand size clastics from river systems and coastal erosion should temporarily maintain

the lag gravel islands. Introduction of sand size clastics to the islands, however, will eventually decrease as the coast retreats, and the offshore islands will erode below base level.

Table 2 - Tundra Duration On the Offshore Islands.

Pingok Island	
Two Islands35 years
East Island	250 years
West Island	270 years
Bertoncini Island80 years
Bodfish Island.	160 years
Cottle Island (tundra areas east to west)	
East.90 years
Central40 years
West.55 years

Erosional Input Into the Barrier Island-Lagoon System

With the average coastal and island dimensions given in the section on coastal exposure and erosion rates, the total volume, and the volume of peat detritus introduced into the lagoon system were determined (Table 3).

Table 3 - Volume of Detritus Input Into Simpson Lagoon From Coastal Erosion

Total	$-2.5 \times 10^5 \text{ m}^3/\text{yr}$
	$-2.6 \times 10^3 \text{ m}^3/\text{yr}$ per kilometer of coastline
Peat Soils	$-6.0 \times 10^4 \text{ m}^3/\text{yr}$
	$-6.2 \times 10^2 \text{ m}^3/\text{yr}$ per kilometer of coastline

For the low and high topographic areas respective minima of 30% and 20% of the total volume are considered peat soils. These are considered minima because they are based only on the approximate thickness of the tundra mat. Considerable amounts of peat detritus are mixed with the inorganic detritus throughout the bluff. Upon combustion, peat soils show an organic content of 40% (Schell, 1977, personal communication). Densities of 2.0 g/cm^3 and 1.1 g/cm^3 for the inorganic and peat detritus respectively were used for determining the mass of the material introduced into the system by coastal erosion (Table 4).

Table 4 - Mass of Detritus Input Into Simpson Lagoon From Coastal Erosion.

Total	$-4.4 \times 10^8 \text{ kg/yr}$
	$-4.5 \times 10^6 \text{ kg/yr}$ per kilometer of coastline
Peat Soils	$-6.6 \times 10^7 \text{ kg/yr}$
	$-6.8 \times 10^5 \text{ kg/yr}$ per kilometer of coastline

River Detritus Into the Barrier Island-Lagoon System

Prior to ice breakup a large volume of detrital material from the Kuparuk River is deposited on the surface of the sea ice within Simpson Lagoon. Detrital material is also deposited on the sea ice at the mouths of the Sagavanirktok and Colville Rivers. As shown by LANDSAT imagery, little of the over ice flow from these rivers enters the boundaries of Simpson Lagoon. Barnes and Reimnitz (1972) noted westward over ice flow from the Kuparuk River, at least to Kavearak Point. Observations made by this investigator on a June overflight of the area confirm extensive lateral flow from all of the major rivers (Map 4). Flow from the Kuparuk River extended to the offshore islands, and at the channels, past the islands. The Colville River overflow was by far the most extensive, reaching Thetis Island to the west. Eastward, the Colville overflow did not extend beyond Oliktok Point. Perturbations in the sea and lagoonal ice covers created by petroleum exploration activities near the offshore islands and the Colville Delta, had little affect on the flow of detrital material. In all observed cases, flow was not significantly diverted or obstructed.

Carlson (1976 a and b) states that for the Kuparuk River, the initial spring thaw flow, lasting from three to four weeks in late May and early June, represents from 60 to 80 percent of the total annual flow, and that 70% of the spring thaw flow is probably beneath the lagoon ice cover. If this is the case, volume and mass figures presented in this report may be conservative. The bulk of detrital material, however, is probably carried in the initial stages of river breakup prior to the destruction

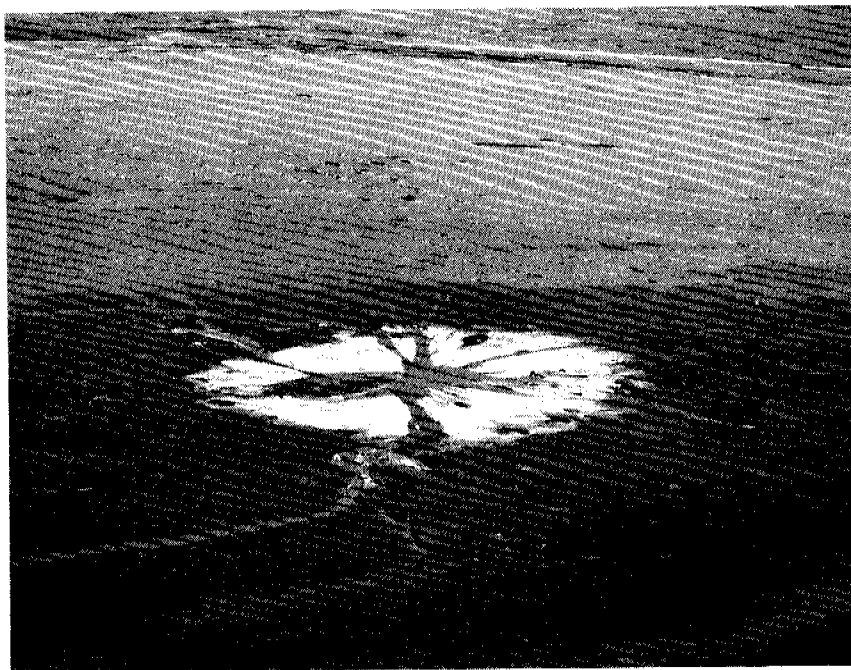


Figure 4 - Strudle hole in the sea ice near the Colville River.
(Photograph by P. Jan Cannon)

of shorefast ice and the development of palinas, resulting in deposition on the surface of the lagoon ice. This detrital material on the lagoon ice is then introduced into the lagoon and open ocean through cracks and strudle holes in the ice (Figure 4).

Mass and volume estimates of detritus are presented here only for the Kuparuk River since it is the major contributor of river introduced material into Simpson Lagoon. An estimate of average detrital thickness covering the lagoon ice is 0.02 meters. A representative overflow coverage of 54 kilometers² was measured from June 1973 LANDSAT imagery. Based on estimated percentages of organic detritus for the Colville River (Schell, 1977, personal communication), 1.0% of the total Kuparuk River spring thaw detritus is considered peat soils. Densities for the organic and inorganic fractions are assumed to be 1.1 g/cm³ and 2.0 g/cm³ respectively. Results are shown in Table 5.

Table 5 - Detritus Input Into Simpson Lagoon From the Kuparuk River Spring Runoff.

Volume of total detritus	$-1.08 \times 10^6 \text{ m}^3$
Volume of inorganic detritus	$-1.07 \times 10^6 \text{ m}^3$
Mass of inorganic detritus	$-2.14 \times 10^9 \text{ kg}$
Volume of peat detritus	$-1.08 \times 10^4 \text{ m}^3$
Mass of peat detritus	$-1.19 \times 10^7 \text{ kg}$

Storm Surge

Areas of possible inundation by storm surge are shown on Map 5. The positions of driftwood on the gravel islands indicate that all of the gravel islands could be completely washed over during periods of maximum storm surge.

Low-lying tundra areas on the mainland coast and offshore islands can also be inundated during storms. Driftwood and steel barrels were observed in some areas as much as one kilometer inland. The position of the wood and barrels, however, may not represent the maximum inundation for a given surge if their deposition occurred during recession of the surge. The extent of maximum storm surge, therefore, should include a safety zone beyond the inundation areas shown on Map 5.

Source of Material

Most of the coarse clastic material is derived from the erosion of tundra covered areas. On the tundra islands and the mainland, constituent gravel has been brought to the surface by frost heave. Coarse clastics are also observed in the coastal bluffs and in the detrital wedge at the base of the bluffs.

Origin and Evolution of the Barrier Islands and Coastal Lagoons

The nature and evolution of the Arctic Coastal Plain is not well understood. This investigator believes that the coastal plain, at least in part, may represent a pre-Wisconsin ground moraine. The clastics composing the coastal plain have similar characteristics to most glacial tills, i.e. multiple lithologies, angular clasts, oriented surface striations and polished surfaces on boulders, and a wide range of clast

sizes. Recently acquired low sun angle LANDSAT imagery shows many features analogous to features in known glaciated areas of Alaska. The same imagery shows definite lobate moraine deposits extending to within 30 kilometers of the present coastline in the Canning River region, east of the study area.

Lithologies found on the offshore islands have several distinct provenances. Carboniferous age limestone and dolomite gravels are present on all of the offshore islands. Carboniferous carbonates were found to compose up to 8% of the material in random gravel samples collected from the islands. These carbonate rocks are most likely derived from the eastern Brooks Range, as large areas of Carboniferous carbonates are presently exposed there. Other suggested provenances, detailed descriptions, and possible transport mechanisms (such as ice rafting) for the gravels found within the study area are in MacCarthy (1958), Mowatt and Naidu (1974), and Naidu and Mowatt (1974).

In light of, and for the purposes of this study, the ultimate provenances of the rocks composing the Arctic Coastal Plain and offshore islands are irrelevant. What is relevant, however, is the fact that the coastal plain did in the past extend beyond its present limits.

The tundra islands are remnant features (in a sense, not true barrier islands) of this once more extensive coastal plain. Indications of this are the morphology of surface lakes and drained lakes, similar stratigraphy for the islands and mainland, and similar lithologies. The tundra islands become isolated from the mainland by communication of inland lakes or topographic lows with the ocean through inundation by erosion (Figure 5). Initially, inundation may be local; subsequent coalescence

of adjacent lakes enlarges the inundated area, and if inland morphology permits, communication from two directions can result creating a lagoon. The size and shape of the barrier island-lagoon system is then modified by the same erosional processes.

An area having potential for one day becoming an island-lagoon system is located immediately west of Harrison Bay. The Kogru River illustrates coalescence of inland lakes; further coalescence will someday form a channel connecting Techekpuk Lake with Harrison Bay. Coalescence of Techekpuk Lake with, say, Imakruak Lake would then isolate the entire area west of Harrison Bay to Smith Bay. On a smaller scale, preferential erosion along Garrey Creek in the same area could isolate the present-day peninsula north of the Kogru River, forming an offshore remnant island (Figure 6). Figure 6A shows the present-day morphology of the area west of Harrison Bay. Figure 6B illustrates the hypothetical morphology after erosion.

The gravel islands of the Jones and Return groups are, in part, remnant coastline, the tundra covers having been completely eroded leaving the constituent sand and gravel as lag. Gravel is not presently being renewed to the islands from other than local sources.

Large boulders observed eroding from the bluffs of tundra covered islands and found on the beaches, were not observed on the gravel islands. These large boulders may be buried in the gravel islands; reworking processes such as wave impact and ice shove would bury the larger heavier clastics.

As constructional features, the islands probably receive sand size clastics eroded from local tundra covered areas and from major rivers, especially the Kuparuk and Sagavanirktok.

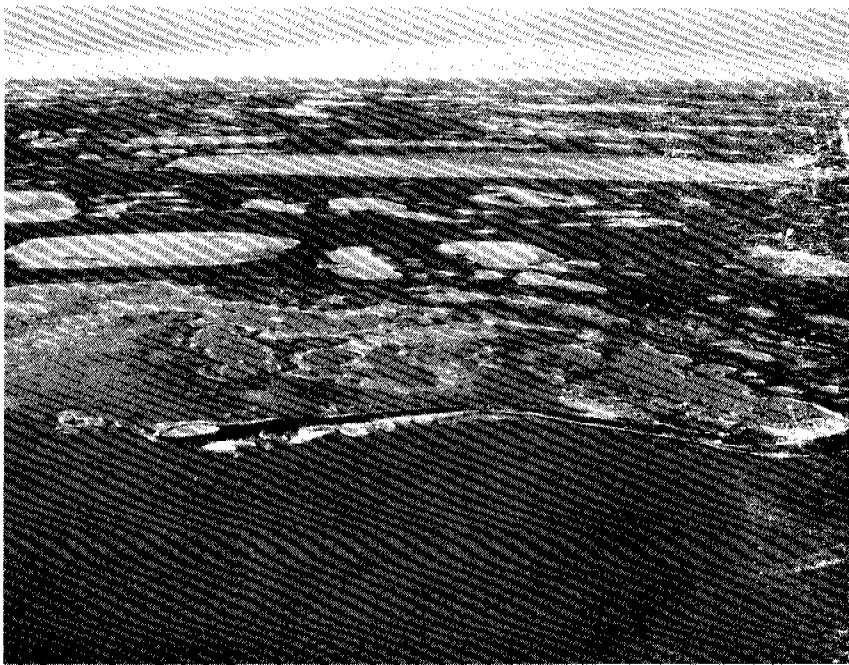


Figure 5 - Lake bed being inundated along the Arctic coast.
(Photograph by S. E. Rawlinson)

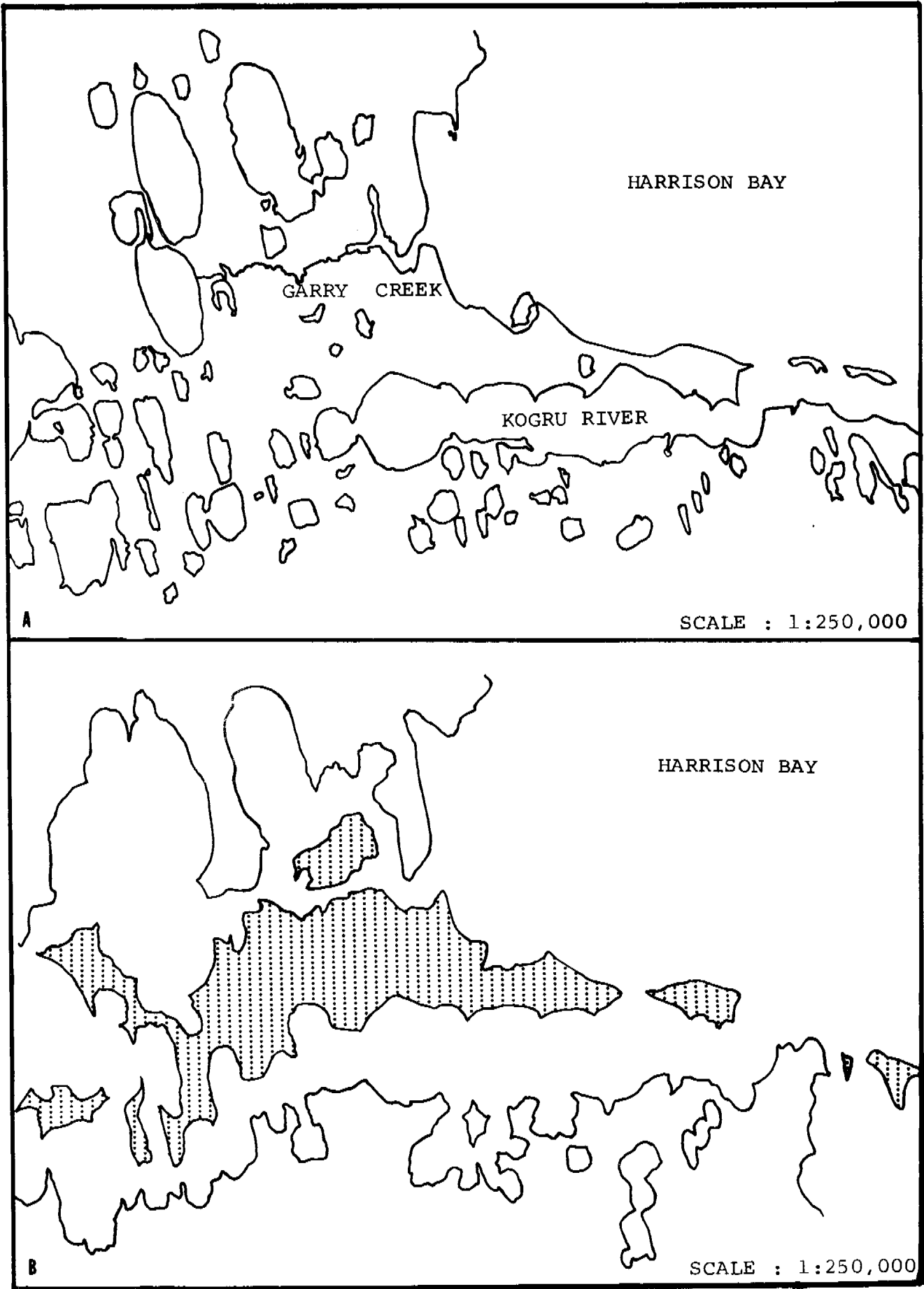


Figure 6- Idealized development of an offshore remnant island by coalescence of lakes.

REFERENCES CITED

- Barnes, P. W., and Reimnitz, Erk, 1972, River overflow into sea ice off the northern coast of Alaska, spring 1972: *Trans. Am. Geophys. Union*, v. 53, p. 1020.
- Black, Robert F. and Barksdale, William L., 1949, Orientated lakes of northern Alaska: *Jour. of Geol.*, v. 57, pp. 108-118.
- Carlson, R. F., 1976a, A theory of spring river discharge into the arctic icepack, *in* D.C. Burrell and D.W. Hood, conveners, *Proceedings of the Third Int. Conf. Port., Ocean Engin. Arctic Condition*, v. 1, *Inst. Mar. Sci., Univ. of Alaska, Fairbanks*, pp. 165-166.
- Carlson, R. F., 1976b, Environmental assessment of the Alaskan Continental Shelf, Unpubl. rept. to NOAA, Water Res. Inst., Univ. of Alaska, Fairbanks.
- Carson, Charles E. and Hussey, Feith M., 1959, The multiple-working hypothesis as applied to Alaska's oriented lakes: *Iowa Acad. of Science, Proc.*, v. 66, pp. 334-349.
- Hartwell, Allen D., 1973, Classification and relief characteristics of northern Alaska's coastal zone: *Arctic*, v. 26, no. 3, pp. 244-252 (Sept.).
- Lewellen, Robert, 1976, A study of Beaufort Sea coastal erosion, northern Alaska, *in* D.W. Hood and D.C. Burrell, eds., *Assessment of the Arctic Marine Environment: Selected Topics*, Occas. Publ. No. 4, *Inst. Mar. Sci., Univ. of Alaska, Fairbanks*, 469 p..
- MacCarthy, Gerald R., 1958, Glacial boulders on the Arctic coast of Alaska: *Arctic*, v. 2, pp. 71-85.
- Mowatt, T. C. and Naidu, A. S., 1974, Gravels from the Alaskan Continental Shelf, Beaufort Sea, Arctic Ocean: petrologic character and implications for sediment source and transport: *Alaska State Div. of Geol. and Geophysical Surveys, Open File Rept. 43*.
- Naidu, A. S. and Mowatt, T. C., 1974, Aspects of size distributions, mineralogy and geochemistry of deltaic and adjacent shallow marine sediments, North Arctic Alaska, *Inst. Mar. Sci., Univ. of Alaska, Conf. 30*, pp. 238-268, *in* Hufford, Gary L., et al., eds., 1974, *U.S. Coast Guard Oceanographic Rept. CG 373-64*.
- Short, A. D., Coleman, J. M. and Wright, L. D., 1974, Beach dynamics and nearshore morphology of the Beaufort Sea coast, Alaska: *in* *The Coast and Shelf of the Beaufort Sea, Proc., AINA Symposium* (eds. J.C. Reed and J.E. Sater), AINA, Arlington, Va., pp. 477-488.
- Tucker, Robert W. and Burrell, David C., 1977, The sedimentary environment of a lagoon on the beaufort Sea coast of Alaska: *Marine Sci. Comm.*, 3(2), *Inst. Mar. Sci., Univ. of Alaska, Fairbanks*, pp. 93-116.

GLOSSARY

- Bar - a generic term for various elongate offshore ridges, banks, or mounds of sand and gravel, submerged at high tide, and built up by the action of waves or currents on the water bottom.
- Barrier island - a long, low, narrow wave-built sandy island representing a broadened barrier beach that is sufficiently above high tide and parallel to the shore.
- Braided stream - a stream flowing in several dividing and reuniting channels resembling the strands of a braid.
- Carboniferous - the Mississippian and Pennsylvanian periods; from 345 to 280 million years ago.
- Clastic - pertaining to a rock or sediment composed principally of broken fragments that are derived from preexisting rocks that have been transported some distance from their places of origin.
- Coastal plain - any lowland area bordering a sea or ocean, extending inland to the nearest elevated land and sloping gently seaward.
- Delta - a low, nearly flat, alluvial tract of land deposited at or near the mouth of a river; commonly forming a triangle or fan shaped plain.
- Dune - a low mound or ridge of loose windblown material (usually sand) capable of movement from place to place, but always retaining its own characteristic shape.
- Eolian - Pertaining to the wind, e.g. wind deposits.
- Estuary - the seaward end of a river valley where fresh water mixes and measurably dilutes sea water and where tidal effects are evident.
- Fluvial - Of or pertaining to a river or rivers.
- Frost heave - the upward movement and distortion due to internal frost action resulting from subsurface freezing of water and growth of ice masses.
- Geomorphology - the science that treats the general configuration of the Earth's surface especially applied to the genetic interpretation of landforms.
- Ice rafting - the transporting of rock of all sizes, on or within icebergs, ice floes, river drift, or other forms of floating ice.

- Ice shove - the lateral pressure exerted by the expansion of shoreward moving ice; the ridge or mound of material formed by ice shove.
- Ice wedge - a vertical, wedge-shaped vein of ground ice.
- Lag deposits - a residual accumulation of coarse, usually very hard rock fragments remaining on a surface after the finer material has been blown away.
- Lagoon - a shallow stretch of sea water, such as a sound, channel, bay, or salt water lake, near or communicating with the sea and partly or completely separated from it by a low, narrow elongated strip of land.
- Lithology - the description of rocks on the basis of such characteristics as color, structure, mineralogic composition, and grain size.
- Longshore transport - material transported by an ocean current; caused by the approach of waves to a coast at an angle. It flows parallel to and near to the shore.
- Lug - the remnant centers of raised polygons left by select erosion along the cracks in patterned ground.
- Moraine - a mound or ridge of unsorted, unstratified glacial drift deposited by direct action of glacier ice in a variety of topographic land forms that are independent of the surface.
- Offshore islands - a general term used to include tundra islands and barrier islands.
- Palinas - open water area where a river mouth enters an ice-covered ocean or lagoon, usually formed prior to and during spring breakup.
- Patterned ground - more or less symmetrical forms such as circles, polygons, nets, steps, and stripes that are characteristic of, but not necessarily confined to, surficial material subject to intensive frost action.
- Permafrost - any soil, subsoil, or other surficial deposit, even bedrock, occurring in Arctic or sub-Arctic regions at variable depth beneath the Earth's surface at a temperature below zero for over two years.
- Pingo - a frost mound; conical mound (commonly 3- to 50 meters high) raised by hydrostatic pressure of water within or below the permafrost of Arctic regions.
- Glacial striations - a superficial scratch, a tiny furrow, or a thread-like line inscribed on a rock surface by a glacier.
- Polished surface - a polished and smoothly striated surface that results from friction along a fault plane.

Remote sensing - the measurement or acquisition of information of some property of an object or phenomenon, by a recording device that is not in physical or intimate contact with the object or phenomenon under study, i.e. satellite imagery.

Spit - a finger-like projection of the beach commonly consisting of sand and gravel deposited by longshore drifting.

Storm surge - a surge of water caused by storm activity.

Strudle holes - a hole in sea ice through which fresh water enters the ocean.

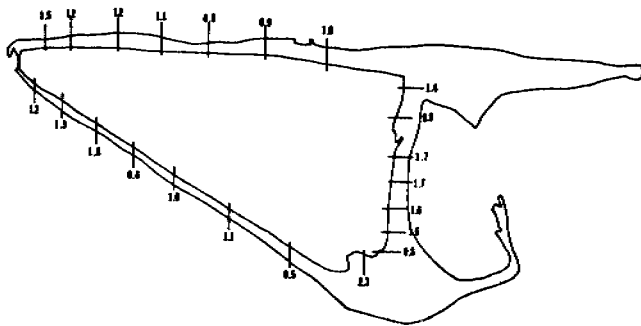
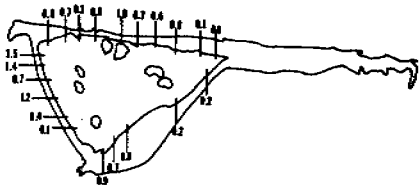
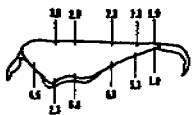
Talik lake - a thaw lake occurring in permafrost terrains.

Thermal erosion - erosion that is enhanced by the melting of underlying ice or permafrost.

Tundra island - any offshore island possessing tundra cover; generally formed as erosional remnants of a coastal plain.

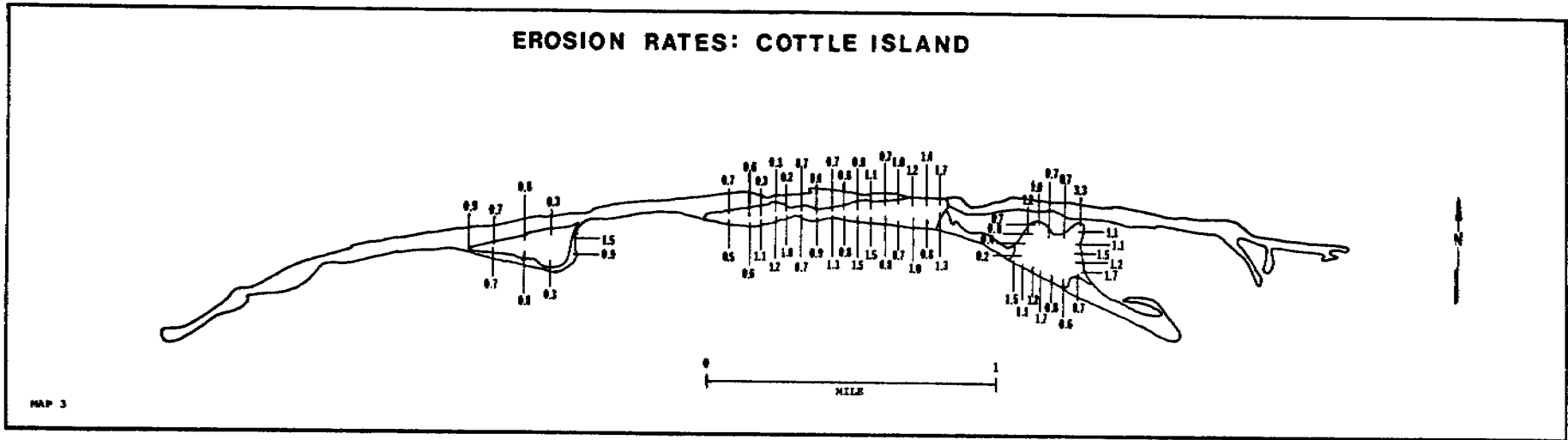
Wisconsin Pleistocene - pertaining to the fourth glacial stage of the Pleistocene Epoch in North America, following the Sangamon interglacial stage: active 7,000 to 15,000 years ago.

EROSION RATES: UNNAMED ISLAND, BERTONCINI ISLAND, AND BODFISH ISLAND

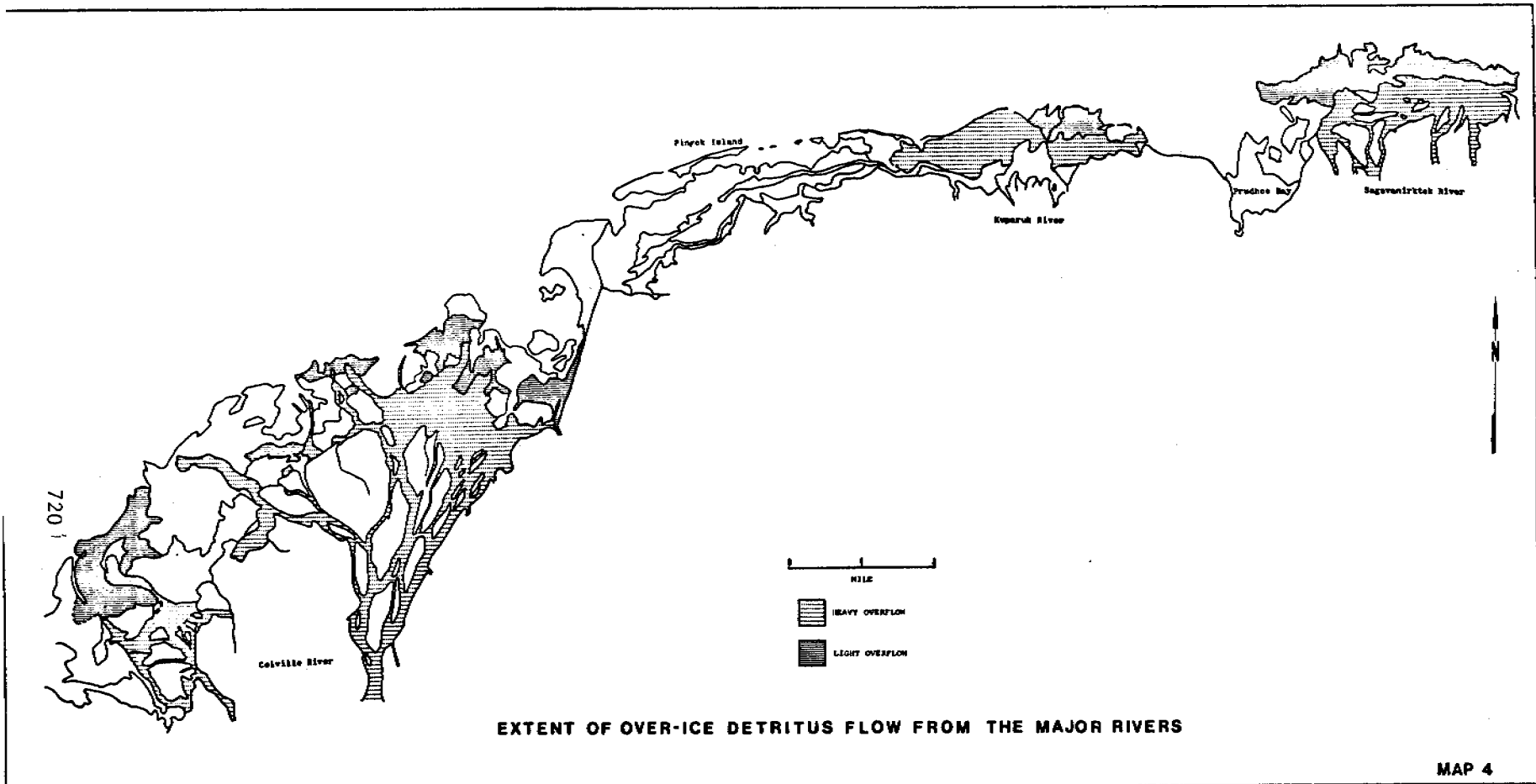


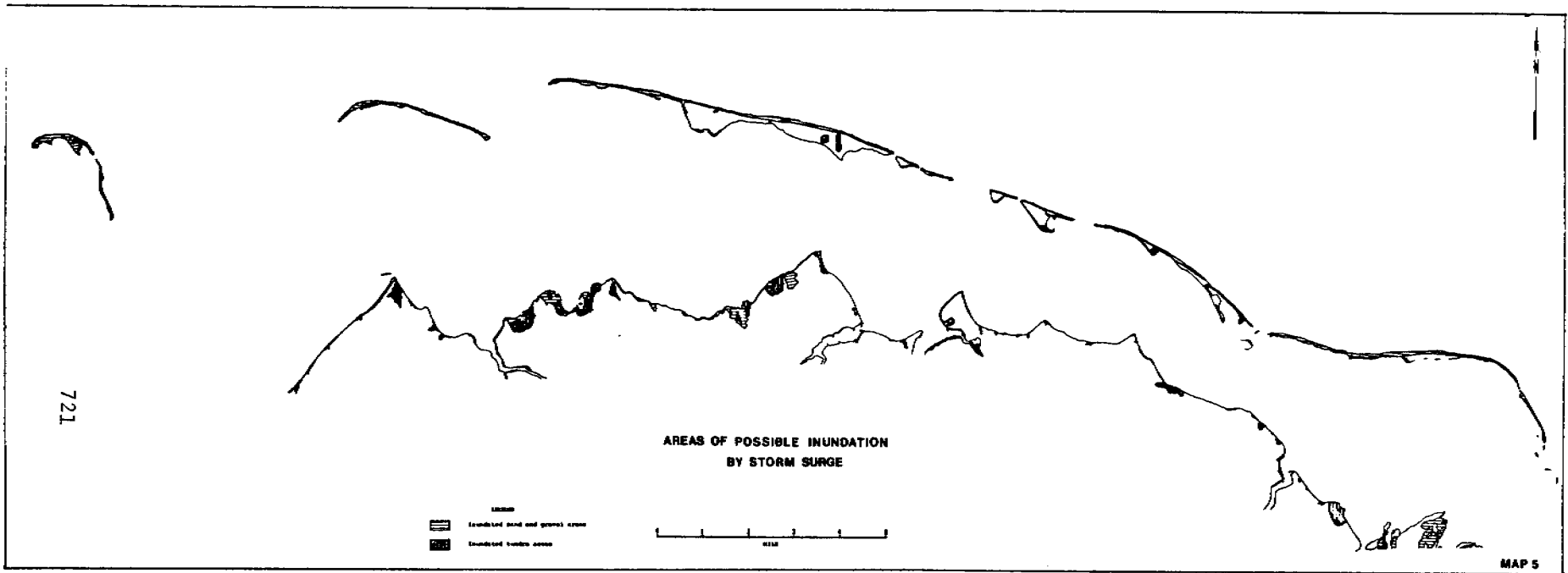
MEASUREMENTS IN FEET PER YEAR

MAP 2



MAP 3



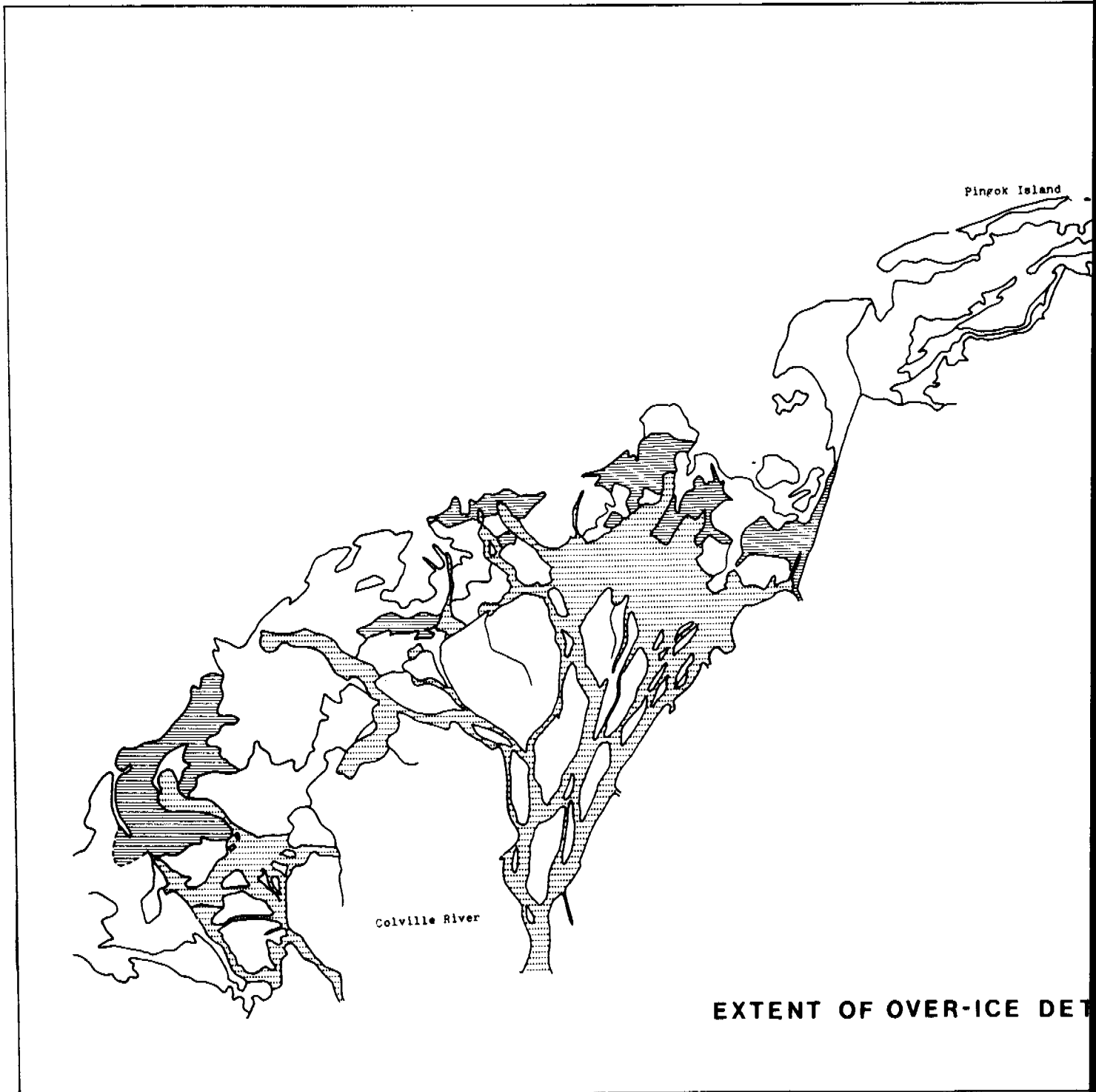


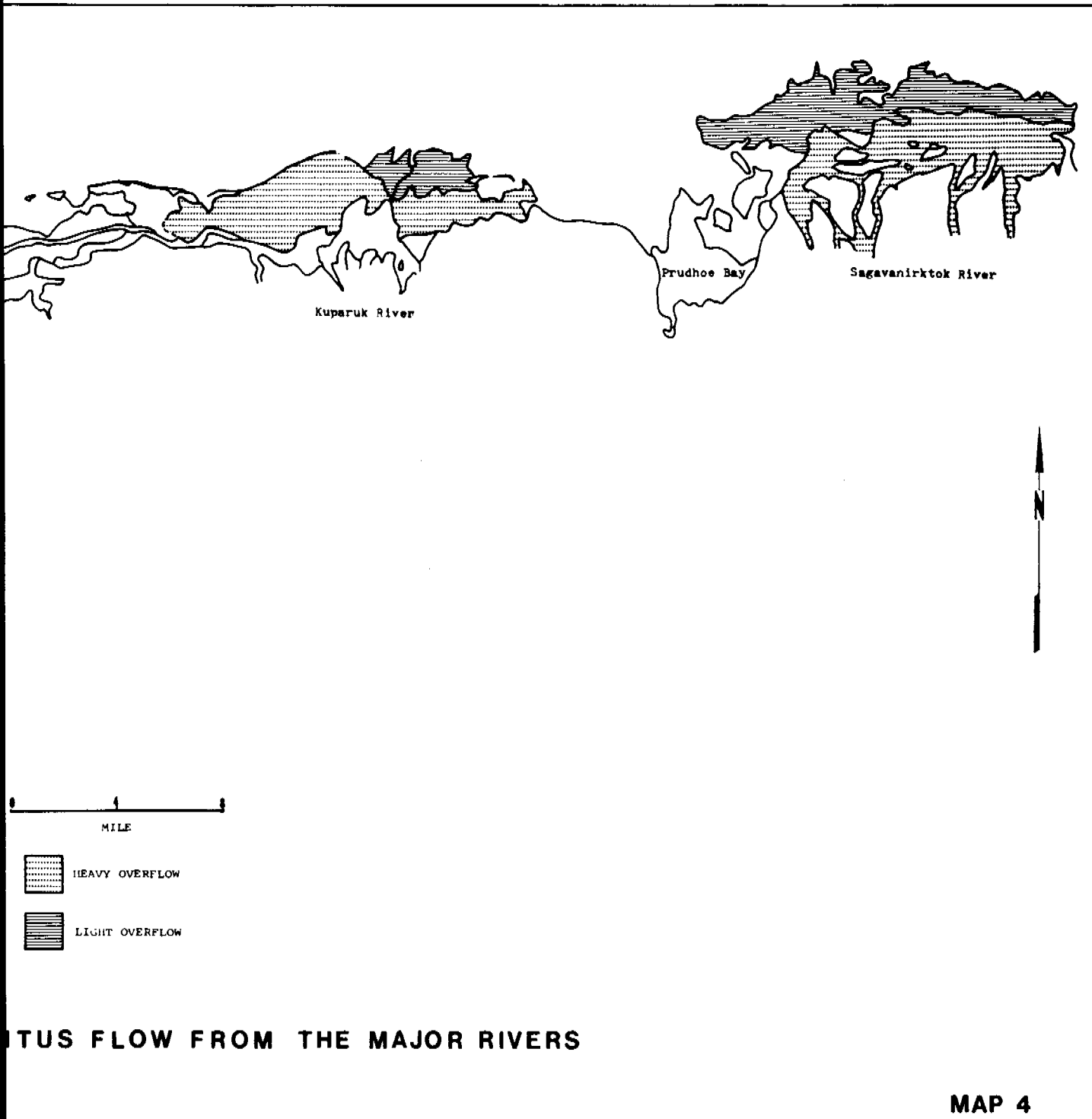




1 M SURGE

MAP 5

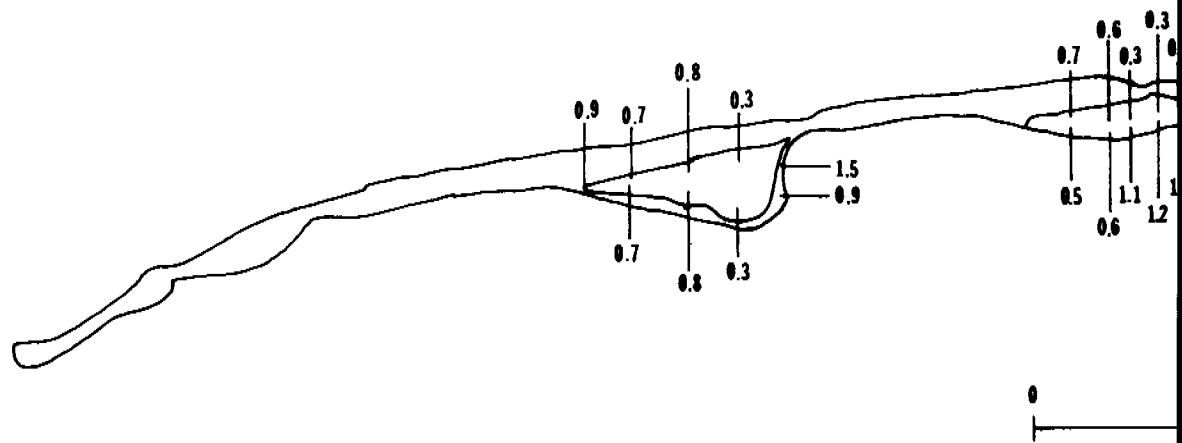




TUS FLOW FROM THE MAJOR RIVERS

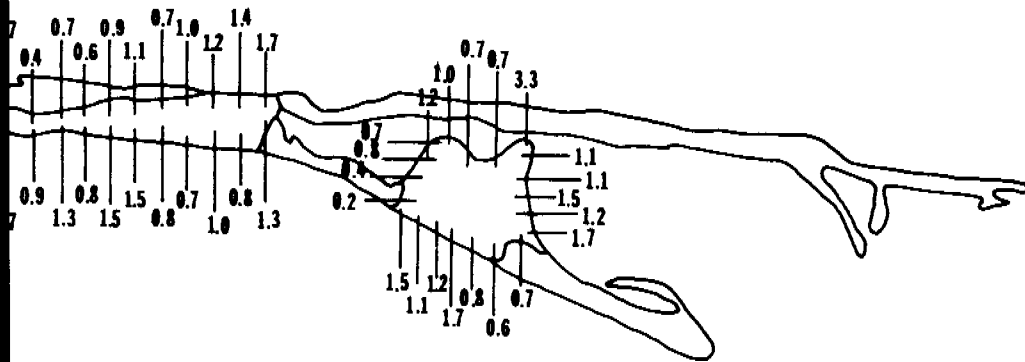
MAP 4

EROSION RATES: CO



MAP 3

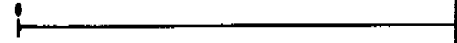
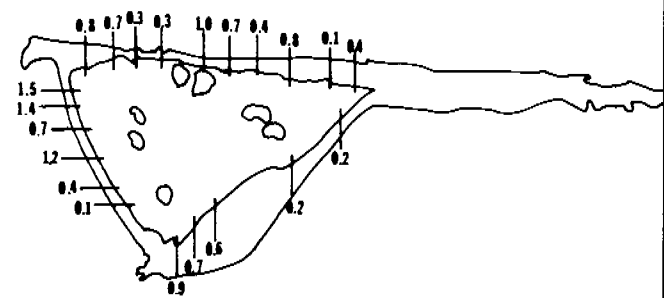
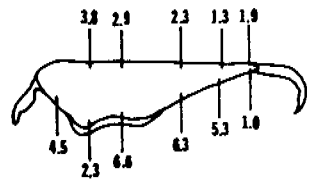
TITLE ISLAND



1
MILE



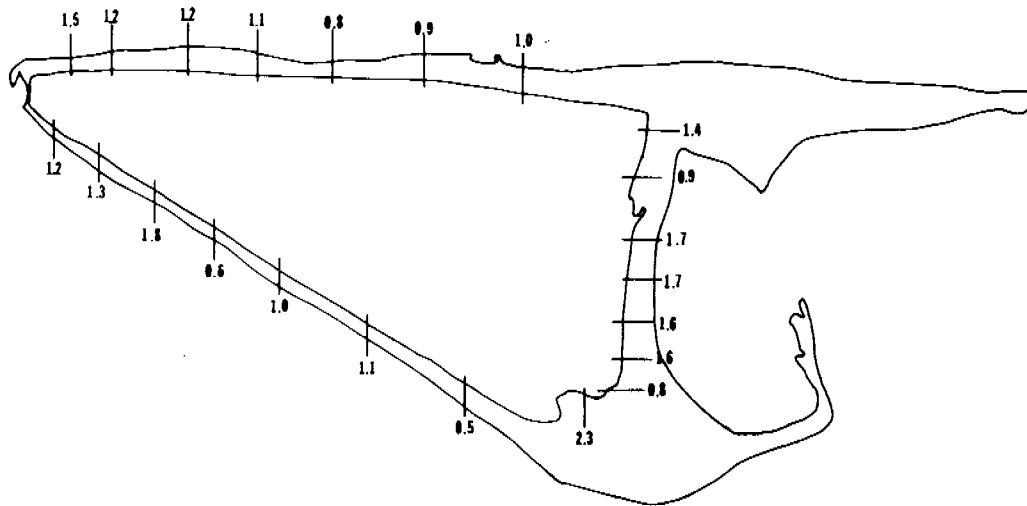
EROSION RATES: UNNAMED ISLAND, B



MAP 2

MEASUREMENT

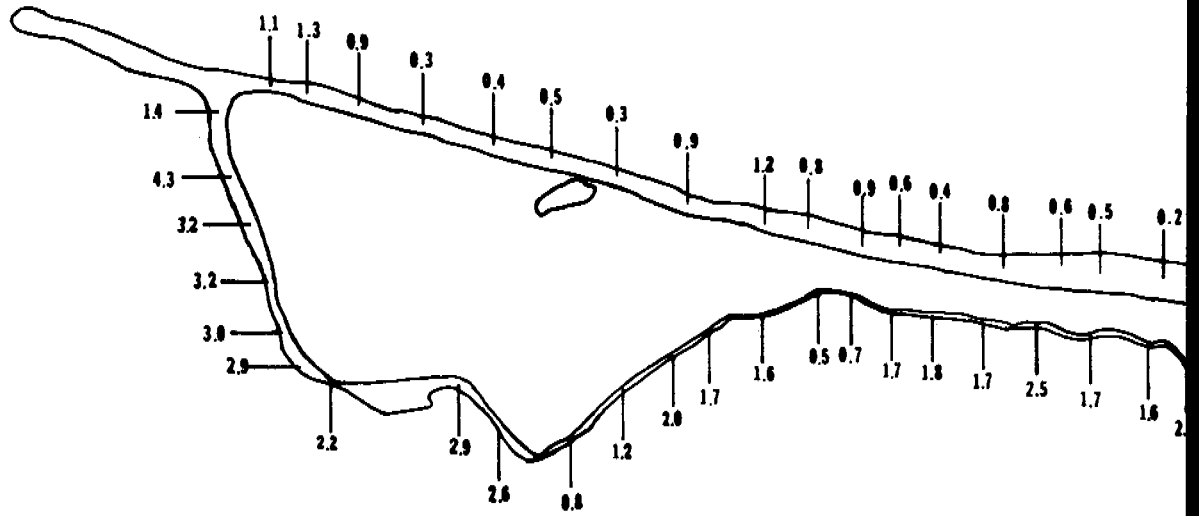
ERTONCINI ISLAND, AND BODFISH ISLAND



0.5 1
MILE

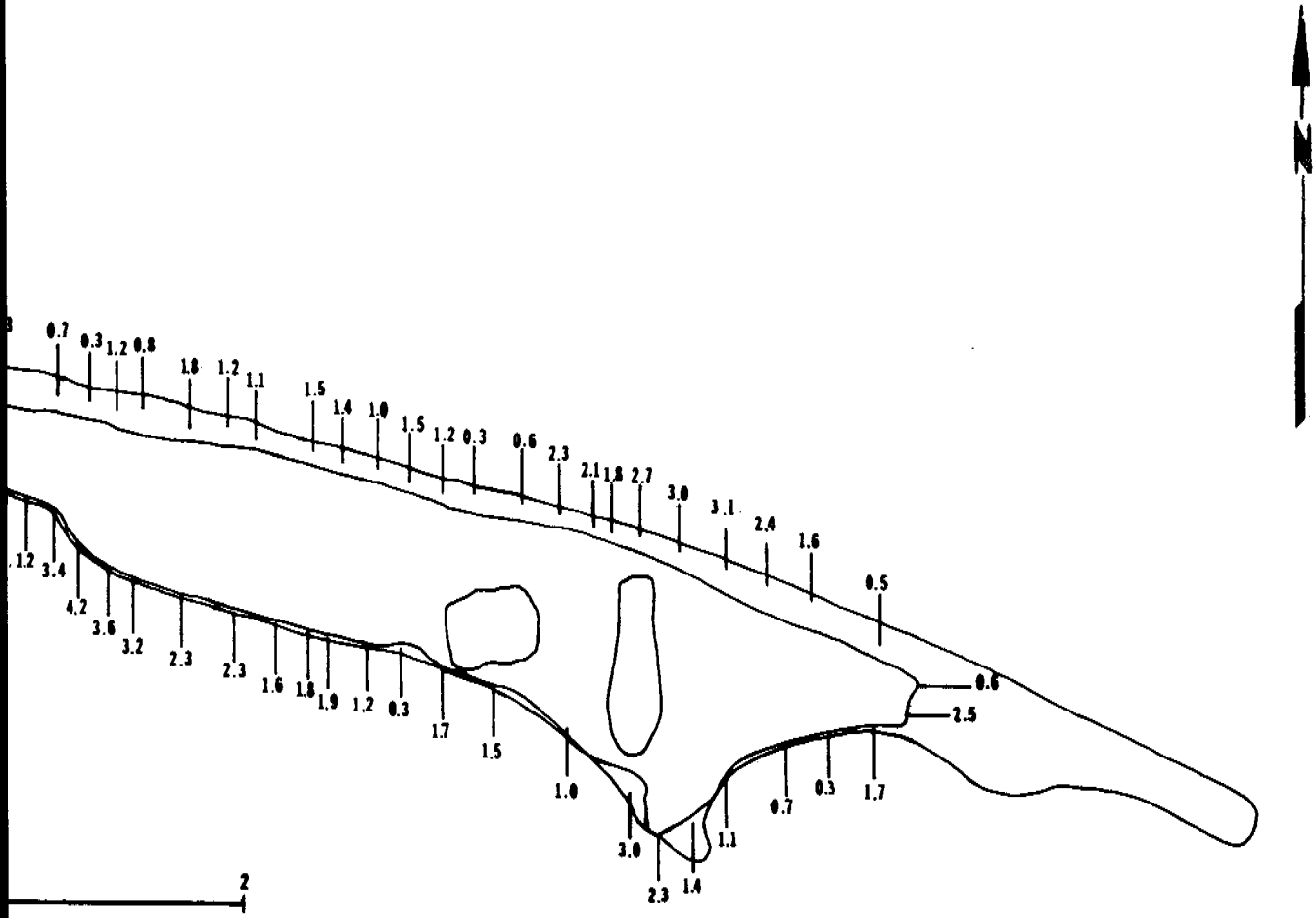
IN METERS PER YEAR

EROSION RATES: PINGO



MAP 1

ISLAND



Contract # 03-7-022-35182

Research Unit # 531

Reporting Period: June 13, 1977-February 28, 1978

Oceanographic Processes in a Beaufort Sea
Barrier Island-Lagoon System:
Numerical Modeling and Current Measurements

1st Annual Report

J. C. H. Mungall, R. W. Hann, Jr., D. J. Horne,
R. E. Whitaker, C. E. Abel
Department of Oceanography
Texas A&M University
College Station, TX 77843
(713)845-1443

March 1978

LIST OF CONTENTS

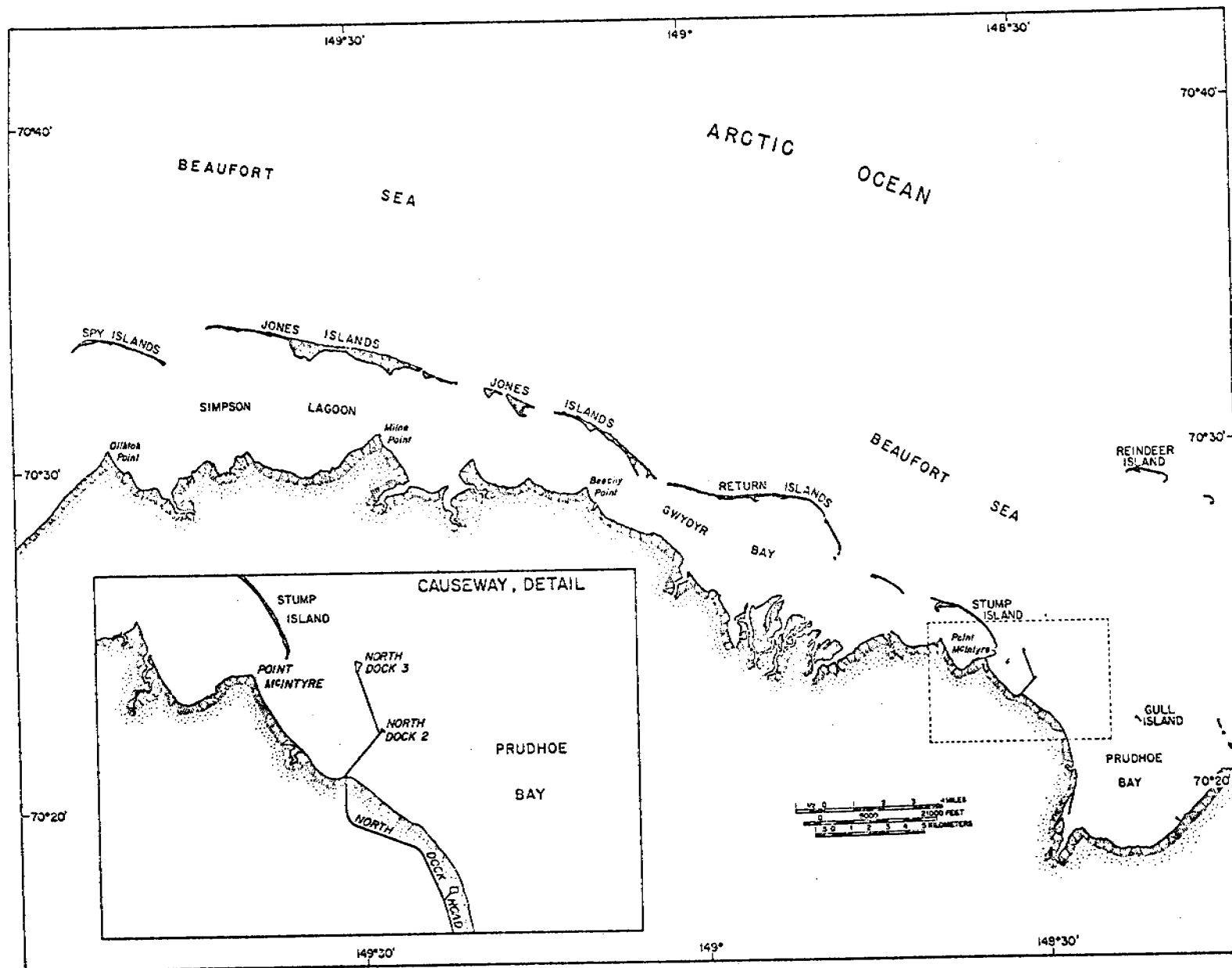
	Page
I and II. Summary and Introduction	2
III and IV. Simpson Lagoon - General Description	5
V. Numerical Modeling Experiments	6
VI. Summer 1977 Field Program	30
VII. Information Gaps and Research Proposed for 1978	43
VIII. Synopsis of Results	46
References	47
Appendix A Two-dimensional modeling results: Unverified depth-mean current vectors and water parcel tracks	48

I. and II. Summary and Introduction

Simpson Lagoon, the principal study area of this contract, is located on the shore of the north coast of Alaska at approximately 70°31'N, 149°15'W. The lagoon, considered a typical example of an arctic barrier island lagoon system, lies some 10 miles to the west of Prudhoe Bay. The region being studied, which is shown in Figure 1, will of course be subject to development should exploratory drilling occur offshore in the wake of the initial success of the Prudhoe Bay oilfield. One of the most likely points of impact will be the barrier islands, since they constitute convenient locations for offshore drilling. Due to the shallow nature of the lagoon the building of causeways is practical in order to provide access to cargo facilities (see Figure 1) or to the barrier islands.

Following discussions with the Texas office of LGL Limited during the last quarter of 1976, a proposal was submitted to NOAA by the Texas A&M Research Foundation on December 21, 1976. The objective of the proposal was to assist other disciplines with their physical oceanography needs for the overall purpose of assessing the susceptibility of Arctic Barrier Island Lagoon systems to modification by nearshore development. This was to be accomplished through numerical modeling and through measurements. Prior to the award of the contract, two ecological modeling workshops held at the University of British Columbia were attended (December 1976 and April 1977) for the purpose of participation in the identification of key data needs. The contract, for \$47,688.00, was awarded in June 1977 to cover the period June 13, 1977 through February 28, 1978.

The modeling part of the investigation concentrated around the development of a two-dimensional vertically-integrated transport model and a three-dimensional multi-level model -- both having the same 1 km × 2 km grid



735

Figure 1. Map of Simpson Lagoon and Prudhoe Bay. The inset shows details of the causeway.

spacing and the same bottom topography. Simulations with the former model have led to a knowledge of the variation of exchange rates with wind speed and direction, of likely water parcel trajectories, and of the probable effect (or lack of effect) of the ARCO causeway on currents. The measurement program (some 3 weeks during August 1977) concentrated on the effects of the causeway on temperature and salinity distribution, on the entrances in the eastern part of the lagoon, and on a near-synoptic survey (using a helicopter) of the lagoon and its surroundings.

Findings from the modeling are that exchange rates and currents vary primarily with the angle between the wind and the lagoon axis (regardless of whether the wind is westerly or easterly) and of course with wind speed. Due to the numerous entrances, exchange rates versus wind speed for the water above the bottom layer vary linearly and are of the order of 20% of the lagoon volume per day for prevailing 5 ms^{-1} ENE winds. Currents are typically of the order of 3% of the wind speed, and it appears that, at distances of more than 10 km, the effect of the causeway on currents is minimal. The measurement program indicated that large differences in temperature and salinity (reaching 7°C and 18 ‰) can occur across the causeway, with the warmer and less saline water tending to be found on the upwind side of the causeway. The helicopter survey indicated that temperatures tend to be highest along the mainland side of the lagoon, a feature which is probably related to the preferential nearshore movement of fish.

Any discussion of the implications of these preliminary findings on OCS oil and gas development would be premature at this instant (March 1978), since any such implications are primarily related to possible biological impacts. The reader is cautioned that a coarse grid spacing was used in the first year's modeling, that the modeling results await verification, and that the field measurements are limited in extent.

III. and IV. Simpson Lagoon -- General Description

Simpson Lagoon (see Figure 1) is bounded by Harrison Bay on the west and Prudhoe Bay on the east. The lagoon is 50 km in length, narrowing from 9 km in the west to 1 km in the east. Depths within the lagoon typically range between 1 and 2 m, although entrance depths can reach 6 m or more. Depths are generally greatest on the western sides of entrances, and the existence of the entrances themselves can change with time.

The lagoon appears to be strongly wind-driven, with flushing rates and currents being closely related to local winds. The lagoon is influenced by fresh water inflows -- particularly those of the Colville River, the Kuparuk River, and the Sagavanirktok River, which flow, respectively, into Harrison Bay, Simpson Lagoon, and Prudhoe Bay. Noteworthy is the short duration of the peak river discharge, much of which can occur before the ice has left the lagoon. Considerable lateral variations in salinity and temperature can occur; these variations probably have a first order effect on the biology of the region but only a second order effect on the circulation within the lagoon.

Local winds are predominantly from the ENE (some 70% of the time). Storms tend to be from the NW. Associated with these storms are possible sea level rises of 2 to 3 meters. (The tidal range is small in comparison -- of the order of 30 cm.) Useful summaries of knowledge concerning the region can be found in Kinney *et al.* (1972), Wiseman *et al.* (1973), Alexander *et al.* (1975), and Barnes *et al.* (1977).

considered) and three-dimensional modeling (in which density and current are permitted to vary in the vertical, as well as laterally). The two classes will be presented sequentially.

Two-dimensional Modeling

Initial efforts have been directed towards the implementation of a model which addressed the following needs:

- 1) independent variables of transport per unit width (instead of current) as needed for computing exchange rates,
- 2) the capability of modeling islands as subgrid scale barriers (instead of using rectangles with a minimum width of one full grid-space interval), since many of the islands, and of course, causeways, are thin,
- 3) provision for recession and flooding of water on grid-squares, since parts of the floor of Simpson Lagoon can be exposed under certain wind conditions, and flooding of the land (with the attendant possibility of pollution) is possible,
- 4) inclusion of algorithms for the computation of flow over broad-crested wiers or over partially or fully submerged narrow-crested barriers,
and
- 5) the inclusion of Coriolis acceleration effects.

The above needs were met by making a small (but non-trivial) extension to the model used by Reid and Bodine (1968) for the study of storm surges in the shallow Galveston Bay region of Texas. The equations, as presently (February 1978) modeled, are

V. Numerical Modeling Experiments

Prior to the hydrodynamic numerical modeling to be described in this section, previous modeling of value (soon to be summarized in a final project report) had been carried out by Richard Callaway, Marine and Freshwater Ecology Branch, Corvallis Environmental Research Laboratory, Environmental Protection Agency, under the title "Transport of Pollutants in the Vicinity of Prudhoe Bay, Alaska (R.U. 335)." This work was directed principally towards the computation of currents in Simpson Lagoon and Prudhoe Bay (using fine grids), and in the region extending from Oliktok Point to Challenge Point using a coarse grid. Both single and multi-layer situations were studied, and the results will be of particular use in providing estimates of river, astronomic and wind-induced current magnitudes and for making preliminary estimates as to the effect of the ARCO causeway on water circulation in the region.

The modeling undertaken in the Simpson Lagoon study differs from the above in that it has been oriented, as much as is possible, to the needs of the biological studies. In addition, since the need for flexibility in the study is essential if the modelers are to be responsive to changing requirements, our philosophy during the first eight months has been that of providing a limited amount of background information and of preparation. In this fashion, instead of running an exhaustive series of simulations, we have concentrated on developing models and displays that can rapidly be altered so as to meet the more specific requests for information that can be expected at the start of the 1978 program.

The modeling effort is divided into two sections: two-dimensional modeling (in which transports per unit width or depth-mean currents are

$$\frac{\partial U}{\partial t} = -gD \frac{\partial H}{\partial x} + \gamma V - fQU + X \quad (1)$$

$$\frac{\partial V}{\partial t} = -gD \frac{\partial H}{\partial y} - \gamma U - fQV + Y \quad (2)$$

and

$$\frac{\partial H}{\partial t} + \frac{\partial U}{\partial x} + \frac{\partial V}{\partial y} = R, \quad (3)$$

in which x and y are horizontal coordinates; t is time; U and V are the vertically averaged components of transport per unit width; g is the acceleration due to gravity; H is the water surface elevation relative to local mean sea level; D is the total water depth; γ is the Coriolis parameter [$2 \times$ earth's angular rate of rotation \times \sin (latitude)]; f is a non-dimensional friction parameter; Q is the magnitude of the vertically averaged transport per unit width; R is the rainfall rate, and X and Y are the components of wind stress divided by water density.

With the exception of simulations run before the start of the project, the grid used for modeling Simpson Lagoon has been that shown in Figure 2, where crosses denote the corners of computational rectangles with dimensions 1 km by 2 km. (Heights were evaluated at the center of each rectangle; normal transports at the centers of the four sides.) The relatively coarse grid spacing was selected as a compromise between the needs of the ecological model and the need for economy. Runs with the above grid spacing typically cost around \$10, those with a grid spacing sufficient for detailed modeling of the effects of the causeway (say, $\frac{1}{2}$ km by $\frac{1}{2}$ km) would probably have cost around \$150.

To date (February 1978) the cases studied have been ones to investigate the response of the lagoon to steady winds; astronomical tide and river influences have been neglected. Winds from five different directions

have been studied in order to estimate the dependence of depth-mean currents and exchange rates on wind direction; details of the cases studied are shown in Table 1. Tests 1 through 3 represent simulations under prevailing wind directions, with the exception of the 35 m s^{-1} wind from east northeast -- the latter test being one to demonstrate water recession and currents under extreme conditions. Since the first three tests indicated that the key parameter influencing currents and exchange rates was the magnitude of the angle between the wind (whether from an easterly or a westerly direction) and the lagoon axis, two more tests were run. Tests 4 and 5 were conducted in an effort first to investigate further the above finding, and secondly (anticipating that these wind directions would cause the largest currents) to investigate probable causeway effects.

The modeling of the region, surrounded by open boundaries on three sides, presented a problem since it is necessary to specify either height or transports on every boundary. As data were lacking on the open sides of the model, and since steady state conditions were to be modeled, the decision was made to use so-called "flow-through" boundary conditions of the type $\partial U/\partial x = 0$ (assuming no local change of depth with distance). The only relevant output of such a model is the *steady-state* output -- the intermediate results indicate only how the simulation is settling down, not how the lagoon behaves during this period. Three additional columns of computational rectangles were added to the east and west ends of the grid shown in Figure 2 to improve the modeling of east/west flow through the region, and in these, and in the last two rows of the northern boundary of the region, no change of depth normal to the open boundaries was permitted to occur. The resulting grid thus consisted of 17×34

Table 1
Summary of two-dimensional tests

Test category	Wind direction (from, degrees true)	Speeds (ms ⁻¹)
1	ENE	5, 10, 15, 20, 35
2	N	5, 10
3	NW	5, 10, 15, 20
4	WNW	5 [*] , 10
5	ESE	5 [*] , 10

* with and without causeway present.

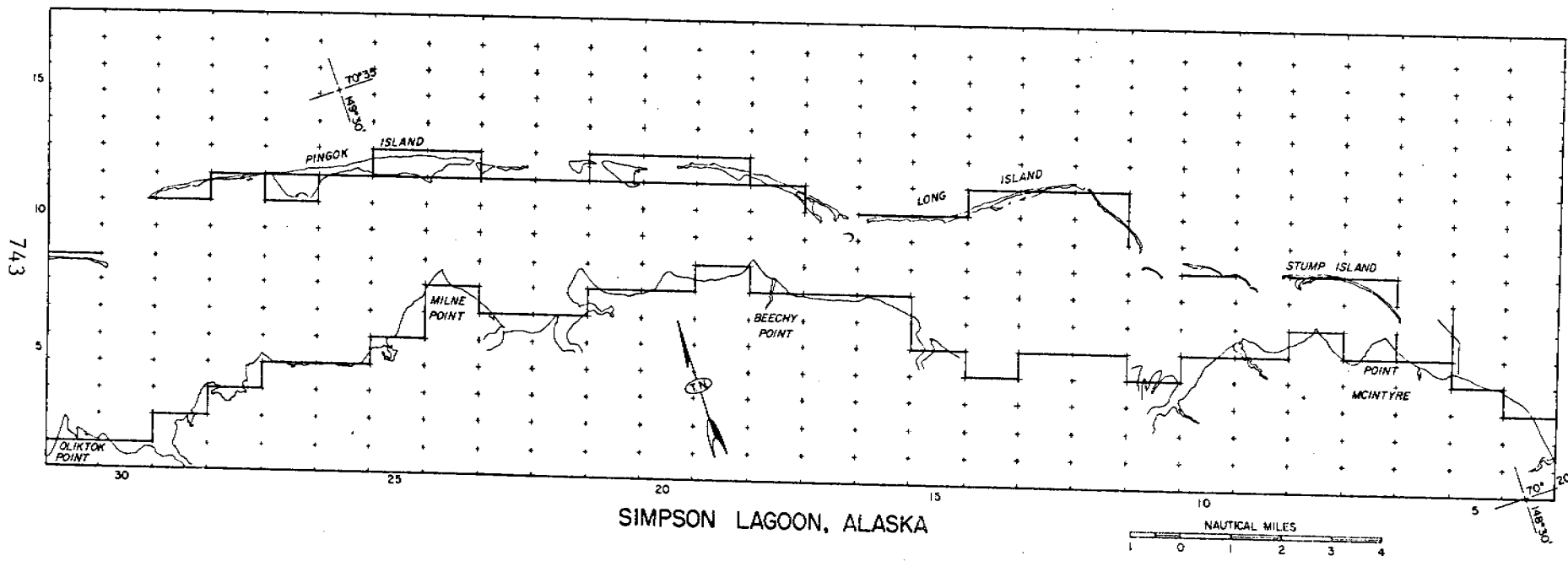


Figure 2. Grid scheme for Simpson Lagoon, Alaska. Crosses denote corners of 1 km x 2 km computational rectangles.

computational rectangles.

Outputs from each run consisted of printouts of water elevations, transport per unit width and depth-mean currents, and of plots of depth-mean currents and water mass trajectories. For convenience, volume flows through the entrances were computed and printed along with estimates of the lagoon exchange rate for the 0.31 km^3 volume lying between the causeway and Pingok Island.

Useful summaries of the numerical modeling results are shown in Figures 3 and 4. Figure 3 shows mid-channel current magnitudes calculated off Milne Point. Clearly to be seen is the near linear relationship between currents and wind velocity: the depth-mean current typically being approximately three percent of the speed, ie 15 cms^{-1} for 5 ms^{-1} ENE winds, 55 cms^{-1} for 20 ms^{-1} ENE winds. The relationship is probably due to a steady-state balance existing between wind stress and bottom stress -- there being little contribution from the surface slope along the lagoon axis. The chief factor in the magnitude of the current appears to be the angle between the wind and the lagoon axis. Probably because of all the entrances, currents are the same for a given wind speed and angle between wind and axis whether the wind blows from an easterly or a westerly direction.

Of interest are the exchange rates that were computed; these are shown in Figure 4. As can be seen, for a typical wind of 5 ms^{-1} from the ENE, one fifth of the volume of the lagoon is exchanged per day. The exchange rate for ENE winds rises almost linearly to 0.8 of the lagoon volume exchanged per day at 20 ms^{-1} . (These figures are of course based on depth-mean currents.)

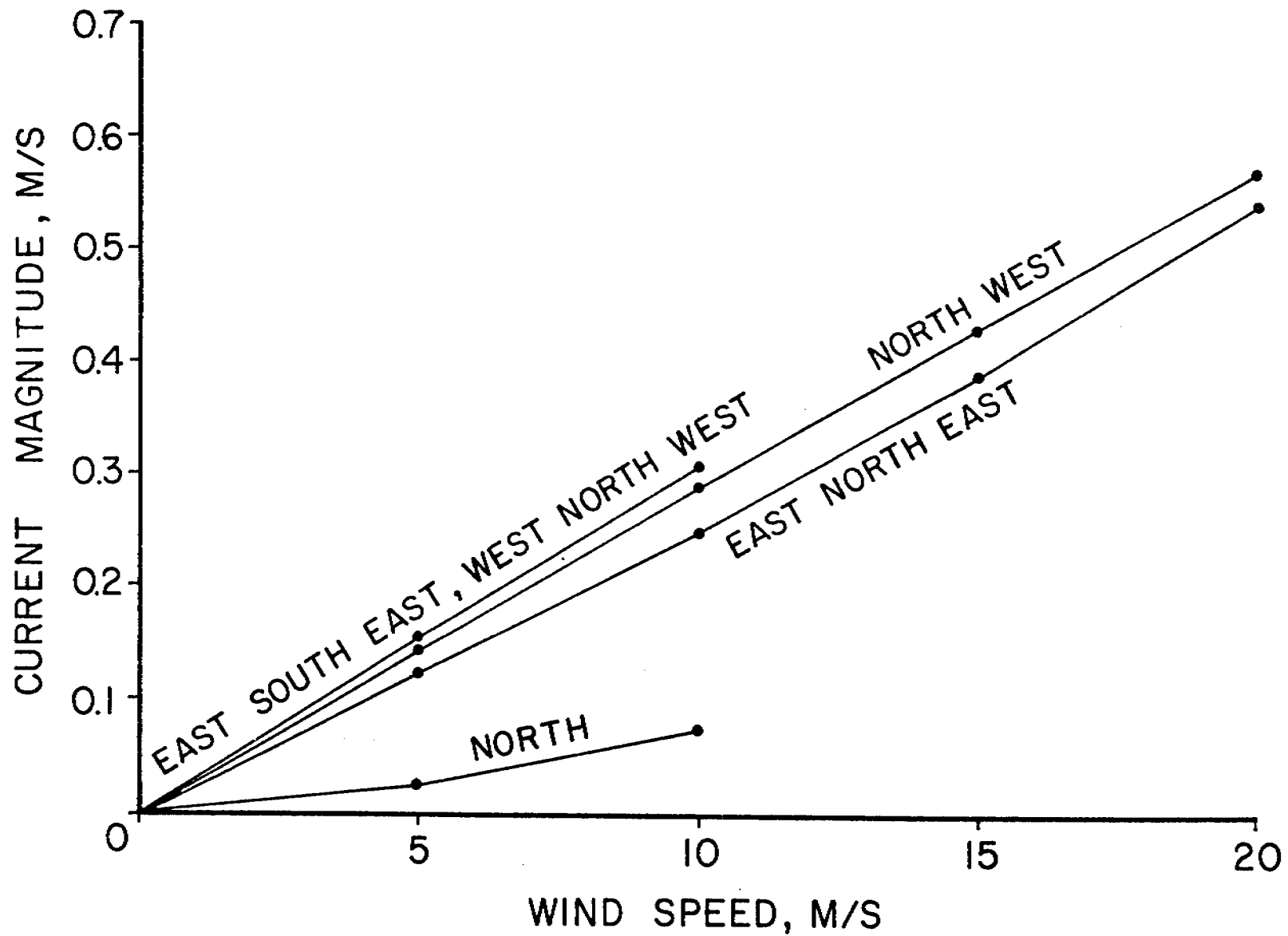


Figure 3. Simpson Lagoon 2-D model results (unverified): Mid-channel current magnitude off Milne Point.

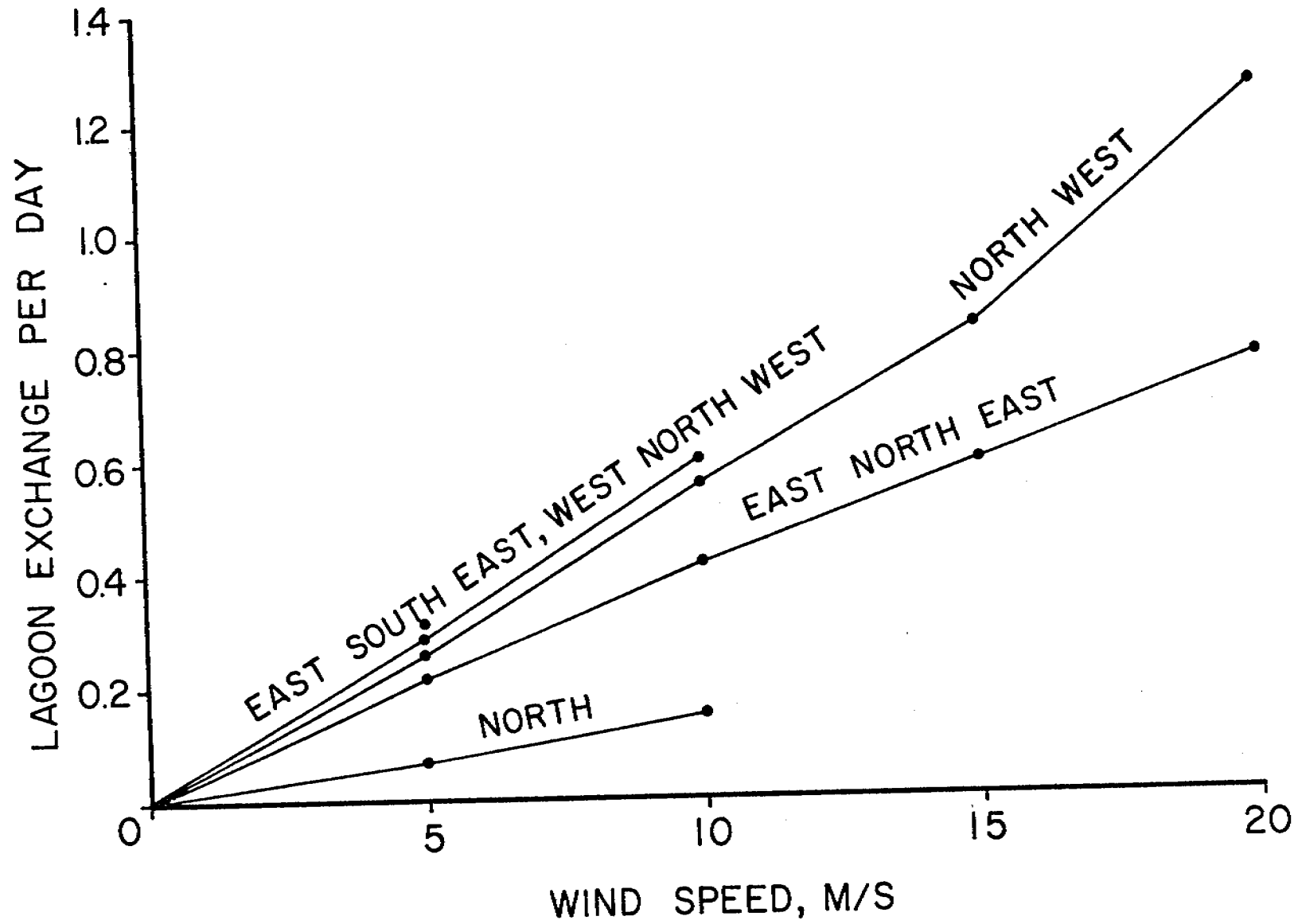
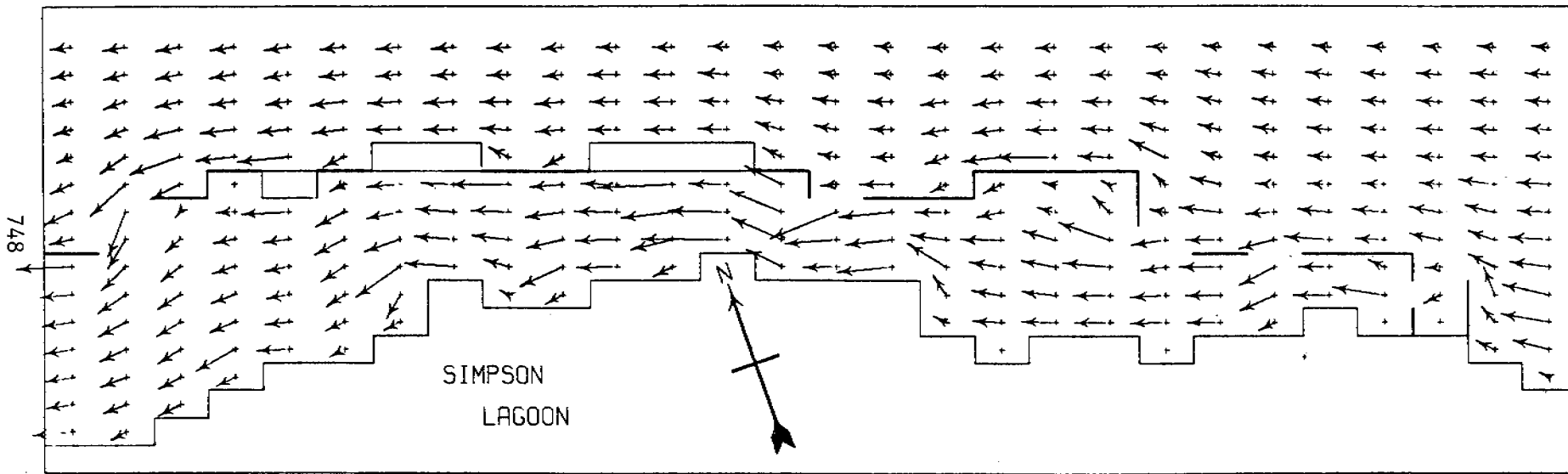


Figure 4. Simpson Lagoon 2-D model results (unverified): Lagoon volume exchange rates.

Computer-drawn plots of unverified depth-mean current vectors were made for each case modeled. An example for the most common case -- 5 ms^{-1} winds from the ENE -- is shown in Figure 5. Water parcel tracks, averaged over the water column, were calculated for 6 starting points for each wind case modeled. An example is shown for the 5 ms^{-1} ENE wind case (see Figure 6).

The depth-mean current vector plots for every remaining wind speed and direction combination run can be seen in Appendix A. Also shown are a large variety of simulated water parcel tracks.



2-D MODEL DEPTH-MEAN CURRENT VECTORS
WIND AT 5 M/S FROM ENE

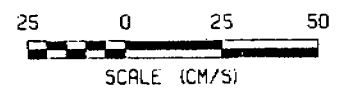
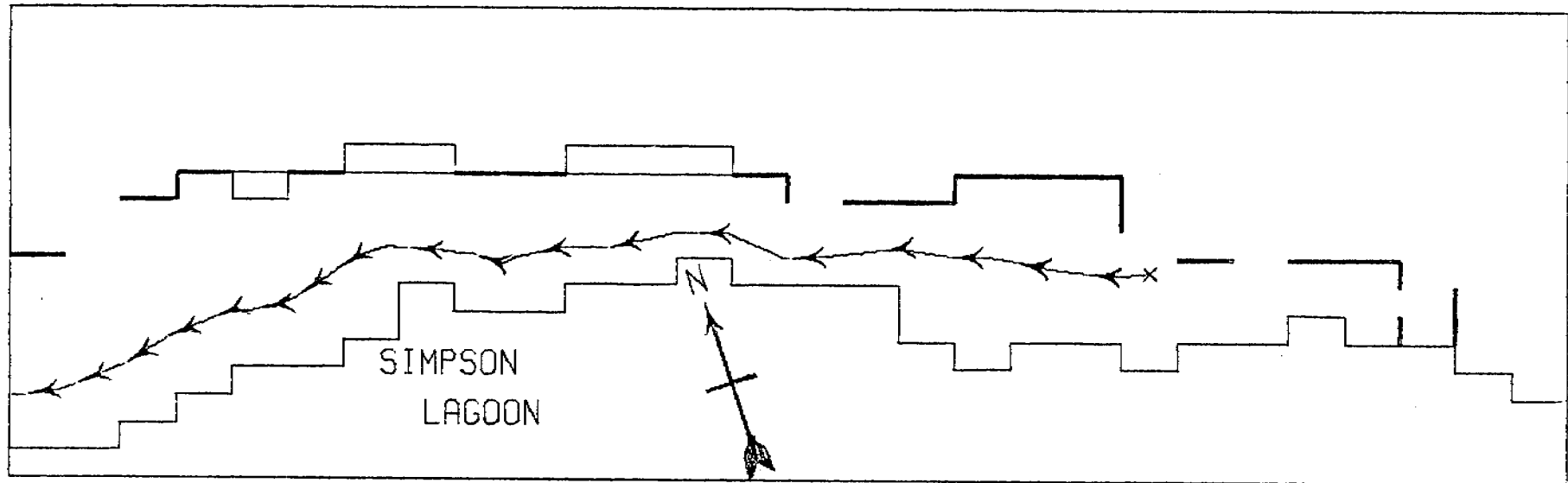


Figure 5. Simpson Lagoon 2-D model results (unverified): current vectors for 5 ms^{-1} wind from ENE.



2-D MODEL WIND AT 5 M/S FROM ENE
ELAPSED TIME MARKER EVERY 6 HOURS

Figure 6. Simpson Lagoon 2-D model results (unverified): Water parcel track for 5 ms^{-1} wind from ENE.

Three-dimensional Modeling [R. E. Whitaker]

The three-space modeling effort has been devoted to modifying an existing N-level variable density numerical model for future computations of the current structure within Simpson Lagoon and the nearshore region. The extension of the algorithm's capability to model islands as subgrid scale barriers was the most significant modification.

The N-level variable density model is the finite-difference analogs of the following time averaged, vertically-integrated equations:

$$\begin{aligned} \frac{\partial(hu)_k}{\partial t} + \frac{\partial(huu)_k}{\partial x} + \frac{\partial(huv)_k}{\partial y} + (wu)_{k-\frac{1}{2}} - (wu)_{k+\frac{1}{2}} - \gamma(hv)_k \\ + \left(\frac{h}{\rho}\right)_k \frac{\partial P_k}{\partial x} - \left(\frac{\tau_{xz}}{\rho}\right)_{k-\frac{1}{2}} + \left(\frac{\tau_{xz}}{\rho}\right)_{k+\frac{1}{2}} = 0, \end{aligned} \quad (4)$$

$$\begin{aligned} \frac{\partial(hv)_k}{\partial t} + \frac{\partial(huv)_k}{\partial x} + \frac{\partial(hvv)_k}{\partial y} + (wv)_{k-\frac{1}{2}} - (wv)_{k+\frac{1}{2}} + \gamma(hu)_k \\ + \left(\frac{h}{\rho}\right)_k \frac{\partial P_k}{\partial y} - \left(\frac{\tau_{yz}}{\rho}\right)_{k-\frac{1}{2}} + \left(\frac{\tau_{yz}}{\rho}\right)_{k+\frac{1}{2}} = 0, \end{aligned} \quad (5)$$

$$\frac{\partial H}{\partial t} + \sum_{k=1}^N \left[\frac{\partial(hu)_K}{x} + \frac{\partial(hv)_K}{y} \right]_{K=N-k+1} = 0, \quad (6)$$

and

$$\begin{aligned} \frac{\partial(hc)_k}{\partial t} + \frac{\partial(huC)_k}{\partial x} + \frac{\partial(hvC)_k}{\partial y} + (wC)_{k-\frac{1}{2}} - (wC)_{k+\frac{1}{2}} \\ - \frac{\partial}{\partial x} \left[D_x \frac{\partial(hC)_k}{\partial x} \right] - \frac{\partial}{\partial y} \left[D_y \frac{\partial(hC)_k}{\partial y} \right] - D_z \frac{\partial C}{\partial z} \Big|_{k-\frac{1}{2}} + D_z \frac{\partial C}{\partial z} \Big|_{k+\frac{1}{2}} = 0, \end{aligned} \quad (7)$$

where k is the level index, h is the depth increment between levels, and C represents temperature or salinity. All other symbols retain their traditional definitions.

The equations of motion for contiguous levels are coupled through the vertical advection terms, pressure gradients and stresses. At the free surface the kinematic stress is taken in the form

$$\left. \frac{\tau_{xz}}{\rho} \right|_{\text{SFC}} = \frac{\rho A}{\rho} C_D |w| w_x, \quad (8)$$

where the usual definition for each term is retained. The bottom stress is assumed to be of the form

$$\left. \frac{\tau_{xz}}{\rho} \right|_{\text{BOT}} = Kqu, \quad (9)$$

where K is a drag coefficient and $q = (u^2 + v^2)^{1/2}$. The interior stresses are taken in various forms. In general the stresses between levels are taken in the form

$$\frac{\tau_{xz}}{\rho} = A_{xz} \frac{\partial u}{\partial z}, \quad (10)$$

where the kinematic eddy viscosity is defined in the form

$$A_{xz} = \ell_o^2 \left| \frac{\partial q}{\partial z} \right| e^{-mRi}, \quad (11)$$

where

$$\ell_o = k_o (D - z)z/D, \quad (12)$$

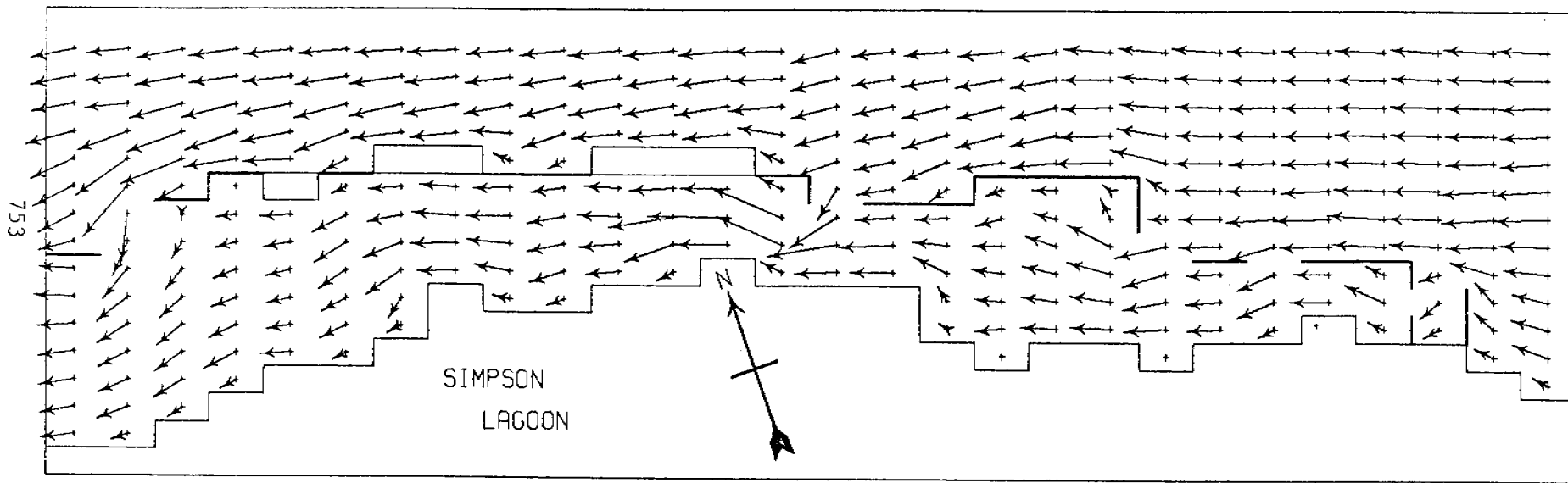
and Ri is a gradient Richardson number.

Five levels were taken to model the Simpson Lagoon and nearshore bottom topography. The levels were defined by depth increments of 0.91 m (3 ft), 0.91 m, 1.83 m (6 ft), 3.96 m (13 ft) and 4.57 m (15 ft), respectively. The lateral extent of the top level is identical to that shown in Figure 2. Although the five-level model does not utilize depths explicitly, the horizontal area delineating each level was specified so as to coincide with the depth field used in the two-dimensional model. Runs with the three-dimensional model cost around \$30 while simulations with a finer spatial resolution ($\frac{1}{2}$ km \times $\frac{1}{2}$ km) would probably have cost \$300.

Since the application of the five-level model to Simpson Lagoon was simply a numerical experiment the only wind case studied has been the response of the lagoon to a steady 5 ms^{-1} wind from the ENE. Tidal and river influences have been neglected. Due to the lack of temperature and salinity data, the density was taken as constant as was the eddy viscosity.

The initial conditions, boundary conditions, wind spin-up and simulation time were identical to the two-dimensional case. Output consisted of listings of the free surface elevation and current components at each level. Plots of the current vector fields at each level were also provided. These plots are shown in Figures 7 through 11.

Offshore, the current vectors show a significant rotation with depth. Notice that compared with the depth averaged currents given in Figure 5, the surface (level 1) currents have larger components into the lagoon through the passes at the western ends of Long and Pingok Islands. There are no significant differences between the surface and depth-averaged currents



3-D MODEL LEVEL 1 CURRENT VECTORS
WIND AT 5 M/S FROM ENE

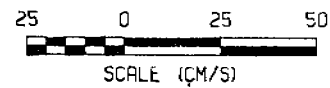
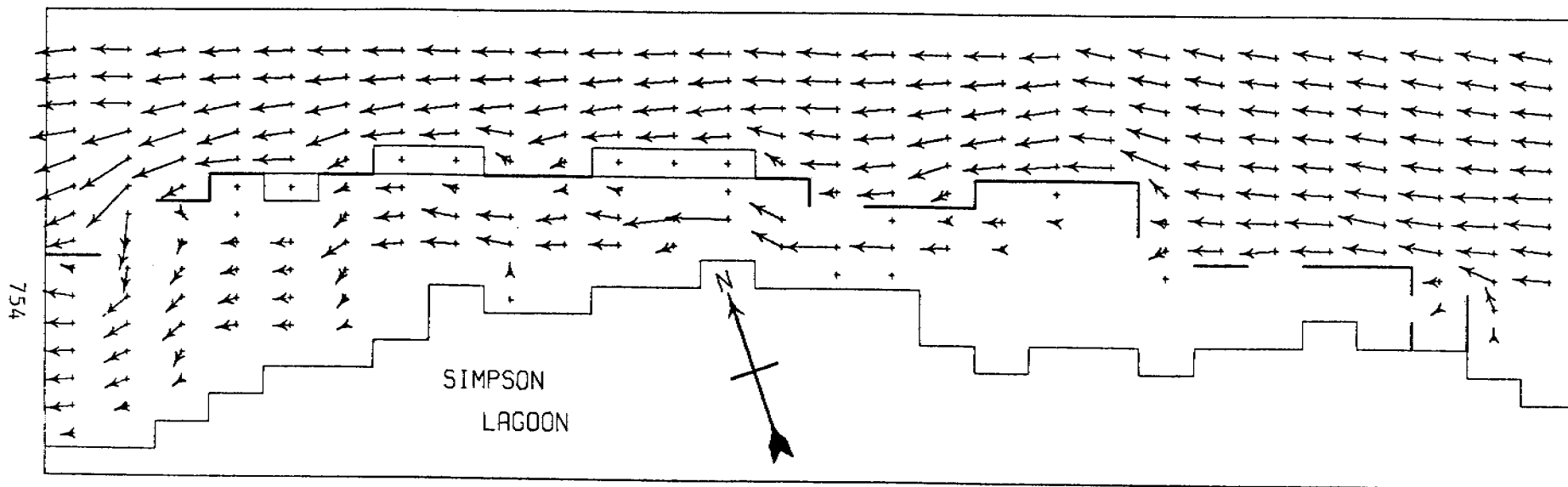
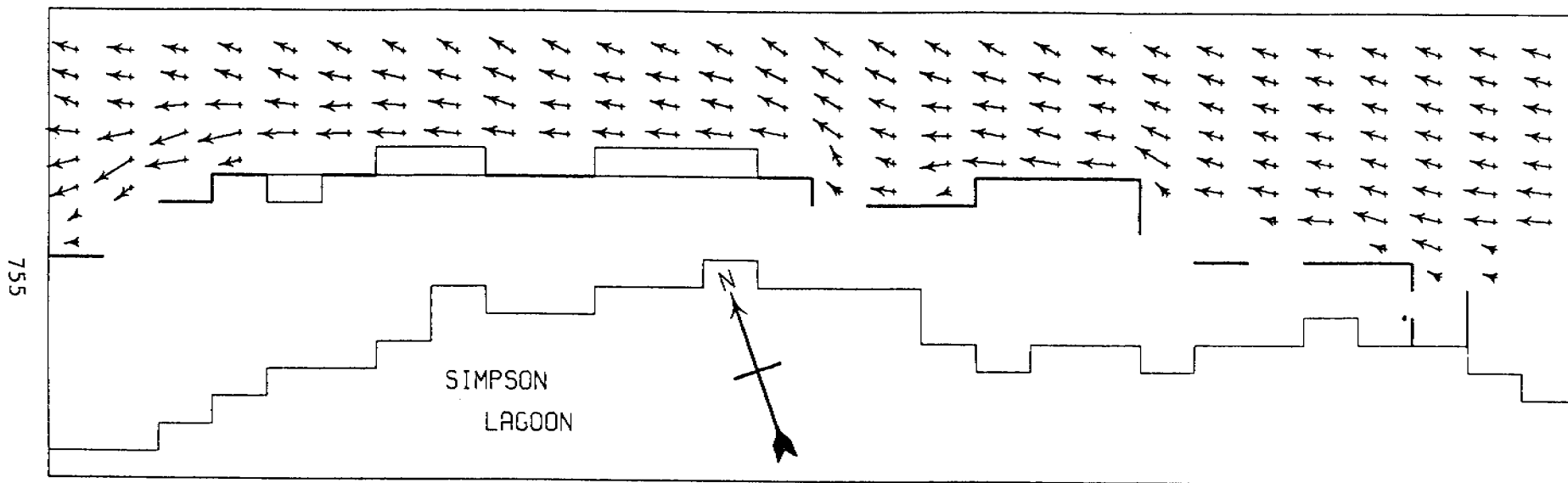


Figure 7. Simpson Lagoon 3-D model results. Horizontal current vector field at 0.46 m (1.5 ft) depth level.



3-D MODEL LEVEL 2 CURRENT VECTORS
WIND AT 5 M/S FROM ENE

Figure 8. Simpson Lagoon 3-D model results. Horizontal current vector field at 1.37 m (4.5 ft) depth level.



3-D MODEL LEVEL 3 CURRENT VECTORS
WIND AT 5 M/S FROM ENE

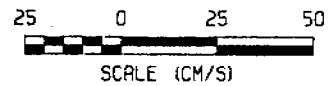
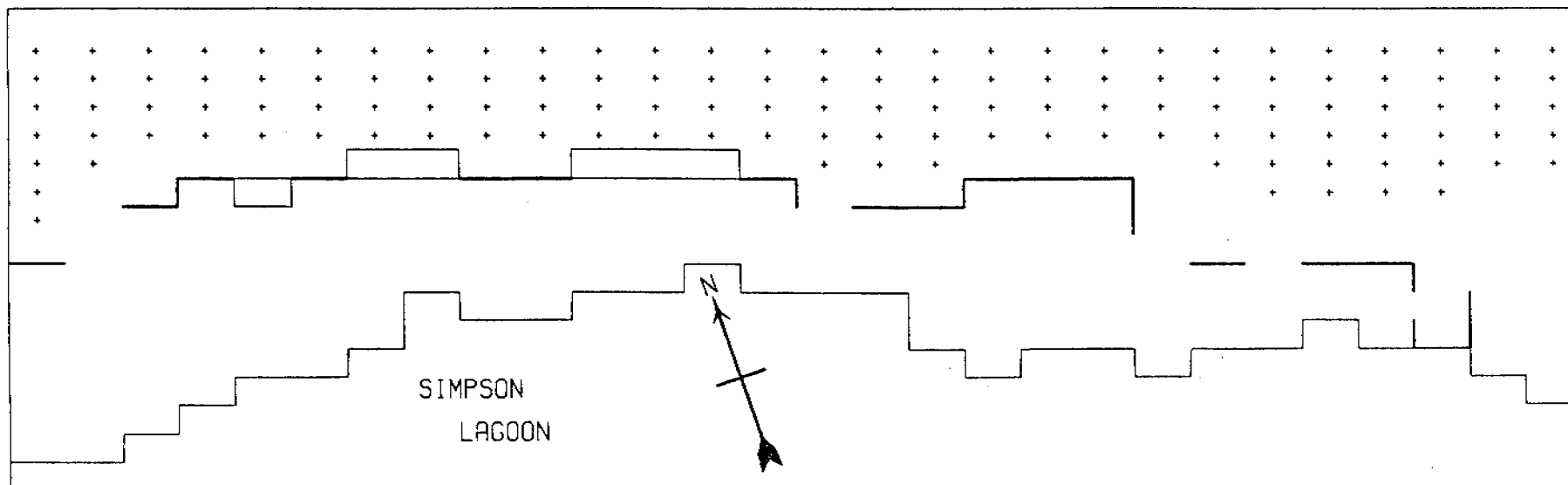


Figure 9. Simpson Lagoon 3-D model results. Horizontal current vector field at 2.74 m (9 ft) depth level.



3-D MODEL LEVEL 4 CURRENT VECTORS
WIND AT 5 M/S FROM ENE

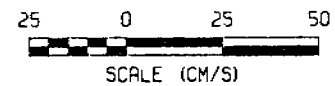
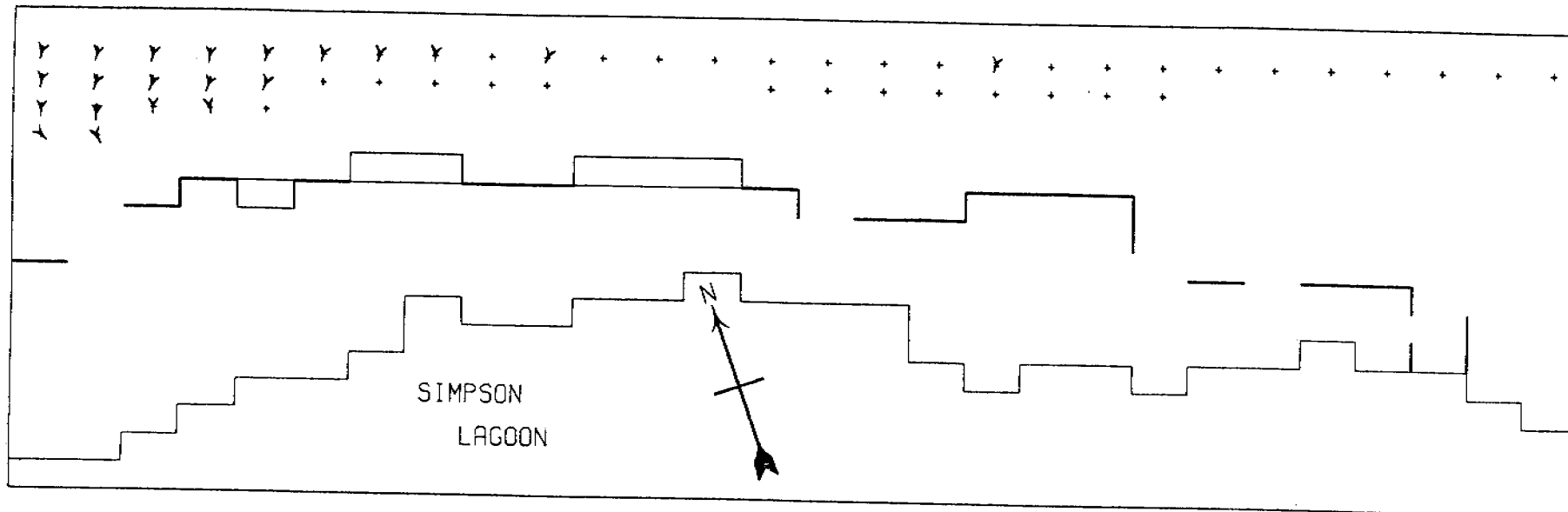


Figure 10. Simpson Lagoon 3-D model results. Horizontal current vector field at 5.64 m (18.5 ft) depth level.



3-D MODEL LEVEL 5 CURRENT VECTORS
WIND AT 5 M/S FROM ENE

25 0 25 50
SCALE (CM/S)

Figure 11. Simpson Lagoon 3-D model results. Horizontal current vector field at 9.91 m (32.5 ft) depth level.

over most of the lagoon proper. This is as it should be since the lagoon is defined by two levels at most.

Figure 12 gives the isotach field in a vertical section extending seaward from Milne Point. Another section extending from Point Storkersen is given in Figure 13. In the Milne Point section relatively high speed (14 to 16 cm s^{-1}) cores are found in the lagoon and just offshore. The large vertical shear within the lagoon is due to the lateral and vertical discretization. A predictable near-linear vertical gradient is obtained in the region offshore from Pingok Island and Point Storkersen. The computed currents off Point Storkersen reveal a broad shallow region of speeds greater than 14 cm s^{-1} with intense lateral shear nearshore.

Hodographs constructed from the computed currents sampled at two points along the Milne Point and Point Storkersen vertical sections are given in Figure 14. The shallow water hodographs representing the lagoon proper display only a slight rotation and weakening over the 0.91 m depth change. In the deeper water the computed currents reveal a rather complicated structure. The current vector obtained for the fourth level along the Point Storkersen section was too small to plot.

Additional numerical experiments related to alternate eddy viscosity parameterizations are continuing.

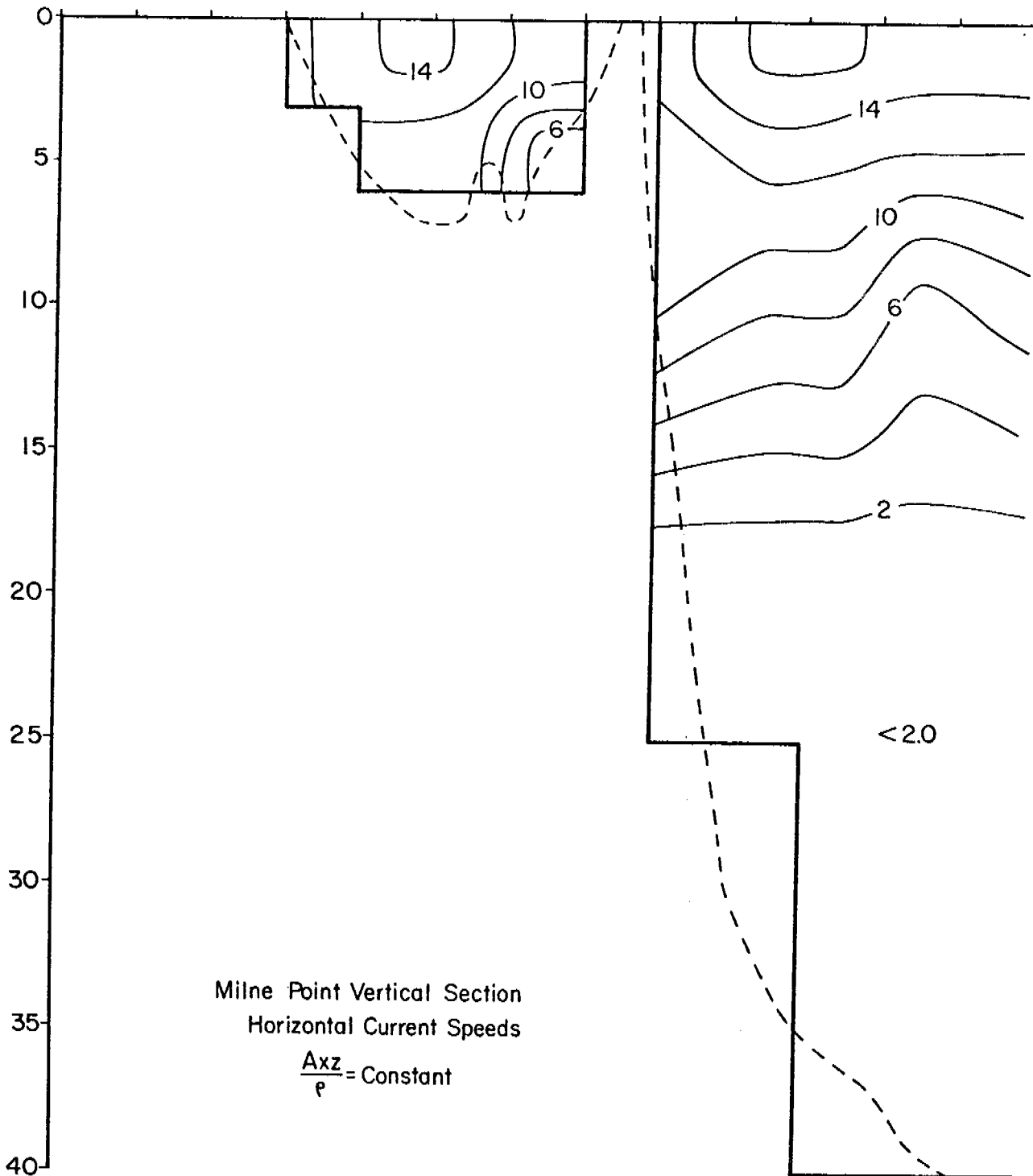


Figure 12. Isotach field in a vertical section extending seaward from Milne Point. Depth in feet, speed in cm s^{-1} . Dashed line is actual bottom profile.

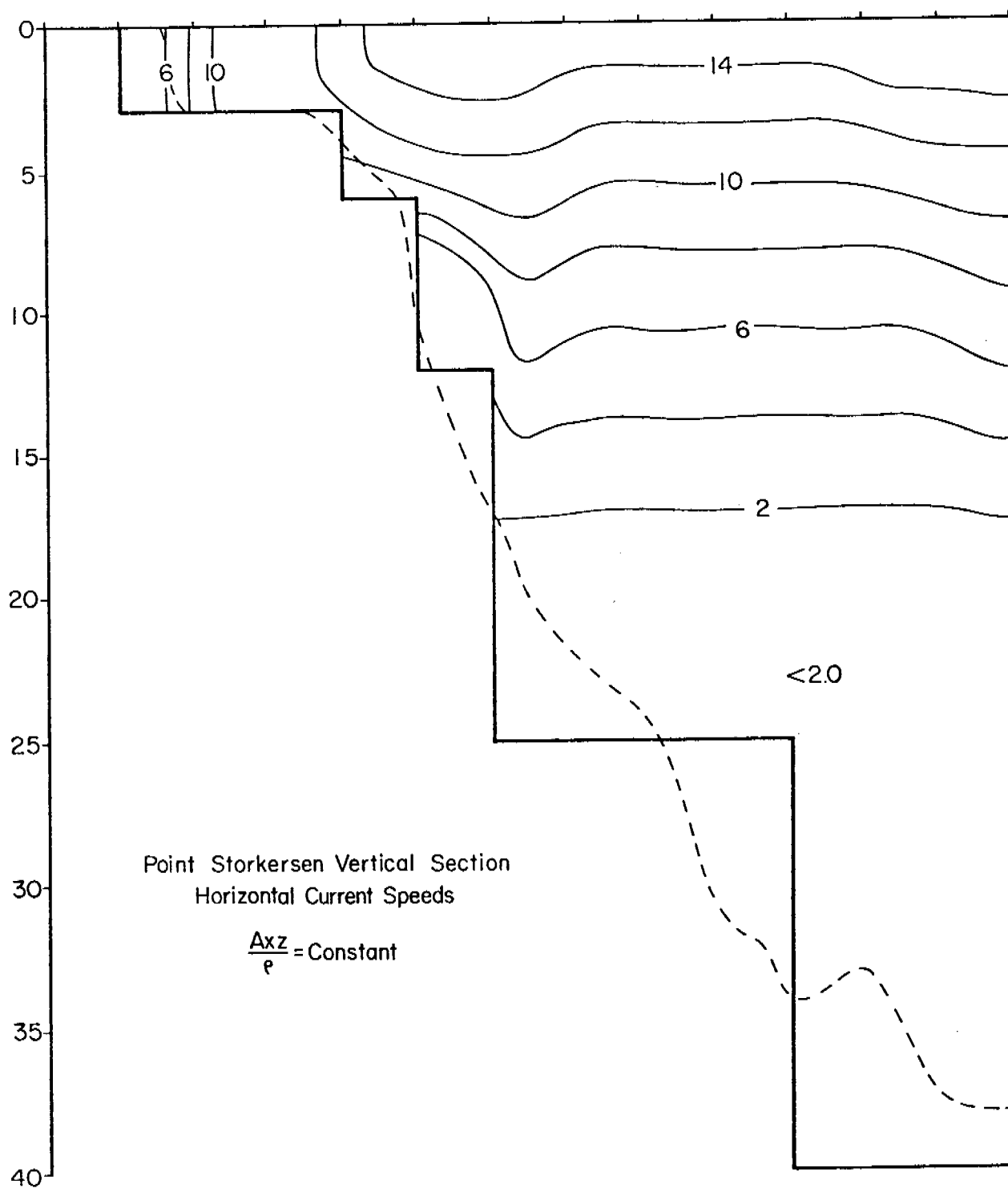


Figure 13. Isotach field in a vertical section extending seaward from Point Storkersen. Depth in feet, speed in cm s^{-1} . Dashed line is actual bottom profile.

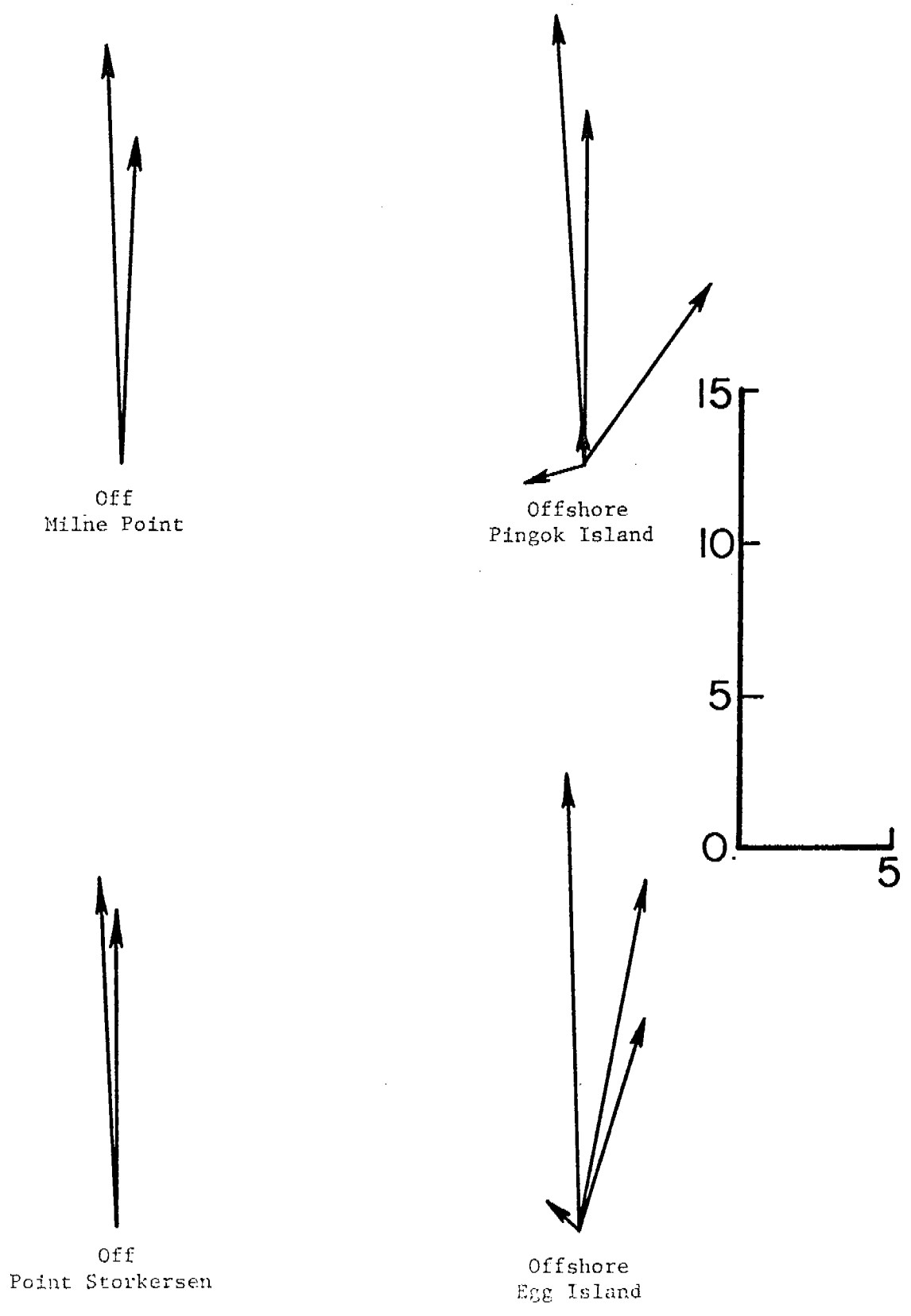


Figure 14. Shallow and deep water hodographs.

VI. Summer 1977 Field Program

The principal measurement objectives of the combined physical oceanography programs were

- a) to gather data for improving our understanding of the circulation and hydrography of Simpson Lagoon, and
- b) to gather hydrographic data in the vicinity of the ARCO causeway in order to assess the nature of its impact, if any, on the surrounding region.

Since biologists of LGL Limited were to take hydrographic data at their sampling stations near Milne Point and Pingok Island, the decision was made to concentrate our efforts at the principal eastern and western entrances; areal coverage of the lagoon was planned through the use of a float plane on a weekly basis.

The base of operations for RU #531 was the VE construction camp at Prudhoe Bay, which, thanks to the efficiency and good nature of oil field maintenance personnel, proved to be an entirely satisfactory choice. Preceded by Roy Hann, Jr., two project members (C. Mungall and D. Horne) operated out of Prudhoe Bay from August 7 to August 25, 1977. Boat support, in the form of a 16-foot Boston Whaler, was available from August 12. The boat, thanks to the courtesy of the Atlantic Richfield Company, was berthed on the causeway and was reached daily by a 30-minute drive from the base camp. Although the float plane was unavailable during August, we were lucky to gain access to a NOAA helicopter for one day and were thus able to make one hydrographic survey of the near-shore waters around Simpson Lagoon. Due to certain flight limitations of helicopters, measurements could only be taken near points where the

helicopter could be set down on land (hence the initial request for a float plane). Unfortunately, owing to the short (less than 2 months) interval between the start of the project and the field season, and to the near omnipresence of fog at the Deadhorse and Prudhoe Bay land strips, some of the current measuring equipment failed to arrive.

The measurements fall into three categories: a) the eastern part of Simpson Lagoon and its environs, b) the helicopter survey, and c) the entrances. These will be dealt with sequentially.

Measurements in the eastern part of Simpson

Lagoon and its environs

Before the arrival of the Boston Whaler measurements were initiated at a series of points around Prudhoe Bay such as were accessible by road: the East Dock, the end of the causeway, and the east and west sides just before the bend in the causeway. In the interests of data continuity, measurements were continued at these locations after the delivery of the boat aboard the NARL Alumiak. The data thus taken supplement the near absent time series data contained in the publication *Final Report on Environmental Studies Associated with the Prudhoe Bay Lock: Coastal Processes and Marine Benthos* (Grider, et al., 1977).

With the arrival of the Boston Whaler measurements were extended to the following locations: between Stump Island and Point McIntyre, at the University of Alaska current meter site (approximately midway between the end of the causeway and the eastern end of Stump Island), and occasionally at the next two entrances towards the west.

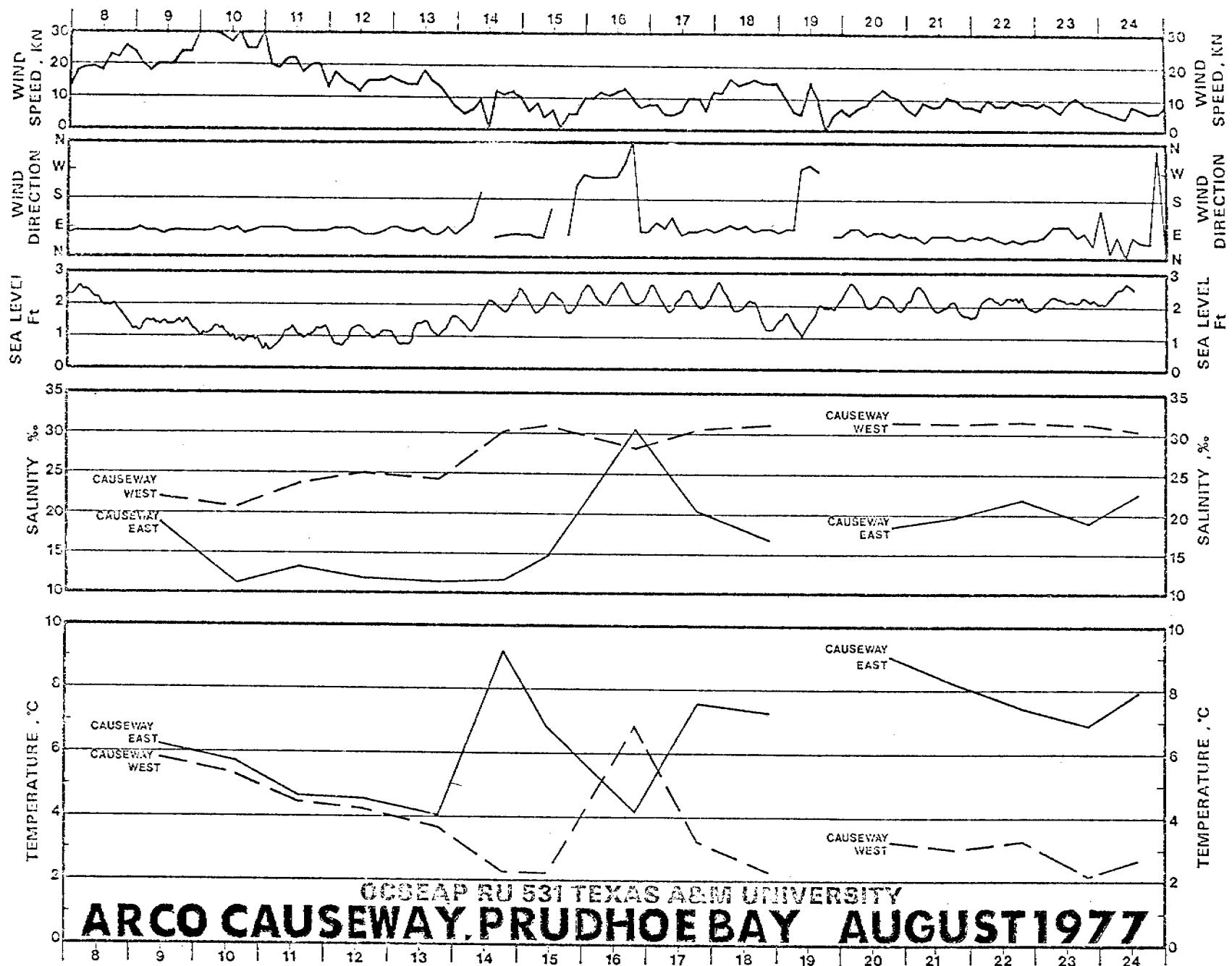
The data collected were chiefly conductivity, temperature and

salinity using a Beckman model RS5-3 (modified to measure down to -2°C), which is considered accurate to 0.1 ‰ and 0.1°C . Additional data (wind, waves, depth, etc.) were taken where appropriate. The data can be combined with meteorological measurements (at Deadhorse) and tide measurements (at the eastern side of the middle of the causeway) taken by NOAA. Furthermore, we look forward to including in the general synthesis the current, salinity and temperature time series data recorded at the nearby University of Alaska current meter as soon as it becomes available.

The principal results of the measurements taken around the causeway are summarized in Figure 15. Wind and sea level data were provided by the National Oceanic and Atmospheric Administration (NOAA); the wind data were measured at Deadhorse Airport (some 20 km from the causeway) and the sea level data (uncorrected for atmospheric pressure effects) were measured at the North Dock 2 site on the causeway.

Winds for the period start with a storm with winds from the ENE of 20 to 30 knots, gusting to 35 or more knots. Throughout the period the prevailing wind direction was from the ENE with wind speeds after the first week being of the order of 10 knots. Changes of wind direction occurred on the 14th, on the 15th, and on the 19th. In each of these cases the wind shifted towards blowing from a westerly direction.

The response of the sea level to local and offshore conditions indicates a decrease 1 ft. (30 cm) or more during the storm. It is likely that the set-down was due to sea level sloping downwards towards the south in geostrophic balance with so-called Coriolis forces (caused by currents flowing to the west) acting in a northerly direction. The



CCSEAP RU 531 TEXAS A&M UNIVERSITY
ARCO CAUSEWAY, PRUDHOE BAY AUGUST 1977

Figure 15. Summary of salinity and temperature measurements taken on the east and west side of the middle of the causeway, 9 through 24 August 1977. Wind and sea level data provided by NOAA.

range of the tide during the middle of August can be seen to be of the order of about 0.75 ft (approximately 20 cm).

A salinity difference of as much as 18 ‰ occurred between measurements taken on the eastern and western sides of the causeway; the lower salinities on the east were probably due to an accumulation of water having its origin in the Sagavanirktok River. This difference was reduced to zero on the 16th when the wind altered to blowing from the west, at which time presumably the accumulated water was flushed out.

The temperature was, in almost all cases, warmer on the east of the causeway than on the west. The difference increased dramatically after the storm, rising to a difference of some 7°C. At this time maximum and minimum temperatures (respectively, for the east and west sides) occurred. Following the storm period, the temperature on the east of the causeway was generally warmer than that on the west by 4 to 5°C with the exception of the time of wind reversal, when the winds changed from easterly to westerly. Further information can be gleaned from Figure 16 which contains summaries of nearly all salinity values taken, including some taken at LGL station 1 off Milne Point. The following points are evident:

1. Although rapid salinity changes can occur at the causeway (e.g. from 14.7 to 30.7 ‰ -- a change of 16 ‰) in one day, changes of a similar magnitude can occur at points less likely to be influenced by the causeway (e.g. from 13.4 to 27.4 ‰ -- a change of 14 ‰ at the East Dock, on the eastern side of Prudhoe Bay).

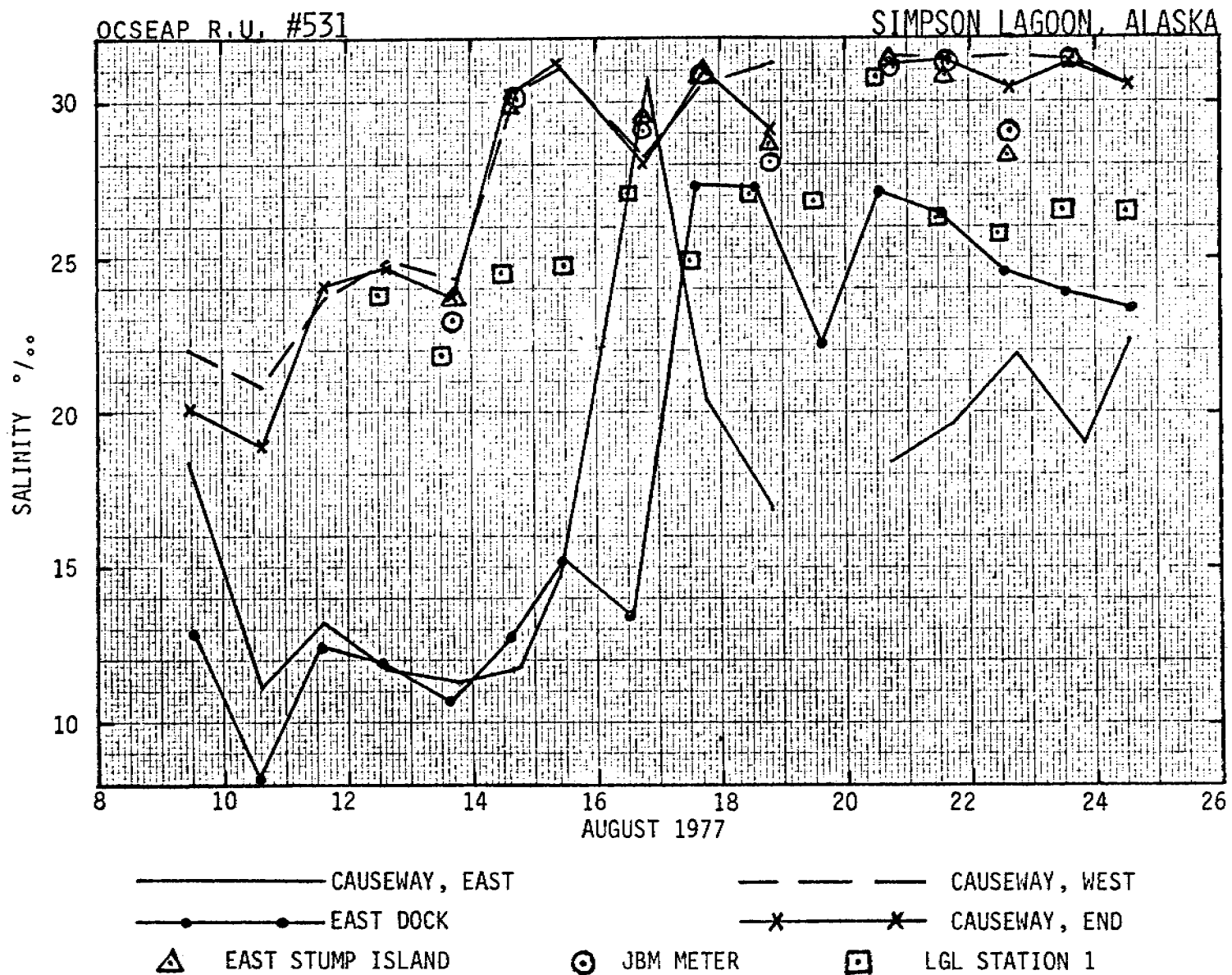


Figure 16. Summary of salinity measurements taken in the eastern part of Simpson Lagoon and its environs.

2. The above changes -- on the order of 15 ‰ in one day -- indicate the need for consideration of self-contained recording instruments should further measurements be required.
3. Measurements taken at the end of the causeway, on the west of the middle of the causeway, at the lagoon entrance between Point McIntyre and the east end of Stump Island, and at the University of Alaska's JBM current meter were generally similar.
4. Salinities measured on the east of the middle of the causeway tended to follow those measured at the east dock for most of the period. In the last week, after a period of relatively consistent winds, salinities were lower at the causeway than at the east dock.
5. Measurements taken at LGL station 1 in general show a rising trend -- perturbations occurring on the 13th, 16th, 17th, and 20th. It is likely that these periods coincided with shifts in the wind direction from east to west and *vice versa*.

Figure 17 contains a summary of nearly all the temperature measurements made during the period. The following points are evident:

1. Large temperature changes--of the order of 6°C can occur in one day.
2. The coldest temperatures measured usually occurred at the end of the causeway.
3. Temperatures at the East Dock tended to have a similar trend to those taken many kilometers away at LGL station 1. The warmest

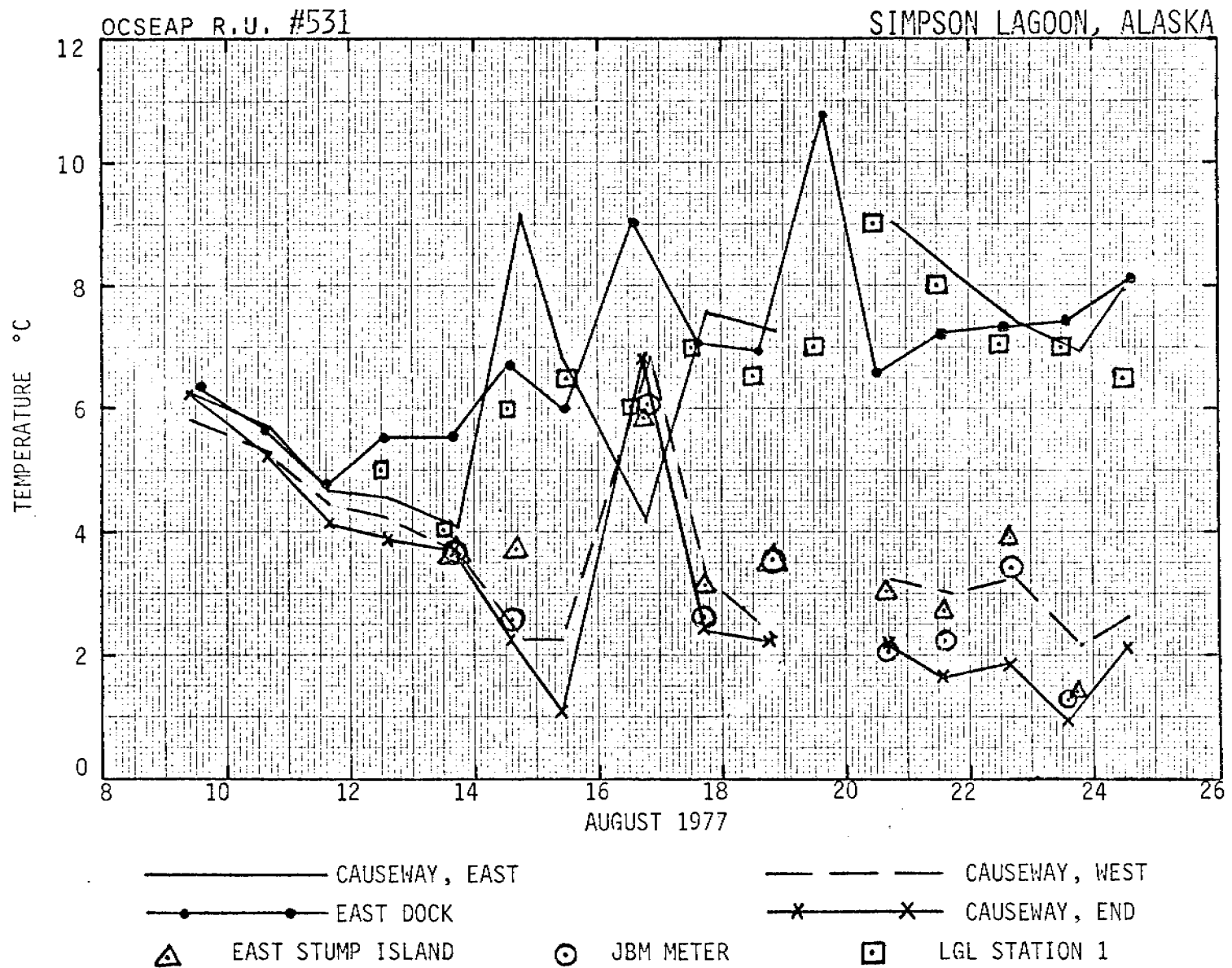


Figure 17. Summary of temperature measurements taken in the eastern part of Simpson Lagoon and its environs.

periods at these two points seem to be associated with periods of little or no wind; elsewhere temperatures at these times tended to be at their coldest.

4. Temperatures at the end of the causeway and to the west are similar with the exception of those at LGL station 1. Except during the storm, the above temperatures had a trend which was the opposite of that just to the east of the causeway.

In conclusion, locally, the causeway has a containing effect--permitting water upwind to be warmed. There is an obvious effect of the causeway on salinity, particularly when the wind is from the east; the consideration of this effect should, however, take into account the distance over which the effect is noticeable, and the magnitude of the change relative to those already experienced in the region.

Measurements taken during the helicopter survey of August 15, 1977

A total of 22 points were visited by a NOAA helicopter (piloted by Mike Barnhill) between 14:20 and 19:40 hours. The measurement locations ranged from Thetis Island in the west to Gull Island in the east. Measurements were taken of conductivity, temperature and salinity at depths of 1 ft. At 14 of these locations sediment samples were obtained by S. Naidu, following his joining the Flight at Pingok Island. Prior to the trip the regular series of measurements had been taken at the East Dock and at the causeway. Meteorological conditions were such that winds were small, following a short period of ENE winds.

The data are summarised in Figure 18. Immediately apparent is the fact that temperatures are warmer along the landward shores of the lagoon -- typically having temperatures of 6 to 8°C versus 2 to 5°C.

SIMPSON LAGOON, ALASKA
OCSEAP R.U. #531

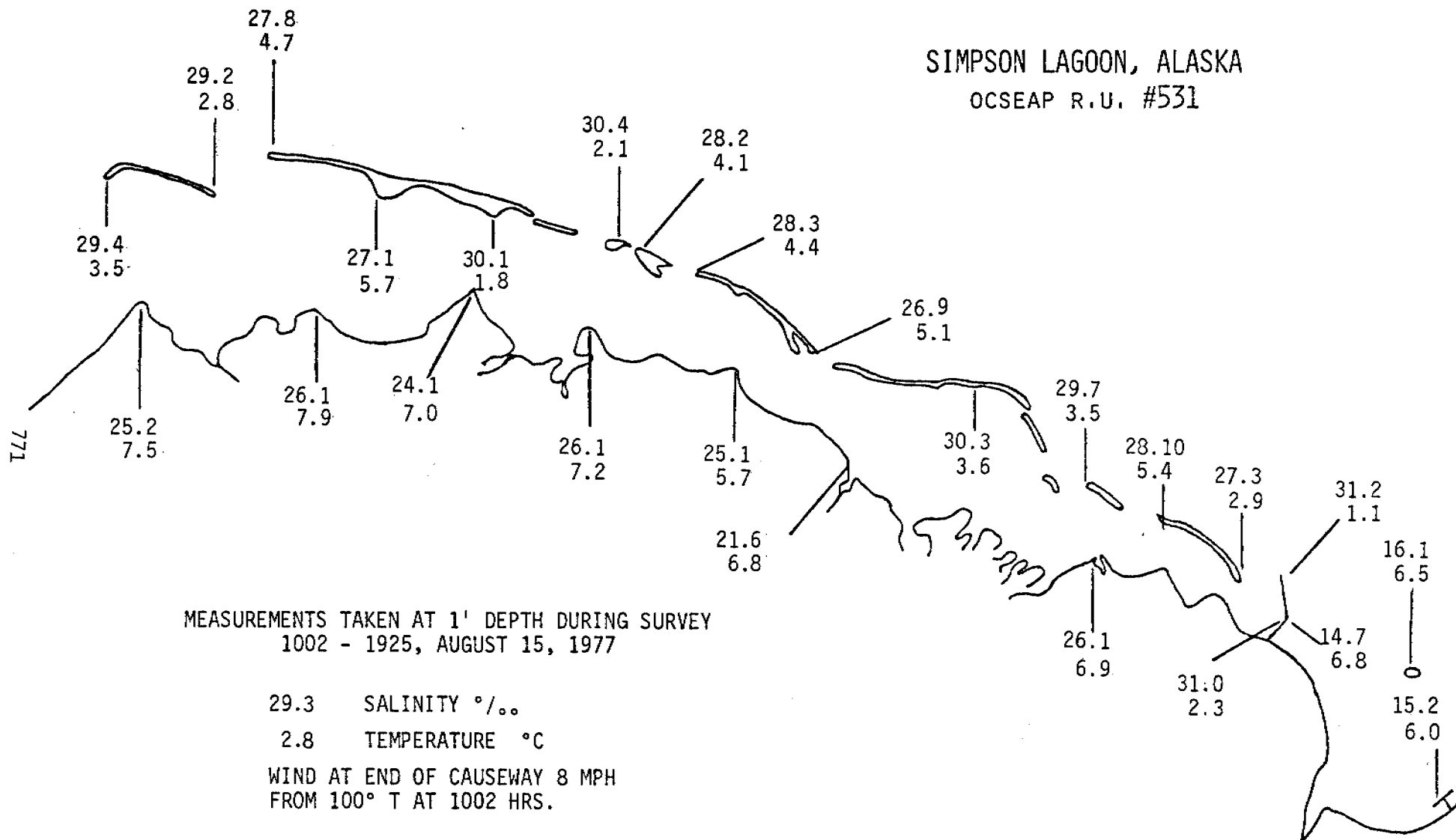


Figure 18. Measurements taken at depth of 1 ft during survey of August 15, 1977.

The coldest temperature (1.1°C) and the highest salinity (31.2‰) were measured at the end of the causeway. Of interest is that although the causeway appears to have caused large differences between conditions in Prudhoe Bay and immediately to the west of the causeway, conditions appear to have returned to 'normal' (in this case 'warm') by the western end of Stump Island -- a distance of 9 km.

Densities [in the form $\sigma_T = (\text{density} - 1) \times 1000$] computed from the measurements are shown in Figure 19. They range from a high value of 25.0 at the end of the causeway to a low value of 11.6 nearby. A considerable cross-channel density gradient exists, which at times can attain as much as $7 \sigma_T$ units over a distance of 7 km. In general however the crosslagoon difference is some 2 to $4 \sigma_T$ units.

Entrance measurements

Visual estimates were made during the helicopter survey of the significance, or lack of significance, of the various entrances. This is a matter of importance for the biological investigations, for selection of possible instrument deployment sites, and for realistic numerical modeling. In addition to the obvious western entrances between Oliktok Point, Spy Island and Pingok Islands, the main entrances seem to be those lying between Cottle Island, Long Island, Egg Island, Stump Island and Point McIntyre.

Soundings of a somewhat crude nature (using poles or weighted ropes marked in feet) were taken at the three easternmost entrances.

1. Point McIntyre -- Stump Island entrance: maximum depth of 1.5 m in middle observed at 17:34 hours Alaska time on August 22, 1977.

SIMPSON LAGOON, ALASKA
 OCSEAP R.U. #531

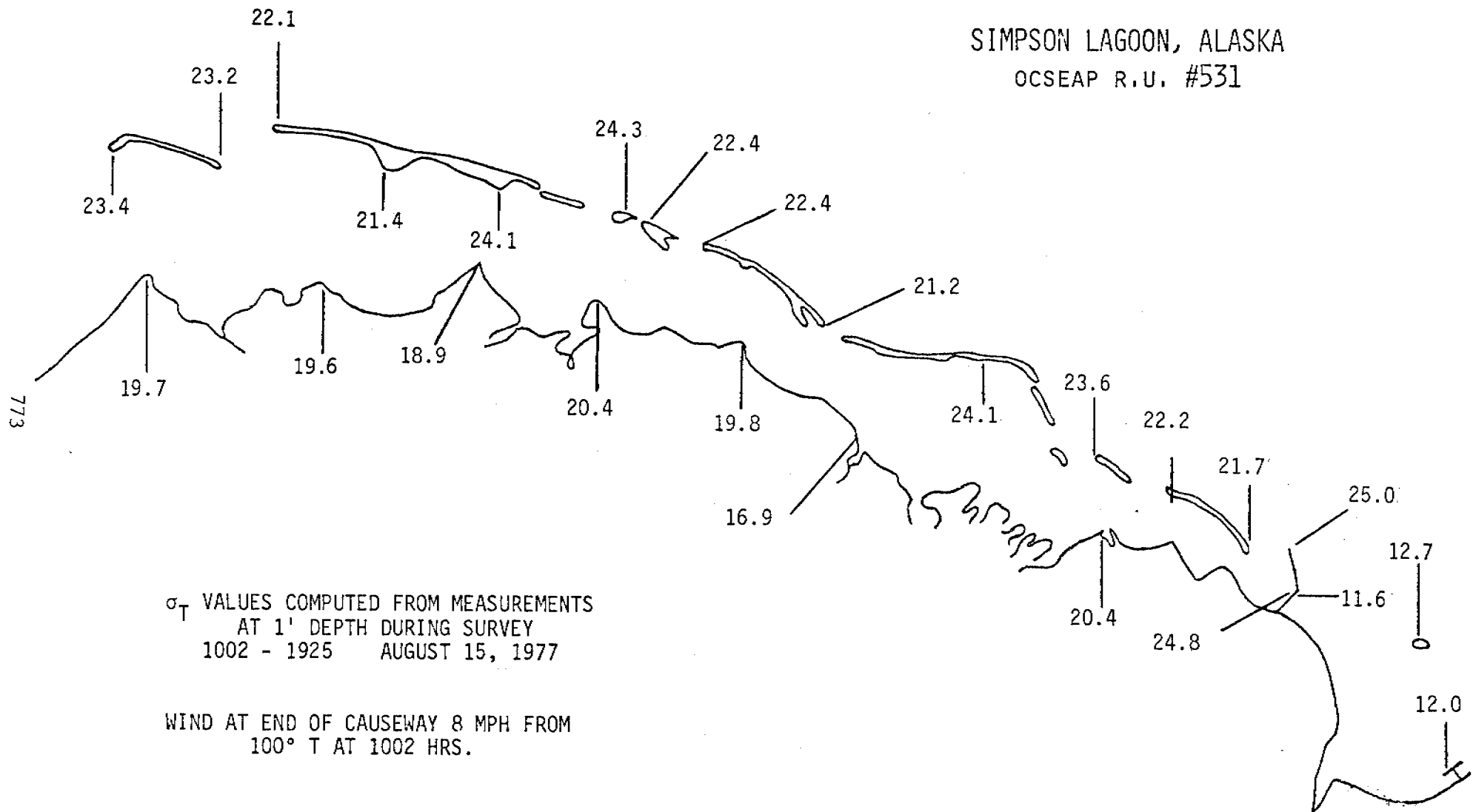


Figure 19. σ_T values computed from measurements taken at depth of 1 ft during survey of August 15, 1977.

2. Stump Island -- Egg Island entrance: maximum depth of 1.6 m very close to Egg Island observed at 15:45 hours Alaska time on August 23, 1977.
3. Egg Island -- small island between Egg Island and Long Island: maximum depth at least 4.8 m close to small island observed at 16:55 hours Alaska time on August 23, 1977.

As can be seen, depths tend to be greatest on the *western* sides of entrances; evidence for this is also to be seen in the steep banks on the *eastern* ends of islands.

Meaningful variations of salinity and temperature with depth were very rare. Only on August 14 were significant gradients noticed: in the Stump Island -- Egg Island entrance we measured 6.4°C and 23.7‰ at a depth of 1 ft, and 3.0°C and 30.0‰ at a depth of 3 ft (in a total water depth of 3.5 ft at 15:50 on August 14 when windspeeds at Deadhorse dropped to zero).

Current measurements were limited by the lack of arrival of the specially-ordered meters. Some measurements were attempted using a Hydroproducts deck readout current meter with a Savonius rotor. Due to the continuous read out, measurements showing wave induced variations could readily be discarded; direction measurements were also recorded but regrettably were suspect. Currents in the Point McIntyre -- Stump Island entrance were of the order of 0.2 to 0.4 knots; those between Stump Island and Egg Island reached 0.55 knots.

VII. Information Gaps and Research Proposed for 1978

Although a statement concerning physical oceanography information gaps should really be formulated in conjunction with all the other Research Units, a beginning attempt will be made here.

1. Water origins, residence times and detritus transport (sources, distribution, transport mechanism): A knowledge of the origin(s) of the water entering Simpson Lagoon -- particularly as to whether the water came from inshore or offshore -- is probably desirable. More detailed information concerning residence times -- particular inshore -- is likely to be necessary. Detritus seems to be a key subject; statements have been made concerning the presence of a 'mat-like, yet fluffy, detritus layer' on the lagoon bottom. Presumably at some stage this detritus becomes suspended. The importance of detritus, and the nature of the information required must be made clear.
2. Current and wave measurements: If sound modeling results are needed that can be used for supplying the basis upon which important decisions are to be made -- e.g. the need for gaps in causeways -- verification is essential. Depending on the requirement for knowledge on detritus movement, certain sophisticated measurements may be necessary, ranging from current profiles that can ultimately be related empirically to detritus suspension, to turbulence and wave measurements. The need for offshore wave and current measurements has been expressed; since these requests may conflict economically with nearshore requests, choices have to be made.

At this time (February 1978) we are in a position to direct our research efforts into several areas. In the proposal that was submitted for 1978 the following areas were addressed:

1. Numerical modeling of water movement.
2. Nearshore wave and current measurements at Pingok Island.
3. Drifter tracking using a radar site at Milne Point.
4. Hydrographic measurements from Boston Whaler and float plane.

Following the submission of the proposal in July 1977 considerable effort has been spent in consultation with Marsh-McBirney, Inc. regarding the development of an electro-magnetic current sensor and land based display for showing mean and wave induced currents (see Figure 20) to be located near the main LGL nearshore station. Waves could also be measured at this point. The design of an economical rapid data acquisition system, capable of obtaining data at intervals of the order of tenths of a second, is underway.

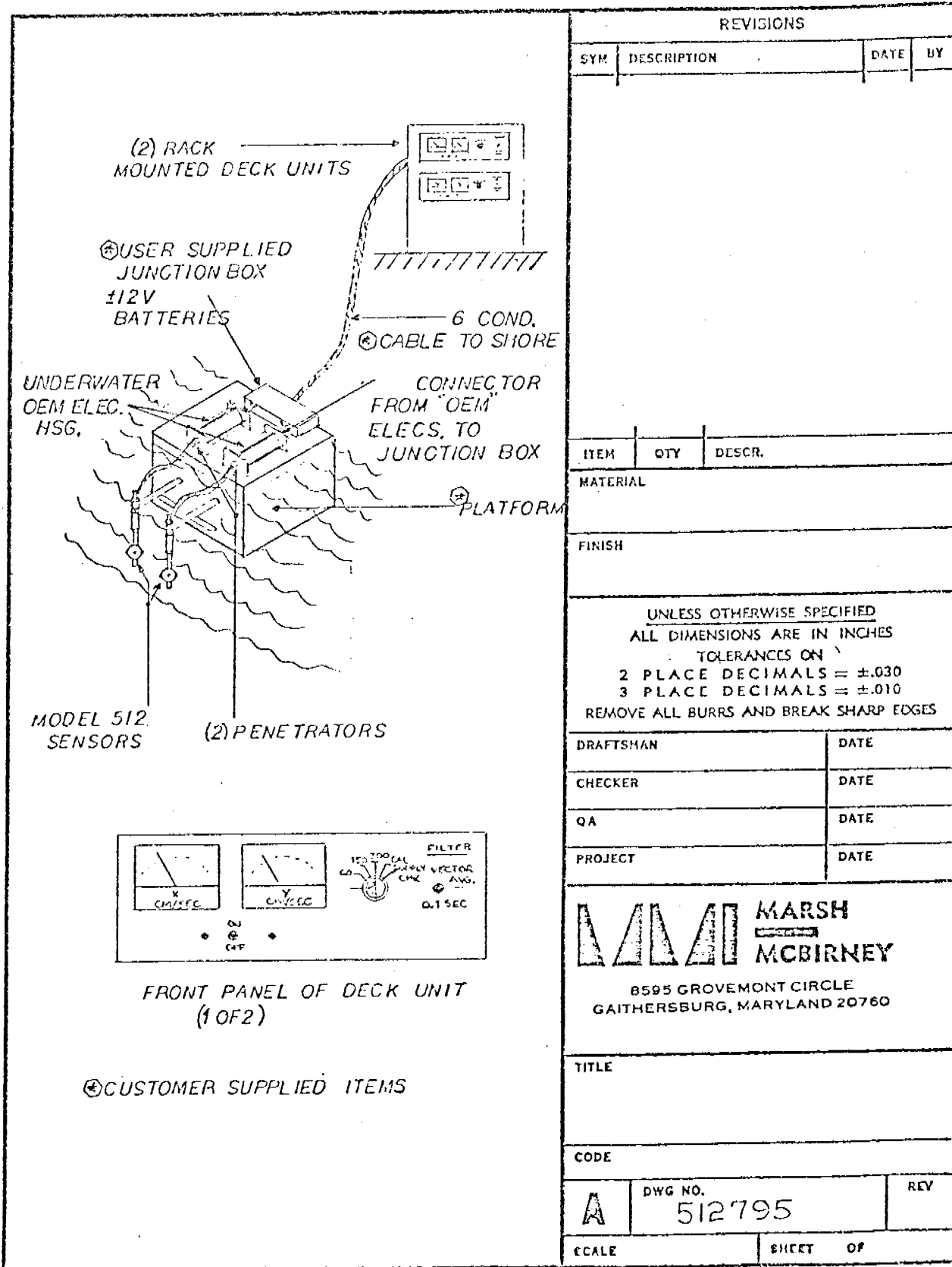


Figure 20. Electro-magnetic current sensor and data display system designed for use at Milne Point, Simpson Lagoon.

VIII. Synopsis of Results

Modeling

Simpson Lagoon seems to be primarily wind-driven. Due to the several openings, currents and exchange rates depend primarily on the angle between the wind and the lagoon axis. Currents tend to be about 3% of the wind-speed, directed along the longitudinal axis of the lagoon. Exchange rates for the water in the lagoon vary from 0.2 of the volume exchanged per day for 5 ms^{-1} ENE winds -- the prevailing windspeed and direction -- to 0.8 for 20 ms^{-1} ENE winds. It is to be stressed that these are unverified results based on depth-mean currents. The hydraulic effect of the causeway on currents probably only extends 5-10 km due to the numerous entrances.

Measurements

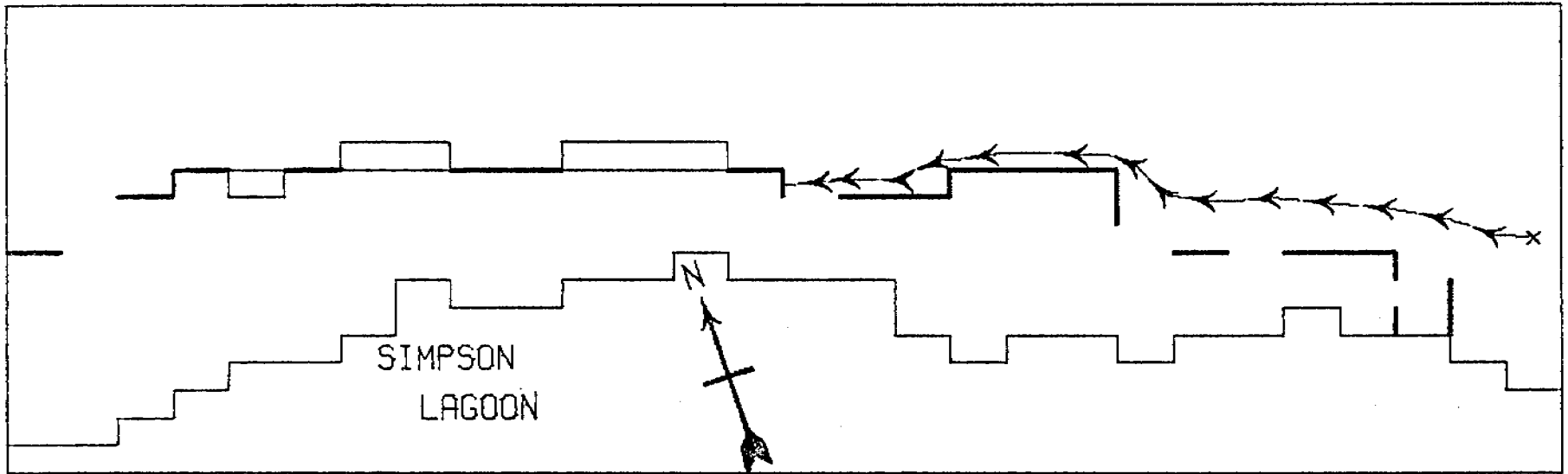
Although strong lateral salinity and temperature gradients usually are present, only very rarely are there vertical gradients. Temperatures seem to be warmer along the landward shores of the lagoon and at points lying upwind from the causeway. The causeway itself has a strong local effect on salinity and temperature. Large differences occur across the causeway, reaching 18 ‰ and 7°C .

References

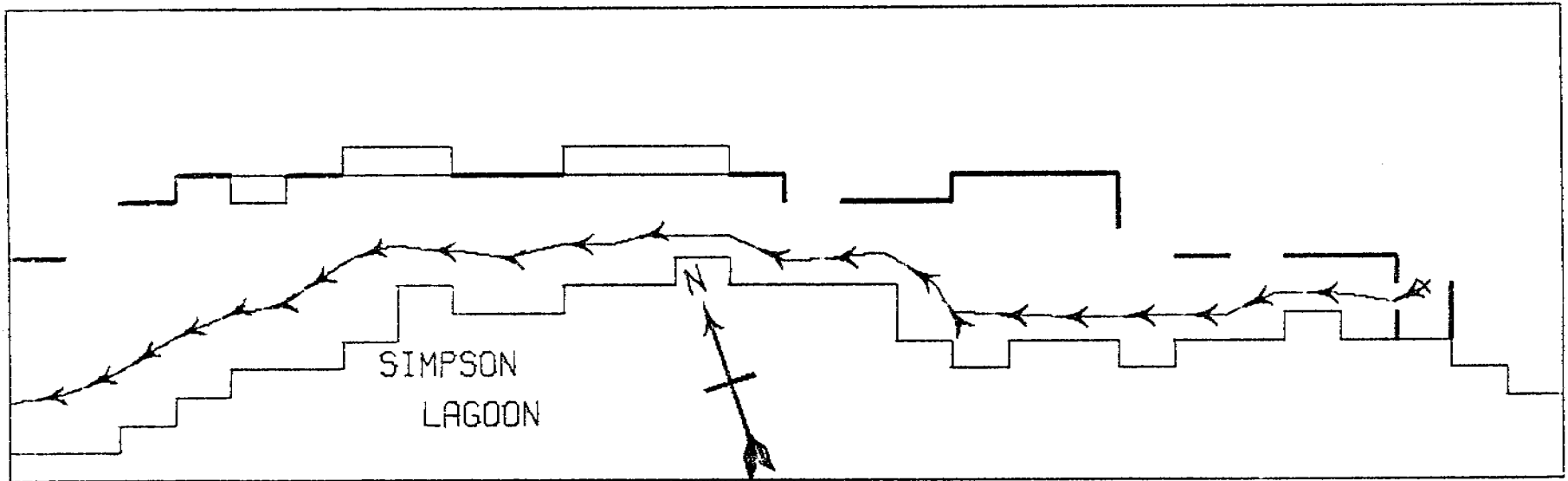
- Alexander, V., et al: Environmental Studies of an Arctic Estuarine System - Final Report. EPA-660/3-73-026. National Environmental Research Center. June 1975. 536 pp.
- Barnes, P., et al: Miscellaneous hydrologic and geologic observations on the inner Beaufort Sea Shelf, Alaska. Open File Report 77-477. United States Department of the Interior Geological Survey. April 1977. 95 pp.
- Grider, G. M., Jr., G. A. Robilliard and R. W. Firth: Final Report on Environmental Studies Associated with the Prudhoe Bay Dock: Coastal Processes and Marine Benthos. Woodward-Clyde, Consultants, 4791 Business Park Blvd., Anchorage, Alaska 99503. April 1977.
- Kinney, P. J., et al: Baseline Data Study of the Alaskan Arctic Aquatic Environment. Tech. Report No. R72-3. Institute of Marine Science, Fairbanks, Alaska. March 1972. 275 pp.
- Reid, R. O. and B. R. Bodine: Numerical model for storm surges in Galveston Bay. *J. Waterways and Harbors Div., A.S.C.E.* (94) WWI, Feb. 1968. pp. 33-57.
- Wiseman, W. J., et al: Alaskan Arctic Coastal Processes and Morphology. Coastal Studies Inst. Tech. Report No. 149. Louisiana State University, Baton Rouge, La. 1973. 171 pp.

APPENDIX A

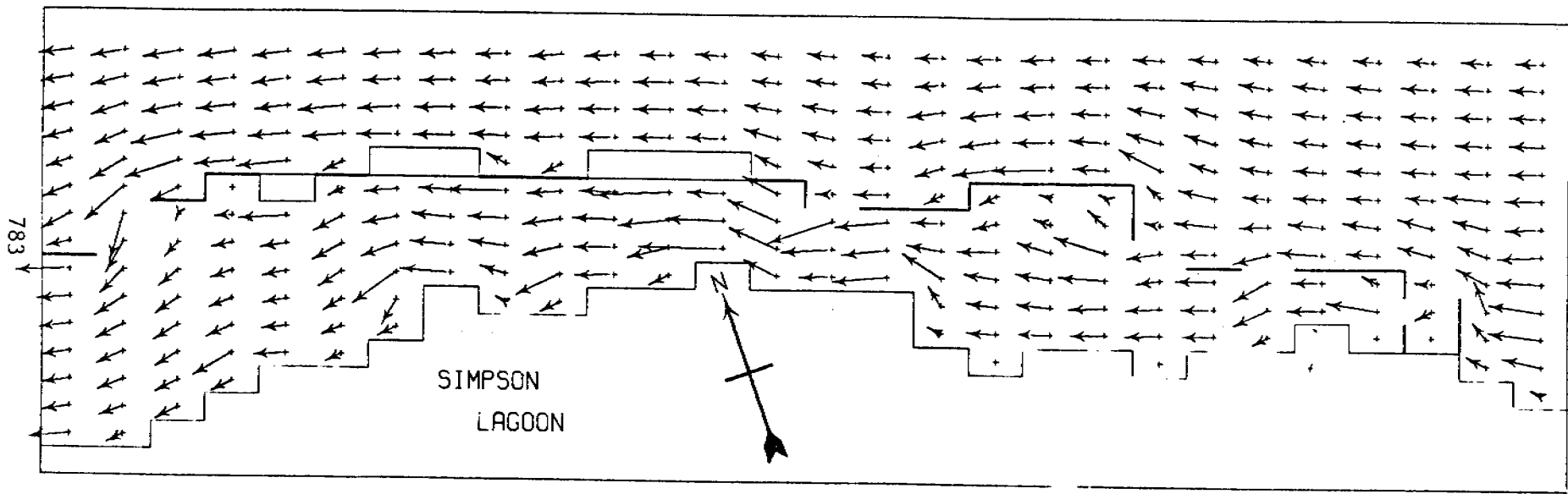
Two-dimensional modeling results: unverified depth-mean current vectors
and water parcel tracks



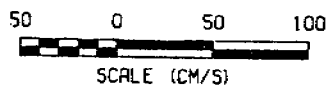
2-D MODEL WIND AT 5 M/S FROM ENE
ELAPSED TIME MARKER EVERY 6 HOURS

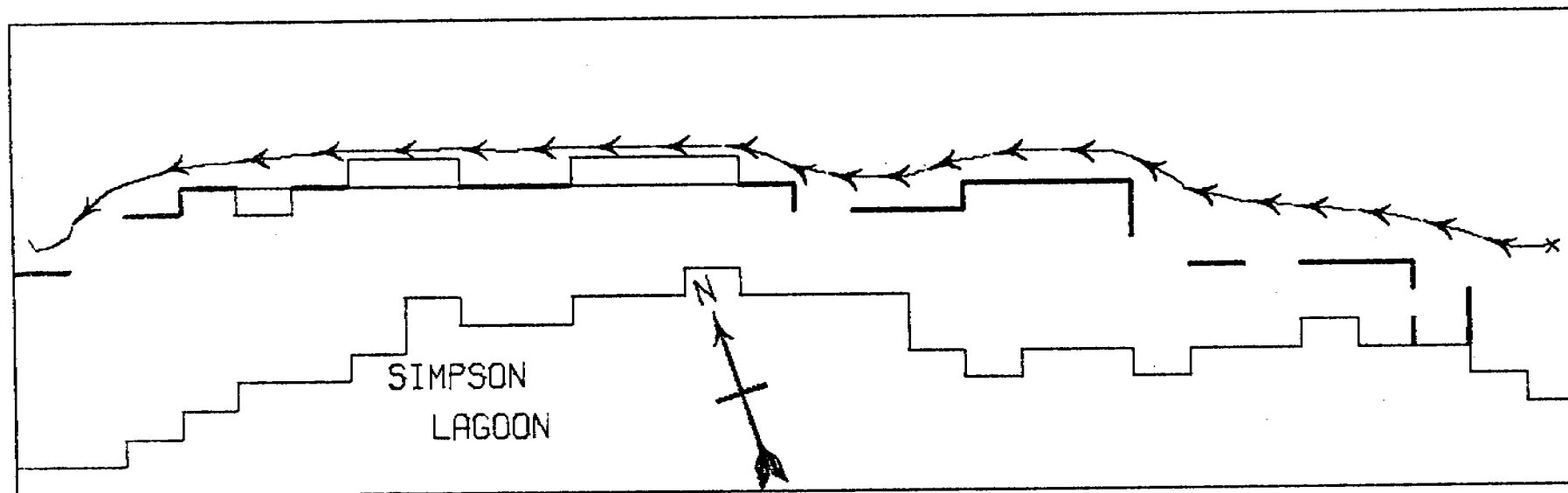


2-D MODEL WIND AT 5 M/S FROM ENE
ELAPSED TIME MARKER EVERY 6 HOURS

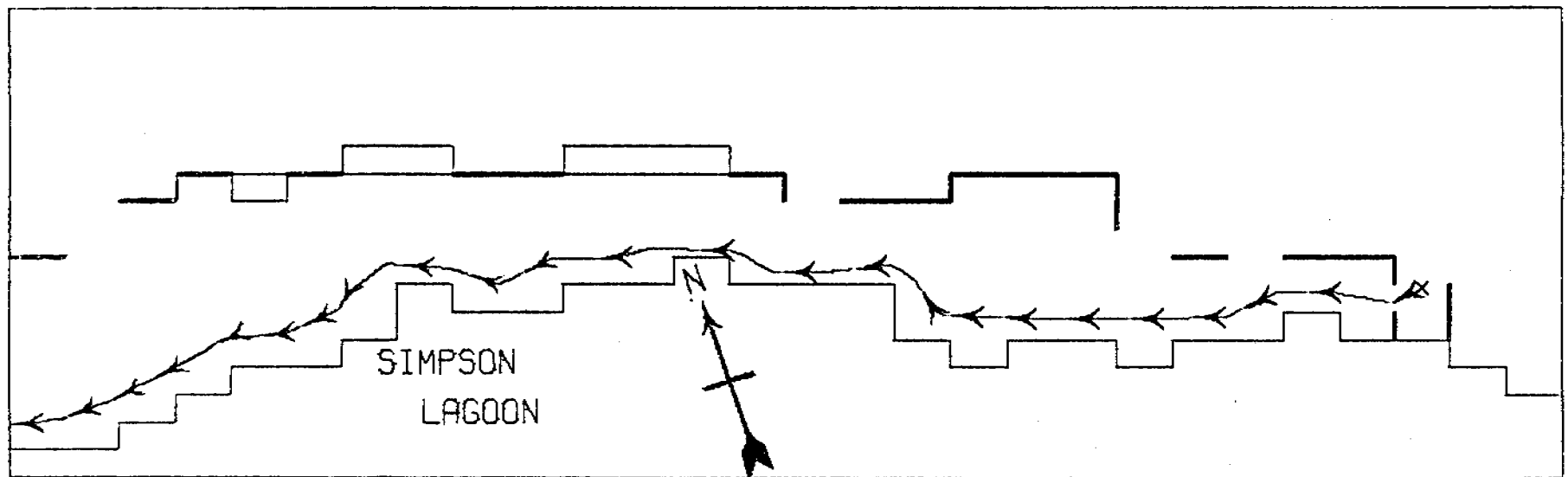


2-D MODEL DEPTH-MEAN CURRENT VECTORS
 WIND AT 10 M/S FROM ENE

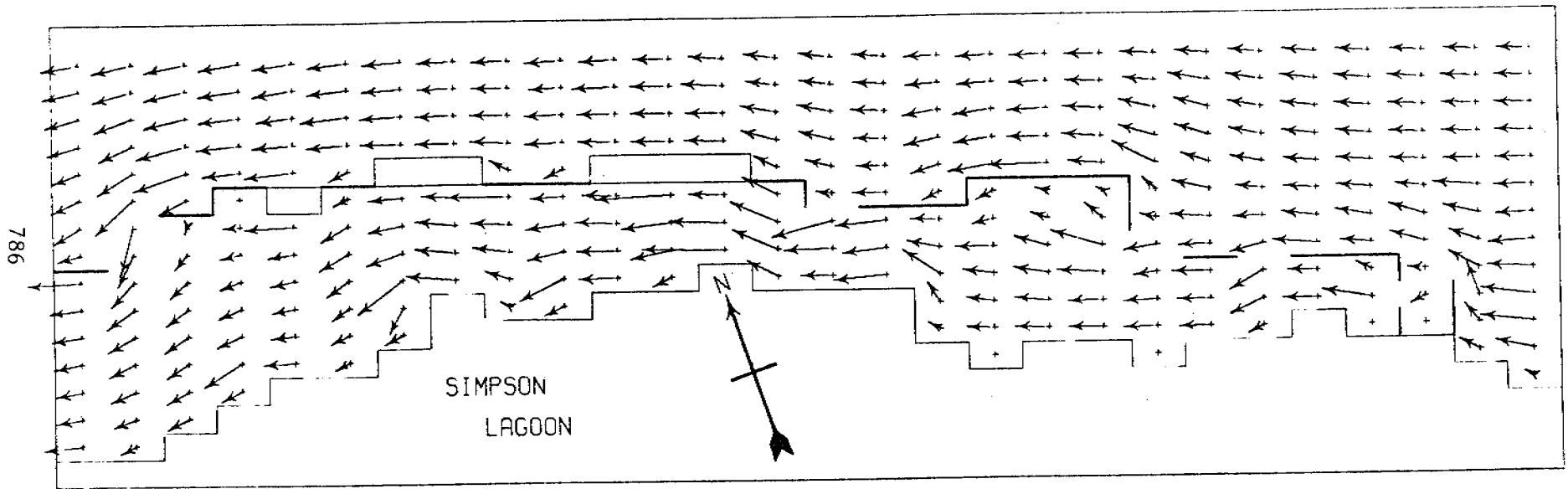




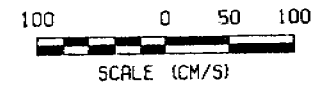
2-D MODEL WIND AT 10 M/S FROM ENE
ELAPSED TIME MARKER EVERY 3 HOURS



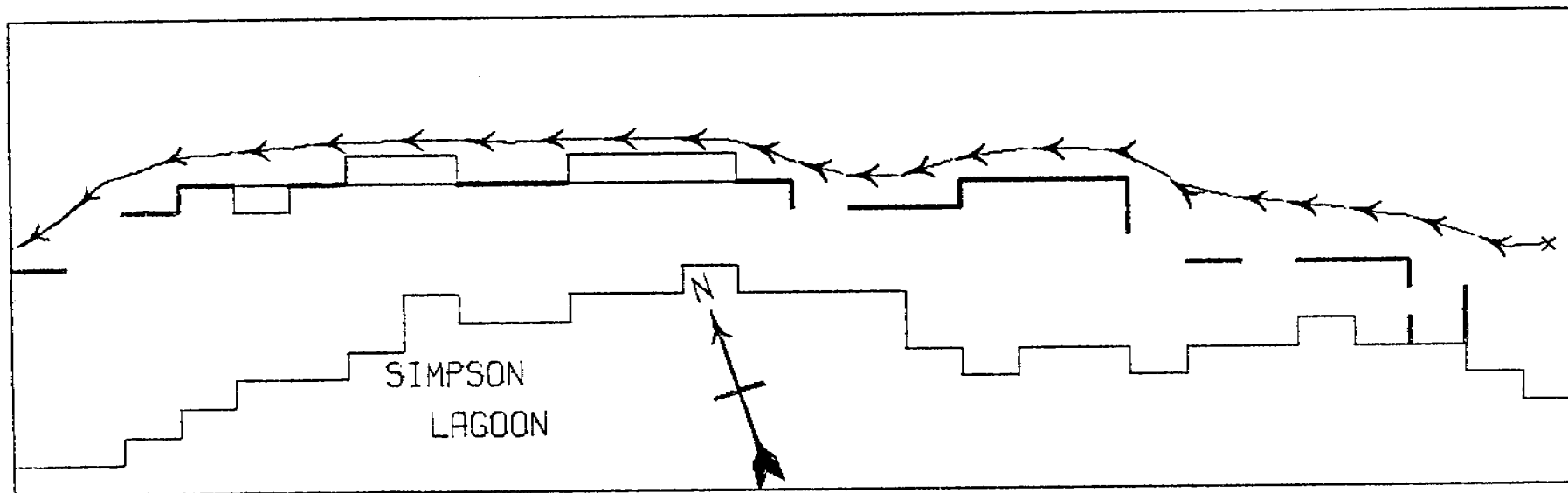
2-D MODEL WIND AT 10 M/S FROM ENE
ELAPSED TIME MARKER EVERY 3 HOURS



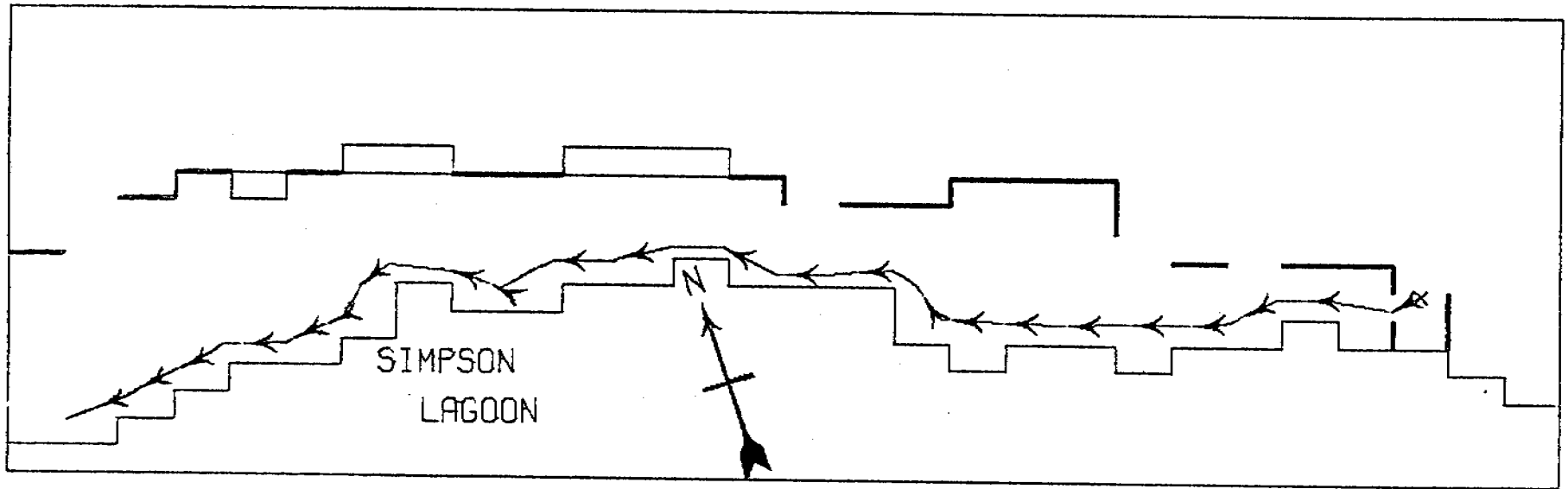
2-D MODEL DEPTH-MEAN CURRENT VECTORS
WIND AT 15 M/S FROM ENE



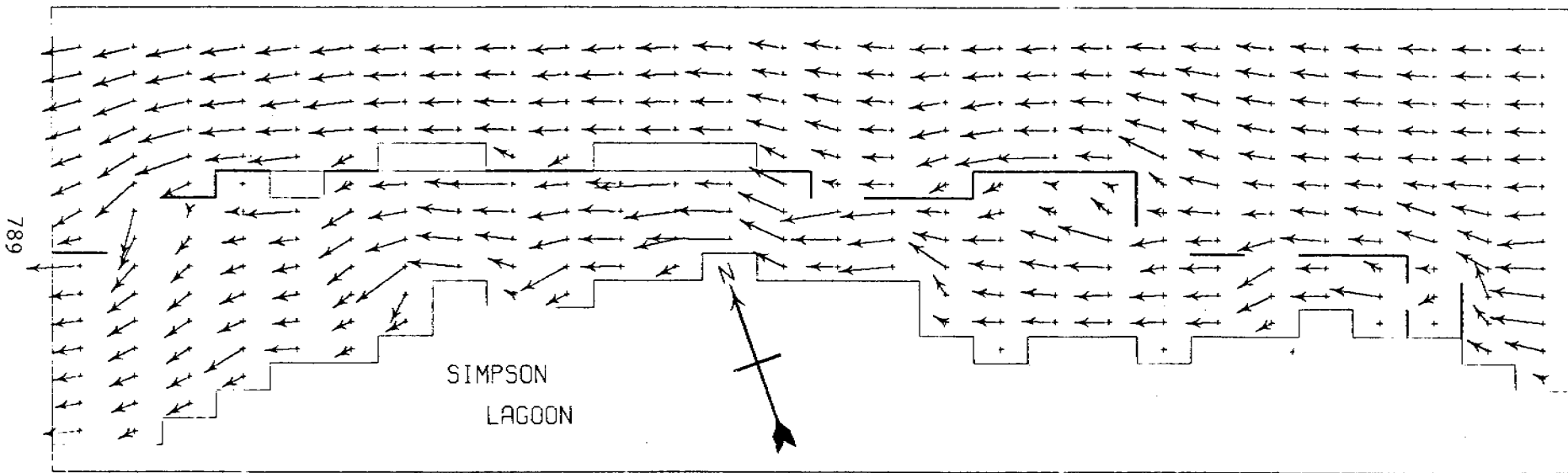
787



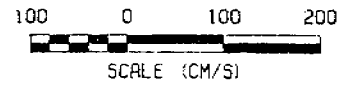
2-D MODEL WIND AT 15 M/S FROM ENE
ELAPSED TIME MARKER EVERY 2 HOURS

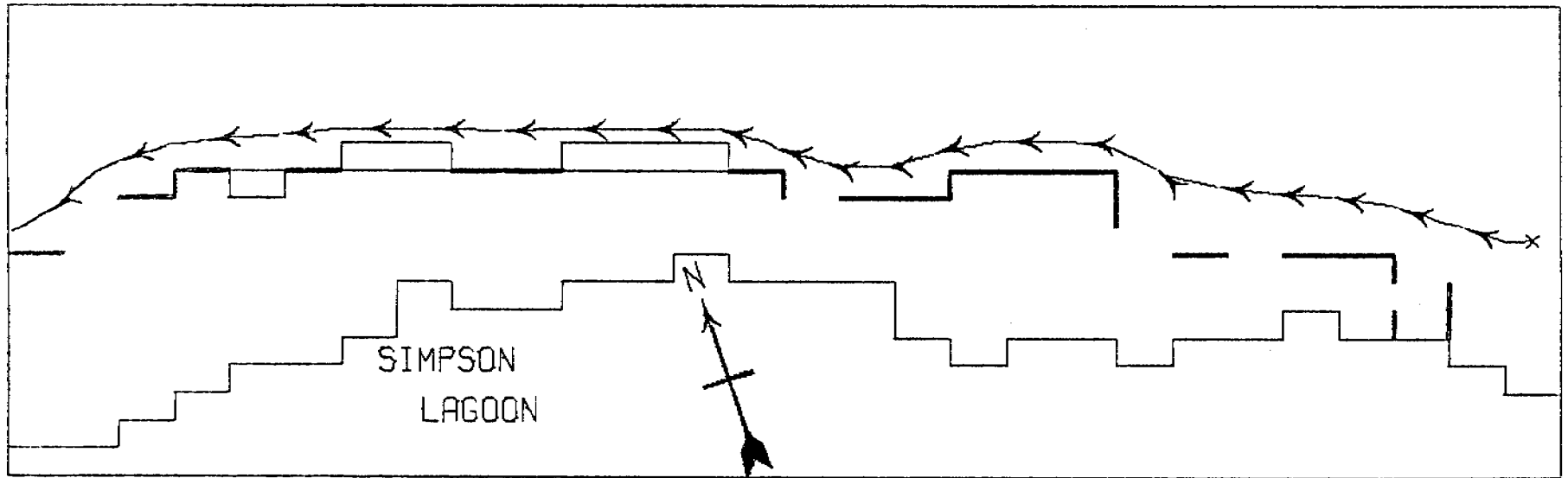


2-D MODEL WIND AT 15 M/S FROM ENE
ELAPSED TIME MARKER EVERY 2 HOURS

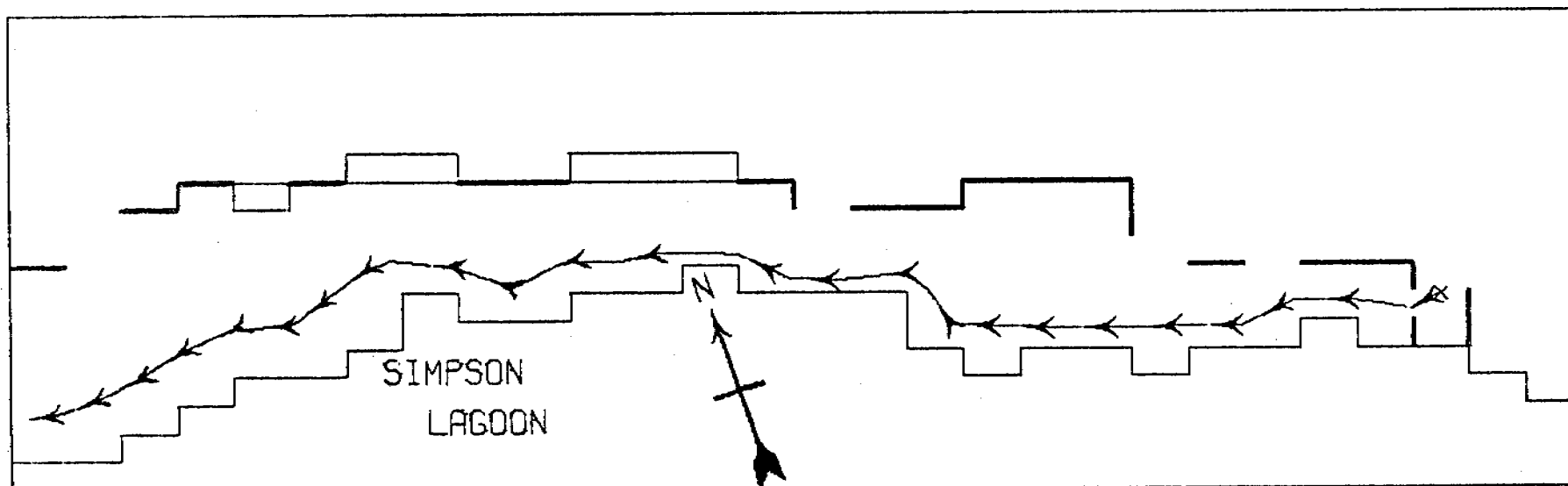


2-D MODEL DEPTH-MEAN CURRENT VECTORS
WIND AT 20 M/S FROM ENE

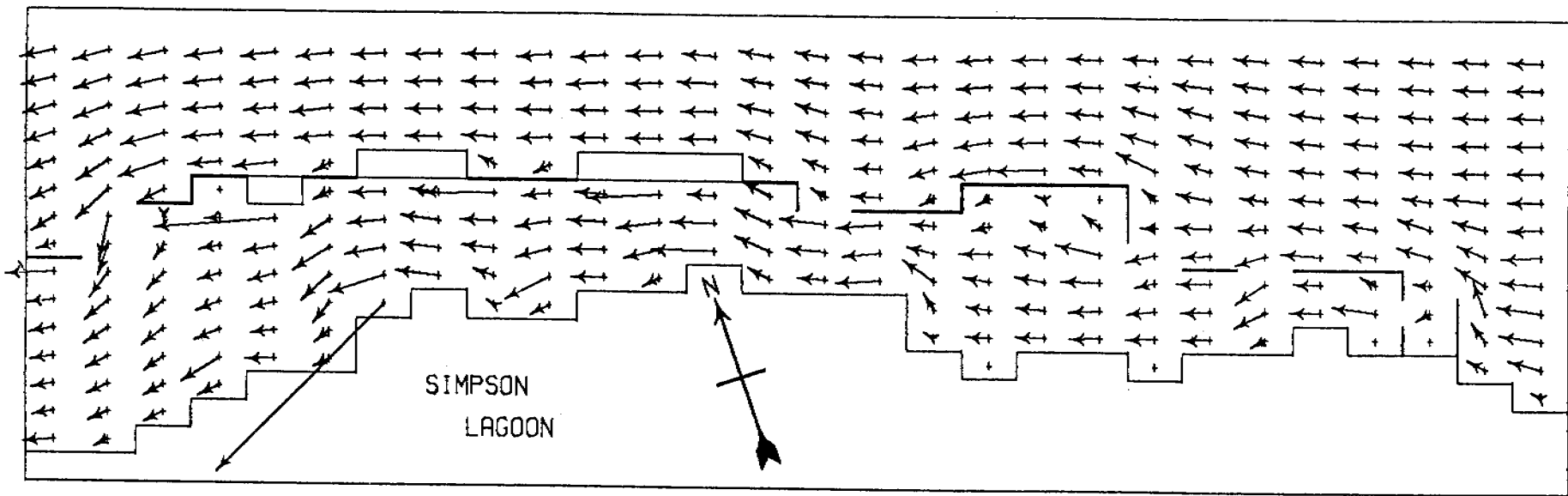




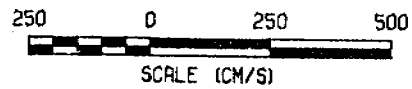
2-D MODEL WIND AT 20 M/S FROM ENE
ELAPSED TIME MARKER EVERY 1.5 HOURS

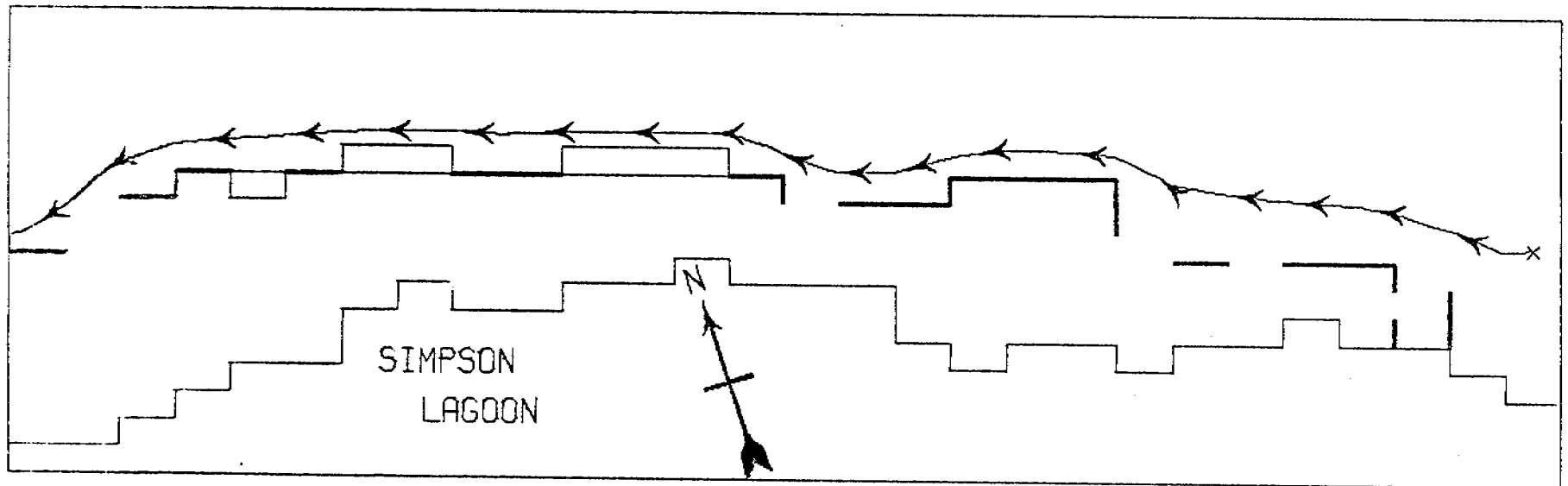


2-D MODEL WIND AT 20 M/S FROM ENE
ELAPSED TIME MARKER EVERY 1.5 HOURS



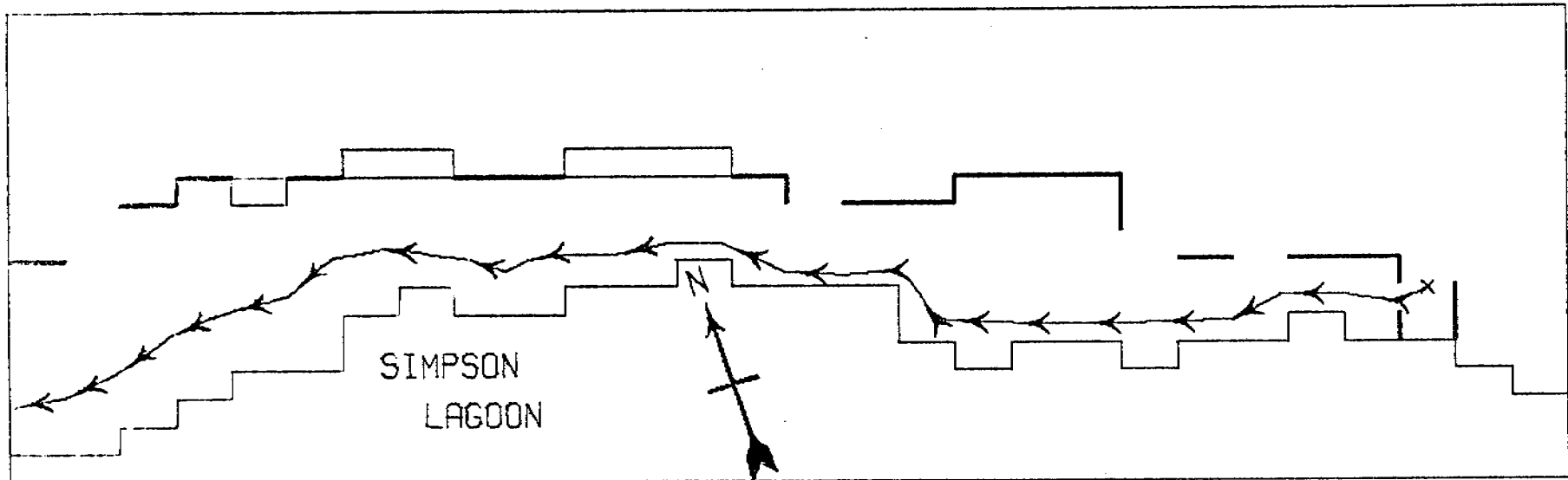
2-D MODEL DEPTH-MEAN CURRENT VECTORS
WIND AT 35 M/S FROM ENE





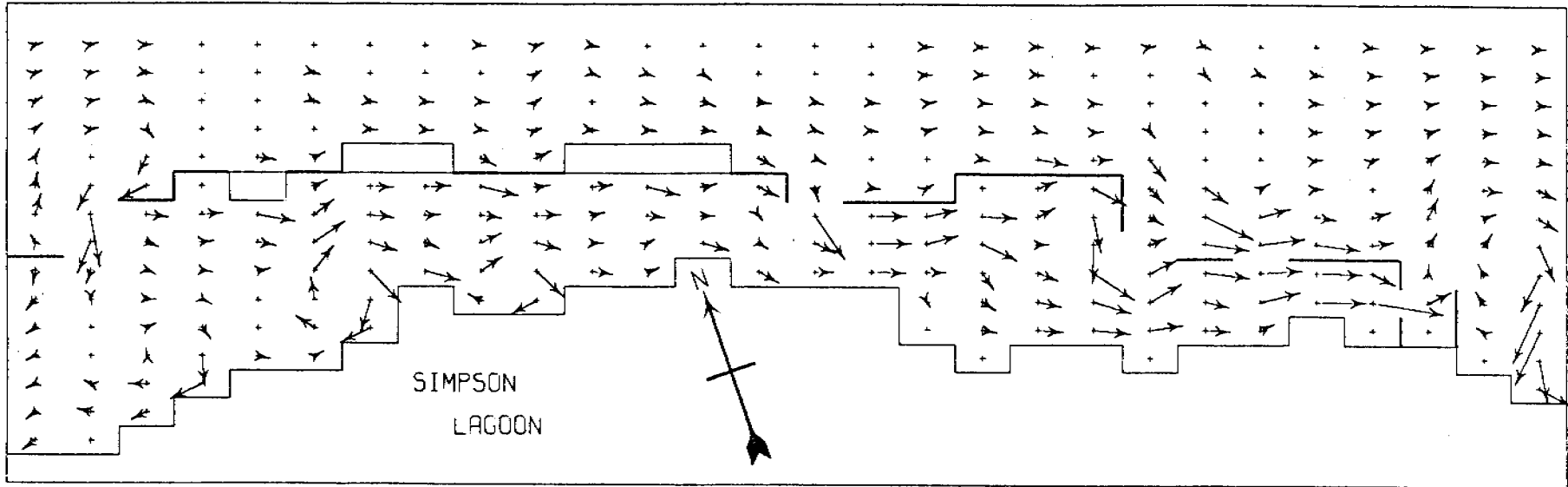
2-D MODEL WIND AT 35 M/S FROM ENE
ELAPSED TIME MARKER EVERY HOUR

794

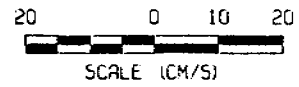


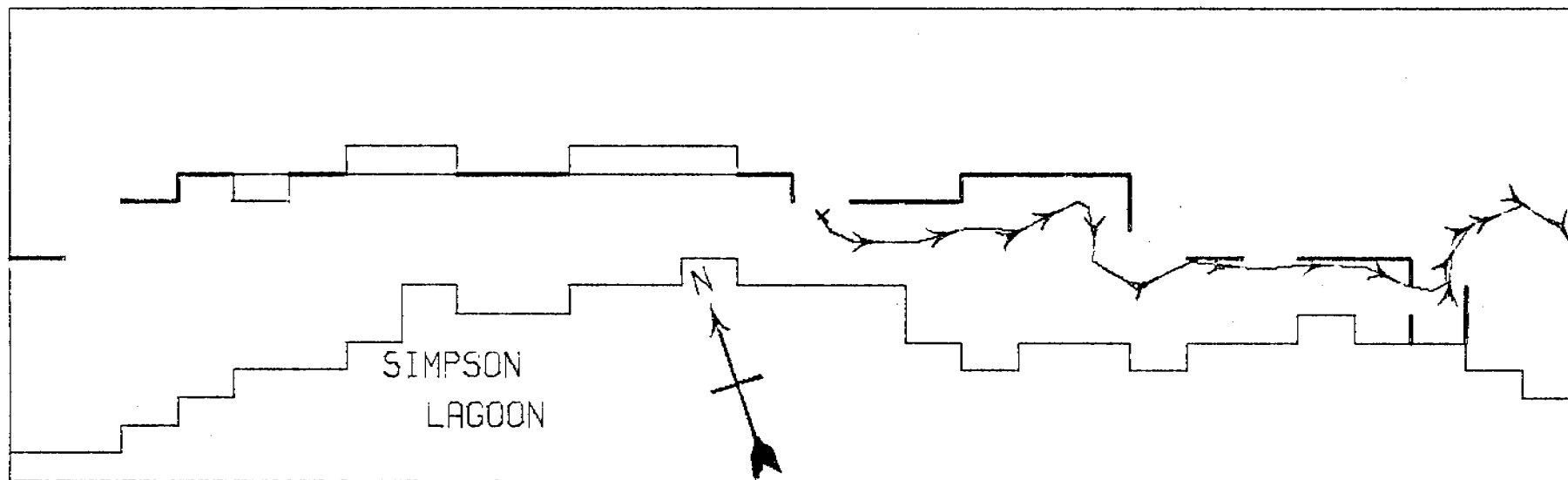
2-D MODEL WIND AT 35 M/S FROM ENE
ELAPSED TIME MARKER EVERY HOUR

795

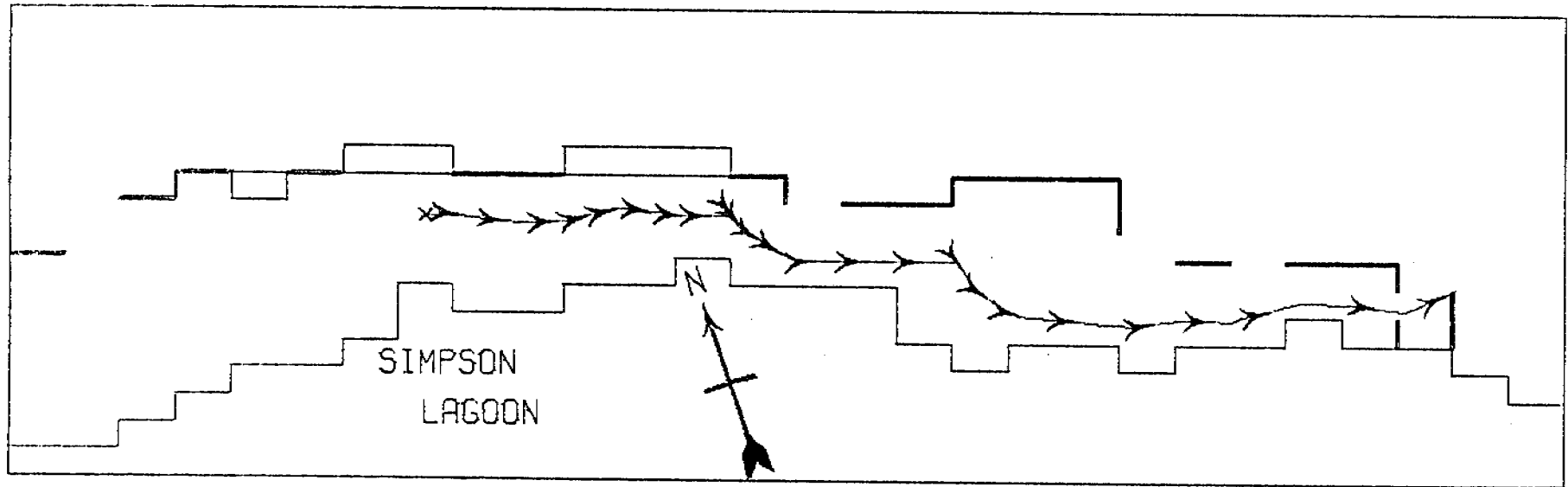


2-D MODEL DEPTH-MEAN CURRENT VECTORS
WIND AT 5 M/S FROM N

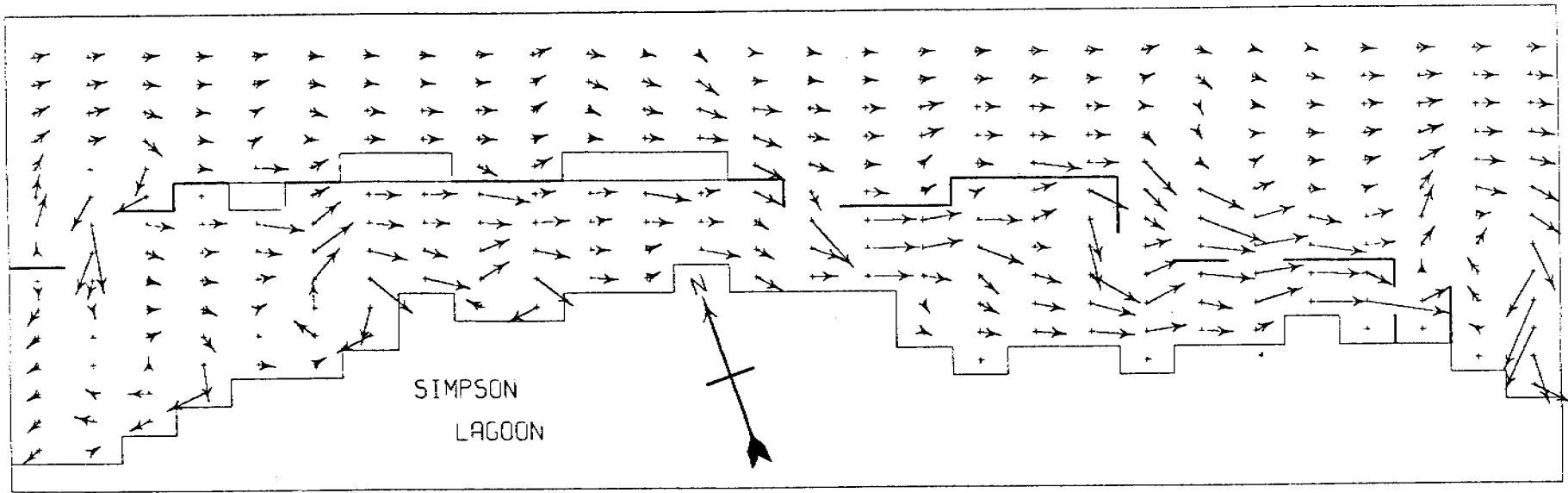




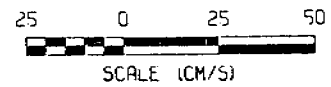
2-D MODEL WIND AT 5 M/S FROM N
ELAPSED TIME MARKER EVERY 12 HOURS

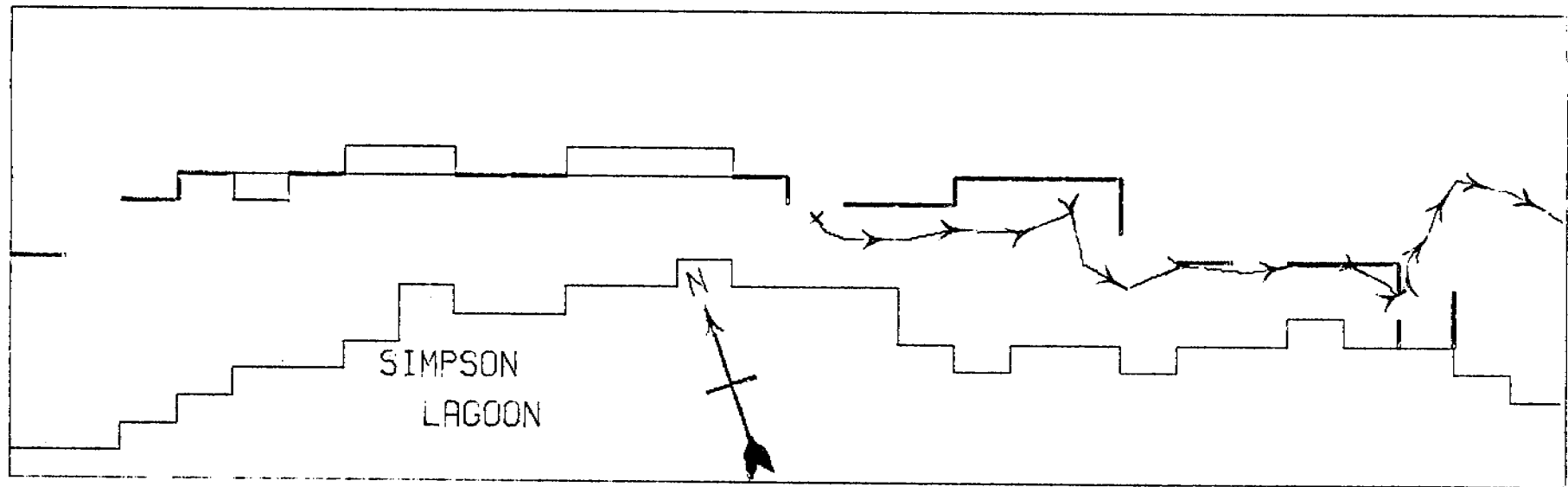


2-D MODEL WIND AT 5 M/S FROM N
ELAPSED TIME MARKER EVERY 12 HOURS



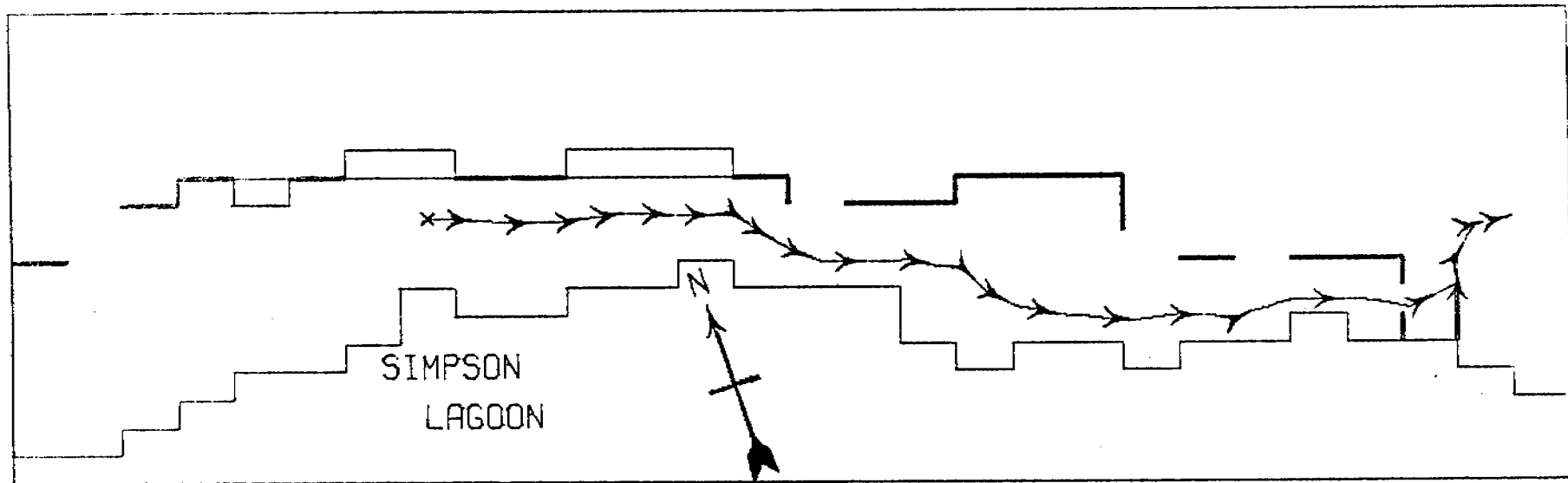
2-D MODEL DEPTH-MEAN CURRENT VECTORS
WIND AT 10 M/S FROM N





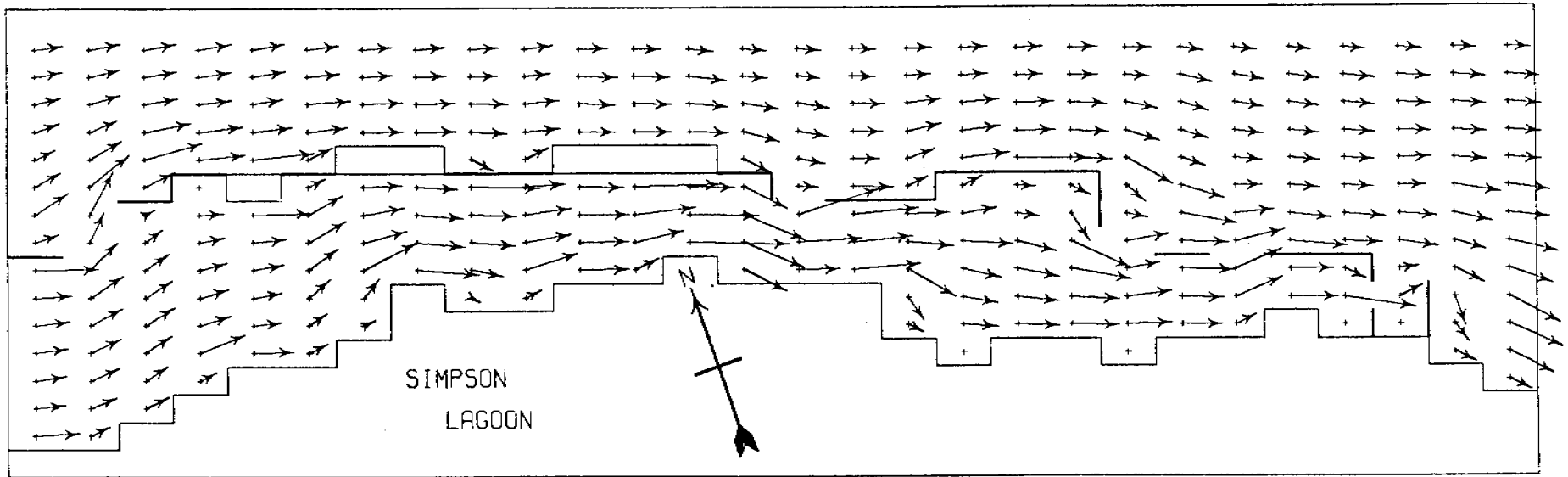
2-D MODEL WIND AT 10 M/S FROM N
ELAPSED TIME MARKER EVERY 6 HOURS

008

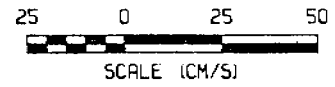


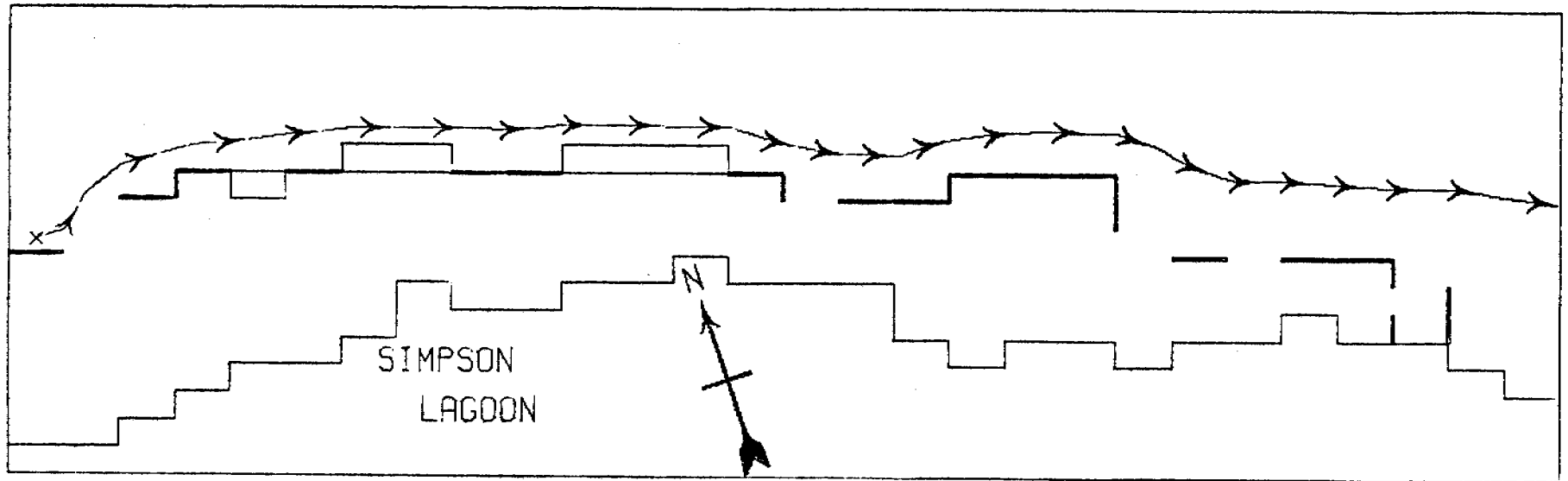
2-D MODEL WIND AT 10 M/S FROM N
ELAPSED TIME MARKER EVERY 6 HOURS

108

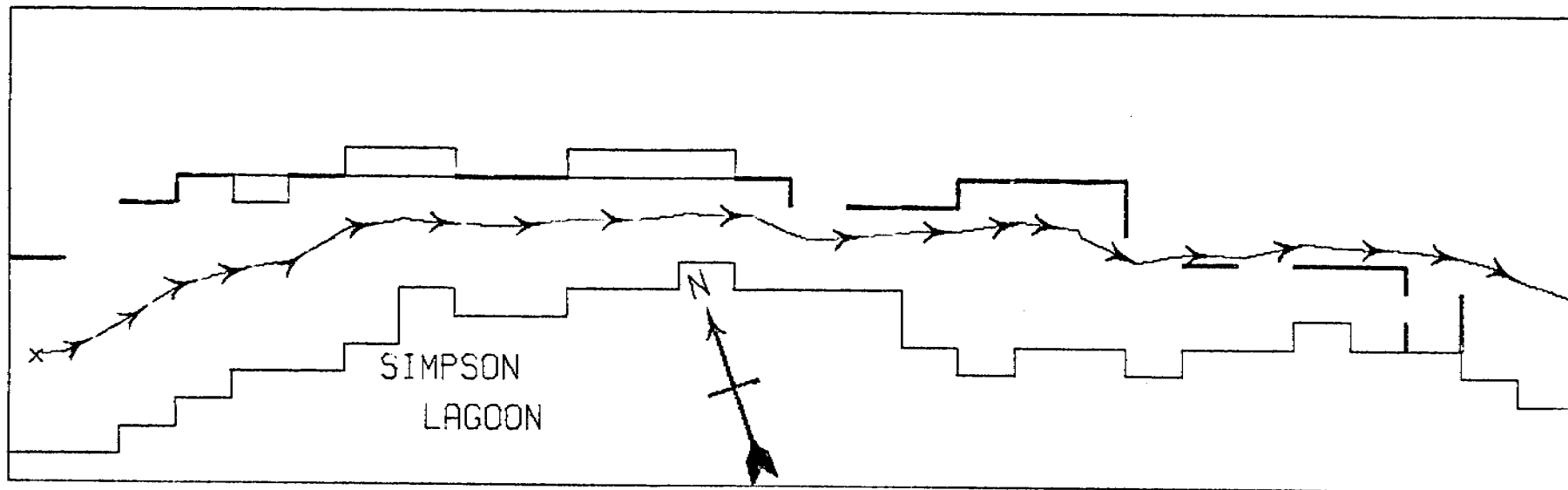


2-D MODEL DEPTH-MEAN CURRENT VECTORS
WIND AT 5 M/S FROM NW



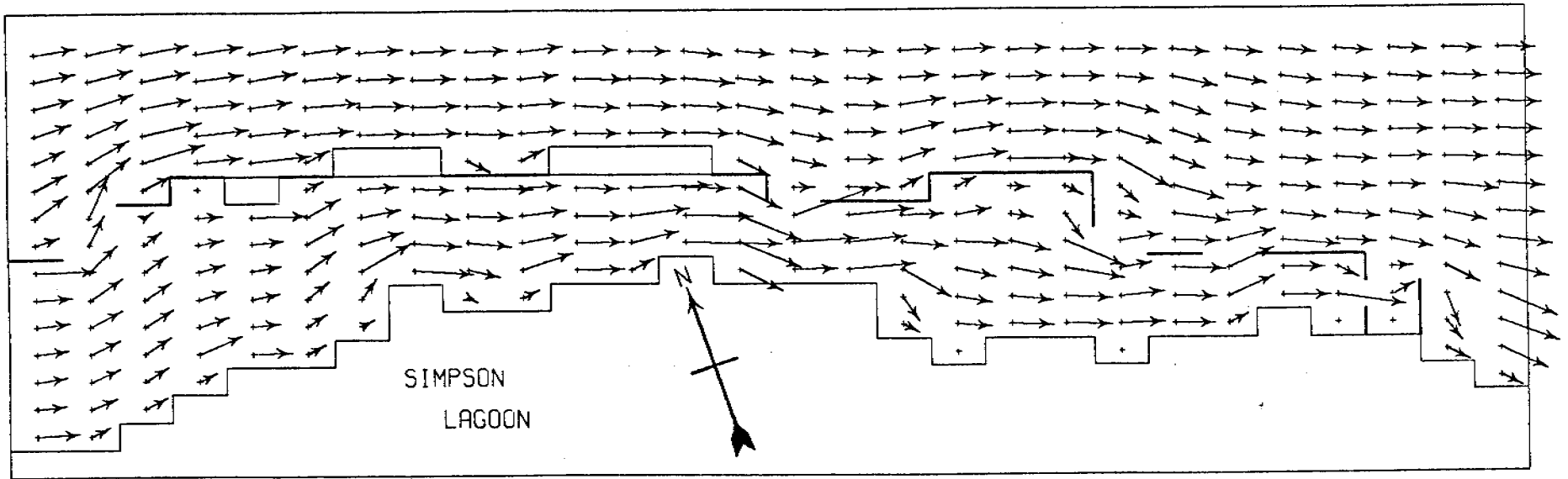


2-D MODEL WIND AT 5 M/S FROM NW
ELAPSED TIME MARKER EVERY 6 HOURS

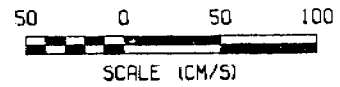


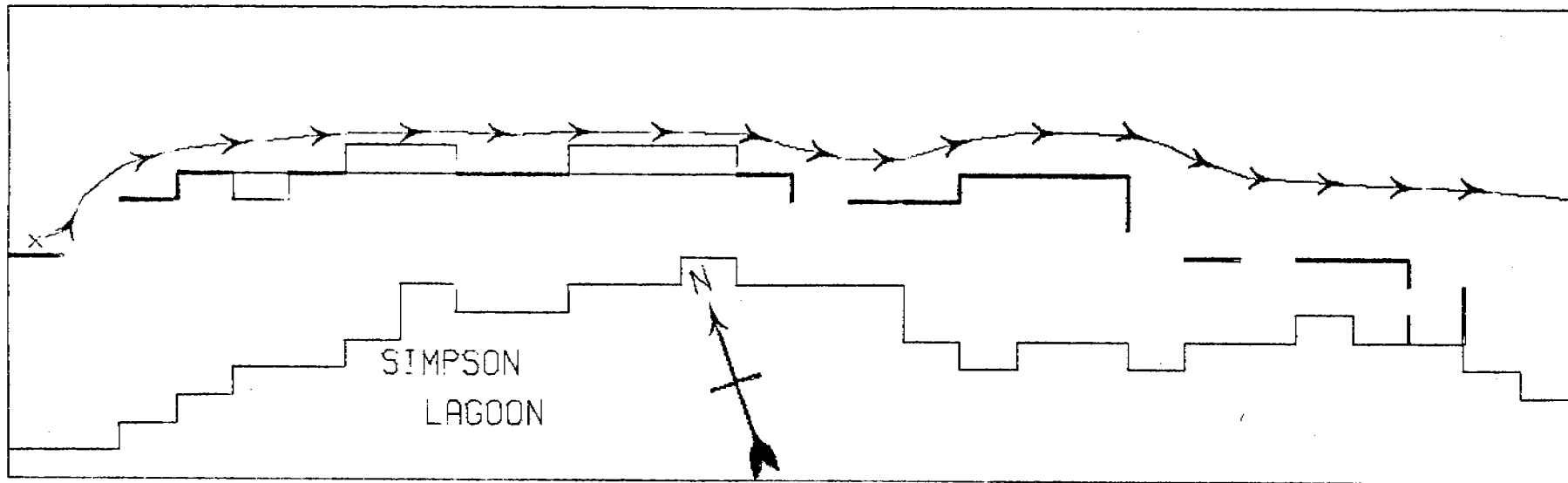
2-D MODEL WIND AT 5 M/S FROM NW
ELAPSED TIME MARKER EVERY 6 HOURS

804

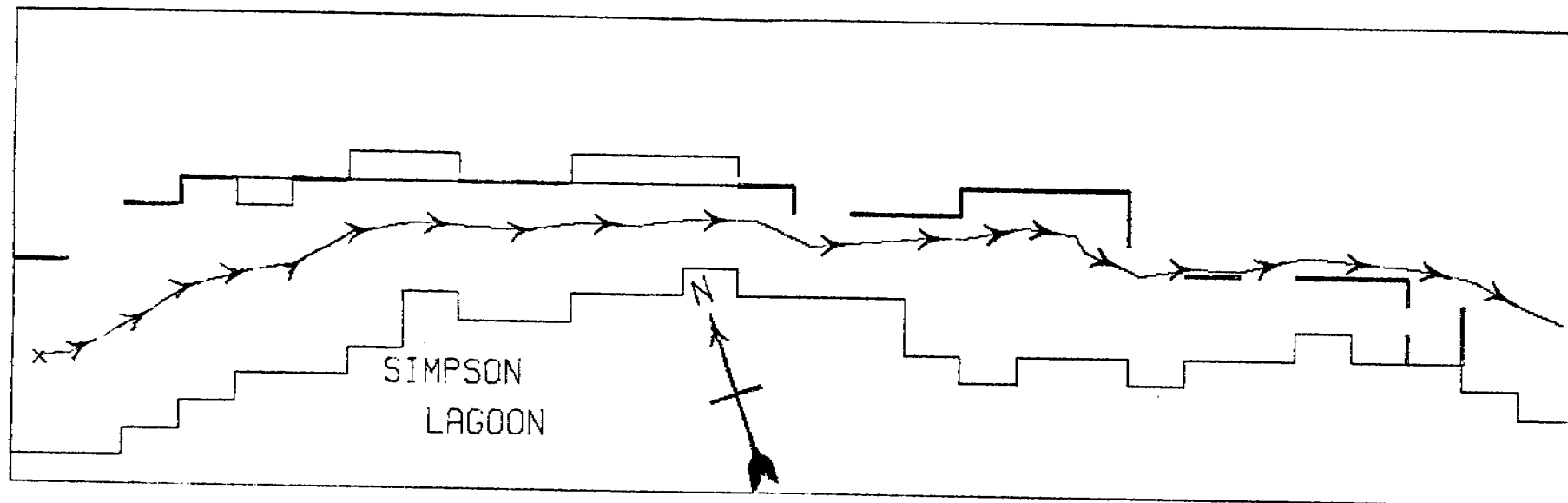


2-D MODEL DEPTH-MEAN CURRENT VECTORS
WIND AT 10 M/S FROM NW

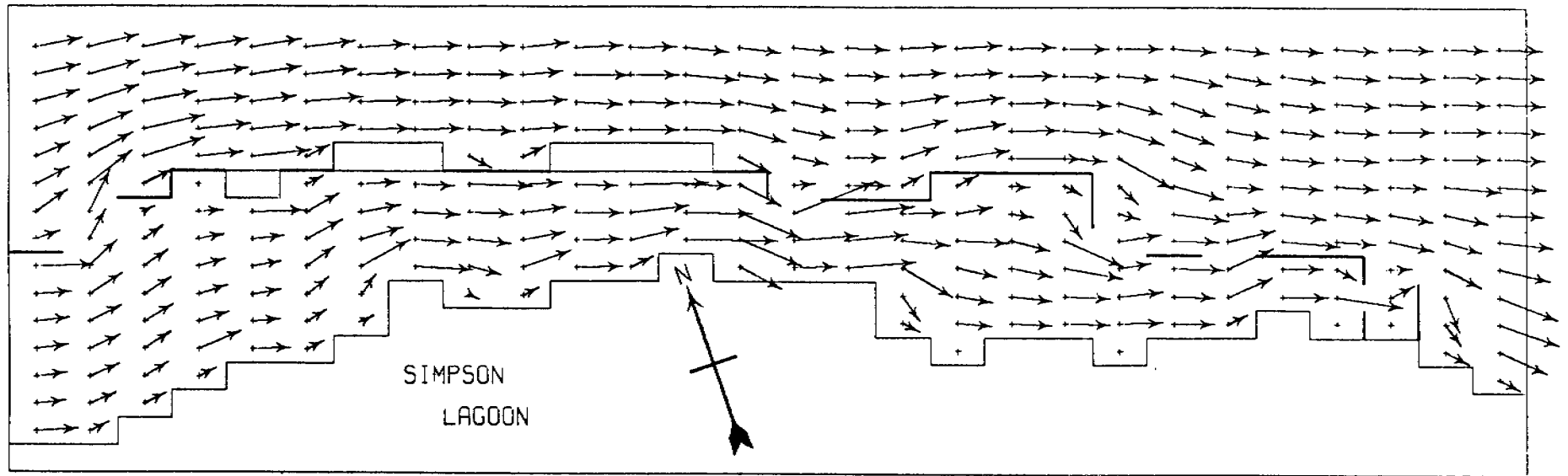




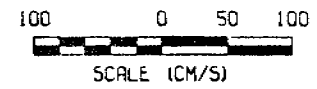
2-D MODEL WIND AT 10 M/S FROM NW
ELAPSED TIME MARKER EVERY 3 HOURS

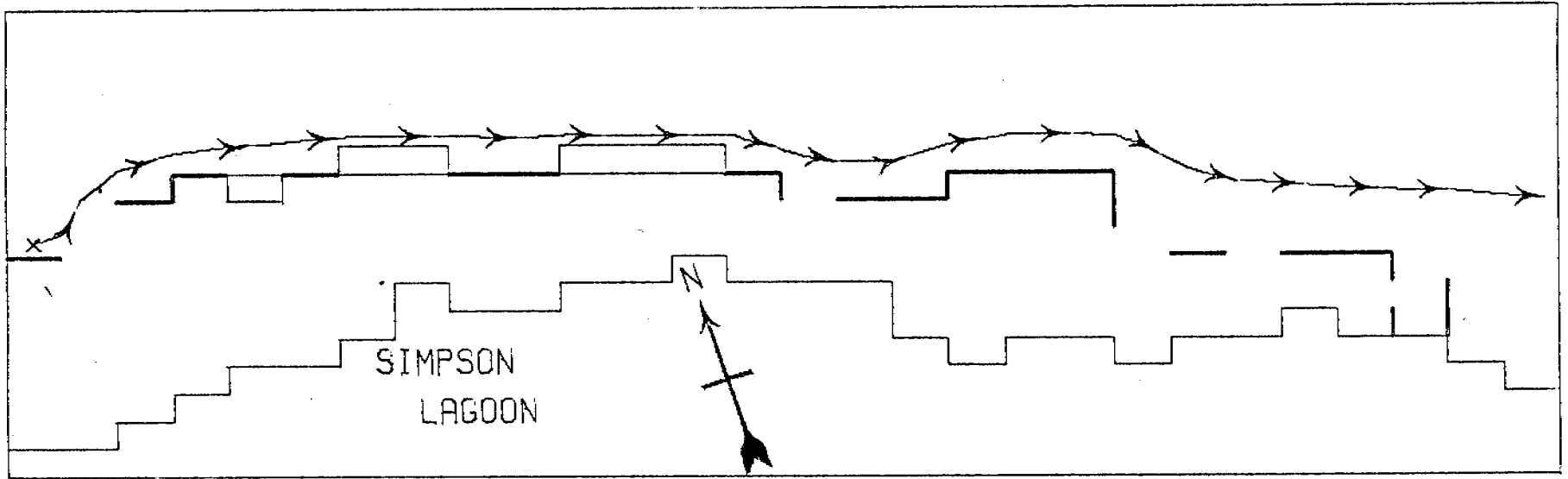


2-D MODEL WIND AT 10 M/S FROM NW
ELAPSED TIME MARKER EVERY 3 HOURS

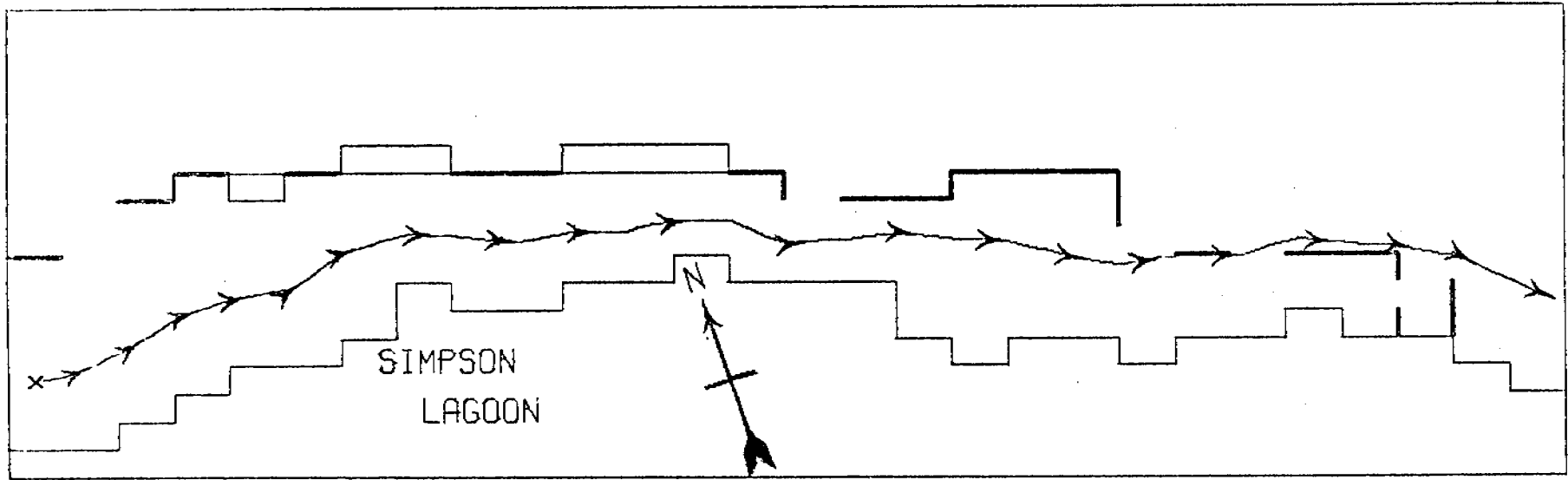


2-D MODEL DEPTH-MEAN CURRENT VECTORS
WIND AT 15 M/S FROM NW

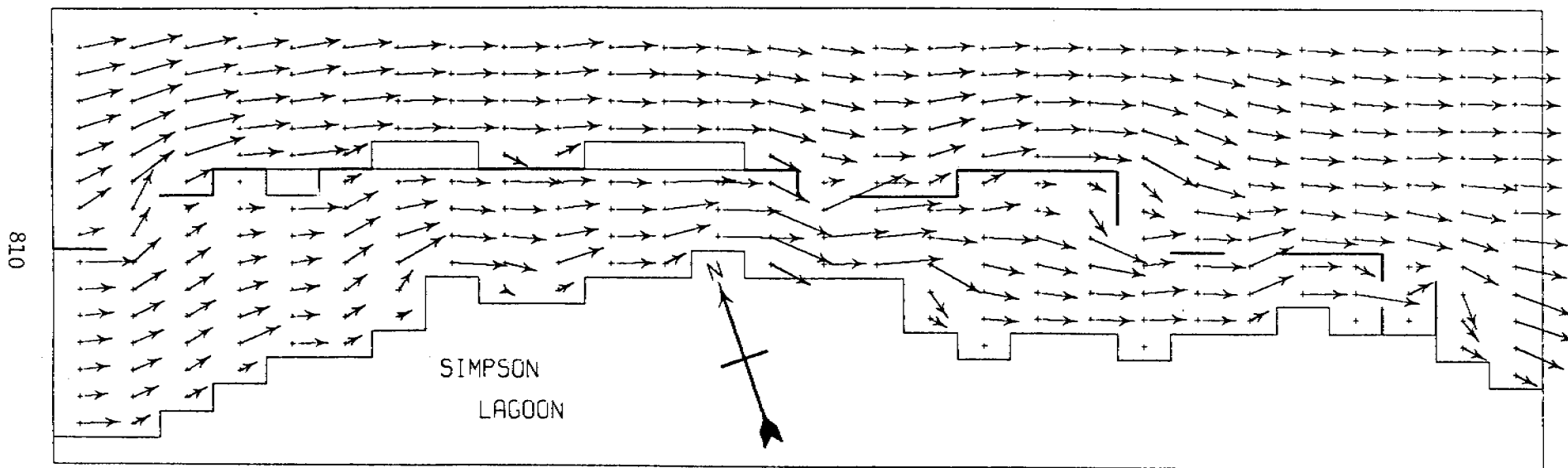




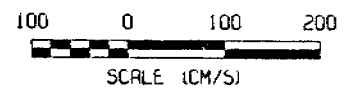
2-D MODEL WIND AT 15 M/S FROM NW
ELAPSED TIME MARKER EVERY 2 HOURS

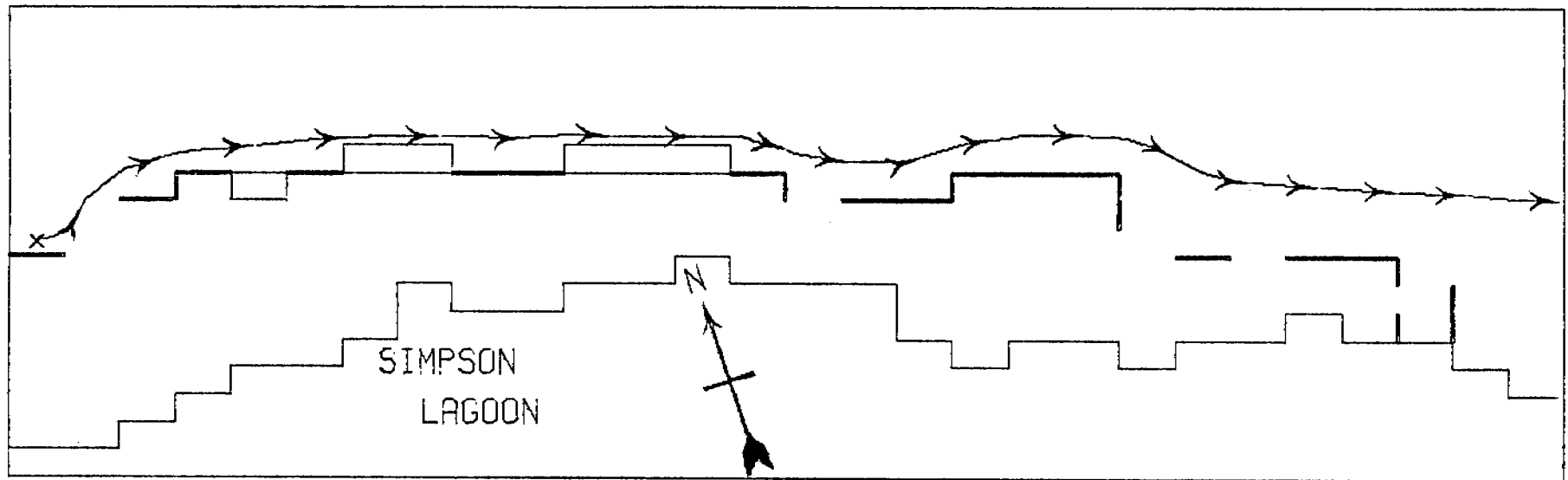


2-D MODEL WIND AT 15 M/S FROM NW
ELAPSED TIME MARKER EVERY 2 HOURS

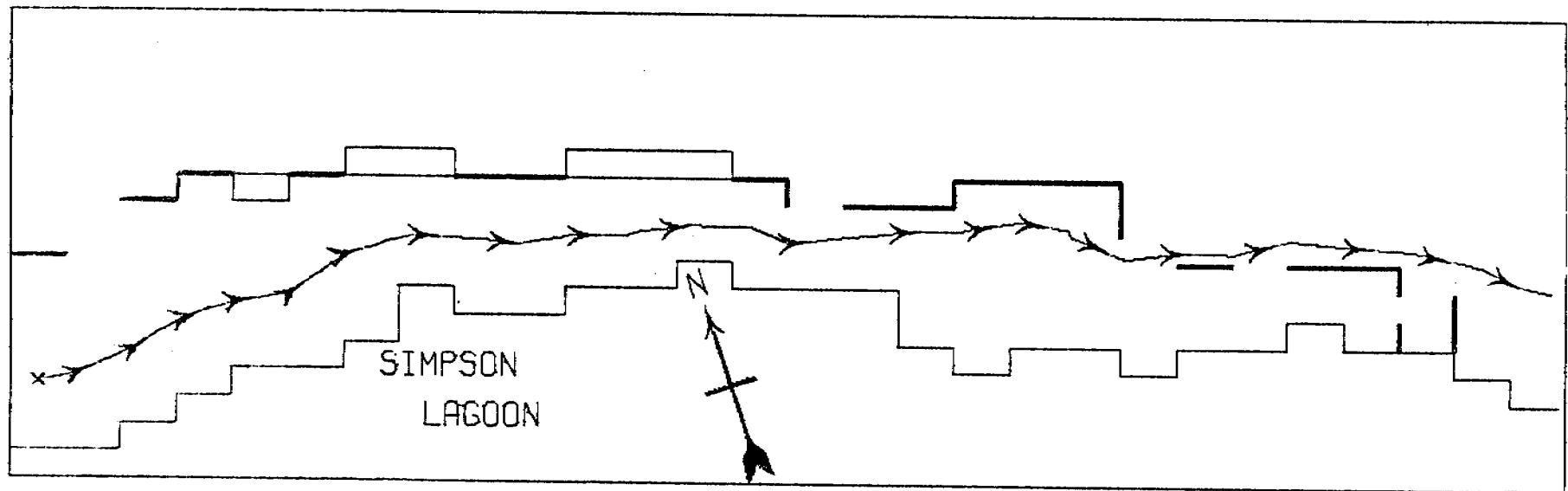


2-D MODEL DEPTH-MEAN CURRENT VECTORS
WIND AT 20 M/S FROM NW

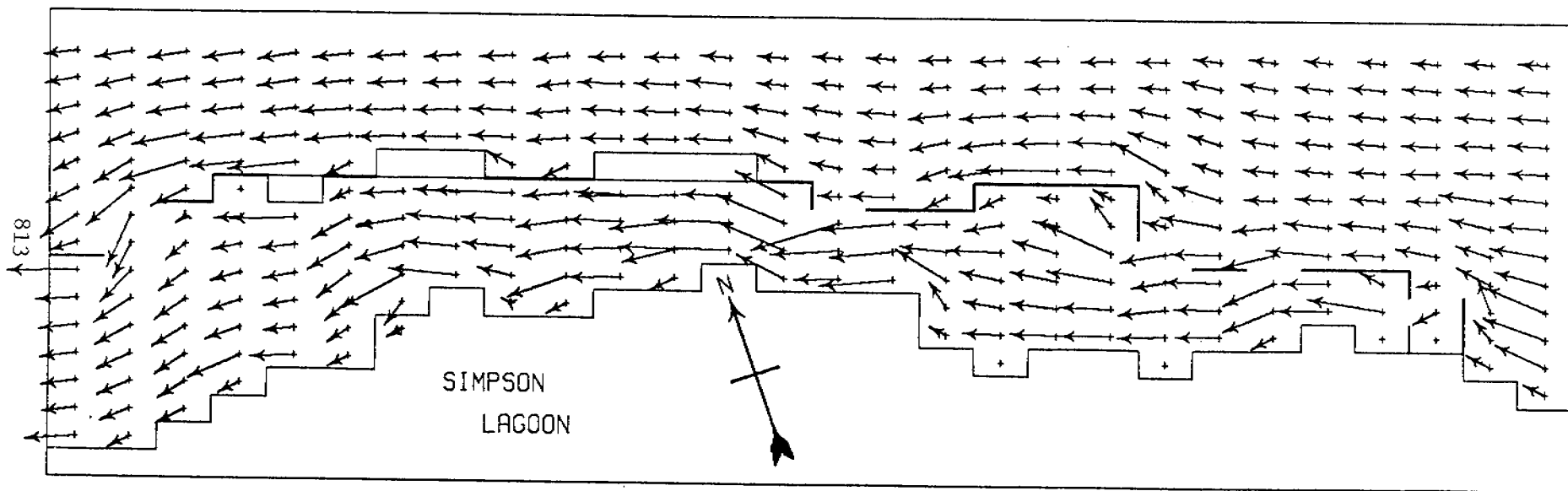




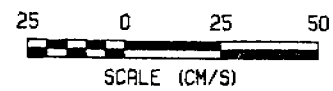
2-D MODEL WIND AT 20 M/S FROM NW
 ELAPSED TIME MARKER EVERY 1.5 HOURS

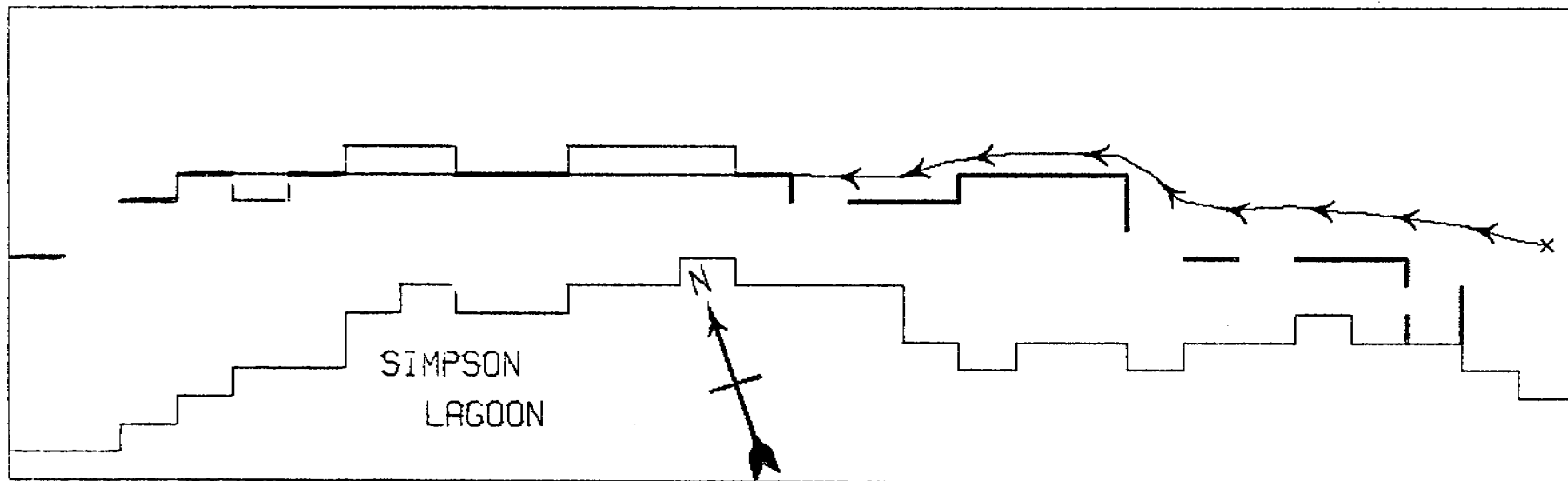


2-D MODEL WIND AT 20 M/S FROM NW
ELAPSED TIME MARKER EVERY 1.5 HOURS

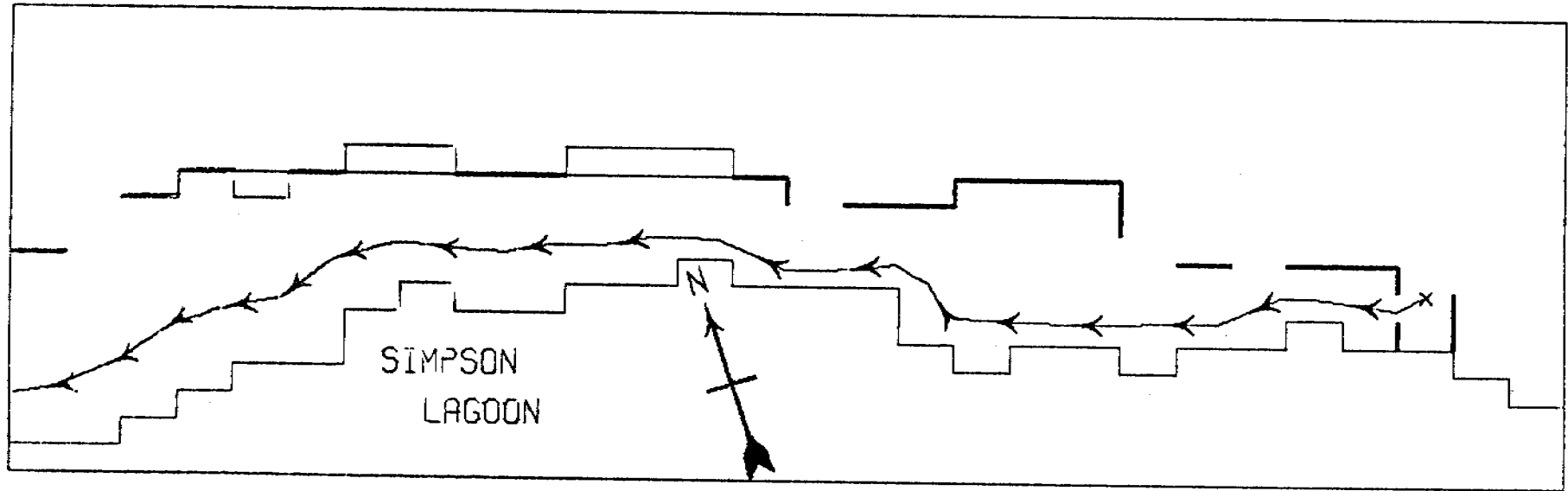


2-D MODEL DEPTH-MEAN CURRENT VECTORS
WIND AT 5 M/S FROM ESE

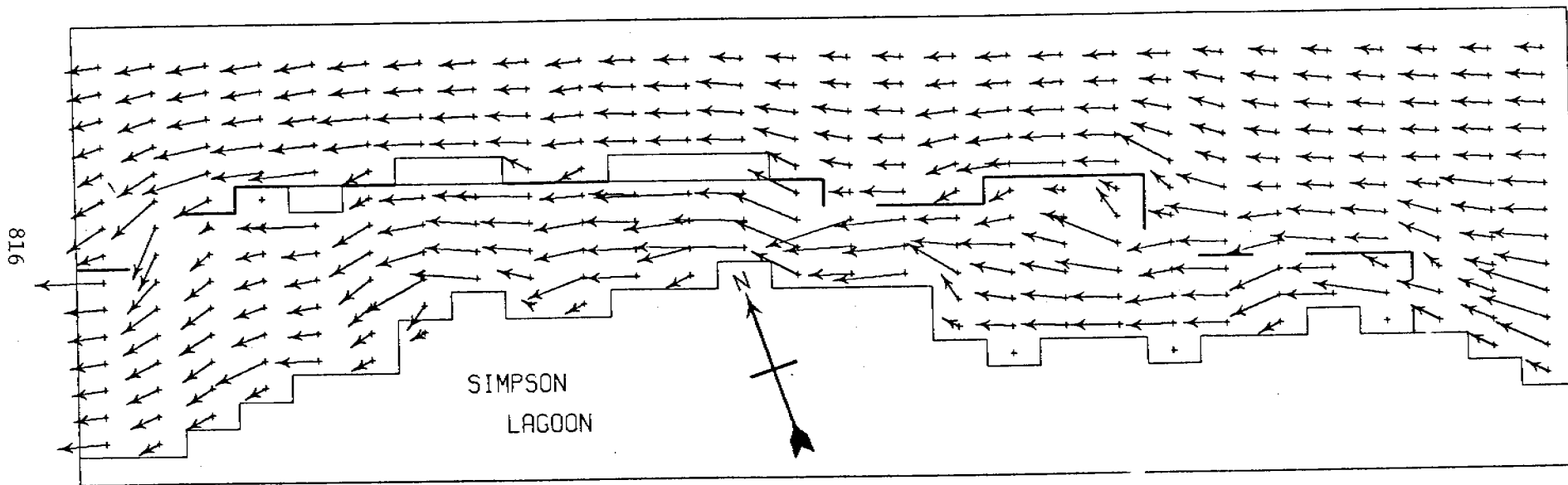




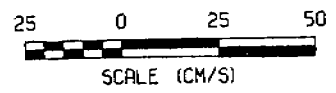
2-D MODEL WIND AT 5 M/S FROM ESE
ELAPSED TIME MARKER EVERY 6 HOURS

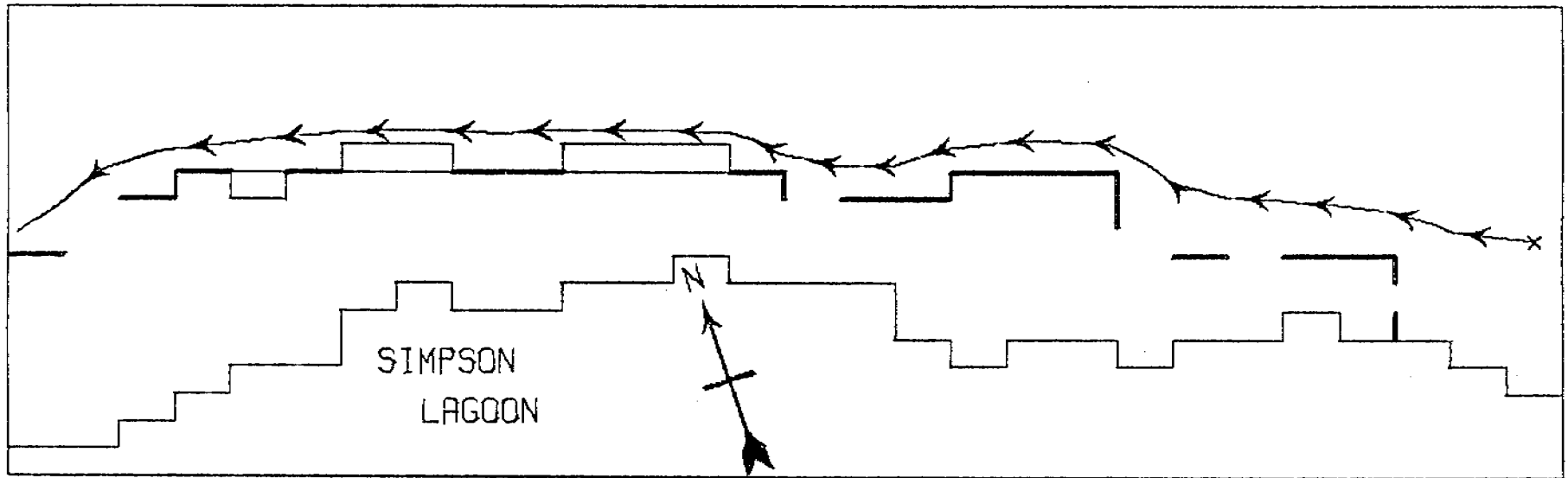


2-D MODEL WIND AT 5 M/S FROM ESE
ELAPSED TIME MARKER EVERY 6 HOURS

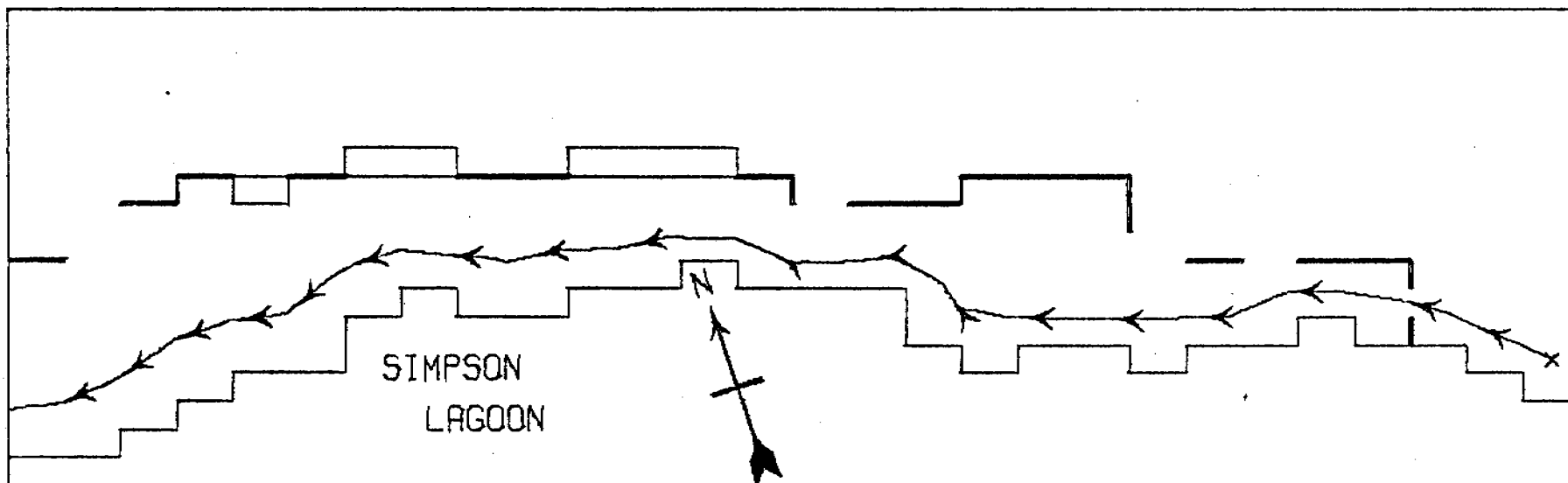


2-D MODEL DEPTH-MEAN CURRENT VECTORS
 WIND AT 5 M/S FROM ESE (NO CAUSEWAY)

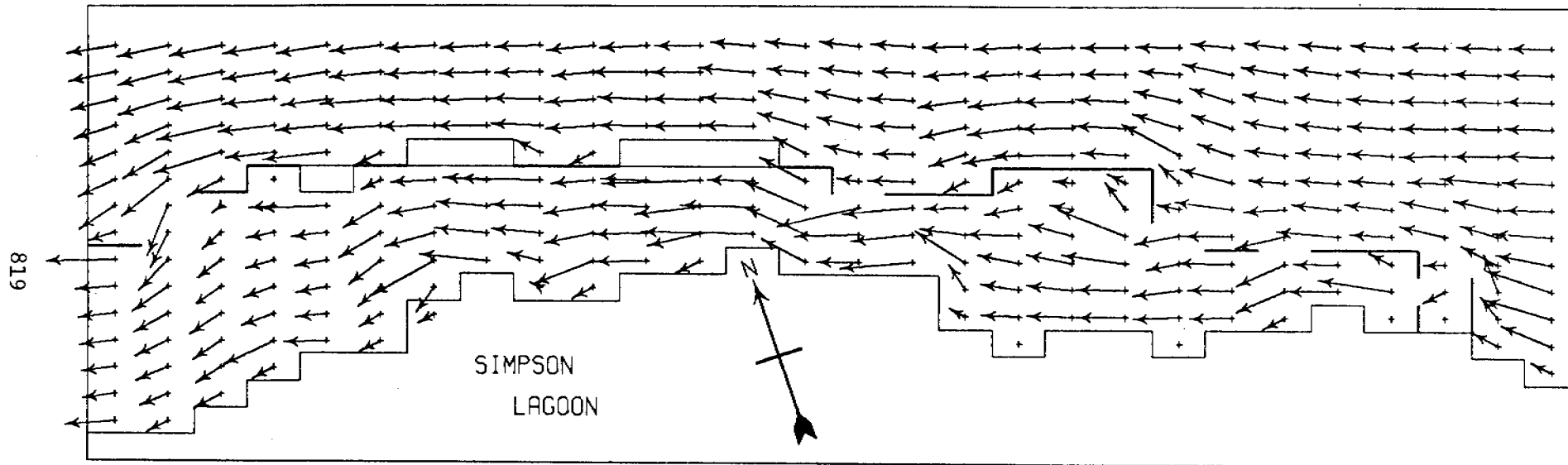




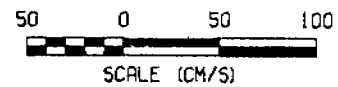
2-D MODEL WIND AT 5 M/S FROM ESE
ELAPSED TIME MARKER EVERY 6 HOURS
(NO CAUSEWAY)

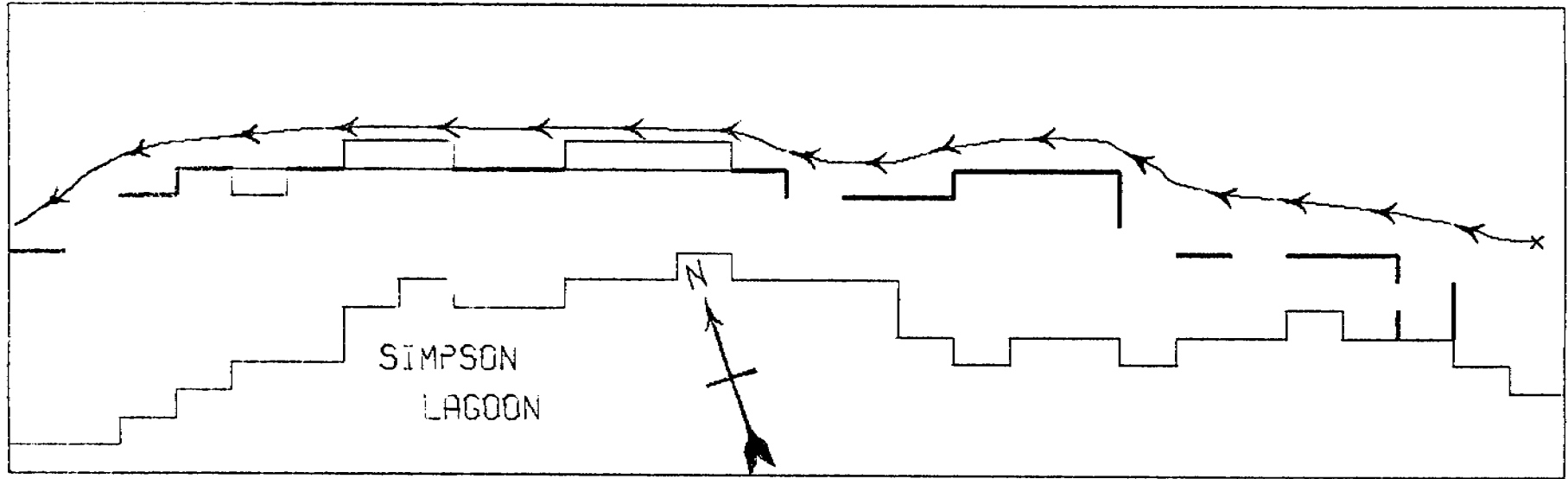


2-D MODEL WIND AT 5 M/S FROM ESE
ELAPSED TIME MARKER EVERY 6 HOURS
(NO CAUSEWAY)

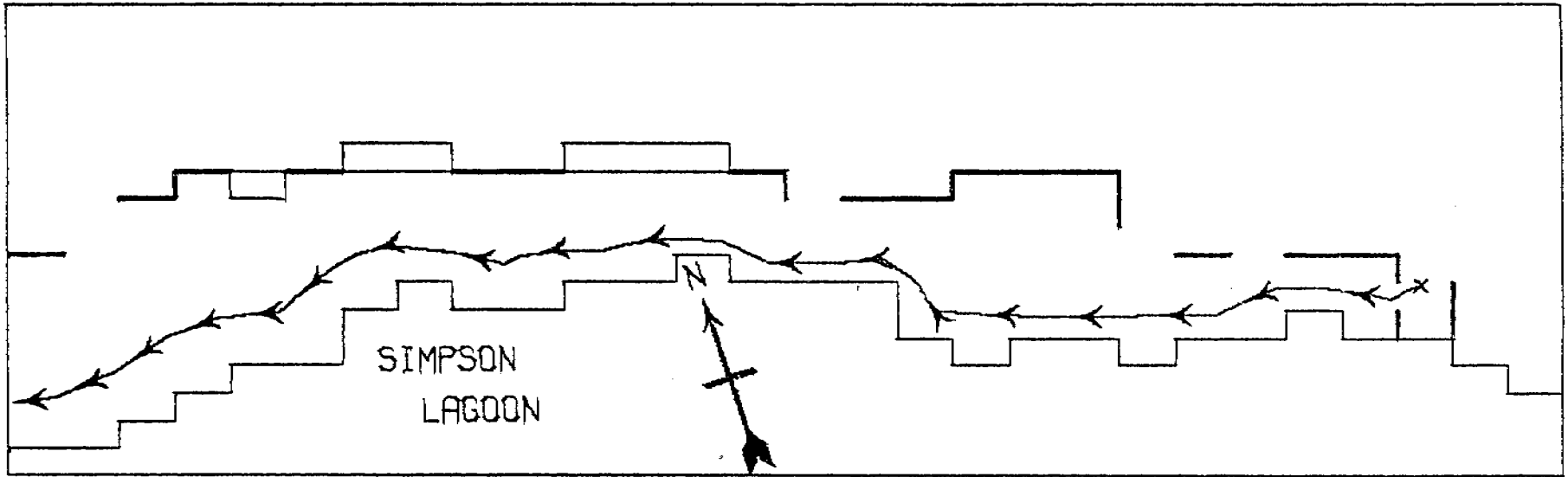


2-D MODEL DEPTH-MEAN CURRENT VECTORS
WIND AT 10 M/S FROM ESE



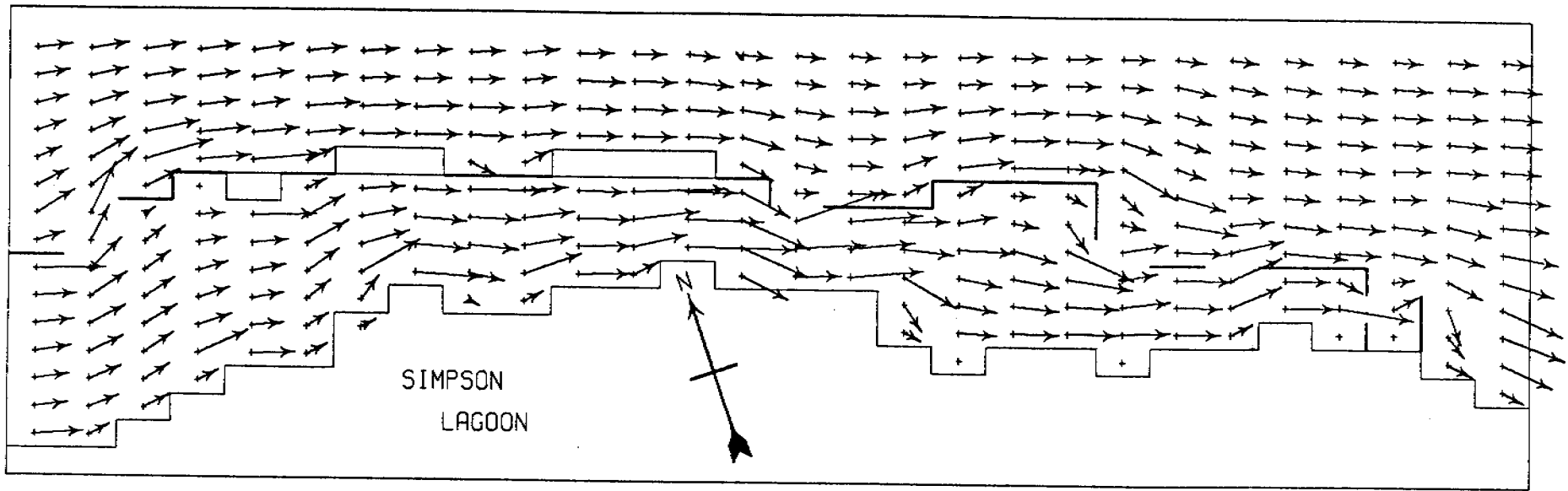


2-D MODEL WIND AT 10 M/S FROM ESE
ELAPSED TIME MARKER EVERY 3 HOURS

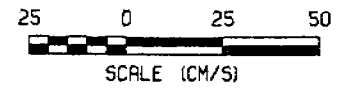


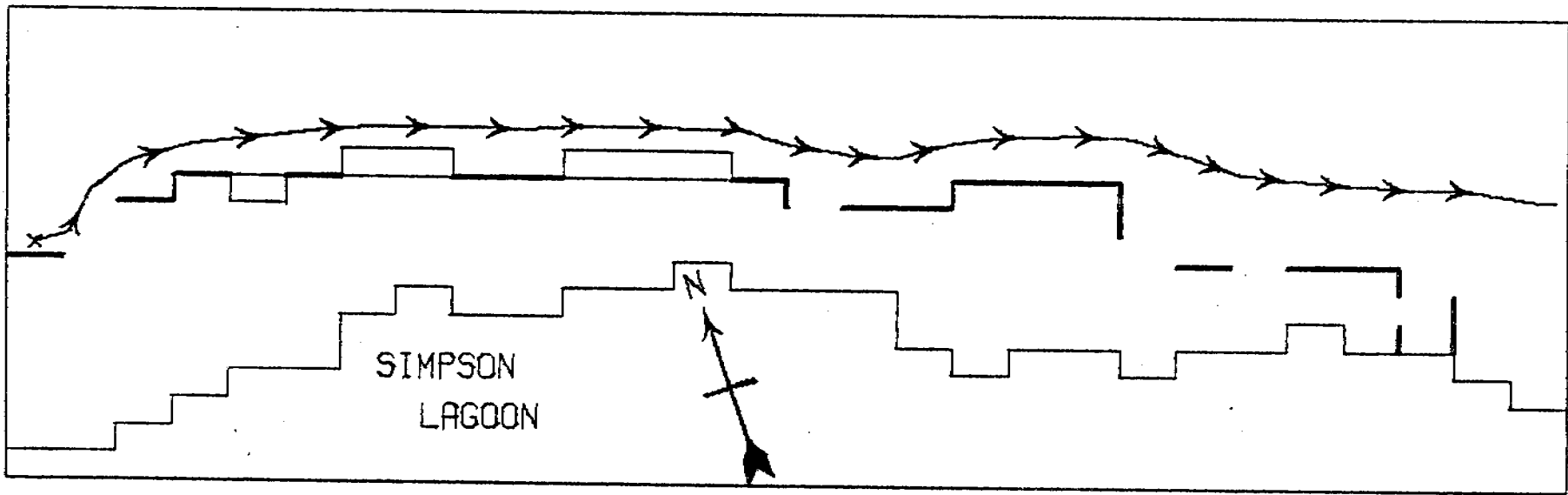
2-D MODEL WIND AT 10 M/S FROM ESE
ELAPSED TIME MARKER EVERY 3 HOURS

822

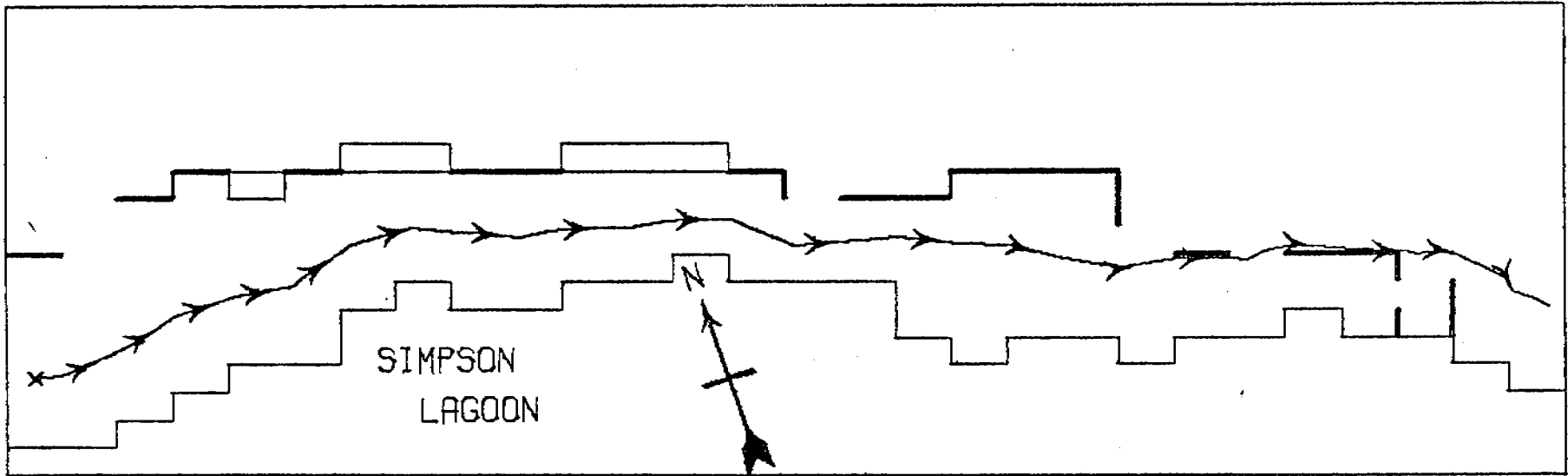


2-D MODEL DEPTH-MEAN CURRENT VECTORS
WIND AT 5 M/S FROM WNW



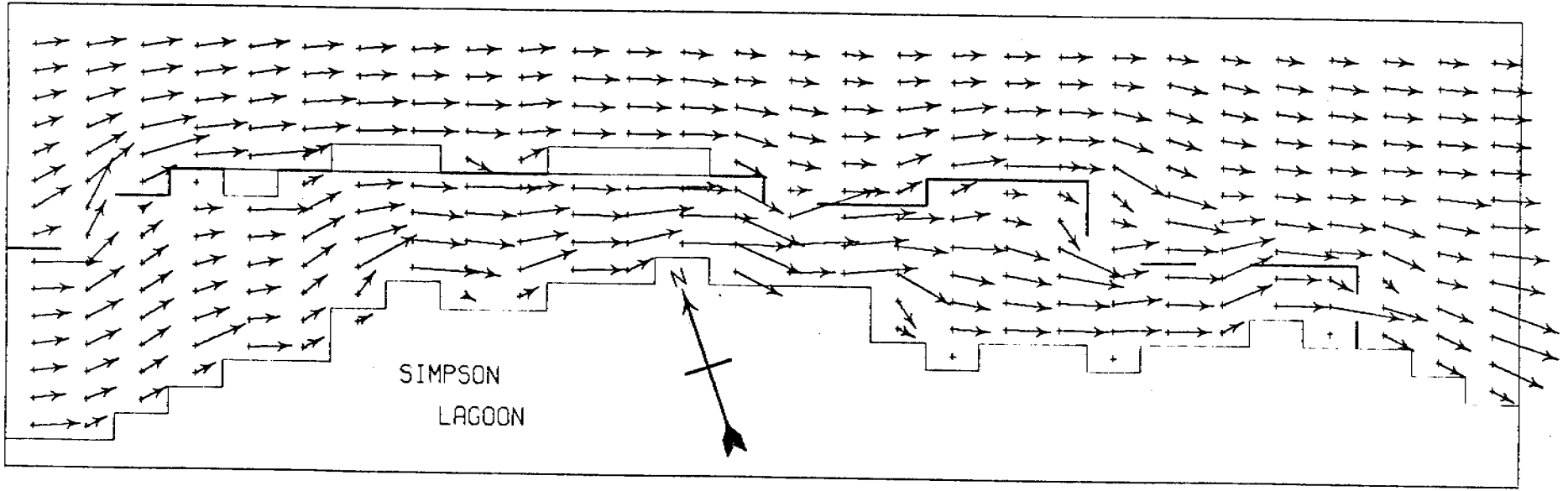


2-D MODEL WIND AT 5 M/S FROM WNW
ELAPSED TIME MARKER EVERY 6 HOURS

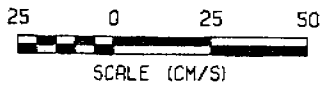


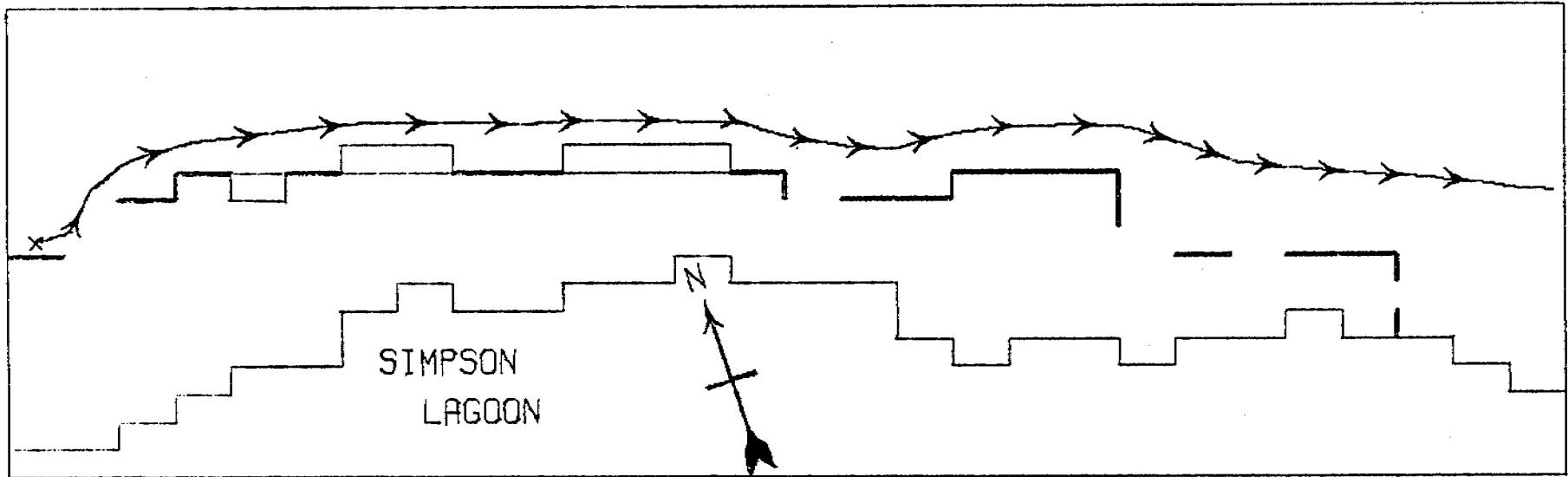
2-D MODEL WIND AT 5 M/S FROM WNW
ELAPSED TIME MARKER EVERY 6 HOURS

825

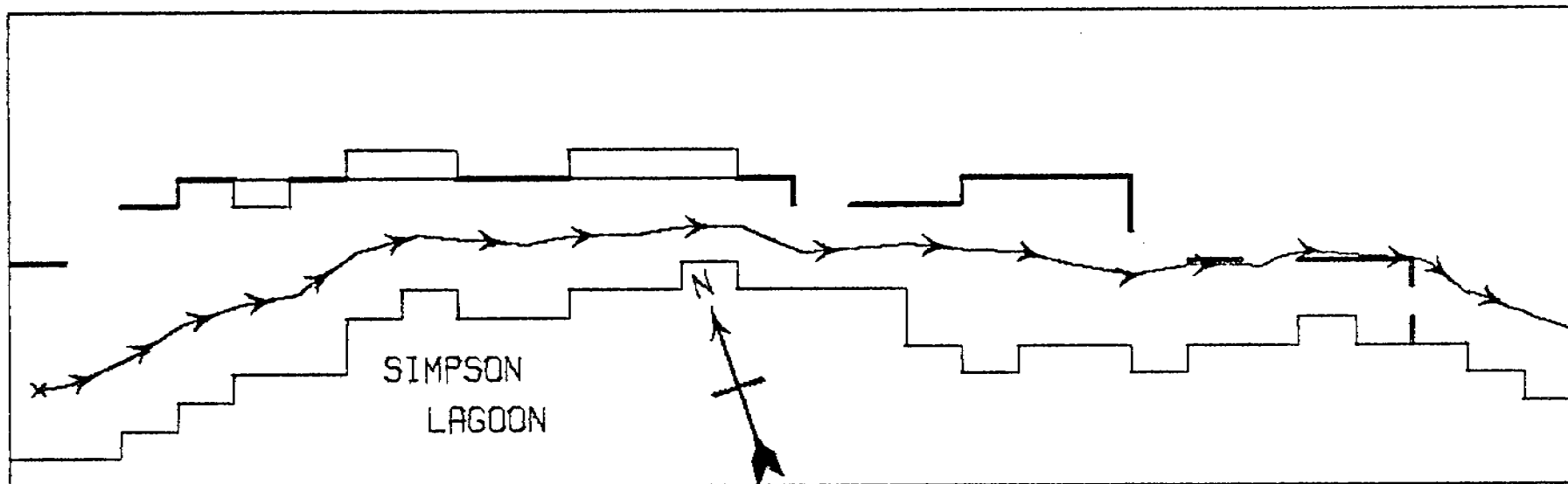


2-D MODEL DEPTH-MEAN CURRENT VECTORS
WIND AT 5 M/S FROM WNW (NO CAUSEWAY)



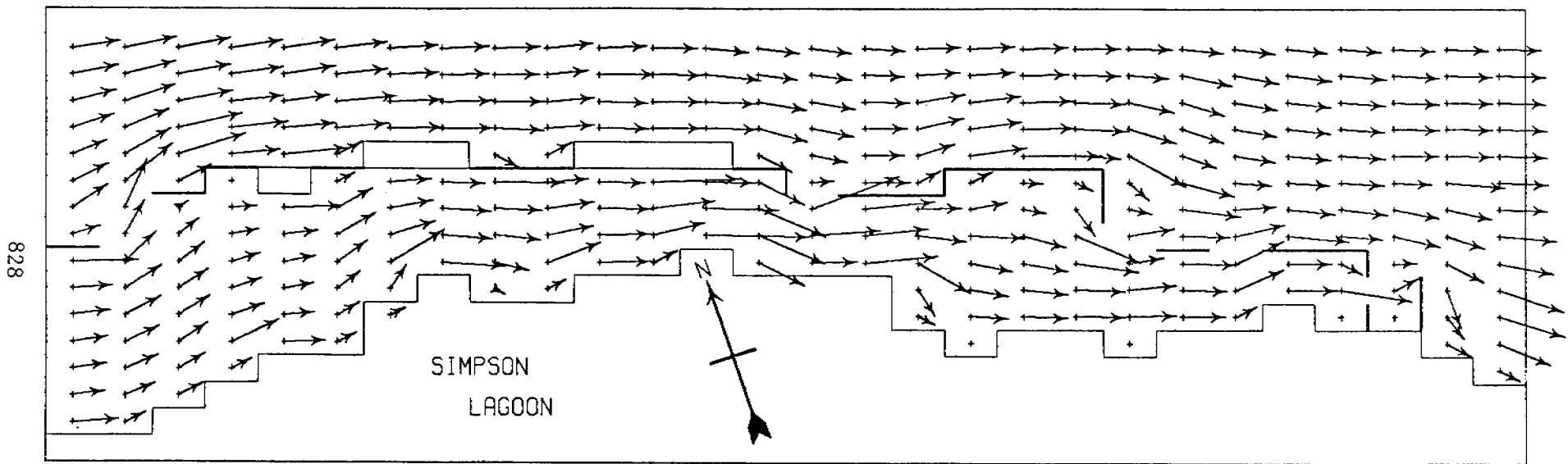


2-D MODEL WIND AT 5 M/S FROM WNW
ELAPSED TIME MARKER EVERY 6 HOURS
(NO CAUSEWAY)

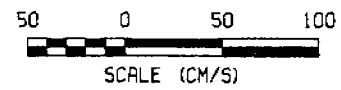


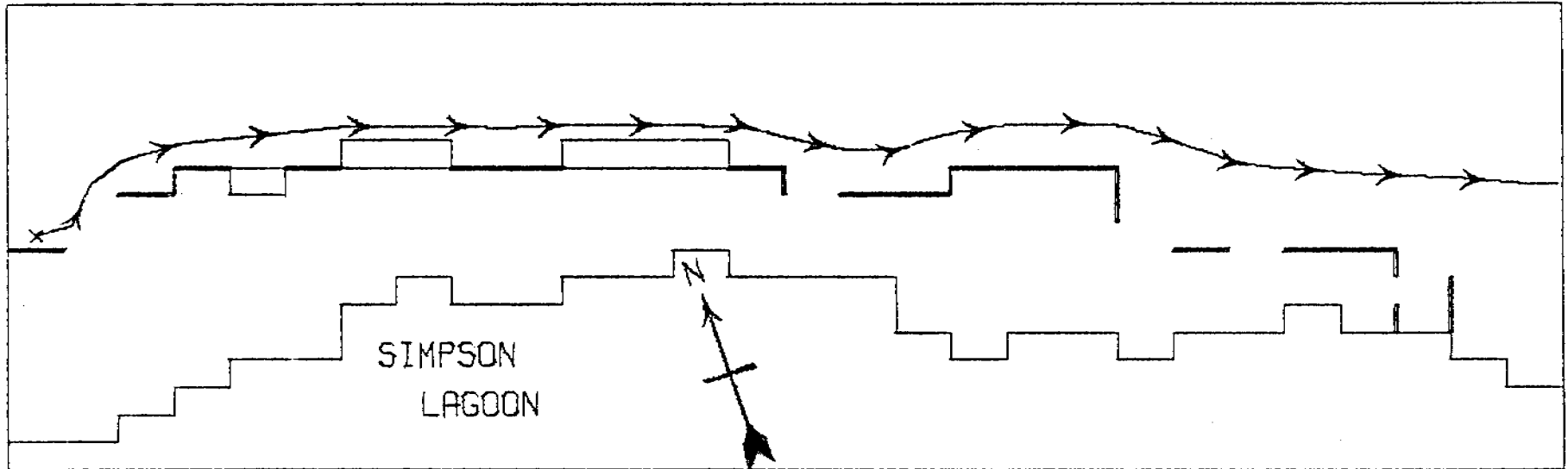
2-D MODEL WIND AT 5 M/S FROM WNW
ELAPSED TIME MARKER EVERY 6 HOURS

(NO CAUSEWAY)



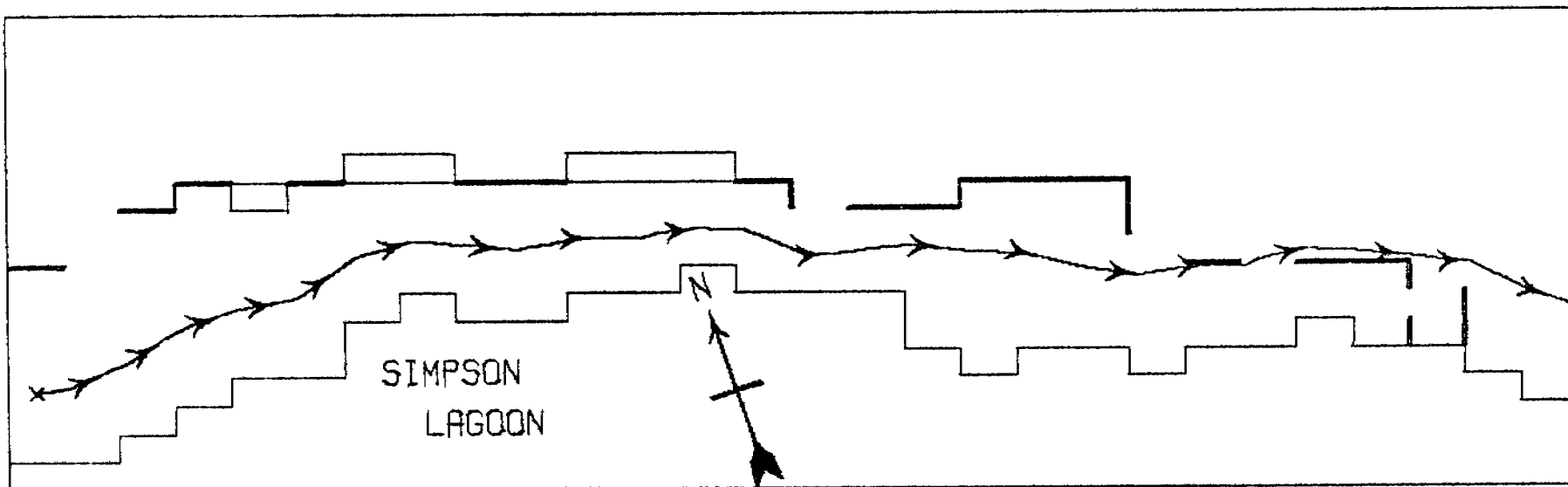
2-D MODEL DEPTH-MEAN CURRENT VECTORS
WIND AT 10 M/S FROM WNW





2-D MODEL WIND AT 10 M/S FROM WNW
ELAPSED TIME MARKER EVERY 3 HOURS

830



2-D MODEL WIND AT 10 M/S FROM WNW
ELAPSED TIME MARKER EVERY 3 HOURS

Contract # 03-7-022-35182
Research Unit # 531
Reporting Period: 1 January 1978-31 March 1978
Number of pages: 3 pages

Oceanographic Processes in a Beaufort Sea
Barrier Island-Lagoon System:
Numerical Modelling and Current Measurements

Principal Investigator: J. C. H. Mungall
Department of Oceanography
Texas A&M University
College Station, TX 77843
(713)845/1443

14 April 1978

A. Field or Laboratory Activities

1. Attendance/participation in meetings

- a) Working Conference on Current Measurements (sponsored by the NOAA Office of Ocean Engineering with the Delaware Sea Grant College Program) at Newark, DE, January 11-13, 1978.

The workshop centered on topics such as meter design and response, mooring line motion, need for calibration, etc. Discussions were held after the sessions with Marsh-McBirny, Inc. and with General Oceanics.

- b) Beaufort Sea Synthesis meeting at Barrow, AK, January 23-27, 1978.
c) Beaufort Sea Meteorological and Oceanographic Measurement Program meeting at Gulf Research & Development Company, Houston, TX, February 28, 1978.

This meeting, held by interested Industry parties to discuss a joint wave/tide/current measurement program along the Beaufort Sea coast, was attended so as to represent Dr. Gunter Weller.

- d) Presentation to the BLM Anchorage, AK Office, March 7, 1978.

Presentation of research efforts during 1977/78.

- e) Coastal Studies Institute, Louisiana State University, Baton Rouge, LA, March 29, 1978.

Accompanied by R. E. Whitaker, a meeting was held with W. Wiseman, S. Murray, and Rod Fredericks to discuss capacitance-gauge wave measurements and RDF drifter-tracking experiments in the Prudhoe Bay area. This meeting has led to the specification of a wave gauge and recording system suitable for deployment on either side of the Barrier Islands this summer. In addition, we were given a demonstration of the use of radio direction finding

(RDF) equipment, and received advice on drifter design for use in shallow waters.

2. Numerical modeling

The numerical experiments performed during the previous quarter were extended to cover additional cases of interest. A program was developed to track selected water parcels by making use of nearby computed currents. Results from the program can be seen in the annual report. Initial experiments were conducted to test several types of eddy-viscosity parameterizations; the first results of these are shown in the annual report.

B. 1978 Research and Measurement Capabilities

We are now in a position to respond to requests from the BLM and from the NOAA-OCSEAP Arctic Project Office for certain types of studies. We are currently programming a long wave numerical model to cover the Beaufort Sea coast from Cape Halkett to the Stockton Islands. The model will consist of $2 \text{ km} \times 2 \text{ km}$ grid squares and will interface, if necessary, with the Simpson Lagoon model. Since simulations with this model are likely to be expensive, say \$50 per run, we will only expend funds sufficient to achieve a demonstration of the capabilities of the model; further runs will only be made at the request of the Arctic Project Office.

Steps have been initiated for the procurement of the following equipment:

- a) A Marsh-McBirney two-axis electromagnetic current meter and display panel.
- b) Two capacitance wave gauge systems, capable of being located some 100 m offshore. Easily-repairable staffs have been selected, and

electronics and strip-chart recording facilities have been planned so as to have the following capabilities:

- 1) A 2-channel system capable of recording wave heights from 2 staffs (superimposed, if necessary),
 - 2) A 3-channel system capable of monitoring simultaneously 1 wave staff and the 2 outputs from the E-M meter.
- c) We have obtained estimates for a Beckman RS5-3 conductivity and temperature cell with 400 ft of cable suitable for permitting frequent measurements at some offshore location.

The above will permit us to respond to a variety of requests for measurements with real-time readout capability.

In addition to the above, we have explored two types of approach to drifter tracking: Precision Radar (with perhaps a 5-mile range), and lower precision 4 MHz RDF (with perhaps a 40 mile plus over water range). The former system would let us track drifters within Simpson Lagoon, the latter would, at the expense of accuracy, let us track drifter motion inside the Lagoon and throughout Prudhoe Bay. The latter capability may be of interest to the BLM and to the Arctic Project Office since there appears to be a growing concern concerning water movements outside Simpson Lagoon. It should be noted that the first method above was the subject of our proposal; the latter would require additional support both in terms of one or two additional personnel to help man the second RDF station, and of the need for transportation. (There may be a problem with renting the 2 RDF sets; they cost some \$3,000 each.)

Permission was received to extend the contract (at no extra cost) to September 30, 1978.

ANNUAL REPORT

Research Unit	#536
Reporting Period	1 Oct. 1977 to 30 Sept. 1978
Number of Pages	15

DEVELOPMENT AND OPERATION OF A
REMOTE SENSING DATA ACQUISITION PLATFORM FOR
OCS STUDIES

Mr. Michael Frank

and

Dr. Gary A. Laursen

Naval Arctic Research Laboratory
Barrow, Alaska 99723

1 April 1978

TABLE OF CONTENTS

- I. Summary of Objectives
- II. Introduction
 - A. General nature and scope of study
 - B. Objectives
 - C. Relevance of study to problems of petroleum development
- III. Current state of knowledge
- IV. Study area
- V. Sources, methods and rationale of data collection
- VI. Results
- VII. Discussion
- VIII. Conclusions
- IX. Needs for further study
- X. Summary of quarterly operations
 - A. Aircraft activities
 - B. Problems encountered
 - C. Recommendations
 - D. Funds expended

SUMMARY OF OBJECTIVES

The primary objective of the proposed program is to establish, operate and maintain a remote sensing data acquisition system using primarily side looking airborne radar (SLAR), a precision radiation thermometer (PRT-5) and aerial photo mapping cameras. Other systems capable of producing valuable insights toward furthering our understanding of the continental shelf barrier islands and marginal ice zone environments exist in infrared thermal imagery, laser profilometry and multispectral, 9.5" format photography that are yet to be developed.

The SLAR, a Motorola APS94D prototype, has been installed into the dedicated NARL aircraft C117-D (31310) in a modular configuration. This allows for easy access to the equipment and movement within the aircraft for the installation of additional equipment for greater flexibility and program expansion. SLAR imagery is easily obtained through most weather conditions. It then becomes a valuable tool for navigation, for reconnaissance, for mapping highlighted terrain, for determining sea ice thickness and fracture configurations, to evaluate terrestrial drainage and erosional patterns and to ascertain relative significances of certain landforms. It becomes a potentially important tool for determining the magnitude of an oil spill under sea ice. It can then be used to map the movements of oil slicks as they are moved by currents and winds.

The precision radiation thermometer (PRT-5), or remote thermometer, measures the effective emission-surface temperature ($^{\circ}\text{C}$) using broad spectrum infrared. Pointedly, ground, snow surface, water, oil slick and oil seep temperatures can be determined quickly and with a high degree of accuracy.

Photo mapping, using a KC1B T-11 9.5" format mapping camera, provides color or black and white imagery that can be used for ground truthing weather permitting. This NARL system has been installed and used in both the C117-D and C-180 aircraft.

INTRODUCTION

General Nature and Scope of the Study:

The need for a total remote sensing program on the North Slope of Alaska has existed for a long while. Certain imagery has been acquired, but the needs for a variety of imagery types is ever increasing. Elements of the North Slope environment are in need of imagery work. Such elements are: land forms, drainage patterns, erosional characteristics at the marine and terrestrial interface, vegetational analyses, soil identification, sea ice distribution, age, thickness and gouging, wind patterns, current patterns, weather sequences, ice island locations and tracking, and the net effects of oil spillage and seep perturbations.

The nature of this study is to initiate a program that will, in short, yield data for environmental assessment that is being requested by the scientific community. The results of many detailed terrestrial, littoral, estuarian and offshore island studies completed by OCSEAP provide a potentially valuable source of ground truthing that will enhance the data produced from the remote sensing platform.

The scope of the program and its development has always been contained within Alaskan borders with specific interests dedicated to the North Slope of Alaska. This area is defined by the Brooks Mountain Range to the south, the Arctic Ocean to the north, and international boundaries on the east and west. The dedicated C117-D aircraft is based at NARL. It has a range of approximately 1500 NM and a cruise speed of 160 knots with an equipment and personnel payload of approximately 2500 lbs. These characteristics allow for extensive penetration to accomplish most North Slope objectives and return to NARL in one day. Anchorage may be used as an overnight station for missions extending into Southern Alaska.

Objectives:

Specific objectives for the most part, are long range and project far beyond a one year program. They are best enumerated as short and long term objectives:

1. Short term objectives - FY78 contract period.
 - a. to dedicate a NARL C117-D to the development of a remote sensing platform;
 - b. to install the side looking airborne radar SLAR modules and antennae;
 - c. to test and calibrate the SLAR at Ft. Huachuca, Arizona;
 - d. to fly monthly missions of the Arctic coast east and west of Barrow, Alaska;
 - e. to modify the platform for aerial photomapping using a T-11, 9.5" format, camera;
 - f. to install a PRT-5 and make it operable;
 - g. to establish means by which imagery (negative) output could be processed via the companion proposal (Belon RU 267).
2. Long term objectives - FY78 and beyond.
 - a. to maintain and insure the operational status of the remote sensing platform with backup material and personnel support;
 - b. to meet the objectives of remote sensing needs as requested and coordinated through the OCSEAP Arctic Project Office;
 - c. to continue building the program with emphasis on thermal imagery (IR), laser profilometry, microwave testing (Mini Micrad Systems, China Lake) and multispectral scanning.

Relevance to Problem of Petroleum Development:

The potential of the remote sensing program to gather data on problems of petroleum development with equipment presently up and working on the platform is substantial. SLAR and photomapping imagery and spot thermal determinations will aide in detecting, mapping and monitoring oil spillage, natural seeps and oil slicks in marine and terrestrial/ aquatic ecosystems such as the Coastal Plains Province on the North Slope of Alaska. Classification and quantification of oil spills cannot be accomplished with SLAR, however.

CURRENT STATE OF KNOWLEDGE

At this writing, very little data has been collected from North Slope remoste sensing missions. Virtually no imagery of coastal zones has been collected during winter periods. Some spring ice work has been accomplished both prior to and during this program. However, the greatest majority of what little has been done by this or other aircraft based platforms, was accomplished during summer months.

STUDY AREA

The study area is contained primarily within Alaska's North Slope boundaries, but will include all coastal zones from the Bering Sea, the Chuckchi Sea, the Beaufort Sea, and terrestrial provinces south to the Brooks Mountain Range. Other locations as usage demands.

SOURCES, METHODS AND RATIONALE OF DATA COLLECTION

The Remote Sensing program was initiated in March 1977. Together with the first six months of FY78, time has been spent acquiring and checking equipment, retro-fitting the aircraft platforms so electrical systems were compatible and building up the equipment for installation.

The SLAR equipment was shipped to NARL on 1 April and arrived by mid-May 1977. Its transfer from CRREL, New Hampshire to NARL marked the beginning. The assembly of equipment was begun and concomitant events included the complete reviewing, repanelling the instrumentation of 310 to become compatible with other NARL aircraft. The installation of the Ontrack III navigation system will complete navaides required for complete navigation and proper data collection. The laser profilometer, multi-spectral camera, mini-micrad system and infrared thermal imager are still being sought. Components or complete systems of all but the laser have been found, requested and are in various stages of coming to NARL.

In August of 1977, the C117-D aircraft N722NR was ready for the amassed and bench tested equipment to be installed. Arrangements were made at Fort Huachuca, Arizona, where similar installations had been made previously into C47 and DC-3 aircraft. Paper work was completed by October and the NARL aircraft was ferried to Fort Huachuca, Arizona, where the

antenna was mounted, systems checked out completed, and the platform flown and calibrated over a unique calibrating range. A great deal of redesigning was necessary for the installations of SLAR equipment into a C117-D as blueprint schematics had only been prepared for C47 aircraft (Figure 1).

The C117-D platform is configured to accept a variety of sensors. However, only the SLAR, PRT-5 radiometer, and the T-11 photomapping camera are in use. The laser and other camera types have been mounted and used in the past. The multi-equipment configuration will allow the simultaneous collection of several types of information along a chosen flight path. Within the aircraft the equipment is completely accessible. The SLAR antenna is the only exception to this as it is attached externally. Easy repair and adjustment can be made in the air while the equipment is operating, a decided advantage over older configurations. The ANS/APS 94D SLAR is one of two prototype models.

During calibration of the SLAR system it was found that several modifications had been made to the film processor and to the film magazine. The wet film processor presented problems to previous users of the equipment and parts of the system had been removed or lost. Film could only be exposed and processed in the lab at a later date. For this program on-board processing is a must, hence parts had to be refabricated.

The first flight during which imagery was taken resulted in the detection of antenna interference. Corrections were made through multiple adjustments of the antenna downward and away from the aircraft. Precision spacer blocks were installed on the mounts and diminished some of what was later found to be inherent antennae "noise". Delays due to Navy science, aircraft failures, malfunctioning equipment and logistical support, caused the program to slide on several occasions. Steps are now being taken to reduce delays.

100

Figure 1-A NARL aircraft C117-D N722NR with antenna forward installation.

Figure 1-B NARL aircraft C117-D N722NR with antenna aft installation.

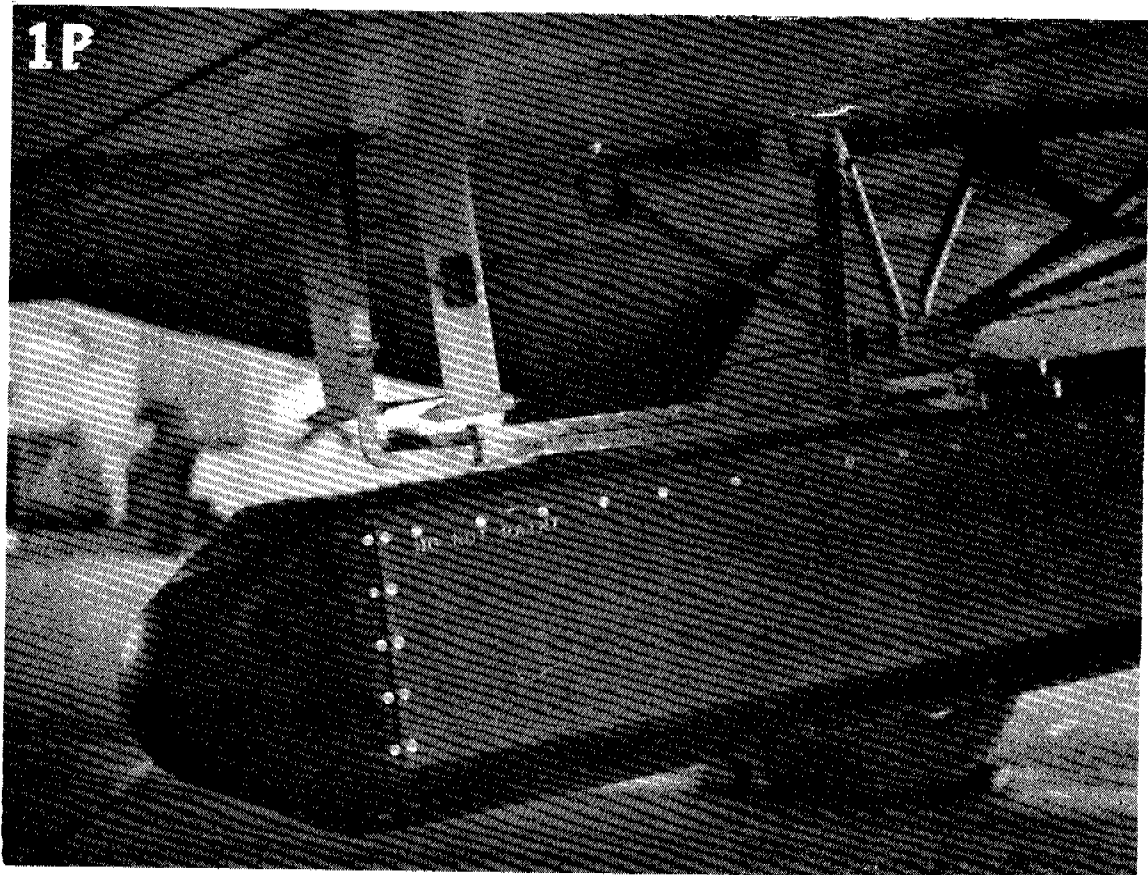
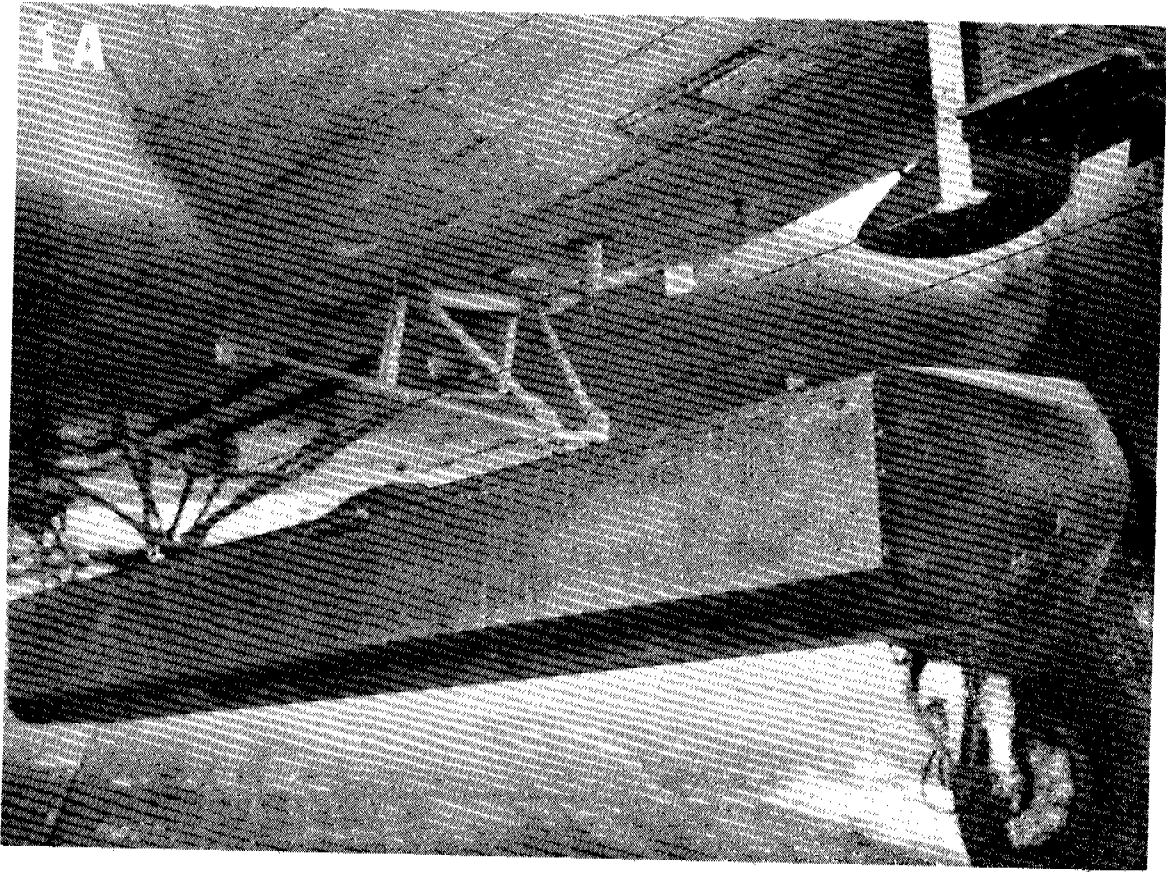
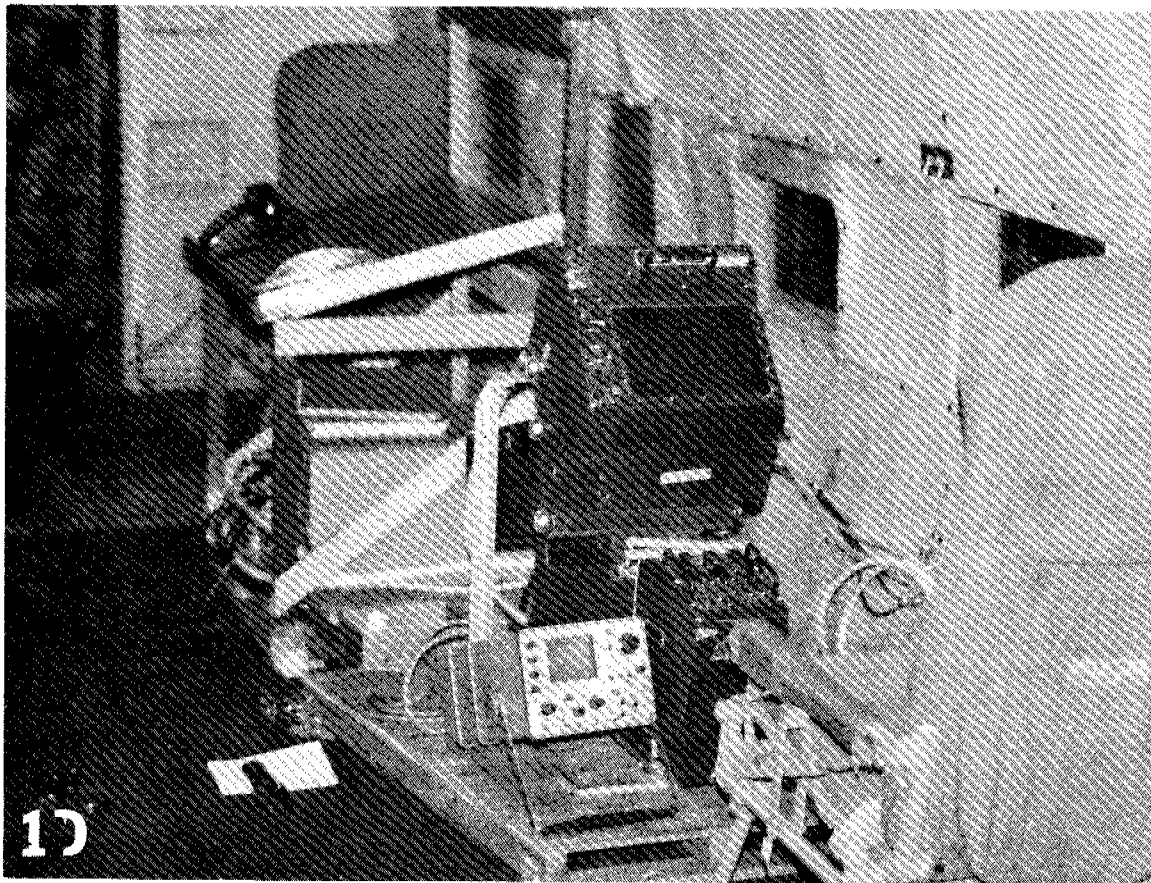
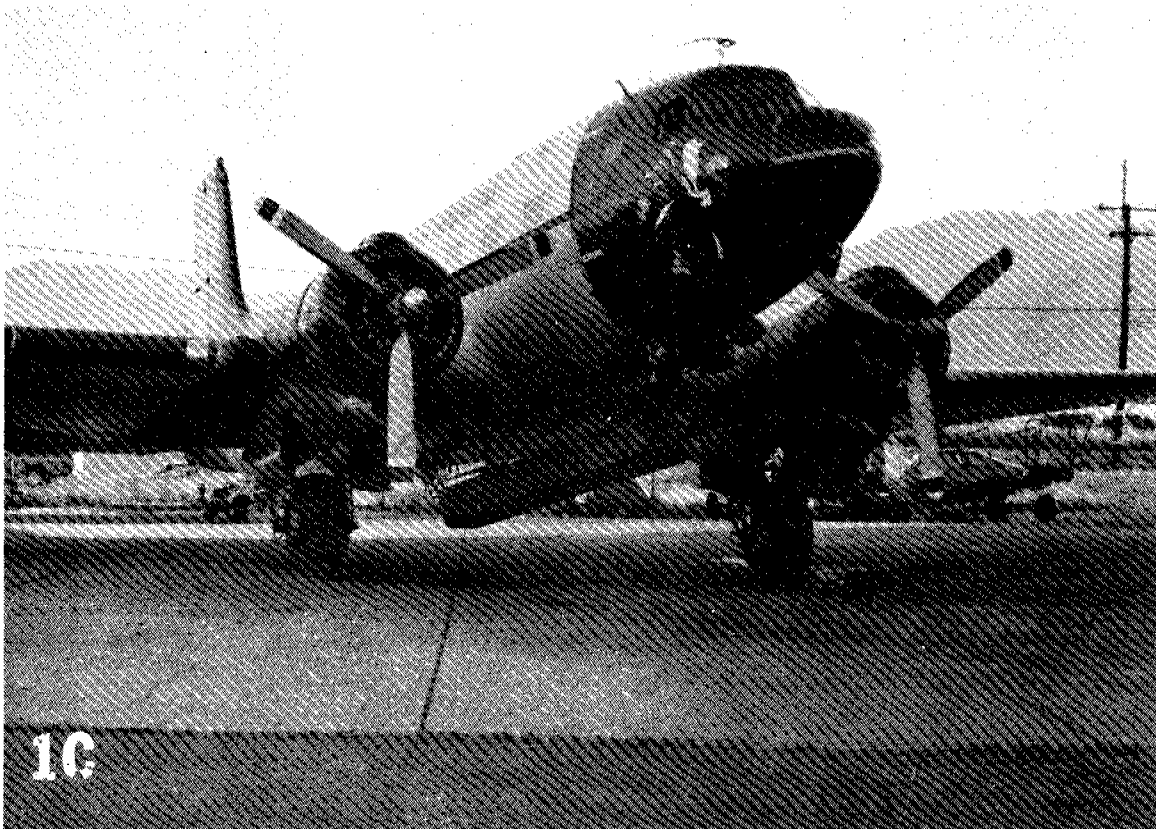


Figure 1-C External antenna configuration for Side Looking Airborne Radar (SLAR) on NARL aircraft N722NR.

Figure 1-D Internal configuration of SLAR and associated components on NARL aircraft 31310.



RESULTS

To date, approximately 6800 km of SLAR imagery have been collected with the C117-D. The quality of the imagery varies with the stability of the platform. Yaw, pitch, and roll motion as well as heading changes, will affect imagery quality. Thus, data must be collected and interpreted with this knowledge to gain maximum usable information.

Figure 2, is imagery of sea ice collected between Barrow and Deadhorse on the operational test flight after relocation of the system. In this example, roll and heading change effects can be easily seen as light or dark streaks across the imagery, indicative of wing up or wing down situations. Heading changes cause wide streaks and vary with the amount of correction. Antenna pattern interference can be seen in the near range in this figure.

Light areas are caused by strong radar return. Thus, the light mesh of lines indicates ice ridges. Dark or black areas in this figure are smooth reflections of refrozen leads or open water. The width of coverage in this figure is 25 km with range marks at 20 km.

Figure 3, a section of imagery taken in Arizona during installation and calibration, shows the affects of ground speed on image quality. The mapping speed of the radar is a function of the aircraft ground speed, and must be constantly fed into the radar set. Round irrigation fields would appear oblong and square fields would appear rectangular if correct ground speed was not fed into the radar set.

The SLAR system was then transferred to NARL's C117-D 310 in preparation of that aircraft as a backup to the remote sensing program. The auto-pilot failed during its test flight and greatly reduced the value of the imagery obtained. The left cathode ray tube (CRT) in the radar system also failed in that it could not be focused. A replacement is being obtained through Fort Huachuca.

Sea ice reconnaissance missions began in late February. The areas from Anchorage to Bristol Bay and Bristol Bay to the Bering Straits were covered. During this mission no inertial navigation or VLF equipment was functioning. Only flight paths along coast lines were flown as land marks were needed for reference points. Severe turbulence greatly affected the product of the mission and led to its eventual discontinuation.

A component, which will enable us to install the Ontrack III VLF navigational system in the aircraft, is presently enroute to NARL. This system will allow accurate determination of such conditions as true ground speed, present position, (latitude and longitude) drift angle, and will eventually be configured to display this data onto the image.

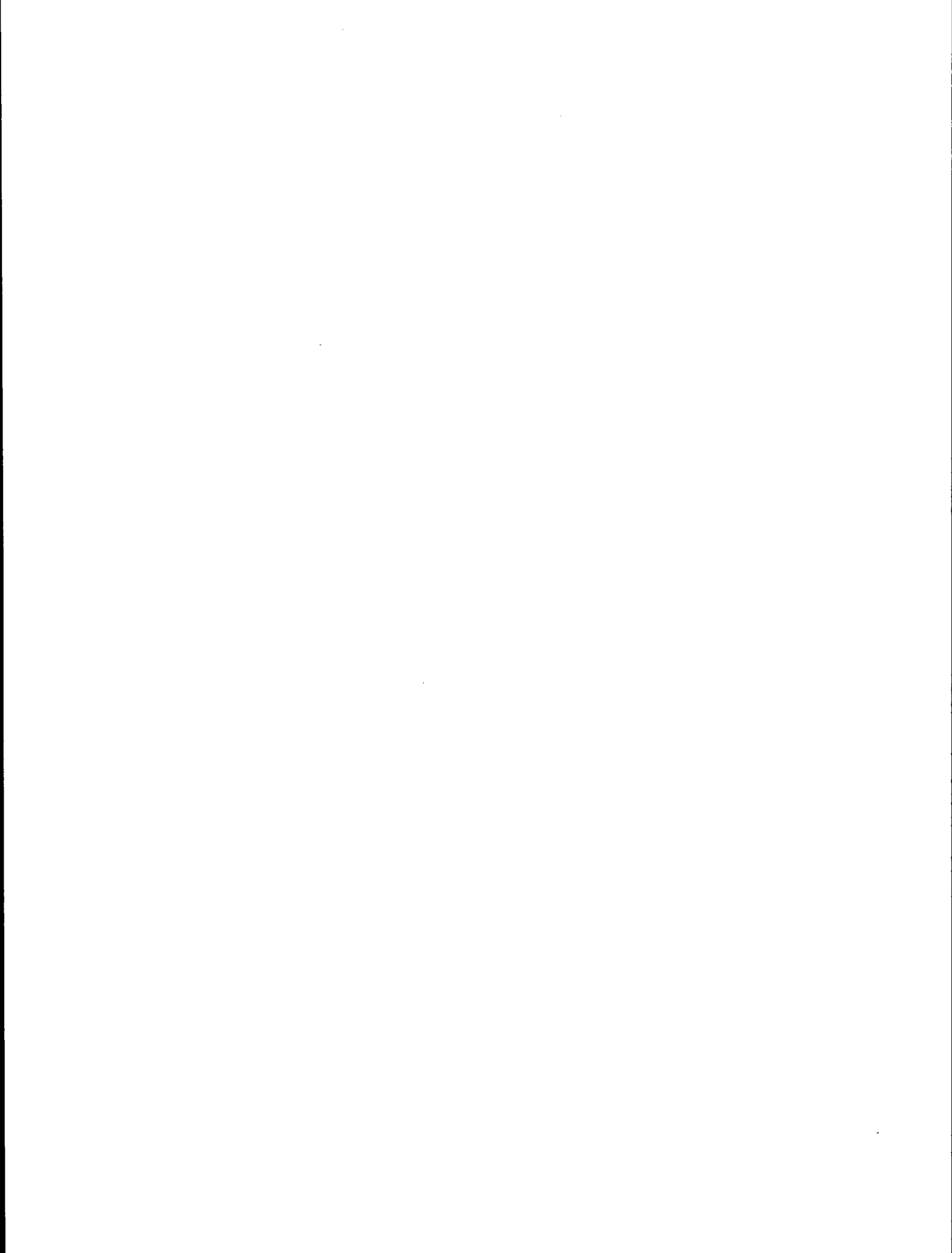
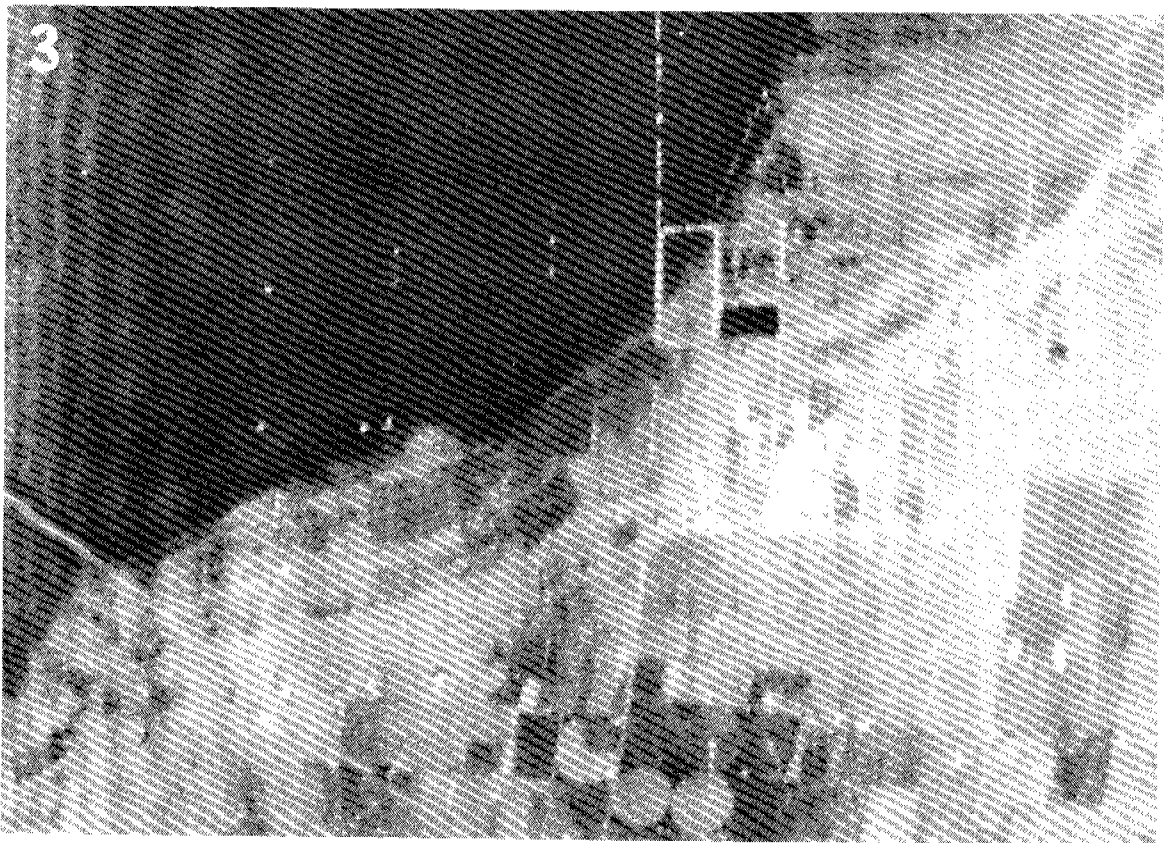
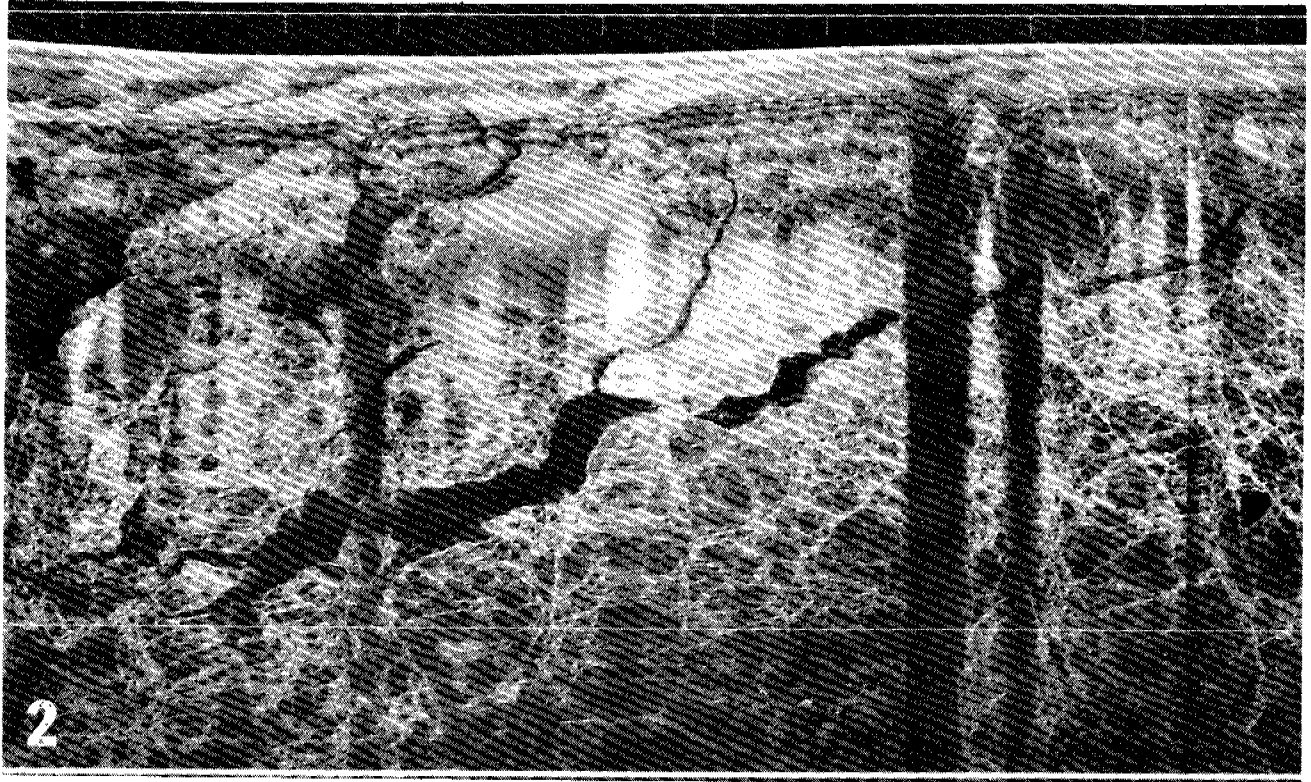


Figure 2 SLAR imagery of sea ice at 3500' elevation showing a 25 km swath width with effects heading changes (large dark blotches).

Figure 3 SLAR imagery taken at 7,000' elevation during inflight system calibration and the stretching and compressing effect of ground speed on emage quality.



A second mission (Figure 4) flown in early March and destined for Demarcation Point ended 50 NM north of Deadhorse due to engine failure. The aircraft awaits its replacement engine that is presently being built up by the aviation department for mounting and return to NARL for installation of the Ontrack III global navigation system.

DISCUSSION

The collection of quality SLAR imagery requires a very stable platform, and a working knowledge of what the system is capable of providing. This knowledge comes from experience of gathering similar data at various system settings, such as range of coverage, altitude and speed. An example of how data quality is changed can be seen in comparing Figures 2 and 4. Both images are of the sea ice between Barrow and Deadhorse. They are not in the same location, but are quite similar. The difference in image quality between these figures is remarkable. Figure 2 was flown at an altitude of 3500 feet with the radar only looking 25 km on each side. Figure 4 was collected from 7000 feet examining 50 km on each side. Figure 2 is much easier to interpret, but it does not contain the area of coverage seen in Figure 4.

Speed will also affect image quality. The slower the aircraft flies, the more radar signals that will hit a particular target. Thus, more radar signal is returned to be processed. The SLAR system is limited to 150 kt minimum speed. If the aircraft flies any slower than the mapping speed of the radar, which is set at 150 kt/min, it will cause the image to stretch. With the C117-D aircraft one must constantly monitor ground speed due to the working speed of 160 knots/hr maximum speed of the aircraft.

More imagery must be acquired in order to find optimum conditions under which arctic data can be collected to provide the most useful information.

CONCLUSIONS

With twelve total months of effort, six of which pertain to the FY78 contract, we have been successful in initiating a remote sensing program at NARL. The program has not been without its administrative and mechanical delays. However, a dedicated NARL C117-D Super DC-3 aircraft, 31310, has been dedicated and retrofitted as the remote sensing platform. The platform has been fitted with the APS94D SLAR, PRT-5 radiometer and T-11 9" format camera. All systems are currently functioning and two missions were completed in Alaska after several weeks of calibration of the SLAR system at Fort Huachuca, Arizona. An engine failure resulted in a complete change in the field. The aircraft will return to NARL April 11 and with the return of Mr. Frank from an equipment gathering trip to Fort Huachuca and China Lake, remote sensing missions will continue.

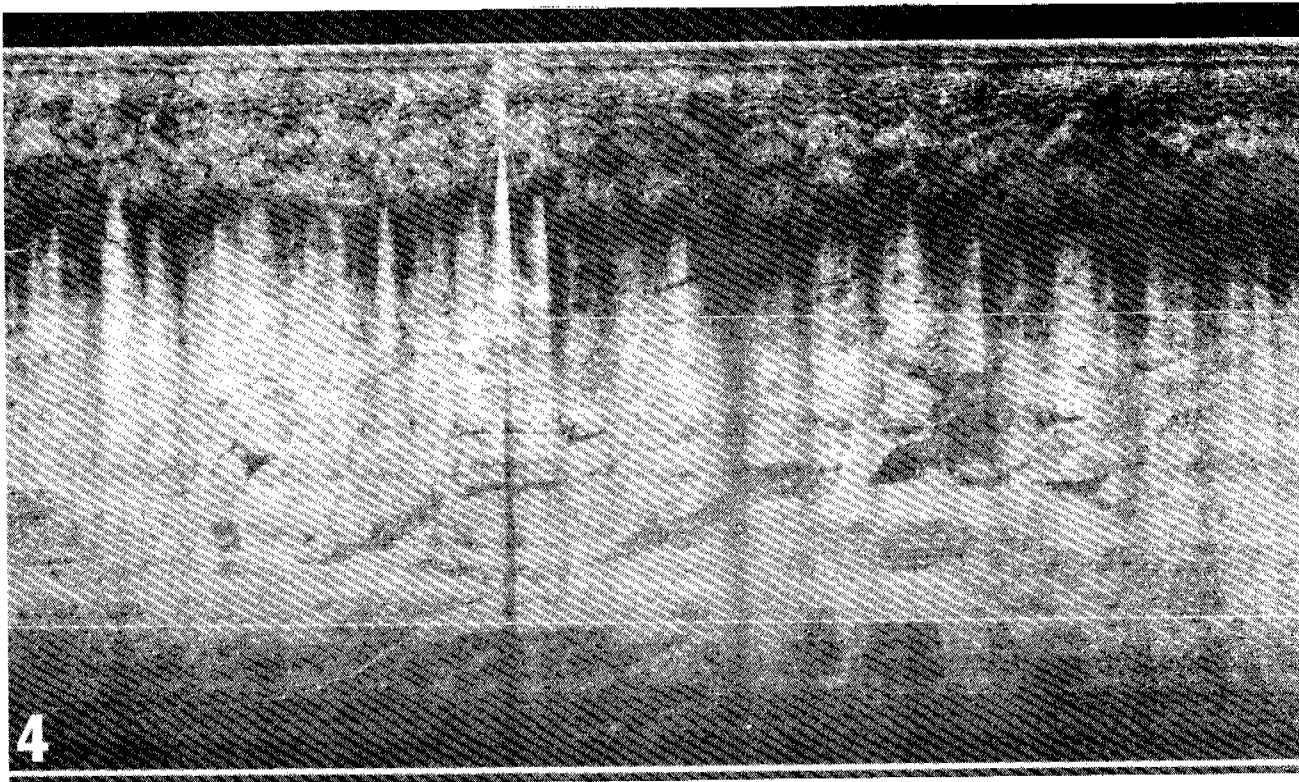


Figure 4 SLAR imagery of sea ice at 7000' elevation showing a 50 km swath width with the effects of aircraft roll (light and dark streaking).

NEEDS FOR FURTHER STUDY

As oil and gas field development continues and increases along the North Slope, the need for a remote sensing platform with expanded capabilities also increase. More imagery of sea ice through all seasons is needed before a complete understanding of off-shore operations can be made. Environmental assessments and monitoring of oil field development can be accomplished by using a remote sensing approach. The use of remote sensing equipment is gaining sophistication in the areas of exploring new oil fields and supporting already established fields in that remote sensing imagery provides valuable weather information for navigation of supply ships, and environmental monitoring of field operations.

SUMMARY OF QUARTERLY OPERATIONS

Aircraft Activities:

The NARL C117-D 31310 has flown approximately 6800 km (28.5 hrs.) of SLAR since early February 1978. This included two flights to Deadhorse from Barrow, and a flight track from Anchorage, down the Cook Inlet area, and out into Bristol Bay, Alaska. This later flight continued up the western coast of Alaska to Tin City. The flight was done for a National Weather Service project. During this quarter, the SLAR system was transferred from NARL aircraft C117-D 722NR to C117-D 31310.

Problems Encountered:

During this quarter, we have encountered numerous aircraft problems which have caused timely delays to the program. Other problems existed with the lack of qualified pilots and maintenance staff to completely support the remote sensing aircraft. Two fully rated DC-3 pilots have been brought to the laboratory for this purpose. A third pilot recently became IFR type-rated in the DC-3 and the fourth will do likewise. Recommended changes would increase the number of qualified support personnel and a larger spare parts inventory to keep the aircraft operational.

ANNUAL REPORT
April 18, 1978
OCS RESEARCH UNIT #540

"Oil Spill Vulnerability of the Beaufort Sea Coast"

Dag Nummedal, Principal Investigator
Ian A. Fischer and Jeffrey S. Knoth, Co-Investigators

I. Objectives

A. Project Objectives

1. To characterize the morphology of the barrier islands and the mainland shoreline.
2. To assess the retention potential for spilled hydrocarbons within the coastal environment.

B. Report Objectives

Summarize all available data on coarse-grained (sand and gravel) transport along the Beaufort beaches.

Coastal Research Division
Department of Geology
University of South Carolina
Columbia, S. C. 29208

II. Field Studies - Field observations of the surf zone. At 5 different days during August 1977, measurements were made of breaker conditions at selected sites along the coast. Two sets of observations, Aug. 8 and 10, were taken during a northeast storm at Pt. Barrow. The measurements are thought to be representative of energy levels occurring a few days every open-water season. Measurements at Pt. Barrow on Aug. 7 and along the western shore of Prudhoe Bay on Aug. 5 are typical of the majority of the days during summer.

The following parameters were measured in the surf as outlined:

Wave height (H_b): measured by sighting along a graduated measurement rod on the horizon.

Wave orthogonal angle (α_b): measured by protractor; angle is relative to the local shoreline trend.

Wave period (T): determined by measuring the average period of ten successive breakers.

Longshore current velocity (V): measured by timing the drift of a neutrally buoyant float along a pre-determined distance of beach.

Wind speed (W): measured by hand-held anemometer.

Wind direction (S): determined by Brunton compass.

The longshore wave energy flux and sediment transport rate are calculated by the following equations (these are the metric equivalents to eqs. 4-35 and 4-40 in the Shore Protection Manual, Coastal Engineering Research Center, 1973):

$$P_{1s} = 2.784 \times 10^{-2} H_b^{5/2} \sin 2\alpha_b \quad (1)$$

where the longshore energy flux, P_{1s} , has the dimension Joules per meter per second. H_b is measured in centimeters and α_b in degrees. The sediment transport rate is calculated by:

$$Q_s = 1.277 \times 10^3 P_{1s} \quad (2)$$

where Q_s has the dimension cubic meters per year.

All field observations and calculations based on equations 1 and 2 are

between longshore sediment transport rates and the longshore component of wave energy flux to be used in the field should be based on field observations only. Thus, by excluding wave tank data used in T.M. 4 (Coastal Engineering Research Center, 1966), the updated Shore Protection Manual (Coastal Engineering Research Center, 1973) recommends using a rating curve which gives a higher transport rate for a given energy flux than was the case with the old version. The new rating curve is equation 2 in this paper.

Observations by Short (1973) along the outer beaches of the Jones Islands, during the 1972 open-water season, indicate a westward transport along the outer beaches of about 10^4 cubic meters of sediment. Most of this transport appears to have occurred during September, a period of unusually high easterly waves.

IV. Summary

Measurements of littoral process variables along the mainland and island shores of the Beaufort Coast of Alaska are much too sparse to permit an evaluation of the spatial and temporal variations of beach sediment transport.

Data presented in this report and those obtained by Short (1973), however, are suggestive of a typical annual net transport rate of about 10^4 cubic meters to the west along the seaward beaches of the Beaufort barriers.

Data obtained by Dygas and Burrell (1975) suggest that annual transport rates along the mainland shore near Oliktok Point are somewhat less, perhaps of the order of some thousand cubic meters per year. The direction of net transport along the mainland shore is highly dependent on location.

For purposes of perspective, these transport rates of the Arctic should be compared to typical rates of a few hundred thousand cubic meters,

summarized in Table 1. Figures 1 and 2 present graphically the variability in transport rates around the cusate foreland of Pt. Barrow.

III. Results and Interpretation.

A. Results. - The rate of longshore movement of coarse-grained beach material (sand and gravel) is found to range from essentially zero up to 4100 cubic meters per day. The average rate along the Beaufort shore of Plover Spit and Pt. Barrow during August 8 and 10, is 1663 cubic meters per day. The storm maintained essentially undiminished vigor for about 3 days. Thus, this storm alone could have moved about 5000 cubic meters to the west past Pt. Barrow. The dramatic decrease in transport rate between stations BE 88 and BE 89 is in excellent accord with the morphology: a series of recurved beach ridges on the west-northwest side of Pt. Barrow attest to a rapid transport from the beaches further east, at least for the last few years.

Few littoral wave observations have previously been made along the Beaufort Coast. The ones that exist, however, demonstrate fair agreement with the ones presented above. Dygas and Burrell (1975) report on wave conditions and calculated sediment transport rates for the mainland shore at Oliktok Point during the summers of 1971 and 1972. The relatively sheltered location of Oliktok Point and the apparent absence of any high-energy events during their 1971 field season produced quite moderate transport rates compared to those encountered at Pt. Barrow during a storm (Table 2). The maximum recorded wave height reached 32 cm, the maximum transport rate was 384 m³/day. Since Dygas and Burrell's (1975) transport estimates were based on the rating curve presented in Technical Memorandum No. 4 (Coastal Engineering Research Center, 1966), their rates are lower than what is presented in this report based on the same field data. As explained by Galvin and Vitale (1976), the relationship

Table 1. Surf zone parameters and longshore transport rates for the Beaufort Coast of Alaska. Measurements during August 1977.

Station	Date	Time ADT	Wave Hgt. (cm)	Orthogonal angle (deg.)	Period (S)	Longshore current vel. (cm/s) ²	Wind speed (km/h)	Wind direction (deg.)	Longshore energy flux (J/m/s) ²	Sediment transport rate (m ³ /day) ²
Prudhoe Bay										
BE 48	Aug. 5	1540	12	65 ⁰	1.35	+22	32	40	10.6	37
BE 51a	Aug. 5	1730	12	110 ⁰	1.70	-14	0	--	-8.9	-31
Be 51b	Aug. 5	1800	14	145 ⁰	1.70	-10	0	--	-19.1	-67
Pt. Barrow										
BE 86	Aug. 8	1015	65	115 ⁰	3.2	-96	38	80	-725	-2539
BE 86	Aug. 10	----	75	120 ⁰	3.6	-114	64	115	-1173	-4107
BE 87	Aug. 8	----	70	115 ⁰	3.1	-122	38	80	-873	-3056
BE 87	Aug. 10	----	50	110 ⁰	3.6	-78	67	115	-316	-1105
BE 88	Aug. 8	1120	50	110 ⁰	3.2	-116	37	80	-316	-1105
BE 88	Aug. 10	----	45	115 ⁰	3.3	-140	67	115	-289	-1012
BE 89	Aug. 8	----	30	125 ⁰	3.5	-90	37	80	-129	-451
BE 89	Aug. 10	----	20	105 ⁰	3.1	-36	57	110	-24.8	-87
BE 90	Aug. 8	1240	8	93 ⁰	2.4	0	37	80	-.52	-1.8
BE 90	Aug. 10	----	8	92 ⁰	1.6	0	57	110	-.35	-1.2
BE 91a	Aug. 8	1500	20	75 ⁰	2.8	+75	48	80	24.9	87
BE 91a	Aug. 10	----	25	80 ⁰	3.4	65	--	--	29.7	103
BE 91b	Aug. 8	1515	30	111 ⁰	2.9	-77	32	80	-91.7	-321
BE 91b	Aug. 10	----	25	110 ⁰	3.0	-34	--	--	-55.9	-195
BE 91c	Aug. 8	1545	25	80 ⁰	2.7	55	41	80	27.9	104
BE 91d	Aug. 8	1600	35	105 ⁰	3.3	-58	45	80	-100.7	352
Plover Point & Spit										
BE 84a	Aug. 7	2050	5	120 ⁰	1.5	-6	9	25	-1.3	-4.71
BE 84a	Aug. 8	1340	40	105 ⁰	2.8	-44	48	80	-140	-492
BE 84a	Aug. 10	----	45	115 ⁰	3.5	-72	64	115	-289	-1012
BE 84b	Aug. 7	2100	22	90 ⁰	2.0	-1	9	25	.03	.13
BE 84b	Aug. 10	----	55	70 ⁰	3.8	124	38	80	401	1405
BE 85	Aug. 8	1350	45	105 ⁰	3.0	-55	64	115	-188	-660
BE 85	Aug. 10	----	60	110 ⁰	3.7	-84	38	80	-498	-1744
BE 85	Aug. 8	1400	58	108 ⁰	3.0	-34	38	80	-418	-1465

1

ADT: Alaska Daylight Time

2

Negative values refer to currents (transport) to the left. Positive values indicate movement to the right.

generally to the south, along the east coast of the United States (Wiegel, 1964). Nummedal and Stephen (1978) have calculated rates ranging up to 1.4 million cubic meters to the west along the Malaspina Foreland.

Table 2. Summary of littoral observations at Oliktok Point, 1971 (From Dygas & Burrell, 1975).

	Northwest-facing shore	Northeast-facing shore
Mean wave height (cm)	5.8 - 32.2	
Period (s)	1.3 - 3.6	
Longshore currents (cm/s)	0 - 75.5	0 - 58.0
Longshore component of wave energy flux (J/m/s)	1 - 110	0.2 - 21.2
Longshore sediment transport rate ¹ (m ³ /day)	3.5 - 384	.7 - 74

¹ Recalculated from data in Dygas and Burrell (1975) according to the revised rating curve presented in the Shore Protection Manual (Coastal Engineering Research Center, 1973) and given in this paper as equation 2.

REFERENCES CITED

- Coastal Engineering Research Center, 1966, Shore Protection Planning and Design: C.E.R.C. Tech. Memo. no. 4.
- Coastal Engineering Research Center, 1973, Shore Protection Manual: Government Printing Office, Washington, D. C.
- Dygas, J. A., and Burrell, D. C., 1975, Dynamic sedimentological processes along the Beaufort Sea coast of Alaska: in Assessment of the Arctic Marine Environment, Hood, D. W. and Burrell, D. C., (eds.), Occasional Pub. No. 4, Institute of Marine Science, University of Alaska, Fairbanks, p. 189 - 203.
- Galvin, C. J., Jr., and Vitale, P., 1976, Longshore transport prediction - SPM 73 equation: Proceedings of the 15th Coastal Engineering Conference, v. II, p. 1133-1148.
- Nummedal, D., and Stephen, M. F., 1978, Wave climate and littoral sediment transport, northeast Gulf of Alaska: Jour. Sedimentary Petrology, v. 48, p. 359-371.
- Short, A. D., 1973, Beach dynamics and nearshore morphology of the Alaskan Arctic coast: Ph.D. dissertation, Louisiana State University, Baton Rouge, La., 140 p.
- Wiegel, R. L., 1964, Oceanographical Engineering: Prentice-Hall, Inc., New Jersey, 532 p.

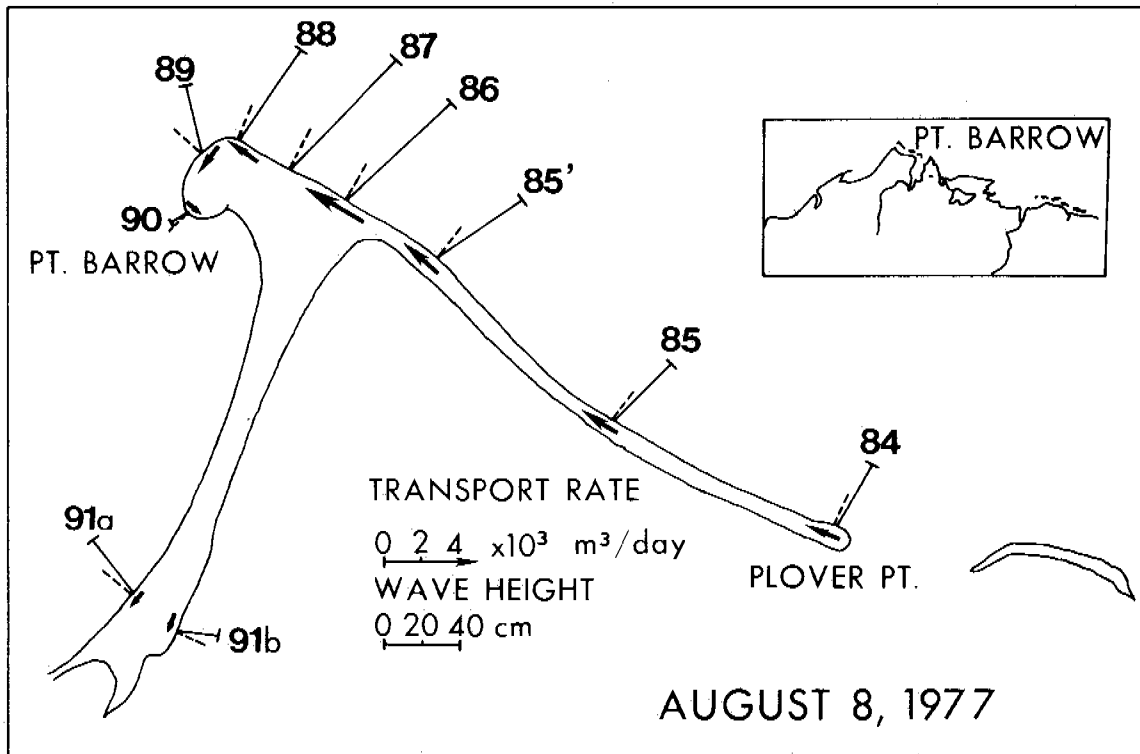


Figure 1. Wave parameters and sediment transport rates along the Pt. Barrow beaches on August 8, 1977.

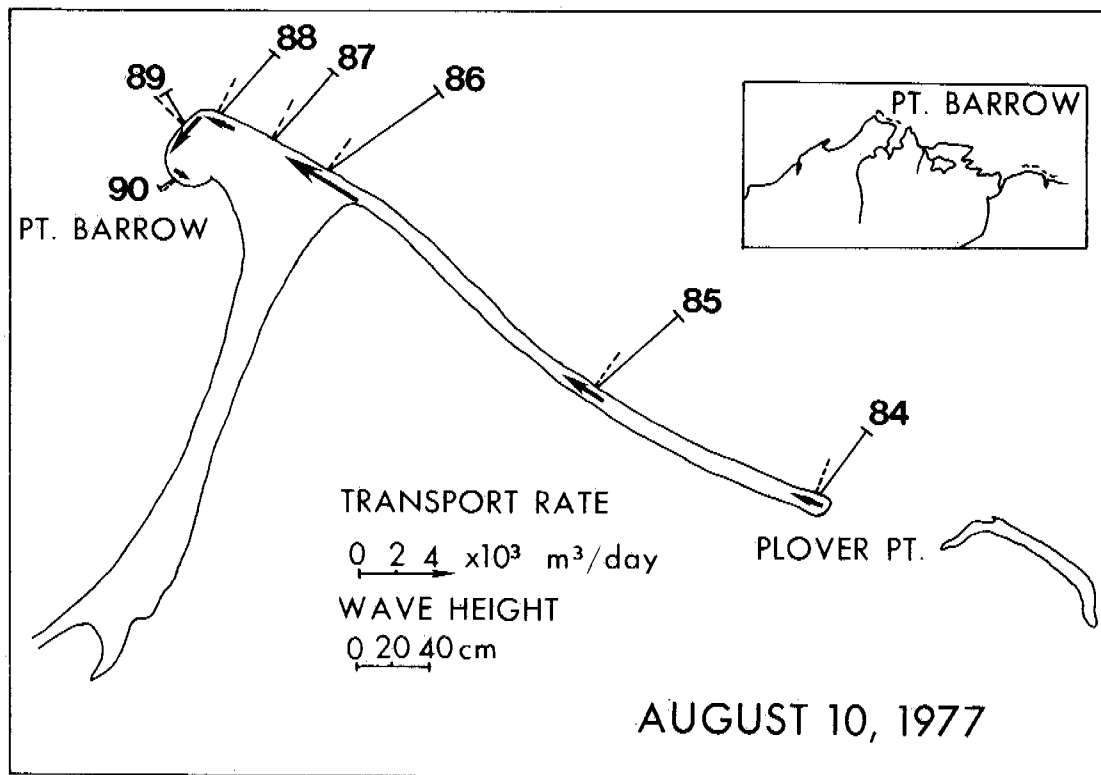


Figure 2. Wave parameters and sediment transport rates along the Pt. Barrow beaches on August 10, 1977.

SECOND ANNUAL REPORT

Contract #R7120840
Research Unit # 541/550
Reporting Period: 1 April 1977-
31 March 1978
Number of Pages: 68

NORTON SOUND/CHUKCHI SEA OCEANOGRAPHIC
PROCESSES (N-COP)

J. D. Schumacher²
R. D. Muench²
T. H. Kinder¹
L. K. Coachman¹
R. L. Charnell²
K. Aagaard¹

1. Department of Oceanography
University of Washington, WB-10
Seattle, Washington 98195
2. Pacific Marine Environmental Laboratory
3711 - 15th Avenue N.E.
Seattle, Washington 98105

31 March 1978

Table of Contents

	<u>Page</u>
I. Summary	1
II. Introduction	2
A. Objectives	
B. Tasks	
III. Present State of Knowledge	4
IV. Study Area	4
V. Data Collection	4
A. Temperature and Salinity Observations	
B. Moored Current Measurements	
C. Meteorological Data	
D. Helicopter Cruise Report	
VI. Present Status	33
A. The Summer 1977 Norton Sound Program	
B. The 1976-77 Moored Current Meter Program	
C. Discussion	
D. Conclusions	
E. References	
VII. Cooperation	63
VIII. Needs for Further Study	63
IX. Conclusions	64
Appendix A. UW Mooring Data Summary	66
Appendix B. UW Budget	68

I. SUMMARY

Analysis of data is beginning to increase our understanding of the physical oceanography of the study region. Specifically, from work done during the past year we conclude:

- A) Net flow through Bering Strait was northward throughout the winter of 1976-77 (September-April), based upon records from moored current meters in Bering Strait and southeast of St. Lawrence Island. Mean current speed in the Strait was about 10 cm sec^{-1} , and southeast of St. Lawrence Island it was about 5 cm sec^{-1} . Large north-south speed fluctuations of 50 cm sec^{-1} were superposed upon the mean northward flow.
- B) There was an overall factor of 2 decrease in kinetic energy density of northern Bering Sea currents at the time of ice formation, as recorded by the overwinter current meters. This energy decrease occurred over all frequencies. There was a more pronounced decrease, by about a factor of five, between diurnal and semidiurnal tidal frequencies.
- C) Tidal currents were extremely complex in the northern Bering Sea and Norton Sound regions. A mixed tide southeast of St. Lawrence Island gave way to a primarily diurnal tide in Norton Sound off Nome. In Bering Strait, there was no diurnal tidal signal and the semidiurnal signal was extremely small. This is attributed to interaction of tidal waves entering the northern Bering Sea region, both from the Arctic Ocean via Bering Strait and from the North Pacific to the south.

D) Two summer hydrographic surveys of Norton Sound revealed a pronounced two-layered structure: a cold, saline near-bottom layer was overlain by a warmer, lower salinity upper layer. The lower layer, a remnant of the preceding winter's convective regime (surface cooling and ice formation) persisted throughout the summer. The overall distribution of temperature and salinity suggested a sluggish horizontal circulation in the eastern sound with a weak cyclonic circulation in the western portion; circulation was weaker in the lower than in the upper layer, and was negligible in the lower layer in the eastern sound. This picture agrees with that derived from summer 1976 field work, and is supported by recorded current measurements obtained about 5 m below the surface at two locations in the sound during July-August 1977.

Our understanding will continue to develop, primarily through analysis of data already in hand. Once we have a basic understanding of processes in sub-regions of the study area (e.g., Norton Sound, Kotzebue Sound, Bering Strait), we will be able to synthesize the regional physical oceanography and to link it with the Bristol Bay study region to the south.

II. INTRODUCTION

A. Objectives

The general objective of this work unit is to relate oceanic advective and diffusive processes to potential pollution problems due to OCS petroleum development. Specific goals are:

1. Verification of fluctuations in transport of the predominantly northward flow through the system;
2. Verification, and temporal and spatial description, of the bifurcation of northward flow which takes place west of Point Hope;

3. Definition of temporal and spatial scales of the eddies ubiquitous in the system, and acquisition of the data needed to contribute to a dynamical description; and,
4. Definition and understanding of circulation in Norton and Kotzebue Sounds.
5. Clarification of interactions in a north-south direction along the Bering Sea shelf, specifically, between the N-COP and B-BOP study areas.

B. Tasks

The overall task is collection of field data to yield a description of the velocity field, improved understanding of mixing processes, and the relative importance of various driving mechanisms which cause and influence water motion. Specific tasks of the program are:

1. Hydrographic data acquisition. We are using hydrographic data: (a) to determine the baroclinic component of the pressure gradient; (b) to examine the hydrographic structure, and (c) for standard water mass techniques. This data contributes to estimating advection and diffusion, and also dynamical balances.
2. Current meter data. Velocity records are used to: (a) define the mean flow; (b) define and explain the low frequency flow components; and (c) analyze the tides.
3. Water level data. These data assist our efforts to estimate the dynamical balances.
4. Atmospheric data. We are attempting to determine the role of meteorological forcing in the velocity fluctuations (i.e., low frequency variability).

III. PRESENT STATE OF KNOWLEDGE

The first annual report (March 1977) summarized the state of knowledge prior to beginning this study. That report, subsequent reports, and Section VI (present status) of this report updates the initial summary.

CORRECTION: Because of an idiosyncrasy in our data processing, some hydrographic distributions presented for Kotzebue Sound in the first annual report are incorrect. We have solved our processing problem, and reported the correct distributions in a technical report (Kinder, T.H., J.D. Schumacher, R.B. Tripp, and D. Pashinski, The Physical Oceanography of Kotzebue Sound, Alaska, during Late Summer, 1976. University of Washington, Department of Oceanography Technical Report, Ref: M77-99, September 1977. 83 pp.

IV. STUDY AREA

The study area remains the southern Chukchi and northern Bering Seas, specifically including Norton Sound, Kotzebue Sound, and Bering Strait (Figure 1). Additionally, during the past year we worked over the shelf between the N-COP and B-BOP areas, attempting to link these two regimes.

V. DATA COLLECTION

In order to address the goals of this work unit, the following research was accomplished from 1 April 1977 to 31 March 1978.

Four field programs were completed during the period (Table 1). The first of these was confined to Norton Sound, and consisted of a CTD station grid occupied from the USGS research vessel *Sea Sounder* from 8-12 July 1977

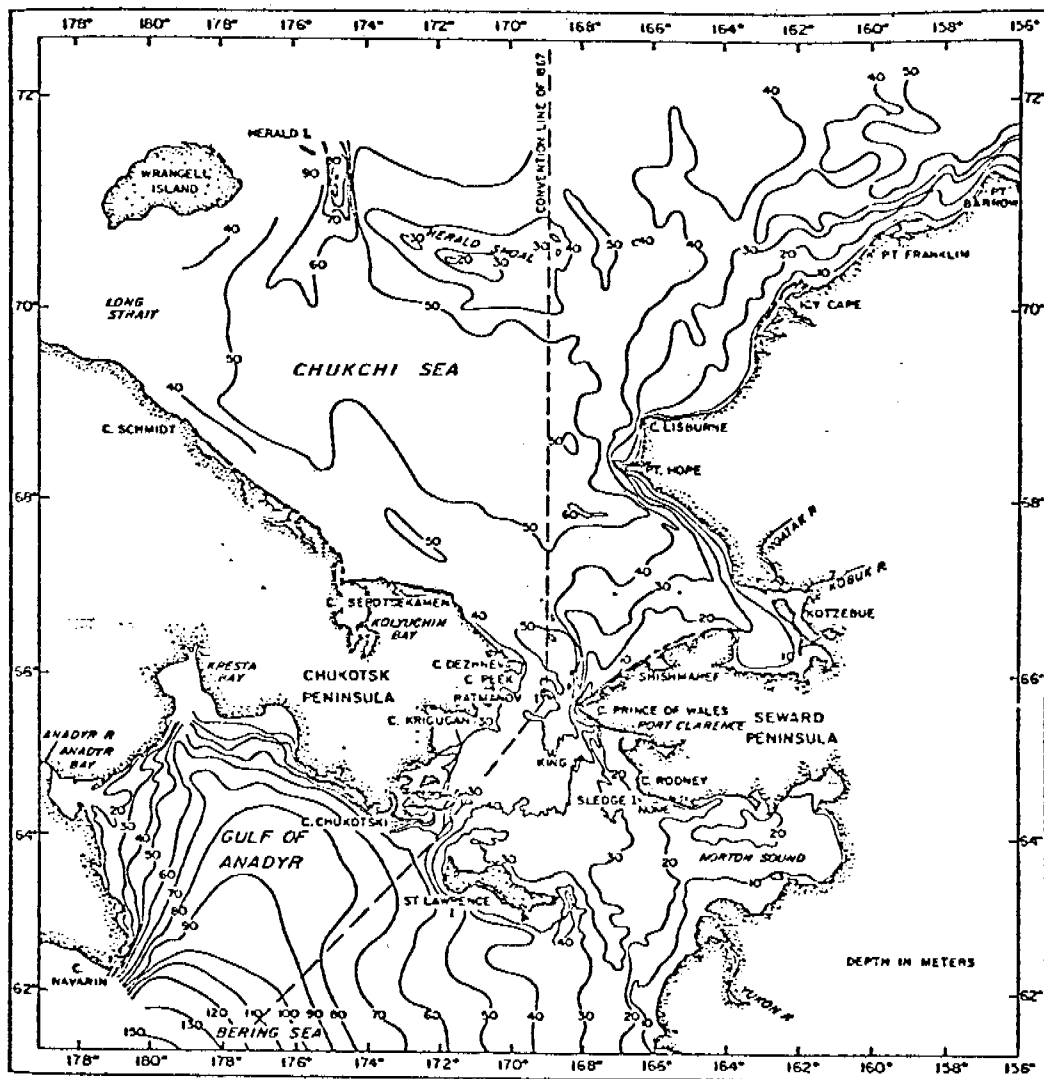


Figure 1. Geographical location and bathymetry of the N-COP study region (after Coachman *et al.*, 1975).

Table 1

Summary of Oceanographic Field Work
 During 1 April 1977-31 March 1978: N-COP

<u>Date</u>	<u>Vessel/ Cruise #</u>	<u>Chief Scientist</u>	<u>CTD Stations</u>	<u>Deploy Moorings</u>	<u>Recover Moorings</u>
7/8/77- 7/12/77	<i>Sea Sounder</i> No Cruise #	D. Cacchione	25	3	--
8/11/77- 9/2/77	<i>Surveyor</i> RP-4-SU-77B-IV	D. Pashinski	134	--	14
9/6/77- 9/29/77	<i>Discoverer*</i> RP-4-DI-77C-I	R.K. Reed	186	9	11
	NOAA Helicopter UH1H N56RF No Cruise #	C.A. Darnall	39	--	--

*Joint cruise to both N-COP and B-BOP areas.

(Figure 2). Since this vessel draws less water than the NOAA research vessels, this cruise allowed the closest penetration toward the Yukon River mouth (into water as shoal as about 5 m). The second field program was carried out from the NOAA vessel *Surveyor* from 11 August-2 September 1977. This cruise occupied 134 CTD stations in Norton Sound, Kotzebue Sound, Bering Strait and the Chukchi Sea (Figure 3) and recovered 14 moored current arrays. Of these, 12 were overwinter arrays which had been moored in October 1976 while two had been moored in July 1977 from *Sea Sounder*. The third program was the first of a series of joint cruises addressing problems in both the northern and southern Bering Sea shelf regions but excluding the region north of Bering Strait. This cruise, from 6-29 September 1977, occupied 186 CTD stations on the Bering Sea shelf, moored 9 overwinter current arrays and recovered 11 additional arrays which had been emplaced during summer (Figure 4). CTD station coverage during this cruise was designed to cover the entire Bering Sea shelf rather than focusing on a specific smaller region. The fourth and final field program for this reporting period was carried out in March 1978 (see Cruise Report, below). This program utilized a helicopter to obtain CTD data through the ice in Norton Sound.

In addition to the oceanographic field work, meteorological data are being routinely collected as detailed below.

A. Temperature and Salinity Observations

Temperature and salinity measurements, except during the helicopter-borne March program, were obtained with Plessey Model 9040 conductivity/temperature/depth (CTD) profiling instruments, Plessey digital data loggers and analog chart recorders. The vessel *Discoverer* had the additional back-up recording capability for CTD data of a PDP-11 computer-based data

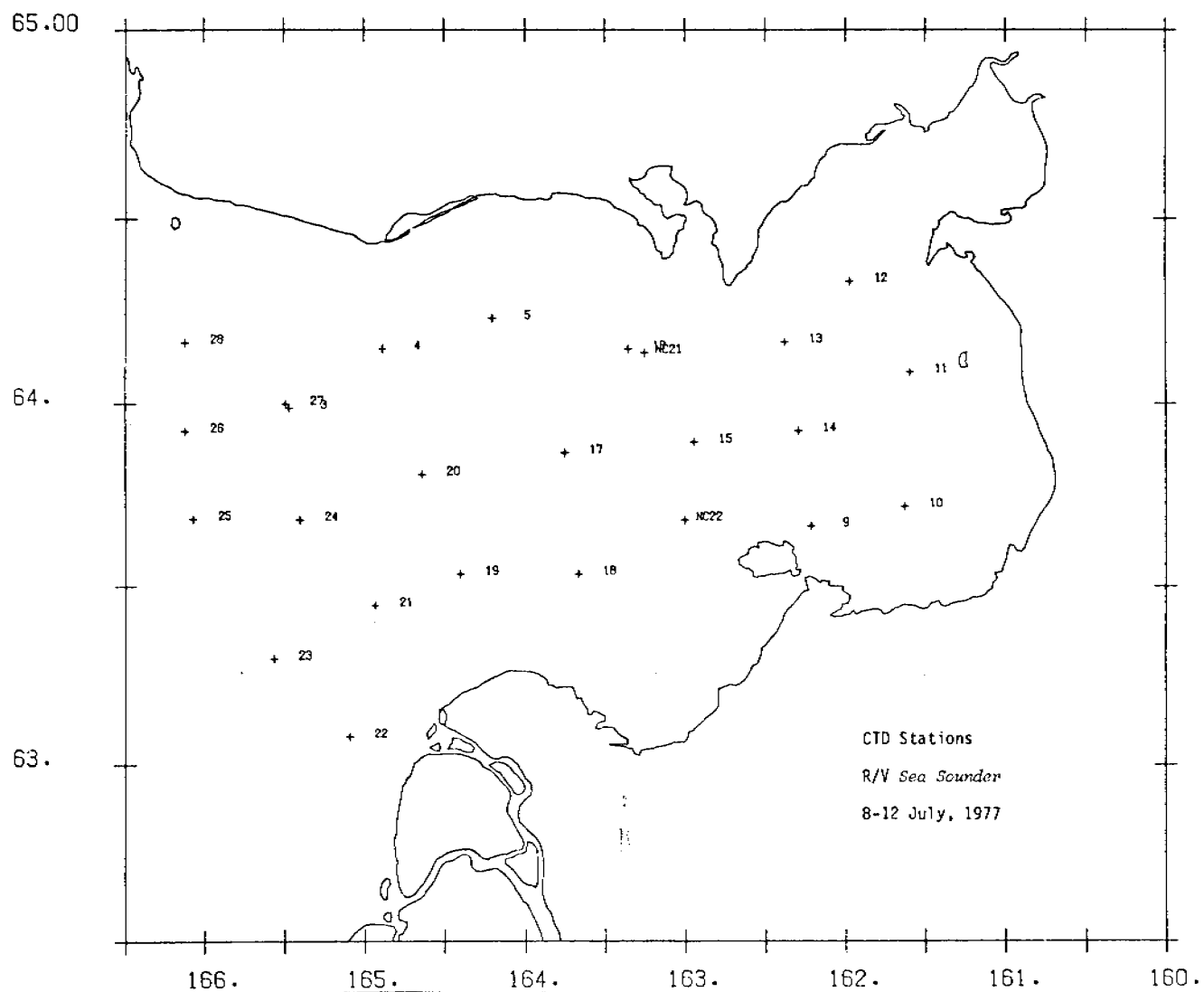
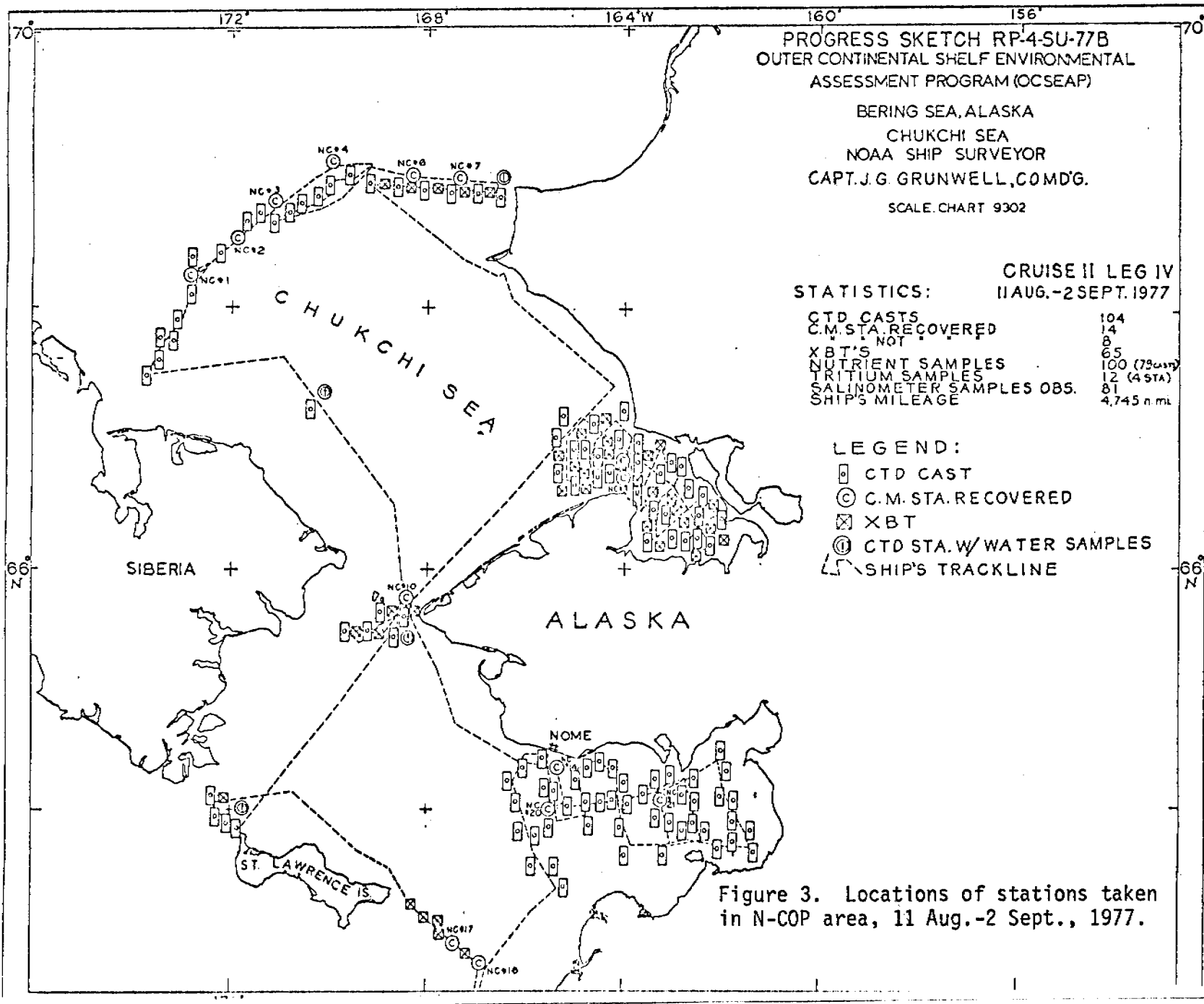


Figure 2. Locations of CTD stations occupied by the USGS vessel *Sea Sounder* in Norton Sound; 8-12 July, 1977. NC21 and NC22 were moored current meter locations (see text).



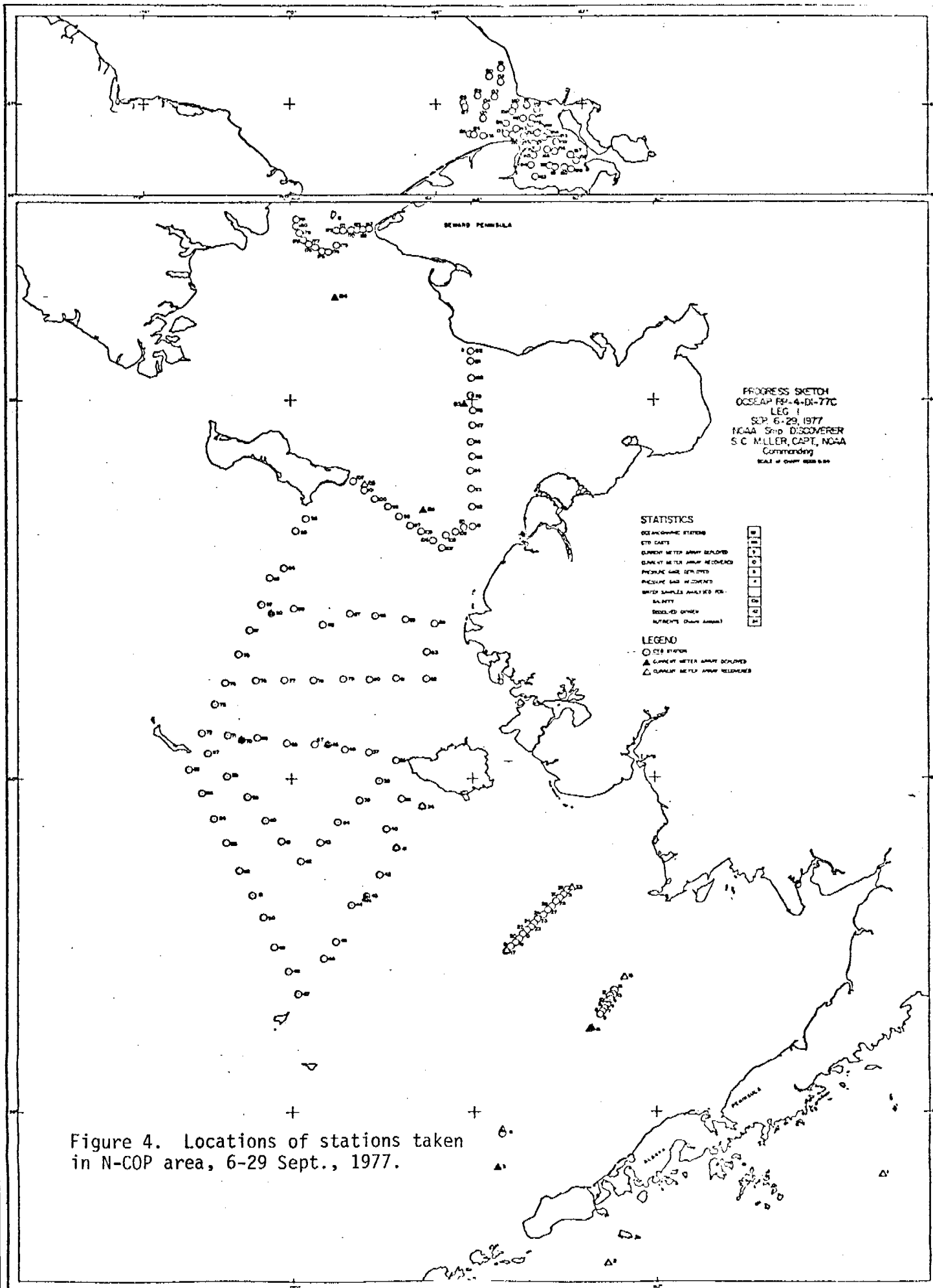


Figure 4. Locations of stations taken in N-COP area, 6-29 Sept., 1977.

acquisition system. The *Surveyor* had the capability, through use of a PDP-8E computer, of printing out and plotting the values recorded on the Plessey system. Both these vessels therefore had the capability of maintaining a continual check on system operation and data quality, and of near-real time monitoring of temperature and salinity. All three vessels allowed real-time monitoring of incoming data via the analog chart recorder; on the *Sea Sounder* this unit provided a sole check on system operation.

All data were acquired and processed aboard ship according to the Pacific Marine Center Oceanographic manual. Calibration samples were obtained using a rosette sampler or sample bottles on every cast. Raw data and calibration values were returned to the Pacific Marine Environmental Laboratory for final processing and analysis. All final temperature and salinity data products meet OCSEA program standards for accuracy and format; all data have been supplied to NODC.

B. Moored Current Measurements

During winter 1976-77, 19 current meter moorings, each containing a single near-bottom meter, were left emplaced in the northern Bering-Chukchi Sea region. Of these, 13 were recovered during late summer 1977 (cf. Figure 5 and Table 1). At the present time, three similar moorings are also deployed in the northern Bering Sea (Figure 5); recovery of these will be attempted in summer 1978.

Regional climatic features dictated certain characteristics of the over-winter moorings in 1977-78, as during the previous winter (Figure 6). In order to reduce chance of contact with surface ice, the flotation was placed about 10 m above the bottom. The meters were modified to record for a full one-year period. AMF releases were provided on each mooring for retrieval.

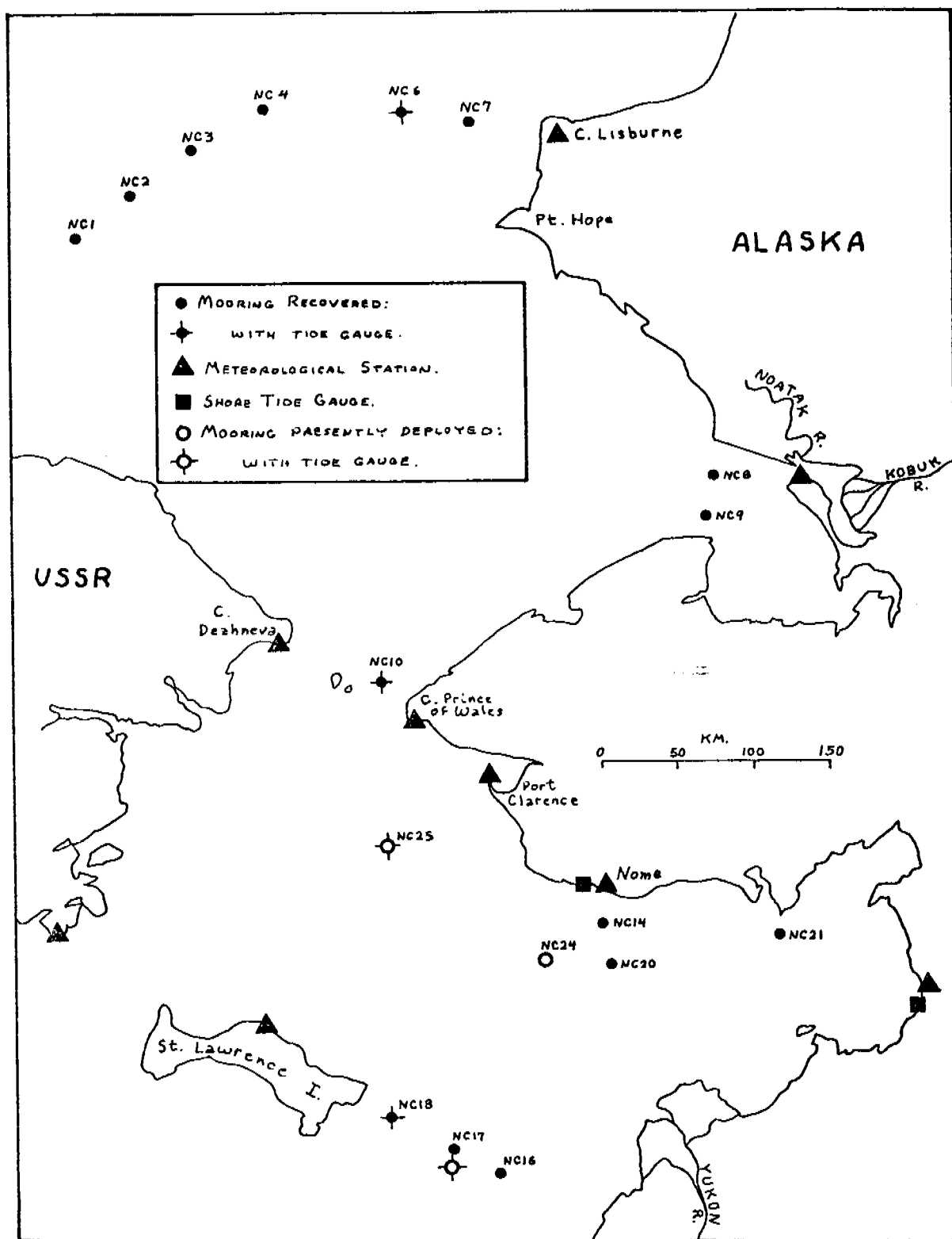


Figure 5. Geographical locations of environmental monitoring (recording) stations, past and present, in the N-COP study region. Those moorings which were not recovered are not shown on the figure.

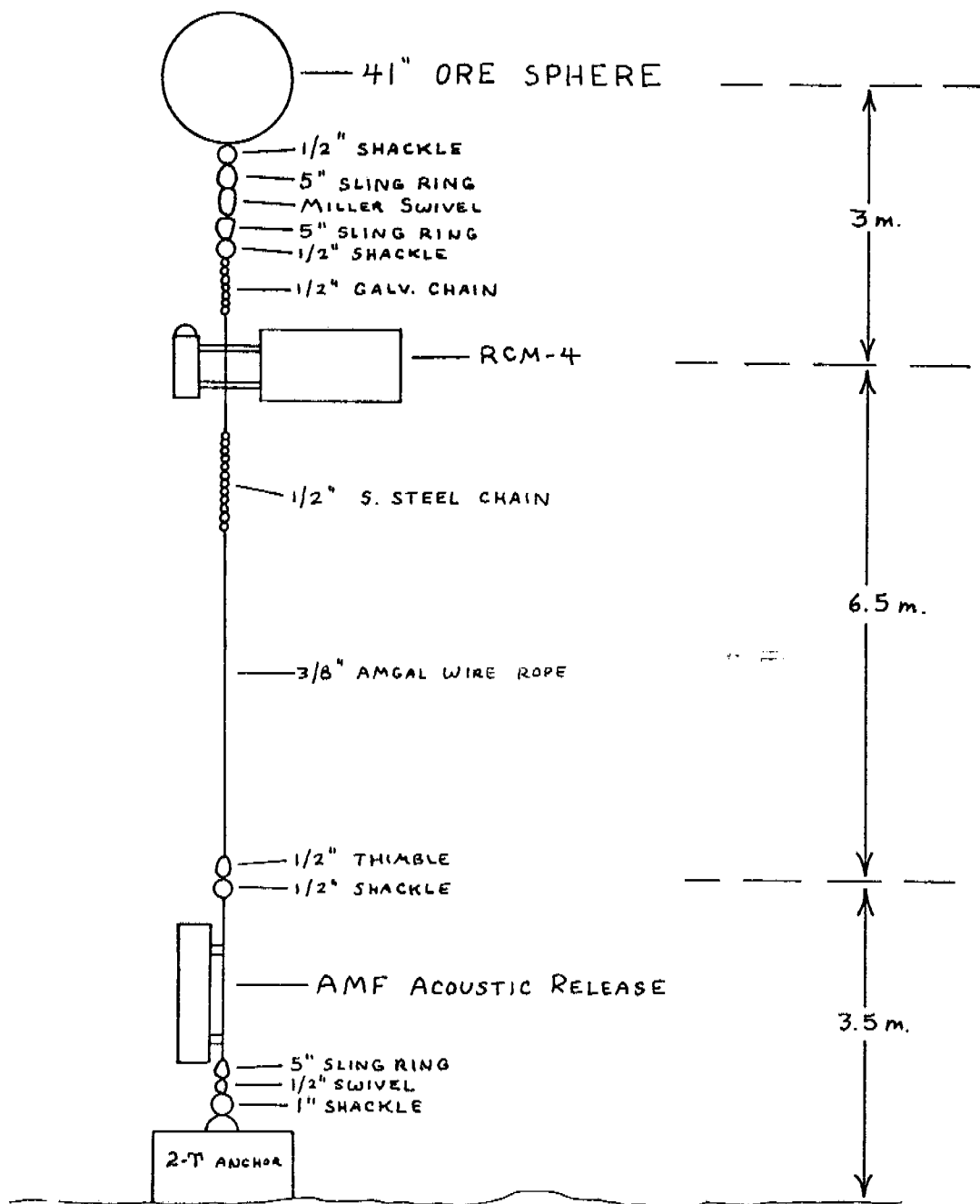


Figure 6. Example of configuration of long-term current meter moorings used in the N-COP program (not drawn to scale).

Based on performance of the 1976-77 moorings, some design modifications were incorporated into the 1977-78 moorings. The streamlined (clamshell) floats used in the earlier moorings apparently had failed due to pressure; these were not used in the 1977-78 moorings. The AMF Model 395 acoustic releases have a higher battery drain than the other AMF releases used; this model was not used during the 1977-78 overwinter program.

During summer 1977, three short-term moorings (about 6 weeks) were deployed in Norton Sound (Figure 5). NC-20 and NC-21 each contained two current meters, while NC-22 (not shown on figure) was in shallower water (about 15 m) and contained a single meter. Each array was equipped with an AMS Model 395 acoustic release. Of the three, only NC-20 and NC-21 were recovered; only the upper meters on these yielded usable data.

C. Meteorological Data

Atmospheric pressure data are being collected from the locations indicated on Figure 5, as during the previous year. Seven of these nine stations were operative prior to the inception of N-COP. Four report data to NWS/NOAA, and barograph charts are obtained from the remaining five by special arrangements. In addition to pressure data, monthly compilations of geostrophic winds (four times daily) are supplied by FNWC, Monterey, for a location midway between Nome and St. Lawrence Island ($63^{\circ}30'N-166^{\circ}00'W$). These winds are computed and compiled according to Bakun (1973).

The geostrophic winds are supplied as print-out and on cards; this information is then placed on magnetic tape. Our geostrophic wind files are kept continually updated. The atmospheric pressure data are received as analog pressure charts or on magnetic tape. The charts must be digitized, while the tapes are transferred, after reformatting, to our data files.

D. Helicopter Cruise Report - 17 February - 5 March 1978

1. Objectives

This cruise was to complete the Norton Sound portion of the winter physical oceanographic survey of Norton Sound, Kotzebue Sound, and the Chukchi Sea. Due to insufficient ice cover in Norton Sound in February 1977, that portion of the survey was not accomplished.

These data, when completed, will: 1) provide comprehensive environmental data on the Alaska Outer Continental Shelf; 2) define the probable ecological impact of petroleum exploration, production, storage, and transportation on the continental shelf; and 3) refine our understanding of key ecological dynamic processes.

2. Narrative

The report of events is as follows:

17 February 1978

Clark Darnall and Steve Harding arrive in Nome, and began searching for our airfreighted equipment. Neither the air shipment nor our personal baggage arrived that day. We settled into our accommodations at the Golden Nugget No. 3. Our rooms and eating arrangements were quite adequate.

18 February 1978

Our personal bags and eight of the 11 pieces of air freight arrived. We telexed Anchorage our urgent need of the other three pieces.

19 February 1978

Dave Drake and Chuck Totman from USGS Menlo Park, California, arrived. Our three missing pieces did not arrive. We continued our search via telephone with Anchorage. NOAA helicopter N56RF arrived at approximately 1630 BST. Lt. Jon Barnhill was the pilot, and Mr. Gary Feldt was the mechanic. The aircraft was not equipped with floats. We decided that an

ice recon flight the following day would be in order.

20 February 1978

Weather, thin cirrostratus; winds, 034^oT 10kt; temperature, -10^oC.

0956 BST

Drake, Totman, and Darnall departed Nome in N56RF (Barnhill). We flew south on proposed section I. The ice was 12-18 inches thick, with many new open small leads (10-100 ft. wide). We encountered fog and winds 040^oT 22kt over the Sound. From the far station on Section I, we flew midway to the far station on Section II. The ice was similar. We returned to Nome for fuel.

Our three missing pieces of equipment had arrived. We planned to survey ice conditions to the east in the afternoon.

1353 BST - Same Crew

Departed Nome in N56RF (Barnhill). Snow and near-zero visibility forced us to abort flight and return to Nome.

Day's Flight Time: 1 Hour, 55 Minutes.

21 February 1978

Weather, clear; winds 020^oT 8 kt, temperature -6^oC.

0818 BST

Drake, Totman, and Darnall departed Nome in N56RF (Barnhill). We were heading east to check ice conditions and burn off fuel in the port fuel bladder (for removal). There was a narrow shore lead from Solomon to Rocky Point. The ice south of this for 3-4 miles was too thin to fly over. Our furthest eastward position was 63^o 52' N, 150^o 50' W. The ice east of this was too thin to work. We returned to Nome. After we arrived, Gary Feldt spent several hours locating and repairing a minor

oil leak in the transmission. We removed the port fuel bladder, loaded our gear and prepared for an early start the following day.

Day's Flight Time: 2 Hours, 10 Minutes

22 February 1978

Weather, light snow; winds, 070^oT 30-35 kt, temperature 0^oC possible icing and white-out conditions prevented flying.

23 February 1978

Weather, snowing winds 080^oT 25-30 kt, temperature -1^oC possible icing and white-out conditions prevented flying.

24 February 1978

Weather, snow showers and low stratus, winds 040T 14 kts, temperature -1^oC. We waited for visibility to improve.

0910 BST

Totman, Harding, Drake and Darnall departed Nome in N56RF (Barnhill). A broken shore lead (100-1000 ft. wide) had developed. We were able to work our way around the widest portions of it. We started the northernmost station of Section I. On the 1st station, the pressure signal of the CTD was very erratic. On the 2nd and 3rd station, the pressure signal was gone completely. We attempted to maintain a uniform descent rate of the CTD sensor package, so that during subsequent data reduction, we would be able to interpolate the depth. After completing station 03, we encountered icing and white out conditions. We returned to Nome. The weather continued to deteriorate, and prevented flying in the afternoon. We used this opportunity to work on the CTD. The people at the FAA Facility kindly allowed us to use their electronics shop, and by that evening we had determined the problem to be bad contacts in an inter board connector

of the power supply/signal return section of the data logger. Cleaning and bending the contact pins appeared to solve the problem. Throughout the remainder of the cruise this intermittent continued to appear, but jarring or flexing the P.C. board mounts always corrected it. Perhaps the vibration of the helicopter was just too much for the electronics.

Day's Flight Time: 40 Minutes

25 February 1978

Weather—thin cirrostratus; wind 070^oT 15 kt, temperature 0^oC.

0840 BST

Harding, Totman, Drake and Darnall departed Nome in N56RF (Barnhill). We proceeded with the stations on Section I. The CTD worked satisfactorily. We were forced to move the 8th Station approximately four miles northward due to a large lead laying to the south. While we were doing these stations, we flew into and under a large weather front moving rapidly northward. By the time we returned to Nome, the weather there had deteriorated and we could fly no more that day. Station 08 was completed.

Day's Flight Time: 1 Hour, 30 Minutes

26 February 1978

Weather—80% cirrostratus, wind 070^oT 25-35 kt, temperature -3^oC.

0832 BST

Totman, Harding, Drake, and Darnall departed Nome in N56RF (Barnhill). We were heading east to start Section II. A considerable amount of flooding and melting had occurred since our ice recon. We took station 009 south of the proposed position due to thin ice to the north. Weather had improved (now 20% cloud cover), but the winds were increasing (100^oT, 35 kt). After completing station 010, we returned to Nome for fuel.

1255 BST - Same crew departed Nome to complete Section II. Winds had increased to 48-50 kt (direct headwind) at 1500 ft. (our ground speed, per GNS500A navigation equipment, 40 kt). When we arrived at the location of station 011, the winds at ground level were 40-45 kt. This was too much for a safe landing with the helicopter, and we returned to Nome (our ground speed -132 kt).

Day's Flight Time: 4 Hours, 22 Minutes

27 February 1978

Weather, cirrostratus, winds 100⁰T 25 kt, temperature -1⁰C, visibility 21 miles.

0754 BST

Harding, Drake, Totman, and Darnall departed Nome in N56RF (Barnhill). We were heading for 4th proposed station on Section II. Off Cape Nome, winds at 1000 ft. were approximately 140⁰T 45 kt. Approximately 40% of the ice in this area had been flooded. The winds were again too high for a safe landing in the area of our desired station. We decided to use our existing fuel to survey ice conditions to the southeast. Due to the high wind from the southeast and to the flooding ice, the edge of workable ice had moved to the northwest (see attached charts of ice cover). We returned to Nome after reaching a position of 63⁰ 54.9' N, 163⁰ 55.2' W (this was the furthest we could safely fly to the southeast).

1104 BST

Same crew departed Nome. We now had 100% stratus cloud cover. We were heading southwest to start Section IV if possible. The winds at the westernmost station of Section IV were 163⁰T 35 kt. At this station (No. 011), the USGS transmissometer failed. We completed station 013 before returning to Nome for fuel. The USGS crew continued to take water samples,

for sediment analysis, at each station.

1458 BST

The same crew departed Nome. We completed station 014. We could see open water at approximately 5 miles to the south. As we were transiting to station 015, we received a radio call asking for the assistance of N56RF in evacuating a burn victim off Little Diomedede (the National Guard helicopter was torn down for inspection). We returned to Nome, unloaded our gear, installed both fuel bladders, and N56RF (Barnhill and Feldt) departed for Little Diomedede.

Day's Flight Time: 4 Hours, 54 Minutes (for our project)

N56RF (Barnhill, Feldt) spent the night at the Tin City after the trip to Little Diomedede.

Pat Wiberg arrived that evening to join the USGS crew.

28 February 1978

Weather clear, wind 080^oT. 13 kt, temperature -2^oC.

0845 BST

N56RF returned. We refueled and reloaded the helicopter. Barnhill had some breakfast and we were ready to go. USGS had been unable to repair their transmissometer, and would continue to take water samples.

0958 BST

Harding, Wiberg, Totman and Darnall departed in N56RF (Barnhill). We completed stations 0015-0019. As we proceeded eastward on Section IV the ice condition deteriorated and we could see open water 5-10 miles to the south. By the time we were at 64^o 04.8' N, 164^o 02.5' W, the ice was 80-90% flooded and quite thin. On our last landing, the ice was less than 10 inches thick,

very soft and weak. Lt. Barnhill decided to not power down the helicopter and we returned to Nome. On our way back, we saw that the ice in this area had experienced considerable flooding (50-70%) and would not be workable. We decided to go west after refueling and try Section VI off Cape Rodney.

1520 BST - Wiberg, Harding, Drake, and Darnall departed Nome in N56RF (Barnhill). The weather continued to be clear, warm, and fairly calm (12 kt). The ice in this direction appeared to be much older with considerable ridging and fewer open leads. We completed all four stations (through Station 023) on Section VI, and we returned to Nome after dark. This had been a very good day, nine stations in all.

Dave Drake planned to return to California the following day. We decided to try Section V next. As this entailed considerable flying time there and return, we would take only two scientific personnel and as much extra fuel as possible.

Day's Flight Time: 3 Hours, 50 Minutes

1 March 1978

Weather clear, some cirrostratus to the south, wind 070⁰T, 9kt, temperature -8⁰C.

0852 BST

Wiberg, Darnall departed Nome in N56RF (Barnhill). We would head south along the open/thin ice to the inshore station of Section V. There were several large northward running leads with workable ice in between as we approached mid-way across the sound. As we moved south it became apparent that the long arm of thicker ice we were flying down was deteriorating and that we would not be able to continue southward. We backtracked north in order to get across to thicker ice to the west. We used over an hour's fuel going down and back this dead end. We returned to Nome to top off

our fuel before flying west and then southward.

1109 BST

Same crew departed Nome. After flying west and then southward, the furthest south or east we could safely fly was just about the position of the far offshore station on Section V $63^{\circ} 27.0' N$; $166^{\circ} 51.5' W$. We did this station 024 and two more (025,026) along a bearing of $287^{\circ} M$ with 10 mile spacing between stations. At the far station, we encountered a tenth of a degree C colder water. This was presumedly colder Gulf of Anadyr water. We arrived Nome at 1545 BST. As our next section VII was distant, we didn't start that afternoon.

Day's Flight Time: 4 Hours, 18 Minutes

2 March 1978

Weather, clear; wind, calm; temperature $-9^{\circ} C$. Again, due to travel time to Section VII, we took only two scientific personnel.

0847 BST

Totman and Darnall departed Nome in N56RF (Barnhill). We completed four stations (027-030), with no difficulties encountered. With the clear weather and close proximity to King Island, this was truly a spectacular section. The ice in this area was old (2-4 ft. thick) with few open narrow leads. We could see what appeared to be open water north and west at a 20-30 mile range. As we were able to return to Nome early, we would try to take stations as deep into the sound as safely possible. Since the position of our stations would be dictated by the availability of workable ice, we would not be able to follow any section lines.

1436 BST

Weather, clear; wind, calm; temperature $-6^{\circ} C$. Wiberg, Totman, Harding and Darnall departed Nome in N56RF (Barnhill). There was a shore

lead open (1/4-1 mile wide) east of Cape Nome, and the ice was unworkable south of Topkok Head. We were able to take four stations (031-034) in the central portion of the sound, before returning to Nome. There appeared to be some workable ice southeasterly toward Pastol Bay, we would try this area the following day.

Day's Flight Time: 4 Hours, 15 Minutes

3 March 1978

Weather, clear; wind, 290°T 4kt; temperature -10°C.

0932 BST

Wiberg, Harding, Totman and Darnall departed Nome in N56RF (Barnhill). By detouring around open water and thin ice, we were able to take three stations (035-037). The furthest eastward position was 63° 40.3' N, 163° 34.8' W. We could see no way to safely work east of this, and returned to Nome. We decided to fly east along the shore to Cape Darby in the afternoon, to see if we could possibly take any stations in the Norton Bay to Stuart Island area.

1422 BST

Wiberg, Darnall departed Nome in N56RF (Barnhill). From Cape Nome to Topkok Head the shore lead was 3-4 miles wide. From Topkok Head to Cape Darby there was either open water or thin new ice as far south as we could see (20-25 miles) Norton Bay and the eastern portion was similar. We returned to Nome without landing.

Day's Flight Time: 3 Hours, 41 Minutes

4 March 1978

Weather, clear; wind, 290°T 12kt; temperature -13°C. We decided to do an additional section southwest from Sledge Island.

0918 BST

Wiberg, Harding and Darnall departed Nome in N56RF (Barnhill). The wind had been from the north, and there was a new shore lead opening from south of Nome, around Sledge Island and continuing to the northwest. The temperature was dropping (-20°C) and the wind was increasing (340°T , 25kt) as we took station 038. By the time we completed station 039, the winds were gusting to over 40kt. We made this our last station, and returned to Nome. This was our last day of helicopter time, so we began packing in the afternoon.

Day's Flight Time: 1 Hour, 4 Minutes

5 March 1978

Weather, clear; wind 010°T , 25kt, temperature -15°C .

1130 BST

Harding and Darnall departed Nome for Barrow, via Wien Air Alaska, to participate in cruise W-30. The USGS personnel departed for California.

3. Methods

CTD casts were taken at each station utilizing a Plessey Model 9400 profiling system with a re-designed sensor package capable of permitting its deployment through an eight-inch auger hole. 110VAC power was supplied by a 2-1/2 KW Onan portable generator. The data signal was transmitted, via a single conductor sea cable and portable winch system, to a Plessey Model 8400 digitizer for formatting and recording on a 7-track Kenedy magnetic tape recorder. In order to determine field correction factors for the conductivity and temperature sensors, a water sample and temperature were obtained from a Nansen bottle one meter above the sensors. The salinity

samples were returned to the University of Washington, Department of Oceanography routine chemistry laboratory for analysis.

The USGS personnel took water samples at selected depths in the water column. These samples were analyzed for suspended sediments on a daily basis. During the first portion of the cruise, suspended sediments in the water column were profiled with an Inter Oceans transmissometer.

The CTD and suspended sediment analysis operations worked quite satisfactorily out of the UH-1H helicopter.

4. Personnel

Clark H. Darnall	Oceanographer	University of Washington
Stephen Harding	Research Aide	University of Washington
Dave Drake	Geologist	USGS
Chuck Totman	Technician	USGS
Pat Wiberg	Technician	USGS
Lt. John Barnhill	Pilot	NOAA
Gary Feldt	Mechanic	NOAA

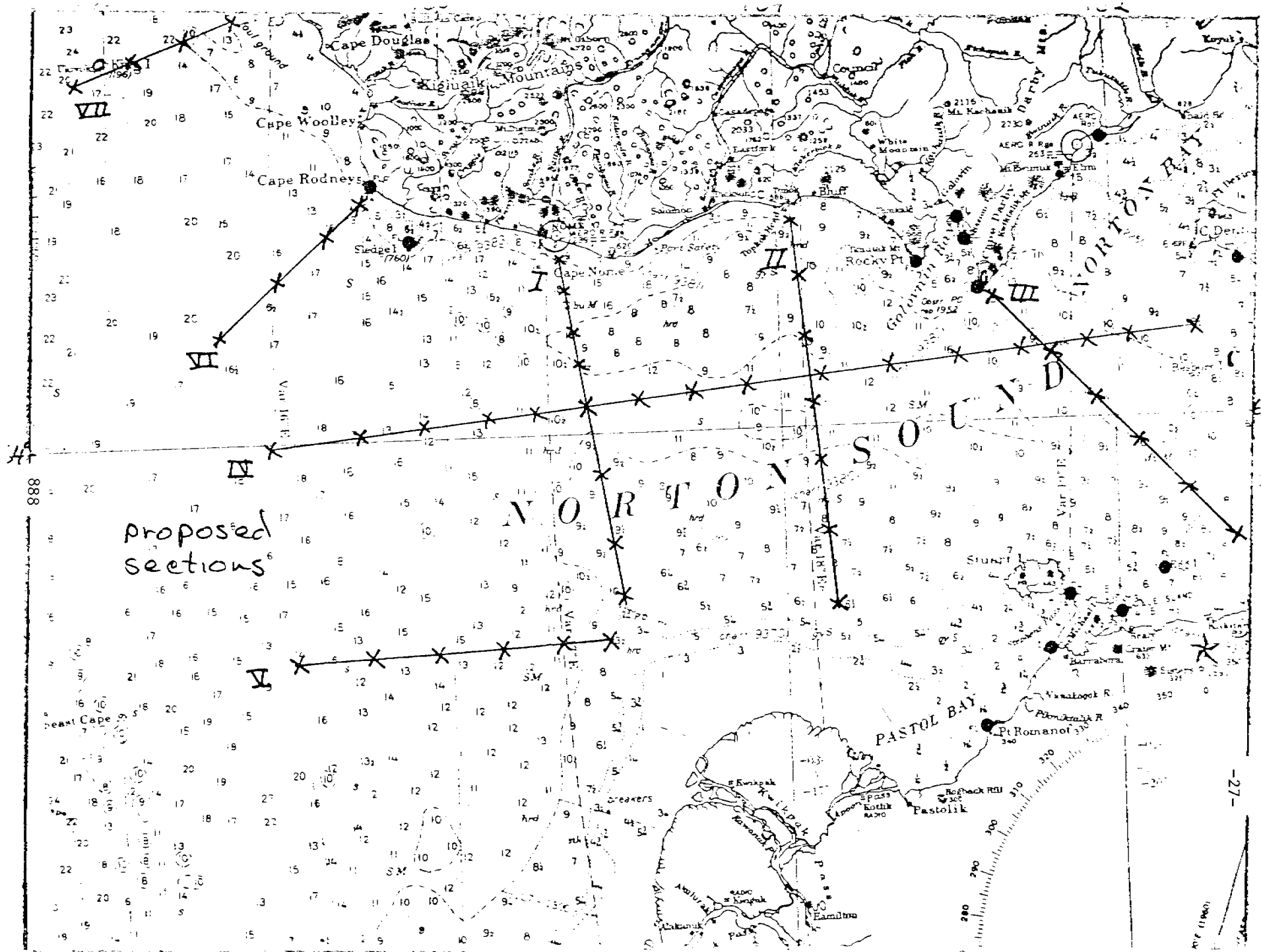
Acknowledgments

Mr. Feldt's and Lt. Barnhill's assistance in completing this project in the presence of difficult conditions was greatly appreciated. The use of the Alaska Air National Guard hangar, and assistance of Captain Doug Dougan was very helpful.

APPENDIX A

Station Number	Date/Time GMT 1978	Latitude North	Longitude West	Water Depth Meters
1	24-02/2100	64° 25.7'	165° 18.6'	23
2	24-02/2209	64° 22.0'	165° 16.2'	31
3	24-02/2258	64° 17.2'	165° 14.5'	23
4	25-02/2013	64° 10.9'	165° 12.1'	19
5	25-02/2059	64° 4.0'	165° 9.9'	19
6	25-02/2146	63° 55.2'	165° 6.5'	19
7	25-02/2232	63° 45.2'	165° 3.2'	18
8	25-02/2324	63° 40.9'	164° 57.0'	19
9	26-02/2131	64° 18.2'	164° 3.0'	19
10	26-02/2215	64° 12.7'	163° 53.3'	19
11	27-02/2316	63° 57.2'	166° 57.7'	34
12	28-02/0013	63° 57.9'	166° 36.6'	34
13	28-02/0056	64° 0.8'	166° 11.4'	27
14	28-02/0243	64° 2.0'	165° 42.5'	22
15	28-02/2135	64° 1.9'	165° 26.9'	20
16	28-02/2213	64° 4.2'	165° 10.0'	19
17	28-02/2250	64° 4.9'	164° 52.1'	20
18	28-02/2337	64° 5.9'	164° 33.5'	21
19	01-03/0037	64° 7.1'	164° 07.6'	22
20	01-03/0316	64° 36.1'	166° 32.0'	24
21	01-03/0350	64° 32.8'	166° 49.1'	28
22	01-03/0425	64° 29.3'	167° 09.5'	31
23	01-03/0455	64° 25.1'	167° 26.9'	31
24	01-03/2330	63° 27.0'	166° 51.5'	27
25	02-03/0027	63° 31.4'	167° 12.7'	27
26	02-03/0120	63° 31.7'	167° 35.0'	30
27	02-03/2114	64° 54.1'	168° 11.7'	41
28	02-03/2202	64° 59.2'	167° 53.8'	43
29	02-03/2248	65° 1.9'	167° 36.5'	36
30	02-03/2338	65° 5.3'	167° 19.7'	23
31	03-03/0219	64° 1.0'	164° 12.0'	21
32	03-03/0258	63° 53.2'	164° 10.9'	20
33	03-03/0338	63° 47.8'	164° 25.3'	18
34	03-03/0412	63° 37.7'	164° 22.2'	16
35	03-03/2142	63° 34.8'	164° 5.7'	15
36	03-03/2224	63° 38.8'	163° 46.4'	16
37	03-03/2257	63° 40.3'	163° 34.8'	16
38	04-03/2106	64° 28.1'	166° 1.5'	22
39	04-03/2158	64° 22.4'	166° 13.9'	28

Total Flight Time in N56RF (OCS Project): 32 Hours 39 Minutes

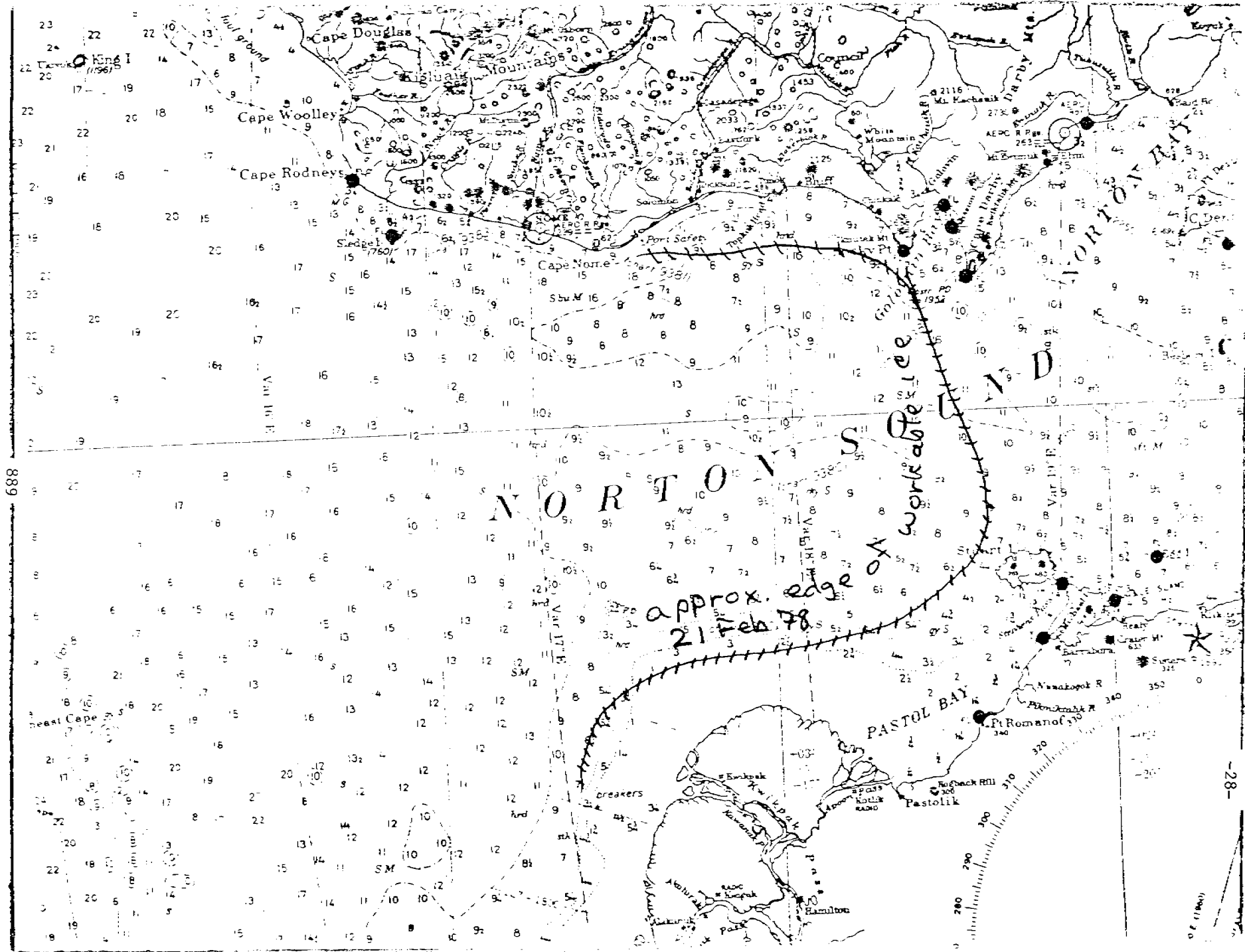


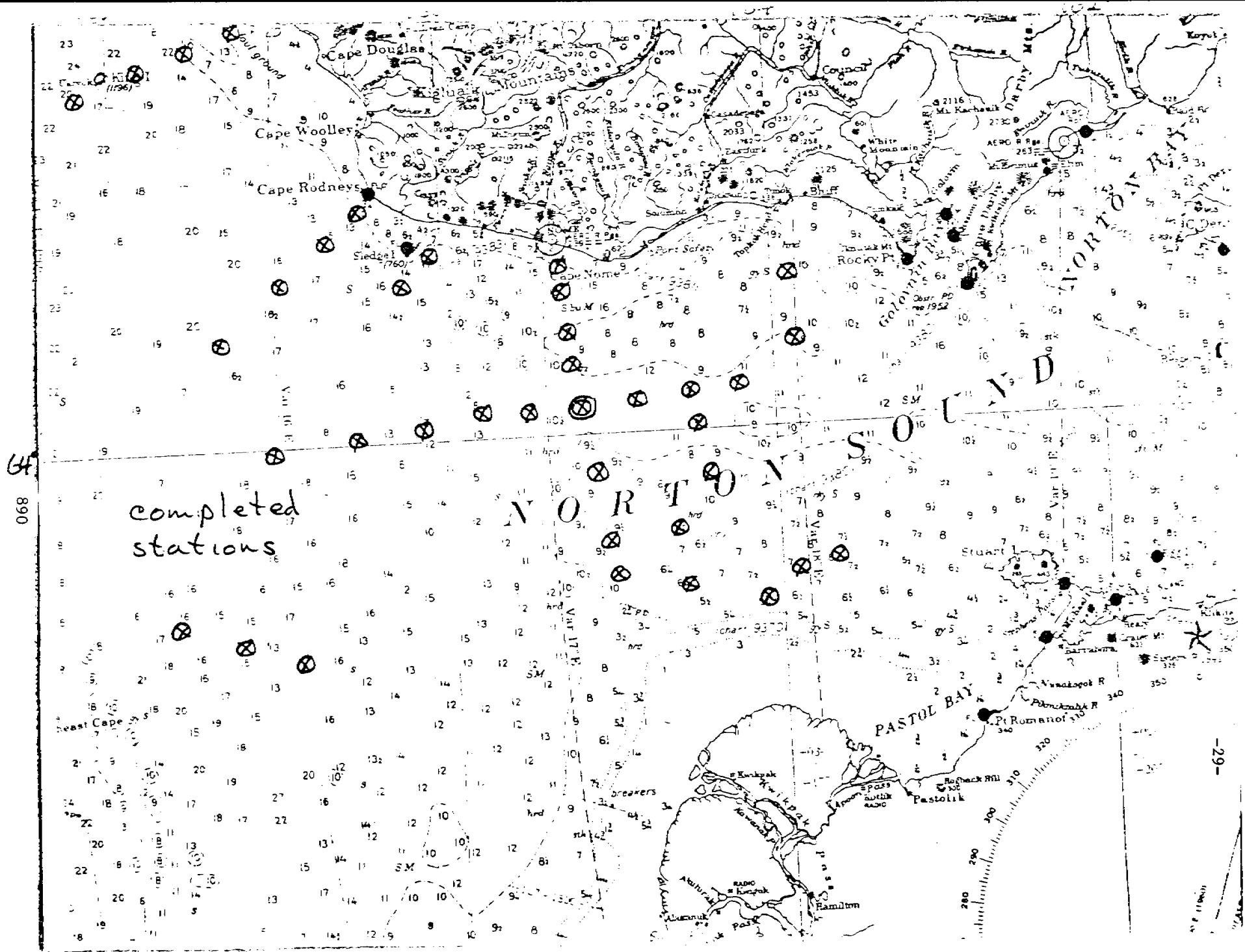
proposed sections

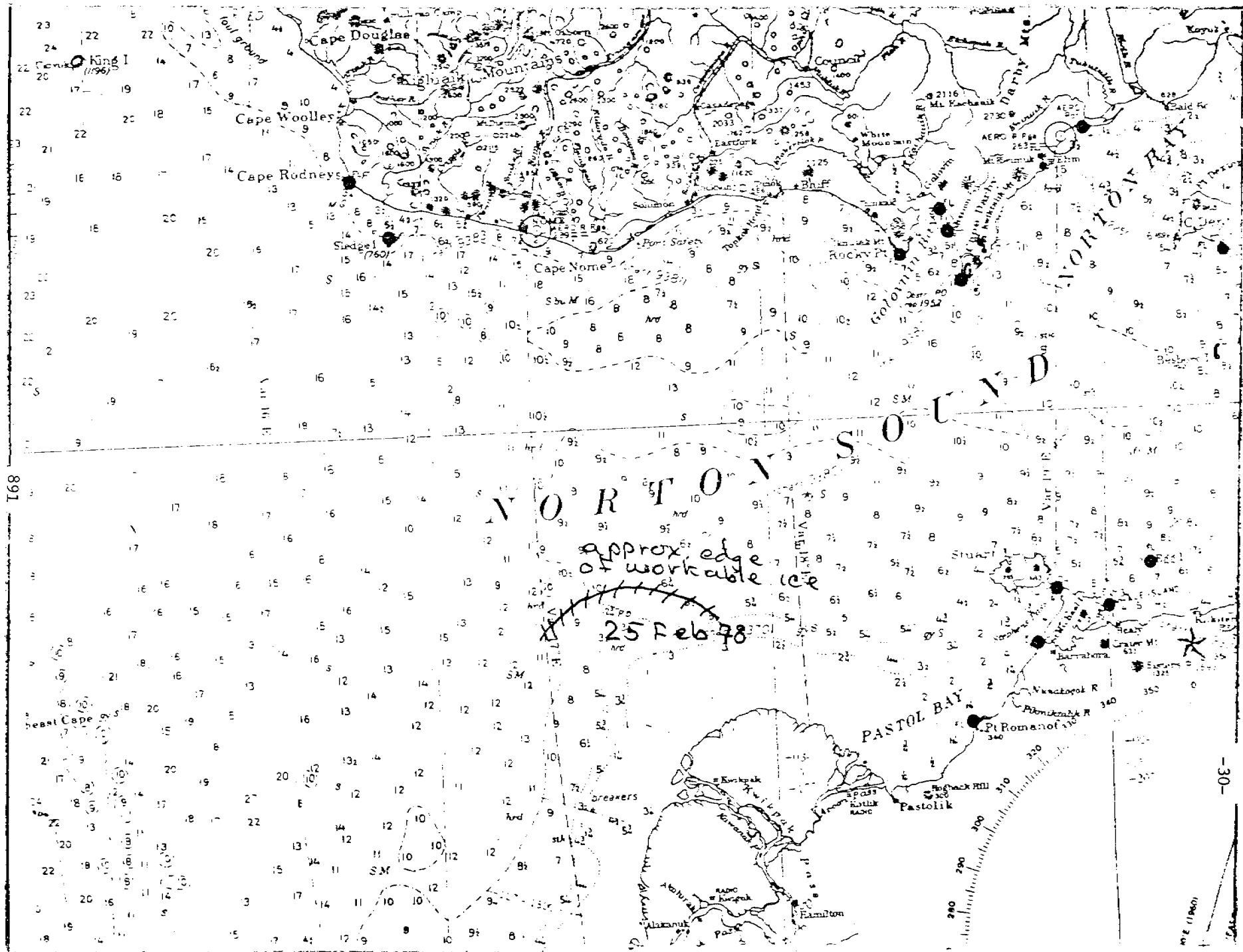
NORTON SOUND

NORTON BAY

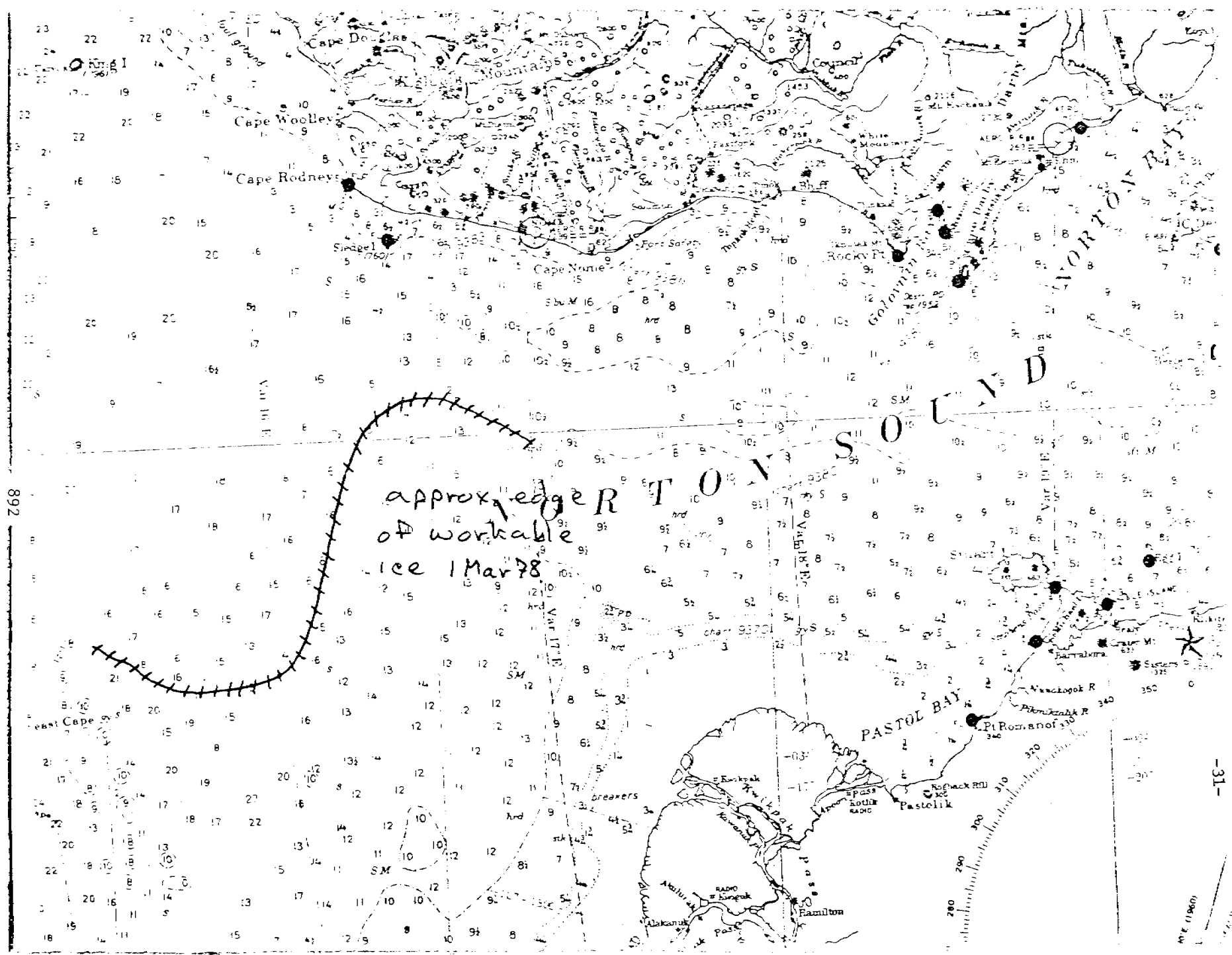
PASTOL BAY

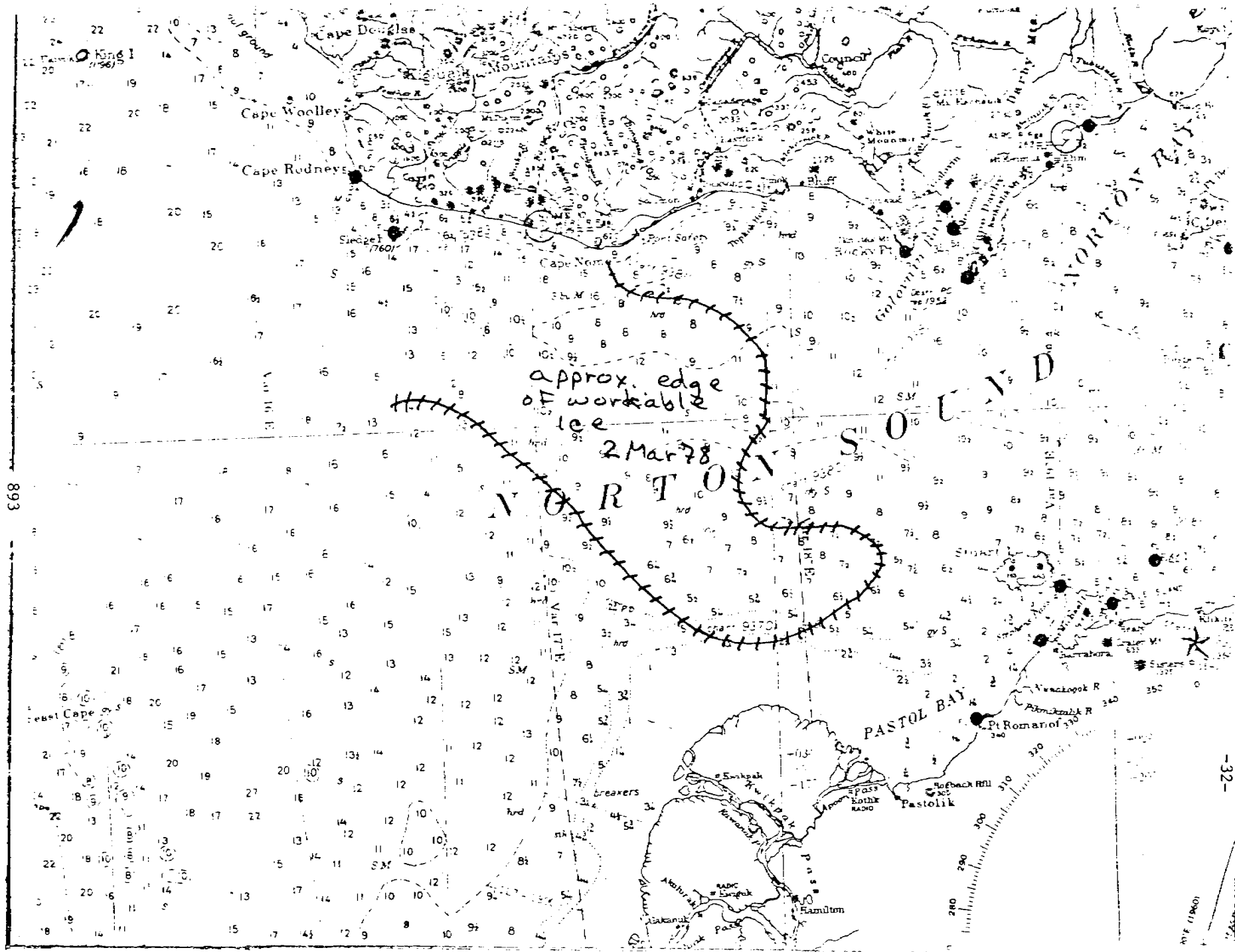






891





VI. PRESENT STATUS

A. The Summer 1977 Norton Sound Program

Sufficient data were obtained during July and August 1977 cruises into Norton Sound to yield insight into processes there. Data from the two summer moorings add additional support. Essential features observed during summer 1977 were similar to those observed during summer 1976.

The horizontal distributions of temperature and salinity in Norton Sound can be characterized by surface and near-bottom plots of temperature and salinity during July and August 1977 (Figures 7-10). In July, the lowest observed surface salinities (<16 ‰) were observed off the Yukon River mouth. Low salinities were also observed in the eastern end of the Sound; it was not, however, possible to trace continuity between the low salinity due to Yukon outflow and that in the eastern Sound. The maximum observed salinities (>31 ‰) occurred in the northwestern Sound just south of Nome; a high salinity (>28 ‰) tongue extended eastward from this area into the central Sound.

By August, maximum surface salinities had become lower (~ 29 ‰) as compared to >31 ‰ in July and still occurred in the northwestern portion of the Sound. Temperatures were higher (15 - 16°C) than earlier (6 - 14°C). Station coverage near the Yukon River mouth was nonexistent in August (water depths were too shallow to permit *Surveyor* to sample there); it was therefore impossible to compare minimum salinities there with those observed in July of >16 ‰. Surface salinities in southeastern Norton Sound were higher (>28 ‰) than in July (<19 ‰).

Near-bottom temperature had increased from <0 to 4°C (outside the shoal coastal parts of the southern Sound) in July to 3 to 8°C by late August. Overall near-bottom salinity did not change appreciably except for a decrease from >34 to >33 ‰ in the central northern Sound. Lack of data off the Yukon River in August preclude a comparison there. The two points showing

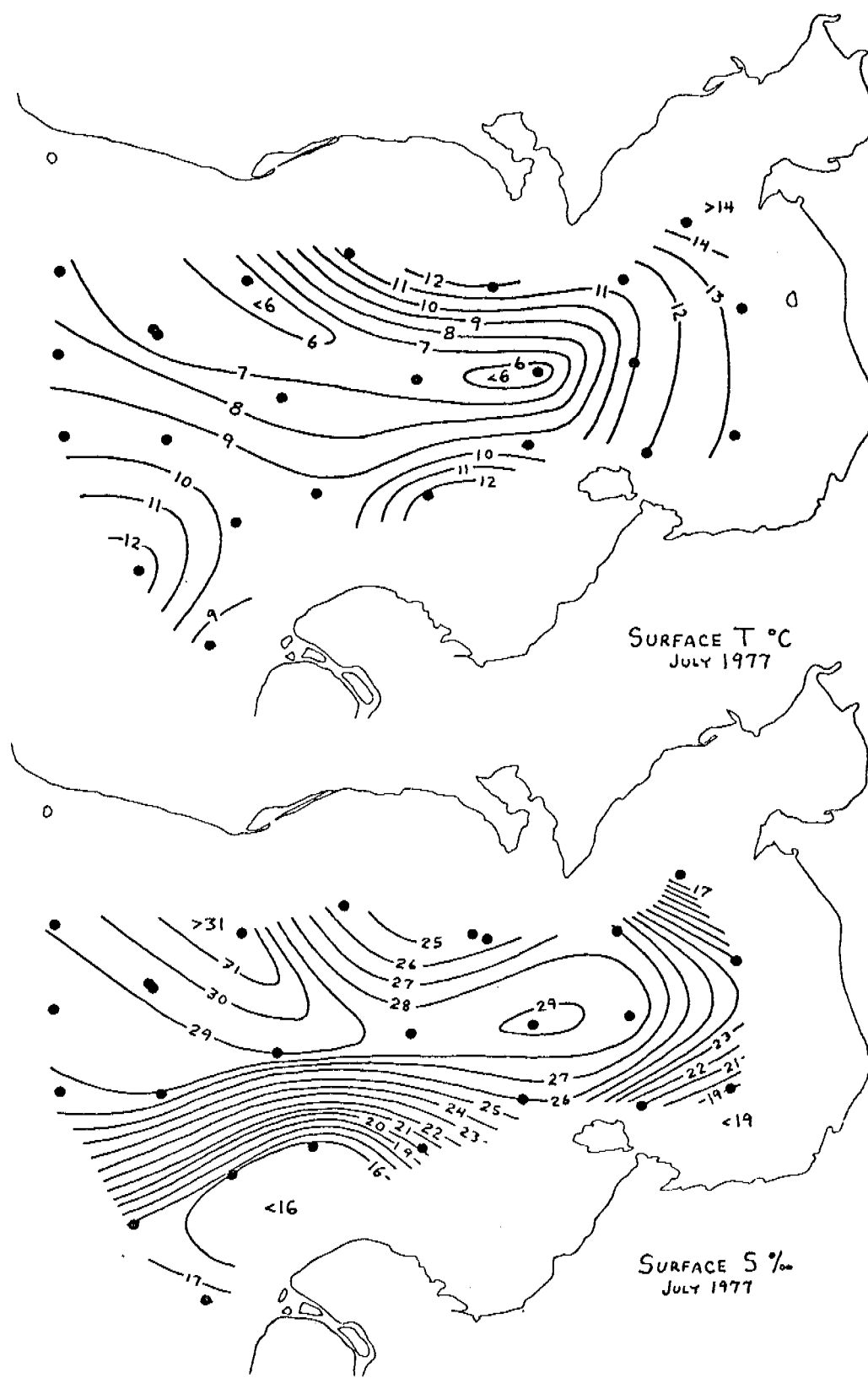


Figure 7. Surface distributions of temperature and salinity, 8-12 July, 1977.

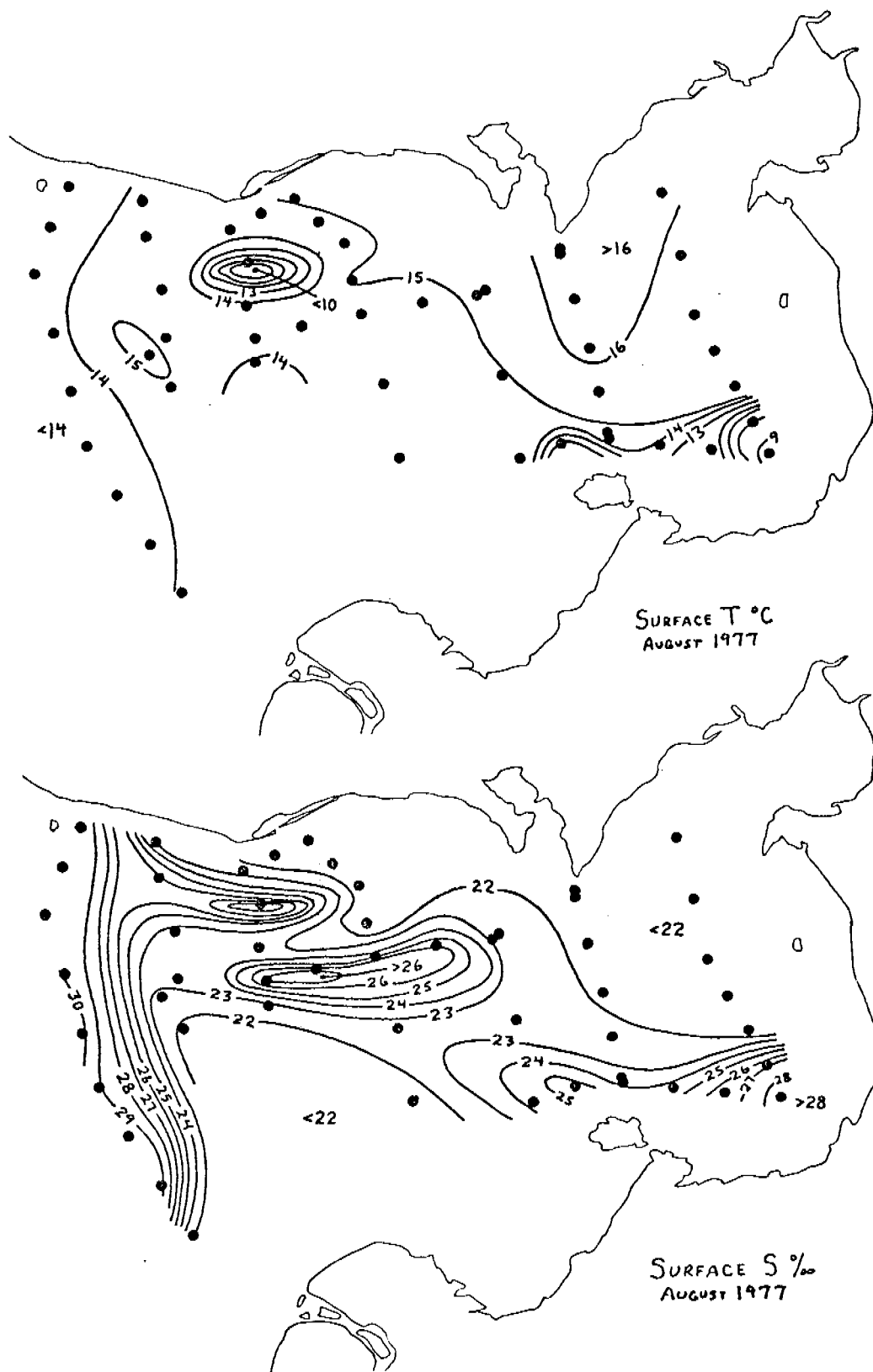


Figure 8. Surface distributions of temperature and salinity in Norton Sd., 26-29 August, 1977. (NOAA vessel *Surveyor*)

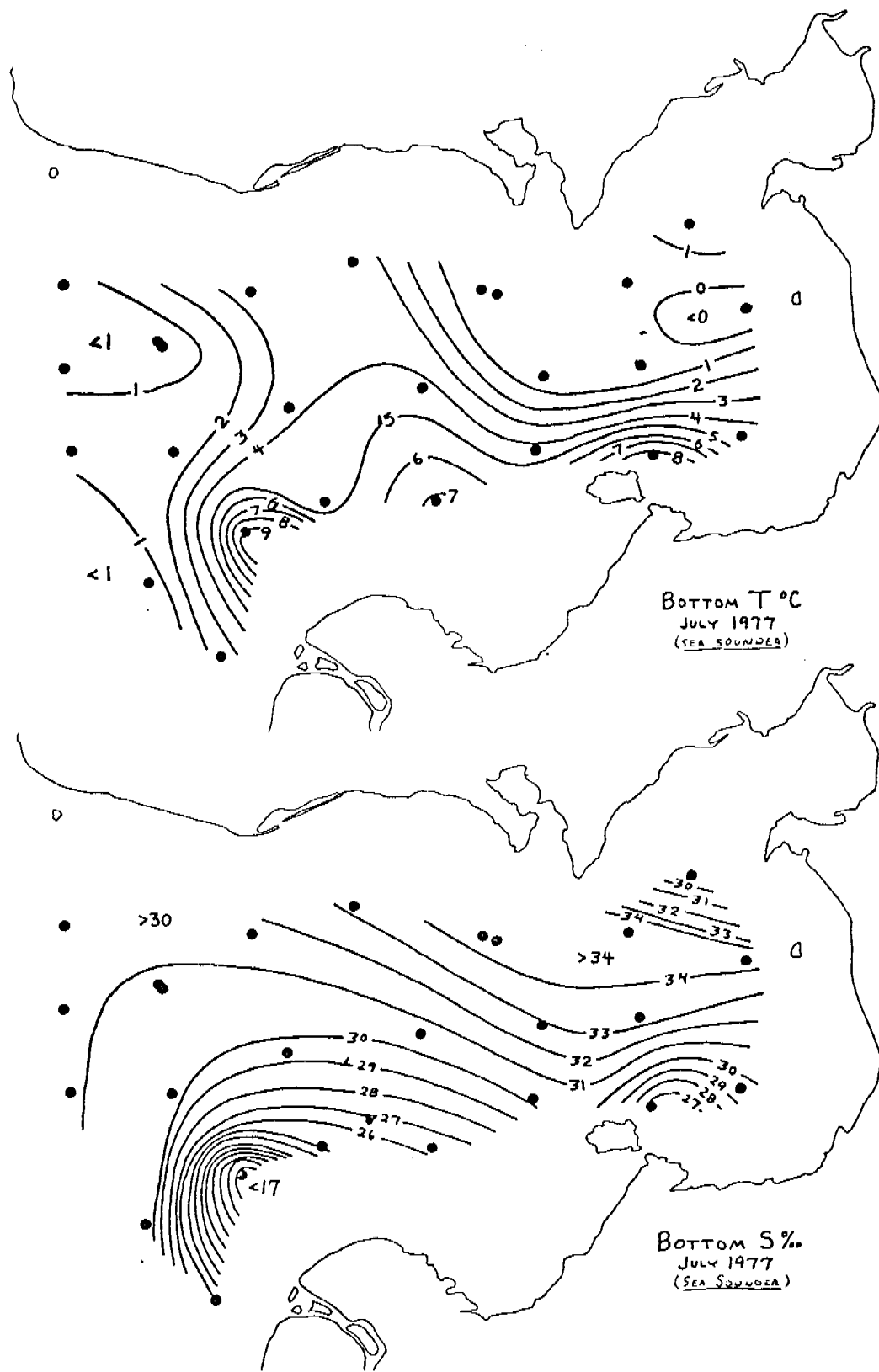


Figure 9. Near-bottom distributions of temperature and salinity, 8-12 July, 1977. (USGS vessel *Sea Sounder*)

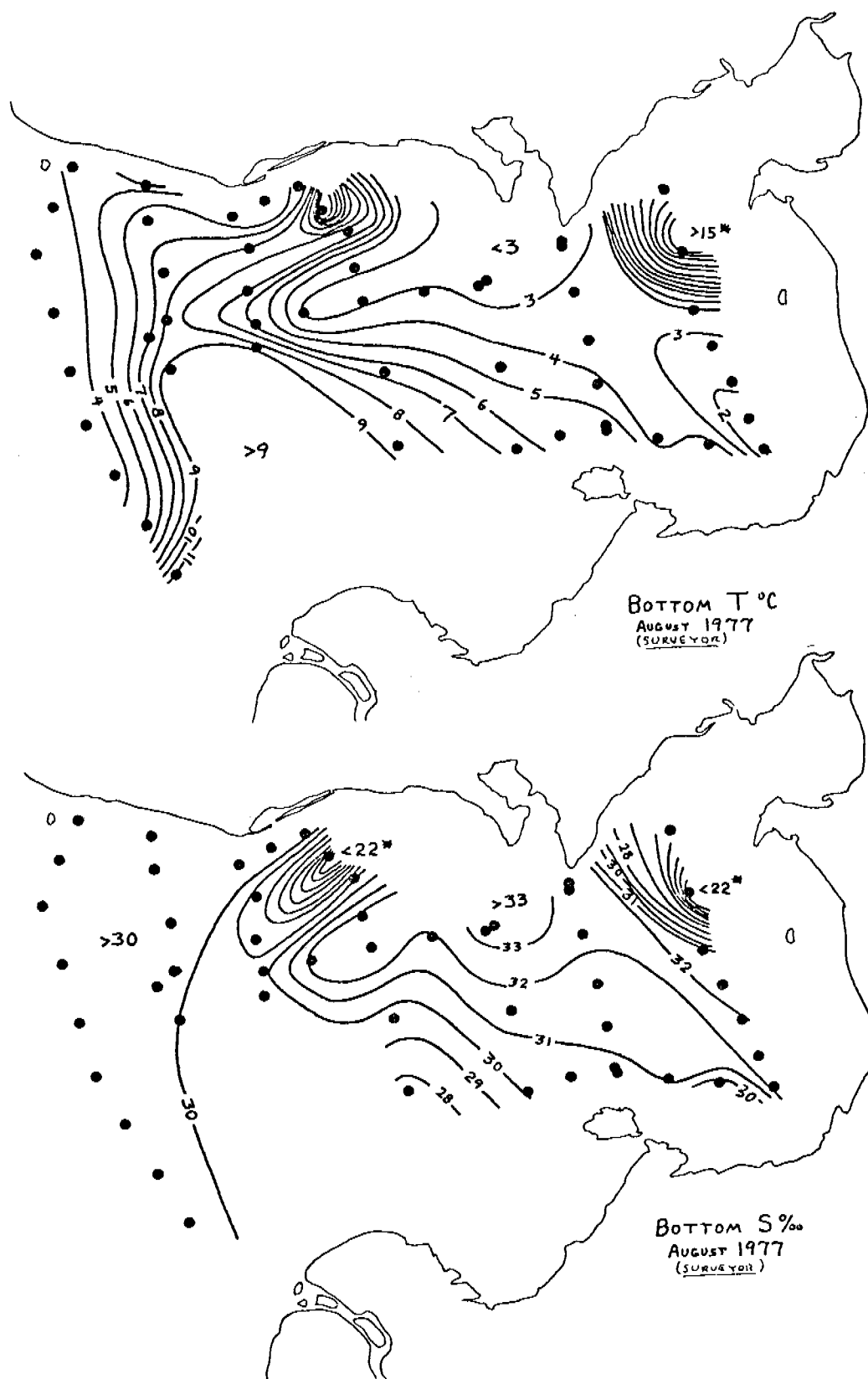


Figure 10. Near-bottom distributions of temperature and salinity, 26-29 August, 1977. (NOAA vessel *Surveyor*)

anomalously warm, fresh water in August ($\sim 15^{\circ}\text{C}$ and $< 22 \text{ }^{\circ}/\text{‰}$), marked with asterisks, actually represent conditions in the upper rather than lower layers because the CTD casts were not continued close enough to the bottom to penetrate the lower layer. These two points therefore do not represent near-bottom conditions.

Selected vertical temperature and density (as sigma-t) sections illustrate that the system was generally strongly two-layered during summer 1977 (Figures 11-14). (An exception was the central western portion, in the region which we characterize below as undergoing vertical mixing). The lower layer was cold ($1-4^{\circ}\text{C}$) and relatively dense ($\sigma_t = 24-27$), while the upper layer was warmer ($7-16^{\circ}\text{C}$) and of lower density ($\sigma_t = 13-23$). The two-layered structure was more pronounced in the eastern than in the western portion of the Sound, and persisted through late summer (July-August).

B. The 1976-77 Moored Current Meter Program

Of the 13 current records recovered from the overwinter 1976-1977 period, only three have been examined in detail to date; NC-10, NC-16 and NC-17. These comprise a set in the northern Bering Sea; southeast of St. Lawrence Island (NC-16 and NC-17), and in Bering Strait (NC-10) (cf. Figure 5). The remainder of the records, those from the Chukchi Sea and Kotzebue Sound, are still undergoing processing.

We present the results from moorings NC-10, NC-16 and NC-17 as spectra and progressive vector diagrams (PVD's) (Figures 15-21). Each of these moorings yielded a long-term (greater than 7 months) current record about 9 m from the bottom. Each record revealed a northward mean flow throughout the measurement period; NC-16 and 17 recorded mean speeds about 5 cm/s, while NC-10 had a mean speed of about 10 cm/s. Large north-south fluctuations

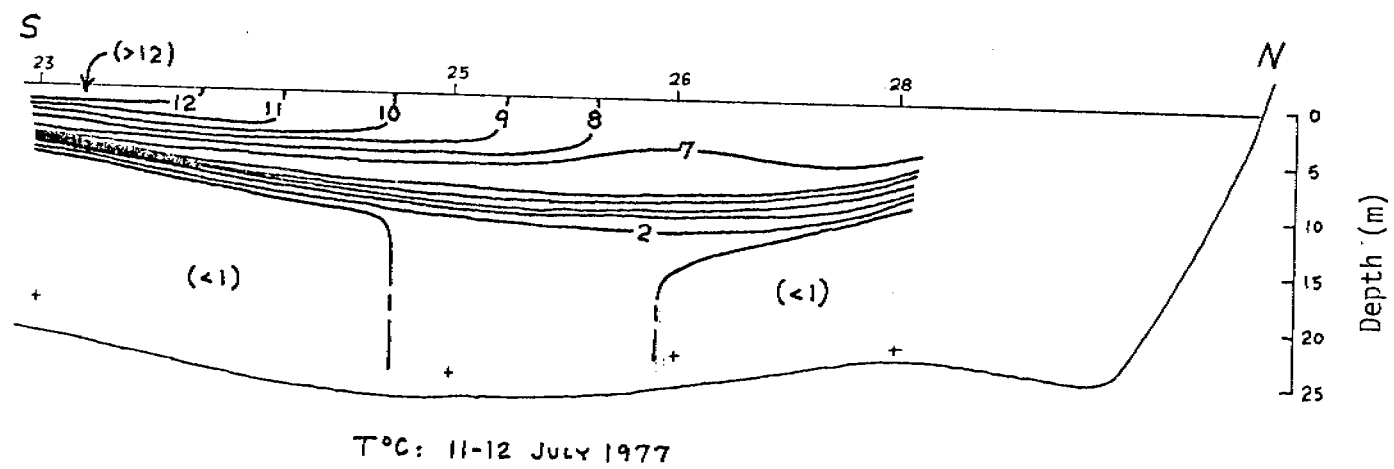
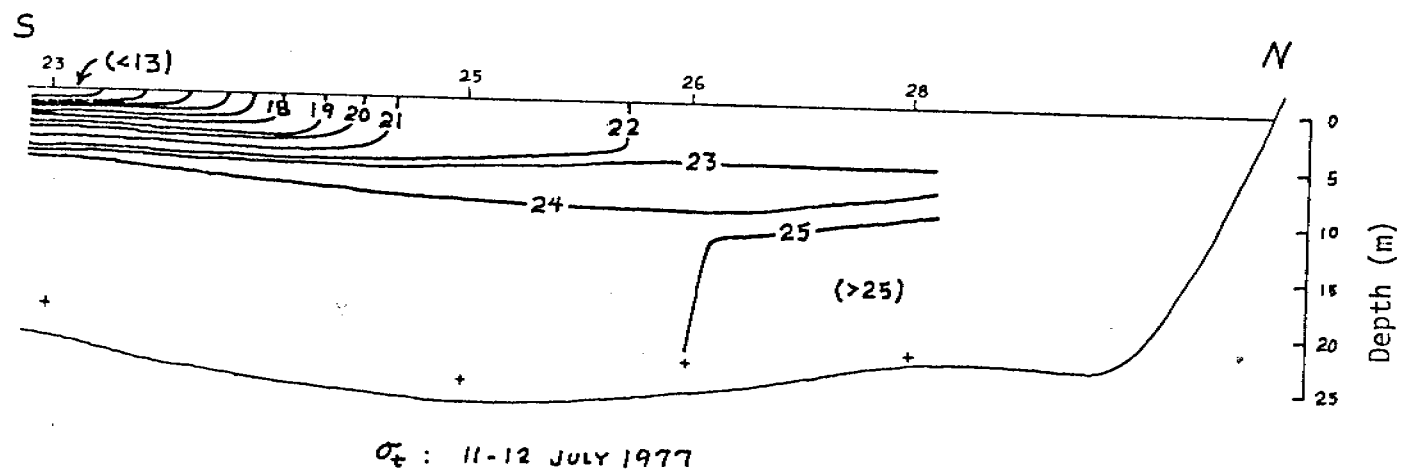


Figure 11. Vertical distributions of density (as sigma-t; upper) and temperature (lower) across western Norton Sound; 11-12 July, 1977.

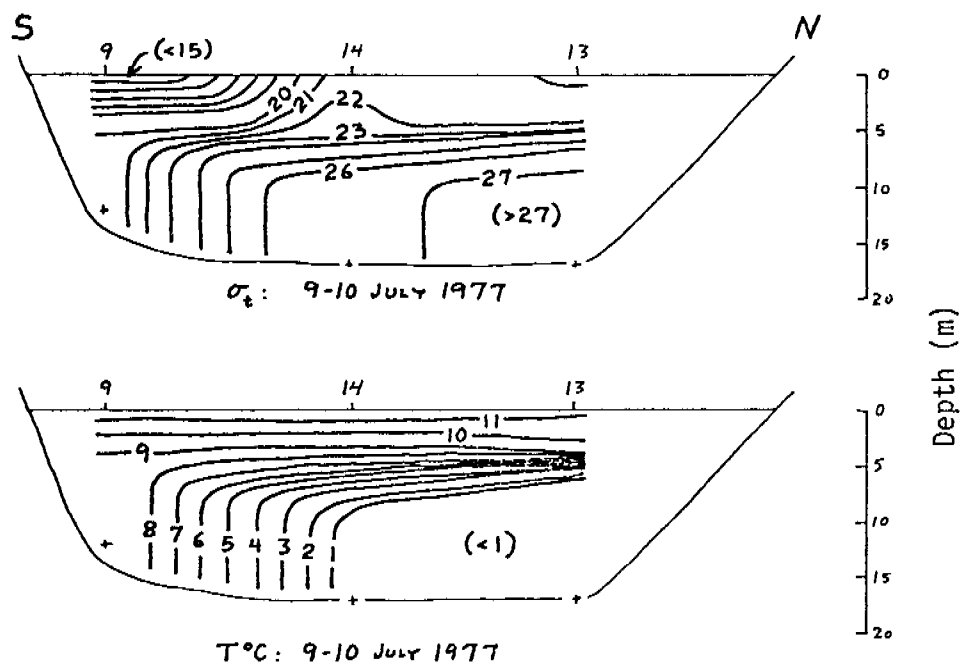


Figure 12. Vertical distributions of density (as sigma-t; upper) and temperature (lower) across eastern Norton Sound; 9-10 July, 1977.

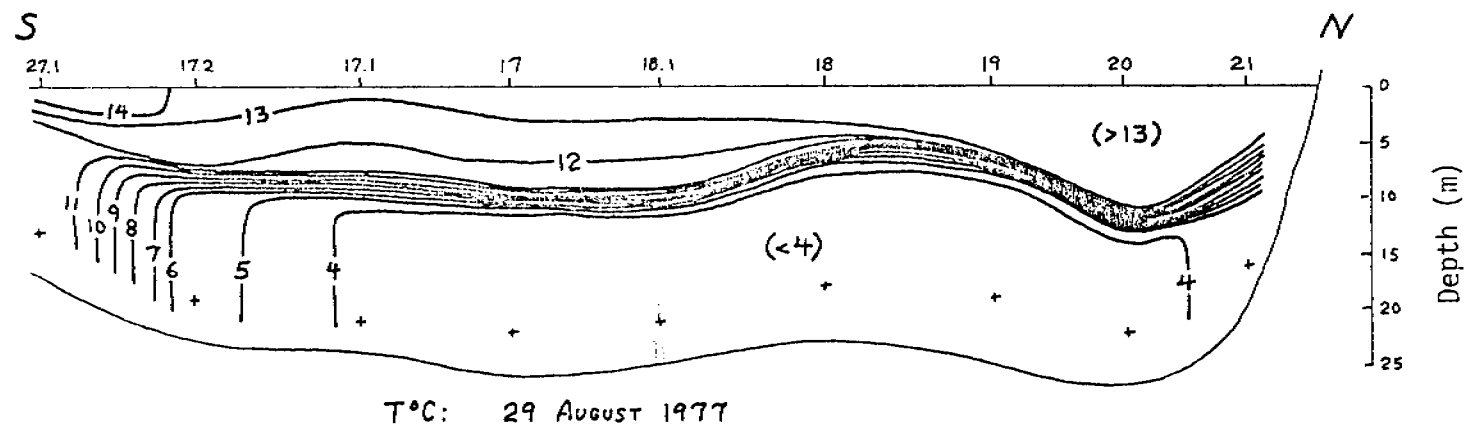
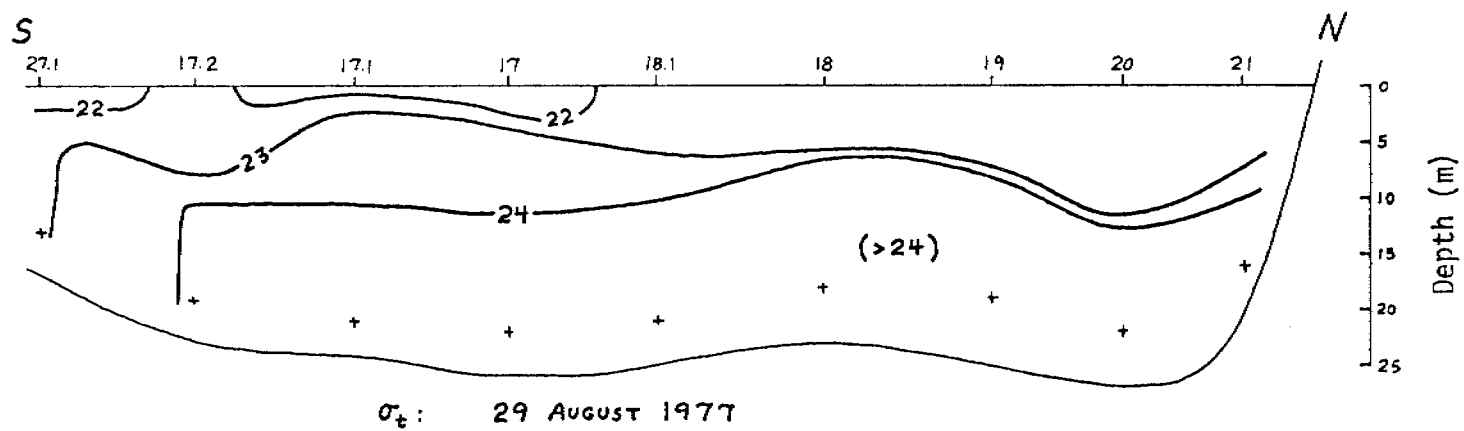


Figure 13. Vertical distributions of density (as sigma-t; upper) and temperature (lower) across western Norton Sound; 29 August, 1977.

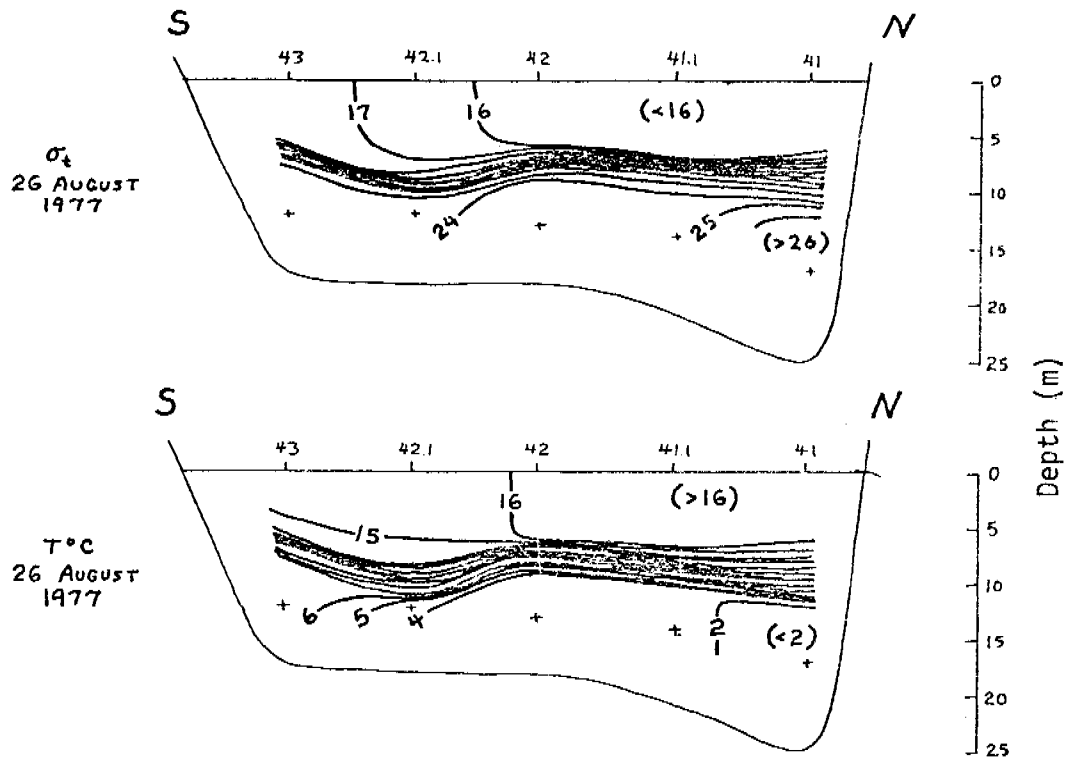


Figure 14. Vertical distributions of density (as sigma-t; upper) and temperature (lower) across eastern Norton Sound; 26 August, 1977.

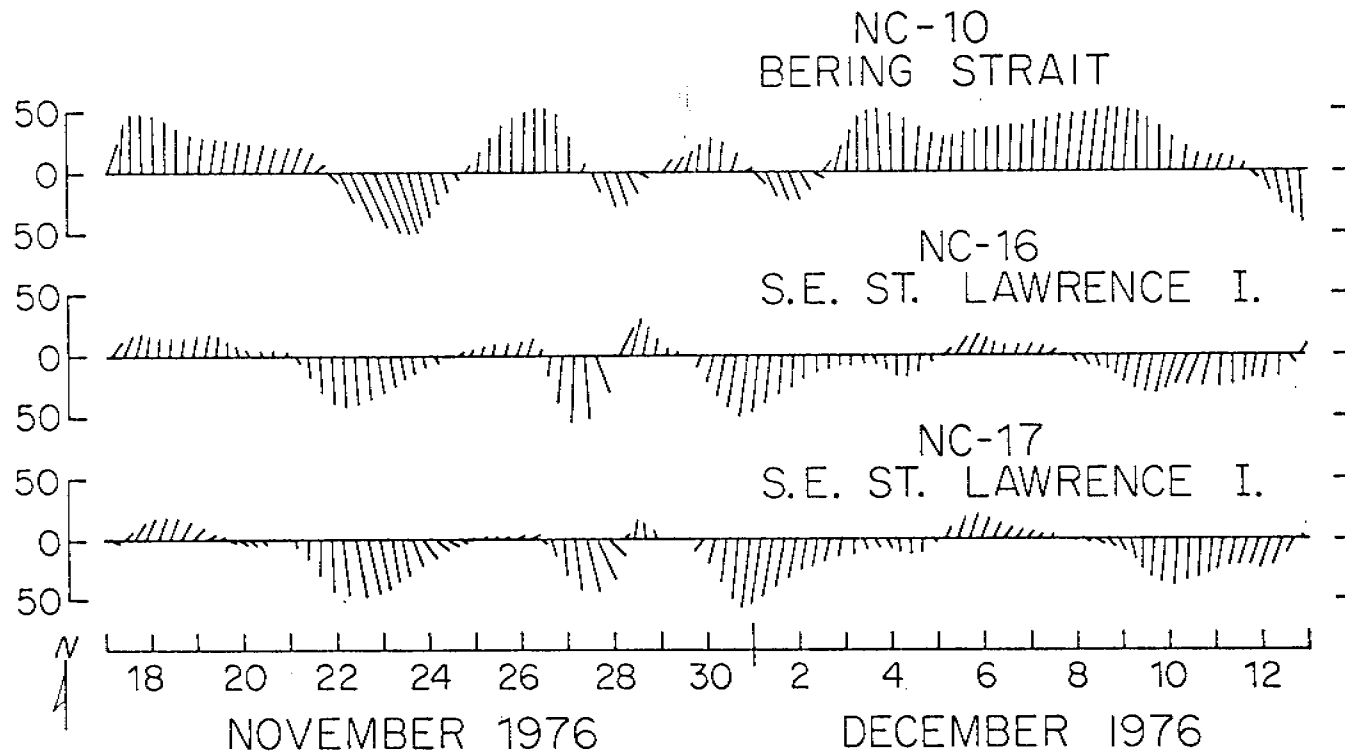
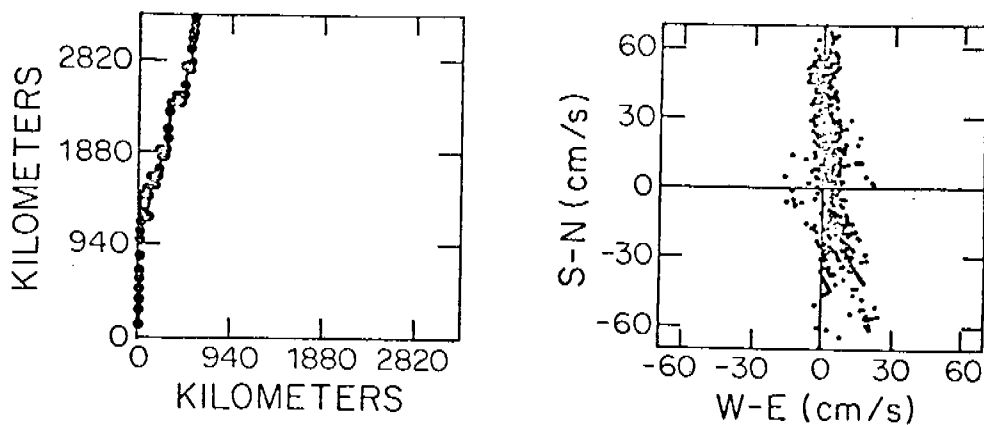
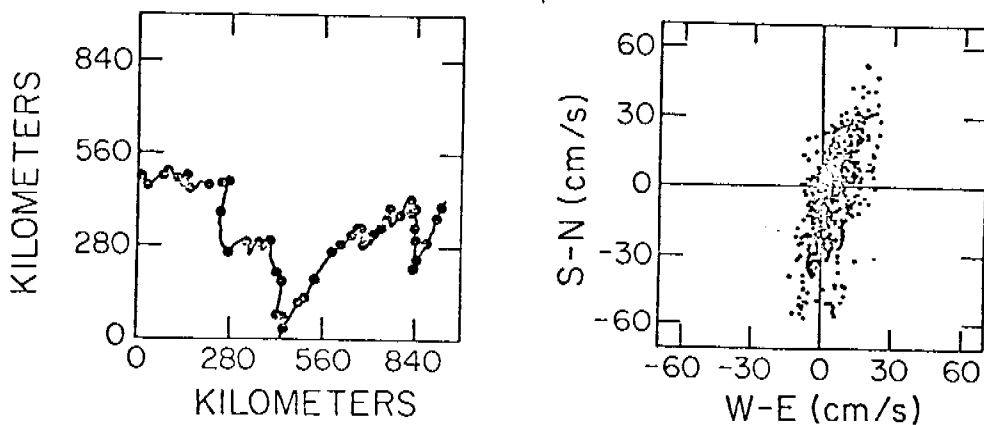


Figure 15. Portion of the 35-hour filtered currents from NC-10, NC-17 and NC-16.

NC-10
BERING STRAIT



NC-17
S.E. ST. LAWRENCE I.



NC-16
S.E. ST. LAWRENCE I.

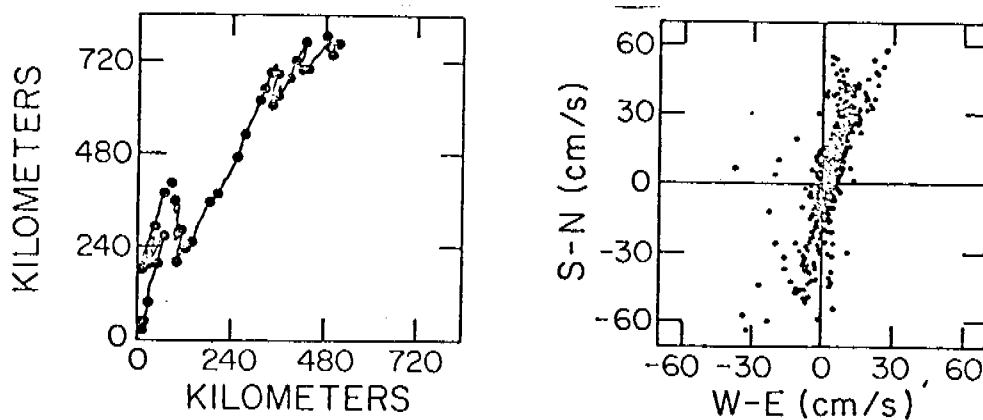


Figure 16 Progressive vector diagrams (left) and scatter plots (right) of NC-10, NC-17 and NC-16 currents.

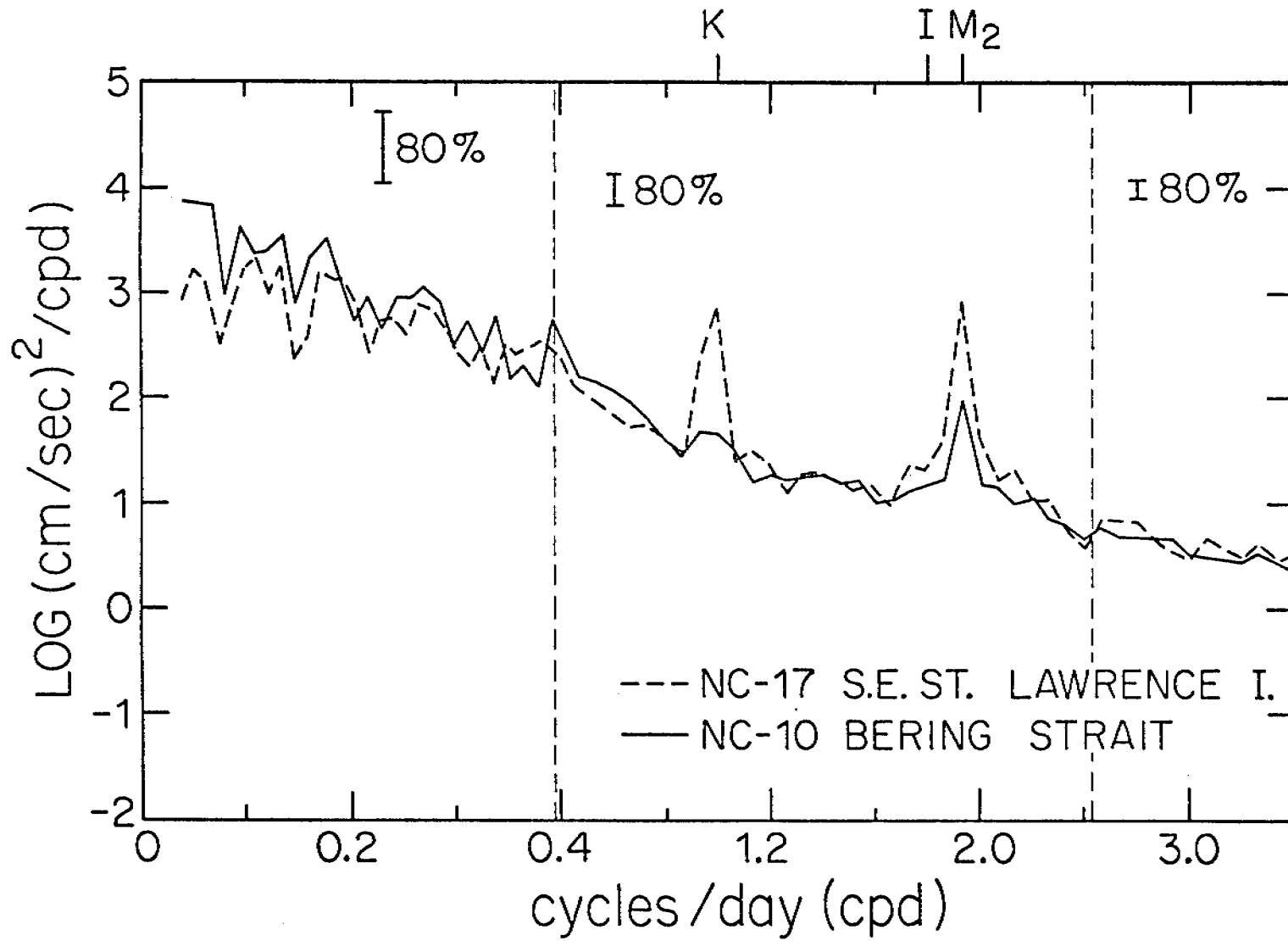


Figure 17. Energy density spectra for NC-10 and NC-17.

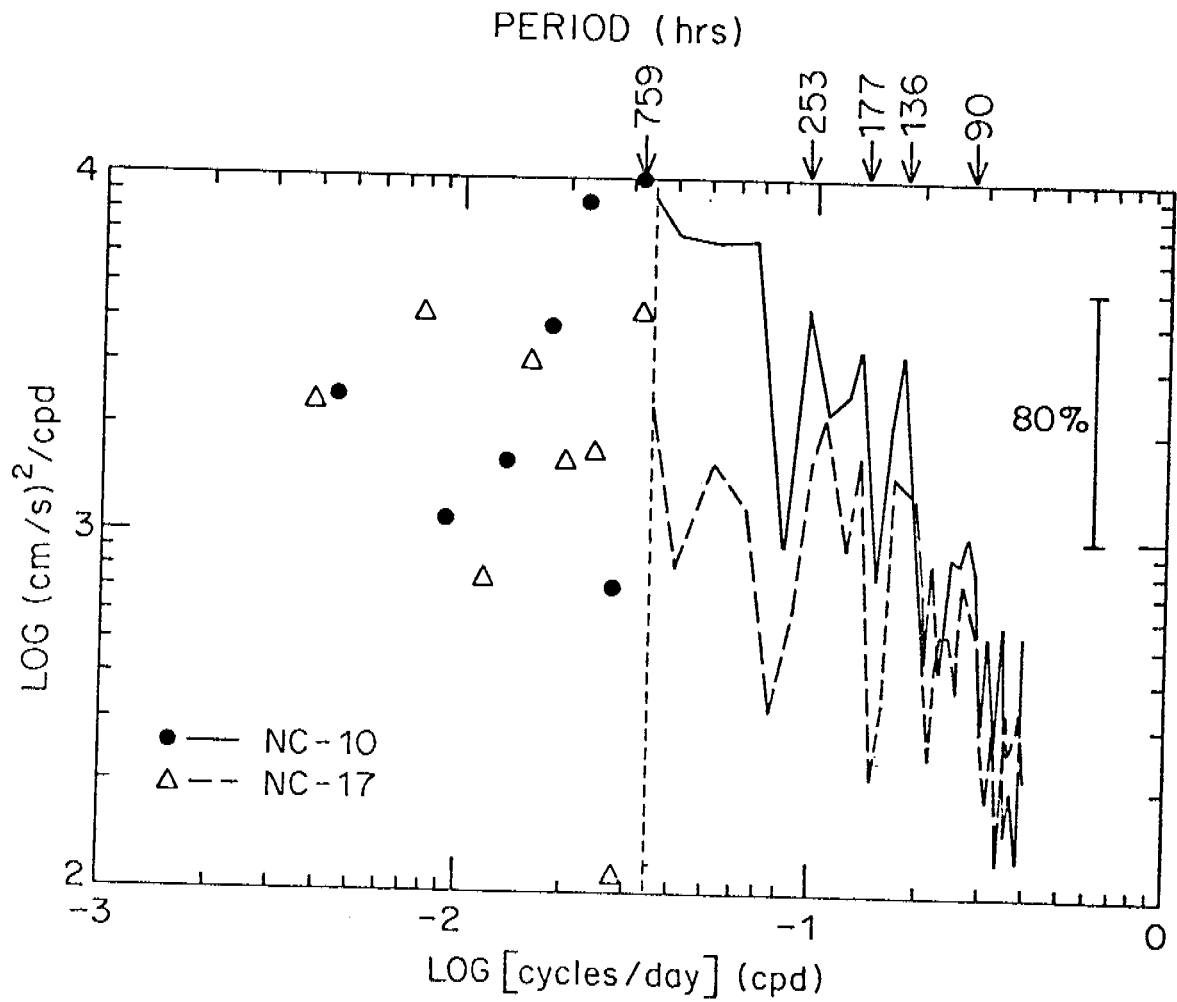


Figure 18. Low frequency portion of the energy spectra from NC-10 and NC-17. The left-hand portion contains the primitive spectral estimates only.

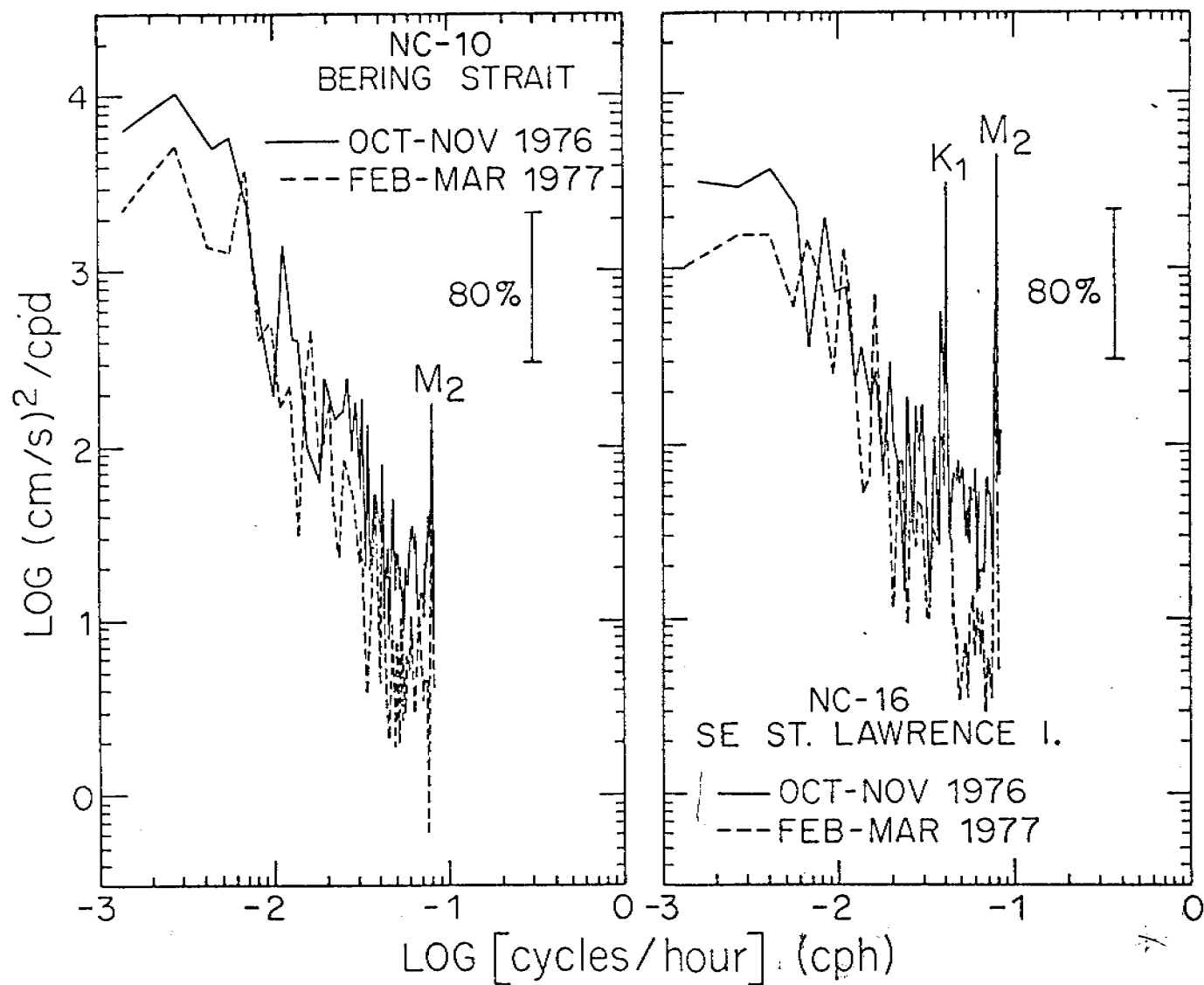


Figure 19. Comparison of energy spectra from NC-10 and NC-17 during two different time intervals; before ice formation (Oct-Nov) and after (Feb-Mar).

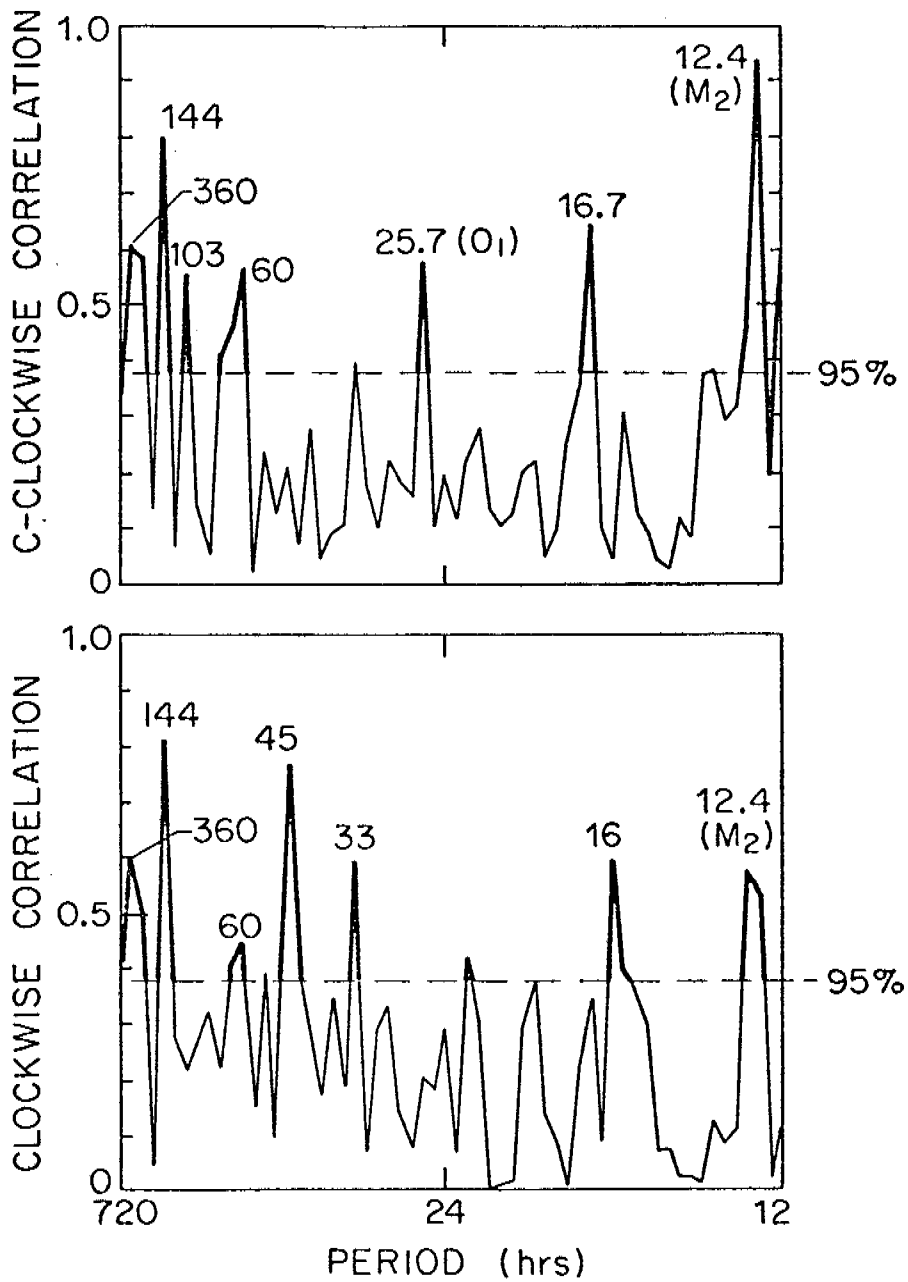


Figure 20. Clockwise and counterclockwise rotary correlations between complete current records from NC-10 and NC-17.

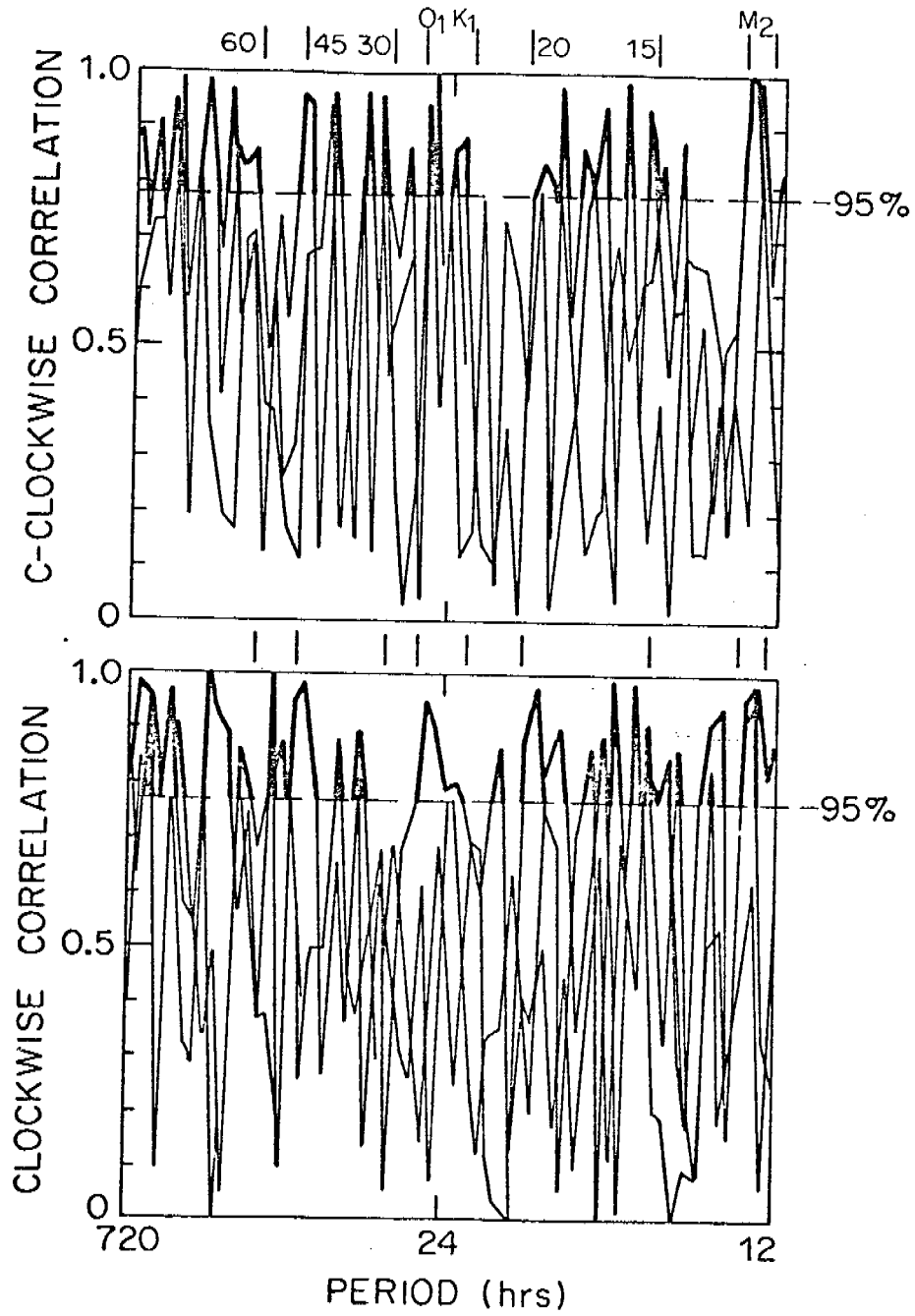


Figure 24. Composite of rotary correlation spectra computed separately for the periods Oct-Nov, Dec-Jan and Feb-Mar 1976-77 at NC-10 and NC-17.

(>50 cm/s) were superposed upon this mean flow at each of the mooring locations, and can be seen in a representative sample of the 35-hour filtered record (Figure 15). Currents were aligned with the local topography, as can be seen from PVD's at the three locations (Figure 16). The alignment in Bering Strait, at NC-10, was more pronounced as might be expected in view of the increased topographic flow constriction there. The scatter diagrams indicate that NC-16 and NC-17 both had the same major flow axes and that there was little cross channel flow, while in the Bering Strait the major axis had rotated slightly to the left in adjustment to the local topography. Maximum event speeds of 50-60 cm/s can be seen on the scatter plots.

Much information can be gained about time series current records by examining the energy spectra. Figure 19 shows the spectra from NC-17 and NC-10. (Records from NC-16 and NC-17 yielded similar spectra, only the NC-17 spectra is plotted for simplicity.) The currents at NC-17 have clearly defined tidal signals (K and M_2 on the figure), and no significant energy in inertial bands (I on the figure). The record from NC-10 has, on the contrary, little energy in the diurnal tidal band (K) and an order of magnitude less energy in the semidiurnal (M_2) band than did NC-17. In the low-frequency (<0.4 cpd) portion of the spectrum, there are several spectral peaks which occur on both the NC-10 and 17 records. A closer examination of this portion of the spectrum (Figure 18) reveals consistent peaks in energy density at periods of 90, 136, 177 and 253 hours. Of these, only the last three were significant at the 80% confidence level.

It was also informative to construct u,v spectra for NC-10 and NC-16 (same as NC-17, as before) over a series of intervals which then serve as subsample intervals of the overall record. The records were broken down into

two-month intervals and spectra constructed for each; the first intervals coincided with the latter portion of the ice-free season, while the second and third coincided with ice-covered seasons. Energy density of the currents decreased by factors of from 2 to 5 when the ice formed, as shown by comparison of the spectra from the different moorings before and after ice formation (cf. Figure 19). The most pronounced decrease occurred in the frequency range between diurnal and semidiurnal tidal (K_1 and M_2); in that range, the nearby order of magnitude decrease was clearly significant at the 80% confidence level.

To clarify relationships between current components at the two locations (Bering Strait and southeast of St. Lawrence Island; basically, a downstream-upstream situation) we computed rotary coherence of the spectra from NC-10 and NC-17 (Mooers, 1973). Computation using the entire series yielded the results shown on Figure 20. Significant correlation was found at semidiurnal tidal frequencies (M_2) for both clockwise and counterclockwise components. There were also correlations at scattered low-frequencies, notable ones being the 60 and 144-hour peaks which occurred in both clockwise and counterclockwise components. Similar computations were then made for each of the two-month subsampling intervals for NC-10 and NC-17, and the results superposed (Figure 21). In this case, if we neglect the O_1 and K_1 tidal peaks, it is apparent that significant correlations occurred in two bands; 15-20 hour periods, and 30-45 hour periods. These bands were pronounced only in the c-clockwise correlation. It appears then that correlated non-tidal periodic motions in this region tend to occupy preferred frequency bands rather than occurring at discrete frequencies.

It may be noted that the segment of the time series record shown in Figure 15 indicates clearly, in the earlier part of the record, a signal having a period of 4-6 days (96-144 hours). These peaks were well correlated at all three locations during the earlier portion of the record shown, as would be expected in view of the scattered correlation peaks in the 90-144 hour (period) spectral range. During the latter portion of the segment shown, however, correlation between the currents at NC-10 and those farther south had broken down. While the currents at NC-16 and NC-17 continued to fluctuate, fluctuating currents at NC-10 were replaced with a continual northward flow. This varying degree of visual correlation is characteristic of these records throughout their duration.

C. Discussion

The Summer 1977 Norton Sound Program

Hydrographic data collected in Norton Sound during summer 1977 support the general results arrived at from analysis of summer 1976 data. The system was two-layered in temperature, salinity and density (as σ_t). The low temperatures (1-2°C) and high densities ($\sigma_t = 26-27$) of the lower layer in the eastern Sound suggest that this was remnant water remaining from the previous winter's convective layer. There is no other local source, during summer, for water having these characteristics; deep water in the western Sound having similar temperatures (1-4°C) was considerably less dense ($\sigma_t = 24-25$) (cf. Figures 11-14).

The temperature increase and concurrent density decrease observed in the deep water from July-August 1977 were due to a combination of diffusive exchange of heat and salt with overlaying water, diffusive exchange with water

to the west and limited advective exchange with water to the west. Any appreciable advection of water into the eastern Sound would have replaced the existing water; low temperature water from the preceding winter would not have been present. The near-bottom current meter on mooring NC-21 failed to operate, so no record of deep currents in the region was available. A near-surface (~ 5 m deep) record from NC-21 revealed a net drift of about 6 cm/s toward 316°T . Due to the shallow depth of the meter, this net drift figure was biased to an uncertain extent by pumping of the meter's rotor by surface wind waves; actual net drift may have been lower. This measurement was in the upper layer of the two-layered system, and it is not likely that it represented flow conditions near the bottom because of probable decoupling of flow across the pycnocline.

South of the channel which parallels the shoreline off Nome, there is a shoal bank-like area having depths of less than about 20 m. There was a breakdown, particularly pronounced during July, of the vertically two-layered structure over this shoal. This resulted in higher salinities and lower temperatures at the surface there than elsewhere in that portion of the Sound (cf. Figures 17 and 18). We believe this is due to vertical mixing over this shoal consequent to impingement of currents on the bottom. Extent of this region is shown, for July, but the distribution of vertically averaged $\delta\sigma_t/\delta z$, where small values indicate a lack of stratification (Figure 22). At that time, the zone of minimum vertical stratification coincided roughly with the region of high surface salinity ($>31 \text{ ‰}$) and low temperatures ($<6^\circ\text{C}$) (cf. Figure 9). In August, the mixed zone appeared far smaller, and coincided with casts which were moreover too shallow to allow averaging of

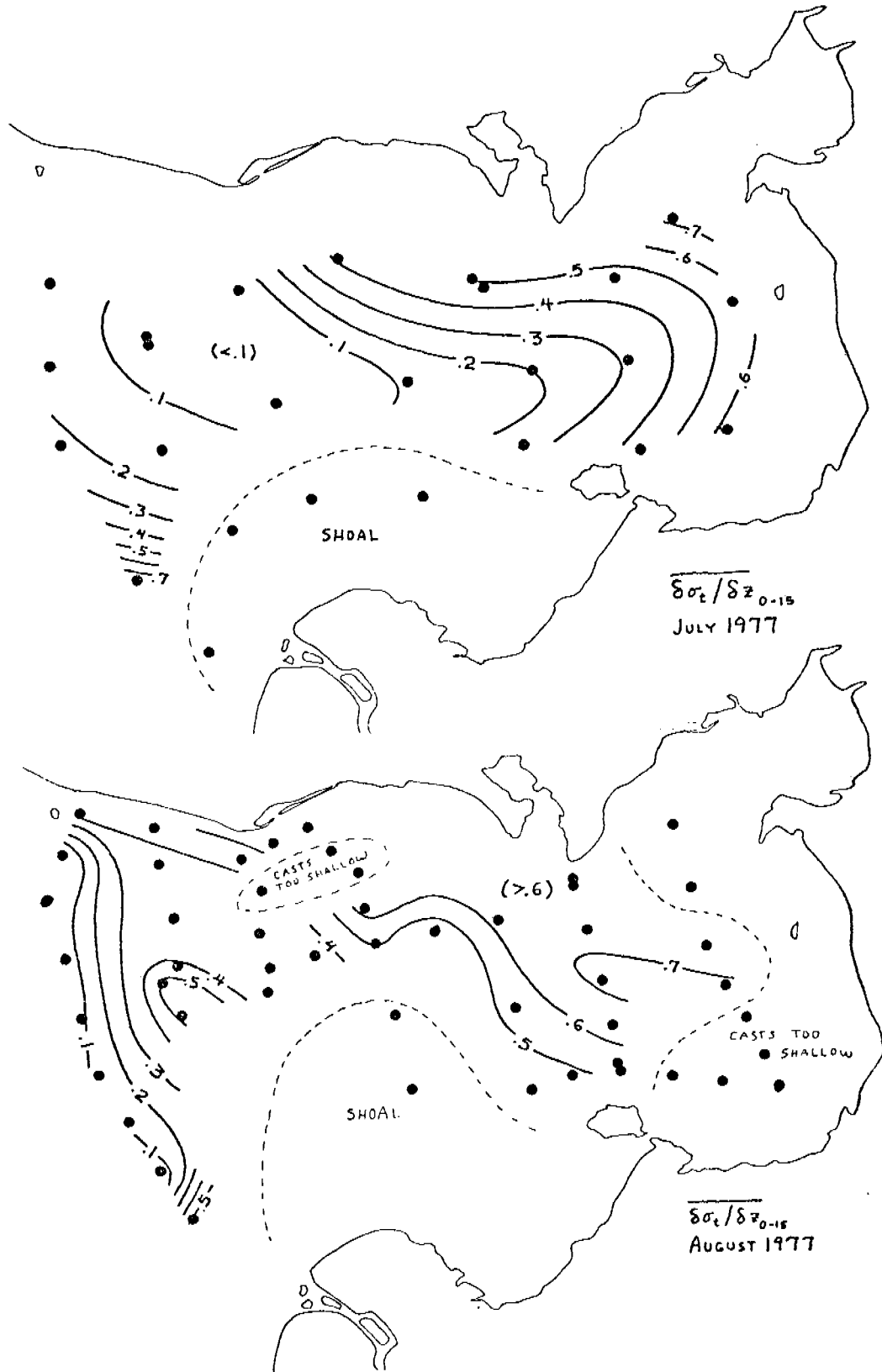


Figure 22. Horizontal distributions of vertically averaged values (computed at 1-m intervals) of $\delta\sigma_t/\delta z$.

$\delta\sigma/\delta z$ down to 15 m. Vertical density structure through the low stratification area is shown in the two lower (eastern) cross-sections of density (Figure 23); the area was centered on stations 31 and 34.1.

The September-October 1976 data from Norton Sound (cf. the last annual report) indicated that a westerly baroclinic coastal flow was present south of Nome. The vertical distribution of density at four sections in this same region during August 1978 gave no indication of such a feature (Figures 13 and 23). The July 1978 data did not extend close enough to shore to detect such a feature if in fact it had been present. The surface distributions of temperature and salinity did suggest, however, that a westerly coastal flow was present near the surface during August; a wedge of warm ($>15^{\circ}\text{C}$), low salinity (22 ‰) water was continuous from the eastern sound to the coastal region near Nome (Figure 9). This was supported by the 5 m recorded currents at NC-21, just south of Cape Darby, which recorded a net flow of about 6 cm/s toward 316°T . While there was considerable fluctuation in the currents at this location during the recording period, there was no reversal to easterly flow (Figure 24). The other recording current meter emplaced during this same period, NC-20, was too far southwest to have sampled any coastal flow. This record did indicate, however, a consistent flow toward the north-northwest (Figure 25) yielding a net drift of about 8 cm/s. This record (obtained, like the NC-21 records, at about 5 m depth) supports the hypothesis advanced using the summer 1976 data that flow in the western Sound is net northerly. It also agrees with circulation deduced from the distribution of dissolved natural gas during summer, 1976 (Cline and Holmes, 1977).

During both July and August, there was no spatial continuity between the low salinity water off the Yukon River north and that in the eastern Sound (Figures 8 and 9). This supports the hypothesis that Yukon water is

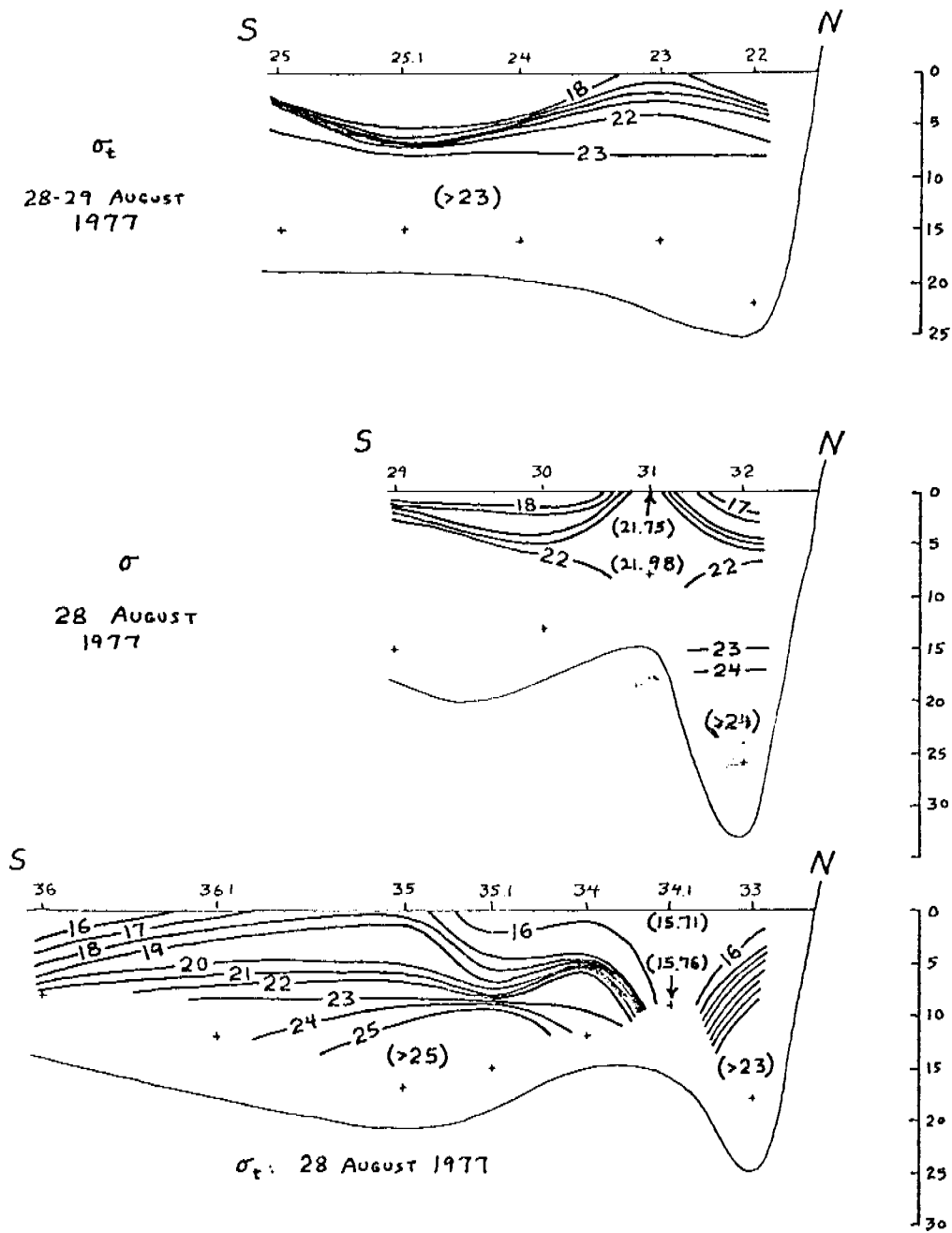


Figure 23. Vertical distributions of density along three sections in northern Norton Sound during August 1977. Upper section extends south from Cape Darby, lower section from Nome, and middle section about halfway between.

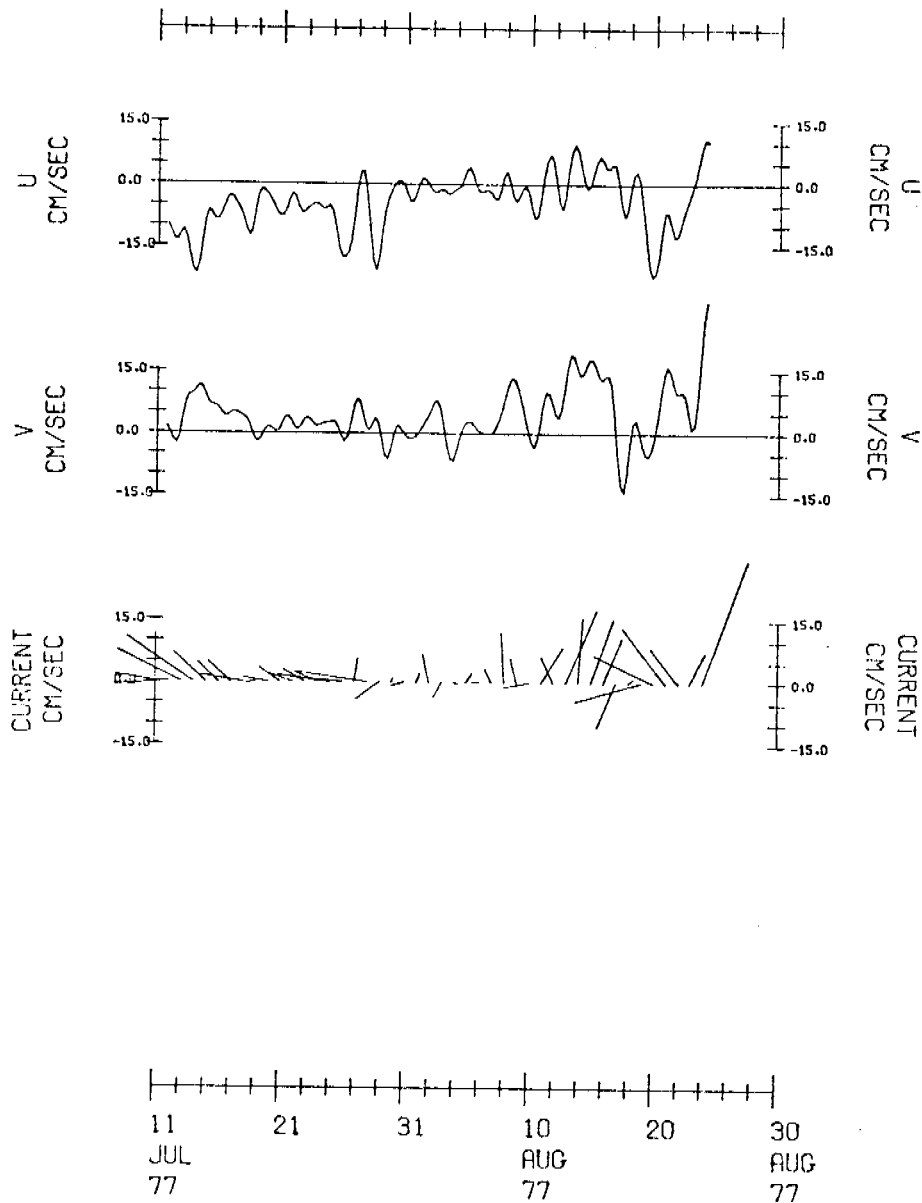


Figure 24. Graphical presentation of 35-hour filtered currents at NC-21, from a depth about 5 m below the surface. Filtering was done according to the methods of Charnell and Krancus (1976).

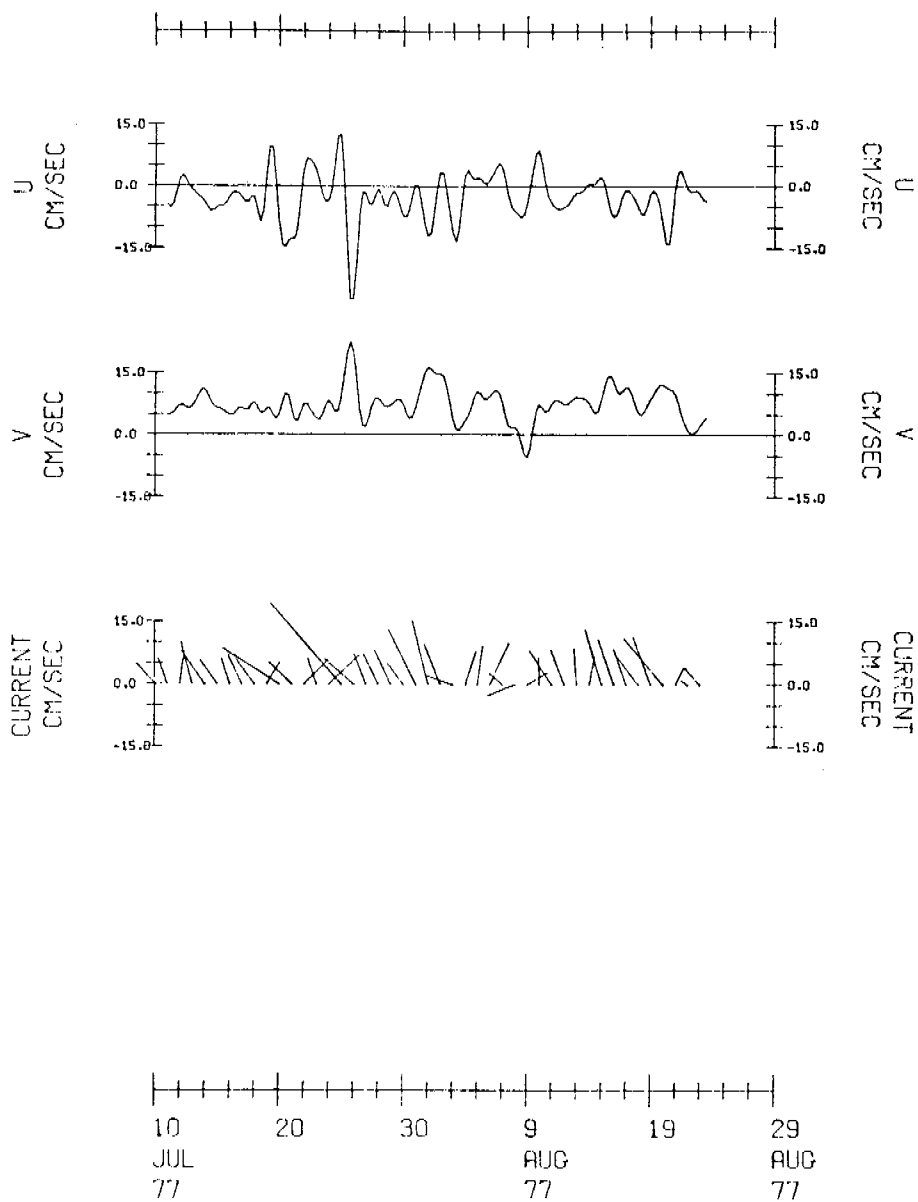


Figure 25. Graphical presentation of 35-hour filtered currents at NC-20, from a depth about 5 m below the surface. Filtering was done according to the methods of Charnell and Krancus (1976).

not regularly advected into the eastern Sound along the coast, though the possibility of irregular pulses of Yukon water to that region remains. Such pulses have not been observed. Based on extrapolation of precipitation figures from Nome, local freshwater runoff is more than adequate to account for the decreased salinities in the eastern Sound. Norton Bay, in particular, appears by its low salinities to contain a freshwater source.

Accumulation of sufficient freshwater in eastern Norton Sound to lower surface salinities there was in part a consequence of sluggish horizontal circulation, while the higher surface salinities in the northwestern Sound are due to continual advection through the system of higher salinity water from offshore on the Bering shelf. Some elevation of surface salinity in the region south of Nome may also be due to vertical mixing leading to upward salt transfer from the deeper, more saline water. The horizontal circulation appears to occur primarily in the western Sound, apparently being prevented by the partial stricture formed by Cape Darby and Stuart Island from entering the eastern Sound. The overall decrease of salinity throughout the Sound during summer 1977 demonstrated accumulation of freshwater in the system.

The 1976-77 Moored Current Meter Program

The overwinter moored current program, whose preliminary results are presented in part above, represents the first successful attempt to obtain current measurements from beneath the northern Bering Sea ice cover. These results have documented and verified that flow through Bering Strait is northerly throughout the winter, a fact which has previously been supposition based on indirect evidence (Coachman *et al.*, 1975). While the flow was observed to reverse on numerous occasions, the reversals never lasted for prolonged periods. We hypothesize that these non-tidal reversals are due to

regional-scale weather disturbances; proof of this awaits further analysis of the current and weather data presently in our possession.

Preliminary estimates, made using spectra, of energy contained in the currents has revealed that energy decreases at the time of ice formation, with the most pronounced decrease being in the higher frequency motions (between semidiurnal and diurnal tidal, especially). This pattern was found in the records for NC-10, NC-16 and NC-17. We hypothesize that this may be due to two separate effects: first, presence of the ice may effectively diminish the amount of higher frequency energy transferred from wind to the water; and second, the ice may act as an upper boundary layer and tend to selectively damp out higher frequency motions. Inevitably, such a boundary effect would also decrease the overall energy in the system, as observed. More rigorous analysis awaits a complete processing of the atmospheric data and of the additional current records which were obtained in the Chukchi Sea (NC-1 through NC-7).

Comparison of current records from southeast of St. Lawrence Island with one from Bering Strait, via rotary coherence analysis, reveals coherence in the tidal bands and in longer period fluctuations. The phase lags in the semidiurnal tidal band yielded an impossible propagation speed; tides in the Bering Strait and farther south appear to behave independently, reflecting their origins in the Arctic Ocean and the Bering Sea, respectively. All evidence suggests that the tides in the area between St. Lawrence Island and Bering Strait, extending into Norton Sound, are extremely complex. For example, the diurnal tidal signal has nearly disappeared between St. Lawrence Island and the Bering Strait. Analysis of tidal currents awaits more rigorous analysis of all available current and sea level measurements from the region, including records from those moorings presently emplaced.

Of the coherent longer-period fluctuations, the two most persistent appear to be the 60 and 144-hour signals. The phasing of these, as derived from the rotary correlations, suggest northward propagation at several meters per second. This is of the same speed as would be expected for northward propagating meteorological disturbances. Seich-like motions in the northern Bering Sea, in the region bounded by St. Lawrence Island, the Bering Strait and Norton Sound, might also generate periodicities in these bands. These problems await more rigorous analysis, particularly of the available atmospheric data. Spectral analyses of the atmospheric pressure records are expected to be particularly informative, as are analyses of the geostrophic winds west of Norton Sound.

D. Conclusions

Hydrographic data obtained in Norton Sound during July-August 1977 supported the overall conclusions arrived at using summer 1976 data. The Sound was vertically two-layered in temperature, salinity and density, except in a school region south of Nome where vertical turbulence appeared to have destroyed the layering. The lower layer was colder and more saline than the upper layer. The interface between layers effectively reduced vertical heat and salt transfer. This, coupled with apparently weak horizontal advection and diffusion, preserved the identity of cold, saline near bottom water remaining from the previous winter's cold, convective regime.

The upper layer appeared to circulate in a generally cyclonic fashion, most of this being confined to the western Sound. Surface temperatures and salinities in August, in conjunction with a recorded series of currents off Cape Darby, support flow of surface water out of the eastern Sound along the northern coast. The vertical density structure indicated, however, that a

westward baroclinic coastal current observed in that region in 1976 was not present in 1977. A northward flow in the western Sound was indicated by an upper layer current record over the summer in agreement with hypotheses based on summer 1976 CTD and dissolved natural gas data.

The Norton Sound lower layer showed virtually no net motion in the eastern Sound, based on presence of remnant water from the preceding winter's regime which remained there until at least late August. Lower layer mean circulation in the western Sound was probably more vigorous, but awaits direct measurements: both of the current meters moored near the bottom in Norton Sound during summer 1977 malfunctioned and yielded no data.

Overwinter moored current data from southeast of St. Lawrence Island and in the Bering Strait have verified the presence of a northward net flow through the Strait during winter. Relatively large non-tidal north-south flow events were superposed on the northward net flow. Kinetic energy density of the currents decreased at the time of surface ice formation, probably due to the frictional influence of the ice cover.

Current data which have been analyzed to date indicate that the tidal regime in the northern Bering Sea-Bering Strait region is exceedingly complex. Preliminary analyses suggest propagation of tidal waves into the region from both the Bering Sea and the Arctic Ocean.

E. References

Bakun, A., Coastal upwelling indices: West coast of North America.

NOAA Technical Report NMFS SSRF-671, 1973.

Charnell, R. and G. Krancus, A processing system for Aanderaa

current meter data, NOAA Technical Memo. ERLPMEL-6, Seattle,

Washington, 1976.

Cline, J.D. and M.L. Holmes, Submarine seepage of natural gas in Norton Sound, Alaska, *Science*, 198, 1149-1153, 1977.

Coachman, L.K., K. Aagaard and R.B. Tripp, *Bering Strait, The Regional Physical Oceanography*, University of Washington Press, Seattle, Washington, 1975.

Mooers, C.N.K., A technique for the cross spectrum analysis of pairs of complex-valued time series, with emphasis on properties of polarized components and rotational invariants, *Deep-Sea Research*, 20, 1129-1141, 1973.

VII. Cooperation

We cooperate with the following research units:

289 (Royer) Satellite imagery displays features of the seasonal ice cover and reveals the northward extension of the structural front.

435 (Leendertse and Liu) We provide hydrographic, current, and pressure data. Together we attempt to understand the tidal regime.

430 (Cacchione and Drake) We are exchanging data and ideas, and trying to understand the physical and sediment transport regimes of Norton Sound.

VIII. NEEDS FOR FURTHER STUDY

Further study under this program should concentrate on analyzing data already obtained, and trying to understand the phenomena thus revealed. This effort can be fruitfully supplemented by selected field work, and by analytical and numerical investigations. Some specific areas of study include:

- A. Synthesize the moored instrument and hydrographic data to develop a coherent picture of the physical oceanography of Norton Sound;
- B. Synthesize the moored instrument and hydrographic data to develop a coherent picture of the physical oceanography of Kotzebue Sound;
- C. Using hydrographic and current meter data, examine the connection between the regime in the N-COP area to the regime farther south in the B-BOP area;
- D. Describe and explain the low frequency (less than diurnal) current regime;
- E. Analyze the tides;
- F. Investigate the structural front that apparently extends from the Bristol Bay region into the N-COP region;
- G. Examine the interaction between wind, current, and sea ice along the ice edge;
- H. Investigate the character and dynamics of the Yukon River plume.

Data are in hand to address most of these topics, so that strong emphasis on data analysis should prove fruitful. Once the individual areas are addressed, a synthesis of the regional physical oceanography should be possible.

IX. CONCLUSIONS

Preliminary analysis of data reveals interesting and important features in the hydrographic and velocity regimes, including:

- A. Cold and salty water, relict from the previous winter, which apparently remains in the bottom layers of Norton and Kotzebue Sounds during summer;

- B. Low frequency current fluctuations near Bering Strait;
- C. Complex tidal behavior; and
- D. An extension of the structural front from the shelf to the south.

Once these and other aspects of the area are comprehensively analyzed and better understood, a synthesis of the regional physical oceanography will be possible.

APPENDIX A.

UW Mooring Data Summary

- 1) Mooring NC-1A
Latitude: 68-15.4 N
Longitude: 172-40.6 W
Current meter depth: 39 meters
Data Period: 8/25/76 to 6/17/77
- 2) Mooring NC-2A
Latitude: 68-29.7 N
Longitude: 171-55.3 W
Current meter depth: 41 meters
Data Period: 8/26/76 to 4/4/77
- 3) Mooring NC-3A
Latitude: 68-44.2 N
Longitude: 171-06.2 W
Current meter depth: 45 meters
Data Period: 8/26/76 to 8/7/77
- 4) Mooring NC-4A
Latitude: 69-00.7 N
Longitude: 169-59.2 W
Current meter depth: 43 meters
Data Period: 8/25/76 to 5/6/77
- 5) Mooring NC-6A
Latitude: 68-57.2 N
Longitude: 168-18.6 W
(a) Current meter depth: 44 meters
Data period: 8/25/76 to ~3/22/77
The quality of data is very poor
towards the end of the record.
(b) Pressure gauge depth: 49.7 meters
Data period: 8/25/76 to 4/30/77
- 6) Mooring NC-7A
Latitude: 68-55.2 N
Longitude: 167-21.3 W
Current meter depth: 36.4 meters
Data period: 8/24/76 to 8/6/77
- 7) Mooring NC-8A Kotzebue Sound
Latitude: 66-54.7 N
Longitude: 164-02.2 W
Current meter depth: 16.1 meters
Data period: 8/23/76 to 4/29/77
No speed data. Rotor fell off after
deployment of mooring.

- 8) Mooring NC-9A
Latitude: 66-43.5 N
Longitude: 164-08.8 W
Current meter depth: 14.5 meters
Data period: 8/23/76 to 5/9/77
Speed data questionable after January
as heavy growth on rotor changed threshold.

The University of Washington has been late in submitting the above data to the OCSEAP Project Office for two reasons. First, the change in computer systems within the department necessitated extensive reprogramming and debugging of the system. Secondly, the quality of some of the data has further burdened us with more than the normal updating of the records. We anticipate that all data will be submitted to the data bank by the end of April.

